International Cryogenics Monograph Series

Franco Pavese
Gianfranco Molinar Min Beciet

Modern Gas-Based Temperature and Pressure Measurements

2nd Edition

Springer

Modern Gas-Based Temperature and Pressure Measurements

For other titles published in this series, go to
http://www.springer.com/series/6086

INTERNATIONAL CRYOGENICS MONOGRAPH SERIES

Franco Pavese • Gianfranco Molinar Min Beciet

Modern Gas-Based Temperature and Pressure Measurements

Second Edition

Springer

Dr. Franco Pavese
Istituto di Metrologia “G. Colonnetti”
(IMGC)
Consiglio Nazionale delle Ricerche (CNR)
(from 2006 merged with IEN into INRIM)
Torino
Italy

Dr. Gianfranco Molinar Min Beciet
Istituto di Metrologia “G. Colonnetti”
(IMGC)
Consiglio Nazionale delle Ricerche (CNR)
(from 2006 merged with IEN into INRIM)
Torino
Italy

ISBN 978-1-4419-8281-0 ISBN 978-1-4419-8282-7 (eBook)
DOI 10.1007/978-1-4419-8282-7
Springer New York Dordrecht Heidelberg London

Library of Congress Control Number: 2012938991

Preface

Since the beginning of the preparation of this book, which is the second edition of a previous book printed in 1992, we have been strongly convinced that temperature and pressure measurements should not be separated, particularly in different applications at low temperatures. This approach has been followed in the preparation of this second edition because advanced applications and modern experimental investigations in science and technology need the combination of various professional experiences, and this is particularly true for the thermodynamic quantities as temperature and pressure.

Although the book is divided in two parts (Part I by Franco Pavese and Part II by Gianfranco Molinar Min Beciet), plus the new Chap. 11 common to the two, we always tried to correlate low temperatures with low-medium pressures as much as possible.

This second edition book has been substantially revised in respect of the first edition, by considering new measurement methods, new systems and devices of the last 20 years. This reflects as well new achievements of metrology in general as the treatment of uncertainty, that is now more stable and well defined, and attention was posed as well to the effects of the BIPM-CIPM 1999 Mutual Recognition Arrangement (MRA) that have produced since 1999 many key comparison results and approval of many calibration and measurement capabilities.

We are pleased to acknowledge our debt to our research group colleagues at the Istituto di Metrologia Gustavo Colonnetti of CNR (IMGC-CNR), merged in 2006 within Istituto Nazionale di Ricerca Metrologica (INRIM) and to many persons at international level to which we have gladly cooperated. In particular, Franco Pavese acknowledges the competent help kindly obtained from INRIM colleague Peter P.M. Steur for the revision of Chaps. 3–5.

However, the persons that we really want to thank are our families; they have been always supporting us and they were able to create around us the "perfect atmosphere" in order to be relaxed and able of working always with great pleasure.

The first edition of our book was dedicated to our wives and sons (Ghita, Carlo and Matteo Pavese; Dida and Daniele Molinar Min Beciet).

This second edition is particularly dedicated to our—present—grand children's (Nicolai, Leonardo, Luca and Viola Pavese; Matteo Molinar Min Beciet) as they are the future of our dreams.

Torino (Italy)

Franco Pavese
Gianfranco Molinar Min Beciet

Contents

Part I Temperature Measurements in the Range from 0.1 to 300 K

1 The Concept of Temperature 3
1.1 Definitions of Temperature 4
1.1.1 The Phenomenological Approach 4
1.1.2 The Axiomatic Approach 10
1.1.3 The Microscopic Approach 13
1.1.4 Negative and Nonequilibrium Thermodynamic Temperatures and for (Fast)-Moving Bodies 16
1.2 Temperature Scales 17
1.2.1 Thermodynamic Temperature 20
1.2.2 Empirical Temperature 24
1.2.3 Official Temperature Scales 29
1.2.4 "Mise en Pratique" for the Definition of the Kelvin 31
1.2.5 Difference Between the Realized Thermodynamic Temperature and the T_{90} 38

2 Gas-Based Reference Points for Thermometry 45
2.1 Thermodynamic States Versus Standard Reference Materials 46
2.1.1 Substances Versus Standard Reference Materials 46
2.1.2 Thermodynamic States and Phase Diagrams 48
2.1.3 Reference Points: Triple, Boiling, and Critical Points 50
2.2 Physical Chemistry Associated with Gas Triple Points 50
2.2.1 Triple Point of a Pure Substance 50
2.2.2 Triple Point of an Impure Substance. Cryoscopy 54
2.3 The Realization of Temperature Fixed Points Using Gas Triple Points 76
2.3.1 Basic Problems in the Design of Cells for Accurate Realization of Triple Points 77
2.3.2 Chemical-Physical Problems in the Realization of Triple Points 85
2.3.3 Thermal Errors in Sealed Cells and Related Problems in Measurement 89

2.4 Modern Design of Temperature Fixed Points Based on the Triple Point of Gases 94
2.4.1 The Technique of Sealed Cells for the Realization of a Temperature Reference 94
2.4.2 Further Checks Necessary to Achieve a Total Uncertainty of ≈50 μK in Triple Point Best Realizations 101
2.4.3 Performance of Sealed Cell Models 109
2.5 Fixed Points Using Other Phase Transitions 123
2.5.1 Liquid-To-Liquid Transitions 123
2.5.2 Solid-To-Solid Transitions 129
2.6 The ITS-90 Between 13.80 and 273.16 K and Scale Approximations Using Sealed Fixed Points 131
2.6.1 Realization of the ITS-90 in the Laboratories 132
2.6.2 Approximating the ITS-90 135
2.7 Gaseous Standard Reference Materials, and Sealed Cells 139

3 Gas Thermometry Between 0.5 and 273.16 K 147
3.1 Constant-Volume Gas Thermometry 148
3.1.1 Influence of Physical Parameters 150
3.1.2 Influence of Technical Parameters 160
3.1.3 Gas Thermometers with a Built-in Pressure-Measuring Device 172
3.2 Interpolating Constant-Volume Gas Thermometers 176
3.2.1 ICVGT Types with Stipulation of the Virial Function 179
3.3 Constant-Volume Gas-Thermometer Realizations 183
3.3.1 CVGTs with Reference at Temperatures Lower than 273.16 K 183
3.3.2 CVGTs with Reference Temperature at 273.16 K 191
3.3.3 CVGTs Using a Cryogenic Pressure Measurement 193
3.3.4 Realizations of Interpolating Gas Thermometers 195
3.3.5 Gas Thermometry in the ITS-90 198
3.4 Dielectric-Constant, Refractive-Index, and Acoustic Gas Thermometers 200
3.4.1 Dielectric-Constant Gas Thermometry 201
3.4.2 Refractive-Index Gas Thermometry 205
3.4.3 Acoustic Gas Thermometry 207
3.4.4 The Boltzmann Project 214

4 Vapor-Pressure Thermometry 221
4.1 Influence of Physical Parameters 224
4.1.1 Purity of the Substance 224
4.1.2 Effect of the Amount of Thermometric Substance 232
4.2 Influence of Technical Parameters 234
4.2.1 Thermometer with Gauge for Pressure Measurement at Room Temperature 234

4.2.2 Use of Sealed Cells for Vapor-Pressure Measurements 239
4.2.3 Thermometer with Gauge for Pressure Measurement at Low Temperature 240
4.2.4 Liquid–Vapor Versus Solid–Vapor Equilibria 241
4.3 Realization of Vapor-Pressure Temperature Scales 242
4.3.1 Equations for Vapor Pressure 243
4.3.2 Helium Vapor Pressure 246

5 Thermometry Based on the Melting Line of ^{3}He 261
5.1 The ^{3}He Melting-Line Thermometer 263
5.1.1 Melting-Line Experiments Below T_{min} 266
5.1.2 Melting-Line Experiments Above T_{min} 267
5.1.3 Pressure and Temperature Measurement 267
5.1.4 The ^{3}He Melting-Line Scale 268

6 Cryostats for Thermometry and Gas-Based Temperature Control ... 269
6.1 Cryostats 269
6.1.1 Refrigerator-Based Cryostats 270
6.1.2 Liquid-Refrigerant Cryostats 274
6.2 Temperature Control in Thermometry and Gas-Based Temperature Controls 278
6.2.1 Control of the Cryogen Bath Temperature 279
6.2.2 Vapor-Flowrate Control 280
6.2.3 Passive Thermostats 280
6.2.4 Self-Regulating Passive Shields 280
6.2.5 Gas-Filled Heat Switches 282

Part II Pressure Measurements in the Range from 10^2 to 10^8 Pa

7 Primary Standards for Pressure Measurements 291
7.1 Liquid-Column Manometers for Pressure Measurements 298
7.1.1 Operating Principles and General Precautions for Absolute Pressure Measurements Below 0.3 MPa 299
7.1.2 Basic Apparatus in Metrological Laboratories: Different Methods for Height Measurements 301
7.1.3 Calculations Applicable with Mercury-Column Manometers: Pressure Measurement Uncertainty 316
7.1.4 Liquid Columns for Different Applications 327
7.2 Gas-Operated Pressure Balances 330
7.2.1 Basic Description 331
7.2.2 Absolute Pressure Measurements to 5 MPa 336
7.2.3 Gauge Pressure Measurements up to 100 MPa 351
7.2.4 Uncertainty of Absolute and Gauge Pressure Measurements with Pressure Balances 368

7.2.5 Results of Comparison Measurements in Gas Media with the Use of Pressure Balances 374
7.2.6 Comparisons of Liquid-Column Manometers and Pressure Balances 379
7.2.7 What Future for Primary Pressure Standards? 389
7.3 Summary of Typical Uncertainty Levels for Liquid-Column Manometers and Pressure Balances 391

8 Pressure Transducers for Gaseous Media 393
8.1 Transfer Standards for Absolute Pressure Measurements Below 120 kPa 395
8.1.1 Transfer Standards for Atmospheric Pressure Measurements 398
8.1.2 Transfer Standards for Gas Pressure Measurements from 100 Pa to 10 kPa 403
8.2 Transfer Standards for Pressure Measurements up to 100 MPa 406
8.3 Transducers Used for Differential Pressure Measurements and as Null Detectors 412
8.3.1 Differential Pressure Transducers for High Line Pressures .. 412
8.3.2 Differential Pressure Transducers Used as Null Detectors ... 416
8.4 Transducers for Pressure Measurements Extended to Cryogenic Environments 418
8.4.1 Strain-Gauge Pressure Transducers for Cryogenic Applications 422
8.4.2 Resonant- and Capacitance-Type Pressure Transducers for Cryogenic Applications 426
8.5 Glossary: Terms Used in the Metrological Characterization of a Pressure Transducer 429
8.6 Typical Procedure for the Static Calibration of a Pressure Transducer in Gaseous Media 430

9 Gas-Based Pressure Fixed Points 433
9.1 The Pressure Scale from 10^2 to 10^8 Pa Based on Pressure Fixed Points 435
9.1.1 Triple Points 436
9.1.2 Other Pressure Fixed Points 437
9.2 Experience in the Use of Fixed Points as Pressure Transfer Standards 438
9.3 Summary of Possible Fixed Points to be Used as Transfer Standards for Gas Pressure Measurements from 100 Pa to Approximately 100 MPa 443
9.4 Appendix: Properties of Substances not Gaseous at Room Temperature of Interest for Realization of Pressure Fixed Point 444

10 The Thermomolecular Pressure Difference Effect 447
10.1 Introduction 447
10.2 The Calculation of the Thermomolecular Pressure Difference 448
10.3 Experimental Measurements of the Thermomolecular Pressure Difference Effect 456
10.4 General Considerations on Experimental Measurements and Theoretical Calculations of the Thermomolecular Pressure Difference 461

11 The Mutual Recognition Arrangement and Its Implementation in Temperature and Pressure 463
11.1 Introduction 463
11.2 The Key Comparisons 464
11.2.1 Key Comparisons Related to Gas Pressure Measurements in the Range from 100 Pa to 100 MPa 465
11.2.2 Key Comparisons Related to Temperature Measurements Extending from 273.16 K Downward 479
11.3 The Calibration and Measurement Capabilities 481
11.3.1 Calibration and Measurement Capabilities for Gas Pressure Measurements in the Range from 100 Pa to 100 MPa 481
11.3.2 Calibration and Measurement Capabilities (CMC) for Cryogenic Temperature Measurements 491
11.4 The BIPM Key Comparison Database (KCDB) 491

Appendix A The International Temperature Scale of 1990 495

Appendix B List of Temperature and Pressure Fixed Points (Table B.1, B.2, and B.3) 511

Appendix C Reference Data on Gases 515

Appendix D Vapor Pressure Equations 541

Appendix E Reference Data for Liquid-Column Manometers (Tables E.1, E.2, E.3, E.4) 549

Appendix F Reference Data for Pressure Balances 555

Appendix G 561

Appendix H General Terminology in Measurements 575

References 581

Index 627

Introduction

The use of substances that are gaseous at room temperature for temperature measurements and for standards realization is traditional in the cryogenic field. Vapor-pressure thermometry and gas thermometry have been since a long time ago the commonest nonelectrical methods for temperature measurements in physics and chemistry. Correspondingly, specific primary and secondary standards have been developed to measure with improved accuracy pressure in gaseous media.

Most of the studies on thermophysical properties of these substances were carried out in the first half of the twentieth century, but work, though with less momentum, progressed especially at NIST (formerly NBS) in the USA and in Russia also in the second half. As far as its use in metrology is concerned, the adoption of the IPTS-68 in 1968 stimulated a new activity both intensive and extensive, as some of these properties form the basis of low-temperature thermometry, which led to the adoption of the new International Temperature Scale which came into effect on 1 January 1990 (ITS-90). Now, after more than 20 years that this scale is adopted, revisions have started. However, with the shift in 2006 of the meaning of "temperature scale" in the definition of the unit kelvin, caused by the introduction of the concept of "*mise en pratique*" of the kelvin, adjustments are now possible without having to promulgate a new ITS-xx.

This activity resulted in a sizeable upgrading of the accuracy in the determination of the gas properties relevant to temperature standards and on standards traceability to the thermodynamic temperature. New techniques were also developed, which greatly improved the reliability of fixed point realization; the possibility of simplifying the use of the existing standards and of adopting new gas-based standards was explored and it is now extensively exploited.

This book is intended to collect up-to-date information on the latest developments in thermometry and manometry that involve the use of gaseous substances and that are likely to be valid methods also in the future. At present, this information is dispersed in a large number of papers published in international journals and most of it is probably available only to a limited number of specialists. While other books on thermometry deal, in a comparable number of pages, with the *whole* range of temperatures and techniques, the part of the present work devoted to thermometry intends, in the first place, to introduce selected methods, leaving the general description of thermometry

to textbooks. Secondly, being limited to low-temperature and gas-based techniques, the present book intends to supply the reader with information about the very tools for their implementation. Instead of the usual "Problems", a synopsis of "Solutions" to problems of thermometry implementation is therefore added at the end of each chapter.

As regards to manometry and pressure measurements in general, this book fills a gap in the international literature, as no other recent book provides a comprehensive survey of methods for pressure measurements in gaseous media used in the medium-to-low pressure range closely connected with thermometry.

Although the two parts of the book on temperature and on pressure measurements both give special attentions to future-oriented techniques, their approach to deal with the subject is very different. Part I deals with thermometric techniques for which, apart few recent exceptions, no commercial devices are available: individual users must directly implement these types of thermometers. Consequently, most of the information collected is intended to help them to select the best design, from both standpoints of simplicity and accuracy, and to be self-sufficient to supply all data necessary for their implementation. On the contrary, for most of the pressure-measuring techniques dealt with in Part II, commercially apparatuses, particularly in the case of modern pressure balances and pressure transducers are available. Accordingly, users can find the basic description of such instruments and all the data necessary for appropriate criteria of selection, in view especially of their use at the best possible accuracy for thermometry and manometry applications.

The methods and the instruments dealt with, which allow medium-to-high temperature and pressure accuracy to be achieved, are *not* intended only for applications which need the top measurement accuracy of interest for standard laboratories (though the error analysis is always pushed to this level), but they can be used in a broader range of applications. However, the book does not include methods or instruments intrinsically limited to low accuracy. This second edition book was revised according to different advances made in the last 20 years in metrology, particularly to give evidence of the important role that the CIPM-MRA have assumed since its starting in 1999.

In Part I, basic concepts of temperature and temperature scale are first introduced together with a short review of the different temperature definitions, so that the reader may be made aware of the difficulties involved in defining temperature, especially when it becomes lower and lower.

The use of well-specified thermodynamic states of condensed gases as temperature fixed points (within the temperature range of 2.2–220 K) are then illustrated, and the most effective method for their realization, the sealed-cell method, is fully described, also concerning the further improvement obtained from year 2000 on thermal issues and on the effect of isotopic composition of the substances used.

In the subsequent chapters, thermometric methods exploiting a pressure-temperature relationship are described. For the gaseous state and for the range 1–300 K, the different types of gas thermometry are discussed, with special emphasis being given to the constant-volume type, not only as an absolute thermometer, but also as an interpolating thermometer (as required by the ITS-90, but in a broader

temperature range) and as a simple and practical self-contained device. Also, the more recent progress in acoustic thermometry is extensively illustrated.

In connection with condensed gases, vapor-pressure thermometry is described for the helium-isotopes in the range 0.3–5 K and for its implementation with other gases in the range up to 300 K; special attention is given to simplified realizations using sealed devices.

The ^{3}He melting-curve thermometry is then introduced as the official, accurate temperature-measuring means below the present range of the ITS-90.

The last chapter of Part I offers a survey of the hardware specifically required for the implementation of these thermometry's and it considers in particular the modern use of closed-cycle refrigerators above 4 K and uses of gases in temperature control.

In Part II, gas pressure measurements are considered in the range from 100 Pa to 100 MPa, in connection with the former applications to thermometry. Modern primary standards for accurate pressure measurements of gaseous media are first reviewed with a detailed and comprehensive description of their best use.

Liquid-column manometers are described for absolute, gauge, and differential pressure measurements in the range from few pascal to less than 0.3 MPa. Subsequently, modern gas-operated pressure balances are extensively discussed for absolute pressure measurements up to about 5 MPa, relative pressure measurements up to 100 MPa and differential pressure measurements.

Liquid manometers and pressure balances will be particularly described analyzing each physical quantity affecting pressure measurement uncertainty.

A survey is made of pressure transducers, particularly of those used for differential measurements and others that can directly be employed in a cryogenic environment. Problems involved in the assessment of their metrological characteristics, mostly stability with time and thermal cycling, are discussed connected with their use as transfer standards. Typical procedures to be used for a correct data acquisition and calibration of significant parameters of pressure transducers are given.

The gas-based fixed points (triple points, critical points,) available in the considered pressure range are reviewed from the standpoint of their use as transfer standards for interlaboratory comparisons.

Physical quantities and phenomena that affect pressure measurements are thoroughly discussed, as they must be taken into account to obtain top accuracy when using primary standards. In this context, special attention is devoted to a specific and controversial problem of cryogenic measurements: the thermomolecular pressure-difference effect.

The last chapter of this book, common to both Part I and II, is new and deals with the CIPM-MRA, putting into evidence the effort that NMIs made to realize pressure and temperature key comparisons, that are shortly reviewed, and the preparation of calibration and measurements capabilities (CMC) available to users in many application fields. Full text of CIPM-MRA is given in Appendix G.

Appendix A introduces the commented text of the International Temperature Scale of 1990 (ITS-90) below 273.15 K, while the modifications contained in the Technical Annex to the *mise en pratique* are reported and commented in the text. Its implementation, which always requires gas-based thermometry below 0 °C, is deeply discussed in Part I.

Reference data are extensively supplied too in Appendices B, C, D, E, F, G and H. They include: a comprehensive list of temperature (with values in ITS-90) and pressure fixed points; relevant thermophysical data and advices for their specific use in thermometric and manometry fields, given in the form of data sheets for each of 15 substances commonly used in manometry and thermometry; tables for the main manometry and pressure balances corrections (according to ITS-90) with specific examples of uncertainty evaluation; the text of the MRA; general terminology in measurements.

Finally, an extensive Bibliography is provided covering all the subjects dealt with, and including a "Further Readings" section for the main topics.

List of Acronyms

AGT	Acoustic gas thermometer
ASMW	Amt für Standardisierung, Messwesen und Warenprüfung (after 1990 merged in PTB) (G)
BCR	Bureau Communautaire de Référence of the European Union (no more existing)
BIPM	Bureau International des Poids et Mesures
CCM	Comité Consultatif pour la Masse et les Grandeurs apparentées
CCT	Comité Consultatif de Thermométrie
CGPM	Conférence Générale des Poids et Mesures
CIAME	Commission Interministerielle des appareils électriques et électroniques de mesure (F)
CIPM	Comité International des Poids et Mesures
CSIRO	Commonwealth Scientific Industrial Research Organization (AU)
CVGT	Constant volume gas thermometer
DCGT	Dielectric constant gas thermometer
GUM	Guide to the expression of uncertainty in measurement (BIPM)
EU	European Union
ICVGT	Interpolating constant volume gas thermometer
IEC	International Electrotechnical Commission
IEN	Istituto Elettrotecnico Nazionale “G. Ferraris” (since 2006 merged with IMGC in INRIM)
IMGC	Istituto di Metrologia “G. Colonnetti” of the Italian National Research Council (since 2006 merged with IEN into INRIM)
INRIM	Istituto Nazionale di Ricerca Metrologica
INTiBS	Instytut Niskich Temperatur i Badan Strukturalnych (PL)
IPRT	Industrial platinum resistance thermometer
IPTS-48	International Practical Temperature Scale of 1948
IPTS-68	International Practical Temperature Scale of 1968
ISA	Instrument Society of America
ISO	International Standards Organization
ITS-90	International Temperature Scale of 1990
IUPAC	International Union of Pure and Applied Chemistry

IUPAP	International Union of Pure and Applied Physics
KCDB	Key Comparison Data Base
KOL	Kamerling Onnes Laboratorium (NL)
KRISS	Korean Research Institute of Standards and Science (ROC)
LCM	Laboratoire Commun de Métrologie LNE/CNAM (F) (formerly Institut National de Métrologie INM/BNM)
LNE	Laboratoire National d'Essais (F)
MRA	Mutual Recognition Agreement (BIPM)
n.b.p.	Normal boiling point (nbp as subscript)
NIM	National Institute of Metrology (CN)
NIST	National Institute of Standards and Technology (formerly NBS) (USA)
NMI	National Metrology Institute
NMIJ	National Institute of Metrology of Japan (AIST, J)
NML	National Measurement Laboratory (also DAP, Division of Applied Physics, of CSIRO), now National Measurement Institute (NMI) (AU)
NPL	National Physical Laboratory (UK)
NPL-I	National Physical Laboratory (India)
NRC	National Research Council (CA)
NRLM/AIST	National Research Laboratory of Metrology (formerly NRLM) (J)
OIML	Organization Internationale de Métrologie Légale
PLTS-2000	Provisional Low Temperature Scale of year 2000
PTB	Physikalische-Technische Bundesanstalt (D)
RIGT	Refractive index gas thermometer
RGA	Residual gas analyzer
RM	Reference Material
SLAP	Standard Light Antarctic Precipitation (Water standard)
SPRT	Standard platinum resistance thermometer
SRM	Standard Reference Material
s.s.t.	Solid-to-solid transition (sst as subscript)
T_{58}	Former ^{4}He vapor-pressure Scale
T_{62}	Former ^{3}He vapor-pressure Scale
T_{68}, t_{68}	Kelvin and Celsius temperature in IPTS-68
T_{76}	Kelvin temperature in EPT-76
T_{90}, t_{90}	Kelvin and Celsius temperature in ITS-90
TC	Thermocouple thermometry
t.p.	Triple point (tp as subscript)
ULT-2000	Ultra-Low Temperature Scale of 2000
VIM	International Vocabulary of Basic and General Terms in Metrology
VNIIFTRI (also PRMI)	State Institute for Physicotechnical and Radiotechnical Measurements (Russia, formerly USSR)
VSL	Van Swinden Laboratory (NL)
V-SMOW	Vienna Standard Mean Ocean Water
WGx	Working Group x of CCT

List of Symbols

Symbols are in order of appearance and by chapter. Some symbols differ from chapter to chapter.

In general, u is used here to indicate the standard uncertainty (also known as the 1 σ or s uncertainty) and $U = ku$ the expanded uncertainty ($k \approx 2$). The symbol u is equivalent to u_c in the GUM notation.

Chapter 1

Q	Amount of heat (energy) (J, joule)
$\dot{Q}$	Heat rate (or "heating"), such as $\delta Q = c \times \delta T$ (W, watt)
c, c_p, c_V	Specific heats
q	Heat flow direction, defined as $q = -k \times \text{grad}\,\theta$
λ	Thermal conductivity (W m^{-1} K^{-1})
k	Boltzmann constant $= 1.380\,6488(13) \times 10^{-23}$ (J K^{-1}) (CODATA 2010)
θ	Empirical temperature $\theta = kT$
T	Thermodynamic temperature
T_{emp} (T_{90})	Empirical International temperature: International Scale temperature
Θ, Θ*	Thompson (Lord Kelvin) temperatures
τ	Norm of a (statistical) distribution, kinetic temperature
t	Celsius temperature (°C, degree Celsius)
t	Celsius-like temperature
t	Time (s, second)
p	(Static) pressure (Pa, pascal)
V	Volume (m^3, cubic meter)
ν	Velocity (m s^{-1})
W	(External) mechanical work (J)
S	Entropy (J K^{-1})
η	Efficiency of a cycle
μ	Carnot function (K^{-1})

μ	Integrating factor of the Pfaffian
J	Mechanical equivalent of heat
m_{B}	Mass of substance B (kg, kilogram)
$M_{\mathrm{r,B}}$	Relative molecular mass
ϕ	Phase of a substance
U	Internal energy of a system (J)
E	(Kinetic) energy (J)
N	Number of molecules
α	Cubic (thermal) expansion coefficient (K^{-1})
P	Physical quantity
n_{B}	Amount of substance B, defined as $\mathrm{n_B/L}$ (mol)
L	Avogadro constant (also indicated N_{A}) $= 6.022\,141\,29(27) \times 10^{23}\ \mathrm{mol}^{-1}$ (CODATA, 2010)
R	Molar gas constant $= 8.314\,4621(75)\ \mathrm{J\ K}^{-1}\ \mathrm{mol}^{-1}$ (CODATA, 2010)
χ	Magnetic susceptibility, defined as $\chi = \mu/\mu_0 - 1$, where $\mu_0 = 4\pi \cdot 10^{-7}\ \mathrm{H\ m}^{-1}$ exactly (henry per meter)

Chapter 2

$T_{\mathrm{r}}, p_{\mathrm{r}}$	Room temperature, room pressure
$T_{\mathrm{tp}}, p_{\mathrm{tp}}$	Triple point temperature, triple point pressure (of an impure substance)
T_{LP}	Liquidus-point temperature at the triple point
$T_{\mathrm{c}}, p_{\mathrm{c}}$	Critical temperature, critical pressure
ρ	Density ($\mathrm{kg\ m}^3$)
T_{tp}^*	Triple point temperature of the pure substance
$\Delta_{\mathrm{fus}}H_{\mathrm{m}}$	Molar enthalpy change in fusion ($\mathrm{J\ mol}^{-1}$)
x	Amount of substance fraction
F	Melted fraction
A	First cryoscopic constant, defined as $A = 1/KT_{m^2}$ (K^{-1}), where $K = R/\Delta_{\mathrm{fus}}H_{\mathrm{m}}$
$E_{\mathrm{f}}, K_{\mathrm{f}}$	First cryoscopic constant, in the literature also E_{f} or $K_{\mathrm{f}} = 1/A$
$\Delta_{\mathrm{fus}}T_{\mathrm{tp}}$	Melting range (K)
μ	Chemical potential ($\mathrm{J\ mol}^{-1}$)
X	"Driving capability" of sealed-cell ($\mathrm{kg\ K\ mol}^{-1}$)
T_λ	^{4}He lambda point temperature
$\Delta_{\mathrm{vap}}H_{\mathrm{m}}$	Molar enthalpy of vaporization

Chapter 3

$B(T)$	Second virial coefficient ($\mathrm{m}^3\ \mathrm{mol}^{-1}$)
$C(T)$	Third virial coefficient ($\mathrm{m}^6\ \mathrm{mol}^{-2}$)

T_b, p_b, n_b	Values of T, p or n for the gas thermometer bulb
N_d, V_d	Amount of substance and volume for the dead volume, including n_r, V_r in the room temperature dead volume, and n_c, V_c for the capillary tube
K	Adsorption coefficient or factor
τ	Adsorbed film thickness (measured in number of layers)
d	Capillary diameter
h	Capillary axial coordinate
H	(Portion of the) capillary length
p^*	Pressure value measured at the manometer (or room-temperature diaphragm) level
Δp_{aer}	Aerostatic pressure head
Δp_{TM}	Thermomolecular pressure difference
K	Compression modulus (Pa)
α_l	Linear (thermal) expansion coefficient (K^{-1})
α	Atomic polarizability, where $\alpha_0 =$ in vacuum
$\Delta V/V_0$	Volume relative change
δp	Pressure error due to manometer uncertainty
c	Velocity of sound (m s^{-1}, meter per second), where in vacuo $c_0 = 299\,792\,458$ m s^{-1} exactly
ε	Relative permittivity (dielectric constant), where in vacuo $\varepsilon_0 = 1/\mu_0 c_0^2$
A_ε	Molar polarizability
b, c	Dielectric virial coefficients
C	Electrical capacitance (F, farad)
γ	Relative capacitance change
n	Refractive index, defined as $n = c_0/c$
E_g	Adiabatic bulk modulus of the gas (Pa)
E	Young's modulus of elasticity (Pa)
g	Acceleration due to gravity (m s^{-2})

Chapter 4

p_i	Partial pressure
ps^0	Pressure of the pure solvent
K_H	Henry's law constant
n^L, m^L, V^L	Quantity of substance, mass and volume of the liquid phase
n^V, m^V, V^V	Same as the vapor phase
n_b, m_b, V_b	Same in the bulb
n_r, m_r, V_r	Same in the room temperature volume
n_c, m_c, V_c	Same in the connecting tube
V_T	Volume of the room-temperature filling reservoir
p_f	Condensation pressure at thermometer filling temperature T_f
H	Magnetic field strength (A m^{-1}, ampere per metre)
s^L	Surface area of the liquid phase

$\dot{n}$	Molar flow rate of refluxing film (mol s^{-1})
h_f	Elevation of the superfluid film above the liquid surface
ΔT_K	Temperature difference caused by the Kapitza effect

Chapter 5

T_{min}, p_{min}	Temperature and pressure at the point of minimum of the melting curve
T_A	Temperature of the second-order transition from normal liquid to superfluid A phase
T_B	Temperature of the first-order transition from superfluid A and B phases
T_S	Temperature of the first-order transition in solid ^{3}He to the ferromagnetically ordered phase
p_m	Melting pressure
η	Dynamic viscosity (Pa s, pascal per second)

Chapter 6

X_x	Gap in a gas-filled heat switch
L	Mean free path of gas molecules, where Λ_0 is at high temperature
K_n	Knudsen number
C	Conductance in the molecular regime (L s^{-1}, liter per second)

Chapter 7

p	Pressure
p_0	Vacuum reference pressure
p_{atm}	Atmospheric pressure
p_v	Mercury vapor pressure
p_j	Operating value of the jacket pressure in a controlled clearance piston-cylinder unit
p_z	Jacket pressure value for zero clearance
Δ_p	Differential pressure
p_L	Line pressure
t	Temperature expressed in °C
T	Temperature expressed in K
t_{ref}	Reference temperature (generally 20 °C)
$\rho_f(t, p)$	Density of a fluid
ρ_o	Mercury density at 20 °C and 101 325 Pa
$\rho(t, p_{atm})$	Mercury density at temperature t and pressure $p_{atm} = 101\,325$ Pa

$\rho(t, (p+p_0)/2)$ or $\rho_{Hg}(t, (p+p_0)/2)$	Mercury density at temperature t and at average pressure between p and p_0
$\rho_{gas}(t, p)$	Density of a gas at temperature t and pressure p (e.g., for nitrogen it will be $\rho_{N2}(t, p)$
ρ_a	Air density
$\gamma(t)$	Surface tension of a fluid at temperature t
$\eta(t, p)$	Dynamic viscosity of a fluid at temperature t and pressure p
g_L	Local acceleration of gravity
h	Difference in height between liquids (case of liquid columns), or distance of a reference level from a fixed position (case of pressure balances)
h	Relative humidity ($h = 0.5$ represents a rate of relative humidity of 50 %)
H	Helmoltz thermodynamic free energy
U	Energy
S	Entropy
V and V_0	Volumes
K_T	Isothermal compressibility
K_S	Adiabatic compressibility
$n(t, p)$	Refractive index (gaseous media must be specified)
N	Number of interferometric fringes
λ	Wavelength of a light source in a gas media
λ_v	Wavelength of a light source in vacuum
C_i	Refractive index correction
c	Speed of sound in mercury
L	Length
l or l_0	Engagement length of a piston in a cylinder
K_{Hg}	Mercury compressibility
M	Molar mass of a gas
R	Molar gas constant ($R = 8.314\,4621(75)$ J mol^{-1} K^{-1}) (CODATA, 2010)
x_v	Mole fraction of water vapor
x_{CO_2}	Mole fraction of carbon dioxide
Z	Compressibility factor for moist air (see Table F.4)
m_i	Mass of the ith weight piece referred to its density ρ_{mi}
ρ_{mi}	Density of the ith weight
m_{icon}	Conventional mass value referred to the conventional density $\rho\ m_{icon}$
$\rho\ m_{icon}$	Conventional density (8000 kg m^{-3})
F	Gravitational force
$A_0\ (t_{ref}, p_{atm})$	Effective area of a piston-cylinder unit measured at the reference temperature t_{ref} and at atmospheric pressure p_{atm}
λ	Pressure distortion coefficient of a piston-cylinder unit (case of pressure balances)
λ_p	Pressure distortion coefficient of the piston (case of pressure balances)

α_p and α_c	Linear expansion coefficients of a piston and cylinder respectively
$A_e(t, p)$	Effective area of a piston-cylinder unit at temperature t and pressure p
h_0	Radial clearance for a piston-cylinder unit at the position $x = 0$
$h(x)$	Radial clearance for a piston-cylinder unit at the position x (x can change between 0 and L)
$u(x)$	Piston deviations from the ideal reference radius
$U(x)$	Cylinder deviations from the ideal reference radius
U_r	Radial displacements (generally on the outer surface of a cylinder)
ν_p, ν_c	Poisson coefficients for piston and cylinder respectively
E_p, E_c	Elasticity moduli (Young) for piston and cylinder respectively
r_0	Piston radius at the position $x = 0$
r_c	Average inner radius of the cylinder
r_p,	Average radius of the piston
R_c	Average outer radius of the cylinder
$A_p(t, p_{atm})$	Effective area of the piston at temperature t and atmospheric pressure
d	Jacket pressure coefficient in a controlled clearance piston-cylinder unit
$A_e(t, p, p_j)$	Effective area of a controlled clearance piston-cylinder unit at pressure p, temperature t and jacket pressure p_j
Δm or Δm_a	Added mass on a pressure balance during differential pressure calibration, typically at a high line pressure
σ^2	Estimated variance
σ	Estimated standard deviation (it can be related to a fitting or to a number of repeated measurements of a physical quantity, or to the combination of different σ's for quantities related between them by a mathematical function)
$p_{sv}(t)$	Saturation vapor pressure of water (see Table F.3.)
$f(p,t)$	Enhancement factor (see Table F.2.)
G	Shear modulus

Chapter 8

Symbols previously reported may be used in the present chapter, but are not all listed here.

$A_e(t,p)$	Effective area of a piston-cylinder unit at temperature t and pressure p
F	Force due to the application of a pressure p to a piston-cylinder unit of effective area A_e (in first approximation $F = p \times A_e$)
p	Pressure
p_L	Line pressure
Δp	Differential pressure
$p_{tr.}$	Pressure reading of a transducer
$p_{pr.\ std.}$	Pressure value measured by a primary standard

$p_{\text{pr. balance}}$ or $p_{\text{p. gauge}}$	Pressure value measured by a pressure balance
$(p_{\text{tr.}} - p_{\text{pr. std.}})$	Pressure calibration difference
$(p_{\text{pr. std.}} - p_{\text{tr.}})$	Pressure calibration correction
t	Temperature expressed in °C
T	Temperature expressed in K
T	(Tesla), SI unit of magnetic flux density
n	Number of measurements
x_i	Result of the ith measurement of the physical quantity x (i variable from 1 to n)
$\overline{x}$	Arithmetic mean of the n measurement results
s	Experimental standard deviation
$p = \text{f}(X)$	Interpolating equation of a transducer
X	Output signal of a transducer, frequently corrected for its zero output value
GF	Gauge factor ($GF = \text{d}R/R$ for a strain gauge transducer)
ε	Strain
C	Electrical capacitance
f.s.	Full scale
LVDT	Linear variable differential transformer
R	Electrical resistance

Chapter 9

Symbols previously reported may be used in the present chapter, but are not all listed here.

p	Pressure
t	Temperature in °C
T	Temperature in K
t.p.	Triple point
p_{tp}	Triple point pressure
T_{tp}	Triple point temperature
v.p.	Vapor pressure
c.p.	Critical point
m.l.	Melting line
$T_{\text{tp, Hg}}$	Mercury triple point (234.3156 K of ITS-90)
d	$= T - T_{\text{tp, Hg}}$
F	Melted fraction ($1/F = 1$ is equivalent to 100% melted, i.e., liquid point)
R	Electrical resistance

Chapter 10

Symbols previously reported may be used in the present chapter, but are not all listed here.

p_c	Cold pressure
p_w	Warm pressure
p_0	$=(p_c+p_w)/2$
T_c	Cold temperature
T_w	Warm temperature
T_0	$=(T_c+T_w)/2$
d	Tube diameter
r	Tube radius
L	Tube length
λ	Mean free path of gas molecules
$\eta(T,p)$	Gas viscosity at temperature T and pressure p
$\eta_0(T_0,p)$	Gas viscosity at temperature T_0 and pressure p
M	Molar mass of a gas
R	Molar gas constant, $R=8.314\,4621$ J mol^{-1} K^{-1}
R'	$=(T_w/T_c)^{1/2}$
R''	$=P_w/p_c$
D	Collisional diameter of a gas molecule
Φ_g	Pressure-shifting factor
f	Momentum accommodation coefficient
γ	Geometry factor
N_G	Number of gas–gas collisions
N_W	Number of gas–surface collisions
Δ_p	Thermo molecular pressure correction calculated on the basis of Weber–Schmidt equation
$\delta(\Delta p)$	Difference between the Weber–Schmidt equation and experimental values of the thermo molecular pressure correction

Appendix A

T_{90}, t_{90}	Kelvin and Celsius temperature for ITS-90 scale
T_{68}, t_{68}	Kelvin and Celsius temperature for IPTS-68 scale
T_{76}	Kelvin temperature for EPT-76 scale
$W(T_{90})$	Ratio $R(T_{90})/R(273.16\ \mathrm{K})$
$W_r(T_{90})$	ITS-90 reference function

Symbols used specifically in particular areas of application or used to define constants or calculation parameters are explained in the text.

Notes to the Reader

1. All temperature data are referred to the new International Temperature Scale 1990 (ITS-90). This is correct except when otherwise stated, because in some cases there are real needs to express some relevant data with reference to the former IPTS-68 temperature scale.
2. All the uncertainties are declared at the one sigma level (u_c in the GUM notation), except when otherwise stated because sometimes we are reporting data from literature where uncertainties either are not declared or it is impossible to recalculate the one sigma level uncertainty. The expanded uncertainty $U = ku_c$ ($k \approx 2$) is also used.
3. All notations are made according to IUPAC recommendations (IUPAC Green Book, third edition, 2009–2010). In some cases, however, American rather than International spelling has been used (e.g., meter rather than metre and liter rather than litre).

Part I
Temperature Measurements in the Range from 0.1 to 300 K

Introduction

In Part I, modern methods which are based on the use of substances gaseous at room temperature, for measuring temperatures lower than 0 °C, are described. The lower limit of the temperature range where these substances can be used is arbitrarily set at ≈ 0.1 K, but ^{3}He melting-curve thermometry, described in Chap. 5, extends down to ≈ 0.001 K.

Figure 1.7 at the end of Chap. 1 shows the typical range for each of these gas-based types of thermometry. The present state-of-the-art allows a top measurement accuracy better than $\pm$ 100 μK for all of them. A recent short digest of the advances in cryogenic thermometry in the last 50 years can be found in Pavese (2006).

Each of the fixed points described in Chap. 2 realizes a single temperature value. Gas thermometry, described in its various forms below 0 °C in Chap. 3, can be used as well above room temperature. Vapor pressure thermometry too, described in Chap. 4, can be used above room temperature: each substance spans only a narrow interval of the whole temperature range, and in some intervals no substance is available.

Finally, Chap. 6 describes thermostats that are used for performing all these thermometric measurements and temperature controls, and devices that are based on the use of gases.

Chapter 1
The Concept of Temperature

This monograph is intended for the use of low-temperature experimentalists, as well as those individuals interested in one or more aspects of thermometry. The concept of temperature, therefore, will only be given a brief introduction and review in this section. For a more complete treatment, the reader is directed to the textbooks listed in the section "Further Readings Part I" after the References.

However, an introduction of the concept of temperature seems desirable for two reasons, one general and one specific. In general, each course or textbook presenting an introduction to thermodynamics or thermometry makes the choice of introducing only one of the several methods of defining temperature. As a consequence, the student or the reader obtains an oversimplified impression of the problems involved with this basic physical quantity, missing some of its more subtle features and developing little sensitivity in dealing experimentally with the associated problems. We will, therefore, provide a brief account of several different approaches to its definition, in order to stimulate further understanding and study.

The range of temperatures considered in cryogenics appears quite small, a few hundred kelvins, when compared with the millions of degrees required to attain the plasma region. However, absolute zero in nature can only be approached asymptotically. Therefore, a logarithmic scale of temperature values is a more realistic way to portray the temperature scale (Fig. 1.1). Since absolute zero is approached as infinity, it becomes similar to the upper boundary of the temperature scale. In the very low temperature range, conditions far away from human experience occur. Temperatures far below the minimum existing in nature (background cosmic radiation, 2.75 K) are commonly attained in laboratories, where equilibrium temperature values may be different for either the lattice or the sublattice (e.g., spin) populations and specific temperature gradients may occur during heat transfer (Kapitza conductance). These conditions directly affect the capability of measuring temperature. Since this text is concerned with temperature measurements based on gases, the concept of the "ideal gas" will be introduced, and before dealing with "the real thing," the limits and limitations of this model relative to the definition of temperature will be elucidated.

F. Pavese, G. Molinar Min Beciet, *Modern Gas-Based Temperature and Pressure Measurements,* International Cryogenics Monograph Series,
DOI 10.1007/978-1-4419-8282-7_1, © Springer Science+Business Media New York 2013

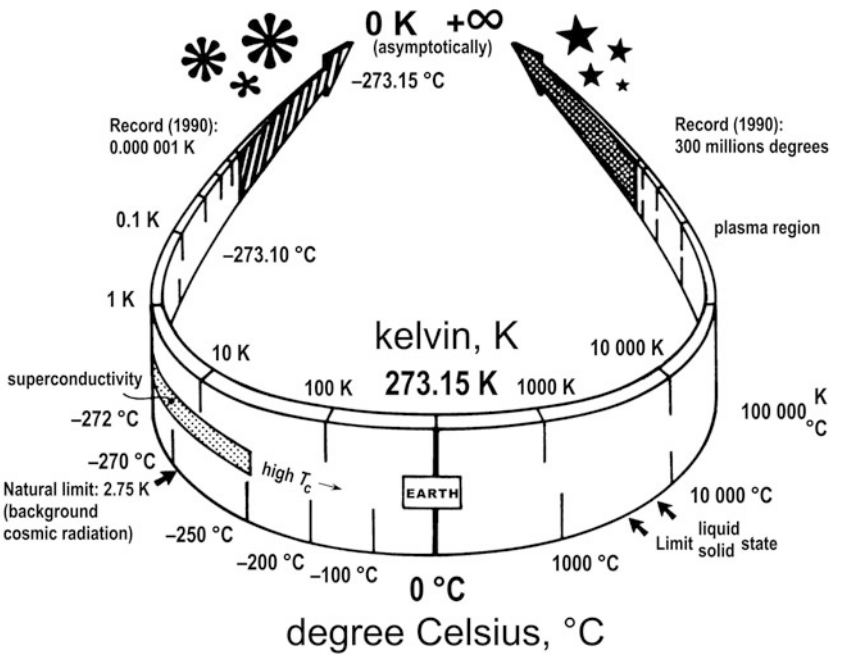

Fig. 1.1 The logarithmic natural scale of temperatures

1.1 Definitions of Temperature

It has long been recognized that people—including scientists and teachers—are divided into two immiscible clusters: "les esprits de justesse" and "les esprits de géométrie" (Pascal 1670). Each of them believes that there is only one approach for explaining the concept of temperature. They follow approaches that are quite different, although consistent. We call the former the *phenomenological approach*, the latter the *axiomatic approach*. A short account will also be given of a third approach, the *microscopic approach*, which is based on the structure of matter.

1.1.1 The Phenomenological Approach

In history, the phenomenological approach came first, but its introduction has not been very straightforward. In fact, the concept of temperature was not separated from the concept of heat until the middle of nineteenth century. This occurred shortly after heat was recognized as not being a substance—the caloric—but energy (a recent concept too). In this respect, Joule's experiment first published in 1845, is traditionally considered crucial. It recognized the relationship between heat and

mechanical work. It is remarkable that the thermal effects of mechanical work and the reverse possibility, of obtaining mechanical work from heat (in steam engines), was recognized and used for decades before this equivalence—namely the first law of thermodynamics—was fully understood.

However, thermodynamics is distinctly different from most mechanics,[1] since for thermodynamics the time arrow is irreversible (Born 1949—see when this irreversibility is claimed to have born in the Planck gas in (Kozlowski et al. 1997)) and the direction of heat flow $\boldsymbol{q}$ is subject to restrictions (Planck 1932; second law of thermodynamics). As described by Born (1949), heat flow $\dot{Q}$ can be described, in general, by a "continuity condition"

$$\dot{Q} + \operatorname{div} \boldsymbol{q} = 0, \tag{1.1}$$

which becomes the familiar equation

$$c\left(\frac{\partial \theta}{\partial t}\right) = \lambda \delta\theta \tag{1.2}$$

when δQ is proportional to the change in temperature $\delta\theta$, c is the specific heat, and if heat flow is proportional to the temperature gradient, $\boldsymbol{q} = -\lambda \operatorname{grad} \theta$. In Eq. (1.2), time t *cannot* be changed to $-t$, since no other variables permit a change in sign (unlike, e.g., Maxwell's equations).

Temperature, as well as entropy, is the concept that stems from this difference. The laws of mechanics involve the independent parameter of temperature and time. Indeed, they could be considered as an outgrowth of the thermodynamic laws with "internal parameters"[2] set to zero (Bazarov 1964).

As noted in Sect. 1.2, the thermodynamic temperature T cannot be measured directly, but only estimated through the measurement of another physical quantity, related to T by a known law. These empirical estimates are indicated in this chapter with the symbol θ. Other definitions of T will be considered, and, when conceptually different, will be represented by other symbols. A summary of these definitions is given in Table 1.1.

From a phenomenological macroscopic point of view, the most common argument for introducing the temperature concept is the one using the concept of *thermal equilibrium*, which is qualitatively obtained simply by recognizing sensations of warmth and cold. This concept leads to the *zeroth law* of thermodynamics, stated as:

> Two systems in thermal equilibrium with a third (system) are in thermal equilibrium with each other (Zemanski 1957).

[1] Also in mechanics the time arrow and irreversibility are not excluded—one example, wear phenomena.

[2] That is parameters depending on the internal structure of the system—such as thermal motion of molecules—as opposed to "external parameters," which are set by the interaction of the system with external systems.

Table 1.1 Summary of temperature definitions (lattice or bulk equilibrium temperature)[a]

Thomson (1848)	$W = (\Theta_2{}^* - \Theta_1{}^*); T \equiv \Theta^* \quad \Theta^* \propto \ln(V/V_0)$
Thomson (1854)	$Q_2/Q_1 = \Theta_1/\Theta_2; T \equiv Q^* \quad \Theta^* = J\ln\Theta + \text{const}$
CGPM (1948)	$T \cong T_{\text{emp}}; \quad t = \theta; \quad (p - p_0)/p_0 = \alpha t, \quad 1/(\alpha/°\text{C}^{-1}) = 273.16,$ $t(\text{nbpH}_2\text{O})/°\text{C} \equiv 100; \quad T_{\text{emp}} = 1/\alpha + t[°\text{K}]$
CGPM (1960)	$T \cong T_{\text{emp}}; \quad T = \theta; \quad (p - p_0)/p_0 = \alpha t, \quad T_{\text{emp}}(\text{tp H}_2\text{O})/\text{K} = 273.16,$ $t/°\text{C} = T_{\text{emp}}/\text{K} - 273.15; \quad t(\text{nbp H}_2\text{O})/°\text{C} \cong 100$
CGPM (1989)	$T_{\text{emp}}(\text{tp H}_2\text{O})/\text{K} - 273.16$ $1/(\alpha/°\text{C}^{-1}) = 273.15, \quad t(\text{nbp H}_2\text{O})/°\text{C} \equiv 99.974$
Carathéodory (1909)	$1/T =$ integrating factor μ of a Pfaffian form $\mathrm{d}x_0 + X_1\mathrm{d}x_1 + X_2\mathrm{d}x_2 + \cdots + X_n\mathrm{d}x_n = 0. \quad \mathrm{d}Q = 1/\mu\mathrm{d}\Phi = T\mathrm{d}S$
Truesdell (1979)	The set of hotnesses (T) is a diffeomorph of $\Re$, equipped with an intrinsic order. An empirical-temperature function (θ) is an order-preserving chart on a bounded segment of the manifold
Owen (1984)	A hotness manifold is a set M whose elements T are called hotness levels together with a set F of functions $\theta{:}M \to \Re$, called empirical temperature scales, satisfying: (1) The range of θ is an open interval for each $\theta \in F$ (2) For every $T_1, T_2 \in M$ and $\theta \in F$, $\theta(T_1) = \theta(T_2) \Rightarrow T_1 = T_2$; (3) For every $\theta_1, \theta_2 \in F$, $\theta \to \theta_2(\theta_1^{-1}(\theta))$ is a continuous, strictly increasing function
Kinetic theory	$T \equiv \Theta = m/3k < v^2 > = 2/3kE_k, \quad v =$ velocity
Statistical mechanics	$T = \tau/k, \quad P(E)\delta E \approx \Omega(E)\mathrm{e}^{-E/\tau}\mathrm{d}E$

[a] T_{emp} in this table indicates the *empirical kelvin* temperature, distinguishing it from T, used for *thermodynamic* temperature
nbp normal boiling point; *tp* triple point

As a third system, an observer can be considered aiming at determining whether the two systems are in thermal equilibrium or not. The following temperature definition follows:

> The temperature of a system is a property that determines whether or not a system is in thermal equilibrium with other systems (Zemanski 1957).

The first consequence of this definition is that it applies only to systems in thermal equilibrium. This restriction is common to all classical thermodynamics, which turns out to be "rate-independent" (Owen 1984; Andresen et al. 1984), i.e., is actually a kind of "thermostatics."

If subjective sensations are not to be used, as is common practice in science after Galileo, it is necessary to find an objective basis for the temperature definition. It was noted long ago that these sensations could be correlated to many measurable phenomena. Historically, they first involved changes in volume—vapors, for example—which were used for performing mechanical work, or changes in length, which were used for moving the dial of an instrument. These observations raise the question as to whether a relationship actually exists between these different empirical

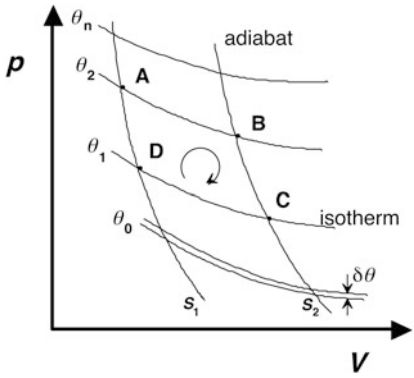

Fig. 1.2 The Carnot cycle (*ABCD*) in the *p*-*V* representation

experiences of temperature, and whether it is possible to define temperature in a way that is independent of any specific substance.

The phenomenological macroscopic answer to these questions was substantiated by Sadi Carnot in 1824 (and published in 1832) when he investigated the problem of determining the efficiency of using heat to obtain mechanical work, an apparently side problem. On the contrary, the problem of finding a relationship between these two quantities is essential. Carnot's principle can be summarized in the following statements:

> (A) Heat can evidently be a cause of motion only by virtue of the changes of volume or of form, which it produces in bodies, (B) The necessary condition of the maximum (efficiency) is, then, that in the bodies employed in realizing the motive power of heat (i.e. mechanical work) there should not occur any change of temperature, which may not be due to a change in volume (Carnot 1832).

Consequently, Carnot's well-known *closed reversible cycle*—three words that also constitute three new basic concepts—*must* be formed by alternating isotherms and adiabats (Fig. 1.2). The fact that a minimum of *two* temperatures is necessary to construct the cycle introduces still another important principle.

The Carnot cycle is represented in Fig. 1.2, with the *p*-*V* coordinates originally used by Carnot. Assume that there are two heat reservoirs able of providing any required amount of heat isothermally, at temperatures θ_1 and $\theta_2 > \theta_1$. The working substance absorbs an amount of heat Q_2 from the hot reservoir in expanding isothermally from A to B; from B to C it does not exchange heat, but performs mechanical work W_2 until it cools down to θ_1; the working substance then undergoes an isothermal reduction in volume from C to D, releasing an amount of heat Q_1 to the cold reservoir; finally, the working substance is returned to its original state A and temperature θ_2 by reversible compression utilizing mechanical work W_1 without any exchange of heat.

If the two isotherms differ by an infinitesimal amount $\mathrm{d}\theta$, and the engine produces a total net work of $\mathrm{d}W$ over the full cycle, the amount of heat Q that is transferred

from the higher to the lower reservoir may be shown to be such that

$$\frac{đW}{Q} = \mu(\theta)\mathrm{d}\theta \tag{1.3}$$

where the differential $đW$ is not exact, since the total work performed along a path depends on the path, and $\mu(\theta)$ is a function of temperature θ *only*—the so-called Carnot function. The latter is true because it may be shown that a Carnot engine does *not* depend on the substance used in performing the work.

There is no agreement among the authors if the last statement is valid for *every* substance. Restricting the discussion to gases, one opinion is that the gas needs *not* to be ideal (Landsberg 1961; Zemansky 1957; Truesdell 1987). For example, Landsberg defines the fluid as

> (a) in each cycle (the fluid) passes through the same physical (equilibrium and non-equilibrium) states; (b) it consists of one and the same phase, and it has a fixed mass, throughout a cycle; (c) . . . [omitted] . . . ; (d) it exchanges no other heat with its surroundings and there are no other entropy changes in the engine (Landsberg 1961).

Therefore, it should not undergo a phase change (Lansdsberg, Truesdell), since it involves a "latent heat" of transformation.[3] In this respect, a phase change is relevant only in connection with requirement (d) (where the term "nonisothermal" should precede the term "entropy changes," according to Carnot principle (B)), according to Carnot's statements about changes in volume, and to changes in internal energy (see also Sect. 1.2).

On the other hand, there is another opinion that the gas in the Carnot cycle must be ideal. For example, Arzeliers states:

> The Carnot temperature is defined by three conditions: (a) for two perfect gases in thermal contact separated by a diathermic wall, $T_1 = T_2$; (b) $\mathrm{d}Q/T$ is an exact differential $\mathrm{d}S$ for all reversible transformations, S being defined the entropy; and (c) for $T = 0$, $S = 0$ (Arzeliers 1968).

Many others are not explicit about this point, including Carnot himself as well as Clausius who first made use of Carnot's ideas.

For a cycle performed between two temperatures θ_1 and θ_2 with $\theta_2 > \theta_1$, Eq. (1.3) defines the efficiency as η equal to W/Q_2 or to $(Q_2 - Q_1)/Q_2$. Then, there is a choice of defining the (absolute) temperature in terms of the mechanical work or the thermal effect of heat.

William Thomson (Lord Kelvin) made the first recognized attempt to define absolute temperature both ways, based on the theory initiated by Carnot that $\mu(\theta)$ in Eq. (1.3) is "universal," as required by an *absolute* temperature.

The first of his definitions (Thomson 1848) states that a unit *difference* of absolute temperature precisely equals the maximum work that can be obtained from "*a unit of heat let down in a cyclic process,*" irrespective of the temperature values involved,

---

[3] *Definition:* "Latent heat is the quantity of heat which must be communicated to a body in a given state in order to convert it into another state without changing its temperature" (Maxwell 1871).

or

$$W = (\Theta_2^* - \Theta_1^*)Q, \tag{1.4a}$$

which is equivalent to setting $\mu(\Theta^*) = 1$ in Eq. (1.3). Using this definition, it would be $\theta = \Theta^*$.

Thomson assumed a "reference" temperature $\Theta_0^* = 0$. In general, the definition holds for $\mu(\Theta^*) = const$. Therefore, temperature intervals are proportioned to increments of efficiency. For an arbitrary "reference" temperature Θ_0^* and any Θ_n^*, one can write

$$\frac{Q_n}{Q_0} = \mu(\Theta^*)^n, \quad \text{or} \quad \Theta^* = \Theta_0^* + \frac{\log(Q/Q_0)}{\mu(\Theta^*)}. \tag{1.4b}$$

When $\Theta^* \to \pm\infty$, $\eta \to 1$.

In his second definition (Thomson 1854), upon the suggestion of Joule who found from experiments on compression of air that $\mu(\theta)$ was rather proportional to $1/\theta$, he stated:

> If any substance, whatever, subjected to a perfectly reversible cycle of operations, takes in heat only in a locality kept at a uniform temperature, and emits heat only in another locality kept at a uniform temperature, the temperatures of these localities are proportional to the quantities of heat taken in or emitted to them in a complete cycle of operations (Thomson 1854).

This statement is equivalent to the well-known relationship that can be derived from Carnot's finite cycle of Fig. 1.2.

$$\frac{Q_2}{Q_1} = \frac{\Theta_2}{\Theta_1}. \tag{1.5}$$

The use of Θ instead of Θ^* marks the fact that this definition of temperature is different from the one in Eq. (1.4a). If chosen as the temperature definition, $\theta = \Theta$ would hold.

Notice that definition in Eq. (1.5) does not place any dimensional constraint on temperature, since only temperature *ratios* are defined, whereas Eq. (1.4a) does, since it is using temperature *differences*.

The relationship between the two definitions is given by

$$\theta^* = J \log\theta + const \tag{1.6}$$

where J is a constant defined as the "mechanical equivalent of a unit of heat" (Truesdell 1980).

Equation (1.5) is the modern definition of thermodynamic temperature, $\Theta = T$, where temperature is assumed proportional to the heat exchanged and where $\Theta \geq 0$.

Equation (1.4a), however, is equivalent to assuming that temperature increases by the same *proportion* as the corresponding increase in the gas volume, i.e., $\Theta^* \propto \ln(V/V_0)$. This definition was also unsuccessfully proposed by Dalton at the beginning of the twentieth century, and also later found some support from scientists working in low-temperature physics (e.g., Simon 1955).

1.1.2 The Axiomatic Approach

Born's statement is a good example of the view of an influential physicist about the type of reasoning reported in the previous section, when he stated:

> These are new and strange conceptions, obviously borrowed from engineering (Born 1949).

though he follows (with some sense of humor):

> It would be ridiculous to feel anything but admiration for the men who invented these methods.

Having said this, we must thank him for having encouraged a mathematician, Carathéodory, to review the problem from an axiomatic point of view and reach quite remarkable conclusions.

However, this new rational thinking about the fundamental principles of thermodynamics gave rise to a dispute, between those who believed that *energy* was the major contributor to temperature and those who thought that *heat* was the more fundamental quantity. Therefore, statements such as: "heat is energy in transit" (i.e., *flowing* energy; Zemansky 1957, 1968), or that a quantity of heat is "the average kinetic energy {of molecules} of the system at equilibrium" (Arzeliers 1968), or "the quantity of energy transmitted by the system without variation of its external parameters" (Bazarov 1964), have not been accepted by the entire thermodynamic community.

Carathéodory started from the point of view of energy, when he stated:

> It is possible to develop the whole {thermodynamic} theory without assuming the existence of heat, that is, of a quantity that is of a different nature than the normal mechanical quantities (Carathéodory 1909).

thereby, incidentally, denying time irreversibility.

Following Gibbs' approach, he needed to define, for a system Σ, only the volume V, the pressure p, and the amount m_k for each kth chemical component of the system. *Equilibrium* is then defined by stating that, when the chemical species are contained in an inert closed vessel, the numerical values of volume, pressure, and concentration remain constant. The vessel is defined *adiabatic* when the components in the vessel remain in equilibrium as the components *outside* the vessel are modified (the vessel itself is assumed not to change shape by external modifications). The vessel is defined as *permeable* when, in order to ensure equilibrium across the wall, a relation must be satisfied of the form

$$F_i\left(V_1, p_1, m_{k,1};\quad V_2, p_2, m_{k,2}\right) = 0 \tag{1.7}$$

for each phase ϕ_i, *as* if no wall were separating them. Finally, he assumed that "external work" could be done on the system, represented as a deformation of the external shape of system Σ (defined as "internal work" in mechanics), driven by forces external to Σ and in contact with Σ, or the reverse. *Forces acting at a distance were ignored*. He concluded from that:

> Every process is characterized by a state variable of the initial and final state, by the external work performed by it, and by the indication of whether it is adiabatic or not.

Carathéodory did not make use of equilibrium states in describing a process, to avoid the possibility of a contradiction, since no change by definition can occur at equilibrium. Thus, a reversible process would have to be a *nonconnected* set of equilibrium states. He preferred to approach the problem by considering an irreversible adiabatic process, such as Joule's experiment, where the system is adiabatically brought from the initial to the final equilibrium state by performing external work. Regardless of how close these states are to each other, this external work cannot be recovered by reversing the process. These conclusions form the basis of Carathéodory's Axiom II:

> In every arbitrarily close neighborhood of a given initial state, there exist states that cannot be approached arbitrarily closely by adiabatic processes.

Incidentally, to counterbalance Born's statement reported at the beginning of this section, this axiom was, in turn, later *deduced* from Kelvin's principle (Landsberg 1964; Arzeliers 1968; Zemansky 1968).

The physical meaning of Carathéodory axiom of "adiabatic unattainability" is that in every equilibrium system a new parameter of state S exists which does not vary in quasistatic adiabatic processes. In fact, assuming that the system is initially in a state 1, where this parameter has a value S_1, while in a state 2 it has a value S_2, it is clear that for a quasistatic[4] adiabatic process occurring at $S = const.$, the state 2 cannot be attained (this occurs, e.g., for an isothermal process where $S \equiv T$) (Bazarov 1964).

Energy U (*not heat*) is introduced by Carathéodory in his Axiom I:

> With every phase ϕ_i of a system Σ, it is possible to define a function ε_i associated with the quantities V_i, p_i and $m_{k,i}$, that is proportional to the total volume V_i of the phase. This function is defined as the internal energy.

The external shape is determined by the "deformation variables," which are functions only of the volume V_i. One parameter must not depend on external shape, since it is known that the initial and final shapes of Σ alone do not uniquely determine the work W performed during an adiabatic process. Therefore, all the state parameters, *but one*, of system Σ must depend on the external shape of the system. The energy U, a state function, must contain this deformation-independent parameter.

From Axiom I, denoting U_0 and U as the initial and final energies, during an adiabatic process energy is conserved $U_0 - U + W = 0$ or, for an infinitesimal state change,

$$\mathrm{d}U + \mathrm{d}W = 0, \tag{1.8}$$

where

$$\mathrm{d}W = p_1 \mathrm{d}x_1 + p_2 \mathrm{d}x_2 + \cdots + p_i \mathrm{d}x_i + \cdots + p_n \mathrm{d}x_n \tag{1.9}$$

---

[4] *Quasi-static:* means that only equilibrium states are involved in the process, despite the fact, that for a process to occur, equilibrium must be perturbed and thus a change of state must occur. It is a limit concept for sufficiently slow variations in time.

and $p_i = f(x_0, x_1, \ldots, x_n)$ are intensive parameters, the forces causing the volume change, and x_i are extensive "mechanical" parameters. Equation (1.9) is a Pfaffian equation, a type of equation well known in mathematics. Carathéodory derived from this a specific theorem, by stating that:

> Given a Pfaffian equation
>
> $$\delta P = dx_0 + X_1 dx_1 + X_2 dx_2 + \cdots + X_n dx_n = 0$$
>
> in which X_i denotes continuous differentiable functions of x_i, and granted that in every neighborhood of a given point P in space with x_i points there exist points that cannot be reached along lines that satisfy this equation, it necessarily follows that the equation possesses a multiplier that converts the equation into a perfect differential.

This theorem is needed since an "integrating factor" μ does not necessarily exist for $n \geq 3$, that is, Pfaffian forms are not necessarily holonomic. Therefore,

$$\mu \delta P = \mathrm{d}\Phi\,(x_1, \ldots, x_n)$$

has an integral

$$\Phi\,(x_1, \ldots, x_n) = \text{const}, \tag{1.10}$$

which represents an adiabatic surface.

It can be demonstrated that, in the case of Eq. (1.8), an integrating factor $\mu(x_1, \ldots, x_n)$ exists, which depends only on temperature. In this case, $\Phi(x_1, \ldots, x_n)$ is the entropy S of the system, and represents the parameter, introduced by Axiom II, that must remain constant on adiabats, and $\mu = 1/T$ is the inverse of thermodynamic temperature. According to the familiar concept of heat, this is given as

$$\mathrm{d}Q = (1/\mu)\mathrm{d}\Phi = T\mathrm{d}S. \tag{1.11}$$

Axiomatic thermodynamics has gone a long way from Carathéodory. In this respect, the reader may consult texts and papers such as Truesdell (1977, 1979, 1980), Serrin (1978), and Owen (1984). For example, Truesdell, whose starting point is opposite to Carathéodory's, assumes that *heat*, not energy, is the primary concept, and replaces the primitive concept of temperature with the primitive concept of "hotness":

> *Axiom 0*: The set of hotnesses is a diffeomorph of the real interval, equipped with an intrinsic order (Truesdell 1979).

This was formalized as

> *Definition 2.1*: A hotness manifold is a set M whose elements L are called hotness levels together with a set F of functions $\phi: M \to \Re$, called empirical temperature scales, satisfying:
> (1) the range of ϕ is an open interval for each $\phi \in F$;
> (2) for every $L_1, L_2 \in M$ and $\phi \in F$, $\phi(L_1) = \phi(L_2) \to L_1 = L_2$;
> (3) for every $\phi_1, \phi_2 \in F$, $\theta \to \phi_2(\phi_1{}^{-1}(\theta))$ is a continuous, strictly increasing function (Owen 1984).

Condition (3) can also be formulated as

Definition 0: An empirical-temperature function is an order-preserving chart on a bounded segment of the hotness manifold (Truesdell 1979).

Fosdick and Rajagopal (1983) provide another demonstration of the existence of such a manifold for temperature.

1.1.3 The Microscopic Approach

Both the preceding approaches are macroscopic as they do not consider the atomic structure of the matter. Let us now examine some approaches based on the atomic structure.

Kinetic Temperature Since the middle of nineteenth century, a kinetic theory of gases developed quite rapidly. From this theory the well-known relationship was established between thermodynamic temperature and a parameter τ (kinetic temperature) that is related to the velocity distribution (Maxwell's distribution) of molecules in thermal equilibrium (a stationary, not a static state, i.e., with stable velocity v distribution)

$$T \equiv \tau = \left(\frac{m}{3k}\right) < v^2 > = \left(\frac{2}{3k}\right) E_k \tag{1.12}$$

where E_k is the kinetic energy (an assumption true only for an *ideal gas*: see Sect. 1.2.1), k is Boltzmann constant and m is the molecular mass. Temperature is proportional to the average kinetic energy of the molecules.

This relationship gave rise to the speculations on whether the concept of temperature is a basic concept or whether it should instead be derived from that of energy (see, for instance, Worthing 1941; De Boer 1965; Arzeliers 1968; Duff et al. 2002; Kalinin et al. 2005).

Temperature in Statistical Mechanics At the turn of the twentieth century, the microscopic structure of matter was studied from a statistical point of view, on the assumption that an *entire system* of n molecules of any substance (not only of gases) can be found in a *continuous* set of "states." Thermal equilibrium was defined as the steady-state distribution of the molecules, by assigning to (Boltzmann–Gibbs) probability P, for energy E, a distribution

$$P(E)\mathrm{d}E \approx \Omega(E)\mathrm{e}^{-E/\tau}\mathrm{d}E \tag{1.13}$$

where τ is the norm of the distribution. It can be demonstrated that

$$\tau = kT \tag{1.14}$$

where k is the Boltzmann constant.

Temperature in Quantum Mechanics Statistical mechanics was the last domain of classical mechanics. Subsequently, only quantum mechanics has been able to explain a wider class of phenomena that remained unexplained in the classical conceptual framework. Many of such phenomena occur at very low temperatures approaching what in the classical definition is the zero of absolute temperature; the amount of energy involved approaches zero as well. Since energy exchanges do not necessarily affect the bulk material (the lattice, in the case of solids), these phenomena may have dramatic effects on macroscopic properties. The ^{3}He-state diagram in Chap. 5 provides an example, others are provided by the variety of solid-state phenomena that occur with decreasing temperatures.

In the distribution of quantum states, a parameter τ is generally defined, which can be interpreted as temperature, as in classical statistical mechanics. The spin systems represent an instance (Simon 1955) where negative values of this parameter (temperature) have been measured in solids.

Gases, too, can be treated as quantum fluids. For helium isotopes, the reader is directed to a textbook in this Monograph Series (Van Sciver 1986), in which macroscopic examples of quantum properties are shown to behave according to the two basic—quite different at low temperatures—statistics: the Bose–Einstein for ^{4}He and the Fermi–Dirac for ^{3}He.

Entropy can be expressed, according to the Boltzmann law, by $S = k\ \ln W$, where W is the number of "microstates" of a macroscopic state of a system. Equilibrium condition is for the maximum number of these microstates and two bodies are said to be in thermal equilibrium when a thermal exchange between the two bodies does not increase that number. Indicating with $W_\mathrm{A} \times W_\mathrm{B}$ the number of degree of freedom of the system, this condition is met when $\mathrm{d}(W_\mathrm{A} \times W_\mathrm{B}) = 0$ or $\mathrm{d}W_\mathrm{A} \times \mathrm{d}W_\mathrm{B} = 0$. Since the total energy of an isolated system cannot increase, $\mathrm{d}W_\mathrm{A} = -\mathrm{d}W_\mathrm{B}$. For constant external parameters, thus for equilibrium $\partial \ln W_\mathrm{A}/\partial \ln W_\mathrm{A} = \partial \ln W_\mathrm{A}/\partial \ln W_\mathrm{A}$, hence the measure of temperature come from $\partial \ln W/\partial U = 1/k\mathrm{T}$.

Only when

$$N/V\left(h^2/2\pi mkT\right)^{2/3} = N/{V_\mathrm{dB}}^3 \ll 1 \tag{1.15}$$

the Maxwell–Boltzmann statistics can be a good approximation of the quantum statistics and quantum effects can be neglected, because the de Broglie wavelength λ_dB is small with respect to the mean distance $(V/N)^{1/3}$ between the gas particles. Otherwise, the ground-state masses of the particles (atoms or electrons) cannot be neglected or one is dealing with quasiparticles (photons, phonons). In these cases, the other two statistics diverge from the high-temperature one, as shown in Fig. 1.3, showing the relationship between the internal energy U and the temperature of the particles. For $T \to 0$, for fermions (spin multiple of 1/2) $U = -3NE_\mathrm{F}/5 \propto T^2$ (E_F Fermi energy), for bosons (integer spin) $U \propto T^{5/2}$ (Strehlow and Seidel 2007).

Is the Boltzmann constant involved also in quantum statistics? The following discussion, taken from Kalinin and Kononogov (2005), well clarifies the issue.

In the equilibrium state, the system of molecules may be expressed by a Gibbs distribution: $F(q, p) = Z^{-1}\exp\{-[U(q) + E(p)]/kT\}$, where Z is the statistical integral, $Z = \int \exp\{-[U(q) + E(p)]/kT\}\mathrm{d}q\mathrm{d}p$, and $U(q)$ is the potential energy of all the

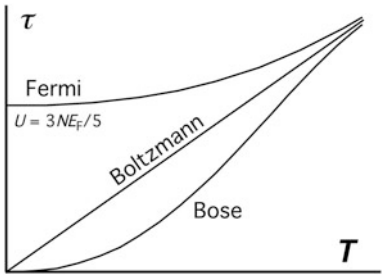

Fig. 1.3 Differences between τ and T in Boltzmann, Fermi, and Bose statistics (a similar graph is obtained by using internal energy U instead of τ)

molecules in the system, including their interaction energy, while $E(p)$ is the kinetic energy of the molecules.

These expressions show that the temperature as an external parameter appears in the definition of the distribution only in the form of the combination $\tau = kT$, as already found in Eq. (1.14). When one calculates all the macroscopic characteristics of the system and the processes in it, we obtain a dependence on τ, not on the thermodynamic temperature T only.

The above expressions describe a classical system of many particles. When that description ceases to be correct, in particular at low temperatures ($kT \to 0$), the quantum effects must be taken into account. An equilibrium system can then be represented as the density matrix $\rho(q, q') = Z^{-1} \sum_n \Psi_n^*(q') \exp(-E_n/kT)\Psi_n(q)$, where the statistical sum Z is defined by $Z = \sum_n \exp(-E_n/kT)$, and $\psi_n(q)$ is an eigenfunction of the hamiltonian H for this molecular system corresponding to the energy level E_n. *The equilibrium State of a quantum system is also dependent on the combination* $kT = \theta$. In equilibrium statistical mechanics in the classical *and* quantum cases, all the characteristics associated with thermal phenomena should be determined by $\theta = kT$. One naturally takes the temperature as that quantity. The unit of measurement for θ should naturally be an *energy level* measurement unit, i.e., the joule in the SI. That suggestion follows from the virial theorem, which directly relates the mean kinetic energy in the molecular motion in the system P_i per degree of freedom to the temperature: $P_i = kT/2$.

It can be shown that in thermodynamics everything that is dependent on temperature T can be reduced to a dependence on $kT = \theta$. When one considers the Carnot cycle on the basis of the first and second laws of thermodynamics, it is found that Eq. (1.5) holds. Thompson (Lord Kelvin) in 1848 adopted a simple linear form for the function $\Theta(\tau)$ and defined $\Theta = \tau$. Subsequently, it was taken $\tau = T$. Should one takes instead $\tau = \theta = kT$, there would be a consequence on entropy.

In fact, while in the first case Eq. (1.11) holds, in the latter case it would be $\mathrm{d}Q/\theta = \mathrm{d}S/k$, where S/k is dimensionless.

In statistical mechanics for a classical system with thermodynamic entropy S, one has $S = -k \int F(t, q, p) \ln F(t, q, p)\, \mathrm{d}q\mathrm{d}p$, and for a quantum system $S = -k \Sigma_n p_n \ln p_n$, in which p_n is the probability of state n. These expressions show that all the content part of the entropy concept is present in the dimensionless integral or sum, while factor k is present in them to provide the necessary dimensions related to the definition

of the thermodynamic temperature T. It would be natural to relate k to the temperature T, not to the entropy S.

1.1.4 Negative and Nonequilibrium Thermodynamic Temperatures and for (Fast)-Moving Bodies

Before closing this chapter, let us briefly consider negative and nonequilibrium temperatures, to make the reader aware of some limitations in the assumptions underlying the foregoing definitions.

Negative Absolute Temperature Let us begin from the second law of thermodynamics: it states that the zero of absolute temperature cannot be *crossed*, as it cannot be reached, but only asymptotically approached. It does *not* state that negative temperatures cannot exist.

This statement is illustrated with an example taken from Bazarov (1964; according to the axiomatic approach, Carnot principle is for Bazarov a *consequence* of the axiomatic temperature definition). Starting from the two laws of thermodynamics for a simple thermodynamic system whose state is determined by an external parameter, a

$$\text{(I)} \quad \delta Q = \mathrm{d}U + A\mathrm{d}a \qquad \text{and} \qquad \text{(II)} \quad \delta Q/T = \mathrm{d}S,$$

a relationship can be found between an empirical temperature θ used to measure the physical laws and the thermodynamic temperature T. Being $\theta = \mathrm{g}(T)$, one obtains

$$\frac{\mathrm{d}T}{T} = \frac{\left\{(\partial A/\partial\theta)_a \mathrm{d}\theta\right\}}{\{(\partial U/\partial a)_\theta + A\}} = \Phi$$

and, by integrating,

$$T = T_0 \mathrm{e}^I \quad \text{where:} \quad I = \int_T^{T_0} \Phi. \tag{1.16}$$

T and T_0 are temperature values according to an absolute scale corresponding to the values of the empirical temperatures θ and θ_0, respectively.

From the definition given in Eq. (1.14), it follows that the sign of temperature T cannot change. However, the sign is not determined, unless it is decided which temperature is higher and which is lower. An *additional* condition must be added, for example, stating that specific heat is positive: $(\delta U/\delta T)_a > 0$, which is a stability condition for the equilibrium of a homogeneous single-component system. In other words, to satisfy this condition, heat must flow from hot to cold bodies.

Negative temperatures are commonly included in studies on thermodynamics (e.g., Ramsey 1956; Landsberg 1961; Bazarov 1964; Dunning-Davies 1976), as a purely academic exercise.

Nonequilibrium Temperatures and Irreversible States All previous definitions apply to equilibrium reversible thermodynamic states. The set of these states is assumed to be connected—though not all states can be reached by all types of processes (see Carathéodory)—but the process that causes the variation from one state to a neighboring one, i.e., time, is in conflict with their definition. "Thermostatics" would actually be a more appropriate term. This difficulty is usually overcome—or is believed to be—by the use of the term quasiequilibrium or quasistatic, defined, according to Carathéodory, as:

> During any quasi-static reversible process, the external work W can be so determined as if the forces that produce it were equal to those required to maintain equilibrium.

For these states, the time arrow is relevant only because time is involved in (heat) flow and this is not reversible. The elapsing-time speed is irrelevant, as far as the above assumption is valid.

This model to approximate natural occurrences is not satisfactory under many circumstances: the application of thermodynamics for practical use almost invariably requires that processes occur in a finite time (Andresen et al. 1984), as the phenomena are either far from equilibrium (subjected to forces far different from those required to maintain equilibrium) or irreversible (as common as: flow, diffusion, friction). In these cases, the question is whether the temperature (and entropy) definition still apply, and whether these concepts can be uniquely defined.

The matter is extremely delicate and complex and is beyond the scope of this monograph, which strictly concerns (*quasi*!) equilibrium states. The reader is directed to the relevant literature (see, e.g., Prigogine 1954, 1962; De Groot and Mazur 1962, Haase 1969).

Temperature of Moving Bodies Readers interested in relativistic thermodynamics can consult articles such as Biro and Van (2010).

1.2 Temperature Scales

Temperature cannot be measured in the same way as other fundamental quantities, e.g., length. The unit size of the degree having been defined, it cannot subsequently be labeled "unit interval" and used to measure temperature in the same way as the meter in length measurements. That is, an additive procedure cannot be used for temperature, by which its value is determined from the number of the "unit intervals" contained in it. Temperature values, instead, can only be determined by comparing two temperatures, one of which is the reference, and by observing whether they are equal—or which one is higher—by observing, in accordance with the zeroth law of thermodynamics, whether there is—or not—a heat flow, and by noting its direction. To assign a numerical value to each temperature, one has to first "order" the measured temperatures, that is, to establish a *scale* in which the heat flows always in the same direction, and then *assign* a sign to the flow. Accordingly, it can be said that $\{\dots T_1 > T_2 > T_3 \dots\}$: temperature is a simply ordered manifold. By this procedure,

one cannot yet assign a numerical value to the different temperatures, but only give them a serial number that will be altered by the arbitrary addition of any new measurement.[5] Nor can one say yet that the value of any T_2 is closer to that of T_1 than to that of T_3 (in fact, one cannot assign a distance between two temperatures), even if he should decide to take the interval, say $\{T_1, T_2\}$, as the unit interval, because neither intervals nor ratios can be compared by means of heat flow ("heating"; Truesdell 1979) measurements.

In other words, the metric of the absolute temperature space $\{T\}$ must be supplied by another physical quantity P whose analytical relationship to temperature can be established and whose metric is known. The metric of $\{T\}$ will be equal, *by definition*, to that of $\{P\}$ only if this relationship is linear: $P \propto T$. Actually, as an empirical temperature θ is measured, $P \propto \theta$. Subsequently, it is demonstrated that $\theta \equiv T$.

As mentioned in the preceding section, the definitions of "absolute" temperature are given only as ratios or differences of values. Therefore, normalization constants are required to make the relationship of temperature with another physical quantity determined. These definitions may be said to provide a "blank tape," which is necessary for temperature measurement, but leaves free the choice as regards both the *size* of the graduation in unit intervals and the *position* of the "zero" value on the tape. These are the two degrees of freedom characteristic of any *linear* scale, that is, as already pointed out, of a scale having the same metric of the space of which is taken to represent the measuring tool. In the case, for instance, of the unit of length, the *meter*, it is appropriate to define it in such a way as to maintain the additive property in the classical isotropic space (though not near a relativistic curvature of the space). In this respect, in the absolute temperature definition of Eq. (1.5) the metric of the space of heat—i.e., of energy—is used; whereas in his first definition (Eq. (1.4)) Lord Kelvin used the metric of the space of mechanical work equivalent to heat. The transformation between the two definitions is not linear, but logarithmic (cfr Eq. (1.6)), as a reflection of the fact that the first defines a temperature ratio, the second a temperature difference.

The definition in the space of heat has been preferred because it closely approximates the numerical values obtained with gaseous substances—already experimentally available at Kelvin's times—and, more specifically, because it matches *exactly* the physical properties of a model state of the matter called "the ideal gas," more or less approximated by real gaseous low-density substances. This limit model has unique characteristics in that the scaling problem, which is usual in natural phenomena (a problem summarized in the question: are the laws of the macroscopic world the same at atomic, subatomic,... level?) is eliminated by assuming that the "gas" constituents are particles like spherical atoms—in the Greek philosophers' sense—not subjected to any external force field (not even to gravity) and not interacting with each other, but only subjected to perfectly elastic (nondissipative) collisions; the model is independent of the size of the atoms and of the scale (e.g., for

[5] This is the type of scale established empirically according to the old method of measuring high temperatures by observing the melting of the tips of a series of refractory cones having different melting temperatures or the familiar thermometers based on glass floaters of different densities.

a model scale of a planetary size, no gravitational forces would be exerted!). In the classical ideal-gas theory, particles are, in fact, not characterized by any parameter, namely mass, but they are identical, so indistinguishable from each other. Starting from the modern generalization of the model of *quantum* ideal gas, they satisfy the equation of state

$$pV = gT \tag{1.17}$$

where g is a constant (Landsberg 1961). In the case of the classical ideal gas, g is defined by Rn (n being the amount of substance and R the gas constant) or by kN (N being the number of particles (entities) and k the Boltzmann constant). Equation (1.17) *alone* defines the ideal gas model for absolute temperature. For an empirical temperature θ, on the contrary, the definition of the model requires, in addition to Eq. (1.17), the condition $(\partial U/\partial V)\theta = 0$, which is no longer implied.

Actually, the plural form "ideal *gases*" is often found. The reason is that other conditions are assumed to be added to the basic model. For example, a common (but *unnecessary*) condition is the definition of a relationship $c(T)$ for the specific heat (e.g., $c(T) = const$); or, of a "structure," e.g., molecular, with an additional kinetic energy associated with each noninteracting particle, as in the microscopic approach (see Sect. 1.1.3). Therefore, we may have different *gases*, depending on whether they are monoatomic or polyatomic, have a spin, etc. In such cases, they can be considered as the limit condition for vanishing intermolecular and external interactions of real gas species.

The ideal gas model was fully developed in the second half of the nineteenth century on the basis of the kinetic theory of gases, which explained the well-known equation of state (Eq. (1.17)). This equation, which establishes a relationship between temperature and other physical quantities, will be treated in detail in Chap. 3.

To summarize, it is because temperature is defined in the heat (energy) space that the absolute lower end of the temperature scale is a zero (only asymptotically approached) and not a (negative) infinity. This, from the standpoint of cryogenics, may be misleading (see Fig. 1.1). Obviously, with decreasing temperatures the quantity of energy associated with all phenomena decreases as well, involving first the material bulk, then only lattice vibrational, molecular, atomic, nuclear, etc. energies, and the relevant effects on the *whole* system decrease accordingly. However, each individual effect on its own scale (viz., atomic heats in the world of atoms, . . .) does not necessarily decrease at the same rate, as is shown by the numerous phenomena occurring at low temperatures (condensation, ordering, etc.; see also Fig. 1.3).

A burning match will hardly heat a cubic meter of water, but will fully burn another match. The problem of scaling according to dimensions was certainly not clear in Kelvin's times and is absent, as already pointed out, in the particular model called the ideal gas, where no "nesting" of levels exist, which, in contrast, is the characteristic of our physical world. A logarithmic temperature scale would let us feel more at ease in this respect (Simon 1955). On a scale of this type, the lowest limit of temperature treated in this monograph, 1 mK, (five and a half orders of magnitude from room temperature) would be *much farther* from room temperature than plasma temperatures (one million degrees) are on the upper side of the scale (see Fig. 1.1).

1.2.1 Thermodynamic Temperature

The previous considerations should be kept in mind when examining the international conventions that set the definition of thermodynamic temperature scales and the values of their standardizing parameters.

First, let us remark again that only an empirical[6] temperature θ can be measured. The aim of this section is to show how a usable relationship can be established between a scale based on θ and the thermodynamic temperature T—it is an interesting question why the decoration "thermodynamic" should be added to "temperature."

Second, it must be pointed out again that none of the definitions of temperature given in the preceding section defines a unique scale. Each only puts constraints on the scale form.

An example is provided by Eq. (1.15) (Bazarov 1964), by which a temperature is defined according to Carathéodory's approach, which relates the empirical temperature θ to the thermodynamic temperature T. T_0 is a reference temperature, a choice on which the size of the unit depends. Should a second reference temperature T_1 be selected, with I_1 denoting the integral of Eq. (1.16) between θ_1 and θ_2, we can write

$$T_1 - T_0 = T_0 \left(\mathrm{e}^I 1 - 1\right). \tag{1.18}$$

Therefore, for any T,

$$T = (T_1 - T_0) \left[\mathrm{e}^I \left(\mathrm{e}^I 1 - 1\right)\right] \tag{1.19}$$

On the assumption that the empirical Celsius temperature is used, $\theta := t$, supplied by the ideal gas, so that $A = p$, $a = V$, and $p = p_0\ (1 + \alpha t)$, with $V = const.$, and that $(\partial U/\partial V)_t = 0$, one obtains

$$I = \ln\left[(1 + \alpha t)/(1 + \alpha t_0)\right] \quad \text{and} \quad I_1 = \ln\left[(1 + \alpha t_1)/(1 + \alpha t_0)\right] \tag{1.20}$$

by assuming that $(T_1 - T_0) = (t_1 - t_0)$, one obtains $T = 1/\alpha + t$, which is a usable relationship between a measured empirical scale and the thermodynamic temperature.

Another example is given in Eq. (1.4b), where the values of two constants can be chosen arbitrarily by setting the zero point in the scale (Kelvin's first definition) and the size of the degree. As a matter of curiosity, with $\theta_1 = 273.16$ K and with the old value 373.16 K for the boiling point of water, one would have: θ*/(unit) = 738 ·log T/K – 1798. On this scale, the value of the tungsten melting point (3,673 K) is 833 (units), smaller in absolute value than that of the normal boiling point of ^{4}He (4.2 K), which would be – 1336 (units) (Wensel 1941).

Kelvin's second definition (Eq. (1.5)) was used as the basis for the first internationally accepted temperature Scale at the first meeting of the Conférence Générale des Poids et Mesures held in 1887 (CIPM 1887; CGPM 1889); it was the "normal hydrogen scale" using a hydrogen gas thermometer developed by Chappuis at the

[6] Here, "empirical" has still the meaning defined in Sect. 1.1, *not* that to be defined in Sect. 1.2.2.

BIPM. Temperature $\theta := t$ was defined with the use of *two* fixed points T_1 and T_0 (according to Bazarov's example), and was assumed to be proportional to the pressure increase (at constant volume), $(p - p_0)/p_0 = \alpha t$. Pressure has a defined value p_0 at the first fixed point T_0, the ice point, which was assumed to be 0 °C (this symbol, and the term "degree Celsius" later adopted in 1948, replaced the *previous*, "degree centigrade"). The second fixed point T_1, necessary to define α, was the normal boiling point of water, defined as 100 °C: $\alpha \approx 0.003\,661\ ^\circ\mathrm{C}^{-1}$. The size of the unit was, therefore, so chosen that the interval between the normal melting point of water and its normal boiling point (see Chap. 2 for the definitions) be *exactly* 100°. In this way, the *size* of the degree Celsius is exactly that of the historical degree centigrade defined by Celsius in 1742. The temperature is defined, as a consequence, in terms of the "Celsius Scale": $T_{\mathrm{emp}} = 1/\alpha + t$, with $1/\alpha = 273.15\ ^\circ\mathrm{C}$ *exactly*. The coefficient of cubic thermal expansion of the gas α is defined as

$$\lim_{P_0 \to 0} \alpha_v = \lim_{P_0 \to 0} \alpha_P = \alpha$$

where α_v and α_p are obtained by measuring the volumes or the pressures, respectively, of a sample of gas enclosed in a bulb thermostated at 0 °C and then at 100 °C. A review of such fundamental measurements can be found in Beattie (1941): values of $1/\alpha$ ranging from 273.25 to 273.08 °C were actually measured. Another critical review can be found in Oishi (1951).

Subsequently, however, international preference moved to the use of only *one* fixed point for the definition of temperature. The main objection to the use of a two-point definition was that (De Boer 1965) with it the definition of absolute temperature is affected by the *experimental* uncertainty in the determination of α (0.01–0.02° at the time), while the Celsius temperature, an empirical scale, is exact by definition. The reverse seemed more appropriate. In 1954, the Comité International des Poids et Mesures endorsed the one-point definition, which was included by the next Conférence Générale des Poids et Mesures in 1960 (CGPM 1960) in the revision of the 1948 Scale. Temperature T_{48} was defined proportional to gas pressure, at a constant volume, $(p/p_0)_V = T$ (as already suggested by Amantons, circa 1700). The size of the temperature unit was then set by defining the numerical value of a *single* thermodynamic state (the meaning of this concept will be discussed in Chap. 2), which is actually the only definition necessary for a scale, which assumes as well $T = 0$ K at zero thermodynamic temperature. This single state was selected to be the triple point of water, because it is today reproducible to within $\pm 50\ \mu$K: it was given the value, *exact by definition*, 273.16 K. The term "kelvin" of this symbol was adopted in 1954; subsequently, in 1968, the symbol of the unit was changed to K, *no longer* °K. At that time, this value was consistent, within the uncertainty of its determination, with the Celsius Scale (in which the triple point of ice is 0.01 °C) since the temperature value of the normal boiling point of water was still 100 °C.

With subsequent measurements (Guildner and Edsinger 1976; Quinn and Martin 1985; Schooley 1988), the "0–100 °C" interval lost its historical exactness (the meter too had lost its exact equivalence to 1/40 000 000 of the earth circumference), when the interval was found shorter by (26 ± 2) mK. However, the Conférence Générale des

Poids et Mesures in 1989 (CIPM 1989) decided to maintain the 1954 definition of the Celsius temperature, i.e., to maintain the *size* of the degree Celsius equal to that of the kelvin. Therefore, the temperature value of water boiling at 101 325 Pa is 99.974 °C, a big change for the more accurate thermodynamic tables. If it had been decided, instead, to maintain *also* the difference between ice point and normal boiling point of water equal to 100 (a decision having no physical basis), the temperature of the triple point of water ought to have been redefined as: $273.16 \times (100/99.975) = 273.23$ K.

This was the situation until a process started in the scientific community and later within the Conférence Internationale des Poids et Measures (CGPM), concerning the possible redefinition of the kelvin by using the Boltzmann constant (see Sect. 3.4.4). In its Resolution 1 of October 2011 (CGPM 2011), the CGPM

> takes note of the intention of the International Committee for Weights and Measures to propose a revision of the SI as follows:
> the International System of Units, the SI, will be the system of units in which:
> the ground state hyperfine splitting frequency of the caesium 133 atom $\Delta\nu(^{133}\mathrm{Cs})_{\mathrm{hfs}}$ is exactly 9 192 631 770 Hz,
> the speed of light in vacuum c is exactly 299 792 458 meter per second,
> the Planck constant h is exactly $6.626\,06\mathrm{X} \times 10^{-34}$ joule second,
> the elementary charge e is exactly $1.602\,17\mathrm{X} \times 10^{-19}$ Coulomb,
> the Boltzmann constant k is exactly $1.380\,6\mathrm{X} \times 10^{-23}$ joule per kelvin,
> the Avogadro constant N_{A} is exactly $6.022\,14\mathrm{X} \times 10^{23}$ reciprocal mole,
> the luminous efficacy K_{cd} of monochromatic radiation of frequency 540×10^{12} Hz is exactly 683 lumen per watt,
> where
> (i) the hertz, joule, coulomb, lumen, and watt, with unit symbols Hz, J, C, lm, and W, respectively, are related to the units second, meter, kilogram, ampere, kelvin, mole, and candela, with unit symbols s, m, kg, A, K, mol, and cd, respectively, according to $\mathrm{Hz} = \mathrm{s}^{-1}$, $\mathrm{J} = \mathrm{m}^2\ \mathrm{kg}\ \mathrm{s}^{-2}$, $\mathrm{C} = \mathrm{s}\ \mathrm{A}$, $\mathrm{lm} = \mathrm{cd}\ \mathrm{m}^2\ \mathrm{m}^{-2} = \mathrm{cd}\ \mathrm{sr}$, and $\mathrm{W} = \mathrm{m}^2\ \mathrm{kg}\ \mathrm{s}^{-3}$,
> (ii) the symbol X in this Draft Resolution represents one or more additional digits to be added to the numerical values of h, e, k, and N_{A}, using values based on the most recent CODATA adjustment,
> from which it follows that the SI will continue to have the present set of seven base units, in particular
> ...
> the kelvin will continue to be the unit of thermodynamic temperature, but its magnitude will be set by fixing the numerical value of the Boltzmann constant to be equal to exactly $1.380\,6\mathrm{X} \times 10^{-23}$ when it is expressed in the SI unit $\mathrm{m}^2\ \mathrm{kg}\ \mathrm{s}^{-2}\ \mathrm{K}^{-1}$, which is equal to $\mathrm{J}\ \mathrm{K}^{-1}$
> ...

Therefore, the CGPM at the date of October 2011 has not yet taken any *final* decision about the above matter, so no change in the kelvin definition is in force after that meeting, at least until the next CGPM meeting would possibly confirm the above intention.

Table 1.2 summarizes chronologically the developments of thermometry.

In principle, any thermodynamic law can be used to assign a metric to the thermodynamic temperature in order to obtain a thermodynamic scale, provided that the law can be reduced from the implicit form

$$T = f(a_1, \ldots, a_m; x_1, \ldots, x_n) \tag{1.21}$$

Table 1.2 A short history of thermometry

1600	Thermoscope invented by Galileo Galilei	The thermoscope has no graduated scale, therefore, temperature evaluation is only qualitative
Mid-1600	Liquid-in-glass graduated thermometers are widely spread	Famous are the alcohol thermometers of the Accademia del Cimento in Florence. Their graduation marks are made of colored glass bits attached to the stem
1694	Melting ice and boiling water adopted by G. Renaldini as fixed points	Fixed points must be established by reference to natural phenomena, whose temperature is assumed to be intrinsically determined
1724	Modern temperature scale proposed by G. Fahrenheit, defined by a thermometer, a law and three fixed points	Fahrenheit's thermometer was a mercury-in-glass one. Thermal expansion vs. temperature was assumed linear. Three fixed points were defined: 0 °F: temperature of a mixture of water, ice, and ammonium chloride; 32 °F: temperature of melting ice; 96 °F: temperature of human body
1742	The temperature interval between melting ice and boiling water subdivided into 100 equal parts by A. Celsius	The degree Celsius (°C) was the one eventually adopted
1821	Thermoelectric effect discovered by T. J. Seebeck	The Seebeck effect is the basis for the thermometers designated as thermocouples
1854	The modern absolute temperature definition suggested by W. Thomson is based on Carnot cycle	A scale whose definition does not depend on a specific substance is called "absolute"
1871	First electrical resistance thermometer built by C.W. Siemens	The electrical resistance thermometer is the best practical thermometer still today
1879	Blackbody radiation law proposed by J. Stefan forms the basis for the radiation thermometers, with Planck's law	The radiation law is strongly nonlinear in temperature, since it depends on T^4
1967	The XIII Conférence Générale des Poids et Mesures adopts the Kelvin scale with a single fixed point: 273.16 K	The unit of temperature is designated "kelvin"; its symbol is K
1990	The XVIII Conférence Générale des Poids et Mesures adopts the present version of the International Temperature Scale, the ITS-90	The ITS-90 provides the best to-date practical approximation of the thermodynamic scale and offers a reproducibility that is better than the thermodynamic scale
2006	Definition of a "*mise en pratique*" of the kelvin	ITS-90, PLTS-2000, and thermodynamic scale transformed in realizations of the "*mise en pratique*" of the kelvin. A Technical Annex contains changes in scales definitions
2011	CGPM takes note of the change of the kelvin definition in the frame of "the possible future revision of the International System of Units, the SI"	If the CCU proposal will stand, the kelvin will be defined by means of the Boltzmann constant set to a stipulated value. This will not have any practical effect on the *mise en pratique* in force since 2006

where x_i ($i = 1 \ldots n$) are independent variables and a_j ($j = 1 \ldots m$) are constants, to a form depending linearly only on one variable, all the others becoming perturbations to be measured or computed (the so-called "corrections")

$$T = g(b_1 \ldots b_p)y \tag{1.22}$$

in which b_k ($k = 1 \ldots m$; $m + 1 \ldots p$ and $p = m + n - 1$) become known constants or variables $b(T)$ measured or independently inferred, and y is a single independent variable (e.g., pressure, for a gas thermometer).

In this form, the thermometer is fully defined by its analytical equation alone and, strictly speaking, it becomes *the* primary thermometer. This would be true, for example, as will be discussed later with the vapor- pressure thermometer (Chap. 4), should its equation be calculated from "first principles," or with the dielectric constant gas thermometer, if polarizability and compressibility modulus could be calculated or independently measured. At present, such a primary definition can only be realized to a modest accuracy, except at sufficiently low temperatures.

However, since temperature is actually *defined* at one fixed point T_0, the triple point of water, *one* free parameter is allowed whose value for each specific implementation of the thermometer is determined by measurement, $y_0 = y(T_0)$, at that fixed point. This is the procedure applied for determining, e.g., the gas density in a constant-volume gas thermometer.

For scales defined only below 100 K, the use of such a fixed point at 273.16 K is quite unsuitable, for it is difficult to optimize a measuring apparatus over a wider temperature range. Therefore, it is common practice to rely on a previous separate thermodynamic determination of the temperature ratio between 273.16 K and a lower temperature (chosen in the range 24–90 K) defined by a well-reproducible thermodynamic state, and to use this state as the reference point for subsequent measurements in the low-temperature range. A thermometer so defined is still considered a "primary" thermodynamic thermometer, because the uncertainty increase due to the contribution of the derived reference point is very small.

The subject of thermodynamic measurements will be fully developed in Chap. 3 in connection with gas thermometry.

1.2.2 Empirical Temperature

The determination of thermodynamic temperature from first principles is a difficult experiment (see Chap. 3 for possible future simplifications). Every measurement is, in fact, only an approximation, because of imperfections in the model used for describing the basic thermodynamic law, of insufficient control of the secondary experimental parameters that are included in the model (the so-called "corrections"), or because of random experimental errors.

In nature, however, a temperature-independent phenomenon is rather the exception than the rule. Any temperature-dependent physical quantity can, in principle,

Fig. 1.4 Nonlinearity in a dial thermometer

be used to measure temperature: thermometers were invented long before the beginning of the science of heat (at the turn of sixteenth century, the alcohol-in-glass thermometers of the Accademia del Cimento in Florence were famous; Middleton 1966). Whether a physical quantity is suitable or not as a thermometer is a matter of convenience; a choice may depend as well on the required precision of the resulting temperature scale.

An important element to consider for the evaluation of a candidate empirical scale, apart from the trivial necessity for the physical quantity to behave monotonically with temperature (e.g., water density is not), is its being or not a linear transformation of absolute temperature—which must be always referred to. If it is not, the metric of the space of absolute temperature is not conserved. This fact does not itself prevent the experimentalist from assigning numerical values sequentially to the thermodynamic states. However, the use of different metrics has several undesirable effects in the comparison of results, a fundamental in the modern conception of science. The relationship between the physical quantity and the thermodynamic temperature must be carefully specified; this specification is often difficult to find in the literature, especially over long periods of time. It is well known that scale-conversion calculations are cumbersome and errors frequently occur. In addition, it is a common experience that it is often impossible to retrieve old data, and that accuracy degradation cannot be avoided. Finally, the functional relationship of derived quantities, e.g., specific heat to absolute temperature, becomes altered.

Most of the possible empirical scales are not linear in thermodynamic temperature, that is, the graduation of the thermometer scale is not uniform with respect to the measured quantity, as many dial thermometers (and manometers) show (Fig. 1.4 shows one example where the measured quantity is dial deflection).

Empirical scales can be subdivided into two subtly but substantially different categories, which will be examined in the following sections.

1.2.2.1 Semiempirical Scales

The only element that makes these scales different from a primary thermodynamic scale is the increased number of conventions stipulated for their definition. Equation (1.20) may be the (to date) exact representation of a thermodynamic law, but the value of some of the parameters b_k either cannot be calculated with sufficient accuracy, or accurate calculations are not estimated convenient. For instance, Curie's law for

paramagnetic substances is

$$\chi = \chi_0 + C/(T + A + B/T). \tag{1.23}$$

This equation, which also is nonlinear in T, can be exploited to determine temperature by measuring the magnetic susceptibility χ, but the three constants must be experimentally determined by measuring the susceptibility values ($\chi_1 \ldots \chi_3$) at three reference temperatures ($T_{r,1}, \ldots, T_{r,3}$), whose values are *defined*. The procedure can then be considered a calibration of the experimental setup. Similar methods can be used in vapor pressure measurements (see Chap. 4) and in gas thermometry (see Chap. 3).

The reference points are at least two. Since they are always selected from well-defined thermodynamic states, it is assumed that, when the state is exactly reproduced, the thermodynamic temperature is too, independently of the experimental setup or of the experimental results.

A scale so defined assumes no approximations in the defining thermodynamic equation and no simplifications in the experiment, as would be the case of a primary thermodynamic measurement. Consequently, the scale definition need *not* specify any characteristics of the experimental equipment or any measurement procedure. Measurements have to be performed according to state-of-the-art techniques required by the accuracy to be achieved. With respect to primary measurements, the measurement procedure is simplified in that calibration at the fixed points avoids measuring several secondary parameters and performing cumbersome and uncertain correction calculations.

Two defining points at least are used, as already said, which, being fixed by the scale definition, are called as well "*fixed points*" of that scale. None need to be the defining point of the kelvin scale. The scale definition assigns them *conventional* temperature values. Though these values are assumed to be *exact* thermodynamic temperature values, they are actually the best up-to-date approximations. The empirical temperature θ defined by these scales is considered to be satisfactory enough as an approximation of the thermodynamic temperature T.

1.2.2.2 Empirical Scales

Quite frequently, the thermodynamic relationship between the measured physical quantity and thermodynamic temperature is not known to sufficient accuracy, or this relationship is not convenient for direct use; it might be as well that measurements are executed with instruments, which cannot or need not to be fully characterized.

A temperature scale stemming from situations such as these is substantially different from semiempirical scales mainly for two reasons.

(a) Approximating Thermodynamic Temperature An equation of the type of Eq. (1.21) becomes a purely computational model to obtain an approximation of the thermodynamic temperature T. The value y_k of the physical quantity is obtained

from the equation at a number of reference temperatures equal to the number p of the free parameters of the model

$$\theta_k = g(a_1 \ldots a_p, y_k) \quad (k = 1 \ldots p) \tag{1.24}$$

where $(a_1 \ldots a_p, y_k)$ are constant parameters. The model must be determined empirically and must prove to fit T over the whole chosen range between the fixed points within the chosen uncertainty, on the basis of *experimental* $T(y)$ data (actually only an estimate $\theta(y)$ is available, as data are affected by experimental errors). The number p of parameters necessary to fit Eq. (1.24) to the required accuracy, determines the number of the fixed points necessary to *calibrate* the thermometer. The optimum spacing between these fixed points on the temperature scale is determined by the characteristics of the model, i.e., by the mathematical function used, but, at the same time, it is obviously constrained by the availability of suitable thermodynamic states in nature. This point will be discussed in connection with the description of the ITS-90.

(b) Interpolating Instrument Since the relationship between the chosen physical property (e.g., electrical resistance) and the thermodynamic temperature is not calculated from first principles, but is derived from experimental data, the use of a temperature scale is limited to a specific device, or at least to a family of devices providing the experimental data.

This point will be made clearer by the example of the platinum resistance thermometer. In first place, the experimental data pertain exclusively to a *specific* substance, platinum, as they cannot be extended, by means of a theory, to be valid for other metals—for an attempt to make the model function valid for a set of metals and starting from first principle calculations, see (Nicholas 1992, 1995a, b). Other restrictions must be considered as well, for instance, the bulk material must be in well- defined chemical (oxidized, ...) and physical (strain-free, ...) states, and the results are valid only for a given range of chemical purity.

When some of the characteristics of the interpolating instrument can be specifically quantified, the range of the accepted values for these parameters must be defined as well in the scale, to enable one following this prescription to reproduce the results, viz. the scale. If this is not possible, with, for example, diode thermometers or thermistors, results, *and that scale*, will be valid only for the specific production lot of devices from which results were obtained.

The thermometer used in a scale of these types is known as an "interpolating instrument," because it is not itself required to reproduce a thermodynamic property, but only precisely the smooth selected function, $y = f(\theta)$, which is used to *interpolate* temperature values between the values assigned to the fixed points.

To summarize, there are three constitutive elements associated with an empirical scale:

1. An interpolating instrument.
2. A mathematical definition.
3. A set of *fixed points*.

The interpolating instrument was discussed in the foregoing point (b). The mathematical definition (see (2)) must conveniently be the simplest function (or set of functions) representing, within the stated accuracy, the relationship between the measured quantity and the thermodynamic temperature; it has a number of free parameters (this is characteristic of an empirical scale), whose numerical values must be obtained from a "calibration" of the interpolation instrument at a number of reference points. The number of these defining fixed points (see (3)) must be equal to the number of free parameters and their position must be such as to permit the best compromise between mathematical requirements and what is available in nature. The temperature value of the reference point is defined, i.e., fixed by the scale definition.

A scale of this type, which is the most common, is affected by a specific shortcoming, which must be kept in mind, called *nonuniqueness*, a *nonstatistical* term expressing the concept that in each particular unit implementing the *interpolating instrument* (i.e., the thermometer) the relationship between the measured quantity and temperature is slightly different. Therefore, the mathematical interpolating procedure defined by the scale *cannot* adequately represent the measurements performed with each individual unit of the thermometer, but can only approximate the physical behavior of these units. In other words, if the scale definition is applied to two specific units of the thermometer placed in an isothermal enclosure, there will be a measurable difference between the temperature values supplied by their calibration tables and the temperatures actually measured. This is true at every temperature *except* at the fixed points, at which the units have originally been calibrated. Calibration at the fixed points means, by definition, to associate the measured numerical value of the property (e.g., of electrical resistance) to each temperature value of the calibration table (expressed in the scale, e.g., T_{90}).

The nonuniqueness effect for a set of platinum resistance thermometers in the temperature range from 13.80–273.16 K is depicted in Fig. 2.46 in Sect. 2.6 (see also Sect. 1.2.3 and Appendix A). The nonuniqueness effect cannot be reduced, since it is a nonstatistical systematic error intrinsic to thermometer fabrication. Consequently, it must not be mixed up with errors in the scale realization, nor must be ascribed to the limited ability of the mathematical definition to match the physical behavior of each individual thermometer; it is due, instead, to technical limits of the interpolating instrument itself. This difference becomes evident in Fig. 1.5, which shows the histogram representing the maximum nonuniqueness value between two fixed points for thermometers obtained from different manufacturers. It also shows an obvious grouping of the deviation values by manufacturer.

Still in connection with these scales, another problem, concerning instead their mathematical definition, is the *smoothness* of the selected mathematical model with respect to the physical relationship between the measured quantity and thermodynamic temperature. In order to model accurately this relationship, high-order polynomials are often required, which tend to oscillate between the constraints. A striking example is the difference between the International Temperature Scale of 1990 (ITS-90), in which the smoothness with respect to the thermodynamic scale has been better controlled, and the former IPTS-68 version, shown in Appendix A (Fig. A1.1). Attempts to show that splines functions could be used instead (Ciarlini

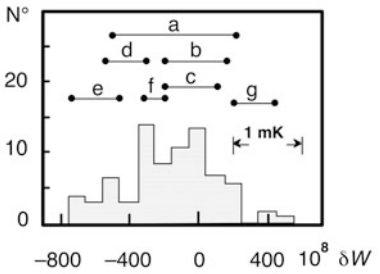

Fig. 1.5 Systematic differences in calibrated platinum-resistance thermometers of different manufacturers (*a–g*). $\Delta W = (R - R_{\text{IPTS-68}})/R_0$ at 120 K, for calibration points at 84 K and 273.16 K. N° = number of thermometers with a given ΔW. (After Pavese and Demonti 1978)

and Pavese 1992b; Pavese and Ciarlini 1992a; Pavese et al. 2012d) did not bring so far to their use in temperature scales definition (see also Sect. 1.2.5).

1.2.3 Official Temperature Scales

Since the measurement of temperature is a necessity in a laboratory, "Laboratory Scales," more of less based on thermodynamic determinations, have always proliferated. In this connection, after it has been demonstrated how delicate a matter the temperature definition is, it seems now appropriate to draw attention on the great care that accurate temperature measurements demand. As a consequence of the accuracy requirements, quite early an international temperature Scale was agreed upon. At its first meeting after the "Convention du Mètre," the Conférence Générale des Poids et Mesures (CGPM is actually a diplomatic body) in 1887 endorsed the "Normal Hydrogen Scale." In 1927, the CGPM adopted the first International Temperature Scale, and in 1937 the Comité International des Poids et Mesures (CIPM) established the Comité Consultatif de Thermométrie, a permanent technical body, which was entrusted with the task of preparing the drafts of revised Scales, to be adopted by the CGPM. A historical review of this process can be found in many texts (e.g., BIPM 1990; Schooley 1986). The last version of the Temperature Scale (ITS-90—see Appendix A) was adopted to begin on January 1, 1990. The preceding versions, after that of 1927, were the ITS-48 (revised in 1960 as the IPTS-48) and the IPTS-68, amended in 1975 (BIPM 1969; Preston-Thomas 1976). The ITS-90 is still in charge when this second edition is published, but in 2006 a basic change in its meaning has been adopted by the CGPM—see Sect. 1.2.4. The history of these scales is summarized in Table 1.3.

The meaning of an "official" scale is not bureaucratic, but scientific and technical. As in all types of measurements, to improve accuracy not only random errors must be reduced, but also the largest possible number of causes of systematic deviations as well has to be eliminated. An international body, within which the recognized specialists in the temperature measurements field meet and discuss their experiences and those of their colleagues, makes it possible to obtain the best approaches for

Table 1.3 The international temperature standards from 1927 to 2011, and future

	ITS-27	IPTS-48 (from 1960)		IPTS-68		ITS-90	PLTS-2000	"*Mise en pratique*"	Future (anticipated)
	1927	ITS 1948	1954[a]	1968	1976	1990	2000	2006	20xx
Unit	Degree centigrade (°C)	Degree Celsius (°C)	Degree kelvin (°K); degree Celsius (°C)	Kelvin (K); degree Celsius (°C)	Kelvin (K); degree Celsius (°C)	Kelvin (K); degree Celsius (°C)	Kelvin (K); degree Celsius (°C)	Kelvin (K); degree Celsius (°C)	*Kelvin (K); degree Celsius (°C)*
Reference T	0.000 and 100.000 °C	0 and 100 °C	273.16 K	273.16 K	273.16 K	273.16 K	273.16 K	273.16 K	None
Range	0.000 °C up	90.2 K up	90.2 K up	13.8 K up	13.8 K up	0.65 K up	0.9 mK–1 K	ITS-90, PLTS-2000, thermodynamic scale realizations; Technical Annex with changes of the above included (see text)	*0.9 mK up*
Interpolating instrument (cryogenic range, K)	None	SPRT	SPRT	SPRT; T_{58} (^{4}He vp), T_{62} (^{3}He vp) recommended	SPRT; T_{58} (^{4}He vp), T_{62} (^{3}He vp) recommended	0.65–3.2 ^{3}He vp, 1.25–5 ^{3}He vp, 3.0–24.6 ICVGT, 13.8 K up SPRT	0.9 mK–1 K melting curve ^{3}He		*Possible redefinition of the kelvin in terms of Boltzmann constant k*
Definition fixed points (cryogenic range)	None	nbp O_2	nbp O_2	tp H_2, vp H_2, nbp H_2, nbp Ne, tp O_2, nbp O_2	tp H_2, vp H_2, nbp H_2, nbp Ne, tp O_2, nbp O_2	ICVGT: 3–5 K ^{3}He or ^{3}He vp, tp H_2, tp Ne; SPRT: tp H_2, vp H_2, nbp H_2, tp Ne, tp O_2, tp Ar, tp Hg	None		*Scale major revisions of: ITS-xx*
Mathematical definition (cryogenic range)	None	Single interpolation polynomial	Single interpolation polynomial	Reference function plus correction polynomial for subranges	Same, but new reference function	vp: polynomials. ICVGT: quadratic polyn. SPRT: new ref. function and corr. polynomials; multiple definitions in some subranges	Polynomial		*Other implementations of the "mise en pratique," Technical Annex*
Thermodynamic scale	Excluded from definition[b]	Excluded from definition	Excluded from definition	Excluded from definition	Excluded from definition	Excluded from definition	Excluded from definition	Included "in due time"	*Included*

[a] In 1964, a provisional definition between 13 K and 90 K was adopted, CCT-64

[b] Before 1927, the thermodynamic hydrogen "normal scale" (CVGT) was the standard; until 2006 the international scales were only empirical and an approximation of the thermodynamic T

nbp normal boiling point; *SPRT* standard platinum resistance thermometer; *tp* triple point; *vp* vapor pressure scale

reducing the error limits. The first task of such a body is to collate the best estimates of the thermodynamic temperature, and then to assess methods for its measurement to the state-of-the-art accuracy. In carrying out this work, it is often realized that the direct measurement of the thermodynamic temperature is affected by an uncertainty larger than the reproducibility level obtainable in empirical temperature measurements. Consequently, so far, it has proved advantageous to define an empirical scale that can be reproduced more accurately and is internationally agreed upon (ITS). Finally, the current best estimate of its difference from the thermodynamic scale is supplied (Fischer et al. 2011; Pavese et al. 2012d), see Sect. 1.2.5.

Should one day the thermodynamic temperature scale be realized with an uncertainty at least equal to that of an ITS, the latter will cease to be the only useful scale, but the role of the international body will not, as it will still have the task of assessing the quality of the methods for scale realizations.

Another equally important role of this body is to assess the traceability of lower level approximations of the thermodynamic scale to the ITS, and to fill a gap of information between the ITS definition and the international codes developed for industry (e.g., by OIML, IEC) or prepared by other international bodies (e.g., IUPAC, IUPAP). At the same time, the body reviews critically the scientific and technical information necessary for code updating.

The change in philosophy of the meaning of the temperature scales occurred in 2006 has an influence also on these matters, as illustrated in the next Section.

1.2.4 "Mise en Pratique" for the Definition of the Kelvin

Following a quite rapid convergence during the 2005 meeting of the CCT, promoted by two different documents (Pavese 2005a; Quinn 2005), it was submitted to, and approved in the same year by, the CGPM a basic change in the meaning of temperature scale, so basic that it is simpler to report entirely the short document now available on the BIPM site (CCT 2006a):

> *Mise en pratique* for the definition of the kelvin (adopted by the CCT in April 2006)
> *Scope*
> This document provides the information needed to perform a practical measurement of temperature in accord with the International System of Units (SI).
> *Introduction*
> The unit of the fundamental physical quantity known as thermodynamic temperature, symbol T, is the kelvin, symbol K, defined as the fraction 1/273.16 of the thermodynamic temperature of the triple point of water. The International Committee for Weights and Measures (CIPM 2005b) recently clarified the definition of the triple point of water by specifying the isotopic composition of the water to be that of Vienna Standard Mean Ocean Water (V-SMOW). Triple-point-of-water cells provide a convenient realization of this definition. For temperatures other than the triple point of water, direct measurements of thermodynamic temperature require a primary thermometer based on a well-understood physical system whose temperature may be derived from measurements of other quantities. In practice, primary thermometry is difficult and time consuming and not a practical means of disseminating the kelvin. As an alternative, the International Temperature Scale provides an internationally

accepted recipe for realizing temperature in a practical way. Beginning in 1927, the CIPM, acting under the authority of the General Conference on Weights and Measures (CGPM) and, since 1937, on the advice of its Consultative Committee for Thermometry (CCT), has adopted a series of International Temperature Scales. Subsequent to the 1927 scale, new scales have been adopted in 1948, 1968, and 1990, with occasional minor revisions in intervening years. The present scale, the International Temperature Scale of 1900 (ITS-90), was extended downward in temperature in 2000, when the CIPM adopted a supplemental scale, the Provisional Low Temperature Scale from 0.9 mK to 1 K (PLTS-2000). The ITS-90 and the PLTS-2000 define temperatures T_{90} and T_{2000} that are good approximations to thermodynamic temperature.

The ITS-90 is the most recent descendant of the original International Temperature Scale of 1927 and replaced the International Practical Temperature Scale of 1968 (IPTS-68) and its extension, the 1976 Provisional 0.5 K to 30 K Temperature Scale. The ITS-90 covers the temperature range from 0.65 K to the highest temperatures that can be determined practically by radiometric means. Supplementary information is available for both the ITS-90 and approximations to the ITS-90.

Considerable research has been conducted on establishing a temperature scale extending to temperatures lower than 0.65 K; the PLTS-2000 is the resulting outcome, defining temperature from 1 K down to 0.9 mK. The PLTS-2000 is explicitly a provisional scale, recognizing that the data sets comprising the basis of the scale were somewhat inconsistent. In the temperature range 0.65 K to 1 K, temperature may be defined on either the ITS-90 or the PLTS-2000. Either scale is acceptable; the choice of scale typically is dictated by convenience or the attainable uncertainty of realization. In those rare cases where use of either scale is convenient, T_{2000} is a better approximation of thermodynamic temperature than T_{90} in the region of overlap.

Historically, the best guide for the realization of the kelvin has been the text and corresponding supplemental information for the International Temperature Scales. Recent developments in thermometry have motivated the creation of a broader, more flexible document that incorporates the temperature scales in current use: the *mise en pratique* for the definition of the kelvin. As envisioned by the CCT, the *mise en pratique* will serve as a reference for:

- the text of the ITS-90 and PLTS-2000;
- a Technical Annex of material deemed essential to realization of the ITS-90 or PLTS-2000, but not included in the scale definitions themselves;
- descriptions of primary thermometers for direct measurement of thermodynamic temperature; and
- assessments of the uncertainty of the ITS-90, PLTS-2000, and measurements made by primary thermometry.

In its present form, the *mise en pratique* consists of the text of the ITS-90, the Technical Annex for the ITS-90 (CCT 2006b), and the text of the PLTS-2000 (see Chap. 4). It is anticipated that future versions of the *mise en pratique* will address the differences $T - T_{90}$ and $T - T_{2000}$ together with their uncertainties, as well as the uncertainty of direct, primary determinations of T.

The rationale of the *mise en pratique* is that, since it was promulgated as the realization of the kelvin, the status of the official temperature scales—and of the thermodynamic scale—is now that of a specific realization of the *mise en pratique*. This drastic change has several important implications that the reader should carefully consider (Pavese 2007a; Ripple et al. 2010).

ITS-90 and PLTS-2000 have not changed their regulatory status, but the new method approved by the CIPM has relaxed some of the previous constraints placed on temperature standards:

1. Adjustments to their definitions can now be implemented by simply updating the Technical Annex. In fact, the specifications for the triple point of water and the e-H_2 fixed points of the ITS-90 have recently been refined to account for isotopic effects (CCT 2006b).
2. Addition "in due course" of other methods to the *mise en pratique* is also foreseen, at present with the explicit mention to thermodynamic temperature.

However, the method introduced by the CIPM intrinsically does not prevent the acceptance of a multiplicity of methods for the *mise en pratique*, even though they may apply to the same temperature range and have different levels of uncertainty. This could mean the addition to the *mise en pratique* of Scales that had previously only the status of "approximations" to the ITS-90, without formal status, showing levels of accuracy—and precision—lower than that of the ITS-90.

1.2.4.1 Different Methods in the Mise en Pratique Must be Compatible with Each Other

The basic requisite of a standard is to be unique within a given uncertainty. In the case of the ITS-90, several mechanisms, usually indicated as type 1–3 (White et al. 2007), give rise to nonuniqueness, which in several range s dominates the uncertainty attributed to the scale. Type 3 nonuniqueness is related to differences in interpolating instruments of the same type (e.g., due to slightly different R–T characteristics of different samples of platinum; or, due to differences in the realizations of the vapor-pressure or gas-thermometer implementations; or, due to the imperfection of the mathematical model used to describe temperature as a function of the response variable of the interpolating instruments).

ITS-90 extensively uses the philosophy of "multiple definitions": this is another independent source of nonuniqueness that also has to be taken into account (type 2 if different types of interpolating instruments are used, type 1 if there is an overlapping subrange with the same interpolating instrument).

Until 2006, the contributions to the uncertainty attributable to a scale realized according to its definition combined the above intrinsic components arising from the definition itself with the state-of-the art uncertainty of its experimental implementation. All significant deviations between realizations, detected through comparison exercises, were attributed to unresolved systematic effects, i.e., to errors in the realizations to be identified and eventually eliminated by the relevant NMI(s). To avoid unduly increasing the uncertainty of the Scale definition, the "multiple definitions" were selected and defined to ensure close agreement with each other, i.e., to realize the same Scale within their individual uncertainty, and, to be of comparable uncertainty.

The effect of having several methods of the same "quality" for the *mise en pratique* defined for the same written standard is analogous with the implementation of "multiple definitions" in the ITS-90. In fact, the metrologist may want to avoid ambiguity by realizing the written standard according to the different methods of

implementing the *mise en pratique*, within a stated uncertainty. In other words, thermometers calibrated using different methods endorsed by the *mise en pratique* should provide the same numerical value for temperature when placed together in the same isothermal enclosure, within the stated uncertainty. The usual way to express this concept is to say that the different implementations of the *mise en pratique* must provide compatible measures (BIPM/ISO 2008) in order to preserve the uniqueness of the definition of the standard. (Metrological) compatibility with one another can be considered the necessary technical metrological requisite of the *mise en pratique* implementations. *It is also a sufficient one*. Other requirements, such as the desire to have only methods with the lowest uncertainties or to keep the *mise en pratique* "simple" may be dictated by what one might consider as nonscientific or "political" arguments, or by a different CIPM vision for the various *mise en pratique* describing the realizations of the SI units.

There are interesting and new implications arising from this single concept in the way that one can conceive a temperature scale. Let us subdivide them into two main categories:

1.2.4.2 Implementations of the Mise en Pratique of Comparable Quality

Traditionally, a temperature written standard, such as the ITS-90, aims at defining procedures that allow the smallest state-of-the-art uncertainty to be attained. Until 2005, different procedures were defined for different ranges within the same written standard, with a possible partial overlap of the definition ranges. In addition, the PLTS-2000 has a small overlap with the other written standard, ITS-90. Therefore, the use of different measurands typical of each procedure (e.g., electrical resistance for the SPRTs and pressure for the ICVGT) was limited to "multiple definitions" in their narrow overlapping ranges.

With the *mise en pratique*, the metrologist is allowed to relax the requirement that a single definition be used to measure temperature in a certain range. Unlike the testing field, the metrologist was already able to select the method to implement a given definition of the written standard. The metrologist is now allowed much more flexibility by choosing among the definitions made available by the *mise en pratique*, and selecting the one that is more convenient in a particular institution for the realization of its standards. The only requirement for this choice is that the definition be included in the list of the allowed implementations of the *mise en pratique*: the only requirement for inclusion in the list is, in principle, that there is firm experimental evidence of the equivalence of the allowed definitions as determined by their "compatibility" with one another.

The definition of "compatibility" according to VIM (BIPM/ISO 2008) is the "property of a set of measurement results for a specified measurand, such that the absolute value of the difference of any pair of measured quantity values from two different measurement results is smaller than some chosen multiple of the standard measurement uncertainty of that difference" (2.47–2007), also noting that "metrological compatibility of measurement results replaces the traditional concept of 'staying

within the error,' as it represents the criterion for deciding whether two measurement results refer to the same measurand or not. If in a set of measurements of a measurand, thought to be constant, a measurement result is not compatible with the others, either the measurement was not correct (e.g., its measurement uncertainty was assessed as being too narrow) or the measured quantity changed between measurements."

This possibility of choice applies to the important case of thermodynamic temperature, with a limit: though the thermodynamic temperature scale is in itself unique, it must be proven that its specific realizations are exempt from significant systematic deviations. This requirement may limit inclusion of the thermodynamic scale in the *mise en pratique* to those ranges where it is compatible with the ITS-90 or PLTS-2000. For those ranges where a persistent incompatibility can be reduced by correcting the significant bias between the ITS-90 or PLTS-2000 scales and the thermodynamic temperature scale, inclusion may be allowed following substantiation of the uncertainty of the correction. Though it may in general be undesirable, the latter solution might be an acceptable means to include top-accuracy written standards in the *mise en pratique* whose state-of-the-art realizations cannot be easily improved.

This requirement should not be confused with the nonuniqueness requirement, typical of a special type of thermodynamic thermometer adopted in the ITS-90, the interpolating constant-volume gas thermometer (ICVGT). There is a basic conceptual—and practical—difference: the ICVGT is an empirical way to use a thermodynamic thermometer. The resulting scale is by definition an approximation, to the thermodynamic scale, as are all other parts of the ITS-90 definition (Pavese 2007a). Consequently, apart from the possibility of significant systematic errors in specific realizations, the lack of specific prescriptions (e.g., density of the gas) for the ICVGT implementation may lead to nonuniqueness of the implementations (Pavese and Steur 1987c; 1989, Steur 1999; Pavese and Molinar 1992c).

Inclusion of the thermodynamic scale among the implementations of the *mise en pratique* of the kelvin is a different case. When this scale is included in the *mise en pratique*, no practical and technical details for its implementation can be further specified, since they would only concern the level of attainable state-of-the-art uncertainty of its technical realizations (Pavese 2007a). Therefore, no specific implementation of the *mise en pratique* method called "thermodynamic temperature scale" need be specified. No type of implementation can be excluded, provided that there is sufficient experimental evidence of the correctness of its uncertainty claims. This is already the case of four implementations of the thermodynamic scale (instead of the ITS-90) included in the comparison CIPM CCT-K1, which supplies the required evidence; it may apply in the future to other implementations (Pavese 2007a). In all instances, no constraints could be placed on a laboratory for its decision to choose, as more convenient for its purposes, the implementation of the thermodynamic temperature scale instead, e.g., of the ITS-90, since there is no ranking of the *mise en pratique* implementations.

According to this philosophy, the written standards *would no longer be ranked* by the type of definition, but according to the level of attainable uncertainty. The latter is often somewhat lower for implementations of the thermodynamic scale than for the

empirical scales. This brings one directly to the second novel possibility introduced by the *mise en pratique*.

1.2.4.3 Implementations of the *Mise en Pratique* of Lesser, But Compatible, Levels of Quality

There is no explicit mention of this possibility in the CIPM decision, but the method introduced by the CIPM does intrinsically allow acceptance of a *multiplicity of methods* for the *mise en pratique*, whether for the same temperature range or for different levels of uncertainty.

The traditional viewpoint in the temperature field, as already pointed out, is that the written standard is intended to define only a top-level temperature scale. In 1990, even the term "practical" was removed from the name of the written standard to avoid confusion between "empirical" and "easy to use." Every user needing temperature measurements of lesser quality needs to show traceability to the top-level definition, even if it is several orders of magnitude lower in uncertainty than required. In fact, all that the CCT has done to address this gap was to prepare a separate Monograph "Techniques for Approximating the ITS-90" (BIPM 1990b; Bedford et al. 1990), whose most recent edition dates to 1990 (a revision is in preparation). The most recent "recommended values of secondary fixed points" dates to 1996 (Bedford et al. 1996). For alternative definitions of the temperature scale, the level of "recommendation" has never been reached. Sometimes a critical review of published work was reported, but none of them were endorsed by the CCT, even when some ISO or regional written standards were adopted for specific thermometers (typically for industrial use, IPRTs, or thermocouples).

This situation has occasionally created some difficulties, and, from time to time, the usefulness of an empirical scale as opposed to the thermodynamic one has been questioned. This may have been a limitation for a large part of the user community, for whom an uncertainty of 0.1 K is often sufficient and who are not interested in the subtleties of a scale made only for submillikelvin uncertainties. Certainly, it has discouraged investigations of methods suitable for scales of lesser quality, but traceable to the ITS-90. For at least 20 years, CCT WG2 has experienced difficulty finding reliable published material in this respect, and these studies are fewer and fewer, since no institution is willing to invest resources in them without a concrete return consisting of their use and endorsement.

The key solution is provided by the basic requirement indicated above: from a technical point of view, different *mise en pratique* implementations need only be consistent with each other, i.e., "compatible" with one another. This requirement does not include the need for all of them to be of the same uncertainty. Consequently, the written standard can offer a majority of its users a wider and more convenient choice of methods, formally accepted as temperature written standards, within the framework of *mise en pratique* implementations, adapted to their needs or having the uncertainty best fitting their purposes. There are several possibilities to implement the criterion. Some are listed here in no particular order (Pavese 2007a):

1. Use of defining fixed points with some relaxed requirements, e.g., use of SRM s for the fixed point realizations or as fixed point devices, instead of realizing thermodynamic states (e.g., this book, Sects. 3.1.2 and 3.1.4).
2. Use of a different list of defining fixed points, or of an abridged list of them (e.g., for SPRTs—this book, Sect. 8.2—or PtRh thermocouples—this book, Sect. 9.5).
3. Use of a stipulated number of empirical calibration temperatures instead of defining fixed points (as used in several CMCs).
4. Use of stipulated model functions instead of a given list of calibration temperatures (e.g., using vapor-pressure thermometry with substances different from helium—Bedford et al. 1990, Sect. 6 and recent developments using dynamic measurements (heat pipes; temperature amplifier for the upper temperature range)).
5. Use of a model function and defining fixed points to find the numerical values of its parameters instead of a stipulated function (e.g., in the temperature range of the superconducting fixed points—this book, Sect. 3.1.1—or, using carbide fixed points at high temperatures).
6. Use of a different scale subfield structure of the definition.
7. Use of different interpolating instruments, or of different quality (e.g., IPRTs—Bedford et al. 1996, Sect. 16; base metal thermocouples—Bedford et al. 1996, Sect. 18—or noble metal thermocouples—Bedford et al. 1996, Sect. 9, and other more recent types; semiconducting thermometers—Bedford et al. 1996, Sects. 11–14 and other more recent types; two-color pyrometers).
8. Use of a stipulated "wire scale."
9. Harmonized use of written standards set by other organizations.

There is a basic difference with respect to a repository of approximations, to the ITS-90, currently represented by the CCT Monograph in (CCT 1990b): those approximations, have no formal status; they are not written standards. On the contrary, all implementations of the *mise en pratique* do, and share equal status with respect to the ITS-90 and PLTS-2000.

Obviously, each of the above alternatives can be considered for inclusion in the list of the endorsed methods for the *mise en pratique* only after sufficient studies are available to prove the level of uncertainty that they provide and the fact that the Scale so defined is compatible with those defined by all the other methods formally endorsed by the *mise en pratique*.

Concluding, when fully exploited, the method of the *mise en pratique* of the kelvin can provide more flexibility to the written standards concerning temperature, thereby coming closer to meeting the needs of most users. In this way, it could balance the impression that temperature metrology as practiced by the national laboratories is becoming an "ivory tower" engaged in the pursuit of scientific subtleties far removed from their needs and interests, an impression that could arise from the decision to move toward a definition of the kelvin linked to a fundamental physical constant.

Extending the principle of "multiple definitions" to a set for the *mise en pratique* implementations covering 2–3 decades of uncertainties would be a step in the direction of users" needs. This would provide standards ranked according to the level of

attainable uncertainty, with the necessary and sufficient technical requirement being that all definitions are compatible.

In particular, the inclusion in the *mise en pratique* of the thermodynamic scale, at least for the temperature range where compatibility with the ITS-90 and PLTS-2000 is proven, will suppress the duality introduced since 1927, when an International Temperature Scale (ITS-27) was preferred for the definition of the international written standard, whose definition was purely empirical. In fact, from then until 2005, the international written standard has always been distinct from the thermodynamic scale.

Every laboratory will be able to choose, as more convenient for its purposes, its own implementation of the thermodynamic temperature scale instead of, for example, the realization of the ITS-90, since there is no ranking of the *mise en pratique* implementations. For the same reason, a laboratory could choose any other method allowed by the *mise en pratique* implementation best fitting its own needs.

1.2.5 Difference Between the Realized Thermodynamic Temperature and the T_{90}

Related to the use, as a temperature scale, of the thermodynamic scale directly, the establishment of the current differences between the latter, as realized in different experiments (Rusby et al. 1996), and the ITS-90 becomes important information. In fact, for the most accurate thermophysical and chemical–physical data, the differences $T - T_{90}$ are significant.[7]

This issue was the task of a Working Group (WG4) of the CCT that annually makes a critical evaluation of the thermodynamic temperature data available (see also a previous work conducted in the frame of IUPAC: Goldberg and Weir 1991). Based on a screened set of data available until early 2010, WG4 delivered interpolating functions (Fischer et al. 2011) for the related differences $T - T_{90}$. To obtain the interpolating functions, the range of the temperature values was subdivided into 42 narrow subranges above the normal boiling point of ^{4}He and below the copper freezing point, and for each of them a consensus mean value for the data in the subrange was computed and attributed to the mean temperature value of the subrange. In addition, from 4.2 K to 35 K and between 77 K and 273.16 K a weighted mean was used. Basically, the choice has been to keep intact the short-range local behavior of the experimental data. In fact, the behavior represented by the set of 42 data so obtained from 4.2 K to 1358 K (copper fixed point)—see Table 1.4—was then fitted using different functions (Tables 1.5 and 1.6):

[7] It is also important to check if the values attributed to the fixed points of the ITS-90 are thermodynamically correct: for example, it has been stated that the value of mercury triple point (see Appendix A) is incorrect (Hill 1995; Benedetto et al. 2004; Moldover et al. 1999a). About correction of thermodynamic data, see the IUPAC Report in Goldberg and Weir (1991) and Pavese (1993).

Table 1.4 Set of the 42 CCT WG4 data used to compute the functions of Tables 1.5 and 1.6 above 4.2 K

T_{90}/K	$(T - T_{90})$/mK	u/mK	T/K	$(T - T_{90})$/mK	u/mK
4.2	− 0.02	0.12	161.405	− 8.43	1.8
5	0.11	0.12	195	− 6.97	1.8
6	0.05	0.13	234.3156	− 3.25	1.0
7	− 0.08	0.10	255	− 1.64	0.9
8	0.02	0.10	273.16	0	0
9.288	0.13	0.11	290	2.19	0.4
11	0.28	0.12	302.9146	4.38	0.4
13.8033	0.44	0.14	335	7.62	0.5
17.035	0.51	0.16	373.124	9.74	0.6
20.27	0.32	0.17	429.7485	10.1	0.8
22.5	0.10	0.18	505.078	11.5	1.3
24.5561	− 0.23	0.20	600.612	9.21	6.1
35	− 0.53	1.0	692.677	13.8	6.9
45	− 0.75	1.4	800	22.4	6.4
54.3584	− 1.06	1.6	903.778	27.6	7.6
70	− 1.57	1.9	933.473	28.7	6.6
77.657	− 3.80	1.2	1052.78	40.9	26
83.8058	− 4.38	1.3	1150	46.3	20
90	− 5.30	1.1	1234.93	46.2	14
100	− 6.19	1.2	1337.33	39.9	20
130	− 8.07	1.6	1357.77	52.1	20

u standard uncertainty

1. Between 8.0 K and 273.16 K, a logarithmic polynomial of degree 7.
2. Between 273.16 K and 1358 K, a rational polynomial of degree 4.
3. Between 2.0 K and 8.0 K, the difference was set to zero, exactly.
4. Between 1.0 K and 2.0 K, $(T - T_{2006})$ was adopted, where the PTB realization of the ^{3}He vapor pressure scale (Engert et al. 2003, 2007) is coincident with the PLTS-2000 Scale. The corresponding interpolating equation is not provided, nor is in the reference.
5. Between 0.65 K and 1.0 K, $(T - T_{2006})$ was adopted (Engert et al. 2007), but the corresponding interpolating equation is not provided, nor is in the reference.

The basic features of the results obtained by CCT WG4 using the set of interpolating functions of Table 1.5 is the following:

1. The functions fit the 42 data points well within their uncertainty.
2. The discontinuity of the first derivative $\mathrm{d}(T - T_{90})/\mathrm{d}T$ at 273.16 K arising from the ITS-90 *reference functions* was maintained (left value 0.7×10^{-4}, right value 1.01×10^{-4}): however, the value of this discontinuity in the ITS-90 calibration of any specific thermometer can slightly be different, due to a nonuniqueness of the ITS-90 in this respect, arising from the correction functions.[8]

[8] A study on 47 SPRTs (Rusby 2010) showed differences between the upper and lower derivatives in a range of 6×10^{-5}: a dispersion of 2×10^{-5} corresponds to "an error or change of ≈0.6 mK in the gallium point or ≈0.8 mK in the mercury point," so quite relevant in top-accuracy metrology.

Table 1.5 Functions used in Fischer et al. (2011) to interpolate the data in Table 1.4

Range (K)	Interpolating function	Parameters	
0.65–1.0 K[a,b]	$T - T_{90} \equiv T - T_{2000}$ $(T - T_{90})/\mathrm{mK} =$ $\sum_{i=0\ldots3} d_i\ (T_{90}/\mathrm{K})^{i}$ [d]	$d_0 = -14.0651$ $d_1 = 40.9970$ $d_2 = -44.1079$	$d_3 = 16.5315$
1.0–2.0[c] K[a,b]	$T - T_{90} \equiv T_{2006} - T_{2000}$ $(T - T_{90})/\mathrm{mK} =$ $\sum_{i=0\ldots5} a_i\ (T_{90}/\mathrm{K})^{i}$ [e]	$a_0 = 8.7999$ $a_1 = -54.8216$ $a_2 = 101.4590$	$a_3 = -83.5816$ $a_4 = 32.2307$ $a_5 = -4{,}7513$
2.0[c]–8.0 K[a]	$T - T_{90} := 0$	–	–
8.0–273.16 K[a]	$(T - T_{90})/\mathrm{mK} = \sum_{i=0\ldots7} b_i$ $(\log_{10}(T_{90}/273.16\mathrm{K}))^{i+1}$	$b_0 = 4.42457 \times 10^{1}$ $b_1 = -1.76311 \times 10^{2}$ $b_2 = -1.53985 \times 10^{3}$ $b_3 = -3.63685 \times 10^{3}$	$b_4 = -4.19898 \times 10^{3}$ $b_5 = -2.61319 \times 10^{3}$ $b_6 = -8.41922 \times 10^{2}$ $b_7 = -1.10322 \times 10^{2}$
273.16–1358 K[a]	$(T - T_{90})/\mathrm{mK} = (T_{90}/\mathrm{K})$ $\sum_{i=0\ldots4} c_i\ (273.16\ \mathrm{K}/T_{90})^{2i}$	$c_0 = 0.0497$ $c_1 = -0.3032$ $c_2 = 1.0254$	$c_3 = -1.2895$ $c_4 = 0.5176$

[a] Fischer et al. (2011): the used data (42 local averages) are reported in Table 1.4

[b] $T_{2006} = {}^3$He Scale PTB-2006. Between 0.64 K (lower limit of ITS-90) and 1.0 K, $T_{2006} = T_{2000}$ (T_{2000} = Scale PLTS-2000). Between 1.0 K and 2.0[c] K, temperatures are calculated using thermodynamic ^{3}He vapor-pressure relations according to scale PTB-2006 (Engert et al. 2007)

[c] According to the data in (Engert et al. 2007), the exact joining point, where $\mathrm{d}(T_{2006} - T_{2000})/\mathrm{d}T = 0$, so joining without second-order discontinuity with the range 2.0–8.0 K, is actually 1.9335 K

[d] This function is not supplied in Fischer et al. (2011), so it has been unofficially computed from the data reported in Fig. 3 of (Engert et al. 2007)—as indicated in Fischer et al. (2011)—, with a standard deviation of 0.006 mK It joins the function above 1 K (see[e]) with a small discontinuity of the first derivative $\mathrm{d}\Delta T/\mathrm{d}T$: 2.4 instead of 2.5 for the upper function

[e] Same as[d]: standard deviation of 0.002 mK

3. The function set to zero between 4.2 K and 8 K produces another discontinuity of the first derivative at 8 K.

Considering that second-order discontinuities in interpolating functions are quite inconvenient outside strict metrological applications, namely for the correction of thermophysical or physical–chemical data (see this book, Sect. 4.3 and Appendix D; and Pavese 1993; Bedford et al. 1996), an additional different interpolating function was made available between 2.3 K and 1238 K for these specific purposes (Pavese et al. 2012d), having the following characteristics:

1. To directly interpolate the whole set of 1046 original experimental data selected by the CCT WG4, without any further assumptions—like weighting—and without the intermediate step bringing to the 42 local-average points.
2. To cover the full range 2.3 K to 1238 K with a single function, continuous up to the first derivative over the full range: the function is a cubic spline (so being the smoothest interpolating function by definition of spline (Ciarlini and Pavese 1992; Pavese and Ciarlini 1992a), with explicit polynomial representation provided between pairs of knots (Cox-de Boor recursion formula), i.e., for each subinterval.

Table 1.6 Functions used in Pavese et al. (2011)[a] to interpolate the experimental data above 2.3 K

Four subintervals spline			Six subintervals spline		
Spline function[b] (Full range)	Cubic polynomials[c] Subinterval (T_{knots})	Coefficients a_{ij}	Spline function[b] (Full range)	Cubic polynomials[c] Subinterval (T_{knots})	Coefficients a_{ij}
− 0.003073048	2.3–90 K a_0	− 0.000593965	0.001339230	2.3–30 K a_0	0.000302995
0.002521906	a_1	0.000084027	− 0.000983408	a_1	− 0.000113512
− 0.007092070	a_2	− 0.000003974	0.002272960	a_2	0.000015650
− 0.007160607	a_3	0.000000052	− 0.007928971	a_3	− 0.000000743
0.011774420	90–300 K a_0	− 0.002642255	− 0.006855934	30–90 K a_0	0.000530791
0.015114007	a_1	− 0.000063857	0.004725796	a_1	0.000034942
0.000330789	a_2	0.000000602	0.010749938	a_2	− 0.000004931
0.060097369	a_3	0.000000004	0.010966562	a_3	0.000000099
0.042668756	300–450 K a_0	0.003884825	0.014062012	90–273.16 K a_0	− 0.002667189
	a_1	0.000157792	0.055697738	a_1	− 0.000081847
	a_2	− 0.000001213	0.042510764	a_2	0.000001038
	a_3	− 0.000000002		a_3	0.000000001
	450–1238 K a_0	0.012749953		273.16–380 K a_0	0.000458927
	a_1	− 0.000047281		a_1	0.000119811
	a_2	0.000000582		a_2	0.000000924
	a_3	− 0.000000001		a_3	− 0.000000038
				380–800 K a_0	0.010793868
				a_1	0.000001234
				a_2	0.000000046
				a_3	0.000000001
				800–1238 K a_0	0.022102959
				a_1	0.000068722
				a_2	0.000000276
				a_3	− 0.000000002

[a]The used original 1046 experimental data are reported in (CCT WG4 2008)
[b]Spline coefficients b_j
[c]Coefficients a_{ij} of the corresponding cubic polynomial (Cox-de Boor recursion formula: $p_i = a_{1i} + h(a_{2i} + h/2\ (a_{3i}h + 1/3\ a_{4i}\ h^2)$, $h = x - \tau_i$, where τ_i is the x value of the lower knot of the ith subinterval) for each of the four or six subintervals, respectively

3. To allow, by this way, the user to compute the $T - T_{90}$ function only in the temperature subinterval(s) of one's interest.
4. To *not* retain the discontinuity of the first derivative at 273.16 K and to *not* retain the difference $(T - T_{90}) := 0$ at 273.16 K, though the resulting value is <0.0005 K (the spline does not force at any knot the function to any specific value).
5. To also remove the second-order discontinuity at 8.0 K.

The set of coefficients to be used to compute the spline function is reported in Table 1.6: two sets are available, the more complex one better matching the WG4 set of functions.

The cost for these features of the spline function consists in some unavoidable deviations—minor for many users—from the WG4 set of interpolating functions. However, these deviations are all within one standard deviation of the data, as shown in Fig. 1.6a for the range: (1) full range, detailed below 50 K and (2) above 273.16 K, respectively (Fig. 1.6b). In Fig. 1.7 a pictorial view of the temperature ranges covered by the different types of thermometry illustrated in this book is shown.

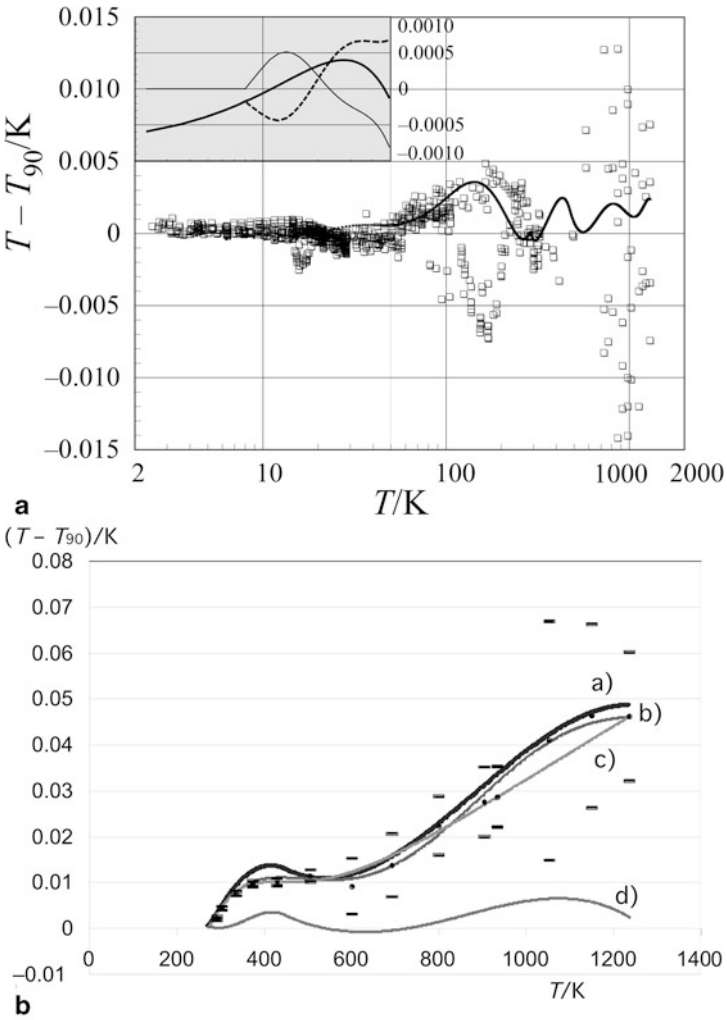

Fig. 1.6 $T - T_{90}$ as computed by different functions: **a** Full range: using the *four* subintervals spline in Table 1.6, with knots at 2.30, 90, 300 (multiplicity 2), 450 (multiplicity 2), and 1238 K. No first-derivative discontinuity at 8.0 K nor at 273.16 K. *Thick line*: difference between the spline function and the functions in Table 1.5 ($\sigma = 0.00091$ K). *Open squares*: residuals of the spline fit, indicating the dispersion of the original experimental data. In the insert: for $T < 50$ K the spline function (*thick line*), the functions in Table 1.5 (*thin line*) and the difference between the two (*broken line*). (From Pavese et al. 2011). **b** Range above 273.16 K: (*A*) using the *six* subintervals spline in Table 1.6, with knots at 2.30, 30, 90, 273.16 (multiplicity 2), 380 (multiplicity 2), 800 and 1238 K (Pavese et al. 2011); (*B*) polynomial (CCT WG4 2008); (*C*) polynomial (Fischer et al. 2011); (*D*) difference (*A*) − (*C*). The short segments are the uncertainty limits of the standard uncertainty of each of the 42 local averages (u in Table 1.4) shown as *thick dots*. (From Pavese 2011a)

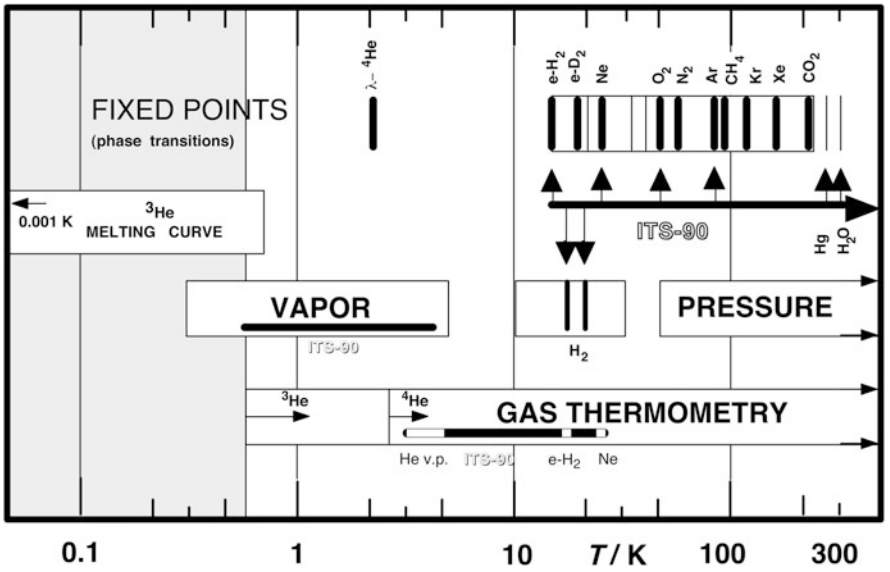

Fig. 1.7 Typical range of gas-based thermometry types

Summary 1.7 Summary of a Temperature Scale Definition

Scale type		Thermometer fabrication[b]	Mathematical definition (model)[c]	Fixed points (reference temperatures)	Example[d]
Thermodynamic	Systematic effects[a]	According to the "state-of-the-art"[e]	Measured property: $P = f(T)$ exact physical law or with calculable corrections	None or triple point of water (sets the size of the kelvin)	CVGT, DCGT, RIGT, AGT
Semithermo-dynamic		Same as thermodynamic	Physical law with empirical corrections: all numerical values of the empirical parameters are specified	None	Vapor pressure (ITS-90) CVGT virials (ITS-90)
Semiempiric		Interpolating instrument: specified range of fabrication (technical) parameters	Same as above, but the numerical values of the free empirical parameters are set by calibration at the fixed points	Two or more reference temperatures, according to the number of free empirical parameters	ICVGT, (ITS-90), $\chi(T)$
Empiric applicable to a class of devices	Nonuniqueness	Interpolating instrument: specified range of fabrication (technical) parameters	Empirical model, with the numerical values of the free parameters set by calibration at the fixed points	Two or more reference temperatures, according to the number of free parameters	SPRT, IPRT, TC
Empiric applicable to each device		Larger tolerances admitted for fabrication parameters	Calibration by comparison with a standard thermometer for a large number of temperatures; data fitted to an empirical model	Various temperatures, whose numerical value is generally set by a standard thermometer	Semiconductor-type thermometers

[a] Main effect, which limits the accuracy of the scale definition. Systematic deviations of the model from actual physical laws are prevailing in the (semi-) thermodynamic scales, nonuniqueness effects in the (semi-)empirical scales

[b] Thermometric substance (gas, metal or alloy wire or film, salt, . . .) must be specified, for example: purity, composition, chemicophysical conditions

[c] The temperature range of the scale is limited by the applicability of the model within a stated accuracy

[d] See list of acronyms

[e] "State-of-the-art" are techniques available to-date that, within a stated accuracy, ensure thermal equilibrium of the thermometer with the body whose temperature is to be measured, and limit the deviations from the defining function $f(T)$ here

Chapter 2
Gas-Based Reference Points for Thermometry

For more than half a century after the fabrication of the first real thermometers, the only way to compare the values obtained from measurements made with two different thermometers was to place both instruments in the same "thermal bath", e.g., air or water (chilled with ice or heated), and compare their readings. The idea that a certain physical state reproduces a unique temperature value, and consequently can be used to calibrate *subsequently* (or in different locations) different thermometers, was in fact not clearly understood until the second half of the seventeenth century, when experimental evidence arose from the readings of the thermometers, and freezing ice was first used for this purpose (Hooke 1664; Renaldini 1694). A kind of ice point is reported to be in use for a similar application in ancient China about 2000 years ago (Chen Xi-guong 1986). The concept of fixed temperature can also be found in the work of Aristotle (circa A.D. 380), and, following his writings, Galen, the famous Greek physician (A.D. 130–200), introduced a "neutral degree of heat" obtained by mixing equal quantities of ice (his maximum degree of cold) and boiling water (his maximum degree of heat). However, the "neutral" degree so obtained was said to be halfway between these extremes, since at that time heat and cold both were considered substances. We know today that such a mixture has actually a temperature of only about 10 °C because of ice enthalpy of fusion and of the variable specific heat of water in that range. These concepts only became clear in the nineteenth century.

Today, reference points are commonly used, though generally speaking, they are not given sufficient attention outside specialized laboratories.

First of all, let the term "reference point" be given a meaning more restrictive than is usually associated to it:

> *Definition* A thermometric reference point is an equilibrium state of a specified substance, the realization of which does not depend on the measurement of any other quantity but temperature, except substance purity or composition—e.g. isotopic.

Accordingly, as will be discussed in Sect. 2.1.3, the very common "boiling points" cannot be termed reference points, as their temperature is defined only through a temperature-pressure relationship, so that *pressure* must be measured too.

From Gibbs' rule, it follows that, for a pure substance, this definition applies only to "triple points". In fact, the general definition of the triple point is applicable to

F. Pavese, G. Molinar Min Beciet, *Modern Gas-Based Temperature and Pressure Measurements,* International Cryogenics Monograph Series,
DOI 10.1007/978-1-4419-8282-7_2, © Springer Science+Business Media New York 2013

any thermodynamic state in which three phases are coexisting. From Gibbs' rule

$$F = c - \phi + 2 \tag{2.1}$$

where F are the degrees of freedom, c the number of chemical substances, and ϕ the number of phases involved. This implies that both temperature and pressure values at a triple point are unique.

Reference points are of great importance in thermometry, not only because they allow empirical scales (where they become "fixed points": see Sect. 1.2.2) to be defined, but because each of them provides a reference temperature available, at which the *stability* of the calibration[1] of a thermometer of any type can be checked in any laboratory without resorting to the help of another.

The three coexisting phases can be combined in different ways, the most common combinations being:

a. solid—liquid—vapor
b. solid—liquid I—liquid II
c. solid I—solid II—liquid
d. solid I—solid II—vapor
e. liquid I—liquid II—vapor

Not all of them are equally suitable as fixed points for thermometry. When no vapor phase is in equilibrium (combinations type (b) and (c)), the points are characterized by a high equilibrium pressure and may be better considered as *pressure* fixed points (see Part II, Chap. 9). Types (d) and (e) are not generally referred to as triple points, but respectively as solid-to-solid and liquid-to-liquid transitions; they will be considered in Sect. 2.5. In the following sections, only type (a) will be considered, which is *the* triple point of a gas.

2.1 Thermodynamic States Versus Standard Reference Materials

2.1.1 Substances Versus Standard Reference Materials

A reference temperature is obtained by defining the values of as many additional parameters as are necessary to uniquely determine a single temperature-dependent state of a substance.

This definition can be specified by simple reference to the *ideal* substance or, instead, by specifying a sufficient number of its relevant physical properties, whose values must be checked empirically. The difference between the two alternative

[1] This means determining the stability in time of the value $y(T_r)$ of its thermometric parameter (e.g., for resistance thermometers, $y = R$).

definitions is equivalent to that existing between a thermodynamic and an empirical temperature scale.

In the first case, the substance is defined only by means of its basic physical parameters so that anyone can reproduce the thermodynamic state in an independent way. Such parameters need to be listed and *defined*, specifying also the uncertainty of the temperature value. These parameters can be the maximum level of impurities (or of a single impurity), the physical state (annealed,. . .), the composition (including the isotopic one, when relevant) and its tolerance in the case of mixtures. It is to be noted that substance with different isotopic composition are generally to be considered as *different* substances. Impurities, either chemical or isotopic, should be considered as such only when one aims at using pure substances.

Each experiment aiming at reproducing the real thermodynamic state and complying with the above specifications is expected to reproduce the same temperature value within a given uncertainty. Each of such experiments is independent of the others and no specific procedures need be defined. In this respect, the exercises usually performed by major laboratories, especially metrological, such as round-robin tests or intercomparisons of results, are normally to be considered as checks of their ability to perform the experiment correctly, not as checks of the quality of the substance employed. They are neither aimed at "calibrating" the fixed points.

In the second case, on the contrary, a certain amount of a substance is prepared to have uniform characteristics though the substance batch and to be stable in time, and is made available by an organization. The physical-chemical characteristics of the substance, and its temperature value—besides its reproducibility between samples—are determined by measuring samples taken from the batch and are assigned to the whole batch of material considered. Subsequently, samples of that batch are made available to other laboratories together with a certificate of compliance with the characteristics of the batch. The materials used for this purpose are called "reference materials" (RM), and the word "standard" (SRM) is added when an official body certifies them. In principle, they need not comply with any of the specifications that an "absolute" reference point has to. The batch of material needs only to be uniform enough to allow the desired reproducibility of certain property characteristics to be obtained between samples and stable in time, in order to achieve the required accuracy of the temperature value. The exact meaning of these requirements is better specified in Sect. 2.7. The users of these materials must rely on the certificate issued by the supplier, and so is, consequently, the temperature scale based on these reference materials.

Sometimes, when it is not even possible to establish a certified value of the property for a whole batch of a material, each sample is certified individually. An example is provided by the realization of the fixed points based on superconducting transitions. The transition temperature value cannot be guaranteed to represent *the* value of a *physical* state; is therefore usually certified as the transition value realized by the individual device and is said to be a "device temperature" value. The same consideration applies—as will be fully discussed in Sect. 2.3—to some triple-point devices, e.g., to a sealed cell realizing the triple point of e-D_2, when commercial-grade gas is used. In this case, the temperature value can be assigned only by calibrating each

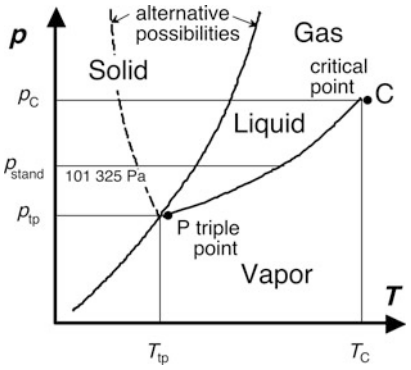

Fig. 2.1 Pressure versus temperature representation of equilibrium thermodynamic states for a constant amount of substance

individual cell as HD contamination of unpredictable amount may occur during cell preparation. In both examples, such a type of SRM relies only on the *stability* in time (and homogeneity of the batch, if a mixture) of the property certified.

In the cryogenic region, the reference points mainly belong to the two groups of those based on a phase transition of gases and those based on superconducting transitions. In this book, only the first group will be treated. In it several reference temperatures are available above 13.8 K (and one near 2.2 K). As already pointed out, vapor pressures are not considered here as serving as set of reference points, but are treated in Chap. 4 as a type of thermometry. Superconducting transitions are useful for reference point realizations below 9 K, as, so far, no attempt has been made to use the high-T_c superconducting materials for this purpose (but the interested reader can look at Pavese and Peroni 2000a; Camacho 2002). The reader is also directed to the relevant literature (e.g., Bedford et al. 1990; Pavese 1979a; Hill and Rudtsch 2005).

2.1.2 Thermodynamic States and Phase Diagrams

In this section, a representation that will be used throughout this text, the so-called phase diagram is briefly described. For complete information, the reader is directed to the "Further reading" Section at the beginning of the References for textbooks on thermodynamics. The thermodynamics involved in this book is strictly equilibrium. No irreversible phenomena are assumed to take place when a substance is being used for accurate temperature measurements.

This assumption allows us to apply, without imposing other conditions, the laws of equilibrium thermodynamics and use their graphical representations, the phase diagrams, which describe connected sets of equilibrium states. The most straightforward representations are that of the p–T and V–T planes. Figure 2.1 shows the main features of the p–T plane. With most substances, the three boundary lines for the existence of a single phase (the two-phase equilibrium lines) join at a single point P, called the triple point. The boundary lines of the gaseous phase are called

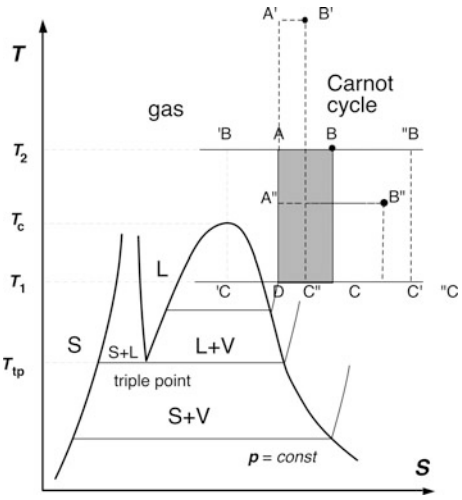

Fig. 2.2 Temperature versus entropy representation of equilibrium thermodynamic states for a constant amount of substance. Carnot cycles (ABCD) are also shown. (see text)

vapor-pressure lines (in sublimation from the solid or vaporization from the liquid, respectively), since a gas is called vapor below the critical point isobar (Fig. 2.1).

These representations do not, however, bring into evidence the internal energy changes associated with most phase transitions. This is an important point in most technical applications and is useful as well for the discussion of the gas-based types of thermometry, since most of them are based on phase transitions.

Instead, a temperature-entropy (*T*–*S*) representation (in Fig. 2.2, for a typical simple substance) is more useful. In this representation, the states of co-existence of two phases are clearly visible, as there are no longer lines, but regions of the *T*–*S* plane, and the triple point is no longer a *point*, but a *line*.

As a rule, the area circumscribed by the cycle line represents the net work performed by any thermodynamic cycle. Since the adiabats are vertical lines, the Carnot cycle has, in this representation, a simple rectangular shape.

A remarkable property of this cycle, inherent in Eq. 1.5, is clearly shown in Fig. 2.2. The ratio of the amounts of heat exchanged with the reservoirs at the two temperatures is *independent* of the work done, i.e. of the distance of the two adiabats.[2] The relationship between heat and work expressed by Eq. 1.6 also becomes evident. For a given area of a Carnot cycle, work *W* is constant. With point D remaining constant, each point of the *T*–*S* plane can be considered as the opposite corner B of a Carnot cycle. The $W = const$ line described by it (B′BB″) is a hyperbola having origin D. In particular, when D = O the hyperbolas represent also the iso-enthalpic lines of a gas in the ideal state.

Another significant property illustrated in the *T*–*S* diagram is the coincidence of the isobars with the isotherms during a phase transition.

[2] In Fig. 2.2 the Carnot cycles are completely included in a *T*–*S* region where no phase transitions occur, as required by Bazarov and Truesdell (see Chap. 1.1).

2.1.3 Reference Points: Triple, Boiling, and Critical Points

It is now evident that the so-called "boiling points" are nothing but points of the saturated vapor pressure line (the "normal boiling point" being the one at a pressure of 101 325 Pa). Their being considered as reference points (and as fixed points of temperature scales) has its historical origin in freely boiling liquids, mainly oxygen, nitrogen, hydrogen, and helium, in storage dewars or open cryostats at atmospheric pressure. As the value of atmospheric pressure is not constant at 101 325 Pa in every location on the Earth and for all times, it has to be corrected to a standard value. Today international codes still require that some engineering tests of temperature-dependent properties should be performed by direct immersion of the device in boiling liquids, and that the temperature value of the boiling refrigerant should be obtained from measurement of atmospheric pressure or of the storage dewar pressure, if the latter is different (generally lower, as it is obtained by pumping on the refrigerant bath, but sometimes higher; see a case discussed in Sect. 2.4.3, and Chap. 6).

Discussion of "boiling points" will be extensively done in Chap. 4 on vapor pressure thermometry, as their realization requires a thermometer of this type.

The triple point and the critical point are also points of the vapor pressure line, and solid-to-solid transitions are part of a pressure dependent line. However, they are states on these lines, which are uniquely defined without having to measure pressure.

Critical points are difficult to realize to a satisfactory level of accuracy, not only because of problems common to all transitions not involving enthalpy changes, but also owing to the usually high critical pressure, a characteristic that makes them, possibly, more suitable for consideration as *pressure* fixed points.

2.2 Physical Chemistry Associated with Gas Triple Points

The triple point is the transition between the liquid and the solid phases in equilibrium with the vapor phase (the subject was introduced in Sect. 2.1 (Fig. 2.1)). It represents the joining at a point of the three two-phase equilibrium lines: solid-liquid, solid-vapor and liquid-vapor (the two last lines being called *vapor-pressure* lines). With all gases having simple molecules, the three transition lines are concurrent at a single point P (Fig. 2.1), with the exception of helium isotopes (see ^{4}He in Fig. 2.3—and ^{3}He in Fig. 5.1, Keller 1969). The effect of isotopic composition is not considered in the rest of the Chapter, except in Sect. 2.2.2.5.

2.2.1 Triple Point of a Pure Substance

As mentioned in Sect. 2.1, for discussion of the phase transitions the representation in the *T*–*S* plane is preferred, in order to make it evident that an enthalpy change takes place at the triple point. This representation illustrates as well in detail the

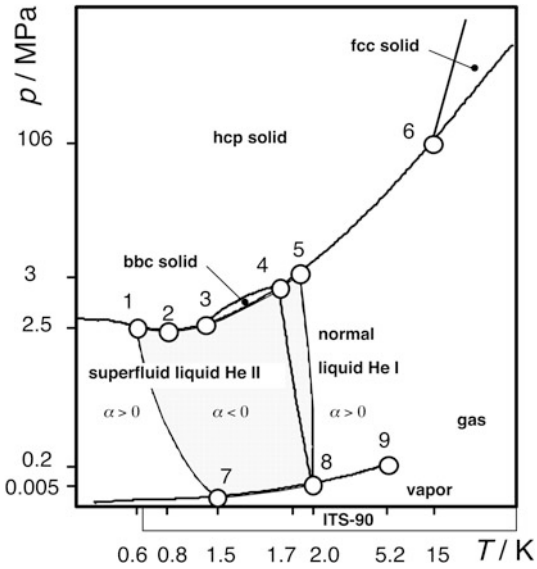

Fig. 2.3 Pressure versus temperature representation of equilibrium thermodynamic states for a constant amount of ^{4}He. (After Keller 1969; BIPM 1990b). *Not to scale*. Key features of the melting line: *1* lower point with thermal expansion coefficient $\alpha = 0$: $T = 0.59$ K, $p = 2.53$ MPa; *2* pressure minimum: $T = 0.775$ K, $p = 2.529$ MPa; *3* lower limit for bcc solid: $T = 1.463$ K, $p = 2.627$ MPa; *4* upper limit for bcc solid and λ-line: $T = 1.771$ K, $p = 3.006$ MPa; *5* upper point with $\alpha = 0$: $T = 1.80$ K, $p = 3.13$ MPa; *6* lower limit for fcc solid: $T = 14.9$ K, $p = 106$ MPa. Key features of the vapor pressure line: *7* lower point with thermal expansion coefficient $\alpha = 0$: $T = 1.14$ K, $p = 71$ Pa; *8* upper point with $\alpha = 0$ and lower end of the λ-line: $T = 2.1768$ K, $p = 5.042$ kPa; *9* critical point: $T = 5.1953$ K, $p = 227.46$ kPa

condensation, and the subsequent solidification process, taking place in a sample of gas being cooled in a container. Figure 2.4b shows such a container in its general form, consisting essentially of two connected volumes, a reservoir R having volume V_1 kept at room temperature T_r and a container C having volume V_2 cooled to lower temperatures. The connecting tube has a volume that can be neglected. The cooldown of the gas in C can follow quite different patterns, as is shown in Fig. 2.4a, depending on the ratio V_1/V_2. When one starts from point O with both containers at room temperature and pressure (T_r, p_r) (with the constraints $p_r \gg p_{tp}$ but $< p_c$, where p_{tp} is the pressure value at the triple point and p_c is that at the critical point) and with a total mass of gas $m_0 = m_1 + m_2$, there are two limiting situations depending on the volume of container R.

Case A, Infinite volume V_1 When cooling container C, pressure remains constant at the value p_r, as more gas simply moves to V_2. The gas follows the isobar p_r from the initial point O, but the mass of the sample in container C varies from $m_2 = \rho_r V_2$ to $m_2' = \rho_2 V_2$, where ρ_r and ρ_1 denote, respectively, the gas density at room and at low temperature (point F in Fig. 2.4a).

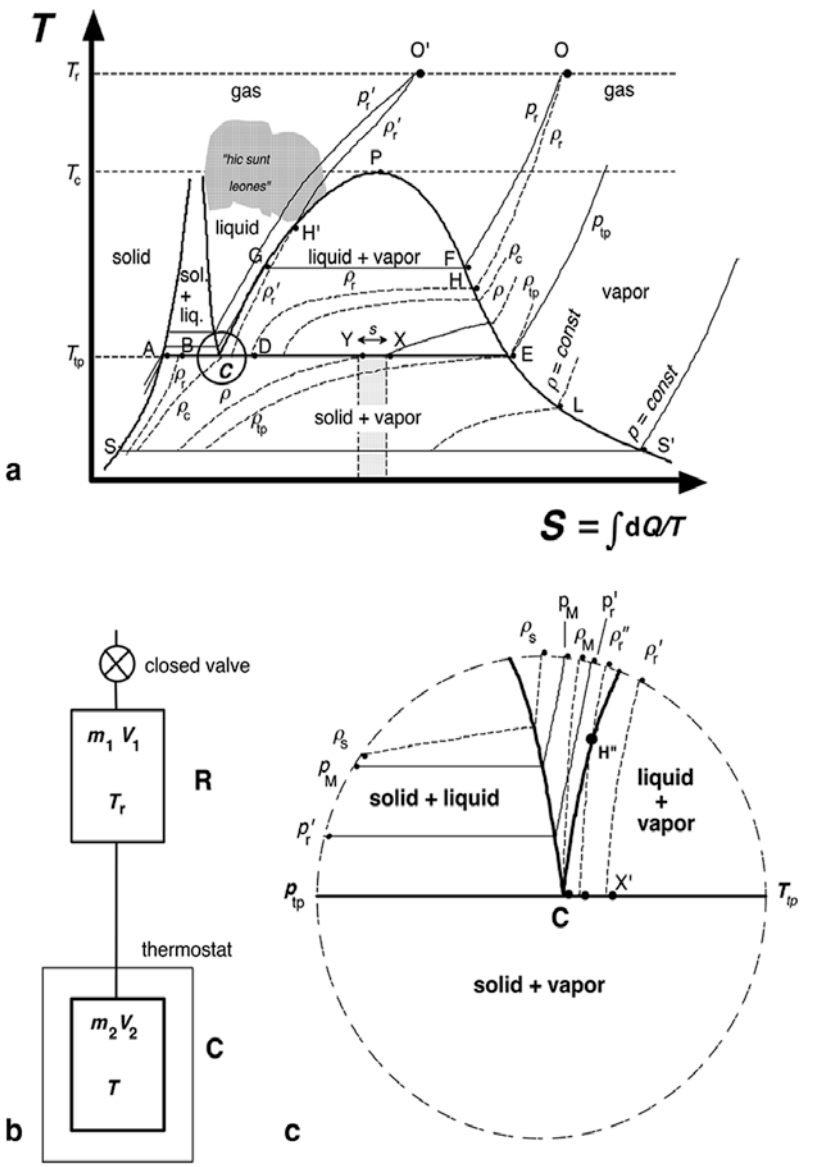

Fig. 2.4 Cooling a sample of gas. **a** General view in the *T*–*S* plane. **b** Layout of the gas container. **c** Enlarged view of the states around the minimum of coexistence *C* of the liquid state (*circled* in **a**)

In this respect, the use of this representation is not strictly correct, as it applies only to transformations involving a *constant amount of substance*. In Case A, the enthalpy changes involved in cooldown are increasingly larger as an increasing amount of gas moves to V_2. Nevertheless, the significant features of cooldown remain the same, as represented in the figure.

Upon further cooling, the sample contained in C crosses the dew-point line at the pressure p_r in F, where a liquid phase begins to condense. The liquid saturates at constant pressure in G (with a mass $m_2'' = \rho_G V_2$); subsequently the temperature decreases again following the liquid saturation line G–C until the first particle of solid phase forms in C. Then, the fraction of solid increases isothermally until the liquid phase is no longer present at A. Finally, the temperature decreases again, following the saturation line of the solid in equilibrium with the vapor, down to the minimum temperature, that of the refrigerant in point S.

Case B, Zero volume V_1 In this case all the gas is contained in C, of volume $V_2 = const.$ Consequently, $m_0 = m_2$ and the density $\rho_r = m_0/V_2$ remains constant. Starting again from the same initial room-temperature point O, the cooldown process now follows the isochoric line ρ_r. This line has a *steeper* slope than the isobar p_r. As the cooling pressure obviously decreases, the *dew point* H is lower than F on the dew point line. Pressure and temperature continues to decrease during liquefaction of the sample and the value p_{tp}, and T_{tp}, is reached at a point D of the triple point line, *without* reaching the line G–C of the saturated liquid. It must be noticed that phase separation occurs in the two-phase region; therefore, density remains constant in that the *total* sample mass m_2 is constant since *total* volume V_2 is, but at each temperature the densities of the liquid and of the vapor phases differ according to their values at the corresponding saturation lines. The sample is fully isothermally solidified at a point B $\neq$ A, then temperature begins to drop again following the lower branch of the same line $\rho_r = const.$ Let us generally denote with a point X on the diagram the liquidus point and with point Y the solidus point of the triple point plateau. The triple point always begins with a value $S(X) > S(C)$. The length $s(X–Y)$ on the isotherm T_{tp} followed during liquid-solid(-vapor) equilibrium depends on the initial density ρ_r. Considering first the case when $\rho_r \leq \rho_{tp}$, it is obvious that no triple-point plateau can be observed, since no liquid condensation can occur. The solid phase begins to form directly from the vapor at the frost point L. This process is valid up to $\rho_r = \rho_{v,tp}$, where L $\neq$ E and $s(X–Y) = 0$. For ρ_r slightly higher than $\rho_{v,tp}$, a small quantity of liquid condenses at a point of the dew line E–F. This small quantity of liquid begins to solidify at X and is wholly solidified at Y. The enthalpy of solidification—corresponding to the dashed area in the diagram—is also small, since most of the sample mass remains in the vapor phase. Point Y lies on the *right* of C. At a certain value $\rho_r = \rho_c$, Y $\equiv$ C, then, with higher densities, which are the most commonly used for fixed points realizations, Y is located on segment A–C, whereas X still lies on segment C–E.

The question arises whether the process now described always occurs. Let us consider this point in detail, since the region of the phase diagram characterized by densities higher than the critical pressure and by low temperatures, close to the triple point, is not often a matter of discussion in the literature. Figure 2.4c shows an enlarged portion of this region in Fig. 2.4a near point C. For these high densities no such a point H exists on the dew point line P–E (Fig. 2.4a), but the high-density isochore ρ_r' from a room temperature point O′ crosses the *liquid* saturation line on the *left* of the critical point P, say at point H′. Then, the isochore penetrates the

unsaturated liquid region (which the isobar p'_r does not): the vapor fraction *increases* until the triple point is reached, with X still on the right of C. Obviously, Y is nearly coincident with A. Notice that, on the contrary, the value of the corresponding isobar p'_r is higher than p_{tp}—that is it does not cross the triple point line—and totally runs in the upper region, that of the (solid + liquid) equilibrium. With even higher values of density ρ'_r, the point H′ shifts to lower temperatures, say H′ in Fig. 2.4c, until a limit situation is reached with ρ_M, where H′ ≡ C. With ρ_r values greater than this, such as ρ_S, the condensation line no longer reaches the triple point line.

Therefore, *the triple point can be obtained by simple refrigeration of a closed container only in the density interval* $\rho_M > \rho_r > \rho_{v,tp}$.

Finally, it is interesting to note that in the region on the left of the critical point, the cooldown process may lead to solidification (at pressures higher than that of the triple point) *by condensation*. In fact, this region of single-phase equilibrium is commonly labeled "gas" at high temperatures and "liquid" in the narrow region above point C, without any phase transition line being crossed!For finite values of the volume V_1 of R, an intermediate line between the isobaric p_r and the isochore ρ_r is followed during refrigeration.

Except in Case B, the variability of the sample mass in C, where the temperature T is measured, prevents a correct use of all the properties of the diagram of Fig. 2.4. For example, one cannot directly obtain the enthalpy of fusion of the sample.

The foregoing considerations are necessary to fully understand the different ways to perform a triple point experiment, which will be described fully in Sect. 2.3.

It must be stressed again that, when starting with a gas in a container with an initial density $\rho_M > \rho_r > \rho_{v,tp}$ (see also Table 2.1) the triple point state will *always* be crossed by simple refrigeration of the sample below T_{tp}. However, not all the density values in this range are equally suitable for an accurate realization of a temperature fixed point, particularly the low values because the resultant available enthalpy of fusion is too small.

2.2.2 Triple Point of an Impure Substance. Cryoscopy

The phase diagram illustrated in the former section requires the substance to be ideally pure. Only in this case do all the properties illustrated in that section apply, such as the isobaric condensation being isothermal.

Real experiments, however, can in fact only be carried out with impure substances—that is with dilute mixtures. The need for high gas purity is treated in detail in Sect. 2.3.

In Sect. 2.2.1 a freezing experiment of an ideally pure gas has been described with the use of phase diagrams. Now we will discuss the same experiment and the inverse melting process using a real gas, displayed as a temperature-versus-time plot in Fig. 2.5a, b, such as it would be displayed by a (chart) recorder.

Table 2.1 Significant parameters for substances

Substance[a]	T_{tp} K	$\Delta_{fus}H_m$ (J mol^{-1})	$\Delta_{vap}H_{m,tp}$ (kJ mol^{-1})	$c_{p,Cu}$ (J K^{-1} g^{-1})	Λ (W K^{-1} m^{-1})	ρ_{tp}/ρ_{NTP}[b]	p_{msc} (bar)[c]	p_M (bar)[d]
Hydrogen[e]	*13.8033*	117	0.91	0.0022	0.12	1040	35	96
Deuterium[e]	18.689	199	1.27	0.005	0.13	1040	39	97
Neon	*24.5561*	335	1.80	0.014	0.13	1730	50	140
Oxygen	*54.3584*	444	7.76	0.117	0.15	980	30	90
Nitrogen	63.151	724	6.03	0.147	0.14	815	25	75
Argon	*83.8058*	1190	6.56	0.213	0.12	980	30	90
Propane	85.528	3525	24.92	0.216		310	11	32
Methane	90.6935	938	8.73	0.225	0.19	680	22	68
Ethane	90.360	582	17.88	0.225		480	16	48
Krypton	115.776	1640	9.13	0.280	0.09	910	24	75
Xenon	161.406	2315	12.75	0.330	0.07	650	19	60
Carbon dioxide	216.591	8650	13.55	0.360	0.13	820	24	76
Mercury	*234.3156*	2295	63.60[f]	0.365	8.39[g]			
Water	*273.16*	6010			5.6			

T_{tp} triple point temperature. In italics the exact definition values of the ITS-90, $\Delta_{fus}H_m$ molar enthalpy of fusion, $\Delta_{vap}H_{m,tp}$ molar enthalpy of vaporization at T_{tp}, $c_{p,Cu}$ specific heat capacity of copper at T_{tp}, λ thermal conductivity of the liquid near the normal boiling point

[a]All substances of natural isotopic composition. Revised values with respect to Bedford et al. (1990) and BIPM (1990b). Mercury and water are reported being necessary to ITS-90 definition below 273.16 K

[b]Density ratio between the liquid (in cm^3) at T_{tp} and the gas (in L at 20 °C)

[c]Minimum pressure at 0 °C for a supercritical isochore (as ρ'_r in Fig. 2.4a), $p_{nsc}\ \mu\ \rho_c/\rho_{0°C}$

[d]Room temperature pressure for the supercritical isochore passing from C (ρ_M in Fig. 2.4c), $p_M \propto \rho_{tp}/\rho_{0°C}$

[e]In spin equilibrium

[f]Molar enthalpy of sublimation

[g]At 25 °C

A constant freezing, or heating, rate (i.e., constant heat exchange) being assumed and the heat capacity of the gas in the experimental temperature interval being considered nearly constant, an ideal pure substance would give rise to record I in the figure in both experiments. An experiment carried out with a real-gas sample of fairly high purity will give rise to record II in freezing or in melting, even in the absence of thermal errors due to experimental artifacts, i.e. for freezing or melting occurring at a sufficiently low rate (see Sect. 2.3.1.1).

a. *Freezing plateau*. The fact that temperature drops below T_{tp} before suddenly recovering is due to a *metastable* state of the liquid phase called subcooling, which may amount to less than 0.1 K or to several kelvin, depending on the substance and on its purity. Then, temperature recovers sharply, when the release of the solidification heat begins at nucleation (or at surface melting (Frenken and van der Veen 1990), and reaches a maximum value. During the subsequent freezing "plateau", temperature does not remain perfectly constant, but tends gradually to decrease, to a greater or smaller extent, depending on the purity of the substance

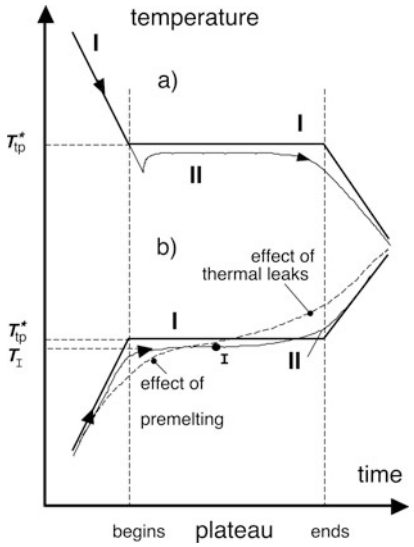

Fig. 2.5 Ideal freezing *a* and melting *b* plateaus for a pure and impure gas in temperature versus time representation. *I* inflection point at T_λ; T^*_{tp} triple point of the pure substance

and on the freezing rate, until it drops again abruptly when the whole sample is solidified. The shape of the plateau becomes rounded with respect to that of a pure substance, and the solidification process is not exactly isothermal.

b. *Melting plateau*. No overheating of the solid phase can generally take place before melting.[3] The beginning of the melting "plateau" may show a substantial rounding off (broken line) starting from as low as a few kelvin (generally much fewer with pure substances) below the T_{tp}. This phenomenon is called "pre-melting effect" and is due to an anomalous behavior of the specific heat of the solid phase, which is not associated with chemical impurities but with the behavior of the molecules in the lattice of that specific substance. With substances not showing this anomaly (solid line), the melting plateau shows anyway a rounded beginning of the plateau similar to that observed for the freezing (after the recovery from subcooling). This rounding can be so small that temperature at 0.05 % of melted fraction is already close within − 1 mK to T_{tp}. Thermal problems (see Sect. 2.3.3), on the other hand, may cause again an upward rounding effect at high liquid fractions, as shown by the broken line in the second half of the plateau, which can be very large (see Sect. 2.3.1.1). Anyway, the melting plateau is not isothermal even in between the foregoing two effects, because of the impurities.

Except when specified mixtures are used or with SRMs, a reference point is specified on the simple assumption of a substance perfectly chemically pure. On the contrary, for substances like hydrogen, neon, krypton, and xenon, the isotopic composition must be specified as well, being critical. Eutectic mixtures have never been exploited with gases in the cryogenic region. Therefore, in determining the temperature value

[3] But it might when heating through a solid-to-solid transition.

of the triple point of a pure substance (T^*_{tp}) the effect of chemical impurities must be taken into account and, if necessary, the measured value be corrected, which usually is not an easy task (see Sect. 2.2.2.3).

What value is to be selected for a correct definition of the triple point temperature is a problem not uniquely defined, since a real melting (Fig. 2.5) does not occur isothermally, and the behavior can be different with differing impurities. The cases relevant to the realization of triple points will be extensively reviewed in the following section by considering only the mixture behavior for small impurity concentrations (dilute mixtures). Further reading should be directed to analytical or physical chemistry textbooks—e.g. Doucet (1975). As regards to the realization of a temperature fixed point, the problem of a unique definition of its value will be treated in Sect. 2.3.

2.2.2.1 Solutions of Solid-Insoluble Impurities (Treatment with the van Laar Equation)

Impurity effects are one of the most significant sources of uncertainty in fixed-point realizations. Recent improvements in the accuracy and limits of detection in the chemical analysis of impurities in fixed-point substances have made it feasible to model and correct for some impurities. This has had a considerable impact on both the realization technique and uncertainty analysis.

When different elements are mixed, they may combine chemically in varying degrees to form a wide range of mixtures, from simple solutions to multiphase systems involving many distinguishable compounds.

However, if the fixed-point substance is sufficiently pure, the formation of additional phases is unlikely, and hence impurities in fixed points can usually be treated as independent components of a simple solution, and this is the basis of suitable models.

Before discussing the assessment of uncertainties due to impurities, we provide some background description of impurity effects.

Cryoscopy, i.e. the study of the depression of the triple point temperature during melting for an ideal, non-ionic solution, and for low concentrations of the solute is based on the van Laar equation

$$\ln(1 - x_i) = \left(\Delta_{\mathrm{fus}} H_{\mathrm{m}} / R T_{\mathrm{tp}}^2\right) \int_{T_{\mathrm{tp}}}^{T^*_{\mathrm{tp}}} \left(\Delta_{\mathrm{fus}} H_{\mathrm{m}} / R T_{\mathrm{tp}}^2\right) dT \tag{2.2}$$

The x_i is the amount of solute fractions, $\Delta_{\mathrm{fus}} H_{\mathrm{m}}$ is the molar enthalpy of fusion of the solvent, and R is the gas constant. A temperature depression $\Delta T_{\mathrm{tp}} = (T_{\mathrm{tp}} - T^*_{\mathrm{tp}})$ is defined from the difference between the T_{tp} value of the pure solvent and the value T^*_{tp} of the actual solution. On the assumption that the change in specific heat capacities Δc_p between the pure solvent and the solution does not depend on T in

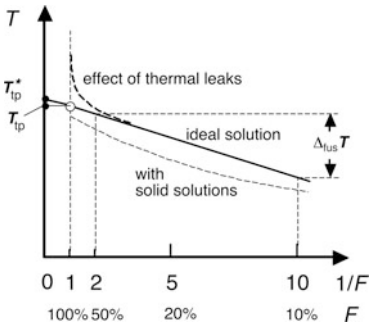

Fig. 2.6 Temperature versus $1/F$ representation of melting (F melted fraction). $\Delta_{fus}T$ definition of the "melting range"; T^*_{tp} triple point of the pure substance; T_{tp} triple point of the impure sample. (See Sect. 2.2.2.2 for the solid solutions case)

the range ΔT_{tp}, Eq. 2.2 can be integrated as follows

$$\ln(1-x_i) = (\Delta_{fus}H_m/R)\cdot\left(1/T^*_{tp} - 1/T\right) + \left(\Delta c_p/R\right)\left(T^*_{tp}/T - 1 - \ln\left(T^*_{tp}/T\right)\right) \tag{2.3}$$

The second term can often be neglected. Then, with $K = R/\Delta_{fus}H_m$,

$$T_{tp} = T^*_{tp}/(1 - KT^*_{tp}\ln(1-x_i)). \tag{2.4}$$

Considering now only binary *dilute* ($x_i \ll 1$, $\Delta T^*_{tp} \ll T^*_{tp}$) solutions, Eq. 2.4 can be written

$$\Delta T_{tp} = T_{tp} - T^*_{tp} \approx -KT^{*2}_{tp}x_i \approx -KT^2_{tp}\,x_i \tag{2.5}$$

and considering the solution *ideal* (i.e. following Raoult's law, where the molar concentration of impurities $x_{i,l}$ in the liquid fraction F, which occurs at a $T < T_{tp}$, is $x_{i,l} = x_i\,(1/F)$), one has, for a melting temperature T at the liquid fraction F,

$$\Delta T = T - T_{tp} = \frac{-x_i}{(AF)} \tag{2.6}$$

with $1/(KT^2_{tp}) = A$ being called the first cryoscopic constant (some authors use a definition corresponding to $1/A$).

Equation 2.5 indicates that temperature depression for low concentrations is proportional to the fraction of impurities. Equation 2.6 shows that the depression is proportional to the inverse of the melted fraction. Therefore, the representation of the melting plateau of the impure gas as T versus $1/F$ of Fig. 2.5 yields a straight line in Fig. 2.6. In this representation, the solidus point (which corresponds to the first melted particle of the sample, i.e. to $F \equiv 0$) must not be considered corresponding to $\Delta T \to -\infty$, since, at very low melted fractions, one can neither actually consider the impurity concentration as uniform nor, consequently, the assumptions of Eq. 2.6 to be valid. For this reason, the values of $1/F$ larger than 10 are rarely taken into account. The liquidus point (which corresponds to the last particle of the sample melted) corresponds to $1/F = 1$, which is the triple point temperature T_{tp} value of

the impure sample. Although values $1/F < 1$ do not correspond to physical states, the extrapolation to $1/F = 0$ gives the temperature value T^*_{tp} for the *pure* substance (cfr Eq. 2.5). Therefore, the difference $\Delta T_{tp} = (T_{tp} - T^*_{tp})$ is the so-called cryoscopic depression, or, from the standpoint of the determination of a temperature fixed point, the impurity error.

Incidentally, the inflection point I in Fig. 2.5b, i.e. the flattest portion of the melting plateau in a T versus time representation, has no physical meaning and the use of its value T_I as T_{tp}, often reported to, would lead to a wrong evaluation of the triple point temperature. These considerations are important in the discussion that follows in Sect. 2.3 about the use of a triple point as a reference point .

A "melting range" $\Delta_{fus}T$ is generally defined to characterize the fusion plateau. It has already been observed that the representation in Fig. 2.6 does not apply to very low liquid fractions (high $1/F$ values). The region of high liquid fractions (low $1/F$ values) may be affected, as will be discussed in Sect. 2.3.3, by experimental artifacts arising from thermal leaks. Therefore, the following definition is used in this text (see next Section as well):

> *Definition* The *melting range* $\Delta_{fus}T$ is the temperature variation occurring, in melting the sample at the triple point, in the range $1/F \approx 2$–10 (≈ 0.1–0.5 liquid fraction) if the melting line is close to a straight line, or in the range $1/F \approx 1.5$–3 (≈ 0.35–0.7 liquid fraction) in the case of upward curvature.

The melting range now defined must not be confused with the *wider* temperature range—discussed in Sect. 2.2.2.2—that is usually spanned with a mixture of any given composition, between the solidus line (generally defined by the first liquid observed in melting) and the liquidus line (generally defined by the first solid observed in freezing, after subcooling).

2.2.2.2 Ideal Solutions of Solid-Insoluble Impurities (Treatment with the van't Hoff Model)

Throughout this section, we refer only to impurity effects. However, the same observations and models apply to isotopic effects. Prince (1966) provides a good tutorial introduction to binary phase equilibria and explains the interpretation of phase diagrams. The derivation of van't Hoff's relation can be found also in Ubbelohde (1965).

Melting and freezing—All chemical reactions and phase transitions involve a balance between the tendency for the system to occupy the lowest energy state, and for the thermal energy in the system to be dispersed as far as possible. The dispersal of thermal energy (i.e., atomic and molecular kinetic energy) is maximized when the system has access to as many microscopic (quantum-mechanical) states as possible. The entropy measures the number of microscopic states. The balance between the two tendencies is described in terms of the thermodynamic potential of the system (Gibbs' free energy). $G = H - TS$, where H is the enthalpy, T is thermodynamic temperature, and S is the entropy. The enthalpy is the total energy of the system, $H = E + pV$, comprising the heat content plus any energy content due to its volume

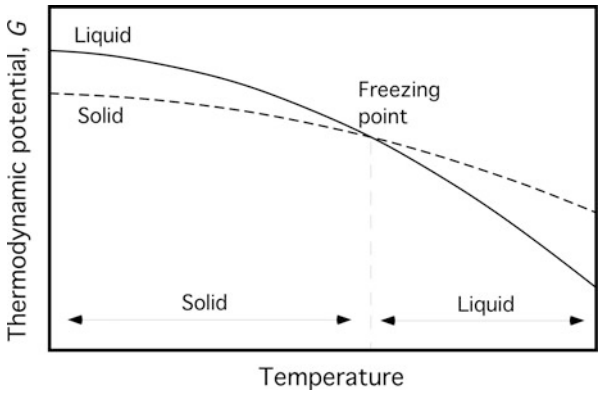

Fig. 2.7 The variation of thermodynamic potential with temperature for the solid and liquid phases

and pressure. Systems tend to reorganize themselves spontaneously to minimize the thermodynamic potential.

In the solid phase, atoms are constrained to move in potential wells (a small volume centered on positions in the crystal lattice) with relatively few microscopic states available. In the liquid phase, atoms are able to move within a large volume with access to a large number and high density of microscopic states. In addition, to move from the solid phase to the liquid phase, the atoms must give up some of their kinetic energy to lift themselves out of the potential wells (the enthalpy of fusion). The liquid phase therefore has both higher entropy and higher enthalpy than the solid phase. Figure 2.7 plots the typical thermodynamic potentials for solid and liquid phases.

Note that the two curves cross so that the minimum thermodynamic potential is achieved with the system in different phases depending on the temperature.

At the freezing point, T_f, the thermodynamic potentials of the solid and liquid phases are equal, that is $H_S - T_f S_S = H_L - T_f H_L$, so that the change in molar enthalpy due to melting $\Delta_{fus} H_m$ in the liquid is exactly offset by an increase in the entropy: $\Delta S_f = \Delta_{fus} H_f / T_f$.

Impurity effects—When two substances are mixed together, the total volume available to both substances is increased, which increases the number of available microscopic states (i.e., the entropy). The presence of impurities in a fixed-point substance therefore alters the entropy of the two phases and the temperature at which the thermodynamic potentials of the solid and liquid phases are the same.

The increase in the entropy due to dilution by an impurity, in either phase, is $\Delta S = -R(x \ln x + x_i \ln x_i)$, where x is the amount fraction of the fixed-point substance, and x_i is the amount of impurity fraction. The first term is the increase in entropy due to the dilution of the fixed-point substance (note $x < 1$, so the entropy is increased), and the second term is due to the dilution of the impurity. In a typical fixed point, the concentration of the impurity is very low and the second term in ΔS can be neglected. This means that the increase in the entropy depends only on the amount fraction of the fixed-point substance. That is, the chemical properties of the impurities have no direct impact on the fixed-point temperature: all that matters is the degree of dilution they cause in the fixed-point substance (Freezing-point depression, boiling-point

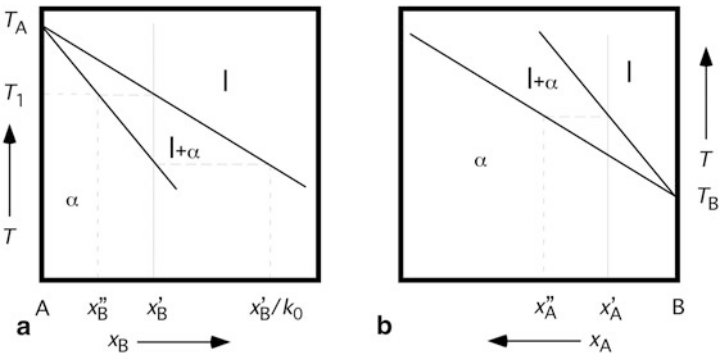

Fig. 2.8 Part of the binary phase diagram concerning substances A and B: in **a** A is the solvent; in **b** B is the solvent. For the meaning of the symbols see text. At temperatures above the liquidus line all the material is liquid, below the solidus line all the material is in the solid phase α, between the two lines solid and liquid phases coexist at equilibrium. (After Prince 1966)

elevation, and osmosis are phenomena that depend only on the number of atoms, and are described as *colligative properties*. Van't Hoff received the Nobel Prize in 1901 for the explanation of the effects). In addition, because x is very close to 1, the expression for the entropy increase can be simplified further, i.e., $R\,x\,\ln x \gg R\ln(1-x) \gg -RX_i$.

The freezing temperature with impurities, T_{tp}, can now be determined by equating the thermodynamic potentials with the increased entropy included for both the solid and liquid phases: $H_{\mathrm{S}} - T_{\mathrm{tp}}\,(S_{\mathrm{S}} + R\,x_{i,\mathrm{S}}) = H_{\mathrm{L}} - T_{\mathrm{tp}}\,(S_{\mathrm{L}} + R\,x_{i,\mathrm{L}})$, and hence, so long as the enthalpy change in fusion is the same in the presence of impurities (which is true for sufficiently low impurity concentrations), and the temperature change is small, then

$$x_{i,\mathrm{S}} - x_{i,\mathrm{L}} = A\left(T^*_{\mathrm{tp}} - T_{\mathrm{tp}}\right), \tag{2.7}$$

where $A = \Delta_{\mathrm{fus}}H_{\mathrm{m}}/RT^2_{\mathrm{m}}$ is the first cryoscopic constant (in the literature, when indicated with E_{f} or K_{f}, is defined as $1/A$). This equation is one of the many variations of van't Hoff's relation. From it, one easily obtains that, for T_{tp} approaching T^*_{tp} (in dilute *ideal* solutions of component i in a solvent having melting temperature T^*_{tp})

$$\left(\mathrm{d}X_{i,\mathrm{S}}/\mathrm{d}T - \mathrm{d}X_{i,\mathrm{L}}/\mathrm{d}T\right)_{T_{f,i}=T_f} = A. \tag{2.8}$$

This equation is important, since it tells that the difference in initial slopes of the solid solidus and liquidus curves, the slopes at $T = T^*_{\mathrm{tp}}$ and $x = 1$, are dependent on the latent heat of fusion of pure solvent $\Delta_{\mathrm{fus}}H_{\mathrm{m}}$ but *independent on the nature of the solute*.

The solidus and liquidus lines in question are those illustrated in Fig. 2.8, which shows a portion of the phase diagram for an *ideal* binary mixture of the same two substances at the melting point, (a) sufficiently close to pure solvent and (b) to pure solute, respectively, so that the curves can be approximated with straight lines.

Table 2.2 Conditions placed on s_S and s_L by specific values of k_0

k_0	Conditions for s_L (Eq. 2.9)	Conditions for s_S (Eq. 2.10)
<0	N.A. ($s_L < -A$, i.e. $s_L > \|A\|$)	N.A. ($s_S = 0$ or $s_S = A$)
0	$s_L = -A$ ($s_S = 0$)	$s_S = 0$
<1	$1 > (1 + A/s_L) > 0$; $s_L < 0$ but $s_L > -A$	$s_S < 0$
0.5	$s_L = -2A$	$s_S = -A$
1	$A/s_L = 0 \rightarrow (s_L \rightarrow \infty)$	$A/s_S = 0 \rightarrow (s_S \rightarrow \infty)$ unless $A \rightarrow 0$
>1	$s_L > 0$	$s_S < 0$
2	$s_L = A$	$s_S = 2A$
3	$s_L = 2A$	$s_S = 3A$

In Fig. 2.8, the symbol $k_0 = x_{i,S}/x_{i,L}$ is introduced, called the *equilibrium for the impurity*, also called the segregation coefficient or partition coefficient, and fractionation coefficient when applied to isotopic impurities. For B indicating the solute, it results from Fig. 2.8a that k_0 can vary from nearly 0 to nearly 1. For B indicating the solvent, it results from Fig. 2.8b that $k_0 > 1$ (typical values ranging from 1–3).

Notice that in the diagrams of Fig. 2.8, the axes are reversed with respect to the ones whose first derivative is reported in Eq. 2.8. Let us consider the slopes at $T = T^*_{tp}$ and $x = 1$, be $s_S = dx_{i,S}/dT$ and $s_L = dx_{i,L}/dT$, which are typically negative for the case A and positive for the case B. Therefore one can express $k_0 = s_S/s_L$.

Equation (2.8) places a *constraint on the difference* $(s_S - s_L)$, but, depending on the *i*th impurity, there is still one degree of freedom in variability, only the degree of divergence of the two lines is constrained to remain the same. This constraint is transferred to k_0, according to the two following relations, expressing it in terms of s_S or s_L, respectively:

$$(s_S - s_L) = s_L(k_0 - 1) = A, \quad k_0 = 1 + A/s_L, \tag{2.9}$$

$$(s_S - s_L) = s_S(1 - 1/k_0) = A, \quad k_0 = 1/(1 - A/s_S) = s_S/(s_S - A). \tag{2.10}$$

The conditions obtained for different values of k_0 are reported in Table 2.2, as obtained from Eqs. 2.9 and 2.10.

For example, for oxygen $A = 0.0181\ K^{-1}$. Therefore, $(s_S - s_L) = 0.0181\ K^{-1}$, i.e. 0.0181 ppm/μK or, as usually indicated, 55 μK/ppm. This is quite higher than observed for any oxygen significant impurity: e.g., $N_2 = 13$ μK/ppm. Differently for neon ($A = 0.0668\ K^{-1}$), $(s_S - s_L) = 15$ μK/ppm, now comparable for significant impurities: e.g., $N_2 = 13$ μK/ppm (Pavese 2009).

Equation 2.8 can be written in order to emphasize instead the effect of the impurity on T_{tp}, as

$$T_{tp} = T^*_{tp} - \left(x_{i,S} - x_{i,L}\right)/A. \tag{2.11}$$

It emphasizes that impurities can both raise and drop freezing points. This can also be seen in Fig. 2.9, where increased entropy for either of the two phases will lower the respective curves. Thus, dilution of the liquid phase causes the freezing point to be depressed, and dilution of the solid phase causes the freezing point to be elevated.

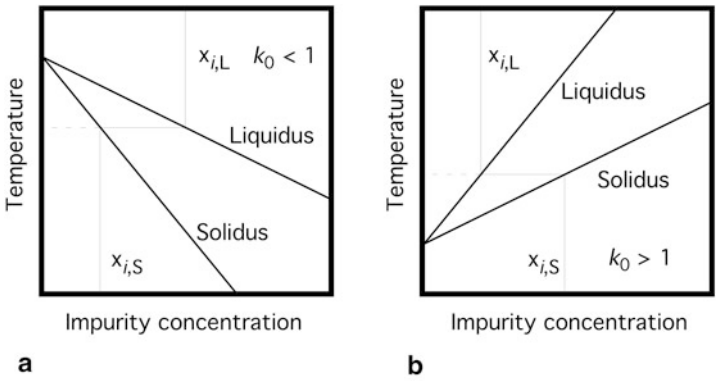

Fig. 2.9 Simplified schematic representation of the binary phase diagrams for impurities at low concentrations with opposite effects in solvent A. (See also Fig. 2.8)

Equation 2.11 can be expressed in terms of the concentration of the impurity in the liquid phase:

$$T_{tp} = T^*_{tp} - x_{i,L}(k_0 - 1)/A = T^*_{tp} - m_L x_{i,L}, \tag{2.12}$$

or in terms of the concentration of the impurity in the solid phase

$$T_{tp} = T^*_{tp} - x_{i,L}(k_0 - 1)/Ak_0 = T^*_{tp} - m_S x_{i,S}, \tag{2.13}$$

where $m_L = 1/s_L$ and $m_S = 1/s_S$ and $k_0 = m_L/m_S$. The conditions in Table 2.2 would be, for the same examples, as follows: for oxygen, to have, for $k_0 = 0$, $m_L = -55\,\mu$K/ppm for all impurities, indicating that a dilute mixture of N_2 in O_2 ($-22\,\mu$K/ppm) is likely to have a $k_0 \approx 0.15$ from Eq. 2.14 (see below); for neon, to have, for $k_0 = 0$, $m_L = -15\,\mu$K/ppm for all impurities, indicating that a dilute mixture of H_2 or N_2 in Ne (-8 K/ppm) is likely to also have $k_0 \approx 0.15$.

In fixed points, the observed behavior with a single impurity in low concentrations is described by one of the two simple binary phase diagrams shown in Fig. 2.9 (Sloan and McGhie 1988).

The diagram (a) is identical to the diagram (a) in Fig. 2.8 for an impurity B in a solvent A depressing the freezing point temperature of A. The diagram (b) corresponds to the diagram (b) in Fig. 2.8, where the concentration of substance A is vanishing into substance B being the solvent, whose freezing temperature is increased by A, but considering instead an impurity C in the same solvent A increasing the freezing point temperature of A.

The figures plot the liquidus temperature (onset of the freezing with cooling, or end of melting with heating) and solidus temperature (onset of melting with heating or end of freezing with cooling) versus impurity concentration. At sufficiently low concentrations, the liquidus and the solidus are straight lines given by Eqs. 2.12 and 2.13, respectively. Now m_L and m_S are the slopes of the actual slopes of the lines in the type of diagrams of Fig. 2.9. The ratio of these slopes is given by the distribution

coefficient $k_0 = x_{i,\mathrm{S}}/x_{i,\mathrm{L}} = m_\mathrm{L}/m_\mathrm{S}$ ($= s_\mathrm{S}/s_\mathrm{L}$, see above). (Note that this is true only at sufficiently low concentrations where the solidus and liquidus are straight lines, it is not true generally.)

Segregation during freezing or dilution during melting—Consider first a fixed point, in a molten state with an impurity B of concentration $x_{i,\mathrm{L}}$, and subject to slow cooling. As it cools from a higher temperature, it eventually reaches to the liquidus temperature. At that point the first amount of solid will form. Under equilibrium conditions, the liquid and solid temperatures must be the same, the latter so crossing the solidus line according to the horizontal full line in Fig. 2.9. This obviously occur at two different concentrations of B for the liquid and the solid (being this initial concentration of the solid $x_{i,\mathrm{Si}}$ lower in (a) and higher in (b)). The segregation of impurities between the solid and liquid phases causes the concentration of the impurities in the remnant liquid to increase ($k_0 < 1$) or decrease ($k_0 > 1$), which in turn causes the liquidus temperature for the remnant liquid to change. The process continues stepwise in a monotonic way in the two cases (decreasing temperature T_tp in (a) and increasing temperature T_tp in (b)), meaning that T_tp is dependant on the liquid fraction, denoted by $F (0 < F < 1)$.

Similar would happen considering a fixed point, in a solidified state and subject to slow heating. As it heats up from a lower temperature, it eventually reaches the solidus line (following the lower vertical full line in Fig. 2.9) and a similar, but opposite description of the melting can be done.

For the case of freezing, if the impurity B is distributed uniformly in the remnant liquid, then the observed fixed-point temperature changes with the liquid fraction of the substance, F according to the following law:

$$T_\mathrm{tp}(F) \approx T^*_\mathrm{tp} + (k_0 - 1)/A\left(x_{i,\mathrm{L}i} F^{k_0 - 1}\right) \tag{2.14}$$

where $x_{i,\mathrm{L}i}$ is the initial concentration of the liquid impurity. This representation of the freezing plateau should not be confused with the representation of the binary mixture in Fig. 2.9: for decreasing F (increasing F in the case of a melting plateau) the concentrations of the liquid and solid phase is located on a segment of either the solidus and liquidus lines. The factor $(k_0 - 1)F^{k_0 - 1}$ is plotted in Fig. 2.10 for several values of k_0 to show the effects of impurities with different k_0 values on the freeze- or melt-plateau shape.

While there is a continuous range of possible k_0 values from zero to large values, there are three distinct families of freezing (or melting) point behavior. The simplest case is for impurities with $k_0 = 1$ (i.e., the impurity is equally soluble in the solid and liquid phases). Such impurities have no effect on the plateau shape or on the fixed-point temperature.

Impurities with $k_0 < 1$ (i.e., the impurity is less soluble in the solid), cause a depression of the plateau liquidus point. A special case is $k_0 = 0$, i.e., the impurity is completely insoluble in the solid, then Eq. 2.14 simplifies to Raoult's law for liquidus-point depression and the observed fixed-point temperature changes with liquid fraction according to

$$T_{\mathrm{f},i}(F) = T_\mathrm{f} - x_{i,\mathrm{L}}/(AF), \tag{2.15}$$

equivalent to Eq. 2.6.

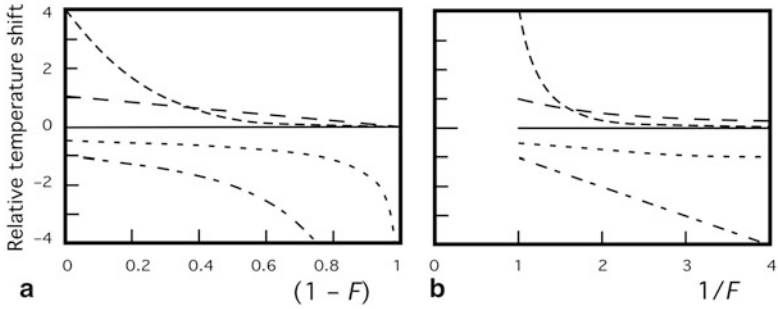

Fig. 2.10 **a** Typical representation of freezing plateaux for fixed points with impurities with different distribution coefficients according to the factor $(k_0 - 1)F^{k_0-1}$ of Eq. 2.14, plotted according to the frozen factor $(1 - F)$—approximately proportional to elapsed time for steady cooling rate. **b** Typical representation of melt plateaus for the same conditions, plotted against $1/F$ (exactly linear in the cases $k_0 = 0$ and $k_0 = 1$). Lines (from *bottom* to *top*): $k_0 = 0$ dash & dot, $k_0 = 0.5$ dots, $k_0 = 1.0$ full line, $k_0 = 2.0$ dash, $k_0 = 5.0$ long dash

Table 2.3 Normalized depression values for values of k_0 at $1/F = 1$ and $1/F = 0$

k_0	$\Delta T_f(1/F = 1)$	$\Delta T_f(1/F = 0)$	Shape
0	− 1	0	Linear
0.05	−0.969	−0.106	Quadratic
0.1	−0.932	−0.194	Quadratic
0.2	−0.848	−0.318	Quadratic
0.3	−0.752	−0.384	Max quadratic
0.5	−0.539	−0.385	Quadratic
0.7	−0.317	−0.272	Quadratic
1.0	0	0	Linear

For systems with impurities with $k_0 = 0$, plots of temperature versus $1/F$ provide a direct measure of the impurity concentration (see Fig. 2.10b), and extrapolations to $1/F = 0$ can be used to determine T^*_{tp}. In practice, few impurities have $k_0 = 0$ exactly, and it is extremely unlikely that a fixed point will have only impurities with $k_0 = 0$, so Eq. 2.15 is at best approximate for most fixed points and quite misleading for others. In fact, in Table 2.3, the computed normalized values of the T^*_{tp} depression for various values of k_0 are reported at $1/F = 1$ (liquidus point of the plateau) and $1/F = 0$ (correct T^*_{tp} when Raoult's law applies). The relationship is exactly linear only for $k_0 = 0$ and $k_0 = 1$, while can be approximated with a quadratic (with modest positive quadratic coefficient) in between these values.

Therefore, only for $k_0 < 0.15$, the deviation from the Raoult's law liquidus-point depression of the plateau is lower than 10 % (as it would happen for the two examples of oxygen and neon reported above) and the error for correction by extrapolation to $1/F = 0$ is greater than 10 % for $0.05 < k_0 < 0.95$, with a maximum of 38 % for $k_0 = 0.3 - 0.5$ using a quadratic approximation, of the relationship (a 25 % deviation for the same two examples).

The third regime in Fig. 2.10 is for impurities with $k_0 > 1$, in which case the observed temperature is always elevated with respect to T^*_{tp}. Note the opposite effect

of the impurities in the curves of Fig. 2.10a, impurities with low values of k_0 have the greatest effect at the end of the freezing plateaus, while impurities with large k_0 values have the greatest effect at the beginning of the freezing plateaus. On the melting plateaus, better represented by Fig. 2.10b, for $k_0 < 1$, the effect is on the slope, which remains close to constant as in the case $k_0 = 0$, while for $k_0 > 1$ the shape bends up and can be confused with the occurrence of thermal effects due to stray exchange in the thermostat.

The ratio $k_0 = K_H/K'_H$ is written here to denote the Henry's law constants related to the distribution equilibrium of the impurity between the solid and the liquid phases (Lewis and Randall 1923). A mathematical procedure for calculating T^*_{tp} in the case of a single impurity, which uses the measured values of T_{tp} at $1/F = 1.0$, 2.0, and 4.0 can be found in Mastrangelo and Dornte (1955).

2.2.2.3 Correction of T_{tp} for Chemical Impurities

As for any systematic effect affecting a measurement, the change in T_{tp} produced by chemical impurities should be estimated and corrected, adding to the uncertainty budget a component due to the uncertainty of this correction. However, the correction is not a trivial issue in most cases, because one should find data about the sensitivity coefficients dT_{tp}/dx_i and for the distribution coefficients k_0 for every diluted binary mixture of the substance (solvent) whose fixed point is of interest and every chemical impurity (solute) that may be present with amount concentrations x_i in the used sample of that substance—see next Section. A critical review of the data on sensitivity coefficients existing in the literature can be found in (Pavese 2009) for the 5 gases more common in the cryogenic range, H_2, Ne, N_2, O_2 and Ar: with respect to metal fixed points, the knowledge is reasonably complete, though often limited to one source—for N_2 in Ne see also (Pavese et al. 2012c). However, also assays providing amount concentrations are equally necessary and they should be reliable and of reasonable accuracy: this cannot be taken for granted. A striking example is the presence of Ar in O_2: long since (Pavese 1984b; Pavese et al. 1988) errors in oxygen T_{tp} up to 2 mK have been observed due to undetected or ill-detected amounts of Ar in O_2—see next Section for a discussion of this case. When oxygen is produced by distillation of air the situation, though improved is not yet solved, especially because often argon is not even counted in oxygen total purity, since it is not of interest to users, outside thermal metrology. Oxygen produced by electrolysis of water is likely to be less affected by the problem. Obviously, if one does not know all the necessary data, a reliable correction cannot be applied.

Methods have been devised, intended to solve this problem in most situations: Tables 2.4 and 2.5 summarize those existing in the literature—the reader is directed to the relevant references for details, in Tables 2.4 and 2.5 only the field of application and the way to apply each of them is summarized.

In some circumstances, the uncertainty that remains associated to the correction is comparable with the uncertainty that must be added to the total uncertainty budget of the fixed-point realization *if no correctionis performed*. The use of uncorrected data

Table 2.4 Correction methods for chemical impurities and related uncertainty increase

Method name	Reference	Correction Δ	Uncertainty u_Δ	Application	Remarks
Correction applied, methods recommended in guidelines					
GUM Eurachem	BIPM 1995 CITAC 2000	"It is assumed that the results of a measurement have been corrected for all *recognised significant* systematic effects" Correction required irrespective of significance of bias			
SIE	BIPM CCT WG1 2005	$\Delta = -\sum_i x_i m_{\mathrm{L},i}$ [a]	$u(\Delta)^2 = \sum_i \left\{ \left[u(x_i)\, m_{\mathrm{L},i} \right]^2 + \left[x_i u\left(m_{\mathrm{L},i}\right) \right]^2 \right\}$	General, but seldom usable in practice	All x_i and $m_{\mathrm{L},i}$ must be known
OME	BIPM CCT WG1 2005	$\Delta = 0$	$u(\Delta)^2 = \left(K_\mathrm{f} x_{\mathrm{L,tot}}\right)/\sqrt{3}$ [b]	In case of failure of all other methods, only	K_f of the substance and total purity $(1 - x_{\mathrm{L,tot}})$ must be known
Hybrid SIE-OME	BIPM CCT WG1 2005	*SIE* and *OME* applied for the relevant parts: as in *SIE* for the known impurities, as in *OME* for the rest			
Correction applied, alternative methods					
One-sided OME	Pavese 2011	$\Delta = -\left(K_\mathrm{f} \cdot x_{\mathrm{L,tot\text{-}rel}}\right)/2$	$u(\Delta)^2 = \left(K_\mathrm{f} \cdot x_{\mathrm{L,tot\text{-}rel}}\right)/2\sqrt{3}$	The effect on T_tp of all impurities have the same sign (depression shown here)	K_f of the substance must be known, and total impurities $x_{\mathrm{L,tot,rel}}$ having an effect on T_tp only
AOE	Pavese 2011	$\Delta = -m_{\mathrm{L,ave}} \cdot x_{\mathrm{L,tot\text{-}rel}}$	$u(\Delta)^2 = (x^2_{\mathrm{L,tot\text{-}rel}}/\sqrt{3})(m_{\mathrm{L,max}} - m_{\mathrm{L,min}})^2 + m^2_{\mathrm{L,ave}} u^2(x_{\mathrm{L,tot\text{-}rel}})$	Same as previous, but also different sign allowed in limited cases. Impurities with $m_\mathrm{L} \approx 0$ excluded from mean	Mean sensitivity m_L value must be computable, and total impurities $x_{\mathrm{L,tot,rel}}$ having an effect on T_tp only
Mixed approaches	Pavese 2011	Applied as in the one-sided *OME* or the *AOE* for the relevant parts. Other methods for the rest			

$\Delta = -b$, b being the estimated 'bias', is the estimated correction required to obtain the corrected value. For all methods, $U = k\sqrt{(u(y_\mathrm{obs})^2 + u(\Delta)^2)}$, where $u(y_\mathrm{obs})$ is the uncertainty of the measured value

SIE summing the Individual Estimates, *OME* Overall Maximum Estimate, *AOE* Average Overall Estimate

[a] x_i is the ith-impurity amount concentration and $m_{\mathrm{L},i}$ is the initial slope of the liquidus curve of that impurity in the solvent

[b] $x_{\mathrm{L,tot}}$ is the "overall impurity fraction at the liquidus point" in amount of substance concentration and K_f is the cryoscopic constant of the solvent. $K_\mathrm{f} = 1/A$, see Eqs. 2.6 and 2.15

Table 2.5 Methods for evaluation of uncertainty increase due chemical impurities

Method name	References[a]	Uncertainty u_Δ	Remarks
Correction not applied			
RSSu	Lira and Wöger 1998a, b; Magnusson et al. 2003; Kallner et al. 2005	$U = k\sqrt{(u(y_{obs})^2 + \Delta^2 + u_\Delta{}^2)}$	Notice that the uncertain Δ *must be known*: however its use in the uncertainty estimation is less critical than performing a correction
RSSU	Thompson et al. 1999; Barwick and Ellison 1999; Franson 1989	$U = k\sqrt{(u(y_{obs})^2 + (\Delta/k)^2 + u_\Delta{}^2)}$	Same as before, but here Δ is not multiplied by k, the coverage factor (for expanded uncertainty U, $k \approx 2$)
SUMU	Phillips et al. 1997	$U_+ = \max\{0, k\sqrt{(u(y_{obs})^2 + u_\Delta^2)} - \Delta\}$ $U_- = \max\{0, k\sqrt{(u(y_{obs})^2 + u_\Delta^2)} + \Delta\}$	Asymmetrical interval. Equation applies when $k\,u(y_{obs})^3 = -x_{L,tot}/A^{b-d}$ (method originally devised for known precisely but not applied)
$SUMU_{max}$	Thompson et al. 1999; Maroto et al. 2002	$U = k\sqrt{(u(y_{obs})^2 + u_\Delta{}^2)} + \lvert\Delta\rvert$	Also described in GUM (F. 2.4.5)
U_e	Synek 2005	$U = k\sqrt{(u(y_{obs})^2 + u_\Delta{}^2)} + E\lvert\Delta\rvert$	Where E is dependent on the bias and is in the range 0–2

The uncertainty of the uncorrected value is $u(y_{obs})$; $\Delta = -b$, where b is the observed 'bias', is the estimated correction required to obtain the corrected value

[a]Reference: Magnusson and Ellison (2008) valid for all

[b]x_i is the ith impurity amount fraction and $m_{L,i}$ is the initial slope of the liquidus curve of that impurity in the solvent

[c]$x_{L,tot}$ is the "overall impurity fraction at the liquidus point" in amount of substance fraction and A is the cryoscopic constant of the solvent

[d]However also the case when $\Delta = -\sum_i c_i\, s_{L,i}$ is used in Table C.1.2b in Appendix C, like in SIE, called "mixed SUMU-SIE" approach

is generally deprecated, but in some casesenough data are not available to do better: note that a zero value for the correction is used in this case by the OME method (see Tables 2.4 and 2.5), basically corresponding to the very minimum knowledge: nominal purity and value of the first cryoscopic constant K_f. The reader can find in the literature other methods proposed for computing the additional uncertainty in the case of the use of uncorrected data: they also involve an estimate of the likely value of the correction. In Tables 2.4 and 2.5, the references to these methods and the basics of their use are reported. At the end of Appendix C, the reader can find a Table with a comparison of the results of application of the different methods and can appreciate the large differences often obtained by using different methods.

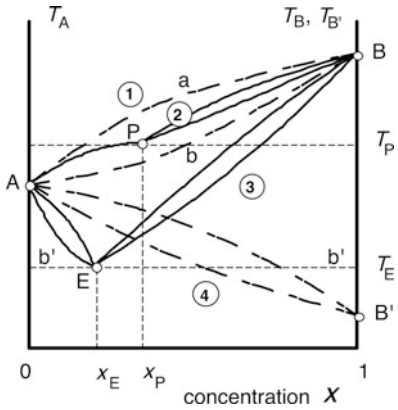

Fig. 2.11 Different types of temperature-composition diagrams of binary mixtures. *1* $T_B > T_A$, *a* liquidus and *b* solidus lines; *2* same for a peritectic *P* mixture, *b′* possible solidus line; *3* same for an eutectic *E* mixture; *4* $T_B < T_A$

2.2.2.4 Phase Diagrams of Binary Mixtures: Eutectic, Peritectic, and Other Mixtures

The values of the sensitivity coefficients dT_{tp}/dx_i for gases are seldom provided in the literature. Very often, this information must be derived from the data of solid–liquid (and vapor) equilibriums in mixtures (Hiza et al. 1975, 1982), and it generally concerns concentrations quite outside the range of interest in thermometry. The values for small concentrations can then be obtained from the slope of an extrapolation to zero solute concentration. Generally, this extrapolation can be obtained graphically from equilibrium diagrams, such as those shown in Fig. 2.11, where some basic behaviors, occurring with substances of interest with respect to the present text, are reported.

Behavior (1) concerns the case of a substance (B) whose triple point temperature is higher than that of substance (A) and their mixtures more or less follow Raoult's law (indicated by the temperature differences between the liquidus (a) and solidus (b) lines). For a pure substance (A) the sensitivity coefficient is *negative*, and positive for substance (B).

Behavior (4) shows the opposite case, namely of a substance (B′) whose triple point temperature is lower than that of substance (A).

With behavior (3) the sensitivity coefficient is positive for both substances, because a characteristic composition x_E of the mixture, which is denoted "eutectic composition", occurs to which corresponds the *minimum* triple point temperature T_E that can be obtained by mixing those two substances. The eutectic point E is easily proved to be invariant according to Gibb's rule. The solidus line, which can be as low as (b′), and the liquidus line coincide at E, i.e., the melting range of a eutectic mixture is very small, *as is with a pure substance*. The eutectic composition has been used at high temperatures to realize accurate reference points (e.g., eutectic Ag-Cu), but at low temperatures there is of little advantage, as a necessary perfect homogeneity of the mixture is not easily achieved and thermal diffusivity is small, which makes the thermal equilibration time quite large.

Behavior (2) is the most insidious for reference triple points. There is an invariant point P, which is denoted "peritectic point", with a characteristic composition x_P of the mixture of two substances (A) and (B) showing a temperature $T_{tp,P}$ *higher* than

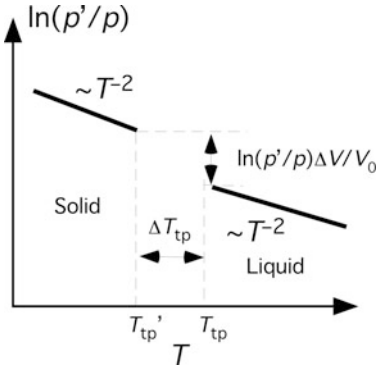

Fig. 2.12 Qualitative features of the normal TPIE for two isotopes: relative volatility versus temperature shows how the triple-point shift coincides with a discontinuityin $\ln(p'/p)$. The features have been exaggerated for clarity, and the figure is not to scale. (After Tew 2008)

$T_{\mathrm{tp,A}}$. The problem arises from the fact that the solidus and liquidus lines between A and P generally show very small or no separation. Therefore, the melting range is almost unaffected by the amount of substance (B) for a sizeable composition range, and consequently the change in the triple point temperature due to impurity (B) *cannot* intrinsically be detected by thermal analysis. Such a problem occurs, e.g., with argon in oxygen (Pavese et al. 1988) or with krypton in argon.

Relevant data on mixtures are given in the gas data sheets in Appendix C, where also a Table of the sensitivity coefficients $\mathrm{d}T_{\mathrm{tp}}/\mathrm{d}x_i$ and of the distribution coefficients k_0 (according to van't Hoff model) is provided for some of the gases (Pavese et al. 2008[4]; CCT WG3 2005; White et al. 2007, 2010).

2.2.2.5 Isotopic Composition

Another difficult case of systematic effect is when the temperature value of the triple point is critically affected by the concentration of different isotopes, which are constituents of most natural substances (Pavese and Tew 2000b; Pavese et al. 2003b; Pavese 2005b).

This is an instance occurring when the pure isotopes show large T_{tp} value differences, as in the cases of hydrogen (Fellmuth et al. 2005, 2012), neon (Pavese et al. 2012b, c), krypton (Inaba and Mitsui 1978; Kemp and Kemp 1978) and xenon (Inaba and Mitsui 1978; Ancsin 1988b; Khnykov et al. 1989b; Hill and Steele 2004, 2005)—also water is affected by isotopic problems (Nicholas et al. 1996; White et al. 2003; White and Tew 2010).

The reader should consult Tew (2008) for a very comprehensive treatment of the subject matter. Here only some basic information will be drawn from that paper concerning the triple point—for the corresponding information concerning the vapor pressure, see Sect. 4.1.1.3.

The qualitative features of the triple-point isotopic effect (TPIE) are illustrated in Fig. 2.12. For the class of substances considered here, all exhibit the so-called

[4] As corrected for the effect of N_2 in Ne according to the new value obtained in Pavese et al. (2012c).

"normal" TPIE where, for two isotopes with atomic masses M and M' ($M > M'$), triple points T_{tp} and T'_{tp} exhibit similar but shifted $p-T$ diagrams. In particular, the triple-point shift $\Delta T_{tp} \equiv T_{tp} - T'_{tp}$ coincides with a discontinuity in the relative volatility, normally expressed as $\ln(p'/p)$ (see Sect. 4.1.1.3 for the vapor-pressure isotopic effect (VPIE) theory), between the solid (s) and liquid (l) phases. At $T = T_{tp}$, one have $\ln(p)_s = \ln(p)_l$ leading to the result,

$$\Delta T_{tp}/T_{tp} \approx k_E \ln\left(p'/p\right)_l \Delta V/2V_S \tag{2.16}$$

where k_E is a "triple-point constant" for the element E (different from one to another), whose value is close to 1, $V = V_l - V_s$ is the change in the molar volume from the liquid-to-solid phase at the triple point and V_s is the molar volume of the solid.

In the limit of small VPIEs, the TPIE is a product of two small quantities and therefore essentially a second-order effect since $\Delta V/V_s$ does not exceed 15 % in the noble gases and is ≤ 16 % for diatomic species of cryogenic interest. In addition, since the VPIE theory predicts that $\ln(p'/p) \approx T^{-2}$ and $\ln(p'/p) \approx \Delta M/MM'$, the same scaling laws should hold true for the TPIE. Furthermore, in a crude way $T_{tp} \approx M$ between elements, so the relative isotope shift T_{tp}/T_{tp} should scale $\approx M/M^3$. This explains why the TPIE is primarily a problem confined to the cryogenic range of light-element fixed points.

Some relevant data are summarized in Sect. 4.1.1.3.

Hydrogen isotopes In the case of hydrogen, the content of deuterium—in the form of HD—is variable from batch to batch and the exact content is normally not included in the supplier certificate issued with the gas. This issue was resolved as the result of an international study (Fellmuth et al. 2005, 2012)—see also Section "Intercomparison of Sealed Cells": it involved the measurement at PTB with an average uncertainty $u = 50$ μK of 32 samples supplied by 7 laboratories, most contained in sealed cells, of HD content ranging (27.2–154.9) μmol D/mol H, certified with a maximum standard uncertainty of the D/H ratio of 1.5 μmol D/mol H. The correction for the HD content is now included in the Technical Annex to the *mise en pratique* of the kelvin (CCT 2006; Steur et al. 2005; Pavese and Tew 2000b; Pavese et al. 2002; Pavese 2005a, b):

"The isotopic composition of commercially available hydrogen varies from an amount-of-substance ratio of about 27 mmol D/mol H to about 150 mmol D/mol H. It has been established that the discrepancies previously found at the triple point are mainly due to the variable deuterium content in the hydrogen used for its realization.

It is therefore specified that the ITS-90 temperature assigned to the triple point of equilibrium hydrogen, $T_{90}(e\text{-}H_2\ TP) = 13.8033$ K, is taken to refer to an isotopic amount-of-substance ratio of 0.000 089 02 mol D/mol H. This is the isotopic ratio determined for SLAP (Gonfiantini 1978).

To correct to the isotopic reference ratio, the following function is specified:

$T_{meas} = T_{90}(e\text{-}H_2TP) + k_D(x - x_0)$, where x denotes the isotopic amount-of-substance ratio of the sample in micromoles D per mole H, $x_0 = 89.02$ μmol/mol the reference ratio specified above, and k_D the slope of the triple-point temperature

dependence on deuterium ratio. The current best value for k_D, and the value specified of the ITS-90, is given (Fellmuth et al. 2005) as 5.42 μK/(μmol/mol)". The standard uncertainty in the slope is 0.27 μK/μmol D/mol H: this corresponds to an uncertainty of the temperature correction lower than 20 μK. An analysis of the same data made using the techniques reported in Sect. 2.4.2 (LSMFE plus bootstrap) evaluated a slope of 5.45 μK/μmol D/mol H and a maximum 95 % bootstrap confidence interval (CI) of (5.29–5.62) μK/μmol D/mol H, which corresponds to a standard uncertainty of 0.08 μK/μmol D/mol H. A Monte Carlo evaluation of the same results brought to a *minimum* triple-point-temperature 95 % CI of (68–102) μK located at 53.3 μmol D/mol H.

In order to perform the correction (the dispersion of temperature values is 0.7 mK in the observed D/H amount range, but is up to ≈ 20 mK for the correction of the H_2 vapor-pressure ITS-90 fixed-point near 17 and 20 K), one therefore needs to get an isotopic composition assay specific for its own sample of hydrogen: a reasonably large number of geochemistry laboratories all round the world can provide this assay. For the way to correct a scale realization for the isotopic effects, see Tew and Meyer 2008; Steur and Giraudi 2012: this issue is very specialistic, so details are not given here, but it is essential for top-level realizations of the ITS-90. If no correction is applied, an additional type B uncertainty component $u = \approx 0.2$ mK if a rectangular probability distribution is assumed. The additional component is nearly one order of magnitude larger than the other uncertainty components of the fixed-point realization.

Incidentally, the effect of deuterium in H_2 also affects the water triple point: also this correction is included, together with the effect of the oxygen isotopic composition, in the same Technical Annex—see reference above.

Neon isotopes In the case of neon, the proportions with respect to ^{20}Ne of the two heavier isotopes, ^{21}Ne and ^{22}Ne, is variable from batch to batch of gas, in particular for gas produced from distillation of air, in practice the only type commercially available, as fractionation occurs during distillation with unpredictable enrichment in ^{22}Ne. The numerous samples examined in addition of those already available in the literature showed a range of ^{22}Ne amount ratios to ^{20}Ne ranging from $n(^{22}\text{Ne})/n(^{20}\text{Ne}) \approx 0.0101$ to ≈ 0.0105, to be compared with the value of the neon isotopic composition recommended by IUPAC CAWIA (now CIAAW) (Wieser 2006; Wieser and Coplen 2011): $^{20}x = 0.9048(3)$, $^{21}x = 0.0027(1)$, $^{22}x = 0.0925(3)$, corresponding to $n(^{22}\text{Ne})/(^{20}\text{Ne}) = 0.01022$ and $n(^{21}\text{Ne})/(^{20}\text{Ne}) = 0.0030$. Therefore, in addition of being much more spread than the IUPAC estimated uncertainty, the IUPAC recommended value is close to the lower bound of the variability interval. The equivalent variability of T_{tp} results to be of ≈ 0.5 mK, about 10 times higher that the rest of the modern best uncertainty budget. The ^{21}Ne amount content, also variable, has no relevance in thermometry.

Also in this case, the issue was resolved as the result of an international study (Pavese 2005a, b; Pavese et al. 2008, 2010a–c, 2011b, 2012b, c; Hill and Fahr 2011; Nakano et al. 2011) and is under way to be incorporated in the Technical Annex. The solution required a quite complicated and comprehensive set of studies, bringing to a method for performing the needed correction of T_{tp} for the actual isotopic

composition of the used neon sample with respect to a reference composition. The measurements on natural isotopic compositions were not sufficient to establish a correction sufficiently accurate, even by using experimental data with an uncertainty $U \approx 50\,\mu\text{K}$ (Pavese et al. 2010b), so that the studies needed including new measurements on the pure[5] isotopes ^{20}Ne and ^{22}Ne, and a theoretical investigation (Pavese et al. 2010c, 2011b, 2012c; Hill and Fahr 2011).

Also in this case, in order to avoid a change in the ITS-90 definition, a neon reference isotopic composition, $^{\text{ref}}x(\text{Ne})$, was eventually preferred, corresponding to the one recommended by IUPAC CAWIA (now CIAAW; Wieser 2006; Wieser and Coplen 2011): $^{20}x = 0.9048(3)$, $^{21}x = 0.0027(1)$, $^{22}x = 0.0925(3)$. However, the correction function spans not only the range of the observed variability of ^{22}x (equivalent to $\approx 0.5\,\text{mK}$), but is valid down to pure ^{20}Ne, just $\approx 14\,\text{mK}$ below the T_{tp} value of the reference isotopic composition, because the experimental determination of the triple point of pure ^{20}Ne is of superior quality. The present best correction function is based on experimental data on high-purity ^{22}Ne and ^{20}Ne and on three artificial certified mixtures of ^{22}Ne in ^{20}Ne (Pavese et al. 2011e, 2012b), confirming the theoretical model (Hill and Fahr 2011) within 10 μK. In the range of interest—^{22}x (in ^{20}Ne) = 0–0.1—the following quadratic correction for T_{LP} with respect to the IUPAC reference isotopic composition applies within 20 μK (Pavese et al. 2012b):

$$T_{\text{LP}}(^{\text{Ne}}x)/\text{K} = T(^{20}\text{Ne})/\text{K} + 0.013\,82 + 0.149\,4188\,{}^{22}x - 0.000\,1448\,{}^{22}x^2 \tag{2.17}$$

where the value of $T(^{20}\text{Ne})$ somewhat depends on its specific realization on an ITS-90 national scale, and on the ITS-90 nonuniqueness until it will be fixed. For the best present value, see Appendix C under "Neon". The equation applies to 'natural' neon that also contains ^{21}Ne, $^{21}x = 0.026$–0.029. For an official correction equation it is necessary to wait for the future CCT decision.

In order to perform the correction, a specific assay of the isotopic composition of the sample used is needed: unfortunately, only very few laboratories in the world are able to provide it with sufficient accuracy. Otherwise, one must resort to the use of^{20}Ne of the best purity, available at a reasonable price: the analytical assay of the chemical and residual isotopic impurities is less critical and some gas manufacturers can provide it.

Other substances with isotopic effects In the case of krypton and xenon, the knowledge about the effect of isotopic composition is limited to a few studies, as their triple points are not definition points of the ITS-90: the most recent are for krypton (Inaba and Mitsui 1978; Kemp and Kemp 1978) and for xenon (Hill and Steele 2004, 2005). Xenon is considered for a possible substitution to the mercury triple point in an approximation to the ITS-90 (see Sect. 2.6), should isotopic variability allow it. Quoting from (Tew 2008), "assuming that this apparent isotopic variability is real, and a sensitivity of 0.75 mK mol g^{-1} derived above, this corresponds to variability in the Xe T_{tp} of only 21 μK".

[5] Isotopic nominal purity of 0.9999 for ^{20}Ne and of 0.999 for ^{22}Ne, sometimes found better from specific assays. Chemical impurities are limited to a total concentration of 1–2 × 10^{-5} of the relevant impurities (N_2, H_2).

Substances with isotopic effect not relevant to thermometry Other substances used for cryogenic fixed points are found exempt from a sizable effect on T_{tp} due to isotopic variability. Specifically for Ar, $\Delta T_{tp} < 1.5\,\mu K$ for $\Delta(^{40}Ar) = 0.003\,\%$ (Pavese 2005b); according to Tew (2008), $\Delta M_{max}(Ar)/M(Ar) < 8 \times 10^{-6}$, corresponding to $\Delta T_{tp} \sim 5\,\mu K$. For O_2, $\Delta T_{tp} < 20\,\mu K$ for $\Delta(^{18}O) = 4\,\%$ (Pavese 2005b); from (Tew 2008), $\Delta T_{tp} < 16\,\mu K$; however it is important in water.

A side effect in isotopic mixtures is a widening in the measured melting range owing to isotopic distillation of the liquid phase during melting (Tiggelman 1973; Tew 2008; Hill and Fahr 2011). The change at the triple point temperature can be computed from the chemical potential μ_A of each component, present with a fraction x_A, by assuming an ideal solution, $\mu_A(p, T, x_A) = \mu_a^*(p, T) + R\,T\,\ln x_A$, where μ^* is the symbol for the pure component. At equilibrium, all chemical potentials must have the same value. For natural neon, the change at the triple point temperature has been calculated by Tiggelman (1973) and Hill and Fahr (2011). During melting, the change of ^{22}Ne concentration in the liquid is 0.08 %, equivalent to a 0.11 mK increase in the melting range, which represents a substantial contribution to the observed total melting range. The distillation effect for mixtures of hydrogen isotopes can be found in Souers (1986).

2.2.2.6 Ortho-Para or Para-Ortho Composition

Some substances are mixtures of isomers with molecules having atoms with different spin combinations. The composition of the mixture changes with temperature, generally for large departures from room temperature, similar to the case of cryogenic temperatures. The use of these substances in thermometry generally requires that spin equilibrium is achieved at the temperature of the fixed point.

Hydrogen and deuterium are the best known in this respect. The nuclear spin of each of the two atoms composing their molecules may assume, at sufficiently high temperatures, different rotational quantum numbers, which are even when they are antiparallel to each other and odd when they are parallel. The two molecular populations—called *para* and *ortho*—are stable unless temperature is changed. In fact, at 0 K only *para*-H_2 or only *ortho*-D_2 can exist. At 0 K, de-excitation occurs of all even states into $J = 0$ and of all odd states into $J = 1$, a metastable condition. The transition from the latter into $J = 0$ is difficult and takes time that may be extremely long, depending upon catalytic effects. The spin composition at any given temperature, i.e., the percent of ortho and para species, is therefore temperature dependent, as Table 2.6 shows (Farkas 1935; Woolley et al. 1948; Souers 1979, 1986). The triple point temperature depends on *ortho-para* composition. In H_2, the equilibrium *ortho* content changes from 75 % at room temperature (the so-called normal hydrogen, n-H_2) to $\ll$0.01 % at the triple point: the value of T_{tp} is 13.951 K and 13.803 K for the two compositions. For the sake of comparison, the equilibrium *ortho* content is 0.2 % at the normal boiling point (20.27 K) and $\approx$ 5 % at the critical point near 33 K. In D_2, the equilibrium *para* content changes from 33.333 % (n-D_2) to 1.51 % and T_{tp} values for the two compositions are 18.724 K and 18.690 K respectively. For the

Table 2.6 *Ortho-para* composition at equilibrium and enthalpy of conversion. (Souers 1986)

T (K)	x(*para*-H_2) (%)	x(*para*-D_2) (%)	$\Delta_{conv}H_{H_2}$ (J mol^{-1})[a]	$\Delta_{conv}H_{D_2}$ (J mol^{-1})[b]
4.2	≈100[d]	1.9×10^{-7}		
10	>99.9999	0.031	0	0.2
13.803[c]	99.996	0.27	0.1	0.8
15	99.99	0.48	0.2	5.5
18.690[d]	99.90	1.51	2	11
20	99.82	2.01[e]	2.6	14
20.271[f]	99.79	2.13	2.8	14
23.66[g]	99.40	3.76	9	28
25	99.02	4.63[e]	14	34
30	97.021	7.864[e]	42	57
40	88.727	14.784	160	109
50	77.054	20.718	326	156
60	65.569	25.131	490	189
70	55.991	28.162	621	207
80	48.537	30.141	750	224
90	42.882	31.395	820	230
100	38.620	32.164	887	236
120	32.959	33.246	1044	237
150	28.603	33.246	1032	238
200	25.974	33.327	1059	238
300	25.072	33.333	1062	238
∞	1/4	1/3		

[a] $\Delta_{conv}H$ molar enthalpy of conversion for n-$H_2 \rightarrow e$-H_2 and n-$D_2 \rightarrow e$-D_2 respectively. For example, converting n-D_2(300 K) into e-D_2(18.69 K) requires $(238 - 11) = 227$ J mol^{-1}

[b] x(*ortho*-H_2) $= 2.1 \times 10^{-17}$

[c,d] Triple points of *para*-H_2 and -D_2, respectively

[e] To this, $J = 2$ population contributes for 0.01 % at 20 K, 0.02 % at 25 K and 0.09 % at 30 K

[f,g] Normal boiling points of *para*-H_2 and -D_2, respectively

sake of comparison, the equilibrium *para* content is 3.76 % at the normal boiling point (23.66 K) and ≈ 14 % at the critical point near 38 K.

The rate of conversion to spin equilibrium can be promoted with the addition of a specific catalyst. When no catalyst is used, the normal composition is initially retained on cooling, but a *natural* conversion in the liquid always takes place (Motizuki 1957, 1962), so that composition—and T_{tp}—slowly drifts with time, faster with hydrogen, slower with deuterium. This "natural" conversion rate is easily increased by paramagnetic impurities, such as O_2. A sizeable enthalpy of conversion is evolved (from normal to equilibrium, at the triple point temperature, about 1.1 kJ mol^{-1} for H_2 and 0.24 kJ mol^{-1} for D_2 (Souers 1986)) which can be a source of thermal problems for an accurate realization of the triple point. Finally, the spin composition change is much faster in the liquid than in the gaseous state. Therefore, once the composition is changed, it will recover back on return to room temperature, but very slowly. Should the sample be condensed again, composition—and T_{tp}—would begin to drift again starting from a value (unpredictably) higher than the one reached at the end of the preceding condensation. Consequently, for the realization of a

reference point, only a sample in spin equilibrium, stabilized by means of addition of a catalyst, can be used.

Hydrous ferric oxide ($Fe_2O_3 \times (H_2O)_n$) is an efficient catalyst commonly used with H_2. With D_2, all hydrates (as catalysts commonly are) greatly increase HD contamination (see preceding section), unless D_2O—commercially available—is used for hydration (McConville and Pavese 1988). They must be baked at a much higher temperature than usually required to remove the exchangeable H radicals, but baking damages their properties and consequently their efficiency risks to reduce in time (Ancsin 1988a; Pavese 1989; Head et al. 1992). Oxides such as Gd_2O_3 are possible alternatives (Head and Rusby 1990; Head et al. 1992; Head 1996, 2001). A more complete list of catalysts used in H_2 sealed cells can be found in (Fellmuth et al. 2005, 2012). Since catalysts are used in the form of powders, they must be carefully baked in situ in order to remove all adsorbed air components, especially water.

Another substance that has different nuclear spin species is methane, CH_4. There are three nuclear spin combinations, generally indicated with A, E and T, or *meta*, *para* and *ortho*. Their proportions at room temperature (n-CH_4) are: A:E:T: = 5:2:9. This composition changes with temperature toward a composition at $T = 0$ K of 100 % A, the only species for which de-excitation can take place directly into $J = 0$, as T de-excitation is into $J = 1$ and E into $J = 2$. In contrast with protium, interconversion time is rapid in the gas, but slows down with a reduction of temperature, so that a room-temperature composition can be considered as only "frozen-in" on rapid condensation, unless a catalyst is specifically used.

During the use of the triple point of methane as a reference point, where generally no catalyst is employed, some anomalies have in fact been observed in some cases (Bonhoure 1984; Inaba and Mitsui 1978), which could be explained with deviations from the n-CH_4 spin composition (Inaba and Mitsui 1980). This composition could easily be checked in situ, as the temperature of the solid-to-solid transition exhibited by solid methane at low temperature (near 20 K) depends to a great extent on spin composition: ≈ 20.5 K for n-CH_4 and ≈ 18.4 K for e-CH_4 (Van Hecke and Van Gerven 1973).

2.3 The Realization of Temperature Fixed Points Using Gas Triple Points

The Working Group 2 of the CCT prepared a list of recommended thermometric fixed points (Bedford et al. 1984, 1996). An update is in preparation from WG2. Another older but more extensive one can be found in Staveley et al. (1981).

Until late in the 1960s, a triple point was considered simply the lowest vapor-pressure point of liquefied gases (or, less commonly, the highest point of solidified gases) and it was performed using the techniques that are described in Chap. 4. However, its unique characteristics as a fixed point are lost with these techniques. Those used in analytical chemistry for purity determinations are more suitable for

fully exploiting the superior quality of this point as a temperature fixed point. In order to understand the meaning of this statement and before examining the modern methods for the realization of triple points, it is necessary to discuss the thermal problems liable to arise in reproducing the thermodynamic state with a sample of real gas enclosed in a container placed inside a cryostat.

2.3.1 Basic Problems in the Design of Cells for Accurate Realization of Triple Points

Let us consider a sample of real gas condensed and then allowed to solidify in a container (usually made of metal), the 'cell', which is part of a cryostat. Any cryostat of the calorimetric type can be used (see Chap. 6), with at least one isothermal shield surrounding the container. Obviously, the thermal quality of the cryostat will contribute to the best precision attainable in the realization of the triple point, but, as will be seen, this influence may be not so critical.

Since a sample of real gas is necessarily more or less impure, the aim of a measurement is to reproduce the triple point as in Fig. 2.6. This can be achieved by freezing or by melting the sample, and, in either case, by continuous exchange of heat with the sample (dynamic technique), or by using the calorimetric technique of intermittent periods of thermal exchange followed by adiabatic return to equilibrium (equilibrium pulse technique). Actually, as the technique of *controlled* removal of heat (by the Peltier effect or with a refrigerator) is not readily applicable in this temperature range, freezing plateaus can be measured only by using the continuous freezing technique.

Devices of different designs have been used for the realization of triple points with different techniques. In the following subsections, two basic cell designs and realization techniques, suitable to represent the two extreme situations, will be described in detail. The first shows that the traditional approach is unsuitable to yield good results for performing triple-point measurements. The second represents the best of the state-of-the-art. Many other intermediate designs are possible, which give results of intermediate quality.

2.3.1.1 Vapor-Pressure Bulb-Type Cell, Used with the Dynamic Technique (Fig. 2.13)

From a thermal point of view, a vapor-pressure bulb is characterized by the following features: (a) a massive copper block, in which the bulb is located, with a large heat capacity, (b) a vapor column thermally connecting, via a small-diameter tube, the condensed sample in the bulb to warmer parts of the apparatus, (c) thermometers fitted in the block, *external* to the bulb, (d) a heater on the outer surface of the block.

During freezing, heat is continuously removed from the surface of the copper block, through a heat-exchange gas in a bath cryostat or, alternately, through a

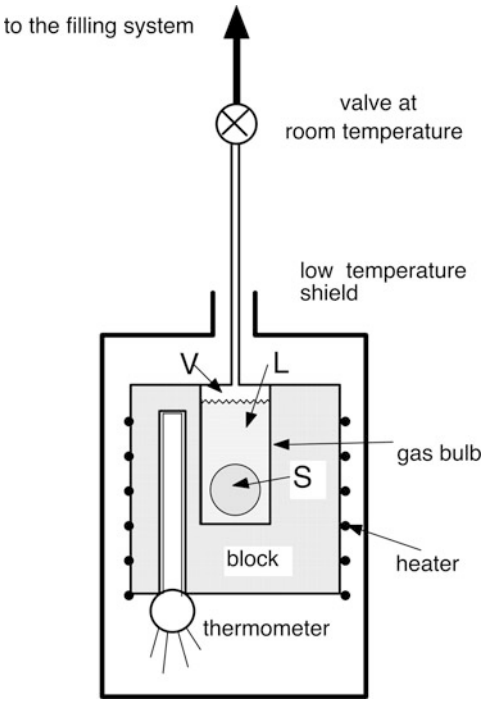

Fig. 2.13 Vapor-pressure-type cell for triple point realization. V vapor, L liquid, S solid phase of the sample

heat-switch when a refrigerator is used. Even if account is not taken of the temperature gradients in the block, the liquefied gas in the bulb begins to cool down from the outside layers and a substantial radial temperature gradient will build up in the sample, owing to the low thermal conductivity of the substance (Table 2.1). The thermometers will indicate a temperature lower than the average one of the liquid.

Moreover, the liquid sample must sub-cool before some solid can nucleate and, consequently, the block must cool below the temperature of the triple point (T_{tp}), from few hundredths of a kelvin to several kelvins depending on the gas and on its purity. In principle, nucleation (or surface melting in the lattice) takes place in the zones where the sample—which cannot be considered uniform as to composition, not being stirred—is less pure; in practice, however, owing to the radial thermal gradient, only the outer layers of the sample will suddenly solidify if the bulb has a simple geometry. Here the heat of solidification is released and temperature increases locally up to T_{tp}. This amount of heat is large when compared with the thermal mass of the sample (see Table 2.1), but the solid phase cannot further increase its temperature without liquefaction occurring again, which prevents the whole sample, initially colder than T_{tp}, from freezing completely. The initial frozen fraction and the maximum temperature of the copper block at this onset of freezing depend on the mass of the copper block and on the cooling rate. The behavior shown in Fig. 2.5 corresponds to a small copper mass and a small cooling rate.

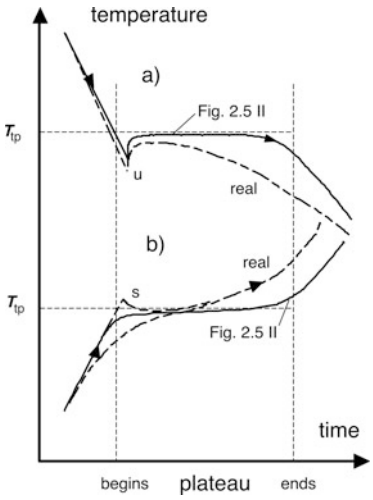

Fig. 2.14 Freezing *a* and melting *b* plateaus for an impure gas *II*, compared with a real experiment, in the temperature versus time representation. **a** Dynamic freezing with a vapor-pressure type cell. *u* liquid subcooling. **b** Dynamic melting with a vapor-pressure type cell. *s* solid superheating (see text)

In a real experiment, the temperature values recorded during the thermal transient depend also on the position of the thermometers with respect to the sample and on the thermal diffusivity of both the copper and the substance, and, consequently, on the geometry of the bulb. In the case considered here, during cooldown, the thermometers indicate the colder block temperature, as is shown in Fig. 2.14a. Then, the temperature rise at the onset of freezing may be limited or prevented from approaching T_{tp} either by the thermal time constant of the block, depending on its mass or by a high freezing rate. The formation of the first solidified layer of the sample then prevents the thermometers from further "sensing" the interface and the internal liquid temperature, where the solidification process takes place nearly isothermally. Further cooling of the block therefore establishes a temperature gradient through the solid phase and the thermometers will monitor temperatures lower and lower than that of the interface.

For subsequent melting of the solidified sample, the bulb is thermally isolated from the refrigerant and a heater on the block is switched on. The heat supplied crosses the block walls reaching first the thermometers, then the external layers of the solidified sample. Under continuous heating conditions, a steady thermal gradient establishes between the heater and the core of the sample, which may be particularly large within the sample, because of the poor thermal conductivity of the solidified gas. Therefore, the temperature value monitored by the thermometer may be substantially higher than the average sample temperature. This means that melting will already occur in some external part of the sample while its mean temperature is still lower than T_{tp}. The total effect is a melting offset (Fig. 2.14b). In addition, the sample is likely to be in very poor thermal contact with the bulb, especially after fast freezing, because of the contraction of most gases on solidification and of the low vapor pressure of the solid. These facts are made evident, in fast heating, by the measured temperature becoming sometimes higher than T_{tp} before the actual onset of melting; subsequently, after some liquid is formed, temperature decreases towards T_{tp}. This effect does

not indicate an overheating of the solid sample—corresponding to subcooling of the freezing liquid—but is simply due to overheating of the *block* and to the initial poor thermal contact between the sample and the block, which gradually improves as the latter is being wetted by the liquid formed from melting of the outer sample layers. The temperature of the whole solid sample slowly becomes uniform and then the sample gradually melts nearly isothermally, but the thermometers fitted in the block are shielded by increasingly thick liquid layers, which get easily overheated due to a continuous heat flow toward the cooler solid phase. A sizeable thermal gradient builds up through the liquid because of its low thermal conductivity. The thermometers will monitor an increasing temperature, higher than that of the solid–liquid interface.

To summarize, in both the cases of continuous freezing and melting, severe limitations to the accuracy of the measurements of the triple point temperature are caused by the use of a cell model as in Fig. 2.13, because the thermometers, (a) are inserted in the thermal path *between* the heat source and the heat sink (which are reversed in the two experiments), and (b) are shielded from the solid–liquid interface, which *alone* remains essentially isothermal during the plateau, by the phase which is free, on the contrary, to overheat (the liquid in melting) or to sub-cool (the solid in freezing), because of its poor thermal conductivity.

2.3.1.2 Small Cell with a Finite Volume at Room Temperature and an Internal Thermometer, Used with the Equilibrium Technique. (Fig. 2.15)

This type of cell is called "open cell" because normally a new sample of gas is condensed in it every time a new experiment is performed, and then is vented out (Ancsin and Phillips 1969). However, it is also possible to use it as a "sealed cell" (see Sect. 2.4.3.1; Pavese et al. 1975b; Pavese 1978b, 1981a). From a thermal point of view, this design is characterized by the following features: (a) a thin-walled high-conductivity metal cell of small heat capacity; (b) a vapor column thermally tied down by means of a heat exchanger to the cell temperature, connecting, via a small-diameter pipe, the condensed sample in the cell to warmer parts of the apparatus up to room temperature; (c) a thermometer fitted in a well at the center of the cell and protruding into the sample; (d) a heater on the outer surface of the cell.

The equilibrium technique requires the use of an adiabatic calorimeter and consists of intermittent exchanges of energy with the sample. After each energy exchange cycle, when the thermal flow produces temperature gradients in the sample, the sample is left undisturbed under adiabatic conditions for a time sufficient to attain thermal re-equilibration.

Freezing plateaus cannot be measured with this technique, as it is not possible to remove a controlled quantity of heat from the sample.[6] Therefore, only melting plateau will be considered here. A (strip) recording of a melting plateau performed

[6] Actually, known amounts of heat can be removed from the sample by making use of the sample enthalpy of evaporation. For instance, heat removal can be carried out by expanding the vapor

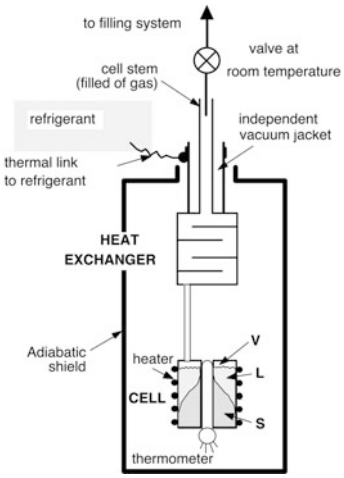

Fig. 2.15 Lower part of a small "long-stem" cell with inner thermometer for triple point realization. The cell stem is the tube connecting the cold cell to the room-temperature valve and filling system

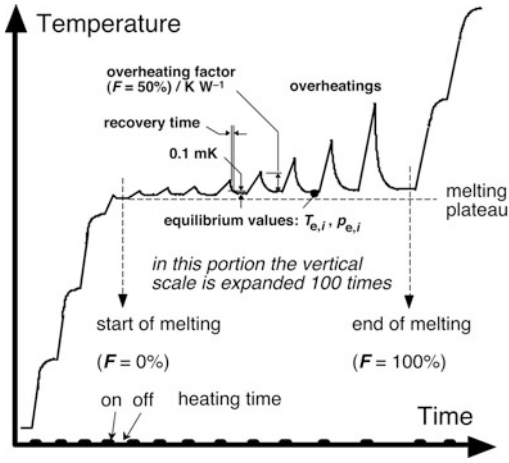

Fig. 2.16 Melting by the calorimetric intermittent-heating method and its definitions. Heating is supplied in equal-energy steps. F melted fraction

with this technique is similar to that in Fig. 2.16, which should be compared with Fig. 2.5. The latter can be considered a melting obtained with the dynamic technique for a vanishing heating rate, so that sample overheating is very small. In a real experiment, an equilibrium plateau is performed in steps, namely only a limited number of experimental points (melted fractions F) are available: a line similar to the one in Fig. 2.5 is often drawn through them only as a visual aid.

When starting from the solidified sample, the thermometer does not monitor a large overheating during each period of the solid sample heating, since the sample is placed between the heater and the thermometer and a very small amount of heat reaches directly the latter only through the thin walls of the cell. The temperature reaches each new equilibrium value in steps having rounded shape because of the thermal gradients that build up in the solid during heating. In the absence of premelting effects

volume of known amounts by means of a calibrated bellows. This technique has been used, so far, only for full sample refreezing or in special studies.

(see Sect. 2.2), the size of the steps—i.e., the heat capacity of the system—remains constant, until very close the onset of melting. When heating causes the first fraction of the sample to melt, suddenly the temperature rise stops; depending on the thermal diffusivity of the substance, on the heat capacity of the container and on the sample purity, a rounded shape of this step or a small overheating is monitored after heating is switched off. This is the very beginning of the melting plateau.

During the melting plateau, heating always builds up some sample overheating (which depends on the cell thermal resistance parameter R_{cs}—see Sect. 2.3.3), whose value often decreases with further sample melting, especially if the sample had been rapidly solidified, because of the improved thermal contact of the sample with the container when it becomes wet by the liquid phase. However, this initial overheating is generally quite small, as the thermometer is in good thermal contact with the sample. It then increases with increasing melted fraction, in a way that depends critically on the cell geometry. Temperatures always return to nearly—though not exactly—the same value at equilibrium, when heating is stopped.

There is an obvious advantage in keeping overheating small for as large a melted fraction as possible, because this reduces the re-equilibration time and makes the equilibrium state less critically affected by stray heat fluxes. The overheating size indicates, in fact, the extent to which the temperature measured by the thermometer is affected by the heat exchange with the cryostat, caused by imperfect adiabatic conditions. In principle, only the solid–liquid interface is assumed to carry the true triple-point temperature. However, according to the experience described in Sect. 2.3.1.1, the best approximation to this condition is to maintain the thermometer as long as possible in good thermal contact with the phase that cannot overheat, i.e. the solid—in melting—which is unlikely to remain sub-cooled using the equilibrium technique. Owing to the unavoidable thermal linkage of the thermometer well with the heater, via the container walls, some liquid also forms between the well and the sample. It must form only a thin layer, to avoid thermal gradients that would "decouple" the thermometer from the interface. This layer can be maintained thin by keeping the sample itself subdivided into thin layers, and (except in applications in zero gravity!), by using horizontal fins connected to the thermometer wells, on which the solid phase can stand in good thermal contact with the thermometer well. With suitable precautions, the overheating can be kept lower than few millikelvin until over 90 % of the liquid fraction F, at the usual heating rates (< 0.01 of increase of liquid fraction F per minute). Otherwise, the plateau temperature would sharply increase as soon as only ≈ 30 % of the sample is melted (as is generally the case with the cell design of Fig. 2.13; Tiggelman 1973). When this increase occurs, the time required to recover equilibrium also increases (see a recovery-time definition in Fig. 2.16), and the equilibrium plateau becomes more and more sensitive to stray heat exchanges. The recovery time largely depends on the thermal diffusivity of the liquid phase and, consequently, on the cell geometry, but can be greatly increased also by a large volume of the vapor phase (see Fig. 4.8 in Chap. 4). The relationship between a real experiment and the $1/F$ vs T plot of Fig. 2.6 is shown in Fig. 2.17.

Effect of the Vapor Column to Room Temperature (Fig. 2.15). The main unavoidable source of heat exchange, is the vapor contained in the tube connecting the cell

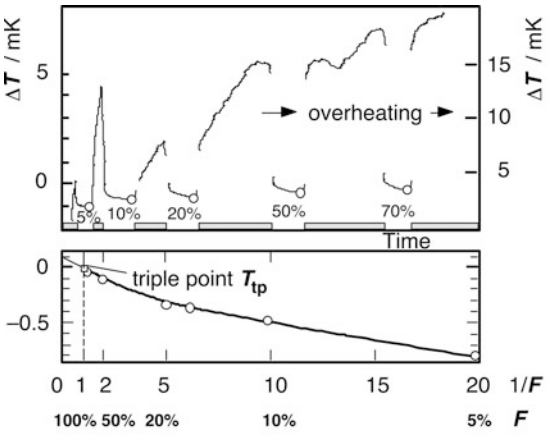

Fig. 2.17 Temperature versus time chart recording of a real experiment (*upper*) and the corresponding T versus $1/F$ plot (*lower*). In the latter, points are the measured equilibrium temperatures. The line is only a visual help drawn for extrapolation to $1/F = 1$. F melted fraction

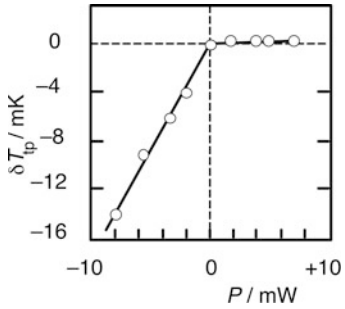

Fig. 2.18 Melting temperature instability at the argon triple point caused by a cold spot produced by heat leak from the cell heat-exchanger. (see Fig. 2.15)

to the external filling circuit (and, possibly, to a pressure measuring apparatus). The precautions necessary to avoid cold spots in this tube are fully discussed in Chap. 4 concerning vapor pressure measurements. It must be pointed out here that cold spots have to be carefully avoided by vacuum jacketing the connecting tube, as they have a very *efficient* pumping effect on the sample. Owing to the large enthalpy of evaporation, the refrigerating effect of pumping is extremely effective and produces an unwanted refreezing of the sample. If the cold spot is large enough, its effect is clearly detected by a dramatic temperature instability downwards (Fig. 2.18), but when it is small, the refrigeration effect is slight and only results in a *stable* lower—and incorrect—temperature value. Cold spots must thus be carefully avoided through control of the connecting tube temperature. This is the reason for the thermal tie-down to the refrigerant shown in Fig. 2.15, which allows the heat exchanger temperature to be carefully controlled and maintained *always* at a value slightly *higher* than that of the cell.

Consequently, a certain amount of heat will always reach the cell by conduction via the connecting tube and by conduction and convection in the vapor. The temperature difference between the cell and the exchanger must be as small as possible; the lowest limit is set by the temperature nonuniformity of the heat exchanger itself (considering

that the tube above the exchanger must be somewhere thermally tied-down to the refrigerant).

Consequently, the small heat input that the cell must always receive tends to keep the liquid phase slightly overheated. This overheating is one leading reason why—when no more of the solid phase is in good thermal contact with the thermometer well—the equilibrium plateau (Figs. 2.5 and 2.6) shows an abnormal upward curvature, which indicates that the true equilibrium conditions are no longer achieved. The overheating amount can be easily checked by changing the heat-exchanger temperature offset, and then corrected by extrapolation of the measured effect to zero offset. For some examples of the dependence of cell overheating on the melted fraction, see Fig. 2.20a in Sect. 2.3.3—and thermal resistance R_{cs} for all-copper cells in Fig. 2.20c.

2.3.1.3 Definition of the Triple Point Temperature

It is now possible to define a procedure for obtaining from each realization of the triple point a temperature value that uniquely defines it as a reference temperature point.

Firstly, no attempt should be made to correct the temperature value for impurities by adding cryoscopic corrections or by extrapolating to $1/F = 0$, because almost invariably the information available about impurities is not enough for a reliable correction. This restriction correspondingly demands that the purity of the substance used for the realization of the reference point be high enough that the uncertainty of the temperature value contributed by the total nominal effect of impurities is lower than the required accuracy of the reference point temperature.

Secondly, the inflection point of the temperature versus time plot should *never* be used, but the temperature versus $1/F$ plot must be used instead. The reference temperature is defined as follows:

> *Definition* The temperature value of a triple point realization, when used as a reference fixed point, is defined by the equilibrium value obtained in melting a sample with the adiabatic calorimetric technique at the liquidus point, defined as $1/F = 1$ and obtained by extrapolation from the melting plateau, within the melting range,[7] by means of the T vs $1/F$ plot.

The uncertainty of the value of T_{tp} thus defined arises from the fact that its value is obtained by extrapolation from a melting range $1/F = 2$–10 (from 1.5 to 3 if the curvature is pronounced, see Sect. 2.2.2.1). The main contribution to uncertainty is caused by the the thermal problems that develop at large liquid fractions and cause the melting plateau to gradually bend upwards. In general, the uncertainty of the T_{tp} value cannot be reliably limited to less than *one tenth* of the melting range.

[7] The melting range has been defined in Sect. 2.2.2.1.

2.3.2 *Chemical-Physical Problems in the Realization of Triple Points*

For accurate triple point realizations, the main problem discussed in the next section (Sect. 2.3.2.1) concerns the purity control of the gases used. Special precautions must be taken with reactive substances, whose use as reference points is, however, avoided whenever possible. With substances whose molecules exhibit different isomeric species, such as hydrogen, deuterium and methane (Sect. 2.3.2.3), equilibrium of the spin-species is necessary for a satisfactory triple point realization.

2.3.2.1 Effect of Substance Purity

In Sect. 2.2, the effect of impurities on the physical properties of a triple point has been analyzed. Considered here are their effects on the accuracy of the realization. A comprehensive database on mixtures can be found in Hiza et al. (1975, 1982). A critical review of literature data for the gases more important in thermometry can be found in Pavese (2009). Some of them are reported in Appendix C. The data indicate that several impurities for many substances affect the triple point temperature up to $\approx 50\ \mu\text{K ppm}^{-1}$ ($\approx 20\ \mu\text{K ppm}^{-1}$ for the most common gases), a value of concern for the most accurate realizations.

The use of a thermometric substance that is gaseous at room temperature is particularly sensitive to the impurity problem. In the first place, it must be noted that the ratio of the amount of substance stored in the container to that of the contaminants present in it is much smaller than with liquids or solids, owing to the much lower density. The walls of the container are covered with several layers of molecules in dynamic equilibrium with walls, not all molecules being of the thermometric substance. Desorption of each layer of such molecules from 1 m^2 of actual surface (equivalent to 0.1–0.3 m^2 of a geometrical surface of usual roughness) is equivalent to a contamination of about 10×10^{-6}/L of gas, which is a sizeable amount. For this reason, even research-quality gases supplied in "lecture bottles" often may result not complying with purity specifications (e.g. see Pavese et al. 1988). Consequently, it is difficult to certify gaseous reference materials (see Sect. 2.7).

Secondly, the substance is unavoidably manipulated when transferred from the storage bottle to the measuring cell and comes into contact with pipes, bottles, valves, ect. that can add to the sample new contamination of air or of different gases formerly used in the system, or because of leaks. A 10^{-8} W (10^{-2} Pa L s^{-1}) leak would introduce a contamination of $4 \times 10^{-7}\ \text{d}^{-1}$ in 1 L of substance.

Therefore, the manipulation of a thermometric substance requires a high-quality handling system and rigorous precautions (for further discussion, see Section "Gas handling systems").

In most cases, the presence of impurities can be detected from the size of the melting range (see Sect. 2.2.2.1), but seldom the triple point temperature value can be reliably corrected for the impurity effect to obtain the required value of T_{tp}. In

some cases, the impurity detection is not even possible with a thermal method—see Sects. 2.2.2.2 and 2.2.2.3. Moreover, when the melting range is wide, the best accuracy in obtaining T_{tp} by means of extrapolation of the melting plateau to $1/F = 1$ (Fig. 2.6) is no longer achievable. As already said, an empirical limit to the best accuracy is set to 1/10 the melting range.

When a substance cannot be obtained with sufficient purity, purification may be attempted. A method successfully tested has been "zone melting" of solidified gases (Ancsin 1972). In the liquid phase, fractional distillation can be applied, when the vapor pressure of the impurities is substantially higher than that of the solvent; higher purity levels have been obtained with ethane and propane (Pavese 1978a; Pavese and Besley 1981b). Distillation was also used for (temporary) purification of deuterium from isotopic impurities (HD and H_2; Ancsin 1988), by increasing in subsequent steps the vapor phase (thus obtaining a distillation of the liquid). A "purification" curve, giving an increasing value of the triple point temperature, was obtained. Extrapolation to 100 % vapor yielded the correct value of pure D_2.

Reactive Substances

Dangerous substances (CO, F_2, Cl) are generally avoided to establish reference points, though the use of permanently-sealed and passivated devices should eliminate all risk for users.

Though not poisonous, some gases interact with the residual gases in the cell, and thus tend to become contaminated; in some cases contamination tends to increase with time. The reference point would then produce a temperature value for the triple point that is not correct by an unpredictable amount, and drifts of this value in time would occur. Contamination due to interaction is probably the case with CO, and it is with D_2. With the latter, the presence of protium (H_2) molecules, unavoidable in any physical system, both in the bulk metals or as H_2O, is troublesome. Protium is easily exchanged, and an isotopic contaminant (HD) forms in large amounts (up to several 0.1 %), which affects the triple point temperature to an extent (2 μK ppm^{-1}) liable to sizeable errors in T_{tp} determination (Pavese and McConville 1987b). The amount of HD, however, proved to remain stable in time once the container is sealed off (Head 2001).

Gas Handling Systems

Handling of "research-grade" gases requires great care and an adequate handling system. Handling procedures, too, must be adequate. However, according to authors' experience, this is not often the case, even concerning the procedures adopted by the manufacturers (see Sect. 2.7). Figure 2.19 shows a high quality system; lesser-quality systems can be (and have been) used when manipulation is very limited, as in preparing sealed cells (see next section), but with some gases they would not ensure impurity stability in time.

Basically, the system shown in Fig. 2.19 is entirely made of ultra-high vacuum components with an internal diameter—just—large enough to permit an effective

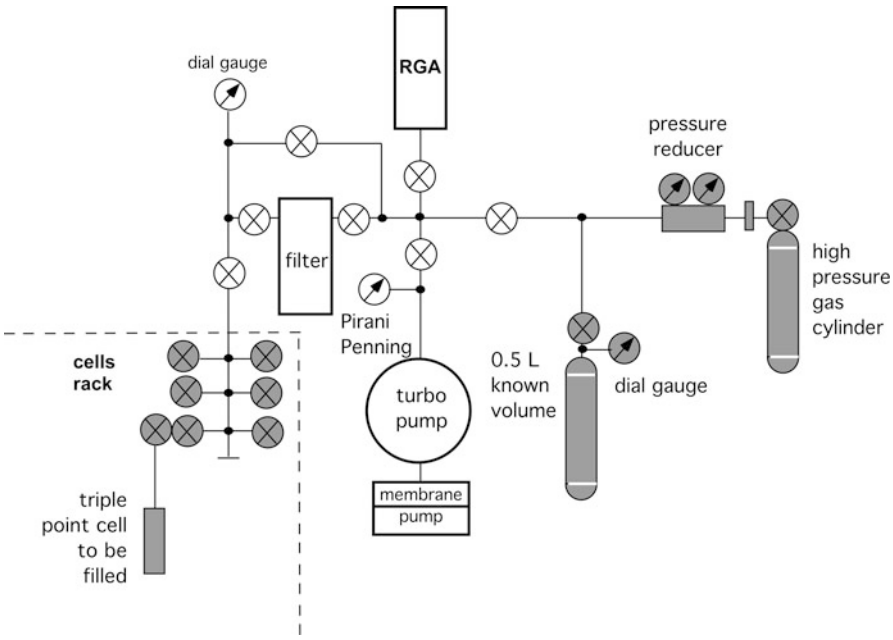

Fig. 2.19 Handling system for ultrapure gases. *RGA* residual gas analyzer

pumping speed (≈ 20 mm). A main pump of the turbomolecular type, backed by a membrane pump, is preferred, as it is clean and pumps nearly equally well all substances and without memory effects (ion, zeolite or cryogenic pumps do have). The latter requirement is a very important one when interchanging gases in the same system (handling system, sample container, etc.). Because memory effects are much more pronounced and difficult to reduce than is usually believed, a residual gas analyzer (RGA), e.g. a simple quadrupole mass spectrometer (having a range at least up to ≈ 50 amu) is *strongly recommended*. The analyzer may be equipped with an *independent* clean pump: a ion pump is convenient for this purpose, which can also be used, instead of the noisier turbomolecular pump, to keep the whole system under active pumping when it remains unattended for long periods of time, since good practice requires to keep the system continuously pumped and to open it to atmospheric pressure as little and for as short a time as possible. All components, including the pressure regulator of the storage cylinder and the manometers, must be of ultra-vacuum quality. The quantity of gas to be transferred is measured with a calibrated (1 %) volumetric setup.

The whole system *must* be repeatedly baked at a temperature that needs not to be higher than 100–150 °C, and subjected, in between baking treatments, to "washing" with the same type and quality of gas that is going to be used; at the same time, the disappearance of the air lines and the stabilization of the set of lines of the new gas in the residual gas spectrum are monitored. Contamination by oils or solvents from new or newly cleaned parts should very strictly be checked and no trace of it must

Table 2.7 Hydrostatic-head effect of condensed phases on triple point temperature

Substance	T_{tp} (K)	$dT_{tp}/dp/10^8$ K Pa^{-1}[a]	$dT_{tp}/dh_L/$ mK m^{-1}[b]
Hydrogen[c]	*13.8033*	34	0.25
Deuterium[c]	18.690	26	0.34
Neon	*24.5561*	16	1.9
Oxygen	*54.3584*	12	1.5
Nitrogen	63.151	24	1.7
Argon	*83.8058*	25	3.3
Methane	90.6935	26	0.9
Krypton	115.776	32	6.8
Xenon	161.406	39	10.4
Carbon dioxide	216.591	11	1.3
Mercury	*234.3156*	5.4	7.1
Water	*273.16*	−7.5	−0.73

Italic denotes the defining ITS-90 value
[a]Equivalent to mK bar^{-1}
[b]h_L = depth of condensed phases
[c]In spin equilibrium

appear in the spectra. Let us remark that, when a new species is introduced in the system, it is then extremely difficult and long to make its line disappear from the spectrum (e.g. Cl^+).

For some applications, e.g., for quantitative isotopic analysis, the RGA has to be equipped with a specific gas inlet system.

2.3.2.2 Effect of Hydrostatic Temperature Gradient

Any column of a substance in the gravitational field is subjected to a vertical pressure gradient caused by its weight. Therefore, in a triple point cell, a vertical temperature gradient occurs in the condensed phases, since the equilibrium temperature is pressure dependent.

In Table 2.7, the size of this effect at the liquidus point is quantified. With a tall cell configuration, in which the cell is filled with a tall column of liquid for use with long-stem thermometers (see Sect. 2.4.2), the correction for this effect can be sizeable. In the special case of helium baths, see Sect. 4.3.2.2.

2.3.2.3 Effect of Pre-melting, Namely Due To a Catalyst Contained in the Cell

It is well known that the melting temperature decreases near crystal defects (e.g. grain boundaries being inner surfaces, dislocations) and surfaces (Papon et al. 2002). This phenomenon can be simply explained by noting that the amplitude of atomic vibrations is higher at these sites than in the ideal bulk state.

Surface melting has been found in a variety of materials (rare gases in the solid state, metals and semiconductors, molecular solids) and at temperatures about 10 %

lower than the melting temperature of the bulk solid. Therefore, pre-melting (melting at temperatures below the melting temperature of the undistorted bulk material) of hydrogen sample portions in direct contact with the catalyst may be caused by either an increase in the distortion of the lattice via mechanical interaction with the catalyst or by an increase in the fraction of the sample at a surface or boundary. The depressed melting temperatures may equally result from the confinement of portions of the hydrogen sample in a restricted geometry such as pores, as has been observed for hydrogen in porous glass—e.g., Tell and Maris (1983), Torii et al. (1990), Schindler et al. (1996), and Beaudoin et al. (1996). In view of these results, this size could yield a melting-temperature depression of the confined hydrogen of about 10 mK. The premelting behavior of the hydrogen samples in cells was found to show premelting effects—see Fellmuth et al. (2005) for details.

The effect can show up (in hydrogen and deuterium samples) as a peak of heat capacity below the triple point temperature, as low as a few tenths of kelvin; or, as a double-peak structure at temperatures of ≈ -70 mK and ≈ -20 mK (about 6 % of the sample for the peak at $T - T_{\mathrm{bulk}} \approx 20$ mK): or as a double peak during the undercooling preceding freezing of the sample. They are definitely not a property of the hydrogen alone. They can be attributed to the presence of a catalyst—in form of powder or sponge-like. The increase of the (cell + sample) heat capacity, C_{c}, starts from ≈ -0.1 K.

To characterize the magnitude of the premelting, it is useful to calculate the ratio $Q_{\mathrm{PM}}/Q_{\mathrm{HF}}$, where Q_{PM} is the portion of the total heat of fusion, Q_{HF} that is necessary for completing the premelting. To determine Q_{PM}, the temperature dependence of C_{c} has to be carefully analyzed by considering a value C_{c0} for the heat capacity that is not influenced by the pre-melting, i.e. a value obtained at a sufficiently low starting temperature. From this analysis (Fellmuth et al. 2005, 2012), premelting results to occur up to 0.2 mK below the triple point temperature, thus a ratio $Q_{\mathrm{PM,0.2\ mK}}/Q_{\mathrm{HF}}$ of about 20 % can be deduced. For many observed cells with small catalyst-to-liquid volume ratio C_{LVR}, the calculated ratios $Q_{\mathrm{PM,0.2\ mK}}/Q_{\mathrm{HF}}$ are smaller than 15 %. In conclusion, one can say with remarkable confidence that the melting plateau of both the hydrogen isotopes becomes extremely flat once all the sample portion embedded in the catalyst mass is melted, and thus a bulk volume of free liquid is formed. The resulting typical shape of a full melting plateau is shown in Fig. 2.20, for cell containing a catalyst with different volume ratios to the sample.

No evidence is presently available of similar effects due to constrained interface in other cryogenic substances, except possibly with neon (Pavese et al. 2012c).

2.3.3 Thermal Errors in Sealed Cells and Related Problems in Measurement

Since the first edition of this textbook was published, important developments have been achieved concerning a better understanding of the thermal behavior of the sealed cells of the types described in Sect. 2.4.3, necessary to develop improved models

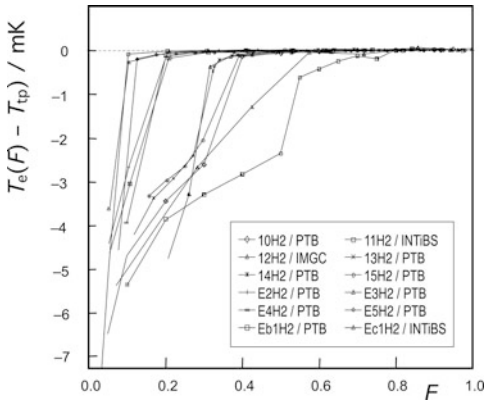

Fig. 2.20 Samples of e-H_2 in sealed cells (all INRIM-types, measured by the indicated laboratory) containing also a catalyst in different volume ratios to the condensed sample: premelting effect due to constrained interface (redrawn from Fellmuth et al. 2005). $T_e(F)$ equilibrium melting temperature at melted fraction F, T_{tp} liquidus point temperature

of these cells, sometimes with contrasting results (see Pavese 2003c; Pavese et al. 2003b, 2010b; Fellmuth and Wolber 2010; Wolber and Fellmuth 2008, 2011; Hill and Fahr 2011). However, different cell models can have quite different geometries, and modeling is generally limited to a simple geometry, applicable only to a few specific types of cells. In general, the spatial distribution between solid and liquid phases is largely a matter of speculation or inference: no experiment has been devised so far to get a picture into the inside of a cells—e.g. using optical fibers and cryogenic cameras as done in other fields of physics.

By thermal behavior, we mean the relationship between the temperature of the solid–liquid interface and the temperature indicated by the thermometers.

There is a thermal transient after each heating pulse with a recovery time constant that can be large or small depending on the cell design. An insufficient recovery causes a dynamic temperature measurement error. On the other hand, if there is a stationary heat flux crossing the cell (due to the residual heat exchange with its surroundings), a stationary temperature value is obtained after the transient, which apparently indicates that thermal equilibrium is reached, while it is in fact wrong. Stationary temperature measurement errors may be caused by the steady temperature difference between the thermometer and the interface due to the heat flux. Therefore, it is generally agreed that there are two types of possible errors occurring in evaluating the equilibrium temperatures—one stationary, called R_{cs} and the other dynamic, called τ.

2.3.3.1 Stationary Temperature-Measurement Errors

For fixed-point realizations, the temperature of the solid-liquid interface must be measured as accurately as possible. Temperature gradients inside a sealed triple-point cell (STPC) are dominated by the liquid phase. Thus, the thermal resistance R_{cs} between the metallic body of the STPC and the solid phase, which cannot overheat during melting, is a crucial parameter for characterizing the thermal conditions. R_{cs} is given by the relation $R_{cs} = \Delta T_{cs}/P_s$, where ΔT_{cs} is the temperature difference

between the metallic body and the condensed phase, and P_s is the thermal power caused by heat leaks or by heating. The magnitude of R_{cs} depends strongly on the STPC geometry, which influences the mean thickness and the area of the liquid layer formed between the metallic body and the solid phase. This means the thickness, and thus R_{cs}, may increase significantly with rising fraction F of sample melted, i.e. especially the end of a measured melting curve may deviate significantly from the equilibrium curve due to heat leaks. If the power P_s is sufficiently small, the difference ΔT_{cs} is nearly constant under steady-state conditions because the relative change of the mean liquid-layer thickness with time is small. If the power is too large during heating, steady-state conditions cannot be reached and a reliable determination of R_{cs} is not possible. Reliable R_{cs} data are necessary for estimating the upper limit for the parasitic heat load P_s during the measurement of the melting curve. If nearly isothermal conditions are realized with sufficient stability, P_s can be determined from the drift of the STPC temperature outside the melting plateau. The limit for this drift is given by the following maximum estimate: the temperature drift dT/dt outside the melting range caused by a parasitic heat load is $P_s = C_c\, dT/dt$, where C_c is the heat capacity of the STPC and t is the time. This heat load causes a temperature difference ΔT_{cs} between the metallic body of the STPC, and thus the thermometer in thermal contact with the metallic body, and the solid phase.

For a maximum estimate, it should be assumed that the whole parasitic heat flows through R_{cs}, i.e. ΔT_{cs} is at most equal to $C_c\, dT/dt\, R_{cs}$. If ΔT_{max} is the maximum allowed stationary error of temperature measurement and $R_{cs,max}$ is the maximum R_{cs} value in the F range of interest, the upper limit for the drift of the STPC temperature outside the melting range is reliably estimated by the expression $(dT/dt)_{max} = \Delta T_{max}/(C_c\, R_{cs,max})$.

Residual stray heat flow is usually evaluated through the measurement of the temperature drift just before the start of the melt. The experience has shown that the thermal drift measured immediately below melting may be erroneously considered valid for the whole duration of the melting—the drift that may additionally be measured at the end of the plateau is generally not reliable at all. Disagreement by up to more than one order of magnitude has been observed. Therefore, another way to evaluate R_{cs} is during the melting, by the size of the overheating during the heat pulses: in this case, the heat supplied is precisely known, but the path followed by this energy can be different with respect to the one applicable to the stray heat, so the values obtained for R_{cs} may be different.

The value of R_{cs} can be widely dependent on the cell model, as shown in Fig. 2.21 for all stainless steel and all copper constructions, using the latter method. In addition, depending on cell model, the R_{cs} also as a function of F can be different, however always increasing with F. As expected, an all-copper cell shows a lower R_{cs}—compare (a) and (c)—and more stable for increasing F—see (c).

Note that, for $R_{cs} = 1$ K/W, an inflow $P = 10$ μW would produce an *increase* of 10 μK of the measured temperature with respect to the true equilibrium value (defined as the one for null P). Such a seemingly irrelevant heat flow value may thus be close to the admissible limit of the total desired uncertainty. It can easily be checked from the measured value of the enthalpy change in melting: in cells containing

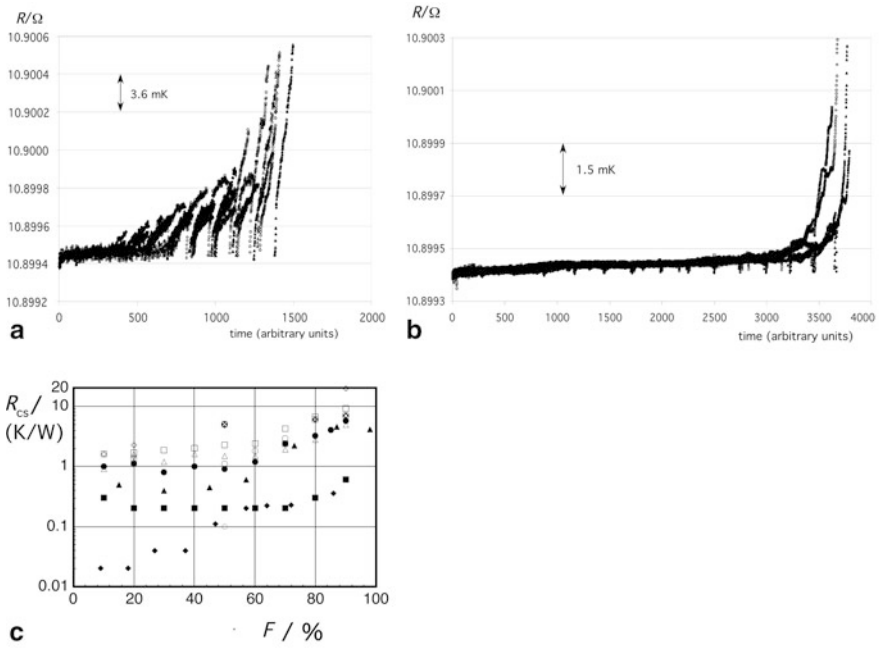

Fig. 2.21 Overheating during heating times in cells. **a** All stainless steel construction. **b** All copper construction, in repeated meltings (compounded un-retouched plots). **c** Values of R_{cs} for several cell models (different symbols) as a function of the melted fraction F. (After Pavese et al. 2010)

about 40 mmol of substance, this inflow introduces an energy of 1.7 J for a melting lasting 24 h. For Ne, H_2, O_2, and Ar, this corresponds to 2.5 mmol, i.e., 6 % of the sample enthalpy change in melting, 7.5 mmol (15 %), 2.0 mmol (5 %), and 0.7 mmol (1.7 %), respectively.

2.3.3.2 Dynamic Temperature-Measurement Errors

The dynamic behavior of the STPC determines the thermal recovery after a heat pulse. This thermal recovery may deviate significantly from a simple exponential law if complex temperature profiles exist in an STPC after heating, i.e. in general, a simple RC model is only a rough approximation. Nevertheless, it is convenient to characterize the order of magnitude of the minimum period required to attain thermal equilibrium by a time constant τ. For a simple RC model, the relation $\tau = R_{cs}\ C_c$ is approximately valid. The minimum necessary recovery period $t_{r,min}$ can be estimated roughly by applying the relation $t_{r,min} = \tau\ \ln(\Delta T_{cs}/\Delta T_{max})$, where ΔT_{cs} is the initial overheating and ΔT_{max} is the maximum allowed dynamic error of temperature measurement. However, the simple RC model holds only for the relatively quick recovery of the metallic body of the STPC with respect to the adjacent layer of liquid phase. Thus, only the first quick part of the recovery corresponds

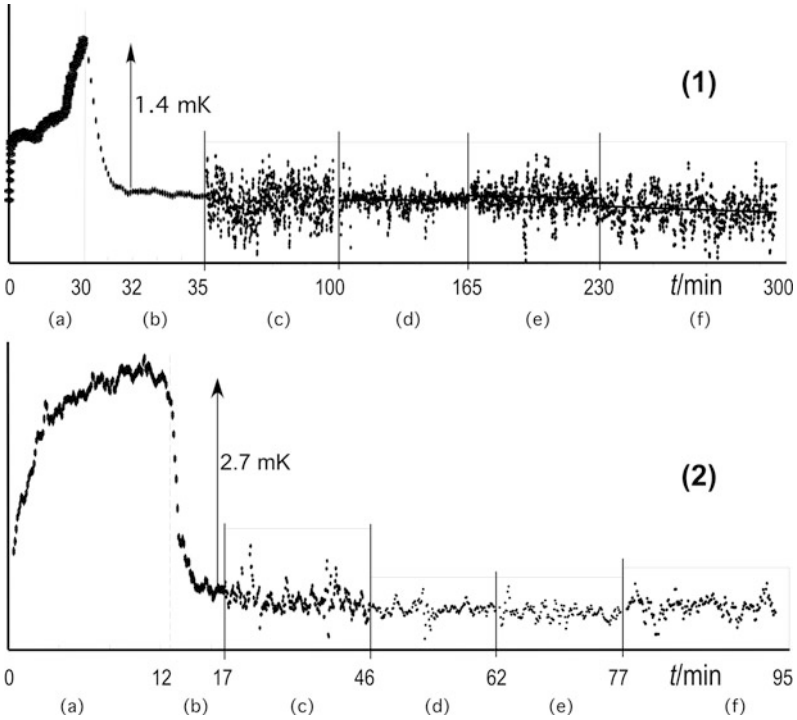

Fig. 2.22 Examples of heat pulse and return to equilibrium for: *1* all copper; *2* all stainless steel cell constructions. Measurements at the neon triple point. Each example is made of six unretouched contiguous computer records. The sequence is measured: *a* during heat pulse, *b* at return to equilibrium, *c–f* to check that equilibrium is effectively reached over the long term. On ordinates, the resistances in ohm, *not to scale*, on abscissas, the time scale in minutes are reported. Case *1*: all-copper cell, $F \approx 85$ %. Total drift: $c + 1$ μK, $d + 2$ μK, $e - 1$ μK, $f - 5$ μK. Case *2*: all-stainless-steel cell, $F \approx 75$ %. Total drift: $c - 10$ μK, $d + 11$ μK, $e - 8$ μK, $f - 3$ μK

roughly to an exponential time dependence, and τ depends strongly on the thermal conductivity of the metallic body of the STPC. Often a long creeping is observed as a second part of the recovery. In this second part, thermal equilibrium is reached in the liquid phase. Because it is dependent on the thickness of the liquid layers and the thermal diffusivity of the liquid, this equalizing process may last much longer than the exponential time dependence. It is, therefore, dangerous to estimate the overall necessary recovery time from the magnitude of the time constant τ only. Also the recovery time of temperature within, e.g., 20 μK from the equilibrium temperature is a useful additional parameter. Its determination requires waiting, for each F value of interest, until the asymptotic (i.e. true equilibrium) temperature is definitely reached. Though in some apparatus τ may be quite longer than expected, requiring hours before full equilibration also at the temperature of the triple point of neon (≈ 25 K), in other apparatuses quite short equilibration times have been observed, as shown in Fig. 2.22 for the two extreme types of cell constructions.

2.4 Modern Design of Temperature Fixed Points Based on the Triple Point of Gases

During a traditional realization of a triple point, after the desired amount of gas has been condensed in a container fitted into the cryostat, the sample of gas is obviously sealed into the apparatus, by closing the valve connecting the cryostat to the filling system (Fig. 2.19). This sample can be further manipulated in different ways by evaporating it back to the filling system, but, at the end of the experiment, the cryostat is warmed up to room temperature and the whole sample is usually discarded. If at a subsequent time, from a few days to many years, another measurement has to be carried out, another sample of gas will be used, generally taken from another storage bottle. In the meantime, the results of the previous measurements remain "stored" and available *only* by means of thermometers, used during the measurements with the reference point and supposed to remain stable in time.

This old procedure has many disadvantages. First, the fixed point is not readily available at all times for a new realization, except during the short period when the measurements are carried out. The storage of results in thermometers has proved to be not reliable, as they often are not stable enough in time (seldom a stability of ± 0.1–0.3 mK in 10 years have been observed). In addition, the old procedures are not routine measurements, but each time they are actually *new experiments*, as a new sample of gas is generally used and, consequently, the degree of its purity has to be ascertained anew, a far from a trivial task. As already pointed out, because of the necessary new manipulation of the gas, it is again possible that the sample will become more contaminated than certified by the supplier. Consequently, it is not surprising that in the past the measurements at the fixed points were not made routinely, and that only calibrated thermometers were used instead, until the technique of permanently sealing the sample in a cell was perfected.

2.4.1 The Technique of Sealed Cells for the Realization of a Temperature Reference

The new technique has been developed since the beginning of the 1970s of the past century (first published paper: Pavese 1975a), though there exist a few examples of an earlier use (Ambrose 1957; Furukawa et al. 1972). With liquids and solids, the method had been used a long time before in calorimetry for the two main reasons, of sample purity preservation, and of thermal contact improvement of powder samples by addition of helium gas. With gaseous substances, purity preservation, as made possible by permanent sealing and the consequent elimination of further gas manipulation, is the aim. Consequently, the sample properties will remain those first measured after sealing. However, this goal is only achieved if the container does not contaminate the sample. This is relatively simple to obtain with most solid or liquid samples, whereas, it is not, generally speaking, easy to achieve with gases

for the reasons already mentioned in Sect. 2.3.2. More than 30 years of experience has shown, however, that this method can be used with most gases (Pavese et al. 1975a, 1984a, 1992b; Bonnier 1975; Pavese and Ferri 1982; Pavese 2003c), and the values of T_{tp} obtained with sealed cells have proved to remain stable within a tenth of millikelvin over a period of time of decades (Pavese 2012a).

The design of a permanently sealed cell substantially differs depending on whether the vapor space must extend to room temperature or need not. In any case, in comparison with a traditional experiment, there is a substantial difference: *the realization of a permanent, accurate, and stable fixed point*.

It is quite inconvenient to use as many different cryostats as there are fixed points. Therefore, the cryostat itself has to be drastically simplified and tailored to the requirements of the triple points, which will be shown to be little demanding; or, conversely, the cells must be made *independent* of the cryostat, so that they can be interchanged in an individual cryostat.

Another special feature of sealed cells is that they must be suitable to withstand a high sample pressure, as the ratio of the condensed to room temperature gas volume typically approaches 1000 (see Table 2.1). This problem is solved in different ways with cells of essentially two types.

2.4.1.1 Cells with Vapor-Space Extending to Room Temperature

This extension is needed only when the vapor pressure is to be measured with a room temperature transducer, that is in the case of the realization of vapor pressure scales (see Chap. 4), or of pressure fixed points (see Part II, Chap. 9). Therefore a full description of this type of use is given in Chaps. 4 and 9. However, this is also the configuration of cells whose sealing valve is located at *room temperature*, even if pressure needs not be measured.

The lower part of the cell in question (called a "*long-stem*" cell) can be similar, in principle, to that shown in Fig. 2.13 and discussed in Sect. 2.3.1.1. The vapor tube connecting the heat exchanger to the sealing valve at room temperature must be vacuum jacketed in order to avoid cold spots during cooldown. The pressure in the sealed cell, when it is stored at room temperature, needs not be particularly high, as a condensed sample of few cubic centimeters is sufficient to fill the measuring chamber, and a 0.5 L to 1 L ballast volume can conveniently be added to the cell at room temperature. The gas pressure at room temperature is therefore typically limited to less than 0.5 MPa, without any other effects than an increase in the vapor space. However, since a large increase of the vapor space may cause a substantial increase of the cell re-equilibration time (see Fig. 4.7), it is advisable to add a valve to seal off the ballast volume after condensation.

2.4.1.2 Totally Cold Cells

As the temperature of a triple point does not depend on pressure, this need not be measured for triple point realization (see Sect. 2.2.1). The sealing device of the cell

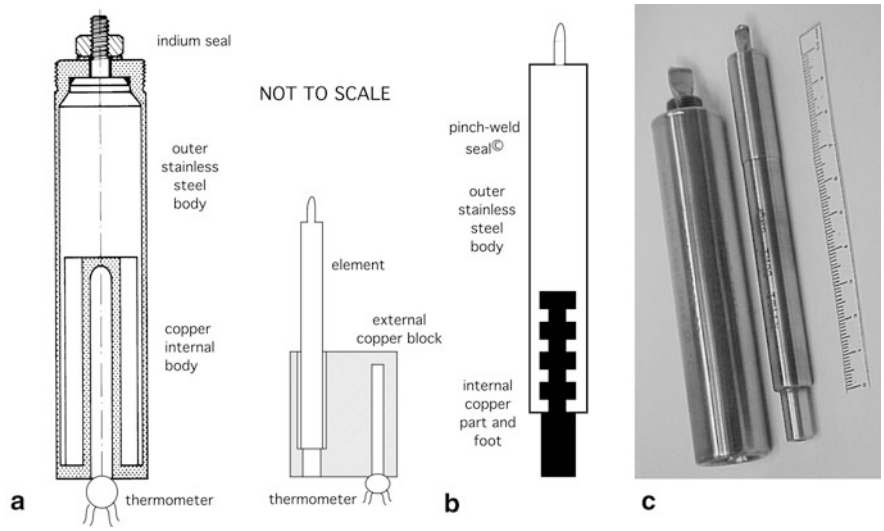

Fig. 2.23 Layout of typical sealed cells for capsule thermometers ("temperature generators"—see text): **a** with inner block and indium seal (old fashioned); **b** with external block (mod. a—see Fig. 2.33): the internal copper body transfers the interface temperature to the external thermometric block; **c** a picture of both models—but (**a**) using a pinch-weld too (rule graduated in centimeters)

can therefore be located at low temperature, on top of the measuring chamber. After chamber filling, this device need not be opened again, as the cell no longer requires to be connected to the filling system. Consequently, the cell can be maintained permanently sealed and *can be totally contained* in the working chamber of the cryostat.

This greatly simplifies cell design because the distinctive features of the cells described in the preceding sections are the necessity of avoiding cold spots in the vapor pressure tube and of avoiding excessive heat exchange via this tube and the vapor contained in it.

With a cold seal (and consequently, without a ballast volume at room temperature), pressure in the cell is quite high, owing to the limited volume of the cell. The cell size in any case depends mainly on its intended application—apart from its use as a thermostat or a shield (see Chap. 6)—and, in particular, on the number and type of thermometers which are to be inserted in it for calibration.

Sealed Cells for Capsule Thermometers (Fig. 2.23a, c)

A small amount of condensed sample is sufficient for a cell of this type. When the size of the inner measuring block (Fig. 2.23a) is large enough to accommodate three standard PRTs, a sample liquid volume from 1 cm^3 to 5 cm^3 is sufficient. With an external block (Fig. 2.23b), 1 cm^3 to 2 cm^3 is a liquid volume sufficient with most gases.

Therefore, most of the cell volume is required *only* in order to limit the gas pressure at room temperature to a value generally less than 20 MPa. This pressure value is the maximum allowed by gas storage cylinders when the direct filling method of the cell is used. On the contrary, filling by cryogenic condensation (see Section "Cell filling" and Summary 2.12) has no intrinsic limitations as to pressure; however, with increasing pressure, the mechanical strength of the cell materials becomes increasingly more critical and the mass of the cell larger (see also Sect. 2.2.1 and Table 2.1 for absolute pressure limits). In all instances, cells of the model shown in Fig. 2.23b should be tested to withstand pressures up to 100 MPa.

The full cell design and procedure for construction is given in Summary Tables 2.12 and 2.13 at the end of this Chapter. Here, only the specific problem of an upper limit for the mass of the cell and of its addenda will be discussed.

The condensed gas temperature is much less affected by thermal exchanges with the environment at the triple point than at any other point of the vapor pressure line, because of the isothermal enthalpy change associated with the solid-liquid phase transition. Energy can be released or adsorbed, up to a maximum amount $\Delta_{\mathrm{fus}} H_m \cdot m_{\mathrm{g}}$ (with $\Delta_{\mathrm{fus}} H_m$ = molar enthalpy of fusion of the cell and m_{g} = sample mass), whereas temperature changes are limited to the melting range (Fig. 2.6). This change can even be much smaller than 1 mK with most of the purest gases listed in Table 2.1. However, this temperature stability can noncritically be achieved only within certain limits for the "thermal mass" ($c_p m_{\mathrm{C}}$, where c_p is the specific heat of the container and m_{C} its mass) of the sample container—i.e. of the cell. These limits are approached when the thermal mass is so large that the energy corresponding to a phase change (freezing or melting) of a large fraction of the sample is required in order to maintain the cell temperature stable. If this energy is too high, thermal gradients can more easily develop and make the cell to behave in a way similar to that observed in the application of the dynamic method (see Sect. 2.3.1.1). Even before this limiting situation occurs, the thermal equilibration time may become longer (because of limited thermal diffusivity), so that it may be more difficult to eventually attain true thermal equilibrium; or else, thermal perturbations may permanently keep the cell in a nonequilibrium state. These problems can be more serious in a cell having an external block (Fig. 2.23b): here also the additional thermal resistance between the cell foot and the block must carefully be minimized.

The last column of Table 2.8 shows the values of a parameter X, denoted here "driving capability", which is an useful indicator allowing to become aware of the approach of the unsafe situation described before: it indicates the mass of copper made to change its temperature by 1 mK, by a 0.1 mol sample changing by 0.1 % its melted fraction. The typical range of values for the main parameters of cell design are also given in Table 2.8, according to the parameter range tested in real cells (see Sect. 2.4.3). However, also cells outside with lower values of X can be measured accurately, but demanding a higher quality to the calorimeter.

The three constitutive elements of a sealed cell are the container, the inner body in thermal contact with the solid-liquid interface, and the sealing device.

Table 2.8 Typical design parameters for triple points in small sealed cells

Substance	T_{tp} (K)	ρ_{tp}/ρ_{NTP}[a]	$X = \Delta_{fus}H_m/c_p$ (kg K mol^{-1})[b]	m_{min} (mmol)[c]	$1/X_c$ range (10^{-6} mK^{-1})[d,e]	X (%)[d,f]
Hydrogen[g]	*13.8033*	1040	50	6	1.5–6	20–70
Deuterium[g]	18.690	1040	40	5	40–130	10–25
Neon	*24.5561*	1730	24	15	2–40	7–160
Oxygen	*54.3584*	980	3.8	100	20–370	6–120
Nitrogen	63.151	815	4.9	100	45–360	6–45
Argon	*83.8058*	980	5.6	100	17–285	6–100
Methane	90.6935	680	4.2	100	18–70	30–120
Propane	85.528	310	16.3	30		
Ethane	90.360	480	2.6	30		
Krypton	115.776	810	5.9	100		
Xenon	161.406	650	7.0	50		
Carbon dioxide	216.591	820	24.0	20		

Italic denotes the defining ITS-90 values
[a] T_{tp} triple point temperature
[b] Density ratio between the liquid (in cm^3) at T_{tp} and the gas (in L) at 20 °C
[c] X = "driving capability" (see Section "Sealed cells for capsule thermometers")
[d] Minimum sample mass recovering a 0.1 mK variation in 0.5 kg of copper with a F variation smaller than 0.1 %
[e] For the cells of Figs. 2.32 and 2.35 (Pavese et al. 1984a)
[f] $1/X_c$ is the ratio of the copper-equivalent cell thermal-mass ($m_c \cdot c_p$) to the sample heat of fusion, in parts per million of F per millikelvin of temperature variation
[g] Value of X_c as a percent of X; values <10 % are typical of multicell devices
[h] In spin equilibrium

1. *Container*. Any material can be used for its fabrication, provided it withstands the high internal room-temperature pressure. It takes account of most of the cell mass. The use of materials having high thermal conductivity promotes uniform temperature throughout the entire sample, but increases the thermal coupling between the heater and the thermometers.
2. *Inner body*. This element may contain the thermometers, as in Fig. 2.23a, or it may be used only to transfer the interface temperature to an external thermometer block, as in Fig. 2.23b. It is usually made of OFHC copper (however, in case A) it can be safely made of stainless steel, since completely surrounded by the sample). It needs fins or baffles, to ensure a good thermal contact with the *solid* phase for as large a melted fraction as possible; however, the larger the inner cell surface is, the more critical the problem of sample contamination may become.
3. *Sealing device*. The seal must remain leak-proof for an indefinitely long time, under thermal cycling from room temperature to that of the cryogenic environment during each cooldown. A variety of types (described in Sect. 2.4.3), ranging from indium O-ring to pinch-off and pinch-weld® seals have been successfully used, the latter being by far the safest one.

A minimum of two cell elements must be assembled: the container and the block. Elements can be assembled by brazing or by welding. Soldering is never considered

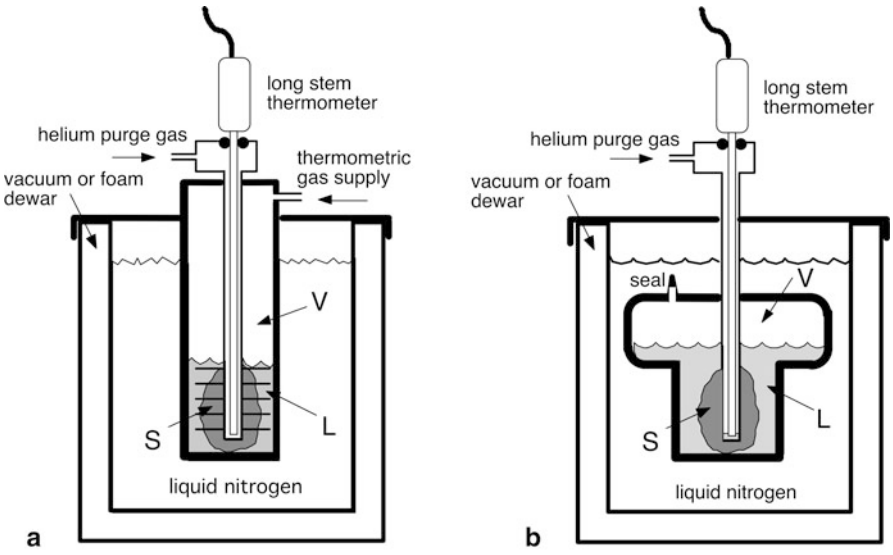

Fig. 2.24 Layout of typical sealed cells for long-stem thermometers. **a** Type with seal (or filling) at room temperature. **b** Totally cold type with permanent seal

for two reasons, (i) the need of using fluxes that cannot possibly be fully removed and, (ii) the need for a high temperature cleaning of the cell for its conditioning prior to filling. From the standpoint of a clean assembly, welding is preferred, but some technological problems may arise when the two elements are made of different materials.

Sealed Cells for Long-Stem Thermometers (Fig. 2.24a, b)

This sealed cell type, not to be confused with the long-stem type for capsule thermometers (Sect. 2.3.3.1), chronologically was first fabricated for carbon dioxide (Ambrose 1957) and argon (Furukawa et al. 1972). Its typical feature, even when the whole sample is kept at a low temperature, is that the thermometer itself must be able to extend up to room temperature (a thermometer of this type is used only down to the liquid nitrogen temperature). A problem peculiar of such thermometers is the so-called "immersion error". The stem above the sensing element (element itself about 5 cm long) and the four wires connected to it bring some heat into the cell, by conduction and through the helium gas used to improve thermal contact between the stem and the cell well. This heat, if not entirely dissipated before flowing into the cell, partially overheats the sensing element or alters the temperature distribution in the cell, producing an extra overheating of the liquid phase. In practical instances, to avoid these effects the cell is required to provide a uniform temperature to a depth of

at least 10 cm from the bottom of the thermometer well—with the usual thermometer stem of 6 mm diameter. A more satisfactory solution is a thermal tie-down of the thermometer stem close to or at the measured temperature, far enough from the sensing element.

A small cell for capsule thermometers can be adapted for this use, provided it features an upper thermometer well and is used with a special cryostat (see Sect. 2.4.3.2).

Alternatively, a special cell can be designed, shown in Fig. 2.28b, used, as described in the same section, for the realization of the triple point of argon (the lowest ITS-90 reference point for a long-stem thermometer). This cell incorporates a cryostat of specific and greatly simplified design, exploiting the fact that the nearby temperature of a convenient refrigerant, liquid nitrogen, is available. These cells uses a much larger sample of gas (about 1–2 mol) than commonly the cells for capsule thermometers are, and the cell container itself is much larger, so as to limit the internal pressure to less than 5 MPa. With samples of this size and warming at slow rates, the dynamic technique for performing the melting plateau can be used.

Cell Filling

Filling is performed through the gas handling system (Section "Gas handling systems"), where the cell has been connected for its initial conditioning (outgassing and, when required, catalyst activation). When the cell is filled at room temperature and at the gas cylinder pressure, a high-pressure valve and a bypass tube from the cylinder to the cell are used as well. However, this technique has the disadvantage that only a small part of the—often costly—gas available in the cylinder can be used.

A better way is the cryogenic filling technique. A quantity of gas measured with the volumetric section is introduced into the gas handling system; then the cell is cooled down until the whole gas sample condenses in it. This is trivial enough with gases condensing at or above liquid nitrogen temperature (≈ 77 K). Even with helium, a complicated dewar system is *not* necessary, as cooling down below about 10 K and for only few minutes is required; this can be achieved simply by placing around the cell (connected to the system with a stem at least 20 cm long) a plastic foam bottle, through the perforated cap of which also the helium transfer tube is inserted. No precooling with liquid nitrogen is necessary. In a few minutes, by evaporating $< \approx 1$ L of liquid helium, one can easily cool the cell enough to achieve full sample condensation.

When the gas vapor pressure at the refrigerant temperature is still high (e.g., in argon condensation by using liquid nitrogen), the part of the gas remaining in the handling system after sealing is a sizeable part of the total amount and must be taken into account when calculating the amount of gas to be actually sealed into the cell. Then the pinch-weld seal can be made (two of such sealed are necessary when using condensation via liquid helium refrigeration, the second in order to remove the 20 cm stem extension.

Finally, *the mass of a sealed sample can be accurately measured*. This is done by weighing the empty cell before mounting—taking into account the air initially contained in it—and then weighing the filled cell after sealing. Weighing of the sample mass cannot be performed accurately only when the cell contains a hydrate catalyst, whose mass change (due to loss of water) during cell conditioning cannot be calculated accurately. In addition, a constant-mass sealing device must obviously be used necessarily (Pavese and Ferri 1990c—see also Patents for the same names).

2.4.2 *Further Checks Necessary to Achieve a Total Uncertainty of ≈ 50 μK in Triple Point Best Realizations*

The following provisions, additional to the parameters of the previous Sections (and Summary Table. 2.14), are also useful to obtain the lowest uncertainties according to the state-of-the-art at the date of this edition, with a higher confidence level, since they allow better understanding of the effects of all influence quantities that affect a fixed-point realization. The modern use of a computer-aided experimental control and data acquisition of a fully automated system is of great help to collect the necessary information (Pavese et al. 2010b).

2.4.2.1 Use of Information Collected During Measurement of a Single Melting

a. *Accuracy and reproducibility of the enthalpy change in melting.* The enthalpy change of melting of the full sample should differ by less than 1 % from a *known value* for the sample obtained preliminarily. This check is possible when the sealed amount of substance is measured by weighing, with an accuracy of a few 0.1 mg, corresponding to a relative standard uncertainty in the amount of substance from a few parts in 10^3 to 5 parts in 10^5, depending on the substance and cell. For cells where the sealed amount of substance is not precisely known, one should ensure an equivalent *reproducibility*. Experience has shown that for a discrepancy higher than about 2 %, anomalous values can be found for the equilibrium temperature values, especially at high F. Enthalpy changes in melting accurate to 0.2–1 % correspond to an average heat intake of 0.6–3 μW for cells containing 40 mmol of neon and for a melting lasting 48 h.
   Various other parameters may also affect the degree of adiabaticity of the calorimeter, such as: (i) the fraction of heating time to total melting duration, during which the temperature of the adiabatic shield might track the cell temperature less accurately due to cell-wall overheating (to some extent also depending on F-item (h)); (ii) the fraction of stray heat to the total supplied heat; (iii) the fraction of heat generated by the thermometers to the total supplied heat.
b. *Temperature difference between cell and adiabatic shield and effect on observed equilibrium temperature.* The plot of the difference $\Delta T_{\text{shield}-\text{cell}}$ between the cell

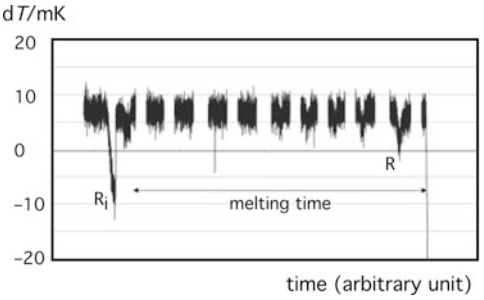

Fig. 2.25 Value of $\Delta T_{\text{shield}-\text{cell}}$ as recorded during a typical melting. R_i initial recovery before melting starts; R recovery after a heat pulse for high F values

and the adiabatic shield *must* be measured over the full melting time. Should any anomaly occur, e.g., slow recovery to thermal equilibrium after a heat pulse, or inversion of $\Delta T_{\text{shield}-\text{cell}}$ at any time during the melting, one should check for possible corresponding anomalies on $T_{e,i}$—the final equilibrium temperatures for increasing F. To understand this effect, it is also necessary to change the cell-shield difference at least once by a known amount during at least one of the meltings, and preferably for more than one F value, because there is always an effect of $\Delta T_{\text{shield}-\text{cell}}$ on $T_{e,i}$, due to the dependence of R_{cs} on F. This check is supplementary to the check of R_{cs} required by the procedure in Sect. 2.3.3.1, and to the information supplied by the overheating observed during the heating pulses using the heater mounted on the cell—see (h). In fact, the effect on the thermometer reading may depend on the path of the stray heat.

Figure 2.25 shows how stable can be $\Delta T_{\text{shield}-\text{cell}}$ during a melting—better than 1 mK after a possible small transient for high F values, where one must ensure that the value does not become negative.

c. *Check of sample thermal re-equilibration after each heat pulse*. The sample overheating, observed during a heat pulse that increases F, recovers after the end of the pulse with a time constant τ—see Sect. 2.3.3.2. The dynamic effects, as re-analyzed in detail in Wolber and Fellmuth 2008, in relation to the samples' thermal history (freezing/melting and annealing cycles), stressed the need to wait, under certain circumstances, a very long time for true thermal equilibrium. Since this effect can produce substantial errors in the evaluation of $T_{e,i}$, true re-equilibration has to be checked by performing various meltings with different re-equilibration times between heat pulses, to ascertain if this issue is confirmed, or one can expect a (even much) shorter equilibration time, as that shown in Fig. 2.22.

d. *Comparison of different thermometers: electrical noise in measurement*. Valuable information is obtained by comparing the values measured by several thermometers mounted on the sealed cell. With old cell models that allowed only one thermometer at a time one obtains only results with a lower confidence level. Electrical noise can contribute considerably to the dispersion of the equilibrium values for increasing values of F. It can vary from day to day or during a day, or due to experimental artifacts such as a scanner channel becoming noisy. In observed extreme cases, the electrical noise level in one channel can be of the order of 1–7 $\times$ 10^{-6} Ω instead of the usual 1–3 $\times$ 10^{-8} Ω preventing a reliable fit of

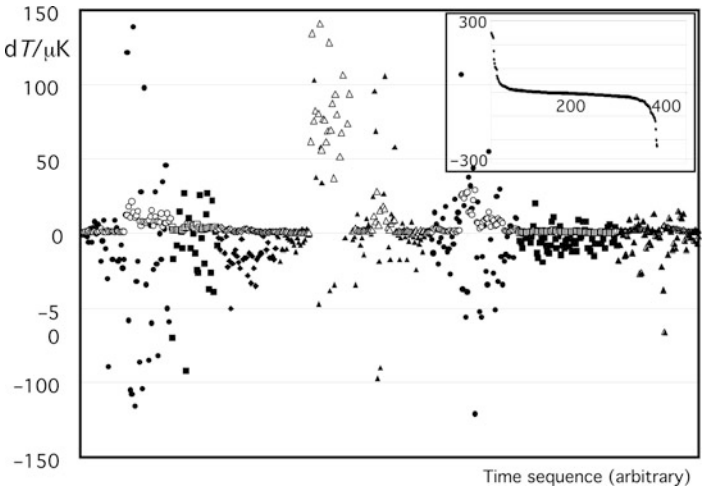

Fig. 2.26 Plots in time sequence (in abscissa) of the maximum drifts ($T_{i,\text{last}} - T_{i,\text{first}}$) (full symbols) observed over each series of readings forming the dataset for computing each of the $T_{e,i}$. Also the corresponding standard deviation of the mean is reported (open symbols), showing the correlation between the measurement electrical noise and the apparent observed drift. The *insert* shows the same ≈ 400 data point ordered according to their values (ordering number on the abscissa). Ten are in total the points outside the figure, with a drift or s.d. value exceeding 150 μK

the melting slope and determination of a reliable value for the liquidus point. In this case, the resulting liquidus point temperature can still be close to the normal value but with a variance quite larger than typical. In fact, a high level of electrical noise does not necessarily affect the values of $T_{e,i}$, if the latter are computed by averaging a large set of readings (typically > 100).

Figure 2.26 shows how large can be the variability of electrical noise during measurements spanning several months.

An additional benefit is that, given the large number of readings, the standard deviation of the mean for each measured value can be used, thus providing a statistically sound ground and more significant than the standard deviation of the set of readings (providing that the thermal drift—see item (i) —is sufficiently small for the readings to be considered repeated measurements).

e. *Comparison of different thermometers: self-heating from the measurement current.* Measured self-heating at several F values of each thermometer provides an additional check of the reliability of the measurements. Variability of the self-heating from cell to cell and from thermometer to thermometer of the same type is indicative of possible problems with the thermometer/cell thermal resistance—see also item (g).

f. *Comparison of different thermometers: calibration stability in time*. When comparing cells the thermometers must be stable in time. When differences between them are reproducible, anomalous values can be used as a criterion to detect unreliable meltings. The use of the Least Squares Method with Fixed Effects (LSMFE)

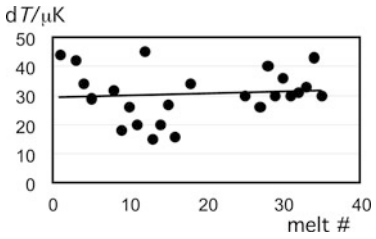

Fig. 2.27 Differences between two calibrated thermometers over the 35 melting plateaus performed in a time span of 12 months: differences obtained from application of LSMFE to all meltings separately for each cell: mean value (30 ± 9) μK. A few values exceeding 50 μK are omitted

(Pavese and Ciarlini 1990b)—see also item (k) —is particularly useful for this computation. Figure 2.27 shows the differences with time of two thermometers measured in subsequent meltings over a period of several months.

2.4.2.2 Use of Features and Information Collected During Data Analysis

The following additional checks, further to the procedure in Sect. 2.3.3, are shown to be useful relative to the comparison of the differences in cell pairs.

g. *Correction for thermometer self-heating (final liquidus-point resistance values only).* When the data used for the final analysis are corrected to zero current, $I = 0$, in the thermometers, the data set is constructed through pairs of resistance measurements performed at currents I and $\sqrt{2} \cdot I$. As indicated ahead, in addition to a 'normal' variation due to electrical noise affecting the measurements at both currents, the self-heating value can be anomalous (e.g., due to incorrect mounting of a thermometer). Therefore, it is important to check if changes in the overheating values affect the overall uncertainty of the dataset. This can be done by comparing two methods of data analysis: (1) by using *each* measured value corrected for the (average) thermometer self-heating measured in the relevant melting; (2) carrying out the whole analysis *without* correction to $I = 0$, and then correcting only the liquidus-point resistance value of each melting (or set of meltings) using an *average* value of the 'normal' self-heating values. Note that the uncertainty related to the self-heating correction can be considered to result from two fully correlated resistance measurements only if a comparable number of measurements are performed for each of the two current levels, which is not a normal procedure.

h. *Cell and sample overheating during heating pulses in different meltings.* The reproducibility of the plot of overheating versus F provides a check on the similarity between meltings of the chemical-physical and spatial conditions of the sample inside the cell. In addition, it provides a different check of R_{cs} from that whose results are indicated in Sect. 2.3.3.1 (see Fig. 2.21), since the heating path to the sample (here from the cell heater) may be different.

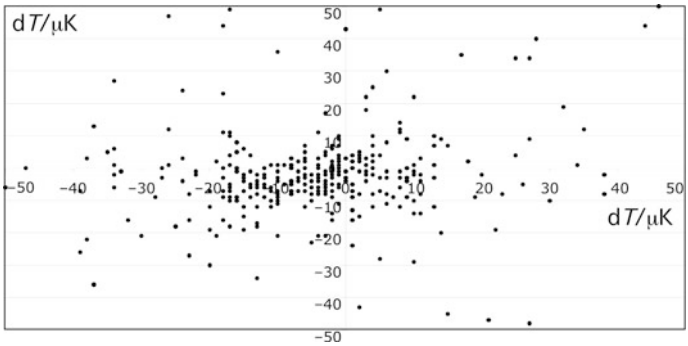

Fig. 2.28 Plot of differences $\delta T = (T_{i,\text{first}} - T_{i,\text{last}}) < 50$ μK observed for each set of readings used to compute the ≈400 equilibrium temperatures $T_{\text{e},i}$. A small part of the latter is out of scale: 61 data > 50 μK and 35 data > 100 μK. On the two axes two different thermometers

i. *Temperature drift in the set of resistance values used to compute each* $T_{\text{e},i}$. The way each equilibrium value $T_{\text{e},i}$ is computed can be crucial for the values and/or their uncertainties. In this respect, for example, the procedure developed in Sect. 2.3.3.4, as recalled in item (c), suggests a thermal drift not higher than 20 μK min^{-1} is needed before computing $T_{\text{e},i}$. Typically, N_i instrumental readings are recorded over the full trend toward re-equilibration, but the computation of $T_{\text{e},i}$ involves only the final part of these readings. Let the first reading be $T_{\text{first},i}$ and the last be $T_{\text{last},i}$ of a total of M_i readings ($M_i < N_i$) used for computing $T_{\text{e},i}$ (for example, $M_i = 60$–900, typically 160, corresponding to a time span of 350–5500 s, typically 900 s). If the criterion of Sect. 2.3.3.4 is used, $T_{\text{first},i}$ will be the first reading after the drift and is smaller than 20 μK min^{-1}. In general, the evaluation of $T_{\text{e},i}$ is performed by averaging the M_i instrumental readings. In Fig. 2.26, some of these results are reported sequentially. In figure 2.28, they are reported for the two used thermometers.
It is noteworthy that the standard deviation of the set of data between T_{first} and T_{last} is approximately 1/4 of the reported differences. In the figure, about 3/4 of the data are within the box {±20, ±20} μK (see figure caption), corresponding to a standard deviation of ≈5 μK. The standard deviation over *all* ≈400 data is 31 μK. No meltings, except the few with very high electrical noise, show values of $(T_{\text{first}} - T_{\text{last}})$ that are systematically greater than about 20 μK, but occasionally the $T_{\text{e},i}$ drift exceeds that value, generally for $F < 10$ % or > 70 %. To be considered real, the drift of one thermometer should confirm the drift value of the other (at least having the same sign), otherwise they should be considered not as real drift values but as arising purely from electrical noise. Drift values within the box {±10, ±10} μK, accounting for 50 % of all the values, are certainly not considered significant. For drift values within the boxes {±20, ±20} μK and {±50, ±50} μK, no correlation between the data of the two thermometers was found (1st and 3rd quadrants). Data in the 2nd and 4th quadrants indicate contrasting drift sign between the two thermometers. This indicates that electrical noise

overall largely dominates the drift data, implying that *sample re-equilibration is achieved* to better than 10 μK, for the set of readings used to compute $T_{e,i}$.
Further, analysis of the re-equilibration data shows that for 270 of the ≈400 data, the differences are negative—i.e. about 2/3—meaning a weak correlation for the expected sign (temperature decreasing during re-equilibration).
In principle, the evaluation of whether or not equilibrium is reached and the computation of $T_{e,i}$ can be done in different ways. The trend to thermal re-equilibration is characterized by a double exponential function, the first (with a very short time constant) due to cooling of the cell assembly and the second (with a longer time constant) due to the thermal re-equilibration of the sample. When the total drift ($T_{\text{first},i} - T_{\text{last},i}$) is comparable with the desired uncertainty (as in Fig. 2.28), the results of three methods for computing $T_{e,i}$ can be compared:

1. the mean value over the M_i readings;
2. the value $T_{\text{last},i}$ obtained from a linear fit to the M_i readings, supposedly closest to true thermal equilibrium;
3. the value $T_{\text{last},i}$ obtained from an exponential fit to all readings after the end of the heating pulse. As explained above, only the second exponential is relevant in this case.

These three methods generally yield different values for $T_{e,i}$, not necessarily leading to different liquidus point values after fitting the $T_{e,i}$ as a function of $1/F$. However, the variation in the values obtained provides additional information about the reliability of the mean value assigned to the liquidus point temperature. For the cases, as in Fig. 2.28, where 'drift' data are within 50 μK one can safely assume that the mean-value method indicated above of computing $T_{e,i}$ is reliable and sufficient within a few microkelvins. Procedures such as the LSMFE—see item (k)—can also be applied to the different sets of data.

j. *Comparison of different meltings of the same sample: melting range and liquidus point.* For a reliable computation for any sample, measuring more than one melting is mandatory, typically three, where at least two thermometers are used for the measurements.
The melting range is evaluated from the same unweighed *linear* fit of $T_{e,i}$ against $1/F$ used to compute the liquidus point by extrapolation. A linear fit is generally sufficient when the melting range is small and the standard deviation of the linear fit is sufficiently low. It has to be considered an *empirical* fit, without suggesting neither that Raoult's law applies nor that the distribution coefficient of impurities be $k_0 = 0$. Only when chemical-physical phenomena can explicitly be found that substantially influence the shape of the meltings, the use of a second-order polynomial is justified.
Some authors define T_{tp} differently, for example as the temperature at $F = 0.5$ (not advised). These values can be easily obtained by decreasing the value of T_{LP} by 1/5 of the reported melting range. The difference ($T_{LP} - T_{F=0.5}$) can be less than 20 μK.

k. *Standard deviation of the melting plateau fit, plateau slope and the use of the LSMFE.* The standard deviation of the fit is a useful indicator of the quality of the melting. However, the meltings do not all have exactly the same slope, and each

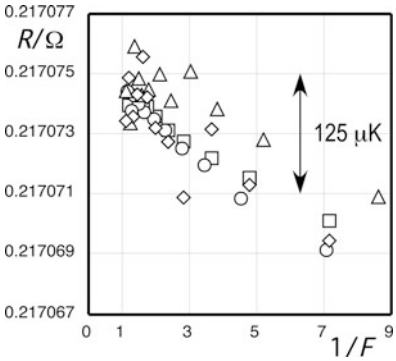

Fig. 2.29 Dataset concerning several meltings realized on a single cell examined with the LSMFE ($u_{\text{fit}} = 16\ \mu\text{K}$): melting #1 is taken as the arbitrary reference. Differences in T_{LP}: 0 (ref), $-1\ \mu\text{K}$, $+4\ \mu\text{K}$, $-38\ \mu\text{K}$ (the latter being anomalous for thermal reasons)

melting can also have a slightly different slope for different thermometers due to the pivoting effect of some data. This indicates a variation in the experimental conditions beyond the parameters that are explicit to the experimenter and that can be acquired and evaluated on a statistical basis, including the differences from thermometer to thermometer.

That said, the cell remains the same for all these measurements, and so does the sample under examination. Therefore, one can expect that the measurements are samples from the same physical condition, except for aspects that depend on the physical-chemical condition of the partially melted sample (e.g., distribution of liquid and solid phases, distribution of impurities, solid undercooling, annealing conditions, distribution of the impurities, isotopic fractionation). The latter are expected to be small or reproducible for ultrapure neon mixtures of isotopes. As a consequence, the data points of different meltings measured using different thermometers *of the same type* can all be fitted together by modelling a fixed effect consisting of a translation parameter for each melting/thermometer. This computation can be carried out using LSMFE (Pavese and Ciarlini 1990b, 1992a; Ciarlini and Pavese 1992), which yields *simultaneously* the linear function *and* the translation values $b_{0,ij}$ (liquidus-point differences and thermometer differences), optimized according to the LS criterion. The same computation can also be performed by *weighing* each individual $T_{\text{e},i}$, typically with the inverse of its associated variance—when acquired, see also Sect. 2.3.3.1. This acts as a double check. In any case, one obtains at the same time the variance of the fit to the overall dataset *and* the differences in T_{LP} between the different meltings. Figure 2.29 shows an application for a series of meltings performed in time on the same cell. The use of LSMFE should be considered the most reliable means of evaluating the differences between liquidus points, taking into account also the dependence on the thermometer.

2.4.2.3 From Checks Involving the Measurement of Several Cells

The melting plateaus obtained with different cells do not have exactly the same shape, due to the reasons discussed in (Pavese 2003c; Pavese et al. 2009b). Differences might

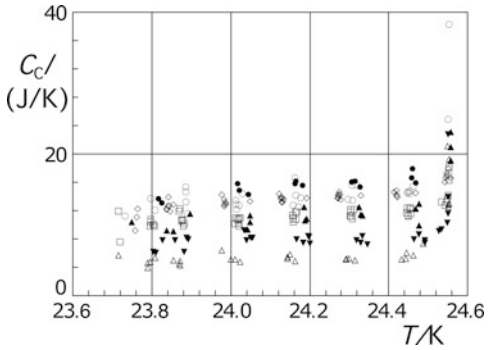

Fig. 2.30 Heat capacity C_C of each cell-assembly as a function of T, as measured on the seven cells (different symbols). No steep increase of heat capacity is observed for any cell for T below ≈ -15 mK from melting

indicate either a different purity between the samples or variations in extent of the thermal effects due to the geometry of the cell. Either of these effects can be totally or partially masked by random effects of $T_{e,i}$ (as distinct from electrical noise, whose effect is generally lower).

When comparing cells, it is normal practice to perform the data analysis separately for each cell and to look at the difference between their liquidus points. However, in the present study of neon samples, of essentially the same purity and similar isotopic composition, one can assume that thermal effects do not significantly affect the liquidus point temperature $T_{\mathrm{LP},j}$, although they may affect other parameters to such an extent as to reduce the reliability of some $T_{\mathrm{LP},j}$. Some further tools are useful therefore, in order to make a more comprehensive comparison.

l. *Check on the quality of heat capacity measurements below melting.* Measurement of accurate values of $\Delta_{\mathrm{fus}}H_{\mathrm{meas}}$ depends also on the accurate detection of the solidus point and on the absence of 'pre-melting' effects. For this purpose, the heat capacity C_C of the cell assembly should be measured at different temperatures, starting from below melting until close to plateau. Figure 2.30 shows examples of these measurements.

m. *Use of the LSMFE technique over all cells and meltings.* The LSMFE (Pavese and Ciarlini 1990b) can be applied to any group of cells (and thermometers), instead of considering each cell individually, for comparing the values for each cell. There are then two options that are worth exploring to get a measure of the variability of the comparison depending on the data treatment:

1. The first, already illustrated before, considers a fixed effect only as a translation of the melting curves due to different isotopic composition (and possibly to measurement artifacts), as in item (k), so a single parameter $b_{0,ij}$ is used in the model;
2. In the second, one allows the cells also to have different melting ranges. For this it is sufficient to extend the fixed-effect model function to include the melting slope, by using a first-order (linear) polynomial $(b_{0,ij} + b_{1,ij} \times 1/F)$ instead of a constant $b_{0,ij}$. In general, the high number of available degrees of freedom (experimental points) allows the much higher number of unknown parameters. For example, if one has on average 5 experimental points for 3 meltings, each concerning 6 cells and using 2 thermometers, one can fit,

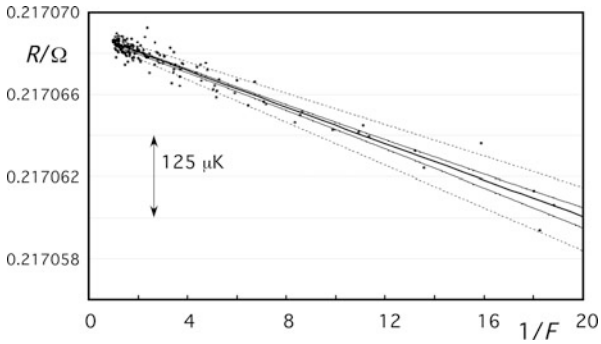

Fig. 2.31 Data of three melting plateaus for three cells with evaluated bootstrap limits after application of the LSMFE. The inner limits are the 95 % bootstrap confidence interval (CI) of the fitted function, the outer limits are the minimum and maximum corresponding to the bootstrap intervals of the two parameters of the linear fit function ($a_0 = (0.21706877 - 0.21706909)\ \Omega(\Delta a_0$ equivalent to 10 mK); $a_1 = (5.19 - 3.81) \times 10^{-7}\ \Omega(1/F)^{-1}$)

using the LSMFE, 36 datasets and 180 data points for a total of 75 unknown parameters—for a linear fit.

In both cases, one obtains (see Fig. 2.29) the whole set of differences for all meltings relative to one, the first one by default, but this is irrelevant since by choosing another the whole set is simply translated by a constant, canceling out when considering differences.

n. *Bootstrap evaluation of the fit parameters*. Especially in the latter case of item (m) (easily applied also to the data of each cell, or of each thermometer), it is useful to carry out, as a final step, a statistical check of the variability of the results obtained. A *bootstrap evaluation* of the fit parameters is a powerful tool in this respect. It consists of a technique of resampling the fit residuals, with typically 1000 replicates being sufficient: it yields average values of the fit parameters and 95 % confidence-interval (CI) for each of them. In addition, it defines 95 % CI upper and lower bounds for the fitted curve—see a similar application in (Ciarlini and Pavese 1992b).

See (Pavese et al. 2010b, c, 2011b, e, 2012c) for applications of these criteria the studies on neon. Figure 2.31 shows an example of use of this method.

2.4.3 Performance of Sealed Cell Models

This Section summarizes the advances in the realization of gas triple point as temperature reference points. Their detailed descriptions are readily available in the literature, and, specifically, in comprehensive papers or books and Journals, such as TMCSI (1982, 1992, 2003, 2012), TEMPMEKO Proceedings (1996, 1999, 2001, 2004, 2007, 2010), Pavese and Ferri (1982), Pavese et al. (1984a), Pavese (1984b), Bedford et al. (1990), etc. The recent ITS-90 primarily uses these fixed points over their proper ranges, by means of the permanent sealing technique recommended in

its "*Supplementary Information for the ITS-90*" (BIPM, 1990a). In addition, as will be more specifically illustrated in Sect. 2.6, they are also useful and easily attained when precision requirements are less stringent.

2.4.3.1 Sealed Cells for Capsule Thermometers

The only reason, today, to use a long-stem cell with capsule thermometers (Sect. 2.3.3.2) is to realize a *pressure* fixed point (see for example Pavese (1981a) in Part II, Chap. 9); otherwise small cells are used.

Some of the initial cell models were firstly tested during an extensive international exercise lasting nearly 6 years, 1978–1984. They are shown in Fig. 2.32. All proved to be essentially of the same quality and stable in time (Pavese 1984b; Pavese et al. 1984a). Only IMGC (now INRIM) cells are known to have then had a longer-term stability; until 2012 checks showed that no changes had occurred in IMGC cells aged for as much as 37 years (Pavese et al. 1992b; Pavese 2003c, 2012a).

A subsequent step improvement in cell best performances occurred starting from 2001, in the frame of a European Project (Pavese et al. 2003b), leading to cells with better performances when used with a new generation of calorimeters. They are shown in Figs. 2.33 and 2.34.

Small sealed cells are of three basic types, (1) those designed to be interchanged, one at a time, in the cryostat (Section "Sealed cells for capsule thermometers"), (2) those designed for multiple fixed-point calibration (Sect. "Multiple cell design") and (3) high-enthalpy cells (Sect. "High enthalpy cells").

Single Cell Design

This is the normal design, in which the inner thermometer block can have one or, better, several wells, to allow several thermometers to be calibrated at a time. A single substance sealed in the cell provides a reference point at its triple point, *and* additional points in case the substance shows solid-to-solid transitions (O_2, N_2, CH_4: see Sect. 2.5.2 and Appendix B). The cell has conveniently small dimensions to fit most cryostats.

The variety of fabrication techniques used in the 1970s–1990s of the past century (Pavese 1984b; Pavese et al. 1984a) are shown in Fig. 2.32: all-copper (types a, g, j), all-stainless steel (types b, f, h, j, k) copper block and stainless steel body (types c, d, e), stainless steel-cladded copper body (type l); with (in types c, h, j, l) or without inner copper baffles. Sealing is achieved by different means and techniques: indium gaskets fitted inside (types c, d, e) or outside (type l) the cell; pinched copper tube (all other types), then soft soldered (types b, f, g, j, k); stainless steel tube pinched with a gold wire inside (types h, i); pinch-weld stainless steel tube (variant to type d (Pavese and Ferri 1990c; see also related Patents)). All parts are assembled by arc welding (types c, d, e, h, i) or by silver brazing (types a, g, j).

The cell inner volume ranged 2.5–74 cm^3, and cell mass 80–320 g. The sample molar mass ranged 0.015–0.32 mol, with a ratio of the enthalpy of fusion (depending

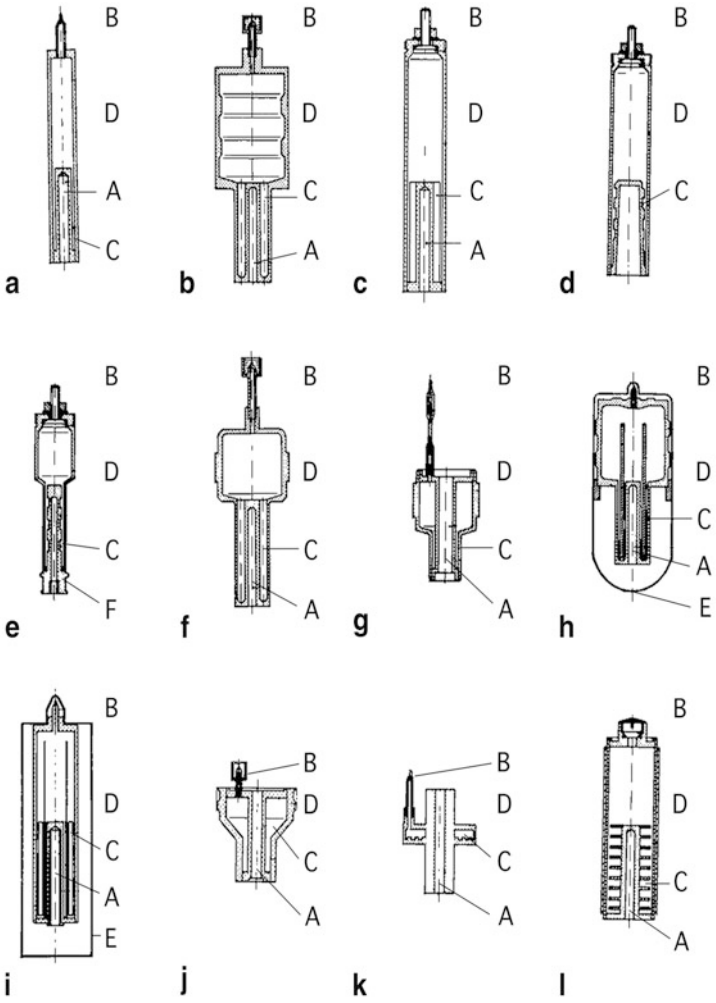

Fig. 2.32 Models of sealed cells, fabricated by the following laboratories and used in an international intercomparison. (After Pavese et al. 1984). **a** ASMW (now part of PTB). **b** BIPM. **c** IMGC (now INRIM, 1–3 well type). **d** IMGC (conical well type). **e** IMGC (miniature type for external block). **f** INM (now LCM). **g** NRLM (now AIST-NMIJ). **h** NBS (now NIST). **i** NBS. **j** NIM. **k** NIM. **l** NRC. For their characteristics, see text. *A* thermometer block with wells; *B* seal; *C* sample chamber; *D* cell body; *E* cell isothermal shield; *F* transfer body of the temperature generator

on the substance) to the cell mass varying from ≈ 0.2 J g^{-1} to ≈ 1.1 J g^{-1} for fixed points above 50 K, and from ≈ 0.025 J g^{-1} to ≈ 0.22 J g^{-1} for fixed points below 25 K. Table 2.8 gives the ranges of the design parameters of these cells, together with some evaluation criteria. One can see that cells designed in different laboratories resulted to behave satisfactorily under widely varying conditions. It is also evident that the

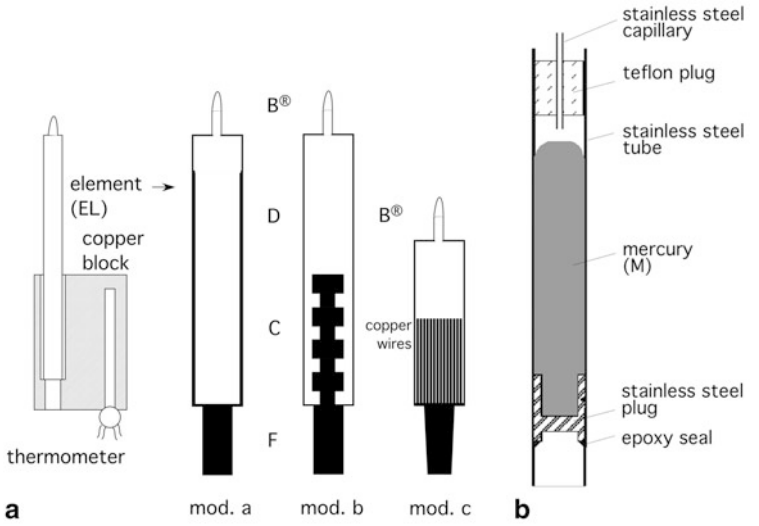

Fig. 2.33 Sealed-cell models developed after 1990 in the frame of the project MULTICELLS (Pavese et al. 2003d)—not to scale: (**a**) IMGC (now INRIM) models of *elements* (EL) (Pavese et al. 2003b): *mod. a* with internal copper clad ($V_{int} = 4.8\,cm^3$); *mod. b* with internal massif copper body, similarly to model (e) in Fig. 2.32, ($V_{int} = 6.2\,cm^3$); *mod. c* with internal body made of a bunch of copper wires, to minimize R_{cs}, and conical foot—also shorter ($V_{int} = 3.8\,cm^3$). *B*–*F* meaning as in Fig. 2.32. The elements can be used either one-by-one or in a multiple assembly. The copper block (see also Fig. 2.23) can accommodate up to four vertical elements plus a central mercury microcell (*M*) (Lipinski et al. 2001). The mercury microcell is shown in (**b**): Ø = 5 mm, *L* = 50 mm, about the size of a capsule SPRT

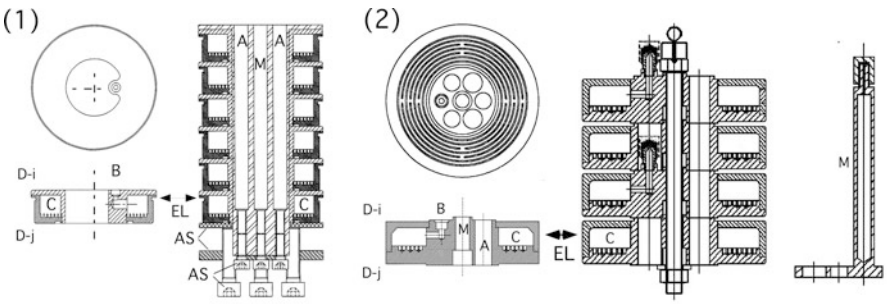

Fig. 2.34 Sealed-cell models developed after 1990 in the frame of the project MULTICELLS (Pavese et al. 2003d): INM (now LCM) models (Hermier et al. 2003). *1* Initial model: up to six horizontal elements (EL) can be accommodated plus a mercury cell in (f). (*C*) sample chamber; (EL) pancake *element* ($V_{int} = 12\,cm^3$); (AP) assembling parts; (*A*) thermometer well; (*M*) well for mercury cell (optional); (*B*) filling tube attachment to pinch; (*D*) body: (*i*) top (stainless steel), (*j*) bottom with heat exchanger (copper). *2* LCM final model: 4 pancake elements, plus possible accommodation of a mercury cell (*M*). Other parts indicated as in model *1*

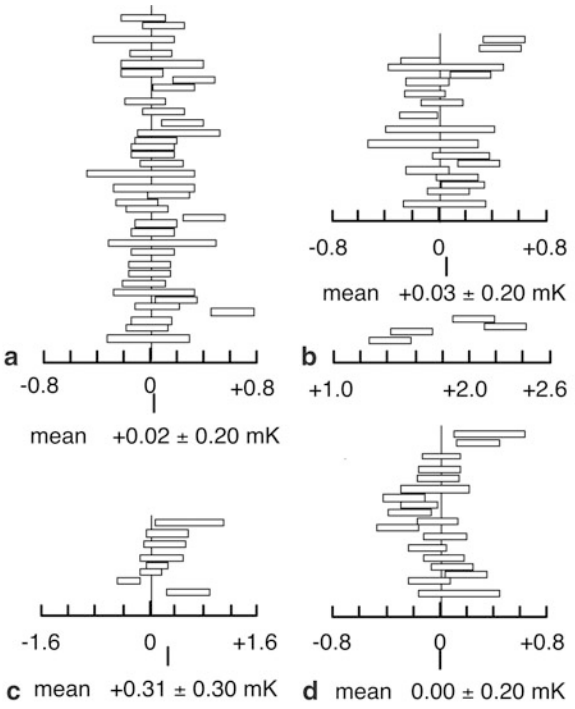

Fig. 2.35 Results of 1978–1984 comparisons of the sealed cells in Fig. 2.32. (After Pavese et al. 1984). **a** argon, 14 cells. **b** oxygen, 9 cells. **c** equilibrium hydrogen, 5 cells. **d** neon, 8 cells

"driving capability" X (Sect. "Sealed cells for capsule thermometers") is close to the upper limit for cell design, and that $\approx 5\ X\ \%$ appears to be close to the desirable limit (however, with the cells of new generation, the amount of sealed substance has generally been reduced without affecting the performance).

The differences of temperature values obtained with these cells with respect to a value used as a reference are shown in Fig. 2.35a–d for the four fixed points of the ITS-90: argon ($u_{LP} = 0.15$ mK), oxygen ($u_{LP} = 0.22$ mK), neon ($u_{LP} = 0.20$ mK), equilibrium hydrogen ($u_{LP} = 0.30$ mK). The larger dispersion observed for last two substances were lately found to be caused by cell-to-cell variability of isotopic composition; for oxygen see Appendix C for a warning about its use. It must be remembered that these figures represent the *best* accuracy achievable *at that date*. Using the same cells with less careful procedures, the uncertainty of the measurements would hardly exceed ± 1 mK, unless the thermometers used to make the measurement have intrinsic limitations.

On the other hand, some of these cells—namely types (c, d, g, and l) in Fig. 2.32—when later used with better calorimeters.

They later proved to allow basically the same improved accuracy of the cells of new generation shown in Figs. 2.33, 2.34, and 2.36. Chapter 6 describes cryostat requirements in the use of these cells.

The elements of Fig. 2.33 can also be used as single cells, but they were specifically designed for multiple-fixed-point use, so more details are provided in this respect in the next section. This is not possible, in general, for the elements of Fig. 2.34.

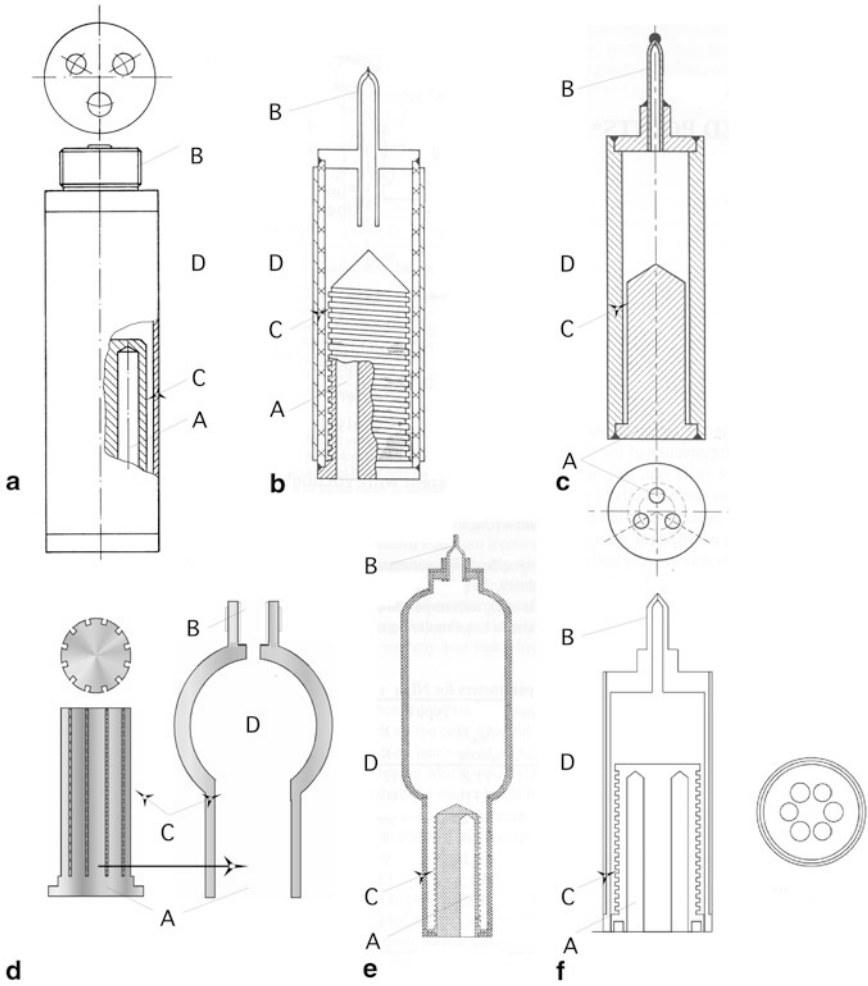

Fig. 2.36 Other second-generation sealed cells of models (*not to scale*) developed at. **a**, **b** NPL (Head 1996, 2001): all stainless-steel (ss), all-copper (externally ss-clad) or fabricated with vacuum-arc remelted (VAR) protium-free stainless steel—see Sect. 2.2.2.6. **c** PTB (Fellmuth et al. 1996): all copper. **d** NMIJ (Nakano et al. 2007): all copper. **e** NIST (Tew 1996): stainless steel with copper block. **f** NRC (Hill 1996): all-copper (externally ss-clad). Meaning of *A–D* as in Fig. 2.32

In the same period, further different models have been designed and used in other laboratories, shown in Fig. 2.36.

In general, the new-generation cells also used a variety of fabrication techniques, from all copper (as NMIJ one) to all stainless steel (as NPL one) type. Their mass ranges from 50 g (one element, INRIM mod. c) to $> \approx 500$ g (LCM, full 4 element type), and the sealed amount per element from 0.02 mol and 0.15 mol. The dispersion

of the results obtained for the cells of Fig. 2.33, for the four fixed points of the ITS-90 *measured separately* and in five different European laboratories, have been: argon ($u_{LP} = 26$ μK), oxygen ($u_{LP} = 24$ μK), neon ($u_{LP} = 26$ μK), equilibrium hydrogen ($u_{LP} = 44$ μK) (Pavese et al. 2003b). Figure 2.36 reports the values of $T_{e,i}$ measured by all laboratories and after treatment with the LSMFE method.

More recently, the expanded uncertainty of the best realizations for hydrogen triple point was reduced to $U \approx 100$ μK (Fellmuth et al. 2005 and 2012), and for neon triple point to $U \approx 50$ μK (Pavese et al. 2010b, see Sect. 2.4.2).

Multiple-Cell Design

Cells of the previous design are useful for single fixed-point realizations, so with cryostats allowing the cells to be quickly interchanged. Otherwise, it may be useful to have more than one fixed-point device (now called "element") mounted in the cryostat at the same time, for a full calibration without having to remove the thermometers from the calibration apparatus. This allows, specifically, to conveniently realizing the four cryogenic fixed point of *e*-H_2, Ne, O_2, and Ar of the ITS-90 subrange 24.5561–273.16 K.

This calibration according to ITS-90 also requires the realization of two triple points of non-gaseous substances: mercury and water. However, it has been shown that the technique of small metal sealed-cells is, in principle, suitable also for an accurate realization of the triple point of water (Ancsin 1982; Bonnier 1982; Pavese and Ferri 1982). A similar technique has been developed for mercury in glass miniature cells (Lipinski et al. 2000, 2001).

The use of multiple cell elements for the realization of the ITS-90 suffers from a peculiar problem: all substances are present during the realization of anyone of the fixed points. Obviously, they do not interfere with each other as far as the value of the realized T_{tp} is concerned, being the four (or up to six if considering also mercury and water) value very far from each other. However, depending on the substance being melted, the others are in the form of gas or solid. Therefore, they contribute to the total heat capacity of the assembly and to its thermal diffusivity: in this respect, one has to remember that heat capacity value is lowering much more slowly with temperature than for metals, and that thermal conductivity of the solid is very low (and the solid can be in bad thermal contact with the container due to thermal contraction—a reason that makes difficult, e.g., to obtain good solid-to-solid transition realizations, see Sect. 2.5). As a result, while these facts do not have influence on static parameters, like T_{tp} is, they can strongly affect the dynamic behavior of the whole assembly, namely (considerably) increasing its re-equilibration dynamic constant τ (see Sect. 2.3.3.2). This effect can make quite more critical the realization of a correct triple point, and more critical the quality of the calorimeter. The advantage to have all the fixed points already all mounted in the cryostat can be vanished by the longer time necessary to perform each melting.

The implementation of multiple devices can be based on two different approaches, one considering a measuring block equipped with several cell elements (Pavese and

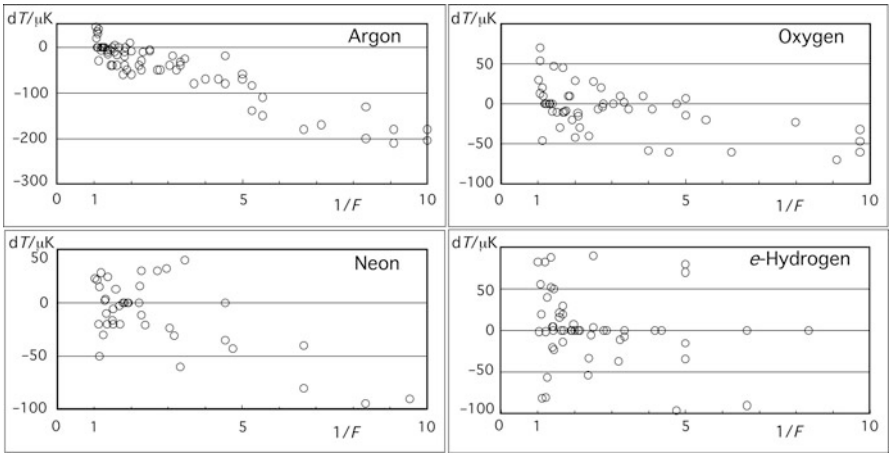

Fig. 2.37 Melting plateau shape for second-generation cells of Fig. 2.33 realizing the four ITS-90 fixed points. F fraction melted. Standard deviation of the linear fitting: argon, $u_{LP} = 26$ μK; oxygen, $u_{LP} = 24$ μK; neon, $u_{LP} = 26$ μK; e-hydrogen, $u_{LP} = 44$ μK. (After Pavese et al. 2003b).

Ferri 1982; Pavese et al. 2003b, c), the other a multicompartment device (Bonnier 1982; Hermier et al. 2003).

Measuring block equipped with several microcells In this case, the principle of the outer block has been adopted (Fig. 2.32f, Pavese and Ferri 1982; Fig. 2.33, Pavese et al. 2003b). This type of cell can actually be considered as a "*temperature generator*"(T-Gen), since its purpose is to keep the assembly temperature constant during the triple point measurement: it acts like a "battery" having a certain amount of (thermal) energy stored in it, and very low internal impedance (i.e. high temperature stability in supplying energy). The mass of the assembly must be as small as possible, in order to accommodate up to four T-Gen. In addition, it must maintain a good thermal conductivity between the cell inner body—transferring the interface temperature value—and the thermometers housed in wells of the external block. In the design of Fig. 2.33c, each T-Gen (element) weights ≈ 50 g and contains ≈ 0.04 mol of substance, while the thermometer block weights another ≈ 100 g. The resulting total weight of a four-element assembly for this design is as little as ≈ 300 g. T-Gens can easily be interchanged in the assembly, whose dimensions can approximately be < 10 cm in length and < 5 cm in diameter.

One-piece multicompartment cells Two approaches to the multicompartment cell design have been implemented.

The first approach produced the cell shown in Fig. 2.38a (Bonnier 1982) and the final ones in Fig. 2.34 (Hermier et al. 2003): they correspond to combining together into a single device all the T-Gens. The difference between the two models is mainly the fact that the older one is made in one-piece, while the modern ones can mount only the desired number of elements. However, differently from the design

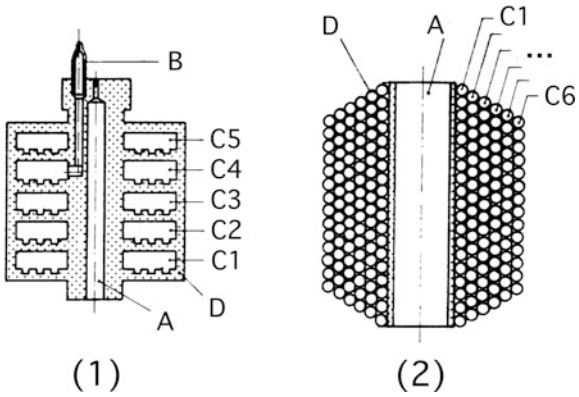

Fig. 2.38 Previous models of multiple sealed cells: *1* INM (later LCM), 5 pancake chambers (C1–C5) in a common body), all stainless steel; *2* VNIIFTRI, up to 6 coiled chambers (C1. . . C6) wound on the same core, all copper. *A*–*D*, meaning as in Fig. 2.32

of Fig. 2.32, each element in Fig. 2.34 is actually like a full cell comprising the thermometer accommodation, only being of a very flat design (while the elements in Fig. 2.33 are of fully vertical design and need an external thermometer block). The overall device dimensions are about the same in both cases. The total weight of the all-stainless steel construction is ≈ 500 g with a filling amount of gas per chamber of ≈ 0.020 mol. Grooves on each chamber floor (made of copper in the last model) improve the thermal contact with the condensed sample.

A second extremely simple and very convenient design is shown in Fig. 2.38b (Khnykov et al. 1989a; Pavese 1984b). A number of copper tubes are separately wound on a central solid-copper core where thermometer wells are drilled. The number of separate coils equals the number of different substances that must be measured (obviously the same fabrication principle can be used also for sealing a single substance). Each tube, welded at one end, is pinched-off at the other after filling, and forms a chamber that can easily withstand very high pressures. Thermal contact between the coils and the copper core can simply be ensured by silver brazing or even by soldering (see also Sect. 6.2.3 for another possible application of this device).

Intercomparison of Sealed Cells

The first intercomparison of sealed cells was organized by IMGC (now INRIM) in 1978–1984 (Pavese 1984b; Pavese et al. 1984a) and involved 41 cells containing seven substances (e-H_2, e-D_2, Ne, O_2, N_2, Ar, CH_4) and nine NMIs. Results are illustrated in Sect. 2.4.3.1.

A second intercomparison of fixed points, where some of the former first-generation sealed cells were used by some NMIs, was organized by the CCT in 1997–1999, and results can be found in the BIPM KCDB under CCT-K2 (Steele et al. 2002)—see Chap. 11.

A third cell intercomparison, of the star type (all cells are measured at the pilot Laboratory), was organized in the years 1995–2007 in the frame of the a EURAMET

and of the MULTICELLS European Projects, including most of the last models, with PTB as pilot, and concerning H_2, Ne, O_2, and Ar. Contrarily to CCT-K2, the sealed cells were all measured directly at the same laboratory. The results for H_2 were used for determining the isotopic correction for this gas (Fellmuth et al. 2005, 2012)—see Sect. 2.2.2.5, and those for neon contributed to determining the isotopic correction for neon (Pavese et al. 2012b). The remaining results are published in Fellmuth et al. (2012): considering only filling gases having nominal purities of 99.999 % or better, which excludes some of the older cells, the following standard deviation of T_{LP} were found: $u_{LP} = (30 \pm 54)$ μK for H_2, 32 cells, (after correcting for the influence of the deuterium content); $u_{LP} = (88 \pm 51)$ μK for Ne, 15 cells, (still uncorrected for the effect of the variability of natural isotopic composition, which is responsible for most of the variability); $u_{LP} = (43 \pm 36)$ μK for O_2, 14 cells, but having excluded four older cells with lower purity gas and possibly responsible for being contaminated with argon; $u_{LP} = (58 \pm 44)$ μK for Ar, 16 cells.

A fourth intercomparison limited to neon, of both natural and pure isotopic composition, was additionally conducted in the years 2003–2011, under an international project (Pavese et al. 2012b), whose results are also reported and discussed in Sect. 2.2.2.5: it involved 30 cells with natural isotopic composition, including the 15 cells measured also at PTB, plus 26 cells of high-purity ^{20}Ne and ^{22}Ne and 3 cells filled with certified artificial mixtures of ^{22}Ne in ^{20}Ne, with an uncertainty $u = 25$–30 μK for the measurements carried out at INRIM.

High Enthalpy Cells

A particular type of temperature generator are the high-enthalpy cells. In fact, the remarkable temperature stability achieved with a *T*-Gen during the triple point plateau can be used as well for stabilizing the temperature of critical experiments or components on Earth and in space (Pavese 1987a; see also Sect. 6.2). Temperature stabilization can be achieved within better than 500 μK using most of the melting plateau ($F = 0.1$–0.9). Even better temperature stability (within < 100 μK) can be obtained allowing only a ± 10 % variation of *F*. The stability is of few microkelvin at short term (≈ 1 h). For space applications, it is easy to calculate that a *T*-Gen, acting as a *passive* thermostat with an average thermal load of 1 mW, would maintain a detector for one year at (24.5561 ± 0.0005) K requiring a volume of only 4 L containing ≈ 96 mol of pure neon at a room temperature pressure of 500 bar. A similar *T*-Gen would maintain a detector at (83.8058 ± 0.0005) K requiring a volume of only 1 L containing 27 mol of argon at the same pressure[8]. Obviously, the energy available is limited, but the process is reversible: the *T*-Gen is very much like a rechargeable battery! An example of cell containing up to 1 mol of substance is shown in Fig. 2.39.

[8] Remember that there also is an upper limit to filling density (i.e. room-temperature pressure) (Sect. 2.2.1 and Table 2.1).

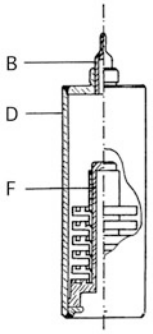

Fig. 2.39 High-enthalpy temperature generator (H 85 mm, Ø 30 mm): the device, kept at fixed temperature by the *T*-Gen, is screwed at the bottom—for use on Earth only. *B*–*F*, like in Fig. 2.32

2.4.3.2 Sealed Cells for Long-Stem Thermometers

In order to satisfy the requirements indicated in Section "Sealed cells for long-stem thermometers", different approaches have been followed. All but one have been, so far, developed for the argon triple point, ≈ 84 K, temperature close to that of liquid nitrogen boiling at atmospheric pressure (≈ 77.3 K). The exception was a sealed cell for carbon dioxide developed by Ambrose (1957).

According to the first approach, a sealed cell containing a large quantity of substance is used, so that the dynamic method (Sect. 2.3.1.1) can be applied for both freezing or melting, the latter being accurate.

Figure 2.40a shows the first argon cell of this type (Furukawa et al. 1972). The cell is a cylinder, extending up to room temperature, featuring a reentrant well in which one long-stem thermometer can be accommodated. The well is purged with precooled helium gas flowing at a controlled rate. The cell is permanently connected to an external ballast cylinder, so that the system can contain about 4 mol of gas with room-temperature pressure limited to 3.4 MPa. When the gas sample is condensed, the liquid depth is 26 cm. The cell is insulated with an evacuated powder insulator from the liquid nitrogen bath, boiling at atmospheric pressure. A copper top cap extending into the refrigerant provides the thermal anchoring for both the cell and the thermometer; cap temperature critically affects the accuracy of the triple point realization. Thermometers can be interchanged during the same melting (or freezing). The phase transition is obtained with the dynamic method and can be controlled to last about 10 h, via the cap heater. The accuracy attained with two cells of this type was ± 0.3 mK.

Figure 2.40b shows an argon cell type (Bonnier 1975; Bloembergen et al. 1990) of wide use in long-stem thermometer calibration. The sealed cell contains about 2 mol of pure argon at a room temperature pressure of about 5.5 MPa. The well for one thermometer extends up to room temperature and is contained in a gas-tight jacket filled with helium gas for improving thermal exchange of the thermometer stem with the liquid nitrogen bath for thermal anchoring, and then with the substance in the cell. In order to reduce temperature gradients due to the poor thermal conductivity

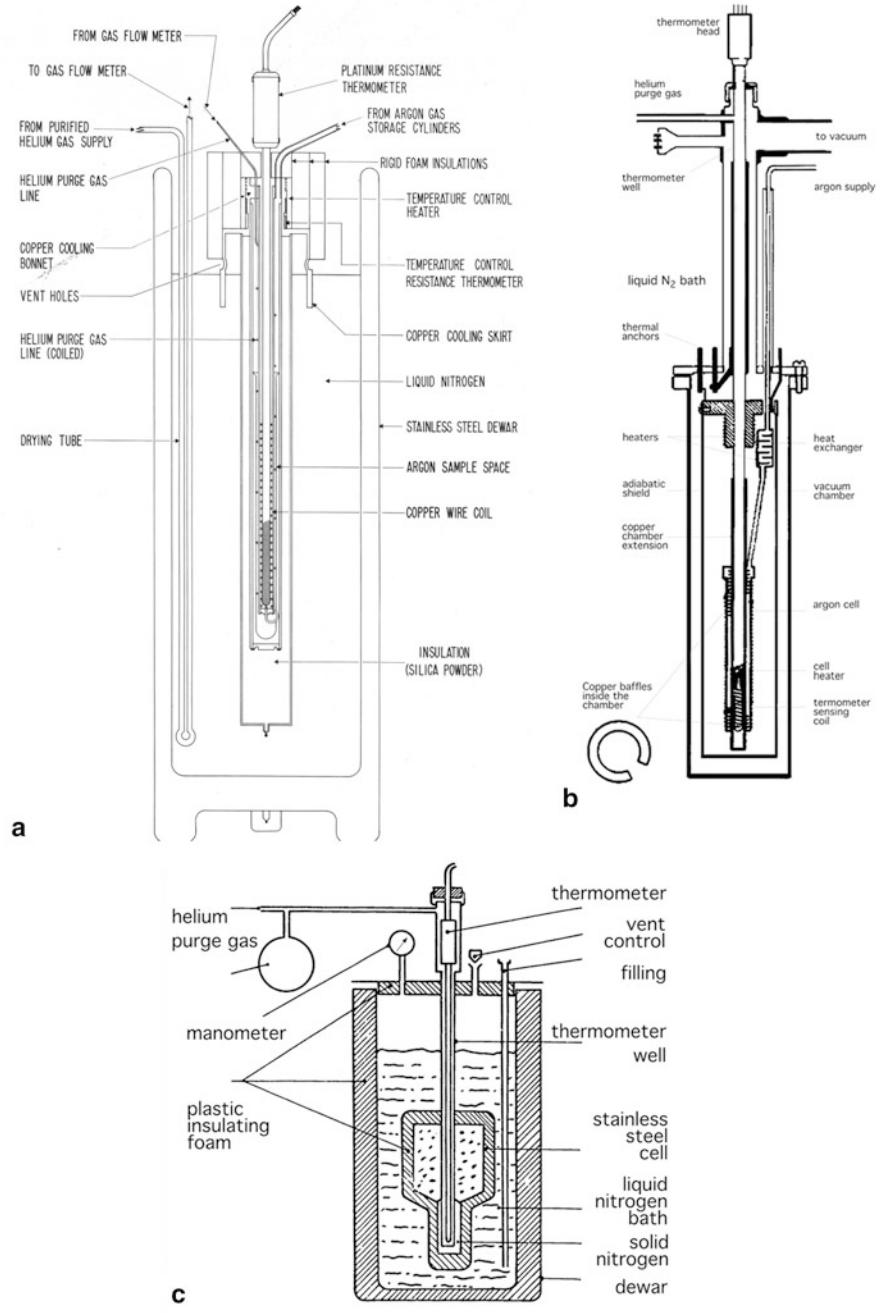

Fig. 2.40 Cells for long-stem thermometers. **a** NBS argon cell with integral dewar. (After Furukawa et al. 1972). **b** NRC argon cell and cryostat: a cylindrical dewar can be used for the cell cryostat (After Ancsin and Phillips 1982). **c** INM (later LCM) argon cell with integral dewar (After Bonnier 1975). **d** IMGC cell (argon and methane) with cryostat; a storage liquid nitrogen dewar can directly be used for the cryostat (After Pavese et al. 1990d). **e** INTiBS argon cell used directly into a liquid nitrogen dewar. (After Szmyrka-Grzebyk et al. 2012a)

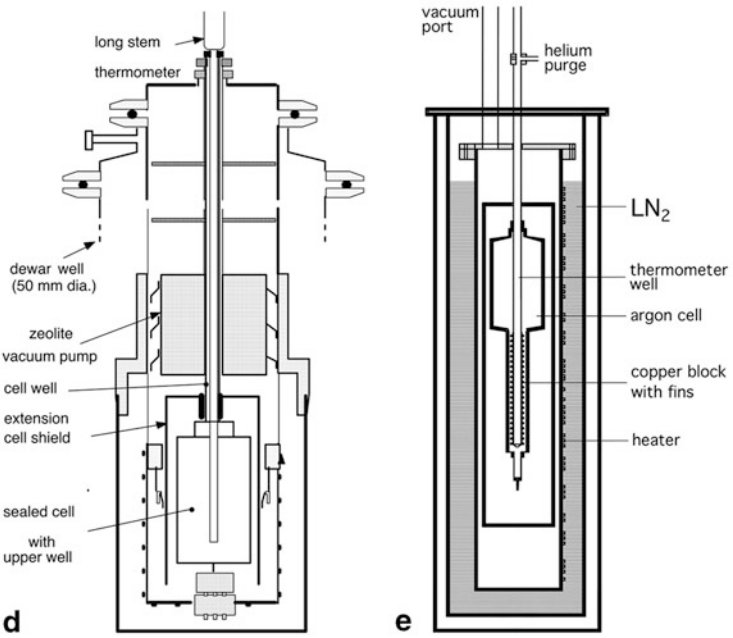

Fig. 2.40 (continued)

of liquid argon, vertical copper concentric tubes are placed in the liquefied phase. The liquid condenses in the cell bottom to a level exceeding the length of the sensing element, and the vapor space extends to about 13 cm length. The temperature of the liquid nitrogen bath is raised to upon 84 K by increasing its boiling pressure up to ≈ 205 kPa. This pressure is obtained with the use of a dewar capable of withstanding high internal pressures by providing a vent to the overpressure through a gravity-type valve. By changing the weight of its cap,[9] the difference of the bath pressure with respect to atmospheric pressure can be trimmed ($\mathrm{d}p/\mathrm{d}\,T = 20.2$ kPa K^{-1}) so as to obtain a bath temperature within $+0.1$ K of the triple point temperature. Under these conditions, melts lasting from 3–4 h are obtained, with $u = 0.3$ mK, and a total uncertainty ± 0.4 mK including the estimate of systematic deviations, as reported from an international intercomparison (Bloembergen et al. 1990).

Incidentally, a cell of this type has also been used as a *pressure* fixed point (Bonhoure and Pello 1983). Instead of a thermometer well, the cell is equipped with a tube extending to room temperature and is connected to a valve and to a diaphragm differential pressure transducer (see Part II, Sect. 9.2).

Subsequently, the same authors (Hermier and Bonnier 1990) used a modified version of their cell in an adiabatic mode of operation. Instead of an overpressurized liquid nitrogen bath, they used as a thermal guard for the cell an external buffer

[9] This must be protected from frost, since the latter would cause a weight change, by keeping it under the escaping dry nitrogen vapors, through a plastic cap.

cell also filled with argon condensed from an external bottle, kept at the triple point temperature by passing cold nitrogen vapors in a coiled tube embedded in it. This method implements the "self-regulated passive shield" principle described in Sect. 6.2.4. The melting is performed with the *continuous heating* (dynamic) method (see Sect. 2.3.1.1) and a value of $u = 0.2$ mK is reported. A later development can be found in Dobre et al. (2011).

As a second approach, the argon cell in Fig. 2.40c (Ancsin and Phillips 1976) is shown, which is a simplified calorimeter cooled with liquid nitrogen at 77 K. The thermometer well extends to room temperature in an evacuated jacket, from a measuring chamber about 20 cm long, in which temperature uniformity is ensured by an isothermal shield regulated with respect to the cell via a differential thermocouple. Ten centimeters of the stem bottom, where the sensing element of the thermometer is located, are inserted into the well of a copper cell where ≈ 6 L of argon are condensed into $\approx 6\,\text{cm}^3$ of liquid for a depth of ≈ 5 cm. The cell is sealed, but not *in* the cryostat, as it is connected to a room temperature 2 L gas ballast to limit pressure when at room-temperature. Therefore a heat exchanger is required as described in Sect. 2.3.3.1. Melting is performed by the intermittent heating (calorimetric) method. The uncertainty of the triple point realization is ± 0.25 mK.

The third approach, illustrated in Fig. 2.40d, uses a small sealed cell about 12 cm long, fully housed in the cryostat, but with a Ø 6 mm thermometer well extending upwards. Therefore, when the cell is not used with a capsule thermometer, a well extension is added, which is filled with helium exchange gas. The assembly can be inserted in the reentrant well of a calorimeter-type cryostat such as that shown in Fig. 6.2 (Pavese et al. 1990d), can be used with a closed-cycle refrigerator (see again Chap. 6). The cell contains about 0.2 mol of gas, which condenses at the cell bottom into about $5\,\text{cm}^3$ of liquid around the sensing element. The melting procedure is the same as that used with the cell of Fig. 2.18 (see Sect. 2.3.1.2), achieving an uncertainty of $\pm$ 0.2–0.3 mK.

The argon cell equipment realized at INTiBS (Szmyrka-Grzebyk et al. 2012a) shown in Fig. 2.40e is similar in principle to the Furukawa type of Fig. 2.40a, but with a different cell and cryostat design. When realized with the continuous heating (dynamic) technique, a melting plateau stable within 0.2 mK is obtained in the F range 0.1–0.7.

Finally, the carbon dioxide cell (≈ 216 K) of Ambrose (1957) and Blanes-Rex et al. (1982) (not shown) has a marked analogy with a cell for the triple point of water. It has been made of metal or of glass (but in this case it must be stored at a temperature near that of the triple point, in order to limit the inner pressure to ≈ 0.5 MPa) or of metal. The metal cell was designed as a standard sampling cylinder, in accordance with the British Standard 1736:1951, and contained about 2 mol of substance at a density such as to allow it to be about 75 % full of liquid at 6 MPa when at room temperature. The cell was completely immersed in a bath of ethanol, chilled with solid carbon dioxide (which has a sublimation temperature at 0.1 MPa that is lower than the triple point, ≈ 195 K), or with a commercial circulator; the bath was maintained stable kept stable at the triple point temperature to within ± 0.5 K. With

a copper cell and the continuous melting technique, the triple point temperature was reproduced with an uncertainty of ± 0.3 mK and with a stainless steel cell, within ± 0.6 mK.

2.5 Fixed Points Using Other Phase Transitions

Apart from the lambda transition in ^{4}He, which is a liquid-to-liquid transition (see Sect. 2.5.1), all other phase transitions useful for thermometry are solid-to-solid transitions (see Sect. 2.5.2). The lambda transition is a reference point of top quality, whereas the accuracy obtainable with the others in the realization of a reference temperature value is much lower. However, some of these transitions occur in temperature regions where no other types of fixed point are available and some are readily available, beside the triple point, in the same sealed device. They can be used in the realization of simple temperature scales for approximating the ITS-90 (see Sect. 2.6).

2.5.1 Liquid-To-Liquid Transitions

It is worthwhile to describe only one of these transitions as a reference point, which is important because it is easily realized to very high accuracy, in a temperature region where no other references of comparable quality are available, except very specialized devices such as the superconducting-transition fixed-point devices. This transition is the ^{4}He lambda-transition from normal to superfluid liquid, at 2.1768 K, a temperature value falling halfway between that of the superconducting transitions of aluminum (1.1810 K) and of indium (3.4145 K). The reader is directed to texts on helium properties, e.g. (Van Sciver 1986), for further reading about its physical properties.

The position of the λ-transition in the p–T plane is shown in Fig. 2.3. It is actually a *line*, as the two liquid phases exist in the pressure range, below the solid phase boundary. The state being discussed is the *lower end point* of this line, where it joins the saturated vapor-pressure line. It is always crossed when lowering pressure on a ^{4}He liquid bath.

The transition is a second-order one, as entropy shows only a slope discontinuity (Fig. 2.41a) and no enthalpy of transition is involved. The value of specific heat shows a logarithmic infinity at T_λ (Fig. 2.41b). Thermal conductivity varies from moderate values in normal liquid (0.02 W K^{-1} m^{-1} in ^{4}He-I, but 0.5 W K^{-1} m^{-1} just below T_λ), to extremely high values in the superfluid phase (>1000 W K^{-1} m^{-1}), much higher than those exhibited by the best metals.

In fact, in the two-fluid model of superfluid helium, the heat transport through ^{4}He-II is accomplished by motion of the normal component. The mechanism is internal convection, far more effective than is heat transfer by diffusion conduction. Heat transport is thus provided by the hydrodynamics of the motions of the normal and

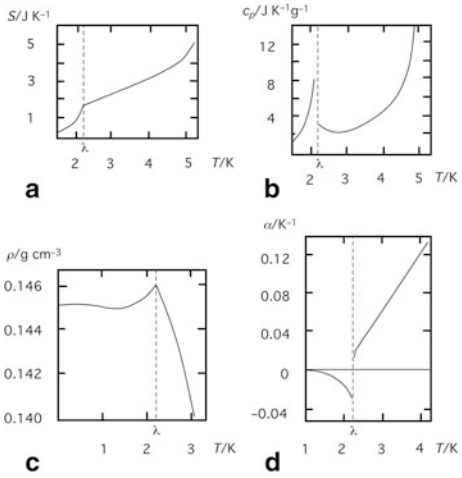

Fig. 2.41 Behavior of ^{4}He at the λ-point. **a** Entropy S. **b** Specific heat c_p. **c** Density ρ. **d** Cubic thermal expansion coefficient α. (After Van Sciver 1986)

superfluid components (Arp 1989). At small thermal flux density, the motion of the normal component is laminar flow: for a 2 mm diameter straight tube, as in a typical cell (Song et al. 1991), thermal conductivity would be $\lambda \gg 5.3 \times 10^9$ W K^{-1} m^{-1}; when the thermal flux density increases beyond a critical value, the motion becomes turbulent and, very close to T_λ, is $\lambda \gg 7.7 \times 10^3$ W K^{-1} m^{-1}. It must be pointed out that in a range of 20 mK just below T_λ, thermal conductivity changes by four orders of magnitude (Alhers 1968, 1969).

In bulk liquid, the transition will take some time to involve all the liquid, as normal liquid helium (so-called liquid ^{4}He-I) shows thermal layering, and the superfluid liquid (so-called liquid ^{4}He-II) has its maximum density near T_λ, as shown in Fig. 2.41c. Therefore, liquid-II tends to leave the surface, where refrigeration takes place, and be replaced by liquid-I. Besides, since no thermal gradients can exist in liquid-II, *all* liquid-II will remain at exactly T_λ until some liquid-I is present. For this reason, a flat temperature (and pressure) plateau is observed, lasting for some time and looking like that of a first-order transition. A thermometer immersed in liquid-II will accurately measure T_λ (account being taken of Kapitza effect—see Sect. 4.3.2.2).

Care must also be taken to limit the hydrostatic temperature gradient in the liquid-II (about 100 mK MPa^{-1}, equivalent to about 1.5 mK/m of liquid (Alhers 1968)) if the bath is deep. The effect of impurities is not critical, equivalent only to -1.4 μK ppm^{-1} with ^{3}He (Hwang et al. 1976), which is the only likely impurity (at a level of 0.5–2 $\times$ 10^{-6} in natural ^{4}He).

Instead of using an open bath and producing the transition by pumping on it (directly, or through a "*lambda*-plate" device (see Chap. 6), the bath can instead be made colder via a heat link connected to a lower temperature, and then a heating source on the link can be adjusted in order to produce the transition alternately in both directions.

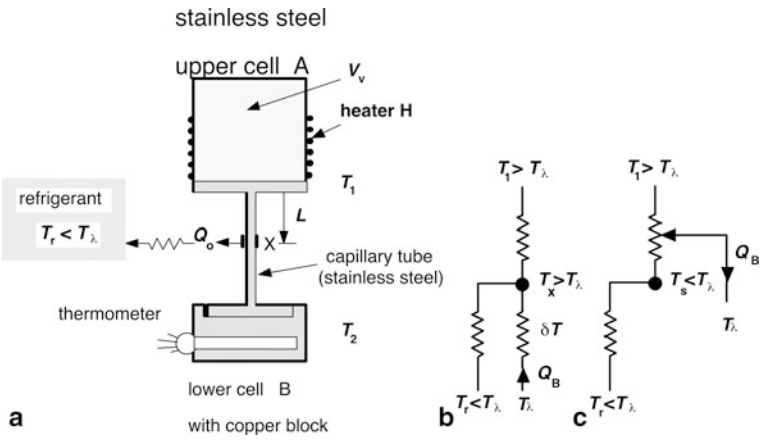

Fig. 2.42 **a** Layout of a sealed cell for the realization of the ^{4}He λ-point. **b**, **c** Schemes of the heat fluxes along the capillary tube for large and small heat inputs, respectively (thermal resistances are indicated; see text)

2.5.1.1 The Lambda-Transition in a Sealed Device

This reference point can also be realized using a *sealed device*. In 1989, a sealed cell, with a capillary, was built in the Cryogenic Laboratory (CL) to realize the transition temperature of liquid helium, using the capillary as a thermal delay-line (Naihao et al. 1989). In 1990, using the same cell, a temperature plateau was obtained at CL with a small heat flow along the capillary such that an interface of He I/He II was maintained within the capillary (Lin Peng et al. 1990, 1997; Song et al. 1991). Because there is a depression of the lambda transition temperature by a heat flux (Alhers 1968b, 1969), the transition temperature measured by thermometer was low. Later a platform was used to control the heat flow passing along the capillary and an extrapolation was employed to determine the transition temperature with zero heat flow (Lin Peng et al. 1997, 2002, 2003, 2011; Peroni et al. 2001). Here a slightly modified arrangement is described in Fig. 2.42. Most of the volume of the two-chamber device is required, as usual, in order to limit room-temperature pressure of the helium contained in it within an acceptable value, 5–7 MPa. The lower small-volume (few cubic centimeter) chamber B is incorporated in a copper block, where the thermometers that are to be calibrated are inserted, and is connected to the upper chamber A only via a small-diameter stainless-steel tube of very low thermal conductivity. When refrigerated to condensation, liquid helium fills, at T_λ, most of the lower chamber, the tube (whose volume is typically 0.1 cm^3) and a few millimeter of the upper chamber. One point X of the tube, near middle length, sinks some heat toward a refrigerant whose temperature $T_r < T_\lambda$.

The cell is first cooled down to about 2.5 K by exchange gas in the cryostat or—under vacuum—by conduction, then is thermally insulated from it and allowed to cool below T_λ by heat leakage. Eventually only liquid-II is present, and, because to

its peculiar heat transport mechanism, $T_1 \equiv T_2 < T_\lambda$. Subsequently, a heater on the upper chamber is switched on. *All* liquid-II warms up and the thermometer block B with it. When the top of the liquid column in the upper chamber crosses the transition temperature, the liquid-I formed will easily and quickly overheat. As soon as an interface is formed, all liquid-II as well as the block attain T_λ and remains at that temperature, $T_1 \equiv T_2 = T_\lambda$. Continuing heating the upper chamber, the level of the transition interface gradually recedes in the tube as more liquid-I is formed, but the temperature of liquid-II and of block B filled with it, remains constant at T_λ. The thermal conductivity of a length L of the stainless-steel tube is almost infinite when filled with liquid-II, but is instead very small when filled with liquid-I: the tube acts as a heat-switch. The thermometer block therefore becomes almost thermally decoupled from the upper chamber and its heating, and only reflects the lambda interface temperature, whatever its level in the tube may be: $T_2 = T_\lambda$. If the energy balance is such that the heat sink point $T_X = T_\lambda$, the interface level L will stabilize there. Should the block B receive more heat Q_B from the environment,[10] the interface level will simply recede in the tube, allowing an extra ΔT to build up along the liquid-I-filled portion of the tube (case (b) in the figure). Should, on the contrary, the block lose heat to the environment, the interface level will rise, and liquid-II will "short-circuit" this additional length of tube (case (c) in the figure). If $T_X \neq T_\lambda$ because of a change in T_r, the level of the interface will move according to case (b) or (c) in Fig. 2.42, depending on whether $T_X > T_\lambda$ or $T_X < T_\lambda$ respectively.

In other words, the device can accommodate a *range* of values of heat exchange with the environment without changes of the block temperature, T_λ. Outside this range, excessive refrigeration or heating brings the interface outside the connecting tube. When the liquid-I/II interface no longer exists there, the reference temperature T_λ is lost. The cell can reproduce T_λ for over 20 min by simply controlling the over-temperature of the upper chamber to a value $\Delta T_\lambda = (10 \pm 5)$ mK (Naihao et al. 1991), and an accuracy of better than ± 0.1 mK has been reported for this device by (Hwang and Khorana 1976; Naihao et al. 1991).

The cell can work even omitting the heat tie down on the tube, like in Figs. 2.42a.

In order to control the heat flow passing through the cell, the top chamber is supported from a copper platform using three brass rods, which act as thermal weak links. On its upper side, the platform is connected through a similar rod system to a copper flange so that the sealed cell and platform assemblage forms an easily handled structure. Finally the device is fixed to the bottom of the ^{4}He pot of the cryostat through the threaded head of the flange.

When the temperature of the cell cools below T_λ, the capillary is fully filled with superfluid helium, He II. The temperature of the bottom chamber, TB, is then set to a value higher than T_λ, say + 15 mK, and the temperature of the platform, TP, is regulated to a value below T_λ. The normal fluid helium, He I, appears at the bottom of capillary and superfluid helium exists in the upper part of the capillary and the top chamber. Because of the great change in thermal conductivity of liquid helium

[10] Actually, some heat comes, at least, from Joule-heating of the thermometers.

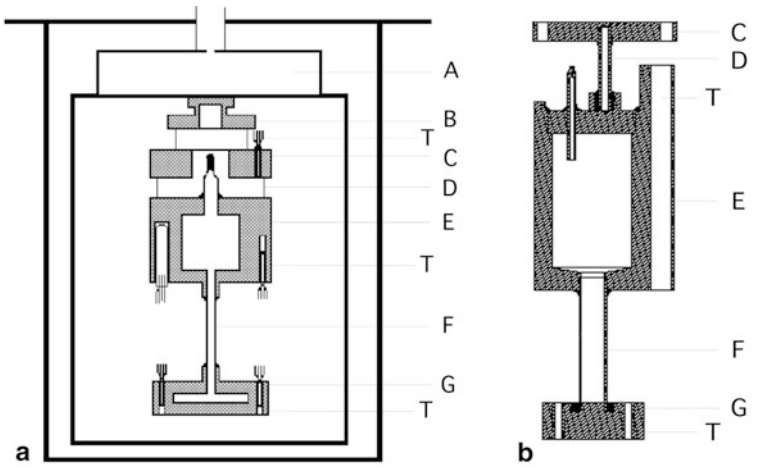

Fig. 2.43 **a** Chinese-type λ-point cell. (After Lin Peng et al. 2003). **b** MULTICELL λ-cell of PTB model. (After Engert et al. 2003; Peroni et al. 2001; Pavese et al. 2003b). *A* upper chamber: ^{4}He-pumped reservoir; *B* λ-cell attachment; *C* upper platform; *D* weak thermal link; *E* upper λ-cell body; *F* low thermal conductivity capillary; *G* lower λ-cell chamber; *T* thermometer. Dimensions of various fabrications are in Table 2.9

at the lambda transition, the column of He I within the capillary provides a self-adjusting heat-link. Under steady conditions, the heat flowing along the capillary to the top chamber will equal the heat leak from the top chamber to the platform, which is governed by the temperature difference between them. The He I/He II interface within the capillary is located so as to maintain the same heat flow, and a stable temperature "plateau" is obtained in the top chamber. On increasing the set point for TP stepwise, the heat flow progressively decreases and a series of new plateaus are reached at slightly different temperatures. These generate a staircase pattern on a chart recorder, each plateau corresponding to a different heat flow. Plotting the readings of the thermometer against the heating power dissipated at the bottom chamber, PB, and extrapolating to zero heat flow, the temperature with no heat flow depression is obtained (Fig. 2.44a; Peroni et al. 2001; Lin et al. 2003). In Lin et al. (2011), a summary result of 34 measurements performed in the period 2002–2008 on cells of the CL model shows a remarkable performance, with $u = 27$ μK, partially due to the contribution of an apparent drift of the RhFe thermometer of ≈ 40 μK in the same time span.

Similar performances were later obtained with a revision of the design by the European Project (Maidanov et al. 2001; Engert et al. 2003; Pavese et al. 2003d). The following main effects have to be taken into account in the design:

- T_λ is depressed by pressure at a rate $\mathrm{d}T_\lambda/\mathrm{d}p = -87.8$ nK/Pa, leading to a depression by a liquid column of height h at a rate $\mathrm{d}T_\lambda/\mathrm{d}h = 1.27$ μK/cm.
- T_λ is depressed by ^{3}He, the only remaining impurity in liquid ^{4}He, at a rate $\mathrm{d}T_\lambda/\mathrm{d}x = -1.45$ K, where x is the molar fraction of diluted ^{3}He.

Table 2.9 Basic data of the measured sealed cells

Data of the cells	Cell C-3[a]	Cell D-1[b]	Cell D-2[b]	Cell D-3[c]	Cell E-1[d]	Cell PTB
Outer diameter of the top chamber (mm)	42	42	42	42	30	35
Total length of the sealed cell (mm)	150	150	150	160	100	93
Outer diameter of the capillary (mm)	3.0	3.0	3.0	3.0	3.0	6.0
Inner diameter of the capillary (mm)	2.0	2.0	2.0	2.0	2.0	5.0
Length of the capillary (mm)	40	47	47	55	20	25
Cavity volume of the cell (cm^3)	9.75	9.75	9.75	10.03	4.88	9.4
Fill pressure[e] (MPa)	10.5	10.0	10.0	10.0	10.5	7.0

[a–d] CL (China) models. Also two cells L1 and L2, with capillary length of 40 mm, were later used
[e] ^{4}He nominal purity 99.9999 %

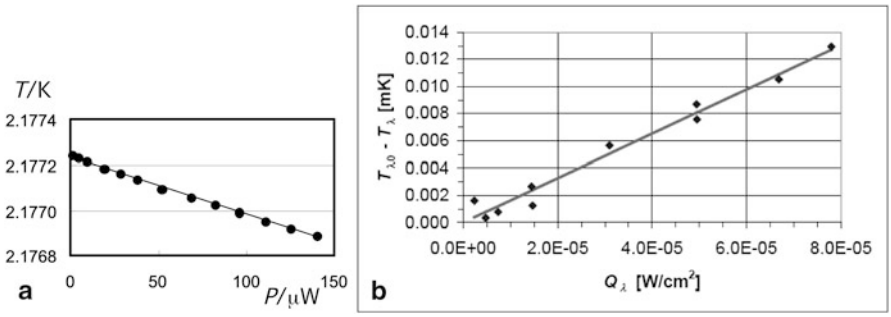

Fig. 2.44 Effect of the heat flux P on the realized T_λ. **a** Chinese type cells, extrapolated values to $P = 0$ are reported in Table 2.10. **b** PTB type cell

Table 2.10 T_λ realization results obtained at CL, IMGC, and NPL

Laboratory	CL	IMGC	NPL	T_λ(NPL)–T_λ(CL)	T_λ(IMGC)–T_λ(NPL)
Cells used	C-3, D-1, D-2	E-1	D-2, D-3		
N° realizations	7	3	8		
T_λ/K	2.177 088	2.176 985	2.177 057	−31 μK	−72 μK
u/μK	44	18	5.8		

- For heat fluxes $Q \leq 10\,\mu W/cm^2$, T_λ is depressed by the heat flux approximately according to the formula $\Delta T_\lambda/T_\lambda = (Q/Q_0)^\alpha$, where $\alpha = 0.813$ and $Q_0 = 570\,W/cm^2$. For larger heat fluxes, the depression may follow another formula, but this has not yet been investigated in detail.

Choosing an appropriate experimental design for realizing the lambda transition, the corrections, which have to be applied to T_λ, amount only to several microkelvins according to the formulas given above.

The SLPC is operated in the following way. The copper flange of the thermal link is connected to the thermal bath of a cryostat that has a temperature T_0 below the temperature T_λ of the superfluid to normal-fluid transition. The temperature T_0 is stabilized at a level of 1 mK. Monitoring the temperature readings of the thermometers in the main body of the SLPC during cooling, one can find a small plateau in their time dependence, indicating the condensation of the ^{4}He gas into the liquid state. After one has cooled the whole SLPC to temperatures below T_λ, there is no measurable temperature difference between the main body and the lower copper plate because of the extremely high thermal conductivity of the superfluid ^{4}He. Turning on the current through the heater, one raises the temperature of the lower copper plate above T_λ. Adjusting the heating power, one can fix the position of the interface between the normal-fluid ^{4}He in the lower part and the superfluid ^{4}He in the upper part at the desired height in the stainless-steel tube. In this configuration, the temperature of the main body of the SLPC and hence the temperature of the thermometers inside the holes of the main body is the measured value of T_λ. This value of T_λ has to be corrected for the depression by the used heat flux, the height of the liquid column above the phase boundary and the temperature difference between the superfluid ^{4}He and the main body. Because of the large heat capacity of the superfluid ^{4}He and the high thermal resistance to the bath temperature T_0, the main body of the SLPC can be held at T_λ over very long periods being only limited by the running time of the cryostat (up to 18 h observed). The standard uncertainty budget of these measurements is less than 50 μK and the repeatability 10 μK at most.

2.5.2 Solid-To-Solid Transitions

Solid-to-solid transitions can be observed in O_2 (two) (Pavese and Ferri 1982; Lipinski et al. 1996, 1997, 2003; Szmyrka-Grzebyk et al. 1998, 2007, 2012a), N_2 (Pavese and Ferri 1982; Lipinski et al. 2007a), CH_4 (Pavese and Ferri 1982), C_2H_6 (two) (Pavese 1978a), C_3H_8 (martensitic type; Pavese and Besley 1981b). In solid-to-solid transitions only the solid and vapor phases are present; only those occurring along the saturated solid-vapor line will be considered here. As vapor is generally at very low pressures, it does not enhance the solid-container thermal contact; helium gas could be added to improve it, as in powder calorimetry, but usually it is not because the triple point is also measured. In addition, the diffusion time constant of the transition through the solidified gas crystals is extremely large, as the interface mobility is very low.

First-order transitions, such as the β–γ in oxygen, exhibits an enthalpy of transition, and behave like, and in principle are realized in the same way as, the triple points. However, the quality required for the calorimeter is much higher, and the equilibration time much longer. It is not unusual to observe overheating of the solid

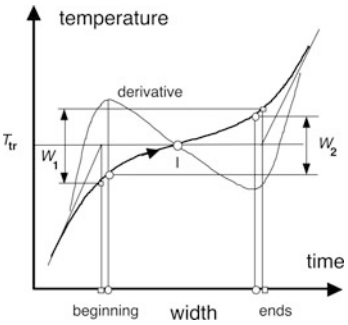

Fig. 2.45 Possible definitions (W_1 and W_2) for width of a reference point based on a second-order solid-to-solid transition with temperature T_{tr}. *I* inflection point

phase at the beginning of the transition, which usually is an experimental artifact, when heating is started from the lower-temperature phase (e.g. for α–β of nitrogen see Kemp and Kemp 1979a). In addition, even when the transition is carefully started with the intermittent-heating method under good adiabatic conditions, and when the heating power is low enough to keep the overheating peak (see e.g., Fig. 2.11) very small, a very long initial re-equilibration time is often observed. In general, this fact can be attributed to an initially poor thermal contact of the low-temperature phase with the cell walls, which later improves due to an expansion of the solid that occurs because of the usually lower density of the upper phase. However, in at least one case (ethane (C_2H_6): Pavese 1978a), it was possible to attribute the peak to a true overheated metastable state of the low-temperature phase.

A problem arises in defining *the* transition temperature, as it is generally impossible to use the $1/F$ versus T plot. The inflection point of the T versus time plot is often used, but its position along the transition is greatly influenced by the experimental procedure. This fact, too, adds to the uncertainty to be assigned to the value of the transition temperature.

Second-order transitions have no enthalpy of transition but only show a heat capacity peak. Therefore the transition, in the T versus time representation, does not show a flat plateau but only an S-shaped behavior, with a maximum derivative value at the inflection point, $(dT/dt)_I \neq 0$ ($c_{p,I} \neq \infty$; Fig. 2.45). A transition width can be defined in two ways: $\Delta T = W_1$, from the transition duration at T_{tr} obtained from the extrapolated lines for constant heat capacity before and after the transition; or $\Delta T = W_2$, between the first derivative maxima.

To be noticed that the α–β transition of oxygen, which in realization looks as a second-order transition (Lipinski et al. 1997, 2003) and has been considered long since second-order (Fagerstroem and Hollins 1969), it has been also stated to be a first-order based on theoretical considerations (LeSar and Etters 1988; Kuchta et al. 1987). The question is still open, since the change in the molar volume is reported to be very small (0.5 %) and values for the possible enthalpy change in the transitions in the range 10–103 J mol^{-1} have been reported. The interest in this transition, in addition to its use for scale approximations (see Sect. 2.5), is increased by the possibility that an argon impurity can be detected in oxygen (not possible at the triple point), because it changes the transition temperature (Pace and Bivens 1970).

Transition temperature values are collected in Appendix B. Their use in temperature scales is described in Sect. 2.6.

2.6 The ITS-90 Between 13.80 and 273.16 K and Scale Approximations Using Sealed Fixed Points

The ITS-90 was conceived in order to reproduce as closely as possible the thermodynamic temperature and to interpolate between fixed points with a nonuniqueness (whose meaning is explained in Sect. 1.2.2.2) limited to ±0.5 mK above 25 K and ±0.1 mK below 25 K. Some complications in satisfying these requirements were due to the fact that no convenient temperature values are available in nature for some of the required fixed points. In the range from 13.80 K to 273.16 K considered in this section, the approach of using only triple points of gases as fixed points has been followed wherever possible and was prompted by the studies performed after the issue of the IPTS-68, and, especially, by the experience gained in an international intercomparison of fixed points of this type (Pavese 1984b; Pavese et al. 1984a). New requirements were also introduced in the ITS-90 with respect to the IPTS-68: as regards to the interpolating function for platinum resistance thermometers,[11] a *single* deviation function for the *full* range was used (instead of several, as in the IPTS-68); as regards to the subdivision in subranges of the temperature range, subranges overlapping was allowed (the subranges are different from those used in the IPTS-68).

These subranges are listed here below, with the indication of the number of required defining fixed points; the same paragraph numbers of the text of the ITS-90 (see Appendix A) are used:

3.3.1 13.8033–273.16 K: 4 triple points of gases, 2 triple points of substances that are liquid at room temperature, 2 points of a vapor-pressure thermometer filled with e-H_2 or of the ICVGT;
3.3.1.1 24.5561–273.16 K: 4 triple points of gases, 2 triple points of substances that are liquid at room temperature;
3.3.1.2 54.3384–273.16 K: 2 triple points of gases, 2 triple points of substances that are liquid at room temperature;
3.3.1.3 83.8058–273.16 K: 1 triple point of a gas, 2 triple points of substances that are liquid at room temperature.

A subrange of marginal interest here and not further discussed in the present monograph, is:

3.3.3 234.3156–302.9146 K: 2 triple points of substances that are liquid at room temperature, 1 fusion point of a metal.

[11] It consists of a reference function and of deviation functions from it.

The basic range given in 3.3.1 overlaps the range of the ICVGT, whose upper limit is 24.5561 K. Therefore, the subrange 3.3.1.1 can be considered the real basic range, unless the standard platinum-resistance thermometer (SPRT) has to be used down to 14 K, or no gas thermometer is available. In 3.3.1, two points from the e-H_2 vapor-pressure scale must be used, namely at ≈ 17.035 K and ≈ 20.27 K, thus introducing the additional requirement of a *pressure* measurement. This definition is similar to, but *not* the same as, the IPTS-68 definition. In the ITS-90, a small temperature range (± 0.01 K) is in fact allowed for the choice of each of the two hydrogen boiling points, and not only the pressure values of hydrogen at the two points, but also its dp/dT, are provided. Therefore, the ITS-90 actually puts *five* constraints (if the triple point temperature is included) to the e-H_2 vapor-pressure equation in the 13.8–20.3 K range. For more on vapor-pressure thermometry, see Chap. 4.

Let us concentrate now on the three ranges 3.1.1.1–3.1.1.3.

2.6.1 Realization of the ITS-90 in the Laboratories

One to four triple points of gases, which can be realized in sealed cells, are necessary to realize the ITS-90. In the range 3.1.1.1, the triple point of e-H_2, which lies outside the range, was necessarily added to impose a further mathematical constraint to the interpolating function, in order to keep the scale nonuniqueness within the aimed limits (± 0.5 mK).

We recall here what has been introduced in Sect. 1.2. The basic requisite of a standard is to be unique within a given uncertainty. In the case of the ITS-90, several mechanisms, usually indicated as Type 1 to Type 3 (White et al. 2007), give rise to nonuniqueness, which in several ranges dominates the uncertainty attributed to the scale. Type 3 nonuniqueness is related to differences in interpolating instruments of the same type (e.g., due to slightly different R–T characteristics of different samples of platinum; or, due to differences in the realizations of the vapor-pressure or gas-thermometer implementations; or, due to the imperfection of the mathematical model used to describe temperature as a function of the response variable of the interpolating instruments). ITS-90 extensively uses the philosophy of 'multiple definitions': this is another independent source of nonuniqueness that also has to be taken into account (Type 2 if different types of interpolating instruments are used, Type 1 if there is an overlapping subrange with the same interpolating instrument). Figure 2.46 shows the effect of Type 1 non-uniqueness below 273.16 K (White et al. 2009, after Meyer and Tew 2006 and Steele 2005).

Additionally, the triple point of water must be realized, which can be done also in a sealed cell (Ancsin 1982; Bonnier 1982, 1987; Pavese and Ferri 1982), and the triple point of mercury, which can be done in miniature glass cells too (Lipinski et al. 2001; see Sects. 2.4.3.1 and "Multiple-cell design"). As regards to the latter, most experience is so far limited to large cells for long-stem thermometers (Furukawa et al. 1976, 1982) and nothing certain is known, at present, about the stability of mercury in metal containers. Should a *long-term* stability be verified, and then this

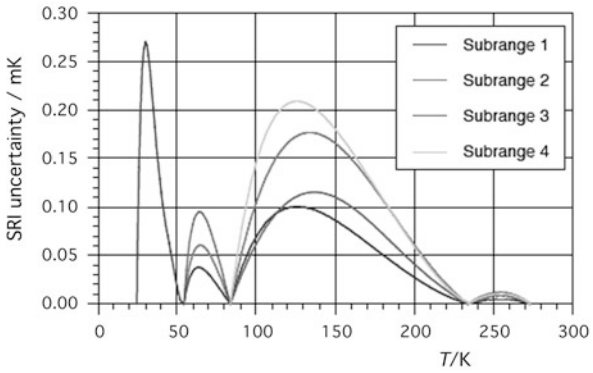

Fig. 2.46 Type 1 nonuniqueness (subrange inconsistency, SRI) of ITS-90 for four subranges over the range 24–273 K. (After White et al. 2009)

triple point too could easily be realized in a metal sealed cell. This point, which is quite close to 0 °C, had to be included in the ITS-90 in order to reduce the scale nonuniqueness between 84 K and 273.16 K. Attempts for replacing it with the xenon triple point (≈ 161.4 K) are under study (see Sect. 2.2.2.5).

The resulting ITS-90 Type 3 nonuniqueness over all ranges below 273.16 K is shown in Fig. 2.47 (Kemp 1989; Hill and Bedford 1990; BIPM 1990a; Hill and Steele 2002).

In principle, all the substances of these fixed points can be included in a single multiple device for the realization of the whole scale (Sect. 2.4.1.2). However, the triple point temperature of the two upper points is much higher than that of liquid nitrogen, commonly used to cool the cryostat. A closed-cycle refrigerator would provide more flexibility in performing all the fixed points and, additionally, would allow cooldown and warmup to be quickly performed.

Today, it seems therefore advisable to consider, unless a refrigerator is used, two different cryostats for the realization of gas triple points and for the realization of the triple point of the substances which are liquid at room temperature, and two different types of devices for their realization.

The sealed cells described in Sects. 2.3.3 and 2.4 are by far the best means to realize the gas triple points, and can be used individually or assembled in one of the devices described in Sect. 2.4.1.2.

For the two upper points, a single liquid (or slush) bath thermostat is the most appropriate. Room-temperature access to the cells is the simplest and traditional glass cells can be used for both water (Sparks and Powell 1972) and mercury (Furukawa et al. 1976, 1982) triple point realizations, where thermometers can be interchanged without difficulty. However, capsule thermometers must be mounted in a stem, the design of which requires specific precautions, otherwise errors as large as 2–3 mK have been observed (Pavese 1984b). A suitable design is shown in Fig. 2.48.

The tendency to make all low-temperature fixed points available as sealed devices is likely to change completely the attitude of users and their attitude to the ITS-90. According to this new approach, a calibration is no longer an “experiment” (often difficult, and always costly and time consuming), but a simple measurement of a self-

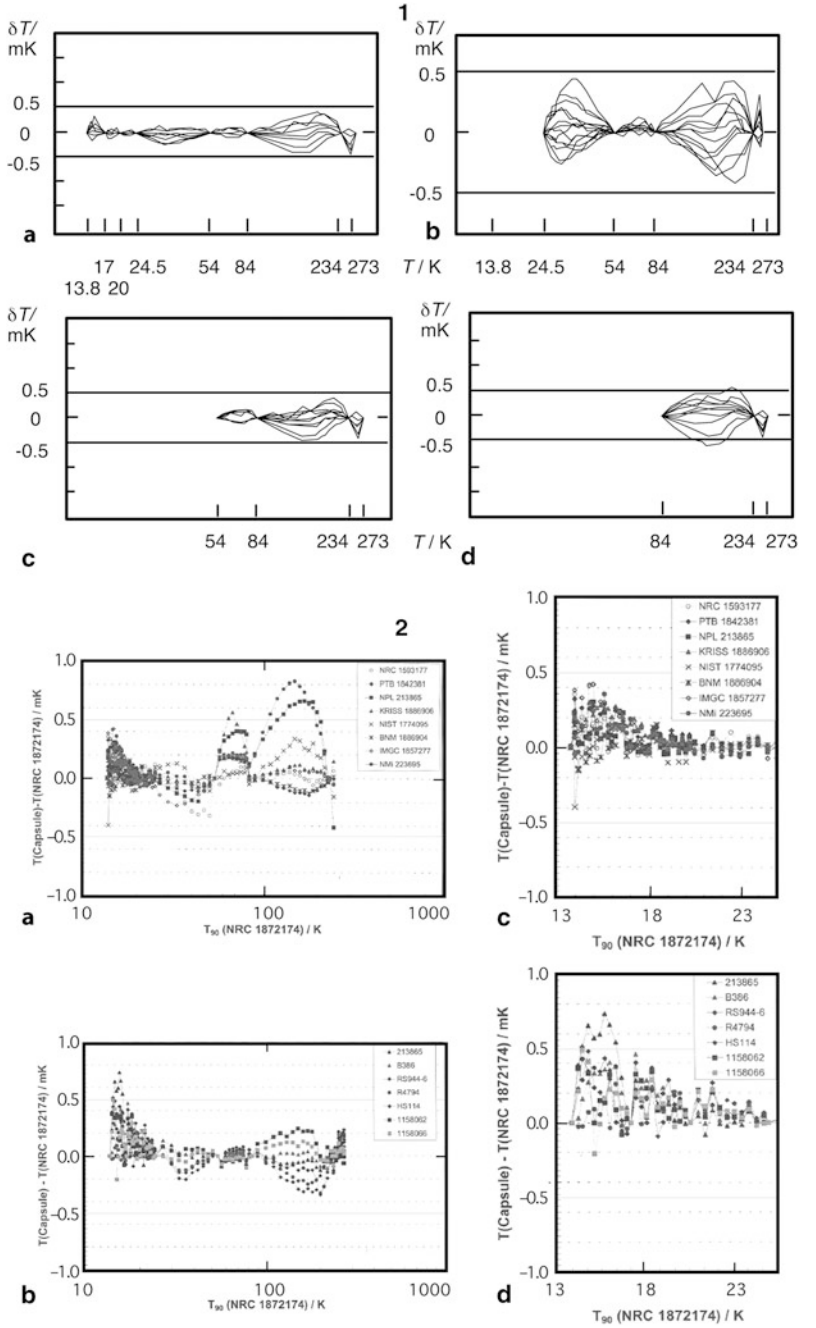

Fig. 2.47 Non-uniqueness of ITS-90 for four subranges: *1* (after Kemp 1989; Hill and Bedford 1990): **a** 13.8–273.16 K; **b** 24.5–273.16 K; **c** 54.4–273.16 K; **d** 83.8–273.16 K. *2* (after Hill and Steele 2003) **a** thermometers used in CCT-K2; **b** other thermometer types (Chino, Hart Scientific, Rosemount, Tinsley); **c** thermometers used in CCT-K2 below 25 K; **d** other thermometer types (Chino, Hart Scientific, Rosemount, Tinsley) below 25 K. Temperature values are those at the fixed points used in the definition

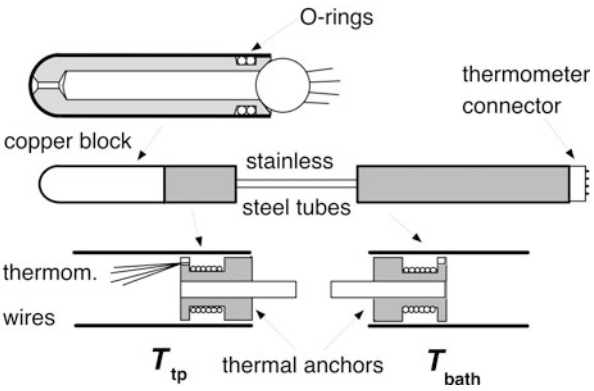

Fig. 2.48 Stem for mounting a capsule thermometer in a long-stem thermometer well. The thermometer connector must be moisture-proof

contained device always ready for use, according to a simple procedure which can be carried out by a computer, especially when a closed-cycle refrigerator is used. This change should encourage a wider dissemination of the temperature scale through a *direct realization of its definition*, namely in an independent way. The role of NMIs is likely to change from a painstaking routine calibration of thermometers, to the certification of the temperature value of fixed-point devices and of the procedures for their use.

The scientists working in these Institutions should not consider such a change as just a time-saving expedient but as a real advantage for the entire scientific community.

2.6.2 Approximating the ITS-90

The high accuracy and reproducibility that the ITS-90 provides are not always needed, and, in such a case, an approximation of the ITS-90 within a specified degree of traceability is sufficient. In other words, if the required uncertainty of the approximation is, say, ± 0.01 K, the approximation should never deviate from ITS-90 by more than ± 0.01 K. This feature must be proved by both mathematical tests and experimental work, which is not the case for most "laboratory scales". The Working Group 2 of the CCT was entrusted with the task of studying these possibilities. A Monograph on the subject was published by the BIPM (Bedford et al. 1990), and referred to in the text covering the ITS-90 definition. This must not be understood as the endorsement of "secondary definitions" of the scale; it means that the traceability to ITS-90 of these scale approximations has been considered, and is known within a stated uncertainty.

In the range from 13.80 K to 273.16 K, there are several possible alternative definitions for approximating the ITS-90, which still use the SPRT quality specified by ITS-90 and provide an accuracy only a little lower than that of ITS-90. A first group uses the ITS-90 mathematical definition and merely *substitutes* one, or more, fixed points, as listed below:

a. The triple point of carbon dioxide (≈ 216.6 K) or of xenon (≈ 161.4 K) is used *instead* of the triple point of mercury. This scale has about the same level of nonuniqueness of ITS-90 (± 0.5 mK in the range 84–273 K), but is traceable to ITS-90 only within ± 1–2 mK because of the uncertainty added by the realization of the substituting triple point, which, at present, is ± 1–2 mK;
b. The triple point of nitrogen (≈ 63.1 K) is used *instead* that of oxygen. This scale has the same level of nonuniqueness of ITS-90, but is traceable to ITS-90 only within ± 1 mK because, until the temperature value of the nitrogen triple point is directly redetermined on the ITS-90, its T_{90} value is known only within ± 1 mK, due to IPTS-68 non-uniqueness;
c. The triple point of methane (≈ 90.7 K) is used *instead* of the triple point of argon. This scale has the same level of non-uniqueness of ITS-90, but is traceable to ITS-90 only within ± 0.5 mK since the realization of the substituting triple point is slightly less reproducible (± 0.3 mK);
d. The triple point of equilibrium deuterium (≈ 18.7 K) is used *instead* of the triple point of equilibrium hydrogen over the range beginning at 25 K. This scale has the same non-uniqueness of ITS-90. The uncertainty of the realization of the substituting triple point is itself within ± 0.2 mK, though more difficult to achieve than using hydrogen, but the scale is traceable to ITS-90 only within ± 1 mK, since e-D_2 T_{90} value is known only within ± 1 mK, due to IPTS-68 nonuniqueness.

Another group of alternative scales still uses an ITS-90-like definition, but omits one or more fixed points. Therefore, these definitions simplify the ITS-90 deviation function;

e. The triple point of mercury is *omitted* in ranges 3.3.1, 3.3.1.1, and 3.3.1.2, and the limit of exponent i in the deviation Eq. A.12 of ITS-90 is accordingly lowered by one. With this scale, the nonuniqueness is increased to ± 1 mK, but only between 84 and 273 K, while remains the same as ITS-90 below 84 K;
f. The triple point of equilibrium deuterium (≈ 18.7 K) is used *instead* of the *two* vapor pressure points of hydrogen in range 3.3.1 and the limit of exponent i of deviation Eq. A.12 of ITS-90 is accordingly lowered by two. With this scale, the non-uniqueness is increased to ± 1 mK, but only between 14 K and 54 K, while remains the same as ITS-90 above 54 K;
g. The triple point of equilibrium hydrogen is *omitted* in the range 3.3.1.1, and the limit of exponent i of deviation Eq. A.12 of ITS-90 is accordingly lowered by one. With this scale the non-uniqueness is increased to ± 1 mK, but only between 25 K and 54 K, while remains the same as ITS-90 above 54 K.
Several of the former alternatives can be applied at the same time, with the stated total accuracy remaining unchanged.

A third group of alternative scales gives a higher uncertainty, of about ± 10 mK, simply because of the lower quality of the selected fixed points which are solid-to-solid transitions (s.s.t.). On the other hand, as they occur in substances that are used as well for the realization of the triple points, fewer calibration devices are necessary. *The triple points of mercury and hydrogen are never included in the*

following alternative scales, owing to the fact that they are no longer necessary to achieve the lower uncertainty level of ± 10 mK:

h. The α–β s.s.t. of oxygen (≈ 23.9 K, accuracy ± 5 mK) is used *instead* of the triple point of neon in range 3.3.1.1. The limit of exponent i of the deviation Eq. A.12 of ITS-90 is lowered by two (having omitted mercury and hydrogen). This scale is traceable to ITS-90 within better than ±10 mK in the whole range, because of the lower accuracy of the substituting fixed point and of the propagation of its uncertainty. For the realization of this scale, extending above 24 K, only *three* cells are required, of oxygen (two points used, plus the included β–γ s.s.t. (≈ 43.8 K, accuracy ±2 mK) which can be used as a check point), argon and water;
i. In addition to the use of the α–β s.s.t. of oxygen as before, the triple point of methane (≈90.7 K) is used instead of that of argon in range 3.3.1.1, and the s.s.t. of methane (≈ 20.5 K, accuracy ±10 mK) is used as well. The limit of exponent i of the deviation Eq. A.12 of ITS-90 is accordingly lowered by one. This scale, which extends above 20.5 K, is traceable to ITS-90 within ±10 mK. Here, too, only *three* cells are required, of oxygen (two points used, plus a check point), methane (two points used), and water.
j. The triple point of nitrogen (≈ 63.1 K) is used *instead* of the triple point of oxygen, and the s.s.t. of nitrogen (≈ 35.6 K, accuracy ± 6 mK) *instead* of the triple point of neon. The limit of exponent i of the deviation Eq. A.12 of ITS-90 is lowered by two. A scale similar to that of range 3.3.1.1 and traceable to ITS-90 within ± 10 mK, but beginning at 36 K, is obtained for which, too, only *three* cells are sufficient. By addition of the triple point of hydrogen (and of one cell, and by raising by one the foregoing limit of the exponent i), this scale can be extended down to 13.8 K to the same accuracy;
k. By using methane *instead* of argon in (j), as in (i), another *three*-cell scale beginning at 20.5 K is obtained.

The addition of the triple point of hydrogen, and of one cell, to the alternatives (h) and (i) (and the raising by one the foregoing limit of the exponent i in the defining equation) allows the scale to be extended down to 13.8 K to the same accuracy. Table 2.11 summarizes all these possibilities.

The application of the *mise en pratique* of the kelvin to obtain scale realizations of different—though traceable—uncertainties, could in future allow to use officially some of them, which can be used today only informally (see Sect. 1.2.4).

On the other hand, there are no possibilities to extend a scale below 84 K with the use of only one gas and water. At present, no calculations exist for ITS-90 approximations confined to lower temperatures, e.g. only *below* 84 K or only *below* 54 K.

For an accuracy level of ± 10–20 mK, as provided by the scales of the third group, some industrial-grade platinum resistance thermometers (IPRT) could seem suitable as interpolating devices, since the stability of some types have been found to be of this level. However, this stability level applies only to *selected* units and it would be, therefore, unwise to rely on a generic IPRT for realizing a scale, until more experience is gained and their quality *certified*.

Table 2.11 Approximations of the ITS-90 in the range from 13.8 K to 273.16 K using different sets of fixed points

Range (K)	Definition		Uncertainty (u/mK)[a]
Same as ITS-90 definition with the following substitutions of fixed points (more than one can be applied at the same time):			
	ITS-90	Approximate scale	
a) 13.8–273.16	Hg (234.3156 K)	CO_2 (216.591 K)	1
b) 13.8–273.16	Hg (234.3156 K)	Xe (161.406 K)	2
c) 13.8–273.16	O_2 (54.3584 K)	N_2 (63.151 K)	1
d) 13.8–273.16	Ar (83.8058 K)	CH_4 (90.6935 K)	0.5
e) 24.5–273.16	H_2 (13.8033 K)	D_2 (18.689 K)	1
Same as ITS-90 definition, except some fixed points are omitted, and defining equation re-adjusted:			
	ITS-90	Approximate Scale	
f) 13.8-273.16	Hg (234.3156 K)	Dropped and $i = 1$ to $n - 1$ Eq. A.12	1[b]
g) 13.8-273.16	H_2 ($\approx$ 17 K) and H_2($\approx$ 20 K)	D_2 (18.689 K) and $i = 1$ to $n - 2$ Eq. A.12	1
h) 24.5-273.16	H_2 (13.8033 K)	Omitted and $i = 1$–4 Eq. A.12	1
Same as ITS-90 definition with the following substitutions of fixed points of lower quality (more than one can be used at the same time):			
	ITS-90	Approximate scale	
For all	H_2 (13.8033 K)	Omitted	
For all	Hg (234.3156 K)	Omitted	
i) 23.9–273.16	Ne (24.5561 K)	$\alpha - \beta$ s.s.t. O_2 (23.867 K)	
(Only O_2, Ar, and H_2O)		$i = 1$–3 Eq. A.12	10
j) 20.5–273.16	Ne (24.5561 K)	$\alpha - \beta$ s.s.t. O_2 (23.867 K)	
	Ar (83.8058 K)	CH_4 (90.6935 K)	
		$\alpha - \beta$ s.s.t. CH_4(20.48 K)	
(Only O_2, CH_4, and H_2O used)		$i = 1$–4 Eq. A.12	10
k) 35.6–273.16	O_2 (54.3584 K)	N_2 (63.151 K)	
	Ne (24.5561 K)	$\alpha - \beta$ s.s.t. N_2 (35.614 K)	
(Only N_2, Ar, and H_2O used)		$i = 1$ to 3 Eq. A.12	10
l) 20.5-273.16	O_2 (54.3584 K)	N_2 (63.151 K)	
	Ne (24.5561 K)	$\alpha - \beta$ s.s.t. N_2 (35.614 K)	
	Ar (83.8058 K)	CH_4 (90.6935 K)	
		$\alpha - \beta$ s.s.t. CH_4(20.48 K)	
(Only N_2, CH_4, and H_2O used)		$i = 1$–4 Eq. A.12	10
13.8–273.16		*For all*, with re-introduction of H_2 (13.803 K) and the maximum i increased again by one	10

Items correspond to those in Sect. 2.6.2

[a]Total uncertainty, mainly determined from the uncertainty in the temperature values of some of the fixed points, which were secondary fixed points of the IPTS-68 or are solid-to-solid transitions

[b]Above 84 K; below, it is still ITS-90's, ± 0.5 mK

2.7 Gaseous Standard Reference Materials, and Sealed Cells

Let us examine now gases from the standpoint of "standard reference materials" concept, which has been introduced in Sect. 2.1.1.

A gaseous substance is necessarily contained in a storage bottle, where, initially, other gases (air or traces from previous fillings) are more or less present. As discussed in the previous sections, and as is well known in vacuum technology, it is very difficult to obtain a clear (gas-free) surface and impossible to keep it gas-free for a long time. Therefore, it is only the matter of the amount of contamination that can be tolerated. It has already been pointed out in connection with temperature fixed points, that most often less than 10^{-5} of total impurities is required. Therefore, the certifications of a material and of its container are both required. It is the authors' experience that a sizeable fraction of lecture bottles of "research grade" gases does not fulfill specifications. A striking example (Pavese et al. 1988) concerned argon in oxygen (see oxygen in Appendix C).

This is a problem apparently not recognized at present. Gases classified as gaseous "reference materials" for certain physical properties resulted to be merely "research grade" materials in manufacturers' catalogues, not special batches, and not specifically (and independently) certified.

Another meaning of the term "reference materials" can be found in reference books from international bodies, e.g. IUPAC (1987), which contain carefully collected and critically evaluated data on thermodynamic properties. By "reference materials" they intend a limited number of substances that are selected and advised, instead of others, for chemical-physical measurements of the "certified" property, e.g., enthalpy. However, the term refers to the physical *substance* itself, and neither applies to nor guarantees any specific available amount of those substances being certified by any body. This meaning does not seem appropriate and will not be considered here.

Indeed, gaseous SRM are necessary, because it is often so difficult to produce a pure specified substance or to keep it pure in time (let us mention, for example, the problem of deuterium with less than 10^{-4} of HD). If the container necessary to preserve in time the properties of a specimen of SRM could be such that the certified property can be measured *without* unsealing the container and removing the substance from it, the reliability of that SRM would be greatly improved.

All this is obviously impossible for gases that must be consumed, e.g., for combustion or pollution tests. It is possible, e.g., when using differential methods, for comparing the reference with the current production of material, as regards to several properties such as purity, enthalpy of melting, specific heat, etc.

For the latter cases, a *method dispensing from container unsealing now exists, because a sealed cellcan be used*, provided that the container is proved to be inert—a common requirement, indeed, for any SRM storage vessel.

The use of fixed points in sealed cells for the dissemination of the temperature scale is now becoming widespread. The experience of the past 15 years has shown that these sealed devices do reproduce the correct thermodynamic state within the lowest uncertainty allowed by the top state-of-the-art (see Chap. 2.6.1). However, for

most users, these cells must be considered only as SRM s, because only standards laboratories have the means for assessing independently their temperature value in an absolute way.

Sealed devices containing gases are not yet been fully exploited. They can be used not only for transition temperature or purity determinations but also when the determination of physical quantities requires an accurate knowledge of the sample mass, since it is possible to produce cells allowing it be measured by weighing, with an uncertainty as low as $\pm$ 1 mg. An example of different use can be found in Pavese et al. (2010c, 2011b); Hill and Fahr (2011); for cells containing a pure isotope, or in (Bosma et al. 2004; Baldan et al. 2009) for pure organic volatile liquids.

Summary 2.12 Summary of triple-point sealed-cell design criteria (most apply also to solid-to-solid and liquid-to-liquid transitions)

	Example	See section
1. Choice of method for fixed-point realization:	Step-melting	
• Continuous melting/freezing		2.3.1.1
• Calorimetric (step-melting)		2.3.1.2
2. Choice of the cell type according to the thermometer type and temperature range:	Three capsule type thermometers only	
• Long stem only: $T > 84$ K		2.4
• Long stem or capsule: $T > 63$ K		
• Capsule only: $T > 13.8$ K		
3. Choice of sealed-cell type:		
• For long-stem thermometers:	Single cell	
Totally cold cells		2.4.1.2
With room-temperature ballast reservoir		2.4.1.1
• For capsule thermometers:		
Single cell, with internal thermometer block		2.4.1.2
Multiple cell device:		2.4.3.1
Multiple cell-bodies fitted to external block		
Multiple-chamber cell		2.4.3.1
4. Choice of sealed amount of substance: (selected according to the "thermal mass" to be driven and to the gas):		
• With continuous melting technique: 0.5–3 mol	H_2, D_2, Ne: 0.05 mol	
• With step-melting technique: 0.03–0.5 mol	O_2, N_2, Ar, CH_4: 0.10 mol	Table 2.8
5. Design of condensed-sample chamber:		
• Volume: condensed sample must cover sufficiently of thermometer block height	Volume: $\approx$ 1–2 cm^3 for 1/4 − 1/2 block submersed.	
• Geometry: thermal contact between interface and thermometer block must be very good; *solid* phase must stay in contact with the block up to high liquid fractions	Copper block with vertical or horizontal fins or grooves.	
Special cases:	Grid mesh size large enough, as sample condensation into the chamber may be prevented by capillarity effects	
• Catalyst use: catalyst volume < 1/2 that of condensed sample; a grid must prevent powder to reach gas handling system		2.2.2.6
• Horizontal cells: vertical cells generally not suitable for horizontal use, and the reverse		
• Cells for zero-gravity applications: special design needed to ensure condensation in the proper part of cell, interface formation and its thermal exchange with thermometers		2.4.3.1
6. Design of ballast chamber (cell main body):		
• Volume: must be calculated to limit cell internal pressure at room temperature below maximum value allowed by body material strength[a]	Typical 20 cm^3 for $p_{max} \approx 100$ bar.	Table 2.1
• Body envelope: generally made of, or reinforced with, stainless steel[b]	Stainless steel 1 mm thick on Ø 20 mm. Copper much thicker or stainless-steel reinforced	

Summary 2.12 (continued)

	Example	See section
7. Design of cold seal[a]:		
• Permanent: most desirable, being the safest	Pinch-weld seal, fully restoring wall strength	2.4.3.1
• Re-openable: generally, also opens the cell to air, therefore requiring subsequent cell re-conditioning		
8. Choice of the sealed substance:		
• Chemical impurities: if no reliable chemical assay is available, the substance with the minimum purity sufficient to make the correction for the effect of the chemical impurities irrelevant should be chosen, if available	All, namely N_2 and H_2 in Ne, Ar in O_2	2.2.2.3 2.3.2.1
• Isotopic composition (impurities): should a substance whose isotopic composition variability is known to sensibly affect the result, an assay for the composition should be obtained. If a high purity isotope is used (namely ^{20}Ne), the amount of isotopic impurities should be reliably known	H_2, Ne, Kr, Xe, H_2O	2.2.2.5
• Otherwise, in both cases, an uncertainty component taking into account the unknown effect should be added to the budget (that may be the dominant component)		

[a]The cell ballast-chamber is not necessary in the case of cells with room-temperature ballast reservoir. In this case, the cell seal is at room temperature

[b]In the case of internal copper thermometer block, it is, generally, the weaker part of the cell because of the thermometer wells

Summary 2.13 Summary of sealed-cell fabrication techniques

	Example	See section
1. Choice of materials:		
• Copper: Best for the body connecting interface and thermometers. OFHC or high conductivity type	(For cell types of Summary Table 2.12)	2.3.1.2
• Stainless steel: Best for cell body strength. For safe arc-welding AISI 304L must be used	Inner block: OFHC copper (Cu)	2.4
No sizeable difference in performance found between all-copper and all-stainless steel cells	Outer body: AISI 304L stainless steel (SS)	
2. Number of cell parts and assembling techniques:		
• Minimum number: Inner block; outer body; sealing device. Each of them can be split in several parts	Cell parts: block (Cu), body cylinder (SS), body top (SS) and	2.3.1.2
• All arc (or plasma) welded: the best, being the cleanest. Difficult to join copper and stainless steel	pinch-weld tube (SS) with inside copper bush	2.4
• Brazing: de-oxidizing resins to be avoided, since cannot be cleaned up (vacuum-brazing better)		
• Soldering: must be avoided due to both low strength and use of soldering flux	All arc-welded	
3. Machining and cleaning of parts:		
• Machining: clean techniques to avoid parts contamination and for easier subsequent cleaning	Alcohol used instead of oil emulsion.	
• Cleaning: all techniques used in ultra-vacuum industry	Ultrasonic bath, distilled water rinsing, (microbead sanding)	
4. Assembly of parts:		
• General: After cleaning, parts stored in clean closed metal boxes until assembling	The total cell mass is about 150 g	2.2.2.6
• Catalyst: included before welding cell top. Confined by means of metal grid: coarse-mesh placed above block for granular catalysts (hydrates); fine-mesh size into filling tube, for fine-powder catalysts (rare-earth oxides)	The total cell-element mass can be as low as 50 g	
• Weighing: after cleaning[a]		
5. Conditioning of cell:		
• Filling tube: fitted to the cell by welding or using compression seal, depending on sealing device	Heating to 100–150 °C generally sufficient with 3–5 heating-rinsing cycles	2.3.2.1
• Clean vacuum system: cell connected to turbomolecular pump and, whenever possible, residual gas analyzer (RGA)	Static vacuum better than 0.01 Pa obtained	
• Procedure: consists of alternate cycles of heating and rinsing with pure filling gas, until residual-gas spectrum shows clean and stable conditions		
• Catalyst conditioning: hydrates (e.g. ferric oxide) lose substantial amount of H_2O (> 10 % of total mass); long pumping time and monitoring 18 amu line with RGA required	Ferric oxide: ≈ 130 °C, except when used with D_2 (≈ 400 °C, 18 % mass loss) Gd_2O_3: ≈ 200 °C	2.2.2.6

Summary 2.13 (continued)

	Example	See section
6. Filling and sealing cell:		
• Gas purity: must be certified in a way independent on manufacturers' specification, and on the actual gas bottle		2.3.2.1 2.4.1.2
• High-pressure filling: by direct connection to the high-pressure cylinder. Limited by its maximum pressure (20 MPa)		2.3.2.1
• Cryogenic-condensation filling: an amount of gas, measured volumetrically, is condensed in the cell, cooled below gas boiling point		
– Liquid nitrogen: only cell bottom is refrigerated, and sealing can easily be performed on cell top	Used with N_2, O_2, Ar, CH_4 and higher condensing gases	
– Liquid helium: full cell and ≈ 10 cm of filling tube kept insulated with a foam bottle, where cold helium vapors are transferred with a standard siphon tube. No liquid needs to be formed; sample condensation occurs in ≈ 10 min, evaporating less than 2 L of liquid helium. In case of pinch-seals, provisional seal initially done 20 cm above cell, then the final one performed close to cell top, after warm up to room temperature	Used with Ne, H_2 and D_2 (In italics gases that may show purity problems. See Appendix C)	
7. Final checks:		
• For leaks: The cell is immersed in a low-viscosity liquid: leaks show up as bubble chains. Mass stability in time is a much more sensitive check	A mass accuracy of ± 1 mg is achieved.	2.4.1.2
• Weighing: useful not only for leak check, but knowledge of sample mass allows the cell use for measuring some thermophysical properties[a]		

[a] By weighing the empty and filled cell the sealed-sample mass is measured. This possibility is prevented with cells containing a hydrated catalyst, as it shows a mass loss during initial conditioning, or when using some sealing techniques

Summary 2.14 Summary of the sealed-cell measurement procedures: step-melting (for top accuracy results)

	See section
1. Mounting cell in cryostat:	
• Cell accessories: Heater: (e.g. kapton-insulated foil heater) mounted on cell body, close to condensed-sample chamber but as much thermally decoupled as possible from thermometers Wire thermal tie-down: thermometer wires thermally tied down to cell body (e.g. via a strip of kapton-insulated foil conductors) Cell attachment: low thermal conductivity fitted to cryostat	Chap. 6
• Cryostat: Mounting internally to isothermal shield: cryostat shield must be regulated to cell temperature using a differential thermocouple Modular cryostats: cell fitted from room temperature into isothermal shield through cryostat well, using a mounting stem. If stem cannot be removed, it must first be thermally tied down to refrigerant temperature, then provided with a thermal guard, regulated at cell temperature using a differential thermocouple fitted to cell attachment *Cryocooler-driven cryostats should preferably be used.* Temperature controls: only control relative to cell temperature required for vacuum better than 2–5 $\times$ 10^{-3} Pa	
2. Cooling cell:	
• No special precautions required with totally cold cells, as no cold-spots can occur. Sample condensation in cells with room-temperature reservoir shows same problems and requires same precautions used in vapor-pressure thermometry	2.2
• *Slow* solidification advisable to limit stress in solid in performing freezing plateaus (not less than 1 h must be allowed)	Chap. 4.5
3. Approaching melting:	
• Sample heating becomes critical at temperature within about -0.5 K the expected triple point value	2.3.2
• Continuous heating must be stopped and temperature allowed to stabilize and to become uniform	
• Then, heating must be performed in steps ΔT with heating power adjusted for heating duration (ON-time) not less than 2–5 min: $\Delta T = 0.1$–0.2 K up to -0.1 K; 0.02 K up to -0.05 K; 0.01 K up to -0.01 K and 0.002 K up to the sharp increase of apparent heat capacity indicating melting onset. No premelting effects should be observed with pure substances, for slow enough operations to ensure true thermal equilibrium. OFF-time: 1–>3 h above 70 K, 10 min–1 h below 30 K	
• At about -0.005 K shield offset must be adjusted to obtain a small drift upward ($<$ 2–3 mK h^{-1}) of cell temperature *The procedure can be simplified for less than top-accuracy measurements*	
4. Performing melting:	
• Use two timers, one set for ON (heating) time and the other for OFF time. Q_m being the total cell heat of melting, heating power must be set to 0.05–0.01 $\times$ Q_m/min. ON and OFF periods are alternated	2.3.1.2

Summary 2.14 (continued)

	See section
• The minimum set of F (melted fraction) values to be obtained after each ON period is (in %): 5 % 10 %, 20 %, 30 %, 50 %, 65 %, and 80 %. During heating, thermometers indicate an over-temperature, increasing with F, gradually vanishing during each OFF period: a temperature stability of microkelvins can eventually be achieved	
• The melting plateau is defined by these equilibrium values $T_{e,i}$	
• All parameters necessary to evaluate the quality and consistency of the data should also be acquired	2.4.2[a]
5. Obtaining T_{tp}:	
• Temperatures $T_{e,i}$ must be plotted versus $1/F$, obtaining a minimum set of points at $1/F = 20$, 10, 5, 3.3, 2, 1.5 and 1.25. A curve fitted through them, of the minimum order possible—usually linear—allows for extrapolation to the liquidus point, $1/F = 1$, defining T_{tp}	2.3.1.2
6. Acquire and process data:	
• Today *it is a must* the use of automatic control of the experiment and of automatic data acquisition. It allows collecting all the information and performing the cross-checks necessary to obtain the best-accuracy level	2.4.2[a]
• When in addition a cryocooler is used, the experiment can be performed in practically unlimited time periods. This is particularly important when working at temperatures where the only possible refrigerant would be liquid helium	6.1.1

[a] See Pavese et al. (2010b)

Chapter 3
Gas Thermometry Between 0.5 and 273.16 K

Chronologically, gas thermometry was the first method used for the accurate measurement of the thermodynamic temperature—with air used as a working substance—the reason being that the very simple law of the ideal gas (Eq. 1.17) is applicable to several real gases with close approximation. Air was soon replaced by hydrogen[1] and then by helium. The reader is directed to "Further Reading," for the history and the developments of gas thermometry.

Though gas thermometry constitutes the solid foundation of thermodynamic temperature measurements (see Chap. 1), its use has traditionally been regarded as very specialized, and as a difficult part of metrology. According to Callendar (1899), "It is impossible for those who have never worked with a gas thermometer to realize the extent of its shortcomings."

It was only in recent years that proposals for the use of a (constant volume) gas thermometer for the practical realization of the International Temperature Scale in its lower range gained attention in the international metrological community. After the first proposal by Barber (1972), gas thermometry was first accepted, as an *interpolating* thermometer, in the EPT-76 (BIPM 1979), and later it was incorporated, as the interpolating gas thermometer between 3 K and 24.5561 K (see Sect. 3.2), in the ITS-90 (BIPM 1989; Preston-Thomas 1990; see Appendix A). Other methods, such as electrical-resistance thermometer practical scales (see Sect. 1.2.2.2) lost the competition in this temperature range because of the insufficient number of suitable fixed points available below 14 K. Besides, it is difficult with alloy thermometers (such as Rh–0.5at%Fe or Pt–0.5at%Co) to reproduce the batch-to-batch characteristics of the material, which is an essential requirement for an empirical scale (see the problem of nonuniqueness in Sect. 1.2.2.2 and 2.6). For magnetic thermometry (Eq. 1.22), it was difficult to maintain a high accuracy over a wide temperature range. More detailed information can be found in a number of recent texts on general thermometry (Quinn 1983, 1990; Schooley 1986; Bedford 1990; Bedford et al. 1990).

Traditionally, gas thermometry is considered for use above 4.2 K, whereas vapor-pressure thermometry is preferred below 4.2 K, with ^{3}He used between 0.5 K and

[1] The advantage of using a low-temperature condensing gas will be made evident in Sect. 3.1.

F. Pavese, G. Molinar Min Beciet, *Modern Gas-Based Temperature and Pressure Measurements,* International Cryogenics Monograph Series,
DOI 10.1007/978-1-4419-8282-7_3, © Springer Science+Business Media New York 2013

3.2 K and ^{4}He used between 1.2 K and 4.2 K. These vapor-pressure scales are now part of the ITS-90 and are widely used all over the world in physical laboratories. Chapter. 4 is devoted to them, and it is compared with gas thermometry in Sect. 4.3.2.4.

Furthermore, ^{4}He has usually been assumed to be *the* thermometric substance; in fact, most of the research work on gas thermometry below 273.16 K has been based on this isotope (Plumb and Cataland 1966; Berry 1979; Colclough 1982b; Kemp et al. 1986; Steur and Durieux 1986; Astrov et al. 1989; Luther et al. 1996; Ewing and Trusler 2000; Benedetto et al. 2004; Pitre et al. 2006; Gaiser et al. 2008; Meyer and Reilly 1997; Hill 2001; Kang et al. 2001; Sakurai 2001; Steur et al. 2002; Tamura et al. 2008; Peruzzi et al. 2010), where the latter seven are interpolating gas-thermometer realizations. However, with the use of ^{3}He, gas thermometry can be carried out at lower temperatures, fully covering the range of ^{3}He vapor-pressure thermometry, and partially covering that of the ^{4}He (Gaiser 2008, thesis; Tamura et al. 2004). The use of ^{3}He used to be affordable, as the lighter isotope was available at a reasonable price and with sufficient purity, however, recently national security reasons have (temporarily) driven up the price. Until some 30 years ago, the use of ^{3}He in accurate gas thermometry was prevented by the insufficient knowledge of its virial corrections (Pavese and Matacotta 1983). They later became available from experiment below 25 K (Matacotta et al. 1987) and from ab initio calculations (Mehl 2007; Hurly and Mehl 2007), and, in fact, both isotopes are considered in the ITS-90 definition for use in gas thermometry between 3 K and 24.6 K. However, the discussion in Sects. 3.1 and 3.2 will not be confined only to subjects relevant to the ITS-90 realization. The full temperature range will be considered, upward to 273.16 K with the use of ^{4}He, and downward to 0.5 K, being ^{3}He the only possible choice in this case.

3.1 Constant-Volume Gas Thermometry

The basic equation of an ideal-gas thermometer, as derived from Eq. 1.17, is (apparently) very simple

$$pV = nRT \tag{3.1a}$$

where p is the gas pressure, V the gas volume, T the thermodynamic temperature, n the amount of gas (in moles), and R the gas constant.

The most direct method of enclosing a known amount of gas n in a known volume V and measuring the pressure p is only used for the determination of the gas constant R at $T = 273.16$ K. Moreover, the relative uncertainty of the value of R (8.314 4621 (75) J K^{-1} mol^{-1}) is, at present (CODATA 2010), $\approx 1 \times 10^{-6}$, which limits the accuracy of a temperature measurement to ± 0.3 mK at 300 K and to $\pm < 0.03$ mK at 30 K. When better accuracy is required, measuring temperature ratios with respect to a reference condition can eliminate the effect of the uncertainty in R:

$$\frac{pV}{p_0V_0} = \frac{T}{T_{\text{ref}}}; \quad T = T_{\text{ref}}\frac{pV}{p_0V_0} \tag{3.1b}$$

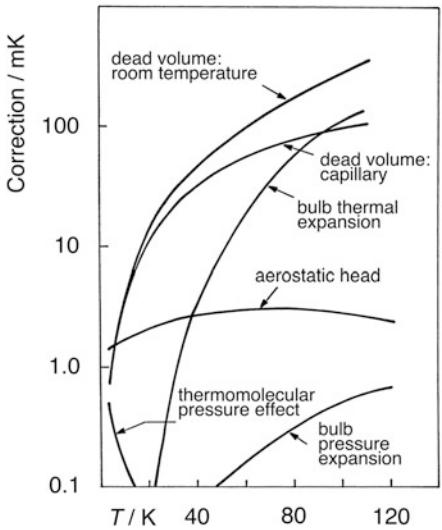

Fig. 3.1 Values of corrections versus temperature, due to departures from Eq. 3.1a, for a typical CVGT with room-temperature pressure measurement and with $T_{\mathrm{ref}} = 27.1$ K. (After Steur and Durieux 1986)

where p_0 and V_0 apply at T_{ref}. This ratio method is universally adopted. It also avoids the necessity of an absolute determination of n.

The volume V and the amount of gas n must remain rigorously constant. The thermometer is then called "constant-volume gas thermometer" (CVGT): $T = T_{\mathrm{ref}}(p/p_0)$. Should, on the other hand, the volume V be measured and the pressure p is kept constant, the thermometer is then called "constant-pressure gas thermometer" (CPGT), which is very rarely used: $T = T_{\mathrm{ref}}(V/V_0)$. Only the CVGT will be illustrated in this monograph.

The constant-volume assumption determines the requirements of the gas container, which are relevant only from the standpoint of the technical realization. On the contrary, the requirement for the amount n of gas to remain constant (as implied in Eq. 3.1b), involves a physical property of the thermometric substance itself, i.e., the number of its "active" molecules N (for the meaning of "active," see Sect. 3.1.1.2 to follow). This number may be affected by an uncertainty because of two physical reasons: (a) the interaction of the molecules with the walls of the container (e.g., adsorption) and (b) the impurities.

In the next two sections, the influence of physical (Sect. 3.1.1) and technical (Sect. 3.3.2) parameters on the accuracy of a CVGT will be discussed separately. Figure 3.1 provides a picture of the number and size of all these influence parameters (requiring the so-called "corrections"), concerning a CVGT with reference temperature $T_{\mathrm{ref}} = 27.1$ K (Steur and Durieux 1986) and Fig. 3.2 shows them for a CVGT with $T_{\mathrm{ref}} = 273.15$ K (Astrov et al. 1989). The uncertainties in these parameters are, obviously, more important than their values, unless the latter are negligible.

The aim of the discussion is to show the best accuracy allowed by the state-of-the-art. When a lower accuracy is sufficient, it will be easy to scale down requirements.

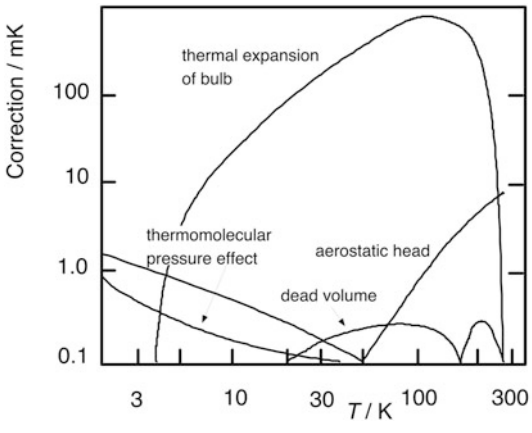

Fig. 3.2 Values of corrections versus temperature, due to departures from Eq. 3.1a, for a typical CVGT with low-temperature separation diaphragm and with $T_{\mathrm{ref}} = 273.16$ K. (After Astrov et al. 1989)

3.1.1 Influence of Physical Parameters

The picture of the gas thermometer given in the former section is oversimplified, since a real gas does not exactly behave as an ideal gas, that is, it does not follow exactly the ideal-gas law (Eq. 3.1a); corrections must therefore be applied, except in the case when very low accuracy is acceptable (lower than 0.1 K with moderate pressures). Several models are available to describe the (p–v–T) behavior of a real gas. For example, in physical chemistry one commonly uses the Van der Waal's equation. In thermometry, the more general virial expansion is used, which describes the real behavior in terms of a linear term (Eq. 3.1a) and of deviations from linearity by adding corrective density terms

$$pV = nRT\left(1 + B(T)\left(\frac{n}{V}\right) + C(T)\left(\frac{n}{V}\right)^2 + \cdots\right). \tag{3.2}$$

Each of the terms added in Eq. 3.2 has a physical meaning and describes a particular form of interaction between the molecules. Thus $B(T)$, which is the so-called second virial coefficient, accounts for the two-particle interactions; the third virial coefficient $C(T)$ accounts for the three-particle interactions. When molar density n/V is sufficiently low, higher order terms are negligible.

In total, there are three types of physical parameters that constrain the accuracy of the realization of temperature measurements with a gas thermometer, and are discussed separately in the following subsections: the virial coefficients, the purity, and the "active" amount of thermometric substance.

3.1.1.1 Virial Coefficients

The temperature-equivalent size of the corrections $B(T)$ and $C(T)$ for both ^{4}He and ^{3}He for a typical case are given in Figs. 3.3 and 3.4 as functions of temperature.

With ^{4}He, the second virial coefficient $^4B(T)$ from 300 K down to 2.6 K is known to a high degree of accuracy.

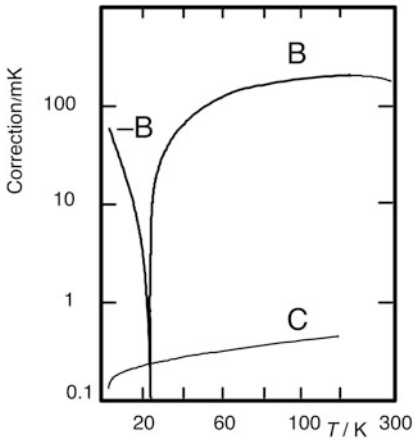

Fig. 3.3 Temperature correction for virials with ^{4}He. $T_{ref} = 27.1$ K; $n/V = 160$ mol m^{-3}. (After Steur and Durieux 1986)

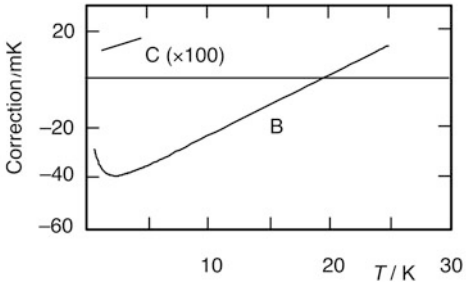

Fig. 3.4 Temperature correction for virials with ^{3}He. $T_{ref} = 24.5$ K; $n/V = 160$ mol m^{-3}. (After Pavese and Steur 1987a)

Most important are the two sets of measurements made by Berry (1979) between 2.6 K and 27.1 K and by Kemp et al. (1986) from 13.8 K to room temperature. Both show comparable uncertainty, $\pm$ (0.03–0.1) cm^3 mol^{-1},[2] and for each of the cases an equation for $^4B(T)$ was derived in the measured temperature ranges; in the overlapping part of their range the two equations agree very closely. These data were carefully analyzed by Steur et al. (1987) and a consistent expression for both $^4B(T)$ and $^4C(T)$ was derived in the range from 2.6 K to 300 K. Other results include Gammon's (1976) very accurate data above 98 K, the dielectric gas thermometer results of Gugan and Mitchell (1980; see also Sect. 3.3), Plumb's (1982) recalculation of the acoustic data of Plumb and Cataland (1966), and the more recent data obtained by Astrov et al. (1989), Pitre et al. (2006), and Gaiser et al. (2008).

The best set of *experimental* values, and their uncertainties, for the second virial coefficient $^4B(T)$ are given in Table 3.1; the uncertainty is ± 0.15 cm^3 mol^{-1} near 3 K and less than ± 0.03 cm^3 mol^{-1} above 20 K. An equation accurately representing these data between 3 K and 24.6 K is given in Appendix A (Eq. A.6a).

[2] Note: all uncertainty values, u, are for $k = 1$.

Table 3.1 Best values for the second virial coefficient $B(T)$ of ^{3}He and ^{4}He

T (K)	$^4B(T)$ (cm^3 mol^{-1})	$\Delta T(^4B)$ (mK) [a]	$^3B(T)$ (cm^3 mol^{-1})	$\Delta T(^3B)$ (mK)[a]
1.0	*−476*[c]	−76.2	*−236.3*[c]	*−37.8*
1.2	*−370.4*[c]	−71.1	*−205.5*[c]	*−39.4*
1.4	*−302.5*[c]	−67.8	*−181.0*[c]	*−40.5*
1.5	*−275.7*[c]	−66.2	−171.6 ± 0.3[d]	−41.2 ± 0.1
1.6	*−255.4*[c]	−65.4	*−161.0*[c]	*−41.2*
1.8	*−220.9*[c]	−63.6	*−144.6*[c]	*−41.6*
2.0	*−194.5*[c]	−62.2	−130.9 ± 0.3[d]	−41.9 ± 0.1
2.25	*−169.0*[c]	−60.8	*−116.54*[c]	*−42.0*
2.6	−142.41 ± 0.3[d]	−59.2	*−99.65*[c]	*−41.5*
3.0[b]	−120.36 ± 0.15	−57.7 ±0.07	−86.03 ± 0.2	−41.3 ± 0.1
3.7	−93.45 ± 0.09	−55.32 ± 0.05	*−69.75*[c]	*−41.3*
4.0	−85.06 ± 0.07	−54.44 ± 0.04	−62.08	−39.7
4.2221	−79.61 ± 0.05	−53.78 ± 0.03	−58.20	−39.4
5.0	−64.37 ± 0.03	−51.49 ± 0.02	−47.18 ± 0.1	−37.7
6.0	−50.59	−48.56 ± 0.03	−37.01	−35.5
7.0	−40.76	−45.65	−29.63	−33.2
8.0	−33.39	−42.74	−24.04	−30.8
9.0	−27.67 ± 0.02	−39.85	−19.65	−28.3
10.0	−23.11	−36.97	−16.11	−25.8 ± 0.1
11.0	−19.37	−34.10 ± 0.04	−13.20	−23.2
12.0	−16.27	−31.24	−10.77	−20.7
13.0	−13.65	−28.39	−8.70	−18.1 ± 0.15
13.8033	−11.82	−26.11	−7.25	−16.0
14.0	−11.41	−25.55	−6.92	−15.5
15.0	−9.47 ± 0.02	−22.72 ± 0.05	−5.37	−12.9
16.0	−7.77	−19.90	−4.02	−10.3
17.0	−6.28	−17.09	−2.82	−7.7
17.0357	−6.23	−16.99	−2.78	−7.7
18.0	−4.96	−14.29	−1.75	−5.0
19.0	−3.78	−11.50 ± 0.06	−0.80	−2.4
20.0	−2.73	−8.72	+0.07 ± 0.1	+0.2 ± 0.2
20.2711	−2.46	−7.97	+0.29	+0.9
21.0	−1.77	−5.96	+0.85	+2.9
22.0	−0.91	−3.20 ± 0.07	+1.56	+5.5
23.0	−0.12	−0.45	+2.21	+8.1
24.0	+0.60	+2.29 ± 0.08	+2.81	+10.8
24.5561	+0.97	+3.81	+3.12	+12.4
25.0	+1.25 ± 0.02	+5.02	+3.36	+13.4
26.0	+1.86 ± 0.02[d]	+7.74 ± 0.08	*+3.8829*[c]	*+16.153*
27.0	+2.36	+10.2 ± 0.15	*+4.3355*[c]	*+18.729*
40.0	+6.90	+42.0	*+8.1528*[c]	*+52.178*
60.0	+9.74	+93.5 ± 0.20	*+10.552*[c]	*+101.30*
80.0	+10.97	+140.4	*+11.561*[c]	*+147.98*
100.0	+11.68	+186.9 ± 0.30	*+12.038*[c]	*+192.61*
120.0	+11.90	+228.5	*+12.267*[c]	*+235.53*
140.0	+12.07	+270.4	*+12.364*[c]	*+277.0*
160.0	+12.15	+312.1 ± 0.50	*+12.386*[c]	*+317.1*
200.0	+12.17	+389.1	*+12.314*[c]	*+394.1*
250.0	+12.06	+480.8 ± 0.80	*+12.128*[c]	*+485.1*
273.16	+11.99	+521.4	*+12.028*[c]	*+525.7*
300.0	+11.82 ± 0.02	+567.4 ± 0.90	*+11.908*[c]	*+571.6*

[a] Calculated as $\Delta T(B) = B(n/V)T$, for $n/V = 160$ mol m^{-3}. Corrections have the opposite sign

[b] In the 3–24.6 K range, the experimental values differ less than 0.05 cm^3 mol^{-1} from the stipulated values of the ITS-90 ((A.6a) (^{3}He) and (A.6b) (^{4}He)), only below 6 K the difference increases up to 0.7 cm^3 mol^{-1} at 3 K (0.35 mK)

[c] No experimental data available. *Theoretical* calculation (Bich et al. 2007)

[d] *Experimental* values and uncertainties (from Gaiser and Fellmuth, 3.7 K < T < 26 K; otherwise from Berry (1976)

Table 3.2 Best values for the third virial coefficient $C(T)$ of ^{3}He and ^{4}He

T (K)	$^4C(T)$ (cm^6 mol^{-2})	$\Delta T(^4C)$ (mK)[a]	$^3C(T)$ (cm^6 mol^{-2})	$\Delta T(^3C)$ (mK)[a]
0.5[b]				
1.0[b]				
1.5			-1100 ± 1600[e]	
2.0			$+2340 \pm 1300$	0.09 ± 0.02
2.6	-588 ± 200[c]	-0.03 ± 0.01	$+2030 \pm 820$	0.10 ± 0.02
3.0	$+715 \pm 90$	$+0.06 < \pm 0.01$	$+1660 \pm 140$	$0.12 < \pm 0.01$
4.0	$+1109 \pm 40$[d]	$+0.116 \pm 0.002$	$+1430 \pm 300$	$0.15 < \pm 0.01$
6.0	$+843 \pm 30$	$+0.141$		
8.0	$+660 \pm 20$	$+0.139$		
10.0	$+547 \pm 15$	$+0.137$		
13.8033	$+422$	$+0.139$		
15.0	$+396 \pm 20$	$+0.141$		
17.0357	$+367$	$+0.147$		
20.0	$+320 \pm 10$	$+0.157 \pm 0.003$		
20.2711	$+318$	$+0.158$		
24.5561	$+271$	$+0.167 \pm 0.006$		
25.0	$+275 \pm 10$	$+0.178$		
30.0	$+244 \pm 10$[c]	$+0.18 < \pm 0.01$		

[a]Calculated as $\Delta T(C) = C(n/V)^2 T$, for $n/V = 160$ mol m^{-3}. Corrections have the opposite sign
[b]No measurements available
[c]From Steur et al. (1987); *experimental* uncertainties are shown
[d]From Gaiser and Fellmuth (2009); *experimental* uncertainties are shown
[e]From Keller (1955); *estimated* uncertainties

An accurate knowledge of the third virial coefficient $^4C(T)$ is less important. The best set of values, and their uncertainties, for the third virial coefficient $^4C(T)$ are given in Table 3.2.

For densities up to 300 mol m^{-3}, the contribution of this coefficient to the overall uncertainty is less than 0.5 mK. Above 5 K, $^4C(T) \propto T^{-1}$, but at lower temperatures there is experimental evidence (Berry 1979) of a downturn (Fig. 3.3), which may be a source of nonlinearity (max 0.5 mK) for a ^{4}He gas thermometer.

As regards ^{3}He, the values of the virial coefficients were much less satisfactorily known until 1987, when new accurate measurements made it possible to acquire a better knowledge of $^3B(T)$ (Matacotta et al. 1987), which is essential in ^{3}He gas thermometry.

Until 1987, only Keller's (1955a, b) measurements between 1.5 K and 3.8 K were available, together with some acoustical data of Grimsrud and Werntz (1967) between 1.4 K and 2.2 K, and the less accurate data of Cameron and Seidel (1985) between 0.6 K and 1.3 K. However, Keller's data are affected by an uncertainty depending on whether they are fitted for both $^3B(T)$ and $^3C(T)$ or only for $^3B(T)$, and the other data have an uncertainty of $\pm$ 1–2 cm^3 mol^{-1}. The uncertainty in $^3B(T)$ of the measurements of Matacotta et al. (1987) between 1.5 K and 20.3 K is $\pm$ 0.2–0.5 cm^3 mol^{-1}. They were carried out with reference to the value ^3B(20.3 K), *calculated* to be 0.30 cm^3 mol^{-1} with an uncertainty estimated to be lower than $\pm$ 0.03 cm^3 mol^{-1} (equivalent to $\pm$ 0.1 mK at a molar density of 160 mol m^{-3}). The use of these

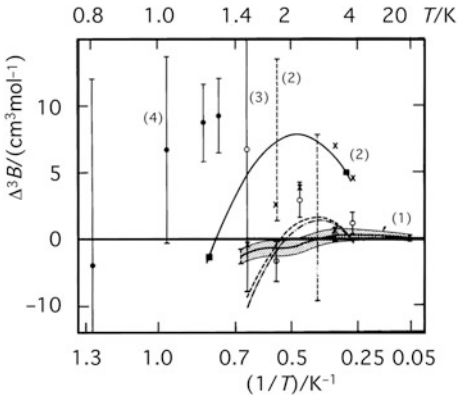

Fig. 3.5 Various experimental determinations of ^{3}B(T) compared with calculations. (After Matacotta et al. 1987) (*baseline*). *1* (*shaded*) fitting of experimental data of Matacotta et al. (1987); *2* data and 95 % CI error bar of Grimsrud and Werntz (1967); *3* data of Keller (1955a, b); *4* data of Cameron and Seidel (1985). The other *curves* are previous calculations

data with a reference point *other* than 20.3 K ($^3B(T)$ passes through zero at about 20 K—see Fig. 3.4, the so-called Boyle point, which marks the change of the dominant interaction potential) may cause some additional uncertainty.

Figure 3.5 shows the deviations of all the available data on $^3B(T)$ below 20 K from the theoretical calculations (HFDHE3 potential; Matacotta et al. 1987). The best set of values, and their uncertainties, for the second virial coefficient $^3B(T)$ are given in Table 3.1. Appendix A reports an equation that accurately represents these data between 3 K and 25 K (Eq. 1.6b).

Less is known about $^3C(T)$ than about $^4C(T)$. The best set of values, and their uncertainties, for the third virial coefficient $^3C(T)$ are given in Table 3.2.

The only data available are those of Keller (1955a, b), which indicate values of the order of 2000 cm^6 mol^{-2}, i.e., about the same order of magnitude as for ^{4}He. At present, no information is available about the existence of a downturn in $^4C(T)$ behavior at lower temperatures, but even if it exists, as suggested by Keller's value $(-1.1 \pm 1.6) \times 10^4$ cm^6 mol^{-2} at 1.5 K, the correction would amount, at this temperature, to -0.4 mK at a molar density of 160 mol m^{-3}.

The accuracy to which $B(T)$ for both ^{3}He and ^{4}He is obtained from theoretical calculations has improved considerably in recent years, through better knowledge of the intermolecular potential function of helium atoms. From classical mechanics, the second virial coefficient $B(T)$ can be written in closed form as

$$B_{c,1} = -\frac{n}{2}\int_0^\infty \left(e^{-b\phi(r)} - 1\right)4r^2 dr \tag{3.3}$$

where $\phi(r)$ is the intermolecular potential assumed to be spherically symmetric and the quantity $\beta = 1/kT$ accounts for the thermal energy of the system. At low temperatures, quantum effects must be taken into account, otherwise large differences would result with respect to experimental data. For example, at temperatures below about 10 K, the classical and quantum values of $B(T)$ for ^{4}He (Keller 1969; Van Sciver 1986) differ by a factor of two.

Any theoretical description of the virial coefficients requires that a physically realistic intermolecular potential function be used. From the initial Hartree–Fock dispersion form, the HFDHE2 calculation of Aziz et al. (1979) has been able to reproduce many properties of helium within the uncertainty of the experimental data then available. When later the new $^4B(T)$ data of Berry (1979) became available, these were observed to deviate significantly from previous theoretical calculations, and it appeared necessary to assume a deeper potential well depth. Through the work of McConville (1984), McConville and Hurly (1991), Aziz (1987), Aziz and Slaman (1990), Cencek et al. (2004), Mehl (2007), Hurly and Mehl (2007), and Hellmann et al. (2007),[3] the potential form was modified (changing e/k from 10.80 K through 10.94 K up to 10.998 K). The different potential forms developed since 1982 show agreement down to 4 K to better than $\pm 0.2\,\mathrm{cm^3\ mol^{-1}}$ in the calculation of $^4B(T)$. The latest forms (Hurly and Mehl 2007; Hellmann et al. 2007) agree with each other within $0.02\,\mathrm{cm^3\ mol^{-1}}$ or better above 20 K, but diverge up to $0.13\,\mathrm{cm^3\ mol^{-1}}$ at 4 K and to $0.30\,\mathrm{cm^3\ mol^{-1}}$ at 2 K. These differences reflect mainly the higher weight given by Hurly and Mehl to the high-temperature results in the fit to their calculated values. The improvement with time in the ab initio calculations is evident in the associated uncertainty estimates. The analysis in McConville (1991) indicates a maximum uncertainty in the computer code calculations of $\pm 0.15\,\mathrm{cm^3\ mol^{-1}}$ at 2.6 K, which decreases to less than $\pm 0.03\,\mathrm{cm^3\ mol^{-1}}$ above 10 K, whereas Hellmann et al. (2007) estimate an uncertainty of ± 0.02 % above 15 K (about $\pm 0.004\,\mathrm{cm^3\ mol^{-1}}$) increasing to ± 0.2 % at 1 K ($\pm 1\,\mathrm{cm^3\ mol^{-1}}$). The increase of the well depth to 10.998 K produces a bound state for two ^{4}He atoms at $\approx(-1.7\ k)$ mK, which reduces $^4B(T)$ slightly at very low temperatures. With ^{3}He, there is no bound state, since the $\lambda = 0$ phase shift is zero at zero energy.

Assuming ^{4}He and ^{3}He to be represented by the same potential function, a comparison of the ^{3}He data of Matacotta et al. (1987) with the most recent HFD-2B function of Aziz (1990) showed an agreement within $\pm 0.3\,\mathrm{cm^3\ mol^{-1}}$. However, a critical comparison performed by McConville (1991) using the HFD-2B function and several other recent potential functions, put into evidence a statistically significant systematic difference between the best fit to the data and these calculations. It amounts to $+1.0\,\mathrm{cm^3\ mol^{-1}}$ at 1.5 K, decreases to zero at 1.75 K, then becomes as large as $-0.5\,\mathrm{cm^3\ mol^{-1}}$ at 2.7 K, and vanishes near 20 K. This systematic difference might be interpreted as due to the neglected contribution of $^3C(T)$ to the data. Agreement between theory and experiment to within $\pm 1\,\mathrm{cm^3\ mol^{-1}}$ at 1.5 K and $\pm 0.3\,\mathrm{cm^3\ mol^{-1}}$ above 4 K, is equivalent to an uncertainty of ± 0.24 mK of the derived gas- thermometer temperature value at 1.5 K, of ± 0.14 mK at 3 K and of ± 0.48 mK at 10 K, for $n/V = 160\,\mathrm{mol\ m^{-3}}$. In Gaiser and Fellmuth (2009), a detailed analysis can be found regarding the agreement between experiment and theory.

Accurate experimental knowledge of the virial coefficients is still limited to $T > 2.6$ K for ^{4}He and to $T > 1.5$ K for ^{3}He, although theoretical models are

[3] Further developments about helium potential energy curve can be found in Hellmann et al. (2007) and Cencek et al. (2012).

Table 3.3 Limits to pressure and density ranges imposed by the vapor-pressure boundary

T (K)	p_{vp} (kPa)	p_{safe} (kPa)	$(n/V)_{max} = p_{safe}/RT$ (mol m^{-3})[b]	$(\delta p/p)$ (%)[a]
(a) ^{3}He				
0.5	*0.021*	*0.014*	*3.37*	*0.95*
0.6	*0.071*	*0.043*	*8.73*	*0.31*
0.7	*0.180*	*0.121*	*19.0*	*0.12*
0.8	*0.378*	*0.23*	*34.1*	*0.058*
1.0	*1.16*	*0.67*	*83.7*	*0.019*
1.1	*1.80*	*1.08*	*118*	*0.012*
1.2	2.65	1.59	159	0.008
1.3	3.74	2.24	207	0.006
1.4	5.08	3.05	262	0.004
1.5	6.71	4.03	323	0.003
2.0	20.0	12.0	722	0.001
3.0	81.8	49.1	1968	<0.001
(b) ^{4}He				
1.0	*0.016*	*0.0096*	*1.15*	*1.39*
1.5	*0.472*	*0.283*	*22.7*	*0.047*
2.0	3.1	1.88	113	0.007
3.0	24.0	14.4	577	0.001
4.0	81.6	49.0	1473	<0.001
5.0	196.0	117.6	2829	

[a] $\delta T/T = \delta p/p$, for $\delta p = \pm 0.133$ Pa (1 mTorr)
[b] In order to have $\delta T \leq \pm 1$ mK, must have $(n/V)_{min} \geq 16$ mol m^{-3}

becoming more and more sophisticated, up to the point where they are even superior to experiment. An extension to lower temperatures, such as down to 0.5 K, requires new measurements, which will be much more difficult with ^{4}He than with ^{3}He. The main difficulty at these temperatures far below the critical temperature, is a restriction set to the range of pressure values over which isotherm measurements can be made, imposed by the departure from ideal-state conditions of the gas, which rapidly increases when approaching the vapor-pressure boundary. This restriction is much more severe with ^{4}He than with ^{3}He. The vapor-pressure boundary places an upper limit to the usable density range for each isotherm, above which higher virial coefficient, such as $C(T)$, has to be taken into account. A safe rule-of-thumb is to take only pressures below 50 % of the saturated vapor pressure.

Two temperature limits can result for the gas thermometer. One is that, in the most accurate gas thermometry, the overall temperature (i.e., pressure) relative uncertainty should not be greater than ± 0.003 % at 30 K and ± 0.02 % at 0.5 K. Table 3.3 shows in column 4 the pressure and molar density range where this level is achieved, the pressure uncertainty being assumed to be $u_p = 0.13$ Pa, which is obtainable only with the best instruments available (see Part II). In the case of ^{4}He, the relative uncertainty can no longer be kept within those limits below about 2 K (close to Berry's (1979) lowest temperature), and below 1.0 K in the case of ^{3}He.

The other, more restrictive, limit is imposed by the necessity to span a *range* of density values (typically in a ratio 1:3), for example, when measuring isotherms, in order to allow an extrapolation with sufficient accuracy to ideal-gas conditions at zero density. This limit sets itself a temperature limit higher than the former by about 0.3 K for ^{3}He and about 0.5 K for ^{4}He.

Obviously, lower temperatures at lower densities can be measured with higher uncertainty. In this respect, the uncertainty increases to 0.9 % with ^{3}He close to 0.5 K, while with ^{4}He it is 1.4 % already at 1 K. Alternatively, uncertainty can be kept constant by improving the accuracy of pressure measurement to about ± 0.01 Pa for pressures below 1 kPa. However, this improvement is meaningful only if the uncertainty arising from the thermomolecular pressure correction at these low pressures can be kept small enough (see Sect. 3.1.2 and Part II, Chap. 10).

3.1.1.2 Amount of "Active" Substance

Only the amount of substance n_b contained in the gaseous state *inside* the bulb volume of the gas thermometer is "active," i.e., it is directly related to its temperature T_b. It must remain constant and must accurately be known during each measurement run. Its constancy cannot be achieved for different reasons and corrections are therefore needed, increasing the uncertainty of the measurements.

One reason for the departure from constant conditions, which will be discussed in the next section, is technical. As a rule—except with some of the techniques described in Sect. 3.1.3—an additional (small) volume is connected to the thermometer bulb, the so-called dead-volume, which is the volume of the connecting pipe to the pressure gauge (usually at room temperature). With different values of T_b, and/or with changes in the temperature distribution in the dead-volume, it will contain different amounts n_d of substance. Since only $n = n_\mathrm{b} + n_\mathrm{d}$ is actually constant, n_b changes accordingly. These changes must be carefully taken into account.

Another reason, which will be discussed in the next subsection on the effects of gas purity, is condensation of impurities present in the thermometric substance.

A third reason, discussed here, is the adsorption of the thermometric gas by the bulb walls (actually, by any part of the gas circuit). As the magnitude of the adsorption depends on temperature, data cannot safely be extrapolated outside their experimental range. Even with helium, the most widely used thermometric substance in recent times, not many adsorption data are available, and nearly all concern only the heavier isotope ^{4}He. In the cryogenic range, one of the few reliable experiments (bulb surface increased by a factor of 4.4 by means of inner disks (Berry 1979)) showed no effect on gas- thermometer behavior within the measurement sensitivity of ± 0.1 mK from room temperature down to 2.6 K. Less empirically, Gershanik (1978) has determined the following relationship:

$$\ln\left(\frac{V_{m,\mathrm{g}}}{V_0}\right) = \underbrace{\ln\left(\frac{\tau}{\zeta}\right)}_{\text{(I)}} + \underbrace{\left(\frac{\zeta \Delta_{\mathrm{vap}} H_m}{\mathrm{R}T\tau}\right) + \left(\frac{\alpha}{\mathrm{R}T\tau^3}\right)}_{\text{(II)}} \tag{3.4a}$$

$$\tau = 0.686 + 0.18\zeta + 0.82\zeta e^{-4/\zeta} \quad \zeta = \frac{K}{1.13K_m} \tag{3.4b}$$

where $V_{m,g}$ is the molar volume of the gas, $V_0 = 30\,\mathrm{cm^3\ mol^{-1}}$, $\Delta_{vap}H_m$ is the molar enthalpy of vaporization ($\Delta_{vap}H_m/R = 10\,\mathrm{K}$), R the gas constant, τ the adsorbed film thickness (expressed in number of molecule layers), a is a coefficient of interaction between the gas and the walls (such that $\alpha/R = (38–40)\cdot\tau^3$ K for a wide variety of materials), K the adsorption coefficient, and K_m the same for a monolayer of argon or nitrogen.

For temperatures below 5 K, where $\zeta \geq 2.5$, term (I) in Eq. 3.4a can more accurately be written as

$$\frac{\left(\Delta_{vap}H_m - RT\right)\left(\dfrac{\zeta}{\tau - 1}\right)}{RT\left(\dfrac{\zeta - 0.5}{2}\right)^3}. \tag{3.4c}$$

The resulting temperature correction obviously decreases with an increasing amount (i.e., pressure) of the thermometric gas. With a bulb having an inner *geometrical* surface of 450 $\mathrm{cm^2}$ and a gas filling of 0.1 MPa at room temperature (about 40 $\mathrm{mol\ m^{-3}}$, Astrov et al. 1989), the required correction has been found to be about 0.3 mK between 2 K and 10 K, to decrease to <0.1 mK above 20 K (Gershanik et al. 1978).

From Eq. 3.4b, the adsorbed coverage is $\tau \approx 1.2$ layers at helium temperatures (see also Daunt and Lerner 1972, Dash 1979, and Dash and Schick 1978), i.e., about 0.5 $\mathrm{mm^3}$ of gas at standard temperature and pressure. At ≈ 5 K, pressure is actually ≈ 60 times less, therefore the correction, as calculated from the equation, is 6×10^{-5}, or 0.3 mK.

In addition, some parts of the apparatus could suffer from sizeable permeability of the walls to the thermometric gas. This is a major problem at very high temperatures, but, with helium, the problem may also arise from the use of glass, e.g., for the bulb. In this case, Sakurai (1982) showed that the gas leakage through a 0.5 L Pyrex bulb with 1 mm-thick walls was less than 4×10^{-9} W ($4 \times 10^{-6}\,\mathrm{Pa\,L\,s^{-1}}$), corresponding to a negligible loss of substance during the period of time required by the experiment.

3.1.1.3 Gas Purity

If an amount fraction x of an impurity is contained in helium (essentially H_2 in ^{4}He and ^{4}He in ^{3}He),[4] then the actual total virial coefficient is

$$(1 - x)^3 B(T) + x^{\mathrm{gas}} B(T). \tag{3.5}$$

An error

$$x\left[{}^3B(T) - {}^{\mathrm{gas}}B(T)\right] = x\delta B \tag{3.6}$$

[4] Water and air are not considered an impurity only in the case of a low-temperature CVGT, as they are assumed to remain trapped outside the bulb. See Sect. 3.3.2.

Table 3.4 Effect of condensation of impurities in ^{3}He and ^{4}He

(a) ^{4}He in ^{3}He or ^{3}He in ^{4}He

T (K)	p (Pa)[a]	$p_{vp}(^4\text{He})$ (Pa)	$p_{vp}(^3\text{He})$ (Pa)	$x(^4\text{He})$ (corresponding to p_{vp})[b]	$x(^3\text{He})$ (corresponding to p_{vp})[b]	Impurity fraction ($\delta p/p$[c])
0.5	665	0.0021	21	3.1×10^{-6}	3.2×10^{-2}	2.0×10^{-4}
0.6	798	0.036	71	4.5×10^{-5}	8.9×10^{-2}	1.6×10^{-4}
0.7	931	0.292	180	3.1×10^{-4}	1.9×10^{-1}	1.4×10^{-4}
0.8	1064	1.5	378	1.4×10^{-3}	3.6×10^{-1}	1.2×10^{-4}
1.0	1330	15.6	1160	1.2×10^{-2}	8.7×10^{-1}	1.0×10^{-4}
2.0	2660	3129				5.0×10^{-5}
3.0	3990	24047				3.3×10^{-5}

(b) H_2 in ^{3}He or ^{4}He

T (K)	p (Pa)[a]	$p_{vp}(H_2)$(Pa)[d]	$x(H_2)$[b] (corresponding to p_{vp})	impurity fraction ($\delta p/p$[c])
4.0	5320	2.8×10^{-5}	5.0×10^{-9}	2.5×10^{-5}
5.0	6650	4.8×10^{-3}	6.7×10^{-7}	2.0×10^{-5}
6.0	7980	0.16	1.9×10^{-5}	1.7×10^{-5}
8.0	10640	15.7	1.5×10^{-3}	1.2×10^{-5}
11.0	14630	74	4.5×10^{-2}	0.9×10^{-5}

[a] $p = (n/V)RT$, with $n/V = 160\,\text{mol m}^{-3}$
[b] Equivalent to p_{vp}/p. For example, for a molar impurity fraction of 1.3×10^{-3}, condensation occurs at temperatures lower than 0.8 K with ^{4}He and than 8.0 K with H_2
[c] $\delta p/p = \delta T/T$; the δp and δT admitted limits are 0.1 mK and 0.133 Pa
[d] From Mullins et al. (1961)

arises from the *difference* in the virial coefficients of the thermometric gas and of the impurity, and from the *change* of x, if condensation, or adsorption, of the impurities occurs. In this latter case, however, the effect of the disappearing gas on the total available amount of measuring gas is much larger than that of the effect through the (apparent) virial coefficient.

The temperature-equivalent error due to ^{4}He impurity in ^{3}He, caused by the difference between the virial coefficients, is very small: for a 10^{-3} molar fraction it is always less than ± 0.05 mK down to 0.5 K.

Considering now the possibility of condensation, Table 3.4a shows the pressure for an ideal-gas thermometer at a molar density of $160\,\text{mol m}^{-3}$ and the ^{4}He vapor pressure, at the same temperatures. Obviously, a molar fraction x of ^{4}He will condense when $xp = p_{vp}$; for example, a 10^{-3} molar fraction condenses only below about 0.8 K, while at 0.5 K condensation does already occur with impurities of the order of 10^{-6} molar fraction. On the other hand, a molar impurity level of 10^{-4} can be tolerated whose maximum contribution to the overall uncertainty is ± 0.05 mK at 0.5 K. The reverse unlikely situation of a ^{3}He impurity in ^{4}He is even more favorable.

In Table 3.4b, the same figures concern a hydrogen impurity in both ^{3}He and ^{4}He. In this case, a 10^{-5} molar impurity fraction can be tolerated whose contribution to the overall uncertainty is less than ± 0.1 mK.

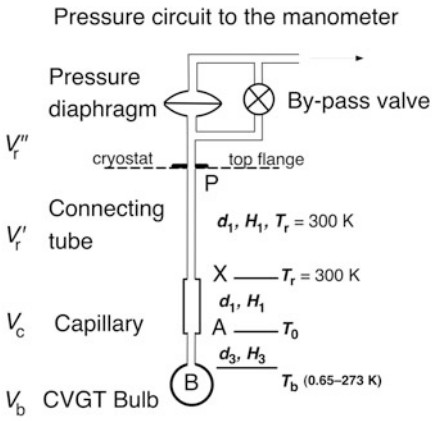

Fig. 3.6 General layout of a gas thermometer. d and H tube diameter and length

In conclusion, in order that the derived temperatures be affected by less than ± 0.1 mK, the measuring gas must contain an impurity level of $^4\text{He} < 10^{-4}$ in ^3He and of $\text{H}_2 < 10^{-5}$ in both ^3He or ^4He. Common grades of commercial-type helium isotopes meet these requirements.

3.1.2 Influence of Technical Parameters

The state-of-the-art of the measurement of the relevant physical parameters puts constraints on the design of a thermometer. Quoting from the "*Supplementary Information for the IPTS-68 and the EPT-76*":

> The design of a constant volume gas thermometer always involves compromises between opposing and often interrelated constraints: the filling pressure [i.e., density] must be sufficiently high to give enough sensitivity, but not so high that departures from ideality of the gas become too large. The ratio of the bulb volume to the dead volume should be large enough to allow the dead-volume correction [relevant at the higher bulb temperatures] to be adequately estimated or measured, but the sensing tube must not be so small that it supports too large a thermomolecular pressure difference [relevant at the lower bulb temperatures]. The effect of adsorption, which is not readily estimated, can be reduced by using as large a volume-to-surface ratio for the bulb as is practicable. (BIPM 1983)

These requirements may be better understood if the traditional technical implementation of the CVGT, which is shown in Fig. 3.6, is recalled.

Bulb B at a temperature T_b, which is to be measured, is connected to the manometer through a diaphragm pressure transducer P that is maintained at room temperature and isolates the pure thermometric substance from the manometric gas. A (capillary) pressure-measuring line is therefore required between the bulb and the transducer. It is represented in the figure, for the general discussion that will follow, with three diameters, d_1 to d_3; most commonly, the capillary diameter is uniform, but it will be shown that this is not always the best solution.

The use of a connecting capillary, until recently unavoidable, is the source of most of the CVGT uncertainty. Let us first point out that in Eq. 3.2 the different quantities involve the bulb, i.e., $p \equiv p_b$, $V \equiv V_b$, $n \equiv n_b$, and $T \equiv T_b$. Instead, with an apparatus such as that in Fig. 3.6, the following equation applies:

$$\left(p^* + \Delta p_{TM} + \Delta p_{aer}\right) V_b = RT_b \left(n_b + n_c + n_r\right) \left(1 + \frac{B\left(n_b + n_c + n_r\right)}{V_b}\right) \quad (3.7)$$

where the influence of the parameters relative to a technical realization is made explicit.

The measured pressure p^* can be related to p_b through correction terms for the thermomolecular pressure effect Δp_{TM} and the aerostatic pressure head Δp_{aer}.

Furthermore, not all the amount of substance n is in the bulb, but some of it fills the capillary (n_c) and some the volumes of the pressure-measuring apparatus at room temperature (n_r): they are commonly denoted as "dead-volume." The total loss of substance $\Delta n_b = (n_c + n_r)$ from the bulb is the main problem of a CVGT, since it is *variable*, obviously depending on pressure, and therefore on temperature. Should it be possible to compensate for the change in the amount of substance needed to fill these volumes external to the bulb when pressure (i.e., temperature) changes from the reference value, to prevent a single molecule of the substance from crossing the bulb volume V_b boundary, then the dead-volume would no longer be critical, and could be designed to minimize the pressure corrections, as in vapor-pressure thermometry (Chap. 4). However, no such a solution has so far been found.

Therefore, unless the tube itself is eliminated by placing a pressure transducer at low temperature *on* the bulb (this special and interesting solution is discussed separately in Sect. 3.1.3), the correction $\Delta n_b = n - n_b$ must be calculated. To minimize the uncertainty of the calculated value, the correction must be made as small as possible, by minimizing the dead-volume; consequently, the choice of all the parameters in Eq. 3.7 does have an influence, more or less significant, on the final measurement uncertainty of the CVGT. This choice will be thoroughly discussed in the following section.

3.1.2.1 The Gas Bulb

Corrections concerning the bulb itself have to be made for volume changes either due: (a) to a pressure difference across the bulb walls or (b) to thermal expansion. Both effects are independent of the gas used and are only small in the temperature range below 30 K.

Pressure Difference Effect

Table 3.5 gives the calculated values of changes in a copper bulb when there is a pressure difference across the wall. The calculation assumes a bulb made of a free-expanding infinite-like cylinder and of two bottom plates having freely supported edges (Steur 1983).

Table 3.5 Effect of pressure deformation for an unguarded copper bulb[a]

Cylinder: $\frac{\Delta V}{V_0} = \frac{1}{E}\left\{\frac{d}{t_c} + \frac{d/t_c}{4 + t_c/d}\right\} p$

Plates: $\frac{\Delta V}{V_0} = \frac{1}{E}\frac{55 \times 10^{-3} d^4}{L t_p^3} p$

T (K)	$\Delta V/V_0$ (10^{-6})[a]	ΔT (mK)[b]
1.0	0.10	
4.2	0.40	< 0.01
10.0	0.95	0.01
20.0	1.9	0.04
30.0	2.8	0.09
50.0	4.8	0.24
100.0	9.5	0.95
200.0	19.0	3.8
273.16	25.9	7.1
300.0	28.5	8.6

d Diameter, t thickness, L cylinder length, E modulus of elasticity

[a]For $V_b = 1$ L, $d = 85$ mm, $L = 176$ mm, $t_c = 14$ mm, $t_p = 30$ mm, $E_{Cu} = 130$ GPa, $T_{ref} = 20$ K; $\Delta V/pV = 7.1 \times 10^{-11}$ Pa^{-1} at $n/V = 160$ mol m^{-3}

[b]$\Delta T = T(\Delta V/V_0)$

The pressure difference can be eliminated by means of a compensating chamber surrounding the bulb, where a pressure value is maintained close to that of the bulb (see Fig. 3.21 to follow Astrov et al. 1989). This precaution is mandatory when a glass bulb is used (Sakurai 1982).

Thermal Expansion

The correction for thermal expansion is important and critical with CVGTs used above 100 K. One good reason for considering the use of a glass bulb is the reduction of the size of this correction and of the associated uncertainty; however, copper bulbs are generally employed to avoid the permeability of glass to helium, the gas most often employed for gas thermometry. The thermal expansion of copper has been studied repeatedly (e.g., White and Collins 1972). A large database exists (TPRC 1975) and new data have been added and often critically reviewed since then (NBS 1975; Kroeger and Swenson 1977; Pavese and Ciarlini 1990b). It is indisputably established that high-purity copper samples, even of different origins, differ very little from one another. The values for the thermal expansion of high-purity copper are known with $u = 5 \times 10^{-6}$ below 300 K (equivalent to ± 0.15 % of the thermal expansion at 77 K) and $u = 6 \times 10^{-8}$ below 35 K. These uncertainties are of the same size as that of the best *individual* experiments. The corresponding linear expansion coefficient a_l is known to ± 0.1–0.2 % above 20 K. The total relative *volume* contraction is 3 times the linear relative contraction, and when corrected with an uncertainty of ± 0.3 %, the uncertainty in the value of the bulb volume is

Table 3.6 Cubic expansion coefficient, volume relative change, and bulk modulus of elasticity (Young's modulus) of polycrystalline copper

T (K)	$3 \times a_l$ (10^{-6} K^{-1})[a]	$\Delta V/V_{0K}$	ΔT (mK)[b]	E_{Cu} (GPa)[c]
1	0.00069	0.0003×10^{-6}		
3	0.00399	0.0045		
5	0.01385	0.02205	138.62	
10	0.09009	0.2417	<0.01	
15	0.30846	1.157	0.02	
20	0.79032	3.764	0.08	138.57
25	1.66719	9.725	0.24	
30	2.99505	21.19	0.64	
40	6.8334	69.22	2.8	138.40
50	11.5566	0.1608×10^{-3}	8.0	138.10
70	21.0105	0.4888	34	137.60
100	31.569	1.290	129	136.55
150	41.007	3.138	471	134.45
200	45.615	5.324	1065	132.35
250	48.330	7.693	1923	130.20
293.15	49.918	9.801	2873	128.25
300	50.133	10.18	3054	127.95

[a] $3 \times a_l = \dfrac{1}{V_{0K}} \dfrac{dV}{dT}$ (McLean et al. 1972); for $T \geq 5$ K (Kroeger and Swenson 1977)

[b] $\Delta T = T \dfrac{\Delta V}{V_{0K}}$

[c] From Leadbetter (1981)

equivalent to a temperature uncertainty of ± 2.4 mK at 170 K, ± 2.0 mK at 84 K, and ± 0.5 mK at 20 K for a CVGT referenced to 273.15 K. For a CVGT referenced to 20 K, the corresponding figures are ± 0.2 mK at 84 K, ± 2.1 mK at 170 K, and ± 7.2 mK at 273 K. The best $\Delta V/V_0$ and a_l data for copper are given in Table 3.6.

Recently (CCT WG4 2008), concern has arisen about the influence of gold plating of the bulb surface, which is suspected (in the absence of hard scientific data) to change the thermal expansion coefficient at temperatures above, say, 30 K.

For practical reasons, the bulb volume is generally on the order of 0.5–1 L, because larger volumes would require more thermometric gas and sizeable temperature gradients could arise.[5] The use of smaller volumes is only for applications of lower accuracy or when using a built-in pressure transducer (see Sect. 3.1.3) as the selection of the bulb volume is conditioned by the need to minimize the effect of the "dead-volume," which will be discussed in the next subsection.

3.1.2.2 Pressure-Measuring Line

A well-known fact in gas thermometry is that the tube connecting the bulb containing the thermometric gas at low temperature to a manometer at room temperature makes

[5] A case where very large volumes are required is discussed in Sect. 3.3.2.

a substantial contribution to the measurement uncertainty. Surprisingly, however, in the thermal design of a CVGT care is usually mostly devoted only to the temperature uniformity of the gas bulb, though the thermal design of the pressure line needs as much care. This design will be discussed in detail in Sect. 3.3, on the basis of the points that will presently be discussed.

The pressure line has two adverse effects: (a) it constitutes the dead-volume, which is filled with a variable amount of gas that is *not* part of the thermometric ("active") substance, thus making the latter $n_b \neq n$ and variable and (b) modifies the pressure value measured at ambient temperature p^*, so that $p^* \neq p_b$, though it is the p_b value *that must be known*.

Corrections for Amount of Thermometric Substance n_b

Dead-Volume The dead-volume V_d is the sum of all the volumes in the pressure-measuring system containing the thermometric gas, between the bulb of volume V_b and the diaphragm of the differential pressure transducer. This volume is considered to be made up of two parts: (i) the volumes at constant (room) temperature (V_r in Fig. 3.6) and (ii) the volume V_C connecting V_r to the bulb. In Fig. 3.6, the volumes in (i) include the tubes connecting point X inside the cryostat to its top flange (V'_r), to the valve V and to the membrane of the differential pressure transducer P (V''_r), including the internal volume of all the valves present in the system; the volume in (ii) includes the capillary tube subjected to temperature gradients, connecting point X to the bulb. Table 3.7 shows the dead-volume corrections for a density of 160 mol m^{-3}.

The geometrical volume of the capillary can be measured to within a δV_C of ± 0.5 %, at the best, and the room-temperature dead-volume to within a δV_r of ± 0.2 %. This corresponds to an uncertainty of the bulb temperature that, for δV_r, can easily be calculated

$$\frac{\delta T}{T} = \frac{dV_r}{V}\frac{T}{T_r}.$$

This equation shows that the associated uncertainty, and also the correction ΔT_r itself scales with the square of T. On the assumption of the same parameters of Table 3.7 and a 1 L bulb at $T = 30$ K, $\delta T/T$ will be $\pm 1.4 \times 10^{-6}$, corresponding to ± 0.04 mK.

The same calculation when applied to determine the effect of δV_C is much more complex, since the source of the dead-volume effect is the (variable) amount Δn_b of the gas it contains.

The uncertainty of the correction values sums up the uncertainty of the geometrical measurement of the volume, and through it also the uncertainty in the determination of the density distribution $\rho(T)$ of the gas in the capillary, which determines the effective amount of the gas in the capillary.

The density distribution is generally obtained by means of a measurement of the temperature distribution in the capillary. This very important point will be discussed in the next subsection. An additional uncertainty of ± 0.3 %, at the best, is inherent

Table 3.7 Dead-volume temperature correction for a 1 L bulb and for the capillary design of Fig. 3.6 with temperature distributions of Table 3.8

$$\frac{\Delta T_c}{T} = \frac{n_c}{n}, \text{ where } n_c = \frac{p}{4R} d^2 p^* \int_B^X \frac{dh}{T(h)}$$

$$\frac{\Delta T_c}{T} = \frac{n_c}{n} = \frac{V_r \dfrac{p^*}{RT_r}}{V \dfrac{p^*}{RT}} = \frac{V_r}{V}\frac{T}{T_r} \quad \Rightarrow \Delta T_r \propto T^2$$

T (K)	Correction ΔT_c on capillary (V_c) (mK)		Correction ΔT_r on T_{room} volume (V_r) (mK)
	(1)[a]	(2)[a]	(3)[a]
0.5	< 0.01	< 0.0	< 0.01
1.2	0.01	0.06	0.06
3.0	0.09	0.31	0.21
5.0	0.18	0.71	0.58
10	0.71	2.5	2.3
15	1.6	5.0	5.3
20	2.7	6.2	9.3
25	4.2	12.3	14.6
30	5.9	17.6	20.9
50	14.9		58.3
100	49.5		233
150	96.4		525
200	152		933
250	215		1458
273.16	245		1740
300	283		2100

[a](1) $H_1 = 0$; $H_2 = H_3 = 50$ cm (300 K – $T_0 = 77$ K – T_b); $d_2 = d_3 = 1.0$ mm; 0.94 cm^3 total volume. (2) $H_1 = 100$ cm (300 K), $d_1 = 1$ mm; $H_2 = 10$ cm (300 − $T_0 = 4.2$ K), $d_2 = 3$ mm; $H_3 = 10$ cm ($T_0 = 4.2$ K – T_b), $d_3 = 1$ mm; 1.57 cm^3 total volume. (3) 7 cm^3 volume

in the evaluation of density distribution, so that the total uncertainty δV_C associated with the variable-temperature part of the dead-volume must be increased to ± 0.8 %.

These effects depend to a small extent on the type of gas used through the second virial coefficient. With helium isotopes, however, the second virial coefficient values tend to become constant at higher temperatures, so that only those tube portions at temperatures below 30 K may contribute to the differences. If this contribution is estimated 30 % of the total effective capillary volume, the isotopic effect with helium on the capillary dead-volume correction will never amount to more than 1 μK.

Temperature Distribution in the Capillary Tube[6] The temperature distribution will be analyzed in two sections of the capillary tube, X–A and A–B in Fig. 3.6. In the

[6] Only the axial temperature distribution is considered. The radial distribution of a capillary whose temperature is measured, as usual, at the outer surface of the tube wall, is reported not to contribute significantly to the dead-volume correction uncertainty by Razumovskii (1990).

following discussion, the capillary will be assumed to have reached thermal equilibrium, a condition, which may take a long time to achieve, and often much longer than expected. The way the temperature distribution is measured will be discussed in Sect. 3.3.1.2. In an interpolating CVGT, its measurement is not necessary, though it is essential to assume that it remains *stable* and it is *reproducible* for each bulb temperature.

The temperature distribution can also be calculated, since, for a tube with different end temperatures in vacuum the energy balance equation can easily be established. It has to be assumed, however, that no heat transfer by radiation occurs, a condition that can only be approximated. Four typical end-temperature combinations will be examined: 0.65–4.2 K; 4.2–24.6 K; 4.2–300 K; and 77–300 K. The first two apply to a tube like A–B, the other two to a tube like X–A. In the calculation, account must be taken of the real thermal conductivity $\lambda(T)$ of both the tube, which will be assumed to be made of stainless steel, and of the gas contained in it, assumed to be ^{4}He. It will be assumed in addition that no convection phenomena take place in the tube, as it would be quite difficult to take them into account, though the occurrence of such phenomena cannot be excluded, even in small-diameter tubes.

Let us first consider the contribution of the gas to the total thermal conductivity of the capillary. The contribution of the gas at 0.1 MPa in a tube with diameter (1×1.5) mm accounts for only $\approx$3 % of the total thermal conductivity in the 0.65–25 K range, less than 2 % in the 4–25 K range, and in a tube with diameters (3×3.5) or (4×4.5) mm about 2–4 % in the 4–300 K range. Obviously, this is also the maximum effect that can be expected when the gas pressure varies in the tube according to temperature or to different filling densities. In addition, due to the different functional dependence $\lambda(T)$ of the gas and of stainless steel, the gas in the tube has a larger influence on the temperature distribution in capillary tubes of *smaller* thickness: with a tube thickness up to 0.25 mm, a maximum perturbation of $\approx$2.5 % due to the gas can be calculated in the 4–300 K range. Therefore, the temperature distribution along the capillary can be assumed essentially independent of tube diameter and thickness for a wide range of values. For example, tubes with diameters (1×1.5) mm, (3×4) mm, or (6×6.25) mm give about the same temperature distribution $T(h)$, h being the axial coordinate of the tube.

Let us now consider the dependence $T(h)$ of the temperature distribution over the capillary length. It can be shown that $T \sim h^n$ where n ranges from ≈ 1 with narrow temperature ranges, to ≈ 2 with wide temperature ranges.

Figure 3.7a shows the evolution of the behavior of the temperature distribution when, over the same tube length and with $T = 4.2$ K at one end, the temperature of the other end (typically, the bulb side) is changed from 5 K to 25 K: the change from a nearly linear to a nearly quadratic behavior is evident. The figure shows as well, for the 4–25 K range, the behavior for $n \equiv 2$: the maximum departure from the real distributions is $\approx$ 10 % at 20 % of the *total* length H (i.e., $-$ 1.0 K at 12.5 K). The same considerations apply to the 4–300 K range (Fig. 3.7b) when changing the lower end temperature (e.g., T_0 in Fig. 3.6), and to the 0.65–4.2 K range. Table 3.8 gives the temperature distribution values for some of these cases.

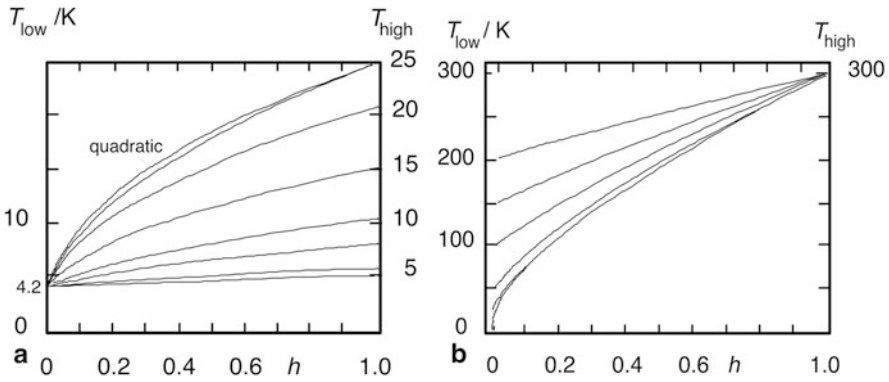

Fig. 3.7 Change of the temperature distribution in a capillary for different end temperature. **a** 4.2 K (fixed)–25 K (max). **b** 4.2 K (min)–300 K (fixed)

Table 3.8 Temperature distributions in capillary tubes[a]

Range (K)					
h (% H)	0.8–4.2 (K)	4.2–25 (K)	100–300 (K)	4.2–300 (K)	n/V (mol m^{-3})[b]
0 low end	0.80	4.20	100.0	4.2	290
2.5	1.11	6.17	106.8	37.1	33
5	1.33	7.55	113.4	51.8	23
10	1.67	9.61	126.0	74.3	16
20	2.16	12.56	149.5	109.7	11.1
40	2.86	16.69	191.8	166.4	7.3
60	3.38	19.79	230.2	214.8	5.6
80	3.82	22.36	266.0	258.9	4.6
100 high end	4.20	24.60	300.0	300.0	4.0

[a] In vacuo; no radiation; filled with ^{4}He at 0.1 MPa
[b] For a bulb at 4.2 K; $p = 0.01$ MPa (^{4}He filling: $n/V = 290$ mol m^{-3})

Attention must be given to the very large temperature gradients that arise from a quadratic behavior. Let us consider the range from 4.2 K to 300 K, and the corresponding large density variation (in the last column of Table 3.8): in only 2.5 % of H, temperature rises from 4.2 K to ≈ 37 K, at which density is already ≈ 9 times less (Arp and McCarty 1989); after 10 % of H, $T \approx 74$ K! Therefore, the *initial* gradient is larger than 10 K for each percent change of H. With a quiescent gas in a vertical tube with $\mathrm{d}T/\mathrm{d}h > 0$, a strong stratification will take place; with $\mathrm{d}T/\mathrm{d}h < 0$ (i.e., with a temperature inversion as with thermal anchoring), convection will occur.

It must also be pointed out that, during changes in bulb temperature, the capillary volume V_C (≈ 1 cm^3 in Table 3.7) is subjected to a substantial flow of gas, from (with increasing temperatures) or to (with decreasing temperatures) the bulb, due to the change in pressure of the gas in the bulb. At $n/V = 160$ mol m^{-3}, the tenfold pressure increase from 3 K to 30 K causes about ≈ 0.02 % of the thermometric gas to cross

Table 3.9 Relative values of the main corrections on pressure[a]

T (K)	^{4}He $\Delta p/p$ (%)[b]		^{3}He $\Delta p/p$ (%)[c]	
	Aerostatic head[d]	Thermomolecular pressure effect[e]	Aerostatic head[d]	Thermomolecular pressure effect[e]
0.5			0.060	0.077
1.0		0.177	0.045	0.015
2.0		0.047	0.030	< 0.001
3.0		0.021	0.022	
4.0	0.038	0.011	0.018	
5.0	0.030	0.008	0.016	
10.0	0.017	0.002	0.010	
15.0	0.013	< 0.001	0.008	
20.0	0.011		0.007	
25.0	0.009		0.006	

[a]Calculated for $n/V = 160\,\text{mol m}^{-3}$
[b]Capillary as in Table 3.7 (a)
[c]Capillary as in Table 3.7 (b)
[d]Calculated from: $\Delta p_{\text{aer}} \approx \frac{gm}{R}\, p^* \int_B^P \frac{dh}{T(h)} \Rightarrow \quad \Delta p_{\text{aer}} \propto T^2$
[e]Calculated from the Weber–Schmitt equation

to or from the capillary. The enthalpy change in this amount of gas, ≈ 0.02 J from 4 K to 37 K, is comparable with the heat capacity of the portion of the capillary where this temperature change occurs (≈ 0.06 J), and is therefore likely to produce a large thermal transient in the temperature distribution of the tube leading to the long time needed for renewed thermal equilibrium.

Corrections for the Bulb Pressure p_b

Corrections to the pressure measurement are made either: (a) for the aerostatic-head effect and (b) for the thermomolecular pressure effect. As both are characteristic of most pressure measurements, the reader is directed also to Part II.

Aerostatic-Head Correction The aerostatic head is the pressure exerted by the column of gas above the bulb. The extent of this effect is, of course, independent of the diameter and length of the capillary tube, and depends on the elevation difference between the bulb and the manometer, on the gas density distribution and its atomic mass. Typical values for ^{4}He and for ^{3}He are reported in Table 3.9, which compares two capillary designs, with different *temperature distributions* in the gas that affects the density distribution in the capillary, as discussed in the section "Corrections for the Bulb Pressure p_b". The uncertainty of the aerostatic-head correction is essentially due to the uncertainty in the knowledge of the temperature distribution in the gas.

Therefore, in principle, it can be made negligible by placing horizontally all nonisothermal portions of the capillary tube, as was done by Kemp et al. (1986); on the other hand, this can promote convection in the tube where temperature gradients

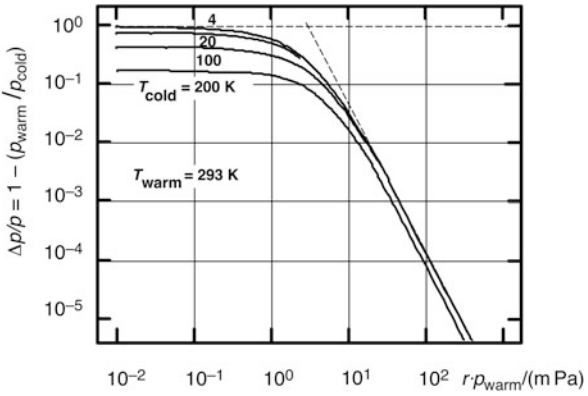

Fig. 3.8 Plot of Weber–Schmitt equation for the relative pressure error due to the thermomolecular pressure effect. r tube radius. (After Steur 1990)

are sharp. A full discussion of this correction, extended to the case of the two-bulb CVGT design (Sect. 3.3.2), can be found in Israilov (1969).

Thermomolecular Pressure Correction The thermomolecular pressure effect consists of a pressure difference in a tube whose end temperatures are different. It arises from phenomena at the metal/gas interface. It decreases with increasing pressure or the tube bore, and decreases with decreasing temperature of the warm end. The theoretical equation theoretically derived by Weber and Schmidt (1936), which accurately describes the thermomolecular pressure effect (see Part II, Chap. 10), is generally adopted for this correction. There is no measurable dependence of this correction on the gas used, but it depends on the condition of the surface (rough or smooth; McConville 1972). Figure 3.8 (Steur 1990) permits calculation of the correction and Table 3.9 compares it with the aerostatic-head correction.

The common choice of a uniform 1.0 mm diameter for the capillary, to minimize the dead-volume, makes the uncertainty of this correction relatively large only below 2 K. Table 3.10 gives the equivalent temperature uncertainty, on the assumption of an uncertainty of $\pm$ 25 % of the *total* thermomolecular correction; the table compares as well, for different capillary designs, the uncertainty of this effect with the uncertainty due to the other main sources.

A larger diameter facilitates the problem of the thermomolecular pressure correction to some extent, but, obviously, involves a larger dead-volume correction (cases [1] and [2]).

Table 3.10 shows clearly that the thermomolecular pressure and the dead-volume corrections, both connected with the pressure-line design, give large contributions to the measurement uncertainty. Therefore, the design of the connecting tube is determinant for obtaining the best accuracy from a CVGT, and a simple uniform tube is not necessarily the best choice. The CVGT design is discussed in Sect. 3.1.3 and provides the most elegant solution to these problems. However, a low-temperature pressure transducer of suitable characteristics is still not readily available.

Let us refer again to Fig. 3.6. All the parameters of the tube must be taken into account for design optimization. First of all, let us consider the length of the variable-temperature portion H(BX), which does not necessarily match the cryostat depth

Table 3.10 Comparison of the main sources of uncertainty δT/mK[a,b]

	Thermomolecular[c]				Virial coefficient		Dead-volume[d]			
T (K)	(1)[e]	(2)	(3)	(4)	$B(T)$	$C(T)$	(1)[e]	(2)	(3)	(4)
^{3}He										
0.5	0.78	0.39	0.10							
0.8	0.53	0.27	0.05							
1.0	0.44	0.22	0.04							
1.5	0.34	0.16	0.01		0.10	0.02				
2.0	0.25	0.13	< 0.01	0.08	0.10	0.01				
3.0	0.16	0.08		0.05	0.10	< 0.01				
4.0	0.11	0.05		0.03	0.10				< 0.01	< 0.01
5.0	0.08	0.04		0.02	0.10		< 0.01	0.01	0.01	< 0.01
10				0.01	0.15		0.01	0.04	0.02	0.01
15				< 0.01	0.15		0.03	0.06	0.05	0.02
20					0.20		0.04	0.11	0.08	0.05
25					0.25		0.06	0.17	0.11	0.07
^{4}He										
30					0.15		0.09	0.25	0.16	0.10
50					0.20		0.24			
100					0.30		0.86			
200					0.50		3.1			
300					0.90		6.5			

[a] Calculated for $n/V = 160\,\text{mol m}^{-3}$

[b] Italic indicates ITS-90 range

[c] Estimated as ± 25 % of the correction

[d] Assuming ± 0.8 % total error for V_c and ± 0.2 % for V_r

[e] *Capillary design*: (1) as in Table 3.7 (1) + (3); (2) as in Table 3.7 (1, with $d_3 = 1.4\,\text{mm}$) + (3); (3) as in Table 3.7 (2) + (3); (4) $H_1 = 0$; $d_2 = 2.0\,\text{mm}$, $H_2 = 25\,\text{cm}$ (300 K–$T_0 = 80$ K, linear temperature distribution); $d_3 = 1.0\,\text{mm}$, $H_3 = 25\,\text{cm}$ ($T_0 = 80$ K – T_{bulb}, quadratic temperature distribution). $V_c = 0.98\,\text{cm}^3$; $V_r = 7\,\text{cm}^3$ (Swenson 1989)

H(BP), i.e., point X is not necessarily at the top of the cryostat. If the cryostat is deep, as traditional bath types are, point X may be situated deep down in the cryostat if $H(\text{BX})_{\text{opt}} < H(\text{BP})$. In this case, the length H_1 of tube above X simply needs to be maintained at room temperature by compensating for its heat losses: this tube portion *must* be considered as an integral part V_r' of the total *room-temperature* dead-volume V_r, at constant temperature T_r. On the other hand, with the use of a much shorter cryostat, of the types employed with closed-cycle refrigerator or a flow cryostat, X can easily be kept at the cryostat top-flange level ($H_1 = 0$), thus reducing $V_r = (V_r' = 0)$.

A capillary design allowing the thermomolecular correction to be kept smaller without increasing the dead-volume correction is to make the variable-temperature portion of the tube, where most of the thermomolecular pressure effect occurs, as short as possible, so that its diameter can be accordingly increased without an increase of the total dead-volume. If the length of the upper tube portion H(XA) is limited to $H_2 = 10\,\text{cm}$ (in the same cryostat, one has $H_1 = 100\,\text{cm}$, $H_3 = 10\,\text{cm}$), the diameter can

be made about 3 times larger (to 3 mm i.d.), causing only a small variation of the total dead-volume correction, but substantially decreasing the thermomolecular effect, as shown in Table 3.7, case (2), and Table 3.10, case (3). There is also advantage in thermal anchoring the temperature T_0 of the middle point A to a fixed value at ≈ 30 K, in order to keep the portion X–A, in which most of the temperature change takes place, between two fixed temperatures: this will be discussed in Sect. 3.3.1.2. In the lower portion A–B, the thermomolecular pressure effect is much smaller, since both end temperatures are low, and therefore a small-diameter tube can be used ($d_3 \leq 1$ mm).

Another equivalent design is the one based, instead of a short length for H_2, on the use of the liquid nitrogen temperature as the fixed temperature of point A ($T_0 \approx 77$ K). This takes advantage of the temperature dependence as T^4 of the thermomolecular pressure effect, whereas the dead-volume correction obeys a T^2 relation. Therefore, density is small in the upper tube portion—which can be optimized with a larger diameter—while the thermomolecular pressure effect is small in the lower tube portion—which can be optimized with a smaller diameter (Table 3.10, case [4]).

3.1.2.3 Filling Density: A Compromise Between Sensitivity and Accuracy

As Table 3.1 shows, the uncertainty in the $B(T)$ values results in a temperature uncertainty between $< \pm 0.1$ mK for ^{4}He between 4 K and 60 K (up to ± 0.9 mK at 300 K) and of ± 0.1 mK for ^{3}He between 4 K and 30 K, for a molar density value of 160 mol m^{-3}. This molar density value is a good compromise, for both ^{3}He and ^{4}He above 2.6 K, especially as regards sensitivity, which is ≈ 1.3 kPa K^{-1}, and thus limits uncertainty to ± 0.1 mK for a pressure uncertainty of ± 0.13 Pa.

The extension of the CVGT to lower temperatures requires further consideration and applies only to ^{3}He, since ^{4}He thermometry is not advisable below 2.6 K (see Sect. 3.1.1.1). If the absolute limit for pressure measurement uncertainty cannot be improved to values better than ± 0.13 Pa, the *relative* temperature uncertainty dT/T of ± 0.01 % can no longer be maintained below 1.2 K. Furthermore, a molar density of 160 mol m^{-3} can no longer be used below 1.2 K without applying a correction also for $C(T)$ and, possibly, for higher virials; however, these corrections are affected by a large uncertainty. Below 1.2 K, the filling molar density must therefore be lowered. At 0.5 K, only about 3.5 mol m^{-3} can be used, as indicated in Table 3.3; the sensitivity of pressure measurements is thus reduced by more than a factor of 40 and the corresponding temperature uncertainty increases to about ± 4.5 mK. More accuracy can be achieved only by keeping the *relative* pressure accuracy constant down to 200 Pa, but the design of a CVGT capillary to be used with that value is more complex, as the correction for the thermomolecular pressure effect easily becomes preponderant at very low pressures and thus also its large uncertainty.

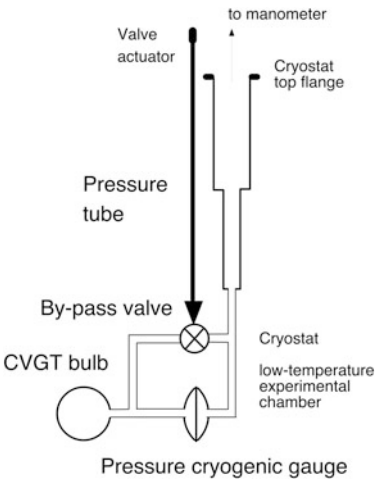

Fig. 3.9 General layout of a gas thermometer with a cryogenic diaphragm pressure transducer

3.1.3 Gas Thermometers with a Built-in Pressure-Measuring Device

The general layout of a gas thermometer using a cryogenic pressure transducer is shown in Fig. 3.9, which includes all possible options to be discussed in the following subsections (compare with Fig. 3.6). A design of this type has been implemented, until now, for a ^{4}He gas thermometer by Astrov et al. (1969) in the 4–20 K range, by Astrov et al. (1989) in the 12–300 K range, and by Van Degrift et al. (1978a, b) for measurements below 10 K. This design has also been used by Steur et al. (2002), but for an interpolating gas thermometer—see Sect. 3.2.

From the discussion of the preceding sections, it is evident that all major corrections, except the virial and adsorption correction, are avoided with the new design. On the other hand, the required pressure transducer must be of a special type (see Part II).

3.1.3.1 Use of a CVGT with a Differential Cryogenic Pressure Transducer

The use of this type of CVGT is the least demanding as regards a pressure transducer for use at cryogenic temperatures, but still requires a pressure-measuring line from the differential transducer to room temperature (Fig. 3.9). Only the zero stability of the transducer is relevant and must be of the same order of magnitude as that required for the room-temperature types.

Design options depend on the actual characteristics of the transducer actually employed. It may be mounted directly as part of the gas bulb, thus eliminating the dead-volume completely, if the transducer has a small and reproducible temperature coefficient of the diaphragm zero, considering that its temperature will change according to the measured bulb temperature. If this is not the case, the transducer

can be attached to the bulb by means of a short tube (which constitutes a small dead-volume), and maintained at a constant temperature (4.2 K, 1.5 K pot of the refrigerator, or that of a fixed point); thus a small thermomolecular pressure correction (and one for the aerostatic head, if the tube is not placed horizontally) is necessary again.

In all cases, and when the gas thermometer is used only below 30 K, the elastic characteristic of the diaphragm is likely to be much improved with respect to room temperature. However, thermal cycling to 300 K is unavoidable. If the diaphragm zero is stable enough on thermal cycling, no checks are necessary during operation, and the (bulb + transducer) system can, in principle, be sealed off. However, with pressure rising as high as 0.4–0.5 MPa at 300 K, the transducer diaphragm must be rugged enough and creep must not develop when it is maintained at room temperature. If these requirements cannot be met, a cryogenic valve (not shown in the figure) has to be placed between the bulb and the transducer, in order to isolate it from the bulb.

If the transducer zero is not stable enough on thermal cycling, in order to check it in situ, a cryogenic by-pass valve will be necessary, which is a critical component since it has to be operated repeatedly and must be of the constant-volume type. Besides, any leakage would affect the measurements, as it would change the amount of sealed substance n. However, it has to be considered that thermal cycling is likely to produce not a sensitivity change but only a zero shift, which can be checked with a temperature fixed-point device connected to the pressure transducer, the temperature of which can be kept at the constant value of the fixed point.

Being a differential transducer, it must be connected to the standard pressure-measuring apparatus at room temperature by means of a tube, which can be filled only with helium gas. Therefore, if the manometer that is to be used cannot use helium as a working gas, a second diaphragm transducer of suitable precision—though of the conventional type—is necessary in the room-temperature manometric circuit, which, however, will have to be calibrated with the same gas combination (Meyer and Reilly 1993/1994). When a pressure balance is used, a diaphragm at room temperature is always necessary, *because of the gas leakage* intrinsic in a manometer of that type (see Part II), especially when using the more costly ^{3}He.

The pressure tube, however, is a much less crucial element than in the case illustrated in Fig. 3.6, since only a correction for the aerostatic head is necessary, not for the thermomolecular pressure or dead-space effects. Its design is the same as used for vapor-pressure measurements, when large bores can be used, to minimize the thermomolecular pressure effect (Sect. 4.2).

3.1.3.2 Use of a CVGT with an Absolute Cryogenic Pressure Transducer

The measurement uncertainty of this transducer must range from ± 0.005 to ± 0.02 % over a pressure interval from about 0.1 MPa to less than 1 kPa, respectively. Its sensitivity must be better by about one order of magnitude. These requirements are not easily met, and in fact a special transducer has to be developed. However, stability to

thermal cycling is generally a much more severe requirement than stability to pressure cycling up to 0.4 MPa, provided that no inversion of the pressure sign occurs (or hysteresis would greatly affect reproducibility). Consequently, a transducer having a good zero reproducibility in thermal cycling is likely to be a good one also when pressure is cycled. Linearity is not strictly a requirement, as nonlinearity complicates the transducer calibration only slightly. In any case, in situ calibration against an absolute pressure standard is required.

A substantial part of the nonreproducibility of pressure readings for $p \neq 0$ is caused by the instability of the electronics of commercial units. This may be greatly reduced by the use of high-precision instrumentation.

With the use of an absolute pressure transducer, a tube connecting the gas thermometer to room temperature is no longer necessary, and the device becomes fully self-contained, only if it can be permanently sealed off. However, such a device shows the same problems (high room-temperature pressure) already pointed out in connection with the use of a differential-type transducer.

3.1.3.3 The Bulb Volume of the Gas Thermometer

The use of a pressure transducer built into the gas-thermometer bulb requires a complete change in the bulb design parameters. Only some hints can be given here, as a thermometer design would require a specific knowledge of the characteristics of the actual pressure transducer.

The most outstanding modification is the bulb size. Since the dead-volume effect is zero (or is greatly reduced), the volume of the gas bulb may become much smaller. However, a question arises as to whether there is a minimum volume.

This question is essentially equivalent to asking whether there is a minimum amount of gas sufficient to keep the uncertainty due to unwanted changes in the active amount of gas n in a CVGT within a stated limit.

Obviously, even with a self-contained small gas thermometer, one cannot avoid corrections for the virials and the variation of the bulb volume V_b as well. The discussion of Sects. 3.1.1.1 (virials), 3.1.1.3 (gas purity), and 3.1.2.1 (bulb deformation) still applies. In addition, the volume variation due to the diaphragm deflection of the pressure transducer, which usually can be neglected being of few cubic millimeters, should be carefully corrected on reduction of the bulb volume, and the deflection itself must be minimized.

As regards the variation of the amount of substance n, a first limit is set by the value of *static* vacuum that the bulb is able to maintain. For 1 mPa (see Sect. 3.2.1.2 for a discussion of this limit), the minimum pressure that can be measured with an uncertainty within ± 0.01 % is 10 Pa. This limit is not very stringent below 30 K, as most of the impurities remain "frozen" on the surfaces. On the other hand, these impurities may affect the accuracy of pressure measurement, because an impurity layer on the capacitor plates of a pressure transducer may alter the capacitance value if the dielectric constant of the layer is different from that of helium (or from ε_0, see Sect. 3.3.1). In a typical transducer (capacitor gap 0.15 mm, diameter 10 mm: see

Sect. 8.4.2), a 10^{-5} relative change in capacitance is caused by a layer of frozen air 1.5 nm thick—the thickness of 3–4 molecular layers—equivalent, for example, of the frozen air in the capacitor (8 mm^3) at a pressure of 3–1500 Pa, depending on the calculations.[7]

Only helium and hydrogen isotopes are not fully cryopumped at helium temperatures and remain in the gas phase (see Sect. 3.1.1.2). Unless their total amount is already below the required limit (for this limit, see Sect. 3.1.1.3), any change in the volume of one of these gases, due to adsorption on the walls at the working temperature, will cause an error. This error can be evaluated starting from the fact that helium is known (Daunt and Lerner 1972; Dash 1979) to build up only a little more than a monolayer on copper at $T < 20$ K (≈ 1.2 layers according to Eq. 3.4; Gershanik et al. 1978). Using a capacitance transducer results in a relative change in the pressure value of $\approx 10^{-4}$ (Gugan and Mitchell 1980), 10 times larger than the change caused by the previous effect.[8] The atom capacity of such a monolayer will affect the amount of active gas n. For helium at 0.1 MPa in a thermometer volume equal to that (8 mm^3) of the capacitor gap itself, values of δn from 0.01 to 20 % can be computed.[9]

Failing other reasons, the volume of the gas bulb might be made comparable to that of the pressure transducer itself; the original question can be shifted to whether one can define a practical size of a cryogenic pressure transducer. Apart from fabrication limitations, from the possible need to add fixed-point devices, or from the possible necessity of keeping the transducer thermally insulated from the gas bulb, the previous calculations indicate that a limit to transducer dimensions is set by the effect of the gas molecules partially on the walls and partially in dynamic equilibrium. These molecules particularly affect capacitive transducers, as they can alter the effective dielectric constant in the capacitor gap, causing the measured capacitance (i.e., pressure) values to fluctuate or become irreproducible.

---

[7] Calculations that follow are performed based on different assumptions, since the situation on the surface is very complex, and often ill defined (Dash and Schick 1978; Gershanik 1984). In addition, a strong temperature dependence exists: the atomic coverage increases by a factor of $\gg 10$ from 18 K to 4.2 K (Daunt and Lerner 1972). One is the extremely simplified assumption that the volume of the adsorbed layer is the geometric surface (generally smaller than the real surface) multiplied by the layer thickness taken equal to the molecular diameter. The volume of gas on the plates is: (1.5×10^{-9} m) $\times$ (78.5 mm^2) $\times$ 2 = 2.36×10^{-7} mm^3 of solid; assuming a ratio $V(\text{gas}_{\text{STP}})/V(\text{solid}) = 1000$, a volume of 2.4×10^{-4} mm^3 of gas results in the capacitor volume of 8 mm^3, corresponding to a pressure of 3 Pa. However, Daunt and Lerner (1972) give, for helium isotopes on copper sponge or gold, a *one* monolayer capacity of the order of 0.5 cm^3 m^{-2}, which leads, for the same area of 157 mm^2, to $\gg 8 \times 10^{-2}$ mm^3. Such a coverage in a bulb of 0.045 m^2 inner area (Sect. 3.1.1.2), would affect n by 22×10^{-6}, corresponding at 10 K to a δT of 0.2 mK, *in accordance with Gershanik's results on adsorption*.

[8] Calculation is as follows: on the assumption of a polarizability parameter of $\approx 2 \times 10^{-2}$ for the adsorbed helium and of 10^{-3} for the thermometric gas at 0.1 MPa, one obtains (2×10^{-2}:10^{-3}) $\times$ (2 $\times$ (plates) $\times$ (0.3×10^{-9} m)):0.1 = 10^{-4}.

[9] Calculation follows again the two previous approaches: on the first assumption, and assuming that the density of the adsorbed layer is in the same ratio of its polarizability, one obtains $5 \times 10^{-5} \times 20 = 10^{-3}$ mm^3 of gas; it is instead 1.6 mm^3 using Daunt and Lerner's data.

3.2 Interpolating Constant-Volume Gas Thermometers

In Chap. 1, the meaning of "interpolating instrument" was introduced as one of the three elements necessary to define an empirical temperature scale. The decision to use a CVGT for defining an empirical scale instead of directly measuring the thermodynamic temperature is prompted by different considerations. One is, for instance, the interest to improve measurement reproducibility beyond the thermodynamic accuracy limit. Another is the simplification when the gas thermometer is used as an *interpolating instrument*. This use, first proposed by Barber (1972), was subsequently and carefully discussed within the CCT (Swenson 1976; CCT 1980, 1984; Steur and Pavese 1987; Steur et al. 1987; Steur and Pavese 1989a, b), until it became part of the ITS-90 between 3 K and 24.6 K.

In general terms, an interpolating constant-volume gas thermometer (ICVGT) differs from a CVGT in that it is calibrated at more than one fixed point (i.e., pressure is measured at temperatures whose values are determined by *independent* means—for example, by a CVGT). Then, a *stipulated*[10] functional relationship is used for interpolating between these fixed points, or for limited extrapolations (the term ICVGT will be retained also for such cases). There is a substantial difference and the biggest simplification with respect to using an "absolute" gas thermometer for thermodynamic measurements, since the corrections for the instrumental (previously also called technical) parameters of the dead-volume or for the measured pressure values are no longer necessarily calculated or measured.[11] In fact, all corrections are taken into account in the "calibration" of the ICVGT at the fixed points. At the same time, one has to assume that the physical conditions of the experiments and the thermal conditions of the apparatus are reproduced in subsequent measurements and perfectly maintained the same as they were at the moment of the calibration. This basic assumption involves, for example, *the temperature distribution in the capillary*, which is not necessarily measured with an ICVGT, when precaution is taken that it remains stable and reproducible.

The reproducibility of an empirical, ICVGT-defined scale depends both on the selection and reproducibility of the technical parameters of the ICVGT noted previously, and on the reproducibility of the fixed points, as well as on the capability of the stipulated interpolating functional relationship to approximate the thermodynamic (T, p) relationship in different experiments (the so-called nonuniqueness: see Sect. 1.2.2.2). The accuracy of the scale depends on the accuracy of the thermodynamic temperature values *assigned* to the fixed points.

These considerations apply in the same way as with another well-known interpolating instrument, the platinum resistance thermometer (PRT). The $R(T)$ relationship

[10] The term "stipulated" is used in metrology to indicate that a certain definition is agreed upon by international bodies, and, possibly, incorporated in the text of an international code, such as the ITS-90. It is equivalent to "agreed," "specified," or else, depending on the sentence.

[11] Except, obviously, the corrections related to the whole manometric system, including the separation diaphragm pressure transducer (Fig. 3.6), which must still be applied.

of a PRT must, after calibration at the fixed points, accurately represent the pure-platinum resistance versus temperature characteristic. To achieve this result, however, the instrument must fulfill well-defined technical specifications, concerning, e.g., platinum purity, lack of mechanical stress in the wire, etc., and be stable in time.

The main reason for the more simple ICVGT use with respect to a CVGT lies in the fact that pressure p^* at the diaphragm level (Fig. 3.6) can be *used* instead of the pressure p at the bulb level,[12] so most of the secondary parameters need no longer to be measured, since most of the corrections, which affect a CVGT must no longer be explicitly made. On the other hand, whatever the stipulated functional relationship

$$T = I(p^*) \tag{3.8}$$

may be, it must apply to any actual implementation of an ICVGT within a selected accuracy. However, since real ICVGTs will differ from each other owing to different choices of the technical parameters, there will be small but experimentally undetermined differences between different ICVGTs, and departures of the chosen approximation $I(p^*)$ from the actual physical behavior. Consequently, these ICVGT instruments, as realized by different laboratories, will not realize *exactly* the same scale, but there will be a *nonuniqueness* error (see Sect. 1.2.2.2). Keeping this nonuniqueness small puts restrictions on the possible $I(p^*)$ functions and on the design parameters of an ICVGT.

Differently from the case of a PRT, the physics underlying an ICVGT is understood sufficiently to make it possible to calculate the exact functional relationship between the thermodynamic temperature T and the pressure p, provided that the experimental conditions are described sufficiently well (e.g., thermal anchoring, variation of cryogenic liquid). The relation is the same as with a CVGT—see Sect. 3.1. Consequently, it is possible to compute the difference between the exact functional relationship and its mathematical approximation $I(p^*)$. This is used for selecting the ICVGT definition, as well as to check its suitability from both standpoints of approximating the thermodynamic temperature and of limiting the nonuniqueness effects.

Linear ICVGT Function Let us start considering for the interpolating Eq. 3.8 a simple linear expression

$$p^* = a + bT. \tag{3.9}$$

This equation has not been written to match the form of Eq. 3.8 but in a form that can be compared directly with the real gas Eq. 3.2. In addition, considering the simplest temperature dependence of the virial coefficients (Barber 1972) as

$$B(T) = c + d/T, \quad C = 0 \tag{3.10}$$

[12] This may produce a nonuniqueness in the definition of the ICVGT. In fact, the use of either p or p^* is allowed by the text of the ITS-90, in that no explicit specification is made regarding the definition of pressure p. It just states "... the pressure p in the gas thermometer." The text in a new edition of the *Supplementary Information to the ITS-90* might resolve this ambiguity. In this book, we assume that measured pressure p^* is directly used.

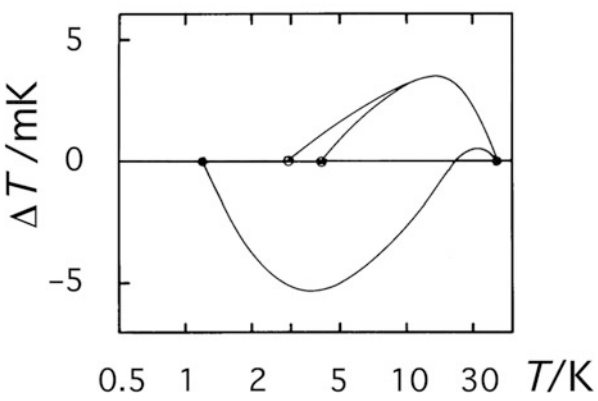

Fig. 3.10 Examples of ^{3}He and ^{4}He ICVGTs' nonlinearity for different sets of fixed points: ^{4}He between 4.2 (or 3 K) and 24.5 K; ^{3}He between 1.2 K and 24.5 K

then Eq. 3.2 becomes

$$p = Rd\left(\frac{n}{V}\right)^2 + R\left(\frac{n}{V}\right)\left(1 + \frac{cn}{V}\right)T. \tag{3.11}$$

Combining Eqs. 3.11 and 3.9 with the approximation $p \equiv p^*$, one obtains

$$a = Rd\left(\frac{n}{V}\right)^2 \neq 0 \quad \text{and} \quad b = R\left(\frac{n}{V}\right)\left(1 + \frac{cn}{V}\right). \tag{3.12}$$

Two calibration points are necessary to determine the value of the two parameters.

In practice, the behavior of $B(T)$ is complicated, $C(T)$ cannot be always ignored and, instead of pressure p, a pressure p^* is measured. The latter is related to p by a *nonlinear* relationship, because of the aerostatic, thermomolecular, and dead-volume corrections. All these effects would cause departures from the linear behavior of Eq. 3.9, which are sources of uncertainty if not taken into consideration in the ICVGT definition. Figure 3.10 shows these departures from linearity below 24.6 K as a function of temperature for some typical cases. The linear approximation of Eq. 3.9 is only useful for an accuracy of about $\pm$ 10 mK.

Nonlinear ICVGT Functions When the required accuracy of the linear function of Eq. 3.9 is not enough, the definition Eq. 3.8 can be transformed to explicitly take account of the different contributions to nonlinearity. This can be done in different ways. One method is to explicitly define some of the correction terms, by modeling them separately. Equation 3.8 then can be modified, by adding one term, as

$$T + v(T) = I'(p^*). \tag{3.13}$$

A typical case is that of $v(T)$ modeling a *physical* parameter of the gas such as the virial coefficients (i.e., the nonideality, Figs. 3.3 and 3.4). The advantage of this model is that $v(T)$ is valid for each gas, i.e., independent of technical implementation. Therefore, the same numerical values of the function $v(T)$ apply to *all* ICVGTs using the same gas and the function can simply be treated as the definition of an empirical temperature $\theta = T + v(T)$.

Another advantage of this model is to simplify the residual function $I'(p^*)$ with a possible reduction of the number of the required fixed points. Using Eq. 3.10 for v(T), for example, only one calibration point is still necessary, to obtain n/V. For greater accuracy, a more complicated function $I'(p^*)$ must be selected; however, the number of its free parameters, which equals the number of the necessary calibration points, must be kept to a minimum.

The first choice in selecting $I(p^*)$ is whether to use a stipulated function for the virials ($I(p^*) = I'(p^*) - v(T)$, as in Eq. 3.13) or to rely only on the calibration of the ICVGT at the fixed points. The second choice is whether to use a purely empirical equation or to use the theoretical exact functional relationship for the CVGT, which was given in Sect. 3.1.

The ITS-90 definition prescribes the choice for the 3–25 K range, by stipulating an equation for $B(T)$, by *assuming* $C(T) \equiv 0$, which implicitly limits the *molar density to less than* $\approx 250\,\text{mol m}^{-3}$, and by using a quadratic model for $I'(p^*)$, thus requiring three fixed points.

Here, only a small part of the possible ICVGT definitions treated in the first edition of this book (Pavese and Molinar 1992c) will be discussed: in Sect. 3.2.1 the one adopted by the ITS-90. For the others, see the first edition.

The upper limit of the temperature range will be set to 30 K, since other interpolating instruments are more suitable in the higher temperature range.

Summarizing, in the following the reader must be aware of the fact that there are three main sources of uncertainty in an ICVGT:

(a) *Fixed point realization*: This subject is treated in detail in Chap. 2. A list of fixed points and their characteristics are given in Appendices B and C. The accuracy of the vapor-pressure scales can be found in Chap. 4.
(b) *Pressure measurement*: This is a subject specifically treated in Part II, but in Sect. 3.1 the required manometer sensitivity is discussed in connection with the filling molar density n/V. Molar density range must be limited to avoid the contribution of the third virial coefficient (Table 3.3). With ^{3}He, this requirement sets a lower temperature limit at 1.2 K for a molar density of $n/V = 160\,\text{mol m}^{-3}$, if one needs to exploit the best accuracy with a manometer uncertainty of ± 0.13 Pa. An ICVGT can be used at lower temperatures when relaxing the accuracy requirements.
With ^{4}He, the lower temperature limit is always restricted to ≈ 2.5 K.
(c) *Choice of the interpolating function and temperature range*: This subject will be treated in this section. Gas purity is assumed to be more than adequate (Table 3.4) and gas adsorption not to occur, thus not contributing to the overall uncertainty.

Hints on ICVGT technical implementation can be found in Sect. 3.3.

3.2.1 ICVGT Types with Stipulation of the Virial Function

A close examination of the analytical expressions for the correction parameters of a CVGT, given in Sect. 3.1 shows that all the *technical* corrections, but that for the

thermomolecular pressure effect below 3 K, can be approximated below 30 K with first- or second-order functions, provided that experimental conditions are adequately taken into account. They do not, of course, depend on the helium isotope used. The behavior of $B(T)$ is different for ^{3}He and ^{4}He. Above 3 K, for an ICVGT filled with $n/V = 160\,\text{mol m}^{-3}$, $^4B(T)$ is quadratic within ± 0.2 mK, whereas $^3B(T)$ is quadratic within ± 0.8 mK, with most of the deviation being concentrated below 5 K. Below 3 K and for the same ICVGT, $^3B(T)$ shows deviations rapidly increasing to more than 1 mK, while ^{4}He can no longer be used below ≈ 2.5 K.

Consequently, considering that the thermomolecular effect must in any case be kept small because the correction of this effect is affected by a large uncertainty, a stipulation of the virial has the following three advantages: (a) the residual interpolation function $I'(p^*)$ becomes independent of the isotope; (b) a simple quadratic function is likely to be suitable for a wide range of technical parameters, i.e., of different ICVGT implementations; and (c) the use of either helium isotopes is perfectly equivalent (except for the lower admissible limit of the temperature range, which is ≈ 2.5 K for ^{4}He and ≈ 0.5 K for ^{3}He).

The disadvantage of a stipulation, at least in an official scale definition, is that it fixes in time not only a functional representation of the virials—probably not critical—but also the actual *numerical values* of the coefficients at the time of the stipulation, values, which might later prove to be different when more precisely determined by subsequent measurements or theory.

Several different ICVGT definitions have been developed: see Table 3.12 (Pavese and Molinar 1992c).

3.2.1.1 Three-Fixed-Point ICVGTs (Quadratic)

Between 3.0 K and 24.5 K, this type of ICVGT is *the one defined by the ITS-90*

$$T\left(1 + B(T)\left(\frac{n}{V}\right)\right) = a + bp^* + cp^{*2} \tag{3.14}$$

where p^* is the pressure measured in the gas thermometer, *in this book always intended to be that measured at the differential pressure transducer*.

The ITS-90 stipulations for $^3B(T)$ or $^4B(T)$ are given in Appendix A (Eqs. 1.6a and 1.6b) and a, b, and c are the coefficients to be determined by calibration of the ICVGT at the triple points of neon (24.5561 K) and of *e*-hydrogen (13.8033 K), and at a temperature between 3.0 K and 5.0 K, measured on either the ^{3}He or ^{4}He vapor-pressure scales. The superconducting transition of indium at 3.4145 K could, in principle, also be considered for non-ITS-90 use. Obviously, the stipulation of a quadratic function assumes that no influence parameter needs be modeled with a polynomial of degree higher than the second (namely the thermomolecular effect).

Under this assumption, the nonuniqueness can be kept smaller than ± 0.1 mK with capillary designs (3) and (4) of Table 3.10 and a very wide range of parameters (Fig. 3.11), including the case of *zero dead-volume*, relevant to the ICVGT discussed in Sect. 3.3.3. This type of ICVGT can actually be used up to 30 K with nonuniqueness still limited to ± 0.3 mK.

The ± 0.1 mK nonuniqueness level is maintained down to 2.5 K for both isotopes and down to 2.18 K *only for* ^{3}He.

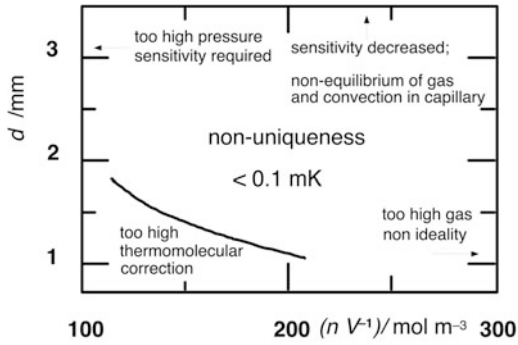

Fig. 3.11 Limits of main ICVGT design parameters for ICVGT types of Sect. 3.2.1.1. d capillary diameter (d_2 in Fig. 3.6); n/V molar density; TM boundary for a ± 0.1 mK uncertainty on the thermomolecular pressure effect correction. Nonuniqueness is $< \pm 0.1$ mK within the indicated limits for the ICVGTs defined by the ITS-90 and for any three-fixed-point ICVGT with stipulated virial (Eq. 3.18) down to 2.5 K using ^{4}He and down to 2.18 K using ^{3}He

Table 3.11 Reduced density and sensitivity limit for a ^{3}He ICVGT below 2.2 K

Temperature (T (K))	Molar density upper limit (n/V (mol m^{-3}))	Sensitivity limit (δT (mK))[a]
2.2–1.2	160	0.1
1.2–1.0	80	0.2
1.0–0.8	30	0.5
0.8–0.65	16	1.0

[a]For a manometer sensitivity of ± 0.133 Pa

Below 2.18 K, the influence of the thermomolecular pressure effect can be limited only by a careful choice of the capillary design, and a lower fixed point is advisable. This case will be discussed in Sects. 3.2.1.3 and 3.2.2.3.

Below 1.2 K, accuracy degradation occurs more markedly, as the molar density must be reduced in order to avoid the ill-known influence of the third virial coefficient $C(T)$ (see Table 3.3 in Sect. 3.1.1.1). Table 3.11 shows the molar density limits, and the consequent uncertainty, caused by the reduced sensitivity of the measurements. It must be pointed out that, for every selected lower temperature limit, i.e., the selected molar density value, the ICVGT must then be used within this same filling molar density *up to the upper temperature limit* (≈ 25 K), as the ICVGT calibration applies specifically to that molar density value.

3.2.1.2 Other Possible ICVGT Definitions

The interested reader should consult the previous edition (Pavese and Molinar 1992c) for the following other types of ICVGT definitions: for ICVGTs with stipulated virial functions, using two or four fixed points; for ICVGTs without stipulated virial functions, two, three, or four fixed points, and suitable for use down to 1.18 K. Table 3.12 summarizes all the types of definitions, for convenience.

Table 3.12 Summary of interpolating CVGT possible definitions

Definition[b]	Range (K)[c]	Accuracy (mK)[d]
(a) With stipulation of the virial function (for ^{3}He use Eq. 1.6a; for ^{4}He use Eq. 1.6b)		
(a.1) *3 fixed points*		
$T(1+B(T)(n/V))=a+bp^*+cp^{*2}$		
3–5 K, 13.8 K, 24.5 K (*ITS-90*)	3–24.5	±0.1
2.18 K, 13.8 K, 24.5 K (*ITS-90*, ^{3}He only)	2–25	±0.1
2.18 K, 13.8 K, 24.5 K	2–30	±0.3
1.18 K, 13.8 K, 24.5 K	1.2–30	±1
(a.2) *2 fixed points*		
same as (a.1) with		
$a/\mathrm{K}=-5\times10^{-4}+5\times10^{-6}\{[p^*(24.6\ \mathrm{K})/(24.6\ \mathrm{K})R]/$ mol m$^{-3}-160\}$ 13.8 K, 24.5 K	2.2–30	±0.3
(a.3) *4 fixed points* (^{3}He only)		
$T(1+B(T)(n/V))=a+bx+cx^2+dx^3,\ x=[\ln(p^*)]^{1.3}$		
1.18 K[e], 4.2 K, 13.8 K, 24.5 K	1.2[e]–25	±0.3
(b) Without stipulations		
(b.1) *Linear*		
$T=a+bp^*$		
4.2 K, 24.5 K (^{4}He)	4–30	±4
1.18 K, 24.5 K (^{3}He only)	1.2–30	±6
(b.2) *3 fixed points*		
(i) $T=a+bp^*+cp^{*2}$		
4.2 K, 13.8 K, 24.5 K (^{4}He)	4–25	±0.1
3.0 K, 13.8 K, 24.5 K (^{4}He)	3–25	±0.2
(^{3}He)	4–25	±0.8
(ii) $T=(b_0p^*+c_0p^{*2})+A+B\ln p^*+C(\ln p^*)^2$		
2.5 K, 13.8 K, 24.5 K (^{3}He only)	2.5–25	±0.1
2.18 K, 13.8 K, 24.5 K (^{3}He only)	2.2–30	±0.15
(b.3) *2 fixed points*		
(^{4}He) same as (b.2 i) with		
$a/\mathrm{K}=4.958\times10^{-5}$ [p^*(24.5 K)/Pa)/24.5 K]		
13.8 K, 24.5 K	3–25	±0.5
(^{3}He)$T/\mathrm{K}=b_0(p^*/\mathrm{Pa})+c_0(p^*/\mathrm{Pa})^2+[a'_0+b'_0\ D/(p^*/\mathrm{Pa})]$		
$a'_0=8.68\times10^{-4}$; $b'_0=-4.225\times10^{-4}$		
$D/\mathrm{K}^{1.5}\mathrm{Pa}^{-1.5}=(p^*(24.5\ \mathrm{K})/24.5\ \mathrm{K})^{1.5}$		
13.8 K, 24.5 K	2–25	±0.5
	2–30	±1
(b.4) *4 fixed points* (^{3}He only)		
(i) $p^*=A+Bx+Cx^2+Dx^3,\ x=[\ln(T)]^{1.3}$		
(ii) $T=\sum_{i=0}^{3}a_i(\ln p^*)^{i(1+V_r/25)}$		
V_r = dead-volume at T_r		
(iii) $T=b_0(p^*-p_1)/(p_3-p_1)+a+bx+cx^2+dx^3,\ x=[\ln(p^*)]^2$		
$p_1=p^*(2.1768\ \mathrm{K}),\ p_3=p^*(24.5561\ \mathrm{K})$		
$b_0/\mathrm{K}=24.5561-2.1768$		
(ii, iii) 1.18[e] K, 3.41 K, 13.8 K, 24.5 K	1.2[e]–25	±0.5
(i, iii) 2.18 K, 4.2 K,13.8 K, 24.5 K	1.8–25	±0.3

[a] Only (a.1) illustrated in this edition; for the others, see first edition (Pavese and Molinar 1992)
[b] $n/V \le 250\ \mathrm{mol\ m^{-3}}$
[c] $T \ge 1.2$ K, as must be $n/V \ge 160\ \mathrm{mol\ m^{-3}}$
[d] In some cases, only some capillary design is suitable
[e] The range can be extended down to 0.8 K, and zinc superconductive transition added, with $n/V \le 160\ \mathrm{mol\ m^{-3}}$ and lower accuracy (Table 3.11)

3.3 Constant-Volume Gas-Thermometer Realizations

In this section, some guidelines will be given about the implementation of the principles discussed in the preceding sections. The guidelines will be provided only for the design of the basic parts of a CVGT. References will be given for the implementations available in the literature.

In order to attain working temperatures, refrigeration of the thermometer is obtained by locating it in a cryostat. Though very often in the past the cryostat was considered integral with the thermometer, it is conceptually distinct and, with proper designing, the thermometer can actually be maintained quite independent of the cryostat. Cryostats for thermometry are treated in Chap. 6.

Constant-volume gas thermometers can be classified, as far as design is concerned, into three groups: the truly absolute, with the working temperature range extending up to 273.16 K, the reference temperature; those using a low-temperature reference temperature; and those exploiting a cryogenic pressure transducer. They will be treated separately.

Interpolating gas thermometers are essentially designed as CVGTs, but some checks and the measurements of a number of correction parameters are avoided. They are generally calibrated at the fixed points by means of calibrated thermometers and not by direct connection of fixed-point realizations to the bulb.

3.3.1 CVGTs with Reference at Temperatures Lower than 273.16 K

This type is treated first, as it is the most common. Only few gas thermometers for low temperatures were made which can also be used in the true absolute mode, owing to the difficulty in optimizing the design over such a wide temperature range. More commonly, thermometers are designed to have a working temperature range of approximately 50–200 K.

A CVGT is made up of essentially three parts: (a) the measuring bulb whose temperature defines the thermodynamic temperature; (b) the pressure capillary, connecting the bulb to the pressure-measuring system at room temperature; and (c) the pressure-measuring system.

3.3.1.1 Measuring Bulb

A 1 L volume is typical for top-accuracy apparatuses, but volumes smaller by a factor of two or three can still be used yielding the same accuracy. A larger bulb volume makes the effect of the dead-volume less critical, but temperature uniformity is more difficult to achieve, the surface adsorbing the thermometric gas becomes larger, and so does the size of the entire experimental apparatus.

The bulb is generally a cylinder of about equal diameter and length, made of OFHC copper of carefully checked thermal expansion (especially for work above 100 K). It is recommended to carry out this check *before* fabrication and use of the instrument, on specimens drawn from the same bar of material. High-purity copper is known to have an extremely reproducible behavior (White and Collins 1972; Kroeger and Swenson 1977; Pavese and Ciarlini 1990b). Therefore, any anomaly can only be due either to errors in thermal expansion measurements, or to coarse problems of the material composition, which could affect as well its geometrical stability and other important properties such as the necessary high thermal conductivity. Should any such anomaly be observed, the material must be replaced. It is *not* recommended to anneal copper to high temperature, but only, if necessary, to release strain after machining by heating it up to 200–300 °C in an inert or slightly reducing atmosphere.

The wall thickness is generally chosen such as to give a substantial rigidity to the bulb, and thus avoid large volume changes when the inner pressure changes. Alternatively, thin walls can be used and the bulb, instead of being subjected to vacuum on one side, is enclosed in a can kept at the same pressure of the bulb (Astrov et al. 1989). This *must* be done when the bulb is made of glass (in this case the bulb is spherical; Sakurai 1982).

Accurate machining of the bulb is necessary so that a real surface area as close as possible to the geometrical one is obtained, in order to minimize gas adsorption. In this respect, polishing with abrasive paste can "splash" the ductile material onto the surface, thus trapping impurities; similarly, gold plating (usually used to limit adsorption) by wet methods (chemical or electrochemical) may cause the same problems. Electroerosion for final machining (easily smooth to better than 1 μm) and vacuum deposition of gold are well suited. The use of a glass bulb eliminates all these difficulties.

In the 2008 report of CCT WG4 (CCT WG4 2008), an attempt is made to explain the observed differences in thermodynamic temperature in the range between about 80 K and 273.15 K, with a maximum of about 10 mK around 150 K. The hypothesis is made that gold plating and cold working may cause unforeseen changes in the thermal expansion of copper. In at least two experiments (Steur and Durieux 1986; Kemp et al. 1986), the carefully machined copper bulb was covered by double gold plating. In the work of Steur and Durieux, a first (inner) gold plating was absorbed into the copper wall by annealing at too high a temperature, leading to a second (inner) gold plating. In the work of Kemp et al., gold plating was performed at both the inner and outer surface of the bulb.

The effect of the gold plating and cold working was estimated to contribute to no more than 2 mK and 1 mK, respectively.

The bulb is constructed in two or three parts (by machining, hydraulic forming [for spherical shape], diamond turning, etc.) and consequently requires one or two seals. In the past, sealing was occasionally made by soft soldering (e.g., using indium, which melts at 157 °C). This method has the distinct advantage, if the correct amount of solder is used, of eliminating gaps in the inner volume, but it has the disadvantage of damaging gold plating, which easily diffuses in the copper even at moderate temperatures. Any other type of low-temperature seal on copper is based on the

extrusion of a wire of ductile materials, such as indium or gold, which leaves a more or less large gap between the two parts, and both size and extrusion cannot be controlled accurately. Edge-cut gaskets (like in ConFlat ultravacuum flanges) cannot be used, since copper is too soft. Consequently, the geometrical definition of the inner volume cannot be calculated better than $\approx 10^{-4}$, even if the inner dimensions are measured to within ± 1 µm. Moldover's method (Moldover and Trusler 1988) of a light vacuum-grease coating, which fills the gap *inside* the gasket, was proven effective in eliminating the gap volume irreproducibility, however, a substantial contribution to bulb volume uncertainty is made by the geometrical definition of the inner edges.[13]

Accurate knowledge of the bulb volume is not strictly necessary, even for an absolute CVGT, as the ratio n/V is determined by calibration at the reference point. However, when possible, it would permit a double check to be made, which is always useful for systematic-error detection. The bulb volume can be measured by filling it with a density-reference substance and by weighing, or by comparison with a calibrated volume applying the expansion method. Mercury cannot be used as a filling substance as in Moldover's experiment, because of the gold plating and the much narrower filling tube (≈ 1 mm diameter). Water can be used, but trapped or evolved air bubbles must be carefully avoided (1 mm^3 bubble means 10^{-6} volume error in a 1 L bulb). Bubbles can only be eliminated by gently boiling the water under reduced pressure. If temperature gradients during weighing can be kept within a few hundredths of a kelvin (for water $\Delta V/V_0 = 50 \times 10^{-6}$ K^{-1}), with this method the volume can be determined within a few parts per million.

In the cryostat, the bulb must be kept in an adiabatic environment. An isothermal heavy copper shield is generally used, which can either be kept well insulated from the bulb, or be thermally linked to the bulb, but only at one point, so that in any case no heat flux can cross the bulb walls.

3.3.1.2 Pressure Capillary

A capillary tube is unnecessary for the case of the CVGT design discussed in Sect. 3.1.3. In all other cases, including the ICVGTs, its design involves many of the most difficult compromises between conflicting requirements.

On the other hand, while the greatest care has always been taken in order to build strictly controlled thermal conditions around the bulb, the capillary tube has almost invariably being designed to pass through the less temperature-controlled regions of the cryostat, on its path to room temperature, apart from its being kept in the evacuated space.

---

[13] Calculations are as follows (assuming for inner bulb dimensions: diameter 100 mm, length 120 mm): 1 µm over an inner surface of 55 cm^2 = 55 $\times$ 10^{-6}. An uncertainty of ± 0.1 mm on a 45° cut edge with a size of 0.5 $\times$ 0.5 mm over the diameter of 100 mm is equivalent to 16 $\times$ 10^{-6} each and to 32 $\times$ 10^{-6} in total. A 0.1 mm-thick and 2 mm-large gap inside each gasket on 100 mm diameter amounts to 63 $\times$ 10^{-6}; an uncertainty of 30 % yields 19 $\times$ 10^{-6}, 38 $\times$ 10^{-6} in total.

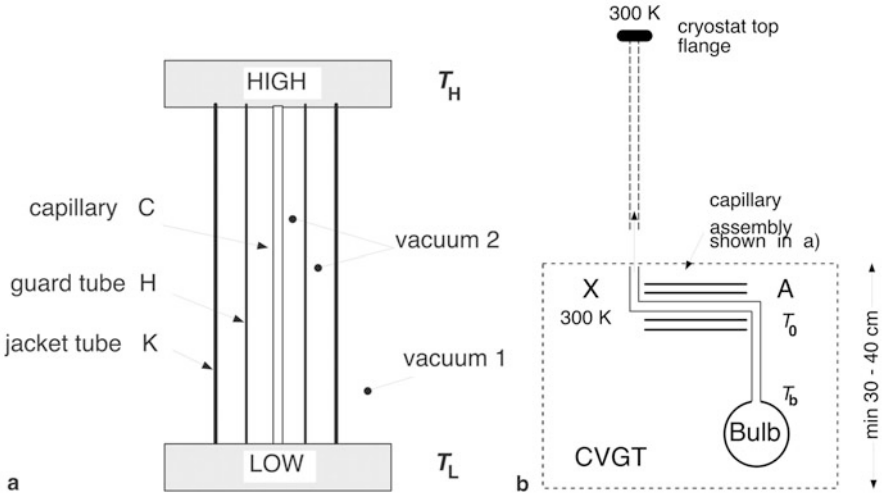

Fig. 3.12 **a** Principle of controlled thermal environment for the capillary. **b** Implementation with section (a) placed horizontally and a short capillary. Points A and X are the same as in Fig. 3.6

It seems therefore necessary, especially in the use of the ICVGT, where the capillary parameters are not necessarily *measured*, to stress the need for a capillary design allowing it to operate in *stable* and *controlled* thermal conditions, in order to have a *stable and reproducible* temperature distribution.

This goal may be achieved by building a calorimetric environment around this tube, as is usually done with the bulb. There is, however, one difference—for the bulb an adiabatic environment is necessary, while for the tube an *isothermal* environment is needed.

In fact, as a certain temperature distribution builds up between the bulb and room temperature, the calorimeter must provide the same temperature *distribution*, so as to minimize the heat transmitted by radiation (the only possible mechanism in *vacuum*), as is done, e.g., in accurate thermal conductivity measurements with the steady-state method. The principle is shown in Fig. 3.12a. The very thin capillary tube C, vacuum insulated between T_H and T_L, faces an isothermal surface, e.g., a concentric tube H between these two temperatures. Very little heat is transmitted by radiation between the two tubes for angles $\alpha \neq 0$, provided the temperature distributions of C and H are the same. This thermal situation may be achieved easily if the tube H is itself shielded from radiation (with a multilayer insulation or/and by a second tube K); the tube C will assume a temperature distribution close to that of H.

It is common practice to put several thermometers (generally thermocouples) on the capillary, in order to check or measure the temperature distribution. However, the thermocouples and their connecting wires are likely to perturb the capillary to such an extent as to *fully* change its temperature distribution with respect to the "natural" one (unperturbed, as calculated using the thermal conductivity). In addition, tube C is so small that it is not easy to mount the thermometers. On the other hand, the size

of tube H can be quite suitable to be instrumented in a much easier way, and be much less perturbed.

Other problems relate to the *time* required to develop a stable—and thus reproducible—temperature distribution in the capillary tube. It has commonly been observed that considerable time is required for the capillary to achieve a stable temperature distribution, because of the low thermal diffusivity of stainless steel. Avoiding any addenda to the tube (especially plastic materials or ill-defined thermal connections) is also advantageous in this respect.

Obviously, maintaining both end temperatures of the tube, T_H and T_L, fixed also improves the stability of its temperature distribution (nevertheless, a transient can occur when the gas flows in the tube owing to bulb temperature changes, see the section "Corrections for the Bulb Pressure p_b"). A comparison of Figs. 3.12a and 3.6, suggests that $T_H \equiv T_{room}$ and $T_L \equiv T_A$. In fact, only the section X–A (Fig. 3.6) of the capillary, where most of the temperature change takes place (at least with a CVGT working below 100 K), will require carefully controlled thermal conditions. In addition, this section takes account of most of the thermomolecular pressure effect requiring a larger tube diameter. Last, to make the capillary temperature distribution independent of the cryostat operation, the vacuum space (2) of the assembly jacket H–K in Fig. 3.12a should be independent of the main cryostat vacuum (1).

The section A–B (Fig. 3.6) of the tube, on the contrary, does show a variable end temperature T_b of the bulb, but there the thermomolecular pressure effect being small, its design is not critical.

The capillary tube assembly should be put into a cryostat reentrant well, in order to be easily demountable. A vertical position is not necessary, on the contrary. If the cryostat can be conveniently designed, there is an advantage in keeping the nonisothermal parts horizontal (Fig. 3.12b), bending if necessary to save space, as this position reduces the uncertainty of the aerostatic correction (see Sect. 3.1.2.2).

There is no great advantage in a long capillary tube since, from a thermal point of view; difficulties increase with length, as already discussed in Sect. 3.2. On the other hand, thermal conduction decreases with length, thereby improving thermal insulation. Therefore, both the tube lengths X–A and A–B (Fig. 3.6) should be kept as short as practical, *independent* of the cryostat depth. Should a tall cryostat be required (see Chap. 6), the portion of tube from point X and the cryostat top flange must be kept *isothermal* at T_{room}. This may, however, lead to other negative aspects such as higher evaporation rates of the cryogenic liquid and problems related to accurate thermal control of a length of tube. *This portion is not part of the capillary dead-volume V_r but of the room-temperature portion of the dead-volume V_r*; therefore, the tube diameter can be relatively small.

The volume of the capillary (and of V_r) must be carefully measured in a CVGT. Sometimes, measurements are carried out by filling the tube with mercury and then weighing the mercury. Another—cleaner—way, with a better accuracy, is the volumetric expansion method. A small reference volume ($\approx 50\,cm^3$, which can be calibrated to an accuracy better than 0.01 %) is filled with an amount of gas, then the pressure is measured with comparable accuracy and the gas is allowed to expand into the capillary. From the two pressure values (after correction for possible small

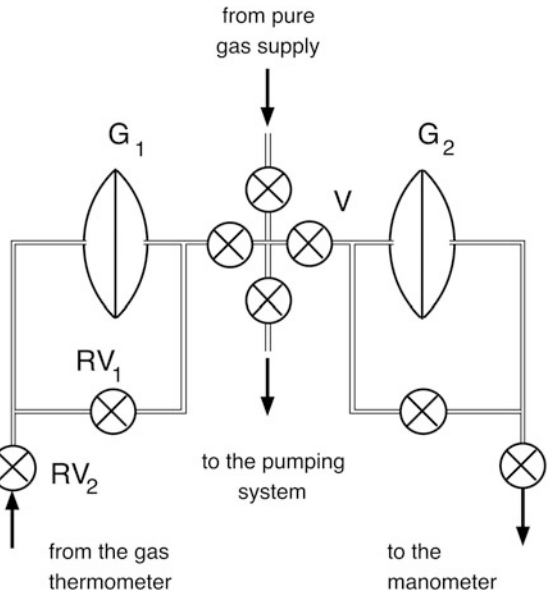

Fig. 3.13 Pressure-measuring system. G_1, G_2 differential gauges; RV_1, RV_2 valves with reproducible volume

temperature changes), it is straightforward to obtain the capillary volume. A similar method can be used for measuring the room-temperature dead-volume. Volume-reproducible valves (discussed in the next section) must necessarily be used for the relevant operations.

As discussed in the section "Corrections for the Bulb Pressure p_b", the geometrical calibration of the dead-volume is not sufficient to calculate the corresponding correction; also the density distribution of the gas in the dead-volume must be known. Besides, the aerostatic head and the thermomolecular correction s also affect the pressure-measuring line. Therefore, one can "calibrate" the whole bulb addenda by replacing the bulb with a blank flange and by performing a number of measurements with "zero bulb volume," which reproduce the $p(T)$ working conditions of the CVGT, at various "bulb" temperatures. The only, though important, difference is that it is not possible to simulate the gas flow from or to the bulb when temperature (i.e., pressure) is changed. Such a flow may alter, at least temporarily, the temperature distribution in the capillary.

3.3.1.3 Pressure-Measuring System

Pressure gauges are described in Part II. Here, a description will be given of the specific characteristics of the room-temperature parts of the thermometric gas system whose general layout is shown in Fig. 3.13.

The purity and integrity of the amount of the thermometric substance must be preserved throughout the operations required to perform the pressure measurements.

A differential pressure gauge G_1, of very small internal volume—to limit the increase of the room-temperature dead-volume, is necessary to isolate the thermometric gas from the manometric gas, possibly of a different type and, in any case, less pure than the former. The operation of this gauge needs a check of the zero, which must be carried out by directly applying the *same* pressure to both sides by opening a by-pass valve. This operation risks contamination of thermometric gas with some of the manometric gas filling in the by-pass section, or loss of some of the thermometric gas. The valve RV_1 sealing the bulb during these operations and the by-pass valve RV_2 must have *reproducible* volume, when open and when closed, since the dead-volume must be reproducible. Many special designs for such a valve are described in the literature (e.g., Anderson et al. 1970; Kemp and Smart 1979; Spencer and Ihas 1985; Siegwarth and Voth 1988). In addition, the volume is required to remain *constant* during the open/close operation with some specific types of CVGT (like the one in Fig. 3.21: see Sect. 3.3.2). Obviously, the gas trapped between RV_1 and V becomes a mixture of the thermometric and the manometric gases, and therefore must be pumped away after each by-pass operation; in the case of ^{3}He, a cryogenic adsorption pump (integral with the cryostat) should be used to recover the gas for subsequent purification. Before RV_1 is reopened, the tubes must be refilled with fresh *pure* gas at the *working* pressure. For the highest accuracy, a second differential gauge G_2 is advisable, of normal internal volume but of comparable accuracy, so that the by-pass operation can be performed with less risk of contaminating the thermometric substance. This gauge is necessary when a piston gauge is used as manometer, especially using ^{3}He.

3.3.1.4 Modern Realizations

High-accuracy realizations (reproducibility $\pm$(0.2–0.5) mK, accuracy few millikelvin) will be first considered, limiting reference to the past to realizations that took part in the definition of the thermodynamic basis of the ITS-90. Mention must be made of the low-temperature CVGT of Kemp et al. (1986) at NML ($4\ \mathrm{K} < T < 273.15\ \mathrm{K}$), of that of Steur and Durieux (1986) at KOL ($4\ \mathrm{K} < T < 100\ \mathrm{K}$), and that of Astrov et al. (1989, 1995), all using ^{4}He as the thermometric gas. The first also used a reference temperature at 273.15 K via calibrated thermometers, but the apparatus was essentially designed for measurements at low temperatures. With ^{3}He, accurate measurements were carried out by Matacotta et al. (1987), mainly with the aim of redetermining the values of the virial coefficients, and—more recently—by Tamura et al. (2008), intended primarily as a direct check of the workings of an ICVGT.

Worth noting is the work, at three different temperatures below 100 K, performed at PTB by Weber (1984, 1991) using a 1 L OFHC bulb *without gold plating*. This work was not officially published at the time in view of the apparent conflict with the work at NML and KOL.

The NML CVGT consisted of a 1 L OFHC copper bulb, gold-plated inside as well as outside, contained in a sophisticated flow cryostat (shown in Fig. 6.4) working in the 10–300 K range. The 1.8 mm i.d. cupro-nickel capillary is connected at the

bottom of the bulb and is thermally anchored to the various shields in such a way that the vertical portions are kept isothermal at the known shield temperatures by means of copper braids, in order to minimize the uncertainty of the aerostatic-head correction. The pressure-measuring system includes a capacitance differential pressure gauge, of 1.3 kPa full scale, equipped with two constant-volume valves (RV_1 and RV_2 in Fig. 3.13), and a precision Bourdon-type pressure gauge, frequently calibrated against a pressure balance-type gauge.

A 60 L ballast needed to be connected to the manometer system in order to achieve a sufficient reading stability for small changes in room temperature. The CVGT was operated at fixed densities in the range 95–235 mol m^{-3} or, when performing isotherms, in a molar density range 16–440 mol m^{-3}, depending on temperature. The purity of the thermometric gas was monitored on-line with a quadrupole mass spectrometer and a moisture analyzer. A great many problems had to be dealt with to achieve the following specifications: total impurities $< 10^{-5}$, moisture $< 2.5 \times 10^{-6}$. Such impurity levels were only achieved by following a long procedure based on repeated baking and purging of all the tubes for several weeks, and trapping of the impurities in the supply gas at 4.2 K.

In the KOL CVGT (Steur and Durieux 1986), a 1 L OFHC gold-plated copper bulb is housed in a conventional bath cryostat. Actually, the (inside) gold plating was performed twice, since the first layer happened to be absorbed into the copper wall during annealing at a too high temperature. The 1 mm i.d. stainless-steel capillary is connected to the top of the bulb and comes straight out from the cryostat in a vacuum jacket. It is thermally anchored only at the bottom, to a block that is independently regulated at the bulb temperature and acts as a thermal guard. The temperature distribution along the capillary is measured at 13 points by means of thermocouples. The pressure system includes a capacitance differential pressure transducer, of 133 Pa full scale, and a precision pressure balance. The CVGT was operated mainly at 160 mol m^{-3}. The purity of the gas samples was measured off-line. Total impurities resulted to be $< 10^{-5}$, except moisture, which was $< 25 \times 10^{-6}$. This CVGT was not intended for use above 100 K. The apparatus was subsequently transferred to VSL to be used for the construction of their ICVGT (Peruzzi et al. 2010).

Also, the measurements performed with the VNIIFTRI gas thermometer were included during the construction of the ITS-90. Their copper bulb (0.55 L) was not gold-plated. The main characteristic (see Fig. 3.15) is that it incorporates a cryogenic differential pressure transducer to isolate the thermometric gas from the manobarometer gas, consisting of a double diaphragm of sapphire, thereby completely suppressing the dead-volume correction. Initially, their results were higher that the NML-KOL data but lower than the results by Martin et al. (1988). However, in 1995 VNIIFTRI published a recalculation of their data based on a revision of the thermal expansion values (Astrov et al. 1995). This recalculation resulted in a strong decrease of the temperature values in the temperature range above 70 K, by as much as 10 mK at about 150 K. This deviation, although apparently confirmed by recent acoustic thermometry, is still of major concern to CCT.

The measurements on ^{3}He were made in cooperation by IMGC and KOL (Matacotta et al. 1987) using the KOL CVGT just described, from 20.3 K down

to 1.47 K. The temperatures below 4.2 K were obtained by continuous pumping on the cryostat helium bath. Filling densities in the range 188–309 mol m^{-3} were used.

At IMGC (now INRIM), a new CVGT realization has been under construction since 1991, intended for use with ^{3}He used as the thermometric gas in the 0.5–100 K range (Pavese and Steur 1987c; Steur and Pavese 1989a, b); its cryostat is shown in Fig. 6.2. A 1 L OFHC gold-plated copper bulb is used with a short composite stainless-steel capillary attached at the top, according to design (b) of Table 3.7, shown in Fig. 3.12b. The pressure-measuring system includes a double differential pressure assembly, as shown in Fig. 3.13, and a high-accuracy mercury manometer operated with nitrogen gas.

The more recent realization by Tamura et al. (2008), with ^{3}He as working gas as well, also used a 1 L OFHC with gold plating, but pressure was measured with an absolute capacitive transducer. Measured temperatures ranged from 3 K up to the triple point of neon at $T_{90} = 24.5561$ K.

Gas thermometers are also used when much lower accuracy is required. Some examples will be given in the next section.

3.3.2 CVGTs with Reference Temperature at 273.16 K

As a rule, a gas thermometer of this design is used only when the *full* range from low to room temperature must be covered. There are two inherent specific problems: thermal expansion of the bulb and moisture in the gas.

As noted in Table 3.6, most of the thermal expansion of a copper bulb takes place above 100 K, consequently, the knowledge of and the correction for this effect is essential for a CVGT of this type. In fact, when the relative contraction of the volume is corrected for accuracy no better than 0.3 %, the uncertainty in the bulb volume value corresponds to a temperature uncertainty of 2.4 mK at 172 K, 2.0 mK at 84 K, and 0.5 mK at 20 K. For comparison, the same volume uncertainty in a CVGT referenced at 20 K, corresponds to an uncertainty of 0.2 mK at 84 K, 2.1 mK at 172 K, and 7.2 mK at 273 K.

The problem with moisture is that it condenses in the bulb within the measurement range, producing a change in n in Eq. 3.1, an effect already discussed in Sect. 3.1.1.3.

A high-accuracy CVGT whose results have been considered as a reference for many years, is that made at NPL by Berry (1979, 1982). He used a type of gas thermometer with which some of the problems discussed before can be avoided, namely an instrument, which implements the two-bulb (or constant bulb-temperature) method. Kirenkov et al. (1974) also developed a similar instrument for work at higher temperatures. The principle is shown in Fig. 3.14. The temperature of the bulb A, instead of being alternatively changed from the value T to the reference value T_0, is always kept at T_0, and temperatures T are measured by a bulb B. Pressures p_0 and p are first measured in the two bulbs separately, then the two bulbs are connected by means of a three-way valve (which must be of the constant-volume type) and pressure p_c is measured.

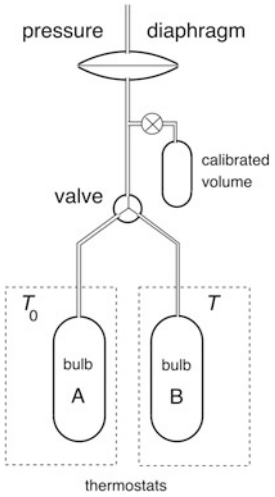

Fig. 3.14 The two-bulb design of a CVGT

It is easy to show that

$$T = T_0 \frac{V}{V_0} \frac{p - p_c}{p_c - p_0}. \tag{3.15}$$

The maximum sensitivity is obtained when $g = V/V_0 \equiv T/T_0$, but a departure from equality is not critical. The volume ratio g can be determined by maintaining the two bulbs at the same temperature, say at T_0. This method has several advantages. First of all, the use of the "primary" reference temperature (273.16 K or, more commonly, 273.15 K) is simpler than is generally possible with a low-temperature CVGT. Then, the uncertainty due to the virial coefficient $B(T)$, δB, can be shown to be $\{p_0 + p_c - (p_0^\tau - p^\tau)\}$, the superscript τ denoting that these pressures are measured in the bulbs when both are maintained at T_0. This relation allows one to minimize δB. Finally, the problem of the condensation of impurities or of sorption are minimized, as bulb B is not required to cover the full range from low to room temperature, and bulb A never changes its temperature.

A disadvantage is the large volume of the reference bulb A necessary to measure temperatures below 30 K; Berry's CVGT size for the two bulbs is 1 and 6 L, respectively. It is difficult to ensure good temperature uniformity and to determine accurately the volume ratio. The dead-volume can be calibrated "on-line" by adding to the circuit the small (39 cm^3) calibrated volume, as shown in Fig. 3.14; its sealing valve must be of the constant-volume type.

In Berry's experiment, the 1 L low-temperature bulb, placed in a conventional bath cryostat, was connected to the differential pressure transducer at room temperature by means of a stainless-steel capillary of 0.98 mm i.d., constant over the entire 1 m length. The tube was thermally tied down, very close to the bulb, to the adiabatic shield and next to the refrigerant temperature. Above this point, the capillary freely reached room temperature in the evacuated cryostat space and its temperature distribution was monitored by means of seven differential thermocouples. The pressure

system included a home-made capacitance differential pressure transducer, of 400 Pa full scale, and (for the first time) a precision pressure balance. The CVGT was operated over a wide molar density range when performing isotherm measurements, 82–618 mol m^{-3} for the absolute (20.2712 ± 0.0003) K isotherm, and 67–1035 mol m^{-3} for the isotherms relative to the 20.3 K one, or at a fixed value of 100 mol m^{-3}.

The more recent precision CVGT (Astrov et al. 1989) will be illustrated in the next section, since it uses a cryogenic pressure transducer.

Lower Accuracy CVGTs It is worth mentioning as well some realizations of CVGTs intended for use when the required accuracy is much lower.

Bedin et al. (1980) reported on a CVGT enclosed in a conventional bath cryostat, fabricated of a 0.12 L copper bulb (only 2 mm thick) with a capillary having 0.45 mm i.d. and 2.3 m length. When used with a manometric system including a differential gauge (± 0.03 % f.s. zero stability) and a mercury manometer (accuracy ± 10 Pa), in the 4–300 K range the CVGT uncertainty was ± 0.8 % at both ends of the range, to improve to about ± 0.1 % near 100 K, for a filling density such that pressure was 0.1 MPa at 300 K.

Winteler (1981) described a high-pressure CVGT made up of a demountable bulb-capillary system connected to a dial manometer. For a filling pressure of 10 MPa (which limits, of course, the minimum working temperature), an uncertainty of 1 % f.s. was still achieved up to a dead-to-bulb volume ratio of 0.1.

3.3.3 CVGTs Using a Cryogenic Pressure Measurement

Most of the discussion in Sect. 3.1.3 also applies to the CVGTs of this type. Also, Sect. 8.4 in Part II is relevant to the subject as the major problem is the availability of a cryogenic pressure gauge of suitable precision.

In the attempt to implement an *absolute* cryogenic pressure gauge, a microwave resonator (462 MHz) was used as a pressure gauge (Van Degrift et al. 1978a, b, 1984; Jones et al. 1977). The body of the transducer and the entire gas-thermometer device are made of "coin silver," a silver alloy containing 10 % copper (Van Degrift 1981); the gas fills a chamber separated from the oscillator, on the other side of a 0.64 mm thick diaphragm machined in the transducer body. When tested between 0.1 K and 10 K with a 0.008 MPa ^{3}He filling, a nonlinearity of $\pm \approx 10$ mK was observed in the 1.5–10 K range, possibly partially due to the temperature scale used. A lower temperature limit of ≈0.7 K was set by the condensation of ^{3}He (therefore, below ≈1.5 K the observed 20 mK nonlinearity was almost certainly due to the uncorrected nonideality of the gas). This condensation, on the other hand, supplied a built-in "fixed point," quite reproducible in the same device and useful for re-calibration of the gauge when it shifts in thermal cycling, since the dew point is sharply defined by a slope discontinuity on the cooling curve. On the other hand, the creep problems of the diaphragm, arising from the need to find an acceptable compromise between excellent electrical conductivity and satisfactory elastic properties, has never been solved

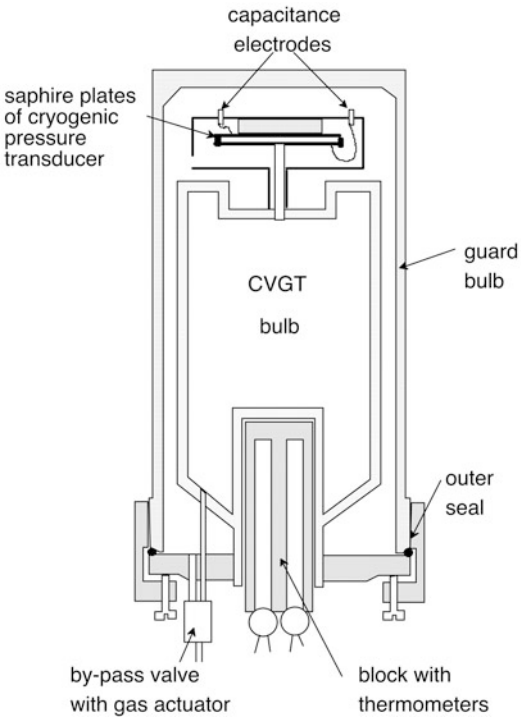

Fig. 3.15 Self-contained CVGT bulb with sapphire diaphragms differential pressure gauge. (After Astrov et al. 1989)

properly. See also Jones et al. (1977) in the References of Part II for a modification of Van Degrift transducer.

In all other realizations, the differential gauge G_1 of Fig. 3.13 was simply moved down from the top of the cryostat (point H in Fig. 3.12a) to the top of the bulb. Metal diaphragms have been used, but these do not allow the best accuracy to be obtained (Astrov et al. 1969; Nara et al. 1989).

More recently, a sapphire transducer has been developed (see Sect. 8.4.2) whose exceptional qualities were investigated. A CVGT utilizing this type of transducer (Fig. 3.15) has been developed by (Astrov et al. 1989; Astrov 1990). The bulb is still large, 0.55 L, but is light in weight, being enclosed in a guard volume maintained at the bulb pressure, and containing the differential sapphire double-diaphragm pressure gauge as well. In order to check the gauge zero, a gas-operated by-pass valve is used. The far from trivial problem of developing a reliable by-pass cryogenic valve was successfully solved with a ball-and-edge sealing technique, but an unknown amount of gas is lost from the measuring bulb every time the valve is operated. Therefore, the reproducibility of the transducer zero and its temperature dependence needed to be evaluated separately and *could not* be checked *during* measurements. However, these parameters have proved to remain stable within ± 0.1 Pa, down to 2.5 K.

Two main advantages of such a construction are that the CVGT can be baked to high temperature (300 °C) and pumped through a short and large pipe, and that it can

be filled with gas *before* it is placed into the cryostat. As the dead-volume correction, obviously, is almost nil and, consequently, a large diameter (2.8 mm) can be used for the short tube connecting the bulb to the transducer, the maximum value of the total correction for the thermomolecular pressure effect was reduced to 0.8 mK at 2 K. The filling molar density can be as low as 26 mol m^{-3},[14] which also minimizes the effects of gas sorption on the walls (see Sect. 3.1.1.2).

Great care was taken in purifying the ^{4}He samples, using a high-temperature zeolite and a fused-silica gas diffusion system. The residual impurities measured off-line with a mass spectrometer were: H_2 (1.3 ± 2) 10^{-6}, Ne (0.2 ± 0.3) 10^{-6}, $(N_2 + CO)$ (1.0 ± 1) 10^{-6}, CO_2 0.8×10^{-6}, and H_2O 0.2×10^{-6}. The CVGT was mounted in a bath cryostat with the parts of the *manometric* tube placed horizontally where thermal gradients are present, in order to avoid increase of the uncertainty due to the aerostatic-head correction. Here, this correction does *not* relate to the CVGT, but to the pressure-measuring system, which includes a high-accuracy mercury manometer.

The use of one or more fixed points, thermally connected to the bulb could allow the pressure gauge to be easily recalibrated in situ. This is actually performed, by definition, each time an ICVGT is calibrated. An ICVGT with a built-in pressure gauge can conveniently replace a conventional CVGT when the required accuracy is well below the high levels indicated so far. When this is the case, several low-temperature *commercial* pressure gauges are already available, suitable for this use, since the quality of the metal-diaphragm gauges becomes a less critical factor (see Sect. 8.4.2). Besides, sensitivity can be increased considerably by increasing the gas pressure. The only restrictive parameter, in this case, is the condensation temperature of the gas in the device, as it sets the lower limit of the usable temperature range. In this respect, helium is always the best choice. Of course, with an increasing pressure the effect of the third order and higher order virial coefficients increases as well. This simply means that nonlinearity is much more pronounced, especially near the lower end of the temperature range, which increases the number of the fixed points necessary for the ICVGT calibration.

3.3.4 Realizations of Interpolating Gas Thermometers

Any CVGT instrument can also, in principle, be used as an ICVGT if an interpolating function is selected and the instrument is calibrated at the corresponding fixed points, simplifying its use. However, no such specific use was ever attempted until recently.

A few preliminary attempts to implement an ICVGT have recently been reported. All are based on a low-temperature pressure transducer. The first was attempted by Van Degrift et al. (1978a, b) and has already been described as a CVGT in the preceding section.

The second has been performed by Nara et al. (1989, 1990). It has the shape of a $\approx 40\,cm^3$ cylindrical sealed cell entirely fabricated of copper, incorporating at

[14] Filling densities up to 128 mol m^{-3} were used.

its bottom a 0.5 mm thick beryllium-copper diaphragm, of 28 mm diameter whose deformation with pressure is detected by means of a three-electrode capacitance technique. The dielectric spacers of the capacitor are fabricated of fused silica and the cell seals utilize indium. The ICVGT is filled with ^{4}He at a room-temperature pressure of ≈ 0.85 MPa, corresponding to a molar density of 350 mol m^{-3}. Condensation of the gas occurs at ≈ 2.2 K.[15]

Several contributions to nonlinearity in this device have been evaluated. Most are caused by the capacitance transducer, such as the thermal expansion of the electrodes (2.6 mK) or edge and tilting effects, each contribution amounting to more than 3 mK. A background change of capacitance was observed to occur when the device was empty, amounting to as much as 0.18 K in the 4–24 K range. When calibrated at 5 K, 14 K, and 24 K (and without any virial stipulation), the maximum deviations from a quadratic behavior of the ICVGT resulted to amount to 1 mK between 5 K and 14 K and 3 mK between 14 K and 24 K.

Later, the ICVGT has been implemented by several laboratories (Meyer and Reilly 1996; Kang 2001; Hill 2001; Sakurai 2001; Steur et al. 2004; Tamura et al. 2003, 2004, 2008; Peruzzi et al. 2010). Notable among these are Tamura et al. (2004, 2008) for the use of ^{3}He, Steur et al. (2004) for the use of a cryogenic pressure transducer, and Hill (2002) for applying the ITS-90 definition in the mode considered in this book, i.e., without explicit corrections beyond the correction for nonideality. In all these experiments, with exception for Steur et al. and Hill, full corrections have been applied as is necessary only for a CVGT. The interpolation characteristics of a sealed ^{4}He CVGT was studied by Nara et al. (1990) and found to be principally determined by the mechanical properties of its cryogenic pressure transducer.

Some of the implementations have yielded contradictory deviations from the modeling results given in the Supplementary Information (BIPM 1990a), showing the importance of the experimental conditions that probably have not been taken properly into account in the modeling. The modeling indicated that for a lower temperature fixed point at either 3 K or 5 K the interpolation errors remain limited to less than 0.5 mK. However, in one experiment (Meyer and Reilly 1996) the interpolation errors using different values for the lower fixed point appeared to be larger, by up to 1 mK, while in a more recent experiment (Peruzzi et al. 2010) these values appear to be limited to less than 0.2 mK. Shortly after publication of the work by Meyer and Reilly at least part of their deviating results could be explained, by more explicit modeling, as being caused by their use of thermal anchoring (Steur 1999) and the remainder of 0.2–0.3 mK may represent the actual interpolation errors.

In one case (Tamura et al. 2008), a direct comparison was made between a CVGT and an ICVGT using for both the same experimental data. Full measurements were first made using the three fixed points prescribed by the ITS-90. Subsequently, the obtained experimental data were recalculated using only the neon fixed point as a reference, converting the experiment essentially in a (relative) CVGT. Comparing the results of the two sets of data, the difference between the two appears to be limited

[15] Therefore, from vapor-pressure measurements one can calibrate *in situ* the pressure transducer.

to about 1 mK. Considering that errors in the hydrogen fixed-point realization can be of the size of 0.7 mK, the NMIJ results seem to largely confirm the ICVGT concept.

Other interpretations of the ICVGT concept regard the use of a DCGT as an interpolating device. Results from such an interpretation are not published specifically, but they are compared with other ICVGT realizations (and ICVGT approximations) among the results of the CCT-K1 comparison. This comparison has shown that the average values for the thermometers submitted from all the different realizations (and approximations) agree to within ± 0.5 mK, in agreement with the value expected at the time of the ITS-90 definition.

Of particular interest is the design reported in Steur et al. (2003) and (1997) and references therein, for an Interpolating Constant-Volume Gas Thermometer exhibiting a small-volume copper bulb (50 cm^3) because it uses a cryogenic pressure-transducer (Pavese et al. 1998) based on the sapphire double-diaphragm technique developed by Astrov et al. (1984). The fact that the vacuum space around the pressure- sensing capillary was not separated from the main vacuum space around the bulb, did not compromise the measurements at the lower temperatures, specifically due to the presence of the cryogenic pressure-transducer, even in the presence of some exchange gas. The reference pressure was measured by means of a commercial high-accuracy pressure balance, the effective area of which was calibrated against the IMGC/JAEGER primary mercury manobarometer, in the pressure range from 1.4 kPa up to 100 kPa. Incidentally, these calibrations showed the exquisite care that must be taken to avoid unwanted errors in the pressure range below 8 kPa (see also Part II). The zero capacity (about 24 pF) of the differential pressure transducer was characterized at pressures up to 60 kPa and at temperatures up to 24.6 K, leading to an expression describing its behavior with an uncertainty of less than 1×10^{-4} pF (Fig. 3.16).

Subsequently, the transducer was calibrated in situ at temperatures of 4.2 K, 8 K, 13.8 K, 18 K, and 24.6 K, for differential pressures up to 5 kPa. Residuals from an overall fit were within ± 2 Pa. Calibration for the ICVGT fixed points were taken from an NPL calibration. All in all, the results for the ICVGT agreed with the NPL calibration of the RhFe thermometer to 1.0 mK (negative below 13.8 K and positive above 13.8 K).

A few years later, with the same cryostat, the same transducer was used in the absolute mode (Steur et al. 2004). Again, the transducer was calibrated in situ against the pressure balance, for pressure values up to 70 kPa. The ICVGT results, obtained in this way, largely agree with those obtained previously in differential mode, with values lower than the reference by 1.5 mK for temperatures below 13.8 K, and higher than that value above. It must be taken into account that the major uncertainty component (2.4 mK equivalent) derives from the calibration of the transducer.

This INRIM ICVGT with cryogenic pressure transducer (i.e., with no dead-volume) has been compared with the realization of the thermodynamic scale at PTB by means of the bilateral intercomparison CCT K1.1 (see Chap. 11), just being ended at the date of this book. The ICVGT has been calibrated at INRIM at the three required fixed points: normal boiling point of ^{4}He at 4.1994 K, with $u = 100$ μK,

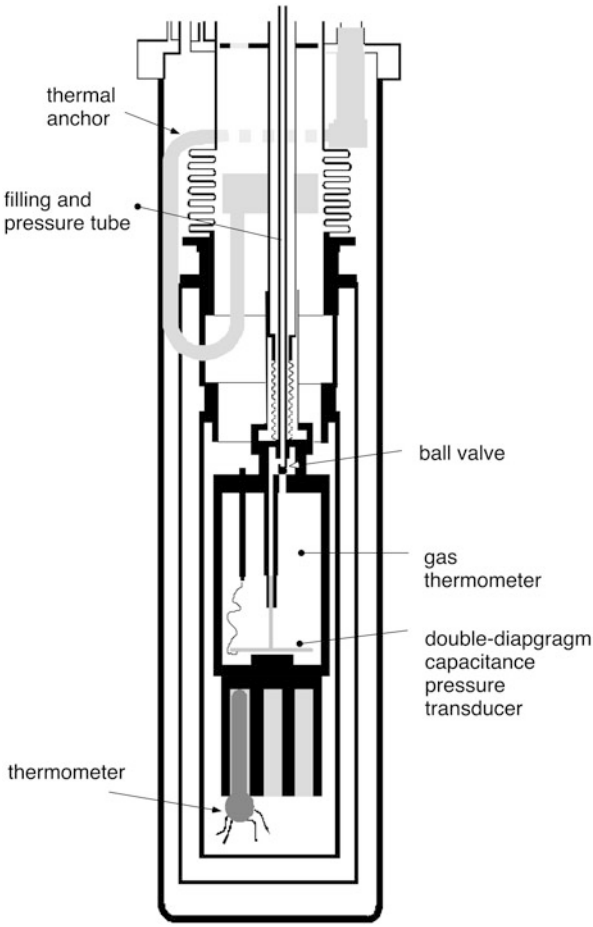

Fig. 3.16 ICVGT with cryogenic pressure transducer contained in the bulb. (After Steur et al. 1997, 2003, 2004)

e-H_2 triple point (corrected for isotopic composition) with $u = 43$ μK, and Ne triple point with $u = 163$ μK (*uncorrected* for isotopic composition, accounting for 160 μK; Steur and Giraudi 2012). The total uncertainty budget of the INRIM measurements on the ICVGT is $U = 1.31$ mK (expanded, $k = 2$), of which 1.30 mK from the initial measurements on the ICVGT (Steur et al. 2003) and using the maximum contribution from propagation of the fixed-point uncertainty.

3.3.5 Gas Thermometry in the ITS-90

The original idea that led to incorporating the ICVGT into the ITS-90 was advanced by Barber (1972). It was assumed to use a *linear* equation with *two* fixed points (^{4}He and e-H_2 normal boiling points), along with the specification of a virial equation

of a simple quadratic form. The 1972 ICVGT parameters specified were as follows: 1 L bulb, 8 cm^3 dead-volume, 80-cm-long 1-mm-bore capillary, 190 mol m^{-3} filling of ^{4}He, range from 4 K to 20 K (compare with the parameters given in the preceding sections). These specifications would have led to a maximum error of 1.9 mK at 12 K.

The ITS-90 below 0 °C is based on the thermodynamic measurements on which the EPT-76 below 14 K had been based and on five new sets of thermodynamic determinations above 14 K, four of which were ^{4}He gas-thermometric determinations (Berry 1979; Kemp et al. 1985; Steur and Durieux 1986; Astrov et al. 1989) and one a radiometric determination (Quinn and Martin 1985; Martin et al. 1988). In addition, some fixed points were determined by means of other types of absolute thermometry. The entire set of these determinations has been used to formulate the equation for the virial coefficient $^4B(T)$; this equation is supported and refined by theoretical potential calculations (Aziz 1990; McConville 1991; Hurly and Moldover 2000; Hurly and Mehl 2007; Cencek et al. 2004; Bich et al. 2007; Hellmann et al. 2007). For ^{3}He, the formulation of the equation for the virial coefficient $^3B(T)$ was made possible by using the experimental and theoretical work developed in cooperation with IMGC, KOL, and Mound Applied Technologies (Matacotta et al. 1987; Pavese and Steur 1987c; McConville 1991), theoretically refined by the potential calculations mentioned before. The shift of the lower limit of the ICVGT from 4.2 K to 3 K and the extension of the use to ^{3}He were questions thoroughly debated before inclusion in the ITS-90 (Pavese and Steur 1987c; Steur and Pavese 1989; Swenson 1989).

The initial agreement between the results of the thermodynamic measurements above 14 K resulted in a great improvement with respect to the measurements performed before the 1970s, though the range from 100 K to 200 K remains problematic (Rusby et al. 1991). However, some 5 years after the promulgation of the ITS-90, Astrov et al. modified their 1989 results by a recalculation of the thermal expansion for their copper bulb, with a subsequent lowering of their temperature values by as much as 10 mK (max around 150 K). This change has still not found a satisfactory explanation (see also previous sections).

A study on the results of the thermodynamic determinations at the base of the ITS-90, performed with the aim of detecting the extent of the nonrandom differences between the different series of measurements (Pavese and Steur 1987d; Pavese 1989; Pavese and Ciarlini 1990b), showed that differences are as high as 3.6 mK.

However, the overall SPRT resistance versus temperature characteristics can be established, on the basis of the 534 experimental data examined, within ± 0.9 mK (Fig. 3.17); for each of the five independent determinations, separately, u lies between 0.3 mK and 0.5 mK. The difference between this overall fit and the ITS-90 reference function Eq. 1.9a in Appendix A is shown in Fig. 3.18.

After the adoption of the *mise en pratique* of the kelvin, it is now expected that in due time the thermodynamic scale also will officially become part of the realizations of the *mise en pratique*. However, it is also expected that the types of thermodynamic thermometers taken in considerations will not be restricted to the CVGT, but will also include other types illustrated in the next section.

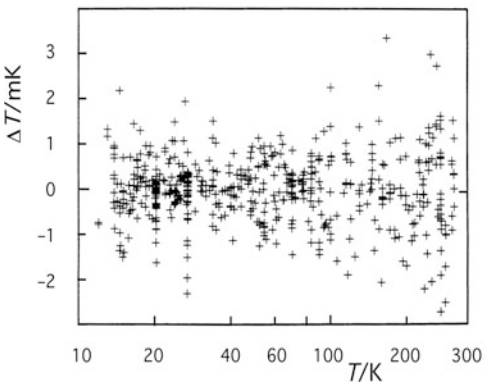

Fig. 3.17 Scatter of the thermodynamic data forming the basis of ITS-90 below 273.16 K. (After Pavese and Ciarlini 1990)

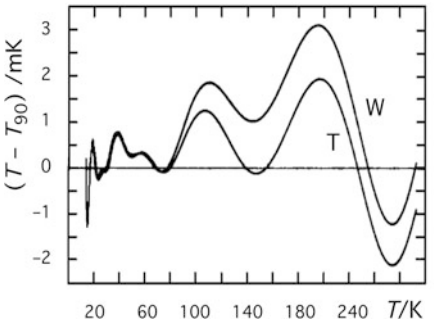

Fig. 3.18 Comparison of the ITS-90 reference function T_{90} below 273.16 K (Eq. 1.9a) with the fitting model of Fig. 3.17. *T* fitting model including the effect of nonrandom translational effects; *W* conventional all-random fitting model. (After Pavese and Ciarlini 1990)

3.4 Dielectric-Constant, Refractive-Index, and Acoustic Gas Thermometers

The preceding sections clearly indicate that a CVGT is not, generally speaking, a simple instrument to design and use. The main difficulties derive from the necessity of very accurately measuring an *extensive* thermodynamic quantity, by which the effects of dead-volume and of gas adsorption on the bulb walls are made critical. A continuous effort has therefore been made to overcome these difficulties by using certain *intensive* thermodynamic properties.

Three of such intensive properties have been exploited in gas thermometry, namely dielectric constant, refractive index, and sound velocity. It cannot be affirmed, at present, that, by such an approach, expectations have been entirely fulfilled and that an instrument based on these properties has superseded the CVGT. The uncertainty is, at best, more or less the same as that of a CVGT and the experimental techniques associated with them are not easier.

Even if this monograph is not intended to be a handbook of possible techniques, they will be reviewed briefly, since these types of thermometry, in principle, provide alternative methods, for application in laboratories that have already acquired specific experience in capacitance, optical, or acoustical measurements. These techniques are

likely to improve in the future, both as regards accuracy and simplicity of realization, as it happened recently, in particular to acoustic gas thermometry.

3.4.1 Dielectric-Constant Gas Thermometry

The Dielectric-Constant Gas Thermometry (DCGT) differs from traditional CVGT by the measurement of the temperature-dependent dielectric constant of the working gas, usually helium, which allows determining the density in situ, thus eliminating the problems involved with the dead-volume affecting CVGT.

The dielectric-constant gas thermometer (DCGT), which has been developed in the 1970s by Gugan and Michel (1980) for work in the 4–27 K range, and more recently by Grohmann and Koch (1984), is based on the use of the Clausius-Mossotti equation to eliminate the volume from the equation of gases. For an ideal gas

$$\begin{aligned} \frac{\varepsilon - 1}{\varepsilon + 1} &= \frac{A_\varepsilon n}{V} \\ pV &= nRT. \end{aligned} \tag{3.16a}$$

Then,

$$p = T\left(\frac{R}{A_\varepsilon}\right)\frac{\varepsilon - 1}{\varepsilon + 2} \tag{3.16b}$$

where ε is the relative permittivity (dielectric constant) of the gas at a pressure p and temperature T and A_ε is the molar polarizability.

As already discussed in Sect. 3.1, the nonideality of a real gas must be taken into account.

Experiments implementing DCGT are based on the virial expansions for the equation of state and for the dielectric constant ε_r, as follows:

$$p = \frac{RT\left(1 + \dfrac{B^*}{V_\mathrm{m}} + \dfrac{C^*}{V_\mathrm{m}^2} + \cdots\right)}{V_\mathrm{m}} \tag{3.17a}$$

with

$$B^* = \frac{B - 3A_\varepsilon b^* D^2}{2RT\varepsilon_0}$$

$$C^* = \frac{C - 3A_\varepsilon c^* D^2}{RT\varepsilon_0}$$

and

$$\frac{(\varepsilon_\mathrm{r} - 1)}{\varepsilon_\mathrm{r}} = \frac{3A_\varepsilon\left(1 + \dfrac{b^*}{V_\mathrm{M}} + \dfrac{c^*}{V_\mathrm{M}^2} + \cdots\right)}{V_\mathrm{M}}. \tag{3.17b}$$

Here, p denotes the pressure, T the temperature, R the molar gas constant, V_m the molar volume, B and C the second and third density virial coefficients, b^* and c^* the second and third dielectric virial coefficients, A_ε the molar polarizability, ε_0 the permittivity of vacuum, and D the electric displacement. Except over narrow temperature intervals near the zeros of $B(T)$ and $C(T)$, the absolute values of b and c are more than two orders of magnitude smaller than B and C, respectively, and can usually be neglected.

From Eq. 3.17b, one can easily obtain the virial expansion of the Clausius–Mosotti equation

$$\frac{(\varepsilon_r - 1)}{(\varepsilon_r + 2)} = \frac{A_\varepsilon \left(1 + \frac{b}{V_m} + \frac{c}{V_m^2} + \cdots\right)}{V_m} \tag{3.17c}$$

where $b = b^* + 2A_\varepsilon$ and $c = c^* + 4A_\varepsilon b^* + aA_\varepsilon^2$.

By combining Eqs. 3.17a and 3.17c, it is possible to eliminate the molar volume V_m.

In a DCGT, the relative permittivity is *not* measured directly, but indirectly through another physical quantity related to it. The dielectric constant is determined by measurement of the capacitance $C(p)$ of a capacitor. In order to measure the zero-pressure limit of this capacitance, one could evacuate the capacitor any time it is needed, but a much simpler solution was identified in the use of a second, identical, capacitor, which is kept under vacuum. Exchanging their roles and using the average of the two types of measurement can then eliminate any residual differences between the two capacitors. This two-cryocapacitor design was first used by Gugan (1980, 1991), and since 1992 it has been taken up by Grohmann and Koch (1984) and continuously improved upon since then.

A ratio of capacitances, with and without the dielectric medium, is determined. However, because of the dimensional change of the capacitor with pressure, the ratio will depend also on the compressibility modulus of the plate material. It can be shown (Smythe 1968) that, for a capacitor consisting of cylindrical inner and outer electrodes, its pressure dependence can be described satisfactorily by

$$C(p) = \varepsilon_r C(0)\,(1 + \kappa_{\text{eff}} p), \tag{3.18}$$

even for eccentric and nonparallel axes; κ_{eff} represents an effective compressibility of the whole capacitor assembly. By using an appropriate combination of the available equations, it is possible to obtain a series expansion of p at a temperature T:

$$p = A_1 \mu \left(1 + A_2 \mu + A_3 \mu^2 + \cdots\right). \tag{3.19}$$

By neglecting the contribution from the dielectric virial coefficients b and c, as well as higher order terms, one obtains the following expressions for the coefficients in Eq. (3.19):

$$A_1 = \left(\frac{A_\varepsilon}{RT} + \frac{\kappa_{\text{eff}}}{3}\right)^{-1} \tag{3.20a}$$

$$A_2 = \frac{B(T)}{A_\varepsilon} \tag{3.20b}$$

$$A_3 = \frac{C(T)}{A_\varepsilon^2}. \tag{3.20c}$$

When measuring a sufficient number of pairs (p_i, μ_i) on a single isotherm, the thermodynamic temperature can then be calculated from the value of A_1 obtained by a fit to these data.

A constant term $A_0 = -A_1(\delta C(0)/3C(0))$ can possibly be added, in order to take into account nonrandom errors in the determination of $C(0)$ (Gugan and Michel 1980).[16] Two parameters are unknown: (A_ε/R) and the linear compressibility modulus K_1.

For a DCGT to work as a primary thermometer, independent values for A_ε/R and k_{eff} have to be available with sufficient accuracy. Ab initio calculations have yielded a value for the molar polarizability of helium $A_\varepsilon = 0.517\,253\,(10)\ \text{cm}^3\ \text{mol}^{-1}$ (Weinhold 1982; Bhatia and Drachman 1994). Experimentally, values for k_{eff} can be obtained by two methods:

(a) An isotherm is measured for each capacitor and using Eq. 3.20a and the literature values for A_ε and R; for $p < 0.3$ MPa and $T > 83.8$ K only the first two terms of Eq. 3.31 are required.
(b) The pressure dependence of the capacitance ratio C_1/C_2 is measured for the two capacitors connected to the same pressure line; omitting higher order terms, it follows that $\kappa_{\text{eff1}} - \kappa_{\text{eff2}} = [C_1(p)C_2(0)/C_2(p)C_1(0) - 1]/p$.

For work at low temperature ($T < 30$ K), use can be made of the fact that κ_{eff} can be taken as a constant (Leadbetter 1983), and only a small correction seems to be required for the temperature difference between 84 K, where the experimental value(s) was obtained and 30 K, where the value(s) is used in a correction term. For the 1996 work, at PTB $U = 1.2$ mK ($k \approx 2$) was claimed.

The various improvements applied on their apparatus over the years culminated in more recent publications (Gaiser et al. 2008, 2010). They show updates with respect to the 1996 work, and various improvements with essentially a lower uncertainty budget and better values for the second and third virial coefficients $B(T)$ and $C(T)$. Impressive agreement is reported for $B(T)$ and $C(T)$ between theory and experiment for temperature above 3.3 K. Mention is also made of unexpected sudden deviations in the ^{4}He gas properties at the lowest temperatures, tentatively attributed to bosonic clustering effects (see Sect. 1.1.3). The most recent paper reports on experiments using ^{3}He, ^{4}He, and Neon in different temperature ranges between 2.5 K and 36 K. Combination of the results obtained for the three gases yields temperatures in agreement with ITS-90 to within a few tenths of a millikelvin up to the highest temperature, in disagreement with the tendency for a deviation above 27 K suggested

[16] The A_0 term is not typical of DCGT. It was introduced by Gugan and Mitchell (1980) due to an unintentional shift of the $C(0)$ value observed in their apparatus. It has never been observed by others (Grohmann 1990).

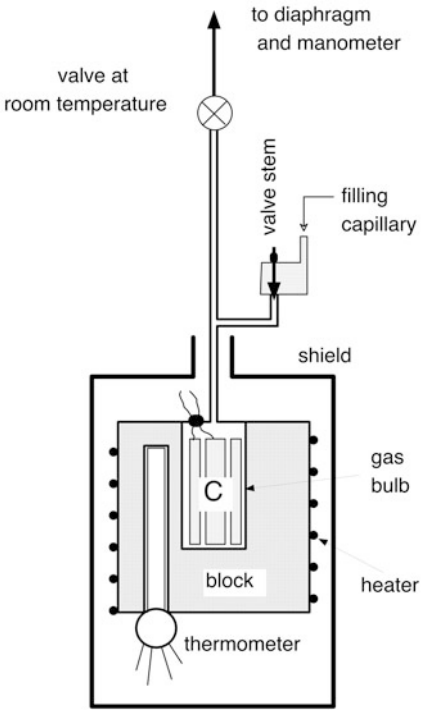

Fig. 3.19 Layout of a dielectric-constant gas thermometer (DCGT). *C* precision capacitor

by the survey of CCT WG4 (CCT WG4 2008), in particular regarding the revised Astrov et al. data and the AGT results by Pitre et al.

It was shown by Gugan (1984) that a sufficiently accurate value for the true linear compressibility modulus K_1 can be obtained with a refined data processing. Consequently, the DCGT might also be used as a primary thermometer, not requiring any calibration at reference temperatures, by application of the values available for A_ε, accurate to 1×10^{-6} (Weinhold 1982), and for R (Cohen and Taylor 1986) for the other parameter: $A_\varepsilon/R = (6.221\,124 \pm 0.000\,05) \times 10^{-8}$ K Pa^{-1}, using the CODATA 2010 value for R.

Implementation of the thermometer is shown in Fig. 3.19. Basically, it is like a vapor-pressure thermometer, as the dead-volume does not represent a problem, and consequently the pressure tube can be kept conveniently large to avoid difficulties concerning the uncertainty of the thermomolecular correction. It may be useful in using a smaller diameter pressure-measuring tube, separate from a larger pumping/filling tube, which may be isolated with a cryogenic needle valve.

The bulb includes one or two precision capacitors. The plate distance in the 10 pF capacitor shown in Fig. 3.19 is 1.5 mm to minimize the effects of capacitor instability due to the gas (see later discussion). One must have a relative accuracy in the capacitance measurements of 10^{-8}, because of the small value of the helium polarizability. This accuracy level is close to the present state-of-the-art. The use of

two nominally identical (when in vacuum) capacitors improves measurement accuracy. Gugan's work has shown that in thermal and pressure cycling a reproducibility of $C(0)$ of few parts in 10^{-9} during several hours can be obtained in the 4–30 K range. The capacitor temperature dependence resulted to be the same as that of pure copper, but the *values* of the thermal expansion coefficient proved to be greater than expected by a few percent, and different for the two nominally identical capacitors.[17]

At higher temperatures (80–300 K), another copper capacitor design (Younglove 1980) proved to have a $C(0)$ stability of 2.5×10^{-6} and a quadratic temperature dependence, reproducible upon thermal and pressure (up to 13 MPa) cycling within 15×10^{-6}.

The capacitor design must also be such that no electric field lines pass through the dielectric instead of the gas.

There are two main chemical-physical sources of errors.

Surface Film Effect An impurity film may alter the nominal distance d between the plates by a relative amount δd ($\ll 1$). The change is represented by $\gamma' = (\varepsilon - 1)(1 - \delta d\varepsilon/\varepsilon')$. The relative error is $\approx -\delta d\varepsilon/\varepsilon'$; therefore, the most troublesome impurity is solid air ($\varepsilon' \approx 1$). When $d = 1.5$ mm, the aimed uncertainty of 10^{-5} on γ' is reached with a film thickness of 150×10^{-10} m, about 20–50 monolayers, depending on the gas.

Absorbed Gas Film With helium, the molecule coverage of a surface shows a strongly nonlinear dependence on pressure, most of it occurring at quite low pressures. A monolayer is almost entirely built-up at the low pressures used in a DCGT; the high-pressure limit coverage is only a little more than one monolayer (about 1.2, see Sect. 3.1.1.2). The uncertainty can again be kept within 10^{-5} for a plate distance of 1.5 mm (see also Sect. 3.1.3.3).

3.4.2 Refractive-Index Gas Thermometry

The refractive-index gas thermometer (RIGT) is the equivalent of the dielectric-constant gas thermometer, where expertise in precision optical measurements in necessary instead of that in precision capacitance measurements.

Starting from the Lorenz-Lorenz law, which is derived from the Clausius-Mossotti law by substituting $\boldsymbol{n}^2$ to ε (Colclough 1974, 1982a), one obtains

$$\frac{\boldsymbol{n}^2 - 1}{\boldsymbol{n}^2 + 2} = \frac{A_\varepsilon n}{V} \tag{3.21}$$

with

$$A_\varepsilon = \frac{\alpha L}{3\varepsilon_0}$$

[17] The value of the thermal expansion coefficient is not critical for a DCGT since all the measurements are performed on isotherms, i.e., $C(p)$ and $C(0)$ measurements are determined at the same temperature.

where $\boldsymbol{n}$ is the refractive index of the thermometric gas at a pressure p and temperature T, n/V is the gas molar density, A_ε is the molar polarizability, a is the atomic polarizability, L Avogadro number, and ε_0 the permittivity in vacuum. Since $(\boldsymbol{n}-1) \ll 1$, for an ideal gas Eq. 3.21 reduces to

$$\boldsymbol{n} - 1 \propto \frac{n}{V} \tag{3.22}$$

The nonideality of the gas, however, must be taken into account. Following a virial expansion truncated to the quadratic term for n/V (coefficients $B(T)$ and $C(T)$) and with $a = a_0[1 + bn/V) + \mathrm{c}(n/V)^2]$, one obtains

$$L = \frac{\boldsymbol{n}^2 - 1}{\boldsymbol{n}^2 + 2} = \frac{L\alpha_0}{3\varepsilon_0 RT} p \left[1 + L_1(T)\left(\frac{n}{V}\right) + L_2(T)\left(\frac{n}{V}\right)^2 + \cdots\right] \tag{3.23}$$

where $L_1(T) = b - B/\mathrm{R}T$ and $L_2(T) = 2B^2 - C - 2bB + c/(RT)^2$ are the relative permittivity virial coefficients. In general, $(\boldsymbol{n} - 1)$ and not L, is measured. The two quantities are related by

$$L = \frac{2}{3}(\boldsymbol{n} - 1)\left[1 - (\boldsymbol{n} - 1)/6 - 2(\boldsymbol{n} - 1)^2/9 - \cdots\right] \tag{3.24}$$

A thermometer implementation is shown in Fig. 3.20: the upper part may be identical to that of a DCGT. The copper block whose temperature is to be measured contains an interferometer with the gas cell placed in one of its branches.

The value of $(\boldsymbol{n} - 1)$ for ^{4}He is 3.5×10^{-5}, at 0.1 MPa, room temperature and 633 nm (He–Ne laser radiation). The dependence on temperature and pressure is: $(\boldsymbol{n} - 1) = 9.40 \times 10^{-8} p/\mathrm{Pa})/(T/\mathrm{K})$. With a 20-cm-long cell, at 0.33 MPa, a phase resolution of 1/1000 of a fringe is necessary to resolve a temperature-relative change of 10^{-6} (10 μK at 10 K, 0.3 mK at the triple point of water, the reference calibration point necessary for a primary thermometer). This phase resolution in fringe measurements proved achievable with a cell immersed in a bath of liquid ^{4}He (Colclough 1982a).

With copper, the contribution of a ± 0.1 % uncertainty in the determination of the cell thermal contraction corresponds to a temperature uncertainty of $\pm 3 \times 10^{-6}$, $\pm 0.3 \times 10^{-6}$, and $\ll \pm 0.1 \times 10^{-6}$ at 273 K, 90 K, and 25 K, respectively. Hydrostatic compression (assuming a modulus of elasticity for copper of $E_{\mathrm{Cu}} = 130$ GPa, temperature independent—in the first approximation, see Table 3.6) contributes to the temperature uncertainty for a maximum of 4.7 mK at 136 K at a reference temperature, $T_\mathrm{r} = 273$ K, for 0.5 mK at $T_\mathrm{r} = 90$ K and for < 0.1 mK at $T_\mathrm{r} = 25$ K. Should the RIGT be used as an interpolating instrument with two fixed points, the hydrostatic compression effect becomes a second-order effect.

The effect of impurities in the gas is quite important, in RIGTs in comparison with DCGTs or acoustic thermometers, as the polarizability of most impurities is likely to be much greater than that of ^{4}He and acts as a multiplier on their molar presence in the thermometric gas.

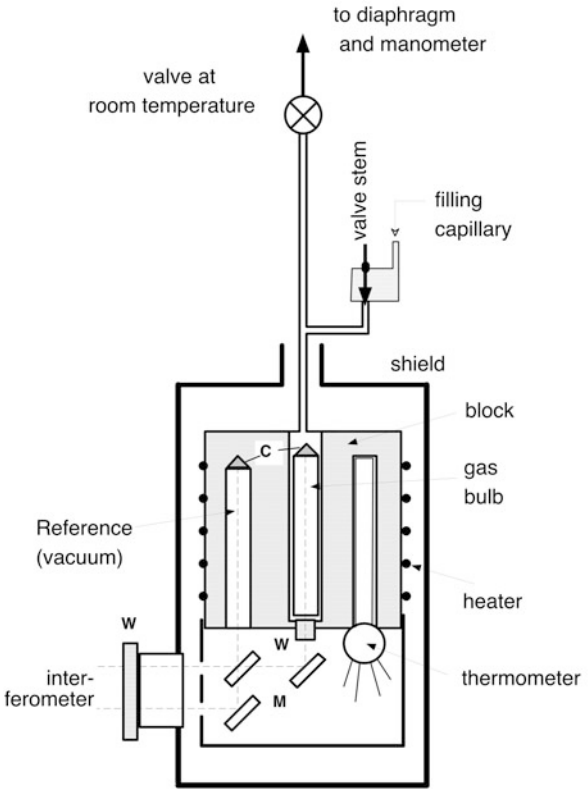

Fig. 3.20 Layout of a refractive-index gas thermometer (RIGT). *C* cube-corner reflector; *W* optical window; *M* mirror

3.4.3 Acoustic Gas Thermometry

Acoustic low-temperature thermometry has been pioneered since the 1960s and has undergone important developments. It is based on the relationship between the (zero pressure) speed of sound in (monatomic) gases and thermodynamic temperature.

When sound propagates in a gas, at frequencies not approaching the mean collision frequency, practically no energy is transmitted and its velocity u in an unbounded medium is

$$u = \sqrt{\frac{E_g}{\left(\frac{n}{V}\right)}} \tag{3.25}$$

where E_g is the adiabatic modulus of elasticity of the gas and n/V is the molar density. For an ideal gas

$$\frac{n}{V} = \frac{p}{RT} \quad \text{and} \quad E_g = \left(\frac{c_p}{c_v}\right) p$$

Thus,

$$u_{\mathrm{id}}^2 = \left(\frac{c_p}{c_v}\right) RT. \tag{3.26}$$

With a real gas, nonideality must be taken into account.

The principle difference between acoustic gas thermometry (AGT) and CVGT is that the determination of gas density in CVGT is replaced by the measurement of the velocity of sound. Use is made of the relationship between the zero-pressure velocity of sound in a monatomic gas u_0, as defined by Laplace, and thermodynamic temperature:

$$u_0^2 = \gamma \frac{RT}{M}. \tag{3.27}$$

With γ the ratio of the ideal-gas heat capacities, R the molar gas constant and M the molar mass. The quantity u_0 is the zero-pressure limit of the expansion

$$u^2 = u_0 \left(1 + \beta_{\mathrm{a}} \rho_n + \gamma_{\mathrm{a}} \rho_n^2 + \cdots\right) \tag{3.28}$$

with β_{a}, γ_{a}, ... the acoustic virial coefficient s that depend only on temperature.

As in gas thermometry of all types, the experiment consists in measuring $u = \{f(p)\}_{T = const}$. It must be noted again that accurate determinations of volume or density are avoided. The accuracy in the measurement of pressure also does not need to be very high.

In addition, if the exact theoretical value of $(c_p/c_v)_{\mathrm{id}}$ is taken (e.g., 5/3 for helium), and the best accepted value for R (*obtained by independent means*) is used, the acoustic thermometer does not need *any* calibration point (not even the 273.16 K point). The thermometer is independent of the amount of gas used, as sound velocity is an intensive quantity. The same would apply to the DCGT (Sect. 3.4.1) in the case A_ε and K_1 are known with sufficient accuracy. In this latter case, an experiment using the thermometer at 273.16 K allows an independent determination of R and, using Avogadro number, of the Boltzmann constant. This experiment has been performed by Quinn et al. (1976), Moldover et al. (1988), and Boyes et al. (1990), but this use of the thermometer will not be described here. However, mention should be made, see Sect. 3.4.4, of the Boltzmann Project, where many different techniques are employed toward obtaining a better value of the Boltzmann constant k_{B}. On the contrary, if the accepted value of R is used, n/V cannot be measured with sufficient accuracy, at least at present, for use with a CVGT and calibration at the defining point of the thermodynamic scale is needed.

Just as in CVGT work, the relatively high uncertainty associated with the molar gas constant R (and with the molar mass M) can be eliminated by measuring the ratio of two temperatures, one of the two being a reference, preferably the triple-point temperature of water, T_{W}:

$$\frac{T}{T_W} = \frac{u_0^2(T)}{u_0^2(T_W)}. \tag{3.29}$$

The velocity of sound is determined through the excitation and the detection of resonances in the working volume. The measured frequencies of these resonances require a set of correction terms, which account for the presence of a thermal boundary layer near the wall of the bulb (main contribution), for coupling of gas and wall motion, and for perturbations due to small holes in the wall for the passage of the gas.

Three different high-accuracy approaches have so far been followed to implement the acoustic thermometer, with the use of *high-frequency interferometers* (Cataland et al. 1962; Plumb and Cataland 1966; Plumb 1982) operated in the 2–20 K range in a cylindrical bulb (resonator); of *low-frequency interferometers* (De Laet 1960; Grimsrud and Werntz 1967; Colclough 1972, 1973, 1979, 1982b) operated in the 1.2–20 K range, also in a cylindrical resonator; and of *spherical resonators* (Moldover and Trusler 1988) applying acoustic resonances, first operated only close to room temperature and later on also at other temperatures, both toward higher (Moldover et al. 1999; Ripple et al. 2007; Strouse et al. 2003) and lower temperatures (Ewing et al. 1986; Ewing and Trusler 1989; Ewing and Goodwin 1992; Benedetto et al. 2004; Pitre et al. 2006). The three experimental approaches are quite different from one another. The reader is directed to the relevant papers for full description.

The high-frequency device of Plumb and Cataland is schematically illustrated in Fig. 3.21a. It is based on the principle of creating standing waves in gaseous helium inside a cylindrical chamber with a diameter of about 10 mm by using an apparatus working at a fixed frequency and with a variable path (i.e., chamber length, few millimeters long), as in the well-known Kundt's tube. A high-frequency wave (>1 MHz) may produce an ill-defined wave field in the resonant cavity, and consequently generate nonrandom errors, which resulted to be of the order of several millikelvin.

De Laet's apparatus used ^{4}He, a fixed chamber length and a variable frequency; Grimsrud's apparatus used both ^{4}He and ^{3}He, and Plumb's method. Colclough's low-frequency apparatus, schematically shown in Fig. 3.21a, used a cylindrical cavity whose dimensions ($f \approx 30$ mm, ≈ 100 mm long) are necessarily larger than Plumb's because of the much lower frequency—a few kilohertz. The low-frequency method has inherent difficulties concerning an accurate definition of boundary layer effects. An exhaustive discussion of the nonrandom errors in both high- and low-frequency cylindrical resonators can be found in Colclough (1973).

Moldover's first *spherical* resonator at NIST is schematized in Fig. 3.21b. With a resonator diameter of ≈ 89 mm, the resonance frequency is in the 2.5–10 kHz range, depending on the mode selected. Argon gas has been used for thermometry experiments performed at the triple point of water and at the triple point of gallium (≈ 303 K), with a resulting total error in u_{id}^2 of about 1.5×10^{-6} (equivalent to ± 0.5 mK for the latter point). Helium could not be used, since growth of impurities has been observed from drift in the measured u^2 value. With this experimental setup, the *natural* resonance frequency of a geometrically well-defined spherical cavity is measured. In the Moldover 1986 work, the cavity volume was measured accurately with a total uncertainty of 0.8×10^{-6}, by using a mercury filling at the working temperature, and by weighing the mercury. With this technique, it is possible to avoid any correction for thermal expansion, though it is only applicable over a narrow

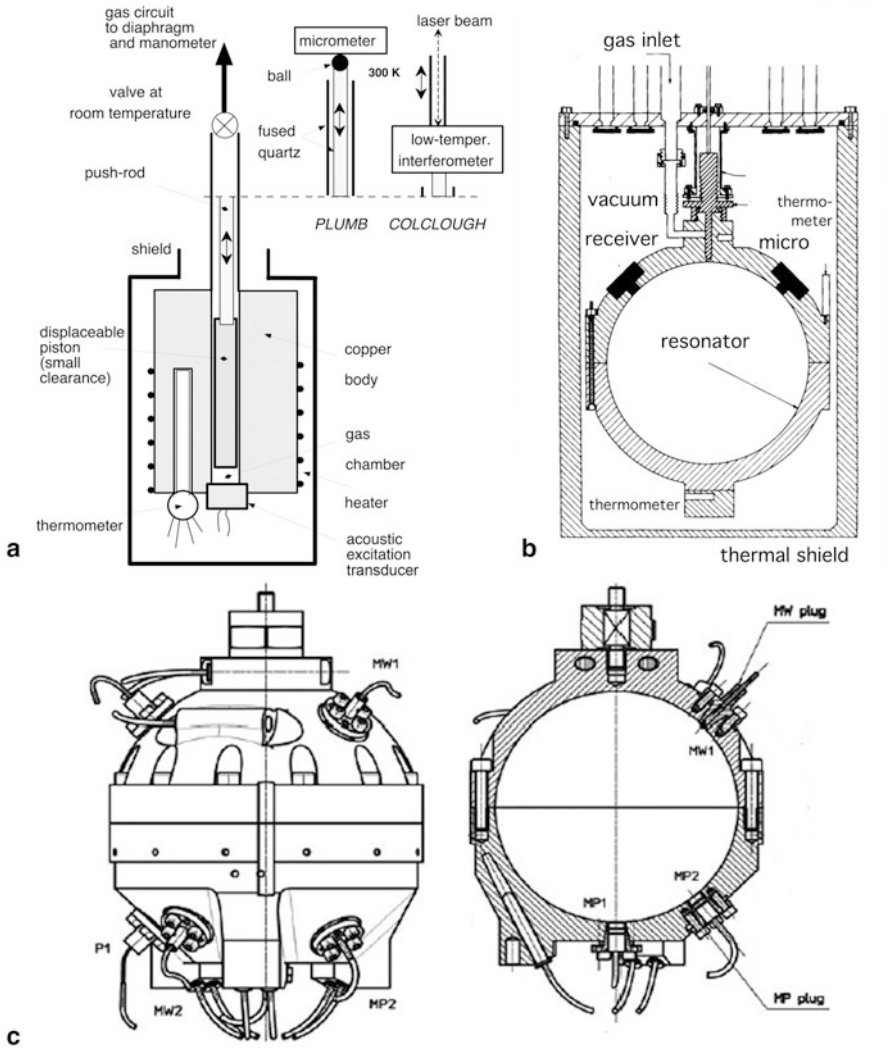

Fig. 3.21 Layout of acoustic gas thermometers (AGT). **a** Variable-length type with translation detected by a room-temperature micrometer (after Plumb 1982), or by a low-temperature interferometer (after Colclough 1982b). **b** First spherical low-frequency resonator type (after Moldover et al. 1988). **c** Recent quasispherical (trielliptical) resonator type (Gavioso et al. 2011). The symbols indicate the various acoustic microwave and temperature transducers

temperature range. On the other hand, the accurate measurement of internal dimensions is not required, provided radially symmetric modes are only used (Moldover et al. 1986). However, at temperatures further away from the triple point of water, thermal expansion of the resonator becomes relevant. All experiments since 1998 were essentially based on Moldover's design, and the effect from thermal expansion was explicitly measured by means of electromagnetic microwave resonances in the

resonator. The continuing work at NIST in acoustic thermometry (Moldover et al. 1999a, b and references therein) brought to a new apparatus designed for a working range up to 800 K, but also used for measurements down to 217 K (Ripple et al. 1999). The design of the resonator is very similar to that shown in Fig. 3.21b, but the experiment has new peculiarities that are illustrated in Sect. 3.4.3.4.

The experiment of Ewing and Trusler (2000) used instead a small aluminum spherical resonator with a diameter of 80 mm, working at microwave frequencies (2–19 GHz) for the determination of thermal expansion, and using argon as thermometric substance. The results report an uncertainty of about $\pm$ 1 mK in the 90–300 K range.

Another improvement was later the use of a *quasispherical* resonator (Gavioso et al. 2011; Troung et al. 2011), for the separation of the various resonance triplets.

The results by Pitre et al. (2006) derive from measurements with helium gas in the temperature range from 7 K up to the triple point of water, and later from additional work (Pitre et al. 2011)—also intended to redetermine the Boltzmann constant (Pitre et al. 2011)—with also adding argon as a working gas, which confirmed the 2006 results. In the work of Benedetto et al. (2004), temperature was measured in the range 234–380 K, using argon as measuring gas. Others are starting to use the same method (Segovia et al. 2010).

Finally, it must be noted that most of the experiments with acoustic thermometers illustrated above, after year 1986, use practically the same experimental techniques and the same theory and procedure for the correction of the boundary layer, the most critical correction (see Sect. 3.4.3.1 below). Therefore, some possible systematic effects that would affect all these experiments remain concealed. In this respect, therefore, it must be also reported the experiment of Zhang et al. (2011) and Sun et al. (2011), that, though so far reporting an uncertainty higher by approximately a factor of five, makes use of a *cylindrical* resonator and other features partially providing a check for systematic effects in spherical resonators.

The results from acoustic gas thermometry after year 2000 seem to corroborate the recalculated values by Astrov et al. (1995), locating thermodynamic temperature in the range 100 K $< T <$ 280 K at values about 10 mK lower than those derived from the ITS-90. But, where Astrov's values show a kind of jump near 100 K, the acoustic data change smoothly, systematically about 3–4 mK below those of Astrov et al. (1996), to join with the experimental data close to 50 K.

Notwithstanding the low uncertainties claimed by AGT, it must be born in mind, that, although the latest AGT experiments have done a great job in limiting the uncertainties by a great many cross-checks, the still unresolved discrepancy with the results from CVGT strongly suggests that AGT and/or CVGT may still be affected by unrecognized systematic errors. This lack of knowledge is underlined by the most recent DCGT measurements (see below) reporting agreement with ITS-90 up to 36 K, contrary to the (preliminary) AGT findings in this temperature range. It is not presently possible to conclude that temperatures derived by AGT represent thermodynamic temperature better than those obtained by CVGT.

For a more detailed discussion of the intricacies of acoustic thermometry the reader is referred to the cited literature.

3.4.3.1 Correction of the Effect of the Acoustic Boundary Layer

The pioneering work by Plumb and Cataland (1966) and Colclough (1973) still relied on an interferometric method for the determination of thermodynamic temperature, and was still affected by the problematics related to the acoustic boundary layer limiting the obtainable uncertainty. Ideally, the normal component of the particle velocity is expected to vanish at the boundary (wall), and for a viscous fluid (gas) also the tangential component should vanish. Furthermore, the solid boundary should disturb the temperature field associated with the velocity field. Thus, near the interface, the acoustic propagation would be more isothermal than adiabatic due to the very high thermal conductivity of the wall with respect to the gas.

The calculation of this correction requires the knowledge of the density and heat capacity of the gas as a function of temperature and pressure. These can be obtained by inversion of the second-order virial equation. The second virial coefficient and its temperature derivative needed can be calculated, e.g., from the expression given in Moldover (1999) or from the recent theoretical calculations (see Sect. 3.2). Similarly, values for the thermal conductivity can be found in the literature, e.g., Moldover (1999). The importance of the boundary layer correction is indicated by the fact that it leads overall to the largest correction and that it can assume relative values as high as $5 \cdot 10^{-4}$.

3.4.3.2 Measurement of the Acoustic Thermometer Volume

Great progress has been made in acoustic thermometry by the subsequent use of a spherical bulb (the resonator) allowing the employment of resonances, and by improved quantification of the boundary layer effect through an appropriate choice of the available acoustic modes. This led to the first high-accuracy measurement of the Ga MP (Moldover 1988) by acoustic means. However, the volume of the resonator was still measured separately by weighting with mercury.

Later on, the radius of the resonator, and its variation due to thermal expansion, were measured by the application of microwaves, using the expression:

$$\frac{T}{T_W} = \frac{\lim_{p\to 0}\left(\dfrac{f_\mathrm{a}+\Delta f_\mathrm{a}}{\langle f_\mathrm{m}+\Delta f_\mathrm{m}\rangle}\right)^2_T}{\lim_{p\to 0}\left(\dfrac{f_\mathrm{a}+\Delta f_\mathrm{a}}{\langle f_\mathrm{m}+\Delta f_\mathrm{m}\rangle}\right)^2_{T_W}} = \frac{\lim_{p\to 0}\left(\dfrac{u}{c}\right)^2_T}{\lim_{p\to 0}\left(\dfrac{u}{c}\right)^2_{T_W}} \tag{3.30}$$

where the subscripts "a" and "m" refer to acoustic and microwave modes, respectively, while Δf_a and Δf_m are corrections to the frequencies f_a and f_m.

These improvements resulted in the first high-accuracy determination of the thermodynamic temperature of the gallium fixed point by Moldover et al. (1999), and in the work by Ewing and Trusler (2000) between 90 and 300 K. Later, Benedetto et al. (2004) also applied these techniques in the temperature range of 234–380 K.

In these three experiments, the microwave measurements were performed separately, in vacuum. The work by Pitre et al. (2006) down to 77 K with preliminary data going as far down as 7 K, introduced further improvements. First, the microwave measurements were performed while taking the acoustic data. Second, a quasispherical resonator was used, in order to resolve the degenerate microwave resonance triplets TE1n and TM1n, allowing a reduction in the uncertainty. Then, as working gas helium was used, while previous experiments used argon, at overlapping temperatures. Since the diffusivity in helium is about 10 times larger than in argon, the use of different gases is an important check on the correctness of the corrections Δf_a, accounting for the heat exchange between the gas and the wall. Similarly, the use of different metals for the resonator allows a check on the correctness of the term Δf_m, accounting for the penetration of the electromagnetic field into the walls. Pitre et al. used a copper wall while previous experiments used either stainless steel or aluminum, and the conductivities of copper and stainless steel differ by a factor of about 300 at 77 K and of about 50 at the triple point of water. The use of helium has, however, one drawback with respect to argon: helium is much more sensitive to impurities. It is therefore advisable in such a case to apply a small flow of the measuring gas for the determination of impurities in a gas chromatograph, passing through a liquid-helium-cooled trap, as used by Benedetto and Pitre, with the drawback, however, that the total amount of gas n is not constant anymore.

3.4.3.3 Effects from Other Acoustic Parameters

Some effects, already recognized by Pitre et al. (2006), include increase in acoustic noise from the bubbling helium bath, perturbation of the acoustic modes by the coil-terminated coaxial cables used for coupling microwaves into the cavity, the condition of the inner surface of the resonator. It is expected that an electropolished surface, as compared with the as-machined one used in the experiment, will reduce the apparent precondensation of argon at 95 K and of helium at 4 K. Pitre et al.'s (2006) work spans a much wider temperature range, with both argon and helium at overlapping temperatures. At the higher temperatures, high-purity argon is used, while for temperatures below, say, 100 K, the use of helium is more appropriate.

A theory for the thermal boundary layer has been developed by Ewing et al. (1986).

3.4.3.4 Effect of the Amount of Gas Contained in the Acoustic Gas Thermometer and of Impurities in the Gas

In an acoustic gas thermometer, the influence of the quantity of gas enclosed in the resonator is by far less critical than in a CVGT, a great advantage. This advantage has been used to allow a real-time verification of a much more important influence factor, the effect of chemical impurities in the gas. These issues were resolved in the work of Ripple et al. (1999) in a unique way. The apparatus includes continuous (slow) flushing of the gas (3×10^{-5} to 3×10^{-4} mol s^{-1}) through the resonator,

and the outgoing gas is analyzed by an inline gas chromatograph, able to measure the presence of H_2, N_2, CO, CO_2, and C_xH_y at a level of 0.3×10^{-6} amount of substance fraction.

Impurities affect helium much more than argon (10^{-6} of H_2O causes a shift of -3.93×10^{-6} and 0.12×10^{-6}, respectively) (de Podesta et al. 2011). Also, isotopic composition affects the measurements when argon is used (Valkiers et al. 2010).

3.4.4 The Boltzmann Project

Following CIPM Recommendation 1 of 2005 (CIPM 2005a), a dedicated Task Group was set up to study the implications of changing the definition of the base-unit kelvin. This Task Group arrived at the proposal of a new definition of the kelvin in terms of a fixed value of the Boltzmann constant, with the condition, however, that the overall experimental relative uncertainty in the Boltzmann constant be 1×10^{-6} or better, and supported by experiments based on different principles (Fischer et al. 2007). Shortly after that, an International Collaboration was set up with the aim of pursuing different methods for the measurement of the Boltzmann constant. Progress over the years is documented by the various Workshops organized within the framework of the Collaboration (C.R. Physique [Acad. des Sciences] 2009; IJOT Special Issue 2010) and by published papers, most already cited. The methods pursued are: acoustic gas thermometry (e.g., Sutton et al. 2010; Gavioso et al. 2010; de Podesta et al. 2011; Zhang et al. 2011), dielectric-constant gas thermometry, Johnson noise thermometry, and Doppler broadening thermometry, each with their own level of uncertainty (see, e.g., Benz et al. 2011; Lemarchand et al. 2011). The best results are presently obtained by acoustic means (now close to 10^{-6} relative uncertainty, IJOT Special Issue 2010). For details about the different approaches, the reader is referred to the original papers and can consult NIST (2011) bibliography (see "Further Readings" Section; Summaries 3.13, 3.14, 3.15, and 3.16)

Summary 3.13 Summary of design criteria for an absolute CVGT in the low-temperature range (T<273.16 K)

	See section
1. *Choice of temperature range and of span* $T_{min} \ll T_{max}$ This choice is preliminary to the choice of most of the design parameters	3.1
• Below 273.16 K, ^{4}He gas thermometry is limited down to 2.5 K. With ^{3}He, accurate virial corrections available down to 1.5 K	3.1.1.1
• Only CVGTs of special design can be used in full span. Being $p \propto T$, the 2.5–273.16 K range corresponds to $p_{max}/p_{min} > 100$. For top accuracy, $dp/p < 0.01$ %, corresponding at p_{min} to $dp < 10^{-6} p_{max}$, generally not achievable	
• Being $p \propto n/V$, molar density must generally be changed over the range to optimize accuracy, but a too high value of n/V must be avoided to not require third virial correction, especially below ≈2 K	
• In general, a CVGT is designed for work only below or only above a temperature between 25 and 100 K	
	3.1

Summary 3.13 (continued)

2. *Choice of reference temperature T_0:*
   Truly absolute thermometer: only one choice possible, 273.16 K
   - Two-bulb CVGT: avoids necessity to bring up to T_0 the bulb measuring $T_{min} > T < T_{max}$. Useful with thermometers designed for use at $T \ll T_0$ 3.3.2
   - Single-bulb CVGT: same bulb spans the entire range up to T_0 3.3.3

   Low-temperature reference temperature T_0^* (from ≈25 K to ≈90 K):
   - Single-bulb CVGT commonly used. T_0 value assigned by an independent experiment, and, therefore, not exact by definition. However, the additional uncertainty is a minor inconvenience with respect to the advantage of limiting bulb temperature within the span $T_{min} \ll T_{max}$ 3.3.1 3.3.3

3. *Choice of thermometric gas and filling density:*
   Thermometric gas:
   - *e*-hydrogen: no more used since half a century, but still suitable for lower accuracy and temperature range above ≈20 K 3.1.1.3
   - ^{4}He: commonly employed in recent gas thermometers. Use limited to above 2.5 K
   - ^{3}He: more considered in modern gas thermometry. Use presently limited to above 1.5 K; potential use down to <1 K

   Filling density: $p \propto n/V$ and $\mathrm{d}p/\mathrm{d}\,T \propto n/V$ (1 kPa K^{-1} $\triangleq$ 121 mol m^{-3}). Always advantageous increasing n/V, up to an upper boundary set by need of third virial correc- tion. As a rule, n/V <250 mol m^{-3} above ≈2.5 K, n/V <160 mol m^{-3} down to 1.2 K and n/V <30 mol m^{-3} at 0.8 K 3.1.2.3 3.1.1.1

4. *Choice of pressure-measuring system:*
   Most important choice determining thermometer accuracy
   - Without separating diaphragm: can be used only for low–medium accuracy, as thermometric gas also fills the entire manometer, with contamination problems and increase of dead-volume
     – Dial manometers: used only for accuracy >±1 %
     – Metal diaphragm or bellows (electronic) manometers: can achieve a ±0.1–0.03 % accuracy
     – Quartz bourdon gauges: can approach ±0.01 % accuracy, but helium leaks through quartz
     – Cryogenic pressure transducers: none commercially available with accuracy better than ±0.1 % (after cryogenic calibration). They eliminate, fully or partially, dead-volume and aerostatic-head corrections 3.1.3.2
   - With separation diaphragm: mandatory for high or top accuracy. Only zero reproducibility and a moderate linearity near zero are important
     – Capacitive diaphragms: several commercial models, when properly used, can allow zero sensitivity and reproducibility better than ±0.1 Pa 3.3.1.3
     – Cryogenic diaphragms: only laboratory-made diaphragms available, some with high zero reproducibility. Confine the thermometric gas at low temperature, totally suppressing dead-volume correction. The tube connecting the diaphragm to room-temperature manometer designed as for vapor-pressure thermometry 3.1.3.1
     – Room-temperature manometers: when a cryogenic diaphragm is used, they are the only manometers allowing helium to be used as manometric gas 3.3.3

5. *CVGT parameter design:*
   A) Room-temperature pressure transducer
   - Bulb: top accuracy, 1 L volume typical; low accuracy, as low as 50 m^3 3.1.3.3
   - Dead-volume: top accuracy, <10 cm^3; low accuracy: up to 10 % of bulb volume 3.3.1.1

   B) Cryogenic pressure transducer
   - Bulb: minimum volume limited only by its invariance, affected by adsorption and wall deflection. It can reduce to the transducer chamber 3.3.3
   - Dead-volume: none (or very small) 3.1.2.2

Summary 3.13 (continued)

6. *Bulb design:*	
Volume V_b may not be constant, because of:	
• Compression modulus: walls must be thick to limit deflection due to pressure or bulb must be enclosed in a guard chamber kept at bulb pressure. Stress in bulb material must be relieved by annealing after machining	3.1.1
• Thermal expansion: nothing can be done to suppress this effect, except using glass; must be corrected for. Small effect below ≈30 K	3.1.2.1
Amount of "active" gas n_b may not be constant, because of:	
• Gas adsorption: physical-chemical interaction of bulb walls with the gas determining the amount adsorbed. Copper often gold-plated to limit adsorption: this prevents heating the bulb above 50–70 °C	3.1.1.2
• Impurity molecules on walls and leaks: clean machining used for metal bulbs followed by physical-chemical cleaning. The bulb-sealing gaskets must be stable in shape and leak-proof at working temperatures	3.1.1.3
7. *Dead-volume design (case A):*	
Dead-volume effect comes from combination of geometrical volume, working pressure, and gas density distribution, i.e., from the amount n_d of substance contained in it	3.1.2.2
• Room-temperature dead-volume n_r: consists of all volumes of the gas-measuring system at room temperature T_r. Must be kept at uniform temperature (except diaphragm, often thermostatted at ≈40 °C), to be measured within 0.1–1 °C	3.1.3
• Low-temperature dead-volume n_c: (part of) capillary tube between room and bulb temperature.	
– Temperature T_c and density ρ_c change from one end to the other. Tube diameter is a tradeoff between geometric volume and thermomolecular pressure effect: typical values between 0.5 and 3 mm.	3.1.2
– Advantageous keeping the parts of tube where temperature variations occur as short as possible. For medium–high accuracy, temperature distribution must accurately be known	3.1.2.2
8. *Gas handling and measuring system (for nonsealed CVGTs):*	
• Handling system: must ensure purity, possibly checked on-line with a mass spectrometer, and includes gas recovery with cryogenic pumps and clean storage (or purification). Similar to the one used for filling triple-point sealed cells	2.2.2.6
• Measuring system (case A): separating diaphragm requires valve system for zero check, including constant-volume valves and provisions to avoid (or to restore) thermometric gas losses and contamination from the manometric gas. For this purpose, a second diaphragm separator may be used	3.1.3

Summary 3.14 Summary of differences and simplifications in design criteria of an ICVGT

	See section
1. *Choice of temperature range and span $T_{min} \ll T_{max}$:*	
• An ICVGT can usefully replace other types of thermometers between 5 and 30 K	3.2
• ITS-90 defines two types, between 4.2 and 24.5 K and between 3 and 24.5 K	
• ICVGT definitions always assume constant molar density n/V in the whole range. According to the CVGT limits, T_{min} is set at ≈2.5 K for $n/V = 250\ \text{mol m}^{-3}$ and at ≈1.2 K for $n/V = 160\ \text{mol m}^{-3}$. Pushing the definition below requires much lower density (i.e., sensitivity) values in *whole* range (e.g., for $T_{min} = 0.8$ K is $n/V = 30\ \text{mol m}^{-3}$), or lower accuracy must be accepted	
2. *Choice of definition range and of reference temperatures $T_{r,i}$:*	
An ICVGT is always of the single-bulb type. Its definition range can be extended below 1.2 K, down to 0.8 K using lower values of n/V, thus with lower accuracy	3.2

Summary 3.14 (continued)

	See section
The number N of reference temperatures $T_{r,i}$, where the ICVGT has to be *calibrated*, set by the number of free parameters in definition equation. Fixed points are selected among the available (choice is not always possible) to: minimize nonuniqueness; allow easiest realization; allow maximum *extrapolation* interval (in order of importance)	Table 3.11
• ITS-90 definitions: $n = 3$. Two triple points (Ne and e-H_2). The lowest is a ^{4}He or ^{3}He vapor-pressure point of ITS-90 definition	3.2.1.1.4
• *Other possible definitions (see details in Pavese and Molinar 1992—first edition of this book): n = 2–4*	3.2.1.2
• *Three main categories, using:* – *Only triple points: n = 2. Definitions with some stipulated parameters, in the 2–30 K range; only triple points of Ne and e-H_2* – *Only fixed points, not requiring pressure measurements: n=3. Definitions in 2–30 K range; triple points of Ne and e-H_2 and the λ-point of ^{4}He* – *Only triple points and superconducting transitions: n=3–4. Definitions in 0.8–30 K range; triple points of Ne and e-H_2 and superconducting transitions: zinc, aluminum, or indium*	
3. *Choice of thermometric gas and filling density:* • Thermometric gas: – No difference with respect to a CVGT • Filling density: can be higher than with a CVGT, as calibration can also take into account third virial coefficient effect.[a] For the ITS-90 definitions, the same limits of a CVGT apply	3.1.1.1
4. *Choice of pressure-measuring system:* No difference with respect to a CVGT, but ICVGT calibration can also incorporate (re)calibration of some of the pressure transducer parameters[a]	3.3.4
5. *ICVGT parameter design:* A) room-temperature pressure transducer: • Bulb: volume V_b can be smaller than that of a CVGT, even for top accuracy, since calibration takes into account dead-volume effects[a] • Dead-volume V_d: the ratio V_b/V_d can be smaller	3.3.4
B) cryogenic pressure transducer: no difference with respect to a CVGT	3.1.2.2
6. *Bulb design:* • Variations of ICVGT volume V_b: due to wall modulus of elasticity and to thermal expansion, taken into account by calibration[a]	3.3.1.1
• Change of the quantity of "active" gas n_b: due to gas adsorption, taken into account by calibration,[a] if reversible and reproducible. As regards impurity molecules on the walls and to leaks, same problems as a CVGT	3.1.1.2 3.1.1.3
7. *Dead-volume design (case A):* All dead-volume effects fully taken into account by calibration[a]	3.1.2.2a
8. *Gas handling and measuring system (for nonsealed CVGT):* No difference with respect to a CVGT	2.2.2.6

[a]Within the validity of the mathematical model used for the definition

Summary 3.15 Summary of the measurements procedures for a CVGT[a] in the low temperature range ($T < 273.16$ K)

	See section
1. *Preliminary procedures and measurements:*	
• Bulb volume (optional): ratio n_b/V_b calibrated at reference temperature T_0, but independent measurement of V_b is a useful check of nonrandom errors	3.3.1.1
• Dead-volume (geometrical measurement): dead-space volume measurements, both of room- and low-temperature parts, need an accuracy as high as ± 0.01 %. Done at room temperature with gas-expansion method, using a $\approx 50\,cm^3$ calibrated volume. For the capillary only, mercury filling and weighing is often used	3.1.2.2
• Dead-volume (total correction): more effective than the former. The whole dead-volume system is *calibrate*d, by fitting the capillary into the cryostat without the bulb and blanking its lower end with a flange. Then, dead-volume is filled with known amount of gas, flange temperature is stabilized at different temperatures spanning the entire working range, and pressure values are measured with the manometer as in normal thermometer measurement. Temperature distribution is also measured with differential thermocouples	3.1.2.2
• Gas purity: at higher temperatures, especially water vapor, difficult to remove, can cause nonrandom errors. Gas purity check is highly desirable and, for high-accuracy measurements, done on-line, as the bulb itself can be a contamination source, especially in sealed CVGTs	3.1.1.3
• CVGT filling: filling is not itself a delicate operation, since the amount of gas sealed in need not be known accurately	2.2.2.6
2. *Performing the measurements of the manometer pressure (p^*):*	
• Measurement at the reference temperature T_0 or T_0*: bulb is first stabilized to T_0: fixed point rarely used, but instead a calibrated thermometer. After capillary temperature distribution stabilization, which can take more time than bulb, pressure measurement and all manometric system corrections are performed; a p_0* value is obtained. Dead-volume temperature distribution is also measured	3.1.2.2
• Measurement at a temperature T: same procedure; a p^* value is obtained	
• Isotherm method: used, in general, only for new virial coefficient value determinations. The thermometer is filled by steps with increasing (or decreasing) amounts $n_{b.k}$ of gas, and pressure p_k* is measured at T_0, to obtain $n_{b.k}/V_b$, and at a fixed temperature T_I of the chosen isotherm	
3. *Calculation of pressure p_b and temperature T_b:*	
• Calculation of p_b: is calculated from p^* applying aerostatic and thermomolecular corrections, depending on ICVGT design and capillary temperature distribution	3.1.2.2 3.1
• Calculation of T_b: temperature values of the bulb, where thermometers are fitted, are calculated from p_b, mainly involving virial and dead-volume corrections (dead-volume "calibration" is used, when performed)	3.1.1.1 3.1.2.2
• Calculation of T_b with the isotherm method: same procedure, excluding virial correction; $T'_{b.k}$, values computed and plotted versus $n_{b.k}/V_b$. Extrapolation to zero density gives T_I value	

[a]A one-bulb CVGT is considered

Summary 3.16 Summary of differences and simplifications in measurement procedures for an ICVGT

	See section
1. *Preliminary procedures and measurements:*	
• Only gas purity check is necessary. Then, the ICVGT filling can be performed	3.1.1.3
• Realization of the fixed points: one or more thermometers must be calibrated at the fixed points realizing the ICVGT reference temperatures	3.2, 3.4
2. *Measurements of the manometer pressure (p^*):*	
• Measurement at the reference temperatures T_i: the bulb is first stabilized at each T_i. After capillary temperature distribution stabilization, which can take more time than bulb, pressure measurement and all manometric system corrections are performed; a $p_i{}^*$ value is obtained. No auxiliary measurements need be done	3.1.2.2 3.1.2.2
• Measurement at any other temperature θ: same procedure; a p^* value is obtained. With the ICVGT, temperature distributions and, in general, all corrections taken into account by calibration procedure, must remain the same in subsequent measurements, at least in between calibrations	
3. *Calculation of temperature θ_b:*	
The $p_i{}^*$ values are *directly* used in the defining equation	3.2
• The numerical values of the equation coefficients are obtained by solving the system of equations obtained by substitution of the $p_i{}^*$ values	
• The defining equation (e.g., T_{90}) is then used with each p^* value to compute the corresponding value of θ_b of the bulb where thermometers are fitted	

Chapter 4
Vapor-Pressure Thermometry

Vapor pressures have been used for a long time for temperature measurements or for calibrating thermometers against a physical property, since the saturated vapor pressure of a pure substance above its liquid phase depends only on temperature. The physical basis of vapor-pressure thermometry has already been discussed in Sect. 2.1 (see Fig. 2.1).

Vapor pressures are very commonly used as well for the realization of the fixed points called "*boiling points.*" These fixed points are simply specific points on the vapor-pressure line, generally those at 101 325 Pa (normal boiling point). They do not deserve special attention, as they differ in no way from any other point of the vapor-pressure line, and are often simply the highest point attained by the experimenter.

The *pressure* fixed points based on triple points, treated in Chap. 9, are another application of a specific point of the vapor-pressure line.

Present knowledge of the physics is adequate to provide an accurate analytical description of the relationship existing between pressure p and thermodynamic temperature T. The following equation was established in the 1950s and can be found in many textbooks (see, e.g., Keller 1969):

$$\ln\, p = i_0 - \frac{\Delta_{\mathrm{vap}} H_{m,0\ \mathrm{K}}}{RT} + \frac{5}{2}\ln T - \frac{1}{RT}\int_0^T S^{\mathrm{L}}(T)\mathrm{d}T + \frac{1}{RT}\int_0^p V^{\mathrm{L}}(p)\mathrm{d}p + \varepsilon(T), \tag{4.1a}$$

where:

$\Delta_{\mathrm{vap}} H_{m,0\,\mathrm{K}}$ is the molar enthalpy of vaporization at 0 K;
i_0 defined by $\ln[g_\sigma(2\pi\ m_\mathrm{a})^{3/2}k^{5/2}h^{-3}]$ is the chemical constant, with m_a being the mass of a single atom and g_σ the degeneracy due to nuclear spin;
$\varepsilon\ (T)$ defined by $\ln \frac{pV^{\mathrm{V}}}{nRT} - 2B(T)\frac{n}{V^{\mathrm{V}}} - \frac{3}{2}C(T)\left(\frac{n}{V^{\mathrm{V}}}\right)^2$ is the vapor virial correction, with $B(T)$ and $C(T)$ being the virial coefficients;
$S^{\mathrm{L}}(T)$ is the molar entropy of the liquid along the saturation line, and $V^{\mathrm{V}}(p)$ and $V^{\mathrm{L}}(p)$ are the volumes of the vapor and the liquid along the saturation line.

F. Pavese, G. Molinar Min Beciet, *Modern Gas-Based Temperature and Pressure Measurements,* International Cryogenics Monograph Series,
DOI 10.1007/978-1-4419-8282-7_4, © Springer Science+Business Media New York 2013

In the case of ^{3}He, the (nuclear spin) specific heat capacity below say 0.5 K is not known well enough, therefore Sydoriak and Sherman (1964) used instead of Eq. (4.1a) a form with two constants a and b, as

$$\ln p = i_0 - \frac{a}{RT} + \frac{b}{T} + \frac{5}{2}\ln T - \frac{1}{RT}\int_{0.5\ \mathrm{K}}^{T} S^{\mathrm{L}}(T)\mathrm{d}T + \cdots, \tag{4.1b}$$

where a is defined by $\{\Delta_{\mathrm{vap}}H_{m,0\ \mathrm{K}} - \int_{0}^{T=0.5\ \mathrm{K}} c^{\mathrm{L}}\ \mathrm{d}T\}$ and b is $S^{\mathrm{L}}(0.5\ \mathrm{K})$.

However, not all the parameters involved in Eq. (4.1a, b) can be calculated from first principles with the accuracy desired for high-precision thermometry. This is similar, for example, to the situation occurring with the nuclear quadrupole resonance thermometry.

Below the λ-point with ^{4}He Eq. (4.1a) and below ≈ 1 K with ^{3}He Eq. (4.1b), respectively, allow calculation of a vapor-pressure scale accurate to within ±0.5 mK, with only one unknown parameter, $\Delta_{\mathrm{vap}}H_{m,0\ \mathrm{K}}$. Only the first three terms are significant contributors; however, for higher temperatures, the other three terms must be taken into account as well, especially the contribution of entropy. With ^{4}He, a 0.1 % uncertainty in each of these three terms contributes to the uncertainty in the vapor-pressure scale by ≈ 2 mK at 3 K and by ≈ 4 mK at 4 K (see Sect. 4.3.2 for a discussion of the helium scales).

Apart from helium, the uncertainty is much higher for most substances. Therefore, vapor-pressure scales cannot be used, at present, as accurate thermodynamic thermometers.

On the other hand, in the implementation of such a thermometer, the choice of the *technical* parameters is not critical (with few exceptions, which will be discussed). Therefore, the exact relationship of Eq.(4.1a, b) is replaced by a semiempirical, or even empirical, equation. The following is often used when only low accuracy is required:

$$\ln p = \alpha + \beta/T + \gamma \ln T. \tag{4.2}$$

This relation is based on the Clapeyron equation and assumes that the heat of vaporization is a linear function of temperature and that $V^{\mathrm{L}} \ll V^{\mathrm{v}}$ and the vapor is an ideal gas. The parameters α, β, and γ are found experimentally for each substance.

Vapor-pressure equations are expected to be valid for a broad variety of experimental conditions, and, in general, no calibration is necessary at *any* fixed point, as the values of *all* coefficients are specified (and tabulated as *defining* values). In fact, the *p–T* relationship of a specific pure substance, after being determined experimentally following careful procedures and being compared with a thermodynamic thermometer (such as a gas thermometer), is assumed to be valid, within the stated accuracy, irrespective of any specific implementation. This procedure has been followed for the realization of ^{3}He and ^{4}He vapor-pressure scales, T_{62} (Sydoriak and Sherman 1964) and T_{58} (Brickwedde et al. 1960), respectively. Lately, new definitions of ^{3}He and ^{4}He vapor-pressure scales were included in the ITS-90.

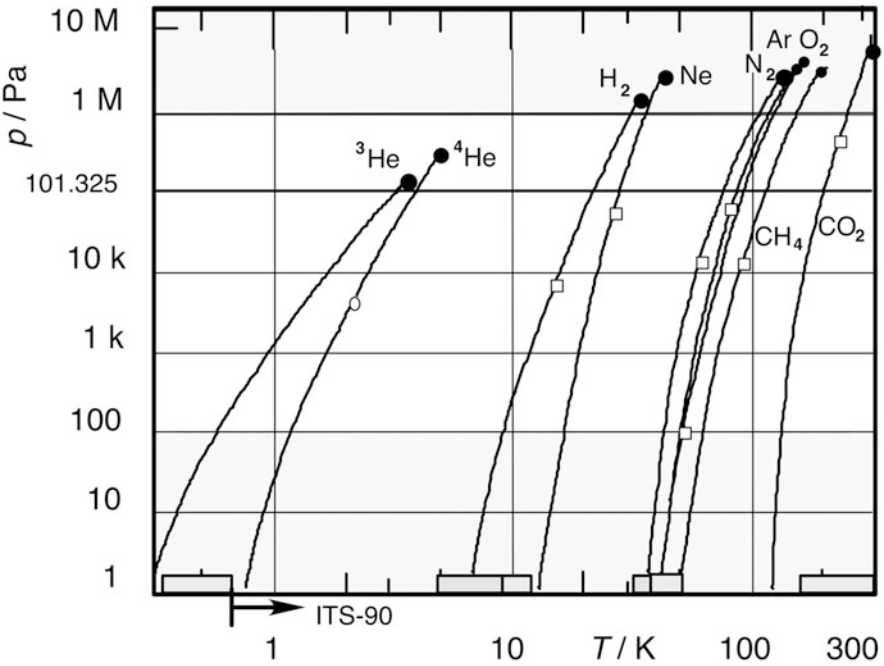

Fig. 4.1 Range for vapor-pressure thermometry of various gases (for quantitative data, see Appendix C). The *shaded parts* indicate regions where it is less common or less accurate. not available lower accuracy. ● critical point; O triple point; **0** λ-point

A scale of this type differs from an empirical scale, in that the realization of the latter requires a specific interpolating instrument, as discussed in Sect. 1.2.2.2. The vapor-pressure scale is, instead, a particular type of the semiempirical scales discussed in Sect. 1.2.2.1. In general, a semiempirical scale also requires the definition of a number of fixed points (such as those of Chap. 2), to determine the values of (some of) the equation coefficients. With the vapor-pressure scale definition, on the contrary, no fixed points are needed as *all* these values are *defined*.

The basic criteria of the vapor-pressure scale differ as well from those of gas thermometry (Chap. 3), where the technical design may seriously affect the accuracy obtainable with individual apparatuses. From this reason, when a gas thermometer is used as an interpolating instrument, the value of a certain number of parameters of the defining equation must be obtained from calibration. No such requirement exists with vapor-pressure thermometry, since only the physical properties of a substance are significant.

On the other hand, each substance allows a scale of this type to be realized only over a rather narrow temperature interval, as shown in Fig. 4.1; unfortunately, over certain temperature intervals vapor-pressure scale realization is not even possible or, at least, not to a high accuracy.

Both liquid–vapor and solid–vapor equilibria will be considered here, within a pressure interval discussed in Sect. 4.2.4; with solid –vapor equilibria greater thermal problems are involved, which may limit the accuracy of the realization.

4.1 Influence of Physical Parameters

Let us first refer to Fig. 2.4 and then to Sect. 2.2.1. With a pure gas, after some liquid has been condensed in the bottom[1] of the container C, after crossing the dew point line L′, pressure remains at a fixed value if the temperature is maintained at a fixed value—by removing the heat of condensation—during further condensation of gas in C from container R. This may occur in two ways:

1. By changing the volume of R, thus reducing the vapor volume: no rise in pressure occurs, only further condensation.
2. By allowing additional gas to flow from a gas storage into R, by opening the inlet valve V.

In both cases, there may be a temperature transient during condensation heat removal. In addition, temperature will become unstable if so much liquid is condensed that it overflows the container C, simply because there will be no more vapor in equilibrium with the liquid at the temperature of container C.

When both these conditions are avoided, the vapor pressure in the bulb realizes the same and unique vapor-pressure scale of a given pure real gas. Virial corrections are always the same on the saturated line, and saturation always occurs, at equilibrium, when some liquid is present.

4.1.1 Purity of the Substance

As discussed in Sect. 2.1, no substance is perfectly pure, but forms a mixture with other substances, which have, at each temperature, different vapor pressures.

4.1.1.1 Effect of Impurities

This discussion of mixtures will be limited to high dilutions ($x_i \ll 0.001$), so that the following assumptions can apply:

- Each of the impurities is present in both the liquid and the vapor phases, though generally in different concentrations x_i^{L} and x_i^{V}.
- The vapor phase is a mixture of ideal gases.
- The surface tensions are negligible.
- The solution in the liquid phase is ideal (no volume change, no heat of mixing).

The matter is extensively discussed in Bedford et al. (1990). Only a short account is given here. The errors contributed by impurities originate from essentially three different sources:

[1] At least for experiments in the earth's gravitational field.

1. The vapor pressure p of a liquid mixture with a main component (the solvent) and impurity components i can be written as the sum of the partial pressures p_i of all the components, in accordance with Dalton's Law

$$p = \sum_{i=1}^{n} p_i = \sum_{i=1}^{n} x_i^{\mathrm{V}} p \tag{4.3}$$

   Impurities almost insoluble in the liquid (those whose normal boiling temperature is much lower) may easily affect the measurements, as they behave in the vapor space nearly as an ideal gas.
2. The vapor pressure of the solvent p_1 in the mixture is lower than the saturated vapor pressure of the pure component p_1^0 (Raoult's law), as

$$p_1 = \left(1 - \sum_{i=2}^{n} x_i^{\mathrm{L}}\right) p_1^0 \tag{4.4a}$$

   The partial pressures of the impurity components ($i = 2$ to n) are, according to Henry's Law, proportional to their concentrations in the liquid: $p_{i=2,n} = x_i^{\mathrm{L}} K_{\mathrm{H},i}$. When this equation is combined with Eq. (4.3), one obtains

$$p = p_1^0 - \sum_{i=2}^{n} x_i^{\mathrm{L}} \left(p_1^0 - K_{\mathrm{H},i}\right). \tag{4.4b}$$

   The measured pressure is a linear function of impurity concentrations in the liquid. The second term is positive or negative, depending on the volatility of the impurities relative to the solvent.
3. The impurity concentration in both phases does not remain constant when varying the liquid fraction.[2] Figure 4.2 shows the isobaric T–x diagram for a two-component mixture in the condensation region.

Let us consider the case of an impurity more volatile than the solvent ($T_1 > T_2$). For a given composition of the totally gaseous mixture (the impurity concentration is exaggerated for clarity), at the crossing of the dew line in A, with $x_i^{\mathrm{V}} = x$, the impurity concentration in the first drop of liquid in B will be $x_i^{\mathrm{L}} = x'$, much lower than x_i^{V}. The condensation temperature is T_{A} ($< T_1$ of the pure solvent). As condensation proceeds, the liquid must have recovered the composition $x_i^{\mathrm{L}} = x$ when virtually the entire sample is condensed. This occurs at a temperature $T_{\mathrm{C}} < T_{\mathrm{A}}$ and the compositions of the liquid between the two limit conditions follow the line B–C. A similar description applies for the case of an impurity that is less volatile than the solvent ($T_1 < T_2$). In both cases, the saturated vapor pressure is no longer independent of the condensed fraction of the sample; this fact is commonly used as a useful diagnostic tool. However, a real situation with mixtures including both types of impurities is more complicated, and one can hardly estimate the correction for the impurity content with sufficient accuracy.

[2] This always occurs when working, as usual, with a fixed total amount of substance in the thermometer: $n = n^{\mathrm{L}} + n^{\mathrm{V}} = const$, so that when pressure increases—in the same volume—n^{L} decreases and n^{V} increases.

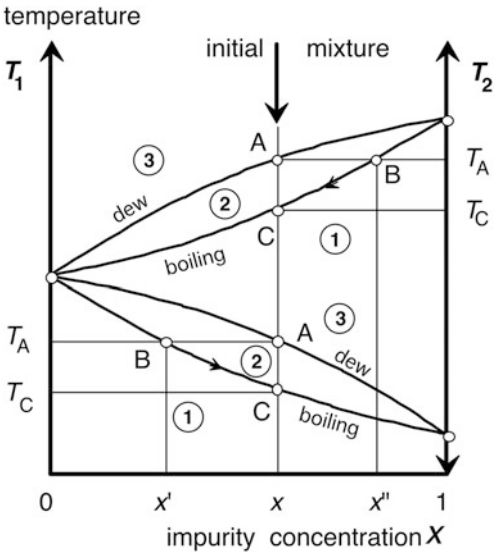

Fig. 4.2 Effect of impurities on condensation pressure, on the T–x plane (see text). (*1*) liquid, (*2*) liquid + vapor, and (*3*) vapor region

Table 4.1 Effect of the most significant impurity in vapor-pressure thermometry for selected gases

Gas	Impurity	Uncertainty[a] (δT/mK)
^{4}He	^{3}He	0.7 @ 1.5 K 0.2 @ 2.6 K
^{3}He	^{4}He	0.07
e-H_2	Ne	0.2
Ne	N_2	− 0.1
N_2	O_2	− 2
Ar	N_2	− 3
O_2	N_2, Ar	1[b]

[a]For a 10^{-4} impurity in the *liquid* phase, at the boiling point (≈ 100 % liquid) and 0.1 MPa, unless otherwise indicated
[b]Maximum. See Fig. 4.3c

4.1.1.2 Scale Errors Due to Chemical Impurities

Chemical impurities are a major source of uncertainty in vapor-pressure thermometry. Table 4.1 summarizes the effect of the main impurity on the normal boiling point of some gases.

When the values of the normal boiling-point and/or the triple-point temperatures of two vapor-pressure scale realizations are different, very often a linear correction is applied to the equation between these two points. This procedure is adequate for volatile impurities that change their volume in the vapor space according to the ideal-gas law.

Conversely, when specific experiments have been performed (Ancsin 1973, 1974a, b, 1977, 1978; Compton and Ward 1976), the effect of most nonvolatile

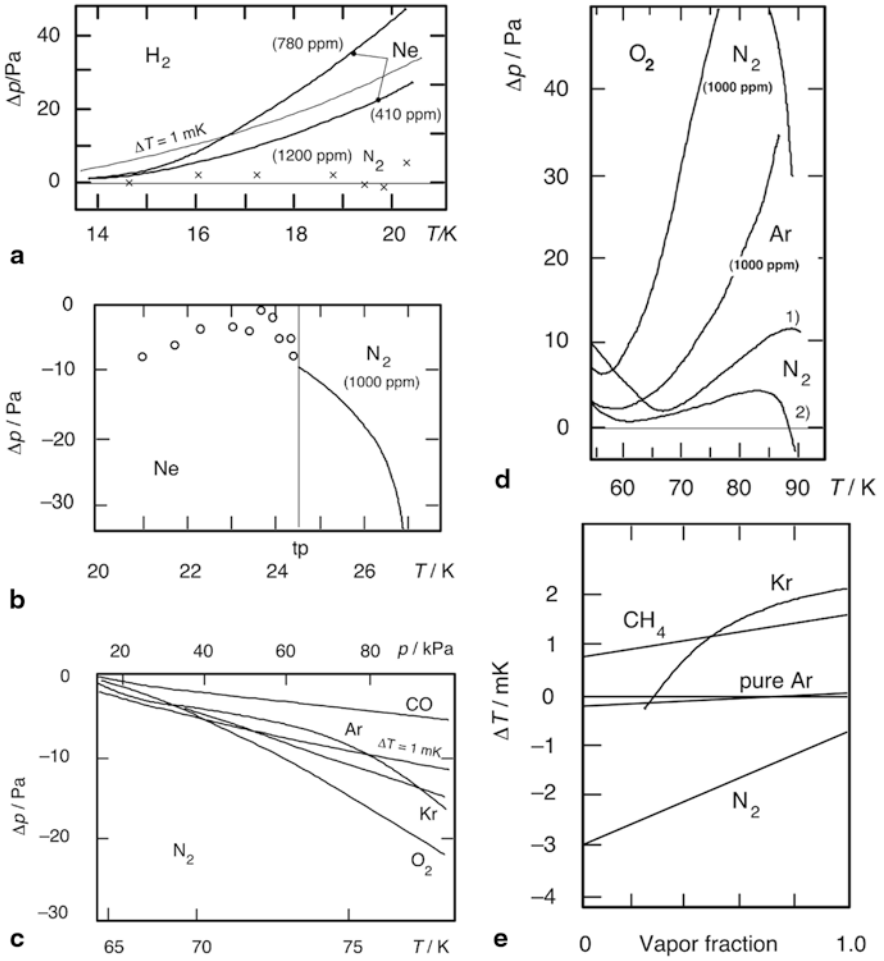

Fig. 4.3 Errors in vapor-pressure thermometry due to a 10^{-4} amount fraction of impurity in the *liquid* phase (unless otherwise indicated): **a** Hydrogen; **b** Neon; **c** Nitrogen; **d** Oxygen: *1)* 0.4 L and *2)* 1.6 L of vapor phase; **e** Argon. (After Ancsin 1973, 1974a, b, 1977, 1978)

impurities on $p = f(T)$ has resulted to be nonlinear, and thus involving a change in *all* equation coefficients. Figure 4.3 illustrates this effect, which was obtained by deliberately adding small quantities of selected impurities to the pure thermometric substance.

The effect of impurities provides a possible explanation for discrepancies, as high as tens of millikelvin, that have often been observed in the past between the temperature scales realized in different laboratories, when they were based on vapor pressures (for neon and oxygen see Fig. 4.4 (Ancsin 1974b, 1978)).

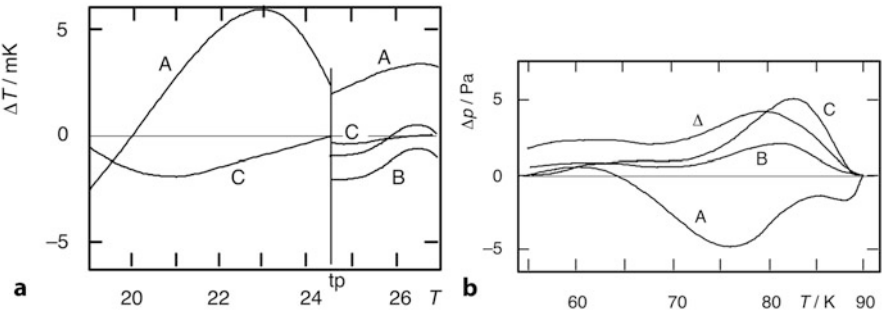

Fig. 4.4 Impurity-due differences between vapor-pressure scales (temperatures according to IPTS-68; after Ancsin 1974b, 1978): **a** Neon. *A*) (Ancsin 1978; Grilly 1962); *B*) (Ancsin 1978; Furukawa et al. 1970); *C*) (Ancsin 1978; Tiggelman 1973). The *broken line* is *B*) with normal boiling-point temperature readjusted. **b** Oxygen (baseline: home-made). *A*) (Ancsin 1974b; Muijlwijk 1968); *B*) (Ancsin 1974b; Muijlwijk 1968), commercial gas; *C*) (Ancsin 1974b; Tiggelman 1973); *D*) same as *B*) with 10^{-4} of N_2 added in sample

4.1.1.3 Isotopic- and Isomeric-Composition Errors

Isotopes and isomers usually have different values for the triple-point temperature. When the difference is significant, and the natural composition is considered, the accuracy of the reference point may be affected by the reproducibility of the composition. This question has been debated, for example, in connection with hydrogen (a mixture of H_2 and HD) and neon (a mixture of ^{20}Ne, ^{21}Ne, and ^{22}Ne). Since the results of a 1978–1984 international intercomparison (Pavese 1984; Pavese et al. 1984), it has been ascertained that the contribution of possible isotopic effects on the dispersion of the triple-point temperature of hydrogen may amount up to 1 mK and that of neon up to 0.6 mK.

In more recent years, both cases have been confirmed, and these effects started to be carefully taken into due consideration in temperature metrology (Pavese and Tew 2000b; Pavese 2003c, 2005b). As a consequence, the effect of isotopic composition on the triple-point temperature of (equilibrium-)hydrogen has been ascertained by a dedicated research program involving the major metrological institutes in the world (Pavese et al. 2003d; Fellmuth et al. 2005, 2012) and a similar dedicated research program (Pavese et al. 2010a, 2012b) has confirmed that the contribution of isotopic effects on the spread of the triple-point temperature of natural neon amounts to ≈ 0.5 mK. In both cases, see Sect. 2.2.2.5 for full details.

The reader should consult Tew (2008) for a comprehensive discussion on the effect on vapor pressures; here, only some basic concepts are drawn from that reference (for the triple-point temperature isotopic effect (TPIE), see Sect. 2.2.2.5).

The qualitative features of the vapor-pressure isotopic effect (VPIE) are illustrated in Fig. 4.5.

For the class of substances considered in this article, all exhibit the so-called "normal" VPIE where the vapor pressure of the lighter isotope is always greater

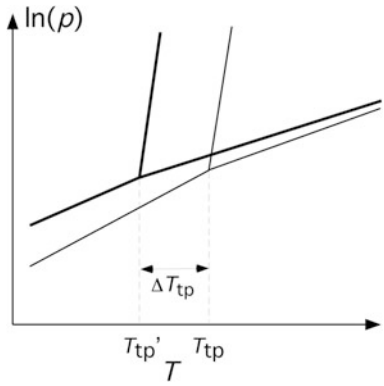

Fig. 4.5 Qualitative features of the normal VPIE for two isotopes: p–T diagram for two isotopes shows higher vapor pressures for the lighter isotope. The features have been exaggerated for clarity, and the figure is not to scale. (After Tew 2008)

than that of the heavier isotope at all temperatures in which a condensed phase exists (Jansco and Van Hook 1974). In this case, two isotopes with atomic masses M and M' ($M > M'$), vapor pressures p and p ($p < p'$) exhibit similar but shifted $p-T$ diagram. Results of the VPIE theory have been combined with the Eyring liquid structure theory by Jeevanandam (1971) to explain the magnitude of the discontinuity $\ln(p'/p) \equiv \ln(p'/p)_s - \ln(p'/p)_l$ in terms of the change in molar volumes V_s and V_l between the two phases. A simplified form of Jeevanandam's result is

$$\ln(p'/p)_l \approx (V_s/V_l)\ln(p'/p)_s, \tag{4.5}$$

if one neglects the nonideal behavior in both the liquid and the vapor and any isotopic dependence in the molar volumes. The subsequent considerations further restrict the discussion to systems exhibiting small VPIEs, or $\ln(p'/p) \ll 1$, which necessarily excludes H_2 and He. Equation 4.5 has been experimentally verified for the noble gases and the isotopic forms of CO.

The theoretical treatment of the VPIE involves thermodynamic relations for the reduced partition function ratio f for the condensed phase "c" (s or l) and the vapor phase "v" that are closely related to the relative volatility. By neglecting the nonideal gas correction, which is ≤ 10 % at the triple points of the substances considered here, the theoretical expressions for $\ln(f_c/f_v)$ could be simplified in terms of the lowest order quantum corrections associated with both external and internal degrees of freedom commonly expressed as

$$\ln(p' - p)_c \approx \ln(f_c/f_v) \approx (A_c/T^2 - B_c/T), \tag{4.6}$$

where the coefficient A_c involves differences of summations $\sum(\nu_i'^2 - \nu_i^2)_c$ over external modes ν_i' of the condensed phase and B_c involves differences of summations over the internal modes in both condensed and vapor phases (Jansco and Van Hook 1974). Hence, the B term plays no role in the calculations of the noble-gas VPIEs, and in practice, it is often acceptable to neglect the B term for some diatomic molecules as well.

Table 4.2 VPIE and TPIE data and estimates for the noble-gas series. (After Tew 2008)

Isotope pair	$\ln(p'/p)_l$[a]	$\Delta V/V_s$[b]	T_{tp}/K[c]	$\Delta T_{tp}/T_{tp}$	k_E
^{20}Ne, ^{22}Ne[d]	0.046	0.150	24.69	6.0×10^{-3}	1.7
^{36}Ar, ^{40}Ar[e]	0.0066	0.146	83.806	7.0×10^{-4}	1.5
^{80}Kr, ^{84}Kr[f]	0.0010	0.144	115.78	8.6×10^{-5}	1.15
^{130}Xe, ^{136}Xe[g]	0.00031	0.148	161.4	2.8×10^{-5}	1.2

[a]Values taken at $T = T_{tp} > T'_{tp}$
[b]Values derived from tabulated molar densities (Pavese and Molinar 1992c)
[c]Approximate temperatures for the heavier isotope on ITS-90
[d]Values for $\ln(p'/p)_l$ and ΔT_{tp} from Bigeleisen and Roth (1961) and Furukawa (1972)
[e]Values for $\ln(p'/p)_l$ and ΔT_{tp} from Lee et al. (1970)
[f]Values for $\ln(p'/p)_l$ and ΔT_{tp} from Lee et al. (1972)
[g]Values for $\ln(p'/p)_l$ and ΔT_{tp} (extrapolated, see Tew 2008) from Canongia et al. (2003) and Chialvo and Horita (2003)

Given these considerations, it is natural to approximate the total vapor pressure of a condensed phase in the following form,

$$\ln(p)_c \approx F_c(T) + a_c/T^2, \tag{4.7}$$

where $F_c(T)$ contains the phase-dependent but isotope-independent functional form for the vapor pressure and a_c contains the isotope dependence implied by Eq. (4.6) such that $A_c = a'_c - a_c$ (from this point the discussion in Sect. 2.2.2.5 about the effects on the triple-point temperature follows). Thus, the VPIE theory predicts that $\ln(p'/p) \sim T^{-2}$ and $\ln(p'/p) \sim \Delta M/MM'$.

For the noble gases Ne, Ar, and Kr, reasonably complete data for both the VPIE (and TPIE) exist (Jansco and Van Hook 1974). Instead, for Xe, there are no experimental VPIE data derived from differential pressure measurements; however, recent theoretical calculations of $\ln(f_c/f_v)$ are available from Canongia Lopes et al. (2003). Further relevant data can be found in Chialvo and Horita (2003). Some of the previous data are summarized in Table 4.2 (Tew 2008).

The effect on vapor pressure could also increase the melting range because of the "distillation" effect, i.e., of the change in isotopic content of the liquid phase when the temperature is changed. This phenomenon is governed by the Gibb's chemical potential μ_A for each phase, as indicated in Sect. 2.2.2.2. It was calculated by Tiggelman (1973) for neon that at ≈ 27 K, where the vapor pressure is about 0.1 MPa, that this effect is equivalent to about 0.4 mK. A more recent estimate of this effect for the vapor-pressure fixed-points of hydrogen, at ≈ 17 and ≈ 20.3 K and a way of correcting for it is given by CCT WG1 (Steur et al. 2005).

Isotopes or isomers can be considered "impurities" only when a pure isotope *must* be used—otherwise they are different substances (Pavese 2005b). This is the case with hydrogen isotopes, where one needs to use pure H_2 or pure D_2 free from any other protium isotope, chiefly from HD.

In addition, these substances have to be used in equilibrium spin composition at the working temperature, as discussed in Sect. 2.2.2.6. This means that, in order to accelerate the attainment of equilibrium, a catalyst must be used, even if at the risk of contamination. The ortho-para composition is temperature-dependent, as

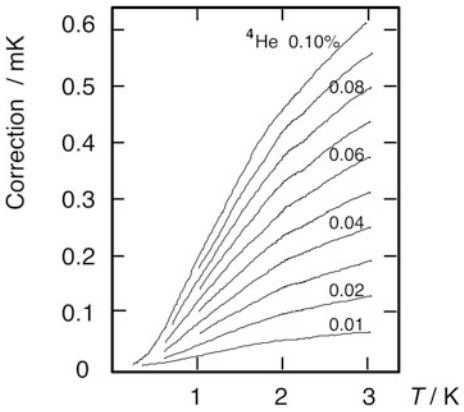

Fig. 4.6 Vapor-pressure error due to ^{4}He in ^{3}He. (After Sydoriak and Roberts 1960)

shown in Table 2.5. Therefore, the new equilibrium composition must be fully established before measurements can be performed correctly whenever the temperature value is changed. In fact, the vapor pressure of isomers is different. For example, $p(n\text{-}H_2) - p(p\text{-}H_2) = (650\ \text{Pa} + 0.030\ p)$ in the 25–110 kPa range (Esel'son et al. 1971).

Another case involves the helium isotopes. The effect of diluted ^{4}He in ^{3}He is shown in Fig. 4.6.

The correction, to be *added* to the uncorrected temperatures, is calculated from

$$\Delta T \approx (1 - x)\frac{d(\ln p)}{dx} \Big/ \frac{d(\ln p)}{dT}, \tag{4.8}$$

assuming that d(ln p)/dx is constant in the range $x(^3\text{He}) = 0$–10 % (Sydoriak and Roberts 1960; Esel'son and Berezniak 1956) and that Raoult's Law applies above 2 K. Between 0.6 and 2 K Sydoriak's experimental data are used and below 0.6 K a linear extrapolation to zero for $T = 0$ K is assumed. The temperature derivatives in Eq. (4.8) are calculated according to T_{62} (see Sect. 3.3.2.1), but, for present purposes, also apply to T_{90}.

The reverse contamination is usually limited to the effect of natural composition (0.5–2 $\times$ 10^{-6} amount of ^{3}He in ^{4}He), which affects ^{4}He vapor-pressure thermometry by much less than 0.1 mK (see also Sect. 2.5). If ^{4}He becomes contaminated (in dilution experiments or when interchanging the two isotopes in the same apparatus with insufficient care), a 10^{-4} of ^{3}He causes an error of 0.2 mK at 2.6 K and of 0.7 mK at 1.5 K.

4.1.1.4 Effect of Magnetic Fields

Vapor-pressure thermometry (like gas thermometry) is well suited—considering the persistent difficulties of employing electrical thermometers for this purpose (Pavese 1990a)—since they are affected very little by magnetic fields, with the exception of a

few paramagnetic substances. Calculations for N_2, O_2, and Ar are given in Meachin and Biddulph (1978). In measurements in magnetic fields up to 9.5×10^6 A m^{-1} using a 13 T magnet, no vapor-pressure changes were detected for N_2 and Ar, while a pressure change μB^2 in vapor pressure was observed for oxygen, amounting, at 12 T, to +1 % (equivalent to +18 mK) at 77.4 K and to +0.4 % (equivalent to +35 mK) at 90.2 K.

With ^{3}He, a pressure change up to 0.2 % at 8×10^7 A m^{-1} was measured at 3.05 K, while no field dependence was detected with ^{4}He (Berman and Kopp 1968).

4.1.2 Effect of the Amount of Thermometric Substance

A basic difference of the vapor-pressure thermometer, with respect to the gas thermometer, is that the amount of thermometric substance is of no consequence, as long as some liquid is present in the measuring bulb and provided that it does not spill over. The reasons were explained in the preceding section.

In principle, a large liquid filling of the bulb is best for minimizing the effect of impurities less volatile than the thermometric substance, whereas a small liquid filling is best for minimizing the effect of impurities more volatile than the thermometric substance. However, the choice is not simple, as in most cases not enough information of the actual impurities is available or impurities of both types are present. It is always recommended that the pressure dependence on the vapor/liquid ratio be checked to determine whether it is small enough not to affect the required accuracy.

The amount of liquid that avoids bulb over is filling easily calculated at the lowest vapor pressure (the lowest temperature T_m to be measured). Since this pressure is usually very low, this is equivalent to calculating the volume $V^\mathrm{L}(T_\mathrm{m})$ using the whole mass m of the sample. This defines the minimum bulb volume V_bm. The liquid filling can be much smaller than V_bm, but one must avoid, at the same time, leaving no liquid in the bulb before the highest vapor pressure (the highest temperature T_M to be measured) is reached. Near T_M, a substantial part of the sample is in the vapor phase. The calculation of m^V is more complex, unless V^V is very small, as it involves the density $\rho(T)$ distribution of the vapor:

$$m^\mathrm{V} = \int_\mathrm{bulb}^\mathrm{room} \rho(T) V^\mathrm{V} \mathrm{d}V. \tag{4.9}$$

From $m^\mathrm{L} = m - m^\mathrm{V}$, V^V can be calculated and must be substantially greater than zero; V^L determines the ratio $r = V_\mathrm{b}/V^\mathrm{V}$. Table 4.3 lists the limiting parameters of vapor-pressure thermometer design (see Bedford et al. (1990), Appendix D for calculation details).

Still in Table 4.3, one can note that with several gases 1 L of gas at room temperature and at 0.1 MPa requires a bulb volume larger than 1 cm^3 and that, conversely, when all the gas is at room temperature, it will attain, with a 1 L ballast, a pressure

Table 4.3 Filling limits for vapor-pressure thermometers with selected gases

Gas	Temperature range (K)[a]	[b]n_{max} (10^{-3} mol)	[c]n_{min} (10^{-3} mol)		$\frac{V_{gasSPT}}{V^{L}_{T_{min}}}$ (L cm^{-3})	$(\rho^{L}/\rho_{s})_{tp}$
			(1)	(2)		
Helium-3	0.65–3.3	27.4	47.8	15.8 + 1.0	0.660	–
Helium-4	1.25–2.18	36.3	2.0	0.30 + 0.04	0.905	–
Helium-4	2.18–5.0	36.5	80.2	9.93 + 1.61	0.910	–
Hydrogen	9–20	43.8	41.5	0.67 + 0.63	1.058	0.89
Neon	19–27	71.7	41.5	0.48 + 0.63	1.731	0.86
Nitrogen	50–77	34.5	41.5	0.16 + 0.46	0.832	0.92
Argon	70–87	40.8	41.5	0.14 + 0.44	0.984	0.87
Oxygen	65–90	39.4	41.5	0.14 + 0.40	0.969	1.02
Methane	90–112	28.1	41.5	0.11 + 0.39	0.677	0.80
Krypton	85–120	34.9	41.4	0.11 + 0.38	0.841	0.87
Xenon	115–160	27.9	41.5	0.09 + 0.32	0.669	0.87
Carbon dioxide	150–217	39	206	0.60 + 1.36	0.189	0.79

[a] T_{min}: see Sect. 4.2.4; T_{max}: at 0.1 MPa, except helium isotopes (0.115 and 0.2 MPa, respectively, near the critical point) and CO_2 (0.52 MPa at the triple point)

[b] For each cubic centimeter of bulb volume V_b filled with liquid at T_{min} (or solid: a maximum liquid–solid volume variation of 15 % can be expected). At T_{min}, p^{v} is small enough ($\approx$ 1 kPa) to neglect n^{v}. $\left[\equiv \rho T^{L}_{min}\right]$

[c] At $p(T_{max})$, for liquid fraction just vanishing and: (1) per liter of vapor space V_{room} at T_{room} (volume V_b and that V_t of the pressure line from T_b to T_{room} can be omitted for $V_b + V_t \leq \approx 10\,cm^3$). $[\equiv \rho_{gasSPT}$ (except for ^{3}He, ^{4}He and CO_2) $= 0.0415 \pm 0.0002$ mol L^{-1}]; (2) per cubic centimeter of bulb volume at T_{max} and for $V_t = 5\,cm^3$ of pressure line, assuming a quadratic temperature distribution, and $V_{room} = 0$ $\left[\rho_t = \rho T^{V}_{max} + \rho\overline{T_t}$ where $\overline{T_t} = T_{max} + \frac{1}{4}(T_{room} - T_{max})\right]$

higher than 0.1 MPa if the bulb is filled with more than 1 cm^3 of liquid. It should also be noted that the term "vapor space" has an obviously different meaning from "dead volume" in a gas thermometer.

It is necessary that *all* of the liquid phase remain in the thermometer bulb where the temperature T is intended to be measured, otherwise pressure values will be altered. This will be further discussed later in this chapter. The most critical effect is the so-called "cold spot," a zone outside the bulb of the thermometer wall where the temperature is *lower* than that of the bulb. This cold surface exerts an extremely *effective* pumping action on the liquid in the bulb, since pressure always tends to equilibrate at a value corresponding to the lowest (wall) temperature, and since the large change in volume due to condensation at the cold spot causes a steady vapor flow. The mass flow, i.e., the mass of liquid transported, is very large, when compared with that obtained by a pumping action from room temperature, since the low-temperature density is much higher and the vapor flow takes place inside a much shorter tube. Even when mass transfer is very small, pressure alteration due to "cold spots" has very serious consequences in the measurement accuracy (see Sect. 4.2.1.2).

4.2 Influence of Technical Parameters

A vapor-pressure thermometer is constructed of a bulb, where the temperature is measured, and a manometer, connected to the bulb with a tube. In most cases, when the manometric gas is different from the thermometric substance, and when the high purity of the latter must be preserved, a diaphragm differential pressure transducer is used to separate the two gas circuits. This most common case will be treated in Sect. 4.2.1. A connecting tube is not necessary when the manometer is directly fitted to the thermometer bulb. This less common configuration will be discussed in Sect. 4.2.3.

As purity requirements are as stringent as those for the realization of triple points, from the standpoint of reliability and simplicity one should consider the advantage of using a sealed device also for a vapor-pressure thermometer. The special problems arising, in this case, for pressure measurements are discussed in Sect. 4.2.2.

Finally, the extension of vapor-pressure measurements to the solidified substance, in order to obtain lower temperatures, is introduced in Sect. 4.2.5.

The specific problems involved in the implementation of an accurate vapor-pressure thermometer with helium isotopes will be fully treated in Sect. 4.3.

4.2.1 Thermometer with Gauge for Pressure Measurement at Room Temperature

The layout of a vapor-pressure thermometer of this type is illustrated in Fig. 4.7; the lower part is the same as that of the apparatus of Fig. 2.13 and some features are similar to those in Fig. 2.15. Very often in the past the tube connecting the bulb to the manometer was designed to pass simply through the cryostat structure, so that the thermometer was integral with the cryostat. However, the thermometer does not necessarily require a dedicated cryostat and therefore the cryostat will not be shown. The thermometer can be adapted to any cryostat of the calorimetric type, provided that the connecting pressure tube is fitted into a reentrant well of the cryostat and has access to room temperature, similar to the design discussed for the gas thermometer (see also Chap. 6 for cryostats).

Figure 4.7 can also be compared with Fig. 3.6 that illustrates a gas thermometer. Even though both units appear to be similar their design parameters are substantially different, as they play a very different role in the accuracy of the thermometer.

4.2.1.1 Thermometer Volume

The thermometer volume is irrelevant within a wide range of values with respect to both the bulb volume V_b and the total volume $V = V_b + V_t + V_r$, where V_t is the volume up to room temperature of the connecting tube and V_r is the room-temperature volume. Let us recall also that $V = V^L + V^V$ and that the relation $0 < V^L < V_b$ must

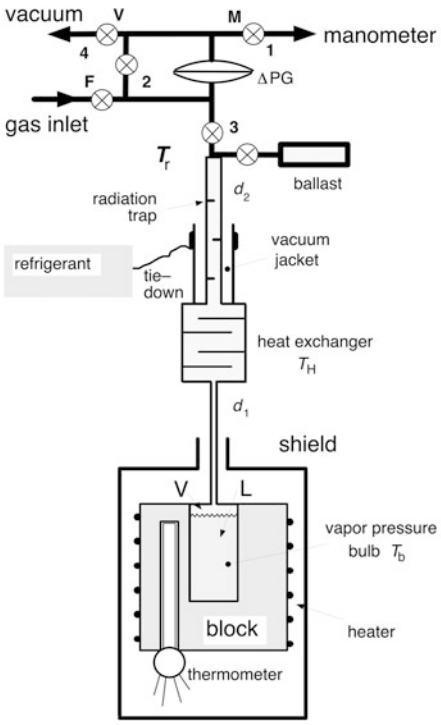

Fig. 4.7 Layout of a typical vapor-pressure thermometer. *DPG* differential pressure gauge

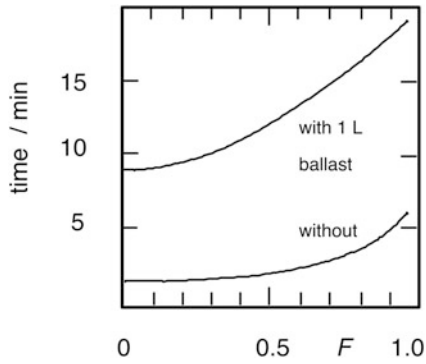

Fig. 4.8 Time constant dependence on vapor volume (argon at the triple point)

apply. Therefore, $V^{\mathrm{V}} = V_{\mathrm{b}}^{\mathrm{V}} + V_{\mathrm{t}} + V_{\mathrm{r}}$. A large value of V^{L} or in the ratio $r^* = V^{\mathrm{V}}/V^{\mathrm{L}}$ only affects the thermal time constant of the instrument (see example in Fig. 4.8).

The larger the bulb volume, the easier temperature gradients will appear in the volume and the slower they will vanish. In the case of a large total volume, every temperature variation requires a large change in vapor mass m^{V}, i.e., a large amount of heat will be involved in condensation or evaporation. In both cases, thermal exchanges with the environment will become more and more difficult to control. Conversely, recall that in a gas thermometer $(V_{\mathrm{t}} + V_{\mathrm{r}})/V_{\mathrm{b}}$ must be as small as possible

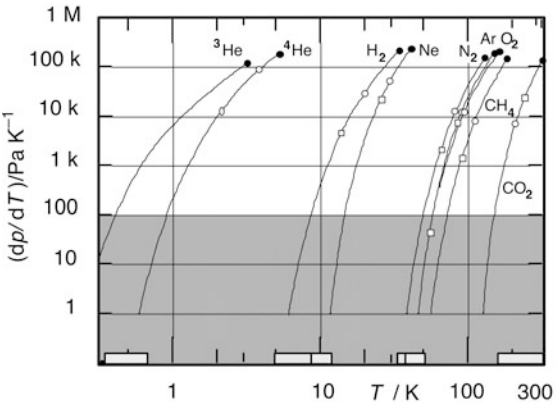

Fig. 4.9 Sensitivity dp/dT of vapor-pressure thermometry for selected gases—compare with Fig. 4.1 (for quantitative data, see Appendix C)

and that the knowledge of the exact values of the volumes V_b, V_t,and V_r and of the mass of substance contained in them under any experimental condition is also a very critical factor.

Therefore, in vapor-pressure thermometry the bulb, which must be massive to ensure temperature uniformity, does not require a large volume V_b, as is necessary in gas thermometry where the effect of the dead volume must be minimized. Instead of 1 L, the typical size for the bulb is a few cubic centimeters. See Sect. 4.3.2 for special problems with helium, particularly in connection with correction for the hydrostatic temperature gradients in the liquid (Sect. 2.3.2.2).

Accordingly, the volume of the connecting tube V_t is insignificant to a large extent, and the tube need not be a "capillary," as is required for a gas thermometer. The diameter d_2 can then be several millimeters large and, if necessary, be widened in steps up to several centimeters, according to the density decrease, in order to limit the effect of thermomolecular pressure difference. An upper value for V_t is mostly a matter of convenience, or can be determined by the need to limit thermal exchange by convection, as will be discussed later.

Finally, no special low-internal-volume pressure diaphragm gauges are necessary, nor are special constant-volume valves to keep V_r small and constant.

4.2.1.2 Pressure Measurement

The general problems involved in accurate pressure measurements with diaphragm gauges and with manometers are treated in Part II. Pressure-measurement accuracy requirements increase with decreasing temperature, because the thermometer sensitivity quickly decreases. Figure 4.9 shows, for the same gases of Fig. 4.1, the dependence of sensitivity dp/dT on temperature. The upper limit of the thermometer range is set by the maximum pressure that the manometer can measure, or by the value of the critical pressure (always less than 10 MPa). The lower limit, on the contrary, is set by the absolute measurement uncertainty of the manometer, as sensitivity decreases with pressure (though *relative* sensitivity may increase). Of course, a

lower-range manometer could be used for this purpose, but a lower limit for *absolute* uncertainty is generally set at about 0.1 Pa, at best, by other unavoidable factors (see below).

Let us assume that the gas system is evacuated as carefully as practical, and that an "empty-cell" experiment is performed. Even considering the cryopumping effect of the cold surfaces (especially at helium temperatures), and considering, on the other hand, that the system also extends to room temperature and that it is made of narrow, long tubes, which are not—and cannot be—baked at high temperature, the "zero" pressure manometer reading will hardly be better than 0.1 Pa for *long-term* and under *static vacuum* conditions. This is the actual lower absolute pressure limit set by system outgassing, irrespective of the manometer sensitivity. When the thermometric gas is let in, the situation may be made even worse by volatile impurities (see Sect. 4.1.1), the presence of which can be checked (though not always easily) by lowering the temperature sufficiently so that the vapor pressure of the pure substance is itself lower than 0.1 Pa.

Compared with the sensitivity of a gas thermometer, that of a vapor-pressure thermometer at any temperature is higher by a factor of two, at least, as explained in Sect. 3.1.1.1 (Table 3.3).

Some precautions are required in the operation of the by-pass valve system (for a general introduction to the use of differential pressure transducers, see Sect. 8.3). The procedure requires closing valves (M) and (3) *before* opening the by-pass valve (2); then, to avoid contamination, completely evacuating through valve (V) the trapped mixture of manometric gas and of thermometric substance, before reopening valve (3). Then the tubes between valves (3), (2), and (F) will be refilled with vapor obtained from evaporation of some of the liquid. This evaporation will produce a thermal transient at the end of the diaphragm-zero calibration procedure, with a sudden drop in temperature, from which it will only slowly recover. Time must be allowed for full recovery. It is not recommended to refill the tubes with fresh gas by opening (F) to restore the current pressure value before reopening (3), as this increases the risk of contamination, unless the vapor space to be refilled is large.

Any pumping effect on the cell will depress the value of the measured pressure. Mild "cold spots," which cannot be detected through temperature instability, are very insidious since they can produce a nearly stationary pressure depression. The same effect (and contamination in addition) would be caused by small leakages in the system.

To give an idea of how critical leakage is in a typical cell, Pavese (1978b) has determined that gas leaking into a mass spectrometer at a rate of 10^{-5} W (10^{-2} Pa L s^{-1}) produced a pressure change $\Delta p = -25$ Pa in oxygen maintained at a $p_{tp} = 146$ Pa. Therefore, a pressure accuracy of 0.1 Pa required that these effects be equivalent to less than 10^{-7} W (10^{-4} Pa L s^{-1}).

4.2.1.3 Pressure Corrections

The temperature value is obtained from a $p = f(T)$ relationship such as Eqs. 4.1 or 4.2 (see also Sect. 4.3.1), where p is the pressure value *at the liquid*. The pressure

value p^* measured with the room-temperature manometer is different from p, as fully discussed in Sect. 3.1.2.2. In vapor-pressure thermometry, the measuring line, extending from the bulb to the manometer at room temperature, plays the same role and involves all the same problems as discussed in that chapter. However, the line parameters can be optimized more satisfactorily and more easily, as there is no conflict between design requirements as in gas thermometry.

The reason is that there is no "dead volume" to be minimized and consequently the diameter of the connecting tube can be large enough to reduce the uncertainty due to the thermomolecular effect.

The magnitude of the *aerostatic correction*, conversely, remains unchanged with respect to gas thermometry, as it depends only on the difference in elevation between the liquid–vapor interface and the mercury surface (or membrane) of the manometer, and on the *vertical temperaturedistribution* in the vapor column. Most of the uncertainty in the aerostatic correction comes from the contribution of the latter. The problems related to its calculation or to measurement have already been discussed in Chap. 3 under the section "Corrections for the Bulb Pressure p_b " and Sect. 3.3.1.2. To reduce this correction, both in size and uncertainty, the nonisothermal portions of the connecting tube can be placed horizontally, whereas the vertical portions are kept isothermal (e.g., using copper tubes or copper cladding). In gas thermometers, this simple arrangement is often impractical since it would increase tube length and thus correspondingly the dead volume.

4.2.1.4 Thermal Problems

The upper limit to the diameter of the connecting tube is set only by the thermal problems connected with the vapor column above the bulb (at T_b), which extends up to the manometer at room temperature T_r.

With reference to Fig. 4.6, this tube must be thermally tied down at a point, to prevent the heat flowing from room temperature from reaching the bulb, which must remain under the best possible adiabatic conditions. The usual anchoring to the refrigerant temperature $T_{ref,r} < T_b$ *cannot* be used in this case, as it would produce a cold spot. The only way to intercept the heat (transmitted by *both* the tube *and* the gas in it, and by the vacuum jacket that *must* surround the pressure tube to avoid cold spots) is to use a heat exchanger kept at a temperature $T_H > Tv$. Actually, T_H must be only *slightly* higher than T_b, otherwise the surface of the liquid in the bulb may become overheated and the vapor pressure will be higher than correct. The larger the tube diameter d_1, the larger this effect will be, especially at temperatures below 30 K.

The design of the thermal tie-down for the heat exchanger (see Fig. 4.6) is not trivial, as it is necessary to dissipate into the refrigerant all the heat conveyed from ambient temperature, while at the same time avoiding that any point of it becomes colder than T_b, and keeping T_H as close as possible to T_b (ΔT as low as 0.01 K). Furthermore, this condition must apply also to the gas inside the heat exchanger,

despite some mass flow always occurring on changing T_b (or the temperature distribution in the vapor space). The mass transferred is proportional to the volume of the vapor space, i.e., to the square of the tube diameter, unless the room-temperature volume V_r is dominant. An amount of heat $\delta Q = \Delta_{vap} H\ \delta m^V$ is exchanged with the liquid surface $s^L = \frac{\pi}{4}(d_{ib})^2$ in the bulb. There is an advantage in having s^L as large as possible, to keep the specific energy exchange $\delta Q/s^L$ low, since the gradient δT^L established by heat flow in the liquid is proportional to the liquid surface. Therefore, δT^L is proportional to the square of the tube diameter. However, the main problem is not the heat flow mechanism, but the fact that, because of the poor thermal conductivity of the liquid, the heat exchanged is produced only by the enthalpy of evaporation of a thin layer of liquid with a thickness δh

$$dT^L = dQ/m^L c_p = -\Delta_{vap} H \delta m^V/(\rho^L s^L dh c_p), \tag{4.10}$$

where the negative sign indicates that the temperature decreases during evaporation. Therefore, δT^L is again inversely proportional to the surface of the liquid and proportional to the square of the connecting tube diameter.

4.2.2 Use of Sealed Cells for Vapor-Pressure Measurements

Sealed vapor-pressure thermometers are the most common in the industrial applications of this type of thermometers. In cryogenics they are most often used filled with helium, but not for medium–high accuracy.

However, the technique of sealing permanently the thermometric substance in a cell described in Sect. 2.4.1, thus eliminating handling problems, is the best for preserving the substance purity in time, which is a critical factor also in vapor-pressure thermometry.

The basic difference of a sealed vapor-pressure thermometer with respect to a sealed cell for triple-point temperature measurements is that pressure must be measured. Unless a cryogenic pressure transducer is used (see next section), only the long-stem type of cell (Sect. 2.4.1.1) can be used, in which the vapor space extends up to room temperature. Such a cell, which is shown in one of its configurations in Fig. 2.13, still is constructed as in Fig. 4.6. Only few considerations must be added:

(a) After the first filling, valve (F) is kept closed (or the tube pinched off). The cell is connected through valve (M) to a manometer during measurements.
(b) Operation of the by-pass valve system is more critical. The procedure described in Sect. 4.2.1.3, which must be followed to check the pressure-transducer zero, produces a loss of a (small) amount of thermometric substance at each operation. Therefore, checks in a sealed cell must be kept as few as possible. With most substances, when the vapor pressure at the refrigerant temperature is lower than 0.01 Pa, the by-pass valve (2) could even be eliminated, since simply lowering enough the temperature of the bulb allows checking the zero of the diaphragm.

However, some substances, namely argon, nitrogen,[3] and helium isotopes, do not allow the use of this procedure.

(c) In a sealed device at room temperature, the pressure is generally very high, owing to the much lower density of the substance (see Table 2.4), requiring heavy walls of the connecting tube and the use of a high-pressure valve for (3). However, pressure can be kept below 0.5 MPa by adding a ≈ 1 L ballast volume, as shown in Fig. 4.6; it is convenient to isolate this volume with a valve after condensation of the gas in the bulb, in order to avoid a large increase in the room-temperature vapor volume V_r (see Sect. 4.2.1.1).

A common criticism to a vapor-pressure-sealed device is that it prevents verification of the sample purity by the method of the vapor-volume change. With the aforementioned ballast volume, this becomes possible. However, it is *not* necessary, as verification must obviously be made *before* sealing the device, by means of a volume-changing device external to valve (F). Only after purity is proved satisfactory, is the cell to be sealed, thus permanently preserving the verified purity level. Anyway, the ballast volume can be useful for subsequent purity checks.

Each sealed cell reproduces a temperature *scale* in full, and, in addition, incorporates a high-quality fixed point, the triple point (with the obvious exception of the helium isotopes). As a set of cells can easily be made interchangeable in the same cryostat, the problem of each substance performing only over a narrow temperature range is alleviated.

4.2.3 Thermometer with Gauge for Pressure Measurement at Low Temperature

This section is equivalent to Sect. 3.1.4 in the chapter on gas thermometry, as also a design of this type requires a cryogenic pressure transducer (one of those described in Sect. 8.4). Let us refer to Fig. 3.9, which is reproduced here as Fig. 4.10 for convenience.

Essentially, all considerations made in Sect. 3.1.4 about the pressure transducer also apply in the case of vapor-pressure thermometers, of both the conventional and sealed types, with few additional considerations. The use of a differential cryogenic transducer in conventional vapor-pressure thermometry has no real advantage, as the connecting tube from low to room temperature is never a critical element as it is in gas thermometry. Besides, in a sealed device incorporating a cryogenic pressure transducer necessarily the room-temperature pressure is very high (much higher than in a sealed gas thermometer), because the cell volume is small. Therefore, this design requires a high-quality pressure transducer having, at the same time, the capability of withstanding pressures up to 2–20 MPa without calibration shift—a very difficult demand to meet. On the other hand, when the cell includes a high-quality calibration

[3] When solid nitrogen is used also as a refrigerant, allowing a minimum temperature of 45–50 K.

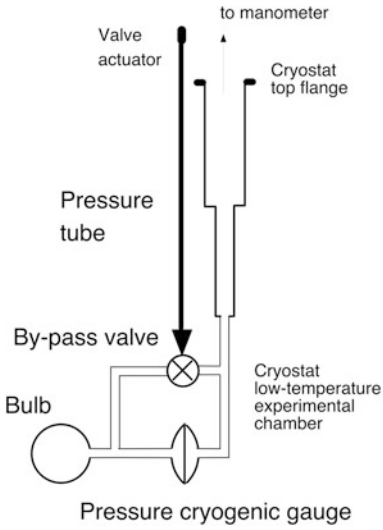

Fig. 4.10 General layout of a vapor-pressure thermometer using a cryogenic pressure transducer. (See also Sect. 3.1.3, Fig. 3.9)

point, such as the triple point (which is not available in the gas-thermometer cell),[4] the pressure transducer could easily be recalibrated in situ. Alternatively, a cryogenic filling valve (V) could be used, but the device would not be self-contained anymore, and the most convenient feature would be lost.

4.2.4 Liquid–Vapor Versus Solid–Vapor Equilibria

As already discussed in connection with the solid-to-solid transitions, thermal problems are much more critical with the solid phase, when no liquid is present, because of the very poor thermal characteristics of the solid phase. It is therefore comparatively much more difficult to obtain true thermal equilibrium, and, consequently to obtain accurate values for vapor pressures of the solid–vapor interface.

However, this is not impossible, and, with some substances, the extension of vapor-pressure measurements down to solid–vapor equilibrium appreciably extends the range, and enhances the usefulness, of a vapor-pressure thermometer. This extension is possible, in particular, when the triple-point pressure is high, e.g., with CO_2, Ar, N_2, Ne, and *e*-H_2 (Fig. 4.1). This extension is also the only way allowing temperature scales based on this type of thermometry to cover certain temperature intervals.

(9–14 K) *e*-H_2 This extension is the most important, as 13.8033 K is the lowest available triple point and no other vapor-pressure scale is available above 5.2 K (^{4}He critical point). The closest thermometric fixed point is the superconducting transition

[4] It can include only a dew point, which is only a *slope* discontinuity (see Sect. 3.3).

of niobium (9.2885 K). At 9 K, e-H_2 has a pressure of ≈ 75 Pa with a sensitivity that is still sufficient for many purposes, i.e., $dp/dT \approx 100$ Pa K^{-1} (at 10 K, $p \approx 260$ Pa and $dp/dT = 315$ Pa K^{-1}).

(19–25 K) Ne An extension of the neon vapor-pressure thermometer is the only way that an overlap can be obtained with the e-H_2 vapor-pressure thermometer, when the latter can only use a 0.1 MPa full-scale manometer (corresponding to ≈ 20 K). Both the absolute pressure value (1.9 kPa) and the sensitivity (1.4 kPa K^{-1}) at 19 K are still high. Sensitivity is ≈ 100 Pa K^{-1} and pressure 390 Pa at 17 K.

(50–63 K) N_2 Above 27 K (where neon vapor pressure is ≈ 0.1 MPa), there is another possible gap in the use of vapor-pressure thermometers, which cannot be filled by any suitable substance. Nitrogen is the only one that can approach neon: at 60 K its vapor pressure is 6.35 kPa and sensitivity 1 kPa K^{-1}; at 50 K pressure is 410 Pa and sensitivity 135 Pa K^{-1}.

(70–84 K) Ar Argon is the highest purity gas that substantially overlaps nitrogen (≈ 77 K at ≈ 0.1 MPa). Its triple-point pressure is quite high (69 kPa) and vapor pressure decreases slowly with temperature, so that a 1 kPa K^{-1} sensitivity is reached at about 70 K. For many uses, argon can still be considered down to 58 K, where the pressure is 420 Pa and the sensitivity about 120 Pa K^{-1}.

(150–217 K) CO_2 Above ≈ 100 K, there is a lack of simple-molecule substances that can be used for vapor-pressure thermometry below 0.1 MPa, as the two noble gases, Kr and Xe (see Table 4.3) are expensive isotopic mixtures, which in addition have distillation problems. Methane can be used up to ≈ 180 K only by measuring higher pressures (up to 3.2 MPa)—or CF_4 up to ≈ 179 K (and to 0.5 MPa; Lobo and Staveley 1979). Above that temperature, substances that are liquid at room temperature are generally used (e.g., dimethyl ether). Solid carbon dioxide, the pressure of whose triple point is the highest (0.52 MPa), can be considered as well. At 194.7 K, its vapor pressure is 0.1 MPa; at 170 K pressure is 9.95 kPa and sensitivity 1.1 kPa K^{-1}, and at 150 K pressure is 843 Pa and sensitivity 120 Pa K^{-1}.

4.3 Realization of Vapor-Pressure Temperature Scales

The main shortcoming in the use of vapor pressures as temperature scales is the very narrow temperature interval in which each substance shows a sufficient sensitivity (which sets the lower limit) and in which the pressure can be measured with commonly available means (which set the upper limit). It is even difficult or impossible to find a suitable substance in some temperature intervals, as Figs. 4.1 and 4.9 clearly show. There is a gap between 5.2 K (upper limit for ^{4}He) and the minimum temperature where solid e-H_2 can be used, ≈ 9 K. Solid neon must be used to join hydrogen unless the latter is used up to a pressure of ≈ 3 MPa, to reach the temperature of the neon triple point at 24.6 K. Further on, no substance is available to fill the gap between neon, even if used up to the critical point (44 K and 2.6 MPa), and the lowest

temperature for which the use of nitrogen can be envisaged, ≈ 50 K. Above 90 K, pressures higher than 0.1 MPa must be measured (using argon or methane) in order to join with the vapor pressure of another substance, such as ethane at ≈ 110 K, whose 0.1 MPa boiling point is at ≈ 185 K. Above this temperature, only propane (which can be used from ≈ 130 K) is available to join liquid carbon dioxide at 216 K, unless high pressures are to be measured. In this respect, methane can be used up to ≈ 180 K (1.3 MPa), or CF_4 up to ≈ 179 K (0.5 MPa; Lobo and Staveley 1979). Alternatively, solid carbon dioxide can be used down to 170 K (9.95 kPa, sensitivity 1.1 kPa K^{-1}) or even down to 150 K (843 Pa, sensitivity 120 Pa K^{-1}). For higher temperatures, in general, substances that are liquid at room temperatures are used.

Since vapor-pressure thermometry is semiempirical, an interpolating instrument is not defined, and only an equation is specified. Should some of its coefficients be not defined, their value is to be determined at an equal number of fixed points, in this way "calibrating" the specific apparatus used. If all of the coefficients are stipulated, fixed points are no longer necessary (Sect. 1.2.2.1). International bodies generally prefer the latter solution when they officially endorse a vapor-pressure scale. When no such an endorsement exists for a given substance (actually all substances except helium isotopes: see Sect. 4.3.2), the first concern for any user must be to select an equation suitable to represent the $p=f(T)$ relationship, where its *traceabilityis reliably established with sufficient accuracy*. This problem will be treated in Sect. 4.3.1.

The next concern for a laboratory (or an industry) desiring to use a vapor-pressure thermometer is how to design an apparatus convenient to use and ensuring the required accuracy level. The aim is *not* to realize an empirical scale, but to reproduce thermodynamic equilibrium states; therefore, nonequilibrium conditions or experimental artifacts must be avoided to affect the measurements within the stated uncertainty. The criteria and precautions deriving from the discussion in the former sections are the basis for such a design, irrespective of the accuracy level. Design can be less careful (e.g., lower substance purity) when lower accuracy is sufficient. Some specific technical implementations, especially for the helium scales, will be described in Sect. 4.3.2.

4.3.1 Equations for Vapor Pressure

For liquid–vapor equilibrium, the semiempirical Eq. (4.2) has been used often supplemented with a linear term

$$\ln p = A + BT + C/T + D\ln T. \tag{4.11}$$

This equation is as well often found simplified, especially for the solid–vapor equilibria, by suppressing the logarithmic term. Sometimes a quadratic term in T is also added (e.g., in the equations recommended in the text of IPTS-68), especially when the range has to be extended to near the critical point. However, these additions cause the model to switch from a semiempirical to a purely empirical model, a field where a wide set of mathematical tools is available for experimental data fitting. Actually, the literature abounds with far more papers on data fitting than on new experimental data.

Very few of the experimental papers specify the temperature scale. The lack of such an indication does not mean, in general, that the temperature values are obtained *directly* on the thermodynamic scale. Most often, practical thermometers calibrated on an empirical scale are used for measurements. Very seldom an explicit reference to any version of the International Scale is given, so that traceability to thermodynamic values is questionable. The equations derived from such papers are themselves affected by the same lack of traceability.

Therefore, when vapor-pressure measurements are used in thermometry, it is advisable to use those equations that have been subjected to international peer review, even in the absence of a formal endorsement. This type of review has been performed specifically for several gases by the Comité Consultatif de Thermométrie (CCT), and more in general by IUPAC.

Prior to the 1975 revision of the IPTS-68, the CCT provided a number of vapor-pressure equations *in* the text of the scale. After 1975, including the International Temperature Scale of 1990 (ITS-90), this list has become a separate publication (the last version is in Bedford et al. 1984, subsequently updated on the ITS-90 in Bedford et al. 1996), prepared by the Working Group 2 of CCT on Secondary Thermometry and issued by BIPM. This indicates that, until these equations are part of the definition of the scale, the international body does not endorse them, though they are, indeed, "recommended." They concern liquid–vapor pressures of e-H_2, Ne, N_2, Ar, and O_2, and solid–vapor pressures of Ne, N_2, and Ar. Until these equations are recalculated for the ITS-90, the temperature values for the latter can *only* be obtained by adding to the temperatures calculated according the IPTS-68 the tabulated differences $(T_{90} - T_{68})$ reported in Table A.6.

For the liquid–vapor pressure values of e-H_2 alone this procedure could not, in principle, be followed, as the ITS-90 definition puts several constraints on the p–T relationship. In fact, it makes use of two points from the e-H_2 vapor pressure as defining points in the range where the platinum resistance thermometer is used. For these two points, the values of both pressure p *and* the first derivative $\mathrm{d}p/\mathrm{d}T$ are specified:

T_{90}/K	p/kPa	$\mathrm{d}p/\mathrm{d}T$/(kPa K^{-1})
17.035	33.321 3	13.320
20.27	101.292	30.000

These are four conditions, which, along with the value of the temperature at the triple point, would overdetermine, for example, an equation such as Eq. (4.12a). Actually, in Bedford et al. (1984, 1996) nine coefficients are used.

CCT equations are reported in Appendix D and tabulated in Appendix C; they allow an accuracy of 1–2 mK in the range between the triple and the normal boiling points, with liquids, and from the triple point down to the indicated temperature with solids.

IUPAC issued a book on "recommended reference materials for the realization of physicochemical properties" (IUPAC 1987), which also reports recommendations on vapor-pressure equations for gaseous substances above 100 K, with reference to a

series of "IUPAC International Thermodynamic Tables of the Fluid State," covering also, as far as the matter of interest here is concerned—in addition to the CCT recommendations—CO_2 (IUPAC 1976) and CH_4 (IUPAC 1978). These equations are also reported in Appendix D and tabulated in Appendix C.

For vapor-pressure equations of other substances not included in these recommendations, well-established models are reported in Appendix C using reference data. Among these models, worth mentioning specifically is Zhokhovskii's (1975, 1990) equation. Zhokhovskii showed that for an extremely wide number of substances the equilibrium vapor pressure over the saturated liquid, or over the saturated solid, could be represented in a wide temperature range, with limits T_0 and T_1, by the equation

$$p = \left\{ p_0^{1-c} + \frac{\left(p_1^{1-c} - p_0^{1-c}\right)\left[1 - \left(\frac{T_0}{T}\right)^n\right]}{\left[1 - \left(\frac{T_0}{T_1}\right)^n\right]} \right\}^{\frac{1}{1-c}}, \tag{4.12a}$$

where p_0 and p_1 are the vapor pressures at the temperatures T_0 and T_1, n and c are constants that are determined by fitting the equation to experimental p–T data in the range T_0 to T_1. Equation 4.9a has no real thermodynamic basis but it can be derived by integrating Clapeyron's equation $\mathrm{d}p/\mathrm{d}T = \Delta_{\mathrm{vap}}H_m n/T\ \delta V$, where $\Delta_{\mathrm{vap}}H_m$ is the molar heat of vaporization and $\delta V = (V^{\mathrm{V}} - V^{\mathrm{L}})$ is the difference between the vapor and liquid volumes, assuming

$$\frac{\Delta_{\mathrm{vap}}H_m}{\delta V} = \frac{\Delta_{\mathrm{vap}}H_{m,0\ \mathrm{K}}}{(\Delta V)_{0\ \mathrm{K}}}\left(\frac{T_0}{T}\right)^n\left(\frac{p}{p_0}\right)^n. \tag{4.13a}$$

The assumption made in Eq. (4.12a) can perhaps be elucidated by reminding that if $\Delta_{\mathrm{vap}}H_m$ is independent of T and $\Delta V = V^{\mathrm{V}} = nRT/p$ it is exact with $n = 1$ and $c = 1$.

With this equation, with only two free coefficients, Zhokhovskii was able to fit vapor–liquid equilibrium data in a pressure range often of several decades (of pressure values), from the triple point ($T_0 = T_{\mathrm{tp}}$; $p_0 = p_{\mathrm{tp}}$) up to near the critical point ($T_1 = T_{\mathrm{c}}$; $p_1 = p_{\mathrm{c}}$), to an accuracy essentially that of the original data (up to better than $\pm$ 1 mK). The equation can also be used for vapor–solid equilibria, in this case the upper end being the triple point and the lower end being the lowest data. Of the two parameters, the value of c is close to one for most substances, while the value of n is found to be specific for each substance.

Another model with only two free coefficients, a and b, recently proposed in connection with helium vapor pressure, requires an integral equation (Elsner 1990)

$$\ln p = \ln T + \ln p_{\mathrm{c}} - \ln T_{\mathrm{c}} \int_{\ln T}^{\ln T_c} \frac{1}{e^{y(\ln T)}}\, \mathrm{d}\ln T \tag{4.12b}$$

with

$$y = \ln T - \ln\frac{5}{2} - a \exp\left[\frac{\ln T - \ln T_c}{b}\right]. \tag{4.13b}$$

However, this equation will not be considered here: e.g., its application to ^{3}He vapor pressure gives less satisfactory results (maximum deviation of the fit from +1.5 mK to −2.8 mK in the range from 0.2 K to the critical point) than Zhokhovskii's (see next section).

Most of the equations reported in Appendix C are in T_{90}, having been recomputed in Pavese (1993) in ITS-90 (using a nonlinear correction) and using the two equations of Rusby (1991) for the difference $T_{90} - T_{68}$ (see Appendix A), but joining at ≈ 63 K instead of ≈ 80 K.

4.3.2 Helium Vapor Pressure

Helium vapor-pressure thermometry will be considered in more detail, because of its widespread use and of the high accuracy that it can achieve. International bodies endorsed it since the turn of the 1950s (T_{58} and T_{62} Scales; a ^{4}He scale actually since 1948). In the ITS-90, ^{3}He and ^{4}He vapor-pressures equations constituted the only definition below 3 K before the definition of the Provisional Low Temperature Scale of 2000 (PLTS-2000, see BIPM web site and Sect. 4.3.2.3), and must also be used for the determination of the lower fixed point of the ICVGT. For ^{3}He and ^{4}He vapor-pressures equations proposed more recently, see Durieux and Reesing (1997).

Many NMIs have realized the parts of the ITS-90 defined by means of ^{4}He, or both ^{4}He and ^{3}He, vapor pressure (Meyer and Reilly 1996; De Groot et al. 1997; Steele 1997; Hill 2002; Shimazaki and Tamura 2003, 2005; Engert et al. 2003, 2007; Sparasci et al. 2011a). Some of these realizations have been intercompared in CCT-K1 (see Chap. 11).

Besides, an accurate measurement of helium vapor pressure involves specific precautions, especially when superfluid ^{4}He is measured below 2.1768 K and when ^{3}He is measured below 1 K. Only the basic information will be given here. The reader is directed to the "*Supplementary Information for the ITS-90*" (BIPM 1990a), to the "*Techniques for Approximating the ITS-90*" (Bedford et al. 1990), and to the relevant literature cited in the following subsections.

4.3.2.1 ^{3}He Scales

Former T_{62}: Scale Definition

Before being included in the ITS-90, in 1962 a *p–T* relationship for ^{4}He had been established by international agreement (T_{62} Scale).

The table of values defining T_{62} was based on measurements by Sydoriak (1964), consisting of an intercomparison with the ^{4}He Scale T_{58}, then already well established, between 1.0 K and 5.2 K (a table of values was available down to 0.5 K). Since no thermodynamic temperature measurements were available below 0.9 K, a *theoretical* calculation using thermodynamic data formed the basis of the T_{62} from 0.9 K down to 0.2 K. Later, evidence of inconsistency with respect to thermodynamic

Table 4.4 Differences $(T_{62} - T_{90})$ and $(T_{58} - T_{90})$

T_{90}/K	ΔT_{vap}/mK	T_{90}/K	ΔT_{vap}/mK	T_{90}/K	ΔT_{58}/mK
0.5	− 1.9	1.8	− 3.9	3.2	− 6.6
0.6	− 2.1	2.0	− 4.1	3.4	− 6.8
0.8	− 2.5	2.2	− 4.4	3.6	− 7.0
1.0	− 2.9	2.4	− 4.9	3.8	− 7.0
1.2	− 3.2	2.6	− 5.4	4.0	− 7.1
1.4	− 3.5	2.8	− 5.9	4.2	− 7.1
1.6	− 3.7	3.0	− 6.3	4.5	− 7.1
		3.2	− 6.6	5.0	− 7.1

T_{vap} denotes the average of T_{58} and T_{62} up to 3.2 K

temperature accumulated. The T_{58} Scale itself was found to deviate from it roughly αT below 4.2 K where the deviation amounted to about −8 mK. On the basis of a broad international intercomparison of the available realizations of thermodynamic scales (Besley and Kemp 1977), the 1976 Provisional Scale EPT-76 took account of the *deviations* of the T_{62} from the thermodynamic temperature. In particular, in the range below 2 K, where no gas thermometry results were available, magnetic scales were considered. Below 1 K, cerium magnesium nitrate (CMN) was used as a paramagnetic salt down to 0.5 K. The parameters of these semiempirical Scales (see Sect. 1.2.2.1) were adjusted so as to smoothly join the ^{4}He vapor-pressure scale. In 1983, on the basis of new vapor-pressure measurements (El Samahy 1979; Rusby and Swenson 1980), a new p–T relationship was established for the EPT-76, and the T_{62} Scale was fully superseded.

It is interesting to note that, by application of Zhokhovskii's Eq. (4.12a) to the T_{62} data, it is impossible to match with any reasonable accuracy the T_{62} definition table for ^{3}He over the *whole* 0.3–3.3 K range. Only by fitting two separate subranges, joining at (0.9 ± 0.1) K is it possible to obtain $u = 0.2$ mK (with $c = 0.952\,888$, $n = 0.345\,556$; maximum deviation 0.17 mK) in the lower 0.3–0.9 K subrange, and $u = 1$ mK (with $c = 0.706\,538$, $n = -0.821\,269$; maximum deviation 2.1 mK) in the upper 0.9–3.3 K subrange (Zhokhovskii 1990; Durieux 1991). Since no phase transition occurs in ^{3}He over the entire temperature range, Zhokhovskii assumed a correlation of this occurrence with an inconsistency within the old T_{62} Scale above and below 0.9 K.

The ITS-90 is based on the previous experimental vapor-pressure data, whose thermodynamic accuracy is estimated to be ± 0.5 mK above 1 K and ± 1 mK at 0.5 K, making use of the entire set of thermodynamic temperature data available until 1989. The differences $(T_{62} - T_{90})$ are given in Table 4.4. The differences in ^{3}He vapor-pressure thermometry below 1 K with respect to thermodynamic scales (*magnetic thermometry*) are shown in Fig. 4.11a (Durieux et al. 1982).

Current T_{2006}: Scale Definition

The T_{2006} ^{3}He Scale has been realized at PTB In 2006: details of the realization can be found in Engers et al. (2007). Current differences $(T_{2006} - T_{90})$ between the scales PTB-2006 and ITS-90 are reported in Fig. 4.11b. Below 1 K the temperature scale T_{2006} coincides with the PLTS-2000, and is based on a thermodynamic

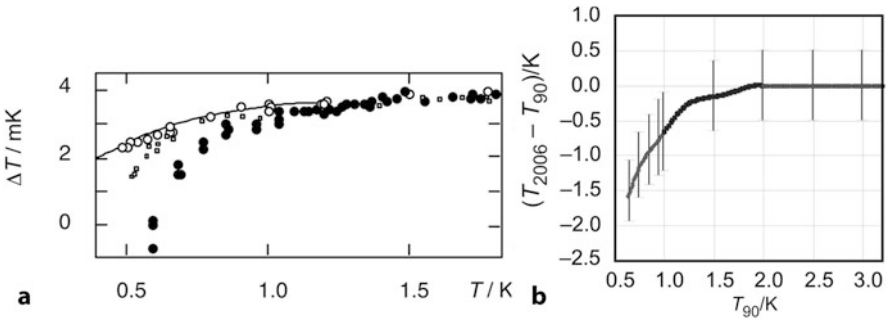

Fig. 4.11 **a** Errors in ^{3}He vapor-pressure thermometry below 1 K. *Baseline:* magnetic thermometry. (After Durieux et al. 1982). • 5-mm tube (Rusby and Swenson 1980); **O** 9-mm tube, □ 13-mm tube (El Samahy 1979). The *solid curve* is the thermodynamic extrapolation below 1 K of the vapor-pressure curve above 1 K at those dates. **b** Current difference ($T_{^3\mathrm{He}} - T_{90}$; Fischer et al. 2011): differences between the scales PTB-2006 and ITS-90 (after Engert et al. 1997). The temperature scale PTB 2006 is based on the PLTS-2000 (below 1 K), on a thermodynamic vapor-pressure relation (1.0–2.0 K); above 2.0 K the difference is equal to zero. See also Sect. 1.2.5., Table 1.5a

^{3}He vapor-pressure relation in the range1.0–2.0 K; above 2.0 K the difference is $(T_{2006} - T_{90}) := 0$. See also Sect. 1.2.5, Table 1.5a.

Specific Difficulties of the Realization

With both helium isotopes, a peculiar thermal stratification occurs in the liquid,[5] which makes the usual correction for the hydrostatic temperature gradient (see Sect. 2.3.2.2) incorrect:

(a) *Thermomolecular error*: The correction for the thermomolecular pressure effect (see Sect. 3.1.2.2 and Chap. 10) is critical below 1 K, as very low pressure values must be measured (20 Pa at 0.5 K). The magnitude of this correction was 4.5 mK at 0.9 K in Sydoriak et al. (1964); as large as 3.5 mK at 0.5 K in El Samahy (1979); 1 mK at 0.65 K in Rusby and Swenson (1980). The correction will be even larger and affected by a higher uncertainty than is normal with the use of an inappropriate tube material or diameter and by surface contamination. Corrections should thus be kept as small as possible by keeping the bore of the connecting tube as large as is practical.

(b) *Inappropriate bulb filling*: As a consequence of the above requirement, the vapor space volume V_V is large in respect of the cell volume V_C. Because of the high vapor density, at least up to the level of the heat exchanger (Fig. 4.7), the vapor mass m^V is so predominant over the liquid mass m^L that is relatively easy to overfill the bulb at low temperatures or, conversely, to evaporate all the liquid phase at high pressures (see Sect. 4.2.1.1). Therefore, a check that the derivative $\mathrm{d}p/\mathrm{d}T$ has approximately the correct value must always be made to be sure that

[5] Most of the studies having been carried out using ^{4}He, this phenomenon will be discussed in the next subsection.

there is a proper liquid–vapor interface. This check fails only near the critical point.

(c) *Thermal-acoustic oscillations*: In a closed tube connecting room to helium (or hydrogen) temperatures, thermal-acoustic oscillations can spontaneously take place when the pressure in it is higher than a few kilopascal (Wexter 1961; Ditmars and Furukawa 1965; Gu and Timmerhaus 1991b). The phenomenon has been thoroughly studied (Taconis et al. 1949; Kramers 1949; Rott and Angew 1969; Yazaki et al. 1979). It is important in cryogenic engineering to avoid its occurrence (Bannister 1966; Tward and Mason 1972), as such oscillations increase heat transfer to liquid helium by as much as 1,000 times the contribution due to gas thermal conductivity (this increase is clearly visible in laboratory when it occurs during liquid helium transfer). This effect is also important in helium vapor-pressure thermometry, as it alters the temperature distribution (though the aerostatic head correction is usually very small) and is a source of liquid–vapor interface overheating.

Vacuum jacketing of the pressure tube, necessary also to avoid cold spots, can prevent the occurrence of these oscillations; however, it must be recalled here that if the inner pressure tube is not thermally tied down (e.g., as shown in Fig. 4.7), it will transfer a substantial amount of heat down to the bulb. Should thermal oscillations occur, they can be damped by adjusting the room-temperature vapor volume V_r (which acts as an acoustic resonator), by inserting some cotton wool *in* the tube (but not in those portions where the diameter is important for thermomolecular correction), or by changing the cold-to-warm length ratio of the tube, or by using, when possible, a narrower tube (Gu and Timmerhaus 1991a).

4.3.2.2 ^{4}He Scales

Formerly T_{58}: Scale Definition

The literature on ^{4}He vapor-pressure scales is extremely extensive. Here it will be only briefly reviewed, while the reader is directed to specialized papers, such as (Durieux et al. 1982; Cataland et al. 1982). Figure 4.12 shows a comparison between the old ^{4}He Scales, which are discussed in Van Dijk and Durieux (1957).

In Eq. (4.1a), only the first three terms are significant at low temperatures, the residual contribution of the other three being equivalent to less than 5 mK below 1.5 K. Below this temperature, the accuracy of the theoretical calculation of the vapor pressure of ^{4}He is determined mainly by that of $\Delta_{vap}H_{m,0K}$, the molar enthalpy of vaporization at 0 K. The theoretical calculation below 1.6 K has been available with great accuracy since 1924 in a region where no thermodynamic temperature measurements were available for a long time (see Fig. 4.12).[6]

In fact, the ^{4}He gas thermometer cannot be used and accurate magnetic thermometry was not available until the end of the 1940s. The T_{58} Scale, in its lower part, relied on magnetic thermometry (defined by Eq. (1.22), where only C and A terms

[6] On the contrary, the 1929, 1932, and 1937 scales were empirical scales.

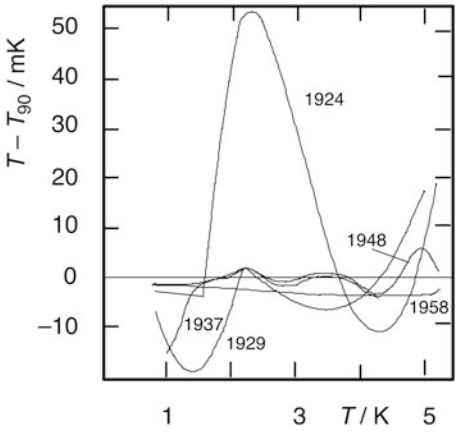

Fig. 4.12 Differences between old ^{4}He vapor-pressure scales. (After Durieux et al. 1982)

are considered). It was defined on the basis of the experimental data and laboratory scales available until 1958, which exhibited a scatter of 4 mK and were estimated to have an accuracy of ± 2 mK between 1 K and 4.5 K. However, later thermodynamic measurements showed with increasing evidence that T_{58} was deviating almost linearly from thermodynamic temperature, by as much as ≈ 7 mK at 4.2 K. In 1976, a provisional Scale (EPT-76) was assembled for the range below the IPTS-68 (with an overlap up to 30 K), down to 0.5 K. The differences between all the temperature scales then available were determined by means of a wide international intercomparison (Besley and Kemp 1977). In 1983, on the basis of new vapor-pressure measurements (El Samahy 1979; Rusby and Swenson 1980), a new p–T relationship was established for the EPT-76, which fully superseded T_{58}.

By application of Zhokhovskii's Eq. (4.12a) to T_{58} data, it is impossible to match with any reasonable accuracy the T_{58} definition table across the ^{4}He superfluid transition by using the same value of n, whereas, by fitting separately the subranges from 2.18 K to 5.2 K ($c = 0.966\,056$, $n = -1.036\,13$) and from 0.5 K to 2.18 K ($c = 0.983\,028$, $n = 0.580\,486$), one obtains $u = 1.0$ and 0.6 mK, respectively, for the two subranges.

The ITS-90 was based on the same experimental vapor-pressure data, whose thermodynamic accuracy is estimated to be of ± 0.5 mK, making use of the whole set of thermodynamic temperature data available until 1989. The differences $T_{58} - T_{90}$ are given in Table 4.4.

Thermodynamic calculations based on Eq. (4.1a) are, at present, accurate to within better than $(-0.1$ to $+0.2)$ mK up to about 2.5 K, then deviating to a maximum of $+0.8$ mK at ≈ 4 K.

Specific Difficulties of the Realization

In addition to some of the problems already discussed in connection with ^{3}He, there are specific difficulties with ^{4}He:

(a) *Normal liquid ^{4}He* (HeI, above 2.1768 K): The temperature gradient in normal liquid ^{4}He (important, e.g., in the realization of the lowest fixed point of an ICVGT—see Chap. 3) resulted different from that expected from the effect of the hydrostatic pressure increase with bath depth.[7]

(b) *Thermal gradient error*: Studies on the temperature distribution in a liquid bath have shown that it may be quite different in a glass or in a metal dewar (Plumb 1959; Crooks 1969). The temperature gradient with depth differs the more from the hydrostatic gradient the lower the bath temperature is; differences as large as 10 mK were found for a bath depth of 20 cm (Hoare and Zimmerman 1959; Swim 1960). At 4.2 K, at a few millimeters below the liquid surface temperatures 5 mK higher than that of the surface have been observed (Durieux 1960): consequently, if the temperature of an immersed body is deduced from the pressure in the vapor phase and accounted for only with the hydrostatic correction, large errors would arise. Such measurements are quite difficult, not very reproducible and dependent on the geometry of the experimental setup and on the evaporation rate. In conclusion, the depth temperature correction for a thermometer immersed in a liquid helium bath cannot be calculated reliably and, consequently, a small bulb should always be used, instead of a deep bath, for accurate vapor-pressure thermometry.

These conclusions are relevant in test procedures for the temperature correction of engineering properties, where the helium storage dewar itself is often directly used as a cryostat and the temperature value must be referred to that of helium boiling under one standard atmosphere (4.2221 K). In order to obtain the temperature value of the immersed test module, often atmospheric or dewar pressure (therefore a *bath* pressure) is measured with a pressure gauge and due to the high $\mathrm{d}p/\mathrm{d}T$ near 4.2 K with ^{4}He (≈ 95 Pa mK^{-1}), it is usually assumed easy to obtain millikelvin accuracy, which may not always be the case.

(c) *Superfluid ^{4}He* (HeII): As problems with superfluid helium are much more serious, the ^{4}He vapor-pressure thermometry below the λ-point should be considered quite specialized, and not be attempted unless it is actually impossible to use ^{3}He or other thermometry types. A full discussion of the problem, which remained unsolved for many years, can be found in Sydoriak and Sherman (1964). Only the basic practical conclusion will be reported here. The physical reason for the difficulties in a closed bulb is the superfluid film reflux with a consequent recondensation that produces a pressure drop, and a heat flux across the liquid-wall interface. A temperature jump there occurs owing to the Kapitza resistance (Kapitza 1941; Van Sciver 1986). The magnitude of this temperature jump is significant in the temperature region below a few kelvins, in the presence of an interface between dissimilar materials where electronic transport of heat does not contribute. Therefore, it is relevant also to ^{3}He vapor-pressure thermometry.

(d) *Errors due to superfluid film reflux*: There is a pressure difference Δp between the vapor-(bulk liquid) interface in the thermometric bulb and the location, at an

[7] Below the first 4 mm from the surface, the hydrostatic pressure gradient in ^{4}He is of 0.14 mK cm^{-1} at 4.2 K, of 0.27 mK cm^{-1} at 4.2 K, and of 1 mK cm^{-1} at 2.2 K.

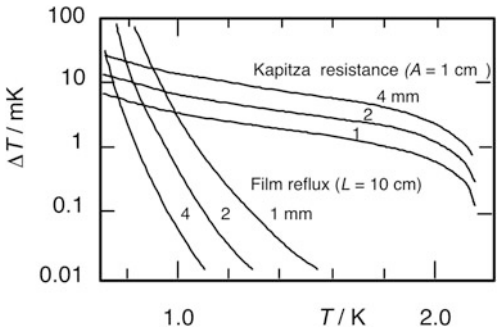

Fig. 4.13 Special problems with superfluid ^{4}He: film reflux and Kapitza effect corrections for different tube diameters. (After Sydoriak and Sherman 1964)

elevation h_f above the bulb, where the superfluid film, which climbs along the connecting tube walls, actually vaporizes (Sydoriak and Sherman 1964)

$$p\Delta p = 8[(aT + b)Th_f\dot{n}]/d^3. \tag{4.14}$$

Here $\dot{n}$ is the specific (per unit of tube circumference) molar film flow rate and d the tube diameter. The equivalent temperature error of Eq. (4.14) is shown in Fig. 4.13, for a *strictly* clean tube.

Conditions of low cleanliness (due to impurities, simply gases on the surface other than helium) can make the reflux to be higher by as much as 10 times, and the error as well. In addition, h_f depends very much on the tube pattern and on whether it is (vacuum) jacketed or not. Therefore, a correction for reflux is quite unreliable.

(e) *Error due to Kapitza resistance*: When a heat flux $\dot{Q}$ crosses a liquid–solid boundary, such as that between condensed helium and the wall of its container, there is, at temperatures low enough, an additional sizeable temperature jump ΔT_K because of the Kapitza effect. This effect depends on a phonon "mismatch" between the two materials, and consequently depends on both materials *actually* crossed by the heat flux (e.g., possible oxide films or molecules of other gases on the surface). It is therefore clear that a correction is again quite unreliable. The temperature dependence is given by Sydoriak and Sherman (1964)

$$\Delta T_K = k\dot{Q}/AT^n, \tag{4.15}$$

where A is the interface area crossed by the flux $\dot{Q}$. The coefficients k and n depend on the materials. For ^{4}He and copper, $n = 2$–3 and $k = 6$–21 in the 0.6–2.1 K range. The magnitude of this error is also shown in Fig. 4.13, being again a *minimum*, as impurities can increase it by a factor of more than 10. Equation 4.15 shows that the heat-flux density must be reduced, thus increasing the constant area A. Contrarily to normal ^{4}He, there is advantage in superfluid ^{4}He to use a *bath temperature*, i.e., to use a large cell—or a cell with a large exchange surface with the liquid.

These considerations indicate the necessity for a careful design and fabrication of a vapor-pressure thermometer to be used below 2.1768 K. A small orifice with a

sharp edge should be placed at the top of the cell to reduce film reflux. In this way, film evaporation will occur just above the orifice. Therefore, the related refrigeration effect will not affect the bulk liquid in the bulb, and the pressure drop will be small in the pumping line near the bulb, where vapor density is higher. A separate sensing tube for vapor-pressure measurement can be connected few centimeters (typically 4–5 cm) above the orifice to the pumping tube used to reduce the ^{4}He bath temperature.

4.3.2.3 ITS-90 Between 0.65 and 5.0 K and Deviations from Thermodynamic Temperature

The T_{58} and T_{62} scales were incorporated in the "*Provisional Temperature Scale 0.5–30 K*" of 1976 (EPT-76; BIPM 1979; Durieux et al. 1979), which was essentially a collection of recognized methods for realizing a temperature scale in that range, related to each other by means of tables of differences. In 1990, it has been replaced by the ITS-90 (see Appendix A), which starts at 0.65 K instead of at 0.5 K for two reasons. First, the existing experimental determinations begin diverging below 1 K, as already pointed out in Sect. 4.3.2.1; second, at 0.65 K the ^{3}He vapor pressure becomes 116 Pa and the thermometer sensitivity $\mathrm{d}p/\mathrm{d}T = 1.08$ kPa K^{-1}, which was considered the minimum acceptable.

The defining equations are purely empirical seventh- to ninth-order logarithmic polynomials with normalized arguments, in order to reduce to the minimum the number of significant digits required for an accurate computation of temperature values. Three sets of coefficients are given: for ^{3}He between 0.65 and 3.2 K (about the normal boiling point); for ^{4}He between the λ-point at 2.1768 K and 5.0 K, near the critical point; and for ^{4}He in the superfluid range between 1.25 K and 2.1768 K, as an alternative to the use of ^{3}He. The interpolating CVGT (3.0–24.5 K), which can join directly the ^{3}He vapor pressures, is actually an alternative to the use of ^{4}He vapor pressure. Either of the two vapor-pressure scales is necessary for the realization of the lower fixed point of the ICVGT.

Table 4.4 reports the differences $(T_{62} - T_{90})$ and $(T_{58} - T_{90})$.

Although a full treatment of liquid helium properties is outside the scope of this monograph, it is useful to dedicate it some attention because of its implications regarding the ITS-90 at temperatures below 1 K.

4.3.2.4 Gas Thermometry Versus Vapor-Pressure Thermometry Below 5 K

In order to be able to compare helium gas thermometry with helium vapor-pressure thermometry, the reader must have become familiar also with the contents of Chap. 3. Table 4.5 collects the error analyses for both thermometry types.

Impurity effects in ^{3}He, mainly due to ^{4}He contamination, are more serious in vapor-pressure thermometry, except at very low temperatures. As discussed in Sect. 4.1.1.3, for a 0.001 ^{4}He fraction, the errors on vapor-pressure thermometry are equivalent to 0.7 mK at 3.2 K, 0.35 mK at 1.5 K, and decreasing to 0.02 mK at 0.5 K (Fig. 4.6). In gas thermometry, the same ^{4}He fraction contributes only

Table 4.5 Comparison of the best accuracy levels in vapor-pressure thermometry and (absolute) gas thermometry

	Vapor pressure (mK)						Gas thermometry (absolute)[a] (mK)							
	^{4}He			^{3}He			^{4}He				^{3}He			
Temperature (K)	Scale (1)[b]	δp (2)	t.m. (3)	Scale (1)[b]	δp (2)	t.m. (3)	δp (2)[b]	t.m. (4)	Virial (5)	d.v. (6)	δp (2)[b]	t.m. (4)	Virial (5)	d.v. (6)
0.5	1.5	–	–	1.5	0.44	0.7								
0.8	1.0	–	–	1.0	0.05	0.1					0.5	0.05		
1.0	0.7	0.87[c]	0.1	0.7	0.02	0.005	13.9	0.22			0.2	0.04		
2.0	0.3	0.01[c]	<0.001	0.3	0.003	<0.001	0.2	0.13			0.1	<0.01	0.10	
3.0	0.2	0.004	<0.001	0.2	0.001	<0.001	0.1	0.08	0.07		<0.1		0.10	
4.0	0.2	0.002	<0.001				<0.1	0.05	0.08	<0.01			0.10	<0.01
5.0	0.2	0.001	<0.001					0.04	0.08	0.01			0.10	0.01
10.0								<0.01	0.10	0.04			0.10	0.02
15.0									0.10	0.06			0.15	0.05
20.0									0.10	0.11			0.20	0.08
25.0									0.15	0.17			0.20	0.11
30.0									0.15	0.25				0.16

[a] Low-temperature reference point (estimated uncertainty ± 0.1 mK)

[b] (1) Uncertainty of the T_{X_1} magnetic temperature scale. (Rusby and Swenson 1980)

(2) Uncertainty corresponding to a pressure uncertainty of ± 0.13 Pa ($dp/dT = 1.33$ kPa K^{-1} with gas thermometers, except below 1.5 K for ^{3}He see note 5) and 2.6 K for ^{4}He

(3) Thermomolecular pressure-effect uncertainty (± 25 % of the correction): tube Φ 10 mm

(4) Same as (3), but tube design as in Table 3.10, case (2) with ^{4}He and case (3) with ^{3}He (for density see Table 3.3)

(5) Combined $B(T)$ and $C(T)$ virial 1σ uncertainty (from Tables 3.1 and 3.2). $n/V = 160$ mol m^{-3} down to 1.2 K with ^{3}He and 2.5 K with ^{4}He: see Table 3.3 for density values at lower temperatures

(6) Tube design: Table 3.10, case (2) with ^{4}He and case (3) with ^{3}He

[c] Additional problems are related to ^{4}He superfluidity

through the virial difference (less than 50 mK) until its condensation that, for a filling of $n/V = 160\,\text{mol m}^{-3}$, occurs at about 0.8 K (Table 3.4a), causing a $\mathrm{d}p \cong 1$ Pa, equivalent to an error of 0.8 mK and, at 0.5 K, of 0.5 mK.

With ^{4}He, only ^{3}He can affect the vapor pressure, but this impurity is likely to be present only in experiments where the two isotopes are alternatively used in the same apparatus, or in dilution studies or apparatuses. A gaseous 10^{-4} ^{3}He amount fraction in the liquid produces an error in ^{4}He vapor-pressure equivalent to 0.7 mK at 1.5 K and to 0.2 mK at 2.6 K (Table 4.1). In gas thermometry, the same ^{3}He fraction never produces errors larger than 10 mK, as it would condense only below 0.25 K, outside the range of gas thermometry.

A large contribution to the uncertainty in measuring the pressure of the vapor at the lowest temperatures is made by the thermomolecular pressure effect. In order to reduce it, a large tube diameter (often more than 10 mm) is used in vapor-pressure thermometry. However, errors difficult to quantify may be caused by the use of large-bore tubes, since overheating of the surface layer of the liquid—which alone is significant in the vapor-pressure determination—can occur, owing to thermal radiation, with respect to the temperature of the bulk liquid, the only one that is measured.

Should any discrepancy with published data occur, it is most likely that it can only be resolved by new measurements using apparatuses with wider tube bores, to lower the uncertainty due to the thermomolecular pressure effect, and larger room-temperature volume, to limit backflow of impurities.

The accuracy of the pressure-measuring apparatus does not limit vapor-pressure measurement accuracy, as it does in gas thermometry, except at the lowest temperatures. Not only are pressures at least twice as large with respect to gas thermometry (Table 3.3), but the sensitivity $\mathrm{d}p/\mathrm{d}T$ is conveniently high, except at the lowest temperatures, where it decreases substantially (1 kPa K^{-1} at 0.64 K with ^{3}He and at 1.31 K with ^{4}He; 300 Pa K^{-1} at 0.5 K with ^{3}He and at 1.1 K with ^{4}He).

However, in vapor-pressure thermometry the largest source of uncertainty arises from the temperature scale, on which vapor-pressure measurements are necessarily based, since vapor pressure is not itself an accurate absolute thermodynamic thermometer, at least above 1 K.

Up to the 1990s, all the published measurements below 2.6 K were made with magnetic thermometers (Rusby and Swenson 1980). An estimate of their uncertainty is given in Table 4.4, which clearly shows that with ^{3}He gas thermometry, which, in principle, is more accurate than magnetic thermometry, can the present uncertainty of measurements below 2 K be substantially reduced, although, below 1 K, application of the PLTS-2000 (or PTB-2006, see the section "Current T_{2006}: Scale Definition" and Fig. 4.11b) has already reduced this uncertainty considerably.

Consequently, vapor-pressure scales are necessarily somewhat less accurate than the best realization of a thermodynamic scale, as they must rely on this for the definition of their temperature values, but they constitute a valuable means as a check on the smoothness of the thermodynamic scale. Besides the uncertainty of temperature values, one has to add the uncertainty inherent in the realization of the vapor-pressure scale itself. Yet vapor-pressure thermometry is more reproducible than gas thermometry, and in most cases the realization is considerably easier.

Summary 4.6 Summary of Design Criteria for Vapor-Pressure Thermometers

	Example	Reference
1. Choice of working substance	T_{max} @ p_c	
• Temperature range: each substance spans only a narrow temperature interval	T_{min} @ 100 Pa K^{-1}	4.2.4
$T_{max}/T_{min} < 2$–3 (including solid–vapor range), except helium. The limit:	T_{max}/T_{min} =	
T_{max} set by maximum manometer pressure;	^{3}He ≈ 10	
T_{min} set by manometer sensitivity	^{3}He ≈ 9	
• Accuracy:	H_2 ≈ 3	Fig. 4.1
Manometer: no single manometer spans whole range from ≈ 1 Pa ($dp/dT \approx 100$ Pa K^{-1}) and critical point	Ne ≈ 3	Table 4.2
($p_c > 10^6$ Pa, except helium) with high or constant accuracy, or with sufficient sensitivity	N_2 ≈ 2.5	
Substance: not all substances allow obtaining top accuracy, due to purity or to thermal problems related to	O_2 ≈ 2.5	4.1.1.1
a low thermal diffusivity value	Ar ≈ 2.5	4.1.1.2
	CO_2 ≈ 2 (solid ≈ 1.5)	4.1.1.3
2. Choice of pressure-measuring system:		
Less critical than with a CVGT, as sensitivity is at least twice.		
Sensitivity and accuracy must be matched to the range of dp/dT and of p, i.e., T, to be measured		4.2.1.2
• Without separating diaphragm: can be used only for low–medium accuracy, as thermometric gas also fills whole manometric apparatus, with problems of contamination and increase of vapor volume		
Dial manometers: used only for accuracy > ± 1 %		
Metal diaphragm or bellows (electronic) manometers: can achieve a ± 0.1 to 0.03 % accuracy		
Quartz bourdon gauges: can approach ± 0.01 % accuracy, but helium leaks through quartz		
Cryogenic pressure transducers: none commercially available with accuracy better than ± 0.1 % (after cryogenic		3.3.3
calibration). Eliminate need of the connecting tube in sealed thermometers, but transducer must withstand high		4.2.3
room-temperature pressure		
• With separation diaphragm: mandatory for high or top accuracy. Only zero reproducibility and a moderate linearity near zero are important		3.3.1.3
Capacitive diaphragms: several commercial models, when properly used, allow zero sensitivity and reproducibility better than ± 0.1 Pa		
Cryogenic diaphragms: only laboratory-made diaphragms available, some with high zero reproducibility. Allow confining thermometric gas at low temperatures, but the tube connecting the diaphragm to room-temperature manometer is still necessary		3.1.3.1
Room-temperature manometers: when a cryogenic diaphragm is used, only manometers allowing helium as manometric gas can be used		4.2.3

Summary 4.6 (continued)

	Example	Reference
3. Choice of sealed versus "open" thermometer:		
• Sealed: low accuracy only (e.g., dial) thermometers		4.2.2
Medium-accuracy sealed thermometers still very simple when using cryogenic manometer and reducing vapor volume, but room-temperature pressure can be higher than 10 MPa. Therefore, only low-sensitivity manometers can be used and thermometer measures only upper part of vapor-pressure scale		4.2.3
High-accuracy sealed thermometers can be made, using ballast room-temperature volume and precision room-temperature diaphragm		
• "Open": vapor-pressure thermometers using gases are open only since working substance does not stay permanently in working bulb, but (new) samples are condensed in it only during measurements. Requires permanent use of a gas-handling system.		2.2.2.6
4. Gas purity, isotopic composition, and spin equilibrium:		
• Purity: must be known, and possibly checked, e.g., by performing a triple-point temperature measurement. Dew-boiling-point difference measurement must also routinely be performed, before sealing in the case of sealed devices		3.1.1.3
• Isotopic composition: some gases show irreproducibility in results due to sample-to-sample changes in isotopic composition. It is impossible to obtain top accuracy with these substances, unless pure isotopes are used.	Kr, Xe	
• Spin equilibrium: with some gases, showing different spin species, equilibrium must be ensured with use of a suitable catalyst. All procedures described for preparing triple-point cells apply	H_2, D_2	3.1.1.3

Summary 4.6 (continued)

	Example	Reference
5. Thermometer filling: • Amount of substance n_{max} at $T_{min} \rightarrow V^L \approx V_b$: $n_{max} \leq \frac{p_{min}}{RT_r}\left[\frac{2V_cT_r}{T_r+T_{min}} + V_r\right] + \frac{V_b}{M}\rho_{min}$ Amount of substance n_{min} @ $T_{max} \rightarrow V^L = V_\varepsilon^L \approx 0$ $n_{min} \geq \frac{V_\varepsilon^L \rho_{max}}{M} + \frac{p_{max}}{RT_r}\left[\frac{2V_cT_r}{T_r+T_{max}} + V_r + \frac{T_r}{T_{max}}\left(V_{max} - V\frac{L}{\varepsilon}\right)\right]$ Bulb volume V_b: $V_b\left(\frac{\rho_{min}}{M} - \frac{p_{max}}{RT_{max}}\right) \leq \frac{V_r}{RT_r}(p_{max} - p_{min}) + \left\{\boldsymbol{V^L\left[\frac{\rho_{max}}{M} - \frac{p_{max}}{RT_{max}}\right]} + \frac{2V_c}{R}\left(\frac{\boldsymbol{p_{max}}}{\boldsymbol{T_r + T_{max}}} - \frac{\boldsymbol{p_{min}}}{\boldsymbol{T_r + V_{min}}}\right)\right\}$ to a first approximation the terms in **bold** can be omitted	^{4}He thermometer $T_{min} = 2.2$ K $p_{min} = 5.263$ kPa $p_{min} = 146\,kg\,m^{-3}$ $T_{max} = 5.2$ K $p_{max} = 227.5$ kPa $p_{max} = 67.5\,kg\,m^{-3}$ $T_f = 4.2$ K $p_f = 100$ kPa $T_r = 300$ K $p_r = 200$ kPa $V_r = 220\,cm^3$ $V_c = 16\,cm^3$ $V_T = 500\,cm^3$ $M = 4\,g\,mol^{-1}$	4.1.2, 4.2.1.1
• Calculation of the amount of substance n to condense in the thermometer: the gas is stored at p_r in the room-temperature reservoir of volume V_T. When the substance is condensed in the thermometer bulb at a temperature T_f, a residual $n_0 = \frac{p_f V_T}{RT_r}$ remains in V_T. Therefore, in order to condense a quantity N, one must have in the system: $n' = \frac{p_r V_T}{RT_r}\left[1 - \frac{p_f}{p_r}\right] + (V_b + V_c + V_r)$	It follows: $V_b \geq \approx 2\,cm^3$ Taking the minimum volume $0.074 \geq n$ $n \geq 0.034$ In order to seal-in 0.05 mol, the filling system must contain 0.069 mol	

Summary 4.7 Summary of Fabrication Techniques for Vapor-Pressure Thermometers

	Reference
1. Design and fabrication of bulb:	
Bulb material must have high thermal conductivity	
• High room-temperature pressure-sealed type	4.2.3
With cryogenic manometer directly fitted to it: only bulb is needed to build the thermometer, of design similar to that of triple-point sealed cells, except that here large cell mass (large heat capacity) helps in temperature stabilization	
With room-temperature absolute manometer: a (relatively) small-diameter low-conductivity tube, connecting bulb to room-temperature manometer, must to be added	
• Low room-temperature pressure type (sealed or "open")	
With room-temperature pressure measurement: traditionally the bulb is a cavity of few cubic centimeters in massive OFHC copper block, where thermometers are also fitted. In sealed types, a ballast volume limits room-temperature pressure	Fig. 2.4 2.1
2. Design and fabrication of connecting tube	4.2.1.3
• Volume and diameter: importance of vapor volume is much less than dead volume in a CVGT; tube diameter choice is almost free to limit thermomolecular effect. At the lowest pressures (below 1 K with ^{3}He), this needs a tube with 2–3 diameters increasing in sequence, the upper part being of several centimeters. Care must be taken to avoid convection and, at helium temperatures, acoustic oscillations Low-accuracy ($\pm$ 1 %) thermometers can have the tube up to several meters long	4.3.2.1
• Cold spots: peculiar and extremely insidious error source, as some substances condensing outside bulb alters saturated pressure value. Best way to avoid them is vacuum jacketing the connecting tube, up to above refrigerated region of cryostat. Jacket can make a proper tube thermal tie-down difficult a proper tube thermal tie-down	4.2.1.4
• Thermal leaks: in vacuum cryostats the connecting tube is the largest source of thermal exchange from environment to bulb, and, before reaching bulb, must be thermally tied down to cryostat isothermal shield surrounding bulb, or to an independent block, acting as thermal guard, kept slightly above bulb temperature to avoid cold spots. Great care must be taken to shield liquid surface from heat exchange by radiation and by convection	4.2.1.4
• Temperature distribution: must be calculable or be measured, to compute an accurate aerostatic correction	4.2.1.3 4.3.2.1
• Special problems: special design needed to measure ^{4}He below λ-point and ^{3}He below 1 K	4.3.2.2
3. Design of room-temperature parts and gas-handling system	
• Thermometer room-temperature parts: when necessary, they can reduce to a dial manometer, or be more complex, in sealed high-accuracy thermometers, which require a ballast volume for room-temperature storage of gas at moderate pressure, and a diaphragm manometer separating thermometric from manometric gas. A set of valves allows operations	4.2.1.2
• Gas-handling system: similar to that used for filling triple-point cells. Is necessary, for initial filling, or for measurements of "open" thermometers. System must ensure purity, possibly checked online with a mass spectrometer in top-accuracy work, and provide cryogenic pumps for recovery of low-condensing gases and clean storage (or purification means). Must include bellows allowing an increased vapor volume sufficient to fully vaporize liquid at T_{min}, for purity check	2.2.2.6

Summary 4.8 Summary of Measurement Procedures with Vapor-Pressure Thermometers

	Reference
1. Preliminary measurements	
• Gas filling: in nonsealed thermometers must be done at each cooldown. The calculated amount of gas is measured with volumetric technique and condensed into bulb kept at low T_f. Full connecting tube must carefully be kept at temperatures $> T_f$ to avoid cold spots, which could even occlude it. Very difficult then to evaporate out substance condensed (or solidified) outside bulb. Its occurrence often indicated by unstable or irreproducible pressure readings at stable bulb temperature, or by sudden temperature (and pressure) rise on heating tube	4.1.2 4.2.1
• Check for gas purity: may affect measurement accuracy, so its check is highly recommended, especially in high-accuracy measurements, to be done in situ, as bulb itself can be a source of contamination, in particular in sealed devices. Check must also be performed with isotherm method at different V^L/V^v ratios, obtained by increasing or decreasing in steps vapor volume at constant n, using bellows built in handling system, and measuring pressure values. The gas, the more it is impure, the more its pressure value will vary, i.e., the pressure difference between dew and boiling points is large	4.1.1.1
2. Performing measurement of manometer pressure (p^*) at θ_b	
• The bulb is first stabilized at θ_b. When connecting-tube temperature distribution has also stabilized, which can take more time than bulb, pressure measurement is performed and all manometric system corrections computed to obtain p^* value. Temperature distribution in connecting tube is measured when it cannot be reliably calculated	
3. Calculation of pressure p and temperature θ_b	
• Calculation of p_b *is* calculated from p^* applying aerostatic and thermomolecular corrections, depending on thermometer design and on tube temperature distribution	4.2.1.3
• Calculation of θ_b temperature values of the bulb, where the thermometers are fitted, are computed using p_b in defining (e.g., T_{90}), or selected, equation	4.3.1

Chapter 5
Thermometry Based on the Melting Line of ^{3}He

Few types of thermometry are available below 1 K, and none is sufficiently well established, readily available, or widely used in laboratories around the world. As discussed in the preceding chapters, even the ITS-90 below 1 K is affected by the degradation of the experimental data forming its basis. As far as the use of gases is concerned, the choice is restricted to ^{3}He. In both vapor-pressure thermometry and gas thermometry, increasing experimental difficulties are encountered below 1000 mK[1]. In no way, can these techniques be applied much below 500 mK.

For these reasons, an increasing number of laboratories, studying physics in the millikelvin region are interested to develop a practical scale, based on certain thermodynamic properties that could be linked to sufficient accuracy to the thermodynamic temperature. The most promising answer to this problem is the possibility of utilizing of the melting line of ^{3}He. In principle, the qualitatively similar melting line of ^{4}He could be used as well (see Fig. 2.3: $p_{\min} = 2.529$ MPa, $T_{\min} = 0.775$ K (Straty and Adams 1966)), but its application up to this time has not been considered.

On the contrary, starting with the work by Greywall (1986) over the years a lot of attention has been given to the ^{3}He melting curve for thermometric use in the temperature range from $\approx$ 1 mK up to 1 K, a range spanning three decades. The attractive feature of the melting curve is that it comes with its own four fixed points. They include three phase transitions, the Néel's transition at 0.9 mK—the B transition at 1.9 mK and the A transition at 2.5 mK, plus a fixed point for pressure calibration: the pressure minimum at about 315 mK.

Figure 5.1 shows the full low-temperature ^{3}He phase diagram (not to scale) along with its relevant features (Keller 1969). Table 5.1 provides the key numerical values.

Several specific features are useful for an accurate thermometer. The melting line itself represents a connected set of thermodynamic states that, as in vapor-pressure thermometry, can become a thermometer through pressure measurements, if the p–T relationship is established with sufficient accuracy. Incidentally, if T is measured instead, the line can be used as a continuous set of reference *pressure* values, or as a pressure scale (see Chap. 9).

[1] Note that in this chapter the prefix *milli* for the kelvin will normally be used, since this type of thermometry essentially extends below 1 K, in the millikelvin region of absolute temperatures.

F. Pavese, G. Molinar Min Beciet, *Modern Gas-Based Temperature and Pressure Measurements,* International Cryogenics Monograph Series,
DOI 10.1007/978-1-4419-8282-7_5, © Springer Science+Business Media New York 2013

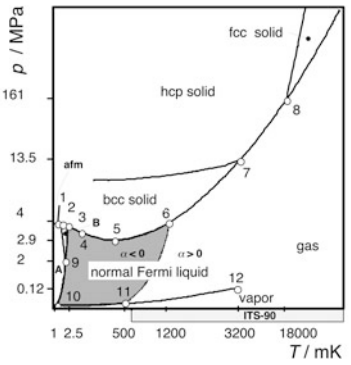

Fig. 5.1 Thermodynamic properties of ^{3}He below 1 K. *Not to scale*. See Table 5.1 for caption of the specific points; *afm* antiferromagnetic ordering transition; *A, B* superfluid phases. (After Keller 1969)

Table 5.1 Key thermodynamic features of condensed ^{3}He

Point[a]		T/mK	p/MPa	References
On the melting line				
1	Antiferromagnetic transition	0.931	3.4846	Greywall (1985, 1986)
2	Superfluid A—superfuid B	1.932	3.4813	Greywall (1985, 1986)
3	Normal liquid—superfluid A	2.491	3.4793	Greywall (1985, 1986)
4	Inflection point $(\mathrm{d}p/\mathrm{d}T)_{\max} = 4.08\,\mathrm{MPa\,K^{-1}}$	≈ 8	≈ 3.457	
5	Minimum pressure	319	2.97060	Greywall (1985); Grilly (1971)
6	Change from negative to positive thermal expansion in liquid	1260	4.76	Keller (1969)
7	Solid bcc–solid hcp transition	3138	13.724	Keller (1969)
8	Solid hcp–solid fcc transition	17780	162.9	Keller (1969)
In the liquid				
9	$p_{\min}$ for superfluid B	2.273	2.150	Greywall (1986)
10	$T_{\min}$ for superfluid	0.929	≈ 0	Greywall (1986)
11	Joining-point of zero thermal-expansion line with vapor-pressure line	502	0.00002	Keller (1969)
12	Critical point	3316.2	0.11466	Durieux and Rusby (1983)

[a]With reference to Fig. 5.1

In addition, the line has several distinctive points that can be used as reference *points*, in the same sense as defined in Chap. 2. They are:

1. The minimum of the melting line (5) occurring at $\approx$ 319 mK, obviously much more effectively used as a *pressure* fixed point.
2. The second-order transition (3) from normal liquid to superfluid A phase, occurring at $T_{\mathrm{A}} \approx$ 2.5 mK.
3. The first-order transition (2) from superfluid phases A and B, occurring at $T_{\mathrm{B}} \approx$ 1.9 mK.

4. The first-order transition (1) of solid ^{3}He into the ferromagnetically ordered phase, occurring at $T_S \approx 1.0$ mK.

The use of these potential reference points may have important consequences as regards the quality of the thermometry that can be performed using the melting line. In fact, this thermometry is usually not implemented as a thermodynamic scale, but the values of the thermodynamic temperature T corresponding to each value of the pressure p must be assigned by means of a primary thermometer. By using reference points with defined temperatures, the quality required to the pressure transducer (which must be a cryogenic one, as later shown) becomes much less critical, since it can be recalibrated *in situ*. An equivalent possibility in vapor-pressure thermometry consists, as noted in Chap. 4, in using the triple point—or the λ-point with ^{4}He—as a reference point. In melting-line thermometry, more than one reference point is available, so that not only a calibration shift, but also possible changes in the transducer gain and non-linearity, can be corrected for.

It has been shown that, between 5 and 20 mK, an equation based on the Clausius-Clapeyron equation could be computed to sufficient accuracy to provide thermodynamic temperature values accurate to ≈ 1% (Scribner and Adams 1972). This equation would allow the ^{3}He melting-line to be used over that range[2] as a primary thermometer.

On the upper side of the temperature range, the extension of measurements by means of the melting line to higher temperatures shows no particular difficulties, excepting the need to measure increasingly high pressures; for example, at 3 K the pressure value is about 13 MPa and at 4.2 K about 30 MPa. In principle, this extension would make a direct connection of the use of ^{3}He melting-line thermometry possible with the use of the ITS-90 interpolating gas thermometry (Astrov et al. 1990).

A description is now given of the basic features of an experiment designed for the measurement of the melting line of ^{3}He for use as a thermometric scale below 1 K. The very specialized techniques and the refrigeration techniques that are required for measurements below 1 K will not be described. The reader is directed to the relevant literature (see, e.g., Lounasmaa 1974).

5.1 The ^{3}He Melting-Line Thermometer

Thermodynamic temperature in this range was established with a plethora of methods, not using a gas for their definition: noise thermometry, magnetic thermometry (CMN and platinum NMR), and nuclear orientation thermometry. Noise thermometry uses the thermal or Johnson noise voltage across a resistance as the thermometric parameter. The basic equation is the Nyquist relation $<V^2(t)> = 4\ kTR\Delta\nu$ where $V(t)$ is the measured noise voltage in a frequency interval $\Delta\nu$ across a resistance R which is at a thermodynamic temperature T, and k is the Boltzmann constant. The

[2] Note that the 5–20 mK range is not so narrow as appears at first glance, since it spans a temperature ratio $T_{max}/T_{min} = 4$, wider, for example, than the range of the ITS-90 ICVGT (3–24.6 K).

thermometer is absolute in the sense that it gives the thermodynamic temperature without any calibrations at known temperatures (Soulen et al. 1994; Schuster et al. 1994).

CMN thermometry has been used for many years. The CMN sample (for metrological applications it should be a spherically shaped high-purity single crystal) is placed in the centre of a set of coils forming a mutual inductance. The reading of an inductance bridge X is related to T by the equation $X = A + B/(T + \Delta)$. The constants A and B which depend on the Curie constant of CMN and on the dimensions of the coil system are determined from calibrations of the thermometer at temperatures above 1 K. In platinum NMR thermometry, the nuclear-magnetic moment due to the applied induction B is determined using standard pulsed-NMR techniques.

The nuclear-orientation thermometer (NOT) is based on the anisotropy of γ-ray emission by radioactive nuclei that possess a nuclear-spin magnetic moment, μ_N. In a magnetic induction B, if $\mu_N B \ll kT$, the magnetic moments of the nuclei will be oriented randomly and no anisotropy will appear in the resulting radiation. When the temperature drops to a level $kT \approx \mu_N B$ anisotropy in the γ-ray emission will become apparent and the degree of anisotropy will be a direct measure of the thermodynamic temperature of the assembly. The thermometer does not follow Curie's law, but it does have sufficient sensitivity between, approximately, 30 and 2 mK.

From the viewpoint of the assignment of thermodynamic *temperature* values, the serious discrepancies in absolute measurements detected below 15 mK (Greywall 1986) suggest this value as a convenient lower limit for a temperature scale based on the ^{3}He melting line. This limit does not necessarily prevent the use of reference points even lower than 2.5 mK, since they are essentially pressure calibration points, easily and uniquely identified by first—or second-order—discontinuities in thermal measurements. Therefore, these points are "reference points" according to definition used in the present monograph (see beginning of Chap. 2), and need not be assigned a temperature value.

From the viewpoint of *pressure* measurements, $\mathrm{d}p/\mathrm{d}T$ is conveniently high, being higher than 1 MPa K^{-1} between 200 mK and 1 K. On the other hand, for required constant 0.1% accuracy over the entire range of the temperature scale, equivalent to 0.7 mK at 0.65 K but 1 μK at 1 mK, as it spans almost three orders of magnitude, the equivalent requirements on pressure *relative* accuracy are not so trivial (Table 5.2). No more than 3×10^{-5} is required for $T > 30$ mK, except in a narrow interval across the pressure minimum (≈ 250–350 mK); below 30 mK, accuracy demands becomes increasingly severe, since $\mathrm{d}p/p$ decreases as $\approx 1/T$ (i.e., 1×10^{-5} at 10 mK and 1×10^{-6} at 1 mK). It may be useful to note that pressure must actually be measured over an interval of only ≈ 0.5 MPa, between 1 mK and 650 mK (only ≈ 0.4 MPa in the 15–650 mK range), being the absolute value about 3 MPa. Therefore, the relative accuracy demands would decrease by about one order of magnitude, should only the *differential* pressure be measured. For example, pressure could be measured against the value of its *minimum* value, kept stable to within ± 60 Pa (see Table 5.2), which can be generated by maintaining some of the ^{3}He slush at 319 ± 4 mK (only a 1% temperature stability).

For the realization of this scale, a liquid–solid ^{3}He mixture is used, contained in a small copper cell of about 0.1 cm^3 volume. The cell can be cooled down to

Table 5.2 Melting line of ^{3}He: pressure accuracy requirements

T (mK)	$\delta T = 0.001T$ (mK)	pm (MPa)	dp/dT (MPa K^{-1})	$\delta p/p^a$ (10^{-6})
1	1	3.45	− 2.9	1
2.7	≈ 3	3.4	− 3.6	3
10	10	3.4	− 4.0[b]	12
15	15	3.35	− 3.9	17
30	30	3.3	− 3.6	33
100	100	3.15	− 2.2	70
250	250	3.0	− 0.4	33
319	319	2.97	0	0[c]
400	400	3.0	+ 0.5	70
600	600	3.2	+ 1.4	260
1000	1000	4.0	+ 2.7	670
1800	1800	6.9	+ 4.3	1120

[a]Relative pressure accuracy required to achieve δT
[b]The maximum dp/dT is at ≈ 8 mK
[c]There is a gap of 100–150 mK across the pressure minimum at T = 319 mK where dp/dT is too small to be of any practical use

about 10 K or 5 mK by means of a ^{3}He/^{4}He dilution refrigerator. For reaching lower temperatures it is necessary to attach a nuclear demagnetization stage. Pressures are measured *in situ* by means of a capacitive pressure transducer. The upper wall of the cell, a beryllium-copper flexible membrane, forms the moveable plate of the capacitor. A fixed copper plate forms the other plate. The gap between the plates is about 0.05 mm. The displacement of the membrane is typically only about 8 μm MPa^{-1}. Nevertheless, pressure differences of a few pascal can be detected. The device was first used by Straty and Adams (1969) and is standard in ^{3}He melting-pressure thermometry. A narrow capillary connects the cell to the ^{3}He supply and a pressure balance at room temperature. Calibration of the pressure transducer against the pressure balance is usually performed with the cell at about 1 K. At temperatures below the pressure minimum, *in situ* pressure measurements are unavoidable because a solid plug will be formed in the filling line of the cell. Pressures range from 2.93 MPa to 3.44 MPa.

The two branches of the melting line must be considered separately, not only because the line minimum causes a scale gap between ≈250 mK and ≈400 mK owing to lack of sensitivity, but also because a different experimental approach is required for the two branches.

In fact, a tube, filled with ^{3}He and with a temperature distribution including $T_{\min}$ will become blocked by solid ^{3}He at $T_{\min}$ as soon as pressure is increased above $p_{\min}$. Therefore, a cell containing ^{3}He kept at a $T < T_{\min}$ will become isolated from the outside gas circuit and cannot be pressurized to higher values unless a *mechanical* action is exerted on the cell walls. From another viewpoint, this blocking has the advantage of making a cryogenic sealing valve in the cell unnecessary. The experimental procedures for performing measurements of the two branches of the melting line are therefore different in that a valve is required only for measurements above $T_{\min}$ and a cryogenic pressure transducer is required only below $T_{\min}$.

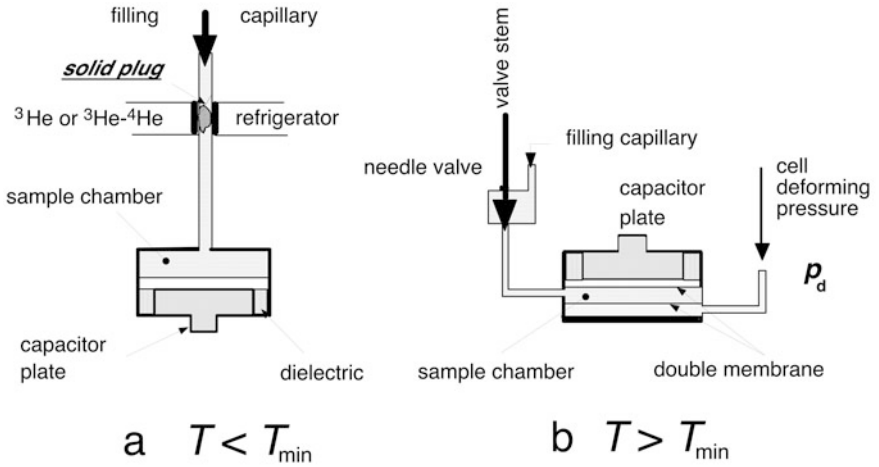

Fig. 5.2 Layout of experimental arrangements for ^{3}He melting-curve thermometry: **a** for $T < T_{min}$; **b** for $T > T_{min}$

The experiment does not need a large amount of substance, therefore advantage is gained in using only few cubic millimeters of liquid to improve thermal response. The liquid is an excellent thermal conductor (λ/W m^{-1} K^{-1} = 4 $\times$ 10^{-5}/(T/K), approaching, below 10 mK, that of pure copper) but liquid–solid slush is not, because of the poor thermal conductivity of the solid phase. Therefore, the cryogenic pressure transducer is usually integrated with the cell, and is also used for performing the measurements on upper branch of the melting line (Grilly 1971). At such low temperatures and fairly high pressures, it is necessary to check whether hydrostatic conditions actually apply (i.e., whether pressure is uniquely defined in the experimental chamber, see Chap. 7), because the dynamic viscosity of liquid ^{3}He is rapidly increasing with decreasing temperature, h/Pa s $\approx$ 2.5 $\times$ 10^{-8}/(T/K)^2. Therefore care must be taken to ensure that the slush is not too rich in solid content, so that the liquid paths are connected and the liquid–solid interfaces are in thermal equilibrium.

It is difficult to show a typical arrangement for a melting-line thermometer, since it is essentially conditioned by the specific pressure gauge used. However, Fig. 5.2a, b very schematically shows two experimental arrangements, for work below and above T_{min}, respectively. The measurements of the (capacitive) pressure gauge can even be automated, thus making the melting-line thermometer to operate automatically at fixed temperatures (Schuster and Wolber 1986).

5.1.1 Melting-Line Experiments Below T_{min}

The blocked-capillary method is generally used. It must be kept in mind that, in this pressure *negative*-slope region, solid ^{3}He tends to form in the *warmer* parts of

the apparatus. Therefore, solid plugs could also form where they are not expected to, if *heater* locations are placed incorrectly (Lounasmaa 1974). Notice that this phenomenon is equivalent to the *opposite* "cold spots."

The sample chamber and the filling capillary (Fig. 5.2a), where liquid ^{3}He is condensed must be maintained initially at a temperature higher than the freezing. The liquid must be compressed by a sufficient gas head to reach the minimum density required (≈ 0.12 g cm^{-3}). The capillary is then cooled rapidly (with a dilution refrigerator), so as to cause plugging of the capillary by the solid phase. The sample trapped in the sample chamber will cool down following an isochore. Starting with the minimum indicated density, it will cross the melting line at 750–800 mK. A slush of solid and liquid phases will form, which on cooling will follow the melting line and become more and more rich in solid phase. It must be noted that in this way the different points on the melting line can only be measured for different liquid/solid ratios and that this lack of flexibility prevents the melting range of the slush from being verified.

5.1.2 Melting-Line Experiments Above $T_{\min}$

The apparatus, shown in Fig. 5.2b, requires a cryogenic sealing valve. It has as well the capability for changing the volume of the sample chamber, by deformation of a supplementary diaphragm (Grilly 1971). This way, the melting line can be crossed along any isotherm. In fact, when p_d is increased from an all-liquid sample, the pressure will increase until the first solid will form, at p_m. A further increase in p_d will cause more solid to form, until the sample pressure again starts rising when the entire sample is solidified. This device could, in principle, be added also to the experiment of Fig. 5.2a. A good ^{3}He refrigerator (able to reach 250–280 mK) is adequate for this experiment. The time required for full sample freezing has been reported to increase when lowering temperature (2 h at 0.3 K; Grilly 1971).

5.1.3 Pressure and Temperature Measurement

The cryogenic pressure gauges used for these measurements were all of the capacitive type, but one, which was based on a microwave resonator (Van Degrift 1982). These gauges are described in Sect. 8.4.2. of Part II. They showed excellent sensitivity and good reproducibility in the working temperature range, but poor reproducibility upon thermal cycling from room temperature. This is not surprising as creep develops only at higher temperatures. However, the reference points existing on the melting line can be used for *in situ* recalibration.

At present, the p–T relationship cannot be calculated from first principles to sufficient accuracy, so that temperature must be obtained from other thermometers.

Above 0.65 K, the ITS-90 can be used, by including in the apparatus a ^{3}He vapor-pressure thermometer. Below 0.65 K, the old T_{62} Scale, which is tabulated down to 0.2 mK, could still be used, or any one of the several choices available in this temperature region (Schooley 1986), directly or by means of calibrated electrical thermometers.

In the (common) case that the temperature of the sample cell has to be measured, or the cell is used for measuring the temperature of another device, one must remember, and take due precautions (Lounasmaa 1974), the special problems arising in this temperature range, including the Kapitza thermal boundary resistance (see also Sect. 4.3.2.2) between ^{3}He and the walls of the cell.

5.1.4 The ^{3}He Melting-Line Scale

During its 19th session of 1996, the CCT recommended that the ITS-90 be extended to the mK range based on the melting pressure/temperature relation of ^{3}He. Such a scale was developed and accepted in 2000 as the "*Provisional Low Temperature Scale of 2000*" (PLTS-2000). It was termed "provisional" because of still-existing discrepancies between the various sets of data forming its basis. The PLTS-2000 was based on three sets of data: from NIST (Fogle et al. 1992a, b; Colwell et al. 1992), PTB (Schuster and Hechtfischer 1992; Schuster et al. 1993), and the University of Florida (Ni et al. 1995a, b).

As early as 1992, indications were forthcoming, specifically from the experiments that later formed the basis for the PLTS-2000, for a deviation from thermodynamic temperature of the ^{3}He vapor pressure scale incorporated into the ITS-90 by as much as 1.5 mK, with the ITS-90 being too high. Documentation throughout the years on this deviation can be found in the Reports to CCT by Working Group 4 (see BIPM website). This deviation was later confirmed by various authors (e.g., Engert et al. 2007). For other realizations of the ^{3}He melting curve see Ni et al. (1995a, b).

Chapter 6
Cryostats for Thermometry and Gas-Based Temperature Control

The "universal" cryostat and "the best" cryostat are utopic terms. The literature contains a very large number of papers describing cryostats. No attempt will be made to review them all, which are extremely numerous and varied. Besides, many of them are only specific for other types of applications; indeed most are too specialized, since their function as thermostats has been unnecessarily confused with the requirements of a specific experiment mounted in them. This is largely unnecessary in many cases.

The most convenient way in which to design a cryostat, based on the (few) specific needs of thermometry, will be shown in the following, in order to overcome the two main problems that arise in cryogenics, namely, difficulty in access to the experimental space, and long cool down and warm up times. In addition, two basic changes occurred in experimental work in the past 20 years from the first edition of this book: the first is in the cooling method, because a basic improvement, and a basic change in methodology, was made possible by the development of new closed-cycle ("dry," not using liquid refrigerants) have been developed that today allow to operate down to 4 K in a very simple manner, and down to $\approx$1.5 K (but sometimes down to the millikelvin region), still without resorting to liquid refrigerants. In this way, working in cryogenics may become as simple as operating a furnace. The second is the general use of automatic systems, computer driven, for equipment control and data acquisition. The two improvements together allow unattended experiments to be run today for an indefinite period of time also in cryogenics.

In the second part of this chapter, some uses of gases in temperature controls will be described that may be found useful in several applications, including space research.

6.1 Cryostats

Till the 1980s, the choice of a cryostat until recently has been restricted to the types using a liquid refrigerant in a bath or flowing into a coiled pipe. However, the rapid development of closed-cycle refrigerators (cryocoolers) has provided a very attractive simplification in cryogenic work. Therefore, we will begin with cryostats of the latter type.

F. Pavese, G. Molinar Min Beciet, *Modern Gas-Based Temperature and Pressure Measurements,* International Cryogenics Monograph Series,
DOI 10.1007/978-1-4419-8282-7_6, © Springer Science+Business Media New York 2013

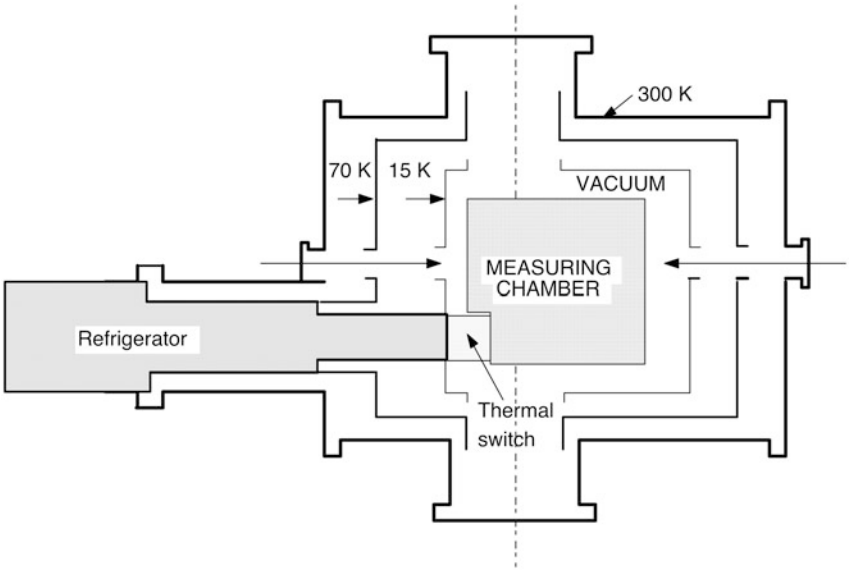

Fig. 6.1 Cryostat for a two-stage closed-cycle ^{4}He refrigerator

6.1.1 Refrigerator-Based Cryostats

6.1.1.1 Closed-Cycle Types (0.3 to 300 K)

Refrigerators (cryocoolers) based on ^{4}He are now available for temperatures down to about 30–50 K with one stage, near 10 K with low-power two stages, and down to 3–5 K with the most modern two stages, with helium liquefaction capability and with or without a small liquid helium bath available. These refrigerators can cool down in a time frame ≈0–4 h, if we include microrefrigerators for detectors: otherwise about 1–2 h is the minimum cool down time for a refrigerator of several watts. These cool down times can be considerably increased by the design of the attached cryostat and by the total mass to be cooled down. Warm up can be achieved as rapidly as desired with addition of heaters. In most applications the refrigerators do not require vacuum cryogenic seals, but only a room-temperature vacuum chamber. They may run for thousands of hours continuously, without cryogenic refilling or maintenance. These units do not require accessories like storage dewars, transfer lines, liquid level detectors, and any associated expertise. These are not manufacturer's claims, but are basic differences with respect to the traditional style of cryogenic experiments. The refrigeration requirements of a cryostat for thermometric use never exceed 1–2 W at 4.5 K and 5–10 W at 77 K.

Figure 6.1 shows schematic of a cryostat designed for a two-stage closed-cycle refrigerator for general purpose and with horizontal refrigerator, needing a so-called thermal—or heat—switch (see Sect. 6.2.5) for its operation.

The shields are directly cooled by the different stages. With the old-style three-stage refrigerators, a third innermost shield is added and the heat switch shown in the figure is included in the refrigerator (generally hydrogen-filled: see Sect. 6.2.4). A high-vacuum pumping system is often not even necessary, since sufficient cryopumping action can be built in the first and second stages. In fact, all internal parts must be thermally insulated from the room-temperature environment by maintaining them under high vacuum during operation. On the other hand, the experiment must be cooled down by the refrigerator, but, during operation, must be thermally disconnected from the refrigerator by means of a switchable connection. Various types of heat switches are described in the literature, including both mechanical and gas-filled types (see Sect. 6.2.5). For example, the measuring chamber shown in Fig. 6.1 is connected to the first shield via a heat switch.

A second example of cryogen-free cryostat operated by a *two-stage* refrigerator with base temperature of ≈10 K, placed vertically upside-down, is shown in Fig. 6.2, extensively used at IMGC (later INRIM) for realizing the fixed points of the ITS-90 down to 13.8 K (Ferri et al. 2003, 2004).

The cryostat is placed on the top of the two-stage refrigerator, and shows one thermal shield connected to each of the stages. The calorimeter is built inside the second-stage shield and is provided with an independent vacuum, so that an exchange gas (typically hydrogen, so that it condenses below 10 K) can be used during cool down. This arrangement requires an additional vacuum-tight feedthrough for the wires inside the cryostat. The cell assembly (shown with three elements mounted) is suspended to the adiabatic shield. The adiabatic shield is mounted on three telescopic spring-loaded supports to damp the refrigerator vibrations. For the same purpose, the cell assembly is further suspended to the shield with carbon-fiber threads. Measurements carried out with an accelerometer showed a strong attenuation of the vibrations: from 20 m s^{-2} at the cold tip to a maximum value of 0.5 m s^{-2} at the fixed-point device.

Should exchange gas be used inside this shield for cool down of an experiment placed in its interior, the chamber itself must be made vacuum tight. The modern refrigerators allow the experiment to remain connected to the lowest stage, even for operation of the experiment up to 300 K. This simply requires more power for the temperature control (up to several tens of watts).

An additional problem may be encountered with vibrations produced by the refrigerator when it uses an alternating piston. If the level of vibration is not acceptable (as is the case when using wire-wound precision thermometers), mechanical decoupling of the refrigerator from the cryostat and of the sensitive parts of the experiment from the equipment is required, however, at the cost of some cooling time lag. Thermal decoupling, such as that required when very high temperature stability must be achieved in the internal experiment, cannot be obtained without an additional lag in the cooling time. A temperature stability of 0.1 mK h^{-1} of the experiment has been reported with residual accelerations lower than 0.5 g (Sakurai and Tamura 1990).

Some types of modern refrigerators are intrinsically vibration-free (e.g., shock-tube refrigerators; Radebough 2009; ter Brake and Wiegerinck 2002).

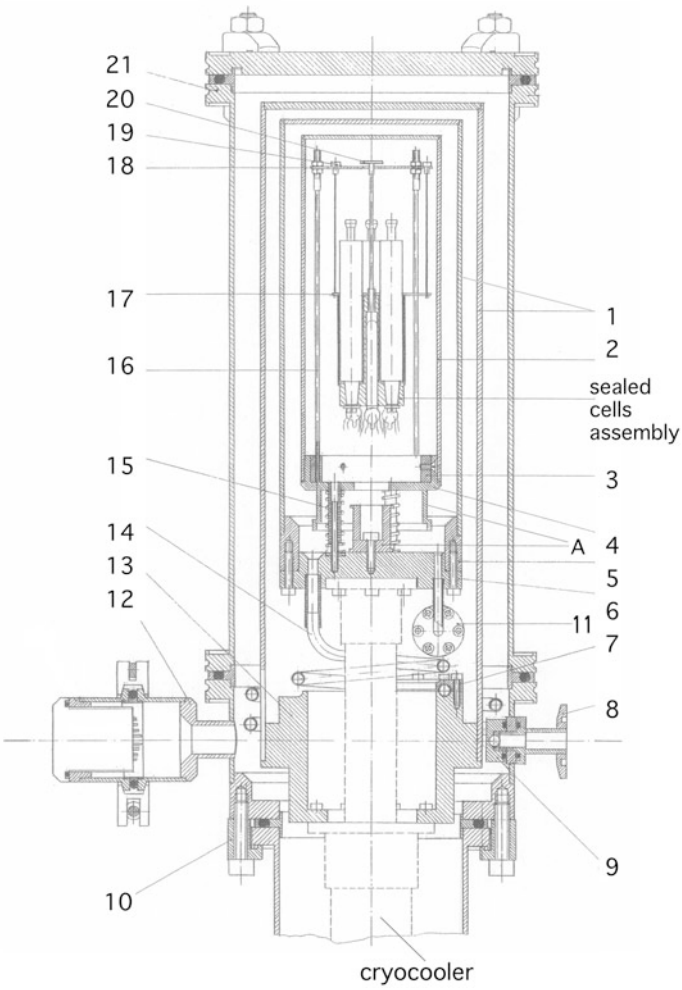

Fig. 6.2 Calorimetric cryostat mounted on the top of a vertical two-stage cryorefrigerator mounted upside-down (see text): *1* First and second cooling-stage cans; *2, 4* calorimeter: adiabatic chamber and shield; *3* mounting of the cell assembly; *6* flange connecting second cooling stage ($T_{\min} \approx 10$ K); A wire thermal anchors; *7* thermal clamp of the pipe at first cooling stage; *8, 9* pumping port for vacuum in the calorimeter; *10* connection to cryocooler body; *11, 12* vacuum-tight wire feedthroughs; *13* flange connecting first cooling stage ($T_{\min} \approx 50$ K); *14* pipe for separate vacuum—or exchange gas—in the calorimeter (inside second-stage can, sealed with indium seal *5*); *15* spring suspension of the calorimeter; *16–20* cage and wire suspension of the cell assembly; *21* general vacuum outer can

This type of cryocooler-based cryostats are widely used—e.g., see Hill and Steele (2003), Sakurai and Tamura (1990), and Sparasci et al. (2011).

The more modern cryogen-free cryostats can reach a base temperature of ≈3.5 K using, e.g., a vertical *two-stage* shock-tube refrigerator. It can be equipped with an

adiabatic calorimeter designed as the one already described in Fig. 6.2 but placed beneath it, because this type of cryocooler cannot be mounted upside-down (nor horizontally).

The latter types of refrigerators allow operation down to 0.65 K (Shimazaki et al. 2008) by using its small ^{4}He-liquefaction capability and an internal module equipped with a pumped ^{4}He bath (see Sect. 6.1.2.1) or, for lower temperatures, a small closed-cycle ^{3}He Joule–Thomson expansion circuit that utilizes the isenthalpic expansion of ^{3}He for cooling (Shimazaki et al. 2008). Even dilution refrigerators can now be used in conjunction with cryocoolers.

For temperatures lower than about 3 K also bath cryostats are still normally used, down to 1.5–2.2 K (see Sect. 6.1.1.2). For lower temperatures, down to approximately 0.3 K, a ^{3}He refrigerator is generally used, which can ensure continuous operation if designed for external pumping on the ^{3}He bath, or intermittent operation (up to several hours per cycle) if designed with a built-in adsorption pump. Figure 6.3 shows an implementation of the latter design. It requires a bath-type cryostat, but not a dedicated one; in fact, the ^{3}He refrigerator is built as a fully independent module fitted into the reentrant well (Ø 115 mm in the figure) of the cryostat. In addition, the refrigerator includes an axial reentrant well (Ø 34 mm) for direct insertion of the experiment into the cryostat cold chamber.[1] This is particularly useful in the case of either vapor-pressure or gas thermometers with room-temperature manometer, because the thermometer setup can be made independent of the cryostat.

6.1.1.2 Refrigerated-Bath Thermostats (200 to 300 K)

In the temperature region above 200 K, which is more properly the domain of traditional "refrigeration" than of "cryogenics" but in which the IPT-90 (or some of its approximations) requires a fixed point, a refrigerated-bath thermostat (using a freezer-type traditional refrigerator) can be considered a more convenient solution instead of a vacuum cryostat, for specific applications or when lower temperatures need not be reached. Refrigerated-bath thermostats generally make interchangeability of experiments or thermometers simpler, as with them vacuum is not used for thermal insulation. These baths can be used at temperatures as low as 150 K (near the melting point of isopentane), but their use becomes increasingly difficult as temperature decreases, especially in connection with trapping of air moisture. Since the liquid in the bath would become contaminated by moisture, its condensation into the liquid must totally be avoided by sealing all inlets from the ambient to the bath, including thermometer wells, or by utilizing a gas purge. A single-stage closed-cycle refrigerator equipped with a "dry" cryostat is probably a better solution in many cases.

[1] Of course, the experiment must be provided with an efficient thermal anchoring, made more difficult, at these temperatures, by the Kapitza boundary resistance.

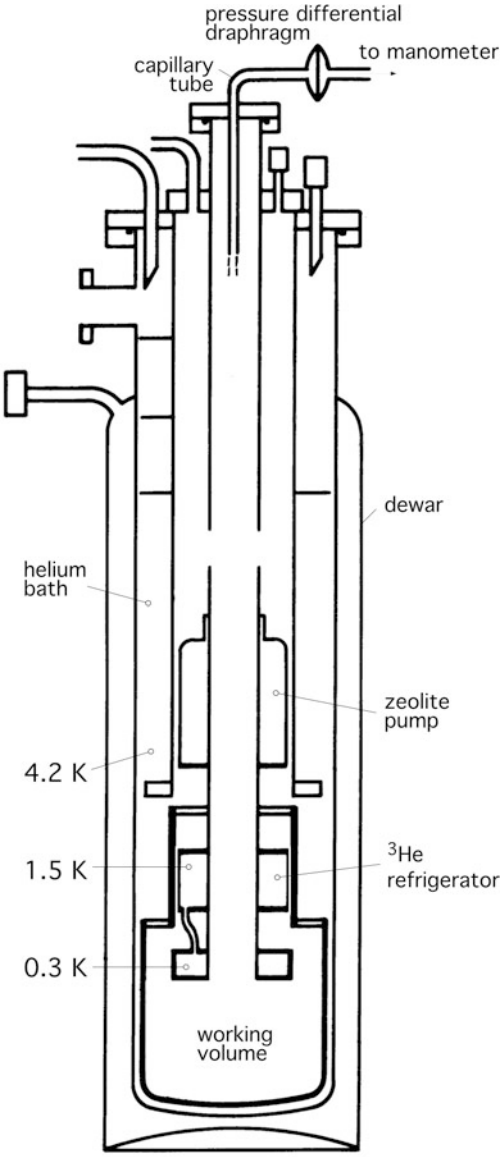

Fig. 6.3 Cryostat with ^{3}He refrigerator. ^{3}He is condensed by cooling via the ^{4}He 1.5 K pot and pumped with the built-in zeolite pump from the lower pot, whose temperature is thereby cooled down to ≈0.3 K

6.1.2 Liquid-Refrigerant Cryostats

The most traditional and widespread type of cryostat is the liquid-refrigerant cryostat. Refrigerants such as liquid nitrogen and helium, more rarely liquid air and hydrogen, are used.

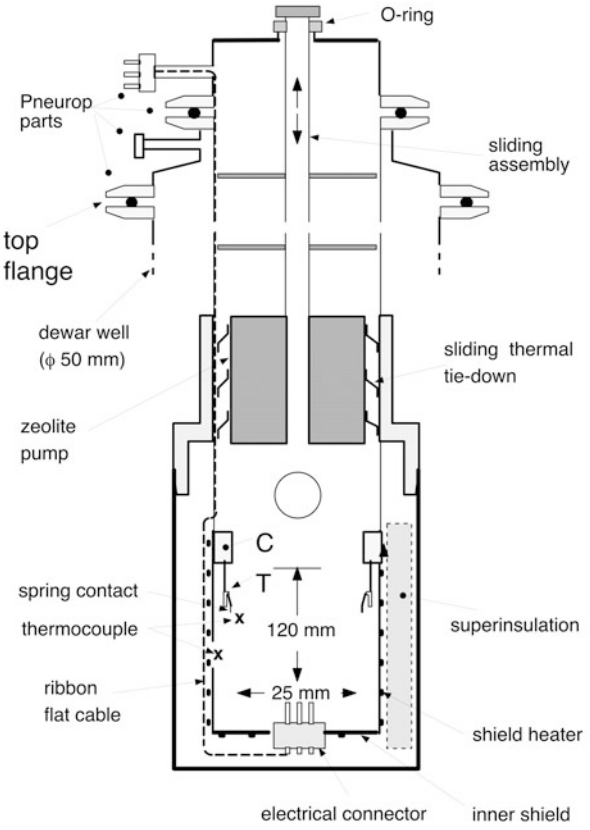

Fig. 6.4 Top-loaded bath cryostat. The cryostat is inserted directly in a ϕ 50-mm-neck storage dewar (*top flange*). Vacuum is provided by a built-in zeolite pump that can be slid down. The experiment is mounted inside the inner shield without the need of a permanent stem connection, and using the built-in connector for the wiring. Shield temperature is regulated with respect to the experiment, which must be in thermal contact only with the sliding contact via the differential thermocouple

6.1.2.1 Bath Cryostats

The experimental chamber of the cryostat is generally immersed in the bath and is thermally insulated from the bath by high vacuum or, occasionally and only for modest-quality measurements, by rough vacuum or, even more simply by foam insulation. Foam insulation can also be used in conjunction with rough vacuum, or multilayer insulation can additionally be used as well. Cool down is obtained by simply admitting some exchange gas, generally ^{4}He, into the cryostat chamber; only in special cases, when helium pumpout would be difficult, heat switches are used.

Bath cryostats may contain refrigerating systems to attain lower temperatures, down to $\approx$0.3 K, by using a pumped ^{3}He bath, as depicted in Fig. 6.4, or too much lower temperatures (typically 10–30 mK) by using a ^{3}He–^{4}He dilution refrigerator or other special refrigerators. The ^{4}He refrigerating bath itself can be further cooled down, by pumping directly on it or on some liquid fed into an annular can (the so-called "lambda plate"), down to the superfluid phase at $\approx$2 K.

In general, one may want to use one refrigerant down to the lowest possible temperature. This means efficient pumping on the liquid—or solid—down to the lowest possible bath pressure. As the heat removed with evaporation gradually decreases with temperature, the bath itself must be thermally well-insulated.[2] Therefore, often, some liquid is admitted from the main bath into an internal smaller container that is maintained at vacuum and insulated from it.

By pumping on the ^{4}He in such a small bath, temperatures of 1.2 to 1.5 K are easily achieved with proper techniques to trap the superfluid ^{4}He film. The lowest temperature attained by combining film trapping and pumping by (zeolite) adsorption was, by chance, coincident with the lower limit of ITS-90 (Goldschvartz et al. 1975). In fact, a temperature lower than 0.65 K was maintained during ≈2 h, but no technical reasons limit the time period.

With any other refrigerant, an additional problem is caused by its solidification, which makes efficient pumping and good heat transfer to the experimental chamber much more difficult. Solid hydrogen is often considered for space applications, not only because temperatures down to about 6 K can be attained, but also since advantage can be gained from the "refrigeration enthalpy" that can be stored because of its high molar enthalpy of sublimation (≈1 kJ mol^{-1}, see, e.g., Bellatreccia et al. 1979). Slush hydrogen is also sometimes used.

Solid nitrogen is often used to the lowest possible temperatures in order to avoid the use of the much more costly liquid helium, difficult to obtain in some countries. Actually, the realization of fixed points down to the triple point of oxygen (≈54.4 K) does not require the use of liquid helium. It is relatively easy to attain temperatures of 40–45 K with solid nitrogen; with special designs (Larin 1976), it is possible to attain temperatures <30 K, i.e., below the $\alpha - \beta$ transition, itself a reference point (see Appendix B and Table 2.5). Of course, the admissible thermal load at these temperatures is very small—of the order of 1 mW.

Instead of submerging the experimental chamber of the cryostat into the bath, it can be thermally connected to some convenient external location on the wall of the refrigerating bath container—generally the bottom. In this case refrigeration inside the chamber is obtained by conduction, while the chamber walls remain at room temperature. Therefore, the experiment must be vacuum insulated from the ambient, as it is when a closed-cycle refrigerator is used.

In both cases this technique has the disadvantages noted at the beginning of this chapter, namely access to the experimental chamber of the cryostat requires not only full evaporation of the refrigerant, but time-consuming warm up of the entire apparatus to room temperature.

The only way to limit the time required to operate this type of cryostat is to avoid removing the entire cryostat whenever something must be changed in the experiment. Consequently, first of all, the experiment must be designed to be *independent* of the cryostat. Second, the cryostat must be designed with a reentrant well, where the experiment can be inserted through a room-temperature top flange. Figure 6.4 presents a schematic drawing of such a "top-loading" arrangement for an immersion cryostat.

[2] In order to reduce heat transmitted by radiation, may even take advantage, today, of the radioactive properties of the new high T_c superconductors (Zeller 1990; Pavese 1995).

When the experiment has to be changed without even breaking vacuum in the cold cryostat, an anticryostat isolated from the cold part by means of a gate valve and possibly including a precooling device, has to be added (not shown). Incidentally, the cryostat shown in the figure is designed (Pavese et al. 1990d) to fit directly into a typical 50-mm-neck storage dewar, thus avoiding the need for a dedicated dewar system and all the cryogenic accessories such as transfer tubes, liquid level probes, etc. as well as the problems involved in the transfer of liquid cryogens. It allows, e.g., in performing an ITS-90 calibration, the sealed cells realizing the different fixed points to be quickly interchanged.

The main problem encountered with a design of this type involves thermal tie-down of the insert, in such a way that the heat transferred from room temperature can be properly dissipated into the refrigerant without perturbing measurements. In addition, thermal anchoring of the removable module must be of the sliding type (Pavese 1975d). Movable or removable thermal contacts at cryogenic temperatures involve serious problems, which become more difficult with decreasing temperatures or with increasing energy dissipation. The possibility of this solution can place a limit to this type of design. The problem is even more difficult when the insert must be removed in a *cold* condition since this requires *dry* contacts under vacuum. Otherwise, thermal contact can be improved considerably by "wetting" the pressed contacts (e.g., by vacuum grease). The experimenter should consult the relevant copious literature.

6.1.2.2 Flow Cryostats

In the past, flow cryostats provided the only solution permitting refrigerant baths and their shortcomings to be avoided, when closed-cycle refrigerators were not readily available. Basically, the design of such a cryostat is similar to the one shown in Fig. 6.1 for the closed-cycle refrigerator, where each shield is refrigerated by means of a coiled tube in which a cold gas flow, obtained from direct evaporation of a liquid refrigerant, is forced to pass. For convenience, particularly when using helium, a cryostat of this type by proper design can stand directly *on* the storage dewar, avoiding an external transfer line, as shown in Fig. 6.5 (Kemp et al. 1986).

The lower temperature is generally limited to about 10 K, since below this temperature the liquid phase also tends to circulate in the coil, thus making the controlled temperature unstable. This inconvenience can be avoided by placing a sintered filter at the coil input, incorporating the evaporation heater. In principle, even subcooled helium could be forced into the tubes. Temperature can be regulated by controlling the flow rate of the flowing gas, and be made extremely stable (within ± 0.1 mK (Kemp et al. 1986)).

Although a cryostat of this type has been used for thermometry work (Blanke and Thomas 1981; Pavese and Ferri 1981c), and in precision gas thermometry (Kemp 1986) as well, its use has presently been replaced with the closed-cycle refrigerator, though it may still be considered in the design of very small cryostats requiring minimal sophistication.

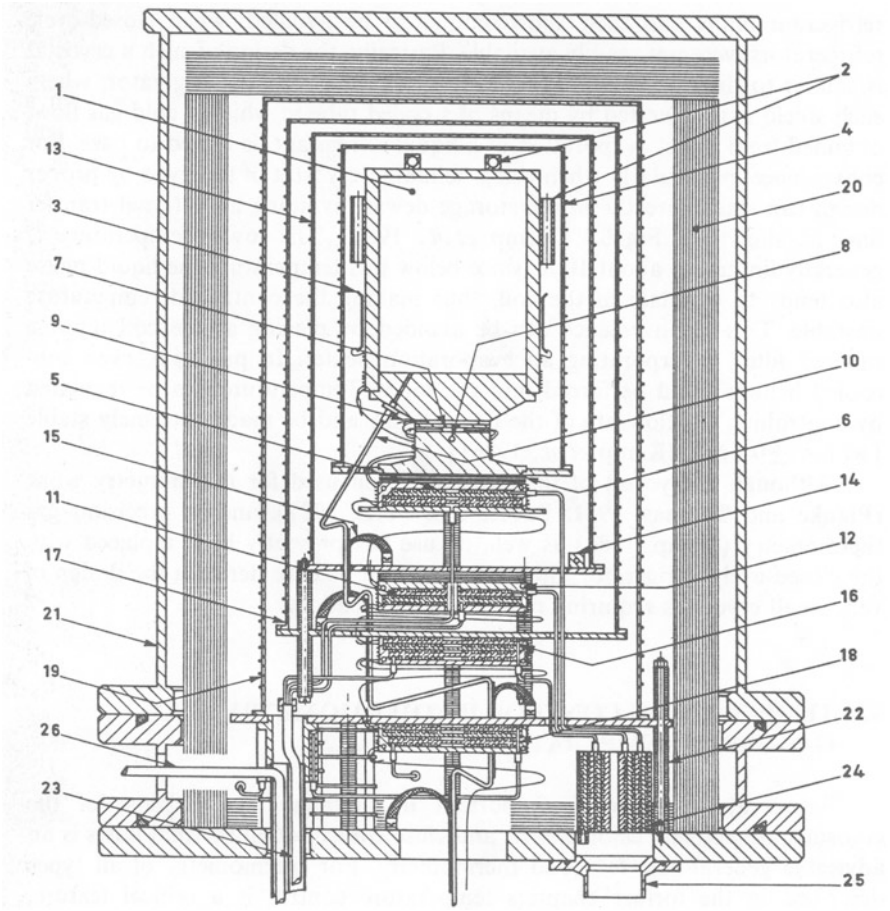

Fig. 6.5 Flow cryostat (shown with a CVGT (*1*) mounted in the experimental chamber); (*2, 7, 9, 12, 14*) thermometers; (*3, 15*) heat sinks; (*4, 13, 17, 19*) shields; (*5, 11, 16, 18, 24*) gas-cooled refrigerators; (*6, 22*) stainless steel spacers; (*8*) heater; (*10*) CVGT capillary; (*20*) multilayer insulation; (*21*) vacuum can; (*23, 26*) liquid helium siphon; (*25*) lead exit. (After Kemp et al. 1986)

6.2 Temperature Control in Thermometry and Gas-Based Temperature Controls

Temperature control is important in thermometry, as most of the cryostats are actually calorimeters, and close control of all thermal flows is an advisable general rule for good thermometry. For thermometry of all types described in the former chapters, temperature control is a critical feature *except for the realizationof triple points*.

Since a triple point is itself self-stabilizing through its melting energy (see Sect. 2.1), the triple-point cell is quite unaffected by thermal exchange with the

environment, apart from thermal gradients, and can thus be used as the reference temperature for temperature control of the cryostat shield(s), simply by means of differential thermocouples. This thermometry type does not need costly and delicate absolute temperature regulators. A single isothermal shield with a differential regulation maintained within ≈0.1 K is sufficient to obtain the highest accuracy. With some triple points, such as that of argon that is close to the refrigerant temperature, a vacuum cryostat is not even necessary. Foam insulation of the isothermal shield in a sealed container immersed in liquid nitrogen is sufficient for an accurate realization of the fixed point (Pavese et al. 1975a).

However, the intention of this section is not to introduce conventional temperature regulations, but to review the techniques that use *gases* for temperature control.

6.2.1 Control of the Cryogen Bath Temperature

Temperature can be controlled through direct control of the cryogen temperature. This is generally attained by control of the cryogen boiling pressure, which is more effective when the dp/dT is large, i.e., at the higher temperatures. The control is performed, in general, on liquids or solids that are subcooled by pumping (see Sect. 6.1.2.1). In the past, the classical approach involved the "Cartesian manostat," a differential device utilizing a short U-tube containing mercury; membrane types were also available. Today, a diaphragm capacitive transducer is generally used, which allows electronic pressure control.

The same principle can also be applied to cryogen baths boiling at temperatures *higher* than the atmospheric. With helium there would be little advantage, since the critical point is at only 5.2 K, but the principle could be applied in laboratories that are located above the sea level, or when the normal boiling point temperature (i.e., at exactly 101 325 Pa) must be exactly reproduced when the atmospheric pressure is lower. This is an alternative to *correct* for the temperature differences, as required by some engineering tests. With liquid nitrogen the advantage is greater, since the boiling temperature can be raised from ≈77 K to about the triple-point temperature of argon, ≈84 K. This has been done in a realization of the argon triple point as a temperature- fixed point (see Sect. 2.4.2). In such cases, a passive pressure regulation can be achieved by using a gravity vent valve, which sets a fixed pressure difference with respect to atmospheric pressure. By changing the load on the cap—which must be protected from moisture condensation by placing it in the dry vent stream—one changes the boiling temperature of the bath.

A temperature control of this type, however, does not avoid the temperature gradients that arise in the bath from the hydrostatic-head effect, unless the liquid is stirred by means, for example, of bubbling some gas through the bath.

6.2.2 Vapor-Flowrate Control

The vapor-flowrate control consists in throttling some liquid from the refrigerant bath, evaporating it, and regulating its temperature (e.g., by sending it through a loosely sintered temperature-controlled copper plug), then allowing the vapors to enter *into* the experimental chamber where they perform the temperature regulation via thermal contact with the experiment. In other words, the vapors act like a circulating, temperature- controlled, exchange gas. Although this technique is claimed to achieve temperature stabilities as good as ±0.01 K, this value seems somewhat quite optimistic. Nevertheless, this technique can be a very efficient one not to control temperature, but to obtain refrigeration in the precooling chamber connected to a top-loaded cryostat as in Fig. 6.5.

A similar control, but with much better results (up to ±0.1 mK), is obtained with the vapors circulating *in the coils* of a flow cryostat (Fig. 6.6), as discussed in Sect. 6.1.2.2.

6.2.3 Passive Thermostats

Accurate temperature regulation (to better than ±1 mK over the long term) is not only difficult to achieve and costly, but also requires resources not always readily available, such as electrical energy in space applications or in unattended locations on the Earth. However, the high-enthalpy triple-point cells described in Sect. 2.4.1.3 can fulfill this task. As indicated there, stability better than ±1 mK can be achieved, depending on the amount of sealed cryogen, over time periods much longer than 1 year, with a convenient choice of temperature values and a short-term stability on the order of few microkelvins. As already discussed, the temperature control of the cell shield is not critical, and requires either a simple electronic controller or a control making use of the stray refrigeration paths available in cold satellites (or from the cold space), resulting almost in an entirely passive system. Furthermore, the thermostat can be regenerated, like a rechargeable battery, by cooling it again just below the triple point.

6.2.4 Self-Regulating Passive Shields

Temperature self-regulated shields represent an extrapolation, for less accurate temperature control, of the concept described in the preceding section. Consider the fabrication of a shield that is similar to the triple-point cell shown in Fig. 2.38(2) (Sect. 2.4.3.1), i.e., consisting of a metal tube coiled in packed helical manner and filled with a high-pressure gas. Calculations of the same type as those reported in Sect. 2.4.1.3: a shield, storing 2 mol of argon (i.e., storing about 2.4 kJ) at 30 MPa and with 40 mm (internal) diameter and 220 mm length (a size suitable to contain a sealed cell for temperature- fixed points), can be constructed from a double-layer

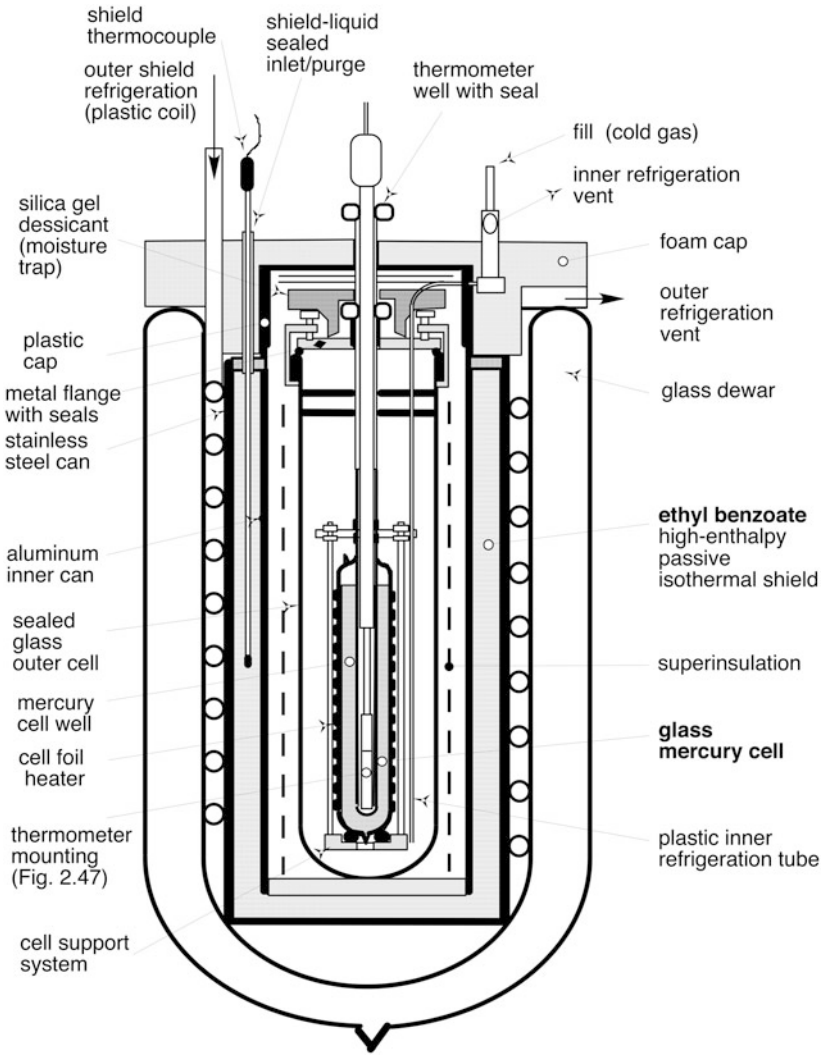

Fig. 6.6 High-enthalpy shield (ethyl benzoate, $T_{tp} = 238.55$ K) used for the realization of a simple, passive thermostat for measuring the triple point of mercury. For the sealed glass outer cell containing the mercury cell, a model used for metal fixed points has been used. For the outer shield refrigeration and for the inner refrigeration, evaporated liquid nitrogen was used. (After Pavese et al. 1999)

coil of stainless steel tube, Ø 4–6 mm. Such a shield, when brought to the triple-point temperature of the enclosed gas, maintains a fixed temperature as long as the three phases are coexistent in the coil, and acts as a passive temperature control, apt to compensate for a thermal exchange up to about the enthalpy of melting of the enclosed amount of substance (2.4 kJ in the example).

Conceptually, this device is similar to the high-enthalpy cells that are sometimes used for wall or floor construction in energy-conscious house design; such cans simply contain a substance undergoing a phase transition with a high-enthalpy change in the 15–25 °C range, and thereby act as heat compensators for room-temperature conditioning.

As an example of application using a liquid, Fig. 6.6 shows a high-enthalpy self-regulating shield using ethyl benzoate, an extremely volatile liquid with $T_{tp} = 238.55$ K—close to mercury triple point $T_{90} = 234.3156$ K—in a thermostat used for the realization of the triple point of mercury (Pavese et al. 1999): it allows, without active regulations, to obtain melting plateaus lasting more than 10 h and to measure mercury T_{tp} with the same accuracy obtained using more sophisticated cryostats.

6.2.5 Gas-Filled Heat Switches

Heat switches are important components in many cryogenic applications. They are on-off devices permitting heat flow with the least temperature drop when ON, and reducing heat flow by several orders of magnitude when OFF.

Heat switches with good performances are difficult to build. They can be divided into two categories, depending on whether they utilize movable metal-to-metal contacts or a gas at different pressures. The literature on the former type of heat switches and on pressed thermal contacts is wide: the same information is useful for the design of sliding thermal contacts also. In the following sections, only the basic design parameters will be discussed for the gas-filled type, which can actually be realized according to different principles, and therefore will be considered separately.

6.2.5.1 Gas-Type Heat Switches

The basic elements for a gas-filled heat switch are shown in Fig. 6.7. The unit is fabricated by facing two surfaces separated by a narrow gap; the so-defined volume is sealed by an external low thermal conductivity envelope—often a plastic material suitable for cryogenics and not permeable to the gas used to fill the switch. The geometrical design can be varied with different solutions of the technical problems involved in the fabrication. A small-diameter tube allows the switch to be filled with some gas (ON condition) and to be evacuated (OFF condition).

Two equations available in any handbook of vacuum technology form the basis for the working principle of this switch.

When the mean free path L of the gas molecules is much greater than the gap x between the two surfaces having an area A, heat transfer is governed by the usual, pressure- independent, thermal conductivity equation

$$\dot{Q} = \lambda \frac{A}{x} \Delta T \tag{6.1}$$

where λ is the thermal conductivity coefficient of the gas.

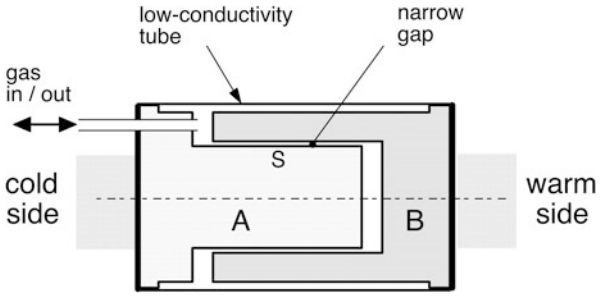

Fig. 6.7 Layout of a gas-filled heat switch

Conversely, for gap dimensions that are small with respect to the mean free path, heat transfer is governed by the pressure-dependent Knudsen equation

$$\dot{Q} = K_s A \, \Delta T p \tag{6.2}$$

where K_s is a constant depending on the geometry of the switch and on the gas.

Between these two regimes, there is a transition regime (Knudsen number s $K_n = L/x$ from $\approx 10^{-2}$ to 0.5) where the thermal conductivity values fall between those calculated from Eqs. 6.1 and 6.2. A detailed analysis of this region is irrelevant here. The mean free path dependence on temperature and pressure can be expressed as

$$\Lambda = \Lambda_0 \left[\left(1 + \frac{\theta_0}{T} \right) \right]^{-1} \tag{6.3}$$

where Λ_0 is the mean free path at high temperature and 0.1 MPa, and θ_0 a temperature characteristic for each gas.

In order to achieve an ON thermal conductivity of $\approx$1 W K^{-1} m^{-1}, it is necessary to use gap values of 20 to 100 mm with surface areas on the order of 10 cm^2 and to use suitable body materials (Nast et al. 1982).

The OFF heat flow depends mainly on the material used for the tube connecting the warm and cold sides of the switch. If some types of reinforced plastic (their permeability to the gas used must be carefully considered) are used instead of the usual stainless steel (titanium could be used as well), ON/OFF ratios of 2000 to 3000 can be achieved.

True OFF condition for the gas thermal conductivity can only be achieved when the gas pressure is sufficiently low ($K_n \gg 0.5$). The free molecular regime is only achieved for pressures $\approx <10^{-2}$ Pa. Therefore, the goal is to obtain a pressure of about 10^{-3} Pa after only a few minutes of pumping; this can be obtained only with the proper design of the filling-/pumping-line parameters. For filling, a capillary tube is obviously adequate, but for quick pump down a large tube diameter is required, unless the tube can be kept very short. The conductance of a tube in the molecular regime can be expressed by

$$C \approx \frac{p}{3} \frac{d^3}{h} \sqrt{\frac{RT}{2\pi M}} \tag{6.4}$$

where d and h are the tube diameter and length, respectively, and M is the molar mass of the gas. The conductance is expressed in liter per second of gas at the pumping pressure p. For ^{4}He at 20 K in a 10-cm-long tube with a 1 mm diameter, $C \cong 200$ mL s^{-1}.

The pressure-versus-time equation of the pressure decrease under constant pumping speed leads to a solution in exponential form, whose time constant is $t = V/C$ ($C \equiv S$, having assumed the pumping speed $S_p \gg C$). Therefore, the time t required to reach the required pressure p_0 from an initial pressure p_i is

$$t = \frac{2.3V}{C} \log \frac{p_i}{p_o} \tag{6.5}$$

For $p_i = 10^4$ Pa, $V = 0.01$ L and $C = 200$ mL s^{-1}, the time required to reach $p_0 = 10^{-3}$ Pa is ≈14 min. In a room-temperature apparatus, considerably more time would actually be required to attain 10^{-3} Pa due to the outgassing from the walls. At low temperatures, this is not a problem, but helium can be adsorbed on the surfaces and its desorption time may be a problem that requires consideration. In addition, some impurities can *condense* onto the cold surfaces and their vapor pressure remains higher than p_0 at the working temperature. A vapor pressure of 10^{-3} Pa is only attained at ≈5 K with H_2, ≈9 K with Ne, ≈30 K with N_2, Ar, and O_2, ≈45 K with Kr, ≈90 K with CO_2, and ≈150 K with H_2O.

A heat switch of this type generally requires a tube for connection to an external filling and pumping system, a configuration that can be quite inconvenient. An elegant, and extremely convenient, solution of this problem (Frank and Nast 1986) is the use of a microscopic sorption pump connected to the switch with a very short capillary tube.[3] A heater on the pump makes it possible to switch ON/OFF the pumping action. An additional advantage of this solution is that the heat switch can be maintained even at an intermediate state of conduction. Ultimately, a heat switch of this type becomes an electrically controlled device instead of a temperature-controlled one, as well as a sealed device.

6.2.5.2 Thermosiphon- and Condensation-Type Heat Switches

A thermosiphon normally consists of a vertical pipe closed at both ends and partially filled with a liquid under its own vapor pressure. Therefore, a heat switch of this type can be a sealed device, if designed to withstand a room-temperature high pressure (up to ≈2 MPa). When the lower pipe end, which is called the "evaporator," is warmer than the upper end, or "condenser," the liquid collected at the bottom evaporates and streams upward as a vapor, condenses at the top, and flows down as a liquid film on the walls. An internal body, often a grid, can be added so shaped as to improve the evaporation and, especially, the condensation process, whose onset during cool down can result somewhat delayed (i.e., the vapor undergoes some subcooling). Facing

[3] A similar solution has been used by Van Degrift in his miniature gas thermometer (see Sect. 3.3.3) for maintaining the reference vacuum in his resonator pressure transducer.

cones have been used for this purpose in one instance (Yamamoto 1984). Obviously, this mechanism works only under (earth) gravity conditions. Heat transport in the ON condition is considerable and very effective ($\lambda \cong 1$ W K^{-1} m^{-1}), even over long distances. It is sustained by an overpressure with respect to the saturated vapor pressure, which is proportional to the temperature drop. When the evaporator is colder than the condenser, the switch is in the OFF condition and only a much smaller amount of heat flows downward owing to the small thermal conductivity of the tube and of the gas. This principle has been used for a long time for cool down of cryogenic equipment (Bewilogua and Knoner 1961).

Obviously, heat switches of this type only act within a fixed and narrow cross-over temperature range, above the normal boiling point of the gas used (N_2, Ne, D_2, H_2, ^{4}He, etc.). In fact, the switch is ON only when there is enough liquid present in the condenser. The switching temperature range therefore depends to some extent on the filling density. As is the case with a sealed container discussed in Sect. 2.2.1, the dew point temperature will depend on the room-temperature filling pressure and on the ratio between the cold and warm volumes. An ON/OFF ratio of $\approx$1000 can easily be achieved, and large quantities of heat can be exchanged effectively with a short time lag (Gifford 1969).

The condensation-type heat switch does not exploit the thermosiphon action, so that its action is orientation (and gravity) independent, but still exploits vapor pressure changes with temperature. Since heat is not transported by a mass flow rate, as in the former type, only the thermal conductivity of the gas and, after condensation, of the vapor carries out, in a switch of this type, the thermal connection, which brings to the ON condition. Therefore, similar to the gas-type switch described in Sect. 6.2.4.1, only allowing a very small gap between cold and warm surfaces of the switch can ensure a sufficiently high thermal conductivity. The difference is that here the filling gas is *sealed* in the switch; care must be taken to ensure that under the OFF condition the solid phase (and also the liquid phase, with high filling density) does not "short-circuit" the switch. The OFF condition is achieved, for most gases, only after the solid is formed, since at the triple point the pressure value is still well within the viscous regime of conduction. A switching ratio $>$500 can easily be achieved (Hilberath and Vowinkel 1983). Helium cannot, of course, be used in a switch of this type. The switching temperature is fixed for each gas and is considerably lower than that of the former type. With nitrogen, for example, it is $\approx$35 K ($\approx T(p_0)$ in Sect. 6.2.4.1), whereas it is $>$80 K for the thermosiphon type. With hydrogen, it is $\approx$6 K. Of course, great care must be taken to keep the partial pressure of the volatile impurities (mainly helium) much below p_0 or the OFF characteristics will be severely degraded.

The use of heat switches of this type is typical in refrigerators, where precooling of the lower stages has to be carried out at the expense of the upper stages or of a liquid refrigerant and, eventually, the refrigerator must be thermally isolated for further cooling.

Summary 6.1 Strategy for Cryostat Selection

1. Minimum-temperature requirement:
   - >200 K: Peltier-effect cooling
   - >150 K: Stirred organic-liquid freezer-type refrigerated bath
     - One-stage closed-cycle refrigerator
   - >≈90 K: liquid-nitrogen flow cryostat
   - >≈50 K: (pumped) liquid nitrogen bath cryostat
     - One-stage closed-cycle refrigerator
   - >12 K: liquid-helium flow cryostat
     - Two-stage closed-cycle refrigerator
   - >4.2 K: liquid helium bath cryostat
     - Three-stage closed-cycle refrigerator
   - >2.1 K: superfluid helium bath cryostat (with l-plate)
   - >1.2 K: cryostat with secondary superfuid helium bath
   - 0.4 K $< T <$ 1.2 K ^{3}He refrigerator (with cyclic/continuous pumping)
   - <0.3 K: dilution refrigerators
     - Adiabatic demagnetization
     - Special techniques
2. Availability of cryogenic experience and ancillary equipment:
   - Stirred organic-liquid freezer-type refrigerated bath: use similar to thermostats in the range 0–300 °C
   - Peltier-effect cooling: no cryogenics expertise required to the user
     Closed-cycle refrigerator: no cryogenics expertise required to the user
   - Flow cryostat: minimum of cryogenic expertise and ancillary equipment
   - Bath cryostat (liquid nitrogen >77 K; liquid helium >4 K): standard expertise
   - Temperatures below ≈3 K: specialized cryogenic work
3. Temperature control:
   - Peltier-effect: all solid-state (stability $\geq \pm 0.0001$ K)
   - Stirred organic-liquid bath: heater electronically controlled ($\geq \pm 0.01$ K)
   - Bath cryostat:
     - Vacuum type, heater electronically controlled ($\geq \pm 0.0001$ K with multistage control)
     - Vapor type, flow control of preheated vapor ($\geq \pm 0.03$ K)
   - Pumped bath type: bath-pressure control or controlled heater ($\geq \pm 0.1 - 0.01$ K depending on pressure; $\geq \pm 0.001$ K)
   - Flow cryostat: flow control plus optional controlled heaters ($\geq \pm 0.03$ K; ± 0.0001 K with multistage control)
   - Closed-cycle refrigerator: heat-load control via controlled heater (Base ± 0.2 K; ± 0.01 K or better with multistage control)
4. Type of cryostat:
   - Open: the experiment can directly be immersed in the cryostat. Type: stirred organic-liquid baths
   - All sealed: requires opening, in order to change the experiment in an experimental chamber confined inside the cryostat, one (or more):
     - Cold seal: most of the bath types
     - Room-temperature seal: upper-bath conduction cryostats
       - Flow cryostats
       - Most closed-cycle refrigerator based
   - All modular: allows to change the experiment without opening the whole cryostat. This can be done when:
     - At room temperature: the cryostat has a well connecting the experimental chamber directly with the outside. The experiment can be inserted with a fixed or removable mounting stem
     - Types: *with closed-cycle refrigerator*; bath; with Peltier cooling

Summary 6.2 (continued)

Cold: the cryostat shows a prechamber at the top of the mounting well, which avoids vacuum breaking and, sometimes, allows some precooling. Types: bath
The minimum working temperature is generally higher than ≈2 K, because of the limited thermal conductivity of pressed contacts, necessary for the movable thermal tie-down. There are noticeable exceptions, such as modules (as narrow as Ø 50 mm) with a built-in ^{3}He refrigerator and a liquid ^{4}He auxiliary bath as a thermal guard

- With removable experiment: it is the common solution for (very) low-temperature modular cryostats, where the experiment is fitted to a module, which can be extracted from the well, but the mounting of the thermal tie-downs requires to open the cryostat Types: bath

5. Thermal cycling speed from room temperature:
   - Very fast (<0.5 h):
     Peltier-effect cooling
     Miniature closed- and open-cycle refrigerator based
     Stirred organic-liquid bath (for sample change only)
     Modular with cold sample removal
   - Fast (<4 h):
     Small flow
     Small closed- and open-cycle cryorefrigerator based
   - Daily operation:
     Flow
     Closed-cycle cryorefrigerator based
     Small liquid-nitrogen bath
     Very small liquid-helium bath
   - Long:
     Bath above 2 K
     Pumped bath
   - Weekly planning:
     Large liquid helium bath
     ^{3}He refrigerator based
   - Very long:
     Refrigeration below 0.3 K
6. The type of experiment. Gas-based types of thermometry with uncertainty:
   <±0.001 K: adiabatic calorimeters. Types: all vacuum types with at least two adiabatic (isothermal) shields (only one for triple-point realizations), with suitable electronic temperature controls. Generally, not available commercially
   <±0.01 K: commercially available best cryostats. Types: as before with one isothermal shield (passive thermal insulation instead of vacuum sufficient for triple-point realizations only). In addition, with flow-type temperature control
   <±0.03 K: same as before, with the addition of the best vapor-type bath cryostats and stirred-bath cryostats
   <±0.1 K: most commercial cryostats and some cryostats with passive thermal insulation

Part II
Pressure Measurements in the Range from 10^2 to 10^8 Pa

Introduction

The pressure range (10^2–10^8) Pa has been selected, as it is the interval covering the highest variety of interests and applications in gas temperature and pressure measurements. Particularly, at low temperatures several gas-based types of thermometry require the most accurate pressure measurements for the exploitation of their potentialities in terms of top accuracy levels. Other specific points are the followings:

- Triple-point pressure determinations require measurements, typically from few pascal (e.g., n-butane, 134.843 K and 0.4 Pa) to a few megapascal (e.g., carbon dioxide, 273.16 K and 3.48608 MPa), of the highest possible accuracy, frequently involving the direct use of pressure primary standards.
- Vapor-pressure measurements are performed mostly in the same pressure range (Fig. 4.1) and the ^{3}He melting curve lies in the (3–4) MPa range.
- Gas thermometry extends typically from 1 to 200 kPa and is the most demanding as to accuracy.
- The determination of the critical point of gases and substances of interest such as water, requires pressure measurements extending from 0.2 to about 22 MPa. The critical point of ^{4}He is at 5.2 K and 0.22 MPa, and that of water is at 647.3 K and 22.12 MPa.
- On one hand, considerations of scientific interest (gas compressibility determination, the study of pressure effects on temperature measurements by secondary standards, the equation of state of gases, transport properties, etc.) and, on the other, considerations of industrial applications, which are very numerous in the range examined here, led us to extend the limit of the present survey to 100 MPa.

The international unit of pressure of the Système International d'Unités (SI) is the pascal (Pa), defined as a force of 1 N applied to a surface of 1 m^2; therefore, 1 Pa = 1 N m^{-2}. In this book, we shall use only the pascal and its multiples, like the kilopascal (kPa) and megapascal (MPa). Another recognized pressure unit is the bar (1 bar = 10^5 Pa). All other units (mm Hg, mm H_2O, at, atm, kgf·cm^{-2}, psi) should

be avoided and will not be used. The mm Hg unit, however, is still internationally accepted only in blood-pressure measurements, owing to its very-large diffusion and to the problems involved in the use of SI unit (e.g., hectopascal or kilopascal). In meteorology, the hectopascal (1 hPa = 1 mbar) is widely used.

Chapter 7
Primary Standards for Pressure Measurements

The primary standards used for pressure measurements are measuring systems that can be metrologically characterized completely and independently with reference only to the basic units of the SI system. When pressure is defined as force per unit area or as the height of a liquid column, pressure is, dimensionally, $p = [\mathrm{M\,L^{-1}\,T^{-2}}]$; a primary pressure standard will thus involve the measurement of mass, length, and time.

The ideal primary standard for pressure measurements operates correctly only when pressure is homogeneous in space, hydrostatic, and time independent.

In the range of pressures under consideration, the primary standards described here, appropriately designed and applying suitably selected working criteria, can reasonably satisfy the above conditions. Homogeneity and hydrostaticity are mainly problems pertaining to dissipative liquids or to solids, where pressure cannot be assumed a priori to be a scalar quantity. These problems are discussed in detail in connection with pressure standards according to the theory of stress by Decker (1972) and by Heydemann (1978). These authors were an invaluable source of information. However, when substances are gaseous, pressure in such media can be considered a scalar quantity.

Generally, a symmetric stress tensor $T_{\mathrm{ij}}(\mathbf{r},t)$ defines stress in space and depends upon position, $\mathbf{r}$ being the vector position and t denoting time.

Pressure $p(\mathbf{r},t)$ is defined as the negative of the average of the three normal stress components

$$p(\mathbf{r},t) = \frac{-(\mathrm{T}_{11} + \mathrm{T}_{22} + \mathrm{T}_{33})}{3}. \tag{7.1}$$

The shear stresses are given by the stress tensor

$$T'(\mathbf{r},t) = T_{\mathrm{ij}}(\mathbf{r},t) - \delta_{\mathrm{ij}}\, p(\mathbf{r},t). \tag{7.2}$$

The hydrostatic pressure condition is characterized by shear stress and isotropic axial stresses both equal to zero. This means that at a single point

$$T'_{\mathrm{ij}}(\mathbf{r},t) = 0 \quad \text{and} \quad -p(\mathbf{r},t) = \mathrm{T}_{11}(\mathbf{r},t) = \mathrm{T}_{22}(\mathbf{r},t) = \mathrm{T}_{33}(\mathbf{r},t). \tag{7.3}$$

F. Pavese, G. Molinar Min Beciet, *Modern Gas-Based Temperature and Pressure Measurements,* International Cryogenics Monograph Series,
DOI 10.1007/978-1-4419-8282-7_7, © Springer Science+Business Media New York 2013

This definition does not require static (i.e., time independent) conditions, although time-dependent changes generally involve shear.

Hydrostaticity in a region of the space implies that each point of the volume must satisfy Eq. 7.3. This, however, does not necessarily imply homogeneous (i.e., constant in space) conditions.

According to the above definition of pressure, nonhomogeneity in a hydrostatic medium in equilibrium may be caused by gravitational, magnetic, or electric forces, which in practice are often quite small, though in some cases not negligible, when compared with the applied pressures. It must be noted that neither homogeneous pressure nor homogeneous stress implies hydrostaticity, but simply constancy in space. In a laboratory pressure system, the time dependence in T_{ij} is generally due to a change of the system from one equilibrium state into another. From a practical standpoint, equilibrium is defined as the state that a system approaches asymptotically within a given time scale. All systems under pressure will undergo time-dependent shear stress with a certain characteristic relaxation time τ when equilibrium is disturbed. In many cases, especially with condensed gases and with liquids at low pressures, τ may be a small fraction of a second and it is usually negligible with respect to measurement times. With liquids, the stress tensor T' will in time tend to a zero value. The way to achieve equilibrium is highly dependent upon system configuration. With systems containing only fluids whose viscosity can be assumed constant throughout the system, the approach to equilibrium is characterized by stress components decreasing approximately exponentially with time. It must be noted that time-dependent shear stresses in condensed matter are generally associated with pressure changes, so that adequate time must be allowed for the system to attain equilibrium before reliable measurements can be made.

To determine pressure experimentally, one must measure the axial stress over a finite area. If pressure is homogeneous over that area, as is the rule in a fluid chamber, the simple force-per-unit-area relationship is valid, and pressure can be uniquely defined and determined to a high accuracy.

Among the different methods that can be applied in pressure measurements at the primary standard level, the following are the most important:

1. Pressure is measured at a fixed and stable temperature in terms of the displacement h of a liquid column of known density ρ_f under a known local acceleration of gravity g_L, in a first approximation (Fig. 7.1).

$$p = p_0 + \rho_f g_L h. \tag{7.4}$$

   Pressure is measured when the applied hydrostatic pressure and the displaced liquid in the column are in static equilibrium.
   Static equilibrium is understood as the absence of fluid motion due either to pressure variation or to disturbance (convective motions, vibrations, temperature changes, ...) in the measuring liquid in the column. The presence of a gas flow, even if very small, prevents the measuring system from reaching complete equilibrium, and this can create a loss in measurement accuracy by an amount unpredictable a priori.

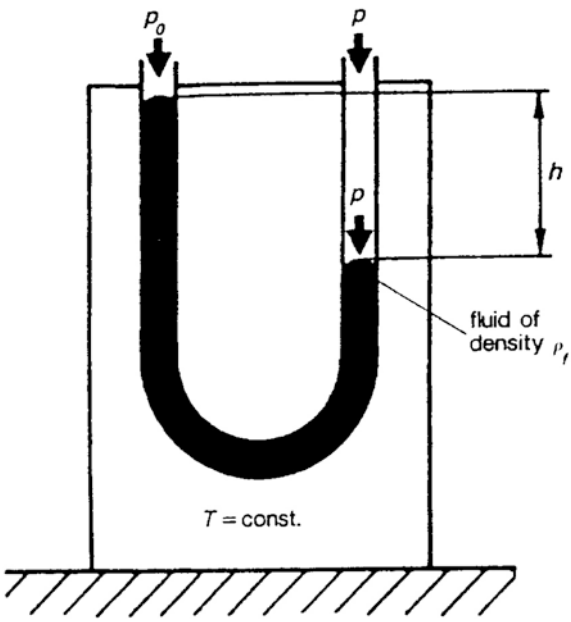

Fig. 7.1 Liquid-column manometer of simple configuration

The conditions of homogeneity, hydrostaticity, and time independence according to laboratory requirements can easily be fulfilled with liquid columns up to approximately 0.3 MPa.

2. Pressure is measured under conditions of equilibrium between the force produced by a mass m in a gravitational field of gravity acceleration g_L and the resulting force produced by the pressure exerted on the end of a cylindrical piston of effective area A_e fitted in a hollow cylinder (Fig. 7.2).

In a first approximation, one has

$$p = \left(\frac{m g_L}{A_e}\right) + p_0. \tag{7.5}$$

The general principle of this system (called pressure balance or piston-gauge, dead-weight tester, manometric balance, dead-weight piston-gauge) is based on the definition of pressure as force per unit area. The homogeneity condition is satisfied in this case when pressures p and p_0 are stable and a well-defined pressure gradient is allowed to stabilize over the whole length of the clearance between the piston and the cylinder through which the gas flows. The pressure gradient is a function of the geometry of the piston-cylinder unit, of the piston and cylinder materials, and of the pressure range and of the type of fluid used. The equilibrium condition is established when, and only when, the piston and the additional standard weights that may be placed on it float in a regular manner, i.e., the standard weights and the piston fall at a constant and reproducible fall rate. The piston fall rate is a function of pressure, temperature, and piston-cylinder geometry. If the geometry of the piston-cylinder unit

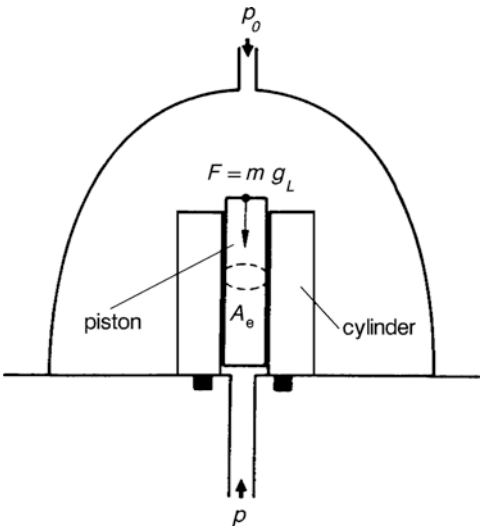

Fig. 7.2 Piston-gauge of simple configuration

is of a sufficiently good mechanical quality, the piston fall does not affect pressure p in the chamber below the piston.

All the above conditions of homogeneity, hydrostaticity, equilibrium, and time independence are generally satisfied, particularly in the case of highly accurate pressure balances, such as those used by national standards laboratories.

In practice, primary instruments both of the liquid column or of the pressure-balance types measure the differential pressure $(p - p_0)$ across the liquid column or across the piston-cylinder unit.

Absolute Pressure Measurements In "*absolute*" pressure measurements, the reference pressure p_0 is theoretically equal to zero. Actually, the reference pressure p_0 is a "vacuum" pressure generally ranging from 0.01 to 0.1 Pa; this reference pressure must be measured and taken into account to obtain the best measurement accuracy.

Differential Pressure Measurements In "*differential*" pressure measurements, the reference pressure p_0 can be any value that is compatible with the types and working ranges of the primary standards employed.

For example, with a liquid-column primary standard, p_0 can range from 0.01 Pa (absolute condition) to the highest pressure typically allowed by the liquid-column apparatus, which is of the order of 0.1–0.3 MPa; with some special metallic columns pressure p_0 may be as high as 10 MPa.

With pressure balances, p_0 typically ranges from 0.01 Pa (absolute condition) to the atmospheric pressure value. Pressure balances are seldom used for p_0 greater than 0.1 MPa, though, in principle, they can operate under such conditions if appropriately designed for this particular use (see Sect. 7.2.5).

Relative or Gauge Pressure Measurements "*Relative*" or "*gauge*" pressure measurements, which are very important and common in pressure metrology, represent

a subcase of differential pressure measurements when p_0 is the atmospheric pressure value. In this instance, particularly when mercury columns are used, fluid contamination by atmospheric agents should be avoided by protecting the liquid columns from air and by using a pure gas maintained at a pressure equal to that of the atmosphere by means of a differential pressure transducer used as a separator. However, pressure balances can directly be maintained at the room atmospheric pressure.

Obviously, measurements must in some cases track out possible variations in the atmospheric pressure value (typical daily variations can be as high as 100–500 Pa; in one week variations are generally lower than 8 000 Pa).

Thermodynamic Methods Beside the two basic measurement criteria, i.e., with liquid columns and pressure balances there exist others for primary pressure determination, for example, those exploiting thermodynamic relationships.

The methods based on such criteria are generally applied for the measurement of pressures higher than the maximum pressure (10^8 Pa) considered here, but in principle they are applicable also in the lower range, as will be discussed in Chap. 9.

High pressures can, for example, be defined as a free energy variation in a known volume V at a constant temperature T

$$p = \left(\frac{\partial H}{\partial V}\right)_{T=const} \tag{7.6}$$

where H is the Helmoltz thermodynamic free energy function $H = U - TS$, with U denoting energy and S entropy.

Since $\mathrm{d}H = p\mathrm{d}V - S\mathrm{d}T$ and, in principle, energy is directly related to force through work, then the definitions of Eqs. 7.5 and 7.6 are equivalent. However, the practical application of Eq. 7.6 is limited to pressures much higher than 100 MPa and therefore will not be considered in this book.

Similar principles are based on the methods by which the pressure value is derived from compressibility measurements and relative variations of volume, V (Smith and Lawson 1954). It can be expressed in the following way

$$p - p_0 = \int_{V(p)}^{V_0(p_0)} \frac{1}{K_T V} dV \tag{7.7}$$

where $K_T = (-1/V)(\partial p/\partial V)_{T=const}$, is isothermal compressibility. The application of a method of this type is difficult. In fact, the measurement of compressibility actually yields adiabatic compressibility values $K_S = (-1/V)(\partial p/\partial V)_{S=const}$, so that it is necessary to introduce a correction term, involving the measurement of thermal expansivity, absolute temperature, volume, and specific heat at a constant pressure, in order to derive K_T from K_S. This method, too, is applied to measure pressures above the range considered in this book.

Pressure Scale The establishment of a primary pressure scale in the range (10^2–10^8) Pa is based on a different philosophy than the realization of the temperature scale described in Chap. 1. In this pressure range, the pressure scale is based on primary

standards that realize the pressure definition without resorting to a practical scale based on fixed points.

As already mentioned, in the SI system pressure is a derived quantity, defined in terms of force per unit area. The pressure scale can be realized with primary instruments, which can be independently characterized by direct measurement of the quantities involved (for example, a primary standard pressure balance requires the measurement of the force and of the effective area to which the force is applied) and by means of an experiment that realizes the definition of pressure.

Once the pressure balance is characterized metrologically, it is still necessary to determine its equilibrium conditions in the pressurizing fluid.

In the range considered in this book (10^2–10^8 Pa), primary pressure standards used to realize the pressure scale are of the liquid column or of the pressure-balance types.

Although the realization of a pressure scale does not require the use of any pressure fixed points, this does not imply that pressure fixed points are not useful; on the contrary, they are indispensable tools to be used as reference or transfer standards.

The use of such reference points, which are very well reproducible, is particularly advantageous to check systematic errors in primary apparatus.

For pressures higher than 2.6 GPa, at which primary pressure standards of the pressure-balance type are not available, the pressure scale is realized and defined on the basis of different pressure fixed points; in this range the analogy with the philosophy underlying the definition and realization of the temperature scale is evident.

In the range of interest in this book, the realization of the pressure scale involves different factors, such as:

- Availability of primary standards, characterized through the determination of base physical quantities and in accordance with their definitions (in our case, liquid-column manometers based on Eq. 7.4 and pressure balances based on Eq. 7.5.
- Availability of transfer or reference standards, to check the pressure scale based on primary standards.
- Availability of secondary standards having high sensitivity, reproducibility, and stability to interpolate the pressure scale and transfer it to users.

Figure 7.3 shows the highest accuracy, typical of gas primary standards in national standards laboratories, for measurements between 10^1 and 10^8 Pa for absolute and gauge pressure measurements based on liquid-column manometers and pressure balances . Both axes of Fig. 7.3 are logarithmic scales for pressure (in pascal) and for the estimated standard uncertainty (in ppm).

The indications given in Fig. 7.3 refer to the present state-of-the-art; research work in different pressure ranges of the scale will possibly improve measurement accuracy. For example, in absolute and gauge modes for pressures up to a few tenths of megapascal, it should be possible, with the use of geometrically improved piston-cylinder units, to achieve an accuracy level of few parts per million (ppm).

Different apparatuses are used over the pressure range considered in Fig. 7.3.

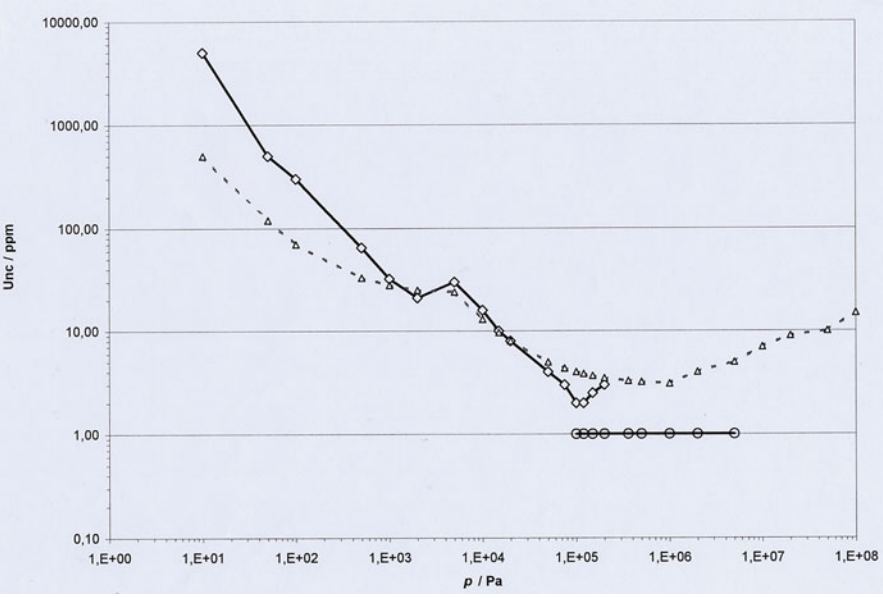

Fig. 7.3 Typical uncertainties of gas primary standards for pressure measurements from 10^1 to 10^8 Pa. Pressure (pascal) and standard uncertainty (ppm) are given using logarithmic scales. (◇ liquid-column manometers, Δ pressure balances, o goal to be reached by special pressure balances to be used in Boltzmann constant experimental determination)

There are liquid-mercury columns for absolute and gauge measurements generally limited to 120 kPa, others extending the range to below 300 kPa, and a few other systems (high-length mercury columns) reaching values typically from about 5 to 8 MPa.

The general tendency is to use different types of primary standard pressure balances to measure pressures from 0.3 to 100 MPa.

In the pressure range from about 1 mPa to about 100 Pa, the measurement method is essentially based on a subdivision of the known measurable pressure to generate lower pressures. This method is implemented by series-expansion calibration systems. The typical range covered is from 133 Pa down to 1.33 mPa, the relative accuracy is approaching 0.1 % depending on the subintervals of the expansions (Poulter 1977; Jousten 2008).

In low and high vacuum, typically in pressure ranges from 10 to about 10^{-4} Pa, even the definition of pressure must resort to kinetic theory of gases, where pressure can be defined in terms of molecular flux or through gas molecular density and temperature. A particular interest is represented by the "transition" range, $(10–10^{-2})$ Pa, where the molecular dynamics are in transition from molecular flow at lower pressures, to the viscous flow at higher pressures. In the transition range, pressure measurements are complicated by the thermomolecular pressure difference effect (see Chap. 10).

The typical range of pressure balances for absolute measurements is 10 kPa–5 MPa, though in some cases the lower limit can be extended down to few Pa by the use of special nonrotating pressure balances.

In the case of absolute differential pressure measurements, whose lower limit can be of the order of 10–20 Pa, the pressure value can be determined by using two absolute pressure balances and by following a specific procedure, which will be described later on.

In gauge pressure measurements, it is possible to arrive at 100 MPa with the use of pressure balances especially designed to operate up to 100 MPa in gas media.

Pressure Fixed Points On the analogy of the temperature scale, as discussed in Chap. 1, the pressure scale, too, can be based on thermodynamic phase transitions of substances occurring at unique and fixed temperatures and pressures.

Let us consider gas-based pressure reference points.

The term "reference point" is defined in this book in Chap. 2. When its value is assigned according to a scale definition, through an international agreement, it becomes a "fixed point" of that scale.

Similarly, as pointed out by Bean (1983), in pressure metrology the term reference point relates to the pressure of a thermodynamic state at which, as a rule, a change of phase occurs in a given substance at a given temperature. On the other hand, below 100 MPa no empirical pressure scale needs to be defined, so that the pressure value of the reference point is not assigned or defined, but only measured, to check that the correct value can be reproduced. When two or more laboratories study the same phase change in the same material, the phase transition should occur at the same pressure: the degree of agreement between the pressure values of different laboratories truly reflects the state of the art as related to the level of the systematic uncertainties in pressure measurements in the laboratories concerned.

The use of a pressure "reference point" as a calibration point or as a check point has consequently acquired increasing importance in recent years, also in the pressure range considered here, particularly for pressure measurements in gases.

A reference point may also be considered a transfer standard, as it has the advantage of being intrinsically highly reproducible and stable at values that are comparable to the accuracy of a primary standard.

The availability and use of gas-based pressure fixed points are discussed in detail in Chap. 9.

Whether a primary standard can be defined with the use of a fixed point is still debatable, but it is undeniable that it is very convenient to use a pressure fixed point as a reference point.

7.1 Liquid-Column Manometers for Pressure Measurements

Liquid-column manometers are still widely employed as primary standards in spite of their being among the oldest pressure-measuring instruments, dating back to the well-known measurement of atmospheric pressure described by Evangelista Torricelli in

1644. Since then, these instruments have undergone many modifications, but they are still fundamental for the measurement of atmospheric pressures and from few Pa to 120 kPa and above as summarized by Tilford (1993/1994). In this range, mercury is the manometric fluid most commonly used.

In the present section, manometers using liquids (often called liquid manometers) will be considered; their use, the required pressure calculations, and the precautions to be taken in carrying out measurements will be described. Although instruments based on liquid-filled columns are still used for gauge pressure measurements at pressures below 10 MPa, the liquid manometers for very high pressures sometimes employed in the past, e.g., Holmann et al. (1995); have been replaced by the more practical pressure balances or equivalent devices. Liquid manometers, however, are still fundamental for the realization of the pressure scale, for the calibration of pressure balances, and for the realization of temperature fixed points. Finally, liquid-column manometers are also employed for small absolute and differential pressure measurements, even at high line pressures.

7.1.1 Operating Principles and General Precautions for Absolute Pressure Measurements Below 0.3 MPa

Pure mercury is used as the manometric fluid for the large majority of instruments measuring absolute gas pressures in the atmospheric pressure range.

To determine pressure p, Eq. 7.4 is used

$$p = p_0 + \rho_f g_L h.$$

All the different parameters, in particular the reference vacuum pressure p_0, the density of the fluid ρ_f, the local acceleration due to gravity g_L and the height difference h, need to be accurately measured and will be discussed in Sect. 7.1.3.

The detection of the mercury surface and the measurement of the difference in the height, h, of the liquid caused by the application of pressure p, is one of the important problems in liquid manometry.

Various methods and techniques are employed, some of which are discussed below and many have been comprehensively reviewed by Brombacker et al. (1960) and by Guildner and Terrien (1975).

The methods and techniques *used to measure height differences* between mercury columns with moderate accuracy are now discussed below:

- *Telescope cathetometers*, equipped with a graduated eyepiece, can be used when mercury is contained in glass tubes. Even if special techniques are adopted to enhance the visual detection of the mercury surface, large systematic errors are likely to occur, owing to imperfect perpendicularity of the two telescopes and to incorrect image focusing. Highly skilled operators, by applying all the relevant corrections, can use such techniques to achieve a length resolution of the order of $\pm$ 10 µm. In the use of these instruments and techniques, possibly still applied by laboratories where accuracy is not better than $\pm$ 100 ppm, too much reliance

is placed on the skill of the operator. Therefore, telescope cathetometers are no longer employed to achieve the best accuracy levels.

- *Electrical continuity* can be used to establish the contact between the mercury and a sliding pointer. The height of the pointer is measured with a cathetometer or vernier and a scale. Unfortunately, because of the surface tension and capillary effects of the mercury, significant errors may be created by the distortion of the surface caused by the pointer. Therefore, such techniques are seldom used.
- *Photocell detectors* of the mercury surface are also now seldom used, only for industrial applications, and in which a cathetometer or a scale is employed for height measurements.

The methods and techniques for the detection and measurement of the mercury position that are still used today and allow high accuracy to be obtained in "state-of-the-art" pressure measurements are discussed below:

- *Capacitance measurements* between the mercury meniscus and an electrically isolated reference plate exploit the high sensitivity achievable by capacitance measurements to determine the difference between the mercury surface and a reference plate. This very sensitive technique for locating the mercury surface can be used only over short distances. A change in the absolute height of the reference plate is measured with other techniques in order to obtain the overall absolute length of the mercury columns.
- *White-light interferometry*, using the mercury surfaces as mirrors, is used because of its high sensitivity in detecting the position of the mercury surface. When this technique is combined with other high-accuracy length-measuring techniques (for example, employing microscope readings on a calibrated scale or laser interferometers), mercury height differences can be determined with a resolution better than 0.5 μm and to an accuracy of a few ppm. To obtain such results, the mercury must be isolated from possible vibrations and its temperature stable to within a few millikelvin.
- *Laser interferometry* techniques employing reflecting mirrors floating in the mercury, are used. Length changes of 0.3 μm, equivalent to pressure changes of about 0.04 Pa, can be detected in this way. With adequate temperature stability, accuracies close to 1 ppm can be achieved in absolute gas pressure measurements around 100 kPa.
- *Ultrasonic interferometers* use a 15 μs wave train of 10 MHz ultrasound, which is transmitted through the mercury columns from the bottom. The ultrasound is reflected from the mercury surface back to the ultrasonic transducers and converted into electrical signals. The phase of the return signal is measured relatively to the transmitted wave. A length change in the mercury column produces a proportional phase change in the ultrasonic return signal. This technique, pioneered by NIST (formerly NBS), is suitable for liquid manometers operating up to 360 kPa, to accuracy generally well below 10 ppm.

The best instruments available, such as those used in national standards laboratories, will be discussed in detail in Sect. 7.1.2.

The use of the foregoing length measurement techniques, especially for high-accuracy pressure measurements, involves a number of common problems. Some of them are listed below:

- Control of the mercury meniscus and the reduction of the error due to capillary action require the use of large-diameter columns. The internal diameters of stainless steel or glass columns are typically from 40 to 110 mm. Some glass columns may have conductive coating (e.g., evaporated nickel–chromium layer) to reduce electrostatic perturbations.
- "Tilt" errors may be produced by the displacement of the center of mass of the instrument when, on pressure application, the mercury is transferred from one column to the other. A "W" or three-column configuration greatly reduces this error.
- Since height must be measured, it is essential that the length measurement axes of the columns are aligned to the vertical.
- Vibrations on the mercury should be minimized, especially when optical interferometry techniques directly using the mercury surface are employed.
- Pure triple-distilled mercury of known density should be employed and acid-distilled water cleaning be used. It is important that the apparatus is filled under vacuum, particularly as regards systems designed to attain ppm accuracy.
- Temperature must be stable and known to within some millikelvin over the whole length of the mercury column, as the overall measurement accuracy is sizably affected by temperature instability and by temperature gradient along the columns, causing a differential thermal expansion.
- The speed of pressure changes may be an important parameter with some calibration systems. Manometers are available, which can cope with pressure change at rates of or higher than 100 Pa s^{-1} without perturbing the manometer output signal. However, it must be remembered that pressure changes affect temperature stability, so that an equilibrium time is needed for the most accurate pressure readings.
- The reference pressure p_0 (vacuum reference) system should be leak-tight and the conductance between the pump and the manometer should be adequate. With a system of this type, the p_0 value is generally limited by mercury-vapor pressure (0.17 Pa at a room temperature around 20 °C). However, if cold traps are used and the pumping speed is appropriate, p_0 can be reduced to below the mercury-vapor pressure. A mercury diffusion pump is the most convenient means for the pumping system. For accurate measurement of p_0, capacitance, McLeod or Pirani gauges are typically used.

7.1.2 Basic Apparatus in Metrological Laboratories: Different Methods for Height Measurements

The manometers existing today at several major national metrology institutions are now described.

Between 1958 and 1980, many standard laboratories directed their efforts to the improvement of their existing apparatuses in order to achieve better accuracies of the pressure measurements needed, for example, for the calibration of new instruments of high resolution and improved accuracy. In the years between 1990 and today, many liquid-column manometers have been improved in their automatic data acquisition and with the main purpose of reducing their measurement uncertainty.

Obviously, not all the different manometers will be discussed here, but only original and/or innovative apparatus designed to achieve the currently available best pressure measurement accuracies in the absolute pressure range to about 120 kPa.

The claimed accuracy at 100 kPa of the mercury-column manometers described here ranges from few ppm to about 20 ppm; with such apparatus a high resolution, from 0.01 to 0.1 Pa, can be normally achieved.

7.1.2.1 White-Light Interferometer Manometers

A very reliable class of instrumentation, still used in a few cases today, though much modified, is the manometer type based on the white-light interferometric technique using the mercury surfaces as mirrors.

These techniques were developed almost at the same time at BIPM by Bonhoure and Terrien (1968) and at NRLM, now NMIJ, by Kaneda et al. (1964). While the instruments are different in detail, they are based on the same principle.

The principle of operation of the BIPM manometer is illustrated in Fig. 7.4.

A white-light beam is split into two parallel beams, which, before reaching the mercury surfaces, are deflected by two optical prisms (5 in Fig. 7.4) and two optical trihedrons (6 in Fig. 7.4). The two trihedrons, joined together, are fixed on a carrier (7) having a graduated rule (8) that can be read by means of a microscope (9). A compensating plate (4) is oscillated through a small angle and produces a low-amplitude sinusoidal variation of the optical path. The beams are deflected again by the optical prisms (5) into two parallel beams perpendicular to the mercury surface. The light reflected back from the mercury surface is recombined at the splitter (3) and the interference fringes are observed by means of a photomultiplier and an oscilloscope.

Fringes are visible only when the optical paths to and from the separate columns are equal. If the voltage applied to the horizontal input of the oscilloscope is sinusoidal and in phase with the oscillation of the compensating plate, the fringe signal appears on the oscilloscope. When in operation, the carrier is displaced until the optical paths are equal and a white fringe is detected. The procedure begins when the two mercury columns are at the same height *in vacuo* (i.e., with "zero" pressure on both columns of the manometer). The scale reading L_0 is the "zero" pressure reading of the interferometer.

Gas (typically nitrogen) pressure is then admitted to one column and produces a height difference h. The carrier is moved to readjust the optical path; interference fringes are detected again with a new carrier reading L_1.

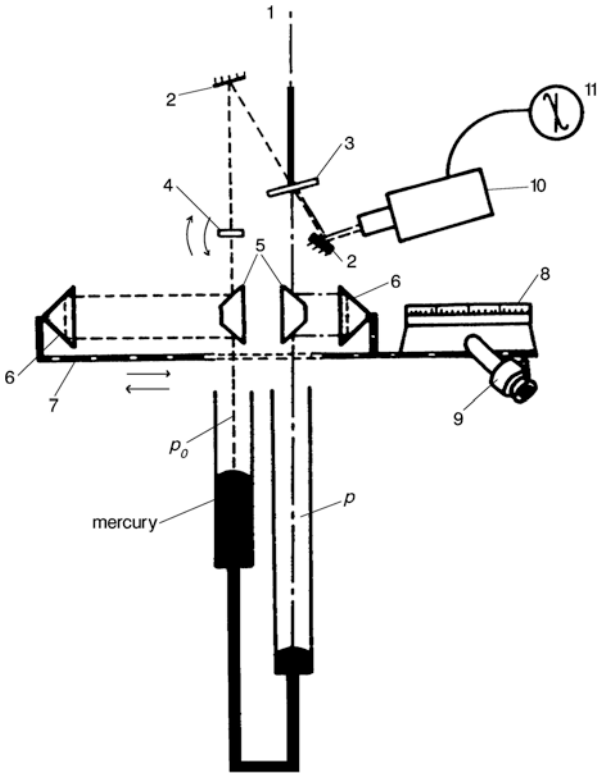

Fig. 7.4 Operation principle of the BIPM manobarometer (*1* white light, *2* reflecting mirrors, *3* separator, *4* oscillating compensator, *5* optical prism, *6* trihedron, *7* carrier, *8* graduated scale, *9* microscope, *10* photomultiplier, *11* oscilloscope). (From Guildner and Terrien 1975 by kind permission of the authors)

To a first approximation, we have

$$h = 4(L_1 - L_0).$$

In order to minimize ripples on the mercury surfaces, the two mercury columns are mounted on three antivibrating springs partially immersed in silicone oil. More than two columns are used to prevent their possible tilting due to mercury movement when pressure is changed. The temperature around the mercury columns is stabilized by means of three concentric layers (aluminum, glass wool, aluminum), all assembled inside a large cylinder. Five differential copper-constantan thermocouples are used to measure the temperature at different heights along the mercury columns and their reading is referred to a reference thermometer. In the most recent version of the manometer, a platinum resistance thermometer, placed close to the graduated scale, is used as the reference. Short-term temperature changes of 10–20 mK/h have been reported for drifts of up to 1 K at room temperature.

The corrected height of the mercury column is calculated from the following equation:

$$h = 4(L_1 - L_0 + C_\mathrm{r})\,[1 + \alpha_\mathrm{r}\,(t_\mathrm{r} - 20)] + C_\mathrm{i} \tag{7.8}$$

where:

- C_r is the scale correction obtained from the calibration of the graduated rule and is referred to 20 °C.
- α_r is the linear thermal expansion coefficient of the scale (specifically, 11.5×10^{-6} °C^{-1} for a steel rule and 0.7×10^{-6} °C^{-1} for an invar rule).
- t_r is the temperature of the rule (°C).
- C_i is a correction, in terms of height, that is required because of the different indices of refraction of the media traversed by each of the two light beams.

For absolute pressure measurements, in the first step of the procedure (with L_0 having been measured), vacuum is present above both mercury surfaces, while in the second step (with L_1 having been measured) vacuum is present in one column and a gas (generally nitrogen) is in the other. In addition, the optical path through air differs between the two procedure steps. The different refractive indices in the two configurations make the optical paths different.

In order to obtain achromatic fringes, equality of the term Σ_i $(m_i l_i)$ for the two optical paths must be obtained. The term l_i is the optical path in medium i and m is defined in terms of the refractive index n at the mean wave number σ of the white light by the relation

$$m = n + \sigma \left(\frac{\mathrm{d}n}{\mathrm{d}\sigma} \right). \tag{7.9}$$

The optical paths Σ_i $(m_i l_i)$ for both columns must be equal in the two procedure steps, that is at the initial reference adjustment (step 1, measurement value L_0) and with the applied pressure (step 2, measurement value L_1). In order to convert the optical path into length, the correction C_i must be made in order to take account of the indices of refraction. This correction is the sum of the different lengths of the optical path multiplied by the appropriate index of refraction, for one column, minus the same sum, for the other. The correction C_i, which depends on h, on the type of gas used and on the mode (absolute or differential) of operation, has a very high absolute value. An important role in this correction is played by the refractive index of air, which is usually calculated by a formula given by Edlén (1966) and subsequently modified by Muijlwijk (1988) in order to take into account the compressibility factor of air in normal laboratory conditions.

Figure 7.5 illustrates the magnitude and the behavior of this correction for absolute pressure measurements and when nitrogen is used as the pressurizing gas.

If helium is used as the pressurizing gas, the shape of the correction, for absolute conditions, changes and becomes almost linear and larger ($C_i = +200$ µm for $h = 800$ mm).

The mercury-column length h having been determined, pressure p is calculated from the general Eq. 7.4.

To do so, the following quantities must be considered:

- Mercury density ρ_f and its change with temperature and pressure.
- The local acceleration due to gravity g_L.
- The reference pressure p_0 (vacuum reference line).

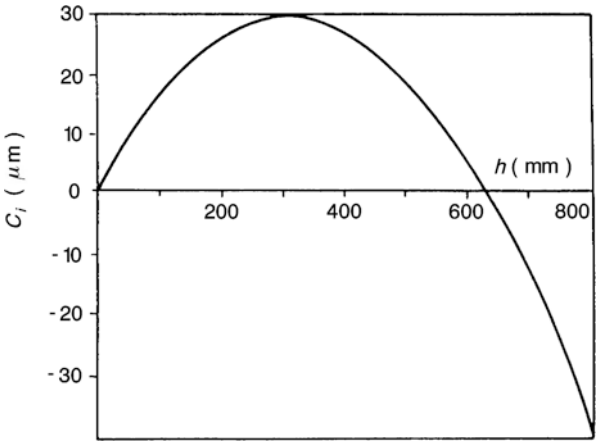

Fig. 7.5 Refractive index correction $C_i = f(h)$ for nitrogen in absolute condition. (From Bonhoure and Terrien 1968 by kind permission of the authors)

Finally, all measured pressures have to be referred to a common height (this is called aerostatic, gas head, or hydrostatic correction). As these problems are common to all types of manometers, they will be discussed together in Sect. 7.1.3.

The uncertainty of the height value of the BIPM manometer is of the order of 1 μm (equivalent to 1.5 ppm at 100 kPa); with all the different corrections and the associated errors taken into account, it was recently estimated that the overall pressure uncertainty at 100 kPa is close to 3 ppm. A similar instrument based on the BIPM prototype was commercialized and is now used in many laboratories. The BIPM design, now modified particularly for temperature measurements and the determination of the displacement of the graduated rule by interferometric techniques, is still employed by many laboratories, and has been used in many international comparisons and in several interesting applications of gas thermometry.

Revised uncertainty of pressure measurements by this type of apparatuses can be found in Stock and Pello (1999) and in Steur and Pavese (1993/1994) where the standard uncertainty of pressure measurements ranges from 16 ppm at 10 kPa to 2.7–2.9 ppm at 100 kPa.

A similar apparatus was designed at NRLM, now NMIJ in Japan by Kaneda et al. (1964). It is based on the same principle as the BIPM instrument, but in the NRLM manometer the height difference between the two mercury columns is measured by means of two Michelson white-light interferometers having a common large beam splitter and a fixed corner cube mounted on the graduated rule. Without analyzing in detail this manometer, mention must be made of the test carried out at NRLM, illustrated in Fig. 7.6, to correct for the refractive index when air is used as a pressurizing gas. Here, too, the correction is large and the behavior of this correction under absolute condition is naturally different from the case of gauge pressure measurements.

The uncertainty of the length measurement values for this instrument, at the 1σ level, taken as the square root of the sum of the squares of the individual contributions to one single measurement value is 2.4 μm (equivalent to a contribution of 3 ppm at

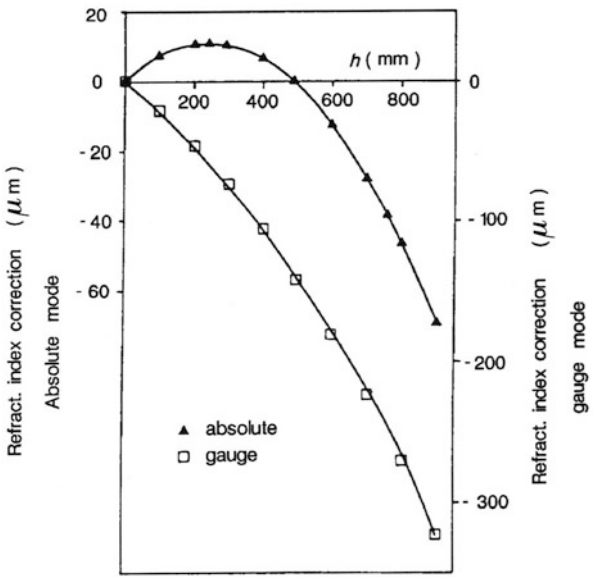

Fig. 7.6 Refractive index correction for air pressure measurements at 20 °C obtained at NRLM under absolute and gauge conditions. (From Kaneda et al. 1964 by kind permission of the authors)

100 kPa). The same instrument was recently modified, in order to make the absolute measurement of the movement of the scale rule by means of a He–Ne laser and have the possibility of using different gases; the instrument has the same good resolution as before.

As it is described by Ooiwa et al. (1993/1994), the revised 1σ estimated uncertainty of the overall pressure measurement value at 100 kPa is 0.4 Pa in both absolute and gauge modes.

Experiments were also carried out with a short-range manometer of 13 kPa full scale by Mitsui et al. (1972). With this instrument, the position of the menisci in the U-tubes are located by a white-light Michelson interferometer, and the displacement of the carrier position is measured by counting the interference fringes produced by a He–Ne laser.

7.1.2.2 Laser Interferometer Manometers

Different attempts were made in the past to use the mercury surface as an interferometer mirror, not only to locate the mercury surfaces but also to make directly, with the interferometric technique, the absolute measurement of the length between the two mercury surfaces. Tilford showed that the 10.6 μm wavelength of a CO_2 laser is sufficiently large to tolerate mercury surface disturbances, provided that they are, in any case, maintained as small as possible by an appropriate treatment of the walls of large-diameter tubes (Tilford 1973). For this experiment, Tilford designed the single interferometer manometer illustrated in Fig. 7.7.

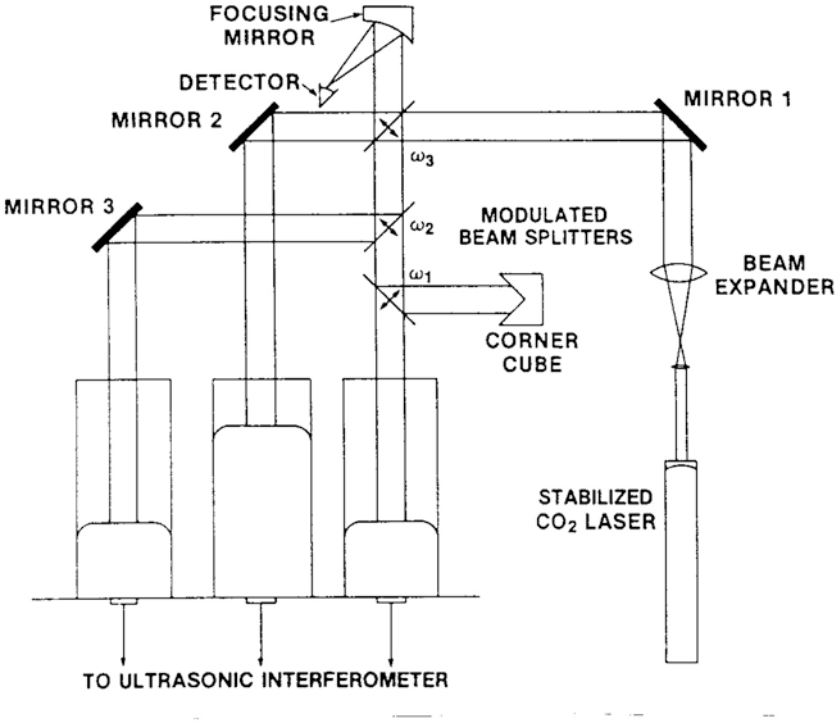

Fig. 7.7 CO_2 laser interferometric manometer. (From Tilford 1987 by kind permission of the author)

Some problems were encountered, owing to transient waves on the mercury surface generated by irregular changes in the meniscus contact angle, particularly during pressure decrease cycles. The prototype was used with pressure changes at a rate of about 11 Pa s^{-1}. Further work was done by combining this technology with the ultrasonic technique; successive approximation calculations were used to arrive at the measurement of mercury height. As this second technology is not of the fringe-counting type, it does not limit the speed of operation.

Further progress was made by Bennett et al. (1975) with the use of especially made lens/mirror cat's eyes floating on the mercury surfaces of both columns. In this way, the laser beam is directly focused on the mercury; the reflection is quite immune from surface ripples and the reflected beams are returned to the beam splitter in a direction parallel to the incident direction without loss of collimation. In such a configuration, a source of difficulties can be laser light focusing, if there is a cat's eye displacement in respect of the mercury surface.

This system, adopted in the NPL-UK long-range primary barometer by Elliott et al. (1960), has given good results both as regards the speed of operation, without failure of fringe counting up to 133 Pa s^{-1}, and the improvement of the overall accuracy of the manometer (better than 6 ppm at 100 kPa).

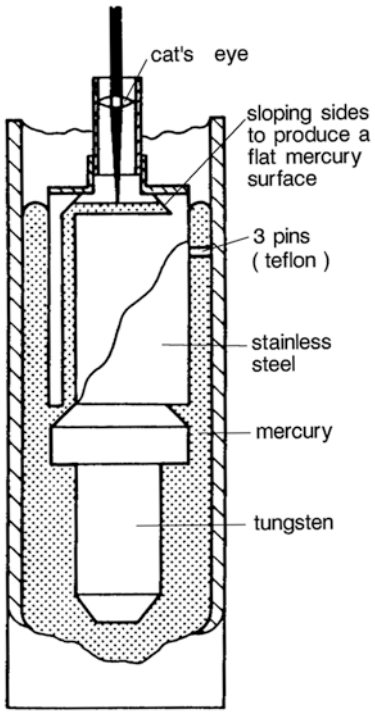

Fig. 7.8 NML floating device and cat's eye designed to reduce vibrations on the mercury surfaces. (From Harrison et al. 1976 by kind permission of the authors)

An apparatus of the same basic conception as the former was built at NML in Australia, now NMIA, by Harrison et al. (1976). Here, too, the mercury surfaces are the mirrors of a Michelson interferometer with a He–Ne laser used to detect directly the height difference of the mercury columns. The difference, in respect of the NPL-UK manometer, is that in Harrison's instrument the two mercury surfaces are part of the same interferometer and the floating cat's eye (see Fig. 7.8) is different from that of the NPL.

The authors reported sensitivity lower than 40 mPa and an overall accuracy of 2 ppm at 100 kPa, essentially limited by the temperature nonuniformity and instability of 10 mK.

All such instruments obviously need refractive index correction on the measuring gas side and for ambient air, beside all the other necessary corrections.

A recent system was installed and characterized at NIM in China by Sheng Yi-Tang et al. (1988).

This apparatus employs devices floating on mercury and two independent interferometric systems, one of which is a laser system working with a floating retroreflector and the other a white-light interferometer working directly on the mercury surface, to detect and measure the mercury height differences. The floating system supports a corner cube mounted on a stainless steel cone. The refractive indices of air and nitrogen were measured experimentally with an uncertainty of the order of 10^{-8}. This manometer has a resolution of 0.01 Pa and a reported overall uncertainty of 2 ppm at 100 kPa.

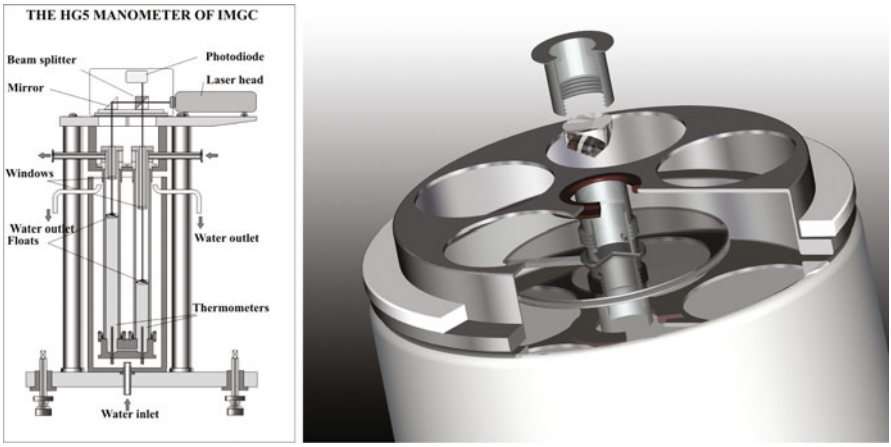

Fig. 7.9 Schematic of the HG5 manometer. *Left:* general schematic, *Right:* reflecting float. (From Alasia et al. 1999a by kind permission of the authors)

A family of mercury-column manometers were designed and fully characterized at IMGC, now INRIM in Italy, by Alasia et al. (1993/1994) All devices use laser interferometry, with lightweight floats supporting cube-corner retroreflectors in order to detect the mercury menisci inside large U-tubes and measure their vertical displacements due to pressure applications. In its last developed version as described by Alasia et al. (1999a), it is as well possible to use cat's eye floats allowing the direct reflection of the laser beams on mercury menisci.

A schematic of this design is given in Fig. 7.9 where on left side are given the general view of the instrument while on the right side the reflecting float is given.

With these types of instruments, absolute and gauge pressure measurements up to 120 kPa are possible with the following standard uncertainties:

Absolute mode, p in Pa: $u(p)/\text{Pa} = 0.153 + 3.79 \times 10^{-7} p + 7.221 \times 10^{-12} p^2$.
Gauge mode, p in Pa: $u(p)/\text{Pa} = 0.153 + 4.22 \times 10^{-7} p + 7.832 \times 10^{-12} p^2$.

While using the cat's eye floats, the standard uncertainty up to 13 kPa is (absolute and gauge mode, p in Pa):

$$u(p)/\text{Pa} = 0.043 + 1.25 \times 10^{-6} p.$$

Similar types of instruments, even with much modern data acquisition and controls, were as well realized by Torres et al. (2005) in Mexico and by Ruiz et al. (2009) in Spain.

The same IMGC/INRIM authors have also realized, as described by Alasia et al. (1999b), short-range micromanometers (still using mercury as a fluid) to allow pressure measurements from 1 Pa to 5 kPa. The pressure standard uncertainty ranges from 12 mPa at 1 Pa to 53 mPa at 5 kPa.

Another instrument worth of mention was realized in Japan and described by Ueki et al. (1993/1994). It is a short-range heterodyne laser interferometry oil manometer

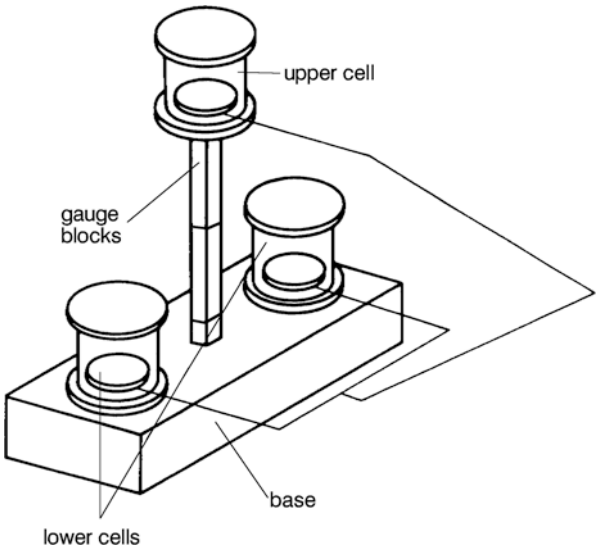

Fig. 7.10 NIST capacitance/gauge-block manometer. (From Guildner et al. 1970 by kind permission of the authors)

operating up to 1 kPa. It uses a Zeeman stabilized He–Ne laser to detect the displacement of oil surfaces by multiple reflection of the laser beams, double U-tubes and double interferometers in order to compensate errors generated by thermal and vibration disturbances. At 1 kPa the estimated standard uncertainty is 34 mPa as obtained in gauge mode only; limitations are related to the need of knowing the oil properties at top-level uncertainty and the general performances in absolute mode.

7.1.2.3 Capacitance/Gauge-Block Manometer

An interesting and unique apparatus is that designed and installed at NIST by Guildner et al. (1970). In this apparatus, the positions of the mercury surfaces are defined by measuring the electrical capacitance between mercury and a precisely located reference plate; calibrated gauge blocks measure the vertical height of the mercury column. Figure 7.10 gives a schematic illustration of this manometer.

At the initial reference vacuum level, the three cells rest on the base and, still at this pressure, the mercury level of the upper cell is adjusted to give a selected capacitance value. Then the upper cell is raised by means of gauge blocks and is fixed in a permanent position. The next step is the evacuation of this cell; the gas is subsequently and gradually introduced into the two lower cells until all the capacitance values in the three cells are equal to that previously obtained at the initial reference level. Capacitance measurements are made with a transformer ratio-arm bridge reproducible to within 1 ppm. The mercury cups have a large 76.2 mm diameter, in order to minimize capillary mercury depression and to have a flat central area. The capacitance plates are of 30.8-mm diameter and are mounted with the use of an optically flat fused silica disc; this configuration represents a compromise by

which high resolution can be achieved and the largest uncertainties can be reduced. Calculations were developed by Guildner et al. (1970) in order to verify that capillary depression and meniscus curvature do not introduce errors into measurement values higher than 0.035 and 3 nm, respectively. Effects resulting from the contact angle of the meniscus with the cup wall, effects of possible ripple on the mercury surface, possible tilting of the base, and column misalignments were carefully investigated as well.

The apparatus is located in a large room, vibration-isolated and electromagnetically shielded, in which temperature uniformity around the mercury columns is of the order of 2 mK in 8 hours; all the basic measurements are remotely controlled. Pressure calculations consider all corrections (see Sect. 7.1.3), for example, those made in gauge-block calibration and those required by the small change produced by pressure variations in the dielectric constant of helium, which is used as the pressurizing gas.

This manometer can operate satisfactorily with helium in the range 10–130 kPa to an estimated uncertainty of about 2 ppm at the 1σ level. In principle, other gases can be used, but each of them requires careful characterization in view of the relevant corrections. Good knowledge of such a sophisticated apparatus is essential for its use. With this manometer, the required predetermination of the operation pressure is, to a certain extent, a limitation, particularly when frequent and quick pressure changes are required. Schooley (1988) checked the different uncertainty contributions of the NIST mercury manometer and confirmed the previous estimated overall pressure uncertainty of 2 ppm for the pressure range from 10 to 130 kPa obtained with helium.

7.1.2.4 Capacitance/Interferometer Manometers

Commercial manometers with which the capacitance technique is used to locate the mercury level are available. Several laboratories employ manometers of this kind, and many have made various modifications to improve accuracy.

Mention has to be made of the apparatus of INM, now LNE in France, by Riety et al. (1977), illustrated in Fig. 7.11.

In this configuration, two capacitance cells (internal diameter 110 mm) are used, one fixed and the other movable vertically along a lead screw; they are connected with a flexible tube containing mercury. After pressure application, the movable cell is displaced until the predetermined reference capacitance (obtained under the zero-pressure condition) is measured again between the mercury surface and the reference electrodes of the cell. Fixed to the movable cell is a corner cube, with which the cell position can be measured by a laser interferometer. The number of fringes, N, being known from the counter, the displacement h is

$$h = \frac{Nv}{2n} \tag{7.10}$$

where v is the wavelength *in vacuo* of the He–Ne stabilized laser and n is the refractive index of air. As it is with different manometers previously described, great care is

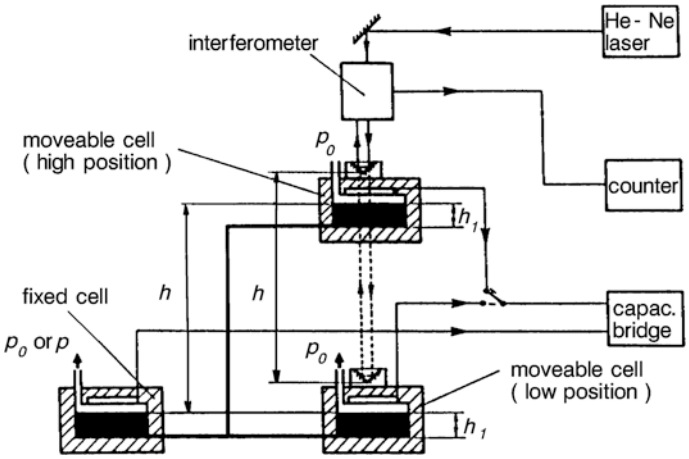

Fig. 7.11 Principle of operation of the INM manometer. (From Riety et al. 1977 by kind permission of the authors)

taken to isolate it from vibrations, to obtain good thermal uniformity on the entire mercury column, to evaluate and compensate for possible deformations in the flexible tube and to measure the reference vacuum pressure to a high accuracy. With this manometer, an absolute uncertainty of 0.2 Pa + 5.0 $\times$ 10^{-6} p/Pa can be achieved, p being the pressure to be measured (Riety 1987). At 100 kPa this is equivalent to 7 ppm. A recent use of the revised manometer was made at LNE by Otal et al. (2008), the manometer having a standard uncertainty of 0.03 Pa + 5.5 $\times$ 10^{-6} p/Pa (equivalent to 5.8 ppm at 100 kPa). The above paper describes as well a pressure comparison in absolute mode with a large effective area (20 cm^2) pressure balance.

An apparatus using the same operation principle and designed for absolute and gauge pressure measurements from 1 to 200 kPa is installed at PTB in Germany and described by Bauer (1979). At 100 kPa the overall pressure accuracy under absolute conditions is stated to be 8 ppm. A revision of this instrument, with different improvements (new mercury from NIST, improved vacuum and temperature stability and associated measurements) and a new uncertainty analysis was made by Jäger (1993/1994). The standard relative uncertainty of absolute pressure measurements is 32.4 ppm at 1 kPa and 2.5 ppm at pressures from 100 to 200 kPa.

Another interesting instrument was build and metrologically characterized in SMU in Slovak Republic, it is described in Farár et al. (1993/1994).The mercury columns of the manometer are in the form of two concentric tubes. Both tubes are equipped with ring (external tube) and disk (internal tube) capacitance sensors. A Michelson interferometer is used and a corner cube reflector is mounted in the bottom of a movable piston that on the other side mounts the capacitance disk sensor. The evaluated type A standard uncertainty is 0.07 Pa and the type B is 0.08 Pa + 1.45 ppm. This instrument, in its revised version was used, with the help of a transfer standard pressure balance, to compare the results of different mercury barometers at NIST, PTB, and the ASMW (former East Germany).

7.1.2.5 Ultrasonic Manometers

An innovative method exploiting an ultrasonic interferometer to measure the mercury-column length began to be developed in 1971 (Heydemann 1971; Heydemann et al. 1976, 1977) at NIST; since then the relevant apparatus has undergone several developments and has been substantially improved (Tilford 1987, 1988a; Tilford et al. 1988).

The range of the initial manometers was about 13 kPa and the column length was measured in terms of the number of wavelengths of the ultrasonic signal with the help of a fringe-counting interferometer having a resolution at the 1σ level of 0.01 μm; a 3σ pressure resolution of 13 mPa is quoted.

Subsequent developments extended the range to 160 kPa (with a 3σ systematic uncertainty of 15 ppm) and, later, to a maximum pressure of 360 kPa.

With the technique used, schematized in Fig. 7.12, an ultrasonic transducer generates a 15 μs-long wave train of 10 MHz ultrasound. The ultrasounds travel in the mercury and are reflected back to the transducer, in which an electrical signal is generated. The phase of this return signal, or *echo*, is measured by correlating it to the original signal.

A length change in the mercury column is revealed by a change in the phase of the ultrasound echo. Originally, a technique for phase change counting by multiples of $\pi/2$ was used. A better system uses a time-of-flight method to measure length, combined with a phase measurement at four frequencies between 9.5 and 10.5 MHz and applies an "exact fraction" algorithm (Tilford 1977). The phase-measuring system and the frequency synthesizer, which generate the different frequencies, are computer controlled (in normal operation, 14 height measurements in the three columns at four different frequencies are made in a time interval of 2–4 seconds). The manometer, of the "W" configuration, is mounted on a heavy aluminum support; three to nine platinum resistance thermometers (PRT) are used to check temperature stability; the weighted mean of the PRT temperatures, which is a function of the mercury height in the center column, is used to calculate the mercury density value. All the relevant corrections are computer controlled. The largest contributions to systematic uncertainty are by the propagation of the ultrasonic wavelength in mercury under operating conditions. These contributions are the uncertainty of the speed of sound in mercury and phase shifts caused by ultrasound diffraction. The speed of sound in mercury was determined by Tilford (1987), by comparing ultrasonically measured lengths with lengths measured by means of an infrared frequency-controlled laser.

The speed of sound in mercury was determined experimentally for mercury columns of 75 mm diameter and lengths variable from 50 to 400 mm, for temperatures between 21.5 and 29.2 °C and pressures to 230 kPa.

The following equation relating the speed of sound in mercury to temperature, pressure, and length was obtained:

$$\begin{aligned} c/\mathrm{mm\ s^{-1}} = 1449441\,[1 - 3.032 \times 10^{-4}\,(t/^{\circ}\mathrm{C} - 23) + \\ 1.42 \times 10^{-10}\,p/\mathrm{Pa} - 1.8 \times 10^{-8}(L/\mathrm{mm} - 400)] \end{aligned} \tag{7.11}$$

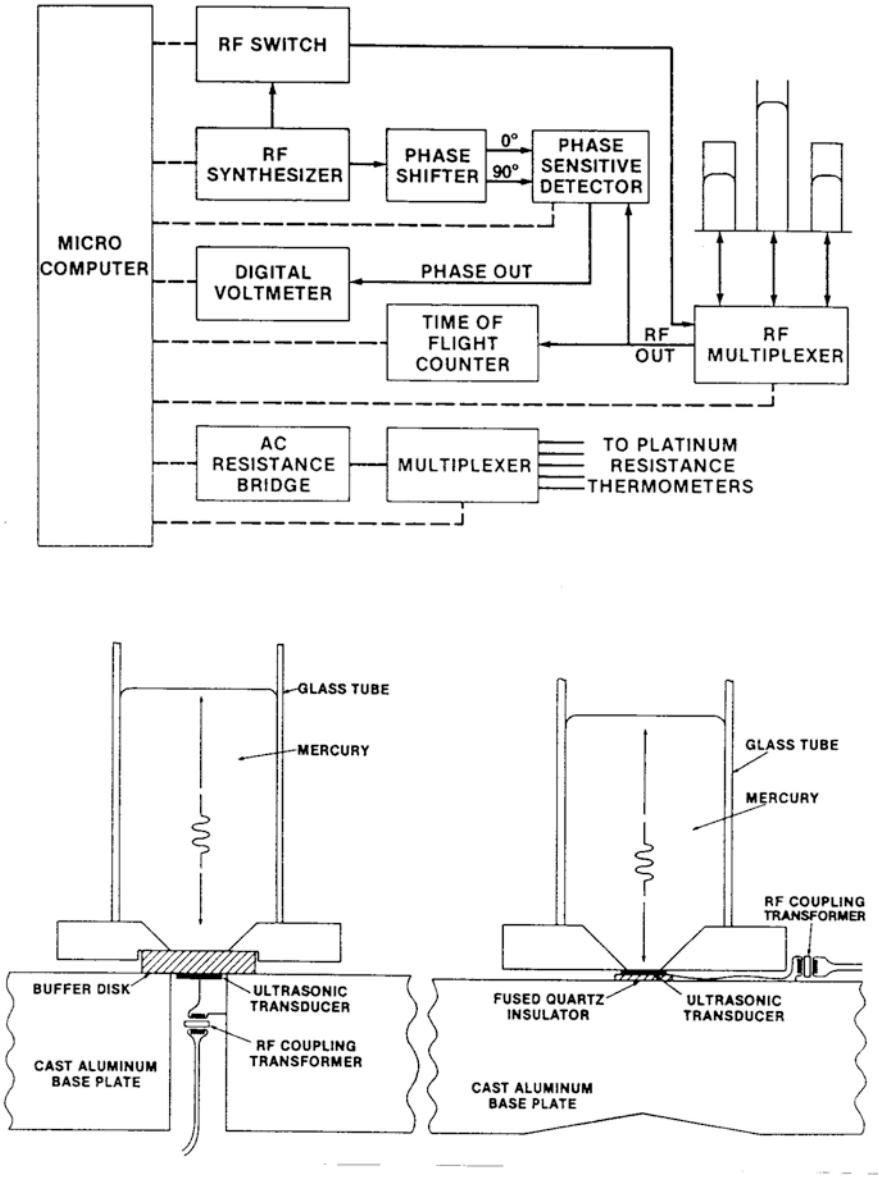

Fig. 7.12 Ultrasonic interferometric mercury manometer of NIST. Ultrasonic transducer installation and schematics of the associated electronics (—— IEEE488 or data-bus connections). (From Tilford 1987 by kind permission of the author)

where c is the speed of sound in mercury, t is the temperature, L is the column length, and p is pressure at the midpoint of the central mercury column.

The length dependence appearing in Eq. 7.11 is probably a diffraction phase shift and decreases as the length increases beyond 400 mm. The temperature coefficient given in Eq. 7.11 adds to the mercury temperature coefficient, so that the overall temperature dependence of the ultrasound manometer is approximately three times the mercury temperature dependence. The total uncertainty of Eq. 7.11 is 4.3 ppm. In the evaluation of pressure uncertainty, an additional 0.75 ppm should be added to take account of possible changes in speed of sound due to isotopic variation in the reference mercury density. Another important source of systematic uncertainty is the fact that the ultrasonic phase measurement value can be affected by imperfections in the individual transducers, strains in transducer mounting, and by diffraction effects, all this representing a contribution lower than 6 ppm to the overall uncertainty.

The total systematic uncertainty of the ultrasonic manometer, in absolute or differential pressure measurements over the whole pressure range and with any gas, was evaluated lower than 15 ppm at the 3σ level. It must be mentioned that 15 ppm is the arithmetic sum of all the systematic uncertainty components, which have to be added up as some of them are correlated. The random uncertainty evaluated at three times the standard deviation is 0.01 Pa + 1.7 ppm (see Table E.3 in Appendix E).

At NIST the family of ultrasonic interferometer manometers (UIM) was further developed to realize, for example, a primary standard for low differential pressure measurements as described by Müller et al. (2005). The low differential pressure UIM standard still uses mercury as a fluid and has a range from 1Pa to 13 kPa, for operations with line pressures up to 200 kPa. This instrument has a standard uncertainty due to systematic effects of $([3 \times 10^{-3}\ \text{Pa}]^2 + [3.2 \times 10^{-6}\, p]^2)^{1/2}$ where p is the differential pressure in pascal. The random uncertainties, mainly due to pressure instabilities, vary from 3 mPa at lowest differential pressures to about 60 mPa at the full scale. At the NPL of India, as described by Mohan et al. (1996) their ultrasonic interferometer manometer was used, in the pressure range from 1 Pa to 1.333 kPa, to evaluate the performances of the static expansion system by using as transfer standard a capacitance diaphragm gauge (CDG).

Table 7.1 contains the mercury-column data of some laboratories at pressures around 100 kPa. All apparatuses have high resolution in the determination of mercury-column height (equivalent to a pressure from 0.01 to 0.04 Pa) and an accuracy, at 100 kPa, lower than 10 ppm.

Still in connection with Table 7.1, it must be mentioned that the uncertainty evaluation is performed in different ways in the various laboratories. After 1993, as a preparatory work done within a EUROMET project (n^{er} 220) by Stuart (1993/1994), the scientific community started to harmonize the uncertainty declarations: a situation that in present day, under the enormous push of the CIPM-MRA, has become more compelling and, generally speaking, universally adopted at least by the national metrology institutions.

Table 7.1 is meant to be informative and cannot be used, strictly speaking, for the purpose of comparing the uncertainties of the different laboratories.

Table 7.1 Some characteristics of the mercury-column primary standards for absolute gas pressure measurements to approximately 100 kPa existing in some national metrology institutes

Laboratory (country)	Principle of operation[a]	Resolution (Pa)	Uncertainty at 100 kPa (ppm)	Relevant papers
BIPM (int.)	w.l.i.	0.01	4	Bonhoure and Terrien (1968)
		0.01	2.9	Stock and Pello (1999)
NRLM, now NMIJ (Japan)	2 w.l.i.	0.01	7	Kaneda et al. (1964)
		0.01	4	Ooiwa et al. (1993/1994)
IMGC, now INRIM (Italy)	w.l.i.	0.03	2.7	Steur and Pavese (1993/1994)
INRIM (Italy)	Ls.i.	0.01	2	Alasia et al. (1999)
CEM (Spain)	Ls.i.	0.01	2.8[c]	Ruiz Gonzáles (2011)
NPL (UK)	Ls.i.	0.04	6	Bennett et al. (1975)
NML, now NMIA (Australia)	Ls.i.	0.04	2	Harrison (1976)
NIM (People's Republic of China)	w.l.i., Ls.i.	0.01	2	Yi-tang et al. (1988)
NIST (USA)	C. gauge b.	0.02	2	Guildner et al. (1970) and Schooley (1988)
NIST (USA)	U.I.M.	0.01	5[b]	Tilford (1988a)
		0.01	2.9	As given in Farár et al. (1993/1994)
SMU (Slovakia)	C., Ls.i.	0.07	2.9	Farár et al. (1993/1994)
INM, now LNE (France)	C., Ls.i.	0.03	7	Riety et al. (1977)
		0.03	5.8	Otal et al. (2008)
PTB (Germany)	C., Ls.i.	0.03	8	Bauer (1979)
		0.03	2.5	Jäger (1993/1994)
VNIIFTRI (Russia)	Ls.i.	0.02	2	Sacharov et al. (1986)

[a] *w.l.i.* White-light interferometer, *Ls.i.* laser interferometer and floating devices, *C.* capacitance, *C. gauge b.* capacitance and gauge blocks, *U.I.M.* ultrasonic interferometer manometer

[b] As the sum of all systematic contributions was evaluated to be 15 ppm at the 3σ level, in the present table the estimated uncertainty is considered to be 5 ppm

[c] Given at $K = 2$ as 5.6 ppm for absolute mode and 6.7 ppm for gauge mode

7.1.3 Calculations Applicable with Mercury-Column Manometers: Pressure Measurement Uncertainty

The different manometers described in the previous sections measure the mercury height h between the columns, after the application of pressure p, in different ways. All the mentioned manometers have high resolution in height measurements (100–10 nm) and high accuracy (a few ppm).

All of them need application of the same calculations, in order to obtain the pressure p through Eq. 7.4. The way of deriving the basic physical quantities to be used in Eq. 7.4 is now examined.

7.1.3.1 Mercury Density

This is one of the most significant parameter to be taken into account. The mercury must therefore be maintained clean and its density, which depends upon its purity, isotopic composition, temperature, and pressure, be known so as to reduce such contributions, which influence the accuracy of mercury density determinations to below a few ppm.

As a rule, impurities are removed by repetitive distillation and by traditional cleaning techniques. After the triple-distillation process, repetitive acid cleaning of mercury (10 % in volume of HNO_3 and distilled water) in a nitrogen atmosphere is essential for the removal of the base materials. At the end of the process, the mercury is transferred under vacuum into carefully cleaned mercury columns. In addition, as mercury must always be maintained pure, conditions of absolute cleanliness must be maintained as well in the normal use of manometers, and all the materials used in column assembling (e.g., glass, stainless steel, Teflon, and nickel) must be mercury compatible. Another precaution is the use of only high-purity dry gas. Attention must be paid to mercury contamination, so that when the manometer is used to perform gauge pressure measurements, direct column connection at environmental-air pressure is generally avoided. As mercury has isotopes of different atomic weights (196, 198, 199, 200, 201, 202, 204), the isotopic composition of various mercury samples can differ according to their origin. This and the type of purification treatment could lead to significant differences in mercury density determinations, which must not be overlooked if an accuracy of a few ppm is to be achieved.

The most significant historical work on mercury density has been carried out by Cook with an "absolute displacement method" (Cook and Stone 1957) and with the so-called "content method" (Cook 1961) applied to measure the density of six samples of mercury. The mean density of four samples was:

$$\rho_0(20\ ^\circ\mathrm{C},\ 101\,325\ \mathrm{Pa}) = 13\,545.884\ \mathrm{kg\ m^{-3}}.$$

To quote directly from Cook, there resulted:

> ... a standard deviation of 0.2 ppm, and there is a high probability that the density of any sample of pure mercury will be within 1 ppm of this value.

The density of the two remaining samples was higher by about 1 ppm in respect of the average value of the other samples, probably owing to a different isotopic composition.

Chattle (1970) corrected the mercury density measured by Cook by relating its value to the IPTS-68 temperature scale, and obtained:

$$\rho_0(20\ ^\circ\mathrm{C_{IPTS\text{-}68}},\ 101\,325\ \mathrm{Pa}) = 13\,545.867\ \mathrm{kg\ m^{-3}}.$$

Chattle also published tables of mercury density values at temperatures from 0 to 40 °C. At 20 °C the change of temperature due to the change of the scale from IPTS-48 to IPTS-68 was of −7 mK.

Another determination of mercury density was made by Fürtig (1973), who obtained:

$$\rho_0(20\ ^\circ\mathrm{C}_{\mathrm{IPTS\text{-}68}},\ 101\,325\ \mathrm{Pa}) = 13\,545.842\ \mathrm{kg\ m^{-3}}$$

with a relative uncertainty of 0.95 ppm.

This value is lower by 0.025 kg m^{-3} (1.8 ppm) than the value obtained by Cook and corrected to IPTS-68. This is another indication of possible differences in mercury samples due to different cleaning techniques and possibly to a different isotopic composition. The typical density variations revealed by different measurements were analyzed by Patterson and Prowse (1985), who found differences from 0.1 to 5 ppm in respect to the Cook value.

To calculate the density of mercury at temperatures other than 20 °C the equation of Beattie et al. (1941) is applied, which was also used by Chattle (1970):

$$\rho(t, p_{atm}) = \frac{\rho_0(20\ ^\circ\mathrm{C}, p_{atm})}{\left[1 + A\,(t - 20\ ^\circ\mathrm{C}) + B(t - 20\ ^\circ\mathrm{C})^2\right]} \tag{7.12}$$

where:

$p_{\mathrm{atm}} = 101\,325$ Pa, t(°C) is related to IPTS-68,
$A = 18115 \times 10^{-8}\ ^\circ\mathrm{C}^{-1}$, $B = 0.8 \times 10^{-8}\ ^\circ\mathrm{C}^{-2}$

As Eq. 7.12 shows, the temperature correction for mercury density is so large (181.16 ppm K^{-1}) that, to obtain a density variation limited to 1 ppm, temperature must be stable along the mercury column to within 5.5 mK, which is the goal to be attained with a mercury manometer of high accuracy.

Another important correction to be applied is for the compressibility of mercury K_{Hg} at a constant temperature, namely, $K_{\mathrm{Hg}} = 4.01 \times 10^{-11}$ Pa^{-1} (Bett et al. 1954). The dependence of the mercury compressibility on pressure and temperature may be neglected in the pressure range of manometry. If the pressure to be measured is p and the reference vacuum pressure is p_0, the density of the mercury can be referred to the mean pressure in the column, which is $(p + p_0)/2$; the density of mercury is then:

$$\rho(t, (p + p_0)/2) = \frac{\rho(t, p_{atm})}{1 - K_{Hg}[((p + p_0)/2) - p_{atm}]}. \tag{7.13}$$

A combination of Eqs. 7.12 and 7.13 makes it possible to compute the density of mercury referred to a temperature value t and to an average pressure value $(p + p_0)/2$ in the column. In Eq. 7.13, pressure p must be always absolute. The compressibility correction is not very large (about 2 ppm for an average absolute pressure of 50 kPa), but it must be applied in all manometer configurations.

Still in connection with the determination of the density of mercury and the relevant correction for temperature, mention must be made of the International Temperature Scale of 1990 (ITS-90), given in Appendix A, for temperatures below 273.16 K.

In the new ITS-90 temperature scale, the 20 °C value of the IPTS-68 scale is lower by 5 mK (i.e., at 20 °C it is $t_{90}/^\circ\mathrm{C} - t_{68}/^\circ\mathrm{C} = -0.005$). The value of the density of

mercury obtained by Cook and corrected for the IPTS-68 temperature scale must now be recorrected for the ITS-90 temperature scale. Using $\rho_0(20\ ^\circ C_{\text{IPTS-68}},\ 101\,325\ \text{Pa}) = 13\,545.867\ \text{kg m}^{-3}$ and correcting this value with the formula (7.12), we obtain

$$\rho_0(20\ ^\circ C_{\text{ITS-90}},\ 101\,325\ \text{Pa}) = 13\,545.855\ \text{kg m}^{-3}.$$

Obviously, this value will be adopted only if the temperature standards, used to measure the temperature in mercury manometers, are calibrated according to the temperature scale ITS-90. In the temperature range from −38.8344 to +29.7646 °C, thermometers are calibrated at the triple points of mercury (−38.8344 °C of ITS-90) and water (+0.01 °C of ITS-90) and at the melting point of gallium (+29.7646 °C of ITS-90).

It is interesting to consider the mercury density measurements made by Adametz and Wloka (1991). Although they used mercury samples of different origin and of unknown concentration impurities and isotopic compositions and with different cleaning methods, the mean values of the mercury density measured in their laboratory, with an estimated uncertainty of 1 ppm, deviate by no more than 0.037 kg m^{-3} (equivalent to 2.7 ppm).

An important paper by Sommer and Poziemski (1993/1994) compares all the data of high-accuracy determinations on mercury density and gives as the most probable estimate of the mercury density at 20 °C (of the ITS-90 temperature scale) and 101 kPa the value of 13 545.850 kg m^{-3} with a standard uncertainty of 0.012 kg m^{-3} (equivalent to 0.9 ppm, based on the relative standard deviation of different measurements from Cook and Stone (1957) to data measured by Sommer et al. in 1991). However, the overall set of measurements differs by 3 ppm from one another, exceeding the typical stated uncertainty of 1 ppm.

In the Sommer and Poziemski (1993/1994) paper, an analysis is also made concerning the thermal expansion and compressibility coefficients of mercury based on previous high-accuracy measurements.

The best data for mercury density $\rho(t, p_{\text{atm}})$ as a function of temperature t (ITS-90 scale) are:

$$\rho(t, p_{atm}) = \frac{\rho_0(0°C, p_{atm})}{\left[1 + \left(a_0 + a_1 t + a_2 t^2 + a_3 t^3\right) t\right]} \tag{7.14}$$

where:

$p_{\text{atm}} = 101$ kPa, $\rho_0(0\ ^\circ C, p_{\text{atm}}) = 13\,595.076\ \text{kg m}^{-3}$ and the coefficients are:
$a_0 = 1.815\,868 \times 10^{-4}\ ^\circ C^{-1}$
$a_1 = 5.458\,43 \times 10^{-9}\ ^\circ C^{-2}$
$a_2 = 3.498\,0 \times 10^{-11}\ ^\circ C^{-3}$
$a_3 = 1.555\,8 \times 10^{-14}\ ^\circ C^{-4}$

and the relative uncertainty of the formula (7.14), in the temperature range from 10 to 20 °C was estimated to be smaller than 1 ppm.

The best data for mercury isothermal compressibility were also analyzed by Sommer and Poziemski (1993/1994) based on the average of different measurements from

1949 to 1971. Based on this analysis, the recommended value for the isothermal compressibility of mercury at 20 °C and 101 kPa is 40.2×10^{-12} Pa^{-1}, with a standard deviation smaller than 0.3×10^{-12} Pa^{-1} at any pressures up to 800 MPa.

Following Sommer and Poziemski (1993/1994), the isothermal compressibility at 20 °C of mercury $\beta_{t=20\,^\circ\mathrm{C}}$ and in the pressure range up to 800 MPa is:

$$\beta_{t=20\,^\circ\mathrm{C}} = \beta_0(1 + b_1 p + b_2 p^2 + b_3 p^3) \tag{7.15}$$

where:

$\beta_0 = 40.25 \times 10^{-12}$ Pa^{-1}
$b_1 = -3.730\,11 \times 10^{-10}$ Pa^{-1}
$b_2 = 1.938\,77 \times 10^{-19}$ Pa^{-2}
$b_3 = -7.299\,26 \times 10^{-29}$ Pa^{-3}

with estimated standard uncertainty of the formula (7.15) between 0.4 and 1 %.

An important paper by Bettin and Krumscheid (1999) describes the growth of a new apparatus for the measurement of the mercury density at 20 °C with a relative standard uncertainty of 0.5 ppm. The new apparatus is based on hydrostatic weighing of sinkers of measured mass and volume, which also allows density comparisons between mercury, samples of different origins and of different isotopic compositions. When this apparatus will be ready (different steps were already reached successfully by construction of tantalum cube and more recently of a tantalum sphere of 7 kg whose volume has to be measured), it will constitute the base for mercury density measurements below 0.5 ppm accuracy, which is a fundamental step to reach pressure-relative uncertainty levels below 1 ppm with mercury manometers.

A fundamental summary paper relating to density of mercury was published by Bettin and Fehlauer (2004); in this paper an important overview of properties of mercury, absolute density determination and density changes with temperature and pressure, role of isotopic composition, dissolved gases, and dissolved impurities, are given for mercury.

Some useful mercury data, very important in manometry, are given in Appendix E, Table E.1, mainly using latest revised data as given in the Bettin and Fehlauer (2004) paper. Other thermophysical data related to mercury are given by the PTB Internal Report (1995) and by the paper by Holman and ten Seldam (1994).

7.1.3.2 Acceleration Due to Gravity

The local acceleration of gravity g_L at the site where a manometer is installed or, in general, at the selected reference measurement level can be known to an accuracy better than 1 ppm. This can be obtained, for example, with the use of a transportable absolute gravimeter, with which the absolute local gravity can be measured to a relative accuracy of few parts in 10^9 (Marson and Faller 1986; Sakuma 1984; Alasia et al. 1982; Niebauer et al. 1995). It must be pointed out, however, that the typical agreement between different absolute gravimeters is of the order of $\pm 6 \times 10^{-9}$ at 2σ level.

A resolution of the same order of magnitude can be obtained also with the use of a relative gravimeter calibrated at a fixed station, where g_L is known by a previous absolute measurement, and with a procedure according to which the relative

apparatus is checked before and after the local measurement of g_L. With such instrumentation, if carefully checked, a typical accuracy of 0.01 ppm can be obtained when the reference points are within a short distance from the site where measurements are carried out and the whole measurement is performed in a few hours. The local gravity acceleration of several reference sites in the world was measured and the relevant values constitute the International Gravity Standardization Net, IGSN-71. The accuracy of this net, which is periodically revised, is of the order of 0.1 ppm only if referred exactly to the previously measured points.

The local acceleration of gravity can also be computed from theoretical formulas. As a rule, these formulas relate the local gravity acceleration to the altitude above sea level and to the latitude of the site; they apply different corrections based on the average altitudes and the average density of the surrounding ground. Such formulas, with which an accuracy limited to few parts in 10^4 can be achieved, are not useful for obtaining the top-level accuracy required for mercury manometers as well as for pressure balances.

Another important correction to be made in the measurement of local acceleration of gravity requires the g_L value to be determined for the altitude at the reference level of the manometer. This correction amounts to $(\delta g_L/\delta h)1/g_L = 3 \times 10^{-7}$ m^{-1}. Daily variations, taking account of the Moon and Sun attraction in respect of the Earth, should also be considered for ppm or better accuracy levels.

7.1.3.3 Aerostatic Head

The reference level to which the calculated pressure p is referred is that of the measuring surface of the mercury column where p is applied. However, since the height of this surface changes with pressure, it is convenient to refer the measured pressure to a fixed and easily measurable level or a reference—mark well identified in the apparatus. As calculations have to take account of the aerostatic head, it is necessary to know the gas density $\rho_{gas}(t, p)$ at a stable temperature t and at the measurement pressure p. If the selected reference level is always above the mercury surface, then the correction is negative, because it is necessary to decrease the absolute manometer-measured pressure p by the gas-head pressure between the measuring surface and the selected reference level.

A typical configuration is illustrated in Fig. 7.13.

The selected reference level is the height h_0 in the mercury manometer when pressure in both columns is at the same vacuum reference p_0.

After pressurization, pressure p at the measurement level will be

$$p = \rho_{Hg}[t, (p + p_0)/2]g_L h + p_0 = \\ = \rho_{Hg}[t, (p + p_0)/2]g_L\,(h_2 - h_1) + p_0$$

and pressure p_r measured at the reference level is

$$p_r = p - \rho_{gas}(t, p)g_L(h_0 - h_1) \tag{7.16}$$

with the g_L value being also referred to the reference level.

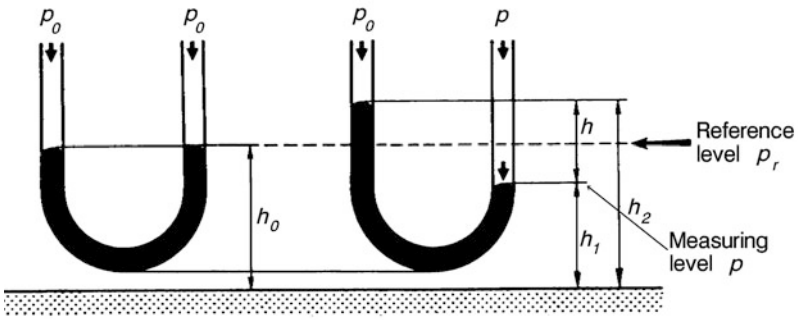

Fig. 7.13 An example of a typical configuration for aerostatic-head calculation (in both manometers temperature is considered uniform and stable in order not to influence mercury density significantly)

In order to calculate $\rho_{\text{gas}}(t, p)$, a simple way is to use the gas equation

$$\rho_{gas}(T, p) = \frac{pM}{TR} \tag{7.17}$$

$$\rho_{gas}(t/°\text{C}, p) = \rho_{gas}(T/\text{K} - 273.15, p)$$

where p/Pa is the *absolute* pressure, T/K is temperature, t/°C is also temperature, M/(kg mol^{-1}) is the molar mass of the gas, and R is the molar gas constant $R = 8.314\,472$ J mol^{-1} K^{-1} as recommended by CODATA 2006 (Mohr et al. 2008), with an estimated standard uncertainty of 1.7 ppm, similar to the value of $R = 8.314\,471$ J mol^{-1} K^{-1} as measured by Moldover et al. (1988). The molar gas constant given by CODATA 2010 is $R = 8.314\,4621\,(75)$ J mol^{-1} K^{-1}.

In Eq. 7.17, $\rho_{\text{gas}}(t, p)$ is expressed in kg m^{-3}, if the above-indicated units are used for p, T, M, and R.

The molecular weights of some common pure gases are:

2.01588×10^{-3} kg mol^{-1} hydrogen,
4.0026×10^{-3} kg mol^{-1} helium,
28.0135×10^{-3} kg mol^{-1} nitrogen, and
39.948×10^{-3} kg mol^{-1} argon.

Another possible way of computing the density, for nitrogen and helium, is to refer to the papers of Span et al. (2000) for nitrogen and McCarty (1973) for helium even if their equations of state have a wider pressure range than the one considered in the present book. Such equations have been used in numerical simulation under the EURAMET Project 1039 aimed to numerical finite element simulation of four pressure balances up to 7.5 MPa to be used for the redetermination of the Boltzmann constant.

The suggested density equations versus pressure are valid at 20 °C, for absolute pressures up to 7 MPa:

$$\rho_{N_2}/(\text{kg m}^{-3}) = 11.550 \cdot \; p/\text{MPa}[1 + 1.1 \cdot 10^{-4} \cdot p/\text{MPa}]$$

with an estimated standard relative uncertainty of 0.005 % and

$$\rho_{^4\text{He}}/(\text{kg m}^{-3}) = 1.6412 \cdot p/\text{MPa}[1 - 4.63 \cdot 10^{-3} \cdot p/\text{MPa}]$$

with an estimated standard relative uncertainty of 0.025 %.

Comparing the above two equations with Eq. 7.17 at 20 °C and in the absolute pressure range from 10 to 101 325 Pa, we have at 0.1 MPa a difference of 0.00576 kg m^{-3} for nitrogen and of 0.000176 kg m^{-3} for helium. These differences are increasing as the absolute pressures increase, an evident limitation of Eq. 7.17.

The aerostatic-head correction depends mainly on the gas density and on the distance $(h_0 - h_1)$.

For a typical case of an absolute pressure of 100 kPa, with nitrogen, with $(h_0 - h_1) = 380$ mm and a temperature of 20 °C, ρ_{N2} (20 °C, 100 kPa) = 1.149 kg m^{-3}, the aerostatic-head value computed at the standard gravity acceleration 9.80665 m s^{-2}, is 4.28 Pa.

The contributions to the uncertainty of the aerostatic-head calculation have always to be considered and are the following:

a. Contribution of the uncertainty of $\rho_{\text{gas}}(t, p)$ determination

$$\Delta_{1p} = \Delta\rho_{gas}(t, p)g_L(h_0 - h_1).$$

Under the conditions specified in the above example, the contribution of an estimated uncertainty of $\Delta\rho_{\text{gas}}(t, p) = 0.01$ kg m^{-3} (probably pessimistic) for nitrogen is equivalent to $\Delta_{1p} = 37$ mPa.

As we have already seen in the case of higher pressures than the ones used typically in manometry, a more precise calculation of gas density should not be based on Eq. 7.17, and should include the virial coefficients and their temperature and pressure variations.

In this case, the Eq. 7.17 may be modified as

$$\rho_{gas}(T, p) = \frac{pM}{RT[1 + (Bp)/RT]}.$$

For example, for nitrogen, the virial coefficient is $B = -6.2 \times 10^{-6}$ (m^3 mol^{-1}). The density of nitrogen, at 101 325 Pa and 293.15 K, obtained with the above equation differs from the value calculated with Eq. 7.17 only for a factor of 3×10^{-4}. Values of the virial coefficients B for different gases can be found in Dymond and Smith (1980). Data of gas thermal properties have also been experimentally measured (e.g., in the case of nitrogen with temperatures from 280 to 360 K and pressures up to 12 MPa) as reported by Blanke et al. (1988).

b. Contribution due to temperature uncertainty

$$\Delta_{2p} = \frac{d\rho_{gas}(t,p)}{dt}\Delta T\, g_L(h_0 - h_1).$$

Under the same foregoing conditions, with ΔT being assumed equal to 10 mK and a density variation of 0.004 kg m^{-3} K^{-1} due to temperature, the contribution to overall uncertainty will be equivalent to $\Delta_{2p} = 0.15$ mPa. Generally, the temperature instability has to be included as well; in such a case generally the estimated temperature uncertainty increase from two to five times the estimated uncertainty of the temperature measurement.

c. Contribution of the uncertainty in h_0 determination

$$\Delta_{3p} = \rho_{gas}(t,p) g_L \Delta(h_0).$$

Still under the same conditions already specified, the contribution of a typical $\Delta h_0 = 0.2$ mm will be equivalent to $\Delta_{3p} = 2.3$ mPa.

d. Contribution of the uncertainty of the g_L value

$$\Delta_{4p} = \rho_{gas}(t,p)(h_0 - h_1)\Delta g_L.$$

Under the specified conditions, the contribution of a relative uncertainty of 1 ppm in the value of the local acceleration due to gravity will be equivalent to $\Delta_{4p} = 0.004$ mPa, a negligible addition.

This contribution must obviously also be taken into account in evaluating the uncertainty of the pressure p value (see Sect. 7.1.3.2).

The above examples, which concern only the aerostatic-head calculation, show that the largest contribution to overall uncertainty is that of gas density, even if temperature is known and stable within 100 mK and the h_0 reference level is determined to within 0.2 or even 0.5 mm.

7.1.3.4 Reference Pressure p_0

When pressure p is measured under absolute conditions (Eqs. 7.4 or 7.5), its value depends on the reference pressure p_0. This (vacuum) reference pressure must be produced by means of, for example, a mercury diffusion pump or a turbomolecular pump appropriately used in the range close to or below 0.1 Pa.

It is advisable to use cold traps in order to prevent mercury-vapor contamination and possible saturation of the pumping system by mercury vapor and it is normal routine to use large-bore tubes to avoid pressure gradients between the columns and the pumping system. It is also necessary that the reference pressure p_0 be measured as close as possible to the mercury column. The reference pressure to be produced should be below 0.1 Pa, this value being conditioned by the mercury-vapor pressure, p_v, ($p_v = 0.170$ Pa at 20 °C, with $dp_v/dt = 0.0147$ Pa °C^{-1} around 20 °C, as measured by Ernsberg et al. (1955).

This conditioning factor makes the measurement of the reference pressure p_0 even more important. In the past years, McLeod and Pirani gauges of appropriate sensitivity were typically used to measure p_0. As the use of Pirani gauges depends on gas composition, these gauges are not very suitable to perform measurements in systems where mercury vapors are to be found. There is now a consolidated tendency to measure p_0 with CDG, with which, for a typical full scale of 1 Pa, the uncertainty is 0.02 Pa. This uncertainty contributes to a systematic uncertainty of 0.2 ppm in the case of absolute pressure measurements at 100 kPa. But, of course, 0.02 Pa estimated uncertainty on p_0 can be a limiting factor, for example, for measurements below 1 kPa. For the measurement of the reference pressure $p_{0,}$ it is necessary to consider as well its uncertainty contribution to the overall pressure uncertainty, see Sect. 7.2.2.7.

7.1.3.5 Uncertainty of Pressure Measurement by Liquid-Column Manometers

It must be mentioned that a detailed analysis of the uncertainty associated with a mercury or a liquid column depends to a high degree on the specific measuring system, especially in connection with the many different techniques applied in mercury height measurements (see Sect. 7.1.2). Besides, there are systems that have special problems needing specific analysis. For example, with an interferometric system equipped with floating devices it is necessary to consider the change that may occur in the shape of the meniscus consequent to a pressure change and to check for the possible effect of surface tension against the tube walls and capillary-depression effects. If a capacitance system is used to locate the mercury position in the columns, an evaluation of the uncertainty inherent in the measurement applying the capacitance technique should be included in the uncertainty budget.

A careful and complete analysis of each contribution to systematic and random uncertainties in the measurement of pressure is a very delicate operation. The estimate of the uncertainty that is frequently associated with the individual parameters is often unrealistic.

Since 1980, the national standards laboratories have adopted the Recommendation of the Comité, International des Poids et Mesures (CIPM Rec. INC-1, 1980) that is given integrally in its English version in Appendix E (Document E.1).

According to this Recommendation, uncertainties are divided into two categories, A (sometimes called improperly random uncertainties) and B (sometimes called systematic uncertainties); this is a useful way of classification, for it requires a careful statement of the different contributions to the overall uncertainty.

With liquid-column manometers, the uncertainties of type A are obtained experimentally from the dispersion of measurement values over the whole pressure range. This dispersion is normally obtained by comparing the basic manometer with another instrument or with a pressure balance of similar uncertainty, in both the absolute and the gauge modes. The reproducibility of zero pressure (when both columns are under the same reference vacuum pressure p_0) is normally also included in the evaluation

of the A-type uncertainties. With mercury manometers, the B-type systematic uncertainties include the several physical quantities (e.g., h, ρ_{Hg}, g_L, t, ...) described in the previous sections, which are indispensable for the measurement of pressure.

Although the uncertainty classification of the BIPM Recommendation is widely accepted, different opinions are held by the individual laboratories as to whether the individual contributions to overall uncertainty should be estimated at the 1σ level (residual standard deviation of the mean) or at the 3σ level. In many papers, however, the method used for uncertainty combination is clearly stated.

At the national-laboratory level, today there is a large agreement to express the individual uncertainty contributions at the 1σ level.

This is also the basic principle followed in the present book, except when otherwise stated, as in the case of some of the literature data reported here, which were evaluated at the 3σ level or in some other cases for which the level had not been specified.

Another debated matter is whether all systematic uncertainties should be related by the arithmetic sum or by the root mean square of the sum of the squares of the different contributions. The choice should depend on the specific case considered. Experience shows, for example, that the arithmetic sum of each uncertainty contribution is a better choice when there are closely correlated physical quantities playing a significant role in the overall uncertainty budget. When some quantities are correlated, it is also possible to consider both their single variances and the covariances of the correlated quantities, all combined together.

Today the situation is more clear and supported by different "Guides to the expression of uncertainty in measurements."

After the approval by CIPM of the Recommendation INC-1 (1980), a Joint Committee for Guides in Metrology (JCGM) was created by different organizations (BIPM, IEC, IFCC, ILAC, ISO, IUPAC, IUPAP, and OIML).

This JCGM produced the first guide for the expression of uncertainty in measurements-GUM in 1995 called "*ISO/IEC Guide 98-GUM (1995).*" This GUM Guide (1995) played an extremely important role of information and clarification and many other documents were developed according to similar structures (e.g., EA, Tech. Report EA-4/02, 1999).

The JCGM revised the 1995 GUM and produced an amended version in 2008, which is called "*JCGM 100:2008*," Evaluation of measurement data. Guide to the expression of uncertainty in measurement, First Edition 2008 together with another guide called "*JCGM 101:2008*," Evaluation of measurement data-Supplement 1 to the "Guide to the expression of uncertainty in measurement-Propagation of distributions using a Monte Carlo method."

Both Guides are the copyright of JCGM and available, for example, in its English version on the BIPM web site http://www.bipm.org/en/pubblications/guides/gum.html.

It is important to also consider the work done by the working group on basic terminology in metrology that produced an International Vocabulary of basic and general terms in Metrology, generally called VIM (1984) and in its last edition as *JCGM 200:2008*, (2008), International Vocabulary of metrology. Basic and general concepts and associated terms (VIM).

Table E.2 in Appendix E gives a typical example of the overall uncertainty budget concerning an absolute/gauge mercury column having a laser interferometric floating device for height measurements as given in Alasia et al. (1999a). In this table, the uncertainty contributed by each parameter is expressed at the 1σ level. The example selected is, to some extent, a little different from some of the cases described in the literature. In fact, a total uncertainty of 0.3 Pa at 120 kPa (at the 1σ level), equivalent to 2.5 ppm, can be considered really good and is the result of all the precautions taken in the measurements of the different parameters appearing in pressure calculation and indicated in Table E.2.

Another example of the uncertainty budget and concerning an ultrasonic manometer (Tilford and Hyland 1988a) is given in Appendix E, Table E.3. In this case, the largest components of the systematic type-B uncertainties are correlated, so that all systematic components are arithmetically summed; a total uncertainty (in this case at the 3σ level) of 0.01 Pa $\pm$ 16.7 ppm can be considered a very good result.

The data reported in Tables E.2 and E.3 in Appendix E and the examples the data refer to, give an idea of how uncertainties in pressure measurements are affected when some measurement conditions are changed. For example, if the estimated temperature uncertainty (also considering uniformity along the mercury columns) is changed from 10 mK to higher values there will be a larger shift of uncertainty due to this condition of measurements.

If a user tries to obtain a typical uncertainty of the same order of magnitude as those reported in Tables E.2 and E.3 without knowing the mercury density, without operating with pure mercury and under the typical laboratory conditions of good temperature uniformity, no vibrations, and stability of the reference pressure p_0, he will find that this is not possible and that uncertainties lower than some pascal are unachieved.

In experiments conducted with "unknown" mercury not perfectly cleaned at the distillation level, with a temperature uniformity of 30 mK, and with vibration problems, the uncertainty may be from 20 to 100 ppm, depending on the specific cases. Under such conditions and at each pressure point, the typical reproducibility, evaluated as the residual standard deviation of the mean (1σ) of the pressure measurements, ranges from 0.4 to 1.5 Pa for pressures from 30 to 115 kPa.

The above examples represent realistically situations in which mercury manometers can be used to the best possible level of accuracy (from a few ppm to about 15 ppm), if several precautions are taken. If this is not the case, even when the resolution of the measurement of mercury height is very good, the typical uncertainty and reproducibility will deteriorate to a level, which is of no interest when a liquid-column manometer is to be used as a primary standard.

7.1.4 Liquid Columns for Different Applications

For the measurement of absolute pressure s, mercury-column manometers can be used to a maximum pressure of 0.36 MPa. Under gauge conditions, different installations of mercury-column systems, generally built at the beginning of the twentieth

century and covering a very high pressure range, are in some cases still used today, though they are now frequently replaced by the more practical pressure balances.

Among different installations, mention must be made of the system of the PTB. It is a 38 m-long mercurycolumn allowing gauge pressure measurements to be made up to 5 MPa. This apparatus was used in the past to evaluate the effective area of pressure balances between 1 and 5 MPa, through pressure determination having an uncertainty of 15 ppm, mainly due to the mercury-column manometer (Bauer et al. 1977). More recently at PTB, Jäger et al. (1990) have reconsidered the accuracy of pressure measurements with the high-pressure mercury manometer, mainly revising different aspects such as temperature measurements, density of mercury data, measurement of column height windows effects, and the localization of mercury menisci. With this revision, the standard deviation of pressure measurements with the 38 m-long column was 7 ppm at 1.2 MPa and 4.8 ppm at 5 MPa. This long mercury column was used at PTB to derive the effective area of gas-operated pressure balances up to 5 MPa. The piston-cylinder units were oil lubricated having 1 cm^2 nominal effective area (the standard deviation of pressure measurements was 8 ppm at 0.8 MPa and 7.2 ppm between 3 and 5 MPa).

Similar apparatus exist in other countries. Meyer and Jessup (1931), in the United States, describe a 1.5 MPa multiple-column manometer; Michels (1932), in Holland, describes a differential 27 m manometer column; Bett and Newitt (1963), in the United Kingdom, describe a differential 9 m mercury column used in differential mode operation up to 250 MPa to calibrate pressure balances; and in Italy, Paratella and Marani (1968) describe a 9 m mercury column used in differential mode to calibrate pressure balances. Even more recently, Holman and ten Seldam (1995), in Holland, describe a revised 30 m mercury column used to calibrate pressure balances up to 300 MPa. In their paper, they mention the difficulties of operation above 260 MPa and quote relative differences in respect to a controlled-clearance pressure balances from 12 to 101 ppm at pressures of 161, 199, and 248 MPa. Giardini (1999) in Australia describe a column of 8.6 m aimed to operate, in five steps of 1.2 MPa, up to a maximum pressure of 5.8 MPa, having a potential standard uncertainty of 8 ppm.

In many cases, however, such instruments were replaced by primary standard pressure balances and some are no longer used.

Another area of important applications (chemical industry, flow of pressurized natural gas, . . .) is that of gas measurements at high line pressures (to a maximum of 20 MPa) and small differential pressures ranging from 0.01 to 0.5 % of the value of the line pressure. In this sector, it is still possible to use some liquid columns having special arrangements and measuring methods, but here, too, some special combinations of pressure balances (see Sect. 7.2.5) have been developed (Daborn 1977).

An interesting apparatus is the one described by Gielessen (1975). It consists of two vessels, one fixed and the other movable vertically; both equipped with high-pressure windows and interconnected by a flexible high-pressure hose. The level of the liquid is measured by a cathetometer. This apparatus operates to a maximum line pressure of 10 MPa with an evaluated measurement uncertainty of 0.2 Pa when water

is used and 2.5 Pa with mercury; differential pressure measurements above 0.5 kPa with water and 6.3 kPa with mercury can be performed.

Other apparatuses are also available for line pressures up to 40 MPa, in which the mercury level is detected by differential transformer devices installed on floating systems; the stated uncertainties range from 0.1 to 0.01 %.

An area where liquid columns of different types are still playing a significant role is that of the measurement of small gas absolute and gauge pressures, generally below 1 kPa. Important papers have been written to review the situation in this sector, in particular Brombacher (1970) and Peggs (1980).

Some of the mercury manometers described in Sect. 7.1.2 also allow absolute and gauge pressure measurements to be made down to 100 Pa, and the same principle of measurement, for example, ultrasonic (Heydemann et al. 1977) can be used on dedicated instruments, for example, covering a range of 13 kPa, with a resolution of 1.4 mPa. Alasia et al. (1999b) describe the interferometry cat's eye mercury micromanometer IMGC-MM1 operative from 1 Pa (standard uncertainty of 12 mPa) to 5 kPa (standard uncertainty of 53 mPa). Yanhua et al. (2011) describe a distilled water micromanometer up to 2 500 Pa using laser interferometer on movable vessel and ultrasonic transit time measurements. Sadkovskaya et al. (2011) describe an oil manometer with floats and laser interferometer used up to 1 000 Pa and Könemann et al. (2011) describe a three-tube mercury micromanometer equipped with floats and plane mirrors and laser interferometer up to 1 kPa.

With a Hess manometer covering a 13 kPa range and using mercury as a fluid, a total uncertainty of 1.1 Pa + 9 $\times$ 10^{-5} p/Pa was reported by Peggs (1980).

Fluids other than mercury and of lower density are frequently used, for example, water and siloxane fluids (Orcutt 1973). A good example of an oil micromanometer was described by Pinot and Riety (1993). This instrument is quoted to be able to perform differential pressure measurements from 0.01 Pa (2σ level uncertainty of 0.005 Pa) to 200 Pa (2σ level uncertainty of 0.13 Pa). Also, diethylhexyl sebacate (DEHS) is sometimes used as fluid for manometry over the range from 1 mPa to 140 Pa and in absolute mode. In such a range, the effect of dissolved gas on the density of oil is nonsignificant, but the decrement of density at higher pressures (e.g., around 100 kPa) become extremely important at pressures from 10 to 100 kPa (Hendricks et al. 2009).

A list of properties of some manometric fluids is given in Appendix E, Table E.4, which is a part of an ample table (Peggs 1980).

For the measurement of small absolute pressure s, it is sometimes convenient to use liquid gallium as the manometric fluid. It is, of course, necessary to operate at stable temperatures higher than that of the gallium melting point, which is 29.7646 °C of the ITS-90 temperature scale. Advantages of this choice are the density of liquid gallium and its vapor pressure, which are, respectively, 2.2 and 7 times smaller than those of mercury. Disadvantages are the need of operating at temperatures higher than 29.8 °C, which must be very stable, and of measuring the gallium density to a high accuracy at the temperature of operation. In addition, the surface tension of gallium is greater than that of mercury.

A new differential gallium manometer of the interferometric capacitance type has been constructed by Legras et al. (1990). This manometer is used in the range from 0.01 to 100 Pa with an estimated sensitivity of 0.001 Pa and repeatability of 0.01 Pa up to 4 Pa and 0.03 Pa for higher pressures.

The use of liquid gallium in manometry is still a debatable and an open question. Still in this area of application, other devices can be used, such as pressure balances in very special configurations or bell-type micromanometers (Jäger et al. 1988) to measure small pressures under absolute or gauge conditions (see Sect. 7.2.5).

7.2 Gas-Operated Pressure Balances

The development of pressure balances dates back to the beginning of the nineteenth century. Essentially, it was stimulated by the need of studying, at pressures higher than those measured by liquid-column manometers, the thermodynamic properties of substances and by the growth of industrial applications, for example, in steam engines.

Galy-Cazalat (1846) describes, for example, an apparatus that is, essentially, a combination of a mercury column and a hydraulic piston multiplier; Seyss (1869) developed a system equipped with two concentric pistons and an automatic large-weight loading device.

Many other contributions were made by different scientists (Desgoffe 1871; Cailletet 1880; Ruchholz 1883; Amagat 1894; Stückrath 1894).

The system conceived by Ruchholz is a very simple device having a carefully machined rotating piston and is not very different from the pressure balances still used today. Amagat used his pressure balance for detailed studies of gas compressibility. At that time, the typical pressure involved was of the order of 150–300 MPa.

The necessity of extending this pressure range further up and of reducing the high leakage between the piston and the cylinder due to the distortions produced on the cylinder and on the piston by pressure increase, led to remarkable progress and to new ideas in the construction of pressure balances of different types.

Examples are the "re-entrant" piston-cylinder unit of Bridgman (1911) and of the controlled-clearance type of Bridgman (1909) and of Newhall (1957), with which devices it was possible to make accurate pressure measurements up to 1.4 GPa in liquid media.

The pressure balances available today have been substantially improved, particularly as regards piston-cylinder geometry, the way of applying the load on the piston, and all the associated measurements (temperature, piston position, piston fall rate, piston rotation and the calculation, or the measurements of piston and cylinder distortions versus pressure).

With gas media, the pressure balances now available are used for:

- Absolute pressure measurements from few kilopascal to approximately 5 MPa.
- Relative pressure measurements from values close to atmospheric pressure up to 100 MPa.

- Differential pressure measurements with line pressures up to approximately 80 MPa, and for small differential pressures from few kilopascal to some megapascal.

Mention has to be made of pressure balances with large piston-cylinder effective areas to be used in absolute and gauge mode around atmospheric pressure values as an alternative to mercury-column manometers. Similarly, there are available today nonrotating force-balanced pressure balances for very low gauge and absolute pressures and pressure balances using conically shaped piston also for very low gauge pressure measurements.

The state of the art of such apparatuses will be described in the following sections together with the procedures for their correct use in order to achieve the best possible accuracy.

Mention must be made of the following review books and survey papers dealing with the same subject described here, in particular: Heydemann et al. (1975), Lewis et al. (1979), Dadson et al. (1982), Peggs (1983), Legras (1988), Ehrlich (1993/1994), Molinar (1993/1994), Sutton (1993/1994), EAL-G26 Guide for the Calibration Of Pressure Balances (1997), and Molinar (2011). See also the section "Further Readings" where relevant papers can be found in Molinar et al. (1994), NCSL International (1998), Molinar et al. (1999), Jousten et al. (2005), Anderson et al. (2005), and Buonanno et al. (2007).

7.2.1 Basic Description

A pressure balance is essentially made up of a piston-cylinder unit and of a system for the application of a known vertical load on the piston (refer to Fig. 7.14a). The piston-cylinder unit is the essential part of the apparatus, as it is used to define the effective area on which pressure is applied. A pressure balance, which measures pressure in terms of force per unit area, looks so simple that its reproducibility and uncertainty are frequently overestimated and its real characteristics are seldom routinely checked, thereby disregarding the advice of the most careful users. The metrological verification of a pressure balance has to be made in its entire range of pressures; too frequently, particularly at lower pressures, such verifications are either not done or are not complete. This gives incorrect information to the user.

In spite of its simplicity, a pressure balance is a very reliable apparatus, but only if appropriately designed and carefully used. Such precautions are even more important when the pressurizing fluid is a gas, because in this case the piston and cylinder are lubricated in the clearance only by the compressed gas: this requires strict conditions of cleanliness.

The main requirements for "ideal" piston-cylinder units are listed below:

- The unit must be made of carefully chosen materials, particularly capable of withstanding high compressive strength under elastic conditions and having a very small linear thermal expansion coefficient.

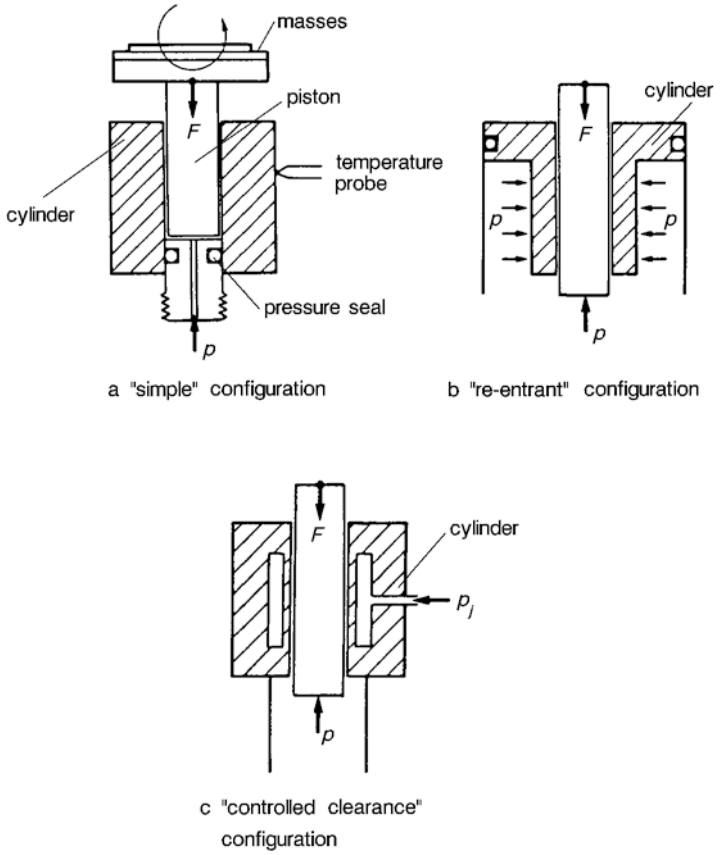

Fig. 7.14 The three basic configurations of a pressure balance (simple or free deformation, reentrant, controlled clearance)

- Unit machining and lapping of the surfaces must be at the submicrometer level, for top-level units the required accuracy is at the level of tenths of nanometers.
- Its effective area at atmospheric pressure must be, as far as possible, constant along the entire engagement length of the piston in the cylinder. This implies an extremely accurate geometry of the piston and of the cylinder, at a level that is achievable only with the very best manufacturing and measurement techniques. Typically, for diameters from few millimeters to 50 mm, diameter and roundness constancy to at least 100 nm or better is considered a good result.
- The clearance between the piston and cylinder diameters must be small (typically from 0.5 μm to less than 1 μm) and uniform along all the engagement length of the piston in the cylinder.
- The piston-cylinder unit must be so designed that the components of the piston-cylinder assembly (e.g., the cylinder retaining nut and the pressure seal, which is

generally fitted to the cylinder) do not exert any sizable force on the cylinder, as unpredictable distortions may be generated on it.

- On application of pressure, the piston must float freely along the engagement length of the cylinder without friction or metal-to-metal contact between the two parts. During pressure measurements, the piston must be in permanent rotation within a selected and appropriate range of revolution frequency in order to reduce possible piston to cylinder friction.
- The rotation decay must be regular, without abrupt stop, and rotation has to last for different minutes. The rotation can be applied to the piston manually or automatically with a revolution frequency of 2–3 Hz. The selection of the appropriate revolution frequency is very important and must be carefully evaluated. If an automatic rotation system is used, it is necessary that it does not introduce any nonvertical force component on the piston that will produce unstable measurements and the motor must be away from piston-cylinder in order not to give too high temperatures changes on piston-cylinder unit.
- The piston fall rate must be small and highly reproducible in the whole pressure range, even if fall rates are comparable only at exactly the same pressure and temperature values. This is an important parameter also used to check the "quality" of the system during the use of the pressure balance.
- The piston-cylinder unit must be designed in such a way as to house an accurate temperature probe usually in contact with the cylinder, in order to correct for the temperature of the unit during the pressure balance operation.

Such requirements are generally entirely fulfilled only by the top-quality pressure balances existing in national standards laboratories. From the point of view of constituent materials, the present tendency, in the pressure range from 0.1 to 100 MPa, is to use tungsten carbide with different percentages of cobalt for the construction of pistons and cylinders.

The elastic characteristics of a material such as this (for example, Young modulus $E = 600$ GPa and a Poisson coefficient of 0.22 for tungsten carbide with 6 % cobalt), its small linear thermal expansion coefficient (generally lower than $5 \times 10^{-6}\ ^{\circ}\mathrm{C}^{-1}$), and its very good machining and polishing characteristics, make it the best choice for the fabrication of pistons and cylinders for pressure balance systems.

As regards load application, the applied force must act vertically on the piston, without parasitic components.

The whole system, consisting of the standard weights and the piston, is in permanent free rotation. If the center of mass of this system is situated on the vertical rotation axis, well below the physical position of the piston, the system stability is improved and the piston can rotate freely for a longer time.

Standard weights used in pressure balances should be designed and used with the same extreme care as that normally reserved for accurate mass standards. It is therefore advisable to use integral weights made of nonmagnetic stainless steel and resort to the soft-cleaning and maintenance procedures employed for mass standards. Such care and attention must be applied to all the pieces (piston, weight carrier, standard weights) used for force generation.

When gas is used as a pressurizing fluid, it is also important that the weight carrier rotate freely in respect of the body of the pressure balance, to avoid creating small clearances and close volumes in which the gas escaping from the piston and the cylinder may be trapped. As gas trapping would create nonmeasurable forces on the piston, normally, large holes along the whole weight carrier are bored in order to prevent such undesirable phenomenon to occur below the weight carrier.

There are *three basic* configurations of pressure balances, depending on the design of the piston-cylinder unit. Such configurations are schematically illustrated in Fig. 7.14.

In the *simple* configuration (Fig. 7.14a), pressure p to be measured is applied to the base of the piston, and the piston and cylinder are so coupled that stresses on piston and cylinder depend solely on the applied pressure and to the pressure distribution all along their engagement length.

The pressure distribution all along the piston-cylinder engagement length is due both to pressure application and to the achievement of pressure equilibrium. In this configuration, also called the *free deformation* type, the piston and cylinder are subjected to free elastic deformations that depend on the value of the measuring pressure p, on the geometry of the piston and cylinder, on pressure distribution along the engagement length of the piston and cylinder, and on the nature of the pressurizing gas. In this configuration, it is important that no parasitic forces should be applied to the cylinder and to the piston.

In the "*re-entrant*" configuration (Fig. 7.14b), the measuring pressure p acts also on a well-defined external part of the cylinder. Measuring pressure p acts on the base of the piston, along the engagement length of the piston and cylinder with an appropriate pressure distribution, and on the external part of the cylinder and produces a change in the clearance between the piston and the cylinder due to cylinder deformation, which is proportional to the differential pressure between the measuring pressure p applied on the external part of the cylinder and the pressure distribution in the piston-cylinder clearance.

In the *controlled-clearance* configuration (Fig. 7.14c), a variable pressure (called jacket pressure) pj, generated, controlled, and measured by an independent system, is applied on the external part of a portion of the cylinder, thus providing control of the clearance between the piston and the cylinder, the clearance being a function of the geometry of the system, the elastic constants of materials used, and of the values of measuring pressure p and pj.

In gas pressure measurements, "simple" piston-cylinder units are the most used for absolute, gauge, and differential measurements; the two other configurations, in principle designed for operations at pressures higher than 100 MPa, can be used as well. Other configurations are frequently used in gas pressure measurements; two types are illustrated in Fig. 7.15.

In the configuration in Fig. 7.15a, the piston-cylinder clearance is oil lubricated, which combines reasonably satisfactory performance with simple use. This configuration can be used with gas media, provided that great care is taken to avoid possible gas contamination brought about by too fast pressure variations. The metrological

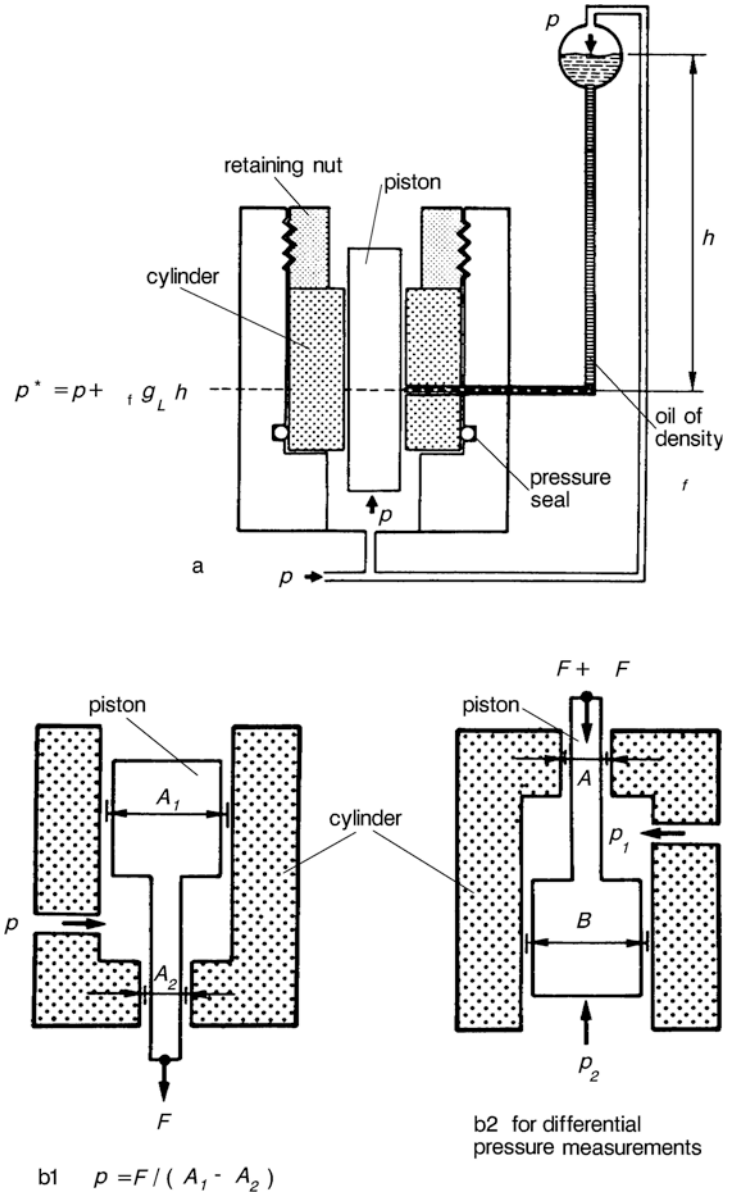

Fig. 7.15 Systems used for gas pressure measurement. **a** Partially "re-entrant" configuration, with oil lubrication between piston and cylinder. **b1** Pressure balance with a double piston. **b2** Pressure balance for differential pressure measurements at high line pressure

characterization of the unit is complicated by the very peculiar liquid pressure distribution along the clearance; the best calibration method consists in the determination of its effective area by *cross-floating* this unit against another standard (taken as primary) working with a completely pure-gas configuration.

"*Cross-floating*" of pressure balances is an experimental technique in which two systems are directly connected and at each measuring pressure value of their overlapping range, the equilibrium between them is detected. Equilibrium is achieved by reproducing the same individual piston fall rate when the two systems are connected together. The equilibrium condition is equivalent to a steady state of the gas flow in the connecting line between the piston-cylinder units. The equilibrium condition is reached by appropriate addition of small standard weights on one of the two systems, and by accurate measurements of piston fall rates at a stable temperature. In order to use this technique at top-level quality, reaching, for example, sensitivities of cross-floats within or below 1 ppm, it is necessary to use top-quality automated fall rates measurements on the two piston-cylinder units, great experience and good practice of pressure measurements.

The two configurations in Fig. 7.15b1, b2 can be used for specific measurement applications. With the first type in Fig. 7.15, pressure p is applied to an effective area, which is the difference $(A1 - A2)$ of the areas of the two piston-cylinder units. With this configuration, the pressure p to be measured can be increased without using too large weight pieces, as the effective area $(A1 - A2)$ can be very small. Modern pressure balances generally are not of this configuration; similar effects can be obtained with a small effective area single-piston-cylinder unit.

The second example in Fig. 7.15b2 illustrates the configuration for the measurement of small differential pressures at a high line pressure (see Sect. 7.2.5) developed at NPL-UK by Daborn (1977).

The pressure balances developed today allow gas pressure to be measured in the ranges specified below:

- Absolute pressures to about 5 MPa. As a rule, different piston-cylinder units must be used to cover the whole range, from large areas piston-cylinder units to the smaller ones. Usually, the lower pressure limit is of the order of few kilopascal, unless particular techniques are used. The "free deformation" piston-cylinder configuration is preferred.
- Gauge pressures to about 100 MPa. In this case too, different units may be used. The pressure balances still cover the entire range to the highest achievable accuracy. The simple, reentrant and the controlled-clearance configurations may all be used, though the first two are preferred in the majority of cases.
- Differential pressures to about 80 MPa line pressure and differential pressures from some kilopascal to some megapascal. Generally, double pressure balance units are used, together with particular measurement procedures.

7.2.2 Absolute Pressure Measurements to 5 MPa

Absolute pressure is measured by a pressure balance, when the force produced by a body of mass mi in a gravitational field and the resulting force produced by a pressure, p, on the piston-cylinder unit of effective area, A_e, are in equilibrium.

Absolute condition is realized when around the weights a stable appropriate vacuum reference pressure, p_0, is generated and measured.

A simplified configuration of systems for absolute measurement has already been given schematically in Fig. 7.2. Pressure, in a first approximation, is computed by means of Eq. 7.5. In this section, only piston-cylinder units of the "simple" type will be discussed, because this is the prevalent configuration in the pressure range from few kilopascal to 5 MPa.

The absolute pressure, p, computed at a reference level h from the base of the piston-cylinder unit (it has to be remembered that the reference level may be the bottom part of the cylinder, or other references, and this level has to be specified at the time of a calibration), is expressed by:

$$p = \frac{\Sigma \mathrm{i} m_{\mathrm{i}} g_{\mathrm{L}}}{A_0(1+\lambda p)(1+(\alpha_{\mathrm{p}}+\alpha_{\mathrm{c}})(t-t_{\mathrm{ref}}))} \pm p_0 \pm \rho_{\mathrm{f}} g_L h. \tag{7.18}$$

The symbols of Eq. 7.18 have the following meanings:

- mi(kg) is the mass of the i$^{\mathrm{th}}$ weight-piece referred to the density $\rho_{\mathrm{m_i}}$ of the i$^{\mathrm{th}}$ weight.
- g_{L} (m s^{-2}) is the local acceleration of gravity.
- A_0 (m^2) is the effective area of the piston-cylinder unit measured at atmospheric pressure and at the reference temperature t_{ref}.
- λ (MPa^{-1}) is the elastic distortion coefficient of the piston-cylinder unit.
- p in the term $(1+\lambda \mathrm{p})$ indicates the effect of pressure on variations in the effective area when a linear variation of effective area versus pressure can be assumed. Pressure p(MPa) in the above parenthesis is computed as $p = 10^{-6}\left(\frac{\Sigma_i m_i g_L}{A_0}\right)$.
- α_{p} and α_{c} (°C^{-1}) are the linear thermal expansion coefficients of the piston and the cylinder, respectively.
- t(°C) is the temperature of the piston-cylinder unit at the time of the pressure measurement.
- t_{ref} (°C) is the reference temperature at which the effective area A_0 was measured; generally, t_{ref} is equal to 20 °C.
- p_0 (Pa) is the vacuum reference pressure.
- ρ_{f} (kg m^{-3}) is the gas density at temperature t and at the absolute pressure p.
- h(m) is the distance between the piston-cylinder level and a selected reference level. If the units indicated above are used, pressure p will be expressed in pascal (Pa).

Equation 7.18 consists of three terms. The first term expresses the absolute pressure generally at the base of the cylinder, which is assumed to be regularly cylindrical, so that no fluid buoyancy correction has to be applied for irregularity in the piston shape.

Sometimes the piston base is also selected as a reference. Other references may be the end of the cylinder, but the best choice is the starting point of the engagement length of the piston and cylinder, at which the pressure in the clearance is maximum

and equal to the measuring pressure p. Reference selection will depend on the design of the piston-cylinder unit. For each system, during its metrological characterization, the reference height selected must be clearly indicated, as it is important for aerostatic-head calculations.

The second term takes account of the measured value of the vacuum reference pressure p_0 surrounding the weights.

The third term is the aerostatic-head pressure correction, to be applied if necessary, for the elevation difference between the piston base and the selected reference level (the sign "+" or "−" depends on the position of the reference level in respect of the base of the piston).

Let us examine in detail each of the physical quantities appearing in Eq. 7.18, when the aim is to use the pressure balance as a primary standard and obtain the best possible accuracy in the measurement of absolute pressures.

7.2.2.1 Mass

The mass of each element, including the piston, of the weight set must be determined. It must be remembered that m_i is not the conventional mass value referred to a conventional density value (generally 8 000 kg m^{-3}), but it is the actual mass value (some authors call this quantity "true" mass or mass referred to vacuum) referred to the actual density ρ_{mi}, to be also determined, of each weight piece.

This question is raised by the fact that mass is normally determined in air, and not *in vacuo*, so that it is necessary to introduce appropriate buoyancy corrections in mass measurements, to take account of the volume difference between the object to be weighed and the standard mass. Unless this correction is applied, generally each mass value is given as a conventional value m_{icon} referred to the conventional value of density of 8 000 kg m^{-3}.

Mass m_i can be related to the conventional mass value m_{icon} by the following equation:

$$m_i = m_{icon} \frac{(1 - \rho_a/8\,000 \text{ kg m}^{-3})}{(1 - \rho_a/\rho_{m_i})} \tag{7.19}$$

where ρ_a is air density (kg m^{-3}) at the time of the mass measurement and ρ_{mi} (kg m^{-3}) is the actual density of the weight-piece expressed in kilograms per cubic meter.

The density, ρ_{mi}, of weights typically used in pressure balances ranges from values around 2 900 kg m^{-3} (typical of weight carriers made out of plated aluminum and nickel) to values around 14 000 kg m^{-3} (typical of pistons made of tungsten carbide).

The best choice is represented by weights entirely made of integral and amagnetic stainless steel, excepting the case of the piston when it is made of tungsten carbide. To give an evaluation of the possible errors occurring in mass determination in carrying out absolute pressure measurements, Fig. 7.16 shows such an error (ppm) in the mass determination (and consequently, in pressure) when the value of the conventional mass m_{icon} is wrongly used instead of the "true" mass value m_i.

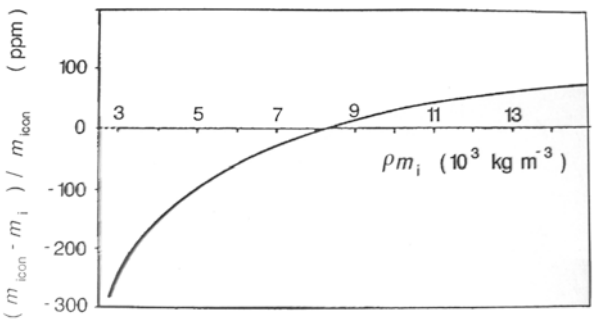

Fig. 7.16 Error in mass evaluation if m_{icon} is used in the place of m_i versus density ρ_{mi}; case of absolute pressure measurements

As can be seen in Fig. 7.16, very large errors, up to −280 ppm and +70 ppm, may occur, depending on the density ρ_{m_i} of the individual weights. Special care is essential in the case of absolute pressure measurements, whereas for gauge pressures it is normal routine to use mass values m_{icon} referred to the conventional reference density of 8 000 kg m^{-3}.

The effects of surface degassing, due to the use of stainless steel weights *in vacuo* and at room temperature, produces mass changes that are generally negligible when compared with the mass stability of about 1 ppm needed for pressure balance application.

Mass determination, with mass values from some grams to some kilograms, is typically possible to an accuracy of 1 ppm or less and residual standard deviations from the mean value around 0.2–0.3 ppm.

Davis and Welch (1988) have demonstrated that the practical uncertainty limits to the mass determination of a 590 g pressure balance weight was equivalent to 0.1 ppm.

7.2.2.2 Local Acceleration Due to Gravity

The value of local gravity acceleration must be measured at the site where the pressure balance is used. The same considerations already mentioned concerning liquid-column manometers (see Sect. 7.1.3.2) apply and are equally important in the case of pressure balances. In laboratories equipped for direct measurement of this quantity, an accuracy of 0.1 ppm is possible, with residual standard deviation from the mean of the order of 0.02 ppm. In this case too, one must not neglect the correction for altitude, which amounts to about 0.3 ppm/m; the value of this correction is comparable to, and in some cases even larger than, the uncertainty with which the local acceleration of gravity g_L is usually measured.

7.2.2.3 The Effective Area

The effective area of the piston-cylinder unit, at atmospheric pressure and at the temperature t_{ref} (generally 20 °C, in some laboratories the reference temperature

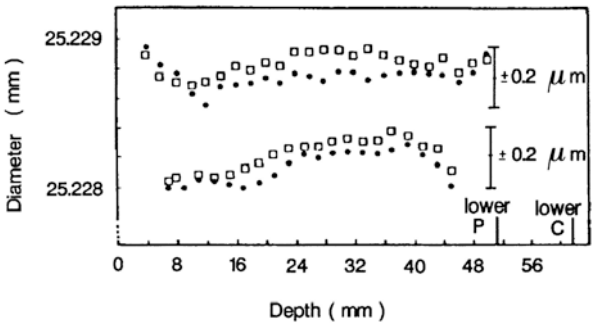

Fig. 7.17 Diameter measurements of a piston (P) and cylinder (C) of a 2 MPa unit (average piston diameter is 25.2282 ± 0.0002 mm, average cylinder diameter is 25.2287 ± 0.0002 mm) along two different generatrices (●, □)

may be selected at 23 °C), can be determined by dimensional measurements or by "cross-floating" techniques against a liquid-column manometer or against another primary standard, e.g., a pressure balance. The primary standard used for cross-floating should obviously be independently characterized at a sufficient level of uncertainty and possess good sensitivity. Experiences in this connection will be analyzed in Sects. 7.2.6 and 7.2.7.

Let us deal here with the method of determining the effective area of a piston-cylinder by dimensional measurements: this method has the advantage of being absolute and independent, but requires sophisticated apparatus, skilled personnel, and very time-consuming measurement procedure.

The diameters of the piston and of the cylinder must be measured over their whole engagement length; generally, one absolute measurement every few millimeters along the piston or cylinder generatrix is sufficient. The same series of measurements must be repeated on another piston-cylinder generatrix 90° apart. It is then necessary to measure the relative displacements, referred to a fixed position, along the selected generatrices (generally at least four), to correlate the absolute diameter measurements with the concomitant displacements along a generatrix and to obtain in this way a continuous indication of the behavior of the displacements along the piston and cylinder generatrices.

Subsequently, roundness measurements are to be made at the same sections where the absolute diameters were measured. In this way, one obtains the necessary information on the geometrical shape of the piston and of the cylinder. Nevertheless, the above measurements are not necessarily fully representative of the actual solid geometries of piston and cylinder. Measurements must be made under very stable temperature conditions, and referred to $t_{ref} = 20$ °C. When measurement uncertainty is required to a few ppm, during the whole measurement temperature shall be maintained at that value, at least within ± 0.2 °C, otherwise dimensional values have to be corrected for thermal variations. The linear thermal expansion coefficients for the piston and the cylinder must therefore be known very accurately (see Sect. 7.2.2.5).

To give an example, Fig. 7.17 illustrates the dimensional measurements carried out on a tungsten carbide piston and a heat-treated steel cylinder of 48 HRC hardness, used for gas pressure measurements to 2 MPa. The roundness measurements made on the same piston and cylinder, over the whole engagement length showed that the maximum roundness error was always less than 0.1 μm.

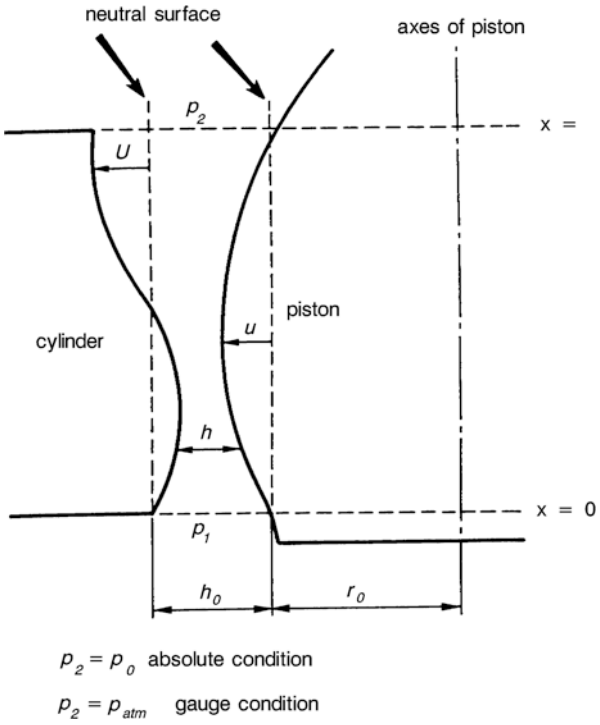

Fig. 7.18 Schematics of a piston-cylinder unit with indication of radial changes between the piston and cylinder in their engagement length (defined as the coupling length of piston and cylinder between $x = 0$ and $x = l$). Absolute condition with $p_2 = p_0$ and gauge condition with $p_2 = p_{atm}$

Although the uncertainty of the diameter measurements was ± 0.1 μm, owing to the piston-cylinder nonuniform geometry illustrated in Fig. 7.18, an uncertainty of ± 0.2 μm was assigned, in order to take account of possible diameter variations outside the four explored generatrices (of the two measured planes), as well as of variations in orthogonality and roundness.

Another example is given by the dimensional measurements on piston-cylinder units of tungsten carbide for a pressure balance unit used for pressure measurements in gauge mode from 10 to 400 kPa (Legras et al. 1986).

In this case, the uncertainty on the measurement of a nominal diameter of about 35 mm was ± 0.04 μm and its geometry (including roundness and orthogonality) resulted constant, typically within ± 0.15 μm, along all the piston-cylinder engagement length.

These are examples of very good results, but unfortunately many other cases exist in practice in which pistons and cylinders have geometric irregularities or tapering along generatrices that may be as high as 1 μm (i.e., 10 times the possible uncertainty of diameter measurements).

It must also be remembered that the effective area based only on the arithmetic average of piston and cylinder areas is possible and correct only for a perfect geometry. For this reason, in the evaluation of the effective area of a piston-cylinder unit, account must be taken of geometric irregularities, of the vertical force distribution on

the piston-cylinder unit, and of the pressure gradient in the whole clearance length between the piston and the cylinder.

Figure 7.18 shows a view of piston-cylinder clearance; in the figure the possible diameter irregularities are emphasized and reference is made to the radius. Therefore, h is the clearance on the radius at a level x, and u and U are the deviations from the ideal reference radius, for the piston and the cylinder, respectively. The h_0 and r_0 are the radial clearance and radius of the piston, respectively, at the level $x = 0$.

The applied pressure to be measured is denoted in Fig. 7.18 by p_1, while p_2 is the pressure around the standard weights (i.e., the reference vacuum pressure p_0 for absolute conditions, or the atmospheric pressure under gauge conditions).

According to the theoretical considerations expressed by Dadson et al. (1982) and Peggs (1977), the effective area A_0 can be derived as

$$A_0 = \pi r_0^2 \left[1 + \frac{h_0}{r_0} - \frac{1}{r_0 (p_1 - p_2)} \int_0^l (u + U) \frac{dp}{dx} dx \right]. \tag{7.20}$$

For a perfect geometry (h = constant, $u = U = 0$), the effective area A_0 computed from Eq. 7.20 is exactly the same as the arithmetic mean between the area of the piston and that of the cylinder.

Such trivial simplification is possible only when the measured dimensional values approach sufficiently well the perfect geometry satisfying the required uncertainty.

For compressible fluids, such as pure gases, and on the assumption of viscosity being constant and of density being proportional to pressure, it was demonstrated (Dadson 1982) that:

$$p(x) = \sqrt{\left[{p_1}^2 - \left({p_1}^2 - {p_2}^2 \right) \frac{\int_0^x h^{-3} dx}{\int_0^l h^{-3} dx} \right]}. \tag{7.21}$$

By replacing $\mathrm{d}p(x)/\mathrm{d}x$ obtained from Eq. 7.21 into Eq. 7.20, for the absolute conditions $p_2 = p_0 = 0$, we obtain

$$A_0 = \pi r_0^2 \left[1 + \frac{h_0}{r_0} + \frac{1}{2r_0} \int_0^l \frac{(u + U) h^{-3}}{\int_0^l h^{-3} dx} \left(1 - \frac{\int_0^x h^{-3} dx}{\int_0^l h^{-3} dx} \right) dx \right]. \tag{7.22}$$

The Eq. 7.22 can be used, with numerical integration techniques, to compute the effective area A_0 in absolute mode.

In the derivation of Eq. 7.22, it is assumed that vertical forces exerted on the cylindrical faces of the piston and cylinder by the fluid are identical, independent of the fluid. Some work with gas-operated pressure balances, to be discussed later (see Sect. 7.2.7), calls this assumption into question.

For a piston-cylinder unit of high geometrical regularity, like that, e.g., of Fig. 7.17, the area difference between A_0 computed using Eq. 7.22 and the simple arithmetic average between the area of the piston and that of the cylinder amounts to only 4 ppm.

This is comparable to the uncertainty of the value of effective area as obtained, in the first approximation, on the estimated uncertainty of the diameter value. For the case given in Fig. 7.17 (having an estimated uncertainty of 0.2 μm for the values of the piston and cylinder diameters), it would correspond to an uncertainty of 16 ppm for the effective-area value A_0. It is interesting to quote the effort made within a EUROMET Project (# 740), and referred in Molinar et al. (2005), where calculations of effective areas for six piston-cylinder assemblies of pressure balances is given. The paper describes the results obtained by six national metrology laboratories for two pressure balances in gas up to 1 MPa and other four pressure balances in liquid up to 1 GPa.

The agreement of the A_0 values between three laboratories using the Dadson theory had maximum difference lower than 1 ppm and the agreement of A_0 values for the two gas units up to 1 MPa was from 13 to 22 ppm.

The estimated A_0 uncertainty ranges from 7 ppm to more than 100 ppm (depending on the specific unit and on the method used to calculate the uncertainty). For piston-cylinders of large effective area (typically with diameters larger than 35 mm), having high regularity from a geometrical view point, it was possible to obtain A_0 uncertainty lower than 10 ppm.

A prevalent way for A_0 calculation gives formulas, that are valid in the case of gauge pressure, and that have the following expressions, which are all equivalent:

$$A_0 = \pi r_0^2 \left[1 + \frac{h_0}{r_0} + \frac{1}{r_0} \int_0^l \frac{(u+U)}{h^3} dx \Big/ \int_0^l \frac{1}{h^3} dx \right]$$

$$A_0 = \pi r_0^2 \left[1 + \frac{1}{r_0} \frac{\int_0^l \frac{1}{h^2} dx}{\int_0^l \frac{1}{h^3} dx} + \frac{2}{r_0} \frac{\int_0^l \frac{r - r_o}{h^3} dx}{\int_0^l \frac{1}{h^3} dx} \right]$$

$$A_0 = \pi r_0 \left[-r_0 + \frac{\int_0^l \frac{r+R}{(R-r)^3} dx}{\int_0^l \frac{1}{(R-r)^3} dx} \right]$$

r and R being the radius of the piston and cylinder, respectively.

Another interesting result is given by Schmidt et al. (2006) where two large-diameter piston-cylinder (35.8 mm), to be used as primary standards in the pressure

range from 0.05 to 1 MPa, have been fully characterized by dimensional measurements and compared with the NIST ultrasonic mercury interferometer. Both piston-cylinders have roundness errors not exceeding 30 nm and are straight within 100 nm and they have average radial clearance of 0.6 μm. The values of A_0 for both units as derived from dimensional measurements and calculation are well in agreement with the standard uncertainty of the results obtained by comparison with NIST mercury manometer and similarly the results are consistent when comparing the ratio of effective areas obtained by cross-floating the two pressure balances. The expanded ($k = 2$) relative uncertainty of the derived effective area for both units is about 6 ppm.

7.2.2.4 Elastic Distortion Coefficient

In Eq. 7.18, the term $A_0 (1 + \lambda p)$ represents a linear relation between the effective area A_0 and pressure p. Variations in the effective area are due to the elastic distortions that the piston and cylinder undergo when pressure is applied.

The linear dependence expressed by the term $(1 + \lambda p)$ is generally acceptable for highly regular piston-cylinder units in free deformation mode and for the range of absolute pressure considered here. The quantity p in the term $(1 + \lambda p)$ is an approximated pressure value, generally calculated as $p = \Sigma \mathrm{i}(m_\mathrm{i} g_\mathrm{L})/A_0$.

The quantity λ denotes the elastic distortion coefficient and, in the absolute pressure range to 5 MPa, it is generally computed according to the theory of elasticity or by finite element analysis (FEA).

There are other possibilities to obtain an absolute derivation of the pressure distortion coefficient, based either on the use of controlled-clearance pressure balances or on the application of the "similarity method." They will be both described in Sect. 7.2.3.2.

Another possibility is to obtain the change of the effective area with pressure by comparison of the pressure balance against another standard (for example, a controlled-clearance pressure balance or a mercury column) if the pressure range overlaps considerably.

More frequently, between pressure balance units of the same type, a comparison technique (often also called "cross-floating") is used to check, from the effective area standpoint, the performances of the two gauges over the whole pressure range for which they are used.

The most widespread method for computing the pressure distortion coefficient is based on the Lamé equation, and is valid for moderate pressures, no end-loading on the cylinder and a pressure distribution assumed as linear (even if it is well known that this assumption is not correct) in the clearance along all the engagement piston-cylinder length. Calculations are performed for a constant mean pressure value equal to $0.5p$ in the clearance.

It was demonstrated (Johnson and Newhall 1953; Tsiklis 1968) that, under these conditions and for the case of a simple piston-cylinder unit,

$$\lambda = \frac{3\nu_p - 1}{2E_p} + \frac{1}{2E_c}\left(\frac{{R_c}^2 + {r_c}^2}{{R_c}^2 - {r_c}^2} + \nu_c\right). \tag{7.23}$$

The first term is the contribution to the distortion of the piston and the second to that of the cylinder. In Eq. 7.23, ν_p, ν_c are the values of the Poisson coefficients for the piston and the cylinder, E_p and E_c are Young's moduli values for the piston and the cylinder, R_c is the outer radius of the cylinder, r_c is the inner radius of the cylinder; the radius of the piston r_p is assumed to be equal to r_c.

The validity of Eq. 7.23 is questionable, particularly as regards the assumptions of a linear pressure distribution and of a $0.5p$ constant pressure value in the clearance, as well as for the implicit constancy of viscosity versus pressure, which is clearly not correct.

The questionable character of Eq. 7.23 was demonstrated by Bass (1978) for pressure systems used up to 160 kPa and equipped with different piston-cylinder units.

Elastic distortion data obtained with the Bass theory were in agreement with the experimental cross-floating results generally within 20 %, but they were in much larger disagreement in respect to the λ value calculated by Eq. 7.23. In particular, the experimental data demonstrated that some of the basic assumptions from which Eq. 7.23 is derived are questionable.

For a tungsten carbide piston-cylinder having a pressure distortion coefficient $\lambda = 2.4 \times 10^{-6}$ MPa^{-1} known with an uncertainty of 20 % at 160 kPa maximum pressure, such uncertainty contributes to the uncertainty of the pressure value to less than 0.1 ppm, and is therefore negligible in practice.

Another experimental study of the pressure profile in the engagement length of a piston-cylinder in liquid media up to 21 MPa, showed a markedly nonlinear pressure profile (Welch et al. 1984). The results about the elastic distortion coefficient for a steel piston-cylinder unit were in very good agreement with the Bass model, but the calculated value of λ with the use of Eq. 7.23 was lower by 24 % than the experimental value.

For a pressure range up to 500 kPa, our experience on the use of Eq. 7.23 is positive, despite the incorrect basic assumptions of this equation, because over this pressure range elastic distortions are small and even a large error in the calculation of the pressure distortion coefficient will not increase the uncertainty of the pressure value too much.

The influence of the distortion coefficient uncertainty is reduced when tungsten carbide is used instead of hard steel for pistons and cylinders. For example, with a tungsten carbide piston-cylinder having a pressure distortion coefficient of 2×10^{-6} MPa^{-1} in a range up to 0.5 MPa, even a 100 % uncertainty on its determination produces a contribution to the pressure uncertainty of only 1 ppm.

The calculation of pressure distortion coefficients become more complicated for pressures from 1 to 5 MPa; in this range, Eq. 7.23 may cause large errors, e.g., of the order from 100 to 200 %.

For a 5 MPa system, with $\lambda = 1.1 \times 10^{-6}$ MPa^{-1}, a 200 % error at 5 MPa pressure is equivalent to 11 ppm, not a negligible contribution.

For a better calculation of pressure distortion coefficients, the many studies that have been carried out generally have been performed with pressures higher than 5 MPa and, mostly, in liquid media (see Sect. 7.2.3.2).

Another approach generally followed is based on finite element methods (FEM) that will be covered in Sect. 7.2.3.2 following the experience of more than 10 years' work (Buonanno et al. 2007).

In conclusion, the use of Eq. 7.23 is advisable only below 0.5 MPa, the estimated uncertainty in the determination of the λ value being about 50 %, if elastic constants are measured with an uncertainty of some percent. It is better to avoid the use of Eq. 7.23 above 0.5 MPa and resort to other means (comparison techniques, experimental measurements, methods of calculations using different techniques as described in Sect. 7.2.3.2), unless uncertainties of the order of some 100 % can be accepted in the determination of the pressure distortion coefficient.

Such contributions for the calculation or the measurement of the pressure distortion coefficient in gas media will be considered in Sect. 7.2.3.2.

Another interesting approach derived from the *EURAMET Project 1039*, started in 2008 with the purpose of computing by FEA the pressure distortion coefficients of gas-operated pressure balances (nitrogen and helium) in both gauge and absolute mode for four special piston-cylinder units up to 7.5 MPa (Coordinator Sabuga-PTB). These pressure balances will be used in experiments on redetermining the Boltzmann constant at PTB (Germany).

Given that the effective area of piston-cylinder assemblies of nonideal geometry depends on pressure, even in absence of elastic distortions, as in the case of low pressures, the effect of the gap geometry on the changes in the effective area due to pressure can be of the same order of magnitude as the effect of elastic distortions. For this reason, within the EURAMET 1039 project, to adequately compare the results obtained for the real and ideal gap models (defined as the model of constant radial clearance), it is suggested attributing to the pressure distortion coefficient only a change in the effective area resulting from the elastic distortions. The following definitions apply:

- $A_0 \equiv A_0(0)$ is effective area at zero pressure.
- $A_0(p)$ is effective area of the undistorted assembly at pressure p. For ideal geometry assemblies, $A_0(p) = A_0$.
- $A_p(p)$ is effective area of the distorted assembly at pressure p.
- λ is pressure distortion coefficient describing the effect of the elastic distortions,

$$\lambda = \frac{A_p(p) - A_0(p)}{A_0 p}.$$

For effective area calculation, the theory by Dadson et al. (1982) is suggested and this will give rise to the following formulas (in this connection z has the same meaning as the previously used x):

- A_0 in gauge mode:

$$A_0 = \pi r_0^2 \left[1 + \frac{h_0}{r_0} + \frac{1}{r_0} \int_0^l \frac{u+U}{h^3} dz \Big/ \int_0^l \frac{1}{h^3} dz \right].$$

- A_0 in absolute mode (which is equivalent to Eq. 7.22):

$$A_0 = \pi r_0^2 \left[1 + \frac{h_0}{r_0} + \frac{1}{r_0} \int_0^l \frac{d(u+U)}{dz} \left\{ 1 - \int_0^z \frac{dz}{h^3} \Big/ \int_0^l \frac{dz}{h^3} \right\}^{0.5} dz \right].$$

- $A_0(p)$ will be:

$$A_0(p) = \pi r_0^2 \left[1 + \frac{h_0}{r_0} + \frac{1}{r_0(p_1 - p_2)} \int_0^l (p_z - p_2) \frac{d(u+U)}{dz} dz \right].$$

- $A_p(p)$ will be:

$$A_p(p) = \pi r_0^2 \left[1 + \frac{h_0}{r_0} + \frac{1}{r_0(p_1 - p_2)} \int_0^l (p_{zp} - p_2) \frac{d(r_p + R_p)}{dz} dz \right].$$

- p_z will be:

$$p_z \equiv p(z) = \left[p_1^2 - (p_1^2 - p_2^2) \int_0^z \frac{dz}{h^3} \Big/ \int_0^l \frac{dz}{h^3} \right]^{0.5}. \tag{7.24}$$

- p_{zp} will be:

$$p_{zp} \equiv p_p(z) = \left[p_1^2 - (p_1^2 - p_2^2) \int_0^z \frac{dz}{h_p^3} \Big/ \int_0^l \frac{dz}{h_p^3} \right]^{0.5} \tag{7.25}$$

where:

- $r_0 = r(0)$; $h_0 = R(0) - r(0)$; $u = r(z) - r(0)$; $U = R(z) - R(0)$; $h = R(z) - r(z)$; $h_p = R_p(z) - r_p(z)$; $p = p_1 - p_2$.
- $R(z)$ and $r(z)$ are radii of undistorted cylinder and piston, respectively.
- $R_p(z)$ and $r_p(z)$ are radii of distorted cylinder and piston, respectively.
- p_1 and p_2 are absolute pressures below and above piston with $p_2 = 0$ in absolute and $p_2 = 0.1$ MPa in gauge mode.
- p_z and p_{zp} are absolute pressure distributions in the undistorted and distorted piston-cylinder clearances, respectively.

Equations 7.24 and 7.25 are valid for ideal gas and do not allow individual properties of gases to be taken into account. To do this, Eqs. 7.24 and 7.25 should be replaced by more general equations

$$p_z = p_1 - (p_1 - p_2)\int_0^z \frac{\eta(p_z)dz}{\rho(p_z)h^3} \Big/ \int_0^l \frac{\eta(p_z)dz}{\rho(p_z)h^3} \tag{7.26}$$

and

$$p_{zp} = p_1 - (p_1 - p_2)\int_0^z \frac{\eta(p_{zp})dz}{\rho(p_{zp})h_p^3} \Big/ \int_0^l \frac{\eta(p_{zp})dz}{\rho(p_{zp})h_p^3} \tag{7.27}$$

where:

η and ρ are viscosity and density of the gas.
Pressure distributions p_z and p_{zp} presented by Eqs. 7.26 and 7.27 can be calculated iteratively.

Two cases of operation, with nitrogen and helium, are considered. At 20 °C and in the absolute pressure range up to 7 MPa, the density and the dynamic viscosity of these gases can be expressed by the equations below with associated uncertainties U ($k = 2$).

- Nitrogen (N_2)
  From Span et al. (2000): $\rho_{N_2}/(\text{kg m}^{-3}) = 11.550 \times (p/\text{MPa}) \times \left[1 + 1.1 \times 10^{-4} \times (p/\text{MPa})\right]$;
  $U(\rho)/\rho = 0.01$ %
  From Stephan et al. (1987): $\eta_{N_2}/(\mu\text{Pa s}) = 8.4 \times 10^{-3} \times (p/\text{MPa})^2 + 0.132 \times (p/\text{MPa}) + 17.58$
  $U(\eta)/\eta = 3$ %.
- Helium (^{4}He)
  From McCarty (1973): $\rho_{^4\text{He}}/\left(\text{kg m}^{-3}\right) = 1.6412 \times (p/\text{MPa}) \times \left[1 - 4.63 \times 10^{-3} \times (p/\text{MPa})\right]$
  $U(\rho)/\rho = 0.05$ %.
  From Kaye and Laby (1973): $\eta_{^4\text{He}}/(\mu\text{Pa s}) = 19.6$, $U(\eta)/\eta = 1$ %.

All the above information has been almost integrally extracted from the guidelines of the EURAMET Project 1039, with the approval of the coordinator.

7.2.2.5 Linear Thermal Expansion Coefficients

The linear thermal expansion coefficients of the piston α_p and of the cylinder α_c must be measured with an uncertainty of the order of few percent.

Thermal expansion coefficients can be measured independently by dilatometer techniques on specimens taken from the same piece used for the fabrication of the piston and the cylinder (Bennett 1977, 1978).

Another possibility is the measurement of the coefficient $2\alpha = (\alpha_p + \alpha_c)$ using the definition:

$$2\alpha = 1/p(\mathrm{d}p/\mathrm{d}t). \tag{7.28}$$

This measurement can be performed with a specific "cross-floating" experiment in which the standard can be another pressure balance or a mercury column of known characteristics. Cross-floating is performed at a pressure p, measured with the standard and selected in such a way as to allow good sensitivity of the cross-floating experiment. The temperature, t, of the pressure balance, whose coefficient 2α must be measured, is changed in steps and accurately measured. A typical temperature accuracy and stability of 0.01 °C is necessary. At each temperature step, pressure is measured with the standard instrument in equilibrium with the pressure balance. The measurement of $\mathrm{d}p/\mathrm{d}t$ is therefore obtained and the coefficient 2α is calculated with the use of Eq. 7.28.

A 1 % uncertainty for a typical value of $2\alpha = 21 \times 10^{-6}$ °C^{-1} for a steel piston-cylinder is equivalent, for a 1 °C temperature variation, to a contribution of 0.2 ppm to the uncertainty of the pressure value. The use of literature data for thermal expansion coefficients of materials used for the fabrication of piston and cylinder is not recommended as it can lead to very large errors, typically from 10 to 20 %. Just to mention one cause; thermal expansion coefficients of steels are influenced largely by their heat treatments, and for tungsten carbide they are affected by the percentage of the binder (cobalt or nickel).

7.2.2.6 Temperature of the Piston-Cylinder Assembly

The temperature, t, of a piston-cylinder must be measured directly on the cylinder of the unit. This is possible with the use of, for example, a miniature platinum resistance thermometer calibrated in the range of use. By regularly checking it at the fixed points of the temperature scale, e.g., at the ice point, a typical uncertainty ranging from 0.005 to 0.02 °C can be obtained. With steel piston-cylinder units, an uncertainty of 0.02 °C in the measurement of temperature contributes 0.4 ppm to overall pressure uncertainty.

It is advisable to also measure the temperature gradient in the cylinder by means of several platinum resistance thermometers installed along the cylinder length. In this way, temperature stability during piston-gauge operation can be better checked. Such a precaution is important for systems of top-level accuracy.

Particularly with gas media, it is equally advisable to install temperature sensors (for example, shielded thermocouples) in the pressurizing gas and close to the piston-cylinder unit, in order to detect the amount of possible temperature changes due to adiabatic expansion or compression of the gas during pressure changes and, consequently, to know the time needed for thermal equilibrium of the measuring apparatus.

The temperature, t_{ref}, in Eq. 7.18 is the temperature at which A_0 has been measured, normally equal to 20 °C.

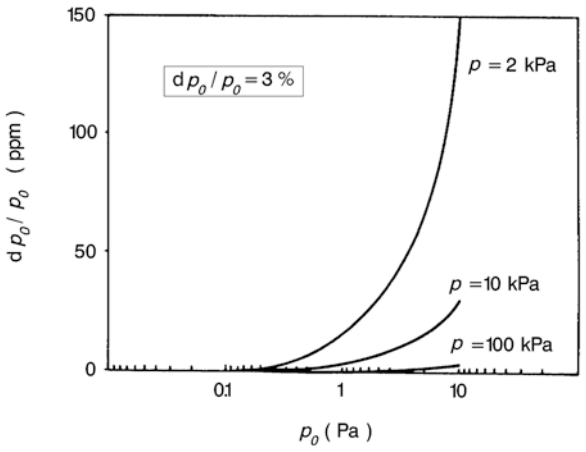

Fig. 7.19 Uncertainty dp_0/p versus p_0 (logarithmic scale) for three different pressure values and with 3 % uncertainty in the p_0 value

7.2.2.7 The Reference Pressure p_0

The reference pressure p_0 is an important quantity that must be measured accurately. For absolute pressure measurements, the best choice would be to operate at so low a p_0 value, that its measurement uncertainty becomes insignificant.

Although this is desirable, the pressure applied in the clearance between the piston-cylinder generates a continuous, though small, gas flow that generally makes it difficult to operate at pressures p_0 below 0.1 Pa (equivalent to 50 ppm at a pressure of 2 kPa). Since at these pressure values, uncertainty on p_0 measurement is not negligible, its contribution must be included as well in the overall measuring pressure uncertainty.

However, from an experimental point of view it is advisable to use large-diameter tubes for the pumping line and for the p_0 measuring line. These two pipes should originate independently from the pressure balance bell jar, because p_0 measurements must not be influenced by a dynamic flow distribution produced close to the pumping system.

For the measurement of p_0, Pirani or capacitance gauges are generally used. In the required pressure range (0.1 to few pascal), the uncertainty needed for the calibration of such devices is of the order of a few percent.

Figure 7.19 shows how the uncertainty of the pressure p_0 is related to the absolute pressure p, and how the absolute uncertainty dp_0 is related to dp_0/p.

These quantities are given as functions (in logarithmic scale) of pressure p_0, for three values of the absolute pressure p (2,10,100 kPa). The uncertainty of the measured value of pressure p_0 is 3 % (the typical measurement uncertainty of a Pirani gauge is of the same order of magnitude).

At $p_0 = 0.1$ Pa the contribution to the uncertainty dp_0/p under the above mentioned condition, is 1.5 ppm at 2 kPa, 0.3 ppm at 10 kPa, and 0.03 ppm at 100 kPa.

It must be added that the above example refers to vacuum gauges frequently calibrated; otherwise deviations and instabilities in the p_0 measurement as high as

10–20 % can be observed. Better results in terms of stability can be obtained with calibrated capacitance transducers of about 100 Pa full scale (see Sect. 8.1.2) used in the lowest part of their full-scale pressure range.

7.2.2.8 Aerostatic-Head Corrections

The aerostatic-head (sometimes also called gas head) correction is important. The same considerations and results already expressed for the determinations of the density of the fluid $\rho_f(t, p)$, which is pressure and temperature dependent, g_L and h and for the uncertainty contributions Δ_{1p}, Δ_{2p}, Δ_{3p}, and Δ_{4p}, in Sect. 7.1.3.3 apply here.

In the last term of Eq. 7.18, the sign will be negative ($-\rho_f g_L h$) if the reference level is at a distance h above the piston-cylinder reference base, and will be positive ($+\rho_f g_L h$) if the reference level is selected to be at a distance h below the piston-cylinder reference base.

All these considerations are based on the same rules already given in the case of liquid-column manometers (see Sect. 7.1.3.3 and Fig. 7.13).

It is a good rule, too, to convert all pressures, that may be of the differential or of the gauge type, into absolute values and to correct (particularly in the case of gauge pressure measurements) for the change in air atmospheric pressure with elevation (for air at 297 K with a nominal molecular weight of 29×10^{-3} kg mol^{-1} the correction is about -1.15 ppm for a centimeter of height increase). This practice may be of importance particularly when high-accuracy transducers are calibrated under gauge or differential conditions (Schultz 1976).

In the case of a pressure balance, very frequently the level to which the measured pressure value has to be referred is selected to be that of the piston base or of the lower end of the cylinder. The selection of the reference level is determined considering the geometric shape of the piston-cylinder unit.

7.2.3 Gauge Pressure Measurements up to 100 MPa

For the measurement of gauge pressure, pressure balances are widely used and the pressure scale (see the introductory text to Chap. 7 for the definition of the pressure scale) can be realized in gaseous media to 100 MPa at least with different types of pressure balances (Ehrlich 1993/1994).

Simple, reentrant and controlled-clearance piston-cylinder configurations, are utilized in this range; frequently, oil-lubricated piston-cylinder units are also employed where the two fluids (the measuring gas and the lubricating oil) are in contact at the piston-cylinder base.

In gauge pressure measurements, the basic design criteria and precautions are those already described in Sect. 7.2.2.

The main difference with respect to absolute measurements is the fact that under gauge conditions load is applied to the piston in ambient air, while under an absolute condition it is referred to the (vacuum) reference pressure p_0.

The gravitational force due to the weights on the piston, which is in equilibrium with the force generated by the pressure p acting on the effective area A_e of the piston-cylinder, is now subjected to an extra force due to the weights buoyancy in air.

With a piston-cylinder unit of the simple or reentrant type, the measured pressure p under gauge (relative to atmospheric pressure) condition is defined by Eq. 7.29, if mass values m_i are referred to the density ρ_{m_i}, or to Eq. 7.30, if conventional mass values m_{icon} and conventional density $\rho_{m_{icon}}$ are used. By convention, $\rho_{m_{icon}} = 8\,000$ kg m^{-3}

$$p = \frac{\sum_i m_i g_L \left(1 - \frac{\rho_a}{\rho m_i}\right)}{A_0 (1 + \lambda p)\left[1 + (\alpha_p + \alpha_c)(t - t_{ref})\right]} \pm \rho_f g_L h \tag{7.29}$$

$$p = \frac{\sum_{icon} m_{icon} g_L \left(1 - \frac{\rho_a}{\rho m_{icon}}\right)}{A_0 (1 + \lambda p)\left[1 + (\alpha_p + \alpha_c)(t - t_{ref})\right]} \pm \rho_f g_L h. \tag{7.30}$$

Although the meanings of the physical quantities in Eqs. 7.29 and 7.30 are exactly the same as those already given in Sect. 7.2.2 and in Eq. 7.18 for the case of absolute pressure measurements, the following additional considerations are necessary:

- The correction for air buoyancy now must always be made. To do so, the value of the density of air ρ_a (kg m^{-3}) must be determined (see Sect. 7.2.3.1) at the time of pressure measurements.
- Any of the two Eqs. 7.29 and 7.30 can be used. Actually, Eq. 7.30 is more frequently used, because it is common practice to have all the pieces of the weight set referred to conventional density values. On the other hand, the pressure balances used for absolute measurements are frequently also used for gauge measurements. In this case, in order to avoid confusion, Eq. 7.29 is more convenient, as it can be used in the gauge mode with the same quantities (m_i, ρm_i) that are used in Eq. 7.18 in the absolute mode. With Eq. 7.29, it is necessary to measure the density ρm_i of each piece of the weight set.
- The pressure distortion coefficient, λ, is not the same for a simple (generally $\lambda > 0$) or for a reentrant (generally $\lambda < 0$) piston-cylinder unit. For a simple piston-cylinder unit, the coefficient λ can be expressed in the same way as in Sect. 7.2.2.4 (Eq. 7.23), in spite of the fact, already mentioned, that this formula may generate very large uncertainties, particularly at high-pressure values.
- In Eqs. 7.29 and 7.30, a linear effective area variation due to pressure has been assumed. There are cases, particularly for extended pressure range or for piston-cylinder systems that undergo very large distortions, or for mixed principle of operation of a piston-cylinder unit (e.g., partially free deformation and partially reentrant unit) in which such linear behavior cannot be automatically predicted. The investigation about the behavior of $A_e = f(p)$ must be experimentally performed and nonlinear relations of $A_e = f(p)$ eventually must be used.

Let us now consider the additional physical quantities ρ_a and λ. The other quantities appearing in Eqs. 7.29 or 7.30 have already been discussed in the previous Sect. 7.2.2.

7.2.3.1 Air Density

For the determination of the density of air ρ_a, the scientific community referred for many years to the document issued by the Comité International des Poids et Measures (CIPM) in 1981 and prepared by the Comité Consultatif pour la Masse et les Grandeurs apparentées (CCM), which gives all the details for the calculation of the density of air.

The absolute value of ρ_a, in the prevalent conditions of use, generally ranges from 1.15 to 1.25 kg m^{-3}. In the use of pressure balances, an acceptable uncertainty in the determination of ρ_a ranges from 0.3 % (corresponding to a pressure uncertainty of 0.4 ppm for a $\rho_{mi} = 8\,000$ kg m^{-3} or 1.0 ppm for a $\rho_{mi} = 2\,900$ kg m^{-3}) to 1 % (corresponding to a pressure uncertainty of 1.3 ppm for a $\rho_{mi} = 8\,000$ kg m^{-3} or 3.5 ppm for a $\rho_{mi} = 2\,900$ kg m^{-3}).

The simplified formula for the calculation of air density ρ_a(kg m^{-3}), derived from the CIPM document of 1981 has been subsequently revised by Davis (1992) and finally by Picard et al. (2008). In the present section, reference is mainly made to the work of Picard et al. (2008) that has reached a widely accepted application and was also approved by the CIPM (96th meeting in 2007). For this reason, the new density of air equation is generally called the CIPM-2007 equation. Formally, the derivation of this equation is similar to the one described in Giacomo (1981) and Davis (1998).

The density of moist air is evaluated using the following equation of state:

$$\rho_a = \frac{pM_a}{ZRT}\left[1 - x_v\left(1 - \frac{M_v}{M_a}\right)\right] \tag{7.31}$$

where the quantities and units in formula (7.31) are:

- p/Pa for the absolute atmospheric pressure.
- T/K for the thermodynamic room temperature = 273.15 + t/ °C where t/ °C is the room air temperature.
- x_v the mole fraction of water vapor.
- M_a/(g mol^{-1}) the molar mass of dry air.
- M_v/(g mol^{-1}) the molar mass of water.
- Z a compressibility factor of moist air.
- R/(J mol^{-1} K^{-1}) the molar gas constant.

For the CIPM-2007 formula, the best recommended choice for the molar gas constant derived from CODATA 2006 (Mohr et al. 2008) with a value of R/(J mol^{-1} K^{-1}) = 8.314 472 and with a standard relative uncertainty of 1.8 ppm. The molar gas constant given by CODATA 2010 is $R = 8.314\,4621\ (75)$ J mol^{-1} K^{-1}.

The details of the calculations of ρ_a, are given in Appendix F, Document F.1; they are taken from Picard et al. (2008).

The logical points of Eq. 7.31 are based on the fact that p, T, relative humidity h, or dew point temperature t_d are measured; the rest is calculated according to different choices based on best available data.

For what concerns temperature, reference is made to the ITS-90 temperature scale and the limits of validity of Eq. 7.31, under the basic assumption defined in its model, are similar to the CIPM-81 equation and are for pressures from 600 to 1 100 hPa and temperatures from 15 to 27 °C.

The molar mass of dry air M_a is based on the mole fractions of the air constituents, with some exceptions related to atmospheric argon and carbon dioxide. Under the conditions given in Picard et al. (2008), if a measurement of x_{CO_2} is available, then the molar mass of dry air can be assumed to be:

$$M_a/\text{g mol}^{-1} = \left[28.965\,46 + 12.011\left(x_{CO_2} - 0.0004\right)\right].$$

If not measured, it is assumed a mole fraction of carbon dioxide in air of 400 µmol mol^{-1}. It is considered preferable, however, to carry out direct measurements of the actual value. Considering that the molar mass of moist air includes the amount fraction of water vapor x_v, it is possible to arrive at the following equation:

$$\rho_a/g\ m^{-3} = \left[3.483\,740 + 1.4446\ \left(x_{CO_2} - 0.0004\right)\right]\frac{p}{ZT}\left(1 - 0.3780x_v\right). \quad (7.32)$$

The quantity x_v is determined from measurements of relative humidity of air h or from air dew point temperature t_d and Z is determined from interpolation equations (See Appendix F, Document F.1).

The uncertainty in the value of ρ_a determined by the Eq. 7.32 is made up of the following contributions.

One is due to the mathematical model itself, used for Eq. 7.32, and it has been evaluated to be of 22 ppm for the case that x_{CO_2} was assumed to be 400 µmol mol^{-1}.

The other contributions to uncertainty are connected with the measurement of pressure p, temperature T, relative humidity h appearing in the determination of x_v, and the measurement of x_{CO_2}.

For a typical calculation of air density, the relative contribution values to the overall uncertainty due to the additional measurements are to be considered as well, so quoting from Picard et al. (2008), we will have:

$$\frac{u_P(\rho_a)}{\rho_a} = \frac{1}{\rho_a}\left(\frac{\partial\rho_a}{\partial p}\right)u(p) \approx +1 \times 10^{-5}\ {\rho_a}^{-1} \quad u(p)$$

for a typical $u(p) = 100$ Pa, we will have a relative contribution on ρ_a of 1×10^{-3}

$$\frac{u_T(\rho_a)}{\rho_a} \approx -4 \times 10^{-3}\ \text{K}^{-1} \quad u(T)$$

for a typical $u(T) = 0.1$ K, we will have a relative contribution on ρ_a of 4×10^{-4}

$$\frac{u_h(\rho_a)}{\rho_a} \approx -9 \times 10^{-3} \quad u(h)$$

for a typical $u(h) = 10$ %, we will have a relative contribution on ρ_a of 9×10^{-4} alternatively, if air dew point is measured, we will have:

$$\frac{ut_d(\rho_a)}{\rho_a} \approx -3 \times 10^{-4} k^{-1} \quad u(t_d)$$

for a typical $u(t_d) = 1$ K, we will have a relative contribution on ρ_a of 3×10^{-4}

$$\frac{ux_{CO_2}(\rho_a)}{\rho_a} \approx +0.4u(x_{CO_2})$$

for a typical $u(x_{CO_2}) = 100$ ppm, we will have a relative contribution on ρ_a of 0.4×10^{-4}.

The quadrature combinations of all these uncertainties plus the uncertainty of Eq. 7.32 give an estimated uncertainty of about 1.5×10^{-3} in the determination of air density.

7.2.3.2 Pressure Distortion Coefficients: Controlled-Clearance Units and Similarity Methods

With a "simple" piston-cylinder under gauge conditions, the pressure distortion coefficient λ can be calculated with the same Eq. 7.23 that is used for absolute conditions. The same calculations (Tsiklis 1968), and the same assumptions of no end-loading and of a linear pressure distribution in the clearance generally used for the free deformation piston-cylinder configuration may also be used in the case of a completely reentrant configuration.

One then obtains

$$\lambda = \frac{3\nu_p - 1}{2E_p} - \frac{1}{r_p}\left(k_1 + \frac{k_2}{2}\right) \tag{7.33}$$

$$k_1 = \frac{r_c}{E_c}\left(\frac{2R_c}{{R_c}^2 - {r_c}^2} - \nu_c\right) + r_p\frac{\upsilon_p}{E_p}$$

$$k_2 = \frac{r_c}{E_c}\left(\frac{{R_c}^2 + {r_c}^2}{{R_c}^2 - {r_c}^2} + \nu_c\right) + \frac{r_p(1 - \upsilon_p)}{E_p}$$

with subscripts "p" and "c" denoting piston and cylinder, respectively. The ν_p and ν_c are Poisson's coefficients, E_p and E_c are Young's moduli, R_c is the outer radius, r_c the inner radius of the cylinder, and r_p is the radius of the piston.

As discussed in Buonanno et al. (2007), for the case of a controlled-clearance unit the distortion coefficient (assuming the same hypothesis made for the free deforming or reentrant models), will be:

$$\lambda = \frac{(3\nu_p - 1)}{2E_p} + \frac{1}{2E_c}\left(\frac{{R_c}^2 + r_c^2 - 2\chi R_c^2}{{R_c}^2 - {r_c}^2} + \nu_c\right) \tag{7.34}$$

where $\chi = p_j/p$ and p_j being the jacket pressure around the cylinder. In the case of $\chi = 0$, Eq. 7.34 coincides with the one related to the case of a free deformation piston-cylinder unit (Eq. 7.23).

As already discussed in Sect. 7.2.2.4, the estimated uncertainty of Eq. 7.23 in the case of a fully free deformation unit, Eq. 7.33 in the case of a fully reentrant unit, and Eq. 7.34 in the case of a fully controlled-clearance unit, which is used to calculate the pressure distortion coefficient, is not satisfactory because the basic assumptions used for these simplified calculations are not correct.

As regards the calculation of λ with Eq. 7.33 for reentrant piston-cylinders, the situation is even worse, because the range of measurement is usually extended to higher pressures, similarly this can be generally applied for the cases of controlled-clearance units.

In order to evaluate the contribution of λ to the uncertainty of the pressure measurement, consider the case of a simple tungsten carbide piston-cylinder, having a 0.2 cm^2 nominal effective area and working to a 100 MPa maximum pressure, with which the value of λ, calculated with Eq. 7.23, is 0.8×10^{-6} MPa^{-1}. If λ is estimated with an uncertainty of 50 % at 100 MPa, the contribution to the overall pressure uncertainty will be 40 ppm, which is a too large value.

In the case of a similar simple piston-cylinder made of hard steel, whose distortions are larger than those of the tungsten carbide unit, the uncertainty contribution of λ will be even larger. This is another reason for preferring tungsten carbide to hard steel in the fabrication of piston-cylinder units.

The uncertainty in the determination of the distortion coefficient λ should typically lie between 5 and 10 %. With reference again to the above example of a tungsten carbide unit, the contribution of λ to the uncertainty of the pressure value will decrease to values from 4 ppm ($\Delta\lambda/\lambda = 5$ %) to 8 ppm ($\Delta\lambda/\lambda = 10$ %).

For gauge pressure measurements up to 100 MPa, the above uncertainties in the determination of the pressure distortion coefficients can be considered good results. Similar rule was considered by the pressure community, in assigning the uncertainty contribution to the pressure distortion coefficient at the time of the MRA application, for the definition of the calibration and measurement capabilities—CMC—generally obtained in the calibration of pressure balances. Such small uncertainties in the determination of pressure distortion coefficients can only be obtained if one of the following methods is adopted:

- Better calculation of λ associated to experimental checks of the calculated results.
- Cross-floating between pressure balances of different types, with the use, for example, of a controlled-clearance pressure balance, in order to define experimentally the behavior of $A_e = f(p)$ of the unit to be characterized.
- Cross-floating and application of the "similarity" method developed at NPL-UK.

The above methods are discussed briefly below, noting that the experience in this area is at present much wider with pressure balances used in liquid than in gaseous media (Buonanno et al. 2007).

In Sect. 7.2.2.4, some calculations and experimental evidence (Bass 1978; Welch 1984; Buonanno et al. 2007) have already been given, which showed the nonlinearity

of the pressure profile in the clearance for some piston-cylinders of the simple type. Other relevant experimental data of this kind were obtained at NIST and INRIM (Bean et al. 1989; Molinar et al. 1989, 1993, 1993/1994a, 1998; Sabuga et al. 2005, 2006). The radial displacements versus applied pressure were measured with capacitance techniques (Bean et al. 1989) and with strain-gauge techniques (Molinar et al. 1989, 1993) on the outer surface of the cylinder in all the engagement length of the piston-cylinder unit. The results of these determinations, when used with appropriate calculations of the distortions in the piston and in the inner diameter of the cylinder, make it possible to obtain better knowledge of the pressure distribution in the clearance and of the distortion coefficients of the piston and of the cylinder as a function of applied pressure.

The calculations for the determination of the distortion coefficient λ can be done in different ways, which are listed below:

- A calculation method (based on the solution of the biharmonic equation representing the piston-cylinder model in its elastic state and with the use of a pressure profile obtained experimentally under appropriate boundary conditions), was developed at NIST (Lazos-Martinez et al. 1986; Bean 1986). This calculation result agrees within 2 % with the λ value obtained from Eq. 7.23.
- A calculation method requiring the solution of the differential equations representing the deformation state, with the unknown functions expressed by the Tschebyschef polynomial, and adopting iterative methods to obtain convergence was developed at INRIM (Molinar et al. 1989, 1993, 1993/1994b, 1998). The pressure distribution in the clearance is calculated through an iterative method derived from the Navier–Stokes equations appropriately modified, in which account is taken of the density and viscosity of the fluid used and, iteratively, of the deformations of the piston-cylinder unit. In Fig. 7.20, the theoretical calculation data of the radial displacement at the outer surface of the cylinder (broken lines) are compared with the experimental determinations obtained with strain gauges. The data refer to a tungsten carbide piston-cylinder used up to 100 MPa. The calculation results agree to within 6 % with the experimental data, and are close to the uncertainty evaluated for the latter. The coefficient λ *c*omputed with Eq. 7.23 is lower by about 4 % than the same coefficient obtained with this method, but only if accurate direct measurements of E and ν for the piston-cylinder materials have been made.

  If literature data are used for E and ν, the discrepancy may be larger, of the order of 20–30 %. A discrepancy of this magnitude was also observed for units made of hard steels, for which the experimental tests and the relevant calculations gave results similar to those indicated above. Similar data were obtained for a piston-cylinder unit operating up to 500 MPa (Molinar et al. 1993).

  It is also interesting to note that similar calculation methods were applied to a NIST unit operating in gas media up to 28 MPa (Molinar et al. 1993/1994). This was a special unit that can be operated in free deformation, reentrant, and controlled-clearance modes. Calculations show that the elastic distortions, the pressure distribution in the clearance, and the pressure distortion coefficients, for

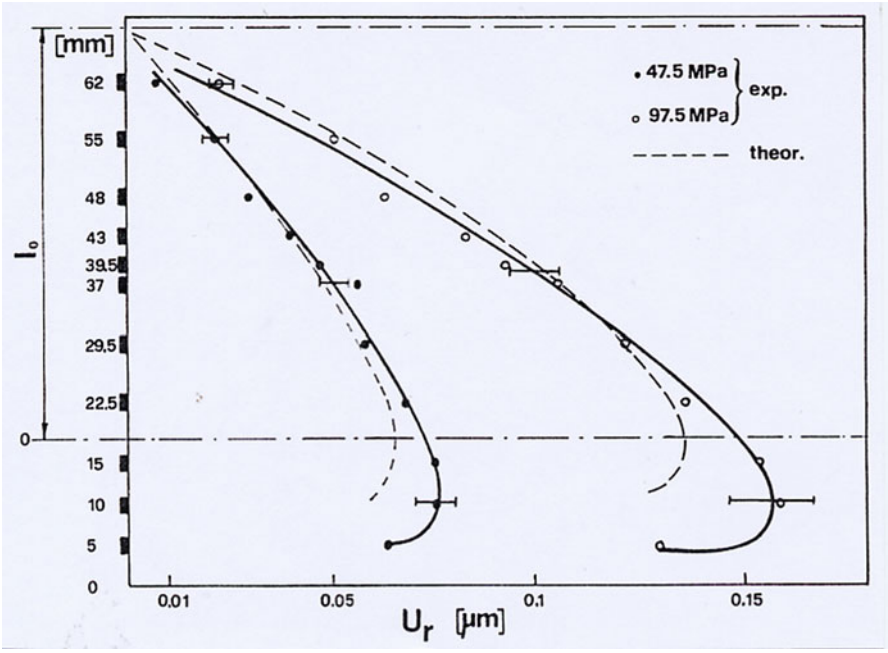

Fig. 7.20 Radial displacements Ur on the outer cylinder surface in the engagement length (l_0) of a tungsten carbide piston-cylinder unit of 100 MPa capacity at two pressure values ($t = 20 \pm 0.05$ °C)

all the three basic configurations, are not fluid dependant. In the free deformation configuration, the maximum radial distortion at the maximum pressure is of the same magnitude (0.527 µm) of the undistorted radial clearance and the agreement between experimental and calculated distortion coefficient is within 1.4 %. In the reentrant configuration, the agreement between experimental and calculated distortion coefficient is within 14.3 %. In the controlled-clearance configuration, the distortion of the cylinder are, on the average, equal to zero and the pressure distribution along the clearance is the most linear of the three configuration studied.

- A general calculation method in which the pressure profile in the clearance is calculated according to the theory of flow in a converging channel was developed at PTB (Klingenberg 1986, 1987, 1989). Results on a tungsten carbide piston-cylinder unit showed pressure distortion coefficients smaller by 20 % than the coefficients calculated with the Eq. 7.23.
- In many laboratories, today it is prevalent to carry out finite elements calculations to determine the pressure distribution into the clearance and the pressure distortion coefficient of a piston-cylinder unit (Wisniewski et al. 1989; Samaan 1990; Samaan et al. 1993/1994; Buonanno et al. 1999; Fitzgerald et al. 1999; Molinar et al. 2005a; Buonanno et al. 2007). Of particular interest is the study of Samaan (1990) on a gas- operated pressure balance of commercial type to a

maximum pressure of 17 MPa. Because of the complex geometry of the piston-cylinder unit (partially simple and partially reentrant), studies and calculations based on finite element techniques represent a powerful tool for understanding elastic distortions. In the case of a simulated constant gap of 1.0 μm, Samaan obtained a pressure distortion coefficient of 0.14 ppm/MPa. Different simulations showed that the distortion coefficient could be made equal to zero by carefully positioning the O-ring seal on the bottom part of the cylinder. In these calculations, compressibility of the gas is taken into account (density is considered linearly proportion with pressure) and the flow rate must be constant everywhere along the piston-cylinder engagement length. Such points have been developed further by many authors. The best example of top-level FEM calculation is represented by the EURAMET Project 1039 (2008–2010), where four piston-cylinder units are considered in gas modes. The units have the following main characteristics (all pistons and cylinders are in tungsten carbide and calculations are performed for nitrogen and helium in gauge and in absolute modes):

- Nominal effective area 10 cm^2 and pressure full scale of 1 MPa.
- Nominal effective area 5 cm^2 and pressure full scale of 2 MPa.
- Nominal effective area 20 cm^2 and pressure full scale of 0.75 MPa.
- Nominal effective area 2 cm^2 and pressure full scale of 7.5 MPa.

The task of the EURAMET project was to minimize the uncertainty contribution produced by a pressure dependence of the effective area up to 7 MPa in order to have calculation and experimental pressure measurement uncertainty $U(p)/p$ close to 1 ppm to be useful in the Boltzmann constant experiment. In order to assess this point, a comparative study is underway by PTB (coordinator), LNE, INRIM-University of Cassino and CMI. It has to be stressed that this effort was made by the use of special pressure balances equipped by special piston-cylinder units and 150 kg masses with automatic mass handler. It has been demonstrated by Sabuga et al. (2011a) that, using three units of 20 cm^2 and three units of 2 cm^2, the effective area ratios derived from cross-floating for all possible units combinations are within 1 ppm, a value similar to the effective area values determined by dimensional measurements.

Preliminary comparative results, Sabuga et al. (2011b), show that:

- A_0, $A_e = f(p)$ and λ are independent of the gas used within viscous flow model, there is fluid dependence for piston fall rates versus pressure.
- Larger contributions on λ uncertainty come from operation mode, uncertainty on dimensional data, and elastic constants.
- Larger differences on λ are due to A_0 discrepancies.
- Agreement in pressure is within 0.34 ppm up to 7 MPa.

The majority of these methods (except when mentioned) were developed mainly for application with liquid media. In this context, the Buonanno et al. (2007) book makes a useful reference, where a comprehensive experience of these calculation methods is given. In last years, different attempts have been made to compare FEM-calculated results between them; they are reported in Molinar et al. (1998) for the EUROMET Project 256; Sabuga et al. (2005, 2006) for the EUROMET Project 463.

As regards the EUROMET Project 463 (Calculations of elastic distortions and associated uncertainty in piston-cylinders operating up to 1 GPa), the numerical results obtained are in better agreement with the ideal than for the real gap model in respect to the experimental data, with very good agreement between FEM and Lamè results for the ideal gap model. The estimated standard uncertainty is $u(\lambda) = (0.04–0.12) \times 10^{-6}$/MPa, which depends on pressure value and operating mode, and the gap dimensions and shape were identified as a main uncertainty source. The numerical model is not very descriptive of the experimental piston fall rates, and the differences between the theoretical and experimental results require further clarification. Further work is needed before FEM can be relied on completely for uncertainty determination, especially when trying to model the behavior of real piston-cylinders. In particular, application of FEM becomes more difficult with increasing distortions and decreasing piston-cylinder clearance. Generally, the following conclusions can be reached:

- The clearance shape is the most important influence parameter in the evaluation, both of the pressure distortion coefficient and piston fall rate. If the aim is only the determination of the pressure distortion coefficient, it is strictly necessary to measure the dimensions of the clearance. For this purpose, without knowing the gap dimensions, the application of the simplified model deduced by the Lamè equation seems to be sufficient and the values obtained by FEM present negligible differences in respect to the theoretical simplified values.
- The influence of the boundary conditions on the pressure distortion coefficient and piston fall rate can be extremely significant, depending also on the type of pressure balance analyzed.
- The influence of the piston and cylinder material mechanical properties on the pressure distortion coefficient varies as a function of the boundary conditions. Particular attention must be paid to the cylinder Poisson ratio ν_c and to the piston Young modulus E_p measurements.
- The most recent experimental and numerical investigations show that the piston fall rates, when numerically evaluated by means of the Stokes theory, are often underestimated compared with the experimental ones. These differences increase with the Reynolds fluid number and might be also due to the inapplicability of the Stokes theory. In order to take into account the differences between theoretical and experimental values of the fall rates, Buonanno et al. (2007) suggest a corrective functional relationship, obtained from a comparison between experimental and calculated values of Poiseuille number. Based on a function between the relative Poiseuille number and the Reynolds number, the numerical values of FEM fall rates can be corrected. From the obtained results, there is strong evidence that the combined effects of small clearances and high pressures are responsible for the deviations from a fully Newtonian fluid behavior. By applying the above mentioned correction, the mean differences between predicted and experimental piston fall rates can be reduced from about 40 % to less than 15 %. This approach validates the hypothesis of piston-cylinder of pressure balances being considered

as microchannels, even if the Navier–Stokes theory cannot, at the moment, be substituted in the calculation of pressure distribution along piston-cylinder clearances and piston-cylinder distortions.

Although these methods have to be carefully considered, they nevertheless represent a very useful attempt to increase confidence in the calculation of pressure distortion coefficients. They prove the importance that dimensional measurements, pressure gradient distribution into the clearance, and elastic-constant determinations have in the uncertainty of calculated elastic distortion coefficients of pistons and cylinders. Dimensional measurements must be made on pistons and cylinders at the submicrometer level. The elastic constants of the piston and cylinder materials (ν and E) must be known with a typical uncertainty of better than 1 %. In this context, it is worth to mention the PTB effort, within the *EURAMET Project 1039*, to measure the elastic constants of materials with resonant ultrasound spectroscopy (Sabuga et al. 2010, 2011) that shows the possibility of performing measurement of E and ν with standard uncertainties as low as 0.03 and 0.05 %, respectively.

The results also confirm the need of determining the properties of the fluid, such as density and viscosity, versus pressure and temperature, and the pressure profile in the clearance. Density and dynamic viscosity of the fluid versus temperature and pressure must be known with typical uncertainties from 0.1 to 1.0 %

The above-mentioned experiences lead to a method for defining the estimated uncertainty budget for the calculation of pressure distortion coefficient; a method that is also valid to investigate the more important parameters affecting its value. Another important aspect, as pointed out by Fitzgerald et al. (1999) is the possibility of using the FEM numerical calculations for the design and analysis of pressure balances under specified user conditions (for example, imposing a specific pressure gradient along the piston-cylinder engagement length and no mounting effects or a specific mode of operation).

The operating principle of controlled-clearance pressure balances is described in detail by Heydemann and Welch (1975). In a system of this type, an auxiliary pressure, the jacket pressure p_j (Fig. 7.14c), is applied onto the outer surface of the cylinder, in order to control its expansion, which is caused by the internal pressure p.

The piston pressure distortion coefficient is computed by means of the simple elastic theory. The cylinder pressure distortion coefficient is determined experimentally, at different values of pressure p, from piston fall-rate measurements when p_j is changed.

The effective area A_e of a controlled-clearance piston-cylinder unit is a function of temperature t, measurement pressure p, and jacket pressure p_j, and is typically

$$A_e\left(t, p, p_j\right) = A_p\left(1 + \lambda_p p\right)\left[1 + \left(\alpha_p + \alpha_c\right)\left(t - t_{ref}\right)\right]\left[1 + d\left(p_z - p_j\right)\right] \tag{7.35}$$

where:

- A_p is the effective area *of the piston*.
- λ_p is the pressure distortion coefficient *of the piston*, that is $\lambda_p = (3\nu_p - 1)/E_p$.

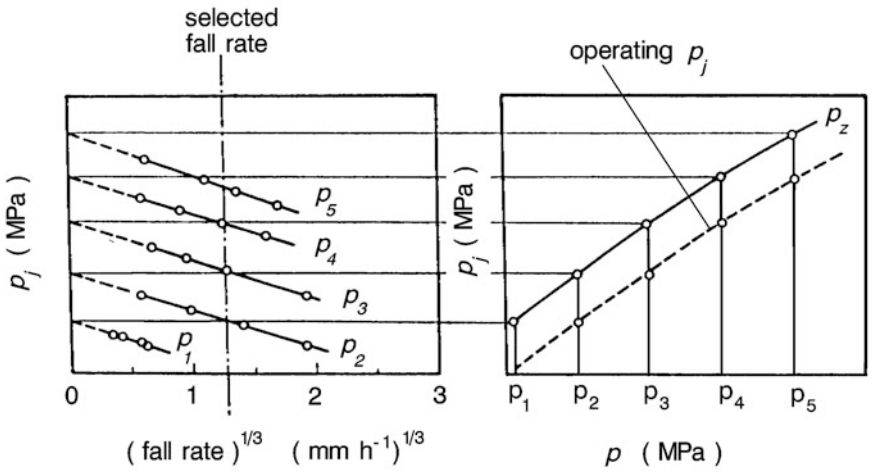

Fig. 7.21 Controlled-clearance pressure balance: zero-clearance jacket pressure p_z, and operating pressure p_j versus measuring pressure p

- d is the jacket pressure coefficient, which can be determined experimentally and whose behavior versus p is frequently of the parabolic type.
- p_z is the value of the jacket pressure at which the clearance in the piston-cylinder unit is zero, on the assumption that the leak rate past the piston is proportional to the third power of the clearance. p_z must be determined experimentally.
- p_j is the operating jacket pressure, as established in order that the cubic root of the piston fall rate is a constant for each selected pressure p.

The other symbols have the same meaning as in the previous sections. Figure 7.21 is an example of the behaviors, experimentally determined, of $p_z = f(p)$ and of the operating jacket pressure $p_j = f(p)$ in arbitrary units.

The behavior of p_j versus the cubic root of the fall rate is determined experimentally at different pressure values ($p1,\ldots,p5$). From the data thus obtained, by extrapolation it is possible to derive $p_z = f(p)$ and, with a selected value of the piston fall rate, to calculate the operating pressure p_j versus the measurement pressure p. This is only the basic principle of the method, whose implementation requires the selection of an appropriate frequency for piston revolution, accurate measurements of piston fall rates, and specific procedures for the determination of the jacket pressure and of the coefficient d, besides careful determination of possible temperature effects on piston fall rates.

Sharma et al. (1988) describe the metrological characterization of a controlled-clearance pressure balance for pressure measurements with different gases up to 5 MPa, and estimate a pressure uncertainty of 26 ppm when nitrogen is used. Controlled-clearance systems can be used, with moderate loss of accuracy, for the characterization of other pressure balances of the simple or the reentrant configurations. The controlled-clearance pressure balance characterized by Sharma and

collaborators was used to obtain the basic characteristics (A_0, λ, ...) of other oil-lubricated piston-cylinder units of the reentrant type of 4 and 8 MPa range, subsequently used in an intercomparison with gas media and under gauge conditions up to 4 MPa (Sharma et al. 1988).

An interesting new approach was presented by Kolb (2011) for controlled-clearance pressure balances used in gas up to 4 MPa (9.8 cm^2). The interest is based on the method, that correlates the exhaust residual pressure over the piston, and this parameter is used to detect the zero-clearance jacket pressure p_z. This method gives different advantages: now p_z characterization can be made over the full jacket pressure range from 0 to p_z without having the risk of damaging the surfaces of piston and cylinder, measurements can be useful to experimentally determine the apparent nonlinearity and to detect more efficiently the value of zero-clearance pressure.

The advantage of a pressure balance of the controlled-clearance type is that it is an alternative to the simple configuration particularly as regards distortions versus pressure applied to the piston-cylinder unit. A pressure balance of this type can be advantageously used, for example, for an experimental check of effective area ratios between systems of different kinds or in the studies of piston-cylinder distortions. A controlled-clearance pressure balance could be also used to check if the $A_e = f(p)$ behavior of, for example, a simple or reentrant piston-cylinder unit, has or has not a linear behavior.

Another convenient way to determine, in absolute terms, the effective area of a pressure balance and, consequently, the pressure distortion coefficient is the application of the *similarity* method developed by Dadson et al. (1965) at NPL-UK.

This method involves cross-floating at different pressures between two pressure balances (denoted here by A and B) of similar dimensions and design but made of materials having widely different Young's moduli (for example, $E_A \gg E_B$). Besides, the materials of the two units should have, ideally, the same Poisson coefficients ($\nu_A = \nu_B$) and, by appropriate machining, the radial clearances between the pistons and the cylinders must be adjusted so as to obtain a relation as close as possible to the equality $r_A/r_B = E_B/E_A$. The annular clearance between the piston and the cylinder of the two devices is assumed to be similarly distorted with increasing pressure, so that the pressure profile may be the same in the two units.

It was demonstrated that if the above conditions are closely satisfied, it is possible to calculate the distortion coefficients λ_A and λ_B of both gauges from the ratio of the effective areas of the two gauges obtained experimentally by cross-floating and with the measurement of Young's moduli E_A and E_B.

The "similarity" method, verified experimentally at NPL-UK also with another technique called the "flow method" (Dadson et al. 1965), yielded good results with liquids media up to 400 MPa.

In conclusion, there are many systems of different configurations that can be used for gauge pressure measurements in gas media up to 100 MPa (Francis and Solis 1989) and there are as many methods and procedures with which the best possible accuracy can be achieved. The different systems, though still based on a simple principle, are nevertheless rapidly and substantially changing as to design and evaluation methods and now their level is that of sophisticated laboratory apparatus requiring specially trained technicians.

7.2.3.3 Pressure Balances of Large Diameters

Nonrotating Pressure Balances (Force-Balanced Pressure Balances)

An original device is, for example, the nonrotational pressure balance for gas operation developed at the NMIJ (Ooiwa 1989). The piston-cylinder clearance is purposely irregular, weight suspension is obtained by means of a special mechanism, and piston inclination is detected by a monitoring technique. This pressure balance is used up to 0.4 MPa (accuracy of 9 ppm) with stability better than 1 ppm, and has the advantage of no piston rotation during operation, a particularly useful feature when absolute pressure measurements are carried out, because it eliminates all the mechanical systems for piston rotation.

The same authors from NMIJ (Ooiwa et al. 1993, Ooiwa 1993/1994b) developed the original idea further. They use an intentionally double-tapered cylinder in order to operate without piston rotation. The piston-cylinder having a nominal effective area of 1.999 cm^2, nominal diameter 15.9 mm, made of 440C stainless steel, is stabilized by a 7 kPa pressure inlet in the central part where the clearance is larger. The second feature is the compensation of the piston weight by the measurement of this force by an electronic balance. The force-balanced principle allows pressure measurements from 1 Pa to 10 kPa with a sensitivity of 5 mPa and an estimated uncertainty of about 15 mPa or 0.01 %.

Haines et al. (2002) and Delajoud et al. (2002) further developed the idea of force balanced pressure balances (FPG) in order to cover the gauge and absolute pressure range from 1 Pa to 15 kPa. The nonrotational piston-cylinder is schematically illustrated in Fig. 7.22.

The piston-cylinder is made in tungsten carbide, the nominal effective area is 9.8 cm^2 and its nominal diameter is about 35 mm. The piston is straight while the cylinder is symmetrically tapered with a typical radial clearance of 1 μm (upper and lower part of the cylinder) and about 4 μm in the cylinder central part. An independent lubricating pressure (40 kPa absolute for absolute mode or 40 kPa above atmospheric pressure for gauge mode) causes gas to flow through the piston-cylinder gap from the middle of the cylinder. A mass comparator measures the force on the piston and an automated pressure controller is used to adjust the flow across the different restrictions and to set and control pressure stability. With this system, that requires clean environment and full knowledge of the controlling part of the instrument, it is possible to have a pressure resolution of 1 mPa and a measurement uncertainty as low as 5 mPa + 3 $\times$ $10^{-5}p$, with p expressed in pascal.

This system can be used to calibrate top-level pressure transducers (e.g., capacitance diaphragm gauges) as well as to check their characteristics by comparison with other pressure balances in their overlapping pressure ranges.

These nonrotating piston devices are now very diffused in national metrology laboratories and different studies have been made. Otal et al. (2005) made a direct comparison of their FPG with a 20 cm^2 pressure balance in gauge and in absolute mode. The relative difference of effective area was only 1.2 ppm and no significant

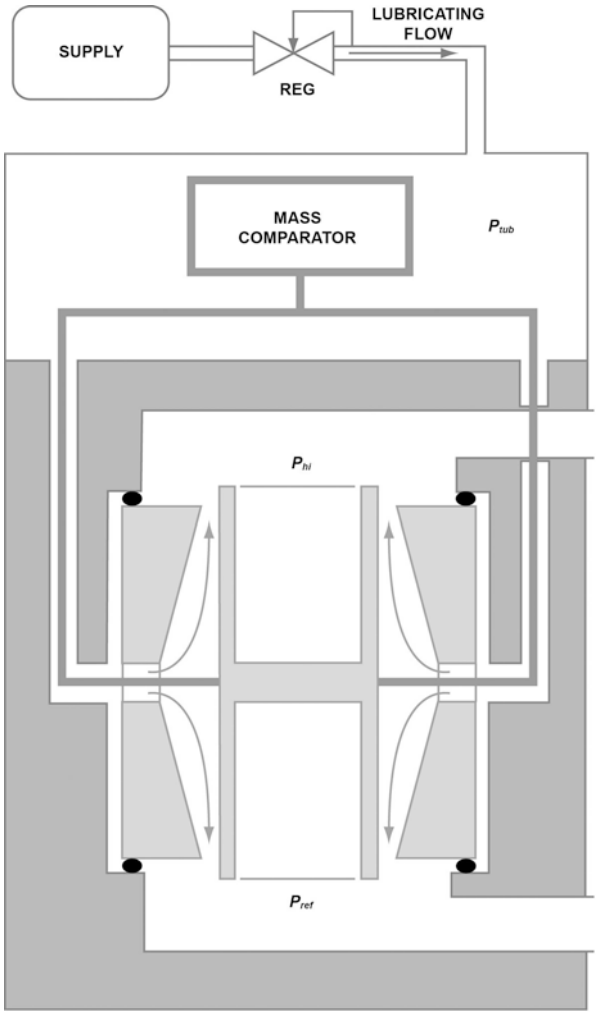

Fig. 7.22 Force-balanced pressure balance (FPG), nonrotating piston principle. (From Delajoud et al. 2002 by kind permission of the authors)

effect of nonlinearity was found between 5 and 15 kPa. The estimated expanded uncertainty has been evaluated to be:

$8\,\text{mPa} + 2.4 \times 10^{-5} p$ in gauge mode, with p expressed in pascal and
$13\,\text{mPa} + 2.3 \times 10^{-5} p$ in absolute mode, with p expressed in pascal.

Rantanen et al. (2005) also made an extensive investigation on this type of instrument with determination of effective area by comparison with pressure balances and mercury manometer and they investigated as well the long-term stability and reproducibility of the instrument over a period of 4 years. They found that the effective area values are the same in gauge and absolute mode and over a period of 4 years there were no evident shift to be quoted.

This type of instrument has been further studied, in order to derive all the input quantities for their correct use, by Haines et al. (2009) and compared at NIST with different primary standards by Hendricks et al. (2009). Four different FPG systems were compared at NIST. All of them in the absolute range from 5 Pa to 15 kPa, compared with the ultrasonic NIST manometer (UIM), were found in agreement within the uncertainty of ($8\,\text{mPa} + 30 \times 10^{-6} p$), however, below 5 Pa some of the comparison results were outside the above specified uncertainty. For comparison, an isolating CDG was used to prevent humidified gas coming from FPG entering the UIM. This is a good recommended practice for applications of FPG and vacuum standards.

As done by different authors, it is worth to mention the device of Woo et al. (2005) where they use a conventional pressure balance of $9.8\,\text{cm}^2$ nominal effective area with a measurement procedure that allows the variation of the pressure in the bell jar and automatic mass handling. With this device, it is possible to operate in absolute mode from 100 Pa to 2 kPa for the calibration of capacitance diaphragm gauges, with a standard uncertainty of the device of $0.11\,\text{Pa} + 1.13 \times 10^{-5} p$, with p expressed in pascal.

Rendle (1993/1994) developed another interesting system. In this case, the elimination of friction between the piston and cylinder (both in Invar) is achieved by a parallelogram suspension system. The piston is very large, having an effective area of $100\,\text{cm}^2$ (diameter of 112.8 mm), the gap between piston and cylinder is about 30 μm. There is flow controller that supplies pressure and controls the flow, which is laminar through the engagement length of the piston-cylinder unit. The piston-cylinder is rigidly mounted on an electronic balance mechanism held at zero when only the piston is balanced. This device gives resolution of 1 mPa from 0 to 1 kPa differential pressure and 10 mPa from 1 to 3.2 kPa. The declared uncertainty is 0.002 Pa + 0.003 % of the reading from 0 to 1 kPa and 0.01 Pa + 0.003 % of the reading from 1 kPa to 3.2 kPa. Similar standards have been successfully used to reduce the uncertainty of the pressure scale from 30 Pa to 11 kPa (e.g., Bock et al. 2009).

Large-Diameter Pressure Balances

Particularly in gas pressure measurements around atmospheric pressure and up to few megapascal, in absolute and in gauge mode, the use of large-diameter piston-cylinder units of top-level geometry is now a reality. Rather, normally piston-cylinder units of (2, 5, 10, 20, 50) cm^2 are used (some time even $100\,\text{cm}^2$). They correspond to nominal diameters of (15.9, 25, 35, 50, 80, or 113) mm, respectively. The large area gives the possibility of reducing the pressure range in its lower part, and if the geometry of the piston-cylinder is dimensionally regular it is also possible to reduce the pressure measurement uncertainty to below 10 ppm tending to approach few ppm. Many of the systems described here are now available commercially from the top pressure metrology companies.

Legras et al. (1995) describe an absolute pressure balance in the pressure range from 150 kPa to 1 MPa. The measuring systems are piston-cylinder units of nominal effective area of 10 and $20\,\text{cm}^2$, and great care was taken in the auxiliary measuring

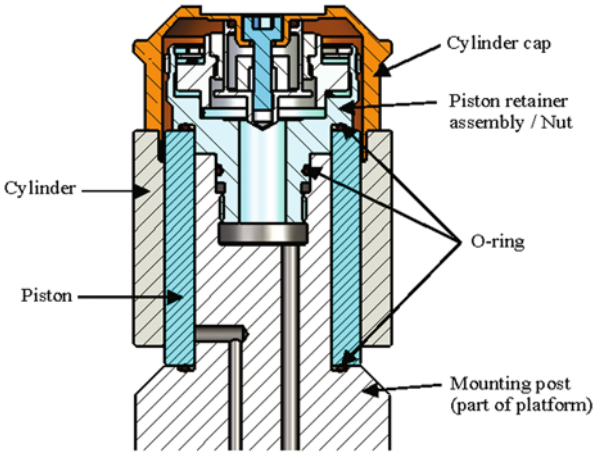

Fig. 7.23 Large-area (nominal 20 cm^2) pressure balance, for gas pressure measurements, gauge and absolute modes up to a maximum pressure of 0.75 MPa. (From material related to *EURAMET Project 1039* by kind permission of Dr. Wladimir Sabuga [EURAMET Project 1039 Coordinator, PTB])

units (e.g., capacitance sensor to measure the reference vacuum with a resolution of 0.01 Pa and uncertainty of 0.05 Pa) in arriving to an estimation of pressure uncertainty of $0.1\ \text{Pa} + 3 \times 10^{-6} p$.

Such systems were ameliorated by Le Guinio et al. (1999) with automated mass loading on the floating elements, using two 20 and 10 cm^2 piston-cylinder units. For the cross-floating of the pressure balances in absolute mode, the authors successfully experimented the use of capacitance diaphragm gauges. The revised standard pressure uncertainty was $0.15\ \text{Pa} + 3 \times 10^{-6} p$ in the pressure range from 10 kPa to 1 MPa.

Delajoud et al. (1999) describe as well the early (1992–1995) NIST experience in using three 50 mm piston-cylinder units (nominal effective area of 20 cm^2), fabricated by DH Instruments, in the absolute mode from 2.5 to 175 kPa with a pressure uncertainty lower than 5×10^{-6}.

The quality of piston-cylinder was investigated by different dimensional measurements where it was demonstrated that radial gap is always lower than 1 μm. The piston and cylinder were made of high-purity alumina oxide, the piston is fixed and the cylinder moves due to pressure application and it is possible, if needed, to supply an external pressure on the inside of the piston in order to vary the radial clearance between piston and cylinder. For the three piston-cylinders used, over a period of 20 months, a long-term repeatability with a relative standard deviation of 2×10^{-6} was obtained. No systematic change of effective area between gauge and absolute mode was reported when changing the fluid (nitrogen and helium).

Almost at the same time, investigations at NIST, reported by Schmidt et al. (1999), are presented for piston-cylinder units of 50 mm in diameter but made in tungsten carbide reaching a relative expanded uncertainty of 5 ppm. Of course, large-diameter piston-cylinder unit can be used as well to measure pressure in liquid media as, for example, reported by Jäger et al. (1999).

Figure 7.23 shows the basic drawing of the tungsten carbide piston-cylinder of 50 mm (0.75 MPa maximum absolute and gauge pressure) that is used within EURAMET Project 1039 for different numerical calculations connected to the

determination of its pressure distortion coefficient, in different conditions of use (gauge, absolute, different gases, different numerical simulations in order to have an idea of influence quantities on the standard uncertainty). Wan Mohamed et al. (2008) developed interchangeable pistons in the same cylinder of nominal 35 mm diameter demonstrating the possibility of interchanging the pistons and that no significant differences can be observed in effective areas when piston rotational frequencies are changed in the range of 30–90 rpm.

7.2.4 Uncertainty of Absolute and Gauge Pressure Measurements with Pressure Balances

In order to define the overall uncertainty of the pressure value measured with pressure balances, the combination of the different uncertainty contributions is now considered. Such contributions are of the same type as those already described for the case of liquid-column manometers primary standards (Sect. 7.1.3 and in Appendix E, Tables E.2, E.3, and E.4).

For primary pressure balance standards, reference is also made to the CIPM Recommendation (CIPM Recommendation INC-1, 1980) given in Appendix E, Document E.1 and to the different guides for the expression of uncertainty in measurements (GUM), such as, for example:

- The "*ISO/IEC Guide 98-GUM (1995).*"
- The more recent "*JCGM 100:2008*," Evaluation of measurement data. Guide to the expression of uncertainty in measurement, First Edition 2008.
- Guide "*JCGM 101:2008*," Evaluation of measurement data-Supplement 1 to the "Guide to the expression of uncertainty in measurement-Propagation of distributions using a Monte Carlo method."

As already discussed, the pressure p to be measured can be expressed in different ways, which depend on the measurement mode (absolute or gauge) and on the configuration of the pressure balance (simple, reentrant, controlled-clearance types).

In the case of a gas pressure measurement under absolute conditions and for a typical piston-cylinder of the "simple" type, pressure p will be expressed by Eq. 7.18, as described in Sect. 7.2.2.

In the case of a gas pressure measurement under gauge conditions, and for a piston-cylinder unit of "simple" or "re-entrant" types, pressure p will be expressed by Eqs. 7.29 or 7.30, as described in Sect. 7.2.3. For a "controlled-clearance" pressure balance, Eqs. 7.29 or 7.30 can be used but the effective area $A_0(1 + \lambda p)$ will be replaced by Eq. 7.35.

The use of these equations implies that a complete measurement and an uncertainty evaluation of all the different physical quantities involved in pressure calculation have been made, in accordance with the indications given in Sect. 7.2.2 (absolute pressure measurements) and in Sect. 7.2.3 (gauge pressure measurements).

As the Eqs. 7.18 and 7.29 or 7.30 indicates, the pressure p to be measured is a function of different physical quantities x_i (m_i, g_L, A_0, ...), so that in general terms

one can write $p = \mathrm{f}(x_\mathrm{i})$. For each physical quantity x_i, an absolute uncertainty $\delta \mathrm{x_i}$ is evaluated on the basis of the residual standard deviation (1σ) of its measurement value. The contribution of each physical quantity x_i to the total uncertainty of the pressure measurement value will be expressed as $1/p(\delta p/\delta x_\mathrm{i})\ \delta x_\mathrm{i}$ (if δx_i are evaluated at the 1σ level, this contribution, too, is referred to the 1σ level).

Consider, as an example, the contributions of the uncertainties of the mass m_i and of temperature t to the pressure uncertainty.

A mass m_i of 10 kg could be measured with a typical uncertainty (at 1σ level) of $6\ \mathrm{mg} = \delta m_\mathrm{i} = \delta x_\mathrm{i}$.

The mass uncertainty will then contribute to pressure uncertainty as

$$\left(\frac{1}{p}\right)\left(\frac{\delta p}{\delta x_\mathrm{i}}\delta x_\mathrm{i}\right) = \left(\frac{\delta x_\mathrm{i}}{x_\mathrm{i}}\right) = \left(\frac{\delta m_\mathrm{i}}{m_\mathrm{i}}\right) = 0.6\ \mathrm{ppm}$$

at the 1σ level. It must be remembered that such an uncertainty contribution is valid only for the specific considered mass of 10 kg. As a weight set of a pressure balance is composed of different pieces, all uncertainty contributions of each single piece have to be considered. This is important especially in the case where different uncertainties' contributions in the weight set are to be considered.

In the case of the measurement of the temperature t of the piston-cylinder unit, a typical $\delta x_\mathrm{i} = \delta t = 0.02$ K comes from the calibration of the temperature probe including also temperature nonuniformity of the piston-cylinder assembly.

For a tungsten carbide piston-cylinder (typical $\alpha_\mathrm{p} + \alpha_\mathrm{c} = 9.8 \times 10^{-6}\ ^\circ\mathrm{C}^{-1}$), the temperature uncertainty contribution to the pressure value uncertainty will be $(1/p)(\delta p/\delta x_\mathrm{i})\delta x_\mathrm{i} = (\alpha_\mathrm{p} + \alpha_\mathrm{c})\delta t = 0.2$ ppm. The contribution of the uncertainty of the value of thermal expansion coefficients must be evaluated separately.

With pressure balances, the type "A" components (CIPM Recommendation INC-1, 1980 and GUM 1995 and 2008) are evaluated experimentally on the basis of sensitivity and repeatability over the whole pressure range. To make this evaluation, it is necessary to perform cross-floating experiments, over the whole common pressure range, between pressure balances of the same nominal effective area and accuracy levels.

The type "B" (systematic) components are the $(1/p)(\delta p/\delta x_i)\delta x_i$ contributions, evaluated for each physical quantity x_i involved in the determination of pressure p. Other additional factors to type "B" errors, not directly involved in the calculation of pressure p, may include, for example, possible errors in the leveling of the piston-cylinder unit, nonvertical or parasitic force components, or long-term instability in the effective area of the pressure balance.

Once the contributions to the uncertainty of the pressure value by all the physical quantities x_i have been determined and all the type "A" components evaluated, all such uncertainty contributions have to be combined.

In the case of pressure balances, a prevalent way of combining all the uncertainties is to take the root mean square of the sum of the squares of all the contributions as

$$\frac{\mathrm{d}p}{p} = \left[\sum\nolimits_\mathrm{i}\left(\left(\frac{1}{p}\right)\left(\frac{\delta p}{\delta x_\mathrm{i}}\delta x_\mathrm{i}\right)\right)^2 + (\text{type "A" comp.})^2\right]^{1/2}.$$

This method is adopted because the majority of the systematic components are not correlated. Sometimes covariance of the correlated quantities is also added into the above parenthesis, to represent the correlation, for example, in the weight mass set, or to correlate the different pressure points made in sequence when the effective area of a pressure balance is derived from cross-floating experiments.

With pressure balances, some contributions (typically by quantities A_0 and λ) are much larger than the others and are prevalent in the uncertainty combination.

The uncertainty thus calculated, of the measured value of pressure p, is at the level of the estimate of one standard deviation. The pressure uncertainty is frequently given at the 2 or 3σ level (i.e., at the level of two or three times the estimated standard deviation). In this case, which must be clearly stated and documented, the 1σ level uncertainty will be multiplied by two (in this case the correct terminology is expanded uncertainty) or three. Some examples (Tables F.2, F.3, and F.4) are given in Appendix F:

- Table F.2 shows a typical example of uncertainty evaluation for absolute pressure measurements to 130 kPa in gas media (nitrogen) with a tungsten carbide piston-cylinder unit.
- Table F.3 gives another example of uncertainty evaluation for gauge pressure measurements to 400 kPa in nitrogen with a tungsten carbide piston-cylinder unit (Legras et al. 1986; Riety et al. 1987).
- Table F.4 gives the pressure uncertainty evaluation for gauge pressure measurements in nitrogen up to 5 MPa (Maghenzani et al. 1987).

These three examples are typical of apparatus available in the main standards laboratories.

Under absolute conditions and with the use of pressure balances, the typical 1σ pressure uncertainty ranges from few ppm for pressures near 100 kPa to less than 8–10 ppm for pressures close to 5 MPa.

Under gauge conditions, the typical pressure uncertainties are again similar to those of absolute conditions up to about 10 MPa, and around 12–15 ppm for pressures up to 100 MPa. The latter higher figure is mainly due to insufficient accuracy in the determination of the effective area and of the pressure distortion coefficient of the piston-cylinder unit.

7.2.4.1 Differential Gas Pressure Measurements with Pressure Balances

The measurement of a gauge pressure is always of the differential type and pressure is measured with reference to atmospheric pressure. More generally, the measurement value of a differential pressure can be related to any pressure value, frequently called the "line pressure" (p_L).

The measurement of a differential pressure, Δp starts from the measurement of the line pressure value. Therefore, we have to measure the differential pressure $\pm\ \Delta p$ with respect to the line pressure p_L.

This differential pressure Δp is generally small in comparison with the p_L value (typically Δp can be of the order of $10^{-3} p_L$).

Attempts have been made to render the value of Δp to be measured with pressure balances as low as possible when the line pressure, p_L, is the atmospheric pressure (full-gauge condition).

The minimum gauge pressure reliably measurable with a gas pressure balance is typically of the order of 2 kPa, though it may, in some cases, be as high as 10 kPa. A relatively high-pressure value is necessary for obtaining a reliable measurement value when the piston alone is rotating and set in equilibrium. If the piston has a small mass and, consequently, small inertia, it decelerates too quickly and measurements are not reliable. If the piston mass is reduced or the piston-cylinder effective area is increased, the aerodynamic forces created by rotation can introduce errors in the evaluation of the force applied to the piston (Prowse et al. 1977).

The construction of a piston-cylinder unit of too large a diameter and having a constant submicrometer-level clearance involves manufacturing difficulties. The manufacturing of special pistons was attempted, with the purpose of achieving a substantial reduction of deceleration in the rotating system, by Dadson and Greig (1965).

Another alternative is the use of nonrotating pistons, where small differential pressures are possible, but only line pressures from vacuum to atmospheric pressure are typically possible.

Tilting-piston apparatus, in which the piston-cylinder is inclined to the horizontal by an angle β, were also used in the past by Hutton (1966). In this case, the force applied on the piston is reduced by a factor $\sin\beta$; for typical ranges from 1 to 14 kPa the uncertainty is of the order of 0.3 Pa (at 1 kPa). Systems of this type are not used for the top-level accuracy because of the problems (friction of piston and cylinder, parasitic force components, . . .) that they may generate.

Another method for the measurement of differential pressures is that requiring two pressure balances of the same type (frequently called "twin" pressure balances), which can be mutually "cross-floated" at a selected line pressure value and are separated when equilibrium is attained. The differential pressure is generated by a mass increase Δm in one of the two pressure balances (Gascoigne 1971; Peggs 1980; Sutton 1986/1987). This method typically allows one to generate high line pressure values. In some cases (e.g., Kojima et al. 2005), the line pressure is close to the atmospheric pressure value and allows differential pressures from 1 Pa to 1 kPa to be measured with standard deviation of repeated measurements of close to 8 mPa.

Another way of operation is to use a system composed of twin balances under absolute conditions; obviously, the line pressure will be an absolute pressure. The advantage of this technique is a reduction of aerodynamic force effects, but to generate the differential pressure a built-in loading system is required for the addition of the necessary weight pieces on one of the balances during the cross-floating.

Sutton (1986/1987) has applied this technique and a twin piston-gauge system was constructed for pressure measurements from 0.5 to 2 000 Pa. The stated overall uncertainty is $0.9\,\text{mPa} + 2 \times 10^{-5} p$. Sutton's system operates with a variable line

pressure; however, since the system was evaluated for an absolute line pressure of 101 kPa, the line pressure in this case is a typical value of a gauge pressure.

Still, another technique was developed by Grohmann et al. (1987) to extend the measurement limit to the lowest possible absolute pressure value with the use of only one absolute piston-cylinder system. With this technique, developed for the calibration of pressure transducers in the 30 Pa pressure range, the pressure lines are used in ways different from the usual. The pressure to be measured (also called "calibration pressure") is that maintained in the bell jar and the pressure applied to the piston-cylinder is the reference pressure. This apparatus is used in calibration work in three steps, according to the principle of the measurement of a small-value pressure in the bell jar (calibration pressure), produced by the addition of small weights on the piston, with the reference pressure (applied to the piston-cylinder unit), to be carefully determined, remaining unchanged during all the calibration. With this method, accuracy, which is also a function of the stability of the reference pressure, is estimated to be 0.6 Pa at a pressure of 30 Pa. To obtain this value, temperature stability and good knowledge of all the metrological parameters of the pressure balance used are necessary.

Another way of performing differential pressure measurements is to use twin balances under gauge conditions. This is advisable only when the line pressure is high enough to obtain a reliable cross-floating condition (see Sect. 7.2.1) between the two balances. Here, too, cross-floating is realized between the two balances at a selected line pressure p_L. The best cross-floating sensitivity is obtained with pressure balances of the same nominal effective area. The two balances are subsequently separated and with a Δm mass increase, by means of additional weight pieces on one balance, the differential pressure Δp can be generated and measured. This Δp value will be referred to the line pressure p_L at which the previous cross-floating was made.

Figure 7.24 gives a typical configuration for differential pressure measurements using twin-pressure balances.

The procedure for performing differential pressure measurements is typically the following:

Step 1. With valves A, B, C open and D, E closed, the system is operated at a line pressure p_L. Fall rates of both units are measured at pressure p_L (with valves A and B closed).

Step 2. Cross-floating of the two units is realized at line pressure p_L and the equilibrium condition between the two units is determined, with the valves as in Step 1.

Step 3. Repetitive checks of the equilibrium condition are made through measurements of fall rates of both pistons-cylinder units.

Step 4. When an equilibrium is reached and temperature on both units is stable at the same value measured during Steps 1 and 2, a mass Δm is added on one unit that will create a Δp pressure on the appropriate line. This Δp is added to the line pressure value. The Δp value will be calculated as the pressure generated by the mass Δm applied on a piston-cylinder unit of known metrological (A_0, λ, ...) characteristics.

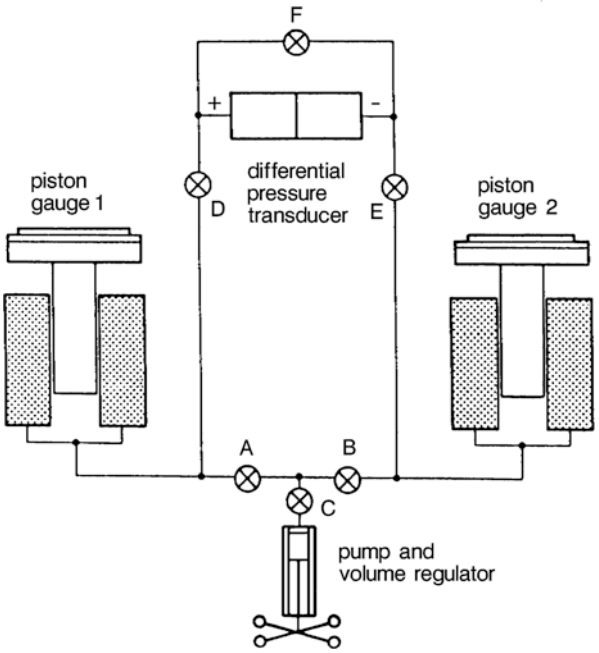

Fig. 7.24 Twin-pressure balance configuration for differential pressure measurements at high line pressure. Typical setup for the calibration of differential pressure transducers

Step 5. The twin-balance configuration can be used for the calibration of a differential pressure transducer. During the calibration operation, valves D and E are open and F closed. Valve F is open only for zero check of the differential transducer, when necessary.

The above-reported procedure is repeated several times and for different mass increases in order to generate the necessary series of differential pressure values up to the full scale needed.

Under the above-described conditions, in determining the overall uncertainty of a differential pressure measurement value, account must be taken of the sensitivity of each of the pressure balances, of the systematic and random uncertainties of the pressure balance used for the Δp generation and measurement, and of the estimated resolution in the "cross-floating" experiment at the selected line pressure. This last element has a large influence in the budget of the differential pressure uncertainty.

When the twin-balance principle is applied, the typical differential pressure uncertainties range from 12 to 30 Pa for pressures from 30 to 150 kPa at a 4 MPa line pressure (Daborn, EUR report 11130 EN 1987) and up to 8 MPa.

For differential pressure measurements at high line pressures, the configuration in Fig. 7.15b2 can also be used. With this configuration, the differential pressure is established across the two ends of a piston of relatively large effective area and the pressure balance of the smaller effective area controls the line pressure.

This system described by Daborn (1977) needs a specific step-calibration procedure, in which pressures p_1 and p_2 (Fig. 7.15b2) are equalized to generate the line pressure and then with a mass Δm_a increase the differential pressure.

$p_2 - p_1 = (\Delta m_a g_L)/B$ is generated, B being the effective area of the larger piston-cylinder unit. The estimated uncertainty for this special pressure balance ranges from 7 to 14 Pa for differential pressures from 30 to 150 kPa and with line pressures from 4 to 8 MPa.

Other systems, e.g., Woo et al. (2009), are using the twin-pressure balance technology coupled with automatic mass charge and care for temperature stability allowing differential pressures from 1 Pa to 31 kPa and line pressures around 100 kPa with an expanded uncertainty (k = 2) of 0.026 Pa + 2.3 $\times$ $10^{-5}p$.

7.2.5 *Results of Comparison Measurements in Gas Media with the Use of Pressure Balances*

The comparisons in gas media reported here and in Sect. 7.2.7 are based, generally speaking, on results obtained before the signing of the Mutual Recognition Arrangement (*CIPM-MRA*, 14 October 1999). See also in references and in Appendix G the Mutual Recognition Arrangement (*CIPM-MRA*) of 1999 and as revised in 2003.

As can be seen in the Sects. 7.2.6 and 7.2.7, the international pressure metrology community, even before the CIPM-MRA, organized a series of gas pressure comparisons in order to internationally validate their measurement results. For more wide information, see also Chap. 11 where an analysis of the important consequences of the CIPM-MRA will be made.

The comparison of standard pressure balances is normal practice in a pressure laboratory and is performed, as a rule, for calibration purposes when it is necessary to determine some of the basic characteristics (A_0, λ, 2α, ...) of a pressure balance. Pressure balance intercomparison can also be necessary to measure or check the ratio of the effective areas of two or more similar systems. Comparisons are frequently performed between different laboratories for the verification of the pressure scale agreement.

The comparison of pressure balances is performed by cross-floating between two different systems at a number of pressure values in the overlapping pressure range. The best reproducibility and sensitivity of cross-floating is obtained when the effective areas of the two systems to be compared are approximately the same and the estimated measurement pressure uncertainties of the systems are of the same level.

For each system to be compared, all the normal precautions must be taken, such as cleaning of piston-cylinder unit, leveling of the instrument also when the weights are added on their carrier, etc. and piston-cylinder temperature, definition of a reference level, frequency of piston revolution and piston fall rate, etc. are determined, which were described in the previous sections.

The two pressure balances to be compared are cross-floated at the same nominal pressure, with the purpose of determining experimentally the pressure value at the equilibrium point of the two units. The first step is the pressurization and the isolation of the two systems; then, when temperature is stable in both units, piston fall rates are measured in both systems. The piston fall rates values, which are pressure and temperature dependent, will be used as references during cross-floating and they can be repeated when necessary in order to verify that their values are the logically expected ones.

The two systems are then interconnected and the weight on one system is gradually changed until the same equilibrium condition achieved, when the systems were isolated, is obtained. This experimental determination, based on the exact reproduction of the fall rates of the isolated systems, is repeated several times and special attention must be given to the temperatures of the units compared. Cross-floating sensitivity, which is defined in terms of the smallest mass increase on one system producing a significant change in the equilibrium of both systems, is an important parameter, as it gives an indication of the sensitivity levels of the systems used. In piston-cylinder units of top-level accuracy, cross-floating sensitivity is generally below a few ppm.

The effective area of one of the systems and their pressure difference can be computed from cross-floating data.

The effective area calculation is normally resorted to for calibration purposes, but it can also be used to compare the basic parameters (A_0, λ, ...) of one system, independently obtained, with the same parameters experimentally determined during the comparison.

For pressure difference calculation, pressure in each system is computed on the basis of the independent metrological characteristics of each piston-cylinder units. In an ideal situation, the pressure difference will be zero over the whole pressure range of the comparison. In this case, the basic characteristics of both piston-cylinder units will prove to be correct at their assigned uncertainty levels. Generally, the pressure difference obtained in the comparison is in agreement within the combined uncertainty of both systems. If this is not the case, it is necessary to identify the responsible systematic errors with a careful check of all physical quantities used to compute pressure on both pressure balances.

These two calculation methods (pressure difference and effective area comparison) are equivalent if all the appropriate corrections (for aerostatic head, buoyancy, temperature differences, ...) have been appropriately applied.

Pressure balance comparisons in gaseous media are generally made under gauge conditions, though, in principle and with ad hoc designed systems equipped with external mass loading devices, it is possible to operate a comparison also under absolute conditions. Cross-floating in absolute conditions is a normal procedure, when pressure balances are to be compared with absolute liquid-column manometers (see Sect. 7.2.7).

Different laboratories have carried out pressure comparisons with pressure balances operating in gaseous media, but until CIPM-MRA they were fewer than comparisons in liquid media. Legras et al. (1988) give, for example, the results

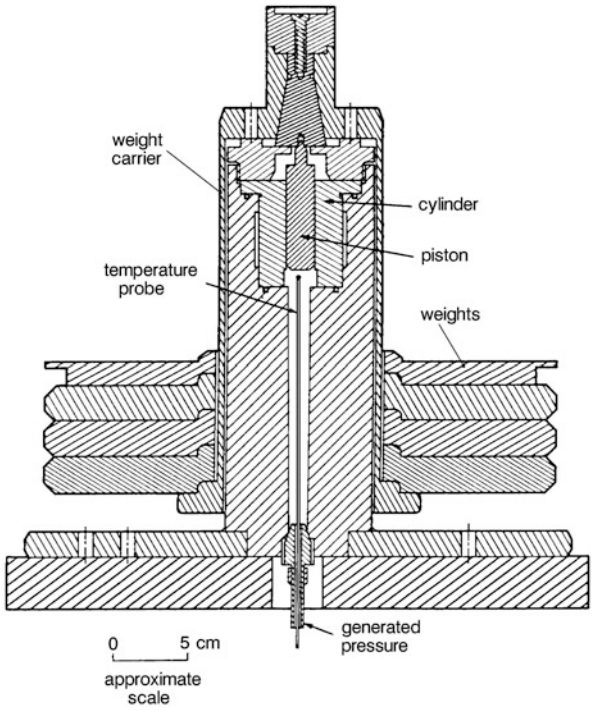

Fig. 7.25 IMGC-5 (now INRIM) free deformation piston-cylinder primary standard used in the IMGC/NBS (INRIM/NIST) comparison between 0.5 and 5 MPa in nitrogen

of an international comparison of 13 laboratories in the pressure range from 20 to 100 MPa in a liquid medium.

It is also possible to compare, over their common pressure range, piston-cylinder units for use with liquids with other units using pure gases, if a reliable fluid separator is used. The liquid-from-gas separator itself must be checked over the whole pressure range, to make sure it does not introduce significant errors during the cross-floating procedure (Driver et al. 1981; see Sect. 8.3.2).

Among the available data, only some typical results obtained in past years by standards laboratories are reported here.

Comparisons in gas media and under gauge conditions up to 5 MPa were made between a primary standard (IMGC-5) of IMGC (now INRIM) and two NIST (formerly NBS) pressure balances (NBS-PG24 primary standard and NBS-PG23 transfer standard; Houck et al. 1983). Figure 7.25 shows the IMGC-5 primary standard (5 MPa pressure range, simple configuration, 2 cm^2 nominal effective area, 24 ppm relative uncertainty) and Fig. 7.26 shows the NBS-PG24 primary standard (1.5 MPa pressure range, controlled-clearance configuration, 5.0 cm^2 nominal effective area, 28 ppm relative uncertainty).

Another NIST system (NBS-PG23, 17.2 MPa pressure range, partially reentrant configuration, 0.084 cm^2 nominal effective area, 30 ppm relative uncertainty) was also used for the comparison, with pressures up to 5 MPa.

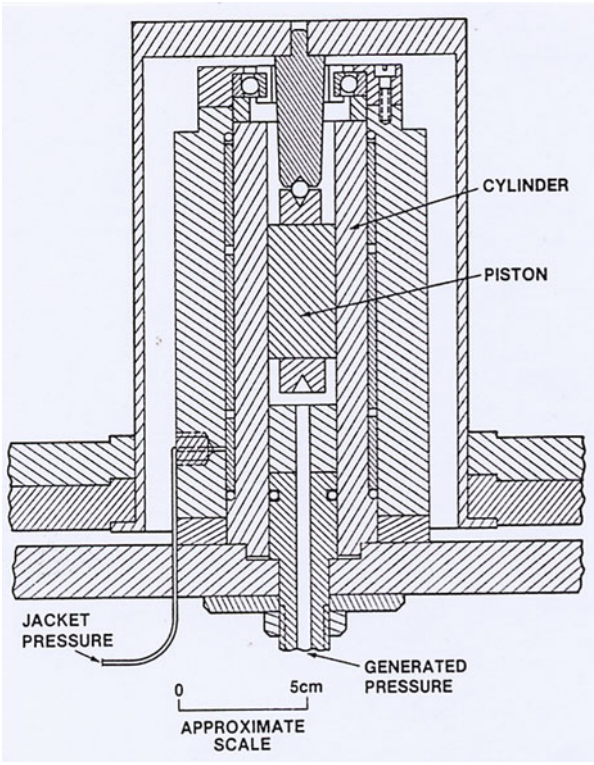

Fig. 7.26 NBS-PG24 controlled-clearance primary standard used in the IMGC/NBS (now INRIM/NIST) comparison between 0.5 and 1.5 MPa in nitrogen

Figure 7.27 gives the pressure differences, resulting from the comparison, between the INRIM (IMGC) primary standard and the NIST(NBS) systems.

The average pressure difference between the IMGC-5 primary standard and the NBS primary standard (NBS-PG24) is within 6 ppm (1.1 Pa is the standard deviation of the mean) in nitrogen over the pressure range from 0.5 to 1.5 MPa.

The average pressure difference between the IMGC-5 primary standard and the NBS transfer standard (NBS-PG23) is within 7 ppm (2.0 Pa is the standard deviation of the mean) in nitrogen over the pressure range from 0.75 to 5 MPa. The same results were obtained when comparing the two systems in terms of their effective areas.

In both cases, the INRIM (IMGC) and NIST (NBS) pressure standards agree to well within the estimated uncertainties of the gauges and this indicates that the pressure uncertainties are correctly estimated.

Other interesting comparison data concerning gas pressure measurements from 0.4 to 4 MPa in nitrogen are given by Sharma et al. (1988) in Fig. 7.28.

A PTB transfer standard (PTB-4 with a total estimated uncertainty of 25 ppm) was compared with the NPL-I transfer standard (NPL-4 having a total estimated uncertainty of 29 ppm) and with another NPL-I reference standard up to 4 MPa. Figure 7.28 shows that the average value of pressure differences between the compared gauges is −7.5 ppm and that the pressure difference values range from −18

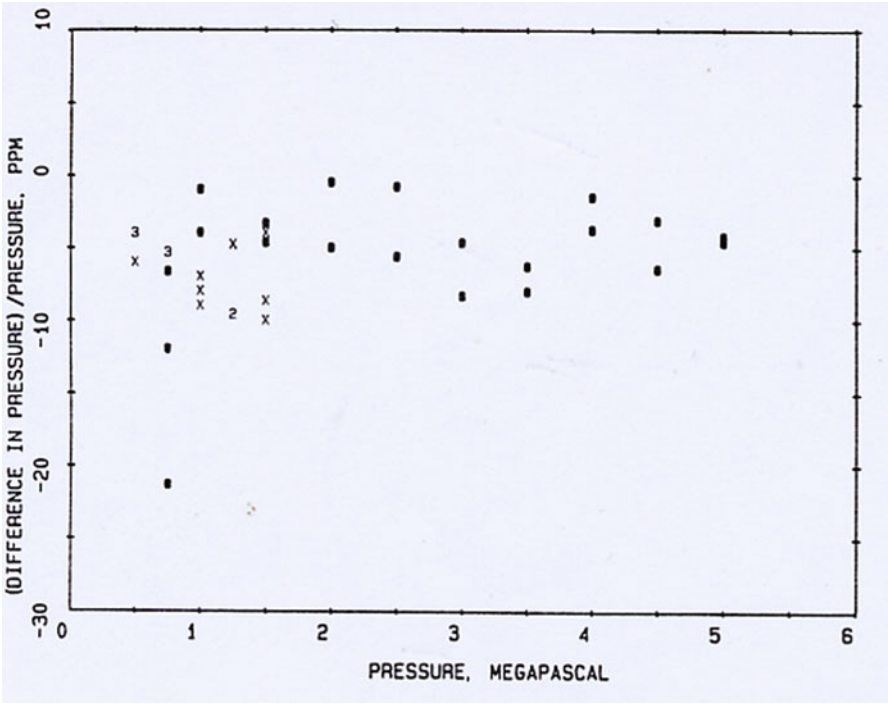

Fig. 7.27 Pressure difference divided by pressure (ppm) versus pressure (MPa) for the following comparisons: • IMGC5/NBS PG23 (0.75–5 MPa). x IMGC5/NBS PG24 (0.5–1.5 MPa)

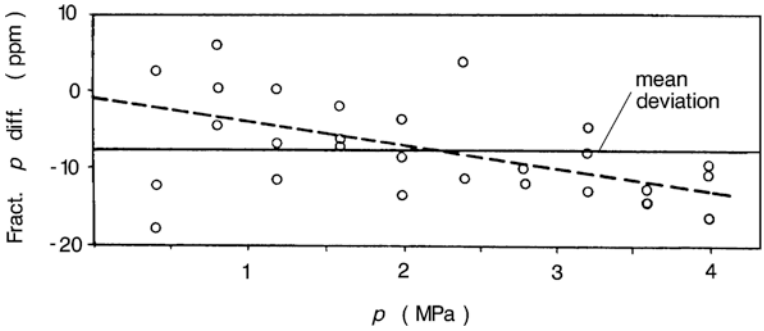

Fig. 7.28 Fractional differences (expressed as $[(p_{\mathrm{NPL-I}} - p_{\mathrm{PTB}})/p_{\mathrm{PTB}}]$, in ppm) of pressure values for measurements in nitrogen up to 4 MPa between NPL-India (NPL-4 pressure balance) and PTB (PTB-4 pressure balance). *Broken line* indicates the effect of the disagreement in the value of λ. (From Sharma et al. 1988 by kind permission of the authors)

to +6.3 ppm over the whole pressure range of the comparison, a value well within the stated uncertainty of the respective transfer standards used in this comparison, as derived from independent evaluations against the standards of both laboratories.

Results of this type confirm the estimated uncertainties of each of the pressure balances used in the comparisons. This is an additional proof that the large uncertainty in pressure balances is mainly due to geometric irregularities in a piston-cylinder unit that influence its effective area. At the same time, it shows that the uncertainty of a pressure balance can be reduced well below 10 ppm with the use of piston-cylinder units of high geometric regularity.

Another important aspect of pressure comparison is their use to find reasons for discrepancies, even if they are small. Klingenberg and Legras (1993/1994) give the results of a gas comparison up to 1 MPa using two transfer standards. It was possible to reproduce the ratio of their effective areas within 1.6 ppm but the absolute values of their effective areas between the two laboratories deviate up to 11.6 ppm. It was proved that this difference was due to problems in performing sufficiently accurate dimensional measurements of the piston-cylinder unit and also in the model used to define the effective area starting from dimensional measurement.

7.2.6 Comparisons of Liquid-Column Manometers and Pressure Balances

Liquid-column manometers, generally using mercury as a fluid, are often compared in the absolute or the differential mode with pressure balances over their overlapping pressure range up to approximately 120 kPa. Although the comparison range is sometimes extended to 360 kPa, in the present section the pressure range considered would be limited to 120 kPa, because it is to this value that the main comparison results have been obtained.

Comparisons of this kind can be performed in the absolute or in the differential mode. The use of the term differential mode here is equivalent to gauge mode and means that the reference pressure may be a value close to atmospheric pressure. The use of mercury-column manometers directly connected at the room air pressure is generally avoided as already pointed out in Sect. 7.1.3.1. In fact, possible mercury contamination and subsequent errors due to the change in the mercury surface due to oxidations may give rise to instabilities in height measurements values and in the course of time produce degradation in column cleanliness.

The mercury-column manometers that are considered here are of top-level accuracy (from few ppm to less than 10 ppm). They are generally to be found in standards laboratories, as mentioned in Sect. 7.1.2; their basic characteristics are of the type summarized in Table 7.1.

Both mercury-column manometers and pressure balances employed in such comparisons should be of top-level accuracy, generally better than 20 ppm, have reproducibility and sensitivity of the order of few ppm, and be equipped for the measurement of temperature, piston fall rate, and revolution frequency of the piston. The pressure balances must be previously fully characterized (see Sects. 7.2.2 and 7.2.3). To achieve all the different purposes of the comparison satisfactorily, a

pressure balance must be equipped with mechanisms for piston rotation, like the device described by Sutton (1980a), which can be easily adapted to any commercially available pressure balance operating in absolute conditions.

With a pressure balance to be used in a comparison and when carrying out absolute pressure measurements, it ought to be possible to change rapidly the weight pieces between one pressure point and the next without having to remove the bell jar. A device allowing the weights to be changed in the bell jar without breaking the vacuum reference pressure p_0 is described by Smart (1982).

The main reasons for comparing mercury manometers and pressure balances, which are the two basic types of primary pressure standards that can be characterized independently, are:

(a) The characterization of an unknown pressure balance over the overlapping pressure range, with the purpose of measuring the effective area of the piston-cylinder unit, instead of calculating it through dimensional measurements.
(b) The use of a specially selected transportable pressure balance as a transfer standard for the comparison of the pressure scale realized by mercury manometers existing in different laboratories.
(c) The study of some particular factors, which can affect the basic characteristics of a pressure balance (e.g., height dependence, frequency of piston revolution, differences between gauge and absolute modes, use of different gases, use of geometrically different weight pieces, which may add aerodynamic force components to the load).

It must be noted that some pressure balance parameter (for example, its effective area) may change with one or a number of the factors mentioned in point c above.

Such comparisons are performed to verify the uncertainty of the pressure scale, because any systematic error, not previously considered, inherent in instruments of both types should be made evident (point b above) and to evaluate nongeometric effects highly significant for the correct use of a pressure balance (point c above).

The comparisons are also useful to ameliorate (reduce the uncertainty) the pressure balances beyond the range of liquid-column manometers.

According to a general comparison procedure, the two instruments must be connected together by a sizable diameter tube (the internal diameter being generally greater than 10 mm) and the two systems must be carefully leak tested with a helium leak detector. The use of an appropriately filtered high-purity dry gas is mandatory.

The pressure balance is mounted together with the nominal-value weight pieces appropriate for the expected pressure value; the bell jar is positioned and sealed over the stack of weights. When the temperature of both systems is stable and the reference zero reading of the manometer is taken, both systems are slowly subjected to pressure. The bell jar of the pressure balance is then evacuated. The two systems are subsequently isolated from each other and the pressure balance is set in equilibrium. When the reference pressure on the pressure balance reaches the required value between 0.1 and 1 Pa and temperature is satisfactorily stable, the two systems are again put into communication; operation in both systems is constantly checked.

Before the two systems are in equilibrium, it is necessary to regulate pressure and isolation and reopening of the pressure line between the two systems may be required to repeatedly check their equilibrium. The residual standard deviation of each pressure measurement value obtained with the mercury column must not change when the pressure balance is compared with the manometer. If a change occurs, it may be that the pressure balance needs cleaning again or that its verticality has to be adjusted, or else the temperatures of the liquid manometer and of the pressure balance are not stable and uniform.

Some typical results of these comparisons between mercury manometers and pressure balances up to 120 kPa are reported here while in Chap. 11 information is given related to pressure comparisons in gas media obtained after the CIPM-MRA (1999).

A comparison was made in 1979 at NPL-UK (Peggs et al. 1979) between a mercury manometer and some pressure balances (four pistons and three cylinders making up four different units), with the purpose of verifying the pressure scale maintained at NPL over the range from 97 to 107 kPa. Nitrogen and helium were used as pressurizing fluids.

The average pressure difference, computed from the independent characterization of each system, between the two standards ($p_{\text{pressure balance}} - p_{\text{manometer}}$) was always positive and amounted to a maximum of +1.2 Pa for 383 observations distributed over the whole pressure range. The average random uncertainty was 0.12 Pa, so that the short-term random uncertainty of the comparisons can be estimated as being not too far from the random uncertainties of the manometer alone (0.05 Pa).

The NPL results show that the pressure difference values are pressure independent in the small tested pressure range from 97 kPa to 107 kPa. The results show as well that there is no significant dependence of pressure difference on the gas used, though larger pressure differences are generally to be found when nitrogen is used. The observed average pressure difference of +1.2 Pa (12 ppm at 100 kPa) is larger than expected, when compared with the average random uncertainties, but is within the total uncertainty of the comparison, calculated to be 14 ppm (1.4 Pa at 100 kPa).

Although these are good results, evidence exists of a sizable unknown systematic error, which is responsible for the +1.2 Pa maximum pressure difference. In order to find an explanation for this difference, the dependence of the effective area on piston fall rate, the use of weight carriers of different designs, temperature errors, and rotational effects were all carefully investigated without finding a satisfactory explanation of the pressure difference. It was eventually suggested that the reported mean pressure difference is correlated to a radial clearance change due to the tilt of the rotational piston axis with respect to the axis of the cylinder. However, no experimental data about tilt measurements have been reported.

The above results are, to some extent, characteristic of such comparisons; agreement is generally satisfactory, in the sense that the pressure difference is lower than the uncertainties, but frequently there is evidence of small systematic and unknown errors.

Another interesting international comparison of mercury manometers with the use of a transfer standard pressure balance has been organized by the Medium-pressure

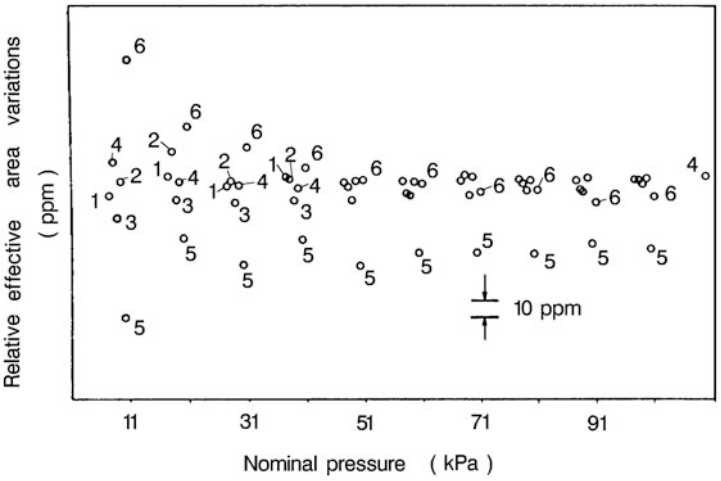

Fig. 7.29 Relative values of the effective area of a pressure balance transfer standard calculated from a comparison with six different manometers. (From Stuart 1989 by kind permission of the author)

Working Group of CCM in the pressure range (10–110) kPa, with NPL-UK acting as the pilot laboratory (Stuart 1989).

The transfer standard pressure balance was especially built in cooperation by NPL, NML, and NIST. It is equipped with a mechanism permitting the ring weight pieces to be changed without breaking the vacuum reference pressure and the piston can be put in rotation by means of an external device with negligible temperature variations. The transfer standard is equipped for the measurement of temperature and of the vacuum reference pressure required for accurate pressure calculation. The effective area of the transfer standard, checked by the pilot laboratory, resulted stable within 0.6 ppm over several years of use.

The participants in the exercise were asked to compare the pressure values obtained with the transfer standard when using some preestablished weight pieces with the values obtained by means of their mercury manometers in absolute mode and optionally in gauge mode. In the calculations, all the pressure values are to be corrected with reference to 20 °C and to the standard acceleration of gravity. The pilot laboratory can thus compute the effective area of the transfer standard and use this value to compare the results of the different participants.

The average results of this intercomparison are given in Fig. 7.29 and show the following:

- The effective area differences are much higher than the typical uncertainty of the manometers and pressure balances of participants and also much higher than the type A (repeatability) uncertainty of participants.
- The repeatability of results improves at higher pressures, which is typical for a pressure balance.

- There is no variation of effective area with pressure, so it is confirmed that the pressure distortion coefficient of the transfer standard pressure balance is equal to zero.
- There is no evidence of effective area variation with time.
- Evidence exists, in some cases, of pressure-proportional systematic errors (see results 5 and 6 in Fig. 7.29) and also of drift errors.

At 100 kPa the results of some laboratories are in agreement to within ±5 ppm, but there are others in which systematic divergences as high as 40 ppm can be observed.

This exercise proves very useful for the verification of the pressure scales maintained in different standards laboratories; by the end of the comparison, a reason for some systematic deviations in respect of the average may be discovered. This comparison will also be useful to verify if there is a consistent difference in effective area of the transfer standard between absolute and gauge modes. The papers by Perkin et al. (1998, 1999) give a full analysis of the results. In absolute mode, the maximum difference between any two laboratories varies from 16 ppm at 11 kPa to 45 ppm at 101 kPa: these differences are greater than the combined uncertainty of participants. Similarly, in gauge mode the maximum difference amounted to 70 ppm at 21 kPa to 35 ppm at 101 kPa.

Cause of errors were found to be related to thermometer instabilities and calibration of Pirani gauge used to measure the reference pressure in absolute mode, even if the size of errors cannot be a reason for the large disagreement reported. The results show as well that there was no consistent variation of effective area with pressure (pressure distortion coefficient equal to zero) but evidenced a difference between the results obtained in absolute mode and those in gauge mode. NIST investigated the reasons of this difference and concluded that it may be the cause of aerodynamic effects on the spinning weights.

More recent comparisons activities between pressure balances of large diameter (50 mm) and mercury-column manometers in absolute mode, e.g., as described by Otal et al. (2008), produced much better and consistent results. The standard uncertainties of mercury column was $0.03\ \text{Pa} + 5.5 \times 10^{-6}\ p/\text{Pa}$ and $0.12\ \text{Pa} + 5.0 \times 10^{-6}\ p/\text{Pa}$ for the pressure balance. The comparison results are extremely good as the relative pressure difference of the two standards is always lower than 4 ppm in all the absolute pressure range from 10 to 100 kPa. Such results are of the same order of magnitude as previous results (1986) obtained in gauge mode.

It is interesting to note that pressure comparisons have also been made for new nonrotating pressure balances (FPG type) and liquid manometers (Girard 2003). The FPG pressure balance was compared in absolute mode to oil manometers from 10 to 100 Pa and to mercury manometers from 100 to 10 000 Pa. The pressure differences are extremely small (below 10 mPa at 100 Pa to below than 50 mPa at 10 kPa) and well within the estimated standard uncertainty of the liquid manometers.

The effective area of a pressure balance obtained from dimensional measurements or by cross-floating against mercury or liquid manometer is normally assumed to be invariant within the uncertainty of its determination. In recent years, some results showed the possibility of reducing the uncertainty of pressure measurements with pressure balances to few ppm (generally below 5–10 ppm).

More investigations have been carried out in order to verify whether the effective area of a pressure balance is really invariant when the pressure balance is used under different conditions (at different heights, with different frequency revolutions of the piston, in absolute or differential mode, with different weight-piece geometries) and with different gases.

Information in connection with these tests is very important, particularly when a pressure balance is to be used when the required uncertainty in pressure determination is of few ppm, that is, of the same order as the pressure uncertainty when measurements are made with mercury manometers.

That present technology can produce piston-cylinder of high geometric regularity is demonstrated, as already cited, by Legras et al. (1986) at LNE, who investigated different piston-cylinder units of nominal effective area of 10 cm^2 for gauge pressure measurements from 10 to 400 kPa. In these units, the dimensional profile of tungsten carbide pistons and cylinders is constant within 100 nm. The uncertainty of their diameter values is 40 nm and the diameter clearance of the piston-cylinder is typically from 500 to 700 nm.

With the use of such pressure balances, the uncertainty of the pressure value was estimated to be $0.3\ \text{Pa} + 4.4 \times 10^{-6}\ p/\text{Pa}$ for the 10–400 kPa pressure range. The largest contribution to the pressure uncertainty is due to the effective area whose uncertainty contributes with 4 ppm. The calculation of the overall standard uncertainty (Legras et al. 1986) is based on the quadratic combinations of all uncertainty contributions.

One of the selected units was compared, in the 10–90 kPa pressure range, in gauge mode and with nitrogen, with a mercury column with which a pressure uncertainty of $0.2\ \text{Pa} + 5.0 \times 10^{-6}\ p/\text{Pa}$ can be achieved (Riety and Legras 1987; Riety 1987). On the average, in the 10–90 kPa range, pressure differences between the pressure balance and the mercury manometer were of the order of 0.2–0.3 Pa. Pressure differences show no systematic pressure effects and are inside the uncertainty of both instruments over the whole pressure range considered. These results show the excellent compatibility between the two primary instruments characterized metrologically in an independent way, when they are used in gauge mode and with nitrogen.

A similar experiment was performed at NIST by Welch et al. (1989b) with the calibration of two absolute pressure balances in nitrogen against their capacitance/gauge-block manometer (see Sect. 7.1.2.3). The effective areas of the two pressure balances were determined with a root-sum-squared 3σ uncertainties of 3 and 4.18 ppm, respectively; a very good result, which allows the pressure scale based on pressure balances to be substantially improved.

Another important measurement was made at PTB by Klingenberg and Lüdicke (1991), who measured the effective area of two 10 cm^2 piston-cylinder units in tungsten carbide from dimensional measurements and from pressure comparisons against the standard PTB mercury manometer. For each piston-cylinder unit, about 5 000 data points were collected from the dimensional measurements of the effective area (relative standard deviation of the effective area was 6 ppm). Each piston-cylinder unit was also compared against the PTB mercury manometer up to about 0.19 MPa and the effective area of each unit was determined (relative standard deviation of

the effective area was 4 ppm). The ratio of effective areas of the two units was also measured up to 1 MPa by a direct cross-floating, and this ratio was found in good agreement with the previously measured one at 0.19 MPa by mercury manometer comparison. Due to this accurate work, the estimated uncertainties (at 3σ level) with these pressure balances at 1 MPa were estimated to be 11 or 19 Pa if only dimensional analysis is performed.

Extensive work in this area is carried out at NIST, with a large variety of pressure balances being compared with their ultrasonic mercury manometer (see Sect. 7.1.2.5) and also with the capacitance/gauge-block mercury manometer. This work is fairly comprehensive, since the comparison is made in gauge and absolute modes, with the different parameters caused to vary, and with the use of different gases.

A first series of results (Tilford 1988; Tilford et al. 1988, 1989) have been obtained in the 5–160 kPa pressure range by comparison of several pressure balances and the NIST ultrasonic mercury manometer. It has been observed that for several pressure balances the effective area value depends on the pressure value, on the gas used and/or on the mode of operation. The change in the effective areas of some of the pressure balances was as large as 25 ppm, while with others random area changes of 2–4 ppm were observed, which are typical values for such comparisons. The study was made in absolute mode (p_0 from 0.2 to 0.5 Pa) and in gauge mode with an established reference pressure of 93 kPa. Nitrogen, helium, and argon were used as pressurizing fluids.

The investigation was first directed to the possible influence of piston height in respect of the cylinder on the effective area of the pressure balance. This is a "geometric" effect, as it is due to imperfections in both piston and cylinder, and may be equivalent to as much as 5 ppm for a height excursion of about 18 mm. But, as Fig. 7.30 shows, with some pressure balances also a larger change has been observed, which may be also dependent on the applied pressure.

As this large change in the effective area (often corresponding to 10–25 ppm for pressures from 5 to 130 kPa) is pressure dependent, it cannot be related to alterations in piston-cylinder geometry because in the considered pressure range elastic distortions do not affect the effective area significantly.

This large effective area variation must be due to changes in gas-piston interaction in the piston-cylinder clearance. The global change in the effective area caused by height variations can be reduced by operating at a well-selected and fixed height, but the mentioned pressure dependence effect, which is the largest of the systematic components under observation, still needs an explanation and cannot be corrected.

Another important factor, not to be overlooked for a correct use of a pressure balance, is the possible effect of hydrodynamic forces on the piston, which are due to the rotational frequency of the piston and, possibly, to the rotation direction. This effect is probably caused by nonuniform piston-cylinder clearance, a nonvertical piston rotation axis, and by nonconcentric weights to the rotation axis. In some commercial units, the rotation frequency of the piston is as high as 19 Hz, whereas it is from 1 to 4 Hz in normal operation. As a rule, in the absolute mode the rotational frequency effect is moderate (few ppm in effective area changes), though in some

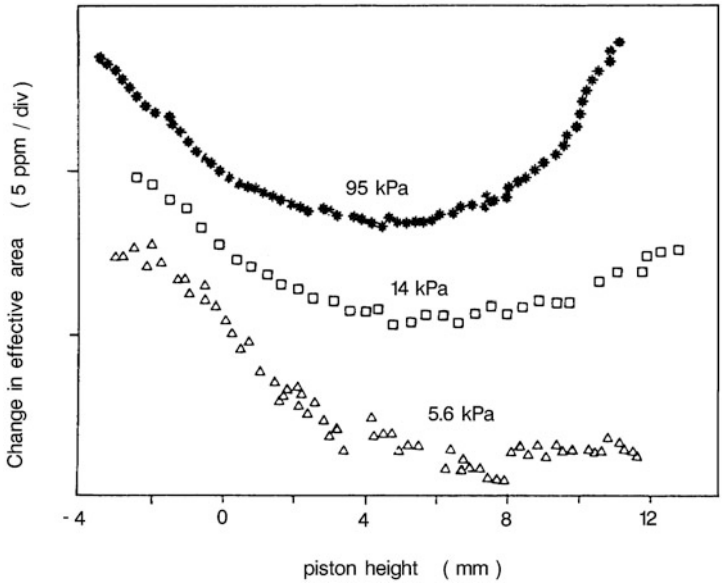

Fig. 7.30 Change in the effective area of a pressure balance as a function of the piston height (absolute mode, nitrogen) for three different pressure values. (From Tilford et al. 1989 by kind permission of the authors)

cases a noticeably different behavior, particularly at low frequencies, may be observed for different directions in piston rotation. This effect is large, sometimes amounting to 40 ppm, in the gauge and differential modes. Results obtained at NIST confirmed that it varies quadratically with the rotation speed, particularly at high frequencies (Sutton 1979). At a fixed rotation speed, the magnitude of this effect is gas dependent, smaller with helium and larger with nitrogen and argon; it varies linearly with the gauge reference pressure and is a function of the outer diameter of the weight pieces.

All these contributions must be taken into account if a pressure balance is to be used when the uncertainty of the pressure value has to be less than 20 ppm. Other investigations at NIST brought into evidence large changes in the effective area at low pressures in absolute mode and showed that in the differential mode effective areas are systematically lower, sometimes by 6 ppm, than in the absolute mode (Welch et al. 1985, 1989a; Tilford et al. 1989). The magnitude of this difference depends on the gas used and on the specific type of piston-cylinder unit. Up to now it is difficult to correlate the observed differences with a particular geometry of the piston-cylinder unit.

Figure 7.31 shows a typical example of the change in the effective area when the pressure balance is used in different operation modes and with different gases.

Similar effects on the effective area, associated with the use of different gases, were also observed when employing gauge piston-cylinder units of the simple type (Maghenzani et al. 1987) and of the controlled-clearance type (Sharma et al. 1989).

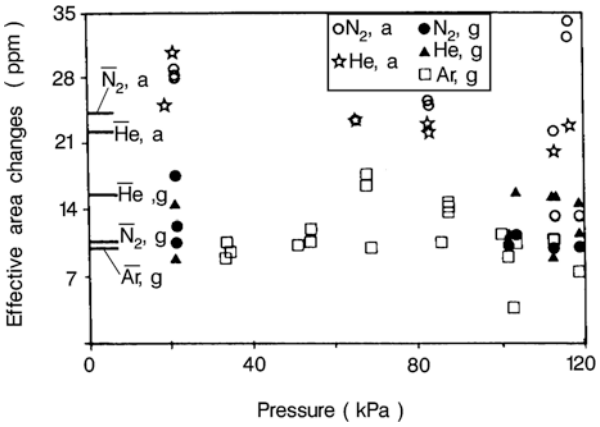

Fig. 7.31 Changes in the effective area of a piston-cylinder unit in absolute (a; ○, ☆, . . .) and gauge (g); (●, ▲, □) modes for different gases. ($\overline{H_e}$,a) is the average value of different determinations obtained in helium and in absolute mode

Meyer and Reilly (1993/1994), at NIST, also investigated the gas (H_2, ^3He, ^4He, N_2, CO_2, and SF_6) dependence for the absolute mode effective area of a pressure balance used from 1.4 to 103 kPa (^3He) and up to 162 kPa for the remaining gas. Variations in area were compared in respect of N_2 and the effective area differences amounted to 26 ppm at 1.4 kPa, only 4 ppm at 45 kPa, and from 100 to 162 kPa the difference was within the resolution of measurements (from 6 to 7 ppm).

Other consistent activity was made at NIST by Schmidt et al. (1993, 1993/1994, 1999a) who studied the effect of the rotational drag in different modes of operation and for different gases. A preliminary model was used to study the rotational dissipation in the piston-cylinder clearance and significant differences were observed for different gases and for different modes of operation. A special three-pressure balances device was created in order to supply data and a model for the gas flow in the crevice (of 1.61 μm) was used. While the model works well to explain the gas species effects for N_2 and He in absolute mode, it predicts a mode effect that is not fully discernable from the experimental data obtained. Lastly, in Schmidt et al. (1999a) the model is examined for drag forces in the clearance on pressure balances when they are used in the viscous-flow (gauge mode) and in the molecular-flow regimes (absolute mode).

The model indicates that the effective area of a pressure balance should vary with viscosity and molecular weight of the used gas. The model was used to verify differences in effective area as reported by Welch et al. (1989) and it explains rather well the large shift with gas species in both gauge and absolute modes, but is unable to explain the magnitude of such shift in effective area between the gauge and the absolute modes. The difficulty is also due to the fact that in the vertical clearance of the piston-cylinder unit there is a pressure distribution that moves from the viscous flow to the molecular one depending on the pressure value and on the gas used.

So far, even if there have been substantial improvements in the prediction of gas and modes effect on the effective area of a pressure balance, still there is not a fully satisfactory theory capable of explaining some large differences particularly between absolute and gauge modes, and also in some cases such differences have

not been reported by experimental data. In this context, it is useful that the Sharipov (2011) paper uses an equation based on rarefied gas flow and not the usual viscous flow equation. At PTB Sabuga et al. (2011d), considering that the gas flow in a gap of a piston-cylinder used in absolute conditions can be partially in molecular regime, partially in transition regime, and partially in the viscous regime, adopted a rarefied gas flow model in gauge and absolute modes (Sharipov 2011) to different piston-cylinder units (10 and 20 cm^2) in order to determine the effective areas well known from dimensional measurements for different gases. The result confirms that for large effective areas (>10 cm^2) the effect of flow regime and gas type should be considered if the uncertainty of pressure measurement is of the order of few ppm and if absolute mode is considered. Effects depend on different pressure distributions in the clearance combined with the nonperfect cylindrical shape of the piston. On the reverse, for piston-cylinder units with $h/r \leq 10^{-4}$ where h is the gap width and r is the radius of the piston, the effect of changes of viscous force due to different flow regime, operation mode and gas produce negligible changes on effective area, typically lower than 3×10^{-7}.

Other important parameters that are necessary to measure and to check from time to time on a pressure balance when the lowest uncertainty levels are required, are the possible *electrostatic charges* and *surface magnetization* effects that can be produced on the piston-cylinder unit.

Electrostatic charges may be produced in the weights of a pressure balance and in the Plexiglas cover of some bell jars of absolute systems and can be measured with resolution of ±25 V. These can deteriorate the reproducibility of a pressure balance, a detrimental effect generally brought into evidence particularly during cross-floating. The best solution is to avoid any plastic or Teflon cover or stopping rings; instead, the use of glass bell jars is highly recommended. It is also important to earth the base and the bell jar of a pressure balance with appropriate metallic nets and wires.

Surface magnetization can be generated in piston and cylinder especially if they are of tungsten carbide. Surface magnetization can be measured with Hall Effect probe whose typical sensitivity is of few $\mu V/10^{-2}\ A^{-1}$ m. It is good practice to measure at regular intervals the surface magnetization of the piston and cylinder, as well as of some parts of the piston-cylinder assembly, and to demagnetize them if the measured magnetic field is greater than 500 A m^{-1}.

Experience has shown that, although such parameters are important and must not be neglected for an appropriate use of a pressure balance, they do not significantly contribute to possible systematic errors in the pressure measurement. Electrostatic charges and surface magnetization are more important with gas absolute pressure balances of typical 130 kPa full scale than in other cases. Our experience concerning gauge pressures of 5 MPa (Maghenzani et al. 1987) showed that such effects can be easily kept under control and appropriately reduced to an insignificant level.

All published results generally demonstrate that the changes observed in effective area of a piston-cylinder unit of a pressure balance are not due to geometric irregularity in the piston-cylinder unit; instead they are likely to be due to changes in the interactions between the piston and the pressurizing gas in the clearance.

If pressure balances are to be used at the ppm pressure uncertainty level, all these effects should be appropriately evaluated and taken into account. A satisfactory

theory is not yet fully available to explain the possible force or momentum transfer between the gas and the piston under all conditions of use, and its dependence and magnitude on the pressure gradient in the clearance and on the type of gas used.

7.2.7 What Future for Primary Pressure Standards?

In the preceding sections, the discussion has been largely concentrated on the improvement of mercury-column manometers for absolute and gauge pressure measurements to 360 kPa and of pressure balances for absolute pressure measurements to 5 MPa and gauge pressures to 100 MPa.

It has been pointed out that there is a tendency to reduce the uncertainty of pressure measurements in gas to few ppm for both these types of primary instruments to about 200 kPa and only for pressure balances to an uncertainty level below 15 ppm with pressures reaching 100 MPa.

As regards mercury-column manometers, it is difficult to predict a future substantial reduction in the uncertainty of pressure determinations and an uncertainty of few ppm will be considered a good result. Its achievement will require the use of instruments of extremely high technological quality and of systems appropriately equipped and carefully maintained (see Sect. 7.1.2) to measure all the associated influence parameters together with the application of automatic techniques, for example, the use of laser and ultrasound interferometers for height determination. It is not to be forgotten, either, that certified reference mercury of known density should be available for wide distribution. One of the major problems is the care needed to preserve the mercury from contamination and the associated safety problems for handling mercury.

With pressure balances too, it has been demonstrated that it is possible to reduce uncertainty to a few ppm level in moderate-pressure ranges (generally below 1 MPa), when they are used in a specified operating condition and with a specific gas. Pressure balances can approach the accuracy of mercury columns only if due account is taken of different parameters or operating conditions (use of different gases, absolute and gauge mode differences, a possible hydrodynamic effect of weights, frequency of revolution of the piston, electrostatic charges, surface magnetization, ...) and if their effects are completely understood and minimized. A better theory explaining the interactions between the piston-cylinder and the molecules of the pressurized gas in the piston-cylinder clearance is necessary.

Lower uncertainty will also imply further improvement of the present technology for the fabrication of pistons and cylinders, to obtain roundness and profiles of the diameters constant to better than 100 nm.

With pressure balances to be used at higher pressures, uncertainty reduction implies better knowledge in the determination of the coefficient of piston and cylinder distortions due to pressure application, as well as a better theory for the calculation of effective area changes with pressure.

Improved pressure balances allowing a substantial uncertainty reduction at few ppm levels are:

- Equipped with automatic mass handling (e.g., Woo et al. 2005; Girard et al. 2006).
- Using piston-cylinder devices that are extremely stable in time (e.g., Legras 1993/1994; Sabuga et al. 2011a).
- Equipped with computerized techniques for handling real time calculation of pressure measurements (e.g., Simpson 1993/1994; Poirier 1999; Caravaggio et al. 2009).
- In some cases, only for higher pressures, they have the possibility of directly measuring the piston-cylinder distortions (e.g., Idowu 1999; Moisoi et al. 2005).
- Using large-diameter (35 or 50 mm) piston-cylinder units, carefully machined at better than 100 nm level.
- Care and specific attentions are paid to harmonic oscillations of piston in the cylinder (e.g., Sutton and Fitzgerald 2009).

The primary standards of both types will play an active role in the future. Liquid-column manometers are expected to be preferred for the smaller measurement pressures (10–100 kPa) even if for this pressure range the nonrotating pressure balances are also available today. Pressure balances for gas pressure measurements are also expected to be available to a few ppm uncertainty for absolute and gauge pressure measurements up to 10 MPa and with a small uncertainty change, 8–10 ppm, if the pressure range is extended to 100 MPa.

One of the major efforts in pressure metrology is linked to the Boltzmann constant determination where there are great expectations particularly for temperature metrology (e.g., Jones 2009). For a determination of the Boltzmann constants, different approaches are on the way using different acoustic thermometry techniques at NIST (Moldover 1997; Schmidt et al. 2006, 2011; Moldover 2011) and other national laboratories in France, United Kingdom, and Italy.

For the determination of the Boltzmann constant by the dielectric-constant gas thermometer technique, pressure standard measuring absolute pressure in helium up to 7 MPa with a relative standard uncertainty of 1 ppm are required (Zandt et al. 2009; Fellmuth et al. 2009; Sabuga 2011c). At PTB this approach is followed with a set of pressure balances (20 and 2 cm^2 effective areas) carefully measured dimensionally and evaluated by improved numerical calculations for their distortions under a EURAMET Project 1039. The pressure balances of 2 cm^2 will be linked by cross-floating to the set of pressure balances of 20 cm^2 effective area, assuring a consistency of results well within 1 ppm (Sabuga 2006; Sabuga et al. 2011a, b).

For the determination of pressure using the acoustic technique of NIST, starting from the very accurate quantum-mechanical calculation of the equation of state of helium it is possible to derive the thermodynamic pressure close to 7 MPa with an estimated uncertainty close to 1 ppm (Moldover 2011). Schmidt et al. (2011) report progress in developing a pressure standard based on the measurements of resonance frequency of a microwave cavity filled with argon at specific temperatures. The pressure standard will be operative from 0.2 to 5 MPa and will rely on the experimentally measured ratio $R(p)$ of refractive index of argon to refractive index of helium. This ratio was measured by resonant frequency measurements in two cavities (one filled with argon and the other with helium) at same pressure and temperatures with an estimated uncertainty of 5×10^{-9}. Using the obtained values

Table 7.2 Pressure measurement uncertainty with a mercury column manometer. Absolute pressure measurements at a full scale of 100 kPa (nitrogen medium)[a]

Parameter	Uncertainty of the parameter for three different cases and contribution of the parameter to pressure uncertainty		
Mercury density	0.02 kg m^{-3}	0.1 kg m^{-3}	1.0 kg m^{-3}
	1.5 ppm	7.5 ppm	75.0 ppm
Mercury thermal expansion	2×10^{-7} K^{-1}	2×10^{-7} K^{-1}	2×10^{-7} K^{-1}
	0.1 ppm	0.1 ppm	0.1 ppm
Temperature	5 mK	20 mK	0.1 K
	1 ppm	4 ppm	20.0 ppm
Gravity acceleration	2×10^{-6} m s^{-2}	1×10^{-5} m s^{-2}	1×10^{-4} m s^{-2}
	0.2 ppm	1.0 ppm	10.0 ppm
Height	1 µm	10 µm	0.1 mm
	1.3 ppm	13.0 ppm	130.0 ppm
Aerostatic head (referred to 750 mm)	0.2 mm	2 mm	20.0 mm
	0.03 ppm	0.3 ppm	3 ppm
Gas density (referred to 750 mm)	0.01 Kg m^{-3}	0.1 kg m^{-3}	0.1 kg m^{-3}
	0.8 ppm	8 ppm	8 ppm
Vacuum reference pressure	0.02 Pa	0.2 Pa	1.0 Pa
	0.2 ppm	2 ppm	10 ppm
Total pressure uncertainty[b]	0.8 Pa	5.3 Pa	45.7 Pa
	equivalent to 8 ppm at 100 kPa	equivalent to 53 ppm at 100 kPa	equivalent to 457 ppm at 100 kPa

[a] See Appendix E, Tables E.2 and E.3
[b] Account is taken of only the listed systematic uncertainties at the pressure of 100 kPa

of $R(p)$ and the helium refractive index, it is possible to reach a totals relative pressure uncertainty of 2.3×10^{-6} (p/MPa) + 2.1×10^{-6} + 0.8×10^{-6} (p/MPa).

Another approach is related to the experiment aimed to use pressure metrology to determine the Planck constant in the watt balance experiment as proposed by Sutton et al. (2010, 2011). In this case, the use of the pressure balance will be related to its short-term repeatability allowing two pressure balances to act as a mass comparator with an estimated uncertainty of 1×10^{-8}.

If this effort will be successfully reached, it will not only constitute an important advance for the determination of the Boltzmann constant or Planck constant and for temperature and mass metrology, but it will also generate important advances to pressure metrology with the possibility of achieving a 1 ppm uncertainty for absolute gas pressure measurements up to 7 MPa with primary standard pressure balances and to assess as well the short-term repeatability using pressure balances in a typical cross-floating experiment.

7.3 Summary of Typical Uncertainty Levels for Liquid-Column Manometers and Pressure Balances

In this section the typical conditions are summarized, to be used only as general examples, which are necessary to obtain a specific pressure uncertainty when liquid-column manometers and pressure balances are used.

Table 7.3 Pressure measurement uncertainty with a pressure balance. Gauge pressure measurement at a full scale of 5 MPa under the same conditions indicated in Appendix F—Table F.4[a]

Parameter	Uncertainty of the parameter for three different cases and contribution of the parameter to the pressure uncertainty		
Masses (10-kg case)	6 mg 0.6 ppm	60 mg 6.0 ppm	0.6 g 60.0 ppm
Gravity acceleration	2×10^{-6} m s^{-2} 0.2 ppm	1×10^{-5} m s^{-2} 1.0 ppm	1×10^{-4} m s^{-2} 10.0 ppm
Air density	$\delta\rho_a/\rho_a = 0.3$ % 0.5 ppm	$\delta\rho_a/\rho_a = 3$ % 5.0 ppm	$\delta\rho_a/\rho_a = 3$ % 5.0 ppm
Density of the masses	1 kg m^{-3} 0.02 ppm	10 kg m^{-3} 0.2 ppm	10 kg m^{-3} 0.2 ppm
Effective area	8.0 ppm by pressure cross-floating	30.0 ppm by dimensional measurements	200.0 ppm by pressure cross-floating
Pressure distortion coefficient	$\delta\lambda/\lambda = 20$ % 3.0 ppm at 5 MPa	$\delta\lambda/\lambda = 50$ % 7.5 ppm at 5 MPa	λ not considered 16.0 ppm
Temperature	0.06 K 1.0 ppm	0.1 K 1.8 ppm	1.0 K 18.0 ppm
Temperature coefficient of the piston-cylinder	5 % 1.0 ppm	20 % 4.0 ppm	50 % 10.0 ppm
Aerostatic-head correction for a level difference of 200 mm at 5 MPa	$\delta\rho_f = 0.01$ kg m^{-3} also compressibility is considered $\delta h = 0.2$ mm 0.23 ppm at 5 MPa	$\delta\rho_f = 0.1$ kg m^{-3} also compressibility is considered $\delta h = 2.0$ mm 0.5 ppm at 5 MPa	Aerostatic-head correction not considered $\delta h = 200$ mm 22.0 ppm at 5 MPa
Total pressure uncertainty[b]	130 Pa equivalent to 26.0 ppm at 5 MPa	485 Pa equivalent to 97.0 ppm at 5 MPa	3.18 kPa equivalent to 636.0 ppm at 5 MPa

[a] See Appendix F, Tables F.2, F.3 and F.4

[b] Account is taken of only the listed systematic uncertainties at the pressure of 5 MPa

In the following tables (Table 7.2 for a mercury manometer and Table 7.3 for a pressure balance), the reported parameters are the main and most important systematic physical quantities affecting the uncertainty of the pressure value.

The "A"-type uncertainties (see Appendix E, Document E.1) are not considered in the following tables, but are discussed in Appendices E and F.

The pressure uncertainty, presented in Tables 7.2 and 7.3, is obtained by the root-mean-square combination of all the systematic components (see the parameter column in the tables). See also Sect. 7.1.3.5 for liquid manometers and Sect. 7.2.4 for pressure balances.

Chapter 8
Pressure Transducers for Gaseous Media

In this chapter, an analysis will be made of the different pressure transducers for gas-static pressure measurements in the pressure ranges from 100 Pa to about 100 MPa, close to the ranges considered for absolute, gauge and differential pressure measurements in previous Chap. 7.

Many of these transducers can work as well in liquid media, but some, particularly those for absolute pressures typically between 100 Pa and some megapascal, are designed for operation only in gas media.

A difference between pressure measurements performed in gas media and in liquids is caused by the different adiabatic compressibility of the media, which during rapid pressure variations produces changes in the transducer temperature and consequently, in its metrological characteristics.

Although the relation between the output of the transducer and the applied pressure is often calculable, as a rule it cannot be estimated with sufficient accuracy. Consequently, transducers need calibration against a primary or secondary standard, appropriately selected as to accuracy and the pressure range. Calibration is necessary for the determination not only of the basic relations between the output signal of the transducer and pressure, but also in order to derive all the metrological characteristics of a transducer: sensitivity, reproducibility, repeatability, linearity, hysteresis, short-term stability, medium- and long-term stability (see Glossary in Sect. 8.5 and Appendix H and the example of the Calibration procedure in Sect. 8.6). For more information on the terminology used to describe the metrological characteristics of a pressure transducer and general laboratory experience regarding pressure measurement systems, the reader is referred to specific texts (e.g. Neubert 1975; Doeblin 1975; Soloman 2009) and also to the section "Further Readings" in the present book.

Many published review papers have already described innovative pressure sensors and general trends, while considering the measurement problems involved in a specific area of application (Alberigi Quaranta 1975; Alberigi Quaranta et al. 1980; Jordan 1985; Jones 1987; Asch 1982; CRIAI 1989; Peggs 1983).

As a reference list documenting the different types of pressure transducers is very long and would take too much room in this book, only some references are cited: Prudenziati et al. (1986) and Middlehoek et al. (1987) for some piezoresistance pressure transducers; Gambling (1987) for optical fibre pressure transducers; Peggs (1983)

F. Pavese, G. Molinar Min Beciet, *Modern Gas-Based Temperature and Pressure Measurements,* International Cryogenics Monograph Series,
DOI 10.1007/978-1-4419-8282-7_8, © Springer Science+Business Media New York 2013

for electrical resistance, ultrasonic, resonant-cavity pressure transducers; Eaton and Smith (1997) for micro-machined sensors; Hyland and Shaffer (1991) for capacitance diaphragm transducers. Many papers related to innovative pressure transducers have been presented at IMEKO TC16 Symposium in China (Zhaohua et al. 2003; Shangchun et al. 2003; Nagashima 2003; Ruifeng et al. 2003; Meiyan et al. 2003). More titles can be found in the "List of References" and "Further Readings" at the end of this book.

Pressure sensors of a large variety and based on different principles are now available. Most of them are suitable for specific applications (different temperature ranges, vibrations, corrosive fluids, nuclear radiations,...) over different pressure ranges and may have quite different measurement uncertainties depending also on individual transducer.

In the last 20 years we have witnessed, in particular, the evolution of the "smart sensors" (Favennec 1987; Document CIAME 1987; Soloman 2009), in which a sensor is connected to some electronics or to a microprocessor for the acquisition and conversion of the digital output signal, and for the electronic computation of all the relevant parameters or quantities affecting the characteristics of the transducer, including its calibration.

Owing to the different measurement techniques now applicable, a detailed analysis of all pressure transducers for any range and application would require a full separate book.

In the different sections of the present chapter, only pressure transducers used as transfer standards for gas pressure measurements of interest in gas-based types of thermometry and in top-level manometry applications will be discussed.

Still in the light of the aim of this book, of such transducers, only those allowing pressure measurements to be carried out with the lowest possible uncertainty when used as pressure transfer standards or those which can work in a cryogenic environment are considered.

Pressure transfer standards are measuring systems of a high technological level; they consist of sensors and the related electronic hardware for output signal conditioning, are compatible with computers for rapid data acquisition, and have excellent (medium-to-high) metrological characteristics, particularly as regards resolution, repeatability, reduced hysteresis, and long-time stability.

The typical uncertainties of pressure measurement values achievable with quality transfer standard are the following:

- For absolute pressure measurements, from 1×10^{-3} (in the 100 Pa to 10 kPa range) to 100 ppm (approximately in the range from 10 kPa to about 10 MPa).
- For gauge pressure measurements, from less than 100 ppm (in the 0.1–10 MPa range) and, typically approximately from 200 to 300 ppm (in the 10–100 MPa range).
- For differential pressure measurements the uncertainty, typically of the order of 1×10^{-3}, depends very much on the differential pressure range and as well on the line pressure value.

The above uncertainty values obviously are obtained only after calibration and generally combine the contributions of the repeatability, hysteresis, long-term stability, residual standard deviation of the calibration equation, and the uncertainty of the primary standard used for calibration (see Sect. 8.6).

Pressure transfer standards are frequently used for high-accuracy pressure measurements, like those in gas or vapor pressure thermometry. For such uses, the transducers must be frequently calibrated against the primary standard. They can also be used for pressure measurement comparisons between laboratories, when the primary standards are not transportable, as it is often the case. More commonly, they are employed to calibrate other pressure measuring devices or transducers for industrial applications of generally less demanding uncertainty. On the other hand also in the last 10 years, different pressure "*calibrators*" were made commercially available. These instruments are on one hand pressure generators and on the other they are transducer-based instruments, where the reference transducers are selected for their optimum stability and superior metrological characteristics, designed for the calibration of other pressure instruments. They have as well the basic characteristics of being digital indication instruments, frequently used for direct measurements and as pressure transfer standards for comparison purposes in a wide range of the pressure scale (Chap. 8 of Anderson et al. 2005; Simon and Pinot 1992).

The following sections will be devoted to an analysis of pressure transducers used as transfer standards in gas media for the following ranges and applications:

- Absolute and gauge pressure measurements below 120 kPa.
- Gauge pressure measurements from few kilopascal to 100 MPa.
- Differential pressure measurements with transducers used as null detectors.
- Pressure measurements in cryogenic environments.

8.1 Transfer Standards for Absolute Pressure Measurements Below 120 kPa

In the range between 100 Pa and 120 kPa, absolute pressure measurements are essential for scientific and technological applications. The measurement of atmospheric pressure is fundamental in mass, density, and dimensional metrology. Besides, in this range most of the gas-based thermometries require, as discussed in Part I, that pressure should be determined with the lowest possible uncertainty. The required uncertainty of pressure determinations around the atmospheric pressure in such top-level applications ranges typically from 1 to 10 Pa.

There exist several areas of application (meteorology, altimetry, avionics and space, wind tunnels,. . .) where pressure has to be measured with transducers of comparable accuracy, sensitivity, and stability.

A large variety of sensors and transducers have been developed, and are now commercially available, to meet the needs of absolute pressure measurement in this range.

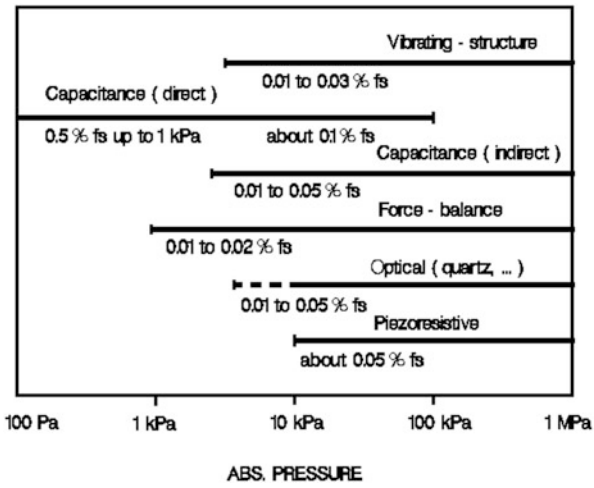

Fig. 8.1 Typical measurement uncertainties and pressure ranges (log scale) for various types of transfer standard transducers for absolute pressure measurements from 100 Pa to 1 MPa

Pressure transducers are sensitive to the force generated by the applied pressure. The force produces a measurable mechanical deflection of a structure or measurable strain or stress changes in the structure, which are then correlated to pressure by specific individual calibration.

As a rule, transducers are strongly affected by temperature, which consequently must be carefully measured during calibration and appropriately taken into account in the normal use of the transducer. Temperature variations may affect transducer readings through the thermal expansion of the mechanical structure of the instrument and of the pressurizing fluid. Temperature variations are caused not only by changes in ambient temperature but also by adiabatic heating and cooling during pressure changes; this effect has also to be accurately evaluated during transducer calibration.

The typical uncertainties and pressure ranges of various types of commonly used, commercially available, absolute transfer standards are illustrated in Fig. 8.1.

A transfer standard must have good resolution and the transducer types in Fig. 8.1 have all a typical resolution from few ppm (which is equivalent to pressure resolution of 0.1–1 Pa at 100 kPa) to 100 ppm (10 Pa at 100 kPa), depending on the pressure range and on the specific type of instrument.

From the standpoint of the various operating principles these transducers can be grouped as the following:

- *Piezoresistive transducers*. Piezoresistive transducers exist in several configurations. Strain in the mechanical structure, which can have different shapes according to the different pressure ranges, is detected by different means and techniques (e.g. strain gauges bonded or evaporated as thin films on the metallic structure, or deposited as thick film on ceramic structures; integrated semiconductors or micro-machined structures). The characteristics of such transducers depend to a large extent on the design of the transducer; the uncertainty in pressure determination usually ranges from 1 % to close to 0.01 %. This wide difference is generally caused by the mechanical design of the sensor, by thermal

compensation, and, sometimes, by electronic signal processing. Such transducers generally exhibit marked hysteresis, particularly when they are used at pressures higher than 1 MPa.

- *Optical transducers*. The deflection or rotation of the mechanical structure is measured by means of an optical system, which is generally servo controlled by means of a force-balancing device. Usually, quartz is the material of the sensor.
- *Force-balance transducers*. The mechanical movement of the sensor is balanced by electromagnetic forces producing an electrical signal proportional to the electromagnetic force used to maintain the sensor in equilibrium. With fused quartz-Bourdon tube transducers, instabilities lower than 0.01 % per year have been reported. The type of pressurizing gas used has to be considered carefully. With helium, very large drift has been observed when pure quartz-Bourdon tubes are employed.
- *Capacitance transducers*. They can be based on the direct measurement of voltage or capacitance variations produced in the sensor by pressure application, or through the change of capacitance inside a resonant circuit whose resonance frequency is measured and is proportional to the applied pressure. These systems are highly temperature-dependent, though with some types the temperature coefficient is only about 10 ppm $^{\circ}C^{-1}$. The measurement uncertainty depends on the pressure range and on the individual transducer, as large differences have frequently been observed between transducers of the same model.
- *Vibrating-structure transducers*. They sense the stress produced by pressure application in a resonant element, which is the sensor of the transducer. Pressure variations produce a change in the resonance frequency of the element, which is measured as the output signal of the transducer. In some transducer configurations, the resonance frequency depends also on the gas used. Different mechanical sensing elements are employed (cylinders, forks,. . .). In some types, pressure is converted into force and then transmitted directly to a crystal quartz oscillator. Temperature effects are generally compensated for through the direct measurement of the temperature of the vibrating element and through a corresponding correction in the signal conditioning circuit, or else by an appropriate cut of the quartz crystal in order to make its temperature coefficient as small as possible or compensated.

The selection of an appropriate transducer to be used as a transfer standard is not easy. The most important feature to be considered is the time stability of all the relevant metrological characteristics.

The initial selection should be based on transducer resolution, with due consideration to the pressure range of interest and to the dependence of its output signal on temperature. The resolution value, along with other information on sensitivity, linearity, hysteresis, and uncertainty, is frequently given in the data sheet prepared by the manufacturer. However, a careful user, even if he already knows the typical performance of a particular kind of pressure transducer, will apply a well-defined calibration method specific for each unit, to make sure that the transducer is good enough to be used as a transfer standard at the uncertainty level of his interest and for its specific application.

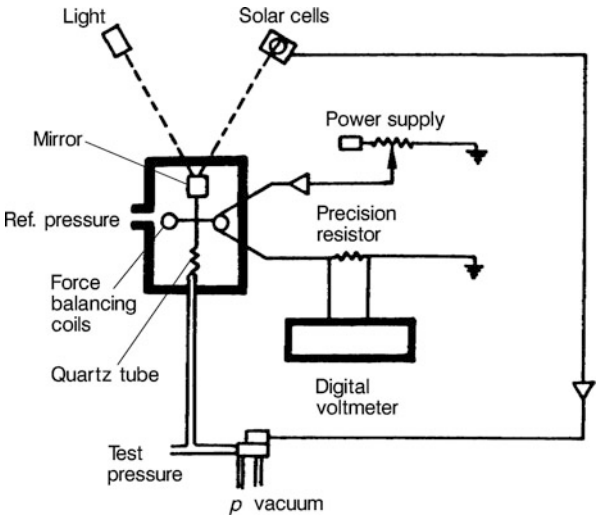

Fig. 8.2 Quartz-Bourdon tube pressure transducer whose rotation is optically detected by a servo-controlled force-balancing system. (With kind permission of Ruska Co., now Fluke, Houston, USA)

There are no "magic rules," but the following considerations will help in understanding how to check the metrological characteristics of a transducer, particularly its stability, for its use as a transfer standard and the definition of its specific calibration interval (see also Sect. 8.6):

- *The stability of the transducer output signal at zero pressure should be carefully determined for a long time and at different temperatures. Calibration shifts are frequently dominated by the zero signal shift of the transducer. Also, effects of temperature on zero signal are often important.*
- *The calibration of the transducer should be carried out with repetitive tests for both increasing and decreasing pressures, made at different times and under controlled and variable-temperature conditions. Appropriate primary standards having adequate uncertainty should be chosen (see Chap. 7).*
- *After some calibration cycles it is good practice to test again the possible zero signal drift of the transducer.*
- *Full-scale pressure drift should also be determined versus time in order to understand whether some fatigue or creep effects may possibly influence transducer readings.*

From the calibration data that can be obtained, which frequently show worse results than expected, it is possible to establish for the individual transducer tested when the zero reference or full-scale checks and successive calibrations have to be repeated.

The following sections give a survey of the most common transfer standards used in gas pressure measurements over different pressure ranges and in different applications.

8.1.1 Transfer Standards for Atmospheric Pressure Measurements

A large variety of pressure transducers exist in this important area of application. Generally, the resolution of many transducers is close to 1 Pa and in some case short-term stability and uncertainties are of the order of some tens of pascal.

Figure 8.2 illustrates the principle of a Bourdon tube pressure transducer having a force-balancing system and in which the tube rotation is detected optically.

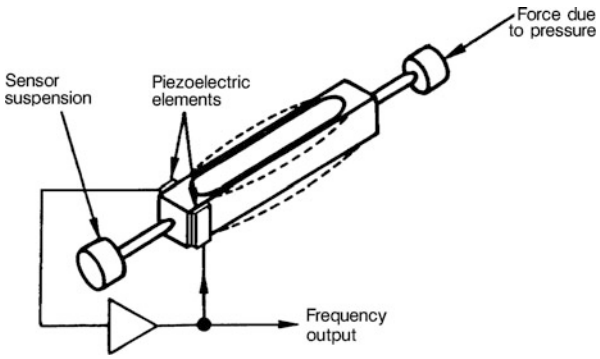

Fig. 8.3 Tuning-fork vibrating pressure sensor. (With kind permission of Yokogawa Electric Company, Japan)

The transducer consists of a quartz helix-shaped tube suspended over two coils in a magnetic field produced by permanent magnets. A curved mirror attached to the free end of the quartz tube reflects the light to photo detectors. When pressure is applied inside the quartz tube, the coil with the mirror rotates and a quantity of light proportional to the rotation is received by a pair of photo detectors producing a current proportional to the applied pressure.

This current signal, amplified and sent to the balancing coils, subjects the quartz tube to a torque equal and opposite to that produced by pressure. The current signal is sent also to a circuit equipped with a calibrated standard resistor; a digital voltmeter is used to measure the voltage at the ends of the standard resistor. The resolution of this system depends on voltage resolution and on electrical noise: it is possible to obtain a resolution of 0.1–0.5 Pa at 100 kPa (corresponding to 0.01–0.05 mV at 10 V). This system can operate with gases, though, when helium is used, diffusion into the quartz tube causes large drifts. In other systems, too, the quartz-Bourdon twisted tube is used, but the mirror movement is detected by optical or electromechanical systems.

In other measuring systems, based on a force equilibrium principle, the sensor is a bellows or a diaphragm balanced by an electromagnetic reaction force controlled by a current proportional to the applied pressure.

Another important family of transducers is that based on a vibrating structure (Halford 1972; Harade et al. 1982). The resonant element (e.g. a tuning fork, a cylinder, . . .), generally made of quartz or of a titanium alloy, is subjected to a force proportional to pressure. The resonant element is caused to vibrate by means of piezoelectric devices and its resonance frequency, which is proportional to the applied force and, consequently, to pressure, is then measured. These measuring systems require a high-level technology, particularly as regards the selection and shaping of the constituent material, in order to optimize the vibrating modes and reduce all parasitic forces on the vibrating element. Generally, systems of this type operate at frequencies close to 50 kHz, with frequency changing by about 5 kHz at full-scale pressure, and are equipped with temperature probes housed close to the vibrating element. An example of a vibrating-structure pressure transducer is given in Fig. 8.3.

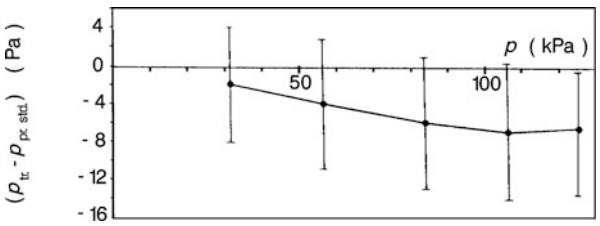

Fig. 8.4 Average calibration difference ($p_{\text{tr.}} - p_{\text{pr.std.}} = f(p)$) for a vibrating-cylinder pressure transducer. Five calibration cycles, from 31 to 126 kPa, were performed in 1 month with nitrogen as the pressurizing medium

In different configurations, equipped as the others with vibrating-cylinder elements, the pressurized gas acts directly on the internal part of a cylinder and in this case the resonance frequency of the system depends on the type of gas used.

In other devices, pressure is converted into a force by a bellows and by a lever mechanism and is then transmitted to a quartz oscillator (Paros 1973, 1975; Schaad 2009). The lever mechanism and the oscillator are made out of the same quartz material for better temperature stability of the system.

Other transducers used for the measurement of atmospheric pressure are of the capacitance type.

Capacitance variations are frequently used inside an oscillator circuit whose resonant frequency is correlated to pressure. In transducers of other types, the capacitance variation is converted into voltage.

It may be desirable to add some remarks applicable to the different families of pressure transducers that can be used as transfer standards in the atmospheric pressure range:

- Fused quartz is increasingly used in the construction of vibrating elements, force balances and capacitance-type pressure transducers, owing to its excellent elastic characteristics and to consequent stability, low hysteresis, small temperature coefficient, good dimensional stability and limited signal shift after repeated pressure cycles.
- Most of the modern transducers are equipped with microprocessors, electronic circuits for data conversion and acquisition, and memory for real-time corrections (for temperature, for example) and for storing the calibration coefficients to be used in polynomial fitting equations to represent the calibration equation in the best way.

Some typical characteristics of the above mentioned transducers are now summarized.

Different short-term tests made in the past on several of these pressure transducers showed that the relative difference between the pressure measured with the transducer and that measured with a primary standard, was generally within some parts in 10^4 (typically 10 Pa at 100 kPa).

Long-term tests, though less common, are very important and are performed in order to check the stability of the calibration curve and the different characteristics of the transducer versus time.

Figure 8.4, which refers to a commercially available vibrating-cylinder pressure transducer, gives the average calibration difference ($p_{\text{tr.}} - p_{\text{pr.std.}}$) with reference

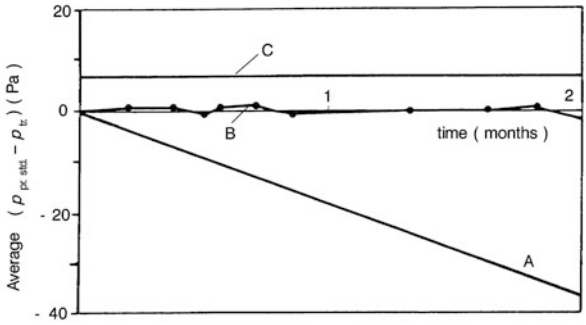

Fig. 8.5 Average calibration correction ($p_{\text{pr.std.}} - p_{\text{tr.}}$) at 100 kPa, in a 2-month period, for three different-type pressure transducers: *A* quartz-Bourdon tube/force balance type (see also extended data in Fig. 8.6); *B* quartz diaphragm/capacitance/resonance frequency oscillator type (see also extended data in Fig. 8.6); *C* vibrating-cylinder type (see also Fig. 8.4 for 1-month period)

to a pressure balance primary standard (the uncertainty of the measured $p_{\text{pr.std.}}$ is 20 ppm) versus pressure. $p_{\text{tr.}}$ is the transducer reading and $p_{\text{pr.std.}}$ is the pressure value measured by the primary standard pressure balance. In Fig. 8.4, the reported segments around the average values denote the maximum fluctuation values of the transducer at the specific calibration pressure.

The calibration cycles illustrated in Fig. 8.4 make it possible to draw the following conclusions, which refer to the transducer in question:

- Repeatability is 1×10^{-4} at full scale and to within 2×10^{-4} over the whole pressure range.
- Hysteresis at the lowest pressures never exceeds 9 Pa (typically 3×10^{-4} at 30 kPa).
- The pressure correction, based on the average calibration difference ($p_{\text{tr.}} - p_{\text{pr.std.}}$), for this transducer ranges from 2 to 7 Pa (Fig. 8.4); at 100 kPa a correction of 7 Pa is still well inside the uncertainty of 1×10^{-4}.
- In a 1-month period and for five complete calibration cycles performed, no appreciable shifts were observed in the calibration differences.

The values given in Fig. 8.4 are obtainable also with most of pressure transducers of other types, however they are valid only at short term and cannot be estimated "a priori"; besides, each specific transducer must be individually calibrated and characterized.

Another example concerning pressure transducers of three types checked over a period of 2 months is given in Fig. 8.5.

The average calibration correction is expressed as the difference between the pressure measured by the primary standard $p_{\text{pr.std.}}$ and the pressure reading of the transducer $p_{\text{tr.}}$.

Transducers A and B were both calibrated only at pressures near 98 and 100 kPa over a 2-month period, whereas for transducer C complete calibration cycles, from 31 to 126 kPa, were repeated several times in 2 months. As Fig. 8.5 shows, the data are quite dissimilar. Transducer C (the same transducer whose data are

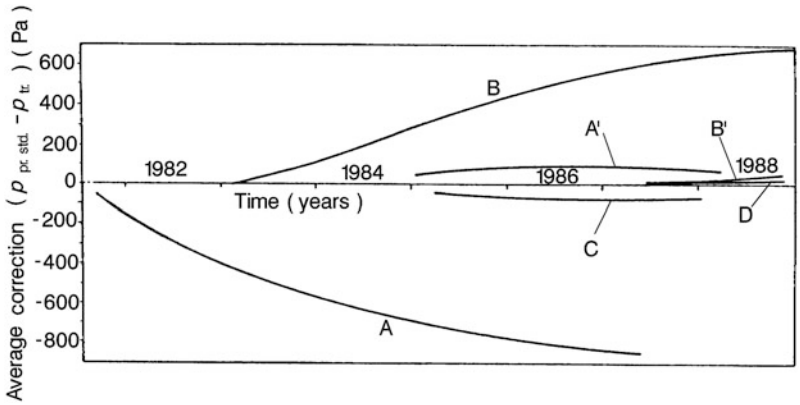

Fig. 8.6 Long-term average calibration corrections ($p_{\text{pr.std.}} - p_{\text{tr.}}$) at 100 kPa for absolute 120 kPa capacity pressure transducers of the following types: *A* quartz-Bourdon tube/force balance type (the same transducer as in Fig. 8.5); *A′* similar type; full scale, model and manufacturer same as *A*; *B* quartz diaphragm/capacitance/resonance frequency oscillator type (the same transducer as in Fig. 8.5); *B′* similar type; full scale, model and manufacturer same as *B*; *C* quartz-Bourdon tube/force balance type (principle similar to *A*, but different manufacturer); *D* force balance quartz oscillator type

given in Fig. 8.4) and transducer B have very good time stability. Transducer A, on the contrary, is affected by continuous drift, amounting to about 18 Pa per month (Girard 1983). The short-term repeatability and hysteresis of the three transducers did not change, but with transducer A, there occurs continuous drift of the average calibration correction. This negative phenomenon, which may be due to relaxation of the quartz element or to loss of vacuum in the sealed system, is impossible to eliminate and can only be taken into account by frequently repeated calibrations. The first indication to be considered concerning transducers of this type is that calibration should be frequently repeated, if such instruments are to be used as transfer standards at uncertainty levels lower than 1×10^{-4}. Short-term repeatability and hysteresis generally remain at a satisfactory level, but they are not completely representative of the overall metrological characteristics of the pressure transducer.

Another example is illustrated in Fig. 8.6, which gives the average calibration corrections (based on the average values of $p_{\text{pr.std.}} - p_{\text{tr.}}$) over a period of about 7 years for six different pressure transducers (for gauge-type identification see captions of Fig. 8.6).

Some of the data in Figs. 8.5 and 8.6 were kindly provided by Girard of BIPM.

The characteristics of the foregoing transducers can be summarized as follows:

- Transducer A showed sizable short-term drift (Fig. 8.5) and a tendency to continuous drifting.
- Transducer A′ showed much better stability than transducer A.
- Transducer B proved to be very stable (Fig. 8.5) for a short period, then began to drift continuously.
- Transducer B′ showed better stability than transducer B.
- Transducers C and D showed excellent stability.

The available data allow us to draw the following general conclusions:

- Transfer standards for gas absolute pressure measurements at the uncertainty level of 1×10^{-4} are commercially available.
- All such transducers need accurate calibration on a long-term basis, in order to obtain the corrections for calibration drift that may be required.
- It is not possible to define a type of transducer having good long-term stability; each unit needs individual and frequent calibration.
- The improved long-term stability of the new-generation transducers of the force balance resonant frequency, and vibrating element types makes them promising instruments for the future.

Miiller (1999) describes a systematic study of repeated calibrations for different types of pressure transducers up to 1 kPa (CDG-Capacitance Diaphragm Gauges, QBG-Quartz-Bourdon Gauges, QRG-Quartz Resonant Gauges, MEMS-Micro Electro Mechanical Systems, PSG-Piezoresistive Silicon Gauges, and RSG-Resonant Silicon Gauges). Key factors limiting their performance were identified as random noise, short-term instability in zero pressure readings, long-term shifts of the transducer calibration with time, and for the heated gauges the effect of thermal transpiration. The study determined that CDGs, QBGs, and QRGs have excellent pressure resolution (about 1×10^{-6} of the full scale) and CDGs, also because they are available for reduced ranges, have the best absolute pressure resolution. QBGs, QRGs, and RSGs have the best long-term stability, with calibration shifts of the order of 1×10^{-4} per year, between one to two orders of magnitude smaller than CDGs.

Such a study was extremely important for the selection of RSGs transfer standards, of 10 and 130 kPa full scales, to be used in NIST-piloted international comparisons (Hendricks and Miiller 2007). The basic characteristics of these transfer standards demonstrated a long-term instability of only few ppm at 130 kPa increasing to 0.01 % at 100 Pa.

An interesting and unique application of pressure balances for atmospheric pressure measurements has been developed at INM, now LNE, by Pinot and Riety (1989). An absolute pressure balance is maintained in permanent equilibrium with atmospheric pressure by means of an electromagnetic servo-controlled system which increases or decreases the force on the piston by an amount corresponding to changes in pressure balance equilibrium caused by atmospheric pressure variations. The signal used for the regulation of the force on the piston is amplified and converted into a voltage, which is proportional to atmospheric pressure. The stated uncertainty obtained with this device for a pressure range from 95 to 105 kPa is better than 3 Pa.

8.1.2 Transfer Standards for Gas Pressure Measurements from 100 Pa to 10 kPa

The pressure transfer standards for atmospheric pressure measurements analysed in Sect. 8.1.1 can be used with reliable uncertainty (0.1 % to some parts in 10^4) down to pressure values close to 10 kPa.

To cover the range from 100 Pa to 10 kPa, for both absolute and differential pressure measurements, different transducers are available, but the devices mostly used at the transfer standard level are of the capacitance types.

Capacitance transducers (in differential and absolute configurations) with typical full scales of 133 Pa, 1.3, 13 and 130 kPa are commercially available. Their capacitance sensors exhibit good resolution and sensitivity but are temperature dependent and for this reason some of these transducers need to be temperature compensated.

However, the best performances are obtained when the whole transducer is temperature controlled, typically at temperatures ranging between 35 and 50 °C. Since a temperature difference may exist between the transducer (at the controlled temperature) and the pressure-measuring apparatus, and because pressure values from 0.01 Pa to 10 kPa are in a transition region between the low-vacuum and the high-pressure ranges, sizable measurement errors may result if no correction is applied for the thermomolecular pressure difference. The thermomolecular pressure difference effect is a physical phenomenon occurring in a gas system, when at particular pressure values, it is subjected to large temperature differences (see Chap. 10). The magnitude of this correction may be very large (a few percent) for pressures below 100 Pa, its value depending not only on the absolute pressure value but also on temperature differences between transducer and measuring apparatus, on the gas species, on apparatus geometry (mainly the diameter of the connecting tube), on surface conditions, and on the constituent materials of the connecting tube.

Published data exist (Poulter et al. 1983; Jitschin et al. 1987; Bergoglio and Calcatelli 2001) for the thermomolecular pressure difference obtained in the calibration of capacitance transducers of 133 Pa and 1.3 kPa full scale and for temperature differences between the transducer and the measuring apparatus ranging from 10 to 30 °C (the temperature of measuring apparatus being 20 °C). These data take account of the use of different gases as well.

Under such conditions, and for the experimental configurations described in the above papers, the thermomolecular pressure difference correction is very small for pressures higher than 100 Pa; but in the pressure region below that considered in the present book and from 0.01 to 100 Pa this correction is as much as 2 % and is heavily dependent on the absolute pressure value. In the pressure range from 100 Pa to 1 kPa, too, the effect of thermomolecular pressure difference plays a significant role when the temperature difference is very high, as in low-temperature gas and vapor pressure thermometry, discussed in Part I, and when a reference transducer (e.g. of the capacitance type) is used at 293 K. In such cases, the thermomolecular pressure difference is small only with absolute pressures above 10 kPa, but at 2.5 kPa it may amount to about 1.3 Pa, a value not to be neglected for the accuracy levels of the order of few parts in 10^4 required by gas thermometry.

The thermomolecular pressure difference effect will be discussed in Chap. 10.

Modern capacitance transducers are instruments of a high technological level because of the great care needed in sensor fabrication and of the sophisticated electronics for signal conversion (capacitance to frequency, or to voltage, conversion). A description of modern developments of such devices is given by Sullivan (1985). In addition to the already-mentioned problems concerning the thermomolecular

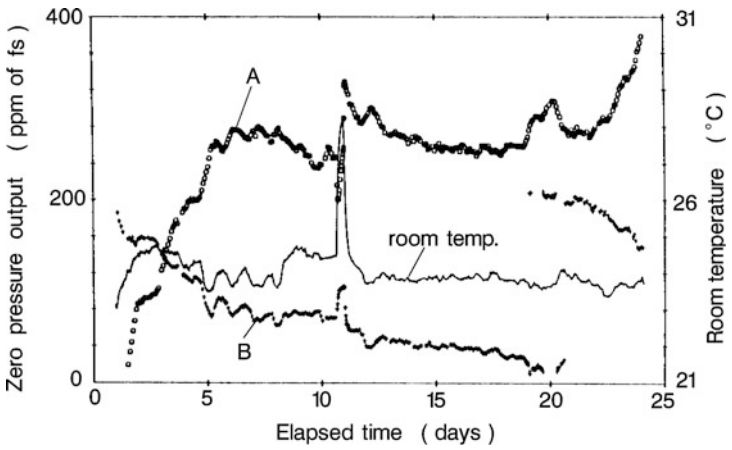

Fig. 8.7 Zero signal versus time for two thermally controlled capacitance pressure transducers (*A* 133 Pa full scale; *B* 1.3 kPa full scale). Room temperature versus time is also plotted. (From Hyland and Tilford (1985) with the kind permission of authors)

pressure difference and the possible transducer instability due to inappropriate selection of the operating temperature of the transducer, the evaluation tests of such transducers generally have to take account of the behavior of the zero output signal as a function of time and temperature, as well as of possible drift of calibration curves with time.

A detailed study of the metrological characteristics of capacitance diaphragm gauges has been carried out by IMGC (now INRIM) and NIST (Bergoglio and Calcatelli 1981; Hyland and Tilford 1985; Tilford 1988b; Hyland and Shaffer 1991) and others (Dwight Adams 1993).

Figure 8.7 illustrates the behavior of the zero signals of capacitance transducers versus time for two devices of 133 Pa and 1.3 kPa full scale, thermally controlled to maintain their temperature at 37 °C.

Room temperature versus time is also plotted in Fig. 8.7.

Zero instabilities are small and typically of about 0.01 Pa at short term (few days), but they become larger, of the order of 0.06 Pa, in long-term tests. The values of these shifts give only a qualitative indication, as different values and behaviors can be observed for different devices. Effects of room temperature variations on the zero signal of transducers can be significant, as Fig. 8.7 shows. Better results can be obtained when both the laboratory room temperature and the operating temperature of the unit are maintained stable, the former within 0.5 °C. If these capacitance transducers are intended for use as transfer standards, frequent checks of the zero output signal are needed, as it is indispensable to follow their evolution in time in relation to temperature changes and possible electronic shift of the control/measuring units.

Capacitance transducers can be calibrated, depending on their full-scale pressures, by means of liquid manometers, pressure balances and in the lowest pressure region, with the use of series expansion apparatuses.

Extensive results of calibrations of capacitance transducers for absolute or differential operating modes and for different pressure ranges and operating conditions can be found in Hyland and Tilford (1985). Calibration shifts differ widely, depending on the individual gauges. With some gauges, calibration stability was of the order of 0.02 % f. s. per year; with other gauges a calibration instability of the order of 2 % f. s. was observed. With the more unstable transducers, often the calibration change is not a continuous drift but an abrupt change. On the average, the typical long-term calibration stability is of the order of 0.4–0.5 % per year, though in some cases better stability can be obtained.

As is the case of transfer standards transducers to be used in the atmospheric pressure region, short-term repeatability and short-term uncertainty are not the most important metrological characteristics of capacitance transducers; long-term evaluation of their metrological characteristics is necessary if the gauges are intended for transfer standards use.

Despite the limitations indicated, capacitance transducers have been widely used as transfer standards in international comparisons (Tilford 1988b). Frequently the analysis of comparison data is complicated by the instability of the capacitance transducers and by the difficulty of a careful evaluation of the thermomolecular pressure difference effect (see Chap. 10), which also causes significant non-linearity's to the transducers.

8.2 Transfer Standards for Pressure Measurements up to 100 MPa

The range of the transfer standards used for absolute pressure measurements and based on the operation principles given in Fig. 8.1, can generally be extended to higher pressures. For example, vibrating-element transducers have been designed for use with absolute pressures to about 4 MPa and force-balance transducers for absolute pressures to about 10 MPa.

In the present section, we will consider only pressure transducers used for gauge pressure measurements whose application, generally different from that in gaseous media described in Part I, requires an extension of the pressure range to about 100 MPa. For gauge pressure measurements in the range from the atmospheric pressure to 100 MPa such transducers are calibrated with primary pressure balance standards covering the appropriate ranges and operating under gauge conditions in gas media.

The calibration method generally adopted in the gauge mode is similar to that used in the absolute mode (see Chap. 7). The sensors used as transfer standards for pressure measurements require an appropriate choice of the mode of operation (absolute or gauge) and of the pressure range. For example, the use of a gauge transducer having too small a pressure range to measure an absolute pressure creates problems of signal stability and requires the correlation of the transducer signal to the atmospheric pressure values, which have obviously to be determined for this purpose.

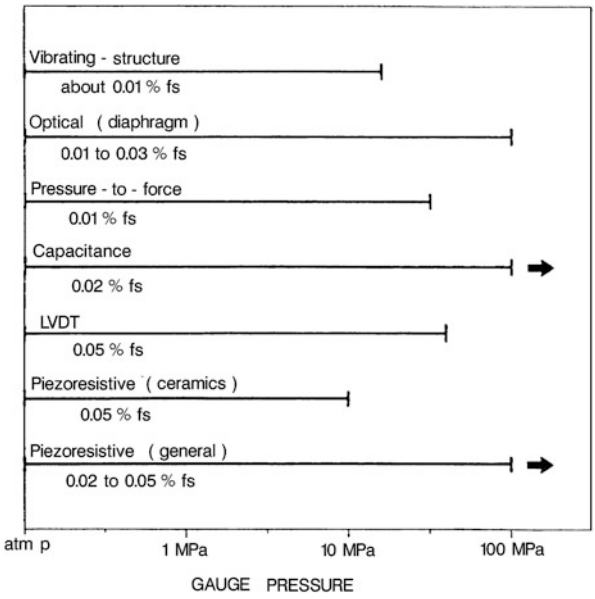

Fig. 8.8 Transfer standard transducers for gauge pressure measurements to 100 MPa, with indication of pressure range (log scale) and typical uncertainty (*arrows* indicate possible extension of the pressure range)

Atmospheric pressure values may typically change daily by about 100 to 200 Pa, and by as much as 8 000 Pa in 1 week. Consequently, in the case of a gauge pressure measurement carried out with a transducer of 0.1 MPa full scale and affected by atmospheric pressure variations of 200 Pa, the operator is compelled to measure the atmospheric pressure and simultaneously correlate it to the transducer signal for correction. If this procedure is not applied, the operator must accept a drift of the transducer signal that may be as high as 0.2 % of the full scale (200 Pa at the full scale of 0.1 MPa).

Another important parameter is the maximum achievable operation pressure, which depends on sensor construction. For example, quartz-Bourdon tubes can be used to about 20 MPa, the working limit of some capacitance sensors can be extended to 100 MPa, and that of some particular types (strain-gauge, manganin gauge, . . .) even to 1 GPa.

Many of the sensors whose operation principles are applied for absolute measurements in gas, are also used for gauge pressure measurements, if appropriately modified.

Figure 8.8 illustrates several types of pressure transfer standards for gauge pressure measurements to 100 MPa and indicates the typical full-scale pressure and uncertainties.

An important group of pressure sensors use the piezoresistive effect and are described as bonded (e.g. Paul 1993/1994) or unbonded, or of the thin-film, ceramic diaphragm-deposited thick film or diffused-semiconductor strain-gauge types. Table 8.1 gives some typical metrological characteristics of piezoresistive sensors of different types.

If metallic thin-film strain-gauge transducers have, on the one hand, a small gauge factor (the *gauge factor* is the ratio of the output signal of the transducer

Table 8.1 Comparison of some metrological characteristics of piezoresistance transducers of three different types

Parameter[a]	Technology		
	Metallic thin film	Semiconductor	Thick film
Gauge factor	2–5	10–180	8–15
Temperature coefficient of resistance $(1/R) \cdot \mathrm{d}R/\mathrm{d}t$ $(\mathrm{ppm} \cdot {}^{\circ}\mathrm{C}^{-1})$	20–4 000	400–3 000	50–200
Temperature coefficient of gauge factor $(1/GF) \cdot \mathrm{d}GF/\mathrm{d}t$ $(\mathrm{ppm} \cdot {}^{\circ}\mathrm{C}^{-1})$	20–100	200–5 000	200–500
Stability in time	Excellent	Good	Good

[a] ε strain, t temperature, R electrical resistance, GF gauge factor $[GF = \varepsilon \times \delta(R/R)]$; See Sect. 8.6

to the applied pressure; see also Sect. 8.6), on the other hand they exhibit limited temperature coefficients both of resistance and of the gauge factor, which ensure excellent signal stability. A sensor of this type is generally preferred as a transfer standard for pressure measurements up to 100 MPa. The typical uncertainty is of the order of 0.05 %, with hysteresis (which may be as high as 0.1 %) being duly taken into account and corrected for.

Semiconductor technology using a silicon diaphragm, with strain gauges, temperature sensors, and signal processing electronics all integrated into the silicon chip, is increasingly employed. The uncertainty level, which is typically of the order of some percent to about 0.1 %, discourages the use of semiconductor transducers, at present at least, as pressure transfer standards.

Thick-film sensors have been extensively investigated (Morten et al. 1979; Canali et al. 1980) below 10 MPa. Ceramic materials are frequently used for the construction of the diaphragm. At present, the stability of thick-film sensors is better than that of semiconductor sensors.

An important feature of metal thin-film strain-gauge pressure transducers is the possibility of their use at low temperatures down to 4.2 K (see Sect. 8.4.1).

Another traditional sensor, which recently underwent a large number of modifications and was substantially improved, is the linear variable differential transformer (LVDT) pressure transducer. In this type, the diaphragm or the tube is appropriately selected so that its movement is reproducible when pressure is applied. Recent improvements include automated temperature corrections, LVDT electronic signal processing, digital conversion, and adaptability to microprocessors. LVDT transducers can be used as transfer standards with an uncertainty of the order of 0.05 % with pressures to 60 MPa.

Another important transducer frequently used in gas gauge-pressure measurements is based on the principle of pressure-to-force conversion; force is measured by means of an electronic balance and is directly related to pressure through calibration. With such gauges, which can be both absolute and differential, pressure measurements are typically possible to about 50 MPa.

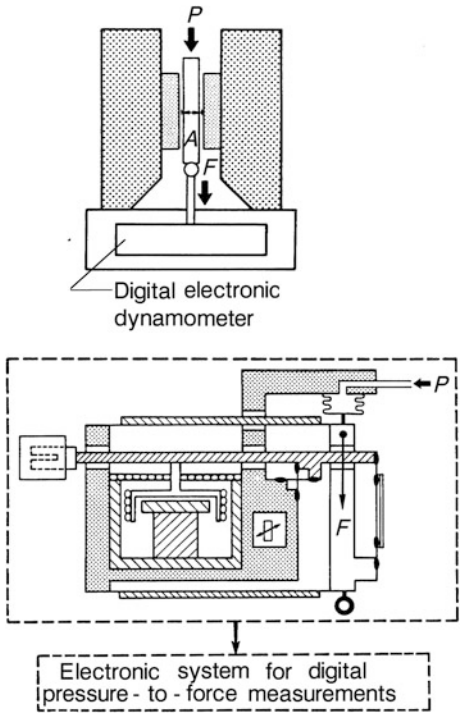

Fig. 8.9 Two configurations of transducers (in the first case it is really a pressure balance) of the pressure-to-force type used as transfer standards for pressure measurements (absolute, gauge, and differential modes of operation are possible)

Figure 8.9 shows schematically two configurations of pressure-to-force transducers.

The first system at the top is a traditional piston-cylinder unit (see Sect. 7.2) of the same quality normally employed in primary standard pressure balances. The pressure p to be measured, applied to the piston-cylinder unit of effective area $A_e(t, p)$, generates on the opposite side of the piston a force $F = p \times A_e$ which is measured by a digital electronic dynamometer.

The effective area $A_e(t, p)$ must be carefully measured by cross-floating against an appropriately selected primary standard (see Sect. 7.2.2.3). The characterization of the piston-cylinder unit must include the determination of the thermal expansion coefficients of the piston and the cylinder and of the pressure distortion coefficient of the assembly, which plays a significant role, particularly when such devices are intended for use at high pressures.

The force to be measured is applied to the pan of an electrodynamics compensation balance of high quality (typically, the same equipment used for mass measurements, in a single pan-configuration). The electromagnetic balance is programmed to give a digital output signal in pressure units. The programme includes the calibration data of the piston-cylinder unit, the temperature reading and all the relevant corrections. The measurement steps and data acquisition are generally computer controlled.

Such devices are highly stable, as good-stability piston-cylinder units and high-quality dynamometers are now available. With such systems of the pressure-to-force

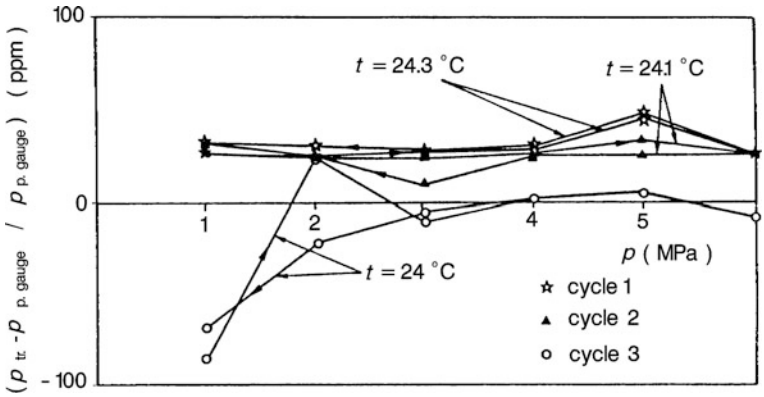

Fig. 8.10 Uncertainty and stability of a pressure-to-force transfer standard for gas gauge pressure measurements from 1 to 6 MPa at different temperatures (three cycles)

type, resolution is typically of the order of 1.0×10^{-5} (equivalent to 100 Pa for a unit of 6 MPa full scale); they can be used as transfer standards over different pressure ranges, depending on the selected effective area of the piston-cylinder unit and on the capacity of the electronic dynamometer.

The advantages of such devices include the possibility of using them as automatically controlled instruments and they allow the separate check and recalibration of their piston-cylinder unit.

Another interesting feature is the possibility of dynamometer recalibration, with the use of standard weights. The piston-cylinder unit is removed and the standard weights are placed on the balance pan. The best results are obtained when operating carefully under laboratory conditions and by regular checking of the planarity of the balance and of the verticality of the piston-cylinder unit.

Figure 8.10 shows the results of different calibrations concerning a commercially available pressure-to-force transducer of the piston-cylinder type having a 6 MPa full scale and 100 Pa resolutions.

The data are expressed as the relative deviation of the transducer readings from the pressure measured with the pressure balance used for calibration; they are based on the averages of different calibration cycles. The transfer standard in question showed deviations well within 100 ppm over the whole pressure range from 1 to 6 MPa in calibrations repeated over a 3-month period.

Similar tests carried out on the same unit but during a 2-year period showed that the maximum deviation is well within 200 ppm over the whole pressure range, even when temperature differences between individual calibration cycles are as large as 5 °C and no temperature corrections are applied.

Such results are typical and show that pressure-to-force transducers are excellent transfer standards for gas gauge pressure measurements in pressure ranges that can be extended to 50 MPa.

Strictly speaking, these systems resemble more a primary pressure standard than a transfer standard, because of their intrinsic capability of calibrating their own

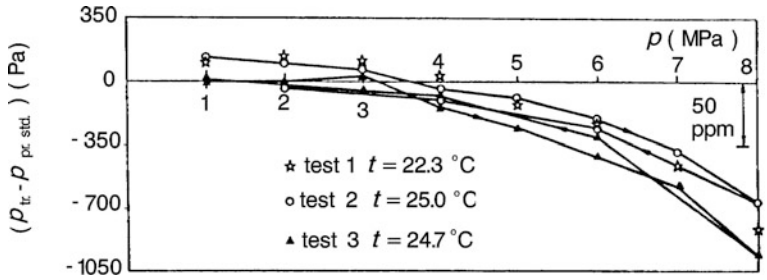

Fig. 8.11 Comparison of three different calibration cycles from 1 to 8 MPa for a quartz resonance-element transfer standard. Temperature measured on the transducer body ranges from 22 to 25 °C. ☆ cycle 1 ($t = 22.3$ °C); ○ cycle 2 ($t = 25.0$ °C); ▲ cycle 3 ($t = 24.7$ °C)

piston-cylinder units and their electronic dynamometers with the specific standard weights assuring in this sense a superior stability.

Another possible configuration is illustrated in Fig. 8.9.

A pressure change in an elastic bellows produces a force variation, which acts on an articulated parallelogram, whose displacement is measured by an optoelectronic sensor. The signal is converted into current and sent to an electromagnet counterbalancing the displacement of the force sensor. The current signal, which is proportional to the applied pressure, is electronically processed directly in pressure units with all the relevant corrections. The electromagnetic force compensation unit is very sensitive and its resulting behavior is linear.

With these systems resolutions from 0.003 to 0.01 % of the full scale are achievable; the typical uncertainty is of the order of 0.03 % and the maximum pressure range measurable is a few tens of megapascal.

Another pressure transducer that may be used as a transfer standard is of the quartz resonance-element type. Figure 8.11 shows three different calibration cycles performed to determine the absolute difference (defined as $p_{tr.} - p_{pr.std.}$) for a transducer of this type.

This transducer proved satisfactory as a transfer standard; short-term repeatability was within 0.003 % of f. s.; repeatability over a 3-month period was within 0.004 % of f. s.; the maximum hysteresis was about 0.005 % of f. s.; linearity was within 0.01 % of f. s.

There is therefore a wide selection of possible transfer standards for pressure measurements under gas-and-gauge conditions with typical uncertainties from 0.01 to 0.05 % of the full scale; however, each individual transducer has to be carefully calibrated and evaluated on a long-term basis. Calibrations must take account of the actual conditions of use of the transducer. Hysteresis and stability at full-scale pressure should be carefully considered.

Some transducers of the above mentioned types can be used at pressures much higher than 100 MPa, for instance, capacitance transducers (Colwell 1979) and some piezoresistance transducers (of manganin and other alloys), which are particularly suitable for pressures from 100 MPa to some gigapascal (Peggs and Wisniewski 1983; Molinar and Bianchi 1989).

A phenomenon that has to be considered, particularly when a pressure transducer is subjected to high pressures, is *adiabatic heating and cooling*. When pressure is rapidly changed, the pressure fluid is subjected to mechanical work, generating in the fluid a temperature change, which is transmitted to the vessel and to the connected instrumentation, including the pressure transducer.

If the process occurs under adiabatic conditions (constant entropy), the temperature change with pressure is directly proportional to the temperature and to the volume expansion coefficient of the fluid and inversely proportional to fluid density and heat capacity at constant pressure. As the operating conditions normally are not adiabatic, the produced temperature changes become attenuated, to extents depending on the fluid and on the apparatus, whose design may make reverting to equilibrium conditions quite a long process. The adiabatic effect can be attenuated by reducing fluid volumes and maintaining a good thermal contact between the main parts of the apparatus with the use of a heat exchanger. It is highly advisable, undoubtedly, to mount a thermometer as close as possible to the pressure sensor, to indicate the time necessary for thermal equilibrium to be achieved again after pressure application. This effect can be highly important for pressure transfer standards, and it must be evaluated with appropriate calibrations.

8.3 Transducers Used for Differential Pressure Measurements and as Null Detectors

Pressure transducers, when used in the differential mode, cover a wide number of applications. In the present section, they will be analysed in connection with their use in gaseous media.

Differential transducers play a very important role in most gas-based thermometry, when they are used as separators between the thermometric and the manometric fluids; in this case the differential transducer is used as a null detector.

More generally, transducers of this type are used for the measurement of small differential pressures (from some hundred pascal to some kilopascal) with a line pressure below or close to atmospheric pressure values (e.g. in wind tunnels, ventilation and air conditioning, gas thermometry), or with line pressures up to some megapascal (in natural-gas flowrate measurements at high pressures, cooling in nuclear reactors, and in connection with the determination of some pressure fixed points).

8.3.1 Differential Pressure Transducers for High Line Pressures

In this field, special primary standards are required (see Sect. 7.2.5) and a specific measurement method has to be applied for transducer characterization (Daborn 1977, 1987), which has to include as well the measurement of the zero signal as a function of the line pressure. The transducer calibration must also include the reproducibility

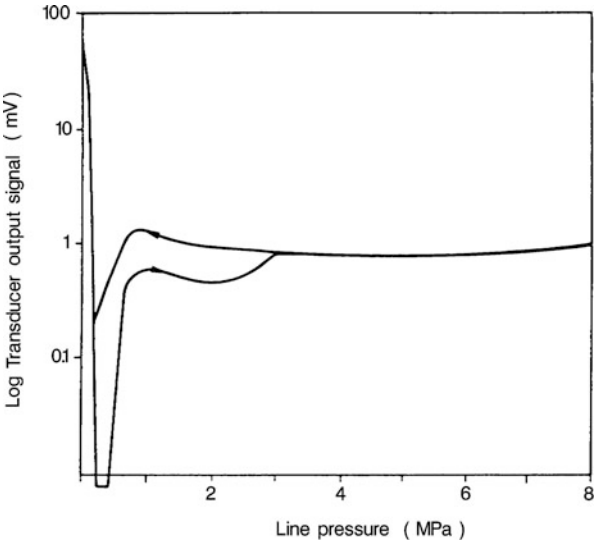

Fig. 8.12 Log of zero signal variation as a function of line pressure up to 8 MPa of a silicon diaphragm semiconductor transducer (differential pressure is always equal to zero)

determination at different line pressure values. These requirements are necessary for minimizing the uncertainty in transducer measurements. Too frequently is a differential transducer calibrated solely at the atmospheric line pressure; which is a correct procedure if the transducer is to be used only at that line pressure. If the transducer will be used at several line pressures, below or above the atmospheric pressure, it must be calibrated at every line pressure value over the whole range of use, because very large differences, dependent on the different line pressure values, have frequently been observed both in the zero signal and in some of the basic characteristics (e.g. calibration equation, reproducibility, . . .) of the transducer.

Figure 8.12 shows an example of the substantial influence of the line pressure on the zero signal of the transducer, as regards a silicon semiconductor-diaphragm differential transducer (maximum differential pressure 150 kPa, maximum line pressure 8 MPa).

To about 3 MPa the zero signal variations with line pressures are so large and non-linear, that it is advisable to use this transducer only for line pressures between 3 and 8 MPa, in which range its zero signal is more stable.

Another example is that of a quartz-Bourdon tube sensor with optomechanical signal detection. In Fig. 8.13, the calibration factor, expressed in this case as the differential pressure divided by the output signal of the transducer, is plotted for four line pressures as a function of the applied differential pressure.

As it can be seen, the calibration factor changes by 3.2 % when the line pressure is caused to vary from atmospheric pressure to about 10 MPa. Other transducers of the same type may exhibit lower, but still significant, changes in the calibration factor with line pressure. Effects on zero stability due to variations of line pressures and for different gases are studied by Sharma (Sharma et al. 1993) for fused quartz-Bourdon tube gauges up to 110 kPa: these effects are extremely important and in this case also

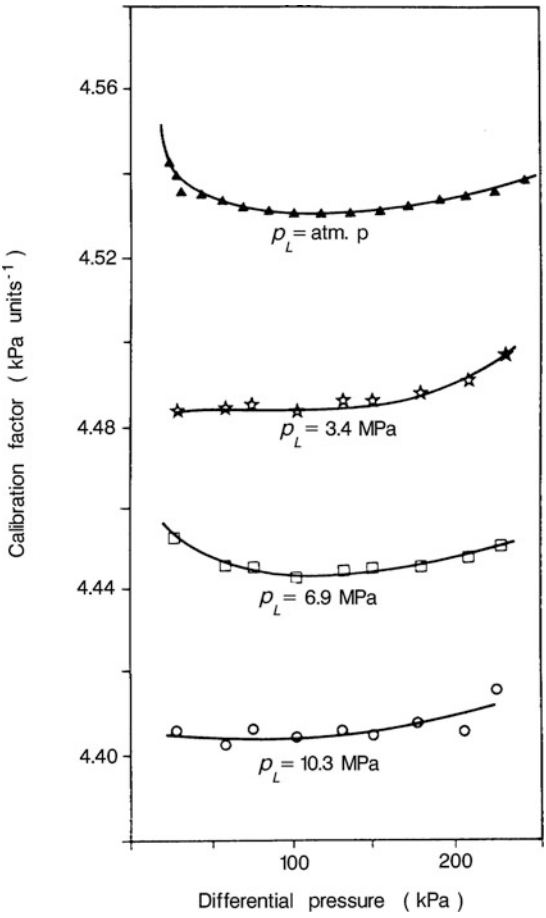

Fig. 8.13 Variation of the calibration factor with line pressure for a quartz-Bourdon tube transducer with optomechanical signal detection (differential pressures to 250 kPa and line pressures to 10 MPa). (From Daborn (1977) with the kind permission of the author)

a gas dependence was reported. Similarly studies have been reported for the case of capacitance diaphragm gauges (Sharma et al. 1991).

The differential transducer types that can safely be used for gas measurements at high line pressures are few; the resonant-frequency, strain gauge, capacitance, and LVDT types are the most common. The capacitance type is noteworthy. For example, one of the designs offers full-scale line pressures to 14 MPa and a differential pressure range of about 50 kPa, with a resolution of 0.7 Pa. The major limitations are zero signal shifts and changes in the calibration factor with different line pressures. Other frequent limitations are signal instability due to the small differential pressure range and inadequate protection from accidental over pressurization.

Actually two contradictory requirements exist in the design of a transducer intended to measure small differential pressures at high line pressures: the sensor must be at the same time very robust for operation at very high line pressures and very sensitive for operation at very low differential pressures with good resolutions.

The procedures for the calibration of differential transducers at high line pressures can help to define the main influence factors, if the following precautions are taken

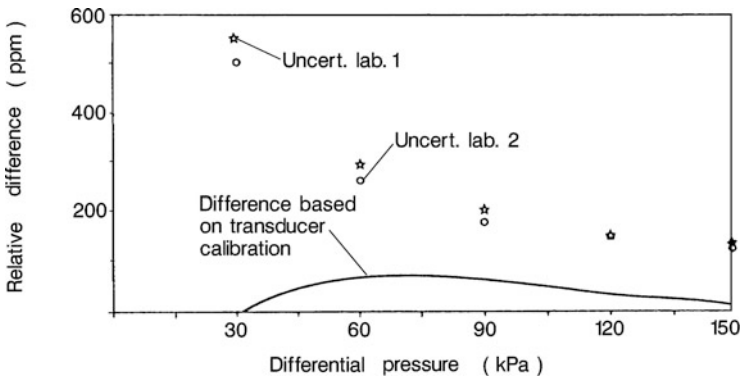

Fig. 8.14 Relative differences between the calibrations by two laboratories of a silicon diaphragm semiconductor differential transducer used as a transfer standard. Measurements were made at 4 MPa line pressure; maximum differential pressure was 150 kPa

(see also Sect. 7.2.5 for the best use of primary standards for differential pressure measurements):

- The differential pressure must be carefully applied so as to avoid over pressurization of the sensor, particularly when the line pressure is generated at the same time.
- No rapidly-varying differential pressures should be applied to the sensor.
- Hysteresis must be carefully evaluated, as it may be very large and also dependent on the line pressure value.
- The transducer must be mounted in the established appropriate position and be stress free; the specified maximum torque value for transducer connection must not be exceeded.
- The positive differential pressure must be applied always on the same side of the transducer.
- Complete calibration cycles should be made at different values of the line pressure; the zero signal of the transducer has to be measured as a function of the line pressure before and after the calibration cycles.
- All calibration cycles must be repeated at regular time intervals, in order to make sure that no zero signal drift has occurred and that the equation representing the calibration characteristics does not need to be changed.

If all such precautions are taken, it is possible, as a rule, to use certain well-studied transducers as transfer standards for accurate differential pressure measurements at high line pressures.

Figure 8.14 shows the calibration data obtained at two laboratories and concerning a transfer standard pressure transducer used for the verification of the differential pressure scale from 30 to 150 kPa at line pressures from 4 to 8 MPa.

The relative difference of the measurement values between the two laboratories is well within 100 ppm over the whole differential pressure range and is well within the stated uncertainty of the primary standards of the laboratories concerned. There

are cases (Daborn 1987) showing that with similar transducers repeatability may be less than 0.05 %, but that differences of differential pressure measurement values between laboratories may be as high as some parts in 10^2, depending on the values of both the line pressure and of the differential pressures.

Other results for the measurement of small differential pressures at high line pressures with capacitance sensors show a typical repeatability of the order of 0.1 %. Transducers of the LVDT type have acceptable repeatability, but generally high hysteresis values.

8.3.2 Differential Pressure Transducers Used as Null Detectors

Differential pressure transducers are often used as separators between pneumatic circuits working with different fluids. In this case, a differential transducer works as a null detector, in the sense that a pressure difference need not be measured, but only the condition of pressure equality on the two sides of the differential pressure transducer must be identified with high reproducibility.

A differential transducer is frequently used to detect equilibrium between two primary standards, for example, two pressure balances (e.g. Kobata and Olson 2005). For this use the differential pressure transducer must have sensitivity and stability, at all the line pressure values of the comparison, of the same order as or better than the sensitivity of pressure balances, which is typically of a few ppm and in some cases even of the order of 0.1–0.5 ppm. The degree of sensitivity can be verified only by frequent checks of the zero of the differential transducer at different line pressure values.

In order to obtain the best results under these conditions, an appropriate configuration of the circuit where the differential transducer is mounted is necessary for checking the zero pressure difference at every line pressure and the metrological characteristics of the transducer.

Figure 8.15 illustrates a typical configuration that allows a differential transducer to be used to detect, for example, the equilibrium condition between two pressure balances or other primary systems operating with different gases.

Valve A in Fig. 8.15 is used to check the zero of the differential transducer at a specific line pressure. The other valves must be appropriately set (see Sect. 7.2.5). After this operation, and before the use of the differential transducer to check pressure equality between the two units under test, the system has to be supplied with the appropriate gases at the selected line-pressure value.

In certain cases, it may be necessary to separate systems using liquid media from other apparatuses operating with gases. The separation between liquid and gas gives rise to considerable problems, as the two fluids must not be mixed (valve A in the configuration of Fig. 8.15 cannot be used). A solution is a diaphragm differential transducer equipped on one side with a free-surface gas–oil interface, which allows the transducer zero to be checked while keeping the fluids separated. When a free-surface interface is used, the operator has also to keep a strict control on the separation

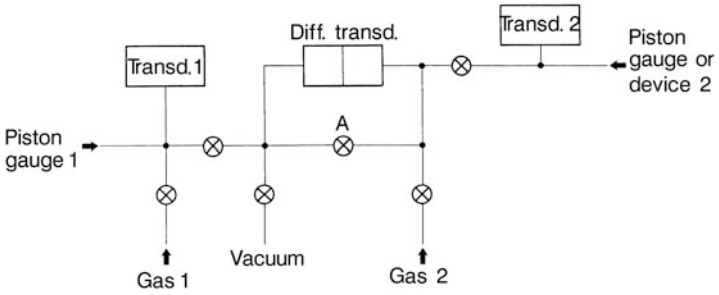

Fig. 8.15 Typical assembly for a differential transducer used as a null detector between two measuring units (pressure balance or device 1 and pressure balance or device 2) working with different gases

level between the liquid and the gas, so that appropriate fluid head corrections may be computed.

Instead of the mentioned interface, one can use specially designed capacitance sensors to locate the level of the liquid–gas interface. An example of such instrumentation, which requires capacitance to be measured with a resolution of 10^{-7} pF, is given in (Tilford and Martin 1984). The system in question is a coaxial three-terminal capacitor partially immersed in oil and partially immersed in gas. With it the hydrostatic heads and differential pressures between two pressure balances operating respectively in oil and in gas can be determined. By means of this capacitance system, hydrostatic pressure changes generated by the displacement of the liquid–gas interface can be detected with a typical sensitivity of 5.8×10^{-3} pF Pa^{-1}. The system was used for a comparison of two pressure balances (one using oil and the other nitrogen) in the pressure range from 0.4 to 4 MPa. The average 4.5 Pa standard deviation of the mean of the pressure differences, measured with the two pressure balances, can be considered a very satisfactory result (Driver et al. 1981).

In the majority of pressure measurements especially in gas thermometry, a differential pressure transducer is used as a null detector for the separation of two different gases. This is the case of the determination of the carbon dioxide vapor pressure, which is 3.48608 ± 0.00017 MPa at 273.16 K (Bignell and Bean 1988). In this experiment, pressure was measured by means of an absolute pressure balance working with nitrogen and of a diaphragm differential transducer of the variable-reluctance type, used to separate nitrogen from carbon dioxide. The differential pressure transducer, placed between the pressure balance and the apparatus used for the measurement of carbon dioxide vapor pressure, was mounted in a configuration similar to that illustrated in Fig. 8.15. The sensitivity of the variable-reluctance differential pressure transducer was 4.5 Pa and its zero signal was stable within this value at a line pressure close to 3.5 MPa.

Another differential transducer used for gas separation and as a null detector is that of the capacitance type. Differential transducers of this type are available for different full-scale pressure values, from 130 Pa to some megapascal. Typically, they

exhibit moderate changes with different line pressure values. Zero stability must always be carefully checked. For a differential capacitance transducer of 1.3 kPa full scale, zero stability well inside 0.1 Pa is quite normal.

Another example of the use of differential capacitance pressure transducers as null detectors is provided by the determination of the triple point of argon (68 890 ± 1.5 Pa at 83.805 8 K of the ITS-90 temperature scale), typically obtained with 1 Pa stability and reproducibility (and in addition, methane: 11 690 Pa and oxygen: 146.25 Pa). In the experiments carried out by Pavese (1981) at IMGC (now INRIM), a differential capacitance pressure transducer of 135 kPa full scale was used to separate the measuring argon cell from the mercury manometer in which nitrogen was used. For this transducer, a 0.5 Pa uncertainty contribution was due to zero signal instability and 0.5 Pa was the uncertainty contribution due to the effect of the line pressure on the zero of the differential transducer.

In another experiment on the argon triple point used as a pressure fixed point (Bonhoure and Pello 1983), a capacitance differential pressure transducer of 1.3 kPa full scale was used as a null detector. Pressure measurements were made only in the vicinity of 69 kPa; the zero stability of the differential transducer was well inside 0.1 Pa.

For the use of pressure fixed points as transfer standards see Chap. 9.

Mention must be made also of the different attempts to optimize the metrological characteristics of LVDT differential pressure transducers.

Holste et al. (1977) developed studies and modifications on LVDT differential pressure transducers to improve their stability in the 100–300 K temperature range. They reported zero stability within 0.005 % for measurements in helium and line pressures from 1 to 3 MPa.

LVDT differential pressure transducers are frequently used as null detectors at room temperatures for the comparison of pressure balances in relative conditions (gauge mode). If zero signal checks at different line pressures are frequently made, the reproducibility of the state of equilibrium between the pressure balances is of the order of a few ppm, a result close to that normally obtained by direct cross-floating through the observation of the fall rates of the compared pistons.

Capacitance-type differential pressure transducers are also widely used in low-pressure ranges (0.1–700 Pa) with typical stabilities of the order of 0.1 Pa/month and stability of the zero signal versus temperature within 0.1 Pa K^{-1} (Abilov et al. 1978).

Capacitance differential transducers have also been developed in very simple configurations for use with corrosive gases, like the gas of laser systems, with resolutions of the order of 0.1 Pa (Shammas and Seguin 1979).

8.4 Transducers for Pressure Measurements Extended to Cryogenic Environments

A complete and exhaustive review of all possible problems connected with pressure measurements under cryogenic conditions will not be attempted. Only pressure transducers recently improved and used at cryogenic temperatures and in high magnetic fields will be analysed.

Pressure measurements at cryogenic temperatures and in high magnetic fields have gained importance owing to the studies connected with large superconducting machines and magnets. Despite the recent discovery of new materials having superconducting properties at high temperatures, the necessity of measuring pressures at temperatures close or below 4.2 K still remains.

In the past 25 years, different pressure transducers have been developed or adapted for use at temperatures down to about 4.2 K.

Gas pressure measurements made directly at low temperatures are certainly preferable to indirect determinations through pressure measurements at room temperature and the use of long thin tubes connecting the low-temperature circuit with a room-temperature pressure transducer. The long-tube configuration may cause difficulties: in fact, at low pressures thermomolecular pressure difference corrections are necessary, because of the very high temperature differences. Thermal instability in the connecting tubes may also cause unstable readings and large drifts in transducer output, even when the instrument is located in a temperature-controlled room. The use of long tubes may cause, in addition, a reduction in the transducer response time to unacceptably low levels and create problems of non-hydrostaticity along the long connecting line.

Today, there is a fairly wide choice of pressure transducers working at the liquid helium temperature, though some are not fully reliable at long term and for applications requiring low uncertainty. For pressure measurements at the liquid helium temperature, it is very difficult to find a reliable transfer standard transducer ensuring medium- and long-term uncertainty between 0.01 and 0.1 %.

For tests and calibrations of pressure transducers at cryogenic temperatures and, in some cases, also in high magnetic fields, different calibration facilities have been proposed (Dean and Flynn 1966; McLellan 1968; Arvidson and Brennan 1976; Edwards and Linon 1978; Krafft et al. 1980; Cerutti et al. 1983; Boyd et al. 1990; Bager et al. 2000).

The design of a calibration unit for testing pressure transducers under cryogenic conditions should be based on the following criteria:

- The pressure transducer to be used in the cryostat should allow operations to be carried out from vacuum to high pressures (typically not exceeding 5 MPa).
- The pressurizing gas should be carefully thermally anchored to the cryostat with the use of different heat exchangers before reaching the transducer under test.
- A variable-temperature cryostat should be used.
- Temperature probes should be used to monitor temperature both around the pressure transducer body and be placed, whenever possible, in the gas as close as possible to the sensing element of the pressure transducer.
- The tubing connecting the transducers at the cryogenic temperature to the reference transducers or the primary standards at room temperature should have a small volume and should be leak tested at the maximum pressure of use.

Figure 8.16 shows a typical set-up for pressure transducer calibration at cryogenic temperatures.

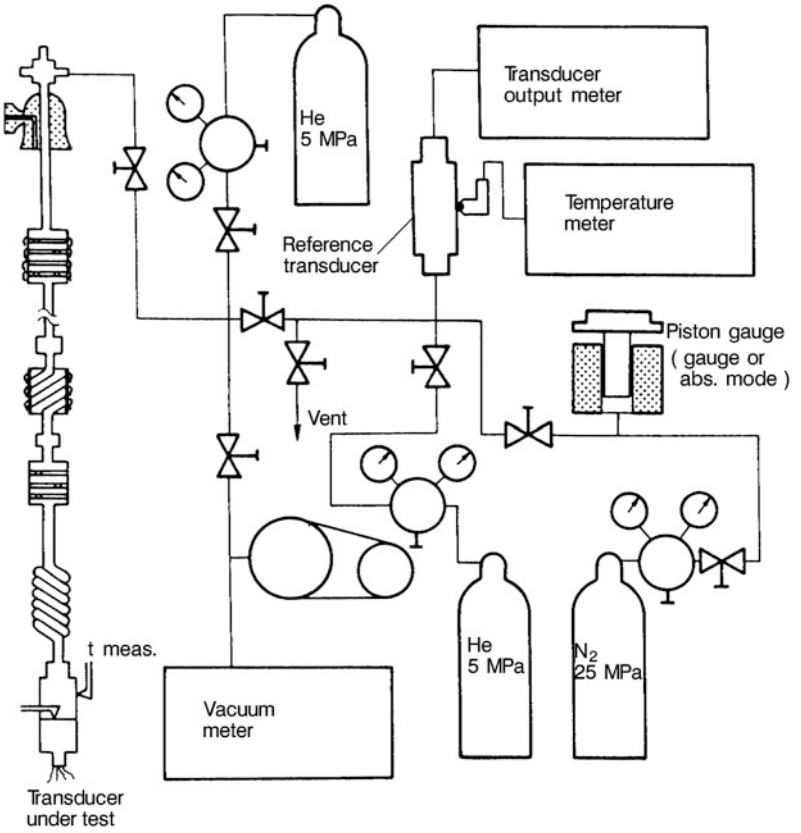

Fig. 8.16 Typical calibration setup for the calibration of pressure transducers at cryogenic temperatures

Each individual pressure transducer requires specific care, as operation at low temperatures is unusual with most of them. For example, with strain-gauge pressure transducers, the selection of the supply current versus measurement sensitivity is a compromise. In fact, at very low current values (generally below 1 mA) temperature gradients in the transducer are limited, but thermoelectric voltage effects in the transducer and wiring may make the output signal of the transducer irreproducible during calibration. With higher currents (typically 10 mA), irreproducibility is reduced, but the higher power dissipation will greatly increase thermal gradients and, even before the transducer becomes thermally unstable large calibration errors may occur, due to the dependence of the transducer temperature coefficient on thermal gradients.

In addition, the procedure for the calibration of a pressure transducer under cryogenic conditions should follow some special rules. Leak tests and careful system washing with the selected pure gas must be carried out, in order to operate under truly homogeneous conditions. This is particularly important when calibrations

have to be made at or below 4.2 K, as at this temperature the use of pure helium is compulsory.

After the transducer to be tested has been mounted into the cryostat, enough time should be allowed to elapse for thermal equilibrium to be achieved. Temperature measurements around and inside the pressure sensor are important to check whether temperature equilibrium is achieved and no thermal gradients are present whenever the operating temperature or pressure have been changed.

It is good practice to carry out some preliminary pressurization cycles to full-scale pressure, in order to observe pressure effects on the transducer and have an idea of the time necessary for temperature to return to equilibrium after each pressure application. In all calibration cycles, pressure should be applied slowly, and at each pressure point thermal stability around and inside the transducer should be checked.

The complete metrological characterization of a pressure transducer under cryogenic conditions should include the evaluation of the following parameters or the execution of the following operations:

- Thermal zero shift of the transducer over the whole temperature range of the test (typically room temperature, liquid nitrogen, and liquid helium temperatures).
- Long-term analysis of the stability of the transducer zero signal at the temperatures of interest.
- Calibration of the transducer at the temperatures of interest (generally room, liquid nitrogen, and liquid helium temperatures).
- An evaluation of the temperature coefficient and of thermal sensitivity at full scale of the pressure transducer at all the temperatures of interest.
- An analysis of repeatability, linearity, and hysteresis obtained from calibration cycles.
- An analysis of magnetic-field effects versus temperature and pressure; the magnetic-field direction with respect to the position of the pressure sensor is to be considered as well.

Since 1960, different pressure transducers have been tested for cryogenic temperature applications. Some of the commercially available units were not specifically designed for operation below 77 K, others were particularly designed for lower temperatures. They will be divided here into two categories.

One group is that of pressure transducers whose output signal changes with the strain applied to the sensor. The instruments belonging to this category generally feature a diaphragm or a bellows, which is deformed when pressure is applied; different techniques are employed for measuring strain. This category includes transducers of the strain-gauge (thin-film, unbonded, semiconductor gauges) and LVDT types. Though they measure an output quantity connected with displacement changes, potentiometric and reluctance pressure transducer types are generally considered in this group, as displacement is frequently produced on a diaphragm. The other group includes capacitance and resonant frequency pressure transducers.

The latest results obtained with the cryogenic pressure transducers of both categories will be analysed in the following sections.

8.4.1 Strain-Gauge Pressure Transducers for Cryogenic Applications

Tests to 1 MPa and at temperatures from 4.2 to 300 K were carried out by Krafft et al. (1980) on unbonded strain-gauge pressure transducers.

With a measured thermal sensitivity shift of about − 3.3 % at 4.2 K, at full scale, the percent change of the transducer output was globally equivalent to 0.01 % K^{-1}. The thermal zero shift was of the order of 0.006 % K^{-1} over the same temperature range. The reproducibility of the zero signal of one of the 1 MPa full-scale transducers for different pressures and temperatures between 300 and 4.2 K was of the order of 2 kPa, which is equivalent to 0.2 % of the transducer full scale. The same transducer was also tested at room temperature with the application of a magnetic field perpendicular to the sensor axis up to approximately 2 T. The observed output signal shifts of the transducer caused by the magnetic field were pressure-independent and were generally inside 20 kPa (2 % of the full scale). Such shifts are mainly due to the magnetization of the resistance wires of the transducer. The above data show that these transducers need no special calibration at 4.2 K, unless the required uncertainty is smaller than 4 %.

Cerutti et al. (1983) tested different strain-gauge pressure transducers (unbonded and thin-film types) to 3.5 MPa, at temperatures from 4.2 to 293 K, and in magnetic fields to 6 T.

The pressure transducers of the unbonded strain-gauge type showed a thermal zero shift of −0.76 % of the full scale and a thermal sensitivity shift equal to −2.2 % of the full scale at temperatures from 4.2 to 293 K. These values are of the same order of magnitude as the results obtained by Krafft with similar transducers. In these transducers, the effect produced by magnetic fields was concentrated below 1 T, at which values it was of about 7 % of the full scale. The effect diminished as the magnetic field was increased from 1 T up to 6 T. The dependence of the signal variation on the magnetic field was moderately affected by pressure and temperature when they were varied over ranges from 3 kPa to 2 MPa and from 6 to 22 K.

The overall results concerning tested thin-film pressure transducers of different types depended critically on the constructional parameters (e.g. the material of the diaphragm, of the strain gauge and of the dielectric substrate). The best results concerning reduction of sensitivity to temperature and magnetic fields were generally obtained with transducers having a stainless steel diaphragm, a dielectric silicon oxide layer and a strain gauge made of a nickel-chromium alloy.

Figure 8.17 shows the calibration factor (see Sect. 8.6 for its definition) versus pressure of one of the thin-film pressure transducers tested at temperatures of 4.2, 77 and 293 K.

The thermal zero shift of this transducer, which represents the worst of the cases considered, was equal to −11.3 % of the full scale and its thermal sensitivity shift was equal to −8.0 % of the full scale over the same temperature range from 4.2 to 293 K. The increase in the calibration factor when temperature is changed from 293 to 4.2 K (Fig. 8.17) cannot be considered typical for such class of transducers and it

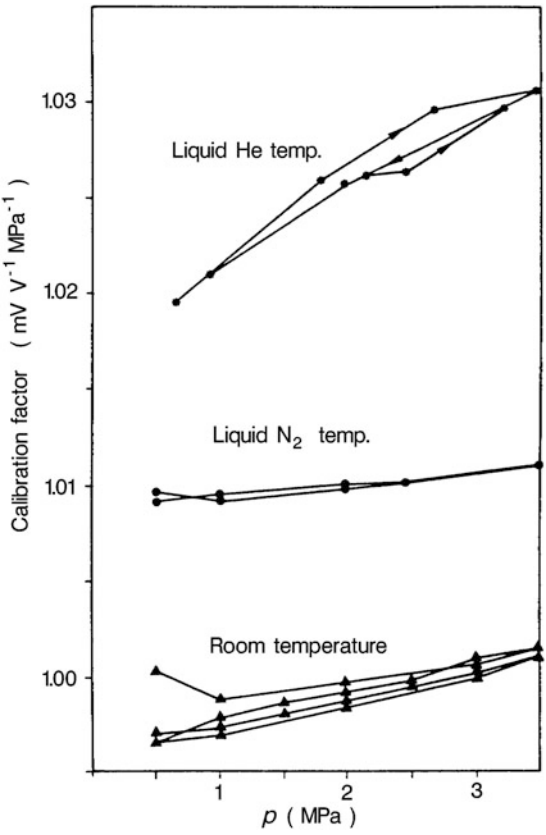

Fig. 8.17 Calibration factor versus pressure of a thin-film pressure transducer at room temperature and at liquid nitrogen and liquid helium temperatures

should be remembered that each transducer needs a specific calibration of its own at the different working temperatures.

The thin-film pressure transducers in question were also tested in magnetic fields up to 6 T with changed temperature and pressure values. Figure 8.18 integrates Fig. 8.17 by showing output signal changes of the same thin-film pressure transducer at pressures from 5 kPa to 3.5 MPa and at temperatures from 5.5 to 7.4 K, versus a magnetic field up to 6 T orthogonal to the plane of the diaphragm.

Figure 8.18 shows that the maximum output signal shift is equal to −3.6 % of the full scale and that output signal changes are less affected by temperature and pressure, than the change produced by the magnetic field.

The results of the tests on the different thin-film pressure transducers (Cerutti et al. 1983) can be summarized in this way:

- Negative zero signal shifts were observed when cooling the transducers from room temperature to 4.2 K. The magnitude of this shift, with the temperature changing from 293 to 4.2 K, ranges from a few percent to −20 % of the full scale, depending on the specific transducer.

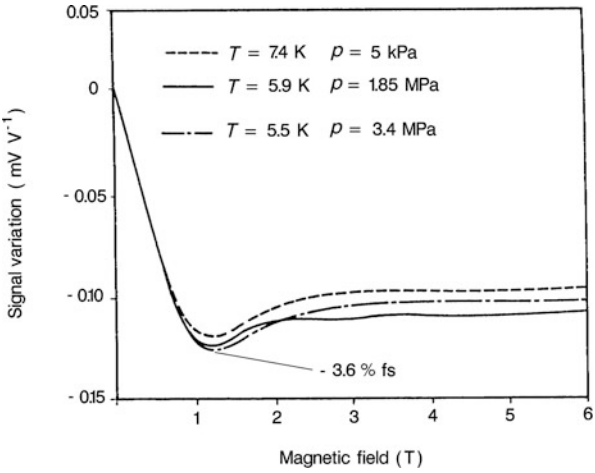

Fig. 8.18 Signal variations at different temperatures and pressures versus a magnetic field orthogonal to the plane of the diaphragm for a thin-film pressure transducer

- Negative thermal-sensitivity shift was also observed during cooling down to low temperatures; typically, the thermal sensitivity shift ranges from -0.2 to -8 % of the full scale with a change of temperature from 293 to 4.2 K. Frequently, a transducer exhibiting a moderate thermal-sensitivity shift has a large thermal zero shift or vice versa. As a general rule, both effects must be evaluated independently.
- Non-linearity and hysteresis errors are typically well below 1 % of the full scale; in the best case, at room temperature, generally they are below 0.1 % of the full scale. At 4.2 K a 0.5 % full-scale error is typical if care is taken to ensure good thermal stability during the tests.
- The calibration factor variation as a function of temperature cannot be predicted to be the same for every transducer of the same type and from the same manufacturer.
- A sizable part of the variation in the transducer output due to the application of a magnetic field parallel to the transducer axis occurs at field values below 1.5 T. Variations can be as high as 7 % of the full scale and are generally affected only to a small extent by pressure and temperature variations. The output signal of the transducer, with magnetic fields from 1.5 to 6 T, remains below the change observed at 1.5 T, its behavior depending on the transducer type.
- When thin-film pressure transducers are used, failure may occur owing to wire rupture during rapid cooling or during the application of a high magnetic field. As occurs with thin-film transducers, strain-gauge transducers may break owing to the same causes. As it is difficult to estimate the probability of failure, it is advisable to use multiple transducer systems to avoid having to interrupt measurements.
- After individual calibrations at the temperature of use, transducers of the strain-gauge type can be used for cryogenic applications, the typical estimated uncertainties being of the order of 1 % of the full scale.

The semiconductor pressure transducer is another type recently tested for measurements under cryogenic conditions. The sensors are miniature resistance elements arranged in a four-arm bridge placed on a semiconductor diaphragm. As they were

not developed for cryogenic applications, they have no sophisticated temperature compensation. Walstrom and Maddocks (1987) made an extensive study of the metrological characteristics of 20 commercially available semiconductor pressure sensors of 0.2 MPa full scale (tested at 13.3 and 133 kPa) over a temperature range from 300 to 1.6 K. From their investigation they drew the following conclusions:

- Semiconductor transducers are inexpensive but far from rugged instruments, as they are liable to be damaged by overpressure; a 20 % failure rate was reported during cooling to liquid helium temperatures.
- Sensor output voltage is approximately 2.5 times greater at the liquid helium temperature than at room temperature.
- Output sensitivity is temperature dependent over the full range from room to liquid helium temperatures.
- Output sensitivity varies by more than 20 % from one unit to another both at room and at liquid helium temperatures, so that an individual calibration of each sensor is necessary.
- Transducer calibration values obtained in the helium II region and calibration values along the helium II saturation curve generally agree well within 1 %.

Boyd et al. (1990) described a sensor calibration system and published the data obtained with silicon semiconductor transducers of 0.2 MPa (absolute and differential) and 1 MPa (absolute) pressure full scales, calibrated between 78 and 300 K. With appropriate calibrations at different temperatures it was observed that, typically, the output sensitivity increases by a factor 1.7 with temperature decreasing from 278 to 78 K. Reproducibility at 78 K, after repetitive cycles from room temperature to 78 K, ranges from 0.05 to 0.2 % of the full scale for the 0.2 MPa and the 1 MPa transducers, respectively.

Another transducer used for cryogenic applications is that of the variable-reluctance type in which pressure acts on a stainless steel diaphragm equipped with inductance coils on both sides. When the differential pressure is zero, the magnetic flux in both coils has equal reluctance; with the application of pressure the magnetic reluctance varies and brings about an inductance change in the coils. The coils are connected to an AC bridge, whose output voltage is proportional to the applied pressure.

Kashani et al. (1988) made different calibration tests on such commercially available pressure transducers for differential pressure measurements from 0.86 to a 34.5 kPa and absolute pressure measurements from 138 to 414 kPa, and from room temperature down to 2.1 K. The transducers had a typical reproducibility of 0.5 % of the full scale at room temperature and maintained their linearity and reproducibility within 1 % also at 77, 4.2 and 2.1 K. As sensitivity is temperature dependent and so is the zero output signal, in order to obtain accurate results, specific calibration tests at the temperatures of use have to be made. It should be noted that although the zero output signal of transducer shifts as the temperature changes between 4.2 and 2.1 K, its sensitivity to pressure remains almost constant. Therefore, it is possible to use the calibration data of the transducer at 4.2 K down to the super-fluid helium regime, provided that its zero signal variation with temperature is taken into account. Kashani

et al. (1990) used a number of transducers of the differential and absolute type for pressure measurements inside a ***s***uperfluid ***h***elium ***o***n-***o***rbit ***t***ransfer (SHOOT) experiment to demonstrate the technological needs in order to transfer superfluid helium in space. Also, micro-machined semiconductor pressure sensors have been designed and investigated (Maryamova et al. 2000).

8.4.2 Resonant- and Capacitance-Type Pressure Transducers for Cryogenic Applications

A different approach is necessary to build high-Q microwave-cavity pressure transducers, which are, essentially, sharply tuned L-C circuits whose resonance frequency shifts with pressure. The L-C circuit is built as a re-entrant microwave cavity having one thin wall which is deformed elastically by pressure, so that a capacitance change and, consequently, a shift in the resonance frequency of the circuit is produced. The resonance frequency value, typically 1.2 GHz, is measured and correlated to pressure variations. This microwave cavity pressure transducer was originally developed by Van Degrift (1974, 1975) and was modified by Jones et al. (1977).

In Van Degrift's configuration, the oscillations are maintained and measured with a tunnel diode housed inside the cavity. The active circuit is DC supplied and the signal output is measured with a high-resolution frequency counter.

A number of problems are apt to arise in pressure measurements carried out with microwave cavity transducers, in particular the following:

- Noise in power input may become frequency noise in the output. The cables of the whole electrical circuit must therefore be carefully shielded.
- A very small gap (approximately 10 μm) should be made for the capacitance element, which makes machining and assembling a delicate and critical operation.
- An appropriate material (copper or beryllium, especially) must be used for the cavity; it must have high electrical conductivity so as to enhance the Q of the cavity and reduce creep when the transducer is thermally cycled down to low temperatures and subjected to high pressures.

Figure 3.15 in Chap. 3 gives the basic configuration of a pressure transducer (Van Degrift et al. 1978a; Astrov et al. 1989 in the list of references of Part I).

Jones et al. (1977) separated the cavity from the active circuit, which is now more simple but less accurate than in the voltage-controlled oscillator in the Van Degrift's design. To reduce output noise, the 1.2 GHz electric components are coupled by means of a long coaxial wire.

Different prototypes have been built with different cavity geometry and gaps, the best results having been obtained with a gap of about 60 μm. Details concerning the design of the cavity and all the associated instrumentation are given in a report by Jones et al. (1977). Calibrations to about 40 kPa at 4, 76 and 298 K showed limited hysteresis and a residual standard deviation of the fit of the calibration curve of typically 0.1 % of the full scale (noise level of the order of 2 mV). Sensitivity values were 2.085×10^{-2} mV Pa^{-1}, 1.707×10^{-2} mV Pa^{-1}, and 1.679×10^{-2} mV Pa^{-1}

at temperatures of 298, 76 and 4 K, respectively. These results are consistent with the increase in the elastic modulus of copper with decreasing temperatures.

Other interesting pressure transducers used at cryogenic temperatures are of the capacitance type, of which Jacobs (1986) published an important survey. The development of very reproducible and highly stable capacitance transducers for pressure measurements at low temperature, e.g. for gas thermometry or for helium-3 melting curve thermometry, constitutes an important part of the pressure metrology work now being carried out in several research institutions (frequently not the national metrology institutes).

The sensor is generally a thin diaphragm made of specially selected materials (copper-beryllium, sapphire) forming the movable electrode of the capacitor having frequently sub-micron gap. The other electrode, generally made of the same material as the movable electrode, is stationary. Pressure applied to the movable electrode produces a capacitance change that can be measured directly or converted into frequency.

In many capacitance sensors, the diaphragm is made of copper-beryllium to minimize temperature effects. Interesting capacitance transducers were built (Straty and Adams 1969; Gonano and Adams 1970; Greywall and Busch 1980; Morii and Adams 1981; Greenberg et al. 1982; Schuster and Wolber 1986; Helvensteijn and Van Sciver 1990; Hieda et al. 2005).

Although these devices differ from one another in full-scale ranges and thermal metrological characteristics, all have good resolution. All may show drifts due to thermal cycling at room temperature and must be calibrated at the temperature of use. Their common feature is the small size, which allows them to be incorporated into low-temperature devices, used, for example, in investigations of the melting curve of helium-3.

An interesting approach was that of Lawless et al. (1985), who designed a multilayer capacitance sensor having a dielectric of a quantum ferroelectric material. The average sensitivity of this device is about 1.51 pF MPa^{-1}, and the sensor output is independent of magnetic field and of temperature when $T < 10$ K. Lawless and collaborators evaluated that the uncertainty of such sensors, for a typical full scale of some hundreds of megapascal is less than 0.1 % for a one-point pressure calibration and resolution is of the order of some hundreds of pascal.

Another interesting application for helium-3 melting curve thermometry is the capacitance pressure sensor designed by Schuster and Wolber (1986). It consists of a copper-beryllium diaphragm (10 mm diameter and 0.5 mm thickness) where a gap of 20 μm is realized between the reference and the movable plates. The calibration of pressure transducers was performed with a pressure balance in absolute mode up to 4 MPa with an experimental uncertainty of 50 Pa. Within the measurement uncertainty, no mechanical hysteresis of the capacitance sensor was found. Schuster and Wolber also designed a computer-controlled capacitance bridge of high resolution and accuracy in order to perform reliable capacitance measurements.

A significant improvement in the quality of capacitance pressure transducers for cryogenic use was obtained by Griffioen and Frossati (1985) with the design and testing of a small (8 mm diameter, 610 μm thickness) absolute pressure transducer of 3.5 MPa capacity made of two sapphire disks.

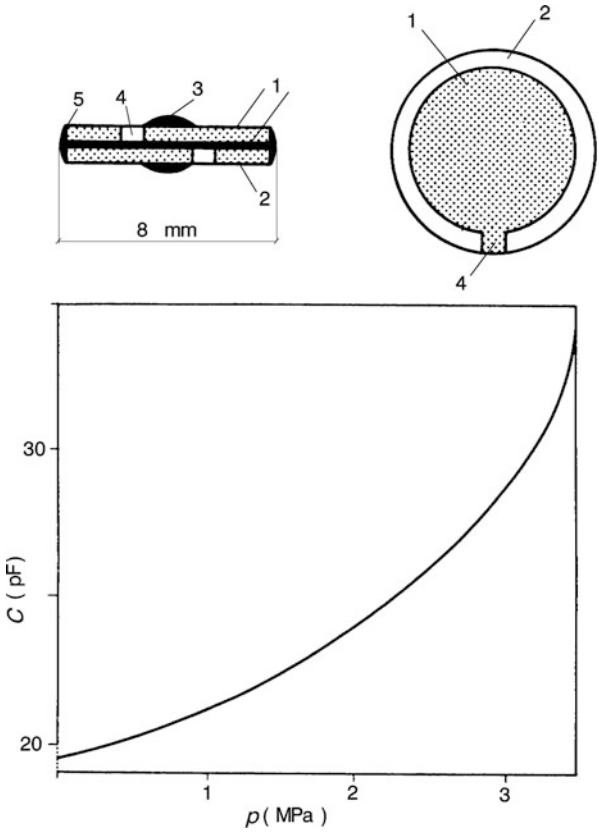

Fig. 8.19 Schematics of a capacitance pressure transducer (*1* platinum electrodes, *2* sapphire disks, *3* electric contacts, *4* platinum duct, *5* glass soldering connection). Behavior of capacitance versus pressure. (From Griffioen and Frossati (1985) with the kind permission of the authors)

Pressure acts on the external part of the two disks, which are soldered together with soft glass in a way that leaves an internal evacuated space and causes a capacitance change between platinum electrodes sputtered on the sapphire disks. Sensitivity at 3.5 MPa was 5 pF MPa^{-1} with a resolution of 1 Pa.

Figure 8.19 is a schematic drawing of this capacitance transducer and illustrates the behavior of capacitance variation versus pressure. Since the sensor is pressurized from the outside, the dielectric constant of the pressurizing fluid does not affect capacitance measurement values. No sizable thermal shift of the output signal was observed for the temperature range from 300 down to 1 K. Warming to room temperature and cooling to about 1 K produced small capacitance changes of the order of 0.02 pF (equivalent to a pressure change of about 6×10^{-4} at 3.5 MPa). The capacitance value, when the device was maintained for 4 weeks at temperatures below 0.3 K, showed no significant shifts.

Another transducer, built according to the same design, having a 100 kPa capacity, 20 mm diameter, 420 µm thickness, proved to be particularly suitable for gas thermometry. This transducer showed a sensitivity of 500 pF MPa^{-1} at full scale and a reproducibility of 0.4 Pa in pressure cycles from vacuum to 13 kPa. These results are very encouraging for the production of very accurate and stable pressure transducers for cryogenic applications.

Another sapphire capacitance pressure transducer, of large diameter, was fabricated at VNIIFTRI (Polunin et al. 1986; see also Astrov in the bibliography of Part I).

Basically, it is a differential pressure transducer, mainly used and tested under absolute conditions, operating to 1 kPa and in a temperature range from 4 to 300 K; its estimated uncertainty is 0.2 Pa. The edges of the two sapphire disks are soldered together by soft glass at a temperature of 950 °C, the internal volume is small and the connection of the inner space to the outside is obtained by means of a platinum tube soldered with soft glass at the centre of one of the sapphire plates. This configuration prevents oxidation of the inner surface of the transducer during heat treatment. Two aluminum-layer electrodes are evaporated on the outer parts of the sapphire disks. The deformation of the elastic element produced by pressure is related to the capacitance measured between the two aluminum electrodes. The sensitivity of this transducer near zero pressure difference is better than 0.05–0.1 pF Pa^{-1} and the temperature coefficient of the zero output signal is 0.05 Pa K^{-1}. Sensitivity and zero shifts can easily be taken into account with appropriate calibration at the different operating temperatures.

In designing differential pressure transducers for cryogenic applications, the most important parameters that have to be minimized are zero instability on thermal cycling and the temperature coefficient.

Monocrystalline sapphire is an excellent material in this respect, but to obtain the best mechanical stability, stresses at the edge of the disks must be minimized. Possibly, results could be improved by techniques (e.g. laser welding or pressure-welding at high temperatures) other than glass brazing of the sapphire disks. Such techniques must ensure reliable sealing and, at the same time, an efficient hinge configuration of the sapphire disks.

More recently, the Russian design of VNIIFTRI has been used as a pressure transducer (Pavese et al. 1998 in references of Part I) in differential (Steur et al. 2003 in references of Part I) and absolute modes (Steur et al. 2004 in references of Part I) in INRIM interpolating gas thermometer.

So far, the experience with capacitance transducers for pressure measurements at cryogenic temperatures has indicated future possibilities of constructing reliable transfer standards (based on sapphire capacitance devices) for cryogenic use having measurement uncertainties of the same order of magnitude as that of transfer standards for pressure measurements at room temperature.

8.5 Glossary: Terms Used in the Metrological Characterization of a Pressure Transducer

See Appendix H, which is valid for any transducer.

The listed terms and definitions are generally taken integrally from the *International vocabulary of metrology—Basic and general concepts and associated terms (VIM), 3rd Ed., JCGM 200:2008.*

Reference is made not only to the International Vocabulary of Metrology (VIM, 3rd Ed., 2008) but also to other relevant documents issued by different international organizations that deal more specifically with the calibration of pressure transducers (for example, British Standard number BS5233, 1986 and the EURAMET Guide N^{er} EURAMET/cg-17/version 01 (2007) which is now largely adopted in Europe).

8.6 Typical Procedure for the Static Calibration of a Pressure Transducer in Gaseous Media

A typical method for the calibration of a pressure transducer under static conditions and in gas media is to compare it with a primary standard pressure balance. The procedure indicated here is simplified and it will not substitute for international standards (e.g. ANSI/ISA-S37.3; CIAME Essais d'evaluation des capteurs de pression 1976; IEC 770; OIML numbers 16, 17, 19, and 53). The EURAMET *Calibration Guidelines on the Calibration of Electromechanical Manometers*, EURAMET/cg-17/v.01, July 2007 is now largely applied in Europe by the accredited laboratories for pressure measurements and constitutes a reference for the calibration of pressure transducers. The present procedure is in agreement with the above-mentioned EURAMET Guideline.

The pressure transducer under calibration must be connected to a pneumatic circuit (see, for example, Figs. 7.21, 8.15 for a typical differential transducer, or Fig. 8.16 for a typical pressure calibration under gauge or absolute conditions at low temperatures). The complete circuit, inclusive of the primary standard and of the pressure transducer, should be tested for possible leaks up to the maximum calibration pressure with the use of the selected gas and, if necessary, also in vacuum.

It must be remembered that the selection of gaseous media may depend on the pressure transducer to be calibrated (some are gas dependent, for instance a number of the vibrating-structure transducers described in Sect. 8.1) or on specific uses (for example, if tests must be performed at the liquid helium temperature, generally only gaseous helium must be used). If particular problems exist for the calibration with the selected fluid (e.g. when primary standards are available only to work in liquid media or work to the best accuracy only with a specific gas), "separators" can be used as null detectors dividing the different fluids (see Sect. 8.3.2). Obviously, the use of the separator must not introduce significant errors in transducer calibration.

The output signal of the pressure transducer under calibration should be measured with the most appropriate device allowing sufficient resolution, stability to be obtained and having an uncertainty at least of the same order of magnitude as the expected uncertainty of the transducer. The instruments for the measurement of the output signal of the transducer, which must be suitable for the type of transducer under calibration, must have low noise levels, well below the expected resolution of the transducer. The dissipation power of the transducer should be maintained as small as possible to avoid creating instability or thermal gradients on the output signal of the transducer, particularly when working at low temperatures (see Sect. 8.4). If the different parameters playing a role in the measurement of the output signal of

the transducer have not been previously determined, it is necessary to evaluate them and to select the most suitable values of the quantities involved. For example, for a strain-gauge pressure transducer, it will be necessary to select a supply voltage value at which, according to the electrical resistance of the strain-gauge bridge, the value for the current circulating in the strain-gauge elements will be acceptable.

In normal calibration operations the apparatuses for the measurement of the output signal should be electrically powered for at least a few hours.

If some quantities affect the values of the output signal (for example, when a capacitance transducer operates at a temperature value higher than room temperature) it is necessary to wait until the effect of the specific influence quantity (temperature, in the example) is complete.

The appropriate primary standard pressure balance to be used for calibration must be selected according to the measurement mode (absolute, gauge, or differential) and to the expected uncertainty level of the pressure transducer to calibrate. Chapter 7, in particular Sect. 7.2, gives the different experimental details and the calculations for the best use of such primary instruments. As regards the way to take account of the different physical quantities contributing to the overall uncertainty of pressure measurement with a pressure balance, the reader is referred to Sect. 7.2.4 and to Tables F.2, F.3, F.4 in Appendix F.

The uncertainty of the primary standard pressure balance to be used for transducer calibration must be lower at least by a factor "*four*" than the expected uncertainty of the transducer. For example, to calibrate a pressure transducer having an estimated measurement uncertainty of 100 ppm at 10 MPa, the uncertainty of the selected standard pressure balance at 10 MPa must be 25 ppm at the utmost. The reason for adopting this criterion is that the pressure balance itself must not introduce significant instability or pressure fluctuations during calibration. There are instances, however, in which this rule cannot be integrally applied, particularly in some cases of small differential pressure measurements.

The calibration of a pressure transducer is normally started with at least three pressurization pre-cycles of the transducer to the maximum pressure, followed by a return to the zero pressure value. In this "pre-cycling", the transducer is compared with the pressure balance operating in equilibrium. The purpose of this preliminary operation is to check the performances of the transducer at the full pressure scale and the way the output signal of the transducer returns to its normal value when zero pressure is restored. Sometimes, during this initial pressurization, it is possible to evaluate some significant parameters (e.g. possible "creep" effects at the pressure full scale can be evaluated directly from a measurement of the output signal at the maximum pressure versus time). When the output signal of the transducer is stable at zero pressure, the calibration cycles can be started.

Typically, a calibration cycle consists of the comparison of the pressure measured by the pressure balance with the measured transducer output signal; the comparison is carried out at ten pressure points equally distributed over the whole scale of the transducer and at increasing and decreasing pressure values. Three calibration cycles are executed at the same pressure points and without interruption.

The three calibration cycles make it possible to compute for each pressure value (see also the glossary in Sect. 8.5 and Appendix H.):

- Repeatability and hysteresis, referred to the pressure reading of the transducer or to its full-scale value (repeatability represents the scatter of the transducer readings at each calibration pressure point and hysteresis is computed by comparing the transducer readings in increasing and decreasing order at the same individual pressure values).
- Linearity of the transducer output signal, which is frequently computed indirectly from the behavior of the gauge factor (sometime also called calibration factor) of the transducer (defined as the output signal-to-applied pressure ratio) versus pressure.
- The best interpolation equation of the type $p = \mathrm{f}(X)$, where X is the output signal of the transducer and p is pressure. The interpolation equation can be a linear or a polynomial function, depending on the type of the transducer and the required level of uncertainty. For each interpolation equation the residual standard deviation (1σ) of the predicted response for the selected fitting can be computed.

All the above items of information constitute the main metrological characteristics of a pressure transducer.

To compute the overall uncertainty to be associated with a pressure transducer, it is necessary to sum the different previously evaluated contributions, namely, pressure balance uncertainty, the maximum repeatability, and hysteresis, the 1σ of the selected interpolating equation and the uncertainty of the measurement of the transducer output signal.

If the output signal of the transducer is converted directly into pressure units (Pa, kPa, bar, mbar, ...), the transducer metrological characteristics can be evaluated in the same way as before, but frequently in this case an average correction (in pressure units), representing the pressure difference between the primary standard and the transducer under calibration can be useful. In such cases, it is necessary to determine also the behavior of this average correction versus the applied pressure, as non-linearity effects may be very large.

The temperature coefficient of the pressure transducer must be determined by repetition of the calibration cycles in the temperature range of interest. It is necessary as well to analyse the output signal of the transducer as a function of temperature, namely thermal zero shift, the change in the gauge factor with temperature, i.e. the temperature coefficient of the gauge factor, and the change in sensitivity with temperature, i.e. thermal sensitivity shift.

A pressure transducer can be subjected to special tests, in order to evaluate its characteristics under particular working conditions such as vibrations, specific temperature ranges, magnetic fields, hostile fluids, etc.

Chapter 9
Gas-Based Pressure Fixed Points

In Chaps. 7 and 8, we discussed the pressure measurements in gaseous media from 100 Pa to 100 MPa, as well as the appropriate primary and secondary pressure standards and the problems connected with their use at the lowest uncertainty level.

Without changing the basic definition of the pressure, which is given, for the pressure range considered in this book, essentially in terms of a force exerted on a known area or of the height of a liquid column, the relationship between well-defined states and pressure values is proving very useful from the metrological standpoint, particularly in view of the possible use of such states as transfer standards for the verification of pressure values obtained from the measurement of force per unit area. The discussion in the present book being limited to gaseous substances, the establishment of a pressure fixed point involves the definition of a pressure-to-temperature relation generally occurring during a phase transition (triple point, melting or freezing curve, vapor-pressure equilibrium, critical point, . . .), which is intrinsically based on some invariant properties of the substance (see Chap. 2).

Therefore, a pressure fixed point can be defined independently of specific implementation and consequently may be an important tool for comparisons, for example, of primary pressure standards. A general advantage of such basic thermodynamic relations is that they do not need correction for the local gravity acceleration, whereas primary pressure standards need an accurate measurement of this physical quantity.

The thermodynamic state used to define a fixed point must be highly reproducible, reversible, uniquely defined as to temperature and pressure, immune, as far as possible, from gas impurities, and detectable with a well-defined procedure in a conveniently short time.

Thermodynamic temperature and pressure relations can be exploited advantageously not only in pressure metrology but also in the definition of the temperature scale, as discussed in Part I. We do not use here strictly the definition of "fixed point" given in Chap. 2, but for simplicity we include in this term all phase transitions.

The realization of pressure fixed points involves different phases of pure substances: solid, liquid and vapor at the triple points (see Chap. 2), liquid or solid and vapor in vapor-pressure equilibrium (see Chap. 4), solid and liquid in melting equilibrium (see Chap. 5).

F. Pavese, G. Molinar Min Beciet, *Modern Gas-Based Temperature and Pressure Measurements,* International Cryogenics Monograph Series,
DOI 10.1007/978-1-4419-8282-7_9, © Springer Science+Business Media New York 2013

In high-pressure metrology, melting or freezing transitions are sometimes used, but the method adopted to detect the phase transition frequently gives rise to high hysteresis or else a long time is required for establishing and measuring the correct temperature–pressure relation.

For pressure measurements using gases in the range considered in the present book, triple points or two-phase equilibrium points could both be used. As the latter are not invariant, pressure fixed points defined by means of a two-phase equilibrium require temperature to be defined, while the pressure value is obtained from the thermodynamic state of the substance employed.

With triple points, both temperature and pressure are uniquely determined through the thermodynamic properties of the substance. A triple point is therefore a superior tool, provided that pure gas is used and that its dp/dT coefficient during melting is small enough to allow pressure to be sufficiently reproducible, account being taken also of temperature reproducibility.

Data about some gas triple points widely used in pressure metrology are given in Table 9.1.

Taking the argon triple point (68 890 Pa at 83.8058 K) as an example, a temperature reproducibility of ± 0.1 mK will produce an expected pressure reproducibility of ± 0.8 Pa. Experimental determinations, e.g., Pavese (1981) showed that it is possible to achieve a pressure reproducibility of the argon triple point of ± 1 Pa, equivalent to ± 15 ppm. That was also confirmed by Bandhyopadhyay et al. (1991) on argon triple point pressure showing a standard deviation of the repeated measurements lower than 0.89 Pa.

Obviously, other requirements (e.g., easy availability, short realization time, compatibility of the used gas with the material of the triple-point cell, ...) must also be taken into account.

From the standpoint of pressure metrology, the necessary characteristics of a gas pressure fixed point are high stability as to temperature and reproducibility of the fixed point, low dp/dT, and minimum possible dependence of the fixed-point pressure value on gas purity. It is the combination of these three parameters that leads to the selection of a gas pressure fixed point.

Sealed devices, which have the advantage of being transportable (see Sects. 2.3 and 4.2) make these requirements even easier to satisfy and the use of fixed points simpler and convenient also in comparisons (see Steur and Pavese 1993/1994).

We have already mentioned in Chap. 8, Sect. 8.3.2 the possible use of a differential pressure transducer, as a null instrument, to separate the gas in the device used in an experiment (e.g., the measurement of vapor pressure in an argon sealed cell) from the gas used in the primary standard (e.g., nitrogen used as the pressurizing fluid in a liquid column manometer or pressure balance).

The selected differential transducer, used in gas pressure fixed-point determination, must be highly stable. If the transducer is used only for purposes of comparison, its pressure reading must be only reproducible. The situation is different when the transducer is used jointly with the primary standard to obtain an absolute value, for example, the determination of the triple-point pressure. In this case, it is necessary to evaluate completely the accuracy of the transducer on the basis of reproducibility, of the line pressure influence on the zero signal, of the effects of hysteresis, of the

aerostatic head corrections, and of the temperature gradient from the experimental cell to the primary pressure standard.

If only a reproducible pressure value is required, as is the case of sealed cells realizing the triple point of a substance to be used as a transfer standard for comparison purposes, the zero adjustment of the transducer can be made on an assumed pressure value, provided that adjustment affects the linearity and sensitivity of the transducer to a small extent. In this case, the aerostatic head correction is not needed, provided that the temperature profile along the pressure tube is stable and reproducible. The change of the zero output signal of the transducer with the line pressure can be neglected.

Pressure transducer complete characterization is a requirement that is added to the basic ones mentioned above for the determination of a gas pressure fixed point.

The basic definitions of the different thermodynamic principles, already discussed in Part I, will not be repeated in the present chapter, which integrates the preceding one only as regards the use of fixed points in gas pressure metrology. It may be partially used as a reference, even if the considered pressure range is much higher than the one used in the present book, the report of Bean et al. (1986) aimed to suggest and recommend a practical pressure scale.

9.1 The Pressure Scale from 10^2 to 10^8 Pa Based on Pressure Fixed Points

In recent years the use of fixed points in temperature metrology was reexamined and improved. The main aim was the realization of the temperature scale by means of fixed points realized as sealed and self-contained devices. As some of them show pressure reproducibility of interest in pressure metrology, they can be used as well as pressure fixed points.

The different methods and techniques used to obtain thermodynamic equilibrium between the different phases of the gaseous substance are fully discussed in Part I.

Among the different thermodynamic relations, the triple points of pure substances that are gaseous at room temperature are used to realize a large number of fixed points. As a rule, triple points are reproducible at the submillikelvin level. When the triple-point temperature changes during melting the reproducible pressure fixed point can be defined at $1/F = 1$, from a plateau definition similar to that shown in Fig. 9.2, Sect. 9.2 widely explained and discussed in Part I.

Over the whole range of pressures from 100 Pa to about 100 MPa, triple points or other fixed points suitable for the realization of a pressure scale can be found in Fig. 9.1 that represents a schematic view of a possible pressure scale.

This scale, however, must not be considered a substitute for the pressure scale based on primary standards previously described in Chap. 7. Rather, some of the fixed points in Fig. 9.1 can be used as transfer standards for the verification of the primary pressure scale or in the study of some systematic effects in primary standards by exploiting the advantage of the high reproducibility of the pressure value they realize and of the fact that a thermodynamic law uniquely defines them.

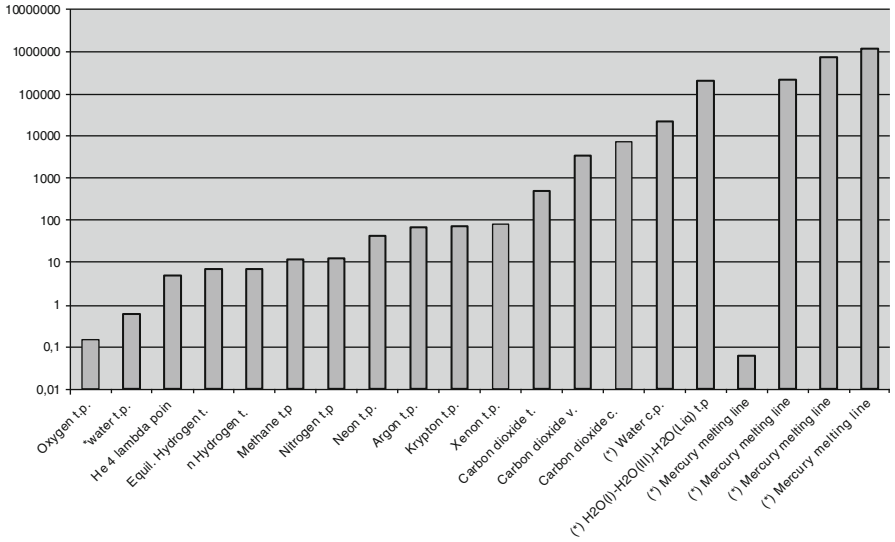

Fig. 9.1 Possible pressure scale based on gas fixed points, all the indicated pressures are absolute one. The y scale is log p/kPa. t.p. = triple point, v.p. = vapor pressure, c.p. = critical point, m.l. = melting line. The fixed points preceded by (*) do not originate, differently from the others, from substances that are gaseous at room temperature. (*) Mercury t.p. (**234.3156 K**; 0.063 kPa), Oxygen t.p. (**54.3584 K**; 0.14625 kPa), (*) Water t.p. (**273.16 K**; 0.611657 kPa), Helium 4 point (**2.1768 K**; 5.0 kPa), Equil. Hydrogen t.p. (**13.8033 K**; 7.034 kPa), n Hydrogen t.p. (13.952 K; 7.21 kPa), Methane t.p. (90.6936 K; 11.696 kPa), Nitrogen t.p. (63.150 K; 12.526 kPa), Neon t.p. (**24.5561 K**; 43.371 kPa), Argon t.p. (**83.8058 K**; 68.890 kPa), Krypton t.p. (115.776 K; 73.100 kPa), Xenon t.p. (161.4037 K; 81.670 kPa), Carbon dioxide t.p. (216.590 K; 517.98 kPa), Carbon dioxide v.p. (273.16 K; 3486.08 kPa), Carbon dioxide c.p. (340.193 K; 7382.5 kPa), (*) Water c.p. (647.256 K; 22120.0 kPa), (*) H_2O(I)-H_2O(III)-H_2O(Liq) t.p. (250.935 K; 208829.0 kPa), (*) Mercury melting line for pressures from atmospheric pressure to 1.2 GPa. $p/\mathrm{MPa} = 19.32845(d/\mathrm{K}) + 0.0018333(d/\mathrm{K})^2 + 0.000059791(d/\mathrm{K})^3$ with $d/\mathrm{K} = T/\mathrm{K} - 234.3156$, T is the ITS-90 temperature and p is the absolute pressure. The above equation is referred to the ITS-90 and uses 234.3156 K as the mercury triple point. For each substance the temperature (K) and the pressure (kPa) of the fixed point are given in parenthesis. All temperatures are related to the ITS-90 temperature scale. The temperatures in **boldface type** indicate points used also as temperature fixed points for the definition of the ITS-90

9.1.1 Triple Points

A triple point marks the transition between the liquid and the solid phase in equilibrium with the vapor phase. For a general definition of a triple point and for the realization of temperature fixed points using triple points of gases the reader is directed to Chap. 2.

The realization of the triple point of a gas simply requires cooling it until condensation of the liquid phase is followed by solidification. Pressure and temperature values decrease until the liquid begins to freeze, then, with pure substances, their values remain constant and fixed until freezing is completed. When the whole liquid

is solidified, pressure and temperature fall again. In order to obtain stable parameters at the triple point in a real experiment, the substance must be maintained under nearly adiabatic conditions by using the techniques, method, and experimental apparatus described in Part I (Chap. 2).

Of particular concern are gas impurities, which, if soluble, may affect the temperature value of the triple point, and, if volatile, affect the pressure value at the triple point. Consequently, impurities must be as low as possible.

Different triple points of gases that can be useful in pressure metrology are listed in Fig. 9.1. In brackets, after the name of the substance, is given the temperature and pressure at the triple point, respectively, in kelvin and kilopascal. The triple-point temperatures of the different substances are referred to the ITS-90 temperature scale.

Tables 9.1 and 9.2 in Sect. 9.3 and Appendix in Sect. 9.4 give triple-point data; similar data are given for other pressure fixed points of substances not gaseous at room temperature.

Figure 9.1 shows that in the pressure range from 100 Pa to more than 100 MPa there are numerous gas triple points, which concentrate mainly in the interval from 1 kPa to about 0.5 MPa. The temperature values of the different triple points lie in a range from about 2 K to room temperature. Not all the listed pressure fixed points are equally useful in terms of expected reproducibility.

The application of triple points for pressure scale verification was greatly improved by the use of gas sealed cells (Pavese 1981). In particular, the argon triple point is well suited for use as a pressure transfer standard (see also Sect. 9.2).

As regards, for example, the realization of the argon triple-point sealed cell, reference is made to Fig. 2.15.

The argon cell used by Bonhoure and Pello (1983) is similar to that used by Bonnier (1975), with the addition of a differential pressure transducer, and also Bonhoure's experiment for the realization of the argon triple point is similar to that of Bonnier (Chap. 2, Sect. 2.4).

It must be noted that, potentially, with an individual sealed cell a large part of the pressure scale can be realized with the use of the vapor-pressure curve. So far, this highly interesting possibility has not been extensively exploited in gas pressure metrology.

9.1.2 Other Pressure Fixed Points

In addition to triple points, the vapor-pressure curves (Ronsin 1987), the critical points, or the melting curves of some substances (e.g., the helium-3 melting curve, the mercury melting curve, ...) can be used to realize fixed points as parts of a pressure scale (Zhokhovskii 1989; Bean et al. 1986). In Fig. 9.1 and Table 9.2, some of these fixed points are given.

Vapor-pressure manometry was recently substantially revitalized by the use of high accuracy pressure transducers for absolute pressure measurements along the vaporization curve. A very interesting experiment is the absolute determination of

the carbon dioxide vapor-pressure value at 273.16 K given by Bignell and Bean (1988). Despite the (moderate) dependence of the basic vapor-pressure parameters on the purity of the gas sample, this pressure point is particularly useful: in fact, given the low-pressure uncertainty of its determination (3.48608 ± 0.000057 MPa equivalent to 16 ppm at the 1σ level), it could be a competitive transfer standard to check the pressure scale realized by means of pressure balances in a range particularly interesting for a better understanding of the uncertainty limits of pressure balances when operating with different gases and under different conditions of use (see Chap. 7, Sect. 7.2.7).

For pressures much higher than the atmospheric and up to 1.2 GPa, substances that are liquid at room temperature, must be used. The mercury melting line should be mentioned in this connection (Molinar et al. 1980, 1991). At pressures of about 227 MPa with the mercury cell maintained at a stable temperature of approximately 246.0 ± 0.002 K, the estimated pressure uncertainty of the mercury melting line used as a pressure fixed point is 0.1 MPa, calculated as the sum of pressure and temperature uncertainties plus 3σ residuals of the polynomial fit (equation in Appendix of Sect. 9.4).

The procedures for the determination of the exact melting conditions must not perturb thermal equilibrium. A procedure generally applied once thermal equilibrium is achieved is to increase slowly pressure until the substance freezes (for mercury, it is necessary to over pressurize by about 50–100 MPa). When thermal equilibrium is reached again, pressure is decreased at a regular rate until the substance starts to melt. With each change of pressure it is necessary to wait for thermal equilibrium to be achieved. Different methods (change of electrical resistance, thermal differential analysis, volume changes, ...) can be used for the detection of the melting phenomenon (e.g, Molinar et al. 1980, 1991; Sharma et al. 1993).

9.2 Experience in the Use of Fixed Points as Pressure Transfer Standards

A large number of fixed points are realized using sealed cells. As an example, the experiment of Pavese (1981) was performed using a sealed cell for the realization of triple points as temperature fixed points, of the type shown in Fig. 2.15 (see Sect. 2.3.1.2). The cell is contained in a vacuum adiabatic calorimeter and it has a room-temperature differential pressure transducer for separation of the small sample (approx. 0.1 mol) of pure gas contained in the cell from the manometric gas, as shown in Fig. 4.7.

Performing a pressure fixed point at the triple point combines the techniques of obtaining a temperature triple point (see Chap. 2) and of realizing a point of the vapor-pressure scale (see Chap. 4). The former technique is necessary to obtain a correct triple-point plateau, i.e., the temperature versus time record shown in Fig. 2.16 (see Sect. 2.3.1.2).

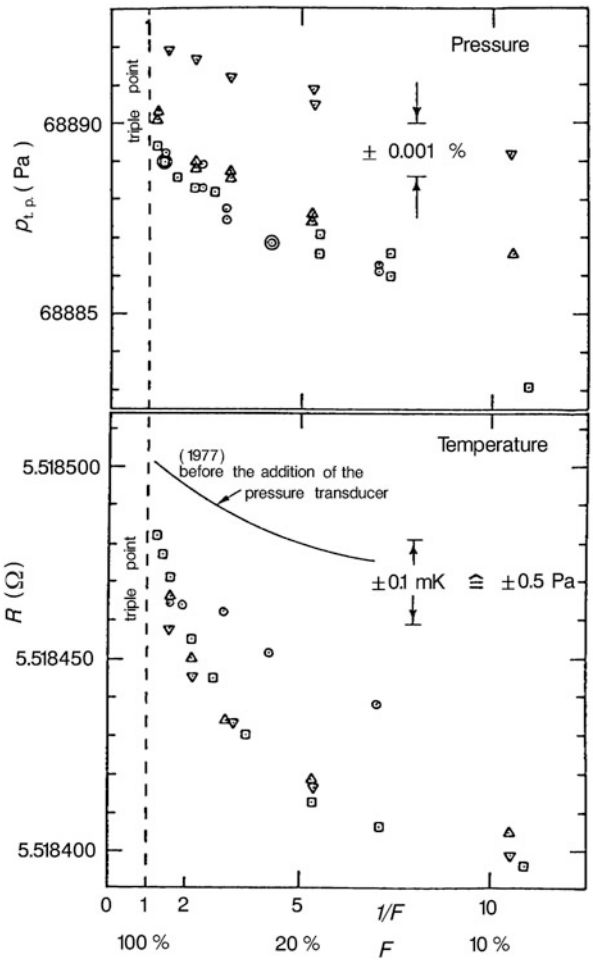

Fig. 9.2 Experimental results of the triple point of argon: pressure and temperature of the triple point versus the melted fraction ($1/F = 1$ is equivalent to 100 % melted)

The latter technique is important in order to perform a correct pressure measurement in a cryogenic environment, considering also that, owing to a generally small value of dp/dT at the triple point, thermal effects are significantly larger on pressure than on temperature. Therefore, for example, the time required for pressure reequilibration after each heating step is larger than for temperature. On the other hand, owing to the extremely high temperature stability and uniformity that can easily be achieved during the triple-point plateau, it is more accurate and by far easier to realize the triple-point pressure fixed point than any other temperature-dependant point of the saturated vapor-pressure curve, even if a larger value of dp/dT seems to be more favorable (as stated, e.g., by Afanas et al. 1987).

For the reasons explained in Chap. 2, the melting temperature shows a slight dependence on the melted fraction. The pressure value changes slightly too, correspondingly, as shown in Fig. 9.2.

Though small, this change must be taken into account for attaining the best accuracy allowed by the fixed point. Therefore, the pressure fixed point, as the temperature one, is defined at the *liquidus point*, $1/F = 1$.

It is interesting to note that Bandyopadhyay et al. (1991) at PTB found for the argon triple-point pressure value a very small dependence from the percentage of the liquid phase. The mean value of 17 determinations, lying between $F = 0.267$ and $F = 0.865$, was 68 890.7 Pa with a standard deviation of 0.85 Pa. If the PTB measured values are linearly fitted for $F = 0.5$, the argon triple point will be 68 890.6 Pa with a standard deviation of 0.86 Pa. If the PTB measured values are linearly fitted for $F = 1$, the argon triple point will be 68 890.8 Pa with a standard deviation of 0.86 Pa.

When the gas sample is large (>1 mol), instead of using the calorimetric stepwise method, the melting plateau can be realized with the continuous heating method (Bonhoure and Pello 1983). This realization has been described, for the cell type shown in Fig. 2.24b, in Sect. 2.3 and Fig. 2.20b in Sect. 2.4.3.2. In the latter case, the melting must be performed with different durations, in order to check that the melting speed does not influence the measured pressure, i.e., a true thermal equilibrium is attained. Also in this case, the liquidus point has to be used.

The fixed point can be used as a transfer standard, in which case no pressure corrections have to be done, such as for the aerostatic head. This avoids measuring (or estimating) the temperature distribution along the pressure tube connecting the cell to the differential pressure transducer. Also, the zero-pressure value of the transducer can be measured at a sufficiently low temperature of the cell, as the small vapor pressure at low temperature (e.g., 9.06 Pa at 47 K for argon) does not need to be known but only to be reproducible, avoiding the delicate and complicated use of the by-pass valve.

However, all these corrections have to be done if the cell is used for the absolute determination of the pressure fixed point. The comparison of experiments on the triple point of argon has shown that the reproducibility of different independent realizations is within their stated uncertainty.

Among the different gas triple points useful at the pressure transfer standard level, the argon triple point is surely the more widely employed for the verification of the pressure scale. The reasons for its application are several.

The argon triple point shows an excellent temperature reproducibility of about ± 0.1 mK and a small $\mathrm{d}p/\mathrm{d}T$ of 8.0 kPa K^{-1} on the vapor-pressure line near the triple point. Therefore, the argon triple point, besides its use as a ITS-90 fixed point, is a very interesting fixed point also in pressure metrology, as both its temperature and pressure values (83.8058 K, 68 890 Pa) are in a temperature range easy to realize and its pressure value lies in a very important range for liquid-column manometry. These advantages have been exploited and a number of realizations of this pressure fixed point were developed at IMGC, now INRIM, (Pavese 1981), at BIPM (Bonhoure and Pello 1983), and at PTB (Bandyopadhyay et al. 1991). The argon triple-point pressures obtained (Pavese (1981) found 68 890 ± 1.5 Pa; Bonhoure et al. (1983) found 68 890.5 ± 0.7 Pa and Bandyopadhyay et al. (1991) found 68 890.8 ± 0.8 Pa) are in very good agreement with each other.

The argon triple point has also been used as a pressure transfer standard to check mercury column manometers for absolute gas pressure measurements. In comparison between laboratories, the use of a transportable sealed cell and, consequently with the same gas, reduces the relevant systematic errors.

The BIPM laboratory used an argon triple-point cell for a comparison between its primary interferometry manometer and a similar instrument installed in the French Centre d'Essais en Vol in Brétigny (Bonhoure and Pello 1983).

The comparison lasted 1 year and involved 15 measurements at each of the laboratories. In the measurements at BIPM, the average argon triple-point pressure was 68 890.0 Pa, with a residual standard deviation of the mean value (1σ) of 0.7 Pa. The measurements made at the Centre d'Essais en Vol in Brétigny gave an average pressure result of 68 890.2 Pa, with a residual standard deviation of the mean value (1σ) of 0.4 Pa. The two average results differ by only 0.2 Pa, a value well inside the estimated uncertainty of the two mercury manometers compared.

A similar comparison experiment was made between BIPM and IMGC (now INRIM), in order to verify the pressure scale maintained with mercury interferometer manometers whose uncertainty was estimated by both laboratories to be well below 10 ppm over the whole pressure range.

The BIPM average argon triple-point pressure was 68 890.0 Pa (also in this case, it was the average of 15 measurements in one year's time) with a residual standard deviation of the mean (1σ) of about 0.2 Pa. The average IMGC-INRIM argon triple-point pressure value was 68 889.4 Pa with a residual standard deviation of the mean (1σ) of about 0.2 Pa, obtained from eight measurements in 1 week. The pressure difference at the argon triple point between BIPM and IMGC-INRIM was 0.6 ± 0.3 Pa, that is, well inside the estimated uncertainties of mercury manometer primary standards for this pressure range.

In other laboratories, research work on the nitrogen triple point (12.526 kPa at 63.150 K) showed that this point can be used also as a satisfactory transfer standard (Harrison et al. 1976).

Other fixed points (carbon dioxide vapor pressure of 3 486.08 kPa at 273.16 K and water I-III-Liquid triple point at 208.829 MPa and 250.935 K investigated in both cases by Bignell and Bean 1988, 1989) proved to be suitable as pressure transfer standards.

The carbon dioxide vapor-pressure fixed point, representing the equilibrium between the vapor and the liquid phase, was determined as 3.48608 MPa at 273.16 K with an estimated uncertainty of 0.000057 MPa (equivalent to a standard uncertainty of 16 ppm at the 1σ level) and with an estimated reproducibility of 24 Pa (equivalent to 7 ppm), and a dp/dT of 92.2 kPa K^{-1} (Bignell and Bean 1988).

Figure 9.3 shows the apparatus used to measure the carbon dioxide vapor pressure.

After initial evacuation and heating, the experimental cylinder housed inside the water triple-point cell is cooled and the carbon dioxide admitted to reach a pressure of about 5 MPa. The cylinder is isolated and the cell is warmed to 0 °C. The zero signal of the differential pressure transducer is adjusted and its bypass valve closed. Nitrogen is admitted on the side of the absolute pressure balance of the differential pressure transducer, and the pressure difference is adjusted by means of small standard weights

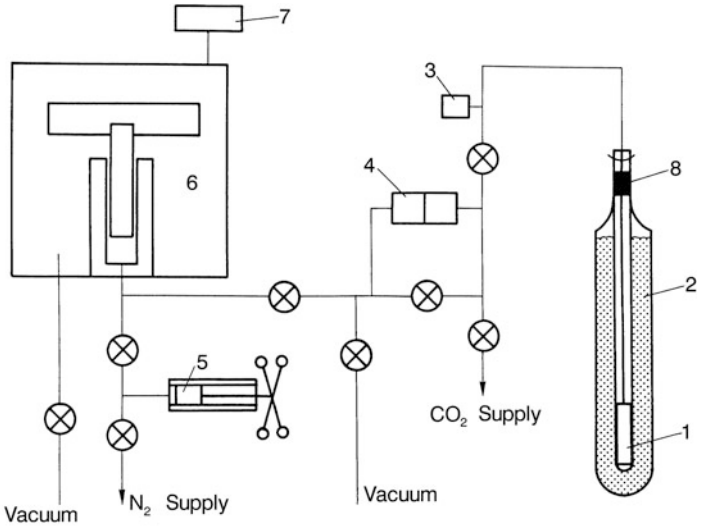

Fig. 9.3 Apparatus used to measure the carbon dioxide vapor pressure at 273.16 K (*1* sample bomb, *2* triple-point cell, *3* pressure transducer, *4* differential pressure transducer, *5* volume adjuster, *6* pressure balance used in absolute mode, *7* vacuum gauge, *8* aluminum block). (From Bignell and Bean (1988) with the kind permission of the authors)

on the pressure balance, until the reading of the differential pressure transducer is lower than 1 kPa. Temperature is checked and controlled, to be maintained at 273.16 K, and the pressure balance and the differential transducer both measure pressure. The vapor pressure of the carbon dioxide sample is the sum of the pressure measured by the pressure balance, the residual vacuum pressure in its bell jar, the aerostatic head pressure between the reference level of the pressure balance and the surface of the liquid in the cylinder (a part of the aerostatic head pressure concerns nitrogen and a part carbon dioxide), plus the pressure reading of the differential pressure transducer.

The experimental determination of the pressure of carbon dioxide vapor showed the substantial influence of the degree of purity of carbon dioxide samples. Among the different ways of preparing a sample, a method is recommended in which sodium bicarbonate of analytical reagent quality is heated and then its water content is removed. This pressure fixed point lies in a very convenient range for checking pressure balances.

The realization of the H_2O(I)-H_2O(III)-H_2O(liq) triple point requires the determination of the solid I-solid III-liquid equilibrium in a way which is not merely confined to determining the pressure and temperature values of the triple point because liquid water is quasistable in the stability region of solids. In fact, it is necessary to penetrate into the stability region of different solid phases, then to approach first the I-III phase transition and finally to identify the triple point, at which the three phases coexist. The experimental reproducibility of this triple point was estimated to

be 3.6 kPa and the temperature reproducibility at the triple point 40 mK. The water (solid I-solid III–liquid) triple point determination as 208.829 MPa at 250.93 K has an estimated uncertainty of 25 kPa (equivalent to 120 ppm at 208.8 MPa; Bignell and Bean 1989).

This pressure fixed point is also useful for testing gas operated pressure balances covering ranges that extend to high pressure values, if an appropriate differential pressure transducer is used for separating the gas from water. The use of water as a fluid, which is easily contaminated when in contact with oxidized metals, would require special attention in the construction of the vessel for triple-point determination and of the part of the apparatus connected to the differential pressure transducer.

In any case, it is essential again to use very stable differential pressure transducers possessing good metrological characteristics for the determination of pressure fixed points (see Chap. 8).

9.3 Summary of Possible Fixed Points to be Used as Transfer Standards for Gas Pressure Measurements from 100 Pa to Approximately 100 MPa

The following tables summarize some characteristics of the pressure fixed points shown in Fig. 9.1.

Tables 9.1 and 9.2 concern gas triple points and Appendix in Sect. 9.4 gives the properties of substances, not gaseous at room temperatures, to be considered for the realization of pressure fixed points. Detailed information on pressure fixed points of gaseous substances can be found also in Afanas et al. (1987).

Table 9.1 Triple points (t.p.) of gases of particular interest in pressure metrology

Property	Substance			
	Carbon dioxide	Argon[a]	Nitrogen	Oxygen[a]
t.p. Temperature referred to ITS-90/K	216.590	83.8058	63.150	54.3584
t.p. pressure/Pa	517.98	68.890	12.538	0.14625
$(\mathrm{d}p/\mathrm{d}T)_{\mathrm{liq}}$/ kPa · K^{-1}	22.6	8.0	2.3	0.046
Temperature reproducibility/mK	0.5	0.1	0.1	0.1
Pressure reproducibility/Pa	11	1.0	0.2	0.1
Pressure uncertainty/Pa	–	1.0	–	0.3
Reference	Meyer and Van Dusen (1933)	Pavese (1981), Bonhoure and Pello (1983), Bandyopadhyay et al. (1991)	Ancsin (1974a)[b]	Pavese (1981)

[a] Fixed point of ITS-90 temperature scale
[b] See references of Part I

Table 9.2 Additional triple points (t.p.) of gases

Property	Substance		
	Equilibrium Hydrogen[a]	Krypton	Xenon
t.p. temperature referred to ITS-90/K	13.8033	115.776	161.406
t.p. pressure/kPa	7.030	73.15	81.71

[a]Fixed point of ITS-90 temperature scale

9.4 Appendix: Properties of Substances not Gaseous at Room Temperature of Interest for Realization of Pressure Fixed Point

Mercury t.p.

- Fixed point on the ITS-90 temperature scale
- t.p. temperature (ITS-90) 234.3156 K
- t.p. pressure 0.063 kPa

See Furukawa et al. (1982)

Water t.p.

- Fixed point of the ITS-90 temperature scale
- t.p. temperature (ITS-90) 273.16 K
- t.p. pressure 0.611657 kPa
- dp/dT liq. 0.0444 kPa K^{-1}
- temperature reproducibility 0.03 mK
- Experimental t.p. pressure reproducibility 0.005 Pa
- Uncertainty of t.p. pressure 0.01 Pa

See Guildner et al. (1976)

$H_2O(I)$-$H_2O(III)$-$H_2O(liq)$ t.p.

- Solid I-solid III-liquid triple point
- t.p. temperature 250.93 K
- t.p. pressure 208829.0 kPa
- Temperature reproducibility 40 mK
- Experimental t.p. pressure reproducibility 3.6 kPa
- Uncertainty of t.p. pressure 25.0 kPa

See Bignell and Bean (1989)

Water c.p.

- c.p. temperature 647.256 K
- c.p. pressure 22120.0 kPa

Mercury Melting Line
The mercury melting line equation is

$$p/\text{MPa} = 19.32845(d/\text{K}) + 0.0018333(d/\text{K})^2 + 0.000059791(d/\text{K})^3$$

with $d/\text{K} = T/\text{K} - 234.3156$; T is the ITS-90 temperature; and p is the absolute pressure.

The above equation is referred to the ITS-90 and uses 234.3156 K as the mercury triple point. The uncertainties achievable in the application of the above equation, when the temperature stability around the mercury cell is maintained at the 2 mK level, are 0.1, 0.16 and 0.39 MPa, respectively, at the absolute pressures of 227.0, 756.0 and 1200.0 MPa. The total uncertainty is calculated as the sum of pressure and temperature uncertainties, plus three times the residual standard deviation of the polynomial fitting equation reported above (Molinar et al. 1980, 1991).

This equation referred to the IPTS-68 temperature scale is given here, too, because of its large use in pressure metrology:

$$p/\text{MPa} = 19.32835(d/\text{K}) + 0.0017068(d/\text{K})^2 + 0.000060867(d/\text{K})^3$$

with $d/\text{K} = T/\text{K} - 234.309$; T is the IPTS-68 temperature; and p is the absolute pressure.

Notes

1. Other relevant data of vapor-pressure properties are given in Chap. 4, Fig. 4.1 (range of pressure and temperature values) and 4.6 (range of dp/dT and temperature values).
2. For the helium-3 melting line, see the relevant data in Chap. 5, Fig. 5.1.

Chapter 10
The Thermomolecular Pressure Difference Effect

10.1 Introduction

The thermomolecular pressure difference is one of the several phenomena which are significant when pressure measurements are made under purely gaseous conditions, particularly when large differences in temperature exist between the place in which pressure measurements have to be carried out and a reference place, where temperature is generally room temperature and where precise pressure measurements can be made by primary or transfer standards. Such phenomena need careful consideration and corrections have to be applied.

Some corrections are specific of the experimental apparatus employed. An example is the *dead-space correction*, which is directly proportional to the volumes and the pressure differences considered and inversely proportional to the reference temperature of the experiment. This correction depends to a large extent on the different temperature gradients between the site used as a reference and the place where the pressure measurements are physically made.

Other corrections depend on the dynamics of pressure variations. An example is provided by the *adiabatic heating and cooling* effects, which also play an important role in gas pressure measurements (see Sect. 8.2).

Other corrections concern the *purity of the fluid* used. There are, for example, gas impurities that heavily affect the reproducibility of some of the most important fixed points (see Sect. 3.1.1, 4.1).

Still, other corrections relate to the conditions of use of the primary and secondary pressure and temperature standards. An example is the aerostatic or gas head correction, (see Sect. 7.1.3.3), which is directly proportional to pressure and inversely proportional to temperature and, as the dead-space correction, depends to a high degree on temperature distribution between the operation levels, as temperature changes produce gas density changes.

There is an effect, evident when a large temperature difference exists between the two ends of a tube connecting the gas volume to the pressure-measuring device, which cannot be corrected in a simple way. This is the *thermomolecular pressure difference*

F. Pavese, G. Molinar Min Beciet, *Modern Gas-Based Temperature and Pressure Measurements,* International Cryogenics Monograph Series,
DOI 10.1007/978-1-4419-8282-7_10, © Springer Science+Business Media New York 2013

effect, also called *thermal transpiration*, a physical phenomenon that produces a measurable pressure difference.

This effect is made evident by the two kinds of molecule collisions occurring in a pressurized gas in a container. At higher pressures, in viscous regime, nearly all collisions occur between gas molecules. At very low pressures, in the Knudsen regime, there are only gas collisions of molecules against tube surface. As pressure is decreased and the change from the viscous to the Knudsen regime is taking place, there is an intermediate region in which the magnitude of the thermomolecular pressure difference is the largest. The physical phenomena occurring are incompletely expressed by the gas kinetic theory.

The thermomolecular pressure difference effect depends on several factors, of which the following, play a key role:

- The different gases used;
- The absolute pressure value;
- The existing regime (viscous, intermediate, Knudsen), which is a function of the pressure value;
- Temperature values or the mean temperature;
- The temperature gradient between the cold and the warm measurement points;
- Gas thermal conductivity;
- The material of the connecting tube;
- The diameter of the connecting tube;
- The state of the internal surface of the connecting tube.

In the present chapter, an analysis will be made of the present theories, the majority of which are semi-empirical, applied in the calculation of the thermomolecular pressure difference effect; the main experimental results described in the literature will be examined as well. Suggestions will be advanced as to the way of performing measurements and calculations of the thermomolecular pressure difference effect, to the highest possible accuracy, for different and typical temperature and pressure ranges of importance in gas thermometry and pressure metrology.

10.2 The Calculation of the Thermomolecular Pressure Difference

Let us investigate two vessels connected by a tube of diameter $d = 2r$ containing a pure gas at different temperatures T_c and T_w, where subscripts "c" and "w" stand for "cold" and "warm" respectively.

According to the kinetic theory, if the mean free path λ of the gas molecules is much smaller than the tube diameter (the situation typical of high-pressure viscous flow regime), the frequent collisions of gas molecules maintain a molecular speed distribution such that, in a steady-state system, the gas temperature and density vary in the tube while the gas pressure remains constant; then $p_c = p_w$ or $p_c/p_w = 1$, where

p_c is the absolute pressure in the vessel maintained at temperature T_c and p_w is the pressure in the vessel at temperature T_w.

At lower pressures, in the molecular flow regime in which the gas mean free path is much larger than the tube diameter, molecule collisions decrease and the temperature of each molecule is known from the temperature of the last collided surface. If the two connected vessels are maintained at different temperatures, T_c and T_w, gas molecules will mix with two different velocity distributions.

In steady-state flow and by the kinetic theory of gases, the pressure ratio is given by the Knudsen value

$$\frac{p_c}{p_w} = \left(\frac{T_c}{T_w}\right)^{1/2} \tag{10.1}$$

which is valid when the molecular speed in each of the two vessels can be related to their temperatures and the probability for the molecules to traverse sections of the connecting tube are equal on both sides of the tube.

Essentially, this is a representation of an ideal case, in which the vessel connection is obtained through an orifice.

When a tube connects the vessels, the mentioned probability depends to a great extent on the reflectivity of the molecule-tube collisions, on surface properties and on the degree of energy exchange. Under these probability conditions the pressure ratio p_c/p_w will be less than the ratio predicted by Eq. ((10.1); Hobson 1969).

In the intermediate pressure region, from 0.01 to 100 Pa, the thermomolecular pressure difference effect plays a significant role even when temperature differences are small (typically, T_c may be the room temperature and T_w may range from 35 to 50 °C).

Obviously, the thermomolecular pressure difference effect plays an important role in vapor pressure thermometry, particularly when temperature differences are as high as 300 K approximately (T_c below 4.2 K and T_w close to 300 K).

It is difficult to establish a reliable and universal model, taking account of all parameters and based on a verified theory, of the thermomolecular pressure difference effect, particularly in the transition or intermediate region between low pressures (where Eq. (10.1) can be used) and high pressures (where Eq. (10.1) becomes $p_c = p_w$).

Models presently available are not wholly satisfactory. The main semi-empirical models now used for the thermomolecular pressure difference calculation will be reviewed here.

The equation of Weber and Schmidt (1936) has been very frequently used for such calculations, particularly in precise vapor pressure thermometry.

Weber and Schmidt proposed a model based on a differential equation to describe the thermomolecular pressure difference effect in all possible pressure and temperature ranges and for any gas.

The differential equation that they proposed is

$$\frac{dp}{dT} = \frac{p}{2T}\left[\frac{\pi}{24 \times K_1}\left(\frac{r^2}{\lambda^2} + 4K_2\frac{r}{\lambda}\right) + \frac{1 + g\left(\frac{r}{\lambda}\right)}{1 + h\left(\frac{r}{\lambda}\right)}\right]^{-1} \tag{10.2}$$

where p is absolute pressure and T is absolute temperature, r is the radius of the tube connecting the two vessels at different temperatures T_c and T_w, and λ is the mean free path of the gas.

The four constants K_1, K_2, $g(r/\lambda)$ and $h(r/\lambda)$ in Eq. (10.2) were so selected as to obtain the best fit of the available data for the different gases. The first two terms of Eq. (10.2) are obtained from the equation for viscous flow and the third term represents the Knudsen behavior $p/(T)^{1/2} = \text{constant}$ at low pressures. Equation (10.2) was solved on the assumption of gas viscosity $\eta(T)$ being a power law in T; the method of partial fractions was used to relate the pressure ratio to the temperature ratio in the following form:

$$\ln\frac{p_c}{p_w} = 0.5\ln\frac{T_c}{T_w} - \left(\frac{2n-1}{2n+2}\right) \times \left(B\ln\frac{y_c + m}{y_w + m} + C\ln\frac{y_c + m'}{y_w + m'} + D\ln\frac{y_c + m''}{y_w + m''}\right) \tag{10.3}$$

where

$$\frac{1}{y} = \frac{\lambda}{r} = \left(\frac{\pi R}{2M}\right)^{1/2} \times \left(\frac{To^{1/2}}{r \times p}\right) \times \eta_o\left(\frac{T}{To}\right)^{1+n}$$

and η_o is the viscosity at $T_o = 273.15$ K, R is the gas constant and M is the molar mass of the gas.

The index "c" and "w" must be appropriately used, depending on the specific case, for the quantities y, λ, p and T.

The constants B, C, D, m, m', m'' and n are determined from the values of K_1, K_2, g and h.

When the constants m' and m'' are complex numbers, an expression other than Eq. (10.3) is used.

The Weber–Schmidt equation has been extensively used particularly in vapor pressure thermometry for thermomolecular pressure difference corrections, but a large number of experimental measurements (e.g. McConville 1969; Freddi and Modena 1968) showed large deviations between experimental values and calculations.

A first attempt to modify the Weber–Schmidt equation in order to obtain a better thermomolecular correction was made by Liang (1953) with an empirical calculation not directly related to the Weber and Schmidt equation and used for different gases. Liang's empirical equation was determined on the basis of experimental data for application in the use of glass tubes and it does not take account of the type of tube

surface. According to Liang, the following empirical equation, which can be used for any gas and for glass tubes, is obtained:

$$\frac{p_w}{p_c} = \frac{\alpha_{He}(\Phi_g \times X)^2 + \beta_{He}(\Phi_g \times X) + R'}{\alpha_{He}(\Phi_g \times X)^2 + \beta_{He}(\Phi_g \times X) + 1} \tag{10.4}$$

where the symbols have the following meaning:

X $= (p_w \times d)$ with d being the diameter of the connecting tube
R' $= (T_w/T_c)^{1/2}$
α_{He} $= 2.52$
β_{He} $= 7.68(1 - R')$
Φ_g is the pressure-shifting factor depending on the type of the gas used;
Φ_g $= 1$ for helium
Φ_g is related to the collisional diameter D by the following equation:

$$0.27 \log \Phi_g = \log D - 0.41$$

The collisional diameter D (expressed in angstrom) is 2.58, 2.80, 2.90, 3.41, 3.70, 3.60, 4.1 respectively for helium, neon, hydrogen, argon, nitrogen, krypton and xenon.

Although this approach can be compared to calculations using the Weber–Schmidt equation, the Liang equation is empirically corrected for collisions between molecules and glass tubes. There is evidence that the Liang Eq. (10.4) cannot be automatically extended to any tube material.

An approach similar to Liang's, for temperatures above room temperature, was adopted by Takaishi and Sensui (1963), who studied experimentally the thermomolecular pressure correction for different gases and for glass tubes and obtained the following equation:

$$\frac{p_w}{p_c} = \left(\frac{f(X) + \left(\frac{T_w}{T_c}\right)^{1/2}}{f(X) + 1} \right) \tag{10.5}$$

where

X $= p_w \times d$
$f(X)$ $= A^*(X/T^*)^2 + B^*(X/T^*) + C^*(X/T^*)^{1/2}$

with $T^* = 0.5(T_w + T_c)$

The parameters A^*, B^* and C^* depend on gas species and were determined by Takaishi and Sensui by fitting their experimental data and those available in the literature. From their results Takaishi and Sensui derived the empirical Eq. (10.5) in which the empirical parameters A^*, B^*, C^* are related to the collisional diameter D of different gas molecules in the following form:

Table 10.1 Values of empirical parameters A^*, B^*, C^* for different gases to be used in Eq. (10.5) for thermomolecular correction. (Takaishi and Sensui 1963)

Gas	A^* $(\mathrm{kPa}^{-1}\,\mathrm{mm}^{-1})^2$	B^* $(\mathrm{kPa}^{-1}\,\mathrm{mm}^{-1})$	C^* $(\mathrm{kPa}^{-1}\,\mathrm{mm}^{-1})^{1/2}$
He	8.44	0.863	1.65
Ne	14.91	1.41	2.60
Ar	60.76	6.06	1.35
Kr	81.58	11.25	1.19
Xe	196.91	31.05	0.87
H_2	6.98	6.0	0.92
N_2	67.51	7.5	1.21
O_2	45.01	13.3	–
CH_4	81.58	11.25	1.13

$$A^* = 1.4 \times 10^4 \exp\left(1.17D \times 10^{10}\right)$$
$$B^* = 5.6 \exp\left(1.4D \times 10^{10}\right)$$
$$C^* = \left(\frac{1.10 \times 10^{-8}}{D}\right) - 14.0$$

with D expressed in meters.

A^*, B^* and C^* are empirical parameters representing the corrections respectively at high, intermediate and low pressures; in the region of transition between viscous and molecular flow their order of magnitude is almost the same. The values of the parameters A^*, B^* and C^* obtained by Takaishi and Sensui for different gases are given in Table 10.1.

It should be remembered that the previous empirical Eqs. (10.4) and (10.5) described by Liang and by Takaishi–Sensui were obtained for glass tubes and for temperatures ranging from room temperature (T_c) to temperature values (T_w) generally not higher than 100 °C, which is a situation very different from the normal in vapor pressure thermometry.

Later in Sect. 10.3, some calculations applying the Liang and the Takaishi–Sensui equations are compared with some experimental values.

McConville also analyzed the discrepancy between the Weber–Schmidt equation and experimental measurement results concerning thermomolecular pressure differences for helium-3 and helium-4 (McConville 1969, 1972). He ascribed the cause of deviations to the fact that the original Weber–Schmidt equation does not take account of the characteristics of the collisions between gas molecules and the tube surface. In addition, the constants in the Weber–Schmidt equation consider the thermomolecular effect specifically for glass tubes; metallic tubes need larger corrections, as molecule–surface collisions depend on surface roughness which can generally be extremely different in metallic tubes than in glasses.

In his investigation on the collision of molecules against the tube wall, McConville (1969, 1972) introduces a specific parameter F that takes account of the reflection of the molecules by the tube wall. This parameter is the momentum accommodation coefficient describing the collision between a molecule and the tube wall and is

introduced to correct the term λ/r for gas viscosity; another coefficient, γ, is also introduced as an undetermined geometry factor. He investigated the role of gas–gas and gas–surface collisions and concluded that the Weber–Schmidt constants can be re-written in the form of physical parameters.

McConville showed that an equation such as (10.2) could be obtained from a steady-state flow equation as a combination of Knudsen and viscous flow, in the following form:

$$N_{\mathrm{w}}\frac{4}{3}\left(\frac{2\pi M}{R}\right)^{1/2}\times r^3\times\frac{d}{dx}\left(\frac{p}{T^{1/2}}\right)+N_{\mathrm{G}}\left\{\frac{\pi pMr^4}{8\eta RT}\left[1+4\left(\frac{2-F}{F}\right)\frac{\lambda}{r}\right]\frac{dp}{dx}\right.$$

$$\left.-\frac{3\pi\eta r^2}{4T}\times\frac{1}{1+4\left(\frac{2-F}{F}\right)\frac{\lambda}{r}}\times\frac{dT}{dx}\right\}=0$$

where N_{W} and N_{G} are the numbers of gas–surface and gas–gas collisions respectively. The assumption of the ratio of N_{G} to N_{W} being proportional to r/λ in the form:

$$\frac{N_{\mathrm{G}}}{N_{\mathrm{W}}}=\frac{8}{9}\gamma\frac{r}{\lambda}$$

simplifies the previous equation, so that the Weber–Schmidt constants can be written in terms of the momentum accommodation coefficient F and of the geometry factor γ as follows:

$$\begin{aligned}
K_1&=1+\frac{1}{\gamma}\\
K_2&=\left(\frac{2-F}{F}\right)\times\left(\frac{1+2\gamma}{1+\gamma}\right)\\
g&=\frac{1}{4\left(\frac{2-F}{F}\right)}\left[1+\frac{2\pi}{3}\left(\frac{2-F}{F}\right)^2\times\frac{\gamma^3}{(1+\gamma)^2}\right]\\
h&=\frac{1}{4\left(\frac{2-F}{F}\right)}\times(1+\gamma)
\end{aligned}\qquad(10.6)$$

The Weber–Schmidt equation, adjusted for McConville's calculation conditions and hypotheses now includes two parameters (F and γ), to be appropriately selected according to the state of the tube surface. Parameter F depends on the nature of the surface, and the geometry factor, γ, can be established by assuming a known value of F for a particular surface, for example, a type of glass. Then, other surfaces can be characterized with an appropriate value of F relatively to glass. This gives the

possibility of establishing a specific procedure for determining the thermomolecular correction for a tube of a specific type from a differential pressure measurement using two tubes of different radii.

Williams III (1970) modified the model for the calculation of thermomolecular pressure difference in the viscous regime so as to include molecular velocity slip at the wall and thermal creep. The author demonstrates that by his mathematical model, based on the gas dynamics theory, one can predict the trends and magnitudes of thermomolecular pressure differences for typical pressure and temperature ranges, as long as the pressure value is reasonably high, that is, as long as the flow regime is viscous.

Other contributions dealing with the calculation of the correction for thermomolecular pressure difference were made by Cha and McCoy (1972) and by Siu (1973).

Siu compared his low-pressure calculation with Hobson's experimental data (Hobson 1969). Siu arrived at a rigorous expression, based on irreversible thermodynamics and statistical mechanics, of the low-pressure limit, which is

$$\frac{dp}{dT} = \left[\frac{1}{2} - \varepsilon(\sigma, \lambda)\right]\left(\frac{p}{T}\right) \tag{10.7}$$

with

$$\varepsilon(\sigma, \lambda) = \gamma(\sigma, \lambda) - 2$$

where $\gamma(\sigma, \lambda)$ is the ratio of moments of a molecular distribution function $f(r, v, \sigma, \lambda)$, which depends on the mean free path, λ, and on a parameter, σ, characterizing the solid surface.

The integration of Eq. (10.7) leads to an expression for the thermomolecular pressure ratio $R'' = p_w/p_c$ but it is complicated by the form of the function $\varepsilon(\sigma, \lambda)$.

Parameter σ depends on p, T and δ which is another parameter that expresses the reflectivity of the surface. The use of the molecular distribution function yields a meaningful description of the ratio R'', but Eq. (10.7) can be integrated only under very limiting conditions.

Siu found, under such conditions, that

$$\left(\frac{R''}{R'}\right) = \left(\frac{T_w}{T_c}\right)^{\varepsilon(\sigma)} \tag{10.8}$$

with $\quad R' = \left(\dfrac{T_w}{T_c}\right)^{1/2}$

where ε now does not depend on λ and $R'' = R'$ when $\varepsilon = 0$.

It is necessary to know the form of the distribution function to determine whether ε is greater or smaller than zero. Siu used the distribution function of Simons (1967), which assumes $L \gg \lambda \gg r$ where L and r are the tube length and radius respectively, to obtain the following equation for $\varepsilon(\sigma)$:

$$\varepsilon(\sigma) = \frac{0.56 \times \sigma}{(1 + 0.1 \times \sigma)} \tag{10.9}$$

With this, Eq. (10.8) leads to $R'' > R'$ for $0 < \sigma < 1$ and $R'' = R'$ only when $\sigma = 0$, that is, when the molecules are scattered completely from the solid surface. If scattering is specular, the deviation of R'' from R' is directly proportional to specularity.

Equation (10.8) is valid only for tubes having $L \gg \lambda$ and surface irregularities uniformly distributed.

Siu compared his calculation data with the experimental data of Hobson (1969) for helium gas and glass tubes with $T_c = 77.4$ K and $T_w = 295$ K, and he found that the values of $R''_{\text{exper.}}$ allow to calculate $R''_{\text{exper.}}/R'$ that ranges from 1 to 1.24.

The parameter σ must be calculated from experimental data, to use it in Eqs. (10.8) and (10.9) for the calculation of R''. In his paper, Siu (1973) gives all the details for the calculation of σ and its relation with $\varepsilon(\sigma)$ and analyzes possible deviation of the thermomolecular pressure difference correction in the Knudsen regime.

The above considerations have brought into evidence the significant role of molecule-tube wall collisions in the determination of thermomolecular corrections in a nearly free molecular flow; it must be noted that $R'' = R'$ only when tubes are long and $\sigma = 0$; when σ is other than 0, an anomalous Knudsen limit is obtained.

Another contribution, useful when considering capillary tubes, was made by Loyalka (Storvick et al. 1978), who started from non-equilibrium thermodynamic relations of the mass flux JM with the thermal energy flux JQ. They developed a theory based on a solution of the linearized Boltzman equation by assuming diffuse specular reflections on the tube wall and by using the BGK model (Bhatnagar et al. 1954) for the collision operator, and with constant collision frequency.

In the paper by Storvick et al. (1978), the values of the steady-state thermomolecular pressure difference are compared with the following Loyalka equation (the density ρ_o is determined at the mean temperature T_o and mean pressure p_o):

$$\frac{\dfrac{\Delta p}{p_o}}{\dfrac{\Delta T}{T_o}} = -\frac{\rho_o}{p_o} \times \frac{\gamma M Q}{\gamma M M}$$

Loyalka's kinetic theory was used for the calculation of the coefficient ratio $(\gamma MQ/\gamma MM)$.

Experimental results, obtained with helium, argon, carbon dioxide and air in capillary tubes having average radii of 0.236 mm, are reported to be in very good agreement with Loyalka's theoretical calculations.

Among the different theoretical methods for the calculation of the thermomolecular pressure difference effect reviewed here, none of them is generally good enough and fully reliable for application in all possible experimental configurations, so that they must always be adapted to a specific experimental condition.

10.3 Experimental Measurements of the Thermomolecular Pressure Difference Effect

It has already been mentioned that the thermomolecular pressure difference depends to a large extent upon the different gas species, upon pressure and temperature values, on instrument configuration (e.g. the diameter of the connecting tube), and on molecule intercollisions and on molecule-tube surface collisions.

As was mentioned in Sect. 10.2, since there are no general theories applicable for all possible configurations, it is advisable to adapt the experimental conditions under which the thermomolecular pressure difference measurement is to be carried out, to make them identical to those of the specific theory used.

The usual way of carrying out experimental measurements of the thermomolecular pressure difference effect is to use a system configuration featuring a large-diameter tube and the small-diameter tube to be studied connecting the two sides having different temperatures T_c (at pressure p_c) and T_w (at pressure p_w), and to measure the pressure difference of the two tubes at T_w with a reliable and carefully calibrated differential pressure transducer. This is an easy procedure, which requires, however, the use of the same material for all tubes in the case of multiple-tube arrangements, since the tube surface condition is an important element to be taken into account.

Another way is to use pressure transducers to measure the pressures p_c and p_w directly in the sites where temperatures T_c and T_w are maintained. The pressure transducer to be employed may be absolute or differential, according to the required measurement. The transducer must have good resolution, sensitivity and long-term stability at the different temperatures where measurements are carried out and over the complete pressure range of interest. For a complete metrological characterization of the pressure transducer careful and repeated calibrations have to be performed at the relevant T_c and T_w temperatures.

An instrument of this type is, for example, the capacitance pressure transducer described by Greywall and Busch (1980), which was used in helium-3 vapor thermometry. It has a good resolution of 2.6×10^{-2} Pa, which is equivalent to 0.3 mK at 0.3 K, and of 13×10^{-2} Pa, equivalent to 0.04 μK at 2 K.

The metrological characteristics of pressure transducers used at low temperatures are fully described in Sect. 8.4.

Capacitance pressure transducers are widely used not only at low temperatures (usually below 77 K), but also at higher temperatures and very frequently in the pressure transition region between the viscous and the Knudsen regimes. Some of the commercial capacitance transducers are thermally isolated and controlled at temperatures from 35 to 50 °C, though they are generally employed at room temperatures.

Such capacitance transducers were used in experimental investigations to measure the thermomolecular pressure difference, typically with $T_c = 20$ °C to 23 °C, $T_w =$ 35 °C to 50 °C and with pressures ranging from 0.01 Pa to 1 kPa; the typical offset at low pressures may range between 2 and 4%, depending on the transducer considered.

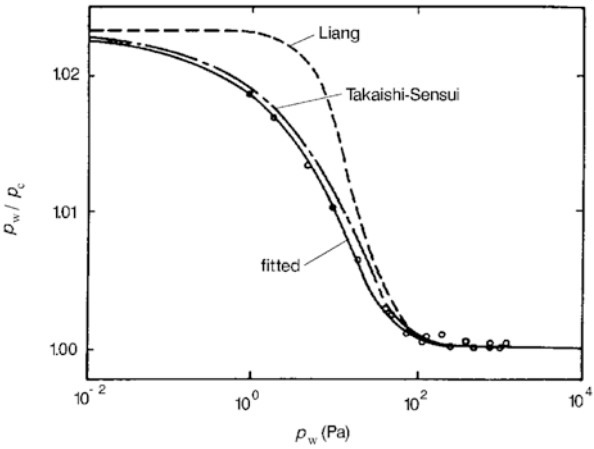

Fig. 10.1 $p_w/p_c = f(p_w)$ for a capacitance transducer of 1 kPa full scale, test in helium. °°°°°°° = Experimental determinations; - - - - - - - = Liang's equation; - · - · - · - = Takaishi-Sensui's equation; (From Jitschin and Röhl (1987), by kind permission of the authors)

Experimental data for different capacitance transducers, for different gases, and different experimental configurations are also given by Baldwin et al. (1973), Poulter et al. (1983) and Jitschin et al. (1987). These experimental data show that at low pressures, generally below 100 Pa, the calibration data of capacitance transducers having temperature controlled heads exhibits marked non-linearity; results indicate as well a calibration factor that varies typically with the gas species and the temperature of the head. The correction p_w/p_c, illustrated in Fig. 10.1 as a function of p_w, concerns a capacitance transducer of 1 kPa full scale tested in helium at temperatures T_c = 26.5 °C and $T_w = 39.0$ °C. In the case illustrated in this figure (Jitschin et al. 1987), it was not only possible to obtain the behavior of transducer calibration but also to compare experimental data with thermomolecular calculations using Liang's (10.4) and Takaishi–Sensui's (10.5) equations.

As Fig. 10.1 shows, Liang's equation is not completely satisfactory and Takaishi–Sensui's one is better for reproducing the experimental behavior even if it shows small but systematic differences with respect to experimental data.

Jousten (1998) considers the temperature corrections in the calibration of different secondary standard gauges (ionisation gauges, spinning rotor gauges and capacitance diaphragm gauges) when these pressure sensors are calibrated or used at different temperatures from the reference one (generally 23 °C) and are aimed to uncertainties lower than 1%. Other studies, particularly in the case of capacitance diaphragm gauges (CDG), are the following:

- Miiller (1999), demonstrated that in the range from 0.5 to 100 Pa, for different gases and absolute mode, controlling the CDG temperature near the room temperature of 23 °C, reduces significantly the thermal transpiration effect.
- Šetina (1999) studied the metrological characteristics of CDG using gases as nitrogen, argon, helium and hydrogen in the pressure range from 0.01 to 100 Pa. The author used a different procedure based on pressure normalisation and considering gas viscosity and average molecule velocity and found that the coefficients

in Takaishi–Sensui equation are not fitting well their calculations for helium and nitrogen.

- Bergoglio and Calcatelli (2001) also studied different CDG's and their purpose was to demonstrate that it is possible, after its first calibration, to arrive at an equation that gives the calibration coefficients as a function of pressure based on a reduced number of calibration experimental points.

From all the above experiences, there is evidence that if interactions between gas molecules and tube surface are not considered, calculations of the thermomolecular pressure effect may yield data largely different from those obtained experimentally. However, Jitschin and his collaborators suggest that if the equations are corrected with the aid of experimental data, an agreement up to 0.1% approximately can be obtained, which is almost of the same order as that of the medium-term stability obtained when the two capacitance pressure transducers investigated by Jitschin were tested.

In numerous experiments on the thermomolecular effect, T_c is generally below 4.2 K and T_w close to room temperature, which are key temperature values in vapor pressure thermometry (Ronsin 1987) and, more generally, in measurements at cryogenic pressures and temperatures.

Hobson (1969) determined the thermomolecular correction when using helium and pyrex tubes of 22 mm diameter in the pressure range from 1×10^{-5} Pa to 13.3 kPa, with $T_c = 77.4$ K and $T_w = 295$ K. In the case studied, the internal surface of the tube was intentionally subjected to the "leaching" process in order to obtain a porous surface layer. Hobson found that in this way molecular collisions were mostly of the cosine reflection type and therefore a nearly perfect materialization of an ideal condition. The experimental measurement values were in very good agreement with Liang's equation. On the contrary, large differences between experimental and theoretical values are generally found when smooth-glass tubes are used.

Other interesting data were obtained at the NPL-UK by Berry (1979) for helium-4 and stainless steel tubes, with temperatures ranging from 4.2 to 293 K and pressures from 2 to 12 kPa. Experimental pressure measurements were made with commercially available diaphragm capacitance-gauges frequently calibrated against a primary pressure balance for careful regular checking. The differential pressure range of such transducers was ± 400 Pa, with a sensitivity allowing 0.002 Pa resolutions. These transducers were checked in particular for stability versus the temperature of operation and for zero signal shifts with a changed line-pressure value; an overall pressure uncertainty of 0.05% was quoted.

The thermomolecular pressure difference was determined experimentally with the use of a diaphragm capacitance-transducer in a range of absolute pressures from 2 to 12 kPa.

The difference $\delta(\Delta p)$ between the Weber–Schmidt equation, in the form of Eqs. (10.2) and (10.3), which do not take account of the momentum transfer accommodation coefficient, and the experimental values obtained by Berry is given in Fig. 10.2. The same figure illustrates as well the absolute value of the thermomolecular correction Δp calculated on the basis of the Weber–Schmidt equation. The segments in

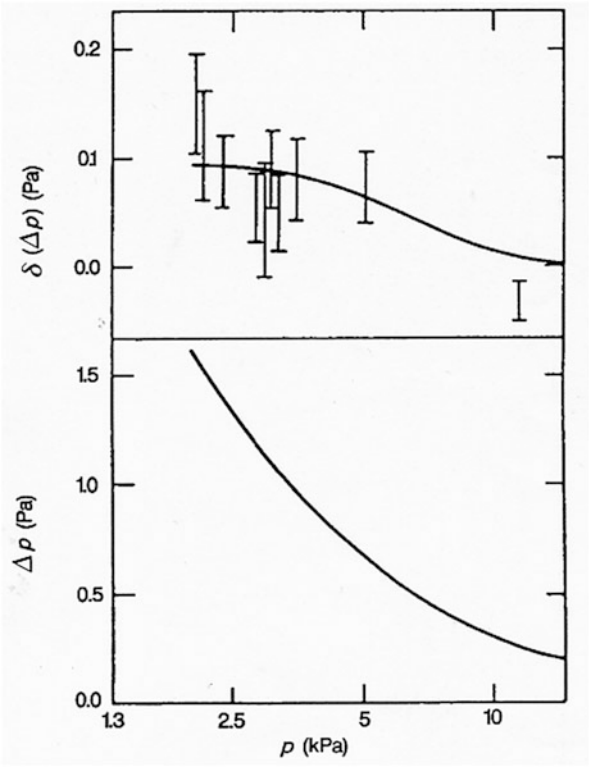

Fig. 10.2 Thermomolecular pressure difference (Δp) versus applied absolute pressure p calculated from Weber–Schmidt's equation for a stainless steel tube for temperatures of $T_c = 4.2$ K and $T_w = 293$ K. $\delta(\Delta p)$ is the difference between the calculated and the experimental values. (From Berry (1979), by kind permission of the author)

Fig. 10.2 are estimates of experimental measurement errors. Berry estimates that the $\delta(\Delta p)$ curve is correct to within 0.07 Pa.

This example once more clearly shows how difficult it is to select an equation allowing the thermomolecular pressure difference to be calculated with acceptable uncertainty.

As already mentioned in Sect. 10.2, McConville determined experimentally the thermomolecular pressure difference (McConville 1969) for helium-3 and helium-4, using stainless tubes of different diameters, and temperatures from 4.2 to about 300 K. It has already been said that evidence exists as to the dependence of the magnitude of the thermomolecular pressure difference correction on the surface state.

In Fig. 10.3, some experimental data taken from McConville's paper are compared with theoretical calculations using the Weber–Schmidt equation.

As Fig. 10.3 shows, the original Weber–Schmidt equation needs systematic adjustment to be in good agreement with experimental data. McConville's adjustment considers the collision of gas molecules against the tube surface (see Eqs. (10.2) and (10.6) in Sect. 10.2). Other investigators (e.g. Freddi and Modena 1968) obtained results similar to those given in Fig. 10.3.

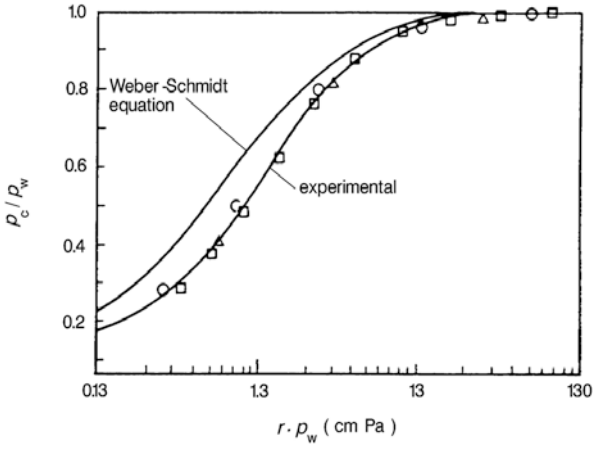

Fig. 10.3 Calculated ratio p_c/p_w versus $(r \cdot p_w)$ based on the original Weber–Schmidt's equation compared with experimental data obtained by McConville (1969) for helium-3 and helium-4 ($T_c = 4.2$ K, $T_w = 303$ K) and different-diameter stainless steel tubes (o $= 0.58 - 0.11$ cm, $\square = 0.58 - 0.28$ cm, $\Delta = 0.58 - 0.05$ cm). (From McConville (1969) by kind permission of the author)

The data obtained by McConville and other authors, which are mutually consistent and in good agreement, confirm that a general theory for thermomolecular pressure difference calculations is a problem that is worth investigating further.

Divergences of the experimental measurement values from calculations made with different models were also reported by Borisov et al. (1973) for different gases, in a temperature range from 77 to 293 K and for glass capillary tubes of radius approximately of 0.148 mm.

The differences between calculations and experimental results were typically of the order of 20%, reduced to about 5% by means of a correction that considered gas molecular diffusion on the wall surface of the tubes. It must also be mentioned that other authors found substantially good agreement when comparing their experimental data with calculations applying the Weber–Schmidt equation.

Bernat and Cohen (1974) give a detailed list of different experiments, some of which showing agreement others discrepancy between experimental data and calculations based on the Weber–Schmidt equation. In particular, very good agreement was obtained with the application of the original Weber–Schmidt equation in the experiment that Bernat and Cohen performed on helium-3 in stainless steel tubes of radii of 2.877 and 1.438 mm, using carefully calibrated capacitance transducers to measure pressure. On the basis of their results, the authors expressed the opinion that the original Weber–Schmidt equation can have a more general application than expected, but that the exact conditions of its applicability still remain to be determined.

Though not excluding the models described by McConville and Siu (McConville 1969; Siu 1973), Bernat and Cohen suggest that not only is gas molecular collision against the tube surface an important element for the thermomolecular correction, but

that the adsorbed gas is also likely to modify drastically gas–surface interactions and that these phenomena may play a significant role, particularly at low temperatures.

McConville, too, arrived at this conclusion, probably not enough forcefully stated, when he reported (McConville 1972) thermomolecular pressure measurements using the same tube as Roberts and Sydoriak (1956) used in their helium-3 vapor pressure work. Roberts and Sydoriak's measurement values were in agreement with the original Weber–Schmidt's constants, whereas McConville's measurement value on the same tube was not. The difference was that in Roberts and Sydoriak's experiments the helium-3 vapor pressure in the tubes was always maintained at about 13 kPa in between the experiments, and this is a condition (different from McConville's experiment) that can also play a significant role to understand the limits of application of the Weber–Schmidt equation.

A systematic study has not yet been carried out to ascertain whether a layer of loosely adsorbed gas always produces thermomolecular pressure differences that can be described by the Weber–Schmidt constants.

To avoid large errors in vapor pressure thermometry, the best solution is to make differential pressure measurements at appropriate temperature and pressure values, so as to determine the thermomolecular pressure difference in a given and well-defined situation or, when possible, to use tubes with diameters large enough to avoid correction for thermomolecular pressure difference.

10.4 General Considerations on Experimental Measurements and Theoretical Calculations of the Thermomolecular Pressure Difference

Different theoretical and empirical approaches for the calculations of the thermomolecular pressure difference effect have been discussed in Sect. 10.2.

At present, there is no "general theory" applicable in all possible experimental cases featuring different tube materials and diameters, different gases and valid for all pressure and temperature ranges.

The original Weber–Schmidt equation is widely used, despite the reported large discrepancies with respect to experimental data. This equation needs to be adapted to the temperature range (for example, Liang's and Takaishi–Sensui's semi-empirical equations can be used for temperatures higher than room temperature), to take account of gas-molecule collisions against the tube wall surface of a specified material and of the effect of adsorbed gas on the surface due to the thermodynamics of the surface under experimental conditions. Time dependency of the surface state, in relation to surface thermodynamics and to gas absorption by the surface, must also be considered.

All theoretical and empirical equations so far employed represent useful attempts to understand these complex phenomena better and, as a rule, they are valid for specific cases and it must be remembered that different investigators have observed differences between theoretical calculations and experimental results.

Probably, the best suggestion is to consider the calculation of the thermomolecular pressure difference, which is a useful indication to derive approximately the quantitative behavior of the effect.

On the contrary, it is certainly possible to obtain better results and better accuracy, if differential pressure measurements are made with much care and attention given in particular to:

- The selection of the tubes, which should have, if possible, a large diameter.
- The selection of the best pressure transducer for differential pressure measurements well considering the pressure range of use (See Chap. 8).
- The metrological characterization of the involved pressure transducers by appropriate short-term calibrations, particularly as regards stability, resolution and accuracy at the different temperatures of the experiment.

It is therefore of primary importance, especially in thermomolecular pressure difference measurements at low temperatures, that capacitance transducers operating directly at low temperatures, like those described in Sect. 8.4.2, and having high resolution and stability and of certified uncertainty should be available.

Chapter 11
The Mutual Recognition Arrangement and Its Implementation in Temperature and Pressure

11.1 Introduction

At a meeting that was held in Paris (France) on 14 October 1999, the directors of National Metrology Institutes (NMIs) of 38 member states belonging to the Meter Convention and two representatives of international organizations signed a Mutual Recognition Arrangement (CIPM-MRA 1999) to support international traceability of national measurement standards and the calibration and measurement certificates issued by NMIs. This document, amended in 2003, is integrally given in English in Appendix G and is freely available on BIPM web site http://www.bipm.org/en/cipm-mra/documents/ in its French and English versions.

This Mutual Recognition Arrangement (MRA) was the response of the internationally organized metrology to have an open, transparent, and comprehensive tool in order to give all potential users a reliable full information on the comparability of national metrology services, so providing the technical basis for wider agreement useful for international trade, commerce, and regulatory matters.

The representatives of 86 Institutes have, in October 2011, signed the CIPM-MRA. The signatory Institutes come from 50 Member States of the Meter Convention, 33 associates of CGPM, and 3 International Organizations: International Atomic Energy Agency (IAEA), Institute for Reference Materials and Measurements (IRMM), and World Meteorological Organization (WMO) and cover a further 138 Institutes designated by the signatory bodies.

The current list of participants is given at: http://www.bipm.org/utils/en/pdf/signatories.pdf. The essential points of the CIPM-MRA are the following as taken almost integrally from BIPM web site:

Objectives:

- To establish the degree of equivalence of national measurement standards maintained by NMIs.
- To provide for the mutual recognition of calibration and measurement certificates issued by NMIs.

F. Pavese, G. Molinar Min Beciet, *Modern Gas-Based Temperature and Pressure Measurements,* International Cryogenics Monograph Series,
DOI 10.1007/978-1-4419-8282-7_11, © Springer Science+Business Media New York 2013

- Thereby to provide governments and other parties with a secure technical foundation for wider agreements related to international trade, commerce, and regulatory affairs.

Process:

- International comparisons of measurements, to be known as key comparisons.
- Supplementary international comparisons of measurements.
- Quality systems and demonstrations of competence by NMIs.

Outcome:

- Statements of the measurement capabilities of each NMI to be included in a database, called the *Key Comparison Data Base* (*KCDB*), maintained by the BIPM and publicly available on the Web.

Engagement NMI Directors sign CIPM-MRA with the approval of the appropriate authorities in their own countries and thereby:

- Accept the process specified in CIPM-MRA for establishing the database.
- Recognize the results of key and supplementary comparisons as stated in the database.
- Recognize the calibration and measurement capabilities (CMC) of other participating NMIs as stated in the database.

Exclusions:

- Signature of MRA engages NMIs but not necessarily any other agency in their country.
- Responsibility for the results of calibrations and measurements rests wholly with NMI that performs them and is not, through MRA, extended to any other participating NMI.

Organizational Structure:

- Overall coordination is by BIPM under the authority of CIPM, which is itself under the authority of the Member States of BIPM.
- The Consultative Committees of CIPM, the Regional Metrology Organizations and BIPM are responsible for carrying out the key and supplementary comparisons.
- A Joint Committee of the Regional Metrology Organizations and BIPM (called JCRB) is responsible for analysing and transmitting entries into the database for the calibration and measurement capabilities declared by NMIs.

11.2 The Key Comparisons

As it can be seen in Appendix G, in order to establish the degree of equivalence of national measurement standards maintained by NMIs, it is necessary to organize key comparisons carried out by the Consultative Committees of CIPM, the BIPM, and the

regional metrology organizations (RMOs), and published by BIPM and maintained in the key comparison database (KCDB). The document CIPM-MRA-D-05, Version 1 (2010) is a useful compendium of all matters related to measurement comparison within the CIPM-MRA.

The results of the comparison will be fully documented, all results will be available in KCDB, and each of the comparisons will be analyzed in terms of degree of equivalence between each participant with an emphasis posed onto the fact that all key comparisons of the same kind, independently of the structure that has organized them (CC of CIPM, RMOs. . .), will be linked together in terms of the degree of equivalence of overall participant results. In the next paragraphs, the key comparisons for gas pressure and temperature measurements will be shortly analyzed.

The data given here are fully extracted from KCDB of the BIPM (available at http://kcdb.bipm.org) in October 2011.

11.2.1 Key Comparisons Related to Gas Pressure Measurements in the Range from 100 Pa to 100 MPa

In October 2011, on KCDB there are 76 results available for pressure measurements.

Between these, 46 are comparisons in gas media, 21 are in liquid media (only gauge mode), and 9 are for vacuum and leaks measurements.

Considering the 46 comparisons in gas media, they can be made in absolute or gauge modes, from a few pascal to a maximum pressure of 7 MPa, generally speaking in gauge mode for pressures higher than some kPa.

Of the 46 key and supplementary comparisons in gas media, for 18 of them there are full results available on KCDB. When full results are published, there are direct links to the reports, or papers published and for each of the participants a degree of equivalence is given as approved by participants and CC of CIPM. The degree of equivalence is built up on the responsibility of participants, it is explained how it is derived starting from the uncertainty of participants at some selected pressure of the comparison. In some cases, the comparisons are just *approved for provisional equivalence*, even if papers are supplied (e.g., the case of *CCM.P-K10*) it means that plans are in progress to start in the near future a new comparison.

For some of the 46 comparisons, there is already a mention of published results, some are in process of conclusions, and some are only at their planning stage.

As a general concept, when the results are available on KCDB, it means that the comparison results have been approved to support the declared measurement equivalence.

For the 46 key and supplementary pressure comparisons in gas media, the following types of transfer standards have been used:

- Pressure balances of different types, with different full scales according to the specific comparison, to be used in absolute or differential (gauge) modes, frequently at the state-of-the-art level and commercially available.

- High-resolution and -precision pressure transducers, almost all commercially available, of the capacitance diaphragm type for the small and moderate pressures and of the resonant silicon gauge type for the medium and high pressures.

From the view point of classification, when the comparison starts with *CCM.P* it means that the comparison has been organized by the Consultative Committee for Mass (CCM) and it is dealing with pressure (*P*). The remaining part is for classification purposes. For example, *CCM.P-K1.c* means a CCM pressure key comparison, under the classification K1.c used to identify a gas pressure comparison in gauge mode from 80 kPa to 7 MPa. In other cases, the comparisons are listed under the name of a regional organization (EUROMET or EURAMET, APMP, COOMET, SIM), so, for example, the name *APMP.M.P-K1.c* means a comparison organized by Asia Pacific Metrology Programme organization, within Mass-Pressure and the use of K1.c means that this comparison has to be linked, even if the pressure range is not completely overlapping, to CCM.P-K1.c comparison.

Considering, as an example, CCM.P-K1.c comparison that was conducted for gauge pressure measurements from 80 kPa to 7 MPa using as transfer standard a pressure balance, on KCDB web site it can be seen that other comparisons have been organized (APMP.M.P-K1.c from 0.4 to 4 MPa, APMP.M.P-K1.c1 from 0.4 to 4 MPa, and EUROMET.M.P-K2 from 1 to 4 MPa) and their results are linked to CCM.P-K1.c comparison in terms of equivalence declarations. To reach these results, a consistent analysis of the data has been undertaken and approved by all participants.

The summary of results for the above comparisons can be found on KCDB at the page http://kcdb.bipm.org/AppendixB/appbresults/ccm.p-k1.c/m.p-k1.c.pdf where all results are given, starting from the results obtained in each of the specific comparison with their declared standard uncertainty of the measurand. It is fully described as well how the key comparison reference value of the measurand were derived for each of the comparisons, how the regional comparisons are linked to the main CCM comparison, and how the degree of equivalence was calculated for each participant. Generally, the degree of equivalence for each participant, at a selected specific pressure value, is given as a difference between the measurand of the participant in respect to the reference value and an uncertainty of this difference is calculated as well.

In Fig. 11.1, the main results of the comparison CCM.P-K1.c and associated regional comparisons are given. The figure is taken from the BIPM-KCDB.

Figure 11.1 gives the degree of equivalence expressed in ppm and its uncertainty for all the 5 participants at CCM original comparisons and the 15 participants in the three regional comparisons. It has to be remembered that not the same transfer standard pressure balance was used in the different regional comparisons in respect to the transfer standard used in CCM.P-K1.c comparison, but this was not a problem even if it was carefully considered in setting up the link between the different comparisons in order to derive a unique degree of equivalence.

Other examples are given for the following comparisons:

- *CCM.P-K2*, a pressure comparison in gas media, absolute mode, from 10 to 120 kPa, nine participants all using mercury manometers as primary standard and a pressure balance as transfer standard. In Fig. 11.2, the degree of equivalence

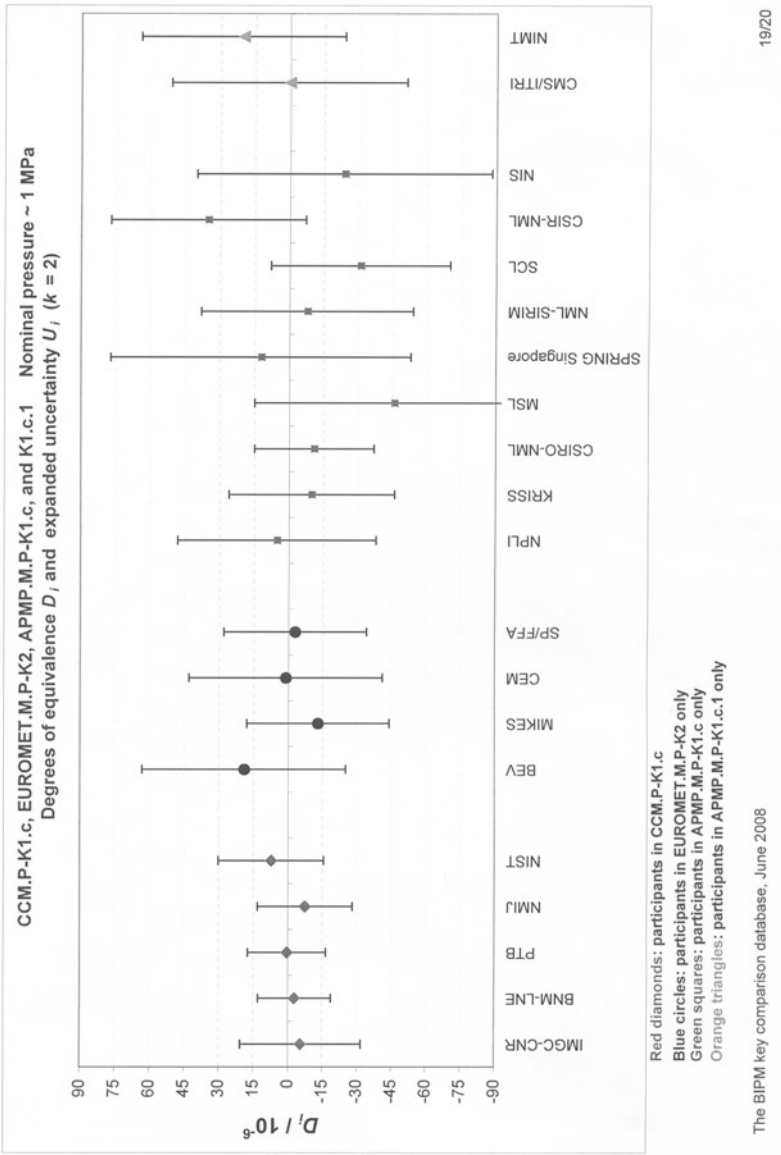

Fig. 11.1 Comparison CCM.P-K1.c and associated regional comparisons. Degree of equivalence (ppm) and its expanded uncertainty (*error bar*), at the nominal pressure of 1 MPa, for the different participants. (Figure extracted from BIPM-KCDB and reproduced with permission of BIPM)

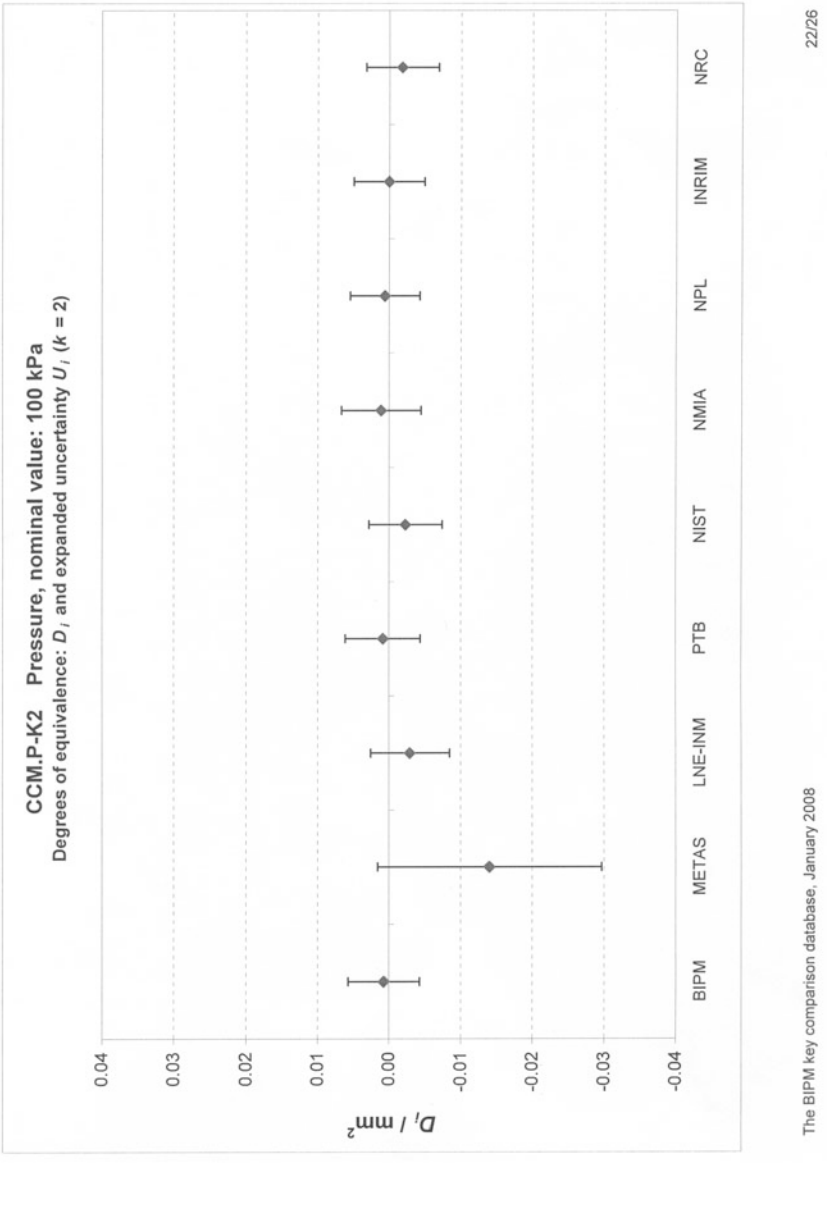

Fig. 11.2 Comparison CCM.P-K2. Degree of equivalence (in mm^2) and its expanded uncertainty (*error bar*), at the nominal pressure of 100 kPa, for the different participants. As the nominal effective area of the transfer standard is 335.70 mm^2, 0.01 mm^2 is approximately equivalent to 30 ppm. (Figure extracted from BIPM-KCDB and reproduced with permission of BIPM)

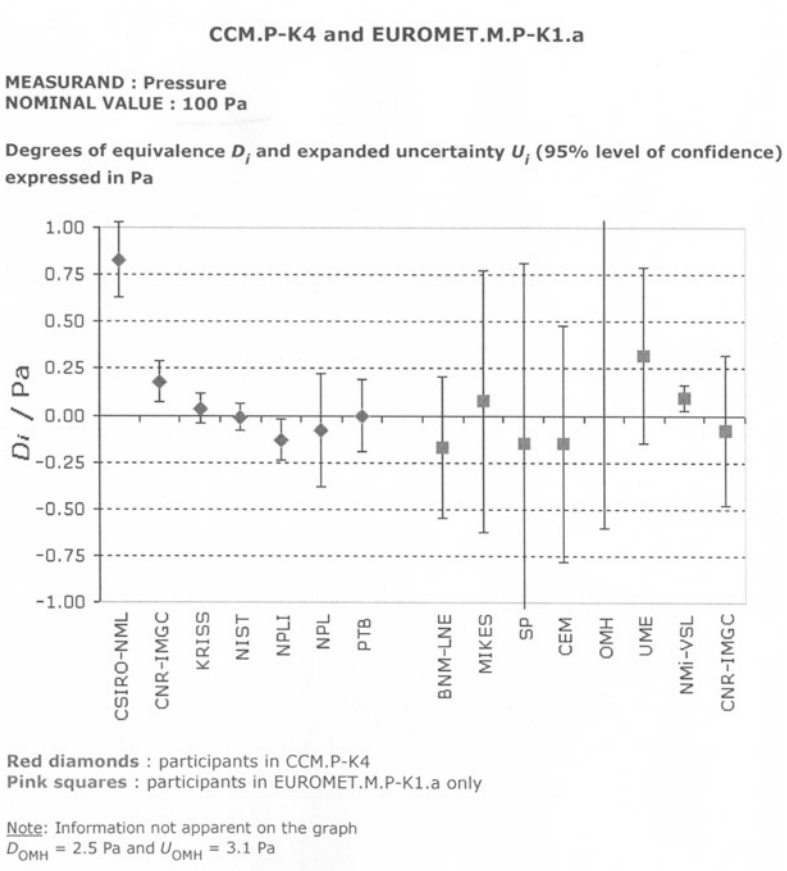

Fig. 11.3 Comparison CCM.P-K4 and associated regional comparisons. Degree of equivalence (in Pa) and its expanded uncertainty (*error bar*), at the nominal pressure of 100 Pa, for the different participants. For CCM.P-K4 comparison, four NMIs used liquid column manometers as primary standards and three NMIs used static expansion systems. (Figure extracted from BIPM-KCDB and reproduced with permission of BIPM)

at the pressure of 100 kPa with its expanded uncertainty is given, this figure was taken from the available results at KCDB. For CCM.P-K2 comparison, a synthesis of the main results is given in Perkin et al. (2008) as well.

- *CCM.P-K4*, a pressure comparison in gas media, absolute mode, from 1 to 1 000 Pa, seven participants some of them using mercury manometers as primary standard and others using static expansion systems. This comparison was followed by regional comparisons (EUROMET.M.P-K1.b, SIM-EUROMET.M.P-BK3, and another EUROMET.M.P-K1.a). The transfer standards were two capacitance diaphragm gauges and two resonant silicon pressure transducers. A synthesis of results for the comparison CCM.P-K4 is given in Miiller et al. (2002). In Figs. 11.3

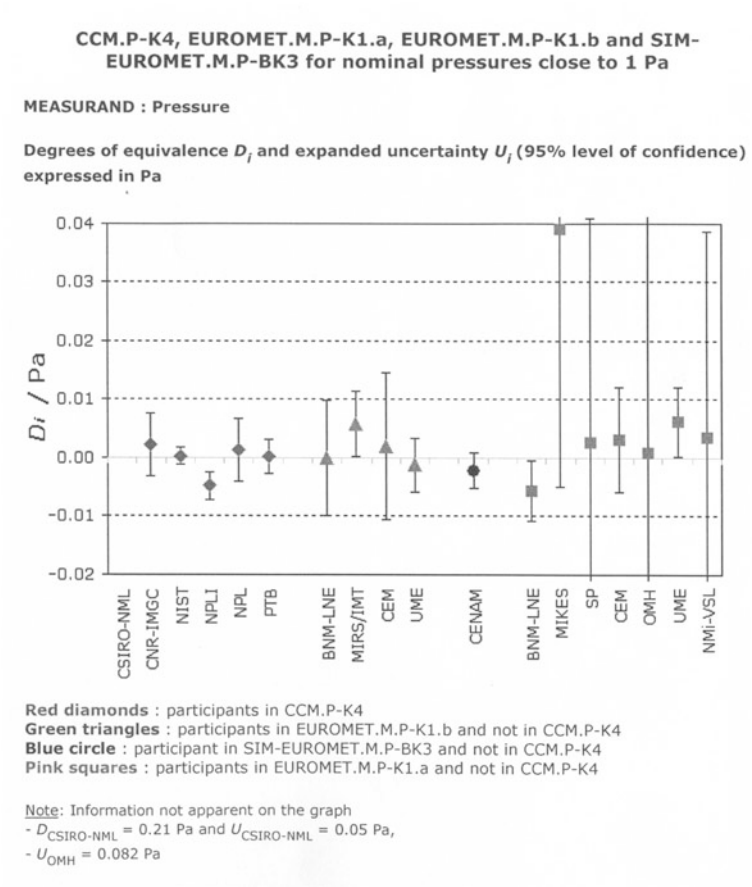

Fig. 11.4 Comparison CCM.P-K4 and associated regional comparisons. Degree of equivalence (in Pa) and its expanded uncertainty (*error bar*), at the nominal pressure of 1 Pa, for the different participants. For CCM.P-K4 comparison, two NMIs used liquid-column manometers as primary standards and four NMIs used static expansion systems. (Figure extracted from BIPM-KCDB and reproduced with permission of BIPM)

and 11.4, the degree of equivalence, at the pressure of 100 and 1 Pa, respectively, is given with its expanded uncertainty, these two figures have been taken from the available results at KCDB.

In Table 11.1, the CIPM main key comparisons for pressure measurements in gas media up to 7 MPa are synthetically summarized. More information is available on the BIPM-KCDB.

Table 11.1 CIPM pressure key comparisons in gas media for pressure range from few Pa to 7 MPa, basic data as described in the BIPM-KCDB. (Reproduced with permission of BIPM)

Comparison identifier	Title	Pressure range	Transfer standard used	Participants	Comparison linked to the present one
CCM.P-K1.a Start date: 1995 End date: 1997 See Molinar et al. (1999)	Pressure measurements, phase A1, gauge mode, determination of effective areas, by calculations, of two piston-cylinder units starting from their dimensional measurements	50 kPa–1 MPa	Two piston-cylinder units (nominal area 10 cm^2) of pressure balances that will be also used with the appropriate pressure balances for the comparison *CCM.P-K1.b*	4	None, but results are related also to *CCM.P-K1.b* comparison as the same transfer standards were used
	Comments: Key comparison reference value x_R is calculated, as the nonweighted mean of the four participants Standard uncertainty of reference value u_R is the standard deviation of the mean u_R/x_R ranges from 1.7 to 2.4 $\times 10^{-6}$ Relative degree of equivalence of participants ranges from 4.3 to -6.0×10^{-6} Expanded uncertainty $U(k \approx 2)$ of degree of equivalence ranges from 5.8 to 22.7 $\times 10^{-6}$ and is largely influenced by the standard uncertainty of participants				
CCM.P-K1.b Start date: 1995 End date: 1997 See Legras et al. (1999)	Pressure measurements, phase A2, gauge mode, determination of effective areas of two piston-cylinder units (the same as *CCM.P-K1.a*) by comparison to participant standards	50 kPa–1 MPa	Two pressure balances, equipped with the same piston-cylinder units used in the *CCM.P-K1.a* comparison	4	*EUROMET.M.P-K3a*, 2000–2001 (seven participants: one was a *CCM.P.K1.b* participant). See Otal et al. (2007) *COOMET.M.P-K1*, 2004–2006 (six participants: one was a *CCM.P.K1.b* participant and another was a *EUROMET.M.P-K3a* participant). See Kiselev et al. (2008) More information on the BIPM-KCDB

Table 11.1 (continued)

Comparison identifier	Title	Pressure range	Transfer standard used	Participants	Comparison linked to the present one
	Comments: Key comparison reference value x_R is calculated as the mean value of 24 individual results (six results for each participants from 100 kPa to 1 MPa) Standard uncertainty of reference value u_R is the standard deviation of the mean u_R/x_R ranges from 0.47 to 0.65×10^{-6} Degree of equivalence is calculated as the difference of participant values in respect of x_R. Relative degree of equivalence of participants ranges from 6.3 to -4.0×10^{-6} Expanded uncertainty U ($k \approx 2$) of degree of equivalence ranges from 5.9 to 26.1×10^{-6} and is largely influenced by the standard uncertainty of participants. Also, degree of equivalence between pair of participants, and their expanded uncertainties, are calculated				
CCM.P-K1.c Start date: 1998 End date: 1999, final report 2000, Molinar et al. (2000)	Pressure measurements, phase B, gauge mode, determination of effective areas of two piston-cylinder units by comparison to participant standards	First p-c unit: 79.4–896.4 kPa Second unit: 0.622–6.792 MPa	Two pressure balances, equipped with piston-cylinder units of nominal effective area of 84 mm^2 and 8.4 mm^2	5	*EUROMET.M.P-K2*, report in 2002 (six participants: two participated also to *CCM.P.K1.c*). See Ban et al. (2002) *APMP.M.P-K1.c*, 1998–2001 (5 + 6 participants: two participated also to *CCM.P.K1.c*). See Bandyopadhyay et al. (2003) *APMP.M.P-K1.c.1*, 2003–2004 (three participants, linked to *APMP.M.P-K1.c*). See Chen-Chuan Hung et al. (2008) *EUROMET.M.P-K3.b*, 2000–2002, report in 2009 (13 participants: two participated also to *CCM.P.K1.c*). See Perkin (2011) More information on the BIPM-KCDB

Table 11.1 (continued)

Comparison identifier	Title	Pressure range	Transfer standard used	Participants	Comparison linked to the present one
	Comments: Key comparison reference value x_R for each transfer standard is calculated as the linear fit $A'_{p'}$ vs. pressure p' of all results from the five participants Standard uncertainty of reference value u_R is taken as the standard deviation of the linear fit u_R/x_R is equal to 2.5×10^{-6} and 7.2×10^{-6}, respectively, for low-pressure unit (C-415) and for high-pressure unit (V-762) Degree of equivalence is calculated as the difference of participant values in respect of x_R. Relative degree of equivalence of participants ranges from 6.3 to -4.9×10^{-6} for unit C-415 and from 14.2 to -12.5×10^{-6} for unit V-762 Expanded uncertainty U ($k \approx 2$) of degree of equivalence ranges from 7.6 to 24.8×10^{-6} (unit C-415) and from 15.6 to 33.2×10^{-6} (unit V-762) and is largely influenced by the standard uncertainty of participants. Also, degree of equivalence between pair of participants, and their expanded uncertainties, are calculated				
CCM.P-K2 Start date: 1998 End date: 2001, final report in Jan 2008, Perkin et al. (2008)	Pressure measurements, absolute mode, determination of effective area of a piston-cylinder unit by comparison to participant standards (mercury manometers)	10–120 kPa	Pressure balance, equipped with piston-cylinder unit of nominal effective area of 335.7 mm^2	9	None
	Comments: Key comparison reference value x_R is calculated at each nominal pressure p as the median of the participants' values obtained at this pressure Standard uncertainty of the key comparison reference value u_R is calculated by the formula $u_R = 1.858\ MAD/(n-1)^{1/2}$ where MAD is the median of absolute deviations from the median and n is the number of participants contributing to the reference value u_R/x_R ranges from 1.5×10^{-6} to 5.1×10^{-6} Degree of equivalence is calculated as the difference of participant values in respect of x_R. Relative degree of equivalence of participants can be pressure dependent. At 10 kPa the relative degree of equivalence ranges from -53×10^{-6} to 19.6×10^{-6}. At 100 kPa the relative degree of equivalence ranges from -42×10^{-6} to 3.3×10^{-6} Expanded uncertainty U ($k \approx 2$) of degree of equivalence is calculated at each pressure and it include the instability of the transfer standard equal to 7.5 ppm as well, a relatively large value. The expanded uncertainty of the degree of equivalence is largely influenced by the standard uncertainty of participants. With the exception of one participant, a generally good agreement was found. Also, degree of equivalence between pair of participants, and their expanded uncertainties, are calculated. For more detailed information at each pressure, see the BIPM-KCDB				

Table 11.1 (continued)

Comparison identifier	Title	Pressure range	Transfer standard used	Participants	Comparison linked to the present one
CCM.P-K4 Start date: 1998 End date: 1999, final report in 2002, Miiller et al. (2002a)	Pressure measurements, absolute mode, determination of pressure measured by a pressure transducer and after appropriate corrections its value compared to participant standards (liquid column manometers and static expansion systems)	1 Pa–1 kPa	Set of pressure transducer all in a thermally controlled box. Two transducers were resonant silicon gauge (RSG), 1 and 10 kPa full scales. Two were capacitance diaphragm gauge (CDG) of 133 Pa full scales	7	*EUROMET.M.P-K1.b*, final report in 2002 (seven participants: three participated also in *CCM.P-K4*). Pressure range from 3×10^{-4} to 0.9 Pa, Two spinning rotor gauge as transfer standards are used. See Jousten et al. (2005) *SIM_EUROMET.M.P-BK3*, final report in 2004 (three participants: one participated also in *CCM.P-K4*). Pressure range from 3×10^{-4} to 0.9 Pa, Two spinning rotor gauge as transfer standards are used. See Jousten et al. (2005a) *EUROMET.M.P-K1.a* final report in 2005 (11 participants: many participated also in *CCM.P-K4*). Pressure range from 0.1 Pa to 1 kPa, Three CDG as transfer standards of 133 and 1 330 Pa full scales are used. See Calcatelli et al. (2005) *EURAMET.M.P-K4.2010*, Planned comparison, 2010–2011, 1 Pa to 15 kPa, absolute and gauge mode, five participants More information on the BIPM-KCDB

Table 11.1 (continued)

Comparison identifier	Title	Pressure range	Transfer standard used	Participants	Comparison linked to the present one
	Comments: In the summary, results on BIPM-KCDB all CCM and regional comparisons are grouped and linked together. Here, we will only mention the data of the *CCM.P.K4* comparison. Four participants used liquid column manometers and four others used static expansion systems, in one case one participant used both. For each of the selected pressures (1, 3, 10, 30, 100, 300, and 1 000 Pa) and for each participant, it was calculated the corrected mean gauge reading, coupled with the standard uncertainty of this corrected reading Key comparison reference value p_R is calculated at each nominal pressure as the unweighted mean of the used measurement method and outliers are excluded. Standard uncertainty of the key comparison reference value u_R is associated to the results after correction, including estimate of uncertainty of the methods and uncertainty of the participant laboratories. See Final Report of the comparison *CCM.P-K4* u_R/p_R ranges from 0.8×10^{-3} at 1 Pa to 0.37×10^{-3} at 1 kPa Degree of equivalence is calculated as the difference of participant values in respect of p_R. Relative degree of equivalence of participants can be pressure dependent. At 1 Pa the relative degree of equivalence ranges from -4.8×10^{-3} to 2.3×10^{-3}. At 1 kPa the relative degree of equivalence ranges from -0.9×10^{-3} to 0.7×10^{-3} Expanded uncertainty $U(k \approx 2)$ of degree of equivalence is calculated at each pressure and it includes the instability of the transfer standard as well. The expanded uncertainty of the degree of equivalence is largely influenced by the standard uncertainty of participants and by need of corrections. At 1 Pa the relative expanded uncertainty of the degree of equivalence ranges from 1.5×10^{-3} to 5.4×10^{-3}. At 1 kPa the relative degree of equivalence ranges from 0.7×10^{-3} to 3.0×10^{-3} Also, degree of equivalence between pair of participants, and their expanded uncertainties, are calculated. For more detailed information at each pressure, see the BIPM-KCDB				
CCM.P-K5 Start date: 1998 End date: 1999, final report in 2002, final paper in Miiller et al. (2002)	Pressure measurements, differential mode (gauge mode), determination of pressure measured by a pressure transducer and after appropriate corrections its value compared to participant standards (liquid column manometers and double pressure balances)	1 Pa–1 kPa	Set of pressure transducers all in a thermally controlled box. Two transducers were resonant silicon gauges (RSG), 1 kPa and 10 kPa full scale. Two were capacitance diaphragm gauges (CDG) of 133 Pa full scale	4	*APMP.M.P-K5*, final report in 2006 (two participants: one participated also in *CCM.P-K5*). Pressure range from 1 to 5 000 Pa., RSG and CDG pressure transducers are used as transfer standards. See Kobata et al. (2007)

Table 11.1 (continued)

Comparison identifier	Title	Pressure range	Transfer standard used	Participants	Comparison linked to the present one
			Similar kind of transducers as used in Key comparison *CCM.P-K4.*		More information on the BIPM-KCDB.
	Comments: In the summary, results on BIPM-KCDB all CCM and regional comparisons are grouped and linked together. Here, we will only mention the data of the *CCM.P.K5* comparison. Three participants used liquid column manometers and one used a double pressure balance. For each of the selected pressures (1, 3, 10, 30, 100, 300, and 1 000 Pa) and for each participant, it was calculated the corrected mean gauge reading, coupled with the standard uncertainty of this corrected reading				
	Key comparison reference value p_R is calculated at each nominal pressure as the unweighted mean of the used measurement method and outliers are excluded. Standard uncertainty of the key comparison reference value u_R is associated to the results after correction, including estimate of uncertainty of the methods and uncertainty of the participant laboratories. See Final Report of the comparison *CCM.P-K5*				
	u_R/p_R ranges from 4.0×10^{-3} at 1 Pa to 0.014×10^{-3} at 1 kPa				
	Degree of equivalence is calculated as the difference of participant values in respect of p_R. Relative degree of equivalence of participants can be pressure dependent. At 1 Pa the relative degree of equivalence ranges from -4.2×10^{-3} to 8.0×10^{-3}. At 1 kPa the relative degree of equivalence ranges from -0.01×10^{-3} to 0.011×10^{-3}				
	Expanded uncertainty $U(k \approx 2)$ of degree of equivalence is calculated at each pressure and it includes the instability of the transfer standard as well. The expanded uncertainty of the degree of equivalence is largely influenced by the standard uncertainty of participants and by need of corrections. At 1 Pa the relative expanded uncertainty of the degree of equivalence ranges from 8.1×10^{-3} to 15.0×10^{-3}. At 1 kPa the relative degree of equivalence ranges from 0.028×10^{-3} to 0.033×10^{-3}				
	Also, degree of equivalence between pair of participants, and their expanded uncertainties, are calculated. For more detailed information at each pressure, see the BIPM-KCDB				

Table 11.1 (continued)

Comparison identifier	Title	Pressure range	Transfer standard used	Participants	Comparison linked to the present one
CCM.P-K6 Start date: 1998 End date: 2001, final report in August 2006	Pressure measurements, gauge mode, determination of effective area of a piston-cylinder unit by comparison to participant standards (mercury manometers and pressure balances)	10–120 kPa	Pressure balance, equipped with piston-cylinder unit of nominal effective area of 335.7 mm^2	7	*APMP.M.P-K6*, 1998–2001(10 participants: one participated also in *CCM.P-K6*). See Bandyopadhyay et al. (2008) *APMP.M.P-K6.1*, 2003–2004, final report in 2009. (three participants: one participated also to *APMP.M.P-K6*). See Chen-Chuan Hung et al. (2009) More information on the BIPM-KCDB

Comments: Key comparison reference value x_R is calculated at each nominal pressure p as the median of the participants' values obtained at this pressure

Standard uncertainty of the key comparison reference value u_R is calculated by the formula $u_R = 1.858\ MAD/(n-1)^{1/2}$ where MAD is the median of absolute deviations from the median and n is the number of participants contributing to the reference value

u_R/x_R ranges from 1.5×10^{-6} to $4{,}5 \times 10^{-6}$

Degree of equivalence is calculated as the difference of participant values in respect of x_R. Relative degree of equivalence of participants can be pressure dependent. At 10 kPa the relative degree of equivalence ranges from -134×10^{-6} to 8.6×10^{-6}. At 100 kPa the relative degree of equivalence ranges from -42.3×10^{-6} to 3.6×10^{-6}

Expanded uncertainty $U(k \approx 2)$ of degree of equivalence is calculated at each pressure and it includes the instability of the transfer standard as well. The expanded uncertainty of the degree of equivalence is largely influenced by the standard uncertainty of participants. All the participants' results were equivalent to the reference value within the quoted uncertainties and all participants' results were in good agreement with all other participants' results

Also, degree of equivalence between pair of participants and their expanded uncertainties are calculated. For more detailed information at each pressure, see the BIPM-KCDB

Table 11.1 (continued)

Comparison identifier	Title	Pressure range	Transfer standard used	Participants	Comparison linked to the present one
CCM.P-K10 Start date: 1983 End date: 1995, final paper in Perkin et al. (1998)	Pressure measurements, absolute and gauge mode, determination of effective area of a piston-cylinder unit by comparison to participant standards (mercury manometers and pressure balances, different participants used more than one primary standard)	10–140 kPa	Pressure balance, equipped with piston-cylinder unit of nominal effective area of 80.6 mm^2	Ten, all in absolute mode and only five in gauge mode	None Approved for provisional equivalence More information on the BIPM-KCDB
	Comments: This comparison was approved for provisional equivalence at the start of BIPM-KCDB. For this reason the usual approach is less solid. It has also to be taken into account the larger time needed for this comparison and in some cases the changes of standards occurred Key comparison reference value x_R is calculated at each nominal pressure p as the unweighted mean value of all participants' values obtained at this pressure Standard uncertainty of the transfer standard effective area is calculated according to each laboratory declaration In absolute mode, the maximum difference between any two laboratories was of the order of 16 ppm at pressure of 11 kPa and of 45 ppm at 101 kPa. The differences are greater than what would be expected from the claimed uncertainties of the participants. Disagreements were also found in gauge mode For more detailed information at each pressure, see the reference paper by Perkin et al. (1998)				

Other CCM or RMO pressure comparisons not listed here belong to the following areas, outside the scope or the pressure range of the present book:

- Ultra-high vacuum (e.g., *CCM.P-K3*, *CCM.P-K3.1*, . . .)
- Leak rates (e.g., *CCM.P-K12*, . . .)
- High pressure in liquid media (e.g., *CCM.P-K7*, *CCM.P-K8*, *CCM.P-K9*, *CCM.P-K11*, . . .)

11.2.2 Key Comparisons Related to Temperature Measurements Extending from 273.16 K Downward

In October 2011, on KCDB, there are 56 results available for temperature measurements. Between these, 18 are comparisons concerning the temperature field covered by this book (excluding three comparisons dedicated to industrial-type thermometers and one to liquid-in-glass thermometers). Of them, only eight concern temperatures below the triple point of argon (≈84 K).

Of the 18 key comparisons, 8 are regional key comparisons. For 6 of the 18, there are full results available on KCDB. When full results are published, there are direct links to the reports, or papers published and for each of the participants a degree of equivalence is given as approved by participants and CC of CIPM. The degree of equivalence is built up on the responsibility of participants, it is explained how it is derived starting from the uncertainty of participants at some selected temperatures of the comparison. A few more of the 18 comparisons are close to completion, while a few others are simply at the planning stage.

The six completed KCs are the following:

1. *CCT-K1* "Realizations of the ITS-90 from 0.65 to 24.6 K", http://kcdb.bipm.org/AppendixB/appbresults/cct-k1_final-report.pdf. The Final Report is published in *Metrologia*, 2006, **43**, *Tech. Suppl.*, 03002. This KC compares ITS-90 realizations in the indicated range, as stored on calibrated Rh-Fe resistance thermometers, between seven participating NMIs. One more NMI is close to completion of supplementary CCT-K1.1.
2. *CCT-K2* "Realizations of the ITS-90 from 13.8 to 273.16 K" (1997–1999), http://kcdb.bipm.org/AppendixB/appbresults/cct-k2_final-report.pdf. The Final Report is published in *Metrologia*, 2002, **39**, 551–571. This KC compares resistance thermometer (SPRT) calibrated at the fixed points of the ITS-90 in the indicated range, between six participating NMIs. One more NMI has completed supplementary comparison CCT-K2.1—see point (4), and others are close to completion of supplementary CCT-K2.2 to CCT-K2.5.
3. *CCT-K3* "Realizations of the ITS-90 from 83.8058 to 933.473 K" (1997–2001), http://kcdb.bipm.org/AppendixB/appbresults/cct-k3.pdf and the Final Report is published in *Metrologia*, 2002, **39**, 179–205. The participating NMIs were 14 plus BIPM. A new comparisons CCT-K3 is at its early stage of planning.
4. *CCT-K2.1* "Realizations of the ITS-90 from 13.8 to 273.16 K" (2003), http://kcdb.bipm.org/AppendixB/appbresults/cct-k2.1_final-report.pdf. See CCT-K2.
5. *EUROMET.T-K3* "Realizations of the ITS-90 from 83.8 to 692.7 K" (2001–2004), http://kcdb.bipm.org/AppendixB/appbresults/euromet.t-k3_final-report.pdf. In addition, from EUROMET there are in progress also supplementary comparisons K3.1–K3.3.
6. *APMP.T-K3* "Realizations of the ITS-90 from 234.3 to 692.7 K" (2000–2003), http://kcdb.bipm.org/AppendixB/appbresults/apmp.t-k3_final-report.pdf. In addition, from APMP there are in progress also supplementary comparisons K3.1–K3.4.

In Figs. 11.5a and b, the main results of the comparison CCT-K1 are given, concerning two different temperature values. The figure is taken from the BIPM-KCDB.

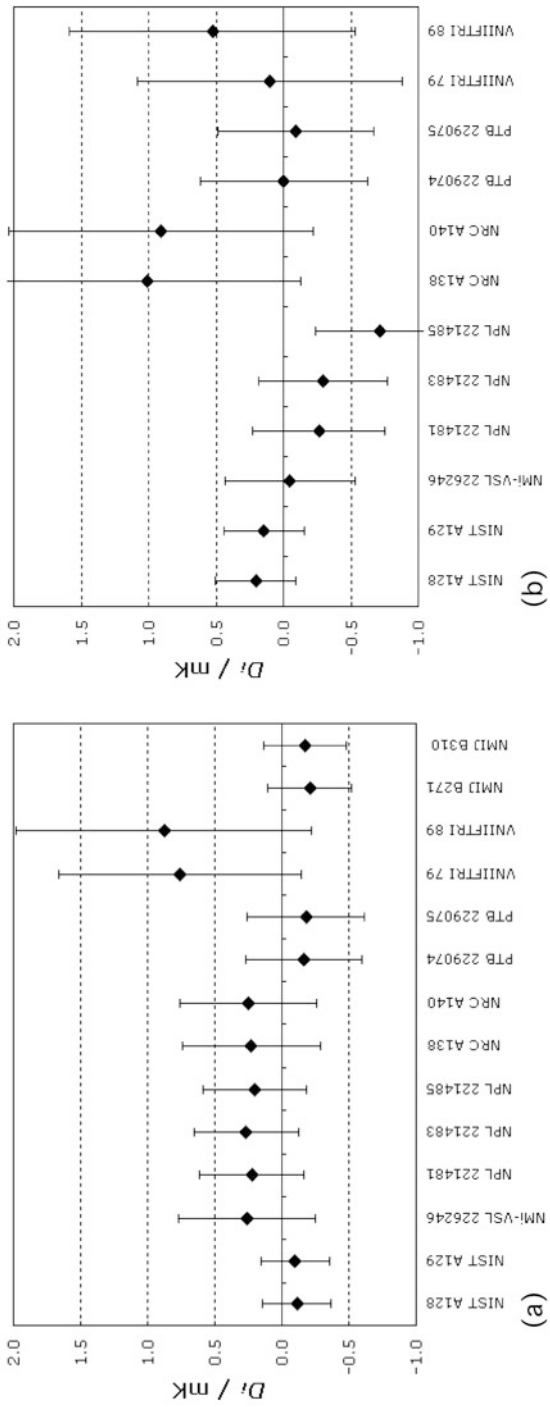

Fig. 11.5 Comparison CCT-K1, for two of the comparison temperatures (see Table 11.2). **a** Point at 2.248 K. **b** Point at 8.400 K. All participants and participating thermometers are shown. The *baseline* is the reference value, with no uncertainty attached to it, and "has no special significance with respect to the ITS-90." The *error bars* are the expanded uncertainty

In Figs. 11.6a and b, the main results of the comparison CCT-K2 and of the supplementary K2.1 are given, concerning two different fixed points.

In Figs. 11.7a and b, the main results of the comparison CCT-K3 are given, concerning the two fixed points below 0 °C and, in Figs. 11.8a and b, the corresponding degree of equivalence with respect to one participant, INRIM.

In Table 11.2, the CIPM key comparisons for cryogenic temperature measurements are synthetically summarized. More information is available on the BIPM-KCDB.

11.3 The Calibration and Measurement Capabilities

As indicated in MRA-approved document (Appendix G) for calibration and measurement certificates, the quantities, ranges and calibration, and measurement capabilities expressed with their uncertainty (normally at a 95 % level of confidence but in some cases it may be at a higher, specified, level), are listed for each participating institute in an appropriate document (Appendix C of the MRA), which is commonly called the list of the CMC. Such uncertainty declarations must be consistent with the results derived from the key comparison as included in Appendix B of the MRA.

If, as a result of a key comparison, a significant unresolved deviation from the key comparison reference value persists for the standard of a particular participating institute, the existence of this deviation is noted in Appendix C. The same applies for significant inconsistencies resulting from a supplementary comparison.

The calibration and measurement capabilities listed in Appendix C of MRA are analyzed by the JCRB following the procedures given in point 7.3 of the MRA document. The calibration and measurement capabilities referred to in the MRA are those that are ordinarily available to the customers of an institute through its calibration and measurement services; they are sometimes referred to as best measurement capabilities.

11.3.1 Calibration and Measurement Capabilities for Gas Pressure Measurements in the Range from 100 Pa to 100 MPa

In October 2011, 43 countries provide CMC for pressure. Forty-two countries for absolute and gauge pressure calibrations for gas and 20 countries for differential pressure calibrations in gas media.

On the KCDB of BIPM, it is possible to visualize the calibration and measurement capabilities for each of the countries, generally NMIs, and from that to visualize different calibrations available.

The information is generally given as in the following Table 11.3, which is taken from KCDB of BIPM and is related to one NMI, *Istituto Nazionale di Ricerca Metrologica* (INRIM).

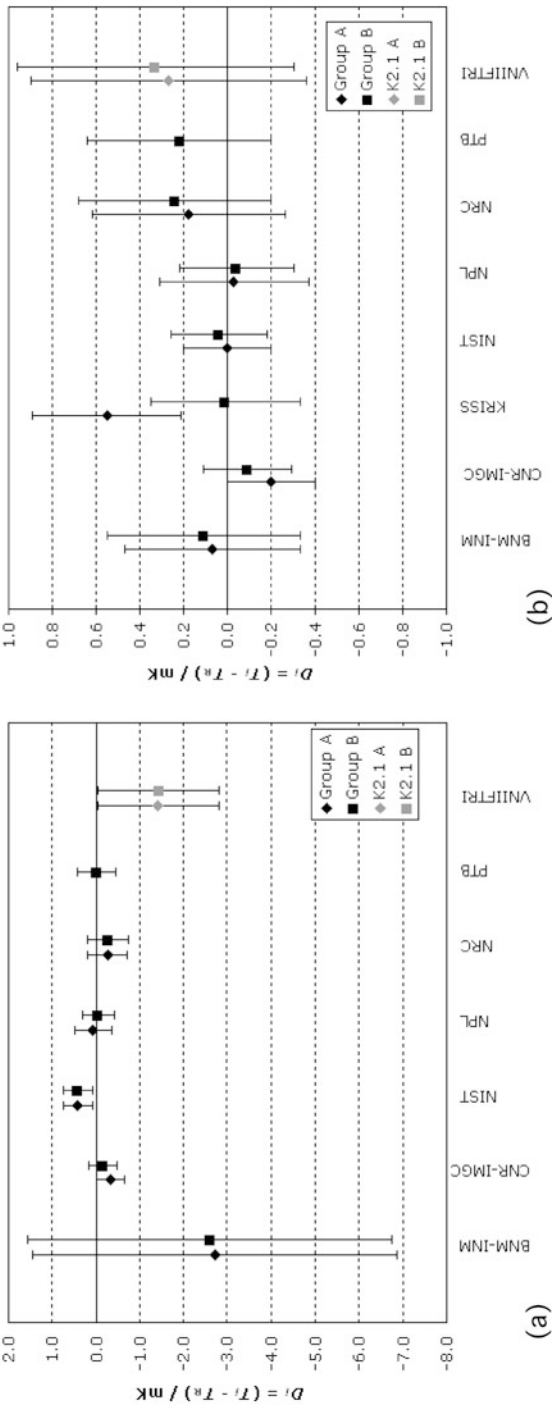

Fig. 11.6 Comparison CCT-K2, for two of the comparison fixed points (see Table 11.2). **a** Hydrogen fixed point. **b** Argon fixed point. Group A and B are for the two groups of participating thermometers. The *baseline* is the reference value, with no uncertainty attached to it, and with no special significance with respect to the ITS-90. The *error bars* are the expanded uncertainty

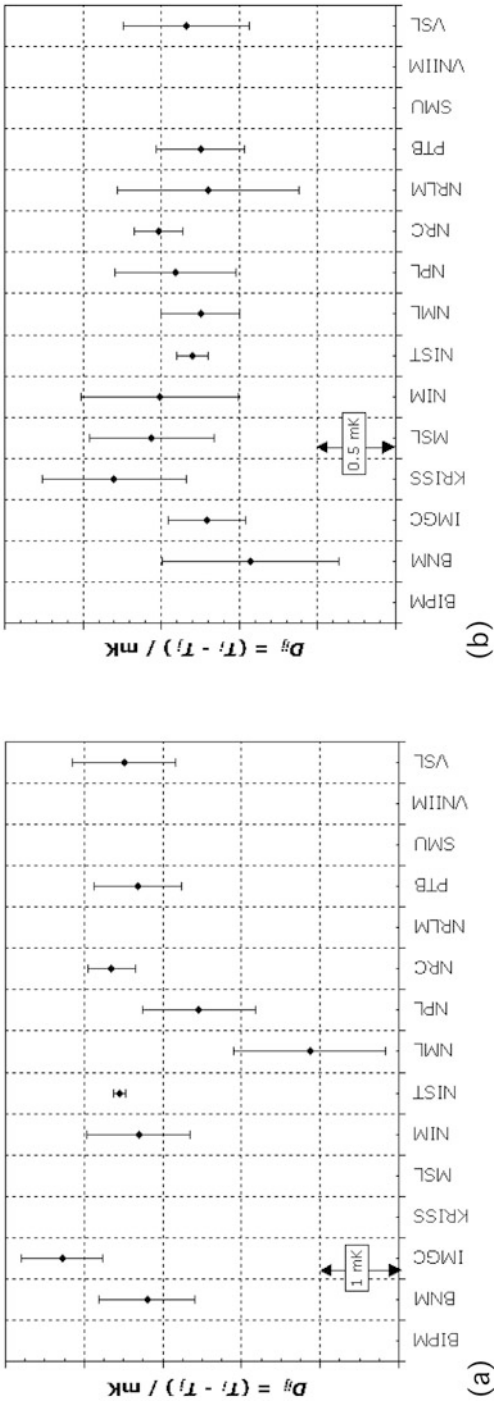

Fig. 11.7 Comparison CCT-K3, for the two comparison fixed points below 0 °C: graph of approximate equivalence (see Table 11.2). **a** Argon fixed point. **b** Mercury fixed point. There is no baseline, since there was no reference value computed. Not all participants provided data for all fixed points. The *error bars* are the expanded uncertainty

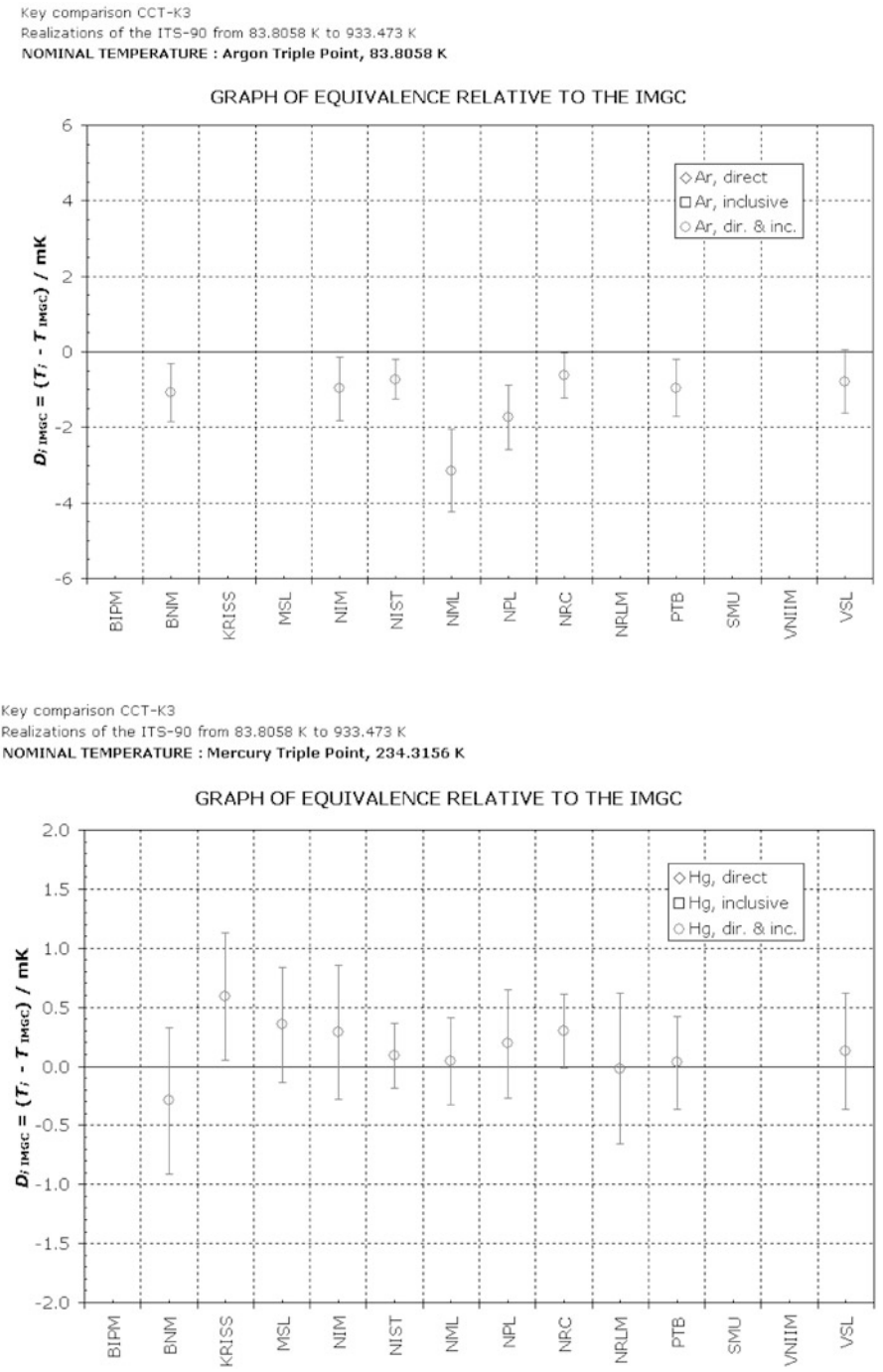

Fig. 11.8 Comparison CCT-K3 for the two comparison fixed points below 0 °C (see Table 11.2). Degree of equivalence relative to one NMI, IMGC (now INRIM), Italy, for the same two fixed points of Fig. 11.7: **a** Argon fixed point. **b** Mercury fixed point. *Baseline* is IMGC. The *error bars* are the expanded uncertainty

Table 11.2 CIPM key comparisons related to temperature measurements extending from 273.16 K downward, basic data as described in the BIPM-KCDB. (Reproduced with permission of BIPM)

Comparison identifier	Title	Pressure range	Transfer standard used	Participants	Comparison linked to the present one
CCT-K1 Start date: 1997 End date: 2001	Realizations of the ITS-90 from 0.65 to 24.6 K	0.65–24.6 K	One to three calibrated Rh-Fe resistance thermometers per participant supplied to the pilot	7	None, except one, K1.1, close to completion More information on the BIPM-KCDB
	Comments: Thermometers are calibrated at a pre-fixed number of temperatures in the range, using local realizations of the ITS-90: 0.650, 0.677, 0.704, 0.762, 0.858, 0.991, 1.032, 1.225, 1.250, 1.503, 1.755, 1.997, 2.248, 2.601, 2.700, 2.897, 2.997, 3.099, 3.400, 3.429, 3.801, 4.225, 4.478, 5.000, 5.948, 7.202, 8.296, 8.400, 9.508, 10.803, 12.297, 13.798, 15.500, 16.999, 18.597, 20.299, 21.575, 22.677, 23.496, 24.102, 24.340, 24.446, and 24.551 K. (From the BIPM-KCDB.) For each temperature in the comparison, the key comparison reference value, T_R, is the weighted mean of T_i, the individual temperature values of thermometers The weighted mean is calculated using the laboratory uncertainty combined with the comparison uncertainty, to set the weights T_R is used as the baseline for the comparison, but has no special significance with respect to the ITS-90, and is used without uncertainty The degree of equivalence of each temperature T_i with respect to the key comparison reference value, T_R, is given by a pair of terms: $D_i = (T_i - T_R)$ and U_i, its expanded uncertainty at 95 % confidence, both expressed in mK. U_i includes the uncertainties in the original laboratory calibrations and in the comparison measurements, but not in T_R The degrees of equivalence between each pair of thermometers is given by: $D_{ij} = (D_i - D_j) = (T_i - T_R) - (T_j - T_R)$ and $U_{ij} = (U_i^2 + U_j^2)^{1/2}$, its expanded uncertainty (at 95 % confidence), both expressed in mK				
CCT-K2 Start date: 1997 End date: 1999	Realizations of the ITS-90 from 13.8 to 273.16 K	13.8–273.16 K	Two calibrated capsule SPRT per participant supplied to the pilot	6	One K2.1 completed. Others, K2.2–K2.5 in progress More information on the BIPM-KCDB

Table 11.2 (continued)

Comparison identifier	Title	Pressure range	Transfer standard used	Participants	Comparison linked to the present one
	Comments: Thermometers are calibrated at the fixed points in the subranges, using local realizations of the ITS-90: 13.8 K, Hydrogen; 17.0 K; 20.3 K; 24.6 K, Neon; 54.4 K, Oxygen; 83.8 K, Argon; 234.3 K, Mercury (and 273.16 K, Water, as the reference). Resistance ratios $W(T) = R(T)/R(273.16\ \mathrm{K})$ are used. (From the BIPM-KCDB.) Key comparison reference value: *there is no single reference value for this comparison* The two measurement runs (groups A and B for the two thermometers) are evaluated separately. Resistance ratios are used with calibration equations for each thermometer to obtain temperature T_i For each group, the key comparison reference temperature, T_R, is the weighted average temperature calculated using the experimental variances to set the weights. They have zero uncertainty by definition The degree of equivalence of each laboratory with respect to the reference value is given by a pair of terms: $D_i = (T_i - T_R)$ and U_i, its expanded uncertainty (at 95 % confidence level), both expressed in mK The degree of equivalence between two laboratories is given by a pair of terms: $D_{ij} = D_i - D_j = (Ti - T_R) - (T_j - T_R)$ and U_{ij}, its expanded uncertainty (95 %), both expressed in mK Linking CCT-K2.1 to CCT-K2 The VNIIFTRI data obtained from CCT-K2.1 are linked to CCT-K2 results via NRC				
CCT-K3 Start date: 1997 End date: 2001	Realizations of the ITS-90 from 83.8058 to 933.473 K (here the interest is limited to temperatures ≤273.16 K)	83.8058–933.473 K	Long-stem SPRTs supplied by the pilot and subpilots	15	Only regional KC_s EUROMET.T-K3 and APMP.T-K3 completed. Others in progress or planned: EUROMET.T-K3.1 to 3.3 and APMP.T-K3.1 and 3.3 More information on the BIPM-KCDB
	Comments: Thermometers are calibrated at the fixed points in the subranges, using local realizations of the ITS-90: Ar, 83.8058 K; Hg, 234.3156 K; (Ga, 302.9146 K; In, 429.7485 K; Sn, 505.078 K; Zn, 692.677 K; Al, 933.473 K;) and H_2O, 273.16 K (reference). Resistance ratios $W(T) = R(T)/R(273.16\ \mathrm{K})$ are used. (From the BIPM-KCDB.) Key comparison reference value: the contents of the Appendix B of the MRA for CCT Key Comparison three were approved by a majority vote of the CCT. Due to the myriad of technical problems, it was *not possible to reach a consensus* on whether: (1) to use a key comparison reference value or (2) not to use a key comparison value. The viewpoints of the NMI participants are contained within the CCT-K3 Final Report (NIST Technical Note 1450)				

Table 11.2 (continued)

Comparison identifier	Title	Pressure range	Transfer standard used	Participants	Comparison linked to the present one
	The CCT agrees by consensus that *the absence of a key comparison reference value* in this appendix does not preclude the use of a key comparison reference value in other key comparisons The degree of equivalence between two laboratories is given by a pair of terms: $D_{ij} = D_i - D_j = T_i - T_j$ and the expanded uncertainty (95 %) U_{ij} of D_{ij}, both expressed in mK The pair-wise temperature differences and their associated uncertainties were calculated for the various laboratories by two paths. Those paths are indicated by the terms "direct" and "inclusive," or the corresponding abbreviations "dir." And "inc.," and yield results that are indicated in the equivalence matrices and graphs by the same terms. In some cases, the paths are identical The "direct" differences are the temperature differences between the realizations of a pair of laboratories that were obtained using the shortest available path linking those laboratories. In some cases, this means that the laboratories are compared using measurements made on the same SPRT or SPRTs. Where necessary, however, NIST or NML serves as an intermediary, linking the measurements of the two laboratories The "inclusive" differences are those in which all of the data obtained by the pair of laboratories involved are used in the calculations of their pair-wise temperature differences and their associated uncertainties. In inclusive differences, whether or not there is a direct linkage between the laboratories, NIST (and possibly also NML) may be used as an intermediary so that the temperature differences can be computed using all relevant data. For the inclusive path, NIST was selected as the intermediate laboratory because, overall, that results in a minimum number of intermediate laboratories in the pair-wise differences The expanded uncertainty, UL (95 %), listed in the matrices of equivalence and used in the "no baseline" graphs of approximate equivalence is derived for each laboratory by combining the type A standard uncertainty for the smallest number of measurements (n) across SPRTs and the type B standard uncertainty for each fixed point. The uncertainty UL (95 %) is only for the respective laboratory with no contribution from the other laboratories *Linking EUROMET.T-K3 to CCT-K3*. The Pilot Laboratory and the five copilots have participated in both comparisons The comparison of their averaged results in both exercises shows that they perform equally within 0.1 mK for all temperatures, except for the Zinc fixed-point temperature (0.23 mK) and the Tin fixed-point temperature (0.14 mK), as explained in Sect. 10.2 of the Final Report The uncertainty linked with the reproducibility between both exercises in also computed (see Table 28 on page 60 of the Final Report) and taken into account for the estimation of the pair-wise degrees of equivalence between participants in EUROMET.T-K3 and CCT-K3 (see Sect. 11.3 of the Final Report)				

Table 11.2 (continued)

Comparison identifier	Title	Pressure range	Transfer standard used	Participants	Comparison linked to the present one
	For each fixed-point temperature, the BIPM key comparison database displays the degrees of equivalence relative to the EUROMET reference value, and the pair-wise degrees of equivalence computed inside the EUROMET key comparison				
	Linking APMP.T-K3 to CCT-K3. The linkage of key comparison APMP.T-K3 to key comparison CCT-K3 is computed using the results of the two common participants, KRISS and NMIA				
	There is no key comparison reference value in CCT-K3. The 22nd CCT, at its meeting of May 2003, however, adopted the proposal to use the "average reference value," ARV, as reference value, for the purposes of CMC review. The ARV is defined as the average of the mean, the weighted mean, and the median. Its uncertainty is the simple average of the respective uncertainties of the mean, the weighted mean, and the median (see Sect. 6 of the 22nd CCT Report)				
	The degree of equivalence of laboratory i with respect to the ARV is given by a pair of terms, both expressed in mK: D_i and U_i, its expanded uncertainty ($k = 2$). The details of the calculation are given in Sect. 7 and 8 of the APMP.T-K3 Final Report				
	The degree of equivalence between two laboratories i and j is given by a pair of terms, both expressed in mK: $D_{ij} = D_i - D_j$, and U_{ij}, its expanded uncertainty ($k = 2$). The details of the calculation are given in Sect. 9 of the APMP.T-K3 Final Report				
	The following table includes the pair-wise degrees of equivalence inside key comparison APMP.T-K3. Pair-wise degrees of equivalence between participants in CCT-K3 and in APMP.T-K3 can be found starting in page 23 of the APMP.T-K3 Final Report				

Table 11.3 INRIM, Italy, partial list of CMC for gas pressure calibrations. (Taken from the BIPM-KCDB and reproduced with the permission of the BIPM. *Mass and Related Quantities, Italy, Istituto Nazionale di Ricerca Metrologica*)

Calibration or measurement service			Measurand level or range (Pa)		Expanded uncertainty				Comments
Quantity	Instrument or artifact	Instrument type or method	Minimum value	Maximum value	Value (Pa)	Coverage factor	Level of confidence (%)	Is the expanded uncertainty a relative one?	
Omissis									
Absolute pressure	Pressure gauge	Gas medium	1E + 03	1.2E + 05	0.5–2.5	2	95	No	Approved on 3 January 2007
Absolute pressure	Pressure gauge	Gas medium	1.2E+05	5.2E + 06	5E-05*p*, *p* pressure in Pa	2	95	No	Uncertainty values range from 6 Pa to 2.6E + 02 Pa Approved on 3 January 2007
Gauge pressure	Digital piston manometer	Gas medium	1	5E + 03	0.05–0.41	2	95	No	Approved on 3 January 2007
Gauge pressure	Pressure gauge	Gas medium	5E + 03	1.2E + 05	1–2.5	2	95	No	Approved on 3 January 2007
Gauge pressure	Pressure balance	Gas medium	6.4E + 03	8E + 06	(0.5 + 2.4E-05*p*), *p* pressure in Pa	2	95	No	Uncertainty values range from 0.7 Pa to 1.9E + 02 Pa Approved on 3 January 2007
Gauge pressure	Pressure balance	Gas medium	8E + 06	2E + 07	(0.5 + 2.8E-05*p*), *p* pressure in Pa	2	95	No	Uncertainty values range from 2.2E + 02 Pa to 5.6E+02 Pa Approved on 3 January 2007
Omissis									

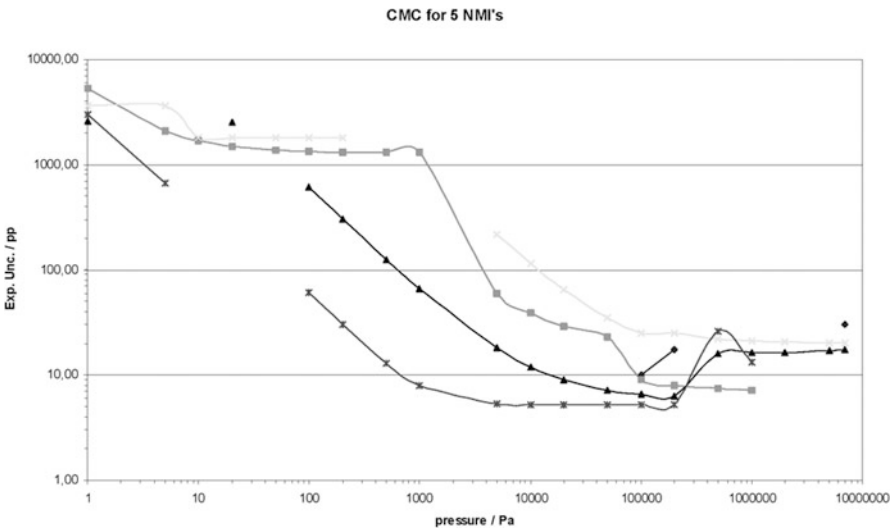

Fig. 11.9 Case of five NMIs: CMC data. Calibrations and measurements for absolute pressures from 1 Pa to 7 MPa. The figure gives the expanded uncertainty (ppm) versus pressure (Pa) in logarithmic scales. All numerical data have been extracted from KCDB

The reported data are not the complete list of pressure CMC for INRIM and they are given here only as an example.

As it can be seen on Table 11.3, which is only reported here as an example, this is what can be viewed from the KCDB search. Information given is as simple as possible and short information is supplied for the type of instrument or artifact under calibration, the condition of measurements, the typical pressure range, and the typical expanded uncertainty.

From the large variety of data in the KCDB different information can be analyzed, for example:

- Calibrations, for absolute pressure measurement calibrations in gas media, are available from 1×10^{-9} Pa to 7 MPa. Figure 11.9 summarizes the expanded uncertainty (in ppm) versus pressure (in Pa) for five different NMIs. As it can be seen, the expanded uncertainty varies with pressures being of the order of 0.1 % for pressures from 1 to 100 Pa, then in some cases typically below 10 ppm for pressures from 10 kPa to 1 MPa and from 1 to 7 MPa close to 20 ppm. This has not to be confused with the best measurement uncertainty of NMIs primary standard, but can be an expression of the best capabilities of the specific NMI to perform the calibrations of a pressure measurement instrument.
- Calibrations, for gauge pressure measurements calibrations in gas media, are available from few kPa to 100 MPa.
- Different calibrations are available for differential pressures in gas, including calibrations of pressure gauges used to perform differential pressure measurements at high line pressure as well.

11.3.2 Calibration and Measurement Capabilities (CMC) for Cryogenic Temperature Measurements

In October 2011, 50 countries provide CMC for temperature. Of them, 23 have CMCs at least down to the triple point of argon (≈84 K), while other 18 limit their CMCs to the refrigeration range (at least down to the triple point of mercury, ≈234 K).

On the KCDB of the BIPM, it is possible to visualize the calibration and measurement capabilities for each of the countries, generally NMIs, and from that to visualize different calibrations available.

The information is generally given as in the following Table 11.4, which is taken from KCDB of the BIPM and is related to one NMI, INRIM.

The reported data are not the complete list of temperature CMC for INRIM and they are given here only as an example, concerning different types of calibrations available to the users in the temperature range below 273.16 K (0 °C).

From the large variety of data in the KCDB, different information can be analyzed.

11.4 The BIPM Key Comparison Database (KCDB)

BIPM-KCDB made available an impressive number of data and it is a great success of the CIPM-MRA (1999) with an extremely high number of visitors. It has been set up under the effort of BIPM in order to give complete visibility to the main results of the CIPM-MRA (1999). It is maintained by the BIPM, which retains complete internationally protected copyright.

The material given in this Chapter is reproduced with the permission of the BIPM.

The BIPM-KCDB is accessible by http://kcdb.bipm.org. Inside the database, the following areas are available:

- *Participants in CIPM-MRA* (*Appendix A*). It contains the list (organized by country) of 86 Institutes, from 50 Member States, plus 33 Associates at CGPM and 3 International Organizations and covers a further 137 Institutes designed by signatory bodies of CIPM-MRA (1999).
- *Key and Supplementary Comparisons* (*Appendix B*). It contains information, data and results, interpreted in terms of equivalence, on CIPM and RMOs key and supplementary comparisons. Search is possible by comparison designation or by an advanced search. The advanced search can be done by *metrology area* (e.g., it is necessary to type Mass to reach the pressure comparisons and Thermometry to reach temperature comparisons), then the *branch* (e.g., pressure), then the *comparison type* (all, key or supplementary), then *organization* (all or different RMO), then *validity* (all or current or archival), and finally *country*. The results will then appear organized following the advanced search defined. All numbers of comparisons and available results are in continuous evolution.
- *Calibration and Measurement Capabilities, CMCs* (*Appendix C*). In this area, it is possible to visualize the CMCs by country (as a general search) or by an

Table 11.4 Partial list of CMC for cryogenic temperature calibrations. (Taken from the BIPM-KCDB and reproduced with the permission of the BIPM. *Thermometry, Italy, Istituto Nazionale di Ricerca Metrologica*)

Calibration or measurement service			Measurand level or range		Measurement conditions/ independent variables		Expanded uncertainty		
Quantity	Instrument or artifact	Instrument type or method	Minimum value	Maximum value			Value	Coverage factor	Level of confidence (%)
Omissis									
Temperature	Fixed point cell for CSPRT	Triple point of Argon	83.8058 K	83.8058 K	Cryostat	Isothermal	0.14 mK	2	95
Temperature	Fixed point cell for CSPRT	Triple point of Mercury	234.3156 K	234.3156 K	Thermostat	Isothermal	0.14 mK	2	95
Omissis									
Temperature	SPRT (capsule)	Fixed points	24.5561 K	273.16 K	Cryostat	Isothermal	0.50 mK	2	95
Omissis									
Temperature	CSPRT	Calibration at triple point of Hydrogen	13.8033 K	13.8033 K	Fixed point	Isothermal	0.35 mK	2	95
Omissis									
Temperature	IPRT	Comparison	−90 °C	0 °C	Stirred liquid bath	Ethanol	0.02 °C	2	95
Omissis									
Temperature	Thermoco-uples	Comparison	−90 °C	250 °C	Stirred liquid baths	Water, ethanol, oil	0.4 °C	2	95
Omissis									
Temperature	Sensors with display unit (only IPRT)	Comparison	−90 °C	0 °C	Stirred liquid baths	Ethanol	0.03 °C	2	95

Three columns on the right, not relevant here, have been omitted

advanced search by metrology area. It gives, as a result, a list or a table prepared and approved by the respective Consultative Committee and the CIPM, involving the JCRB as well.

- *List of Key Comparison* (*Appendix D*). At the time of publication of this book, it contains 764 key comparisons plus 280 supplementary comparisons. These numbers are in continuous evolution. Search is possible by metrology area (for pressure at first type Mass) and connected branch. For pressure 76 key and supplementary comparisons are available, the majority of them with published results in terms of degree of equivalence.
- There are other sections as well, e.g., *What's new?*, providing information and the latest news organized by date. There is an area for *KCDB Newsletter* as well. The KCDB Newsletter is issued twice a year (June and December) and at the moment 15 numbers have been issued, all available in this area. Also, an important *Related links* gives, for example, the KCDB statistics on number of key and supplementary comparisons, graphs of participation in key and supplementary comparisons divided by country, and distribution of calibration and measurement capabilities. A section of the *KCDB FAQs* is available as well to reply to the most common questions.

The BIPM -KCDB is one of the most visited parts of the BIPM web site, extremely useful to give everybody wide information about internationally accepted traceability of measurements as well as information on calibration and measurement services available in the different metrology institutes all over the world.

Appendix A
The International Temperature Scale of 1990

Annotated text of the parts of the definition that concerns the temperature range below 273.16 K.
(BIPM 1989; Preston-Thomas 1990)

The International Temperature Scale of 1990 was adopted by the International Committee of Weights and Measures at its meeting in 1989, in accordance with the request embodied in Resolution 7 of the 18th General Conference of Weights and Measures of 1987. This scale overcomes the International Practical Temperature Scale of 1968 (amended edition of 1975) and the 1976 Provisional 0.5–30 K Temperature Scale.

A.1 Units of Temperature

The unit of the fundamental physical quantity known as thermodynamic temperature, symbol T, is the kelvin, symbol K, defined as the fraction 1/273.16 of the thermodynamic temperature of the triple point of water.[1]

Because of the way earlier temperature scales were defined, it remains common practice to express a temperature in terms of its difference from 273.15 K, the ice point. A thermodynamic temperature, T, expressed in this way is known as a Celsius temperature, symbol t, defined by

$$t/^{\circ}\mathrm{C} = T/\mathrm{K} - 273.15 \tag{A.1}$$

The unit of Celsius temperature is the degree Celsius, symbol °C, which is by definition equal in magnitude to the kelvin. A difference of temperature may be expressed in kelvins or degrees Celsius.

[1] Comptes Rendus des Seances de la Treizième Conférence Générale des Poids et Mesures (1967–1968), Resolutions 3 and 4, p. 104.

F. Pavese, G. Molinar Min Beciet, *Modern Gas-Based Temperature and Pressure Measurements,* International Cryogenics Monograph Series,
DOI 10.1007/978-1-4419-8282-7, © Springer Science+Business Media New York 2013

The International Temperature Scale of 1990 (ITS-90) defines both International Kelvin Temperatures, symbol T_{90}, and International Celsius Temperatures, symbol t_{90}. The relation between T_{90} and t_{90} is the same as that between T and t, that is

$$t_{90}/^{\circ}\mathrm{C} = T_{90}/\mathrm{K} - 273.15 \tag{A.2}$$

The unit of the physical quantity T_{90} is the kelvin, symbol K, and the unit of the physical quantity t_{90} is the degree Celsius, symbol °C, as is the case for the thermodynamic temperature T and the Celsius temperature t.

A.2 Principles of the International Temperature Scale of 1990 (ITS-90)

The ITS-90 extends upwards from 0.65 K to the highest temperature practicably measurable in terms of the Planck radiation law using monochromatic radiation. The ITS-90 comprises a number of ranges and sub-ranges throughout each of which temperatures T_{90} are defined. Several of these ranges or sub-ranges overlap, and where such overlapping occurs, differing definitions of T_{90} exist: these differing definitions have equal status. For measurements of the very highest precision, there may be detectable numerical differences between measurements made at the same temperature but in accordance with differing definitions. Similarly, even using one definition, at a temperature between defining fixed points two acceptable interpolating instruments (e.g., resistance thermometers) may give detectably differing numerical values of T_{90}. In virtually all cases, these differences are of negligible practical importance and are at the minimum level consistent with a scale of no more than reasonable complexity: for further information on this point, see "Supplementary Information for the ITS-90".

> This scale concept is new with respect to the former issues. In the ITS-90, generally near the end of a definition field, a multiple definition is available. All definitions are equivalent and their use is equally allowed. Small differences between the temperature scale—i.e. in the numerical values of T_{90}—obtained using different definitions are known to exist, but they have been studied and checked to be within ITS-90 accuracy.

The ITS-90 has been constructed in such a way that, throughout its range, for any given temperature, the numerical value of T_{90} is a close approximation to the numerical value of T according to best estimates at the time the scale was adopted. By comparison with direct measurements of thermodynamic temperatures, measurements of T_{90} are more easily made, are more precise, and are highly reproducible.

There are significant numerical differences between the values of T_{90} and the corresponding values of T_{68} measured on the International Practical Temperature Scale of 1968 (IPTS-68), see Fig. A.1 and Table A.6.

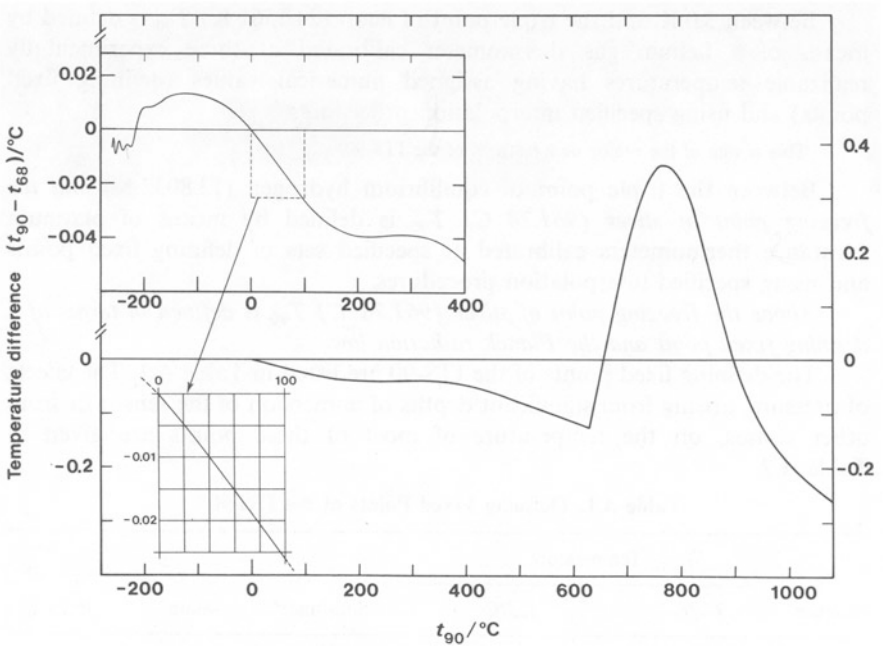

Fig. A.1 Temperatures differences ($t_{90} - t_{68}$)

It must be clearly noted that the accuracy which can be obtained from these differences in no way can be better than that allowed by the less accurate term of the difference, i.e., by the older scale, the IPTS-68. The number of digits of the differences reported in Table A.6 is generally larger than justified by the actual accuracy: it simply permits a smooth interpolation or to compute smooth functions for use in automatic computation. Some of these functions are reported in the Note to Table A.6.

Similarly there were differences between the IPTS-68 and the International Practical Temperature Scale of 1948 (IPTS-48), and between the International Temperature Scale of 1948 (ITS-48) and the International Temperature Scale of 1927 (ITS-27). *See the Appendix and, for more detailed information, "Supplementary Information for the ITS-90".*[2]

A.3 Definition of the International Temperature Scale of 1990

Between 0.65 K and 5.0 K T_{90} is defined in terms of the vapor-pressure temperature relations of ^{3}He and ^{4}He.

The ITS-90 definition supercedes the old scales T_{62} and T_{58}.

[2] The text in italic is out of the scope of this book (*most is omitted*).

Between 3.0 K and the triple point of neon (24.5561 K) T_{90} is defined by means of a helium gas thermometer calibrated at three experimentally realizable temperatures having assigned numerical values (defining fixed points) and using specified interpolation procedures.

This is one of the major new features of the ITS-90.

Between the triple point of equilibrium hydrogen (13.8033 K) *and the freezing point of silver (961.78 °C)*, T_{90} is defined by means of platinum resistance thermometers calibrated at specified sets of defining fixed points and using specified interpolation procedures.

Above the freezing point of silver (961.78 °C) T_{90} is defined in terms of a defining fixed point and the Planck radiation law.

The defining fixed points of the ITS-90 are listed in Table A.1. The effects of pressure, arising from significant depths of immersion of the sensor or from other causes, on the temperature of most of these points are given in Table A.2.

A.3.1 From 0.65 K to 5.0 K: Helium Vapor-Pressure Temperature Equations

In this range, T_{90} is defined in terms of the vapor pressure p of ^{3}He and ^{4}He using equations of the form

$$T_{90}/\mathrm{K} = A_0 + \sum_{i=1}^{9} A_i[(\ln(p/\mathrm{Pa}) - B)/C]^i \qquad \text{(A1.3)}$$

The values of the constants A_0, A_i, B, and C are given in Table A.3 for ^{3}He in the range 0.65–3.2 K and for ^{4}He in the ranges 1.25–2.1768 K (the λ point) and 2.1768–5.0 K.

No fixed points are used in the definition and, consequently, no calibration at fixed points is needed. A thermometer is designed according to the state-of-the-art, then the T_{90} values are obtained from the measured values of p and from Eq. (A.3; see Chap. 4).

A.3.2 From 3.0 K to the Triple Point of Neon (24.5561 K): Gas Thermometer

In this range, T_{90} is defined in terms of a ^{3}He or a ^{4}He gas thermometer of the constant-volume type that has been calibrated at three temperatures. These are the triple point of neon (24.5561 K), the triple point of equilibrium hydrogen (13.8033 K), and a temperature between 3.0 and 5.0 K. This last temperature is determined using a ^{3}He or a ^{4}He vapor pressure thermometer as specified in Sect. A.3.1.

Contrarily to the vapor-pressure thermometer, the gas thermometer is used as an interpolating instrument (ICVGT) between fixed points. Three of them are defined. There are two definitions for the ICVGT. In the first (Sect. A.3.2.1), only the use of ^{4}He is allowed in a range above 4.2 K and with a single Eq. (A.4). In the second (Sect. A.3.2.2), both helium isotopes can be used in the full range above 3 K and two equations are needed: one, Eq. (A.6), with defined coefficients, is specific for each isotope and takes into account the gas non-ideality, the other, Eq. (A.5), similarly to Eq. (A.4), has a quadratic form whose coefficients must be determined by measurements at the fixed points.

A.3.2.1 From 4.2 K to the Triple Point of Neon (24.5561 K) with ^{4}He as the Thermometric Gas

In this range, T_{90} is defined by the relation

$$T_{90} = a + bp + cp^2 \tag{A.4}$$

where p is the pressure in the gas thermometer and a, b, and c are coefficients the numerical values of which are obtained from measurements made at the three defining fixed points given in Sect. A.3.2, but with the further restriction that the lowest one of these points lies between 4.2 and 5.0 K.

A.3.2.2 From 3.0 K to the Triple Point of Neon (24.5561 K) with ^{3}He or ^{4}He as the Thermometric Gas

For a ^{3}He gas thermometer, and for a ^{4}He gas thermometer used below 4.2 K, the non-ideality of the gas must be accounted for explicitly, using the appropriate second virial coefficient $B_3(T_{90})$ or $B_4(T_{90})$. In this range, T_{90} is defined by the relation

$$T_{90} = \frac{a + bp + cp^2}{1 + B_x(T_{90})n/V} \tag{A.5}$$

where p is the pressure in the gas thermometer, a, b, and c are coefficients the numerical values of which are obtained from measurements at three defining temperatures as given in Sect. A.3.2 n/V is the gas density with n being the amount of gas and V the volume of the bulb, x is 3 or 4 according to the isotope used, and the values of the second virial coefficients are given by the relations.

For ^{3}He

$$B_3(T_{90})/\mathrm{m}^3\ \mathrm{mol}^{-1} =$$
$$\left\{16.69 - 336.98(T_{90}/\mathrm{K})^{-1} + 91.04(T_{90}/\mathrm{K})^{-2} - 13.82(T_{90}/\mathrm{K})^{-3}\right\} \times 10^{-6} \tag{A.6a}$$

For ^{4}He

$$B_4(T_{90})/\mathrm{m}^3\ \mathrm{mol}^{-1} = \{16.708 - 374.05(T_{90}/\mathrm{K})^{-1} - 383.53(T_{90}/\mathrm{K})^{-2} + 1799.2(T_{90}/\mathrm{K})^{-3} - 4033.2(T_{90}/\mathrm{K})^{-4} + 3252.8(T_{90}/\mathrm{K})^{-5}\} \times 10^{-6} \quad \text{(A.6b)}$$

Gas molar density (n/V) is obtained with sufficient accuracy from the pressure value measured at the upper fixed point, assuming an ideal gas $(n/V)/\mathrm{mol\ m}^{-3} = \dfrac{p(24.5561)/\mathrm{Pa}}{24.5561\ R}$

The accuracy with which T_{90} can be realized using Eqs. (A.4) and (A.5) depends on the design of the gas thermometer and the gas density used. Design criteria and current good practice required to achieve a selected accuracy are given in "*Supplementary Information for the ITS-90*".

A.3.3 The Triple Point of Equilibrium Hydrogen (13.8033 K) to the Freezing Point of Silver (961.78 °C): Platinum Resistance Thermometer

In this range, T_{90} is defined by means of a platinum resistance thermometer calibrated at specified sets of defining fixed points, and using specified reference and deviation functions for interpolation at intervening temperatures.

Below 0 °C, there are several differences with respect to the IPTS-68 definition that will be noted in the following.

No single platinum resistance thermometer can provide high accuracy, or is even likely to be usable, over the entire range 13.8033 K–961.78 °C. The choice of temperature range, or ranges, from among those listed below for which a particular thermometer can be used is normally limited by its construction.

For practical details and current good practice, in particular concerning types of thermometer available, their acceptable operating ranges, probable accuracies, permissible leakage resistance, resistance values, and thermal treatment, see "*Supplementary Information for the ITS-90*". It is particularly important to take account of the appropriate heat treatments that should be followed each time a platinum resistance thermometer is subjected to a temperature above about 420 °C.

Temperatures are determined in terms of the ratio of the resistance $R(T_{90})$ at a temperature T_{90} and the resistance R(273.16 K) at the triple point of water. This ratio, $W(T_{90})$, is[3]

[3] Note that this definition of $W(T90)$ differs from the corresponding definition used in the ITS-27, ITS-48, IPTS-48, and IPTS-68: for all of these earlier scales $W(T)$ was defined in terms of a reference temperature of 0 °C, which since 1954 has itself been defined as 273.15 K.

$$W(T_{90}) = R(T_{90})/R(273.16\ \mathrm{K}) \tag{A.7}$$

Warning: This definition is different from that of the IPTS-68, where $R(273.15\ \mathrm{K})$ was used. A mistake produces a sizeable error!

An acceptable platinum resistance thermometer must be made from pure, strain-free platinum, and it must satisfy at least one of the following two relations

$$W(29.7646\ ^\circ\mathrm{C}) \geq 1.118\ 07 \tag{A.8a}$$

$$W(-38.8344\ ^\circ\mathrm{C}) \leq 0.844\ 235 \tag{A.8b}$$

These criteria are different from that used in the IPTS-68, where $R(100\ ^\circ\mathrm{C})/R(0\ ^\circ\mathrm{C})$ was used. This is due to the fact that the boiling point of water is no more a definition point of the scale (its numerical value is also different: $T_{90}(H_2O) = 99.974\ ^\circ\mathrm{C}$).

An acceptable platinum resistance thermometer that is to be used up to the freezing point of silver must also satisfy the relation

$$W(961.78\ ^\circ C) \geq 4.2844 \tag{A.8c}$$

In each of the resistance thermometer ranges, T_{90} is obtained from $W_r(T_{90})$ as given by the appropriate reference function (Eq. (A.9b) or Eq. (A.10b)), and the deviation $W(T_{90}) - W_r(T_{90})$. At the defining fixed points, this deviation is obtained directly from the calibration of the thermometer: at intermediate temperatures it is obtained by means of the appropriate deviation function (Eqs. (A.12), (A.13), and (A.14)).

The structure of the ITS-90 definition in this range is the same of that of the IPTS-68: a reference function W_r (with respect to 273.16 K in the ITS-90!) and deviation functions. However, both functions are different, and deviation functions are differently used, as shown in the following. In addition, both $T_{90}(W_r)$ and $W_r(T_{90})$ are defined.

i. For the range 13.8033–273.16 K, the following reference function is defined

$$\ln[W_r(T_{90})] = A_0 + \sum_{i=1}^{12} A_i \left[\frac{\ln(T_{90}/273.16\ \mathrm{K}) + 1.5}{1.5} \right]^i \tag{A.9a}$$

An inverse function, equivalent to Eq. (A.9a) within ±0.1 mK, is

$$T_{90}/273.16\ \mathrm{K} = B_0 + \sum_{i=1}^{15} B_i \left[\frac{W_r(T_{90})^{1/6} - 0.65}{0.35} \right]^i \tag{A.9b}$$

The values of the constants A_0, B_0, A_i and B_i are given in Table A.4.

A thermometer may be calibrated for use throughout this range or, using progressively fewer calibration points, for ranges with low temperature limits of 24.5561, 54.3584, and 83.8058 K, all having an upper limit of 273.16 K.

ii. *For the range 0 °C to 961.78 °C, the following reference function is defined: [. . . text omitted]*

iii. A thermometer may be calibrated for use in the range 234.3156 K (−38.8344 °C) to 29.7646 °C, the calibration being made at these temperatures and at the triple point of water. Both reference functions (Eqs. (A.9a, b) and Eqs. (A.10a, b) omitted) are required to cover this range.

The defining fixed points and deviation functions for the various ranges are given below, and in summary form in Table A.5.

The ITS-90, as the IPTS-68, defines *subranges*, however differently. In fact in the ITS-90 they always extend from the *same* upper limit (273.16 K) down to a decreasing limit (i.e., the subranges are set "in parallel", not "in series" as in the IPTS-68). In addition there is a narrow subrange *crossing* 0 °C.

A.3.3.1 The Triple Point of Equilibrium Hydrogen (13.8033 K) to the Triple Point of Water (273.16 K)

The thermometer is calibrated at the triple points of equilibrium hydrogen (13.8033 K), neon (24.5561 K), oxygen (54.3584 K), argon (83.8058 K), mercury (234.3156 K), and water (273.16 K), and at two additional temperatures close to 17.0 K and 20.3 K. These last two may be determined either: by using a gas thermometer as described in Sect. A.3.2, in which case the two temperatures must lie within the ranges 16.9 K–17.1 K and 20.2–20.4 K respectively; or by using the vapor pressure-temperature relation of equilibrium hydrogen, in which case the two temperatures must lie within the ranges 17.025–17.045 K and 20.26–20.28 K respectively, with the precise values being determined from Eqs. (A.11a) and (A.11b) respectively

$$T_{90}/\mathrm{K} - 17.035 = (p/\mathrm{kPa} - 33.3213)/13.32 \tag{A.11a}$$

$$T_{90}/\mathrm{K} - 20.27 = (p/\mathrm{kPa} - 101.292)/30 \tag{A.11b}$$

The deviation function is[4]

$$W(T_{90}) - W_{\mathrm{r}}(T_{90}) = a[W(T_{90}) - 1] + b[W(T_{90}) - 1]^2 + \sum_{i=1}^{5} c_i [\ln W(T_{90})]^{i+n} \tag{A.12}$$

[4] This deviation function [and also those of Eqs. (A.13) and (A.14)] may be expressed in terms of W_{r}, rather than W; for this procedure see "*Supplementary Information for ITS-90*" (BIPM 1990).

with values for the coefficients *a, b,* and c_i being obtained from measurements at the defining fixed points and with $n = 2$.

For this range and for the subranges "The Triple Point of Neon (24.5561 K) to the Triple Point of Water (273.16 K)", "The Triple Point of Oxygen (54.3584 K) to the Triple Point of Water (273.16 K)", "The Triple Point of Argon (83.8058 K) to the Triple Point of Water (273.16 K)", the required values of $W_r(T_{90})$ are obtained from Eq. (A.9a) or from Table A.1.

There are changes with respect to the fixed points used in the IPTS-68 definition. The triple points of neon and argon are substituted for the normal boiling points of neon and oxygen. The triple point of mercury is substituted for the normal boiling point of water, thus eliminating the need to heat the thermometers above room temperature during calibration. Only in the full range, which extends below the triple point of neon (and overlaps the range of gas thermometry), there is a need for pressure measurements. These points can be realized by means of two *e*-H_2 vapor-pressure points: for both of them, selection of any accurate temperature value in a small interval is allowed, instead of the fixed value required by the IPTS-68. Alternatively, these points can be obtained from the ICVGT used for the realization of the 3–25 K range. All other subranges require the use of triple points only. The same deviation function is defined for the range and most of the subranges, simply omitting some terms according to the number of the fixed points required.

A.3.3.1.1 The Triple Point of Neon (24.5561 K) to the Triple Point of Water (273.16 K)

The thermometer is calibrated at the triple points of equilibrium hydrogen (13.8033 K), neon (24.5561 K), oxygen (54.3584 K), argon (83.8058 K), mercury (234.3156 K), and water (273.16 K).

The deviation function is given by Eq. (A.12) with values for the coefficients *a*, *b*, c_1, c_2, and c_3 being obtained from measurements at the defining fixed points and with $c_4 = c_5 = n = 0$.

A.1.3.3.1.2 The Triple Point of Oxygen (54.3584 K) to the Triple Point of Water (273.16 K)

The thermometer is calibrated at the triple points of oxygen (54.3584 K), argon (83.8058 K), mercury (234.3156 K), and water (273.16 K).

The deviation function is given by Eq. (A.12) with values for the coefficients *a*, *b*, and c_1 being obtained from measurements at the defining fixed points, with $c_2 = c_3 = c_4 = c_5 = 0$ and with $n = 1$.

A.1.3.3.1.3 The Triple Point of Argon (83.8058 K) to the Triple Point of Water (273.16 K)

The thermometer is calibrated at the triple points of argon (83.8058 K), mercury (234.3156 K), and water (273.16 K).

Table A.1 Defining fixed points of the ITS-90*

Number	Temperature		Substance[a]	State[b]	$W_r(T_{90})$
	T_{90}/K	t_{90}/°C			
1	3–5	−270.15 to −268.15	He	V	
2	13.8033	−259.3467	*e*-H_2	T	0.00119007
3	≈17	≈−256.15	*e*-H_2 (or He)	V (or G)	
4	≈20.3	≈−252.85	*e*-H_2 (or He)	V (or G)	
5	24.5561	−248.5939	Ne	T	0.00844974
6	54.3584	−218.7916	O_2	T	0.09171804
7	83.8058	−189.3442	Ar	T	0.2158597
8	234.3156	−38.8344	Hg	T	0.84414211
9	273.16	0.01	H_2O	T	1.00000000
10	*302.9146*	*29.7646*	*Ga*	*M*	*1.11813889*
11	*429.7485*	*156.5985*	*In*	*F*	*1.60980185*
12	*505.078*	*231.928*	*Sn*	*F*	*1.89279768*
13	*692.677*	*419.527*	*Zn*	*F*	*2.56891730*
14	*933.473*	*660.323*	*Al*	*F*	*3.37600860*
15	*1234.93*	*961.78*	*Ag*	*F*	*4.28642053*
16	*1337.33*	*1064.18*	*Au*		
17	*1357.77*	*1084.62*	*Cu*		

[a]All substances except ^{3}He are of natural isotopic composition. e-H_2 is hydrogen at the equilibrium concentration of the *ortho* and *para* molecular forms

[b]For complete definitions and advice on the realization of these various states, see "*Supplementary Information for the ITS-90*". The symbols have the following meanings: *V* vapor pressure point, *T* triple point (temperature at which the solid, liquid, and vapor phases are in equilibrium), *G* gas thermometer point, *M*, *F* melting point, freezing point (temperature, at a pressure of 101 325 Pa, at which the solid and liquid phases are in equilibrium)

Note: Entries in italics are beyond the scope of this book

The deviation function is

$$W(T_{90}) - W_r(T_{90}) = a[W(T_{90}) - 1] + b[W(T_{90}) - 1] \ln W(T_{90}) \qquad \text{(A1.13)}$$

with the numerical values of a and b being obtained from measurements at the defining fixed points.

In this subrange, the deviation function is defined in a different way, being only three of the fixed points involved.

A.3.3.2 From 0 °C to the Freezing Point of Silver (961.78 °C) (... text omitted)

Table A.2 Effect of pressure on the temperature of some defining fixed points

Substance	T_{tp} (K)	$dT_{tp}/dp/10^8$ K Pa^{-1}[a]	$dT_{tp}/dh_L/$ mK m^{-1}[b]
Hydrogen[c]	*13.8033*	34	0.25
Deuterium[c]	18.690	26	0.34
Neon	*24.5561*	16	1.9
Oxygen	*54.3584*	12	1.5
Nitrogen	63.151	24	1.7
Argon	*83.8058*	25	3.3
Methane	90.6935	26	0.9
Krypton	115.776	32	6.8
Xenon	161.406	39	10.4
Carbon dioxide	216.591	11	1.3
Mercury	*234.3156*	5.4	7.1
Water	*273.16*	−7.5	−0.73

Italic denotes the defining ITS-90 value
[a]Equivalent to mK bar^{-1}
[b]h_L = depth of condensed phases
[c]In spin equilibrium

Table A.3 Values of the constants for the helium vapor pressure Eqs. (A.3a, b), and the temperature range for which each equation, identified by its set of constants, is valid

	^{3}He 0.65–3.2 K	^{4}He 1.25–2.1768 K	^{4}He 2.1768–5.0 K
A_0	1.053447	1.392408	3.146631
A_1	0.980106	0.527153	1.357655
A_2	0.676380	0.166756	0.413923
A_3	0.372692	0.050988	0.091159
A_4	0.151656	0.026514	0.016349
A_5	−0.002263	0.001975	0.001826
A_6	0.006596	−0.017976	−0.004325
A_7	0.088966	0.005409	−0.004973
A_8	−0.004770	0.013259	0
A_9	−0.054943	0	0
B	7.3	5.6	10.3
C	4.3	2.9	1.9

Table A.4 The constants A_0, A_i; B_0, B_i in the reference functions of Eqs. (A.9a) and (A.9b), respectively

A_0	−2.135.347.29	B_0	−0.183.324.722	B_{13}	−0.091.173.542
A_1	3.183.247.20	B_1	0.240.975.303	B_{14}	0.001.317.696
A_2	−1.801.435.97	B_2	0.209.108.771	B_{15}	0.026.025.526
A_3	0.717.272.04	B_3	0.190.439.972		
A_4	0.503.440.27	B_4	0.142.648.498		
A_5	−0.618.993.95	B_5	0.077.993.465		
A_6	−0.053.323.22	B_6	0.012.475.611		
A_7	0.280.213.62	B_7	−0.032.267.127		
A_8	0.107.152.24	B_8	−0.075.291.522		
A_9	−0.293.028.65	B_9	−0.056.470.670		
A_{10}	0.044.598.72	B_{10}	0.076.201.285		
A_{11}	0.118.686.32	B_{11}	0.123.893.204		
A_{12}	−0.052.481.34	B_{12}	−0.029.201.193		

Table A.5 Deviation functions and calibration points for platinum resistance thermometers in the various ranges in which they define T_{90}

Section	Lower temperature limit T/K	Deviation function	Calibration points (see Table A.1)
(a) Ranges with an upper limit of 273.16 K			
A.3.3.1	13.8033	$a[W(T_{90})-1]+b[W(T_90)-1]^2 + \sum_{i=1}^{5} c_i[W(T_{90})]^{i+n}$, $n=2$	2–9
A.3.3.1.1	24.5561	As for A.3.3.1 with $c_4=c_5=n=0$	2, 5–9
A.3.3.1.2	54.3584	As for A.3.3.1 with $c_2=c_3=c_4=c_5=0, n=1$	6–9
A.3.3.1.3	83.8058	$a\,[W(T_{90})-1]+b[W(T_{90})-1]\ \ln W(T_{90})$	7–9
Section	Upper temperature limit t/°C	Deviation function	Calibration points (see Table A.1)
(b) Ranges with a lower limit of 0 °C			
A.3.3.2[a]	*961.78*	$a[W(T_{90})-1]+b[W(T_{90})-1]^2+ c[W(T_{90})-1]^3 + d[W(T_{90}) - W(660.323\,°C)]^2$	*9, 11–15*
A.3.3.2.1	*660.323*	*As for A.3.3.2 with $d=0$*	*9, 12–14*
A.3.3.2.2	*419.527*	*As for A.3.3.2 with $c=d=0$*	*9, 12, 13*
A.3.3.2.3	*231.928*	*As for A.3.3.2 with $c=d=0$*	*9, 11, 12*
A.3.3.2.4	*156.5985*	*As for A.3.3.2 with $b=c=d=0$*	*9, 11*
A.3.3.2.5	*29.7646*	*As for A.3.3.2 with $b=c=d=0$*	*9, 10*
(c) Range from 234.3156 K (−38.8344 °C) to 29.7646 °C			
A.3.3.3		As for A.3.3.2 with $c=d=0$	8–10

[a]Calibration points 9, 12–14 are used with $d=0$ for $t_{90} < 660.323$ °C; the values of a, b, and c thus obtained are retained for $t_{90} > 660.323$ °C with d being determined from calibration point 15

Table A.6 Differences between ITS-90 and EPT-76, and between ITS-90 and IPTS-68 for specified values of T_{90} below 273.16 K (and derivatives of these differences)

$dT = (T_{90} - T_{76})$mK $d\delta T/dT \times 10^{-3}$ T_{90}/K	0	1	2	3	4	5	6	7	8	9
0						−0.1	−0.2	−0.3	−0.4	−0.5
						−0.1	*−0.1*	*−0.1*	*−0.1*	*−0.1*
10	−0.6	−0.7	−0.8	−1.0	−1.1	−1.3	−1.4	−1.6	−1.8	−2.0
	−0.1	*−0.1*	*−0.13*	*−0.13*	*−0.13*	*−0.13*	*−0.13*	*−0.20*	*−0.20*	*−0.20*
20	−2.2	−2.5	−2.7	−3.0	−3.2	−3.5	−3.8	−4.1		
	−0.24	*−0.24*	*−0.24*	*−0.24*	*−0.24*	*−0.30*	*−0.30*	*−0.30*		

$dT = (T_{90} - T_{68})$/K $d\delta T/dT \times 10^{-3}$ T_{90}/K	0	1	2	3	4	5	6	7	8	9
10					−0.006	−0.003	−0.004	−0.006	−0.008	−0.009
					5.0	*0.0*	*−0.13*	*−0.20*	*−0.13*	*0.0*
20	−0.009	−0.008	−0.007	−0.007	−0.006	−0.005	−0.004	−0.004	−0.005	−0.006
	0.0	*0.10*	*0.0*	*0.0*	*0.10*	*0.10*	*0.0*	*0.0*	*−0.10*	*0.0*
30	−0.006	−0.007	−0.008	−0.008	−0.008	−0.007	−0.007	−0.007	−0.006	−0.006
	0.0	*−0.10*	*0.0*	*0.0*	*0.0*	*0.0*	*0.0*	*0.0*	*0.0*	*0.0*
40	−0.006	−0.006	−0.006	−0.006	−0.006	−0.007	−0.007	−0.007	−0.006	−0.006
	0.0	*0.0*	*0.0*	*0.0*	*0.0*	*0.0*	*0.0*	*0.0*	*0.0*	*0.0*
50	−0.006	−0.005	−0.005	−0.004	−0.003	−0.002	−0.001	0.000	0.001	0.002
	0.0	*0.0*	*0.0*	*0.10*	*0.10*	*0.10*	*0.10*	*0.10*	*0.10*	*0.10*
60	0.003	0.003	0.004	0.004	0.005	0.005	0.006	0.006	0.007	0.007
	0.0	*0.0*	*0.0*	*0.0*	*0.0*	*0.0*	*0.0*	*0.0*	*0.0*	*0.0*
70	0.007	0.007	0.007	0.007	0.007	0.008	0.008	0.008	0.008	0.008
	0.0	*0.0*	*0.0*	*0.0*	*0.0*	*0.0*	*0.0*	*0.0*	*0.0*	*0.0*
80	0.008	0.008	0.008	0.008	0.008	0.008	0.008	0.008	0.008	0.008
	0.0	*0.0*	*0.0*	*0.0*	*0.0*	*0.0*	*0.0*	*0.0*	*0.0*	*0.0*
90	0.008	0.008	0.008	0.008	0.008	0.008	0.008	0.009	0.009	0.009
	0.0	*0.0*	*0.0*	*0.0*	*0.0*	*0.0*	*0.0*	*0.0*	*0.0*	*0.0*
T_{90}/K	0	10	20	30	40	50	60	70	80	90
100	0.009	0.011	0.013	0.014	0.014	0.014	0.014	0.013	0.012	0.012
	0.0	*0.20*	*0.13*	*0.0*	*0.0*	*0.0*	*0.0*	*−0.10*	*0.0*	*0.0*
200	0.011	0.010	0.009	0.008	0.007	0.005	0.003	0.001	*273.16*	0.0
	−0.10	*−0.10*	*−0.10*	*−0.10*	*−0.13*	*−0.20*	*−0.22*	*−0.21*		*−0.19*

Notes to Table A.6

1. Equations giving the differences $T_{90} - T_{68}$ shown in Table A.6. The polynomial representations of the differences between 13.8 K and 1064.18 °C are due to R. L. Rusby (1990).[5] From 13.8 and 83.8 K (accuracy ±1 mK)

$$(T_{90} - T_{68})/\text{K} = a_0 + \sum_{i=1}^{12} a_i((T_{90} - 40\ \text{K})/40\ \text{K})^i$$

[5] The two functions show a discontinuity of the value of 0.6 mK and of the first derivative at their joining point 83.8053 K. This discontinuity, inconvenient when calculating scale conversion of thermophysical or thermodynamic data, is better removed if the joining point is moved to ≈63 K (Pavese 1993).

From 83.8 K to +630.6 °C (accuracy approximately ±1.5 mK below 0 °C *and* ±*1 mK above* 0 °C)

$$(t_{90} - t_{68})/°\mathrm{C} = \sum_{i=1}^{8} b_i((t_{90}/630\ °\mathrm{C})^i)$$

The coefficients a_i and b_i of the equations are

i	a_i	b_i
0	−0.005 903	0
1	0.008 174	−0.148 759
2	−0.061 924	−0.267 408
3	−0.193 388	1.080 760
4	1.490 793	1.269 056
5	1.252 347	−4.089 591
6	−9.835 868	−1.871 251
7	1.411 912	7.438 081
8	25.277 595	−3.536 296
9	−19.183 815	0
10	−18.437 089	0
11	27.000 895	0
12	−8.716 324	0

(after BIPM 1990)

2. Conversion of thermodynamic quantities (Douglas 1969):
   Enthalpy: $dH = -(T_{90} - T_{68})c_p$
   Specific heat capacity: $\mathrm{d}c_p = -(T_{90} - T_{68})\ \mathrm{d}c_\mathrm{p}/\mathrm{d}T - c_p\ \mathrm{d}(T_{90} - T_{68})/\mathrm{d}T$
   Entropy:

$$\mathrm{d}S = -\int_0^T ((T_{90} - T_{68})\mathrm{d}c_p/\mathrm{d}T^2)\mathrm{d}T - (T_{90} - T_{68})c_p/T$$

   (after Goldberg and Weir (1991))
3. Conversion of T_{90} to thermodynamic temperature T: see discussion and equations for $T - T_{90}$ in Sect. 1.2.5. (Pavese et al. 2011)
4. Conversion between older temperature scales and ITS-90. In general, for a quantity $X(T)$ the conversion from a scale $T_X - T_{90}$ is

$$X(T_{90}) = X(T_{9\mathrm{X}})\mathrm{d}X/\mathrm{d}T(T_{90} - T_X)$$

   a. Scale different from the ITS-90 in the value of the reference temperature T_0^*

$$T_{90} = T^*(273.16/T_0^*)$$

b. Scale with the value of a fixed point T_1^* different from $T_{90,1}$ with $p_{90,1} = p_1^*$ or $p_{90,1} \neq p_1^*$, with $T_{90,1} = T_1^*$. In a vapor pressure equation in the range $(T_1^*,\ T_{\max},)$ or $(T_{\max},\ T_1^*)$ is

$$p \approx A_{90} + f^*(T_{90})$$

where the coefficient $A_{90} = A_1^* + \delta A$ with δA such as $p(T_{90,1}) = p_{90,1}$

c. Scale different from the ITS-90 in the value of the reference temperature T_0^* and of a second fixed point T_1^*. Assuming a linear correction between the two points is

$$T_{90} = (T^* - T_1^*)(273.16 - T_{90,1})/(T_0^* - T_1^*) + T_{90,1}$$

d. Scale IPTS-48

T_{90} (K)	t_{90} (°C)	$\delta T = T_{90} - T_{48}$ (mK)	$\mathrm{d}\delta T$ (dT)
93.15	−180	20	0.0
103.15	−170	17	−0.5
113.15	−160	7	−0.8
123.15	−150	0	0.0
133.15	−140	1	0.2
143.15	−130	8	0.8
153.15	−120	17	−0.9
163.15	−110	26	−0.9
173.15	−100	35	−0.7
183.15	−90	41	−0.5
193.15	−80	45	0.0
203.15	−70	45	−0.0
213.15	−60	42	−0.3
223.15	−50	38	−0.5
233.15	−40	32	−0.7
243.15	−30	24	−0.8
253.15	−20	16	−0.8
263.15	−10	8	−0.8
273.15	0	0	−0.7

e. Scale EPT-76

$$T_{90} - T_{76} = -5.6 \times 10^{-6}\ (T_{76})^2$$

(after BIPM 1990b).

Appendix B
List of Temperature and Pressure Fixed Points (Table B.1, B.2, and B.3)

Table B.1 Best-quality temperature and pressure fixed points (ITS-90 fixed points in italics)

Equilibrium state[a]	T_{90}/K (p/Pa)[b]	Uncertainty δT (mK) (δp/Pa)[c]	Purity of material (%)[d]	References[g]
Triple point of equilibrium hydrogen	*13.8033*	*0.3 (0.5)*[f]	*99.999*	*Ancsin 1977; Pavese and Ferri 1982; Kemp and Kemp 1979b; Hoge and Arnold 1951*
Triple point of equilibrium deuterium	18.6889	0.3	99.99	Pavese and McConville 1987; McConville and Pavese 1988; Ancsin 1988; Kemp 1982; Pavese and Barbero 1979; Schwalbe and Grilly 1984; Khnykov et al. 1978
Triple point of normal deuterium	18.7236	0.3	99.99	Pavese and McConville 1987; McConville and Pavese 1988; Ancsin 1988; Kemp 1982; Pavese and Barbero 1979; Schwalbe and Grilly 1984; Khnykov et al. 1978
Triple point of neon isotope ^{20}Ne	24.5422	0.05	99.99	Pavese et al. 2011b
Triple point of natural neon[e]	*24.5561*	*0.4 (0.2)*[f]	*99.99*	*Pavese et al. 2010b*
		(0.5)[f]		
Triple point of neon isotope ^{22}Ne	24.6888	0.05	99.9	Pavese et al. 2011b
Triple point of oxygen	*54.3584*	*0.2 (1)*[f]	*99.995*[h]	*Kemp et al. 1976; Pavese 1978b; Ancsin 1974b; Compton and Ward 1976*
	(146.25)	(0.1)		Pavese 1981
Triple point of nitrogen	63.1507	0.7 (0.1)[f]	99.999	Pavese 1981; Pavese and Ferri 1982; Ancsin 1974a
Boiling point of nitrogen	77.352	2	99.999	Ancsin 1974a
Triple point of argon	*83.8058*	*0.3 (0.15)*[f]	*99.9999*	*Kemp and Kemp 1978; Seifert 1983; Ancsin 1974a; Tiggelman and Durieux 1972; Ancsin 1973b; Furukawa et al. 1972; Furukawa 1982; Kemp et al. 1976; Khnykov et al. 1978; Blanke and Thomas 1981; Pavese 1978b*
	(68 890)	*(1.5)*[f] (1)		Pavese 1981; Bonhoure and Pello 1983
Boiling point of argon	87.3032	0.3	99.999	Pavese 1981; Ancsin 1973b; Kemp et al. 1976
Triple point of methane	90.6943	0.3[f] (0.3)	99.995	Khnykov et al. 1978; Pavese et al. 1975b; Pavese 1979; Bonhoure and Pello 1978, 1980
	(11 696)	(0.7)		Pavese 1981
Triple point of xenon[k]	161.406	2	99.995	Inaba and Mitsui 1978; Kemp et al. 1982; Ancsin 1988b; Khnykov 1989b; Head et al. 1989; Hill and Steele 2004, 2005
Triple point of carbon dioxide	216.592 (517.980)	1 (50)	99.99	Pavese and Ferri 1982; Ambrose 1957; Bonnier et al. 1984; Head et al. 1990

F. Pavese, G. Molinar Min Beciet, *Modern Gas-Based Temperature and Pressure Measurements,* International Cryogenics Monograph Series,
DOI 10.1007/978-1-4419-8282-7, © Springer Science+Business Media New York 2013

Table B.1 (continued)

Equilibrium state[a]	T_{90}/K (p/(Pa))[b]	Uncertainty δT (mK) (δp(Pa))[c]	Purity of material (%)[d]	References[g]
Triple point of mercury	*234.3083*	*0.5 (1.5)*[f]	*99.9999*	*Furukawa and Bigge 1976 (Furukawa et al. 1982)*
Freezing point of water	273.1500	0.5		
Boiling point of carbon dioxide at t.p. H_2O	273.16			
	(3.38608 MPa)	(170)	99.999	Bignell and Bean 1988
Useful low-melting metals				
Triple point of gallium[i]	*302.9146*	*0.2 (1)*[f]	*99.99999*	(See Bedford et al. 1996; Ambrose and Crovini 1987)
Triple point of gallium[i,j]	302.9166	0.1	99.99999	
Triple point of indium[j]	429.7436	0.2	99.9999	
Freezing point of indium[j]	*429.7485*	*0.2 (3)*[f]	*99.9999*	
Freezing point of tin[j]	*505.078*	*0.2 (5)*[f]	*99.9999*	
Freezing point of bismuth[j]	544.552	1	99.9999	
Freezing point of cadmium[j]	594.219	1	99.9999	
Freezing point of lead[j]	600.612	1	99.9999	

[a]The equilibrium states in this table are for a pressure $p_{\text{ref}} = 101\,325$ Pa (one standard atmosphere), except for the triple points. The defining points of the ITS-90 are shown in italics. For these points, the references are simply a representative subset of the available literature—see Sect. 2 are related references for more recent information

[b]All temperature values are given in ITS-90, and are mostly taken from Bedford et al. (1996), directly from the scale definition for the defining fixed points, and by applying the differences in Table A.6 to the IPTS-68 values for the others, whose accuracy becomes, consequently, limited in general to three decimal figures

[c]The indicated uncertainty is, where possible, the standard deviation of the consensus values—see Bedford et al. (1984, 1996) for details in the uncertainty evaluation. Otherwise, uncertainties are best estimates based upon the information available in the references and upon the agreement between results of comparable experiments. For the points that are not defining points of the ITS-90 below 273 K and are relatively distant from a defining fixed point, the largest contributor to the uncertainty is non-uniqueness of the IPTS-68 (note, *not* of the ITS-90), which has not been suppressed by the temperature recalculation used here (see above, note b). Only direct re-determinations in ITS-90 will allow reducing this uncertainty

[d]The minimum purity of the material to which the listed values of temperature and uncertainty apply is given in percent by volume when the material is liquid or gaseous at 0 °C and 101 325 Pa, and in percent by weight when the material is solid at 0 °C and 101 325 Pa (except for mercury)

[e]These values are for neon with an isotopic composition close to that specified in BIPM (1990)

[f]The inherent accuracy of several triple points is better than indicated. One of the chief contributors to the tabular uncertainties is the nonuniqueness of the IPTS-68 (see above, note c). In the inter-comparison of cryogenic triple-point cells (Pavese et al. 1984), where it was possible to exclude the non-uniqueness component, nor the effect of isotopic composition variability in H_2 and Ne was taken into account. It was found that a group of each of hydrogen, neon, nitrogen, argon and methane triple-point realizations of various manufactures agreed to within ±0.3 mK, ±0.20 mK, ± 0.15 mK, ± 015 mK and ± 0.3 mK, respectively. This reproducibility value, when better, is reported in *round brackets*. In *square brackets* is the estimated thermodynamic standard uncertainty (BIPM 1990) of the ITS-90 defining points. For methane, the T_{90} value was obtained from $T_{68,\text{Ar}}$ the IPTS-68 definition using argon triple point, since it was found that $[T_{68,\text{Ar}}(CH_4) - T_{68,O_2}(CH_4)] = 0.7 \pm 0.7$ mK (Pavese et al. 1984)

[g]Parenthetic reference provides more information but appears to relate to the same experiment as described in the non-parenthetic reference

[h]For possible problems with oxygen purity, see Appendix C

[i]Measured temperatures were based upon samples ranging from 99.9995 to 99.99999 % in purity and were adjusted to the equivalent of purity 99.99999 %

[j]The effect of pressure on these freezing points is the following (see Table 2.7 for the same effect on substances below 273.16 K):

Substance	[a]dT/dp (10^8 K Pa^{-1})[b]	dT/dh_L (10^8 mK m^{-1})
Gallium	*−2.0*	*−1.2*
Indium	*4.9*	*3.3*
Tin	*3.3*	*2.2*
Bismuth	−3.5	−3.4
Cadmium	6.2	4.8
Lead	8.0	8.2

Italics denotes defining ITS-90 fixed points

[a]Equivalent to (mK bar^{-1})

[b]h_L depth of condensed phases

[k]Its reproducibility is limited by isotope composition and distillation effects

Table B.2 Second-quality temperature fixed points

Equilibrium state[a]	T^{90}/K[b]	Uncertainty (mK)[c]	Purity of material (%)[d]	References[i]
Triple point of normal hydrogen	13.952	2	99.99	Ancsin 1977
Boiling point of normal hydrogen	20.388	2	99.99	Ancsin 1977
$\alpha-\beta$ transition point of solid oxygen	23.868	5	99.999	Pavese and Ferri 1982; Ancsin 1975; Kemp and Pickup 1972; Orlova 1962; Muijlwijk et al. 1969
Boiling point of natural neon[e]	27.098	2	99.99	Ancsin 1978
$\alpha-\beta$ transition point of solid nitrogen	35.614	6	99.999	Kemp and Kemp 1979a
$\beta-\gamma$ transition point of solid oxygen	43.796	1	99.999	Pavese and Ferri 1982; Ancsin 1975; Kemp and Pickup 1972; Orlova 1962; Muijlwijk et al. 1969; Cowan et al. 1976
Boiling point of oxygen	90.196	1	99.995	Ancsin 1974b; Compton and Ward 1976
Triple point of krypton	115.775	1	99.995	Seifert 1983; Inaba and Mitsui 1978
Sublimation point of carbon dioxide	194.686	3	99.99	Barber 1966
Low-melting non-gaseous substances				
Triple point of bromobenzene[f]	242.424	10	99.998	(see Bedford et al. 1984; Ambrose and Crovini 1987)
Triple point of phenoxybenzene (diphenyl ether)	300.014[g]	1	99.9999	
Triple point of succinonitrile	331.215	2	99.9995	
Freezing point of sodium	370.944	5	99.99	
Triple point of benzoic acid	395.490	4	99.998	
Triple point of benzoic acid[h]	395.486	2	99.999	

[a]The equilibrium states in this table are for a pressure $p_{\text{ref}} = 101\,325$ Pa (one standard atmosphere), except for the triple points. The defining points of the ITS-90 are shown in italics. For these points, the references are simply a representative subset of the available literature—see Sect. 2 and related references for more recent information

[b]All temperature values are given in ITS-90, and are mostly taken from Bedford et al. (1996), directly from the scale definition for the defining fixed points, and by applying the differences in Table A.6 to the IPTS-68 values for the others, whose accuracy becomes, consequently, limited in general to three decimal figures

[c]The indicated uncertainty is, where possible, the standard deviation of the consensus values—see Bedford et al. (1984, 1996) for details in the uncertainty evaluation. Otherwise, uncertainties are best estimates based upon the information available in the references and upon the agreement between results of comparable experiments. For the points that are not defining points of the ITS-90 below 273 K and are relatively distant from a defining fixed point, the largest contributor to the uncertainty is non-uniqueness of the IPTS-68 (note, *not* of the ITS-90), which has not been suppressed by the temperature recalculation used here (see note[b]). Only direct re-determinations in ITS-90 will allow reducing this uncertainty

[d]The minimum purity of the material to which the listed values of temperature and uncertainty apply is given in percent by volume when the material is liquid or gaseous at 0 °C and 101 325 Pa, and in percent by weight when the material is solid at 0 °C and 101 325 Pa (except for mercury)

[e]These values are for neon with an isotopic composition close to that specified in BIPM (1990b)

[f]The published value has been lowered 2 mK to obtain the temperature corresponding to the liquidus point ($1/F = 1$)

[g]The listed temperature is estimated to be the triple-point temperature of the ideally pure substance. In practice it is difficult to achieve a purity higher than 99.999 %, for which the triple-point temperature is (300.018 ± 0.002) K

[h]Freezing point given is the value under one atmosphere of dry air. Different values are obtained under an atmosphere of nitrogen or oxygen

[i]Parenthetic reference provides more information but appears to relate to the same experiment as described in the non-parenthetic reference

Table B.3 Possible useful points deserving further studies[a]

Equilibrium state	T_{90}/K (p/kPa)	Aimed uncertainty δT (mK) (δp/Pa)	References
$\alpha-\beta$ transition point of solid methane	20.48	5	Pavese and Ferri 1982
Triple point of propane	85.528	1	Pavese and Besley 1981b; Goodwin 1977
Triple point of ethane	90.360	1	Pavese 1978a; Straty and Tsumura 1976; Ziegler et al. 1964b
Boiling point of methane	111.667	0.5	Pavese et al. 1975b; Pavese and Ferri 1982
Boiling point of krypton	119.81	2	Ziegler et al. 1964a; Lovejoy 1963
Boiling point of xenon	165.06	2	Ancsin 1988b
Triple point of sulfur exafluoride	222.35 (225.05)	([b])	Schumb 1947

[a]For a far more complete list of secondary fixed points useful in chemistry (with values in IPTS-68) see (Staveley et al. 1981)
[b]Unknown

Appendix C
Reference Data on Gases

In the first part of Appendix C, the sensitivity coefficient of the triple point temperature to chemical impurities are reported, together with the results of examples of correction of this effect using different methods illustrated in Sect. 2.2 and of the resulting increase of uncertainty.

In the second part, the data sheets of a number of gases are collected. Temperatures are given in ITS-90, except when differently noted in the vapor-pressure tables (for the reason, see Note b in Appendix D, Table D.2). When T_{68} or T_{48} have been used, the linear term of the original vapor-pressure equation (given in Appendix D) has been adjusted so as the equation matches the numerical value of T_{90} at the joining temperature (generally the t.p. or the n.b.p. temperature). The conversion of T_{68} or T_{48} to T_{90} can be found in Appendix A, and Note 3 to Table A.6. Vapor pressure equations in T_{90} can be found in Appendix D (Tables C.1.1, C.1.2).

F. Pavese, G. Molinar Min Beciet, *Modern Gas-Based Temperature and Pressure Measurements,* International Cryogenics Monograph Series,
DOI 10.1007/978-1-4419-8282-7, © Springer Science+Business Media New York 2013

Part C.1—Effect and Correction of Chemical Impurities

Table C.1.1 Effect on T_{tp} per amount of substance fraction of various gaseous chemical impurities on the indicated pure substances (in italics are the principal impurities)—see Sect. 2.2: initial liquidus-line slopes $s_L = dT_{liq}/dc_i$ (in parentheses the initial solidus line slopes s_S) and uncertainties $u(dT_{liq}/dc_i)$ in μK ppm^{-1}; distribution coefficients k_0 and their estimated uncertainties

Chemical impurity	*e*-Hydrogen		Neon		Oxygen		Argon	
	s_L (s_S)	k_0	s_L (s_S)	k_0	s_L (s_S)	k_0	s_L (s_S)	k_0
He	−11(2) (s_S n.a.)	0.21(14)	None		+1.5(0.5)[a] (s_S n.a.)	1.03(1)	n.a.	
H_2	–		−7 ± 3[c] (s_S n.a.)	0.53(20)	n.a.		None	
Ne	−2(0.5) (s_S n.a.)	0.86(4)	–		−1(0.5)[a] (s_S n.a.)	0.98(1)	None	
O_2	None[b]		n.a.		–		−22(3)[a] (−35)[5]	0.57(5)
N_2	None[b]		−6.6(0.5)[a,c] (−21)[d]	0.47(13)	−22(3)[a] (−35)[d]	0.60(4)	−22(3)[a] (−50)[d]	0.52(4)
Ar	n.a.		None		+12(3)[a] ($s_L = s_S$)	1.23(5)	–	
CO			None		n.a.		−24(4)[a] (−50)	0.50(5)
F_2					n.a.		−10(2) ('much larger')	0.80(4)
CH_4					< −30 (s_S n.a.)	0.45(18)	−25(5)[a] (−80)	0.42(5)
Kr					−5(1)[a] (−9)[d]	0.92(2)	+5(3)[a] ($s_L = s_S$)	1.11(5)
Xe					−8(2) (−30)[d]	0.85(4)	−6(2) (s_S n.a.)	0.88(4)

Notes: The entries in italics indicate the main chemical impurities
All s_L (s_S) are from Pavese (2009), except for N_2 in *Ne* that is from Pavese et al. (2012b). All k_0 are from White et al. (2009): for F_2 in *Ar* and *Xe* in O_2, the reported liquidus slopes and solidus slopes are not consistent with each other; for *Ar* in O_2 the value of k_0 is not consistent with experimental data
n.a. no data available
[a]Estimated only from thermal metrology studies
[b]Estimated from solubility data
[c]Both H_2 and N_2 impurities can easily removed today to much less than 10^{-6} amount of substance fraction with the use of a zirconium-getter based commercial filters
[d]s_S provided with no uncertainty estimate, to qualitatively evaluate from ($s_L - s_S$) the value of k_0

Table C.1.2 Simulations of the effect of correcting or not correcting for chemical-impurity bias b in overall triple-point temperature determinations. (Δ, U_{imp}, U_{tot}, U_{obs} in μK). (From Pavese et al. 2011a)

(a) Using methods determining a correction Δ with uncertainty U_Δ (expanded uncertainty, $k \approx 2$).

	e-H_2 ($K_f = -13.5$ μK) [a]						Ne ($K_f = -15$ μK) [a]					
	99.9999 % [b]			99.998 % [b]			99.999 % [b]			99.998 % [b]		
	Ne: $X\cdot10^6 = 0.3$ [c], $u(X\cdot10^6)$/μK = 0.18 [d] ^{4}He: $X\cdot10^6 = 0.5$ [c], $u(X\cdot10^6)$/μK = 1.65 [d] Rest [e]: $X\cdot10^6 = 0.2$			Ne: $X\cdot10^6 = 5$ [c], $u(X\cdot10^6)$/μK = 3 [d] ^{4}He: $X\cdot10^6 = 3$ [c], $u(X\cdot10^6)$/μK = 9.9 [d] Rest [e]: $X\cdot10^6 = 12$			H_2: $X\cdot10^6 = 1$ [c], $u(X\cdot10^6)$/μK = 2.1 [d] N_2: $X\cdot10^6 = 3$ [c], $u(X\cdot10^6)$/μK = 7.2 [d] Rest [e]: $X\cdot10^6 = 6$			H_2: $X\cdot10^6 = 5$ [c], $u(X\cdot10^6)$/μK = 10.5 [d] N_2: $X\cdot10^6 = 5$ [c], $u(X\cdot10^6)$/μK = 12 [d] Rest [e]: $X\cdot10^6 = 10$		
Method/Approach	Δ	U_{imp} [f]	U_{tot} [f] ($U_{\text{obs}} = 60$)	Δ	U_{imp} [f]	U_{tot} [f] ($U_{\text{obs}} = 60$)	Δ	U_{imp} [f]	U_{tot} [f] ($U_{\text{obs}} = 60$)	Δ	U_{imp} [f]	U_{tot} [f] ($U_{\text{obs}} = 60$)
SIE	6	4	60	43	24	65	31	20	63	75	48	77
OME	:= 0	16	62	:= 0	312	317	:= 0	173	183	:= 0	346	352
One-sided OME($U+$)	5	5	60	54	54	81	30	30	67	75	75	96
($U-$)		6	6		62	62		35	69		87	105
AOE	5	11	61	52	114	129	30	19	63	75	47	77

	O_2 ($K_f = -55$ μK) [a]									Ar ($K_f = -49$ μK) [a]					
	99.998 % [b]			99.998 % [b]			99.9995 % [b]			99.999 % [b]			99.998 % [b]		
	N_2: $X\cdot10^6 = 10$ [c], $u(X\cdot10^6)$/μK = 66 [d] Ar: $X\cdot10^6 = 3$ [c], $u(X\cdot10^6)$/μK = 11 [d] Kr: $X\cdot10^6 = 1$ [c], $u(X\cdot10^6)$/μK = 1.5 [d] Rest [e]: $X\cdot10^6 = 6$			N_2: $X\cdot10^6 = 3$ [c], $u(X\cdot10^6)$/μK = 20 [d] Ar: $X\cdot10^6 = 10$ [c], $u(X\cdot10^6)$/μK = 36 [d] Kr: $X\cdot10^6 = 1$ [c], $u(X\cdot10^6)$/μK = 1.5 [d] Rest [e]: $X\cdot10^6 = 6$			N_2: $X\cdot10^6 = 2.5$ [c], $u(X\cdot10^6)$/μK = 16.5 [d] Ar: $X\cdot10^6 = 1$ [c], $u(X\cdot10^6)$/μK = 3.6 [d] Kr: $X\cdot10^6 = 0.1$ [c], $u(X\cdot10^6)$/μK = 1.5 [d] Rest [e]: $X\cdot10^6 = 1.4$			N_2: $X\cdot10^6 = 0.4$ [c], $u(X\cdot10^6)$/μK = 2.6 [d] O_2: $X\cdot10^6 = 0.4$ [c], $u(X\cdot10^6)$/μK = 2.6 [d] Kr: $X\cdot10^6 = 0.05$ [c], $u(X\cdot10^6)$/μK = 0.8 [d] CH_4: $X\cdot10^6 = 0.05$ [c], $u(X\cdot10^6)$/μK = 0.45 [d] Rest [e]: $X\cdot10^6 = 0.4$			N_2: $X\cdot10^6 = 10$ [c], $u(X\cdot10^6)$/μK = 66 [d] O_2: $X\cdot10^6 = 2$ [c], $u(X\cdot10^6)$/μK = 13 [d] Kr: $X\cdot10^6 = 2$ [c], $u(X\cdot10^6)$/μK = 3 [d] CH_4: $X\cdot10^6 = 0$ [c] Rest [e]: $X\cdot10^6 = 1$		
Method/Approach	Δ	U_{imp} [f]	U_{tot} [f] ($U_{\text{obs}} = 80$)	Δ	U_{imp} [f]	U_{tot} [f] ($U_{\text{obs}} = 80$)	Δ	U_{imp} [f]	U_{tot} [f] ($U_{\text{obs}} = 80$)	Δ	U_{imp} [f]	U_{tot} [f] ($U_{\text{obs}} = 80$)	Δ	U_{imp} [f]	U_{tot} [f] ($U_{\text{obs}} = 80$)
SIE	189	148	168	−49	103	131	44	37	88	19	8	80	254	148	169
OME	:= 0	1270	1273	:= 0	1270	1273	:= 0	318	327	:= 0	57	98	:= 0	849	852
One-sided OME($U+$)	*(385)*	*(385)*	n.s.	*(385)*	*(385)*	n.s.	(138)	*(138)*	n.s.	22	22	84	343	343	404
($U-$)		*(445)*	n.s.		*(445)*	n.s.		*(159)*	n.s.		25	91		396	691
AOE	*(70)*	*(725)*	n.s.	*(70)*	*(725)*	n.s.	(18)	*(186)*	n.s.	21	49	94	322	759	763

Table C.1.2 (continued)

(b) Using methods *not* performing a correction Δ with uncertainty U_Δ (expanded uncertainty, $k \approx 2$).

Method/Approach	e-H_2 ($K_f = -13.5$ μK) [a]						Ne ($K_f = -15$ μK) [a]					
	99.9999 % [b]			99.998 % [b]			99.999 % [b]			99.998 % [b]		
	Same as in Table C.1.2(a)			Same as in Table C.1.2(a)			Same as in Table C.1.2(a)			Same as in Table C.1.2(a)		
	Δ	U_{imp} [f]	U_{tot} [f] ($U_{obs} = 60$)	Δ	U_{imp} [f]	U_{tot} [f] ($U_{obs} = 60$)	Δ	U_{imp} [f]	U_{tot} [f] ($U_{obs} = 60$)	Δ	U_{imp} [f]	U_{tot} [f] ($U_{obs} = 60$)
RSSu	n.a.	19	63	n.a.	329	334	n.a.	183	193	n.a.	377	382
RSSU	n.a.	16	62	n.a.	316	322	n.a.	176	186	n.a.	354	359
SUMU ($U+$)	n.a.	26	73	n.a.	420	425	n.a.	233	243	n.a.	496	502
($U-$)		5	51		204	209		113	123		196	202
Mixed SUMU-SIE($U+$)	n.a.	0 [g]	54		0 [g]	22	n.a.	0 [g]	39	n.a.	0 [g]	2
($U-$)		10	66	n.a.	67	108		51	94		123	152

Method/Approach	O_2 ($K_f = -55$ μK) [a]									Ar ($K_f = -49$ μK) [a]					
	99.998 % [b]			99.998 % [b]			99.9995 % [b]			99.999 % [b]			99.998 % [b]		
	Same as in Table C.1.2(a)			Same as in Table C.1.2(a)			Same as in Table C.1.2(a)			Same as in Table C.1.2(a)			Same as in Table C.1.2(a)		
	Δ	U_{imp} [f]	U_{tot} [f] ($U_{obs} = 80$)	Δ	U_{imp} [f]	U_{tot} [f] ($U_{obs} = 80$)	Δ	U_{imp} [f]	U_{tot} [f] ($U_{obs} = 80$)	Δ	U_{imp} [f]	U_{tot} [f] ($U_{obs} = 80$)	Δ	U_{imp} [f]	U_{tot} [f] ($U_{obs} = 80$)
RSSu	n.a.	1485	1487	n.a.	1485	1487	n.a.	420	428	n.a.	70	106	n.a.	1065	1068
RSSU	n.a.	1327	1330	n.a.	1327	1330	n.a.	346	355	n.a.	60	100	n.a.	908	911
SUMU ($U+$)	n.a.	2040	2043	n.a.	2040	2043	n.a.	516	525	n.a.	101	142	n.a.	1535	1538
($U-$)		500	503		500	503		120 [h]	129 [h]		12	54		163	166
Mixed SUMU-SIE($U+$)	n.a.	0 [g]	0 [g]	n.a.	152	180	n.a.	0 [g]	8	n.a.	0 [g]	62	n.a.	0 [g]	0 [g]
($U-$)		337	357		54	82		81 [h]	132 [h]		27	99		402	423

Table C.1.2 (continued)

The main chemical impurities are listed and quantified. n.s. = not suitable approach.
See Sect. 2.2, Table 2.4a for the approach definitions. See Table C.1.1 for the values of dT_{liq}/dx_i and $u(dT_{liq}/dx_i)$ of each chemical impurity. Correction $\Delta = -b$.
n.a. correction *not applied*
[a] K_f = first cryoscopic constant (values from Pavese 2009).
[b] Total nominal chemical purity.
[c] $x = \sum x_i$, total chemical impurities in amount of substance concentrations.
[d] $u(x) = \sum (u(x_i)\,(dT_{liq}/dx_i))$, in μK, sensitivities from Table C.1.1.
[e] Impurities with no effect on T_{tp}.
[f] U_{imp} = contribution of chemical impurities only; U_{tot} = by also adding $U_{obs} = U(y_{obs})$ in quadrature.
[g] Forced to zero.
[h] Not applicable (see Table 2.4) since $U(y_{obs}) < \Delta$.
Other Notes: same as in Table C.1.2(a) above.

Part C.2—Data Sheets of Gases

3-Helium

^{3}He, Relative Molecular Mass: 3.016 605

Critical point parameters			
T_c/K = 3.3162	p_c/MPa = 0.11466	ρ_c/kg m^{-3} = 41.3	
Vapor properties (see note)			
$\rho_{v,nbp}$/kg m^{-3}		$c_{p,v}$(2 K, 1 bar)/J K^{-1} mol^{-1}	
$\rho_{v,tp}$/kg m^{-3}	n.a.	λ_v(2 K, 1 bar)/J K^{-1} m^{-1} s^{-1}	0.013
w_v(3.34 K, 0 Pa)/m s^{-1}	123.8	η_v(25 °C, 1 bar)/10^{-3} Pa s	
Liquid properties			
$\rho_{L,nbp}$/kg L^{-1}	0.062	$\Delta_{vap}H_{m,tp}$/kJ mol^{-1}	n.a.
$\rho_{L,tp}$/kg L^{-1}	n.a.	$c_{s,L}$(2 K)/J K^{-1} mol^{-1}	7.8
T_{nbp}/K	3.1968	$\lambda_{L,nbp}$/J K^{-1} m^{-1} s^{-1}	0.020
$\Delta_{vap}H_{m,nbp}$/kJ mol^{-1}	30	$\eta_{L,nbp}/10^{-3}$ Pa s	6.0

Liquid-vapor pressures (ITS-90; BIPM 1990)

T_{90} (K)	p (kPa)	$\frac{dp}{dT}$ (kPa K^{-1})	$\frac{1}{p}\frac{dp}{dT}$ (%)	T_{90} (K)	p (kPa)	$\frac{dp}{dT}$ (kPa K^{-1})	$\frac{1}{p}\frac{dp}{dT}$ (%)	T_{90} (K)	p (kPa)	$\frac{dp}{dT}$ (kPa K^{-1})	$\frac{1}{p}\frac{dp}{dT}$ (%)
0.65	0.1160	1.080	930	1.50	6.710	17.80	265	2.40	38.217	55.4	145
0.70	0.1799	1.486	825	1.60	8.649	21.03	243	2.50	44.02	60.7	138
0.80	0.3778	2.523	668	1.70	10.924	24.51	224	2.60	50.38	66.3	132
0.90	0.6946	3.863	556	1.80	13.558	28.22	208	2.70	57.30	72.2	126
1.00	1.1603	5.499	474	1.90	16.575	32.16	194	2.80	64.82	78.4	121
1.10	1.8040	7.422	410	2.00	19.999	36.34	182	2.90	72.99	84.9	116
1.20	2.6539	9.622	363	2.10	23.852	40.75	171	3.00	81.82	91.8	112
1.30	3.737	12.09	323	2.20	28.157	45.39	161	3.10	91.37	99.2	109
1.40	5.081	14.82	292	2.30	32.938	50.26	153	3.20	101.67	107.0	105

Notes and Warnings The use of ^{3}He is only considered at low temperatures. Therefore here only the some properties of the vapor (i.e., below the critical point) will be indicated. For use of ^{3}He as a gas in gas thermometry see Chap. 3.

4-Helium

^{4}He, Relative Molecular Mass: 4.002 602

Critical point parameters			
T_c/K = 5.1953	p_c/MPa = 0.22746	ρ_c/kg m^{-3} = 69.64	
Gas properties			
ρ(300 K, 1 bar)/kg m^{-3}	0.1625	w_g(3.8 K, 0 Pa)/m s^{-1}	114.9
ρ(0 °C, 1 bar)/kg m^{-3}	0.1785	$c_{p,g}$(0 °C, 1 bar)/J K^{-1} mol^{-1}	20.8
$\rho_{g,nbp}$/kg m^{-3}	16.0	λ_g(0 °C, 1 bar)/J K^{-1} m^{-1} s^{-1}	0.142
$\rho_{g,tp}$/kg m^{-3}	n.a.	η_g(25 °C, 1 bar)/10^{-6} Pa s	19.6
Liquid properties			
$\rho_{L,nbp}$/kg L^{-1}	0.1250	$\Delta_{vap}H_{m,tp}$/kJ mol^{-1}	n.a.
$\rho_{L,tp}$/kg L^{-1}	n.a.	$c_{s,L,nbp}$/J K^{-1} mol^{-1}	18
T_{nbp}/K	4.2221	$\lambda_{L,nbp}$/J K^{-1} m^{-1} s^{-1}	0.031
$\Delta_{vap}H_{m,nbp}$/kJ mol^{-1}	0.0829	$\eta_{L,nbp}$/10^{-6} Pa s	3.6
Superfluid properties			
T_λ/K	2.1768	$\rho_{g,\lambda}$/kg m^{-3}	20.8
p_λ/kPa	5.0418	$\rho_{L,\lambda}$/kg L^{-1}	0.146

Liquid-vapor pressures (ITS-90; BIPM 1990b)

T_{90} (K)	p (kPa)	$\frac{dp}{dT}$ (kPa K^{-1})	$\frac{1}{p}\frac{dp}{dT}$ (%)	T_{90} (K)	p (kPa)	$\frac{dp}{dT}$ (kPa K^{-1})	$\frac{1}{p}\frac{dp}{dT}$ (%)	T_{90} (K)	p (kPa)	$\frac{dp}{dT}$ (kPa K^{-1})	$\frac{1}{p}\frac{dp}{dT}$ (%)
1.25	0.1147	0.757	660	2.10	4.141	11.04	267	3.70	59.351	66.4	112
1.30	0.1578	0.975	618	2.17	5.0418	12.414	246	3.90	73.67	76.8	104
1.40	0.2820	1.537	545	2.30	6.730	15.05	224	4.10	90.14	88.0	98
1.50	0.4715	2.287	485	2.50	10.228	20.06	196	4.22	101.325	95.306	94
1.60	0.7464	3.245	435	2.70	14.807	25.87	175	4.30	108.94	100.1	92
1.70	1.1279	4.423	392	2.90	20.626	32.45	157	4.50	130.26	113.3	87
1.80	1.6384	5.822	355	3.10	27.836	39.78	143	4.70	154.3	127.5	82
1.90	2.2993	7.427	323	3.30	36.590	47.89	131	4.90	181.3	142.8	79
2.00	3.1293	9.195	284	3.50	47.044	56.8	121	5.00	196.0	151.2	56

Notes and Warnings Thermometric measurements below the λ point are quite specialized.

e-Hydrogen

H_2, Relative Molecular Mass: 2.015 88 (Natural)

Critical point parameters			
T_c/K = 32.968	p_c/MPa = 1.293	ρ_c/kg m^{-3} = n.a.	(20.3 K *e*-H_2)
T_c/K = 33.18	p_c/MPa = 1.315	ρ_c/kg m^{-3} = 31.0.	(*n*-H_2)
		ρ_c/kg m^{-3} = 30.6	(*e*-H_2)
Gas properties (for *n*-H_2: c(*o*-H_2) = 0.749)			
ρ(300 K, 1 bar)/kg m^{-3}	0.080	w_g(0 °C, 1 bar)/m s^{-1}	1276
ρ(0 °C, 1 bar)/kg m^{-3}	0.088	$c_{p,g}$(25 °C, 1 bar)/J K^{-1} mol^{-1}	28.8
$\rho_{g,nbp}$/kg m^{-3}	1.19	λ_g(0 °C, 1 bar)/J K^{-1} m^{-1} s^{-1}	0.17
$\rho_{g,tp}$/kg m^{-3}	0.126	η_g(25 °C, 1 bar)/10^{-6} Pa s	8.9
Liquid properties			
$\rho_{L,nbp}$/kg L^{-1}	0.071	$\Delta_{vap}H_{m,tp}$/kJ mol^{-1}	0.911
$\rho_{L,tp}$/kg L^{-1}	0.077	$c_{s,L,nbp}$/J K^{-1} mol^{-1}	19.3
T_{nbp}/K[c(*o*-H_2) = 2.1 × 10^{-3}]	20.271	$\lambda_{L,nbp}$/J K^{-1} m^{-1} s^{-1}	0.12
$\Delta_{vap}H_{m,nbp}$/kJ mol^{-1}	0.906	$\eta_{L,nbp}$/10^{-6} Pa s	13.3
Solid properties			
$\rho_{s,tp}$/kg L^{-1}	0.087	$\Delta_{fus}H_{m,tp}$/kJ mol^{-1}	0.117
T_{tp}/K [c(*o*-H_2) = 4 × 10^{-5}]	13.8033	$\Delta_{sub}H_{m,tp}$/kJ mol^{-1}	1.028
p_{tp}/kPa	7.03	$c_{t,s,tp}$/J K^{-1} mol^{-1}	6.2
$(dT_{tp}/dp)_{mc}$/10^{-8} K Pa^{-1}	34	$\lambda_{s,tp}$/J K^{-1} m^{-1} s^{-1}	≈0.55

Liquid-vapor and solid-vapor pressures (Pavese 1991: 9–13.8 K; BIPM 1983: 15–23 K; Van Itterbeek et al. 1964)

T_{90} (K)	p (kPa)	$\frac{dp}{dT}$ (kPa K^{-1})	$\frac{1}{p}\frac{dp}{dT}$ (%)	T_{68} (K)	p (kPa)	$\frac{dp}{dT}$ (kPa K^{-1})	$\frac{1}{p}\frac{dp}{dT}$ (%)	T_{68} (K)	p (kPa)	$\frac{dp}{dT}$ (kPa K^{-1})	$\frac{1}{p}\frac{dp}{dT}$ (%)
9	0.0521	0.101	196	13.8	7.030	4.6	66	24	264.25	59.5	22.5
9.5	0.1208	0.180	149	15	13.373	6.7	50	25	328.72	69.5	21.2
10	0.2393	0.302	126	16	21.463	9.59	45	26	403.63	80.4	19.9
10.5	0.4329	0.483	111	17	32.77	13.15	40	27	489.83	92.1	18.8
11	0.7347	0.738	100	18	48.00	17.43	36	28	588.2	104.7	17.8
11.5	1.187	1.089	92	19	67.88	22.46	33	29	699.5	118.1	16.9
12	1.843	1.556	84	20.3	101.325	30,05	30	30	824.7	132.4	16.0
12.5	2.766	2.164	78	21	124.65	34.84	28	31	964.5	147.4	15.3
13	4.035	2.940	73	22	163.11	42.22	26	32	1119.9	163.3	14.6
13.5	5.739	3.91	68	23	209.35	50.41	24				

For *ortho-para* composition, see Table 2.6

Effect of impurities on T_{tp}, $(\delta T_S, \delta T_L)$/μK ppm^{-1} (• = not available)
D2: +(5.5, 3.5); HD: +(3.0, 2.5); Ne: −(•, 2), eutectic point at T = 13.76 K @ x(Ne) = 0.0020
^{4}He: −(•, 11) (on freezing curve + 0.25mK/MPa $\hat{=}$ < 0.01mK at t.p.)
O_2, N_2: none.

Notes and Warnings e-H_2 indicates hydrogen in spin equilibrium at each temperature, obtained with the permanent presence of a catalyst, not hydrogen equilibrated with a catalyst at, say, 20.3 K, and then supposed to equilibrate at other temperatures only by self-conversion (for a full discussion see Souers (1986, p. 24–31).

$\Delta_{rot}H_m$/J mol^{-1} = 2229 for 20.3 K e-H_2. Variations in T_{tp} due to variation in isotopic composition (HD content) of gases of different origins are within U = 0.4 mK: for correction see Sect. 2.2.2.5.

e-Deuterium

D_2, Relative Molecular Mass: 4.028 204 (Pure Isotope)

Critical point parameters			
T_c/K = 32.256	p_c/MPa = 1.650	ρ_c/kg m^{-3} = n.a.	(−20.3 K *e*-D_2)
T_c/K = 38.34	p_c/MPa = 1.665	ρ_c/kg m^{-3} = 67.7	(*n*-D_2)
		ρ_c/kg m^{-3} = 67.3	(*e*-D_2)
Gas properties (for *n*-D_2: c(*p*-D_2) = 0.6667)			
ρ(300 K, 1 bar)/kg m^{-3}	0.16	w_g(0 °C, 1 bar)/m s^{-1}	
ρ(0 °C, 1 bar)/kg m^{-3}	0.18	$c_{p,g}$(0 °C, 1 bar)/J K^{-1} mol^{-1}	28.6
$\rho_{g,nbp}$/kg m^{-3}	1.77	λ_g(0 °C, 1 bar)/J K^{-1} m^{-1} s^{-1}	0.11
$\rho_{g,tp}$/kg m^{-3}	0.455	η_g(25 °C, 1 bar)/10^{-6} Pa s	13
Liquid properties			
$\rho_{L,nbp}$/kg L^{-1} (*n*-D_2)	0.159	$\Delta_{vap}H_{m,tp}$/kJ mol^{-1}	1.27
$\rho_{L,tp}$/kg L^{-1} (*n*-D_2)	0.174	$c_{s,L,nbp}$/J K^{-1} mol^{-1}	25.5
T_{nbp}/K[*n*-D_2: c(*p*-D_2) = 0.0376]	23.66	$\lambda_{L,nbp}$/J K^{-1} m^{-1} s^{-1}	0.13
$\Delta_{vap}H_{m,nbp}$/kJ mol^{-1}	1.22	$\eta_{L,nbp}$/10^{-6} Pa s	29.4
Solid properties			
$\rho_{s,tp}$/kg L^{-1}	0.197	$\Delta_{fus}H_{m,tp}$/kJ mol^{-1}	0.199
T_{tp}/K [*n*-D_2: c(*p*-D_2) = 0.0151]	18.6890	$\Delta_{sub}H_{m,tp}$/kJ mol^{-1}	1.47
p_{tp}/kPa	17.31	$c_{t,s,tp}$/J K^{-1} mol^{-1} (*n*-D_2)	11.8
$(dT_{tp}/dp)_{mc}$/10^{-8} K Pa^{-1}	26	$\lambda_{s,tp}$/J K^{-1} m^{-1} s^{-1} (*n*-D_2)	0.31

Liquid-vapor and solid-vapor pressures (*n*-D_2) (Souers 1979, 1986)

T_{68} (K)	p (kPa)	$\frac{dp}{dT}$ (kPa K^{-1})	$\frac{1}{p}\frac{dp}{dT}$ (%)	T_{68} (K)	p (kPa)	$\frac{dp}{dT}$ (kPa K^{-1})	$\frac{1}{p}\frac{dp}{dT}$ (%)	T_{68} (K)	p (kPa)	$\frac{dp}{dT}$ (kPa K^{-1})	$\frac{1}{p}\frac{dp}{dT}$ (%)
9	0.0011	0.0022	195	18.7	17.03	8.89	52	29	368.5	75.3	20.4
10	0.0066	0.0106	161	20	29.32	11.64	40	30	449.7	87.2	19.4
11	0.0286	0.0386	135	21	42.82	15.48	36	31	543.4	100.4	18.5
12	0.0995	0.1145	115	22	60.51	20.04	33	32	650.9	114.9	17.7
13	0.2901	0.2887	99	23	83.14	25.35	31	33	773.7	130.9	16.9
14	0.7359	0.641	87	23.7	101.325	29.53	29	34	913.4	148.7	16.3
15	1.668	1.284	77	25	146.32	38.38	26.2	35	1071.7	168.3	15.7
16	3.450	2.366	68	26	188.52	46.17	24.5	36	1250.6	190.0	15.2
17	6.608	4.07	61	27	238.97	54.9	23.0	37	1452.5	214.1	14.7
18	11.872	6.62	55	28	298.6	64.6	21.6				

For para-ortho composition, see Table 2.5

Effect of impurities on T_{tp}, $(\delta T_S, \delta T_L)/\mu K\ ppm^{-1}$
H_2: −(6.5, 4.5); HD: −(2.1, 1.5)
Ne: −(16, 8), eutectic point at $T = 18.50$ K @ $x(Ne) = 0.0023$
^{4}He: (on freezing curve $+ 0.20$ mK/MPa $\hat{=} < 0.01$mK at t.p.)

Notes and Warnings *e*-D_2 indicates deuterium in spin equilibrium at each temperature, obtained with the permanent presence of a catalyst, not deuterium equilibrated

with a catalyst at, say, 20.3 K, and then supposed to equilibrate at other temperatures only by self-conversion (for a full discussion see Souers (1986, p. 24–31).

$\Delta_{\mathrm{rot}}H_{\mathrm{m}}/\mathrm{J\ mol^{-1}} = 2375$ for 18.7 K e-D_2. Therefore, at the triple point, $\mathrm{d}H_{\mathrm{rot}}/\mathrm{d}T = 2\ \mathrm{J\ mol^{-1}\ K^{-1}}$, to be applied to the amount of substance still converting. Peculiar freezing plateaux showing a double subcooling peak (Fellmuth et al. 2005), and melting plateaux showing "premelting" effects have been reported when using very pure e-D_2, of no consequences on the measured T_{tp} value.

Neon

Ne, Relative Molecular Mass: 20.179 7

Critical point parameters			
T_c/K = 44.4	p_c/MPa = 2.654	ρ_c/kg m^{-3} = 483.0	
Gas properties			
ρ(300 K, 1 bar)/kg m^{-3}	0.819	w_g(0 °C, 1 bar)/m s^{-1}	435
ρ(0 °C, 1 bar)/kg m^{-3}	0.900	$c_{p,g}$(0 °C, 1 bar)/J K^{-1} mol^{-1} = c_p^0	= 2.5 × R ≅ 20.786
$\rho_{g,nbp}$/kg m^{-3}	9.55	λ_g(0 °C, 1 bar)/J K^{-1} m^{-1} s^{-1}	0.046
$\rho_{g,tp}$/kg m^{-3}	4.6	η_g(25 °C, 1 bar)/10^{-6} Pa s	31.4
Liquid properties			
$\rho_{L,nbp}$/kg L^{-1}	1.206	$\Delta_{vap}H_{m,tp}$/kJ mol^{-1}	1.80
$\rho_{L,tp}$/kg L^{-1}	1.247	$c_{s,L,nbp}$/J K^{-1} mol^{-1}	36.2
T_{nbp}/K	27.098	$\lambda_{L,nbp}$/J K^{-1} m^{-1} s^{-1}	0.13
$\Delta_{vap}H_{m,nbp}$/kJ mol^{-1}	1.74	$\eta_{L,nbp}$/10^{-6} Pa s	124
Solid properties			
$\rho_{s,tp}$/kg L^{-1}	1.444	$\Delta_{fus}H_{m,tp}$/kJ mol^{-1}	0.335
T_{tp}/K	24.5561	$\Delta_{sub}H_{m,tp}$/kJ mol^{-1}	2.14
p_{tp}/kPa	43.379	$c_{t,s,tp}$/J K^{-1} mol^{-1}	24.3
$(dT_{tp}/dp)_{mc}$/10^{-8} K Pa^{-1}	16	$\lambda_{s,tp}$/J K^{-1} m^{-1} s^{-1}	

Liquid-vapor and solid-vapor pressures (Ziegler et al. 1970: 15–19 K (T_{48}); Ancsin 1978: 20–24.6 K; Preston-Thomas: 24.6–40 K)

T_{48} T_{68} (K)	p (kPa)	$\frac{dp}{dT}$ (kPa K^{-1})	$\frac{1}{p}\frac{dp}{dT}$ (%)	T_{68} (K)	p (kPa)	$\frac{dp}{dT}$ (kPa K^{-1})	$\frac{1}{p}\frac{dp}{dT}$ (%)	T_{68} (K)	p (kPa)	$\frac{dp}{dT}$ (kPa K^{-1})	$\frac{1}{p}\frac{dp}{dT}$ (%)
15	0.0515	0.044	85	24.6	43.32	16.00	37.0	34	533.5	103.3	19.4
16	0.150	0.114	77	25	50.88	18.12	35.6	35	644.2	118.3	18.4
17	0.387	0.259	67	26	71.63	23.52	32.8	36	770.5	134.6	17.5
18	0.900	0.541	60	27.1	101.33	30.57	30.2	37	913.7	152.2	16.7
19	1.922	1.035	54	28	131.69	37.19	28.2	38	1075.3	171.2	15.9
20	3.827	2.485	64.9	29	172.97	45.53	26.3	39	1256.6	191.7	15.3
21	7.107	4.195	59.0	30	223.09	54.90	24.6	40	1459.2	213.9	14.7
22	12.495	6.740	53.9	31	283.11	65.33	23.1				
23	20.95	10.38	49.6	32	354.11	76.85	21.7				
24	33.73	15.43	45.7	33	437.18	89.49	20.5				

[a] Incremental

Effect of impurities on T_{tp}, $(\delta T_S, \delta T_L)/\mu K\ ppm^{-1}$ (•, information not available)
^{4}He: none
H_2 (•, D_2): −(•, 7)
N_2: −(•, 6.6)
Ar, CO: none
Pure isotopes: ^{20}Ne T_{tp} = 24.542 28 K, ^{22}Ne T_{tp} = 24.688 85 K,
$^{22}T - {}^{20}T$ = 0.146 57 K.

Notes and Warnings Variations in T_{tp} due to variation in isotopic composition of gases of different origins are within U = 0.3 mK: for correction see Sect. 2.2.2.5. Distillation effects equivalent to less than 0.5 mK at n.b.p.

Nitrogen

N_2, Relative Molecular Mass: 28.013 48

Critical point parameters			
T_c/K = 126.21	p_c/MPa = 3.4000	ρ_c/kg m^{-3} = 314	
Gas properties			
ρ(300 K, 1 bar)/kg m^{-3}	1.11	w_g(0 °C, 1 bar)/m s^{-1}	336.8
ρ(0 °C, 1 bar)/kg m^{-3}	1.12	$c_{p,g}$(0 °C, 1 bar)/J K^{-1} mol^{-1}	29.2
$\rho_{g,nbp}$/kg m^{-3}	4.61	λ_g(0 °C, 1 bar)/J K^{-1} m^{-1} s^{-1}	0.024
$\rho_{g,tp}$/kg m^{-3}	0.674	η_g(25 °C, 1 bar)/10^{-6} Pa s	17.8
Liquid properties			
$\rho_{L,nbp}$/kg L^{-1}	0.809	$\Delta_{vap}H_{m,tp}$/kJ mol^{-1}	6.03
$\rho_{L,tp}$/kg L^{-1}	0.868	$c_{s,L,nbp}$/J K^{-1} mol^{-1}	57.2
T_{nbp}/K	77.352	$\lambda_{L,nbp}$/J K^{-1} m^{-1} s^{-1}	0.14
$\Delta_{vap}H_{m,nbp}$/kJ mol^{-1}	5.56	$\eta_{L,nbp}$/10^{-6} Pa s	165
Solid properties			
$\rho_{s,tp}$/kg L^{-1}	0.945	$\Delta_{fus}H_{m,tp}$/kJ mol^{-1}	0.724
T_{tp}/K	63.151	$\Delta_{sub}H_{m,tp}$/kJ mol^{-1}	6.75
p_{tp}/kPa	12.526	$c_{t,s,tp}$/J K^{-1} mol^{-1}	46
$(dT_{tp}/dp)_{mc}$/10^{-8} K Pa^{-1}	24	$\lambda_{s,tp}$/J K^{-1} m^{-1} s^{-1}	
Solid-to-solid transition (second-order)			
T_{sst} = 35.614 K			

Liquid-vapor and solid-vapor pressures (Frels 1974: 45–55 K; Ancsin 1974a: 57–63 K, 64–75 K; Wagner 1973)

T_{68} (K)	p (kPa)	$\frac{dp}{dT}$ (kPa K^{-1})	$\frac{1}{p}\frac{dp}{dT}$ (%)	T_{68} (K)	p (kPa)	$\frac{dp}{dT}$ (kPa K^{-1})	$\frac{1}{p}\frac{dp}{dT}$ (%)	T_{68} (K)	p (kPa)	$\frac{dp}{dT}$ (kPa K^{-1})	$\frac{1}{p}\frac{dp}{dT}$ (%)
45	0.0659	0.0267	40	64	14.622	2.612	17.9	90	360.15	30.81	8.6
47	0.1431	0.0532	37	65	17.429	3.008	17.2	95	539.84	41.37	7.7
49	0.2918	0.0997	34	67	24.335	3.928	16.1	100	776.95	53.8	6.9
51	0.5627	0.1775	32	69	33.261	5.03	15.1	105	1081.0	68.2	6.3
53	1.0326	0.302	29.2	71	44.591	6.33	14.2	110	1462.1	84.6	5.8
55	1.8129	0.492	27.1	73	58.740	7.85	13.4	115	1931.5	103.6	5.4
57	3.0598	0.781	25.5	75	76.147	9.60	12.6	120	2502.7	125.6	5.0
59	5.006	1.189	23.7	77.35	101.33	11.93	11.8	125	3195.2	152.8	4.8
61	7.919	1.754	22.1	80	136.88	15.00	11.0				
63.15	12.538	2.583	20.6	85	228.77	22.04	10.0				

Effect of impurities on T_{tp}, $(\delta T_S, \delta T_L)$/μK ppm^{-1} (•, information not available)

Ar: −(6, 4.5); up to x(Ar) = 0.30, $(T_S - T_L) < 0.1$ K and the line show a $\Delta T_{min} = -0.53$ K @ x(Ar) = 0.17.

CH_4: −(3, 3); up to $x(CH_4) = 0.238$, $(T_S - T_L)$ is very small, as with argon and the line show a eutectic-like point at $T_{min} = 62.6$ K @ $x(CH_4) = 0.238$.

O_2: −(33, 15), peritectic point at $T_{min} = 50.1$ K @ $x(O_2) = 0.23$.

Kr: +(•, 25); CO: +(2, 8)

Notes and Warnings An impurity x(Ar) < 0.17 affects very little the melting range. Care must be taken to detect argon impurity in nitrogen; δTL values as low as −2.6 μK ppm^{-1} have been reported.

Oxygen

O_2, Relative Molecular Mass: 31.998 8

Critical point parameters			
T_c/K = 154.595	p_c/MPa = 5.0430	ρ_c/kg m^{-3} = 436	
Gas properties			
ρ(300 K, 1 bar)/kg m^{-3}	1.301	w_g(0 °C, 1 bar)/m s^{-1}	317.2
ρ(0 °C, 1 bar)/kg m^{-3}	1.429	$c_{p,g}$(0 °C, 1 bar)/J K^{-1} mol^{-1}	29.33
$\rho_{g,nbp}$/kg m^{-3}	4.47	λ_g(0 °C, 1 bar)/J K^{-1} m^{-1} s^{-1}	0.0245
$\rho_{g,tp}$/kg m^{-3}	0.011	η_g(25 °C, 1 bar)/10^{-6} Pa s	20.6
Liquid properties			
$\rho_{L,nbp}$/kg L^{-1}	1.141	$\Delta_{vap}H_{m,tp}$/kJ mol^{-1}	7.76
$\rho_{L,tp}$/kg L^{-1}	1.307	$c_{s,L,nbp}$/J K^{-1} mol^{-1}	54.3
T_{nbp}/K	90.196	$\lambda_{L,nbp}$/J K^{-1} m^{-1} s^{-1}	0.15
$\Delta_{vap}H_{m,nbp}$/kJ mol^{-1}	6.81	$\eta_{L,nbp}$/10^{-6} Pa s	189
Solid properties			
$\rho_{s,tp}$/kg L^{-1}	1.351	$\Delta_{fus}H_{m,tp}$/kJ mol^{-1}	0.444
T_{tp}/K	54.3584	$\Delta_{sub}H_{m,tp}$/kJ mol^{-1}	8.20
p_{tp}/kPa	0.14625	$c_{t,s,tp}$/J K^{-1} mol^{-1}	46
$(dT_{tp}/dp)_{mc}$/10^{-8} K Pa^{-1}	12	$\lambda_{s,tp}$/J K^{-1} m^{-1} s^{-1}	
Solid-to-solid transition (first-order)[a]			
T_{sst} = 23.867 K	$\rho\beta$ = 1.527	$\rho\alpha$ = 1.537	
$\Delta_{tra}H_m$/kJ mol^{-1} = n.a.[a]			
Solid-to-solid transition (first-order)			
T_{sst} = 43.796 K	$\rho\gamma$ = 1.388	$\rho\beta$ = 1.463	
$\Delta_{tra}H_m$/kJ mol^{-1} = 0.749			

[a]Contentious: theoretical predictions indicate a first-order transition

Liquid-vapor pressures (Wagner et al. 1976)

T_{68} (K)	p (kPa)	$\frac{dp}{dT}$ (kPa K^{-1})	$\frac{1}{p}\frac{dp}{dT}$ (%)	T_{68} (K)	p (kPa)	$\frac{dp}{dT}$ (kPa K^{-1})	$\frac{1}{p}\frac{dp}{dT}$ (%)	T_{68} (K)	p (kPa)	$\frac{dp}{dT}$ (kPa K^{-1})	$\frac{1}{p}\frac{dp}{dT}$ (%)
54.36	0.1459	0.0461	31.6	82	39.186	5.0366	12.9	110	543.2	37.463	6.89
55	0.1782	0.0549	30.8	84	50.336	6.1388	12.2	115	755.3	47.639	6.31
57	0.3225	0.0920	28.5	86	63.847	7.3987	11.6	120	1022.0	59.269	5.80
60	0.7245	0.1848	25.5	88	80.042	8.8254	11.0	125	1350.5	72.404	5.36
63	1.4967	0.3431	22.9	89	89.253	9.6041	10.8	130	1748.7	87.121	4.98
67	3.5272	0.7065	20.0	90.2	101.33	10.5944	10.5	135	2224.5	103.548	4.66
70	6.254	1.1375	18.2	93	134.57	13.1767	9.8	140	2787.3	121.906	4.37
73	10.531	1.7464	16.6	97	195.70	17.5225	9.0	145	3447.5	142.606	4.14
77	19.685	2.9036	14.8	100	253.84	21.3167	8.4	150	4218.7	166.574	3.95
80	30.091	4.0820	13.6	105	378.32	28.7030	7.6	154	4930.6	190.808	3.87

Effect of impurities on T_{tp}, $(\delta T_S, \delta T_L)/\mu K\ ppm^{-1}$ (•, information not available)

Ar: +(12, 12), peritectic point at $T = 55.1$ K @ $x(Ar) = 0.2$. $\delta T_{\alpha,\beta} = -20$, $\delta T_{\beta,\gamma} = -28$

CH_4: −(•, < −30), eutectic point at $T = 51$ K @ $x(CH_4) = 0.08$.

C_2H_4, C_2H_6, C_3H_6, C_3H_8 show a eutectic point at low concentration and a small negative δT_{tp}.

He: +(•, 1.5); Ne: −(•, 1)

Kr: −(9, 5), eutectic point at $T = 53.94$ K @ $x(Kr) = 0.08$.

N_2: −(35, 22), eutectic point at $T = 50.1$ K @ $x(N_2) = 0.23$.

Xe: −(30, 8), eutectic point at unknown temperature @ $x(Xe) < 0.1$.

Warning Detection of argon in oxygen is impossible from thermal analysis, since low-concentration argon has no influence on the melting range. Manufacturers' impurity analyses are unreliable (Pavese 1988). Great care must then be taken in using oxygen obtained from distillation of air, as errors on T_{tp} greater than + 2 mK have been observed.

Argon

Ar, Relative Molecular Mass: 39.948

Critical point parameters			
T_c/K = 150.70	p_c/MPa = 4.8653	ρ_c/kg m^{-3} = 536	
Gas properties			
ρ(300 K, 1 bar)/kg m^{-3}	1.624	w_g(0 °C, 1 bar)/m s^{-1}	307.8
ρ(0 °C, 1 bar)/kg m^{-3}	1.784	$c_{p,g}$(0 °C, 1 bar)/J K^{-1} mol^{-1} = c_p^0	= 2.5 × $R \cong$ 20.786
$\rho_{g,nbp}$/kg m^{-3}	5.78	λ_g(0 °C, 1 bar)/J K^{-1} m^{-1} s^{-1}	0.017
$\rho_{g,tp}$/kg m^{-3}	4.0	η_g(25 °C, 1 bar)/10^{-6} Pa s	22.3
Liquid properties			
$\rho_{L,nbp}$/kg L^{-1}	1.392	$\Delta_{vap}H_{m,tp}$/kJ mol^{-1}	6.56
$\rho_{L,tp}$/kg L^{-1}	1.415	$c_{s,L,nbp}$/J K^{-1} mol^{-1}	45.6
T_{nbp}/K	87.3024	$\lambda_{L,nbp}$/J K^{-1} m^{-1} s^{-1}	0.12
$\Delta_{vap}H_{m,nbp}$/kJ mol^{-1}	6.46	$\eta_{L,nbp}$/10^{-6} Pa s	253
Solid properties			
$\rho_{s,tp}$/kg L^{-1}	1.623	$\Delta_{fus}H_{m,tp}$/kJ mol^{-1}	1.19
T_{tp}/K	83.8058	$\Delta_{sub}H_{m,tp}$/kJ mol^{-1}	7.75
p_{tp}/kPa	68.890	$c_{t,s,tp}$/J K^{-1} mol^{-1}	33.2
$(dT_{tp}/dp)_{mc}$/10^{-8} K Pa^{-1}	25	$\lambda_{s,tp}$/J K^{-1} m^{-1} s^{-1}	

Liquid-vapor and solid-vapor pressures (Ziegler 1962: 52–72 K (T_{48}); Chen 1971: 75–83.8 K; Wagner 1973: (with T_c = 150.70568 K: 84–150 K)

T_{68} (K)	p (kPa)	$\frac{dp}{dT}$ (kPa K^{-1})	$\frac{1}{p}\frac{dp}{dT}$ (%)	T_{68} (K)	p (kPa)	$\frac{dp}{dT}$ (kPa K^{-1})	$\frac{1}{p}\frac{dp}{dT}$ (%)	T_{68} (K)	p (kPa)	$\frac{dp}{dT}$ (kPa K^{-1})	$\frac{1}{p}\frac{dp}{dT}$ (%)
52	0.0613	0.0220	36	81	46.42	6.76	17.0	100	323.74	25.70	7.99
55	0.1697	0.0543	32	83	61.67	8.55	16.1	105	472.22	33.92	7.18
59	0.5590	0.1551	28	83.80	68.890	9.37	15.3	110	665.25	43.53	6.54
63	1.5784	0.383	24	84	70.45	8.08	11.47	115	909.83	54.5	5.99
66	3.161	0.697	22	85	78.90	8.82	11.18	120	1213.1	67.0	5.52
69	5.950	1.199	20	86	88.11	9.61	10.90	125	1582.4	81.0	5.12
72	10.616	1.961	18.5	87.30	101.325	10.700	10.56	130	2025.6	96.6	4.77
75	18.068	3.069	17.0	88	109.00	11.32	10.38	135	2551.1	113.9	4.47
77	25.153	4.053	16.1	90	133.50	13.21	9.90	140	3168.4	133.4	4.21
79	34.435	5.271	15.3	95	213.03	18.81	8.83	150	4733.7	183.6	3.88

Effect of impurities on T_{tp}, $(\delta T_S, \delta T_L)$/μK ppm^{-1} (•, information not available)

H_2: none

CH_4: −(80, 25), eutectic point at T = 71 K @ $x(CH_4)$ = 0.40.

CO: −(50, 24), eutectic point at T = 68 K @ x(CO) = 0.65. For x(CO) > 0.4, behavior like Ar in N_2

F_2: −(250, 10), eutectic point at T = 53 K @ $x(F_2)$ = 0.70. For higher $x(F_2)$, behavior like Ar in N_2

N_2: −(50, 22), eutectic point at T = 63.1 K @ $x(N_2)$ = 0.70.

Ne: $\delta T_L = 0$ within the measurement sensitivity (± 0.1 mK) up to amount concentration of 2×10^{-4}.
O_2: $-(35, 22)$, peritectic point at $T = 55.1$ K @ $x(O_2) = 0.20$. Solubility limit at $x(Ar) < 0.2$.
Kr: +(5, 5)
Xe: $-(\bullet, 6)$, eutectic point at $T = 82.3$ K @ $x(Xe) = 0.23$.

Notes and Warnings The fcc low-temperature phase of argon mixtures with N_2, O_2, and CO is reported to be stable up to the argon triple-point temperature, with the possibility of peritectic behavior just below T_{tp} (Barrett and Meyer 1965a, b). No troubles observed so far on the triple point realization, except few reports of peculiar behaviors in approaching the plateau, of no consequences.

Methane

CH_4, Relative Molecular Mass: 16.043

Critical point parameters			
T_c/K = 190.563	p_c/MPa = 4.5992	ρ_c/kg m^{-3} = 162.7	
Gas properties			
ρ(300 K, 1 bar)/kg m^{-3}	0.687	w_g(0 °C, 1 bar)/m s^{-1}	411
ρ(0 °C, 1 bar)/kg m^{-3}	0.755	$c_{p,g}$(0 °C, 1 bar)/J K^{-1} mol^{-1}	34.95
$\rho_{g,nbp}$/kg m^{-3}	1.816	λ_g(4.5 °C, 1 bar)/J K^{-1} m^{-1} s^{-1}	0.031
$\rho_{g,tp}$/kg m^{-3}	0.251	η_g(25 °C, 1 bar)/10^{-6} Pa s	11.1
Liquid properties			
$\rho_{L,nbp}$/kg L^{-1}	0.422	$\Delta_{vap}H_{m,tp}$/kJ mol^{-1}	8.73
$\rho_{L,tp}$/kg L^{-1}	0.451	$c_{s,L,nbp}$/J K^{-1} mol^{-1}	53
T_{nbp}/K	111.667	$\lambda_{L,nbp}$/J K^{-1} m^{-1} s^{-1}	0.19
$\Delta_{vap}H_{m,nbp}$/kJ mol^{-1}	8.19	$\eta_{L,nbp}$/10^{-3} Pa s	116
Solid properties			
$\rho_{s,tp}$/kg L^{-1}	0.489	$\Delta_{fus}H_{m,tp}$/kJ mol^{-1}	0.938
T_{tp}/K	90.6935	$\Delta_{sub}H_{m,tp}$/kJ mol^{-1}	9.67
p_{tp}/kPa	11.696	$c_{t,s,tp}$/J K^{-1} mol^{-1}	43
$(dT_{tp}/dp)_{mc}$/10^{-8} K Pa^{-1}	26	$\lambda_{s,tp}$/J K^{-1} m^{-1} s^{-1}	
Solid-to-solid transition (second-order)			
T_{sst} = 20.48 K			

Liquid-vapor and solid-vapor pressures (Freeth and Verschoyle 1931: 70–85 K; IUPAC 1978: (with $T_c = 190.6136$ K), 90.7–190 K)

T_{68} (K)	p (kPa)	$\frac{dp}{dT}$ (kPa K^{-1})	$\frac{1}{p}\frac{dp}{dT}$ (%)	T_{68} (K)	p (kPa)	$\frac{dp}{dT}$ (kPa K^{-1})	$\frac{1}{p}\frac{dp}{dT}$ (%)	T_{68} (K)	p (kPa)	$\frac{dp}{dT}$ (kPa K^{-1})	$\frac{1}{p}\frac{dp}{dT}$ (%)
70	0.2572	0.0617	24	102	42.170	4.21	10.0	130	367.128	22.02	6.0
75	0.7873	0.1642	21	104	51.284	4.91	9.6	135	489.98	27.23	56
80	2.0911	0.383	18	106	61.877	5.69	9.2	140	640.53	33.1	5.2
85	4.9417	0.800	16	108	74.106	6.55	8.8	145	822.16	39.7	4.8
90.7	11.697	1.506	12.9	110	88.135	7.49	8.5	150	1038.32	46.9	4.5
92	13.805	1.723	12.5	111.7	101.325	8.34	8.2	155	1292.6	54.9	4.3
94	17.618	2.099	11.9	113	112.924	9.07	8.0	160	1588.6	63.7	4.0
96	22.239	2.532	11.4	115	132.21	10.23	7.7	170	2322.3	83.7	3.6
98	27.786	3.03	10.9	120	191.39	13.54	7.1	180	3276.0	107.9	3.3
100	34.384	3.58	10.4	125	268.66	17.47	6.5	190	4507.2	141.2	3.1

Effect of impurities on T_{tp}, $(\delta T_S, \delta T_L)$/μK ppm^{-1}

Ar: −(70, 35), eutectic point at $T = 71$ K @ $x(\mathrm{Ar}) = 0.60$.

C_2H_4: −(240, 40), eutectic point at $T = 84.5$ K @ $x(C_2H_4) = 0.122$; solubility limit at $x(\mathrm{Ar}) = 0.025$.

C_2H_6: −(120, 70), eutectic point at $T = 73$ K @ $x(C_2H_6) = 0.3$.

C_3H_8: −(100, 60), eutectic point at $T = 70$ K @ $x(C_2H_4) = 0.5$.

Kr: +(12, 20)
N_2: −(65, 40), eutectic point at $T = 62.6$ K @ $x(N_2) = 0.762$; solubility limit at $x(Ar) = 0.45$.
O_2: −(100, 50), eutectic point at $T = 51$ K @ $x(O_2) = 0.92$.
CO_2: −600 μK with 10^{-5} amount of substance fraction, then constant up to 10^{-4}.

Notes and Warnings Methane has atoms with three different spin species; therefore, in principle, a catalyst should be used to ensure spin equilibrium at any temperature, but this is not usually done. However, occasional problems in the realization of the triple points have been reported (see Chap. 2).

Krypton

Kr, Relative Molecular Mass: 83.80

Critical point parameters			
T_c/K = 209.3	p_c/MPa = 5.50	ρ_c/kg m^{-3} = 908	
Gas properties			
ρ(300 K, 1 bar)/kg m^{-3}	3.413	w_g(0 °C, 1 bar)/m s^{-1}	224
ρ(0 °C, 1 bar)/kg m^{-3}	3.749	$c_{p,g}$(0 °C, 1 bar)/J K^{-1} mol^{-1} = c_p^0	= 2.5 × R ≅ 20.786
$\rho_{g,nbp}$/kg m^{-3}	8.7	λ_g(0 °C, 1 bar)/J K^{-1} m^{-1} s^{-1}	0.0087
$\rho_{g,tp}$/kg m^{-3}	6.4	η_g(25 °C, 1 bar)/10^{-6} Pa s	25.0
Liquid properties			
$\rho_{L,nbp}$/kg L^{-1}	2.42	$\Delta_{vap}H_{m,tp}$/kJ mol^{-1}	9.13
$\rho_{L,tp}$/kg L^{-1}	2.44	$c_{s,L,nbp}$/J K^{-1} mol^{-1}	44.2
T_{nbp}/K	119.81	$\lambda_{L,nbp}$/J K^{-1} m^{-1} s^{-1}	0.09
$\Delta_{vap}H_{m,nbp}$/kJ mol^{-1}	9.01	$\eta_{L,nbp}$/10^{-3} Pa s	400
Solid properties			
$\rho_{s,tp}$/kg L^{-1}	2.825	$\Delta_{fus}H_{m,tp}$/kJ mol^{-1}	1.64
T_{tp}/K	115.776	$\Delta_{sub}H_{m,tp}$/kJ mol^{-1}	10.77
p_{tp}/kPa	73.15	$c_{t,s,tp}$/J K^{-1} mol^{-1}	35
$(dT_{tp}/dp)_{mc}$/10^{-8} K Pa^{-1}	32	$\lambda_{s,tp}$/J K^{-1} m^{-1} s^{-1}	

Liquid-vapor and solid-vapor pressures (Ziegler 1964)

T_{48} (K)	p (kPa)	$\frac{dp}{dT}$ (kPa K^{-1})	$\frac{1}{p}\frac{dp}{dT}$ (%)	T_{48} (K)	p (kPa)	$\frac{dp}{dT}$ (kPa K^{-1})	$\frac{1}{p}\frac{dp}{dT}$ (%)	T_{48} (K)	p (kPa)	$\frac{dp}{dT}$ (kPa K^{-1})	$\frac{1}{p}\frac{dp}{dT}$ (%)
70	0.0368	0.010	28	100	11.90	1.59	13.3	116	74.54	6.25	8.39
73	0.0816	0.021	25	102	15.56	2.00	12.8	117	81.00	6.67	8.23
77	0.2142	0.049	23	104	19.88	2.45	12.3	118	87.89	7.11	8.09
80	0.4138	0.087	21	106	25.32	3.00	11.9	119	95.23	7.56	7.94
83	1.116	0.218	20	108	31.96	3.65	11.4	119.8	101.325	7.924	7.82
87	1.606	0.285	18	110	39.99	4.40	11.0				
90	2.688	0.45	17	112	49.27	5.23	10.6				
93	4.348	0.67	15	114	61.16	6.26	10.2				
97	7.87	1.12	14	115.9	73.150	7.205	9.85				

Effect of impurities on T_{tp}, $(\delta T_S, \delta T_L)$/μK ppm^{-1} (•, information not available)

Ar: −(35, 20), close to ideal solution.

CH_4: −(40, 20), close to ideal solution.

O_2: −(•, 60), eutectic point at T = 53.94 K @ $x(O_2)$ = 0.92; solubility limit at $x(K_r) > 0.8$.

Xenon

Xe, Relative Molecular Mass: 131.29

Critical point parameters			
T_c/K = 289.7	p_c/MPa = 5.84	ρ_c/kg m^{-3} = 1100	
Gas properties			
ρ(300 K, 1 bar)/kg m^{-3}	5.369	w_g(0 °C, 1 bar)/m s^{-1}	168
ρ(0 °C, 1 bar)/kg m^{-3}	5.897	$c_{p,g}$(0 °C, 1 bar)/J K^{-1} mol^{-1}	21.08
$\rho_{g,nbp}$/kg m^{-3}	∼12	λ_g(0 °C, 1 bar)/J K^{-1} m^{-1} s^{-1}	0.0051
$\rho_{g,tp}$/kg m^{-3}	8	η_g(25 °C, 1 bar)/10^{-6} Pa s	22.7
Liquid properties			
$\rho_{L,nbp}$/kg L^{-1}	3.06	$\Delta_{vap}H_{m,tp}$/kJ mol^{-1}	12.75
$\rho_{L,tp}$/kg L^{-1}	3.08	$c_{s,L,nbp}$/J K^{-1} mol^{-1}	44.6
T_{nbp}/K	165.06	$\lambda_{L,nbp}$/J K^{-1} m^{-1} s^{-1}	0.073
$\Delta_{vap}H_{m,nbp}$/kJ mol^{-1}	12.64	$\eta_{L,nbp}$/10^{-3} Pa s	528
Solid properties			
$\rho_{s,tp}$/kg L^{-1}	3.54	$\Delta_{fus}H_{m,tp}$/kJ mol^{-1}	2.315
T_{tp}/K	161.406	$\Delta_{sub}H_{m,tp}$/kJ mol^{-1}	15.06
p_{tp}/kPa	81.71	$c_{t,s,tp}$/J K^{-1} mol^{-1}	35.5
$(dT_{tp}/dp)_{mc}$/10^{-8} K Pa^{-1}	39	$\lambda_{s,tp}$/J K^{-1} m^{-1} s^{-1}	

Liquid-vapor and solid-vapor pressures (Ziegler 1966)

T_{48} (K)	p (kPa)	$\frac{dp}{dT}$ (kPa K^{-1})	$\frac{1}{p}\frac{dp}{dT}$ (%)	T_{48} (K)	p (kPa)	$\frac{dp}{dT}$ (kPa K^{-1})	$\frac{1}{p}\frac{dp}{dT}$ (%)	T_{48} (K)	p (kPa)	$\frac{dp}{dT}$ (kPa K^{-1})	$\frac{1}{p}\frac{dp}{dT}$ (%)
90	0.0077	0.0018	24	120	1.505	0.197	13.1	150	34.05	2.82	8.3
93	0.0153	0.0034	22	123	2.206	0.274	12.4	153	43.43	3.45	7.9
97	0.0356	0.0072	20	127	3.57	0.415	11.6	156	54.88	4.20	7.7
100	0.064	0.0122	19	130	5.02	0.556	11.1	159	68.75	5.06	7.4
103	0.112	0.0200	18	133	6.94	0.774	10.6	161.4	81.710	5.84	7.21
107	0.222	0.0368	17	137	10.47	1.041	10.0	162	84.82	5.09	6.00
110	0.360	0.056	16	140	14.02	1334	9.5	163	90.03	5.3	5.90
113	0.568	0.084	14.8	143	18.54	1.69	9.1	164	95.49	5.59	5.85
117	1.006	0.139	13.8	147	26.43	2.28	8.6	165.1	101.325	5.85	5.77

Effect of impurities on T_{tp}, $(\delta T_S, \delta T_L)/\mu K\ ppm^{-1}$ (•, information not available)
O_2: −(•, 100), eutectic point at T unknown and $x(O_2) > 0.9$.

Notes and Warnings Isotopic composition is not reproducible from sample to sample, causing an uncertainty at T_{tp} of more than ± 2 mK. Isotope distillation occurs in vapor pressure measurements.

Carbon Dioxide

CO_2, Relative Molecular Mass: 44.009

Critical point parameters			
T_c/K = 304.20	p_c/MPa = 7.3825	ρ_c/kg m^{-3} = 466	
Gas properties			
ρ(300 K, 1 bar)/kg m^{-3}	1.773	w_g(0 °C, 1 bar)/m s^{-1}	260
ρ(0 °C, 1 bar)/kg m^{-3}	1.951	$c_{p,g}$(0 °C, 1 bar)/J K^{-1} mol^{-1}	36.3
$\rho_{g,nbp}$/kg m^{-3}	n.a.	λ_g(4.5 °C, 1 bar)/J K^{-1} m^{-1} s^{-1}	0.015
$\rho_{g,tp}$/kg m^{-3}	14.0	η_g(25 °C, 1 bar)/10^{-6} Pa s	15.1
Liquid properties			
$\rho_{L,nbp}$/kg L^{-1}	n.a.	$\Delta_{vap}H_{m,tp}$/kJ mol^{-1}	13.55
$\rho_{L,tp}$/kg L^{-1}	1.178	$c_{s,L,nbp}$/J K^{-1} mol^{-1}	64.1
T_{nbp}/K	n.a.	$\lambda_{L,nbp}$/J K^{-1} m^{-1} s^{-1}	130
$\Delta_{vap}H_{m,nbp}$/kJ mol^{-1}	n.a.	$\eta_{L,nbp}$/10^{-3} Pa s	
		p(0.01 °C)/MPa	3.38 608
Solid properties			
$\rho_{s,tp}$/kg L^{-1}	1.530	$\Delta_{fus}H_{m,tp}$/kJ mol^{-1}	8.65
T_{tp}/K	216.591	$\Delta_{sub}H_{m,tp}$/kJ mol^{-1}	22.19
p_{tp}/kPa	517.980	$c_{t,s,tp}$/J K^{-1} mol^{-1}	55.7
$(dT_{tp}/dp)_{mc}$/10^{-8} K Pa^{-1}	11	$\lambda_{s,tp}$/J K^{-1} m^{-1} s^{-1}	
T_{sub}(1 bar)/K	194.68	$\Delta_{sub}H_m$(1 bar)/kJ mol^{-1}	25.2

Liquid-vapor and solid-vapor pressures (Fernandez and Del Rio 1984)

T_{68} (K)	p (kPa)	$\frac{dp}{dT}$ (kPa K^{-1})	$\frac{1}{p}\frac{dp}{dT}$ (%)	T_{68} (K)	p (kPa)	$\frac{dp}{dT}$ (kPa K^{-1})	$\frac{1}{p}\frac{dp}{dT}$ (%)	T_{68} (K)	p (kPa)	$\frac{dp}{dT}$ (kPa K^{-1})	$\frac{1}{p}\frac{dp}{dT}$ (%)
194	95.827	7.88	8.22	212	377.113	26.57	7.04	232	962.78	35.85	3.72
194.7	101.325	8.28	8.17	214	433.669	30.05	6.93	234	1036.48	37.86	3.65
196	112.793	9.11	8.08	216.6	517.980	35.14	6.79	236	1114.27	39.93	3.58
198	132.383	10.51	7.94	218	550.447	23.58	4.28	238	1196.25	42.07	3.52
200	154.943	12.09	7.80	220	599.154	25.14	4.20	240	1282.57	44.27	3.45
202	180.855	13.86	7.66	222	651.048	26.77	4.11	242	1373.36	46.53	3.39
204	210.544	15.86	7.54	224	706.256	28.45	4.03	243	1420.47	47.69	3.36
206	244.475	18.11	7.41	226	764.906	30.21	3.95				
208	283.162	20.62	7.28	228	827.125	32.02	3.87				
210	327.169	23.43	7.16	230	893.042	33.90	3.80				

Effect of impurities on T_{tp}, $(\delta T_S, \delta T_L)/\mu K\ ppm^{-1}$ (•, information not available)
CH_4: −(•, ∼15), nearly no eutectic point (see CH_4 and Davis et al. 1962).
C_2H_6: −(•, ∼30).
C_3H_8: −(•, ∼35).

Notes and Warnings Premelting effects starting as low as −1 K from T_{tp} have been reported to occur sometimes with very pure carbon dioxide, but no explanation is available.

Ethane

C_2H_6, Relative Molecular Mass: 30.070

Critical point parameters			
T_c/K = 305.5	p_c/MPa = 49.1	ρ_c/kg m^{-3} = 212.2	
Gas properties			
ρ(300 K, 1 bar)/kg m^{-3}	1.23	w_g(0 °C, 1 bar)/m s^{-1}	
ρ(0 °C, 1 bar)/kg m^{-3}	1.35	$c_{p,g}$(0 °C, 1 bar)/J K^{-1} mol^{-1}	53.4
$\rho_{g,nbp}$/kg m^{-3}	2.0	λ_g(0 °C, 1 bar)/J K^{-1} m^{-1} s^{-1}	
$\rho_{g,tp}$/kg m^{-3}	∼0	η_g(25 °C, 1 bar)/10^{-6} Pa s	
Liquid properties			
$\rho_{L,nbp}$/kg L^{-1}	0.546	$\Delta_{vap}H_{m,tp}$/kJ mol^{-1}	17.90
$\rho_{L,tp}$/kg L^{-1}	0.659	$c_{s,L,nbp}$/J K^{-1} mol^{-1}	68.5
T_{nbp}/K	184.5	$\lambda_{L,nbp}$/J K^{-1} m^{-1} s^{-1}	
$\Delta_{vap}H_{m,nbp}$/kJ mol^{-1}	14.72	$\eta_{L,nbp}$/10^{-3} Pa s	
Solid properties			
$\rho_{s,tp}$/kg L^{-1}	0.693	$\Delta_{fus}H_{m,tp}$/kJ mol^{-1}	0.582
T_{tp}/K	90.360	$\Delta_{sub}H_{m,tp}$/kJ mol^{-1} (solid I)	18.48
p_{tp}/kPa	0.0010	$c_{l,s,tp}$/J K^{-1} mol^{-1}	
$(dT_{tp}/dp)_{mc}$/10^{-8} K Pa^{-1}	16	$\lambda_{s,tp}$/J K^{-1} m^{-1} s^{-1}	
Solid-to-solid transition (first-order)			
T_{II-I} = 89.842 K	$\Delta_{tra}H_{m,II-I}$/kJ mol^{-1} = 2.05		
Solid-to-solid transition (first-order)			
T_{III-II} = 89.734 K	$\Delta_{tra}H_{m,III-II}$/kJ mol^{-1} = 0.09		
$\Delta H_{m,III-I}$/kJ mol^{-1} = 2.256	$\Delta_{sub}H_{m,tr}$/kJ mol^{-1} (solid III) = 20.84		

Liquid-vapor pressures (Ziegler 1964)

T_{48} (K)	p (kPa)	$\frac{dp}{dT}$ (kPa K^{-1})	$\frac{1}{p}\frac{dp}{dT}$ (%)	T_{48} (K)	p (kPa)	$\frac{dp}{dT}$ (kPa K^{-1})	$\frac{1}{p}\frac{dp}{dT}$ (%)	T_{48} (K)	p (kPa)	$\frac{dp}{dT}$ (kPa K^{-1})	$\frac{1}{p}\frac{dp}{dT}$ (%)
90.4	0.001	0.0003	27	147	7.36	0.66	9.0	180	78.8	4.51	5.7
110	0.073	0.0125	17	150	9.58	0.82	8.6	182	88.2	4.92	5.6
115	0.165	0.0256	16	153	12.3	1.01	8.2	184.5	101.325	5.492	5.42
120	0.347	0.049	14	157	11.0	1.31	7.8				
125	0.684	0.088	13	160	21.3	1.59	7.4				
130	1.27	0.150	12	163	26.6	1.90	7.1				
133	1.80	0.203	11	167	35.1	2.37	6.8				
137	2.78	0.295	10.6	170	42.8	2.78	6.5				
140	3.78	0.378	10.0	173	51.8	3.23	6.3				
143	5.08	0.486	9.6	177	66.1	3.93	5.9				

Effect of impurities on T_{tp}, $(\delta T_S, \delta T_L)/\mu K\ ppm^{-1}$ (•, information not available)
CH_4: −(80, 26), eutectic point at $T = 73$ K @ $x(CH_4) = 0.7$.
C_2H_4: −(30, 25), eutectic point at $T = 87$ K @ $x(C_2H_4) = 0.3$.
C_3H_8: −(40, 25), eutectic point at $T = 72$ K @ $x(C_3H_8) = 0.52$.

N_2: $-(20, 10)$, full diagram not available.
O_2: $< -(\bullet, < 10)$, eutectic point at $T = 84$ K @ $x(O) = 0.26$.
CO_2: soluble up to $x(CO_2) < 0.1$ and form an eutectic with a small T_{tp} depression (available diagram too small to quantify).

Notes and Warnings Solid-to-solid transitions show very long equilibration time; extremely difficult to perform correctly (Pavese 1978b).

Propane

C_3H_8, Relative Molecular Mass: 44.097 21

Critical point parameters			
T_c/K = 369.775	p_c/MPa = 4.242	ρ_c/kg m^{-3} = 219	
Gas properties			
ρ(300 K, 1 bar)/kg m^{-3}	1.80	w_g(0 °C, 1 bar)/m s^{-1}	214
ρ(0 °C, 1 bar)/kg m^{-3}	1.96	$c_{p,g}$(0 °C, 1 bar)/J K^{-1} mol^{-1}	
$\rho_{g,nbp}$/kg m^{-3}	2.20	λ_g(0 °C, 1 bar)/J K^{-1} m^{-1} s^{-1}	
$\rho_{g,tp}$/kg m^{-3}	2×10^{-5}	η_g(25 °C, 1 bar)/10^{-6} Pa s	
Liquid properties			
$\rho_{L,nbp}$/kg L^{-1}	0.528	$\Delta_{vap}H_{m,tp}$/kJ mol^{-1}	23.0
$\rho_{L,tp}$/kg L^{-1}	0.666	$c_{s,L,nbp}$/J K^{-1} mol^{-1}	99.0
T_{nbp}/K	231.079	$\lambda_{L,nbp}$/J K^{-1} m^{-1} s^{-1}	
$\Delta_{vap}H_{m,nbp}$/kJ mol^{-1}	18.9	$\eta_{L,nbp}$/10^{-3} Pa s	
P(300 K)/kPa	999.7	ρ_L(300)/kg L^{-1}	0.489
		$C_{s,L}$(300)/J K^{-1} mol^{-1}	119.2
Solid properties			
$\rho_{s,tp}$/kg L^{-1}		$\Delta_{fus}H_{m,tp}$/kJ mol^{-1}	3.50
T_{tp}/K	85.528	$\Delta_{sub}H_{m,tp}$/kJ mol^{-1}	26.50
p_{tp}/kPa	3×10^{-7}	$c_{t,s,tp}$/J K^{-1} mol^{-1}	
$(dT_{tp}/dp)_{mc}$/10^{-8} K Pa^{-1}		$\lambda_{s,tp}$/J K^{-1} m^{-1} s^{-1}	

Liquid-vapor and solid-vapor pressures (Goodwin 1977)

T_{68} (K)	p (kPa)	$\frac{dp}{dT}$ (kPa K^{-1})	$\frac{1}{p}\frac{dp}{dT}$ (%)	T_{68} (K)	p (kPa)	$\frac{dp}{dT}$ (kPa K^{-1})	$\frac{1}{p}\frac{dp}{dT}$ (%)	T_{68} (K)	p (kPa)	$\frac{dp}{dT}$ (kPa K^{-1})	$\frac{1}{p}\frac{dp}{dT}$ (%)
85,5	3×10^{-6}			175	3.297	0.2760	8.4	225	75.79	3.616	4.77
125	0.0076	0.0013	17.1	180	4.949	0.3886	7.9	231.1	101.325	4.489	4.43
135	0.0378	0.0056	14.8	185	7.238	0.5343	7.4	240	148.0	6.015	4.06
140	0.0770	0.0105	13.6	190	10.35	0.7193	6.9	250	218.2	8.090	3.70
145	0.1487	0.0189	12.7	195	14.51	0.9494	6.5	260	311.2	10.58	3.40
150	0.2741	0.0323	11.8	200	19.93	1.231	6.2	270	431.2	13.50	3.13
155	0.4840	0.0531	11.0	205	26.91	1.570	5.8	275	502.8	15.14	3.01
160	0.8220	0.0841	10.2	210	35.74	1.973	5.5	280	582.8	16.89	2.89
165	1.347	0.1287	9.6	215	46.75	2.444	5.2	290	770.6	20.76	2.69
170	2.139	0.1912	8.9	220	60.31	2.990	5.0	300	999.7	25.14	2.51

Effect of impurities on T_{tp}, $(\delta T_S, \delta T_L)/\mu K\ ppm^{-1}$ (•, information not available)

CH_4: −(•, 40), eutectic point at $T = 70$ K @ $x(CH_4) = 0.5$. "Glassy" state claimed up to near the eutectic composition. For a probable reason see Notes.

C_2H_6: −(•, 40), eutectic point at $T \cong 72$ K @ $x(C_2H_6) = 0.48$. "Glassy" state claimed: see above.

CO_2: soluble up to $x(CO_2) < 0.1$ and form an eutectic with a small T_{tp} depression (available diagram too small to quantify).
O_2: −(•, 20), eutectic point at $T = 83.5$ K @ $x(O_2) = 0.08$.

Notes and Warnings Propane shows a very large liquid subcooling (as large as 8 K). In connection with this, propane has a *metastable phase* undergoing melting at $T_{tp}^{II} = 81.234$ K, with $\Delta_{fus}H_{m,tpII} = 2.4$ kJ mol^{-1}. A solid-to-solid transition between the two phases has been observed from 79.6 to 81.2 K, with $\Delta_{tra}H_{m,tr} = -0.70$ kJ mol^{-1} (the phase transformation is exothermic; Pavese and Besley 1981b).

Appendix D
Vapor Pressure Equations

It is difficult to select vapor pressure equations, not because their number for each substance is small, but because it is difficult either to trace them to ITS-90 or to obtain a reliable uncertainty value for most of them, or because it is difficult, and often impossible, to find a full study of the effect of impurities on the experimental values on which they are based.

Table D.1 reports the equations that are the best according to the aforementioned requirements, many of them having had translated to T_{90} (Pavese 1993). They are generally restricted to a pressure range extending from the lowest pressure values that allows preserving the indicated uncertainty up to about 0.1 MPa.

Table D.2 collects some other equations, which show a higher uncertainty but are usable in an extended pressure range. The sensitivity $\mathrm{d}p/\mathrm{d}T$ at selected temperatures also tabulated (see also Fig. 4.9).

Table D.1 Best vapor pressure equations

Equilibrium state[a]	T (K)[b]	Uncertainty δT (mK)[c]	Purity of material (%)[d]	References
Liquid-vapor phases of ^{3}He	0.65–3.2	0.1 (0.5)	99.999	ITS-90
	$T_{90}/\mathrm{K} = A_0 + \sum_{i=1}^{9} A_i[(\ln(p/\mathrm{Pa}) - B)/C]^i$			
	Coefficients in Table A.3			
Liquid-vapor phases of ^{4}He	1.25–2.18 and 2.18–5.0	0.1 (0.5)	99.999	ITS-90
	$T_{90}/\mathrm{K} = A_0 + \sum_{i=1}^{n} A_i[(\ln(p/\mathrm{Pa}) - B)/C]^i$			
	Coefficients in Table A.3			
Liquid-vapor phases of equilibrium hydrogen	17.025–17.045	0.1	99.99	ITS-90
	$T_{90}/\mathrm{K} - 17.035 = (p/\mathrm{kPa} - 33.3213)/13.32$			
	20.26–20.28			
	$T_{90}/\mathrm{K} - 20.27 = (p/\mathrm{kPa} - 101.292)/30$			
	13.8–20.3	1[e]	99.99	Pavese 1993 (Ancsin 1997[f])

F. Pavese, G. Molinar Min Beciet, *Modern Gas-Based Temperature and Pressure Measurements,* International Cryogenics Monograph Series,
DOI 10.1007/978-1-4419-8282-7, © Springer Science+Business Media New York 2013

Table D.1 Best vapor pressure equations

Equilibrium state[a]	T (K)[b]	Uncertainty δT (mK)[c]	Purity of material (%)[d]	References
	$p/p_0 = \exp\left[A + B/(T_{90}/\mathrm{K}) + CT_{90}/\mathrm{K}\right] + \sum_{i=1}^{5} b_i (T_{90}/\mathrm{K})^i$ $A = 4.037\,592\,968, \quad B = -101.277\,5246,$ $C = 0.047\,833\,3313, \quad b_0 = 1902.885\,683,$ $b_1 = -331.228\,2212, \quad b_2 = 32.253\,417\,74,$ $b_3 = -2.106\,674\,684, \quad b_4 = 0.060\,293\,573,$ $b_5 = 0.000\,645\,154$			
Solid-vapor phases of natural neon[f,g]	20.0–24.6	2	99.99	Pavese 1993 (Ancsin 1974a[f]; Tiggelman 1973)
	$\ln(p/p_0) = A + B/(T_{90}/\mathrm{K}) + C(T_{90}/\mathrm{K}) + D(T_{90}/\mathrm{K})^2$ $A = 11.471\,649\,42, \quad B = -269.697\,6862,$ $C = -0.099\,675\,5105, \quad D = 0.001\,841\,2174$			
Liquid-vapor phases of natural neon[g,h]	24.6–27.1	2	99.99	Pavese 1993 (Ancsin 1978[f]; Tiggelman 1973; Furukawa 1972)
	$\ln(p/p_0) = A + B/(T_{90}/\mathrm{K}) + C(T_{90}/\mathrm{K}) + D(T_{90}/\mathrm{K})^2$ $A = 11.206\,308\,45, \quad B = -249.362\,3787,$ $C = -0.110\,540\,081, \quad D = 0.001\,350\,4837$			
Solid-vapor phases of nitrogen	56.0–63.1	2	99.999	Pavese 1993 (Ancsin 1974a[f])
	$\ln(p/p_0) = A + B/(T_{90}/\mathrm{K}) + C(T_{90}/\mathrm{K})$ $A = 12.078\,566\,55, \quad B = -858.004\,6109,$ $C = -0.009\,224\,098$			
Liquid-vapor phases of nitrogen	63.2–77.4	2	99.999	Pavese 1993 (Ancsin 1974a[f])
	$\ln(p/p_0) = A + B/(T_{90}/\mathrm{K}) + C(T_{90}/\mathrm{K}) + D(T_{90}/\mathrm{K})^2$ $A = 15.260\,171, \quad B = -880.842\,4122,$ $C = -0.070\,838\,754, \quad D = 0.000\,226\,855\,75$			
Liquid-vapor phases of oxygen	67[j]–90.2	1	99.999	Pavese 1993 (Ancsin 1974b[f]; Tiggelman 1973)
	$\ln(p/p_0) = A + B/(T_{90}/\mathrm{K}) + C(T_{90}/\mathrm{K}) + D(T_{90}/\mathrm{K})^2 + E(T_{90}/\mathrm{K})^3 + F(T_{90}/\mathrm{K})^4$ $A = 34.847\,668\,61, \quad B = -1802.699\,664,$ $C = 11\,747.389\,23, \quad D = -0.311\,382\,523$ $E = 0.001\,834\,5399, \quad F = -4.285\,2574 \times 10^{-6}$			
Solid-vapor phases of argon	81.0[i]–83.7	1.5	99.999	Pavese 1993 (Ancsin 1973b[f])
	$\ln p = A + B/(T_{90}/\mathrm{K})$ $A = 22.548\,794, \quad B = -956.102\,217$			
Liquid-vapor phases of argon	83.8–87.3	1	99.999	Pavese 1993 (Ancsin 1973b[f])
	$\ln(p/p_0) = A + B/(T_{90}/\mathrm{K}) + C(T_{90}/\mathrm{K})$ $A = 10.592\,150\,77, \quad B = -864.739\,442,$ $C = -0.007\,870\,4304$			

Table D.1 Best vapor pressure equations

Equilibrium state[a]	T (K)[b]	Uncertainty δT (mK)[c]	Purity of material (%)[d]	References
Liquid-vapor phases of methane	90.7–190	5[k]	99.99	Pavese 1993 (IUPAC 1978)
	$\ln(p/p_c) = T_c/T_{90}[A\tau + B\tau^{1.5} + C\tau^{2.5} + D\tau^5]; \tau = 1 - T_{90}/T_c$			
	$A = -6.047\,641\,425, \quad B = 1.346\,053\,934,$			
	$C = -0.660\,194\,779, \quad D = -1.304\,583\,684$			
	$T_c = 190.568$ K, $\quad p_c = 4.595$ MPa			
Liquid-vapor phases of carbon dioxide	216.6–304	15	99.99	Pavese 1993 (IUPAC 1976)
	$\ln(p/p_c) = A_0(1 - T_{90}/T_c)^{1.935} + \sum_{i=1}^{4} A_i \left(\frac{T_c}{T_{90}} - 1\right)^i$			
	$A_0 = 11.374\,539\,29, \quad A_1 = -6.886\,475\,61,$			
	$A_2 = -9.589\,976\,75, \quad A_3 = 13.674\,8941,$			
	$p_c = 7.3825$ MPa, $\quad T_c = 304.2022$ K			

[a] The vapor pressures equations included in the ITS-90 definition are shown in *first three rows*. ($p_0 = 101\,325$ Pa)

[b] Temperature values are given in ITS-90, T_{90}, when part of the Scale definition. For the other equations, when the uncertainty is better than ≈ 10 mK it is not possible to make a simple correction, because the relationship $(T_{90} - T_{68}) = \Delta T = f(T_{90})$ is not linear. Until the coefficients of these equations are recalculated from the data *individually* corrected to T_{90} or new data become available, T_{68} must still be used in the equations. The pressure value calculated for each T_{68} entry will then be attributed to the corresponding T_{90} value obtained from Table A.6. Few equations are given for a generic temperature θ, as no scale indication was even available. For conversion between temperature scales see Appendix A, Table A.6 and its Notes, and Table 4.4. In the range below 13.8 K the previous scale was not the IPTS-68, but the EPT-76. The deviations $(T_{90} - T_{76})$ are very small, e.g., -0.4 mK at 8 K and -1.0 mK at 13.8 K; consequently in these equations T_{90} can be used instead of T_{76}

[c] The uncertainty value in square brackets is the thermodynamic standard uncertainty (BIPM 1990)

[d] Minimum purity of the material to which the listed values of temperature and uncertainty apply (see Table D.1)

[e] The summation term in the equation adds to the value of p a pressure amounting to the equivalent of 1 mK maximum

[f] Ancsin's equations are reported, as they are the only for which both the uncertainty and the effect of impurities are clearly indicated

[g] These values are for neon with an isotopic composition close to that specified in (BIPM 1990)

[h] There is no convenient way to obtain a "mean value" for vapor-pressure equations from different references. Therefore, for each substance, an equation from a particular reference is used. In every case the differences between it and the equivalent equations in the references in parentheses are within the uncertainty listed

[i] It has been tested (Pavese 1981) that this equation actually represents the vapor pressure of solid argon down to 47 K ($p = 9$ Pa). Below 50 K it agrees with Ziegler et al. (1962a) within ± 2 Pa

[j] Below about 65 K the vapor pressure of oxygen is so low as to be of little use for accurate thermometry

[k] Uncertainty is ± 1 mK between 70 and 95 K

Table D.2 Other vapor pressure equations

Equilibrium state[a]	T (K)[b]	Uncertainty δT (mK)[c]	References	Sensitivity dp/dT (kPa K^{-1})
Liquid-vapor phases of ^{3}He	0.3–0.9	0.2 (0.5)	Zhokhovskii 1974, 1989, 1990	3.86 at 0.9 K
	0.9–3.2	1	Zhokhovskii 1974, 1989, 1990	107 at 3.2 K
	Eq. (a) $p = \left\{ p_0^{1-c} + \frac{\left(p_1^{1-c} - p_0^{1-c}\right)\left[1-\left(\frac{T_0}{T}\right)^n\right]}{\left[1-\left(\frac{T_0}{T}\right)^n\right]} \right\}^{\frac{1}{1-c}}$			
	Subscript: 0 at p, $T_{\min}$; 1 at p, $T_{\max}$ in the range			
	Eq. (a) : $T = T_{62}$;			
	$T_0 = 0.300$ K, $T_1 = 3.324$ K; $c = 0.952\,888$, $n = 0.345\,556$; $p_0 = 0.251\,7$ Pa, $p_1 = 707.193$ Pa			
	$T_0 = 0.900$ K, $T_1 = 3.324$ K; $c = 0.706\,538$, $n = -0.821.269$; $p_0 = 707.193$ Pa, $p_1 = 106.771$ Pa			
	0.2–3.3	T_{62} Scale[d]	Sydoriak et al. 1964	
	$\ln p = A + B\,T + C\,T^2 + D\,T^3 + E\,T^4 + F/T9 + G\ln T$			
	$A = 4.803\,86$, $B = -0{,}286\,001$, $C = 0.198\,608$, $D = -0.050\,223\,7$, $E = 0.005\,054\,86$, $F = -2.491\,74$, $G = 2.248\,46$			
	0.5–3.2	T_{76} Scale[e]	Durieux and Rusby 1983	
Liquid-vapor phases of ^{4}He	0.5–2.18	0.6	Zhokhovskii 1974, 1989, 1990	12.3 at 2.18 K
	2.18–5.2	1	Zhokhovskii 1974, 1989, 1990	173 at 5.2 K
	See Eq. (a) for ^{3}He: $T = T_{90}$;			
	$T_0 = 0.5$, $T_1 = 2.18$ K; $c = 0.983\,028$, $n = 0.580\,486$; $p_0 = 0.002\,063$ Pa, $p_1 = 508\,1.617$ Pa			
	$T_0 = 2.18$, $T_1 = 5.19$ K; $c = 0.966\,056$, $n = -1.036\,13$; $p_0 = 508\,1.617$ Pa, $p_1 = 226642.3$ Pa			
	0.5–5.2	T_{58} Scale[d]	Brickwedde et al. 1960	
	0.5–5.2	T_{76} Scale[e]	Durieux and Rusby 1983	
Solid-vapor phases of equilibrium hydrogen	10.5–13.8	10	Woolley et al. 1948 (Souers 1979, 1986; Mullins et al. 1961)	4.55 at 13.8 K
	$\log(p/\text{Pa}) = 6.74928 - 47.0172/(T_{90}/\text{K}) + 0.03635(T_{90}/\text{K})$			
	8–13.8	3	Pavese 1993 (Zhokhovskii 1974, 1989, 1990)	
	$T_{90}/\text{K} = A_0 + \sum_{i=1}^{4} A_i \left[\ln\left(\frac{p}{133.322}/\text{Pa}\right)\right]^i$			
	$A_0 = 9.445\,740\,15$, $A_1 = 0.783\,155\,123$, $A_2 = 0.055\,608\,068$, $A_3 = 0.004\,665\,781$, $A_4 = 0.000\,331\,861$			

Table D.2 (continued)

Equilibrium state[a]	T (K)[b]	Uncertainty δT (mK)[c]	References	Sensitivity dp/dT (kPa K^{-1})
	8–13.8	2 Pa	Pavese 1993 (Zhokhovskii 1974, 1989, 1990)	
		$p/\text{Pa} = 133.222\left(A_0 + \sum_{i=1}^{5} A_i (T_{90}/\text{K})^i\right)$ $A_0 = -53.520\,874\,9$, $A_1 = 33.679\,913\,7$, $A_2 = -8.832\,540\,10$, $A_3 = 1.204\,628\,68$, $A_4 = 0.085\,197\,66$ $A_5 = 0.002\,492\,82$		
Liquid-vapor phases of equilibrium hydrogen	13.8–23	1.5	Pavese 1993 (BIPM 1983; Ter Harmsel et al. 1967)	30.0 at 20.3 K
		$\ln(p/p_0) = A + B/(T_{90}/\text{K}) + C(T_{90}/\text{K}) + D(T_{90}/\text{K})^2$ $A = 4.060\,002\,052$, $B = -102.229\,7484$, $C = 0.049\,639\,6741$, $D = -0.000\,056\,296\,15$		
	20–32	–	Van Itterbeek et al. 1964 (Weber et al. 1962)	157 at 31.5 K (1 MPa)
		$\ln(p/\text{Pa}) = 7.676\,96 - 71.102/(\theta/\text{K}) + 2.444\,98 \ln \theta/\text{K}$		
Solid-vapor phases of natural neon	13.8–24.5	1.5	Pavese 1993 (Zhokhovskii 1974, 1989, 1990; Ziegler et al. 1970; Grilly 1962)	2.48 at 20 K
	See Eq. (a) for ^{3}He: $T = T_{90}$; $c = 0.995\,3181$, $n = 0.856\,9276$; $T_0 = 10$ K, $T_1 = 24.55$ K $p_1 = 0.012\,761$ Pa, $p_2 = 43\,240.07$ Pa			
Liquid-vapor phases of natural neon	24.6–40	6	Pavese 1993 (Zhokhovskii 1974, 1989, 1990; Ziegler et al. 1970)	16.0 at 24.6 K 30.6 at 27.1 K 214 at 40 K
	See Eq. (a) for ^{3}He: $T = T_{90}$; $c = 0.854\,332$, $n = -0.129\,166$; $T_0 = 24.5622$ K (IPTS-68), $T_1 = 40$ K $p_1 = 43\,400$ Pa, $p_2 = 1\,460\,422$ Pa			
	24.6–40	–	Pavese 1993 (Preston-Thomas 1976)	(1.45 MPa)
		$\ln(p/p_0) = A + B/(T_{90}/\text{K}) + C(T_{90}/\text{K}) + D(T_{90}/\text{K})^2$ $A = 4.619\,489\,43$, $B = -106.478\,268$, $C = -0.036\,993\,7132$, $D = 0.000\,042\,561\,01$		
Solid-vapor phases of nitrogen	35–63.1	20	Frels et al. 1974 (Ziegler et al. 1963)	0.135 at 50 K
Liquid-vapor phases of nitrogen	63.2–84	2	Pavese 1993 (Preston-Thomas 1976; Moussa 1966; Ziegler and Mullins 1963)	2.3 at 63 K 12 at 77.3 K
		$\log p/p_0 = A + B/(T_{90}/\text{K}) + C \log((T_{90}/\text{K})/T_0)$ $+ D(T_{90}/\text{K}) + E(T_{90}/\text{K})^2$		

Table D.2 (continued)

Equilibrium state[a]	T (K)[b]	Uncertainty δT (mK)[c]	References	Sensitivity dp/dT (kPa K^{-1})
	$A = 5.831\,051\,804$, $B = -397.023\,9009$, $C = -2.043\,082\,307$, $D = -0.014\,356\,880$, $E = 68\,890\,944 \times 10^{-6}$, $T_0 = 77.3516$ K			
	64–125	5	Pavese 1993 (Wagner 1973)	86 at 110 K (1.5 MPa)
	$\ln p/p_c = T_c/T_{90}(A\,\tau + B\,\tau^{1.5} + C\,\tau^3 + D\,\tau^6)$; $\tau = 1 - T_{68}/T_c$ $A = -6.102\,733\,65$, $B = 1.153\,844\,492$, $C = -1.087\,106\,903$, $D = -1.759\,094\,154$ $T_c = 126.2124$ K, $p_c = 3.399\,97$ MPa			
Liquid-vapor phases of oxygen	54–154	2	Pavese 1993 (Wagner et al. 1976; Mullins et al. 1962)	0.5 at 65 K
	$\ln(p/p_c) = T_c/T_{90}(A\,\tau + B\,\tau^{1.5} + C\,\tau^3 + D\,\tau^7 + E\,\tau^9)$ $\tau = 1 - T_{90}/T_c$ $A = -6.044\,437\,278$, $B = 1.176\,127\,337$, $C = -0.994\,073\,392$, $D = -3.449\,554\,987$, $E = 3.343\,141\,113$ $T_c = 154.5947$ K, $p_c = 5.0430$ MPa			10.6 at 90 K 59 at 120 K (1 MPa) 1.4 at 70 K
Solid-vapor phases of argon	57–83.8	10	Pavese 1993 (Zhokhovskii 1974, 1989, 1990; Leming and Pollack 1970; Ziegler et al. 1962a)	
	See Eq. (a) for ^{3}He: $T = T_{90}$; $c = 1.033\,500\,172$, $n = -1.300\,578$; $T_0 = 62.0039$ K, $T_1 = 83.8058$ K $p_1 = 1246$ Pa, $p_2 = 68\,890$ Pa			
	75–83.8	3	Pavese 1993 (Chen et al. 1971)	
	$\log(p/\text{Pa}) = 9.788\,783 - 414.898\,553/(T_{90}/\text{K})$			
Liquid-vapor phases of argon	84–150	5	Pavese 1993 (Wagner, 1973)	7.9 at 83.8 K
	$\ln(p/p_c) = T_c/T_{90}(A\,\tau + B\,\tau^{1.5} + C\,\tau^3 + D\,\tau^6)$; $\tau = 1 - T_{90}/T_c$			10.7 at 87.3 K
	$A = -5.906\,852\,299$, $B = 1.132\,416\,723$, $C = -0.772\,007\,200$, $D = -1.671\,235\,815$ $T_c = 150.7037$ K, $p_c = 4.8653$ MPa			26.1 at 100 K
Solid-Liquid phases of methane	65–90.7	20	Freeth and Verschoyle 1931	
	$\ln(p/\text{Pa}) = 9.9089 - 0.001425\,\theta/\text{K} - 517.65/(\theta/\text{K})$			
Liquid-vapor phases of methane	90.7–190	5[f]	Pavese 1993 (Kleinrahm and Wagner 1986; Ziegler et al. 1962b)	1.5 at 90.7 K
	$\ln(p/p_c) = T_c/T_{90}(A\,\tau + B\,\tau^{1.5} + C\,\tau^2 + D\,\tau^{4.5})$ $\tau = 1 - T_{90}/T_c$ $A = -6.036\,690\,537$, $B = 1.412\,275\,294$, $C = -0.498\,639\,547$, $D = -1.438\,177\,00$ $T_c = 190.564$ K, $p_c = 4.5992$ MPa			8.4 at 112 K 64 at 160 K (1.6 MPa)

Table D.2 (continued)

Equilibrium state[a]	T (K)[b]	Uncertainty δT (mK)[c]	References	Sensitivity dp/dT (kPa K^{-1})
Solid-vapor phases of krypton[g]	87–116	10	Freeman and Hasley 1956 (Ziegler et al. 1964a)	0.3 at 87 K 7.2(S), 6.2(L) at tp
	$\log(p/\text{Pa}) = 9.86960 - \frac{579.6}{\theta/\text{K}}$			
Solid-vapor phases of xenon[g]	120–161	20	Freeman and Hasley 1956 (Ziegler et al. 1966)	0.2 at 120 K 5.8(S), 4.9(L) at tp
	$\log(p/\text{Pa}) = 9.86200 - 799.1/(\theta^*/\text{K})$ with $\theta^*/\text{K} = 1.012\,\theta/\text{K} - 1.878$[h]			
Solid-vapor phases of carbon dioxide	194–216.6	2	Pavese 1993 (Fernandez and Del Rio 2005; Mullins et al. 1963; IUPAC 1987; Vukalovich and Altunin 1968)	
	$\log(p/\text{MPa}) = 6.976\,7875 - 1789.6686/(T_{90}/\text{K} + 29.8365)$			36(S), 23(L) at tp
	173–216.6	10	Pavese 1993 (Zhokhovskii 1974, 1989, 1990)	
	See Eq. (a) for ^{3}He: $T = T_{90}$; $c = 0.825\,429\,831$, $n = -1.887\,323\,87$; $T_0 = 173.0137$ K, $T_1 = 216.5905$ K $p_1 = 14\,263$ Pa, $p_2 = 517\,987.5$ Pa			
Liquid-vapor phases of carbon dioxide	216.6–243	2	Pavese 1993 (Fernandez and Del Rio 1984; Mullins et al. 1963; IUPAC 1987; Vukalovich and Altunin 1968)	
	$\log(p/\text{MPa}) = 3.331\,489\,751 - 693.010\,3945/(T_{90}/\text{K} - 25.0085)$			

[a]The vapor pressures equations included in the ITS-90. ($p_0 = 101\,325$ Pa)

[b]Temperature values are given in ITS-90, T_{90}, when part of the Scale definition. For the other equations, when the uncertainty is better than ≈ 10 mK it is not possible to make a simple correction, because the relationship $(T_{90} - T_{68}) = \Delta T = f(T_{90})$ is not linear. Until the coefficients of these equations are recalculated from the data *individually* corrected to T_{90} or new data become available, T_{68} must still be used in the equations. The pressure value calculated for each T_{68} entry will then be attributed to the corresponding T_{90} value obtained from Table A.6. Few equations are given for a generic temperature θ, as no scale indication was even available. For conversion between temperature scales see Appendix A, Table A.6 and its Notes, and Table 4.4. In the range below 13.8 K the previous scale was not the IPTS-68, but the EPT-76. The deviations $(T_{90} - T_{76})$ are very small, e.g., -0.4 mK at 8 K and -1.0 mK at 13.8 K; consequently in these equations T_{90} can be used instead of T_{76}

[c]The uncertainty value in square brackets is the thermodynamic standard uncertainty (BIPM 1990)

[d]See Table 4.3 for the difference of the ITS-90 equation and the T_{62} and T_{58} equation

[e]T_{76} below 5 K is coincident with T_{90} within ± 0.1 mK

[f]Above 100 K. It increases to 15 mK at 91 K and to 10 mK near the critical point

[g]Only the solid-vapor range is considered, because there are only ≈ 4 K between the triple point and the normal boiling point (for the liquid range, see Michels et al. (2008) for krypton and Michels and Wassenaar (1950) for xenon)

[h]Temperature corrected in order to make the equations (29) coincident with (31) within $\pm \approx 10$ mK

Appendix E
Reference Data for Liquid-Column Manometers (Tables E.1, E.2, E.3, E.4)

Table E.1 Some mercury data for use in manometry

Density

- Cook (1957, 1961)
  Density ρ_0 at 20 °C and 101 325 Pa

$$\rho_0(20\ ^\circ\text{C}, 101\,325\ \text{Pa}) = 13545.867\ \text{kg} \cdot \text{m}^{-3}$$

  1σ, except 2 samples is 0.2 ppm; 1σ all samples is 1 ppm
  Value corrected by Chattle (1970) and related to the IPTS-68 temperature scale
- Cook (1957, 1961). Density ρ_0 at 20 °C and 101 325 Pa corrected to ITS-90

$$\rho_0(20\ ^\circ\text{C}, 101\,325\ \text{Pa}) = 13545.855\ \text{kg} \cdot \text{m}^{-3}$$

  This value was computed from the ρ_0 value of Cook calculated in accordance with the IPTS-68 scale and corrected to the new ITS-90 temperature scale at 20 °C. For the definition of the temperature scale ITS-90 below 273.16 K see Appendix A
- Fürtig (1973)
  Density ρ_0 at 20 °C and 101 325 Pa, value referred to the IPTS-68

$$\rho_0(20\ ^\circ\text{C}, p_{\text{atm}}) = 13545.842\ \text{kg} \cdot \text{m}^{-3} \text{ with } p_{\text{atm}} = 101\,325\ \text{Pa}$$

  Relative standard uncertainty 9.5×10^{-7}
- Sommer and Poziemski (1993/1994) and Bettin et al. (2004)
  Density ρ_0 at 20 °C and 101 325 Pa, value referred to the ITS-90

$$\rho_0(20\ ^\circ\text{C}, p_{\text{atm}}) = 13545.850\ \text{kg} \cdot \text{m}^{-3} \text{ with } p_{\text{atm}} = 101\,325\ \text{Pa}$$

  Relative standard uncertainty 8.9×10^{-7}

Thermal expansion coefficient

- Bettin et al. (2004): $(1.812 \pm 0.005) \cdot 10^{-4}\ \text{K}^{-1}$

F. Pavese, G. Molinar Min Beciet, *Modern Gas-Based Temperature and Pressure Measurements,* International Cryogenics Monograph Series,
DOI 10.1007/978-1-4419-8282-7, © Springer Science+Business Media New York 2013

Table E.1 (continued)

Density variation with temperature $\rho(t, p_{atm})$

- Beattie et al. (1941); Chattle (1970)

$$\rho(t, p_{atm}) = \frac{\rho_0(20\ ^\circ\mathrm{C}, p_{atm})}{[1 + A(t - 20\ ^\circ\mathrm{C}) + B(t - 20\ ^\circ\mathrm{C})^2]}$$

  Where
  $p_{\mathrm{atm}} = 101\,325$ Pa, t(°C) is related to IPTS-68
  $A = 18115 \cdot 10^{-8}\ ^\circ\mathrm{C}^{-1}$, $\mathrm{B} = 0.8 \cdot 10^{-8}\ ^\circ\mathrm{C}^{-2}$
- Sommer and Poziemski (1993/1994) and Bettin et al. (2004)

$$\rho(t, p_{atm}) = \frac{\rho_0(0\ ^\circ C, p_{atm})}{[1 + (a_0 + a_1 \cdot t + a_2 \cdot t^2 + a_3 \cdot t^3) \cdot t]}$$

  Where:
  $p_{atm} = 101$ kPa, ρ_0 (0 °C, p_{atm}) = 13595.076 kg · m^{-3} and the coefficients are:
  $a_0 = 1.815\,868 \cdot 10^{-4}\ ^\circ\mathrm{C}^{-1}$
  $a_1 = 5.458\,43 \cdot 10^{-9}\ ^\circ\mathrm{C}^{-2}$
  $a_2 = 3.498\,0 \cdot 10^{-11}\ ^\circ\mathrm{C}^{-3}$
  $a_3 = 1.555\,8 \cdot 10^{-14}\ ^\circ\mathrm{C}^{-4}$
  t (°C) is related to the ITS-90 temperature scale and the relative uncertainty of the above formula, in the temperature range from 10 to 20 °C was estimated to be smaller than 1 ppm

Mercury isothermal compressibility

- Bett et al. (1954)
  If the pressure to be measured is p and the reference vacuum pressure is p_0, the density of the mercury can be referred to the mean pressure in the column, which is $(p + p_0)/2$; the density of mercury is then:

$$\rho(t, (p + p_0)/2) = \frac{\rho(t,\ p_{atm})}{1 - K_{Hg}[(p + p_0)/2 - p_{atm}]}$$

  In the above equation, pressure p must be always absolute. All pressures to be expressed in pascal and temperature in °C. The compressibility correction is not very large (about 2 ppm for an average absolute pressure of 50 kPa), but it must be applied in all manometer configurations
  The compressibility coefficient is $\mathrm{K}_{Hg} = 4.01 \cdot 10^{-11}$ Pa^{-1} at constant temperature
- Sommer and Poziemski (1993/1994) and Bettin et al. (2004)
  The isothermal compressibility at 20 °C of mercury $\beta_{t=20\ ^\circ C}$ and in the pressure range up to 800 MPa is:

$$\beta_{t=20^\circ C} = \beta_0(1 + b_1 \cdot p + b_2 \cdot p^2 + b_3 \cdot p^3)$$

  Where:
  $\beta_0 = 40.25 \cdot 10^{-12}$ Pa^{-1}
  $b_1 = -\ 3.730\,11 \cdot 10^{-10}$ Pa^{-1}
  $b_2 = 1.938\,77 \cdot 10^{-19}$ Pa^{-2}
  $b_3 = -\ 7.299\,26 \cdot 10^{-29}$ Pa^{-3}
  with estimated standard uncertainty between 0.4 % and 1 %

Mercury vapor pressure

- Ernsberg and Pitman (1955)

$$p_{\mathrm{v}} \text{ at } 20\ ^\circ\mathrm{C} = 0.171 \text{ Pa}$$

  The temperature dependence of Hg vapor pressure around
  20 °C is $\mathrm{d}p_{\mathrm{v}}/\mathrm{d}t = 0.0147$ Pa °C^{-1}

Table E.1 (continued)

- Bettin et al. (2004)

$$p_v \text{ at } 20\ ^\circ\text{C} = (0.170 \pm 0.003)\ \text{Pa}$$

Mercury triple point
- Furukawa et al. (1982)
  234.3083 K (−38.8417 °C) related to IPTS-68 scale
  234.3156 K (−38.8344 °C) related to ITS-90 scale
- Hill (1994)
  234.3085 K (−38.8415 °C) related to IPTS-68 scale
  234.3159 K (−38.8341 °C) related to ITS-90 scale

Mercury boiling point

- Ambrose and Sprake (1972)
  629.811 K (356.661 °C) of the IPTS-68 scale at 101 325 Pa

Mercury freezing point

- Furukawa et al. (1982)
  234.3137 K (−38.8363 °C) of the IPTS-68 scale at 101 325 Pa

Mercury surface tension

- Kaye and Laby (1973)
  485×10^{-3} N m^{-1} at 20 °C of the IPTS-68 scale, at 101 325 Pa and at 9.80665 m s^{-2}

Other properties

- From Table 1 in Bettin et al. (2004)
  Thermal conductivity: (8.09 ± 0.24) W m^{-1} K^{-1}
  Compression heating: $(0.028 \pm 0.001)10^{-6}$ K Pa^{-1}
  Molar mass: (200.59 ± 0.01) g mol^{-1}
  Dynamic viscosity: $(1.56 \pm 0.015)10^{-3}$ Pa s
  Electrical conductivity: $(1.044 \pm 0.0035)10^{6}$ S m^{-1}
  See also:
  PTB Internal Report (1995)
  Holman and ten Seldam (1994)

Document E.1 Recommendation of the Working Group on the Statement of Uncertainties Submitted to the Comité International des Poids et Mesures

Assignment of experimental uncertainties

Recommendation INC-1 (1980)

1. The uncertainty in the result of a measurement generally consists of several components which may be grouped into two categories according to the way in which their numerical value is estimated
   A those which are evaluated by statistical methods,

B those which are evaluated by other means.
There is not always a simple correspondence between the classification into categories A and B and the previously used classification into "random" and "systematic" uncertainties. The term "systematic uncertainties" can be misleading and it should be avoided.
Any detailed report of the uncertainty should consist of a complete list of the components, specifying for each of them the method used to obtain its numerical value.

2. The components in category A are characterized by the estimated variance, s_i^2, (or the estimated "standard deviation" s_i) and the number of degrees of freedom, ν_i. Where appropriate, the estimated covariance should be given.
3. The components in category B should be characterized by quantities u_j^2, which may be considered as approximations to the corresponding variances, the existence of which is assumed. The quantities u_j^2 may be treated like variances and the quantities u_j like standard deviations. Where appropriate, the covariances should be treated in a similar way.
4. The combined uncertainty should be characterized by the numerical value obtained by applying the usual method for the combination of variances. The combined uncertainty and its components should be expressed in the form of "standard deviations".
5. If, for particular applications, it is necessary to multiply the combined uncertainty by a factor to obtain an overall uncertainty, the multiplying factor used must always be stated.

The CIPM adopted this recommendation in its 70th session (October 1981).

After the constitution of the Joint Committee for Guides in Metrology (JCGM) different guides for the expression of uncertainty in measurements (GUM) were prepared, mainly:

- "ISO/IEC Guide 98-GUM (1995)";
- "JCGM 100:2008", Evaluation of measurement data. Guide to the expression of uncertainty in measurement, First Edition 2008
- "JCGM 101:2008", Evaluation of measurement data-Supplement 1 to the "Guide to the expression of uncertainty in measurement-Propagation of distributions using a Monte Carlo method.

The last two recent guides, copyrighted of JCGM, are available, for example, in its English version on the BIPM website: http://www.bipm.org/en/pubblications/guides/gum.html.

Table E.2 Typical standard uncertainty contributions for a mercury manometer HG5 (laser-interferometer type, equipped with reflecting floating device or with cat's eye for height measurement) for absolute pressure in nitrogen from 100 Pa to 120 kPa. (Data as in Alasia et al. 1999a)

Ref. #	Source of uncertainty	Quantity	Reflecting floats, stand. dev.	Cat's-eye floats, stand. dev.
1	Reference pressure of the gas	p/mPa	1.2	1.2
2	Acceleration due to gravity	$\Delta g_L/g_L$	$1.5 \cdot 10^{-7}$	$1.5 \cdot 10^{-7}$
3	Density of mercury at 20 °C and 101 325 Pa	$\Delta\rho_{HG}/\rho_{HG}$	$1.0 \cdot 10^{-6}$	1.0×10^{-6}
4	Equation for density of mercury at known p, t	$\Delta\rho_{HG}/\rho_{HG}$	$1.0 \cdot 10^{-7}$	1.0×10^{-7}
5	Average temperature of mercury at mid-height of the U tube	t/mK	10	10
6	Temperature differences of mercury in the two limbs	t/mK	0–5	0–5
7	Interferometer output	$\Delta z/z$	$5.0 \cdot 10^{-8}$	$5.0 \cdot 10^{-8}$
8	Sampling of the signal of the interferometer	z/μm	0.05	0.1
9	Position of mercury menisci and changes of flotation levels	z/μm	1.0	0.2
10	Zero drift of interferometer during measurements	z/μm	0.58	0.23
11	Deviation of laser beams from verticality	$\Delta z/z$	$1.4 \cdot 10^{-7}$	$1.4 \cdot 10^{-7}$
12	Experimental correction for manometer tilt	$\Delta z/z$	$7.0 \cdot 10^{-8}$	$7.0 \cdot 10^{-8}$
13	Actual refractivity of gas (at working conditions)	$\Delta(n-1)/(n-1)$	$1.5 \cdot 10^{-3}$	$1.5 \cdot 10^{-3}$
14	Temperature in both gas columns above mercury	t/mK	100	100
15	Initial vertical separation between both reflecting surfaces and HG5 reference level	a/μm	500	500
16	Actual height of reflecting surfaces above mercury menisci	a'/μm	300	NA
17	Molar mass of gas (dependent on purity)	$\Delta M/M$	$1.0 \cdot 10^{-3}$	$1.0 \cdot 10^{-3}$

The statistical combinations of all the above contributions, assumed to be all mutually independent, yields the combined standard uncertainties of the HG5 mercury manometer used with nitrogen up to 120 kPa:

- Case of absolute pressure measurements with floating devices

$$u(p)/\text{Pa} = 0.153 + 3.79 \cdot 10^{-7} \cdot p/\text{Pa} + (7.221 \cdot 10^{-12}) p^2/\text{Pa}$$

- Case of gauge pressure measurements with floating devices

$$u'(p)/\text{Pa} = 0.153 + 4.22 \cdot 10^{-7} \cdot p/\text{Pa} + (7.832 \cdot 10^{-12}) p^2/\text{Pa}$$

- Case of absolute/gauge pressure measurements with cat's eyes devices, limited to 13 kPa

$$u'(p)/\text{Pa} = 0.043 + 1.25 \cdot 10^{-6} \cdot p/\text{Pa}$$

Table E.3 Uncertainties of the NIST ultrasonic interferometric manometer. (Reproduced from Tilford et al. 1988a by kind permission of the authors)

"A" type uncertainties at 3 times the standard deviation are	0.01 Pa ± 1.7 ppm
"B" type (systematic) uncertainties at 3 times the standard deviation, for each contribution, are	
– Mercury density (Cook's mean value)	0.6 ppm
– Variation due to isotopic composition	1.5 ppm
– Variation due to compressibility	0.2 ppm
– Variation due to thermal expansion	0.05 ppm
– Acceleration of gravity	0.2 ppm
– Temperature	1.0 ppm
– Sound speed, measured value	4.3 ppm
– Sound speed, isotopic variation	0.75 ppm
– Ultrasonic frequency	0.1 ppm
– Verticality	0.1 ppm
– Ultrasonic phase	6.0 ppm
Total systematic uncertainty	15.0 ppm
Total uncertainty as the sum of A and B uncertainties (at the 3σ level) is	0.01Pa ± 16.7 ppm

Table E.4 Some properties of manometric fluids at 20 °C. (Reproduced from Peggs (1980) by kind permission of the author)

Fluid	Density ($kg\,m^{-3}$)	Cubic thermal expansion coefficient ($°C^{-1}$)	Surface tension ($10^{-3}\ N\,m^{-1}$)	Dynamic viscosity ($Pa\,s$)
DEHS	913.6	72.0×10^{-5}	30.0	0.245
DC704	1067.9	72.0×10^{-5}	38.0	0.47
Mercury	13545.8	18.115×10^{-5}	485.0	1.55×10^{-3}
Water	998.2	20.0×10^{-5}	72.8	1.0×10^{-3}
DC200(1)[a]	818.0	135.0×10^{-5}	17.5	1.0×10^{-3}
DC200(2)[b]	953.0	87.9×10^{-5}	20.0	1.0×10^{-3}

Notes: *DEHS* di-ethil-hexyl-sebacate, *DC704* silicone oil (tetrapheniltetramethyltrisiloxane), *DC200* silicone oil (polydimethylsiloxane)
[a]DC200(1) = $10^{-6}\ m^2\,s^{-1}$ grade of kinematic viscosity
[b]DC200(2) = $10^{-5}\ m^2\,s^{-1}$ grade of kinematic viscosity

Appendix F
Reference Data for Pressure Balances

Document F.1 Calculation of the Density of Air ρ_a

The details of the calculations of ρ_a are given in Sect. 7.2.3.1 and they are taken from Picard et al. (2008).

The density of moist air is evaluated using the following equation of state:

$$\rho_a = \frac{p \cdot M_a}{Z \cdot R \cdot T}\left[1 - x_v\left(1 - \frac{M_v}{M_a}\right)\right] \tag{7.31}$$

where the quantities and units in formula (Eq. 7.31) are:

- p/Pa for the absolute atmospheric pressure,
- T/K for the thermodynamic room temperature $= 273.15 + t/°\mathrm{C}$ where $t/°\mathrm{C}$ is the room air temperature,
- x_v the mole fraction of water vapor,
- $M_a/(\mathrm{g} \cdot \mathrm{mol}^{-1})$ the molar mass of dry air,
- $M_v/(\mathrm{g} \cdot \mathrm{mol}^{-1})$ the molar mass of water,
- Z the compressibility factor of moist air,
- $R/(\mathrm{J} \cdot \mathrm{mol}^{-1} \cdot \mathrm{K}^{-1})$ the molar gas constant.

For the CIPM-2007 formula, the best recommended choice for the molar gas constant derive from CODATA 2006 (Mohr et al. 2008) with a value of $R/(\mathrm{J} \cdot \mathrm{mol}^{-1} \cdot \mathrm{K}^{-1}) = 8.314\,472$ with a standard relative uncertainty of 1.8 ppm. The molar gas constant given by CODATA 2010 is $R = 8.314\,4621\ (75)\ \mathrm{J} \cdot \mathrm{mol}^{-1} \cdot \mathrm{K}^{-1}$.

The logical points of Eq. (7.31) are based on the fact that p, T, relative humidity h, or dew point temperature t_d are measured; the rest is calculated according to different choices based on best available data. For what concern temperature reference is made to the ITS-90 temperature scale and the limits of validity of Eq. (7.31), under the basic assumption defined in its model, are similar to the CIPM-1981 equation and are for pressures from 600 hPa to 1100 hPa and temperatures from 15 °C to 27 °C.

The molar mass of dry air M_a is based on the mole fractions of the air constituents, with some exceptions related to atmospheric argon and carbon dioxide. Under the

F. Pavese, G. Molinar Min Beciet, *Modern Gas-Based Temperature and Pressure Measurements,* International Cryogenics Monograph Series,
DOI 10.1007/978-1-4419-8282-7, © Springer Science+Business Media New York 2013

conditions given in Picard et al. (2008), if a measurement of x_{CO_2} is available, then the molar mass of dry air can be assumed to be:

$$M_a/\mathrm{g}\cdot\mathrm{mol}^{-1} = [28.965\,46 + 12.011\cdot(x_{CO_2} - 0.0004)]$$

If not measured, it is assumed a mole fraction of carbon dioxide in air of 400 μmol $\cdot$ mol^{-1}, but there are some precautions expressed for doing it according to the best achievable estimated uncertainty. Considering that the molar mass of moist air includes the amount fraction of water vapor x_v, it is possible to arrive to the following equation:

$$\rho_a/\mathrm{g}\cdot\mathrm{m}^{-3} = \left[3.483\,740 + 1.444\,6\cdot\left(x_{CO_2} - 0.000\,4\right)\right]\cdot\frac{p}{Z\cdot T}\cdot(1 - 0.3780\cdot x_v) \tag{7.32}$$

The quantity x_v is determined from measurements of relative humidity of air h or from air dew point temperature t_d and Z is determined from interpolation equations. *Calculation of x_v from measurements of relative humidity or dew-point temperature* (from Appendix A.1 in Picard et al. (2008)).

The equations and their constants are unchanged from the CIPM-1981/1991 equation.

The first step is the determination of the vapor pressure at saturation p_{sv}.

We will have:

$$p_{sv} = 1\ Pa\cdot\exp\left(A\cdot T^2 + B\cdot T + C + \frac{D}{T}\right)$$

where

$A = 1.237\,884\,7\cdot 10^{-5}\ \mathrm{K}^{-2}$
$B = -1.912\,131\,6\cdot 10^{-2}\ \mathrm{K}^{-1}$
$C = 33.937\,110\,47$
$D = -6.343\,164\,5\cdot 10^{3}\ \mathrm{K}$

The second step is the calculation of the enhancement factor f.

We will have:

$$f = \alpha + \beta\cdot p + \gamma\cdot t^2$$

where

$\alpha = 1.000\,62$
$\beta = 3.14\cdot 10^{-8}\ \mathrm{Pa}^{-1}$
$\gamma = 5.6\cdot 10^{-7}\ \mathrm{K}^{-2}$

where t is in °C and p in pascal.

Using these values, it is possible to derive x_v (from measurements of relative humidity h or dew-point temperature t_d):

$$x_v = h\cdot f(p,t)\cdot\frac{p_{sv}(t)}{p} = f(p,t_d)\cdot\frac{p_{sv}(t_d)}{p}$$

The relative humidity has a range from $0 \leq h \leq 1$ and a relative humidity of 55 % will be expressed as $h = 0.55$.

Calculation of the compressibility factor Z from measurements of pressure p, temperature t or T, and the amount of the fraction of the water vapor x_v (from Appendix A.2 in Picard et al. (2008)).

Also the equation for calculation of Z and its constants are unchanged from the CIPM-1981/1991 equation and are the followings

$$Z = 1 - \frac{p}{T} \cdot \left[a_0 + a_1 \cdot t + a_2 \cdot t^2 + (b_0 + b_1 \cdot t)x_v + (c_0 + c_1 \cdot t) \cdot x_v^2\right] + \frac{p^2}{T^2} \cdot (d + e \cdot x_v^2)$$

where

$a_0 = 1.581\,23 \cdot 10^{-6}\ \mathrm{KPa}^{-1}$
$a_1 = -2.9331 \cdot 10^{-8}\ \mathrm{Pa}^{-1}$
$a_2 = 1.1043 \cdot 10^{-10}\ \mathrm{K}^{-1}\ \mathrm{Pa}^{-1}$
$b_0 = 5.707 \cdot 10^{-6}\ \mathrm{KPa}^{-1}$
$b_1 = -2.051 \cdot 10^{-8}\ \mathrm{Pa}^{-1}$
$c_0 = 1.9898 \cdot 10^{-4}\ \mathrm{KPa}^{-1}$
$c_1 = -2.376 \cdot 10^{-6}\ \mathrm{Pa}^{-1}$
$d = 1.83 \cdot 10^{-11}\ \mathrm{K}^2\ \mathrm{Pa}^{-2}$
$e = -0.765 \cdot 10^{-8}\ \mathrm{K}^2\ \mathrm{Pa}^{-2}$

Equations used to determine p_{sv} and Z are interpolating formulas that are valid only for limited ranges of pressure and temperature.

These ranges determine the region of validity of the CIPM-2007 equation and its predecessors. The recommended ranges of temperature and pressure over which the CIPM-2007 equation may be used are unchanged from the original CIPM-1981 and are for pressure p from 600 to 1100 hPa and temperatures t from 15 °C to 27 °C.

The uncertainty in the value of ρ_a determined by the Eq. (7.32) is made up of the following contributions.

One is due to the mathematical model itself, used for Eq. (7.32), and it has been evaluated to be of 22 ppm for the case that x_{CO_2} was assumed to be 400 µmol mol^{-1}.

The other contributions to uncertainty are connected with the measurement of pressure p, temperature T, relative humidity h appearing in the determination of x_v and the measurement of x_{CO_2}.

For a typical calculation of air density, the relative contribution values to the overall uncertainty due to the additional measurements are to be considered as well, so quoting from Picard et al. (2008) we will have:

$$\frac{u_p(\rho_a)}{\rho_a} = \frac{1}{\rho_a} \cdot \left(\frac{\partial \rho_a}{\partial p}\right) \cdot u(p) \approx +1 \cdot 10^{-5}\mathrm{Pa}^{-1} \cdot u(p)$$

for a typical $u(p) = 100$ Pa, we will have a relative contribution on ρ_a of $1 \cdot 10^{-3}$

$$\frac{u_T(\rho_a)}{\rho_a} \approx -4 \cdot 10^{-3}\mathrm{K}^{-1} \cdot u(T)$$

for a typical $u(T) = 0.1$ K, we will have a relative contribution on ρ_a of $4 \cdot 10^{-4}$

$$\frac{u_h(\rho_a)}{\rho_a} \approx -9 \cdot 10^{-3} \cdot u(h)$$

for a typical $u(h) = 10$ %, we will have a relative contribution on ρ_a of $9 \cdot 10^{-4}$ alternatively if air dew point is measured we will have:

$$\frac{ut_d(\rho_a)}{\rho_a} \approx -3 \cdot 10^{-4} \mathrm{K}^{-1} \cdot u(t_d)$$

for a typical $u(t_d) = 1$ K, we will have a relative contribution on ρ_a of $3 \cdot 10^{-4}$

$$\frac{ux_{CO_2}(\rho_a)}{\rho_a} \approx +0.4 \cdot u(x_{CO_2})$$

for a typical $u(x_{CO_2}) = 100$ ppm, we will have a relative contribution on ρ_a of $0.4 \cdot 10^{-4}$.

The quadrature combinations of all these uncertainties plus the uncertainty of Eq. (7.32) give an estimated uncertainty of about $1.5 \cdot 10^{-3}$ in the determination of air density.

Table F.1 Some characteristics of typical materials used for the construction of piston-cylinder units in pressure balances

Material	Typical characteristics	Typical heat treatment or hardness	E (10^5 MPa)	ν	α (10^{-6} °C^{-1})
T.C. 6 % cobalt	C.S. 4200 MPa		6.47 ± 0.065	0.2178 ± 0.0007	4.9
H. steel		55 HRC	2.18 ± 0.025	0.2868 ± 0.0008	11.0
T.C. various cobalt %	C.S. from 3800 to 5100 MPa		From 6.11 to 6.32	From 0.211 to 0.209	From 4.3 to 5.0
H. steel K9 type	$7.89 \cdot 10^4$ MPa (G)	HRC > 50 tempd. to 750 °C	2.06	0.295	From 9 to 12

T.C. tungsten carbide, *H. steel* hard steel, *C.S.* compressive strength, *tempd.* tempered, *G* Shear modulus

Table F.2 Uncertainty evaluation for absolute pressure measurements with a pressure balance[a] Tungsten carbide piston-cylinder unit of the free deformation type with $2\alpha = \alpha p + \alpha c = 9.1 \cdot 10^{-6}\,°C^{-1}$, A_0 nom. $= 3.36\,cm^2$, pressure range to 137 kPa, with nitrogen as pressurizing gas

See also Eq. (7.18) and Sects. 7.2.2. and 7.2.3
"A" type uncertainties
0.2 Pa + 2 ppm (includes sensitivity and reproducibility)
"B" type (systematic uncertainties)

x_i	$(1/p)(\delta p/\delta x_i)\delta x_i$	$(1/p)(\delta p/\delta x_i)\delta x_i$	Notes
m_i	$\delta m_i/m_i$	0.6 ppm	
g_L	$\delta g_L/g_L$	0.2 ppm	
A_0	$\delta A_0/A_0$	7.0 ppm	
λ	$p \cdot \delta\lambda$		$\lambda = 0$
p in $(1 + \lambda \cdot p)$	$\lambda \cdot \delta p$		$\lambda = 0$
$(\alpha_p + \alpha_c)$	$(t - t_{ref}) \cdot \delta(\alpha_p + \alpha_c)$	0.5 ppm	$\delta 2\alpha/2\alpha = 5\ \%$
T	$(\alpha_p + \alpha_c) \cdot \delta t$	0.2 ppm	$\delta t = 0.02$ K
p_0	$\delta p_0/p_0$	$p_0 = 0.03$ Pa equivalent to 3 ppm at p of 10 kPa	$\delta p_0/p_0 = 5\ \%$ typically $p_0 = 0.5$ Pa
ρ_f	$\delta\rho_f/\rho_f$	0.04 Pa + 0.1 ppm	See Sect. 7.1.3.3 $\delta\rho_f = 0.01\,kg\,m^{-3}$
g_L for height	$\delta g_L/g_L$	0.2 ppm	
h	$\delta h/h$	0.02 Pa + 0.1 ppm	$\delta h = 0.2$ mm

[a]The overall uncertainty of a pressure measurement at the 1σ level is 0.25 Pa + 8 ppm. At the highest pressure of 137 kPa, the uncertainty is 1.35 Pa (equivalent to 9.8 ppm) at the 1σ level

Table F.3 Uncertainty evaluation for gauge pressure measurements to 400 kPa with a pressure balance[a]
Piston-cylinder unit of the free deformation type in tungsten carbide with $2\alpha = \alpha p + \alpha c = (8.8 \pm 0.2)10^{-6}\ °C^{-1}$, nominal diameter of the piston 35.33 mm, pressure range from 10 to 400 kPa, nitrogen

"A" type uncertainties
$0.1\ \text{Pa} + 0.3 \cdot 10^{-6}\ p/\text{Pa}$
"B" type (systematic uncertainties)

Parameter x_i	Maximum uncertainty	Uncertainty (1σ)
m_i	$1 \cdot 10^{-6}\ p$	$0.34 \cdot 10^{-6}\ p$
g_L	$0.5 \cdot 10^{-6}\ p$	$0.2 \cdot 10^{-6}\ p$
$(1 - \rho_a/\rho_{mi})$	$0.01\ \text{Pa} + 0.3 \cdot 10^{-6} p$	$0.003\ \text{Pa} + 0.1 \cdot 10^{-6} p$
A_0	$4 \cdot 10^{-6}\ p$	$1.34 \cdot 10^{-6}\ p$
λ	$0.04 \cdot 10^{-6}\ p$(max)	$0.012 \cdot 10^{-6}\ p$, at max p
t	$0.63 \cdot 10^{-6}\ p$	$0.21 \cdot 10^{-6}\ p$
Level[b]	$0.012\ \text{Pa} + 0.12 \cdot 10^{-6}\ p$	$0.004\ \text{Pa} + 0.04 \cdot 10^{-6}\ p$

[a]The overall pressure uncertainty at the 1σ level is $0.1\ \text{Pa} + 1.45 \cdot 10^{-6} p/\text{Pa}$. At the 3σ level, pressure uncertainty is $\delta p = 0.3\ \text{Pa} + 4.4 \cdot 10^{-6} p/\text{Pa}$. It must be noted that this last figure (obtained as three times the RMS of the squares of all contributions at the 1σ level) is equivalent to the RMS of the squares of all contributions when the maximum uncertainty is used for all the x_i parameters. At the highest 400 kPa pressure, the uncertainty is 2.06 Pa (equivalent to 5.2 ppm) at the 3σ level. The data used here are taken from (Legras et al. 1986; Riety et al. 1987). p is always expressed in pascal. See also Eq. (7.29) and Sects. 7.2.3. and 7.2.4
[b]All quantities ρ_f, g_L and h included

Table F.4 Uncertainty evaluation for gauge pressure measurements to 5 MPa with a pressure balance[a]

Piston-cylinder unit of the free deformation type, piston of tungsten carbide and cylinder of hard steel with $\alpha p + \alpha c = 17.5 \cdot 10^{-6}\ °C^{-1}$, nominal effective area $2\,cm^2$, pressure range from 0.1 to 5 MPa, nitrogen

The data reported here are taken from Maghenzani et al. 1987

See also Eq. (7.29) and Sects. 7.2.3. and 7.2.4

"A" type uncertainties

2 Pa + 2 ppm (includes sensitivity and reproducibility, nitrogen and helium only)

"B" type (systematic uncertainties)

x_i	Uncertainty (1σ level) $(1/p)(\delta p/\delta x_i)\delta x_i$	Notes
m_i	0.6 ppm	
g_L	0.2 ppm	
ρ_a	0.5 ppm	$\delta\rho_a/\rho_a = 0.3\ \%$
ρ_{mi}	0.02 ppm	$\delta\rho_{mi} = 1\,kg \cdot m^{-3}$
A_0	6.0 ppm	Dimensional measurement of diameters with 0.1 µm uncertainty
λ	3 ppm at 5 MPa	$\lambda_{calculated} = 3.3 \cdot 10^{-6}\ MPa^{-1}$ $\delta\lambda/\lambda = 20\ \%$
p in $(1 + \lambda \cdot p)$		Not considered
$(\alpha_p + \alpha_c)$	1.0 ppm	$\delta(\alpha_p + \alpha_c)/(\alpha_p + \alpha_c) = 5\ \%$
t	0.2 ppm	$\delta t = 0.06$ K
ρ_f	0.04 Pa + 0.1 ppm	See Sect. 7.1.3.3
g_L for height	0.2 ppm	See Sect. 7.1.3.3
h	0.002 Pa + 0.1 ppm	See Sect. 7.1.3.3

[a]Overall pressure uncertainty at the 1σ level is 2.4 Pa + 7.2 ppm. At the highest pressure of 5 MPa, the uncertainty is 38.4 Pa (equivalent to 7.7 ppm) at the 1σ level

Appendix G

The text of the Mutual Recognition Arrangement (CIPM-MRA 1999, revision 2003).

Mutual Recognition Arrangement (CIPM-MRA; 1999, revised in 2003), Mutual recognition of national measurement standards and of calibration and measurement certificates issued by national metrology institutes, Paris 14 October 1999, Technical Supplement revised in October 2003, 45 pages, BIPM Editor, Pavillon de Breteuil, F-92312, Sèvres Cedex, France, available on http://www.bipm.org/en/cipm-mra/mra_online.html. (Document reproduced with permission of BIPM.)

Mutual Recognition of National Measurement Standards and of Calibration and Measurement Certificates Issued by National Metrology Institutes Paris, 14 October 1999

Technical Supplement revised in October 2003 (p. 38–41).

Comité international des poids et mesures.

Arrangement drawn up by the International Committee of Weights and Measures under the authority given to it in the Metre Convention.

This document will be open for signature by directors of the national metrology institutes (NMIs) of the Member States of the Metre Convention starting from 14th October 1999, at a meeting of directors that will take place on the occasion of the 21st General Conference of Weights and Measures.

Nom/*Name* **BIPM**

LNM/*NMI** **État/***State*

Signature Signature

This arrangement covers all the institutes listed here.

Declaration to be signed by representatives of intergovernmental and international organizations designated by the CIPM wishing to participate in the arrangement. *I declare as representative of an intergovernmental or international organization designated by the CIPM that my organization wishes to participate in this Mutual Recognition Arrangement and agrees to abide by the rules and procedures of the arrangement.*

F. Pavese, G. Molinar Min Beciet, *Modern Gas-Based Temperature and Pressure Measurements,* International Cryogenics Monograph Series,
DOI 10.1007/978-1-4419-8282-7, © Springer Science+Business Media New York 2013

Mutual Recognition of National Measurement Standards and of Calibration and Measurement Certificates Issued by National Metrology Institutes

The Essential Points The Mutual Recognition Arrangement (MRA) has been drawn up by the International Committee of Weights and Measures (CIPM), under the authority given to it in the Metre Convention, for signature by directors of the national metrology institutes (NMIs) of Member States of the Convention.

Objectives

- to establish the degree of equivalence of national measurement standards maintained by NMIs;
- to provide for the mutual recognition of calibration and measurement certificates issued by NMIs;
- thereby to provide governments and other parties with a secure technical foundation for wider agreements related to international trade, commerce and regulatory affairs.

Process

- international comparisons of measurements, to be known as key comparisons;
- supplementary international comparisons of measurements;
- quality systems and demonstrations of competence by NMIs.

Outcome

- statements of the measurement capabilities of each NMI in a database maintained by the BIPM and publicly available on the Web.

Engagement NMI directors sign the MRA with the approval of the appropriate authorities in their own country and thereby:

- accept the process specified in the MRA for establishing the database;
- recognize the results of key and supplementary comparisons as stated in the database;
- recognize the calibration and measurement capabilities of other participating NMIs as stated in the database.

Exclusions

- signature of the MRA engages NMIs but not necessarily any other agency in their country;
- responsibility for the results of calibrations and measurements rests wholly with the NMI that makes them and is not, through the MRA, extended to any other participating NMI.

Organizational Structure

- overall coordination is by the BIPM under the authority of the CIPM, which itself is under the authority of the Member States of the Metre Convention;

- the Consultative Committees of the CIPM, the Regional Metrology Organizations, and the BIPM are responsible for carrying out the key and supplementary comparisons;
- a Joint Committee of the Regional Metrology Organizations and the BIPM is responsible for analyzing and transmitting entries into the database for the calibration and measurement capabilities declared by the NMIs.

Preamble National accreditation and regulatory bodies require multilateral agreements or arrangements to define the conditions under which they can accept calibration, measurement, and test certificates issued by laboratories accredited in other countries. These agreements or arrangements depend for their validity on the accuracy of national measurement standards and of calibration and measurement certificates issued by national metrology institutes (NMIs). This arrangement provides for the mutual recognition of national measurement standards and of calibration and measurement certificates issued by national metrology institutes, and is founded on the efforts of each individual national metrology institute to base its measurements and measurement uncertainties on SI units.

To put the criteria for mutual recognition on an objective footing, the arrangement calls upon: (a) the results of a set of key comparisons carried out using specified procedures which lead to a quantitative measure of the degree of equivalence of national measurement standards; (b) the operation by each NMI of a suitable way of assuring quality; and (c) successful participation by each NMI in appropriate supplementary comparisons. Together, these three procedures demonstrate to participating institutions the degree to which each may have confidence in the results reported by others, and so promote mutual confidence between them.

For the purposes of this arrangement, the degree of equivalence of measurement standards is taken to mean the degree to which these standards are consistent with reference values determined from the key comparisons and hence are consistent with each other. Each reference value is referred to as a key comparison reference value and, in most cases, it can be considered to be a close, but not necessarily the best, approximation to the SI value. The degree of equivalence of a national measurement standard is expressed quantitatively in terms of its deviation from the key comparison reference value and the uncertainty of this deviation.

This arrangement is in two parts: through part one, signatories recognize the degree of equivalence of national measurement standards of participating national metrology institutes; through part two, the signatories recognize the validity of calibration and measurement certificates issued by participating institutes.

Formally, this document is a technical arrangement among directors of the national metrology institutes of Member States of the Metre Convention and it is not a diplomatic treaty. It is drawn up by the CIPM under the Metre Convention and it is neither an extension to the Convention nor a replacement for any Article of the Convention. The directors who in due course decide to sign the arrangement do so with the approval of the appropriate governmental or other official authorities in their own country. It is expected that participation in this arrangement will open the way to, and provide the technical basis for, wider agreements related to trade, commerce, and regulatory affairs, signed by the competent authorities in each country or region.

Participation in the arrangement through their regional metrology organization is also open to the NMIs of States and Economies that are Associates of the CGPM.

1 The Arrangement

1.1 This is an arrangement between national metrology institutes which specifies terms for the mutual recognition of national measurement standards and for recognition of the validity of calibration and measurement certificates issued by national metrology institutes. It is drawn up by the CIPM with the authority given to it under Article 10 (1921) of the Rules Annexed to the Metre Convention.

1.2 This arrangement is in two parts as specified in paragraph 2 below: part one concerns national measurement standards and part two concerns calibration and measurement certificates.

1.3 Participating national metrology institutes, signatories to this arrangement, may choose to limit their participation to part one, the recognition of national measurement standards.

1.4 Each signatory to this arrangement is the national metrology institute designated by the appropriate national governmental or other official authority of the Member State of the Metre Convention as being responsible for national measurement standards. For any state that has more than one such designated institute, the arrangement is signed by one institute on behalf of all, the names of the other institutes being attached to the document.

1.5 Designated NMIs of States or Economies that are Associates of the CGPM may participate in the arrangement only through their regional metrology organizations by signing a declaration, appended to this arrangement.

1.6 Intergovernmental and international organizations designated by the CIPM may also participate in the arrangement.

2 Scope of the Arrangement

2.1 Participating national metrology institutes, listed in Appendix A, recognize the degree of equivalence of national measurement standards, derived from the results of key comparisons, for the quantities and values specified in Appendix B. This constitutes part one of the arrangement.

2.2 Participating institutes recognize the validity of calibration and measurement certificates issued by other participating institutes for the quantities and ranges specified in Appendix C. This constitutes part two of the arrangement.

3 Technical Basis of the Arrangement

3.1 The technical basis of this arrangement is the set of results obtained in the course of time through key comparisons carried out by the Consultative Committees of the CIPM, the BIPM and the regional metrology organizations (RMOs), and published by the BIPM and maintained in the key comparison database. Detailed technical provisions are given in the Technical Supplement to this arrangement.

3.2 Key comparisons carried out by Consultative Committees or the BIPM are referred to as CIPM key comparisons; key comparisons carried out by regional metrology organizations are referred to as RMO key comparisons; RMO key comparisons must be linked to the corresponding CIPM key comparisons by

means of joint participants. The degree of equivalence derived from an RMO key comparison has the same status as that derived from a CIPM key comparison.

3.3 A Joint Committee of the RMOs and the BIPM (the Joint Committee or JCRB), created by the CIPM, is responsible for the coordination of data provided by the RMOs, and other actions undertaken by them to promote confidence in calibration and measurement certificates (see paragraph 9.3).

4 Responsibilities of the Consultative Committees of the CIPM The Consultative Committees have the responsibility for choosing the key comparisons listed in Appendix D and affirming the validity of the results. The particular responsibilities of the Consultative Committees are detailed in the Technical Supplement.

5 Responsibilities of the Regional Metrology Organizations The national metrology institutes that are signatories to this arrangement undertake to put in place appropriate structures within their RMOs so that the RMOs may:

a. make proposals to the Consultative Committees on the choice of key comparisons;
b. carry out the RMO key comparisons, described in the Technical Supplement, corresponding to the CIPM key comparisons;
c. participate in the JCRB (see paragraphs 9.3 and 9.4 below);
d. carry out supplementary comparisons and other actions designed to support mutual confidence in the validity of calibration and measurement certificates issued by participating institutes (see paragraph 7.3 below).

6 Participation in Key and Supplementary Comparisons

6.1 Participation in a CIPM key comparison is open to laboratories having the highest technical competence and experience, normally the member laboratories of the appropriate Consultative Committee. Those laboratories that are not members of a Consultative Committee and not NMIs must be nominated by the designated national metrology institute referred to in paragraph 1.4 as being responsible for the relevant national measurement standards. In choosing participants, the Consultative Committees should take proper account of regional representation. The number of laboratories participating in CIPM key comparisons may be restricted for technical reasons.

6.2 Participation in key comparisons organized by an RMO is open to all RMO members and to other institutes which meet the rules of the regional organization (including institutes invited from outside the region) and have technical competence appropriate to the particular comparison.

6.3 Participation in RMO supplementary comparisons is open to those institutes meeting the requirements specified in paragraph 6.2.

7 Confidence in Measurements

7.1 Confidence in measurements is an essential prerequisite to international trade and facilitates almost every task in the industrialized world. To a large extent this confidence already exists and is based on the SI, which is the cornerstone of the international measurement system, as realized by the national metrology

institutes. The function of this mutual recognition arrangement is to extend and consolidate preexisting worldwide confidence in measurements.

7.2 Institutes participating in this arrangement are expected to extend existing international confidence in their activities by publishing regular reports on the work of their laboratories and transmitting them to the BIPM, by participation in relevant conferences, and by taking part in the activities organized by the BIPM.

7.3 In addition to participation in the key and supplementary comparisons, identified in paragraph 6, recognition of calibration and measurement certificates requires one of the following procedures in order to establish the necessary mutual confidence:

a. an NMI that chooses for its calibration and measurement services a quality system that meets the requirements of ISO Guide 25 or equivalent for an NMI, assessed by an accreditation body fulfilling the requirements of ISO Guide 58, declares its calibration measurement capabilities (see paragraph T.7) and submits them to the local RMO for review and transmission to the Joint Committee for analysis and inclusion in Appendix C;

b. an NMI that chooses to use a different way of assuring quality or chooses a different quality system, or ISO Guide 25 without third-party assessment, for its calibration and measurement services declares its calibration measurement capabilities (see paragraph T.7) and submits them to the local RMO for review and transmission to the Joint Committee for analysis and inclusion in Appendix C. Demonstration of competence and capability may require visits and examination of procedures by an NMI and/or by peers selected by the local RMO.

7.4 Nothing in this arrangement is intended to limit the freedom of one or more signatories to establish mutual recognition, as specified in paragraphs 2.1 and 2.2, outside this arrangement.

8 Disputes in the Operation of the Arrangement This arrangement is operated by the BIPM in close consultation with the Consultative Committees and the RMOs whose responsibility it is, under paragraphs 4 and 5 above, to carry out and evaluate the results of the key comparisons. Disagreements that arise in the operation of this arrangement are discussed first within the appropriate Consultative Committee, the RMO or the Joint Committee and if not resolved there, are referred to the CIPM.

9 Coordination

9.1 Overall coordination of activities related to this arrangement resides with the CIPM.

9.2 Coordination of the key comparisons is effected through consultations between the Consultative Committees and the RMOs.

9.3 Coordination of the supplementary comparisons and other actions related to confidence in calibration and measurement certificates undertaken by the regional metrology organizations is carried out by the JCRB. The JCRB is created by the CIPM comprising representatives of the RMOs and is chaired by the Director of the BIPM. Its terms of reference are given in Appendix E.

9.4 Under the overall responsibility of the CIPM, the Joint Committee is responsible for analysing and maintaining the content of Appendix C.

10 Responsibility and Liability for Measurements

10.1 It is recognized and accepted by each signatory that this arrangement creates no rights, liabilities, or obligations that will have binding effects in national or international law.

10.2 It is recognized and accepted by each signatory that this arrangement covers, in each country, only the signatory institute and other institutes represented by it. It does not necessarily extend to other metrological or regulatory bodies in that country.

10.3 Responsibility for all measurements made under this arrangement rests wholly with the institute making the measurements. No responsibility for declared uncertainties or statements of quality is assumed by the CIPM, the BIPM, the Consultative Committees, or the RMOs.

11 Signing this Mutual Recognition Arrangement and Bringing it into force

11.1 The procedure for implementing this arrangement is as follows:

- at the meeting of directors of national metrology institutes held on 23–25 February 1998, the directors were invited to initiate a draft of this arrangement;
- at the meeting of directors of national metrology institutes to be held at the time of the 21st CGPM in October 1999, directors will be invited to sign this arrangement for an initial period of four years. New signatories may attach themselves to this arrangement at any time by application to the Director of the BIPM.

11.2 To withdraw from the arrangement, the Director of a signatory institute should notify the Director of the BIPM 6 months prior to the effective date of withdrawal. The Director of the BIPM will notify all other signatories of such notice of withdrawal not later than one month after it has been received.

11.3 During the period from October 1999 until such time as the first round of key and supplementary comparisons has been completed and the quality systems specified in paragraph 7.3 put in place, the arrangement will operate in a transitional mode. Provisional degrees of equivalence (Appendix B) will be based on the results of comparisons carried out since about 1988, reviewed and approved by the Consultative Committee for each field and entered into the key comparison database referred to in paragraph 3.1. Provisional calibration and measurement capabilities (Appendix C) will be based on corresponding data reviewed by the RMOs and analysed by the JCRB, taking into account the procedures specified in paragraph 7.3 and included in the key comparison database.

11.4 After the initial period of four years, signatories may, with the approval of the appropriate governmental or other official authorities in their own country, make changes to this arrangement at meetings organized by the CIPM of directors of the national metrology institutes.

12 Status of National Measurement Standards Calibrated by the BIPM or by a National Metrology Institute Nothing in this arrangement restricts the rights under the Metre Convention of participating national metrology institutes to have their national standards calibrated by the BIPM or by another national metrology institute. The mutual recognition of such standards depends upon subsequent participation in key or supplementary comparisons (see paragraphs 3 and 6 above).

13 NMIs that are not Members of an RMO Those NMIs that wish to participate in this arrangement but are not members of an RMO, should either form a new RMO, or for the purposes of this arrangement, associate themselves with an existing RMO, whichever is the more appropriate. If neither approach is possible, they should seek to make special provisions.

14 NMIs that are Members of more than one RMO Those NMIs that are members of more than one RMO must declare with which RMO they will participate in part two of this arrangement.

15 Entry of new RMOs into the Joint Committee The entry of a new RMO into the Joint Committee is subject to approval by the CIPM.

Technical Supplement to the Arrangement

CIPM Revision 2003 At its 92nd meeting, in October, 2003, the CIPM approved proposals from the JCRB for modifications to the Technical Supplement of the CIPM-MRA. These concern paragraph *T.7*, stating that unresolved inconsistencies resulting from supplementary comparisons will be noted in Appendix C, and paragraph *T.10*, clarifying that supplementary comparisons are only carried out by RMOs.[6] The following is the revised text with the changes highlighted. Underlined text has been added and barred text deleted.

The technical basis for this arrangement is the set of results obtained during the key comparisons carried out by the Consultative Committees, the BIPM and the RMOs (paragraph 3.1). The following specify conventions and responsibilities relating to the key comparisons.

T.1 CIPM key comparisons lead to reference values, known as key comparison reference values.

T.2 For the purposes of this arrangement, the term degree of equivalence of measurement standards is taken to mean the degree to which a standard is consistent with the key comparison reference value. The degree of equivalence of each national measurement standard is expressed quantitatively by two terms: its deviation from the key comparison reference value and the uncertainty of this deviation (at a 95 % level of confidence). The degree of equivalence between pairs of national measurement standards is expressed by the difference of their

[6] The definition of a supplementary comparison in the Glossary (p. 44) has been revised in accordance to this modification.

deviations from the reference value and the uncertainty of this difference (at a 95 % level of confidence).

T.3 Although a key comparison reference value is normally a close approximation to the corresponding SI value, it is possible that some of the values submitted by individual participants may be even closer. In a few instances, for example in some chemical measurements, there may be difficulty in relating results to the SI. Nevertheless, the key comparison reference value and deviations from it are good indicators of the SI value. For this reason, these values are used to express the degree of equivalence between the standards of participating laboratories. In some exceptional cases, a Consultative Committee may conclude that for technical reasons a reference value for a particular key comparison is not appropriate; the results are then expressed directly in terms of the degrees of equivalence between pairs of standards.

T.4 The results of the RMO key comparisons are linked to key comparison reference values established by CIPM key comparisons by the common participation of some institutes in both CIPM and RMO comparisons. The uncertainty with which comparison data are propagated depends on the number of institutes taking part in both comparisons and on the quality of the results reported by these institutes.

T.5 The results of the CIPM and the RMO key comparisons, the key comparison reference values, the deviations from the reference values and their uncertainties, together with other information necessary for their interpretation, are published by the BIPM and entered into the key comparison database.

T.6 CIPM and RMO key comparisons must be carried out following the Guidelines for CIPM key comparisons published by the BIPM and available on the BIPM Web page.

T.7 For calibration and measurement certificates, the quantities, ranges and calibration and measurement capabilities expressed as an uncertainty (normally at a 95 % level of confidence but in some cases it may be at a higher, specified, level), are listed for each participating institute in Appendix C. They must be consistent with the results given in Appendix B, derived from the key comparisons. If, as a result of a key comparison, a significant unresolved deviation from the key comparison reference value persists for the standard of a particular participating institute, the existence of this deviation is noted in Appendix C. *The same applies for significant inconsistencies resulting from a supplementary comparison*. In this case, the institute has the choice of either withdrawing from Appendix C one or more of the relevant calibration and measurement services or increasing the corresponding uncertainties given in Appendix C. The calibration and measurement capabilities listed in Appendix C are analysed by the Joint Committee following the procedures given in 7.3 above. The calibration and measurement capabilities referred to in this paragraph are those that are ordinarily available to the customers of an institute through its calibration and measurement services; they are sometimes referred to as best measurement capabilities.

T.8 Responsibilities of the Consultative Committees: the Consultative Committees have a prime role in choosing and implementing key comparisons and in affirming the validity of the results. Their particular responsibilities are:

a. to identify the key comparisons in each field and maintain a current list (Appendix D);
b. to initiate and organize, with the collaboration of the BIPM, the execution of key comparisons at intervals to be decided individually for each comparison;
c. to review the results of CIPM key comparisons and determine the reference values and degrees of equivalence on the basis of the proposals of the appropriate working groups;
d. to approve the final report of CIPM key comparisons for publication by the BIPM;
e. to examine and confirm the results of RMO key and supplementary comparisons and incorporate them in Appendix B and the key comparison database;
f. to examine and confirm the results of bilateral key comparisons for entry into Appendix B and the key comparison database.

T.9 RMO key comparisons: the RMO key comparisons extend the metrological equivalence established by the CIPM key comparisons to a greater number of national metrology institutes including those of States or Economies that are Associates of the CGPM. Redundancy, coherence and timeliness are important aspects of regional comparisons for they ensure that the overall system of comparisons is robust. Regional organizations therefore have a particular responsibility for ensuring that:

a. links with the CIPM key comparisons provide adequate redundancy through the participation of a sufficient number of laboratories in both sets of comparisons to ensure that links to the key comparison reference values are established with acceptably low uncertainty;
b. the procedures used in regional comparisons, and the evaluation of the results and uncertainties, are compatible with those used in the CIPM key comparisons;
c. the timing of the RMO key comparisons is coordinated with, and is at least as frequent as, those of the CIPM key comparisons;
d. the results of RMO key comparisons are carefully evaluated by the RMO, which also takes responsibility for ensuring that the proper procedures have been followed, and then the results are submitted for publication and to the relevant CC for incorporation in Appendix B and the key comparison database;
e. the results of appropriately performed bilateral comparisons are considered and then submitted to the relevant Consultative Committee for incorporation in Appendix B and the key comparison database;
f. in the case that an RMO key comparison takes place before the corresponding CIPM key comparison, the link to the subsequent key comparison reference value is deferred until both key comparisons are completed.

T.10 Supplementary comparisons: in addition to the key comparisons, *the Consultative Committees*, the RMOs, *and the BIPM* may carry out supplementary comparisons to meet specific needs not covered by key comparisons, including comparisons to support confidence in calibration and measurement certificates.

The Joint Committee of the RMOs and the BIPM (see paragraph 9.3 above) provides a forum for the coordination, among the regions, of the supplementary comparisons carried out by the RMOs in order to bolster confidence in calibration and measurement certificates.

Appendices to the Arrangement

Appendices A, B, C and D are maintained electronically in the key comparison database held at the BIPM. During the initial four-year period, the database (which was designed by the NIST) will be held jointly by the BIPM and the NIST.

Appendix A List of national metrology institutes that are signatories to the arrangement, together with their logos.

Appendix B

B 1: Results of CIPM key comparisons.
B 2: Results of RMO key comparisons.
B 3: Results of supplementary comparisons.

For each key comparison, the following are included:

- individual values for each institute together with their declared uncertainties;
- the key comparison reference value with its associated uncertainty;
- for each institute, the deviation from the key comparison reference value and the uncertainty in that deviation (at a 95 % level of confidence), i.e. its degree of equivalence;
- the degrees of equivalence between the standards of each of the participating institutes.

Appendix C Quantities for which calibration and measurement certificates are recognized by institutes participating in part two of the agreement. The quantities, ranges, and calibration and measurement capabilities expressed as an uncertainty (normally at a 95 % level of confidence) are listed for each participating institute.

Appendix D List of key comparisons.

Appendix E Terms of reference of the Joint Committee of the Regional Metrology Organizations and the BIPM (JCRB).

Glossary of Terms Used in this Arrangement

- BIPM: Bureau International des Poids et Mesures.
- CGPM: General Conference of Weights and Measures.
- CIPM: International Committee of Weights and Measures.
- Calibration and measurement capability (*CMC*): the highest level of calibration or measurement normally offered to clients, expressed in terms of a confidence level of 95 %, sometimes referred to as best measurement capability.
- Calibration or measurement certificate: a certificate issued by a national metrology institute and relating to a test, calibration or measurement of an instrument or a reference material (pertaining either to physical or to chemical measurements).
- CIPM key comparison: a key comparison executed by a Consultative Committee or the BIPM leading to a key comparison reference value.
- Degree of equivalence of a measurement standard: the degree to which the value of a measurement standard is consistent with the key comparison reference value. This is expressed quantitatively by the deviation from the key comparison reference value and the uncertainty of this deviation. The degree of equivalence between two measurement standards is expressed as the difference between their respective deviations from the key comparison reference value and the uncertainty of this difference.
- Key comparison: one of the set of comparisons selected by a Consultative Committee to test the principal techniques and methods in the field (note that key comparisons may include comparisons of representations of multiples and submultiples of SI base and derived units and comparisons of artefacts).
- Key comparison database**:** the database maintained by the BIPM which contains Appendices A–D of this Mutual Recognition Arrangement.
- Key comparison reference value: the reference value accompanied by its uncertainty resulting from a CIPM key comparison.
- National metrology institute: the national metrology institute signatory to this arrangement is the metrology institute designated by the appropriate national governmental or other official authority as that responsible for national measurement standards.
- RMO key comparison: a key comparison executed by an RMO. Note: only key comparisons carried out by a Consultative Committee or the BIPM lead to a key comparison reference value. For a key comparison carried out by a regional metrology organization, the link to the key comparison reference value is obtained by reference to the results from those institutes which have also taken part in the CIPM key comparison.
- Supplementary comparison: comparisons carried out by *the Consultative Committees,* the RMOs, *and the BIPM* to meet specific needs not covered by key comparisons, including comparisons to support confidence in calibration and measurement certificates.

Terms of Reference of the Joint Committee of the Regional Metrology Organizations (RMOs) and the BIPM

1. The Joint Committee is charged with
   a. coordinating the activities among the RMOs in establishing confidence for the recognition of calibration and measurement certificates, according to the terms of the Mutual Recognition Arrangement (MRA);
   b. making policy suggestions to the RMOs and to the CIPM on the operation of the MRA;
   c. analyzing the application by each RMO of the criteria of the MRA;
   d. analyzing and entering into Appendix C the proposals of each RMO in respect of the calibration and measurement capabilities of their member NMIs and reporting to the CIPM;
   e. facilitating appropriate interregional supplementary comparisons;
   f. writing an annual report on the activities of the Joint Committee to the CIPM and to the signatories of the MRA.
2. Membership and meetings of the Joint Committee
   a. each RMO informs the Director of the BIPM of the name of its official representative on the Joint Committee;
   b. at each meeting of the Joint Committee the representatives may be accompanied by appropriate advisors;
   c. the Joint Committee operates by consensus;
   d. the Joint Committee should meet at least once a year.

Appendix H
General Terminology in Measurements

This appendix lists, in alphabetical order, some of the common terminology used to derive the metrological characteristics of a transducer and gives, without pretension of substituting metrological vocabularies or other similar documents, only the most common definitions used to qualify the main metrological characteristics of a transducer.

For the purposes of this book, the present list can be applied to any pressure and temperature transducer.

The listed terms and definitions are either taken integrally (here cited in quotes) and each definition is given with the index number as indicated in VIM 2008. All definitions are based on *International vocabulary of metrology—Basic and general concepts and associated terms (VIM), Third Edition, JCGM 200:2008.* This important document is freely available on the web site of BIPM at: http://www.bipm.org/utils/common/documents/jcgm/JCGM_200_2008.pdf

2.39 Calibration "Operation that, under specified conditions, in a first step, establishes a relation between the quantity values with measurement uncertainties provided by measurement standards and corresponding indications with associated measurement uncertainties and, in a second step, uses this information to establish a relation for obtaining a measurement result from an indication".

> *Note 1* A calibration may be expressed by a statement, calibration function, calibration diagram, calibration curve, or calibration table. In some cases, it may consist of an additive or multiplicative correction of the indication with associated measurement uncertainty.
>
> *Note 2* Calibration should not be confused with adjustment of a measuring system—often mistakenly called "self-calibration"—nor with verification of calibration.
>
> *Note 3* Often, the first step alone in the above definition is perceived as being calibration.

Confidence Level The probability that a measurement error will not exceed the stated uncertainty. For example, if errors are assumed to be normally distributed and the measurement uncertainty is specified as 0.1 % at the three standard deviation levels, there is 99.7 % probability that the measured value is within 0.1 % of the reference quantity value. When confidence levels are used, the type of distribution employed must be absolutely specified.

F. Pavese, G. Molinar Min Beciet, *Modern Gas-Based Temperature and Pressure Measurements,* International Cryogenics Monograph Series,
DOI 10.1007/978-1-4419-8282-7, © Springer Science+Business Media New York 2013

Dead Band The range through a stimulus can be varied without producing a change in the response of a measuring instrument.

Drift The slow variation with time of a metrological characteristic of a measuring instrument.

Experimental Standard Deviation For a series of n measurements of the same measurand, the parameter "s" characterizing the dispersion of the results and is given by the formula:

$$s = \sqrt{\frac{\sum_{i=1}^{n} (x_i - \bar{x})^2}{n-1}}$$

x_{i} being the result of the i^{th} measurement and $\bar{x}$ being the arithmetic mean of the n results considered.

Hysteresis The property of a measuring instrument whereby its response to a given stimulus depends on the sequence of preceding stimuli. Hysteresis is sometimes related to influence quantities.

Linearity The deviation of instrument output from the linear dependence on the input stimulus. More properly, it should be called nonlinearity.

2.13 Measurement Accuracy, Accuracy of Measurement, Accuracy "Closeness of agreement between a measured quantity value and a true quantity value of a measurand".

Note 1 The concept 'measurement accuracy' is not a *quantity* and is not given a numerical quantity value. A measurement is said to be more accurate when it offers a smaller measurement error.

Note 2 The term "measurement accuracy" should not be used for measurement trueness and the term measurement precision should not be used for 'measurement accuracy', which, however, is related to both these concepts.

Note 3 'Measurement accuracy' is sometimes understood as closeness of agreement between measured quantity values that are being attributed to the measurand.

2.16 Measurement Error, Error of Measurement, Error "Measured quantity value minus a reference quantity value".

Note 1 The concept of 'measurement error' can be used both: (a) when there is a single reference quantity value to refer to, which occurs if a calibration is made by means of a measurement standard with a measured quantity value having a negligible measurement uncertainty or if a conventional quantity value is given, in which case the measurement error is known, and (b) if a measurand is supposed to be represented by a unique true quantity value or a set of true quantity values of negligible range, in which case the measurement error is not known.

Note 2 Measurement error should not be confused with production error or mistake.

2.21 Measurement Repeatability, Repeatability "Measurement precision under a set of repeatability conditions of measurement".

2.25 Measurement Reproducibility, Reproducibility "Measurement precision under reproducibility conditions of measurement".

Note Relevant statistical terms are given in ISO 5725–1:1994 and ISO 5725–2:1994.

2.41 Metrological Traceability "Property of a measurement result whereby the result can be related to a reference through a documented unbroken chain of calibrations, each contributing to the measurement uncertainty".

Note 1 For this definition, a 'reference' can be a definition of a measurement unit through its practical realization, or a measurement procedure including the measurement unit for a nonordinal quantity, or a measurement standard.

Note 2 Metrological traceability requires an established calibration hierarchy.

Note 3 Specification of the reference must include the time at which this reference was used in establishing the calibration hierarchy, along with any other relevant metrological information about the reference, such as when the first calibration in the calibration hierarchy was performed.

Note 4 For measurements with more than one input quantity in the measurement model, each of the input quantity values should itself be metrologically traceable and the calibration hierarchy involved may form a branched structure or a network. The effort involved in establishing metrological traceability for each input quantity value should be commensurate with its relative contribution to the measurement result.

Note 5 Metrological traceability of a measurement result does not ensure that the measurement uncertainty is adequate for a given purpose or that there is an absence of mistakes.

Note 6 A comparison between two measurement standards may be viewed as a calibration if the comparison is used to check and, if necessary, correct the quantity value and measurement uncertainty attributed to one of the measurement standards.

Note 7 The ILAC considers the elements for confirming metrological traceability to be an unbroken metrological traceability chain to an international measurement standard or a national measurement standard, a documented measurement uncertainty, a documented measurement procedure, accredited technical competence, metrological traceability to the *SI*, and calibration intervals (see ILAC P-10:2002).

Note 8 The abbreviated term "traceability" is sometimes used to mean 'metrological traceability' as well as other concepts, such as 'sample traceability' or 'document traceability' or 'instrument traceability' or 'material traceability', where the history ("trace") of an item is meant. Therefore, the full term of "metrological traceability" is preferred if there is any risk of confusion.

2.26 Measurement Uncertainty, Uncertainty of Measurement, Uncertainty "Non-negative parameter characterizing the dispersion of the quantity values being attributed to a measurand, based on the information used".

Note 1 Measurement uncertainty includes components arising from systematic effects, such as components associated with corrections and the assigned quantity values of measurement standards, as well as the definitional uncertainty. Sometimes estimated systematic effects are not corrected for but, instead, associated measurement uncertainty components are incorporated.

Note 2 The parameter may be, for example, a standard deviation called standard measurement uncertainty (or a specified multiple of it), or the half-width of an interval, having a stated coverage probability.

Note 3 Measurement uncertainty comprises, in general, many components. Some of these may be evaluated by Type A evaluation of measurement uncertainty from the statistical distribution of the quantity values from series of measurements and can be characterized by standard deviations. The other components, which may be evaluated by Type B evaluation of measurement uncertainty, can also be characterized by standard deviations, evaluated from probability density functions based on experience or other information.

Note 4 In general, for a given set of information, it is understood that the measurement uncertainty is associated with a stated quantity value attributed to the measurand. A modification of this value results in a modification of the associated uncertainty.

2.19 Random Measurement Error, Random Error of Measurement, Random Error "Component of measurement error that in replicate measurements varies in an unpredictable manner".

Note 1 A reference quantity value for a random measurement error is the average that would ensue from an infinite number of replicate measurements of the same measurand.

Note 2 Random measurement errors of a set of replicate measurements form a distribution that can be summarized by its expectation, which is generally assumed to be zero, and its variance.

Note 3 Random measurement error equals measurement error minus systematic measurement error.

Relative Error The absolute error of measurement divided by the reference quantity value of the measurand.

2.20 Repeatability Condition of Measurement, Repeatability Condition "Condition of measurement, out of a set of conditions that includes the same measurement procedure, same operators, same measuring system, same operating conditions, and same location, and replicate measurements on the same or similar objects over a short period of time".

Note 1 A condition of measurement is a repeatability condition only with respect to a specified set of repeatability conditions.

Note 2 In chemistry, the term "intra-serial precision condition of measurement" is sometimes used to designate this concept.

2.24 Reproducibility Condition of Measurement, Reproducibility Condition "Condition of measurement, out of a set of conditions that includes different locations, operators, measuring systems, and replicate measurements on the same or similar objects".

Note 1 The different measuring systems may use different measurement *procedures*.

Note 2 A specification should give the conditions changed and unchanged, to the extent practical.

4.14 Resolution "Smallest change in a quantity being measured that causes a perceptible change in the corresponding indication".

Note Resolution can depend on, for example, noise (internal or external) or friction. It may also depend on the value of a quantity being measured.

4.12 Sensitivity of a Measuring System, Sensitivity "Quotient of the change in an indication of a measuring system and the corresponding change in a value of a quantity being measured".

Note 1 Sensitivity of a measuring system can depend on the value of the quantity being measured.

Note 2 The change considered in a value of a quantity being measured must be large compared with the resolution.

4.19 Stability of a Measuring Instrument, Stability "Property of a measuring instrument, whereby its metrological properties remain constant in time".

Note Stability may be quantified in several ways.

Example 1 In terms of the duration of a time interval over which a metrological property changes by a stated amount.

Example 2 In terms of the change of a property over a stated time interval.

2.17 Systematic Measurement Error, Systematic Error of Measurement, Systematic Error "Component of measurement error that in replicate measurements remains constant or varies in a predictable manner".

Note 1 A reference quantity value for a systematic measurement error is a true quantity value, or a measured quantity value of a measurement standard of negligible measurement uncertainty, or a conventional quantity value.

Note 2 Systematic measurement error, and its causes, can be known or unknown. A correction can be applied to compensate for a known systematic measurement error.

Note 3 Systematic measurement error equals measurement error minus random measurement error.

References

Part I

Alhers G (1968a) Effect of the gravitational field on the superfluid transition of helium-4. Phys Rev 171:275–282

Alhers G (1968b) Thermal conductivity of helium-I near the superfluid transition. Phys Rev Lett 21:1159–1162

Alhers G (1969) Mutual friction in helium-II near the superfluid transition. Phys Rev Lett 22:54–56

Ambrose D (1957) The triple point of carbon dioxide as a thermometric fixed point. Br J Appl Phys 8:32–34

Ambrose D, Crovini L (1987) Temperature. In: March KN (ed) IUPAC, Recommended reference materials for the realization of physicochemical properties, Chap. 8. Blackwell Scientific Publication, Oxford

Ancsin J (1972) Purification of oxygen by zone melting. In: Plumb HH (ed) Temperature, its measurements and control in science and industry, vol 4. Pittsburgh, Washington, pp 211–216

Ancsin J (1973) Studies of phase changes in argon. Metrologia 9:147–154

Ancsin J (1974a) Some thermodynamic properties of pure and impure nitrogen. Can J Phys 52:1521–1531

Ancsin J (1974b) Vapor pressure scale of oxygen. Can J Phys 52:2305–2311

Ancsin J (1975) Crystalline transformations of oxygen. In: Billing BF, Quinn TJ (eds) Institute of physics conference series vol 26, pp 57–64

Ancsin J (1977) Thermometric fixed points of hydrogen. Metrologia 13:79–86

Ancsin J (1978) Vapor pressures and triple point of neon and the influence of impurities on these properties. Metrologia 14:1–7

Ancsin J (1982) Melting curves of water. In: Schooley JF (ed) Temperature, its measurements and control in science and industry, vol 5. AIP, New York, pp 281–284

Ancsin J (1988a) Triple point of pure and impure deuterium. Metrologia 25:155–163 (See also: Pavese F (1989b) Comments to the former. Metrologia 25:207–208)

Ancsin J (1988b) Triple point of xenon. Metrologia 25:221–225

Ancsin J, Phillips MJ (1969) Triple point of argon. Metrologia 5:77–80

Ancsin J, Phillips J (1982) Argon triple point realization cryostat for platinum resistance long stem thermometers. Rev Sci Instrum 47:1519–1521

Anderson RL, Guildner LA, Edsinger RE (1970) Movable and fixed modular vacuum devices with confined fluorocarbon plastic seals. Rev Sci Instrum 41:1076–1082

Andresen B, Salamon P, Berry RS (1984) Thermodynamics in finite time. Phys Today 37:62–70

Arp VD, McCarty RD (1989) Thermophysical properties of helium-4 from 0.8 to 1500 K with pressures to 2000 MPa, NBS technical note 1334. National Bureau of Standards, Boulder

Arzelier H (1968) Thermodynamique Relativistique et Quantique. Gautier-Villars, Paris

Astrov DN (1990) Private communication

F. Pavese, G. Molinar Min Beciet, *Modern Gas-Based Temperature and Pressure Measurements,* International Cryogenics Monograph Series,
DOI 10.1007/978-1-4419-8282-7, © Springer Science+Business Media New York 2013

Astrov DN, Orlova MP, Kytin GA (1969) PRMI temperature scale in the range from 4.2 to 20 K. Metrologia 5:111–118

Astrov DN, Belyansky LB, Dedikov UA, Zacharov AA, Polunin SP (1984) A precision gas thermometer for the 4–273 K range, document CCT/1984-36, Bureau International des Poids et Mesures. Sèvres, France

Astrov DN, Belyanskii LB, Dedikov YuA, Polunin SP, Zakharov AA (1989) Precision gas thermometry between 2.5 and 308 K. Metrologia 26:151–166

Astrov DN, Belyanskii LB, Dedikov YuA, Zakharov AA, Polunin SP (1990) Thermodynamic temperature scale from 13.8 to 308 K. Izmeritel'naya Tekhnika (1):41–46, 72–81 (Jan 1989, english translation)

Astrov DN, Belyansky LB, Dedikov YA (1995/1996) Correction of the gas-thermometry scale of the VNIIFTRI in the range 2,5–308 K. Metrologia 32:393–395

Aziz RA, Slaman MJ (1990) An analysis of the ITS-90 relations for the non-ideality of ^{3}He and ^{4}He: Recommended relations based on a new interatomic potential for helium. Metrologia 27:211–219

Aziz RA, Slaman MJ (1991) An examination of ab initio results for the helium potential energy curve. J Chem Phys 94:8047–8053

Aziz RA, McCourt FRW, Wong CCK (1987) A new determination of the ground state interatomic potential of helium. Mol Phys 61:1487–1493

Aziz RA, Nain PS, Carley JS, Taylor WL, McConville GT (1979) An accurate intermolecular potential for helium. J Chem Phys 70:4330–4342

Baldan A, Bosma Peruzzi A, Van Der Veen AMH, Shimizu Y (2009) Adiabatic calorimetry as support to the certification of high-purity liquid reference materials. Int J Thermophys 30:325–333

Bannister JD (1966) Spontaneous pressure oscillations in tubes connecting liquid helium reservoirs to 300 K environment. In: proceedings IIR conference, annex 1966–5 to bulletin IIR, pp 127–130

Barber CR (1966) The sublimation temperature of carbon dioxide. Br J Appl Phys 17:391–397

Barber CR (1972) A proposal for a practical scale of temperature below 20 K. In: Plumb HH (ed) Temperature, its measurements and control in science and industry, vol 4. Pittsburgh, Washington, pp 99–103

Barrett CS, Meyer L (1965a) Argon-nitrogen phase diagram. J Chem Phys 42:107–112

Barrett CS, Meyer L (1965b) Phase diagram of argon-carbon monoxide. J Chem Phys 43:3502–3506

Barwick VJ, Ellison SLR (1999) Measurement uncertainty: approaches to the evaluation of uncertainties associated with recovery. Analyst 124:981–990

Bazarov IP (1964) Thermodynamics. Pergamon Press, Oxford

Beattie JA (1941) The thermodynamic temperature of the ice point. In: Fairchild CO, Hardy JD, Sosman RB, Wensel HT (eds) Temperature, its measurements and control in science and industry, vol 1. Reinhold Publication Company, New York, pp 74–88

Beaudoin G, Haljan P, Paetkau M, Beamish JR (1996) Freezing of molecular hydrogen and its isotopes in porous vycor glass. J Low Temp Phys 105:113–131

Bedford RE (1990) Physical principles. In: Ricolfi T, Scholz H (eds) Thermal sensors, vol 4. VCH, Weinheim (Sensors—a comprehensive book series in eight volumes)

Bedford RE, Bonnier G, Maas H, Pavese F (1984) Recommended values of temperature for a selected set of secondary reference points. Metrologia 20:145–155

Bedford RE, Bonnier G, Maas H, Pavese F (1990) Techniques for approximating the ITS-90, monograph 1990/1991, Bureau International des Poids et Mesures. Sèvres, France (www.bipm.org)

Bedford RE, Bonnier G, Maas H, Pavese F (1996) Recommended values of temperature on the international temperature scale of 1990 for a selected set of secondary reference points. Metrologia 33:133–154

Bedin E, De Combarieu A, Doulat J (1980) Un thermomètre à gaz à volume constant à basse température (4–300 K). BNM Bull 17:5–13

Bellatreccia A, Martinis L, Scaramuzzi F (1979) Use of solid hydrogen to attain temperatures down to 6–7 K: perspective for cryogenic space satellites. In: proceedings XV International congress of refrigeration, IIR, Paris, pp 41–44

Benedetto G, Gavioso RM, Spagnolo R, Marcarino P, Merlone A (2004) Acoustic measurements of the thermodynamic temperature between the triple point of mercury and 380 K. Metrologia 41:74–98

Benz SP, Pollarolo A, Qu JF, Rogalla H, Urano C, Tew WL, Dresselhaus PD, White DR (2011) An electronic measurement of the Boltzmann constant. Metrologia 48:142–153

Berman R, Kopp J (1968) Measurements of the vapor pressure of helium-3 in high magnetic fields. Cryogenics 8:111–112

Berry KH (1979) A low temperature gas thermometry scale from 2.6–27.1 K. Metrologia 15:89–115

Berry KH (1982) Measurements of thermodynamic temperature from 2.6–27.1 K. In: Schooley JF (ed) Temperature, its measurements and control in science and industry, vol 5. AIP, New York, pp 21–24

Besley LM, Kemp RC (1977) An intercomparison of temperature scales in the range 1–30 K using germanium resistance thrmometry. Metrologia 13:35–51

Bewilogua L, Knoner R (1961) Thermosiphons. IIR Bull Annexe 1961–1965, IIR, London, pp 199–210

Bhatia AK, Drachman RJ (1994) Polarizability of helium and the negative hydrogen ion. J Phys B: At Mol Opt Phys 27:1299–1305

Bich E, Hellmann R, Vogel E (2007) Ab initio potential energy curve for the helium atom pair and thermophysical properties of the dilute helium gas. II. Thermo-physical standard values for low-density helium. Mol Phys 105:3035–3049

Bigeleisen J, Roth E (1961) Vapor pressures of the neon isotopes. J Chem Phys 35:68–77

Bignell N, Bean VE (1988) A fixed point on the pressure scale: carbon dioxide vapor pressure at 273.16 K. Metrologia 25:141–145

BIPM (1969) The international practical temperature scale of 1968. Metrologia 5:35–45

BIPM (1979) The 1976 provisional 0.5–30 K temperature scale. Metrologia 15:65–68

BIPM (1983) Supplementary information for the IPTS-68 and for the EPT-76, monograph, Bureau International des Poids et Mesures. Sèvres, France (http://www.bipm.org)

BIPM (1989) Echelle internationale de température de 1990 (EIT-90), Bureau International des Poids et Mesures, Sèvres, France, extrait des Procès Verbaux du CIPM, 78 Session

BIPM (1990a) Supplementary Information for the ITS-90, monograph, Bureau International des Poids et Mesures. Sèvres, France (http://www.bipm.org)

BIPM (1990b) Techniques for approximating the ITS-90, monograph 1990/1991, Bureau International des Poids et Mesures. Sèvres, France (http://www.bipm.org)

BIPM/ISO (2008) International vocabulary of basic and general terms in metrology (VIM), Bureau International des Poids et Mesures. Sèvres, France (http://www.bipm.org)

BIPM, IEC, IFCC, ISO, IUPAC, IUPAP, OIML (1995) Guide to the expression of uncertainty in measurement (GUM), 2nd edn, Bureau International des Poids et Mesures. Sèvres, France (http://www.bipm.org)

Biro TS, Van P (2010) About the temperature of moving bodies. EPL 89:30001. doi:10.1209/0295-5075/89/30001. www.epljournal.org

Blanes-Rex R, Fernandez EPA, Guzman F (1982) On the triple point temperature of carbon dioxide. Cryogenics 22:113–114

Blanke W, Thomas W (1981) The temperatures of the triple points of methane and argon in the IPTS-68. In: proceedings I symposium IMEKO TC 12, CSVTS, Dum Techniky, Praha, pp 19–24

Bloembergen F, Bonnier G, Ronsin H (1990) An intercomparison of sealed argon triple point calibration facilities accomodating long—stem thermometers. Metrologia 27:101–106

Bonhoure J (1984) Private communication

Bonhoure J, Pello R (1978) Temperature of the triple point of methane. Metrologia 14:175–177

Bonhoure J, Pello R (1980) Points triples de l'argon et du methane: utilization de cellules scellées. Metrologia 16:95–99

Bonhoure J, Pello R (1983) Cellule à point triple de l'argon: instrument de transfer de pression. Metrologia 19:21–23
Bonnier G (1975) Point triple de l'argon (83,798 K) référence de transfert. Bull BNM 22:14–18
Bonnier G (1982) Thermal behavior of thermometric sealed cells and of a multicompartment cell. In: Schooley JF (ed) Temperature, its measurements and control in science and industry, vol 5. AIP, New York, pp 231–238
Bonnier G (1987) Le point triple de l'eau: conception et étude d'une cellule scellée métallique. Bull BNM 70:17–21
Bonnier J, Hermier Y, Wu Biqin (1984) Triple point of carbon dioxide in a multicompartment cell. In: Bernhard F (ed) Proceeding II IMEKO Symposium Suhl, GDR, pp 39–54
Born M (1949) Natural philosophy of cause and chance. Oxford University Press, Oxford
Bosma R, Baldan A, Heemskerk M, Peruzzi A (2004) Adiabatic calorimetry for purity determination of liquid organics at NMi VSL. In: Zvizdic D et al (eds) Proceeding TEMPMEKO 2004, LPM/FSB, Zabreb, pp 745–750
Boyes SJ, Ewing MB, Trusler JPM (1990) Primary acoustic thermometry between 100 and 300 K using a spherical resonator. In: proceeding XI IUPAC conference, pp 530
Brickwedde FG, Durieux M, Clement JR, Logan JK (1960) The 1958 ^{4}He scale of temperatures. J Res NBS 64A:1–17
Callendar GS (1899) On a practical thermodynamic standard. Phil Mag 48:519–547
Camacho D (2002) Superconducting based temperature pseudo-fixed point, PhD Thesis 2000–2002. CERN, Geneva
Cameron JA, Seidel GM (1985) The second virial coefficient of ^{3}He gas below 1.3 K. J Chem Phys 83:3621–3625
Canongia Lopes JN, Pádua AAH, Rebelo LPN, Bigeleisen J (2003) Calculation of vapor pressure isotope effects in the rare gases and their mixtures using an integral equation theory. J Chem Phys 118:5028–5037
Carathéodory C (1909) Untersushungen über die Grundlagen der Thermodynamik. Math Ann 67:355–386 (Berlin)
Carnot S (1832) Réflections sur la Puissance Motrice du Feu et sur les Machines Propres à dévélopper cette Puissance. In: Mendoza E (ed) Reflections on the motive power of fire and other papers (trans: Thurston RH). Dover Publications, New York
Cataland G, Edlow M, Plumb HH (1972) The determination of absolute temperatures from sound velocity measurements. In: Plumb HH (ed) Temperature, its measurements and control in science and industry, vol 4. ISA, Pittsburg, pp 129–132
Cataland G, Edlow M, Plumb HH (1982) Recent experiments on liquid helium vapor pressure measurements from 2 to 4 K. In: Schooley JF (ed) Measurements and control in science and industry, vol 5. AIP, New York, pp 413–420
CCT (1980) Report of working group 5, annexe T6, comptes rendus du CCT, Bureau International des Poids et Mesures. Sèvres, France, pp 105–107
CCT (1984) Report of working group 4, annexe T5, comptes rendus du CCT, Bureau International des Poids et Mesures. Sèvres, France, p 147
CCT (2005) Recommendation T3 (2005) to the CIPM: creation of a mise en pratique of the definition of the kelvin, document 2005-32, Bureau International des Poids et Mesures. Sèvres, France
CCT (2006a) Mise en pratique for the definition of the kelvin, Bureau International des Poids et Mesures. Sèvres, France (http://www.bipm.org/utils/en/pdf/MeP_K.pdf)
CCT (2006b) Technical annex for the International Temperature Scale of 1990 (ITS-90), Bureau International des Poids et Mesures. Sèvres, France (http://www.bipm.org. http://www.bipm.org/utils/en/pdf/MeP_K_Technical_Annex.pdf)
CCT WG1 (2005) Methodologies for the estimation of uncertainties and the correction of fixed-point temperatures attributable to the influence of chemical impurities, CCT/2005-08, Bureau International des Poids et Mesures. Sèvres, France (http://www.bipm.org)
CCT WG3 (2005) WG3 report to CCT, CCT/2005-15. Bureau International des Poids et Measures. Sèvres, France (http://www.bipm.org)

CCT WG4 (2008) Report of working group 4, document CCT/2008-13rev, 2008. Bureau International des Poids et Measures. Sèvres, France (http://www.bipm.org)
Cencek W, Jeziorska M, Bukowski R, Jaszunski M, Jeziorsi B, Szalewicz K (2004) Helium dimer interaction energies from Gaussian geminal and orbital calculations. J Phys Chem A 108:3211–3224
Cencek W, Przybytek M, Komasa J, Mehl GB, Jeziorski B, Szalewicz K (2012) Effects of adiabatic, relativistic, and quantum electrodynamics interactions on the pair potential and thermophysical properties of helium. J Chem Phys (to appear)
CGPM (1889) Comptes Rendus des Séances de la I Conférence Générale, pp 35, Bureau International des Poids et Mesures. Sèvres, France
CGPM (1948) Comptes Rendus des Séances de la IX Conférence Générale, Bureau International des Poids et Mesures. Sèvres, France
CGPM (1960) Comptes Rendus des Séances de la XI Conférence Générale, pp 124–133, Bureau International des Poids et Mesures. Sèvres, France
CGPM (1989) Comptes Rendus des Séances de la XVIII Conférence Générale, Bureau International des Poids et Mesures. Sèvres, France
CGPM (2011) On the possible future revision of the international system of units, the SI, Comptes Rendus des Séances de la XXIV Conférence Générale, Resolution 1, Bureau International des Poids et Mesures, Sèvres, France. http://www.bipm.org/en/convention/cgpm/resolutions.html
CIPM (1887) Procès Verbaux 85, Bureau International des Poids et Mesures. Sèvres, France
CIPM (2005a) Recommendation 1 (CI-2005): preparative steps towards new definitions of the kilogram, the ampere, the Kelvin and the mole in terms of fundamental constants, International Committee for Weights and Measures, Bureau International des Poids et Mesures. Sèvres, France
CIPM (2005b) Recommendation 2 (CI-2005): Clarification of the definition of the kelvin, unit of thermodynamic temperature, International Committee for Weights and Measures, Bureau International des Poids et Mesures. Sèvres, France
Chen X (1986) A brief history of the development of heat and temperature measurement in ancient China. Symposium on temperature, Beijing
Chen HH, Aziz RA, Lim CC (1971) On the vapor pressure of solid argon. Can J Phys 49:1569–1581
Chialvo AA, Horita J (2003) Isotopic effect on phase equilibria of atomic fluids and their mixtures: a direct comparison between molecular simulation and experiment. J Chem Phys 119:4458–4467
Ciarlini P, Pavese F (1992) Computational and statistical analysis of the thermodynamic data which form the basis of the ITS-90 between 13.8 and 273.16 K—I Computational basis. In: Schooley JF (ed) Temperature, its measurement and control in science and industry, vol 6. American Institute of Physics, New York, pp 75–78
CODATA (Committee on Data for Science and Technology), Task Group on Fundamental Constants (TGFC) (2010) CODATA recommended values of the fundamental physical constants: 2010 (NIST), available in press from 2012
Cohen ER, Taylor BN (1986) The 1986 Adjustement of the fundamental physical constants CODATA Bullettin (63), International Council of Scientific Unions, CODATA, 51 Blvd. de Montmerency, 75016 Paris. Also, (1987) J Res NBS 92:85–95
Colclough AR (1972) A low frequency acoustic thermometer for the range 2–20 K. In: Plumb HH (ed) Temperature, its measurements and control in science and industry, vol 4. ISA, Pittsburg, pp 365–372
Colclough AR (1973) Systematic errors in primary acoustic thermometry in the range 2–20 K. Metrologia 9:75–98
Colclough AR (1974) A projected refractive index thermometer for the range 2–20 K. Metrologia 10:73–74
Colclough AR (1979) The temperature dependance of pressure-volume and acoustic second virial coefficient for ^{4}He in the quantum region. Metrologia 15:183–193
Colclough AR (1982a) A refractive index thermometer for use at low temperatures. In: Schooley JF (ed) Temperature, its measurements and control in science and industry, vol 5. AIP, New York, pp 89–94

Colclough AR (1982b) Primary acoustic thermometry: principles and current trends. In: Schooley JF (ed) Temperature, its measurements and control in science and industry, vol 5. AIP, New York, pp 65–75

Colwell JH, Fogle WE, Soulen RJ (1992) The ^{3}He melting curve thermometer as a universal temperature transfer standard. In: Schooley JF (ed) Temperature, its measurements and control in science and industry, vol 6. AIP, New York, pp 101–106

Compton JP (1970) The realization of the normal boiling point of neon. II vapor pressure measurements. Metrologia 6:103–109

Compton JP, Ward SD (1976) Realization of the boiling and triple points of oxygen. Metrologia 12:101–113

Cook GA (1961) Argon, helium and rare gases. Interscience, New York

Cowan JA, Kemp RC, Kemp WRK (1976) An investigation of the β–γ transition in oxygen. Metrologia 12:87–91

Crooks MJ (1969) Temperature profiles in experimental dewars. Cryogenics 9:32–35

Dash JG (1979) Films and solid surfaces. Academic Press, New York

Dash JG, Schick (1978) Helium monolayers. In: Bennemann KH, Ketterson JB (eds) The physics of liquid and solid helium, pt. II. Wiley, New York, pp 497–572

Daunt JG, Lerner E (1972) Adsorption of ^{3}He and ^{4}He on copper and on argon-coated copper below 20 K. J Low Temp Phys 8:79–92

Davis JA, Rodewald N, Kurata F (1962) Solid-liquid-vapor phase behavior of the methane-carbon dioxide system. A I Ch E J 8:537–539

De Boer J (1965) Temperature as a basic physical quantity. Metrologia 1:158–169

De Groot SR, Mazur P (1962) Non-equilibrium thermodynamics. North Holland, Amsterdam

De Groot MJ, Gibb K, Heimeriks H (1997) The measurement of the helium vapour pressure between 0.53 K and 1. In: Szmyrka-Grzebyk A (ed) Proceedings Wroclaw Workshop. Ladek Zdroj, Wroclaw, L 104–109

De Laet J (1960) Verb K Vlaam Acad Wet 66:22

de Podesta M, Sutton G, Underwood R, Bell S, Stevens M, Byrne T, Josephs-Franks P (2011) Outgassing of water vapour, and its significance in experiments to determine the Boltzmann constant. Metrologia 48:1–6

Ditmars DA, Furukawa GT (1965) Detection and damping of thermal-acoustic oscillations in low temperature measurements. J Res NBS 69C:175–178

Dobre M, Didialaoui I, Hermier Y (2011) Argon triple point for long-stem SPRTs: thermal behavior. Int J Thermophys 32:1573–1580

Doucet Y (1975) Liquid-solid phase equilibria II—Cryoscopy. In: Nendre B Le, Vodar B (eds) Experimental thermodynamics, IUPAC, vol II. Butterworths, London, pp 835–900

Duff MJ, Okun LB, Veneziano G (2002) J High Energy Phys JHEP03(2002)023. http://cdsweb.cern.ch/record/523965

Dunning-Davies J (1976) Negative absolute temperatures and Carnot cycles. J Phys A: Math Gen 9:605–609

Durieux M (1960) Thermometry at liquid helium and liquid hydrogen temperatures. Thesis, Kamerling Onnes Laboratorium, Leiden

Durieux M (1991) Private communication

Durieux M, Rusby RL (1983) Helium vapor pressure equations on the EPT-76. Metrologia 19:67–72

Durieux M, Reesing AL (1997) The ^{4}He and ^{3}He vapour-pressure equations. In: Szmyrka-Grzebyk (ed) Proceedings Wroclaw Workshop. Ladek Zdroj, Wroclaw, pp 96–103

Durieux M, Astrov DN, Kemp WRG, Swenson CA (1979) The derivation and development of the 1976 provisional 0.5–30 K temperature scale. Metrologia 15:57–63

Durieux M, van Dijk JE, ter Harmsel H, Rem PC (1982) Helium vapor pressure equations on the EPT-76. In: Schooley JF (ed) Temperature, its measurements and control in science and industry, vol 5. AIP, New York, pp 145–153

Dymond JH, Smith EB (1980) The virial coefficient of pure gases and mixtures—a critical compilation. Clarendon Press, Oxford

El Samahy AA (1979) Thermometry between 0.5 and 30 K. Thesis, Kamerling Onnes Laboratorium, Leiden

Elsner A (1990) Fit function for the vapor pressure of helium-3. Phys Lett A 149:184–190

Engert J, Fellmuth B, Maidanov VA (2003) High-Precision realisation of the lambda transition of ^{4}He as a temperature fixed point. In: Szmyrka-Grzebyk A (ed) Proceedings CELTAM workshop. INTiBS, Wroclaw, pp 37–42

Engert J, Fellmuth B, Jousten K (2007) A new ^{3}He vapour-pressure based temperature scale from 0.65 to 3.2 K consistent with the PLTS-2000. Metrologia 44:40–52

Esel'son BN, Berezniak NG (1956) Diagram of state for liquid-vapour system of helium isotopes ^{3}He and ^{4}He. Soviet Phys JETP 30:628–639

Esel'son BN, Blagoi YuP, Grigor'ev VN, Manzhelii VG, Mikhailenko SA, Neklyudov NP (1971) Properties of liquid and solid hydrogen, Izdatel'stvo Standardtov, Moskva 1969, Israel Program for Scientific Translations, Jerusalem

Eurachem (2000) CITAC Guide, end edn. http://www.eurachem.org

Ewing MB, Goodwin ARH (1992) Speeds of sound, perfect-gas heat capacities, and acoustic virial coefficients for methane determined using a spherical resonator at temperatures between 255 and 300 K and pressures in the range 171 kPa to 7.1 MPa. J Chem Thermodyn 24:1257–1274

Ewing MB, Trusler JPM (1989) Speed of sound in CF4 between 115 and 300 K measured with a spherical resonator. J Chem Phys 90:1106–1115

Ewing MB, Trusler JPM (2000) Primary acoustic thermometry between $T = 90$ K and $T = 300$ K. J Chem Thermodyn 32:1229–1255

Ewing MB, McGlashan ML, Trusler JPM (1986) The temperature-jump effect and the theory of the thermal boundary layer for a spherical resonator. Speed of sound in argon at 273.16 K. Metrologia 22:93–102

Fagerstroem CH, Hollins-Hajjet AC (1969) The specific heat of solid oxygen. J Low Temp Phys 1:3–12

Farkas A (1935) Ortho, para, and heavy hydrogen. Cambridge University Press, Cambridge

Fellmuth B, Maas H (1987) Recommended values of superconducting transition temperatures as reference temperatures for a selected set of materials, document CCT/1987-32, Bureau International des Poids et Mesures. Sèvres, France

Fellmuth B, Wolber L (2010) Investigation of the parameters of sealed triple-point cells for cryogenic gases. Int J Thermophys 32:161–172

Fellmuth B, Maas H, Elefant D (1985) Investigation of the superconducting transition point of niobium as a reference temperature. Metrologia 21:169–180

Fellmuth B, Hill KD, Bloembergen P, de Groot M, Hermier Y, Matveyev M, Pokhodun A, Ripple D, Steur PPM (2005a) Methodologies for the estimation of uncertainties and the correction of fixed-point temperatures attributable to the influence of chemical impurities, Working document of the CCT WG1, CCT/2005-08, Bureau International des Poids et Mesures. Sèvres, France

Fellmuth B, Wolber L, Hermier Y, Pavese F, Steur PPM, Peroni I, Szmyrka-Grzebyk A, Lipinski L, Tew WL, Nakano T, Sakurai H, Tamura O, Head D, Hill KD, Steele AG (2005b) Isotopic and other influences on the realization of the triple point of hydrogen. Metrologia 42:171–193

Fellmuth B, Wolber L, Head D, Hermier Y, Hill Lipinski LKD, Mao YZ, Nakano T, Pavese F, Peruzzi A, Rusby RL, Shkraba V, Steele AG, Steur PPM, Szmyrka-Grzebyk A, Tew WL, Wang L, White DR (2012) Investigation of low-temperature fixed points by an international star intercomparison of sealed-triple point cells. Metrologia 49:257–265

Fernandez-Fassnacht E, Del Rio F (1984) The vapor pressure of carbon dioxide from 194 to 243 K. J Chem Thermodyn 16:469–474

Ferri D, Ichim D, Pavese F, Peroni I, Sparasci F, Steur PPM (2002) Low-temperature fixed points realizations using a cryogen-free refrigerator. In: Zvizdic D et al (eds) Proceedings TEMPMEKO 2004. LPM/FSB, Zabreb, pp 165–170

Ferri D, Ichim D, Pavese F, Peroni I, Sparasci F, Steur PPM (2003) A closed-cycle refrigerator for reslizing low-temperature fixed points. In: Szmyrka-Grzebyk A (ed) Proceedings CELTAM workshop. INTiBS, Wroclaw, pp 102–107

Fischer J, Gerasimov S, Hill KD, Machin G, Moldover MR, Pitre L, Steur P, Stock M, Tamura O, Ugur H et al (2007) Preparative steps towards the new definition of the kelvin in terms of the Boltzmann constant. Int J Thermophys 28:1753–1765

Fischer J, de Podesta M, Hill KD, Moldover M, Pitre L, Rusby RL, Steur PPM, Tamura O, White R, Wolber L (2011) Present estimates of the differences between thermodynamic temperatures and the ITS-90. Int J Thermophys 32:12–25

Fogle WE, Soulen RJ, Colwell JH (1992a) ITS-90 below 1 K: how accurate is it? In: Schooley JF (ed) Temperature, its measurement and control in science and industry, vol 6. American Institute of Physics, New York, pp 85–90

Fogle WE, Soulen RJ, Colwell JH (1992b) A new cryogenic temperature scale from 6.3 mK to 650 mK. In: Schooley JF (ed) Temperature, its measurement and control in science and industry, vol 6. American Institute of Physics, New York, pp 91–96

Fosdick RL, Rajagopal KR (1983) On the existence of a manifold for temperature. Arch Ration Mech Anal 81:317–332

Frank DJ, Nast TC (1986) Getter activated cryogenic thermal switch. Adv Cryog Eng 31:933–940

Franson MAH (1989) Standard methods for examination of water and wastewater. American public health association, Washington

Freeman MP, Hasley GD (1956) Interaction of pairs of gas atoms with surfaces. J Phys Chem 60:1119–1123

Freeth FA, Verschoyle TTH (1931) Physical constants of the system methane-hydrogen. Proc Royal Soc A130:453–463

Frels W, Smith DR, Ashworth T (1974) Vapor pressure of nitrogen below the triple point. Cryogenics 14:3–7

Frenken JWM, Van Der Veen (1990) Suface-melting. Nederlandsch Tijdschr Natuurkunde A56(4):1–6

Furukawa GT (1972) Vapor pressures of natural neon and of the isotopes ^{20}Ne and ^{22}Ne from the triple point to the normal boiling point. Metrologia 8:11–27

Furukawa GT (1982) Reproducibility of the triple point of argon in sealed transportable cells. In: Schooley JF (ed) Temperature, its measurements and control in science and industry, vol 5. AIP, New York, pp 239–248

Furukawa GT, Bigge WR (1976) The triple point of mercury as a thermometric standard, document CCT/1976-18, comptes rendus CCT, annexe T14, Bureau International des Poids et Mesures. Sèvres, France, pp 138–144

Furukawa GT, Saba WG, Sweger DM, Plumb HH (1970) Normal boiling point and triple point temperatures of neon. Metrologia 6:35–37

Furukawa GT, Bigge WR, Riddle JL (1972) Triple point of argon. In: Plumb HH (ed) Temperature, its measurements and control in science and industry, vol 4. ISA, Pittsburg, pp 231–240

Furukawa GT, Riddle JL, Bigge WR, Pfeiffer ER (1982) Application of some metal SRM's as thermometric fixed points. NIST, Gaithersburg (NBS Spec Publ pp 260–277)

Gaiser C (2008) Properties of helium and gas thermometry, PhD Thesis, Humboldt Univ Berlin (Aachen: Shaker). ISBN:978-3-8322-7552-5

Gaiser C, Fellmuth B (2009) Helium virial coefficients—a comparison between new highly accurate theoretical and experimental data. Metrologia 46:525–533

Gaiser C, Fellmuth B, Haft N (2008a) Primary dielectric-constant gas thermometry in the range from 2.4 to 26 K at PTB. Int J Thermophys 29:18–30

Gaiser C, Fellmuth B, Haft N (2008b) Dielectric-constant gas-thermometry scale from 2.5 to 36 K applying ^{3}He, ^{4}He, and neon in different temperature ranges. Int J Thermophys 31:1428–1437

Gammon BE (1976) The velocity of sound with derived state properties in helium at −175 to 150 °C with pressure to 150 atm. J Chem Phys 64:2556–2568

Gavioso RM, Benedetto G, Giuliano Albo PA, Madonna D, Merlone A, Guianvarc'h C, Moro F, Cuccaro R (2010) A determination of the Boltzmann constant from speed of sound measurements in helium at a single thermodynamic state. Metrologia 47:387–409

Gavioso RM, Benedetto G, Madonna Ripa D, Giuliano Albo PA, Guianvarc'h C, Merlone A, Pitre L, Truong D, Moro F, Cuccaro R (2011) Progress in INRIM experiment for the determination of the Boltzmann constant with a quasi-spherical Resonator. Int J Thermophys 32:1339–1354

Gershanik AP (1984) Statistical determination of the volume of an adsorbed layer. Zhurn Fiz Khim (USSR) 68:677–682

Gershanik AP, Glikman MS, Astrov DN (1978) On the sorption correction for the precise gas thermometer, document CCT/1978-45, annexe T11, comptes rendus CCT, Bureau International des Poids et Mesures. Sèvres, France, pp 93–97

Gifford WE (1969) The thermal check valve—a cryogenic tool. Advances in Cryogenic Engineering, vol 7. Plenum Press, New York, pp 551–555

Goldberg RN, Weir RD (1992) Conversion of temperatures and thermodynamic properties to the basis of the ITS-90. Pure Appl Chem 64:1545–1562

Goldschvartz JM, Van Der Merwe WP, Kollen A (1975) Reaching a temperature of 0.64 K in an ^{4}He cryostat with a new geometry. Cryogenics 15:153–154

Gonfiantini R (1978) Standards for stable isotope measurements in natural compounds. Nature 271:534–536

Goodwin RD (1974) The thermophysical properties of methane, from 90 to 500 K at pressures to 700 bar, NBS technical note 653, National Bureau of Standards, Cryogenic Division, Boulder

Goodwin RD (1977) Provisional thermodynamic functions of propane from 85 to 700 K at pressures to 700 bar, NBSIR 77–860, National Bureau of Standards, Cryogenic Division, Boulder

Greywall DS (1985) ^{3}He melting-curve thermometry at millikelvin temperatures. Phys Rev B 31:2675–2683

Greywall DS (1986) ^{3}He specific heat and thermometry at millikelvin temperatures. Phys Rev B 33:7520–7538

Grilly ER (1962) The vapor pressure of solid and liquid neon. Cryogenics 2:226–229

Grilly ER (1971) Pressure-volume-temperature relations in liquid and solid ^{3}He. J Low Temp Phys 4:615–635

Grimsrud DT, Werntz JH Jr (1967) Measurements of the velocity of sound in ^{3}He and ^{4}He gas at low temperatures with applications for the temperature scale. Phys Rev 157:181–190

Grohmann K (1990) Private communication

Grohmann K, Koch H (1984) A dielectric constant gas thermometer. In: Eckern U, Schmid A, Weber W, Wuhl H (eds) Proceedings LT-17. Elsevier Science Publication B. V., Eindhoven, pp 397–398

Gu Y, Timmerhaus KD (1991a) Damping of thermal acoustic oscillations in hydrogen systems. Adv Cryo Eng 37A:265–273 (Theoretical analysis of thermal acoustic oscillation systems. In: proceedings. XVIII IIR congress, Montreal, paper N°20)

Gu Y, Timmerhaus KD (1991b) Thermal acoustic oscillations in triple point liquid hydrogen systems. Int J Refrig 14:282–291

Gugan D (1984) The analysis of ^{4}He isotherms: density and dielectric virial coefficients, and the accuracy of NPL-75. Metrologia 19:147–162

Gugan D, Mitchell GW (1980) Dielectric constant gas thermometry from 4.2 to 27.1 K. Metrologia 16:149–167

Guildner LA, Edsinger RE (1976) Deviation of international practical temperatures from thermodynamic temperatures in the range from 273.16 to 730 K. J Res NBS 80A:703–738

Haase R (1969) Thermodynamics of irreversible processes. Reading, Mass

Head DI (1996) Recent measurements of the deuterium triple point. In: Marcarino P (ed) Proceedings TEMPMEKO 96. Levrotto & Bella Publication, Torino, pp 87–91

Head DI (2001) Recent measurements of European Deuterium cells at NPL. In: Fellmuth B, Seidel J, Scholz G (eds) Proceedings TEMPMEKO 2001. VDE, Berlin, pp 423–428

Head DI, Rusby RL (1990) Cleaner catalyst for the para to ortho conversion in high purity deuterium at low temperatures. Phys B: Phys Condens Matter 165:161–162

Head DI, Mao W, Rusby RL (1989) Comparison of three xenon triple point cells, document CCT/1989-19, Bureau International des Poids et Mesures. Sèvres, France

Head DI, Hermier Y, Rusby RL, Bonnier G, Mao W (1990) Measurements of carbon dioxide and xenon triple point cells. Tempmeko 90, Finnish Society of Automatic Control, Helsinky, pp 118–125

Head DI, Rusby RL, Pavese F (1992) The triple point of pure equilibrium deuterium using Gd_2O_3 spin catalyst. In: Schooley JF (ed) Temperature, its measurement and control in science and industry, vol 6. American Institute of Physics, New York, pp 247–249

Hellmann R, Bich E, Vogel E (2007) Ab initio potential energy curve for the helium atom pair and thermophysical properties of dilute helium gas. I. Helium-helium interatomic potential. Mol Phys 105:3013–3023

Hermier Y, Bonnier G (1990) Réalization du point triple de l'argon par une méthode calorimétrique. Bull BNM 82:23–27

Hermier Y, Pitre L, Geneville C, Vergé A, Bonnier G, Head DI, Fellmuth B, Wolber L (2003) A new generation of multicells for cryogenic fixed points at BNM/INM. In: Ripple DC (ed) Temperature, its measurements and control in science and industry, vol 7. AIP, New York, pp 179–184

Hilberath W, Vowinkel B (1983) An automatic low temperature heat switch. Cryogenics 23:467–468

Hill KD (1995) Inconsistency in the ITS-90 and the triple point of mercury. Metrologia 32:87–94

Hill KD (2001) Realizing the ITS-90 below 13.8 K at NRC. In: Fellmuth B, Seidel J, Scholz G (eds) Proceedings TEMPMEKO 2001. VDE, Berlin, pp 543–548

Hill KD (2002) Realizing the ITS-90 below 4.2 K at the National Research Council of Canada. Metrologia 39:41–49

Hill KD, Bedford RE (1990) Deviation functions below 303 K for consideration in the ITS-90, document CCT/1989-4, Bureau International des Poids et Mesures. Sèvres, France (and, private communication)

Hill KD, Fahr M (2011) Triple-point temperatures of ^{20}Ne and ^{22}Ne. Int J Thermophys 32:173–188

Hill KD, Steele AG (2003) The non-uniqueness of ITS-90: 13.8033–273.15 K. In: Schooley JF (ed) Temperature, its measurement and control in science and industry, vol 6. American Institute of Physics, New York, pp 53–58

Hill KD, Steele AG (2004) The triple point of xenon. In: Zvizdic D et al (eds) Proceeding TEMPMEKO 2004. LPM/FSB, Zabreb, pp 153–158

Hill KD, Steele AG (2005) The triple point of xenon. Metrologia 42:278–288

Hill KD, Rudtsch S (2005) Thermometry's dependence on chemical metrology: a needs-based assessment. Metrologia 42:1–4

Hiza MJ, Kidnay AJ, Miller RC (1975) Equilibrium properties of fluid mixtures, vol 1. Plenum, New York

Hiza MJ, Kidnay AJ, Miller RC (1982) Equilibrium properties of fluid mixtures, vol 2. Plenum, New York

Hoare FE, Zimmerman JE (1959) Helium temperatures from vapor pressure measurements. Rev Sci Instrum 30:184–186

Hoge HJ, Arnold RD (1951) Vapor pressure of hydrogen, deuterium and hydrogen deuteride, and dew-point pressure of their mixtures. J Res NBS 47:63–74

Hurly JJ, Moldover MR (2000) Ab initio values of the thermophysical properties of helium as standards. J Res Natl Inst Stand Technol 105:667–688

Hurly JJ, Mehl JB (2007) ^{4}He thermophysical properties: new ab initio calculations. J Res Natl Inst Stand Technol 112:75–94

Hwang KF, Khorana BM (1976) Lambda transition of liquid helium as thermometric fixed point. Metrologia 12:61–63

IJOT (International Journal of Thermophysics) (2010) Special issue on Boltzmann costant determinations Int J Thermophys 31(7)

Inaba A, Mitsui K (1978a) Effects of impurity and of annealing on the triple point of methane. Jpn J Appl Phys 17:1451–1452

Inaba A, Mitsui K (1978b) Réalization des points triples du kripton et du xénon au moyen de cellules scèllée, Comité Consultatif de Thermométrie, Annexe T17, Bureau International des Poids et Mesures. Sèvres, France, pp 111–113

Inaba A, Mitsui K (1980) Nuclear spin conversion in methane at its triple point. Bull NRLM 42:17–18

Israilov KC (1969) Influence of the thermometric measurements on the results of manometric and gas thermometric measurements. Acta Metrology Institute VNIIM 105 (165), Leningrad, USSR, pp 81–106 (trans: Pavese F). IMGC report IMGC S/271, January 25

IUPAC (1976) International thermodynamic tables of the fluid state—3 carbon dioxide. In: Angus S, Armstrong B, de Reuck KM (eds) Pergamon Press, Oxford (The series includes: 1. Argon; 2. Ethylene)

IUPAC (1978) International thermodynamic tables of the fluid state—5 Methane. In: Angus S, Armstrong B, de Reuck KM (eds) Pergamon Press, Oxford (The series includes: 4. Helium; 6. Nitrogen; 7. Propylene (Propene))

IUPAC (1987) Recommended reference materials for the realization of physicochemical properties. In: March KN (ed) Blackwell Scientific Publication, Oxford (Chap. 5: Pressure-volume-temperature, Collator: Ambrose D)

Jansco G, Van Hook WA (1974) Condensed phase isotope effects. Chem Rev 74:689–750

Jeevanandam M (1971) Vapor pressure isotope effect near the triple point. J Chem Phys 55:5735–5741

Jones MC, Arp VD, Parrish WR, Daney DE, Ludtke PR, Frederick NV, Hands BA (1977) Helium research in support of superconducting power transmission. Annual Report NBSIR 77–853, CONS-3800-1, National Bureau of Standards, Cryogenic Div

Kalinin MI, Kononogov SA (2005) Boltzmann's constant, the energy meaning of temperature an thermodynamic irreversibility. MeasTechn 48:632–636

Kallner A, Khorovskaya L, Petterson T (2005) A method to estimate the uncertainty in measurements in a conglomerate of laboratories/instruments. Scand J Clin Lab Invest 65:551–558

Kang HK, Seong DJ, Kim YG, Gam KS (2001) Construction and performance of the interpolation gas thermometer at KRISS. In: Fellmuth B, Seidel J, Scholz G (eds) Proceedings TEMPMEKO 2001. VDE, Berlin, pp 106–109

Kapitza P (1941) Heat transfer and superfluidity in helium. Phys Rev 60:354–355

Keller WE (1955a) Pressure-volume isotherm of ^{3}He between 1.5 and 3.8 K. Phys Rev 98:1571–1575

Keller WE (1955b) Pressure-volume isotherms of ^{4}He below 4.2 K. Phys Rev 97:1–12

Keller WE (1969) Helium-3 and Helium-4. The international cryogenics monograph series. Plenum Press, New York

Kemp RC (1982) The triple points of equilibrium and normal deuterium. In: Schooley JF (ed) Temperature, its measurements and control in science and industry, vol 5. AIP, New York, pp 249–250

Kemp RC (1989) A test of the interpolation equations of version E of ITS-90 for platinum resistance thermometers below 273.16 K, document CCT/1989-30; comments on the Bloembergen modification, document CCT/1989-31, Bureau International des Poids et Mesures. Sèvres, France

Kemp RC, Kemp WRG (1978) The triple points of krypton, argon, nitrogen and neon. Metrologia 14:83–88

Kemp RC, Kemp WRG (1979a) The α–β transition in nitrogen. Metrologia 15:87–88

Kemp RC, Kemp WRG (1979b) The triple point, boiling point and 17 K point of equilibrium hydrogen. Metrologia 15:155–159

Kemp RC, Smart PW (1979) Simple and compact constant volume valve for use in gas thermometry. Rev Sci Instrum 50:1316–1317

Kemp RC, Kemp WRG, Cowan JA (1976) The boiling points and triple points of oxygen and argon. Metrologia 12:93–100

Kemp RC, Kemp WRG, Smart PW (1982) The triple point of natural xenon. In: Schooley JF (ed) Temperature, its measurements and control in science and industry, vol 5. AIP, New York, pp 229–230

Kemp RC, Kemp WRG, Belsey LM (1986) A determination of thermodynamic temperatures and measurements of the second virial coefficient of ^{4}He between 13.81 and 287 K using a constant-volume gas thermometer. Metrologia 23:61–86

Kemp WRG, Pickup CP (1972) The transition temperatures of solid oxygen. In: Plumb HH (ed) Temperature, its measurements and control in science and industry, vol 4. ISA, Pittsburg, pp 217–223

Kemp WRG, Kemp RC (1981) The triple point of ^{20}Ne. Metrologia 17:67–68

Khnykov VM, Orlova MP, Belyanskii LB, Rabukh LN (1978) The argon triple point: a new reference point for the temperature scale. Zhurnal Fizicheskoi Khimii 52:1483–1484 (English trans: Russian J Phys Chem 52:849–850)

Khnykov VM, Losev MI, Parbuzin VS, Rabuch LI, Astrov DN (1989a) Realization of the triple point of deuterium, document CCT/1989-9, Bureau International des Poids et Mesures. Sèvres, France

Khnykov VM, Losev MI, Gerasimov GM, Rabuch LI, Astrov DN (1989b) Realization of the triple point of xenon, document CCT/1989-8, Bureau International des Poids et Mesures. Sèvres, France

Kleinrahm R, Wagner W (1986) Measurements and correlation of the equilibrium liquid and vapor densities and the vapor pressure along the coexistence curve of methane. J Chem Thermodyn 18:739–760

Kozlowski M, Marciak-Kozlowska J (1997) The time arrow in Plank gas. Found Phys Letters 10:295–299

Kramers HA (1949) Vibrations of a gas column. Physica 15:971–984

Kroeger FR, Swenson CA (1977) Absolute linear thermal expansion measurements on copper and aluminum from 5 to 320 K. J Appl Phys 48:853–864

Kuchta B, Luty T, Meier RJ (1987) The α–β phase transition in solid oxygen. J Phys C: Solid State Phys 20:585–590

Landsberg PT (1961) Thermodynamics. Interscience Publication, New York

Larin MP (1976) Production of temperature over the 29–63 K range using solid nitrogen and its application. Pribory I Teckhnika Eksperimenta (6):208–211 (English trans: Experimental Techniques, pp 1824–1827)

Leadbetter HM (1981) Elastic constants of polycrystalline copper at low temperatures. Phys Stat Sol 66:477–484

Leadbetter HM (1983) Elastic propeties, In: Reed RP, Clark AF (eds) Materials at low temperature, Chap. 1. Am Soc for Metals, Ohio, pp 1–25

Lee MW, Fuks S, Bigeleisen J (1970) Vapor pressures of argon-36 and argon-40 intermolecular forces in solid and liquid argon. J Chem Phys 53:4066–4076

Lee MW, Eshelman DM, Bigeleisen J (1972) Vapor pressures of isotopic krypton mixtures. Intermolecular forces in solid and liquid krypton. J Chem Phys 56:4585–4592

Lemarchand C, Triki M, Darquié B, Bordé CJ, Chardonnet C, Daussy C (2011) Progress towards an accurate determination of the Boltzmann constant by Doppler spectroscopy. New J Phys 13:073028 (online at http://www.njp.org/)

Leming CW, Pollack GL (1970) Sublimation pressures of solid Ar, Ne and Xe (and their lattice mechanics). Phys Rev B 2:3323–3330

LeSar R, Etters RD (1988) Character of the α–β phase transition in solid oxygen. Phys Rev B 37:5364–5370

Levenson MS, Banks DL, Eberhart KR, Gill LM, Guthrie WF, Liu HK, Vangel MG, Yen JH, Zhang NF (2000) An approach to combining results from multiple methods motivated by the ISO GUM. J Res Natl Inst Stand Technol 105:571–579

Lewis GN, Randall M (1923) Thermodynamics and free energy of chemical substances. McGraw-Hill, New York

Lin P, Mao Y, Hong C, Yue Yi, Zhang Q (1990) Study of the realization of ^{4}He λ-transition point temperature by means of a small sealed cell. In: proceedings ICEC 13. Cryogenics 30(Supp):432–436

Lin P, Mao Y, Hong C (1997) Proceedings of international conference of the temperature and thermal measurements (TempBeijing 1997), (Zhang B et al (ed)), Beijing, Standard Press of China, pp 28–34

Lin P, Mao Y, Yu L, Zhang Q, Ho C (2002) Studies on a sealed-cell lambda-point device for use in low temperature thermometry. Cryogenics 42:443–450

Lin P, Mao Y, Hong C, Pavese F, Peroni I, Head D, Rusby RL (2003) Realization of lambda transition temperature of ^{4}He using sealed cells. In: Ripple D (ed) Temperature, its measurement and control in science and industry, vol 7. AIP, New York, pp 191–196

Lin P, Yu L, Yin L (2011) New results for the realization of the superfluid transition temperature of helium. Int J Thermophys 32:153–160

Lipinski L, Szmyrka-Grzebyk A, Manuszkiewicz H (1996) Hysteresis effect in the α–β transition of solid oxygen. Cryogenics 36:921–924

Lipinski L, Szmyrka-Grzebik A, Manuszkiewicz H, Steur PPM, Pavese F (1997) The α–β transition in solid oxygen as a secondary fixed point of the ITS-90. In: Marcarino P (ed) Proceedings TEMPMEKO 96. Levrotto & Bella Publication, Torino, pp 105–109

Lipinski L, Manuszkiewicz H, Szmyrka-Grzebyk A, Steur PPM, Marcarino P (2001) Comparison of temperature values of the mercury triple point realized in miniature and conventional cells. In: Marcarino P (ed) Proceedings TEMPMEKO 96. Levrotto & Bella Publication, Torino, pp 441–446

Lipinski L, Kowal A, Szmyrka-Grzebyk A, Manuszkiewicz H, Steur PPM, Peroni I, Sparasci F, Ferri D (2003) Accurate heat capacity measurements of oxygen at the α–β transition of oxygen. In: Szmyrka-Grzebyk A (ed) Proceedings CELTAM workshop. INTiBS, Wroclaw, pp 119–126

Lipinski L, Kowal A, Szmyrka-Grzebyk A, Manuszkiewicz H, Steur PPM, Pavese F (2007a) The α–β transition of nitrogen. Int J Thermophys 28:1904–1912

Lira IH, Wöger W (1998a) The evaluation of the uncertainty associated with a measurement result not corrected for systematic effects. Meas Sci Technol 9:1010–1011

Lira IH, Wöger W (1998b) The evaluation of the uncertainty in knowing a directly measured quantity. Meas Sci Technol 9:1167–1173

Lobo LQ, Staveley LAK (1979) The vapor pressure of tetrafluoromethane. Cryogenics 19:335–338

Lounasmaa OV (1974) Experimental principles and methods below 1 K. Academic Press, London

Lovejoy DR (1963) Some boiling and triple points below 0 °C. Nature 197:353–354

Luther H, Grohmann K, Fellmuth B (1996) Determination of thermodynamic temperature and ^{4}He virial coeffcients between 4.2 and 27.0 K by dielectric constant gas thermometry. Metrologia 33:341–352

Magnusson B, Naykki T, Hovind H, Krysell M (2003) Handbook for calculation of measurement uncertainty. NORDTEST report TR 537 internet version 2003

Magnusson B, Ellison SLR (2008) Treatment of uncorrected measurement bias in uncertainty estimation for chemical measurements. Anal Bioanal Chem 390:201–213

Maroto A, Boqué R, Riu J, Rius X (2002) Validation of analytical methods. Accred Qual Assur 7:90–94

Martin JE, Quinn TJ, Chu B (1988) Further measurements of thermodynamic temperature using a total radiation thermometer: the range −130 °C to +60 °C. Metrologia 25:107–112

Mastrangelo SVR, Dornte RW (1955) Solid solutions treatment of calorimetric purity data. J Am Chem Soc 77:6200–6201

Matacotta FC, Mc Conville GT, Steur PPM, Durieux M (1987) Measurements and calculations of the ^{3}He second virial coefficient between 1.5 and 20.3 K. Metrologia 24:61–67

Maxwell JC (1871) Theory of Heat. Longmans Green and Company, London

McConville GT (1984) Helium-4 second virial in low temperature gas thermometry: comparison of measured and calculated values. In: proceedings LT17 conference. North Holland, Amsterdam, pp 401–402

McConville GT, Pavese F (1988) Physico-chemical problems involved in measuring thermodynamic properties of normal and equilibrium deuterium at the triple point. J Chem Thermodyn 20:337–358

McConville GT, Hurly JJ (1991) An analysis of the accuracy of the calculations of the second virial coefficient of helium from interatomic potential functions. Metrologia 28 (in press)

McCarty RD, Stewart RB (1965) Thermodynamic properties of neon from 25 to 300 K between 0.1 and 200 atm. Advances in thermophysical properties at extreme temperatures and pressures. The American Society of Mechanical Engineers, New York, pp 84–97

McLean KO, Swenson CA, Case CR (1972) Thermal expansion of copper, silver and gold. J Low Temp Phys 7:77–98

Meachin AJ, Biddulph MW (1978) The effect of high magnetic fields on the vapor pressure of nitrogen, oxygen, and argon. Cryogenics 18:29–32

Mehl JB (2007) He ab initio calculations III, internal NIST report, 2007-11-19

Meyer CW, Reilly ML (1992) Gas dependence of the effective area of the piston gauge to be used for the NIST realization of the ITS-90. In: Schooley JF (ed) Temperature, its measurement and control in science and industry, vol 6. American Institute of Physics, New York, pp 133–138

Meyer CW, Reilly ML (1993/1994) Measurements of the gas dependence of the effective area of a piston gauge using H_2, ^3He, ^4He, N_2, CO_2 and SF_6. Metrologia 30:595–597

Meyer CW, Reilly ML (1996a) Realization of the ITS-90 at the NIST in the range 0.65–5.0 K using the ^3He and ^4He vapor-pressure thermometry. Metrologia 33:383–389

Meyer CW, Reilly M (1996b) Realization of the ITS-90 at the NIST in the range 0.65–5.0 K using the ^3He and ^4He vapour-pressure thermometry. Metrologia 33:383–389

Meyer CW, Reilly ML (2006) Realization of the ITS-90 at NIST in the range 3.0–24.5561 K using an interpolating constant volume gas thermometer. In: Marcarino P (ed) Proceedings TEMPMEKO 96. Levrotto & Bella Publication, Torino, pp 39–44

Meyer CW, Tew W (2006) ITS-90 nonuniqueness from PRT subrange inconsistencies over the range 24.56–273.16 K. Metrologia 43:341–352

Middleton WEK (1966) Thermometer, and its use in metereology. The Johns Hopkins Press, Baltimore

Moldover MR, Mehl JB, Greenspan M (1986) Gas-filled spherical resonator theory and experiment. J Acoust Soc Am 79:253–272

Moldover MR, Trusler JPM, Edwards TJ, Mehl JB, Davis RS (1988) Measurement of the universal gas constant *R* using a spherical acoustic resonator. J Res NBS 93:85–144

Moldover MR, Boyes SJ, Meyer CW, Goodwin ARH (1999a) Thermodynamic temperatures of the triple points of mercury and gallium and in the interval 217–303 K. J Res Natl Inst Stand Technol 104:11–46

Moldover MR, Boyes SJ, Meyer CW, Goodwin ARH (1999b) Primary acoustic thermometry from 217 to 303 K. In: Dubbeldam JF, de Groot MJ (eds) Proceedings TEMPMEKO 99. NMi Van Swinden Laboratorium, Delft, The Netherlands, pp 250–255

Moran DW (1959) Low temperature equilibria in binary systems. Thesis, University of London

Motizuki K (1957) Theory of the ortho-para conversion in solid deuterium. J Phys Soc Jpn 12:163–170

Motizuki K (1962) Note on para-ortho conversion in solid deuterium. J Phys Soc Jpn 17:1192

Moussa MRM (1966) On thermometry between 63 and 273.15 K. Thesis, Kamerling Onnes Laboratorium, Leiden

Muijlwijk R (1968) Vapor pressures of oxygen and platinum resistance thermometry below 100 K. Thesis, Leiden

Muijlwijk R, Durieux M, Van Dijk H (1969) The temperatures at the transition points of solid oxygen. Physica 43:475–480

Mullins JC, Ziegler WT, Kirk BS (1961) Thermodynamic properties of parahydrogen from 1 to 22 K. Engineering Experiment Station, Georgia Institute of Technology, Atlanta, Technical Report N°1, Project A-595

Mullins JC, Ziegler WT, Kirk BS (1962) Thermodynamic properties of oxygen from 20 to 100 K. Engineering Experiment Station, Georgia Institute of Technology, Atlanta, Technical Report N°2, Project A-593

Mullins JC, Ziegler WT, Kirk BS (1963) Calculation of the vapor pressure and heats of vaporization and sublimation of liquid and solids below one atmosphere pressure, Carbon monoxide and carbon dioxide. Georgia Institute of Technology, Engineering Experiment Station

Nakano T, Tamura O, Sakurai H (2007) Realization of low-temperature fixed points of the ITS-90 at NMIJ/AIST. Int J Thermophys 28:1893–1903

Nakano T, Tamura O, Sakurai H (2011) Comparison at NMIJ/AIST of the triple point of neon using different sealed cells. Int J Thermophys 32:1581–1588

Nara K, Rusby RL, Head DI (1989) The interpolation characteristics of a sealed gas thermometer, document CCT/1989-21, Bureau International des Poids et Mesures. Sèvres, France

Nara K, Rusby RL, Head DI (1990) Study of the interpolation characteristics of a sealed gas thermometer. Cryogenics 30:952–958

Nast TC, Bell G, Barnes C (1982) Development of a gas gap cryogenic thermal switch. Adv Cryog Eng 27:1117–1125

NBS (1975) Standard reference material 736; Copper—thermal expansion, revised certificate (Kirby RK, Hahn TA)

Ni W, Xia JS, Adams ED, Haskins PS, McKisson J (1995a) ^{3}He melting pressure temperature scale below 25 mK. J Low Temp Phys 99:167–182

Ni W, Xia JS, Adams ED, Haskins PS, McKisson J (1995b) ^{3}He melting pressure thermometry. J Low Temp Phys 101:305–310

Nicholas JV (1992) Thermodynamic behavior of platinum resistivity. In: Schooley JF (ed) Temperature, its measurement and control in science and industry, vol 6. American Institute of Physics, New York, pp 383–388

Nicholas JV (1995a) Debye functions in temperature metrology. In: Ciarlini P, Cox MG, Pavese F, Richter D (eds) Advances mathematical and computational tools in metrology, vol II. World Scientific, Singapore, pp 194–205

Nicholas JV (1995b) On the thermodynamic accuracy of the ITS-90: platinum resistance thermometry below 273 K. Metrologia 32:71–77

Nicholas JV, Dransfield TD, White DR (1996) Short communication: isotopic composition of water used for triple point of water cells. Metrologia 33:265–267

Oishi J (1951) Absolute temperature of the ice point by isotherm method and its best value. In: proceedings VIII IIR congress, London, pp 207–211

Orlova MP (1962) Temperature of phase transitions in solid oxygen. In: Herzfeld CM (ed) Temperature, its measurements and control in science and industry, vol 3. Reinhold Publication Company, New York, pp 179–183

Owen DR (1984) A first course in the mathematical foundations of thermodynamics. Springer, New York

Pace EL, Bivens RL (1970) Thermodynamic investigation of solid argon-oxygen mixtures. J Chem Phys 53:748–753

Papon P, Leblond J, Meijer PHE (2002) The physics of phase transitions. Springer, New York

Pascal B (1670) Pensées, in Oeuvres Complètes. Bibliotèque de la Pleiade, 1954 Paris

Pavese F (1975c) Realization of the IPTS-68 between 54.361 and 273.15 K and the triple points of oxygen and argon. Inst Phys Conf Series (GB) 26:70–79

Pavese F (1975d) A sliding thermal tie-down suitable for cryogenic temperatures in vacuum. J Phys E: Sci Instrum 8:508–511

Pavese F (1978a) Some thermodynamic properties of ethane between its double solid-to-solid transition and its triple point temperature. J Chem Thermodyn 10:369–379

Pavese F (1978b) The triple point of argon and oxygen. Metrologia 14:93–103

Pavese F (1979a) Gases as reference materials. In: proceedings international symposium on the production and use of reference materials, BAM, Berlin, pp 472–476

Pavese F (1979b) Temperature value of the triple point of methane. Metrologia 15:47–49

Pavese F (1981a) The use of triple point of gases in sealed cells as pressure transfer standards: oxygen (146.25 Pa), methane (11696 Pa) and argon (68890 Pa). Metrologia 17:35–42
Pavese F (1984b) International intercomparison of fixed points by means of sealed cells: 13.81–90.686 K, monograph 1984/4, Bureau International des Poids et Mesures. Sèvres, France
Pavese F (1987a) Passive thermostat with millikelvin temperature stability for space applications. Cryogenics 26:23–26
Pavese F (1989) On the reference function for platinum resistance thermometers below 273.16 K, document CCT/1989-12, Bureau International des Poids et Mesures. Sèvres, France
Pavese F (1990a) Fields of application: cryogenics. In: Ricolfi T, Scholz H (eds) Thermal sensors, Chap. 10, vol 4. VCH, Weinheim (Sensors—a comprehensive book series in eight volumes)
Pavese F (1993) Recalculation on ITS-90 of accurate vapour-pressure equations for e-H_2, Ne, N_2, O_2, Ar, CH_4 and CO_2. J Chem Thermodyn 25:1351–1361
Pavese F (1995) Magnetic shielding using high-Tc superconductors: a large-scale application with peculiar requirements. In: Acquarone M (ed) High temperature superconductivity: models and measurements. World Scientific, Singapore, pp 637–647
Pavese F (2003c) Century stable cryogenic temperature fixed points: problems solved and problems to be solved. In: Ripple D (ed) Temperature, its measurement and control in science and industry, vol 7. AIP, New York, pp 167–172
Pavese F (2005a) Proposed method for tackling in the ITS-90 definition the issue of isotopic composition prescribed for relevant substances used in the Scale definition, document CCT/2005-17, Bureau International des Poids et Mesures. Sèvres, France
Pavese F (2005b) On problems in the definition of the International Temperature Scale arising from the variability of the isotopic composition of some substances used for the fixed-points. Metrologia 42:194–200
Pavese F (2006) Lessons learnt in 50 years of cryogenic thermometry, Chapter 10. In: Timmerhaus, R (eds) Cryogenic engineering: fifty years of progress. Springer, New York, pp 179–221
Pavese F (2007a) Possible implications of the principle of the 'mise en pratique' in its application to the kelvin. Int J Thermophys 28:1766–1774
Pavese F (2007b) The definition of the measurand in key comparisons: lessons learnt with thermal standards. Metrologia 44:327–339
Pavese F (2009) Critical review of information relevant to the correction of the effect of chemical impurities in gases used for the realization of ITS-90 fixed points. Metrologia 46:47–61
Pavese F (2012a) On systematic effects affecting the mise en pratique of the Kelvin, and their correction. In: Meyer CW et al (eds) Temperature, its measurements and control in science and industry, vol 9. AIP, Melville (in press)
Pavese F (2012d) Note on 'Thermodynamic temperature differences from the ITS-90 for the correction of thermodynamic property data' by F. Pavese, P. Ciarlini, and P.P.M. Steur by J. Fischer, Chairman of WG4 of CCT. J Chem Thermodyn 44:179–180
Pavese F, Demonti G (1978c) Sur la possibilité de définir des échelles secondaires sans utilizer de point d'ébullition, annexe T19, comptes rendus CCT, Bureau International des Poids et Mesures. Sèvres, France T 116–121
Pavese F, Barbero C (1979c) The triple point of pure normal deuterium. Cryogenics 19:255–260
Pavese F, Besley LM (1981b) Triple-point temperature of propane: measurements on two solid-to-liquid transitions and one solid-to-solid transition. J Chem Thermodyn 13:1095–1104
Pavese F, Ferri D (1981c) Flow cryostat for accurate measurements of cryogenic transducers in the range 4–300 K. In: proceedings of international ACRI conference, CLEP, Padova, pp 169–176
Pavese F, Ferri D (1982) Ten years of research on sealed cells for phase transition studies of gases at IMGC. In: Schooley JF (ed) Temperature, its measurements and control in science and industry, vol 5. AIP, New York, pp 217–227
Pavese F, Matacotta FC (1983) A project on ^{3}He gas thermometry at low temperatures at IMGC. IMGC Int Report NS/223, Turin, Italy
Pavese F, McConville GT (1987b) The triple-point temperature of pure equilibrium deuterium. Metrologia 24:107–120

Pavese F, Steur PPM (1987c) ^{3}He constant-volume gas thermometry: calculations for a temperature scale between 0.8 and 25 K. J Low Temp Phys 69:91–117

Pavese F, Steur PPM (1987d) On the reference function for PRTs, particularly in the range 60–100 K: new calculations, document CCT/1987-26, Bureau International des Poids et Mesures. Sèvres, France

Pavese F, Ciarlini P (1990b) Accurate modelling of translational bias and its application to reduction of thermodynamic data series. Metrologia 27:145–152

Pavese F, Ferri D (1990c) Pinch-weld method for sealing of large bore tubes suitable for work from ultravacuum to high pressure. Adv Cryog Eng 35:1835–1837

Pavese F, Ciarlini P (1992a) Computational and statistical analysis of the thermodynamic data which form the basis of the ITS-90 between 13.8 and 273.16 K—II Results. In: Schooley JF (ed) Temperature, its measurement and control in science and industry, vol 6. American Institute of Physics, New York, pp 79–83

Pavese F, Molinar GF (1992c) This book, first edition: Plenum Press, New York, ISBN 0-306-44167-5

Pavese F, Peroni I (2000a) Superconductive-transition based thermometer: a proposed new type of thermometer for the cryogenic range, document CCT/2000-21, Bureau International des Poids et Measures. Sèvres, France

Pavese F, Tew WL (2000b) On the isotopic composition of commercial hydrogen vs 'natural isotopic composition' and the problems for the ITS-90 definition, document CCT/2000-19, Bureau International des Poids et Mesures. Sèvres, France

Pavese F, Cagna G, Ferri D (1975a) Miniature sealed cells as an easy-to-use temperature calibration device and a precision thermostat for cryogenic temperatures. In: proceedings VI international cryogenic engineering conference, IPC. Science and Technology Press, Guildford, pp 205–207

Pavese F, Cagna G, Ferri D (1975b) The triple point of pure methane. In: proceedings VI international cryogenic engineering conference, IPC. Science and Technology Press, Guildford, pp 281–285

Pavese F, Ancsin J, Astrov DN, Bonhoure J, Bonnier G, Furukawa GT, Kemp RC, Maas H, Rusby RL, Sakurai H, Ling S (1984a) An international intercomparison of fixed points by means of sealed cells in the range 13.81–90.686 K. Metrologia 20:127–144

Pavese F, Ferri D, Giraudi D (1988) Evidence of unreliability of factory analyses of argon impurity in oxygen. Adv Cryog Eng 33:1039–1043

Pavese F, Giraudi D, Ferri D, Steur PPM (1990d) A simplified cryostat for direct use in storage dewars for accurate measurements down to 4.2 K. Cryogenics 30(Suppl):463–467

Pavese F, Ferri D, Giraudi D, Steur PPM (1992b) Long-term stability of permanent realizations of the triple point of gases in metal sealed cells. In: Schooley JF (ed) Temperature, its measurement and control in science and industry, vol 6. AIP, New York, pp 251–256

Pavese F, Steur PPM, Ferri D, Astrov DN (1998) Development of an accurate double-diaphragm saphire cryogenic pressure transducer. Adv Cryo Eng 43:789–794

Pavese F, Marcarino P, Giraudi D, Dematteis R (1999) IMGC cells for the realisation of the triple point of mercury. In: Dubbeldam JF, de Groot MJ (eds) Proceedings TEMPMEKO 99 NMi Van Swinden Laboratorium, Delft, The Netherlands, pp 112–117

Pavese F, Tew WL, Steele AD (2002) Archival and theoretical considerations for isotopic dependence in the e-H_2 fixed points. In: Fellmuth B, Seidel J, Scholz G (eds) Proceedings TEMPMEKO 2001, VDE, Berlin, pp 429–434

Pavese F, Ichim D, Ciarlini P, Balle C, Casas-Cubillos C (2003a) Detection of thermometer clustering in the calibration of large batches of industrial thermometers for the LHC by automated data processing. In: Ripple DC (ed) Temperature, its measurement and control in science and industry, vol 7. American Institute of Physics, New York, pp 429–433

Pavese F, Ferri D, Peroni I, Pugliese A, Steur PPM, Fellmuth B, Head D, Lipinski L, Peruzzi A, Szmyrka-Grzebyk A, Wolber L (2003b) Cryogenic temperature sealed fixed points: a new-generation of modular cells at IMGC. In: Ripple DC (ed) Temperature, its measurement and control in science and industry, vol 7. American Institute of Physics, New York, pp 173–178

Pavese F, Fellmuth B, Head D, Hermier Y, Peruzzi A, Szmyrka-Grzebyk A, Zanin L (2003d) Multicells: a european project on cryogenic temperature fixed points in sealed cells. In: Ripple DC (ed) Temperature, its measurement and control in science and industry, vol 7. AIP, New York, pp 161–166

Pavese F, Fellmuth B, Head D, Hermier Y, Hill KD, Valkiers S (2005c) Evidence of a systematic deviation of isotopic composition of neon of available sources from the 'Natural Composition'. Analytical Chem 77:5076–5080

Pavese F, Fellmuth B, Hill KD, Head D, Hermier Y, Lipinski L, Nakano T, Peruzzi A, Sakurai H, Smyrka-Grzebyk A, Steele AD, Steur PPM, Tamura O, Tew WL, Valkier S, Wolber L (2008) Progress toward the determination of the relationship triple point temperature vs. isotopic composition of neon. Int J Thermophys 29:57–66

Pavese F, Fahr M, Hermier Y, Hill KD, Lipinski L, Nakano T, Peruzzi A, Sakurai H, Sparasci F, Steur PPM, Szmyrka-Grzebyk A, Tamura O, Tew WL, Valkiers S, van Geel J (2010a) Further progress toward the determination $T_{tp} - x(^{22}Ne)$. Int J Thermophys 31:1633–1643

Pavese F, Steur PPM, Bancone N, Ferri D, Giraudi D (2010b) Comparison with $U \approx 50$ μK of neon samples of different isotopic composition. Metrologia 47:499–518

Pavese F, Valkiers S, Steur PPM, Ferri D, Giraudi D (2010c) An accurate determination of the triple point temperature of pure ^{20}Ne and ^{22}Ne. J Chem Thermodyn 42:1222–1229

Pavese F, Ciarlini P, Steur PPM (2011a) Thermodynamic temperature differences from the ITS-90 for the correction of thermodynamic property data. J Chem Thermodyn 43:75–79

Pavese F, Steur PPM, Kim JS, Giraudi D (2011b) Further results on the triple point temperature of pure ^{20}Ne and ^{22}Ne. J Chem Thermodyn 43:1977–1983

Pavese F, Steur PPM, Fahr M, Hermier Y, Hill KD, Kim JS, Lipinski L, Nagao K, Nakano T, Peruzzi A, Sparasci F, Szmyrka-Grzebyk A, Tamura O, Tew WL, Valkiers S, van Geel J (2012b) Dependence of the triple point temperature of neon on isotopic composition and its implications for the ITS-90. In: Meyer CW et al (eds) Temperature, its measurements and control in science and industry, vol 9. AIP, Melville (in press)

Pavese F, Steur PPM, Giraudi D (2012c) The triple point temperature of pure neon isotopes and the dependence on the nitrogen impurity and on the sealed.cell model. In: Meyer CW et al (eds) Temperature, its measurements and control in science and industry. AIP, Melville (in press)

Pavese F, Steur PPM, Kim JS, Giraudi D (2011e) Results on three calibrated artificial mixtures of ^{22}Ne in ^{20}Ne (To be published)

Peroni I, Pavese F, Ferri D, Lin P, Zhang Q, Yu L (2001) A sealed cell for the accurate realization of the λ-point of ^{4}He. In: Fellmuth B, Seidel J, Scholz G (eds) Proceedings TEMPMEKO 2001. VDE, Berlin, pp 391–396

Peruzzi A, Bosma R, de Groot MJ, Verbeek J (2010) ^{4}He interpolating constant-volume gas thermometry in the range 3.0–24.5561 K. Metrologia 47:325–333

Phillips SD, Eberhardt KR, Parry B (1997) Guidelines for expressing the uncertainty of measurement results containing uncorrected bias. J Res Nat Inst Stand Technol 102:577–585

Pitre L, Moldover MR, Tew WL (2006) Acoustic thermometry: new results from 273 to 77 K and progress towards 4 K. Metrologia 43:142–162

Pitre L, Sparasci F, Truong D, Guillou A, Risegari L (2011) Measurement of the Boltzmann constant k_B using a quasi-spherical acoustic resonator. Int J Thermophys 32:1825–1886

Pitre L, Sparasci F, Guillou A, Truong D, Hermier Y, Himbert ME (2010) New determination of the Boltzmann constant with an acoustic method, 2010 Conference on Precision Electromagnetic Measurements (CPEM), pp 129–130. ISBN:978-1-4244-6795-2

Planck M (1932) Introduction to theoretical physics, Vol V: theory of heat (trans: Brose HL). MacMillan and Co. Ltd., London

Plumb HH (1959) Proceedings X IIR conference. Bull IIR 34:161–163

Plumb HH (1982) He-4 virial coefficients, derived from NBS acoustic thermometry between 2 and 20 K. In: Schooley JF (ed) Measurements and control in science and industry, vol 5. AIP, New York, pp 77–88

Plumb HH, Cataland G (1966) Acoustical thermometer and the NBS provisional temperature scale 2–20 (1965). Metrologia 2:127–139
Plumb HH, Cataland G (1966) Acoustical thermometer and the National Bureau of Standards provisional temperature scale 2–20 (1965). Metrologia 2:127–139
Preston-Thomas H (1976) The international practical temperature scale of 1968. Amended edition of 1975. Metrologia 12:7–17
Preston-Thomas H (1990) The International Temperature Scale of 1990. Metrologia 27:3–10
Prigogine I (1954) Thermodynamics of irreversible processes. Interscience Publication, New York
Prigogine I (1962) Non-equilibrium statistical mechanics. Interscience Publication, New York
Prince A (1966) Alloy phase equilibria. Elsevier, Amsterdam
Physique CR (2009) Special issue on Boltzmann costant determinations. Acad des Sci 10(9):815–893
Quinn TJ (1983) Temperature. Academic Press, London
Quinn TJ (2005) Temperature scales and units and implications for practical thermometry of a possible redefinition of the kelvin in terms of the Boltzmann constant—a Note to the CCT June 2005, document CCT/2005-26, Bureau International des Poids et Mesures. Sèvres, France
Quinn TJ, Martin JE (1985) A radiometric determination of the Stefan–Boltzmann constant and thermodynamic temperatures between −40 and 100 °C. Phil Trans Royal Soc London Series A316:85–189
Quinn TJ, Colclough AR, Chandler TRD (1976) A new determination of the gas constant by an acoustical method. Phil Trans Royal Soc London 283:367–420
Radebaugh R (2009) Cryocoolers: the state of the art and recent developments. J Phys Condens Matter 21(2009). doi:10.1088/0953-8984/21/16/164219
Ramsey NF (1956) Thermodynamics and statistical mechanics at negative temperatures. Phys Rev 103:20–28
Razumovskii NA (1990) Radial temperature inhomogeneity in a gas-thermometer capillary. Izmeritel'naya Tekhnika 4:37–38 (Engl Transl Exp Tech 32:353–355)
Ripple DC, Defibaugh DR, Gillis KA, Moldover MR (1999) Primary acoustic thermometer for use up to 800 K. In: Dubbeldam JF, de Groot MJ (eds) NMi Van Swinden Laboratorium, Delft, The Netherlands, pp 418–423
Ripple DC, Strouse GF, Moldover MR (2007) Acoustic thermometry results from 271–552 K. Int J Thermophys 28:1789–1799
Ripple DC, Davis R, Fellmuth B, Fischer J, Machin G, Quinn TJ, Steur PPM, Tamura O, White DR (2010) The roles of the mise en pratique for the definition of the kelvin. Int J Thermophys 31:1795–1808
Roberts TR, Sherman RH, Sydoriak SG (1964) The 1962 ^{3}He scale of temperatures. III. Evaluation and status. J Res NBS 68A:567–578
Rott N, Angew Z (1969) Math Phys 20:230–235
Rusby RL (1991) The conversion of thermal reference values to the ITS-90. J Chem Thermodyn 23:1153–1161 (Incorporated in (BIPM 1990))
Rusby RL (2010) The discontinuity in the first derivative of the ITS-90 at the triple point of water. Int J Thermophys 31:1567–1572
Rusby RL Swenson CA (1980) A new determination of the helium vapor pressure scales using a CNM magnetic thermometer and the NPL-75 gas thermometer scale. Metrologia 16:73–87
Rusby RL, Hudson RP, Durieux M, Schooley JF, Steur PPM, Swenson CA (1991) The thermodynamic basis of ITS-90. Metrologia 28:9–18
Rusby RL, Hudson RP, Durieux M, Grohmann K, Jung H-J, Steur PPM, Nicholas JV (1996) The status of thermodynamic thermometry. Metrologia 33:409–414
Sakurai H (1982) Constant volume gas thermometer for thermodynamic temperature measurements of the triple point of oxygen. In: Schooley JF (ed) Temperature, its measurements and control in science and industry, vol 5. AIP, New York, pp 39–42
Sakurai H (2001) A Practical interpolation gas thermometer using a closed cycle refrigerator. In: Fellmuth B, Seidel J, Scholz G (eds) Proceedings TEMPMEKO 2001, VDE, Berlin, pp 537–542

Sakurai H, Tamura O (1990) Cryogenic thermometer calibration apparatus using a GM type closed-cycle helium refrigerator. In: proceedings TEMPMEKO 90, Helsinky, pp 112–117
Shimazaki T, Tamura O (2004) Realization of the ^{3}He vapour pressure scale at NMIJ using a continuous operating system. In: Zvizdic D (ed) Proceedings TEMPMEKO 2004 LPM-FSB, Zagreb, pp 383–388
Schindler M, Dertinger A, Kondo Y, Pobell F (1996) Hydrogen in porous Vycor glass. Phys Rev B (Condensed Matter) 53:11451–11461 (Czech J Phys 46(pt S1):509–510)
Schooley JF (1986) Thermometry. CRC Press Inc., Boca Raton
Schooley JF (1988) NBS gas thermometry from 0 to 660 °C. In: proceedings workshop national conference on standards laboratories, 50/1–14
Schumb WC (1947) Ind Eng Chem 39:421–427
Schuster G, Wolber L (1986) Automated helium-3 melting curve thermometer. J Phys E: Sci Instrum 19:701–705
Schuster G, Hechtfischer D (1992) Extrapolation of ITS-90 to lower temperatures. In: Schooley JF (ed) Temperature, its measurement and control in science and industry, vol 6. American Institute of Physics, New York, pp 97–100
Schuster G, Hoffmann A, Hechtfischer D (1993) ^{3}He melting pressure-temperature relation in the range from 1 to 1000 mK. Czech JPhys 46(Suppl 1):481–482. doi:10.1007/BF02569656 (LT21 proceedings)
Schuster G, Hechtfischer D, Fellmuth B (1994) Thermometry below 1 K. Rep Prog Phys 57:187–223
Schwalbe LA, Grilly ER (1984) Pressure-volume—temperature relationship for normal deuterium between 18.7 and 21.0 K. J Res NBS 89:227–250
Scribner RA, Adams ED (1972) ^{3}He melting curve thermometry. In: Plumb HH (ed) Temperature, its measurements and control in science and industry, vol 4. ISA, Pittsburg, pp 37–47
Segovia JJ, Vega-Maza D, Martín MC, Gómez E, Tabacaru C, del Campo D (2010) An apparatus based on a spherical resonator for measuring the speed of sound in gases and for determining the Boltzmann constant. Int J Thermophys 31:1294–1309
Seifert P (1983) Tripelpunkte von Gasen als Fixpunkte im Tieftemperaturbereich. Metrologische Abhandlungen 3:133–146
Serrin J (1978) The concept of thermodynamics. In: La Penha GM, Medeiros LA (eds) Contemporary developments in continuum mechanics and partial differential equations. North-Holland Publication Company, Heidoven, pp 411–451
Shimazaki T, Tamura O (2005) Realization of the ^{3}He vapour pressure scale at NMIJ using a continuous operating system. In: proceedings 9th international symposium on temperature and thermal measurements in industry and science TEMPMEKO 2004, Ed. in Chief Zvizdic D, LPM-FSB (Zagreb, Croatia), pp 383–388
Shimazaki T, Toyoda K, Oota A, Nozato H, Usuda T, Tamura O (2008) Closed-cycle Joule-Thomson cryocooler for resistance thermometer calibration down to 0.65 K. Int J Thermophys 29:42–50
Siegwarth JD, Voth RO (1988) A miniature cryogenic vacuum valve. Adv Cry Eng 33:1153–1159
Simon FE (1955) The concept of temperature near absolute zero. In: Wolfe HC (ed) Temperature, its measurements and control in science and industry, vol 2. Reinhold Publication Company, New York, pp 9–17
Sloan GJ, McGhie AR (1988) Techniques of melt crystallisation. Wiley, New York
Smythe X (1968) Static and dynamic electricity. McGraw-Hill, New York, pp 76–78
Song N, Mao Y, Lin P, Zhang Q, Zhang L (1989) Proceedings of international conference on cryogenics and refrigeration. International Academic Publishers, Hangzhou 1989, pp 227–231
Song N, Hong CS, Mao Y, Ling P, Zhang Q, Zhang L (1991) Realization of the lambda transition temperature of liquid helium-4. Cryogenics 31:87–93
Souers PC (1979) Cryogenic hydrogen data pertinent to magnetic fusion energy, Rpt. UCRL-52628, Lawrence Livermore Laboratory, University of California, Livermore
Souers PC (1986) Hydrogen properties for fusion energy. University of California Press, Los Angeles

Soulen RJ Jr, Fogle WE, Colwell JH (1994) Measurements of absolute temperature below 0.75 K using a Josephson-junction noise thermometer. J Low Temp Phys 94:385–487

Sparasci F, Pitre L, Truong D, Risegari L, Hermier Y (2011a) Realization of a ^{3}He–^{4}He vapor-pressure thermometer for temperatures between 0.65 and 5 K at LNE-CNAM. Int J Thermophys 32:139–152

Sparasci F, Pitre L, Truong D, Risegari L, Hermier Y (2011b) Realization of a ^{3}He–^{4}He vapor-pressure thermometer for temperatures between 0.65 and 5 K at LNE-CNAM. Int J Thermophysics 32:139–152

Sparasci F, Pitre L, Rouillé G, Thermeau J-P, Truong D, Galet F, Hermier Y (2011c) An adiabatic calorimeter for the realization of the ITS-90 in the cryogenic range at the LNE-CNAM. Int J Thermophys 32:201–214

Sparks LL, Powell RL (1972) Calibration of capsule platinum resistance thermometers at the triple point of water. In: Plumb HH (ed) Temperature, its measurements and control in science and industry, vol 4. ISA, Pittsburg, pp 1415–1422, 1569–1578

Spencer GF, Ihas GG (1985) Miniature bellows-free low-temperature valve. Rev Sci Instrum 56:1838–1840

Staveley LAK, Lobo LQ, Calado JCG (1981) Triple-points of low-melting substances and their use in cryogenic work. Cryogenics 21:131–144

Steele AG (1997) Design and preliminary results of a vapour pressure cryostat at NRC. In: Szmyrka-Grzebyk A (ed) Proceedings Wroclaw Workshop Ladek Zdroj, Wroclaw, pp 54–60

Steele AG,(2005) ITS-90 Subrange inconsistency below the triple point of water. Metrologia 42:289–297

Steele AG, Head DI (2004) Comparison of 'VAR' deuterium triple point cells. In: Zvizdic D et al (eds) Proceedings TEMPMEKO 2004, LPM/FSB, Zabreb, pp 301–306

Steele AG, Fellmuth B, Head DI, Hermier Y, Kang KH, Steur PPM, Tew WL (2002) CCT-K2: key comparison of capsule-type standard platinum resistance thermometers from 13.8 to 273.16 K. Metrologia 39:551. doi:10.1088/0026-1394/39/6/6

Steur PPM (1983) Determination of temperatures between 4 and 100 K with a gas thermometer. Thesis, Kamerling Onnes Laboratorium, Leiden

Steur PPM (1987) The gas thermometer as interpolating instrument below 24.6 K, proceeding LT18 conference. Jap J Appl Phys 26(Suppl 26-3-2):1685–1686

Steur PPM (1990) Courtesy of the author

Steur PPM (1999) The interpolating constant-volume gas thermometer and thermal anchoring. Metrologia 36:33–39

Steur PPM, Durieux M (1986) Constant-volume gas thermometry between 4 and 100 K. Metrologia 23:1–18

Steur PPM, Giraudi D (2012) Adjustment to the ICVGT realization of the ITS-90 at INRIM. In: Meyer CW et al (eds) Temperature, its measurements and control in science and industry, vol 9. AIP, Melville (in press)

Steur PPM, Pavese F (1987) ^{3}He scale proposal 0.8–24.6 K, document CCT/1987-10, Bureau International des Poids et Mesures. Sèvres, France

Steur PPM, Pavese F (1989a) ^{3}He constant-volume gas thermometer as interpolating instrument: calculations of the accuracy limit versus temperature range and design parameters. Cryogenics 29:135–138

Steur PPM, Pavese F (1989b) The interpolating gas thermometer in the ITS-90, document CCT/1989-12, Bureau International des Poids et Mesures. Sèvres, France

Steur PPM, Pavese F (2005) On the definition of 'pressure' in the ITS-90 definition of the interpolating CVGT, document CCT/2005-3, Bureau International des Poids et Mesures. Sèvres, France

Steur PPM, Pavese F, Ferri D, Giraudi D (1997) An interpolating gas thermometer with cryogenic pressure transducer, seminar on low temperature thermometry. In: Szmyrka-Grzebyk A (ed) Proceedings low temperature thermometry abd dynamic trmperatuire measurement, INTiBS, Ladek-Zdroj, Wroclaw, pp 20–23

Steur PPM, Pavese F, Peroni I (2003) The IMGC interpolating constant volume gas thermometer—new data. In: Schooley JF (ed) Temperature, its measurement and control in science and industry, vol 6. American Institute of Physics, New York, pp 125–130

Steur PPM, Peroni I, Pavese F, Ferri D, Pugliese A (2003) IMGC's interpolating constant volume gas thermometer: re-evaluation of the 2002 data. In: Szmyrka-Grzebyk A (ed) Proceedings CELTAM Workshop, INTiBS, Wroclaw, pp 86–90

Steur PPM, Durieux M, McConville GT (1986) Analytic expressions for the virial coefficients B(T) and C(T) of ^{4}He between 2.6 and 300 K. Metrologia 24:69–77

Steur PPM, Pavese F, Durieux M (1987) Interpolating helium constant volume gas thermometers, document CCT/1987-5, Bureau International des Poids et Mesures. Sèvres, France

Steur PPM, Peroni I, Ferri D, Pavese F (2004) Interpolating gas thermometry with a cryogenic absolute pressure sensor. In: Zvizdic D et al (eds) Proceedings TEMPMEKO 2004, LPM/FSB, Zabreb, pp 141–146

Steur PPM, Fellmuth B, Gam KS, Hermier Y, Hill KD, Pokhodun AI, Ripple DC (2005) Isotopic effects in the hydrogen fixed points: report to the CCT, working document CCT/2005-06, Bureau International des Poids et Mesures. Sèvres, France

Straty GC, Adams ED (1966) ^{4}He melting curve below 1 K. Phys Rev Lett 17:290–292 (Errata Corrige. IBIDEM 7:505)

Straty GC, Adams ED (1969) Highly sensitive capacitive pressure gauge. Rev Sci Instrum 40:1393–1397

Straty GC, Tsumura R (1976) Phase transition and melting pressures of solid ethane. J Chem Phys 64:859–861

Strouse GF, Defibaugh DR, Moldover MR, Ripple DC (2003) Progress in primary acoustic thermometry at NIST: 273–505 K. In: Ripple DC (ed) Temperature, its measurement and control in science and industry, vol 7. AIP, New York, pp 31–36

Strehlow P, Seidel J (2007) Definition der temperatur und ihre grenzen. PTB Mitteilungen 117:16–22

Sun JP, Zhang JT, Zhang XY, Lin H, Feng XJ (2011) Length determination of a fixed-path cylindrical resonator with the dual wavelength laser interference method. Int J Thermophys 32:1330–1338

Sutton G, Underwood R, Pitre L, de Podesta M, Valkiers S (2010) Acoustic resonator experiments at the triple point of water: first results for the Boltzmann constant and remaining challenges. Int J Thermophys 31:1310–1346

Synek V (2005) Attempts to include uncorrected bias in the measurement uncertainty. Talanta 65:829–837

Swenson CA (1976) The constant volume gas thermometer as an interpolation instrument below 20 K, document CCT/1976-6, annexe T9. Comptes rendus CCT, Bureau International des Poids et Mesures. Sèvres, France T 86–88

Swenson CA (1989) Supplementary information for ITS-90. Draft for the ICVGT, document CCT/1989-27, Bureau International des Poids et Mesures. Sèvres, France

Swim RT (1960) Temperature distribution in liquid and vapor phases of helium in cylindrical dewars. Adv Cryo Eng 6:498–504

Sydoriak SG, Roberts (1960) Vapor pressure of ^{3}He/^{4}He mixtures. Phys Rev 118:901–912

Sydoriak SG, Sherman RH (1964) The 1962 ^{3}He scale of temperatures I. New vapor pressure comparisons. J Res NBS 68A:547–558

Sydoriak SG, Roberts TR, Sherman RH (1964) The 1962 ^{3}He scale of temperatures. II. Derivation. J Res NBS 68A:559–565

Szmyrka-Grzebyk A, Lipiński L, Manuszkiewicz H (1998) Phase transition in solid solid oxygen as thermometric fixed points. J Low Temp Phys 111:399–406

Szmyrka-Grzebyk A, Lipiński L, Manuszkiewicz H, Pavese F, Ferri D, Giraudi D, Steur PPM (2007) Evidence for anomalies in the solid-solid transitions of oxygen and impurity detection. In: Marcarino P (ed) Proceedings TEMPMEKO 96, Levrotto & Bella Publication, Torino, pp 105–110

Szmyrka-Grzebyk A, Manuszkiewicz H, Kołodziej B, Lipiński L, Steur PPM, Pavese F (2012a) System for realization of the argon triple point. In: Meyer CW et al (eds) Temperature, its measurements and control in science and industry, vol 9. AIP, Melville (in press)

Szmyrka-Grzebyk A, Kowal A, Lipiński L, Manuszkiewicz H, Steur PPM, Pavese F (2012b) The β–γ transition of oxygen as secondary fixed point. In: Meyer CW et al (eds) Temperature, its measurements and control in science and industry, vol 9. AIP, Melville (in press)

Taconis KW, Beenakker JJM, Nier AOC, Aldrich LT (1949) Measurements concerning the vapor-liquid equilibrium of solutions of ^{3}He in ^{4}He below 2.19 K. Physica 15:733–739

Tamura O, Takasu S, Murakami Y, Sakurai H (2003) Interpolating gas thermometer for realizing the ITS-90 at NMIJ/AIST. In: Ripple DC (ed) Temperature, its measurement and control in science and industry, vol 7. AIP, New York, pp 131–136

Tamura O, Takasu S, Sakurai H (2004) Realization of the ITS-90 using the ^{3}He interpolating gas thermometer of NMIJ/AIST. In: Zvizdic D et al (eds) Proceedings TEMPMEKO 2004, LPM/FSB, Zabreb, pp 79–84

Tamura O, Takasu S, Nakano T, Sakurai H (2008) NMIJ constant-volume gas thermometer for realization of the ITS-90 and thermodynamic temperature measurement. Int J Thermophys 29:31–41

Tell JL, Maris HJ (1983) Specific heats of hydrogen, deuterium, and neon in porous Vycor glass. Phys Rev B Condens Matter 28:5122–5125

Ter Brake HJM, Wiegerinck GFM (2002) Low-power cryocooler survey. Cryogenics 42:705–718

Ter Harmsel H, Van Dijk H, Durieux M (1967) The heat of vaporization of hydrogen. Physica 33:503–522

Tew WL (1996) Sealed-cell devices for the realization of the triple point of neon at the NIST. In: Marcarino P (ed) Proceedings TEMPMEKO 96, Levrotto & Bella Publication, Torino, pp 81–86

Tew WL (2008) Estimating the triple-point isotope effect and the corresponding uncertainties for cryogenic fixed points. Int J Thermophys 29:67–81

Tew WL, Meyer CW (2008) Adjustments to the NIST realization of the ITS-90 from 5 to 24.5561 K, document CCT/2008-09, Bureau International des Poids et Mesures. Sèvres, France

Thompson W (1848) On an absolute thermometric scale founded on Carnot's theory of the motive power of heat, and calculated from Regnault's observations. Phil Magazine 33:313–317

Thomson W (1854) Trans Royal Soc Edinburgh 21:123

Thompson M, Ellison SLR, Fajgeli A, Willetts P, Wood R (1999) Harmonized guidelines for the use of recovery information in analytical measurement. Pure Appl Chem 71:337–348

Tiggelman JL (1973) Low-temperature platinum thermometry and vapor pressures of neon and oxygen. Kamerling Onnes Laboratorium, Thesis, Leiden

Tiggelman JL, Durieux M (1972) Vapor pressures of liquid oxygen and nitrogen. In: Plumb HH (ed) Temperature, its measurements and control in science and industry, vol 4. ISA, Pittsburg, pp 149–157

TEMPMEKO Proceedings (1996) Proceedings TEMPMEKO 97 (Marcarino P (ed)), Levrotto & Bella Publication, Torino

TEMPMEKO Proceedings (1999) Proceedings TEMPMEKO 99 (Dubbeldam J.F, de Groot MJ (eds)), NMi Van Swinden Laboratorium, Delft, The Netherlands

TEMPMEKO Proceedings (2001) Proceedings TEMPMEKO 2001 (Fellmuth B, Seidel J, Scholz G (eds)), VDE, Berlin

TEMPMEKO Proceedings (2004) Proceedings TEMPMEKO 2004 (Zvizdic D et al (eds)), LPM/FSB, Zabreb

TEMPMEKO Proceedings (2007) See papers on Int J Thermophysics 2008–2009

TEMPMEKO Proceedings (2010) See papers on Int J Thermophysics 2010–2011

TMCSI (1941) Temperature, its measurements and control in science and industry, vol 1. (Fairchild CO, Hardy JD, Sosman RB, Wensel HT (eds)), Reinhold Publication Company, New York

TMCSI (1955) Temperature, its measurements and control in science and industry, vol 2. (Wolfe HC (ed)), Reinhold Publication Company, New York

TMCSI (1962) Temperature, its measurements and control in science and industry, vol 3. (Herzfeld CM (ed)), Reinhold Publication Company, New York
TMCSI (1972) Temperature, its measurements and control in science and industry, vol 4. (Plumb HH (ed)), ISA, Pittsburg
TMCSI (1982) Temperature, its measurements and control in science and industry, vol 5. (Schooley JF (ed)), AIP, New York
TMCSI (1992) Temperature, its measurements and control in science and industry, vol 6**.** (Schooley JF (ed)), AIP, New York
TMCSI (2003) Temperature, its measurements and control in science and industry, vol 7**.** (Ripple D (ed)), AIP, New York TMCSI
TMCSI (ITS9 2012) Temperature, its measurements and control in science and industry, vol 8. (Meyer CW et al. (eds)), AIP, Melville
Torii RH, Maris HJ, Seidel GM (1990) Heat capacity and torsional oscillator studies of molecular hydrogen in porous Vycor glass. Phys Rev B Condens Matter 41:7167–7181
TPRC (1975) Thermophysical properties research center. In: Touloukian YS, Kirby RK, Desai PD (eds) Thermal expansion: metallic elements and alloys (Thermophysical properties of the matter), vol 12. IFI/Plenum, New York
Truesdell CA III (1979) Absolute temperatures as a consequence of Carnot's general Axiom. Arch Hist Exact Sci 20:357–380
Truesdell CA III (1980) The tragicomical history of thermodynamics 1822–1854. Springer, New York
Truesdell CA III (1987) Private communication
Truesdell CA III, Bharatha S (1977) The concepts and logic of classical thermodynamic as a theory of heat engines: rigorously constructed upon the foundation laid by S. Carnot and F. Reech. Springer, New York
Truong D, Sparasci F, Foltê te E, Ouisse M, Pitre L (2011) Measuring shell resonances of spherical acoustic resonators. Int J Thermophys 32:427–440
Tward E, Mason PV (1982) Damping of thermoacoustic oscillations. Adv Cryo Eng 27:807–815
Ubbelohde AR (1965) Melting and crystal structure. Clarendon Press, Oxford, pp 31–36
Valkiers S, Vendelbo D, Berglund M, de Podesta M (2010) Preparation of argon primary measurement standards for the calibration of ion current ratios measured in argon. Int J Mass Spectrom 291:41–47
Van Degrift CT (1981) Coin silver as a construction material in low-temperature experiments. Physica 107B:605–606
Van Degrift CT, Bowers J Jr (1984) A progress report on the development of a small high precision pressure/temperature sensor for use at low temperatures. In: proceedings ICEC 10, Butterworth, London, pp 154–158
Van Degrift CT, Bowers WJ Jr, Wilders DG, Pipes PB (1978a) A small gas thermometer for use at low temperatures. ISA annual conference, ISA, New York, pp 33–38
Van Degrift CT, Bowers WJ Jr, Wilders DG, Pipes PB (1978b) A small gas thermometer for use at low temperatures. J de Physique Colloque C6 39(Suppl°8):1173–1174
Van Dijk H, Durieux M (1959) The temperature scale in the liquid helium region, ch. XIV. In: Gorter CJ (ed) Progress in low temperature physics, vol 2, pp 431–464
Van Hecke P, Van Gerven L (1973) Spin conversion in solid methane: proton magnetization and spin-lattice relaxation. Physica 68:359–381
Van Itterbeek A, Verbeke O, Theewes F, Staes K, De Boelpaep J (1964) The differences in vapor pressure between normal and equilibrium hydrogen. Vapor pressure of normal hydrogen between 20 and 32 K. Physica 30:1238–1244
Van Sciver SW (1986) Helium cryogenics, the international cryogenic monograph series. Plenum Press, New York
Vander Wall EM (1970) Carbon compounds/liquid hydrogen fuels, Technical Report. FR02-W396, Aerojet Liquid Rocket Company, Sacramento, California

Vasserman AA, Kazavchinskii YaZ, Rabinovich VA (1971) Thermophysical properties of air and air components (Zhuravlev AM (ed)). Israel program of scientific translations, Jerusalem (Izdatel'vo 'Nauka', Moskva 1966)
Vukalovich MP, Altunin VV (1968) Thermophysical properties of carbon dioxide (trans: Gaunt DS). Collet's Publication, London
Wagner W (1973) New vapor pressure measurements for argon and nitrogen and a new method for establishing rational vapour pressure equations. Cryogenics 13:470–482
Wagner W, Ewers J, Penterman W (1976) New vapor pressure measurements and a new rational vapor pressure equation for oxygen. J Chem Thermodyn 8:1049–1060
Ward SD (1980) Realizations of the triple points of argon and neon at NPL, document CCT/1980-51, Bureau International des Poids et Mesures. Sèvres, France
Weber LA (1970) P-V-T, thermodynamic and related properties of oxygen from the triple point to 300 K at pressures to 33 MN/m2. J Res NBS A 74:93–129
Weber F (1984) Gas thermometry at 27, 54 and 90 K, CCT/1984-06, consultative committee for thermometry. BIPM, Sèvres, France
Weber F (1991) Physikalisch-Technische Bundesanstalt, Braunschweig, PTB-Bericht W-47
Weber S, Schmidt G (1936) Experimentelle Untersuchungen über die thermomolekulare Druckdifferenz in der Nähe der Grenzbedingung und Vergleichung mit der Theorie, KOL Comm. N°246c, Leiden, from Rapports et Communications N°7. VII Congrès IIR
Weber LA, Diller DE, Roder HM, Goodwin RD (1962) The vapor pressure of 20 °K equilibrium hydrogen. Cryogenics 2:236–238
Weinhold F (1982) Mass polarization and Breit-Pauli corrections for the polarizability of helium-4. J Phys Chem 86:1111–1116
Wensel HT (1941) Temperature, its measurements and control in science and industry, vol 1, pp 3–23. Reinhold Publication Company, New York (Fairchild CO, Hardy JD, Sosman RB, Wensel HT (eds)
Wexter A (1961) Storage and transfer of liquefied gases, Chap. 7. In: Hoare FE, Jackson LC, Kurti N (eds) Experimental cryophysics. Butterworths, London, pp 138–164
White DR (2005) Two issues relating to the harmonisation of uncertainty analyses, CCT/2005-09, Bureau International des Poids et Mesures. Sèvres, France (http://www.bipm.org)
White GK, Collins JG (1972) Thermal expansion of copper, silver and gold at low temperatures. J Low Temp Phys 7:43–75
White DR, Tew WL (2010) Improved estimates of the isotopic correction constants for the triple point of water. Int J Thermophys 31:1644–1653. doi:.1007/s10765-010-0819-4
White DR, Dransfield TD, Strouse GF, Tew WL, Rusby RL, Gray J (2003) Effects of heavy hydrogen and oxygen on the triple-point temperature of water. In: Ripple DC (ed) Temperature, its measurement and control in science and industry, vol 7. AIP, New York, pp 221–226
White DR, Ballico M, del Campo D, Duris S, Filipe E, Ivanova A, Kartal Dogan A, Mendez-Lango E, Meyer C, Pavese F, Peruzzi A, Renaot E, Rudtsch S, Yamazawa K (2007) Uncertainties in the realisation of the SPRT sub-ranges of the ITS-90. Int J Thermophys 28:1868–1881
White DR, Bonnier G, Diril A, Arai M, Ballico M, Chimenti V, Duris S, Filipe E, Ivanova A, Dogan AK, Mendez-Lango E, Meyer C, Pavese F, Peruzzi A, Renaot E, Rudtsch S, Stock M, Ugur S (2009) WG3 report to CCT, CCT/2005-15rev and CCT/2008-19rev. Bureau International des Poids et Measures. Sèvres, France (http://www.bipm.org)
White DR, Ballico M, del Campo D, Duris S, Filipe E, Ivanova A, Kartal Dogan A, Mendez-Lango E, Meyer C, Pavese F, Peruzzi A, Renaot E, Rudtsch S, Yamazawa K, Zhang JT (2010) Uncertainties in the SPRT sub-ranges of ITS-90: topics for further research. Int J Thermophys 31:1749–1761
Wieser ME (2006) Inorganic chemistry division, commission on isotopic abundances and atomic weights. Atomic weights of the elements 2005. Pure Appl Chem 78:2051–2066
Wieser ME, Coplen TB (2011) Atomic weights of the elements 2009 (IUPAC technical report). Pure Appl Chem 83:359–396
Wilks J (1968) The properties of liquid and solid helium. Clarendon Press, London

Winteler HR (1981) High-pressure gas-filled thermometers. In: proceedings I symposium IMEKO TC12, CSVTS, Dum Techniky, Praha, pp 162–168
Wolber L, Fellmuth B (2008) Influence of the freezing and annealing conditions on the realization of cryogenic triple points. Int J Thermophys 29:82–92
Wolber L, Fellmuth B (2011) Improved thermal model for the realization of the triple points of cryogenic gases as temperature fixed points. Int J Thermophys 32:189–200
Woolley HW, Scott RB, Brickwedde FG (1948) Compilation of thermal properties of hydrogen in its various isotopic and ortho-para modifications. J Res NBS 41:379–475
Worthing AG (1941) Is temperature a basic concept? In: Fairchild CO, Hardy JD, Sosman RB, Wensel HT (eds) Temperature, its measurements and control in science and industry, vol 1. Reinhold Publication Company, New York, pp 41–43
Yazaki T, Tominaga A, Narahara Y (1979) Stability limit for thermally driven acoustic oscillation. Cryogenics 19:393–396
Younglove BA (1969) Measurements of the dielectric constant of saturated liquid oxygen. Advances in Cryogenic Engineering, vol 15. Plenum Press, New York, pp 70–75
Zeller AF (1990) High Tc superconductors as thermal radiation shields. Cryogenics 30:545–546
Zemansky MW (1957) Heat and thermodynamics, 5th edn. McGraw-Hill, New York
Zemansky MW (1968) Heat and thermodynamics, 5th edn revised. McGraw-Hill, New York
Zhang JT, Lin H, Feng XJ, Sun JP, Gillis KA, Moldover MR, Duan YY (2011) Progress toward redetermining the Boltzmann constant with a fixed-path-length cylindrical resonator. Int J Thermophys 32:1297–1329
Zhokhovskii MK (1975) Use of p-T equilibrium curves in realizing temperature scales. Izmeritel'naya Tekhnika 11:50–54 (English trans: Exp Tech 1717–1722, 1974)
Zhokhovskii MK (1989) Testing a universal equation for first-order phase transition p-T curves. Izmeritel'naya Tekhnika 3:21–23 (English trans: Exp Tech 31:217–220, 1989)
Zhokhovskii MK (1990) Singularities of the p-T curve universal equation for phase transitions of the first kind. Izmeritel'naya Tekhnika (11):51–53 (English trans: Exp Tech 32:1102–1106)
Ziegler WT, Mullins JC (1963) Calculation of the vapor pressure and heats of vaporization and sublimation of liquid and solids below one atmosphere pressure, nitrogen and fluorine, Engineering Experiment Station, Georgia Institute of Technology, Atlanta, Technical Report N 1
Ziegler WT, Mullins JC, Kirk BS (1962a) Calculation of the vapor pressure and heats of vaporization and sublimation of liquid and solids below one atmosphere pressure, Argon, Engineering Experiment Station, Georgia Institute of Technology, Atlanta, Technical Report N 2
Ziegler WT, Mullins JC, Kirk BS (1962b) Calculation of the vapor pressure and heats of vaporization and sublimation of liquid and solids below one atmosphere pressure, Methane, Engineering Experiment Station, Georgia Institute of Technology, Atlanta, Technical Report N 3
Ziegler WT, Kirk BS, Mullins JC, Berquist AR (1964) Calculation of the vapor pressure and heats of vaporization and sublimation of liquid and solids below one atmosphere pressure, Ethane, Engineering Experiment Station, Georgia Institute of Technology, Atlanta
Ziegler WT, Yarbrough DW, Mullins JC (1964a) Calculation of the vapor pressure and heats of vaporization and sublimation of liquid and solids below one atmosphere pressure, Krypton, Engineering Experiment Station, Georgia Institute of Technology, Atlanta, Technical Report
Ziegler WT, Mullins JC, Berquist AR (1964b) Calculation of the vapor pressure and heats of vaporization and sublimation of liquid and solids below one atmosphere pressure, Propane, Engineering Experiment Station, Georgia Institute of Technology, Atlanta, Technical Report
Ziegler WT, Mullins JC, Berquist AR (1966) Calculation of the vapor pressure and heats of vaporization and sublimation of liquid and solids below one atmosphere pressure, Xenon, Engineering Experiment Station, Georgia Institute of Technology, Atlanta, Technical Report N°3
Ziegler WT, Brown GN, Garber JD (1970) Calculation of the vapor pressure and heats of vaporization and sublimation of liquid and solids below one atmosphere pressure, Neon, Engineering Experiment Station, Georgia Institute of Technology, Atlanta, Technical Report N°1

Part II

Abilov GS, Polunin SP, Astrov DN, Belyanskii LB (1978) Differential membrane manometer for the measurement of low pressures. Instrum Exp Tech 21:1425–1427
Adametz H, Wloka M (1991) Measurements of the absolute density of mercury in the ASMW. Metrologia 28:333–337
Afanas'ev SN, Stepanov AY, Suprunyuk VV (1987) Method of constructing secondary standards for absolute pressure on the basis of fixed points for phase transitions in pure substances. Meas Tech 30(6):532–535
Alasia F, Cannizzo L, Cerutti G, Marson I (1982) Absolute gravity acceleration measurements: experiences with a transportable gravimeter. Metrologia 18:221–229
Alasia F, Capelli A, Cignolo G, Sardi M (1993/1994) A new generation of mercury manometers at the IMGC. Metrologia 30:571–577
Alasia F, Birello G, Capelli A, Cignolo G, Sardi M (1999a) The HG5 laser interferometer mercury manometer of the IMGC. Metrologia 36:499–503
Alasia F, Capelli A, Cignolo G, Goria R, Sardi M (1999b) The MM1 laser interferometer low-range mercury manometer of the IMGC. Metrologia 36:505–509
Alberigi-Quaranta A (1975) Sensori e trasduttori (Sensors and transducers). L'Elettrotecnica 62(11):935–940
Alberigi-Quaranta A, Prudenziati M, Taroni A (1980) Sensori per il controllo e la misura (Sensors for control and measurements). Fisica e Tecnologia 3:139–159
Amagat EH (1894) Memoires sur l'elasticité et la dilatabilité des fluides jusqu'aux trés hautes pressions. Ann Chim Phys 29:68–136, 505–574
Ambrose D (1990) The density of mercury. Metrologia 27:245–247
Ambrose D, Sprake CHS (1972) The vapour pressure of mercury. J Chem Thermody 4:603–620
Ancsin J (1977) Thermometric fixed point of hydrogen. Metrologia 13:79–86
Anderson R et al (2005) Pressure measurement, monograph 7, NMI technology transfer series, 3rd edn. NMI of Australia (Bignell N (ed))
Arvidson JM, Brennan JA (1976) Pressure measurement at low temperatures. In: Advances in Instrumentation 31. Conference paper II, pp 607.1–607.9
Asch G (1982) Les capteurs en instrumentation industrielle, Chap. 13, pp 573–614. Dunod, Paris
Bager T, Casas J, Metral L (2000) Cryogenic pressure calibration facility using a cold force reference. Adv Cryog Eng 45(B):1873–1880
Baldwin GC, Gaerttner MR (1973) Thermal transpiration error in absolute pressure measurement with capacitance manometers. J Vac Sci Technol 10:215–217
Ban S, Jäger J, Legras JC, Matilla C, Rantanen M, Steindl D (2002) Regional Key comparison EUROMET.M.P-K2 within the pressure range (0.5) 1 to 4 (5) MPa. Report on the results of measurements performed in the period from May 1994 to October 1995 in the framework of the EUROMET Project 305, February 28 2002
Bandyopadhyay AK, Blande W, Jäger J (1991) Measurement of argon triple-point pressure. PTB Mitteilungen 101:269–274
Bandyopadhyay AK, Blanke W, Jäger J (1991) Measurements of argon triple- point pressure. PTB-Mitteilungen 101:269–274
Bandyopadhyay AK, Woo SY, Fitzgerald M, Man J, Ooiwa A, Jescheck M, Wu J, Fatt CS, Chan TK, Moore K, El-Tawil AE (2003) Results of the APMP pressure key comparison APMP.M.P-K1c in gas media and gauge mode from 0.4 to 4.0 MPa. Metrologia 40:07002 (Tech Suppl)
Bandyopadhyay AK, Woo SY, Fitzgerald M, Man J, Ooiwa A, Jescheck M, Wu J, Fatt CS, Chan TK, Moore K (2008) Final report of APMP pressure key comparison (APMP.M.P-K6) in gas media and gauge mode from 20 to 105 kPa. Metrologia 45:07001 (Tech Suppl)
Bass AH (1978) Analysis of mechanical pressure generators. J Phys E: Sci Instrum 11:682–688
Bauer H (1979) Die darstellung der druckskala im bereich von 0.01 bis 2 bar durch das quecksilber. PTB Mitteilungen 89:248–255

Bauer H, Gielessen J, Jäger J (1977) Die Darstellung der Druckskala im bereich zwischen 10 und 100 bar durch die Hauptnormalger te der PTB. PTB-Mitteilungen 87:384–395

Bean VE (1983) Fixed points for pressure metrology. In: Peggs GN (ed) High pressure measurement techniques, Chap. 3, pp 93–124. Applied Science Publication, London

Bean VE (1986) Pressure metrology: primary standard piston gauges. Physica 139 and 140B:739–742

Bean VE, Yaw-Poo l (1989) A capacitance method of measuring the radial displacement of the outer diameter of the cylinder of a piston gage In: Molinar GF (ed) High pressure metrology. Monographie 89(1):22–26 (BIPM, Sévres, France)

Bean VE, Akimoto S, Bell PM, Block S, Holzapfel WB, Manghnani MH, Nicol MF, Stishov SM (1986) Another step toward an international practical pressure scale. Second AIRAPT IPPS task group report. Physica 139 and 140B:52–54

Beattie JA, Blaisdell BE, Kaye J, Gerry NT, Jhonson CA (1941) An experimental study of the absolute temperature scale. VIII.The thermal expansion and compressibility of vitreous silica and the thermal dilation of mercury. Proc Am Acad Arts Sci 74:371–388

Bennett SJ (1977) An absolute interferometric dilatometer. J Phys E: Sci Instrum 10:525–530

Bennett SJ (1978) Thermal expansion of tungsten carbide gauge blocks. Metrol Inspect 35–37 (Sept.)

Bennett SJ, Clapham PB, Daborn JE, Simpson DI (1975) Laser interferometry applied to mercury surfaces. J Phys E: Sci Instrum 8:5–7

Bergoglio M, Calcatelli A (1981) Metrological characteristics of some membrane capacitance vacuum gages. In: Proceedings VII Congresso Nazionale Scienza e Tecnica del Vuoto, Bressanone, Bolzano, Italy, pp 193–206

Bergoglio M, Calcatelli A (2001) Some considerations on handling the calibration results of capacitance membrane gauges. Vacuum 60:153–159

Bernat TP, Cohen HD (1974) Thermomolecular corrections to vapor pressure measurements of ^{3}He. J Low Temp Phys 14(5–6):597–601

Berry KH (1979) NPL-75: a low temperature gas thermometry scale from 2.6 to 27.1 K. Metrologia 15:89–115

Bett KE, Newitt DM (1963) The use of a high-pressure differential mercury manometer for the accurate calibration of free-piston gauges. In: the physics and chemistry of high pressures, pp 99–111. Society of Chemical Industry, London

Bett KE, Weale KE, Newitt DM (1954) The critical evaluation of compression data for liquids and a revision of the isotherms of mercury. Br J Appl Phys 5:243–251

Bettin H, Krumscheid H (1999) New apparatus for measuring the density of mercury. Metrologia 36:547–550

Bettin H, Fehlauer H (2004) Density of mercury—measurements and reference values. Metrologia 41:16–23

Bhatnagar PL, Gross EP, Krook M (1954) A model for collision process in gases. I) Small amplitude process in charged and neutral one-component system. Phys Rev 94:511–525

Bignell N, Bean VE (1988) A fixed point on the pressure scale: carbon dioxide vapour pressure at 273.16 K. Metrologia 25:141–145

Bignell N, Bean VE (1989) Pressure fixed points based on the Carbon dioxide vapour pressure at 273.16 K and the H_2O(I)-H_2O(III)-H_2O(L) triple-point, In: Molinar GF (ed) High pressure metrology. Monographie 89(1):175–184 (BIPM, Sévres, France)

BIPM, IMGC (private communication) (1982). Rapport sur la comparaison du Manobarométre interferentiel de l'IMGC(Turin) au Manobarométre interferentiel du BIPM, BIPM (Sevrés-France), 20 July 1982

Blande W, Jescheck M, Rimhus D (1988) Die thermischen Zustandsgrössen des Stickstoffs im Temperaturbereich von 280 bis 360 K bei Drücken bis 12 MPa. PTB-Mitteilungen 98(3):187–192

Bock T, Ahrendt H, Jousten K (2009) Reduction of the uncertainty of the PTB vacuum pressure scale by a new large area non-rotating piston gauge. Metrologia 46:389–396

Bonhoure J, Terrien J (1968) The new standard manobarometer of the Bureau Internationale des Poids et Mesures. Metrologia 4:59–68
Bonhoure J, Pello R (1983) Cellule à point triple de l'argon:instrument de transfer de pression. Metrologia 19:21–23
Borisov SF, Kulev AN, Porodnov BT, Svetin PE (1973) Effect of the interaction of gases with a surface on the effect of the thermomolecular pressure difference. Zh Tech Fiz 43(9):1973–1978
Boyd C, Juanarena D, Rao MG (1990) Cryogenic pressure sensor calibration facility. In: Fast RW (ed) Advances in cryogenic engineering, vol 35B, pp 1573–1581. Plenum Press, New York
Bridgman PW (1909) The measurement of high hydrostatic pressare. I. A simple primary gauge. Proc Am Acad Arts Sci 44:201–217
Bridgman PW (1911) The measurement of hydrostatic pressures up to 20,000 kg/cm^2. Proc Am Acad Arts Sci 47:321–343
British Standard BS5233:1986 (1986) British standard glossary of terms used in metrology (incorporating BS2643). BSI-UK, UK
Brombacher WG (1970) Survey of micromanometers (National Bureau of Standards monograph), vol 114. National Bureau of Standards, Gaithersburg
Brombacher WG, Johnson DP, Cross JL (1960) Mercury barometers and manometers (National Bureau of Standards monograph), vol 8. National Bureau of Standards, Gaithersburg
Buonanno G, Dell'Isola M, Maghenzani R (1999) Finite element analysis of pressure distortion coefficient and piston fall rate in a simple pressure balance. Metrologia 36:579–584
Buonanno G, Ficco G, Giovinco G, Molinar Min Beciet G (2007) In: Buonanno G, Molinar Min Beciet G, (eds) Ten years of experience in modelling pressure balances in liquid media up to few gpa, Collana Scientifica della Facoltà di Ingegneria_02, Università di Cassino, pp 182. ISBN:978-88-8317-037-9, available for free download on: http://cassino.adacto.it/sba/modelling_pressure.cfm
CRIAI (1989) Sensori per applicazioni industriali. Liguori, Napoli
Cailletet L (1880) Sur la mesure des hautes pressions. Ann Chem Phys 19:386–387
Calcatelli A, Arrhen F, Bergoglio M, Greenwood J, Kangi R, Jousten K, Legras JC, Rantanen M, Verbeek J, Matilla Vicente C, Szaulich D (2005). Results of the regional key comparison EUROMET.M.P-K1.a in the pressure range from 0.1 to 1000 Pa. Metrologia 42:07004 (Tech Suppl)
Canali C, Malavasi D, Morten B, Prudenziati M, Taroni A (1980) Piezoresistive effects in thick-film resistors. J Appl Phys 51(6):3282–3288
Caravaggio M, Molinar Min Beciet G, De Maria P (2009) Contribution to the pressure uncertainty measurements due to the "on board" electronic error compensation system, Paper presented at NCSLI Conference, July 2009, San Antonio, TX
Cerutti G, Maghenzani R, Molinar GF (1983) Testing of strain-gauge pressure transducers up to 3.5 MPa at cryogenic temperatures and in magnetic fields up to 6 T. Cryogenics 23:539–545
Cha CY, McCoy BJ (1972) Burnett theory of thermal transpiration with wall accomodation. J Chem Phys 56(7):3273–3277
Chattle MV (1970) The density of mercury over the temperature range 0 to 40 °C (National Physical Laboratory Report, Qu 9). National Physical Laboratory, Teddington
CIPM Recommendation (1981) Formule pour la détermination de la masse volumique de l'air humide, Comité Consultatif pour la Masse et les grandeurs apparentées—First Session, Annexe G2, G19–G33
CIPM MRA-D-05 (2010) Measurement comparisons in the CIPM MRA, Available at BIPM, Version 1, October 2010, p 28
Clifford PN (1985) The international vocabulary of basic and general terms in metrology. Measurements 3(2):72–76
Colwell JH (1979) A solid-dielectric capacitive pressure transducer. In: Timmerhaus KD, Barber MS (eds) High-pressure science and technology, vol 1, pp 798–804. Plenum Press, New York
Cook AH (1961) Precise measurements of the density of mercury at 20 °C. II-Content method. Phil Trans R Soc London Ser A254:125–154

Cook AH, Stone NWB (1957) Precise measurements of the density of mercury at 20 °C I-absolute displacement method. Phil Trans R Soc London Ser A250:279–323
Daborn JE (1977) The accurate measurement of differential pressure at high line pressure. Meas Control 10:377–387
Daborn JE (1987) Report on a BCR audit of measurements of static differential pressures at high line pressures, BCR (European Economic Community), Report EUR 11130EN
Dadson RS, Greig RGP (1965) An improved form of pressure balance for use at relatively low pressure. J Sci Instrum 42:331–333
Dadson RS, Greig RGP, Horner A (1965) Developments in the accurate measurement of high pressures. Metrologia 1:55–68
Dadson RS, Lewis SL, Peggs GN (1982) The pressure balance. Theory and practice. National Physical Laboratory, Teddington
Davis RS (1992) Equation for the determination of the density of moist air (1981/1991). Metrologia 29:67–70
Davis RS, Welch BE (1988) Practical uncertainty limits to the mass determination of a piston-gage weight. J Res NIST 93(4):565–571
Dean JW, Flynn TM (1966) Temperature effects on pressure transducers. ISA Trans 5(3):223–232
Decker DL, Bassett WA, Merrill L, Hall HT, Barnett JD (1972) High pressure calibration, a critical review. J Phys Chem Ref data 1(3):773–836
Delajoud P, Girard M (2002) A force balanced piston gauge for very low gauge and absolute pressure, presented at 2002 NCSL international workshop and symposium, USA
Delajoud P, Girard M, Ehrlich C (1999) Early history of the development and characterization of a 50 mm diameter, gas-operated piston gauge as a primary pressure standard. Metrologie 36:521–524
Desgoffe C (1871) Hochdruck Manometer für hydraulische Pressen. Dinglers Poly J 202:393
Document CIAME (1987) Les capteurs intelligents. CIAME-AFCET, Paris
Doeblin EO (1975) Measurements systems: application and design. McGraw-Hill, New York
Driver RG, Houck JC, Welch BE (1981) An intercomparison of pressure standards between LNE and NBS. J Res NBS 86:277–279
Dwight Adams E (1993) High-resolution capacitance pressure gauges. Rev Sci Instrum 64(3):601–611
Dymond JH, Smith EB (1980) The virial coefficients of pure gases and mixtures: A critical compilation. Oxford University Press, Oxford
EA European Co-operation for Accreditation (1999) Expression of the uncertainty of measurement in calibration, Technical Report EA-4/02
EAL-G26 Reference Guide, EA-4/17 (1997) Calibration of pressure balances, 1st edn, p 29 (now under EURAMET Revision)
Eaton WP, Smith JH (1997) Micromachined pressure sensors: review and recent developments. Smart Mater Struct 6:530–539
Edlén B (1966) The refractive index of air. Metrologia 2:71–80
Edwards D Jr, Linon P (1978) Pressure measurements in a cryogenic environment. J Vac Sci Technol 15(3):1186–1188
Ehrlich C (1993/1994) A review of gas-operated piston gauges. Metrologia 30:585–590
Elliott KWT, Wilson DC, Mason FCP, Bigg PH (1960) Primary standard barometer of range 0–1200 mbar. J Sci Instrum 37:162–166
Ernsberger FM, Pitman HW (1955) New absolute manometer for vapour pressures in the micron range. Rev Sci Instrum 26:584–589
EURAMET Guide EURAMET/cg-17/v.01 (2007) Guidelines on the calibration of electromechanical manometers, previously EA-10/17. www.euramet.org, See also Version 02 (2011).
EURAMET Project 1039 (2008–2010) FEA calculation of pressure distortion coefficients of gas-operated pressure balances, Coordinator Dr. W. Sabuga (PTB). www.euramet.org, See also Final Report 2010-03-25

Farár P, Ŝkrovánec T, Faltus Z, Chytil M (1993/1994) The SMU primary mercury manometer and its comparison with three manometers of different design. Metrologia 30:751–755
Fellmuth B, Fischer J, Gaiser C, Priruenrom T, Sabuga W, Ulbig P (2009) The International Boltzmann project-the contribution of the PTB. C R Physique 10:828–834
Favennec JM (1987) Smart sensors in industry. J Phys E: Sci Instrum 20:1087–1090
Fitzgerald MP, Sutton CM, Jack DG (1999) Design of a pressure balance with a small and calculable change of area with pressure. Metrologia 36:571–573
Francis DB, Solis K (1989) Design considerations for a new high pressure (100 MPa) gas lubricated piston pressure gage. In: Molinar (ed) High pressure metrology. Monographie 89(1):53–61 (BIPM, Sévres, France)
Freddi A, Modena I (1968) Experimental thermomolecular pressure ratio of Helium-3 down to 0.3 K. Cryogenics 8:18–23
Furukawa GT, Riddle JL, Bigge WR, Pfeiffer ER (1982) Application of some metal SRM's as thermometric fixed points (National Bureau of Standards special pubblication), vol 260, p 77. National Bureau of Standards, Gaithersburg
Fürtig M (1973) Absolutmessung der quicksilberdichte im ASMW. Exp Tech Phys XXI:521–534
Galy-Cazalat M (1846) Description d'un manométre court à tube ouvert. Bull Soc Encour Ind Natn 1846:590–592 (Paris (F))
Gambling WA (1987) Novel optical fibres for sensing applications. J Phys E: Sci Instrum 20:1091–1096
Gascoigne J (1971) Precise pressure measurement in the range 0.1–500 torr. Vacuum 21:21–26
Giacomo W (1982) Equation for the determination of the density of moist air (1981). Metrologia 18:33–40
Giardini P (1999) Work towards a new mercury column for high pressure. Metrologia 36:511–515
Gielessen J (1975) Űber Normalgeräte für die Messung des Differenzdrucks im Bereich der Wirkdruckgaszähler (PTB Internal Report W-4), p 24. PTB, Braunscweig
Girard G (1983) Mesure de la pression atmospheric a la section des masses du BIPM (Internal report BIPM-83/2). BIPM, Sévres, France
Girard M (2003) Private communication to Gianfranco Molinar Min Beciet
Girard M, Delajoud P (2006) Automated mass handling for high performance pressure balances. MAPAN J Metrol Soc India 21(3):155–165
Gonano R, Adams ED (1970) In situ vapour pressure measurement for low temperature thermometry. Rev Sci Instrum 41:716–719
Greenberg AS, Guerrier G, Bernier M, Frossati G (1982) A design for an immersible pressure-capacitance gauge. Cryogenics 22:144–145
Greywall DS, Busch PA (1980) High precision ^{3}He-vapour-pressure gauge for use to 0.3 K. Rev Sci Instrum 51:509–510
Griffioen W, Frossati G (1985) Small sensitive pressure transducers for use at low temperatures. Rev Sci Instrum 56:1236–1238
Grohmann K, Lee HK (1987) Extension of the application range of a piston pressure gauge to low pressures. J Phys E: Sci Instrum 20:1169–1172
Guildner LA, Terrien J (1975) Mercury absolute manometers. In: Le Neindre B, Vodar B (eds) Experimental thermodynamics, vol 2, Chap. 4, Part 1, pp 115–131. Butterworths, London
Guildner LA, Stimson HF, Edsinger RE, Anderson RL (1970) An accurate mercury manometer for the NBS thermometer. Metrologia 6:1–18
Guildner LA, Johnson DP, Jones FE (1976) Vapour pressure of water at its triple point. J Res NBS 80A:505–521
Haines R, Blair M (2002) Application of a wide method for the automated calibration od a very low gauge and absolute pressures in a commercial calibration laboratory, Presented at 2002 JAN Measurement Science Conference, Anaeim, CA, USA
Haines R, Blair MA (2009) Method of traceability for FPG8601 force balanced piston gauge to define pressures in the range from 1 Pa to 15 kPa in gauge and absolute measurement modes.

In: XIX IMEKO World Congress, Lisboa, Portugal, 6–11 Sept 2009, conference proceedings pp 2071–2076
Halford RJ (1972) Pressure measurements using vibrating cylinder pressure transducer. Instrum Practice 823:829–833
Harade K, Ikeda K, Ueda T (1982) Precision sensors using mechanical resonators. Yokogawa Tech Bull 26(2):13–19
Harrison ER, Hatt DJ, Prowse DB, Wilbur-Ham J (1976) A new interferometric manometer. Metrologia 12:115–122
Helvensteijn BPM, Van Sciver SW (1990) A symmetrical low temperature pressure transducer. Rev Sci Instrum 61(3):1127–1130
Heydemann PLM (1978). Generation and measurement of pressure. In: Kelm H (ed) High pressure Chemistry, pp 1–49. D. Reidel Publication Company, Dordrecht
Heydemann PLM (1971) A fringe counting pulsed ultrasonic interferometer. Rev Sci Instrum 42:983–986
Heydemann PLM, Welch BE (1975) Piston gages. In: Le Neindre B, Vodar B (eds) Experimental thermodynamics, vol II, Chap. 4, Part 3, pp 147–202. Butterworth, London
Heydemann PLM, Tilford CR, Angel RW (1976) Ultrasonic Interferometer Manometers: 10E-5 torr resolution. In: 22nd ISA symposium proceeding, San Diego (CA), pp 69–75
Heydemann PLM, Tilford CR, Hyland RW (1977) Ultrasonic manometers for low and medium vacua under development at the National Bureau of Standards. J Vac Sci Technol 14:597–605
Hendricks JH, Miiller AP (2007) Development of a new high-stability transfer standard based on resonant silicon gauges for the range 100 Pa to 130 kPa. Metrologia 44:171–176
Hendricks JH, Olson DA (2009) NIST experience with non-rotating force-balanced piston gauges for low pressure metrology. In: XIX IMEKO World Congress, Lisboa, Portugal, 6–11 Sept 2009, conference proceedings pp 2077–2083
Hendricks JH, Ricker JR, Chow JH, Olson DA (2009) Effect of dissolved nitrogen gas on the density of di-2-ethylhexyl sebacate: working fluid of the NIST oil ultrasonic interferometer manometer pressure standard. Measure 4(2):52–59
Hieda M, Kato T, Hirano D, Matsushita T, Wada N (2005) Low temperature performance of miniature capacitive pressure sensor with submicron gap. J Low Temp Phys 138(3–4):917–921
Hill KD (1994) An apparatus for realizing the triple point of mercury. Metrologia 31:39–43
Hobson JP (1969) Surface smoothness in thermal transpiration at very low pressures. J Vac Sci Technol 6:257–259
Holman GJF, Ten Seldman CA (1994) A critical evaluation of the thermophysical properties of mercury. J Phys Chem Ref Data 23(5):807–827
Holman GJF, Ten Seldman CA (1995) A pressurized mercury column up to 300 MPa. Metrologia 32:277–294
Holste JC, Eubank PT, Hall KR (1977) Optimum use of a differential pressure transducer for high-precision measurements. Ind Eng Chem Fundam 16(3):378–380
Houck JC, Molinar GF, Maghenzani R (1983) An intercomparison of pressure standards between the Istituto di Metrologia “G. Colonnetti” and the National Bureau of Standards. J Res NBS 88:253–259
Hung C-C, Jian W, Changpan T (2008) Final report on APMP.M.P-K1.c.1: pneumatic key comparison from 0.4 to 4 MPa in gauge mode. Metrologia 45:07010 (Tech Suppl)
Hung C-C, Jian W, Changpan T (2009) Final report on APMP.M.P-K6.1 pneumatic key comparison from 20 to 105 kPa in gauge mode. Metrologia 46:07004 (Tech Suppl)
Hutton UO (1966) Tilting air-lubricated piston gauge. Instrum Control Syst 9:99–100
Hyland RW, Tilford CR (1985) Zero stability and calibration results for a group of capacitance diaphragm gauges. J Vac Sci Technol A3(3):1731–1737
Hyland RW, Shaffer RL (1991) Recommended practices for the calibration and use of capacitance diaphragm gauges as transfer standards. J Vac Sci Technol A9(6):2843–2863
Idowu A (1999) Feasibility of directly measuring piston-cylinder distortion. Metrologie 36:575–578

ISO Metrology Group (1984) International vocabulary of basic and general terms in metrology (VIM), 1984 edn. ISO, USA (See also JCGM 200:2008)
Jacobs R (1986) Cryogenic applications of capacitance-type pressure sensors. Adv Cryo Eng 31:1277–1284
Jäger J, Sabuga W, Wassmann D (1999) Piston-cylinder assemblies of 5 cm^2 cross-sectional area used in an oil-operated primary pressure balance standard for the 10 MPa range. Metrologie 36:541–544
JCGM 100:2008 (2008) Evaluation of measurement data. Guide to the expression of uncertainty of measurement, © Joint Committee for guides in metrology (JCGM), 1st edn, p 120
JCGM 101:2008 (2008) Evaluation of measurement data. Supplement 1 to the "Guide to the expression of uncertainty of measurement". Propagation of distributions using a Monte Carlo method, © Joint Committee for guides in metrology (JCGM), 1st edn, p 82
JCGM 200:2008 (2008) International Vocabulary of metrology. Basic and general concepts and associated terms (VIM), © Joint Committee for guides in metrology (JCGM), p 90
Jitschin W, Röhl P (1987) Quantitative study of the thermal transpiration effect in vacuum gauges. J Vac Sci Technol A5(3):372–375
Johnson DP, Newhall DH (1953) The piston gauge as a precise pressure-measuring instrument. Trans ASME 75:301–310
Jones BE (1987) Sensors in industrial metrology. J Phys E: Sci Instrum 20:1113–1126
Jones MC, Arp VD, Parrish WR, Daney DE, Ludtke PR, Frederick NV, Hands BA (1977) Helium research in support of superconducting power transmission, annual report (July 1975–Sept 1976) NBS Boulder, Colorado(USA), internal report NBSIR-77-853
Jones N (2009) The new and improved Kelvin. Nature 459:902–904
Jordan GR (1985) Sensor technologies of the future. J Phys E: Sci Instrum 18:729–735
Jäger J (1993/1994) Use of a precision mercury manometer with capacitance sensing of the menisci. Metrologia 30:553–558
Jäger J, Schultz W (1988) Druckvergleichsmessungen zwischen einem Quecksilber—Präzisionmanometer und Tauchglockenmanometern als Normalgeräte zur Messung Kleiner Űberdrücke. PTB Mitteilungen 98:39–44
Jäger J, Klingenberg G, Schultz W (1990) The standard instrument of the PTB for the 5 MPa range of pressure measurements. PTB Mitteilungen 100:429–438
Jousten K (1998) Temperature corrections for thye calibration of vacuum gauges. Vacuum 49(2):81–87
Jousten K, Bergoglio M, Calcatelli A, Durocher JN, Greenwood J, Kangi R, Legras JC, Matilla C, Šetina J (2005) Results of the regional key comparison EUROMET.M.P-K1.b in the pressure range from 3×10^{-4} to 0.9 Pa. Metrologia 42:07001 (Tech Suppl)
Jousten K, Santander Romero LA, Torres-Guzman JC (2005a) Results of the key comparison SIM-EUROMET.M.P-K3.b in the pressure range from 3×10^{-4} to 0.9 Pa. Metrologia 42:07002 (Tech Suppl)
Kaneda R, Sudo S, Nishibata K (1964) An interferometric primary standard barometer. Bull NRLM 9:24–36
Kashani A, Spivak AL, Wilcox RA, Woodhouse CE (1988) Performance of Validyne pressure transducers in liquid helium. In: Scurlock RG, Bailey CA (eds) Proceedings of the 12th ICEC conference, Southampton (UK), pp 379–383. Butterworths, London.
Kashani A, Wilcox RA, Spivak AL, Daney DE, Woodhouse CE (1990) SHOOT flowmeter and pressare transducers. Cryogenics 30:286–291
Kaye GWC, Laby TH (1973) Table of physical and chemical constants, 14th edn. Longman, London
Kisilev Y, Sabuga W, Dapkeviciene K, Farar P, Saczuk K, Sandu I (2008) Final Report on key comparison COOMET.M.P-K1 in the range 0.05 to 0.5 MPa of pneumatic gauge pressure. Metrologia 45:07015 (Tech Suppl)
Klingenberg G (1986) Elastic distortion of piston-cylinder systems of pressure balances. Metrologia 22:259–263

Klingenberg G (1987) The theory of the flow in a converging channel applied to piston-cylinder systems of pressure balances. Metrologia 24:89–95
Klingenberg G (1989) Critical remarks concerning the derivation of the elastic distortion coefficient from the normally used theory. In: Molinar GF (ed) High pressure metrology. BIPM (Sévres) Monographie 89(1):pp 1–11
Klingenberg G, Legras JC (1993/1994) Bilateral comparative pressure measurements of the LNE and the PTB using 10 cm^2 piston-cylinder assemblies. Metrologia 30:603–606
Kobata T, Olson DA (2005) Accurate determination of equilibrium state between two pressure balances using a pressure transducer. Metrologia 42:231–234
Kobata T, Kojima M, Saitou K, Fitzgerald M, Jack D, Sutton C (2007) Final report on key comparison APMP.M.P-K5 in differential pressure from 1 to 5000 Pa. Metrologia 44:07001 (Tech Suppl)
Könemann J, Ehlers S, Jescheck M, Sabuga W (2011) Development of a laser-interferometric mercury micromanometer at PTB, 5th CCM International Conference on pressure and vacuum metrology and 4th International Conference IMEKO TC16, Berlin, Germany, 2–5 May 2011, to be published in PTB Mitteilungen
Kojima M, Kobata T, Saitou K, Hirata M (2005) Development of small differential pressure standard using double pressure balances. Metrologia 42:227–230
Kolb K (2011) Controlled clearance piston gauge research, 5th CCM International Conference on pressure and vacuum metrology and 4th International Conference IMEKO TC16, Berlin, Germany, 2–5 May 2011, to be published in Measurement
Krafft G, Spiegel HJ, Zahn G (1980) Suitability of commercial strain gauge pressure transducers for low temperature application. Cryogenics 20:625–628
Lawless WN, Clark CF, Samara GA (1985) Quantum-ferroelectric pressure sensor for use at low temperatures. Rev Sci Instrum 56(10):1913–1916
Lazos-Martinez RJ, Bean VE (1986) Elastic distortion of piston gauges. Physica 139, 140B:785–787
Legras JC (1988) La mesure des pressions statiques. Chiron, Paris
Legras JC (1993/1994) Stability of piston-cylinder assemblies from an experience of fifteen years. Metrologia 30:625–629
Legras JC, Le Breton D (1990) Le manometre differentielle capacitif interferometrique (M.D.C.I.). Vide Couches Minces Suppl 252:127–129
Legras JC, Le Guinio J (1995) La balance de pression absolue du BNM/LNE dans le domaine de 150 kPa a 1 MPa. In: proceedings of the 7th International Congress Metrologie, France, pp 319–324
Legras JC, Lewis SL, Molinar GF (1988) International comparison in the pressure range 20–100 MPa. Metrologia 25:21–28
Legras JC, Schatz B, Delajoud P (1986) La référence nationale de pression du BNM dans la domaine de 10 à 400 KPa. Bull BNM 17:39–53
Legras JC, Sabuga W, Molinar G, Dchmidt JW (1999) CCM key comparison in the pressure range 50 to 1000 kPa (gas medium, gauge mode). Phase A2: pressure measurements. Metrologia 36:663–668
Le Guinio J, Legras JC, El-Tawil A (1999) New BNM-LNE standard for absolute pressure measurements up to 1 MPa. Metrologie 36:535–539
Lewis S, Peggs GN (1979) The pressure balance, a practical guide to its use. National Physical Laboratory, Teddington
Liang SC (1953) On the calculation of thermal transpiration. J Phys Chem 57:910–911
Maghenzani R, Molinar GF, Marzola L, Kulshrestha RK (1987) Pressure metrology up to 5 MPa in different gas media. J Phys E: Sci Instrum 20:1173–1179
Man J, Molinar Min Beciet G, Buonanno G, Giovinco G (2007) Numerical characterization of a 10 MPa pressure standard based on dimensional data. In: Proceedings of the 7th Metrology Society of Australia conference, Adelaide, Australia, 25–27 July 2007, p 70, 75
Maryamova I, Druzhinin A, Lavitska E, Gortynska I, Yatzuk Y (2000) Low-temperature semiconductor mechanical sensors. Sens Actuator A: Phys 85(1–3):153–157

Marson I, Faller JE (1986) G-the acceleration of gravity: its measurement and its importance. J Phys E: Sci Instrum 19:22–32
McCarty RD (1973) Thermodynamic properties of helium-4 from 2 to 1500 K and pressures to 10^8 Pa. J Phys Chem Ref Data 2(4):923–1041
McConville GT (1969) Thermomolecular pressure corrections in helium vapour pressure thermometry: the effect of the tube surface. Cryogenics 9 (April 1969):122–127
McConville GT (1972) The effect of the measuring tube surface on thermomolecular pressure corrections in vapor pressure thermometry. Temperature 4:159–165
McLellan WH (1968) How to calibrate pressure transducers at 7 K. ISA Transactions 7(1):59–66
Meiyan L, Chen M (2003) Surface acoustic wave resonator pressure sensor, IMEKO TC16 International Symposium on pressure and vacuum, 22–24 Sept 2003, Beijing, China, In: Proceedings of ISPV-2003, Acta Metrologica Sinica Press, China, pp 310–312
Meyer CH, Jessup RS (1931) A multiple manometer and piston gauges for precision measurements. N B S J Res 6:1061–1102
Meyers CH, Van Dusen MS (1933) The vapor pressure of liquid and solid carbon dioxide. J Res NBS 10:381–412
Meyer CW, Reilly ML (1993/1994) Measurements of the gas dependence of the effective area of a piston gauge using H_2, ^3He, N_2, CO_2 and SF_6. Metrologia 30:595–597
Michels A (1932) The calibration of a pressure balance in absolute units. Proc R Acad Amsterdam 35:994–1003
Middlehoek S, Audet SA (1987) Silicon sensors: full of promises and pitfalls. J Phys E: Sci Instrum 20:1091–1096
Miiller AP (1999) Measurement performance of high-accuracy low-pressure transducers. Metrologia 36:617–621
Miiller AP, Bergoglio M, Bignell N, Fen KMK, Hong SS, Jousten K, Mohan P, Redgrave FJ, Sardi M (2002) Final report on key comparison CCM.P-K4 of absolute pressure standards from 1 to 1000 Pa. Metrologia 39:07001 (Tech Suppl)
Miiller AP, Cignolo G, Fitzgeral MP, Perkin MP (2002) Final report of the key comparison CCM-P-K5 of differential pressure standards from 1 to 1000 Pa. Metrologia 39:07002 (Tech Suppl)
Miiller AP, Tilford CR, Hendricks JH (2005) A low differential-pressure primary standard for the range 1 Pa to 13 kPa. Metrologia 42:187–192
Mitsui K, Sakurai H, Mochizuchi T (1972) A gas thermometer measurement below IPTS range. In: Temperature, its measurement and control in science and industry, vol 4, Part 1, Chap. 31, pp 331–338. ISA, Pittsburg
Mohan P, Sharma DR, Gupta AC (1996) Comparison of an ultrasonic interferometer manometer and a static expansion system using a capacitance diaphragm gauge. Metrologia 33:165–171
Mohr PJ, Taylor BN, Newell DB (2008) CODATA recommended values of the fundamental physical constants: 2006. Rev Mod Phys 80(2):633–730
Moisoi N, Severn I, Summer DR (2005) Direct measurements of pressure-induced distortion in a piston-cylinder using a capacitance technique. Metrologia 42:242–245
Moldover MR (1997) Proposed primary pressure standard based on capacitance measurements In: 13th symposium on thermophysical properties, NIST June 1997, p 386
Moldover MR (2011) Gas thermometry and alternative pressure standards In: 5th CCM international conference on pressure and vacuum metrology and 4th international conference IMEKO TC16, Berlin, Germany, 2–5 May 2011, to be published in PTB Mitteilungen
Moldover MR, Trusler JPM, Edwards TJ, Mehl JB, Davis RS (1988) Measurement of the universal gas constant R using a spherical acoustic resonator. Phys Rev Lett 60:249–252
Molinar GF (1993/1994) An old instrument in the new technological scenery: the piston gauge in liquid up to 1 GPa. Metrologia 30:615–623
Molinar GF (2011) Historical perspectives of high pressure metrology using pressure balances In: 5th CCM international conference on pressure and vacuum metrology and 4th international conference IMEKO TC16, Berlin, Germany, 2–5 May 2011, to be published in PTB Mitteilungen

Molinar GF, Bianchi L (1989) Stability and metrological characteristics of manganin gauges up to approximately 1 GPa, In: Molinar GF (ed) High pressure metrology. BIPM (Sévres) Monogr 89(1):147–156

Molinar GF, Bean V, Houck J, Welch B (1980) The mercury melting line up to 1200 MPa. Metrologia 16:21–29

Molinar GF, Cresto PC, Maghenzani R (1989) Elastic distortion in a piston-cylinder unit for pressure measurements in liquids to 100 MPa. Preliminary results. In: Molinar GF (ed) High pressure metrology, Monographie 89(1):12–21 (BIPM, Sèvres, France)

Molinar GF, Bean V, Houck J, Welch B (1991) Pressare measurements with the mercury melting line referred to ITS-90. Metrologia 28:353–354

Molinar GF, Maghenzani R, Cresto PC, Bianchi L (1993) Elastic distortions in piston-cylinder units at pressures up to 0.5 GPa. Metrologia 29:425–440

Molinar GF, Cresto PC, Ehrilch C, Houck J (1993/1994a) Elastic distortion calculations on a special piston gauge (PG27) up to 28 MPa in different operational modes. Metrologia 30:635–640

Molinar GF, Sabuga W, Robinson G, Legras JC (1998) Comparison of methods for calculating distortion in pressure balances up to 400 MPa. EUROMET Project 256. Metrologia 35:739–759

Molinar GF, Rebaglia B, Sacconi A, Legras JC, Vailleau GP, Schmidt JW, Stoup JR, Flack DR, Sabuga W, Jusko O (1999) CCM Key comparison in the pressure range 0.05 to 1 MPa (gas medium, gauge mode). Phase A1: dimensional measurements and calculations of effective area. Metrologia 36:657–662

Molinar GF, Legras JC, Jäger J, Ooiwa A, Schmidt J (2000) Draft B-Results of the CCM pressure key comparison (Phase B) in gas media and gauge mode from 80 kPa to 7 MPa. IMGC-CNR Internal Report number 42

Molinar GF, Bergoglio M, Sabuga W, Otal P, Ayyildiz G, Verbeek J, Farar P (2005) Calculation of effective area A_0 for six piston-cylinder assemblies of pressure balances. Results of the EUROMET project 740. Metrologia 42:197–201

Molinar GF, Buonanno G, Giovinco G, Delajoud P, Haines R (2005a) Effectiveness of finite element calculation methods (FEM) on high performance pressure balances in liquid media up to 200 MPa. Metrologia 42:207–211

Morii Y, Adams ED (1981) Capacitive pressure gauge for use inside a sample cell. Rev Sci Instrum 52:1779–1780

Morten B, Pirozzi L, Prudenziati M, Taroni A (1979) Strain sensitivity in film and cermet resistors: measured and physical quantities. J Phys D: Appl Phys 12:51–54

Muijlwijk R (1988) Update of the Edlén formulae for the refractive index of air. Metrologia 25:189

Mutual Recognition Arrangement (CIPM-MRA) (1999, revised 2003) Mutual recognition of national measurement standards and of calibration and measurement certificates issued by national metrology institutes, Paris 14 Oct 1999, technical supplement revised in Oct 2003, p 45, BIPM Editor, Pavillon de Breteuil, F-92312, Sèvres Cedex, France. http://www.bipm.org/en/cipm-mra/mra_online.html

Nagashima H (2003) Precision digital manometer, MT200 series, IMEKO TC16 International Symposium on pressure and vacuum, 22–24 Sept 2003, Beijing, China In: proceedings of ISPV-2003, Acta Metrologica Sinica Press, China, pp 182–186

Neubert HKP (1975) Instrument transducers: an introduction to their performance and design. Claredon Pres, Oxford

Newhall DH (1957) Pressure Cylinder unit and method, Patent N^{er} 2796229

Niebauer TM, Sasagawa GS, Faller JE, Hilt R, Klopping F (1995) A new generation of absolute gravimeters. Metrologia 32:159–180

Ooiwa A (1989) Development of a highly stable air piston pressure gage with non-rotational piston-cylinder system. In: Molinar GF (ed) High pressure metrology. BIPM (Sévres) Monographie 89(1):67–72

Ooiwa A (1993/1994a) Novel non rotational piston gauge with weight balance mechanism for the measurement of small differential pressures. Metrologia 30:607–610

Ooiwa A, Ueki M (1993) Development of novel air piston gauge for medium vacuum and fine differential pressure measurement. Vacuum 44(5–7):603–605
Ooiwa A, Ueki M, Kaneda R (1993/1994) New mercury interferometric baromanometer as the primary pressure standard in Japan. Metrologia 30:565–570
Orcutt RH (1973) Interlot density variation of a siloxane manometer fluid. J Vac Sci Technol 10:506
Otal P, Legras JC (2005) Metrological Characterization of a new standard, in absolute and gauge pressure modes, in the range 1 to 15000 Pa. Metrologia 42:216–219
Otal P, Verbeek J, Steindtl D, Tesar J, Gorobei VN, Matilla Viciente C, Spohr I (2007) Final Report on key comparison EUROMET.M.P-K3.a in the gauge pressure range 50 to 1000 kPa. Metrologia 44:07010 (Tech Suppl)
Otal P, Harel D, Legras JC (2008) Comparison between the absolute pressure balance and the mercury manometer of LNE. Revue Française de Métrologie 13:25–32
Paratella A, Marani A (1968) Colonna differenziale a mercurio di altezza 9 m per la taratura di bilance manometriche. Mem Acc Patavina di SS LL AA 80:67–82
Paros JM (1973) Precision digital pressure transducer. ISA Trans 12(2):173–179
Paros JM (1975) Digital quartz transducers for absolute pressure measurements. In: Proceedings 21th ISA Symposium, Philadelphia
Patterson JB, Prowse DB (1985) Comparative measurement of the density of mercury Metrologia 21:107–113
Paul H (1993/1994) New high-precision reference pressure transducers from 1 to 50 MPa. Metrologia 30:677–681
Pavese F (1981) The use of triple point of gases in sealed cells as pressure transfer standards: Oxygen (146.25 Pa), Methane (11696 Pa) and Argon (68890 Pa). Metrologia 17:35–42
Peggs GN (1977) A method for computing the effective area of a pressure balance from diametral measurements, National Physical Laboratory Divisional Report MOM 23. National Physical Laboratory, Teddington
Peggs GN (1980) A review of the fundamental methods for measuring gauge pressures up to 1 KPa. J Phys E: Sci Instrum 13:1254–1262
Peggs GN (1983) High pressure measurement technique. Applied Science, London
Peggs GN, Wisniewski R (1983) Electrical resistance gauges. In: Peggs GN (ed) High pressure measurements techniques, Chap. 6, pp 215–248. Applied Science, London
Peggs GN, Elliott KWT, Lewis S (1979) An intercomparison between a primary standard mercury barometer and a gas-operated pressure balance standard. Metrologia 15:77–85
Perkin M (2011) Report on EUROMET key comparison of pressure measurements standards in the range 80 kPa to 7 MPa (EUROMET.M.P-K3.b). Metrologia 48:07006 (Tech Suppl)
Perkin M, Köhler R, Riety P, Skrovanek T, Morris EC, Tilford CR, Ehrlich CD, Ooiwa A, Eichorn G, Jäger J, Molinar GF, Bass AH, Gupta AC (1998) Comparison of pressure standards in the range 10 to 140 kPa. Metrologia 35:161–173. An erratum of this article has been published in: (1999) Metrologia 36:160
Perkin M, Picard A, Lecollinet M, Fen K, Sardi M, Miiller A, Agarwal A, Jescheck M, Wüthrich C (2008) Final report on CCM key comparison CCM.P-K2: pressure (10 to 120 kPa) absolute mode. Metrologia 45:07002 (Tech Suppl)
Picard A, Davis RS, Gläser M, Fujii K (2008) Revised formula for the density of moist air (CIPM-2007). Metrologia 45:149–155
Pinot P, Riety P (1989) Barometre automatique de haute precision. Bull BNM 78:17–25
Pinot P, Riety P (1993) Le micromanomètre à huile de l'Institut National de Métrologie. Bull BNM 92:13–20
Poirier F (1999) APX50, the first fully authomatic absolute pressure balance in the range 10 kPa to 1 MPa. Metrologia 36:531–533
Polunin SP, Astrov DN, Belyanskii LB, Dedikov YA, Zakharov AA (1986) Precision differential capacitance manometer. Instr Exp Tech 29(2):501–503
Poulter KF (1977) The calibration of vacuum gauges. J Phys E: Sci Instrum 1:112–125

Poulter KF, Rodgers MJ, Nash PJ, Thompson TJ, Perkin MP (1983) Thermal transpiration correction in capacitance manometers. Vacuum 33(6):311–316

Prowse DB, Hatt DJ (1977) The effect of rotation on a gas operated free-piston gauge. J Phys E: Sci Instrum 10:450–451

Prudenziati M, Morten B (1986) Sensori e trasduttori a film spesso. Fis Tecnol 9:21–32

PTB Internal Report (1995) (PTB-Stoffdatenblätter SDB 12), Mercury, p 21. ISSN:0942-7821

Rantanen M, Semenoja S (2005) Results on the effective area of the FPG-type digital piston manometer of MIKES. Metrologia 42:165–168

Reccomendation INC-1 (1981) Adopted by the 70th CIPM session, Procéss Verbaux, 49, CIPM

Rendle CG (1993/1994) A large area piston gauge for differential and gauge pressure from zero to 3,2 kPa. Metrologia 30(6):611–613

Riety P (1987) Etalons primaires de pression: Manométre à mercure ou balance manometrique? Bull BNM 70:8–16

Riety P, Lecollinet P (1977) Le systéme de référence des pressions de l'Institut Nationale de Metrologie (Laboratoire Primaire du BNM). Bull BNM 28:13–21

Riety P, Legras JC (1987) Comparaison entre le manométre a mercure de l'INM et la balance de pression de 400 kPa du LNE. Bull BNM 70:3–7

Roberts TR, Sydoriak SG (1956) Thermomolecular pressure ratios for ^{3}He and ^{4}He. Phys Rev 102:304–308

Ronsin H (1987) Thermométres à pression de vapeur saturante. Bull BNM 70:27–47

Ruchholz E (1883) Ruchholz's manometer-Probiapparat. Dinglers Poly J 247:21

Ruifeng Y, Litian L, Zhijian L (2003) Stress sensitive PMOS operational amplifier and its application in silicon pressure sensor In: IMEKO TC16 International Symposium on pressure and vacuum, 22–24 Sept 2003, Beijing, China, proceedings of ISPV-2003, Acta Metrologica Sinica Press, China, pp 232–234

Ruiz Gonzales S (2011) Desarrollo de un nuevo patron nacional de presion. Desde la columna de mercurio a patrones primaries de vacio. PhD Thesis, University of Valladolid, Spain, April 2011

Ruiz Gonzales S, Medina MN, Calvo R (2009) The CEM laser interferometer mercury manobarometer In: XIX IMEKO World Congress, Lisboa, Portugal, 6–11 Sept 2009, conference proceedings, pp 2019–2022

Sabuga W (2006) Towards 7 MPa pressure standards with 1×10^{-6} uncertainty. In: AdMET conference, New Delhi-India, conference proceedings on CD, paper 58, pp 555–564

Sabuga W (2011c) Pressure measurements in gas media up to 7.5 MPa for the Boltzmann constant redetermination. In: 5th CCM international conference on pressure and vacuum metrology and 4th international conference IMEKO TC16, Berlin, Germany, 2–5 May 2011, to be published in PTB Mitteilungen

Sabuga W, Molinar G, Buonanno G, Esward T, Rabault T, Yagmur L (2005) Calculation of the distortion coefficient and associated uncertainty of PTB and LNE 1 GPa pressure balances using finite element analysis-EUROMET Project 463. Metrologia 42:202–206

Sabuga W, Molinar G, Buonanno G, Esward T, Legras JC, Yagmur L (2006) Finite element method used for calculation of the distortion coefficient and associated uncertainty of a PTB 1 GPa pressure balance-EUROMET Project 463. Metrologia 43:311–325

Sabuga W, Ulbig P, Salama AD (2010) Elastic constants of pressure balances' piston-cylinder assemblies measured with the resonant ultrasound spectroscopy. In: proceedings of the International Metrology conference CAFMET 2010, pp 1–8

Sabuga W, Priruenrom T, Haines R, Blair M (2011a) Design and evaluation of pressure balances with 1×10^{-6} uncertainty for the Boltzmann constant project. In: 5th CCM international conference on pressure and vacuum metrology and 4th International Conference IMEKO TC16, Berlin, Germany, 2–5 May 2011, to be published in PTB Mitteilungen

Sabuga W, Priruenrom T, Molinar Min Beciet G, Giovinco G, Rabault T, Wongtherp P, Pražák D (2011b) FEA Calculation of pressure distortion coefficients of gas-operated pressure balances-EURAMET project 1039. In: 5th CCM international conference on pressure and vacuum

metrology and 4th international conference IMEKO TC16, Berlin, Germany, 2–5 May 2011, to be published in measurement
Sabuga W, Sharipov F, Priruenrom T (2011d) Determination of the effective area of piston-cylinder assemblies using a rarefied gas flow model. In: 5th CCM international conference on pressure and vacuum metrology and 4th international conference IMEKO TC16, Berlin, Germany, 2–5 May 2011, to be published in PTB Mitteilungen
Sacharov AA, Astrov DN, Belianski LB, Dedikov YA, Polunin SP (1986) Interferometric mercuri manometer, in Russian. Instrum Exp Tech 3:196–201
Sadkovskaya I, Eichwald A (2011) A laser interferometric oil manometer with floats (The research of the uncertainty and some prospects). In: 5th CCM international conference on pressure and vacuum metrology and 4th international conference IMEKO TC16, Berlin, Germany, 2–5 May 2011, to be published in PTB Mitteilungen
Sakuma A (1984) Gravitational acceleration, mass, and electrical quantities. Present status of the absolute measurement of gravitational acceleration. In: Taylor BN, Phillips WD (ed) Precision measurement and fundamental constants II, vol 617, pp 397–404. NBS (USA) Special Publication, USA
Salama AD, Sabuga W, Ulbig P (2011) Measurement of the elastic constants of pressure balance materials using resonance ultrasound spectroscopy. In: 5th CCM International Conference on pressure and vacuum metrology and 4th International Conference IMEKO TC16, Berlin, Germany, 2–5 May 2011, to be published in Measurement
Samaan ND (1990) Mathematical modelling of instruments for pressure metrology. Ph. D. Thesis, City University of London, Measurement and Instrumentation Centre
Samaan ND, Abdullah F (1993/1994). Computer-aided modelling of pressure balances. Metrologia 30:641–644
Schaad TP (2009) Nano-resolution oceanic, atmospheric and seismic sensors with parts-per-billion resolution. Technical Note document N°G8218 Rev E
Schmidt JW, Moldover MR (2011) Progress toward a pressure standard using argon-filled microwave cavity resonator. In: 5th CCM international conference on pressure and vacuum metrology and 4th international conference IMEKO TC16, Berlin, Germany, 2–5 May 2011, to be published in PTB Mitteilungen
Schmidt JW, Welch BE, Ehrilch CD (1993) Operational mode and gas species effects on rotational drag in pneumatic dead weight pressure gauges. Meas Sci Instrum 4:26–34
Schmidt JW, Welch BE, Ehrilch CD (1993/1994) Gas and mode, vertical and rotational effects with a three piston gauge apparatus. Metrologia 30:599–602
Schmidt JW, Tison SA, Ehrilch CD (1999a) Model for drag forces in the crevice of piston gauges in the viscous-flow and molecular-flow regimes. Metrologia 36:565–570
Schmidt JW, Cen Y, Driver RG, Bowers WJ, Houck JC, Tison SA, Ehrilch C (1999b) A primary pressure standard at 100 kPa. Metrologie 36:525–529
Schmidt JW, Jain K, Miiller AP, Bowers WJ, Olson DA (2006) Primary pressure standards based on dimensionally characterized piston/cylinder assemblies. Metrologia 43:53–59
Schooley JF (1988) NBS gas thermometry from 0 to 660 °C. In: proceedings of workshop and symposium of the national conference of standards laboratories, pp 50.1–50.14
Schultz RA (1976) The calculation of exact gas head corrections. In ISA ASI 76221, pp 89–96
Schuster G, Wolber L (1986) Automated ^{3}He melting curve thermometer. J Phys E: Sci Instrum 19:701–705
Šetina J (1999) New approach to corrections for thermal transpiration effects in capacitance diaphragm gauges. Metrologia 36:623–626
Seyss L (1869) Űber die neue Controle-Pumpe für Manometer. Dinglers Poly J 191:352–354
Shammas S, Seguin HJJ (1979) Simple sensitive capacitance manometer for corrosive gas laser systems. Rev Sci Instrum 50(2):207–209
Shangchun F, Qin J, Guanngyu L (2003) A novel miniature resonant cylinder pressure transducer. In: IMEKO TC16 international symposium on pressure and vacuum, 22–24 Sept 2003, Beijing, China, proceedings of ISPV-2003, Acta Metrologica Sinica Press, China, pp 150–153

Sharipov F (2011) How theoretical flow simulation can help pressure and vacuum metrology. In: 5th CCM international conference on pressure and vacuum metrology and 4th international conference IMEKO TC16, Berlin, Germany, 2–5 May 2011, to be published in Measurement

Sharma JKN, Bandyopadhyay AK (1993) Establishment of the mercury fixed point around 0 °C using volumetric method. PRAMANA J Phys 40(2):129–136

Sharma JKN, Jain KK, Bandyopadhyay AK (1988a) Characterization of a controlled clearance piston gauge using different working fluids up to 5 MPa. Jpn J Appl Phys 27(5):843–848

Sharma JKN, Jain KK, Bandyopadhyay AK, Jäger (1988b) International intercomparison of pressure standards in the pneumatic region 0.4–4.0 MPa between NPL (India) and PTB (FRG). J Phys E: Sci Instrum 21:635–641

Sharma JKN, Jain KK, Bandyopadhyay AK (1989) Effect of different gas media on the operation of the controlled clearance piston gauge up to 5 MPa. In: high pressure science and technology, Kiev (USSR), Naukova Dumka, proceedings XI Airapt conference Vol 4, pp 105–110

Sharma JKN, Sharma DR, Gupta AC (1991) Zero shift in the differential capacitance diaphragm gauges due to the change in line pressure. J Vac Sci Technol A 9(4):2389–2393

Sharma JKN, Sharma DR, Gupta AC (1993) Effect of line pressure on the zero stability of a differential quartz bourdon gauge for various gases. Metrologia 30:37–43

Sheng Y, Han N, Guo C, Duan M, Xu Y (1988) A new primary standard manometer. In: Rutledge WC (ed) Metrology, proceedings of the 11th IMEKO conference, Houston USA Oct 1988, Instrument Society of America, Research Triangle Park, North Carolina, pp 265–270

Simons S (1967) Poiseuille gas flow in the transition regime II. Application of the general theory. In: proceeding R Soc London A301, pp 401–410

Simon J, Pinot P (1992) Générateur de pressions différentielles de 0 à 1000 pascal. Bull BNM 88:11–17

Simpson DI (1993/1994) Computerized techniques for calibrating pressure balance. Metrologia 30:655–658

Siu MCI (1973) Equations for thermal transpiration. J Vac Sci Technol 10(2):368–372

Smart PW (1982) Mass adjuster for pressure balance. Rev Sci Instrum 53(3):366–367

Smith AH, Lawson AW (1954) The velocity of sound in water as a function of temperature and pressure. J Chem Phys 22:351–359

Soloman S (2009) Sensors handbook, 2nd edn. McGraw-Hill Professional, p 1424

Sommer KD, Poziemski J (1993/1994) Density, thermal expansion and compressibility of mercury. Metrologia 30:665–668

Stephan K, Kraus R, Laesecke A (1987) Viscosity and thermal conductivity of nitrogen for a wide range of fluid states. J Phys Chem Ref Data 16(4):993–1023

Span R, Lemmon EW, Jacobsen RT, Wagner W, Yokozeki A (2000) A reference equation of state for the thermodynamic properties of nitrogen for temperatures from 63.151–1000 K and pressures to 2200 MPa. J Phys Chem Ref Data 29(6):1361–1433

Steur PPM, Pavese F (1993/1994). Error budget and accuracy of the IMGC manobarometer model BIPM/JAEGER with automatic data acquisition. Metrologia 30:559–563

Stock M, Pello R (1999) Improved measurement accuracy and uncertainty budget of the BIPM primary standard manobarometer. Metrologia 36:149–153

Storvick TS, Park HS, Loyalka SK (1978) Thermal transpiration: a comparison of experiment and theory. J Vac Sci Technol 15(6):1844–1852

Straty GC, Adams ED (1969) Highly sensitive capacitance pressure gauge. Rev Sci Instrum 40:1393–1397

Stuart PR (1989) Primary barometers and the BIPM International intercomparison in the pressure region 10 kPa to 110 kPa. In: Molinar GF (ed) High pressure metrology. Monographie 89(1):95–104 (BIPM, Sévres, France)

Stuart PR (1993/1994) Measurement uncertainties of U-tube manometers and pressure balances. Metrologia 30:727–735

Stückrath R (1894) Manometer für hohe Druck. PTR Z Instrumde 14:307–308

Sullivan JJ (1985) Development of variable capacitance pressure transducers for vacuum applications. J Vac Sci Technol A3(3):1721–1730
Sutton CM (1979) The rotational frequency dependence of a pressure balance. J Phys E: Sci Instrum 12:1–3
Sutton CM (1980a) An improved mechanism for spinning the floating element of a pressure balance. J Phys E: Sci Instrum 13:825
Sutton CM (1980b) The effective area of a pressure balance at low pressures. J Phys E: Sci Instrum 13:857–859
Sutton CM (1986/1987) The accurate generation of small gauge pressures using twin pressure balances. Metrologia 23:187–195
Sutton CM (1993/1994) The pressure balance as an absolute pressure standard. Metrologia 30:591–594
Sutton CM, Fitzgerald MP (2009) Performance aspects of gas-operated pressure balances as pressure standards. Metrologia 46:655–660
Sutton CM, Fitzgerald MP (2011) A Planck constant measurement using pressure metrology. In: 5th CCM international conference on pressure and vacuum metrology and 4th international conference IMEKO TC16, Berlin, Germany, 2–5 May 2011, to be published in PTB Mitteilungen
Sutton CM, Fitzgerald MP, Jack DG (1999) Conventional pressure balances as reference standards for pressures in the range 10 Pa to 10 kPa. Metrologia 36:517–520
Sutton CM, Fitzgerald MP, Jack DG (2010) The concept of a pressure balance based watt balance. In: CPEM 2010 conference Digest, Daejeon, Korea, 13–18 June 2010, pp 131–132
Takaishi T, Sensui Y (1963) Thermal transpiration effect of Hydrogen, Rare gases and Methane. Trans Faraday Soc 59:2503–2514
Tilford CR (1973) A fringe counting laser interferometer manometer. Rev Sci Instrum 44:180–182
Tilford CR (1977) Analytical procedure for determining lengths from fractional fringes. Appl Opt 16:1857–1860
Tilford CR (1987) The speed of sound in a mercury ultrasonic interferometer manometer. Metrologia 24:121–131
Tilford CR (1988a) New developments in barometric range pressure standards. In: proceedings of NCSL symposium, pp 35–1, 35–15, Washington DC
Tilford CR (1988b) International comparisons of pressure standards: a status report. J Res NBS 93:545–549
Tilford CR (1992) Pressure and vacuum measurements. In: Rossiter BW, Hamilton JF, Baetzhold RC (eds) Physical methods of chemistry, Chap. 2, vol VI. Wiley, New York
Tilford CR (1993/1994) Three and a half centuries later-the modern art of liquid-column manometry. Metrologia 30(6):545–552
Tilford CR, Martin DF (1984) Gas/oil interface and high-sensitivity differential pressure indicators used for the comparison of gas with oil piston gauges. Rev Sci Instrum 55(1):95–98
Tilford CR, Hyland RW (1988) The NBS ultrasonic interferometer manometer and studies of gas-operated piston gages. In: Rutledge WC (ed) Metrology, proceedings of the 11th IMEKO conference, Houston, USA, Oct 1988, Instrument Society of America, Research Triangle Park, North Carolina, pp 277–289
Tilford CR, Hyland RW, Sheng Y (1989) Non geometric dependencies of gas-operated piston gage effective areas. In: Molinar GF (ed) High pressure metrology. BIPM, Sévres. Monographie 89(1):105–113
Torres-Guzman JC, Olvera-Arana P, Alasia F, Sardi M, Zuñiga S, Santander LA, Esparza A (2005) The IMGC/CENAM-HG6 mercury manobarometer. Metrologia 42:161–164
Tsiklis DS (1968) Handbook of techniques in high-pressure research and engineering. Plenum Pres, New York (Translated from Russian)
Ueki M, Ooiwa A (1993/1994) A heterodyne laser interferometric oil manometer. Metrologia 30:579–583
Van Degrift CT (1974) A sensitive dispacement transducer using an extremely reentrant 84 MHz cavity oscillator. Rev Sci Instrum 45(9):1171–1172

Van Degrift CT (1975) Tunnel diode oscillator for 0.001 ppm measurements at low temperatures. Rev Sci Instrum 46(5):599–607

VIM (2008) International Vocabulary of Metrology. Basic and general concepts and associated terms (VIM), 3rd edn, JCGM 200:2008 (Available at the BIPM website: http://www.bipm.org)

Walstrom PL, Maddocks JR (1987) Use of Siemens KPY pressure sensors at liquid helium temperatures. Cryogenics 27:439–441

Wan Mohamed WAM, Petzig JN (2009) The development of novel interchangeable pistons for pressure performance optimisation in a gas-operated dead weight pressure balance. Metrologia 46:315–322

Weber S, Schmidt G (1936) Experimentelle Untersuchungen über die thermomolekulare Druckdifferenz in der Nähe der Grenzbedingung $p_1/p_2 = (T_1/T_2)^{1/2}$ und Vergleichung der Theorie, Leiden Communication 246 C Kamerlingh Onnes Laboratory University, Holland

Welch BE, Bean VE (1984) A method to determine the pressure dependent distorsion of a simple piston gage based on dimensional metrology. In: Materials Research Society Symposium proceeding vol 22, pp 261–264. Elsevier, New York

Welch BE, Guildner LA, Bean VE (1985) Factors affecting the precision of gas operated piston gages at the part per million level. Adv test Meas, 22:303. In: proceeding of 31st International Instrumentation Symposium, San Diego, CA

Welch BE, Edsinger RE, Bean VE, Ehrlich CD (1989a) Observations of gas species and mode of operation effects on effective areas of gas-operated piston gages. In: Molinar GF (ed) High pressure metrology. Monographie 89(1):81–94 (BIPM, Sévres, France)

Welch BE, Edsinger RE, Bean VE, Ehrlich CD (1989b) The reduction of uncertainties for absolute piston gage pressure measurements in the atmospheric pressure range. J Res NIST 94(6):343–346

Williams JC III (1970) Thermal transpiration. A continuum gasdynamic view. J Vac Sci Technol 8(2):446–450

Wisniewski R, Sendys R, Wisniewski D, Rostocki AJ (1989) Determination of pressure coefficient of effective area of simple 0.3 GPa deadweight manometer by means of finite element method of strain calculation. In: Molinar GF (ed) High pressure metrology. Monographie 89(1):27–30 (BIPM, Sévres)

Woo SY, Choi IM (2005) New apparatus for calibrations in the range of 2 kPa absolute pressure. Metrologia 42:193–196

Woo SY, Choi IM, Kim BS (2005) New weight-handling device for commercial pressure balances. Metrologia 42:224–226

Woo SY, Choi IM, Song H-W (2009) A low differential pressure standard in the range 1 Pa to 31 kPa at KRISS. Metrologia 46:125–128

Yanhua L, Jinku W, Yuanchao Y (2011) Recent development on the compensated micro-manometer. In: 5th CCM international conference on pressure and vacuum metrology and 4th international conference IMEKO TC16, Berlin, Germany, 2–5 May 2011, to be published in measurement

Zandt T, Gaiser C, Fellmuth B (2009) Dielectric-constant-gas-thermometry measurement system for the determination of the Boltzmann constant at PTB, IVth International Workshop "Progress in determining the Boltzmann constant", 22–24 Sept 2009, INRIM, Torino, Italy

Zhaohua Z, Ruifeng Y, Litian L (2003) Silicon digital pressure sensor using ring oscillator and mixer. In: IMEKO TC16 international symposium on pressure and vacuum, 22–24 Sept 2003, Beijing, China, proceedings of ISPV-2003, Acta Metrologica Sinica Press, China, pp 108–112

Zhokhovskii MK (1989) Testing a universal equation for first-order phase transition p-T curves. Izmer Tekh 3:21–23 (English trans: Exp Tech 1989, 217–220)

Zolotich EV (ed) (1987) Researches on high pressures. Standard Press, Moscow (in Russian)

Further Readings Part I

Arzeliers H (1968) Thermodynamique Relativistique et Quantique. Gautier Villars, Paris
Bazarov IP (1964) Thermodynamics. Pergamon Press, Oxford
Bedford RE, Bonnier G, Maas H, Pavese F (1990) Techniques for approximating the ITS-90, monograph BIPM, Bureau International des Poids et Mesures. Sèvres, France
BIPM (1990a) Supplementary information for the ITS-90, monograph BIPM, Bureau International des Poids et Mesures. Sèvres, France
BIPM (1990b) Echelle Internationale de Température du 1990, official text, Bureau International des Poids et Mesures. Sèvres, France
Carnot S (1932) Réflection sur la Puissance Motrice du Feu et sur les Machines Propres à Dévélopper cette Puissance (English edition: Mendoza E (1660) Reflections on the motive power of fire and other papers (trans: Thurston RH). Dover Publications Inc., New York
Cook GA (ed) (1961). Argon, helium and rare gases. Interscience Publication, New York
Dash JG (1979) Films and solid surfaces. Academic Press, New York
De Groot SR, Mazur P (1962). Non equilibrium Thermodynamics. North Holland, Amsterdam
Desvillettes L, Villani C (2005) On the trend to global equilibrium for spatially inhomogeneous kinetic systems: the Boltzmann equation. Invent math 159:245–316. doi:.1007/s00222-004-0389-9 (free download from . . .)
Haase R (1969) Thermodynamics of irreversible processes. Addison-Wesley, Mass
Hiza MJ, Kidnay AJ, Miller RC (1982). Equilibrium properties of fluid mixtures, vol 2. IFI/Plenum, New York
IUPAC (1975) Experimental thermodynamics, vol II (Nendre B Le, Vodar B (eds)). Butterworths, London
IUPAC (1974) International thermodynamic tables of the fluid state, vol 1–8 (Angus S, Armstrong B, Reuck K M de (eds)). Pergamon Press, Oxford
Keller WE (1969) Helium-3 and Helium-4, the international cryogenic monograph series. Plenum Press, New York.
Landsberg PT (1961) Thermodynamics. Interscience, New York
Lounasmaa OV (1974) Experimental principles and methods below 1 K. Academic Press, London
Middleton WEK (1966) A history of the thermometer, and its use in metereology. The John Hopkins Press, Baltimore
NIST (n.d.) Fundamental constants bibliographic search results: 38 citations matching “Boltzmann constant”. http://physics.nist.gov/cgi-bin/fundconst/
Owen DR (1984) A first course in the mathematical foundations of thermodynamics. Springer, New York
Prigogine I (1954) Thermodynamics of irreversible processes. Interscience, New York
Prigogine I (1962) Non equilibrium statistical mechanics. Interscience, New York
Quinn TJ (1990) Temperature, IInd edn. Academic Press, London
Schooley JF (1986) Thermometry. CRC Press Inc., Boca Raton
TMSCI (1941–2012) Temperature, its measurements and control in science and industry, vol 1–8 (Various publishers)
Truesdell CA III (1980) The tragicomical history of thermodynamics 1822–1854. Springer, New York
Van Sciver SW (1986) Helium cryogenics, The international cryogenic monograph series. Plenum Press, New York
Zemansky MW (1968) Heat and thermodynamics. McGraw-Hill, New York

Further Readings Part II

Anderson R et al (2005) Pressure measurement, monograph 7, NMI technology transfer series, 3rd edn. NMI of Australia (Bignell N (ed))

Bandyopadhyay AK, Varandani D, Krishan L (eds) (2001) Advances in High Pressure Science and Technology. In: proceedings of the second international pressure metrology workshop and international conference on high pressure science and technology, NPL New Delhi, India

Berman A (1985) Total pressure measurements in vacuum technology. Academic Press, London

Bray A, Barbato G, Levi R (1990) Theory and practice of force measurement (Monograph in physical measurement). Academic Press, London

Bridgman PW (1970) The physics of high pressure. Dover, USA (a reprint of the 1931 Bell G & Sons book)

Buonanno G, Ficco G, Giovinco G, Molinar Min Beciet G, Buonanno G, Molinar Min Beciet G (eds) (2007). Ten years of experience in modelling pressure balances in liquid media up to few GPa, Collana Scientifica della Facoltà di Ingegneria_02, Università di Cassino, pp 182. ISBN:978-88-8317-037-9, available for free download on: http://cassino.adacto.it/sba/modelling_pressure.cfm

CIAME (F) (1981) Essais d'evaluation des capteurs de pression, 2nd edn. Editino La Documentation Française, Paris

Dadson RS, Lewis SL, Peggs GN (1982) The pressure balance: theory and practice. National Physical Laboratory, Teddington

Decker DL, Bassett WA, Merrill L, Hall HT, Barnett JD (1972) High pressure calibration, a critical review. J Phys Chem Ref data 1(3):773–836

Doeblin EO (1975) Measurements systems:application and design. McGraw-Hill, New York

Heydemann PLM, Welch BE (1975) Piston gages. In: LeNeindre B, Vodar B (eds) Experimental thermodynamics, Vol II, Chap. 4, Part 3, pp 147–202. Butterworth, London

Holzapfel WJ, Isaacs NS (1997) High presssure techniques in chemistry and physics. Oxford University Press, Oxford

First IMEKO TC16 (Pressure and Vacuum) International Conference (2001). 17th Conference Force, Mass, Torque and Pressure measurements at present and in the future. In: proceedings by UME, Tutkey. ISBN:975-403-221-1

Second IMEKO TC16 (Pressure and Vacuum) International Conference (2003) Second Conference on Pressure and Vacuum Measurements. In: proceedings of ISPV 2003, Acta Metrologica Sinica, Beijing

Third IMEKO TC16 (Pressure and Vacuum) International Conference (2007) 20th Conference on Measurement of Force, Mass and Torque together with 1st Conference on Vibration Measurements-Cultivating metrological knowledges. In: proceedings by CENAM, Mexico on CD

Jousten K (ed) (2008) Handbook of vacuum technology. Wiley-VCH, Berlin

Lafferty JM (1998) Foundations of vacuum science and technology Wiley, New York

Legras JC (1988) La mesure des pressions statiques. Chiron, Paris

Lewis S, Peggs GN (1979/1992) The pressure balance, a practical guide to its use. National Physical Laboratory, Teddington

Molinar GF (ed) (1989) BIPM Monographie 1989/1991, High Pressure Metrology. In: first seminar proceedings of the "High Pressure" Working Group of the CCM, LNE (Paris), 24 and 25 May 1988

Molinar GF (ed) (1994) Pressure metrology from 1 kPa to 1 GPa, CCM second international conference organised by the high pressure working group of the CCM, conference proceedings. Metrologia 30(6): 543

Molinar GF (1995) The measurement of high pressure, Part 2.1.3. In: Kaye GWC, Laby TH (eds) Table of physical and chemical constants, 16th edn, pp 33–37. Longman, UK

Molinar GF, Simpson D, Tilford CR (eds) (1999) Pressure metrology from ultra high vacuum to very high pressures ($10^{-7\circ}$ Pa to $10^{9\circ}$ Pa), CCM third international conference organised by the

low, medium and high pressure working groups of the ccm, conference proceedings. Metrologia 36:489

Jousten K, Legras JC, Severn I (eds) (2005). Pressure metrology from ultra high vacuum to very high pressures ($10^{-9\circ}$ Pa to $10^{9\circ}$ Pa), CCM fourth international conference organised by the low, medium and high pressure working groups of the CCM, conference proceedings. Metrologia 42(6)

NCSL International (1998) Deadweight pressure gauges-recommended intrinsic/derived standards practice. NCSL International USA

Neubert HKP (1975) Instrument transducers: an introduction to their performance and design. Claredon Pres, Oxford

Peggs GN (1983) High pressure measurement technique. Applied Science, London

Sherman WF, Stadtmuller AA (1987) Experimental techniques in high pressure research. Wiley, London

Spain IL, Paauwe J (1977) High Pressure technology, vol 2. Marcel Deckker, New York

Tabor D (1979) Gases, liquids and solids 2nd edn. Cambridge University Press, Cambridge

Index

A

Ab initio calculations, 148, 155, 203, 246-50
Absolute, *see* Temperature or Pressure
Absolute temperature, 8, 14, 16, 18-21, 23, 25, 176, 183, 185, 199, 214, 254-55, 261, 264
Absolute pressure, 294, 327, 330, 336-338, 350, 368-370, 391, 395-398
Acceleration due to gravity, 320-321, 324
  local, 339
  standard, 323
  uncertainty, 324, 392, 553-554, 559-560
  zero (in space), 19
Accuracy, 1, 29, 44, 80, 101, 113, 126, 136-138, 148, 154, 171, 176-182, 193
  definition of, 576
  of dead volume calibration, 170, 176, 192
  of gas thermometer, 148, 171
    interpolating, 176-81
    lower accuracy, 193
  of pressure measurements, 325, 368, 391-392, 553-554, 559-560
  of temperature
    fixed-point realizations, 77-93, 101-108, 123-130
    scales, 38, 131, 195, 242, 268
  of vapor-pressure thermometry, 222, 243-46, 254
  of virials, 150-59, 170, 177-81, 196, 199, 203, 206, 208, 212, 221, 254
Acoustic gas thermometer, *see also* Gas thermometer, 207
Acoustic gas thermometry, boundary layer, 209-213
Acoustic virial coefficient, 207-208
Absorbed, 184, 190, 205
Absorption, 461
Adiabat, 7, 12, 49
Adiabatic, 12, 77, 80, 84, 101-02, 121, 130, 185-86, 207, 212, 238, 271-73
  definition, 10-11
  calorimetry (calorimeter), 80, 273, 287, 439
  compressibility, *see also* Compression modulus, 295, 393
  heating and cooling, 396, 412, 447
  shield, 101-02, 192, 271
  state of a system, *see* Adiabat
  unattainability, 11
Adsorbed, 76, 97, 158, 175, 216, 284
  layer, 175
Adsorption, 149, 157-60, 175, 179, 184, 189, 200, 273, 276
Aerostatic head, 88, 161, 168-69, 173, 178, 187-90, 195, 238, 249, 305, 321
  calculation, 321-324
  correction, 168
Air
  as liquid refrigerant, 274
  buoyancy, 352
  compression, 9
  density, 353-355, 555-558
  humidity, 356-357
  impurity, 9, 45, 66, 72, 76, 85, 87, 101, 138, 147, 158, 175, 185, 205, 273-74
Ambient, pressure, 50, 279, 294
  effect on air density, 354, 557
Amount, 7, 10, 14, 48, 49, 58, 64, 78, 81, 83-84, 96-97, 116, 139, 184, 232, 235, 238, 249, 280, 285
  concentration, 66-67
  fraction, 60, 68, 159, 227, 255
    of solute, 57

F. Pavese, G. Molinar Min Beciet, *Modern Gas-Based Temperature and Pressure Measurements,* International Cryogenics Monograph Series,
DOI 10.1007/978-1-4419-8282-7, © Springer Science+Business Media New York 2013

of substance (or of a named substance), as opposed to simply "amount", 19, 47-49, 51, 66, 70, 72, 85-86, 94, 100-02, 113-14, 117, 141, 148-150, 157, 161, 164, 173-75, 188, 208, 213-14, 231-32
of substance
active, 150, 157, 164
in fixed point cells, 109
in gas thermometry, 157, 164, 196, 214
in vapor-pressure thermometry, 232
ratio, 71
Annealed, 47
Annealing, 102, 107, 184, 190
Approach, axiomatic, 10
Approach, microscopic, 13
Approach, phenomenological, 4
Approximation, *see* Argon; Deuterium; Helium-3; Helium-4; Fixed point; Hydrogen; Methane; Neon; Nitrogen; Oxygen; Triple point; Uncertainty; Xenon
Approximation, of a Scale, 23, 26, 31-33, 35, 37, 73, 131, 139, 177-78, 197
Area, *see* Effective area of a piston-cylinder unit
Area, 49, 91, 175, 184
effective, 331, 339-344
measurement of effective area, 339-344
real (as opposite to geometric), 184
Argon (Ar)
as adsorbed gas, 76, 158, 175
as a pressure fixed point, 242, 243, 418, 434, 440
as impurity, 66, 70, 118, 131, 138, 158, 227
cell intercomparison, 113, 117
gas thermometry, 209, 211, 213-14
high-enthalpy temperature generator (T-Gen), 117-18
high-enthalpy shield with, 280
impurities in, 70, 516, 518, 530
in Scales, 136-38
isotope, 230
properties, 55, 88, 98, 233, 530
triple point
as pressure fixed point, 46, 50, 95, 110, 121, 221, 436-441
in the ITS-90, 495
realizations, 110-117
sealed cell, 83, 99-100, 113-116, 119-23
vapor pressure, 230, 243, 542, 546
solid, 100, 242
in heat switches, 284
in magnetic fields, 232
Atmospheric pressure, 50, 294-295, 342, 407
measurement of, 398-403
boiling point, *see* Boiling point
Atomic, 13, 19, 59, 71, 88, 175, 206, 208
mass (weight), 71, 169, 229

B

Baking, 76, 87, 190
Balance, *see also* Pressure balance, 330-392, 555-560
Barometer, *see also* Manometer, 190, 197, 301-316, 549-554
Batch, of material, 47-48, 71-72, 139, 147
Bath, 45, 50, 77, 88, 119, 121-25, 129, 135, 170, 190-92, 195, 206, 213, 251-253, 269-70, 273, 275-76, 279-80
Behavior, 28, 39, 56, 63-64, 69, 78, 89, 124, 130, 150, 154, 166-67, 177-80, 196-97, 229
thermal, 89-90
dynamic, 92, 115
Bias, *see* Systematic effect
BIPM-KCDB, *see also* Appendix G, 491-493
Block, 78-80, 190, 206
thermometer, 96, 115-16, 125-27
external, 96-98, 111, 117
internal, 96, 110
Body, 96, 98, 116
inner
Boiling point, 6, 20-22, 30, 38, 45, 50, 74-75, 132, 197-98, 221, 226, 243-44, 253, 279, 285, 495, 511, 520
Boltzmann Project, 214, 390
Bootstrap, 72, 109
Boundary layer, 209-12
Brazing, 98, 110, 117, 143
Bulb, 21, 77-79, 204, 209, 212, 216
contraction, 162, 191, 206
CVGT, 157-60, 161, 162-63, 168, 183-85, 189-91
two bulbs, 169, 191, 193-94, 197-99
deformation, 162, 174
filling, 158, 160, 171, 181, 191, 193, 195, 209, 215-17, 232, 249
gold plating, 163, 175, 184-85, 189-91
ICVGT, 174-75
inner edges, 185
moisture condensation, 279
overfill, 232-33
pressure, *see* Bulb filling
volume, 157, 160-63, 174, 183, 185, 188, 191, 232-35
volume measurement
geometrical, 185

mercury filling, 185, 209, 212, 218
microwave, 210-13
water filling, 185
vapor pressure, 77, 232-34, 236, 251, 259-60
wall, 157, 161, 175, 184, 190, 195, 200, 209, 212-13, 252
Buoyancy correction, 338, 352

C

Calculation, 152, 154-155, 169, 175, 185, 199, 218-19, 229-32, 258-60
ab initio, 27, 148, 155, 203, 246-50
Calibration, 26, 28, 37, 44, 46-47, 103, 110, 115, 119, 135, 136, 176-79, 185, 195, 197, 204, 208, 222-23, 240, 261, 263-65, 277, 373, 393, 414-416, 420, 430-432
correction, 401-402
definition, 575
general rules for pressure devices, 414-416, 420, 430-432
of a pressure transducer, 420, 430-432
of interpolating CVGT, 176-80
of vapor-pressure thermometers, 223, 243
stability in time, 103
Calibration and measurement capabilities (CMC), 37, 356, 464, 481-82, 488, 573
for pressure measurements, 489-90, 573
for temperature measurements, 491-92
Calibration factor, *see* Factor of calibration, 413-414, 424
Caloric, 4
Calorimeter, 80, 97, 101, 109, 115, 122, 129, 186, 271-73
Calorimetry, *see* Adiabatic calorimetry
Capacitance
and gauge block manometers, 310-311
and interferometric manometers, 302-310
manometers, 311-312
pressure transducers, 95, 121, 160-63, 169, 172-76, 180, 183, 198, 234, 237, 240-41, 405, 418, 456-458
for cryogenic applications, 426-429
ratio, 203
Capacitor, *see* Capacitance
Capsule, *see* Thermometer
Capillary tube (in gas thermometry), 125-28, 160-61, 164-71, 176, 180-81, 185-88, 189-93, 197, 236, 265, 266-67, 283-84
Carbon dioxide (CO_2), 98, 122
as impurity, 520
critical point, 536
properties, 536, 543, 547
triple point, 136
sealed cell, 99, 119, 123
vapor pressure, 233, 242-43, 511, 513, 536, 543, 547
Carnot, 7
cycle, 7-9, 15-16, 23, 49
function, 8
Catalyst, 75-76, 88-90, 100-01, 141, 230, 257, 523-25, 533
Cell
block (inner and external), 96-98, 111-12, 116-17
chamber, 96, 111-12, 117, 122, 125-29
element, 98, 112-17
filling, 55, 81, 86-87, 94, 96, 100, 117, 144
by cryogenic condensation, 97, 100, 241
from gas cylinder, 97
foot, 97, 112
for capsule thermometers, 96-98, 110
for lambda point of ^{4}He, 123
for long stem thermometers, 99, 119
glass (or bulb), 115, 122, 132, 133, 158, 162, 184, 281
high-enthalpy, 118
long stem, 81, 95, 110, 239
micro, 112, 116
multiple, 115-17
open, 80
sealed, 94
totally cold, 95
sealed, *see* Cell, long stem
thermometer block (inner), 77-80, 96, 98, 110, 114, 125-27, 194
volume, 97, 240
Celsius, *see* Degree Celsius
Centigrade, *see* Degree Celsius
Characterization
of liquid-column manometers, 298-330, 549-554
of pressure balances, 330-392, 559-560
of pressure transducers, 393-429
Chemical impurity, 57, 66-68, 73, 142, 213, 226-27, 516-18, 520-40
Chemical-physical problem, 46, 50, 85, 150, 224
Chamber, *see* Cell

Change, 5-8, 10-12, 22, 29-32, 49-50, 57, 64, 66, 70-71, 74-76, 91, 101, 104, 110, 125, 157, 161, 167, 174, 186, 196, 227, 229-30, 232, 240, 269
CIPM-MRA, *see* Appendix G, 463-493
Clapeyron equation, 222
Clausius-Clapeyron equation, 263
Clausius-Mossotti equation
Clearance of piston-cylinder, 341-342
  variation with pressure, 344-348
Closed-cycle refrigerator, *see* Cryocooler
Coefficient
  distribution (k_0)
  of equation, 65-66, 70, 106, 516
  sensitivity, 227
Coefficient of
  adsorption of a gas on a wall, 158
  fractionation, *see also* Distribution coefficient
  interpolating CVGT equation, 180, 495
  Kapitza-effect equation, 125, 251-52, 268, 273
  temperature in pressure transducers, 405, 408, 410, 411, 423-425
  thermal conductivity, *see also* Thermal conductivity
  thermal expansion, *see also* Thermal expansion
  thermal expansion
    of a gas, 21, 51, 125, 262
    of copper, 161-63, 184, 190, 199, 205, 209-12
  vapor-pressure equation, 222, 243, 541
  virial, 150-57, 165, 178, 180, 202, 206, 208, 221, 254
    ab initio calculation, 148, 155
    correction for the two-bulb method, 192
Coil, 117, 123, 213, 264, 269, 277, 280-81
Cold spot, 83, 95-96, 233, 237-38, 249, 267
Colligative property, 61
Comparison, *see also* Key comparisons and Intercomparison
Comparison, 25, 33, 35, 44, 68, 74, 95, 102-06, 108, 155, 170, 185, 187, 191, 196, 200, 206, 249, 254
  of liquid column manometers, 379-389, 478
  of pressure balances, 374-379, 471-473, 477
  using pressure transducers, 474-476
Compatibility, *see* Compatible
Compatible, 33-38
Composition, 31, 44-45, 47, 50, 55-56, 59, 69-73, 74-76, 108, 113, 118, 142, 184, 198, 214, 225, 228, 230-31, 257
Compressibility, adiabatic, 295, 393, etc
Compressibility modulus (factor), 24, 202-04
  of moist air, 353, 555-558
Compression, 7, 9, 143, 206, 216, 349
  hydrostatic, 291-294
  modulus, 216
Compressive strength, 558
Concentration, 10, 57-69, 70-74, 224-25, 319, 504, 519
  molar, 58
Condensation, 19, 51, 53-54, 75-76, 95, 97, 100, 125, 129, 141, 145-46, 157-59, 192-96, 213, 224-26, 235, 240, 251, 255, 273, 279, 284-85, 436
Constant, 9, 12, 14, 18, 20, 24, 26-27, 37, 55, 108-09, 165, 192, 203, 222, 225, 231, 245, 252, 264, 283-84, 292
  Avogadro L (N_A), 22
  Boltzmann k_B (k), 13-14, 19, 22-23, 30, 57, 208, 211, 214, 263
  chemical (i_0), 221
  cryoscopic, *see* Cryoscopic constant
  density, 53
  gas molar R, 19, 148, 158, 202, 208
  g, 19
  heat capacity C_P, 82, 130
  mass (or amount of substance), 48-49, 51-53, 101, 149, 157, 213
  Planck h, 22
  pressure, 50-51, 53, 149
  temperature, 55, 91, 116, 126, 170, 173, 191
  time, *see* Time constant
  triple-point (k_E), 71
  volume, 21, 147, 149, 173, 189-92, 236
  work, 49
Constant volume gas thermometer (CVGT), *see* Gas thermometer
Constraint, 9, 20, 28, 32, 35, 51, 62, 132, 160, 244
Container, 51-54, 77, 82, 85-87, 94, 97-100, 115, 130, 133, 138-40, 149, 224, 252, 276, 279, 285, 448
Contamination, 48, 76, 85-87, 98, 139, 143, 189, 215-18, 230-31, 237, 248, 253, 256, 260, 295
Continuous, 6, 10-13, 40, 64, 77, 79-80, 87, 122-23, 141, 145, 191, 200, 202, 213, 261, 270, 273

Control, 77, 80, 83, 85, 101, 119, 125, 126, 145-46, 185-87, 235, 269, 271, 277-81, 284, 301
temperature, 185, 269, 271, 278-81, 284
flow, 286, 366
passive, 118, 122, 279-81
Controlled clearance, 332-334
method, 355, 361-363
piston-cylinder type, 332, 355
Convection, 83, 124, 166-68, 236, 259
Conventional density, 338-339, 352
Conventional mass value, 338-339
Conversion, 25, 394
ortho-para or para-ortho, 75-76
natural, 75
Copper
block, 77-78, 110, 112, 114, 124, 141, 206, 259
high purity, 162, 184
OFHC, 98, 143, 184, 190, 259
Correction, *see also* Aerostatic head, Buoyancy, Dead space correction, Height, Load, Refractive index
Correction, 24, 26, 30, 35, 38-40, 44, 65-68, 71-73, 84, 88, 104, 118, 129, 142, 148-54, 157-75, 176-182, 183, 187-91, 195-97, 203-04, 209-13, 221, 224-27, 229, 231, 236-38, 246, 248-52, 254, 295
Correction for
acoustic boundary layer, 211-12
aerostatic head, 168-169, 321-324, 435
amount of gas, 164
buoyancy, 338, 352
chemical impurity, 66
dead volume, 164
density, 321-324
dynamic thermal errors, 92
hydrostatic head, *see also* Aerostatic head, 88, 321-324, 435
isomeric composition, 228
isotopic composition, 228
non sphericity (of resonator), 210-11
pre-melting effect, 89
stationary thermal errors, 90
Creep, 173, 193, 267
Creeping, 93
Critical
point, 49-52, 54-55, 74-75, 223, 233, 236, 241-46, 249, 253, 279, 520, 541, 288
pressure, 520
temperature, 156
Cross floating of pressure balances, 336, 371
Cryocooler, 145-46, 270-73
vibration, 271
vibration-free, 272
Cryogenics, 19, 239, 269, 273, 282
Cryogenic pressure
measurements, 418-429
transducers, *see also* Pressure transducers, 172-73, 175, 183, 193, 196-98, 217, 239-41, 256, 265-67, 418-429
Cryopumping, 237, 271
Cryorefrigerator, *see* Cryocooler
Cryoscopic, constant (A, K_f), 58, 61, 67-69
depression, 59
Cryoscopy, 54
Cryostat, 50, 77, 82, 94-96, 100, 110, 115, 121-23, 126-27, 129, 133, 135, 145, 164, 169-70, 183, 185-95, 218, 234, 240, 251, 259, 269
bath, 77, 135, 170, 190, 192-95, 269, 273-77
cryogen free or closed-cycle, *see* Cryocooler
flow, 277
top loading, 274-275
Curie law, 25, 264
Cycle, 7-set, 23, 49, 80, 102, 143, 174

D

D_2O, 76
Dalton's Law, 225
Dead volume (in gas thermometry), 157, 160-61, 164-65, 169-72, 174-76, 187, 200, 204, 214-19, 233, 236-38, 263, 265-66, 279, 295
correction, 164-65, 170
measurement, 187
geometrical, 164, 188, 218
zero, 172-74, 180, 190, 195
Deadweight gauge, *see also* Pressure balances, 293
Deadweight gauge, types and design, 293, 322
Deadweight tester, *see also* Deadweight gauge, 293
Definition, 6, 8, 12, 13, 22, 30, 31, 44, 45, 59, 84, 136, 139, 177, 180-82, 246-47, 249, 268
ICVGT
ITS-90, 495
other possible, 181-82
ideal gas, 13, 18, 19
melting range, 59
multiple, 33-34, 37
of the kelvin, 6, 21-22, 495
Definition of pressure, 291-298
Definition, of temperature, 4-5, 6, 10, 13-14, 16

Deformation, *see also* Elastic deformation, 332, 334, 344, 429
Deformation, *see also* Pressure distortion coefficient, Elastic distortion calculations
Deformation
of bulb (in gas thermometry), 161-62
of elastic elements, 332, 334, 344, 429
of piston and cylinder, 344-360
Degree Centigrade, *see also* Degree Celsius
Degree Celsius (SI unit of temperature), 21-23, 30, 495
Density, 15, 18, 24, 35, 51-55, 60, 98, 118, 122, 124-25
critical, 520
molar, in (I)CVGT, 150-51, 153-57, 159-160, 164-168, 171, 175, 179-181, 188, 190, 193-96, 201-02, 206-208, 212, 232-33, 236, 240, 248, 252, 254, 267, 285, 292
molar (in gas thermometry)
upper limit, 98
of a gas, 321-323, 447
at λ-point, 124-25
liquefied, 520
of air, 353-355, 555-558
of gallium, 329
of liquids, 554
of mercury, 549
variation with pressure and temperature, 550-551
of (thermal) heat flux, 252
of water, 554
of weights of pressure balances, 338-339
Depression, 57-58, 60, 64-65, 67, 89, 125, 129, 237, 310
cryoscopic, 58-59
Design, 77, 94, 98, 129, 160, 164-65, 168-70, 172, 177, 181, 183, 186, 191-92, 197, 201, 205, 207, 233, 240, 263, 270, 274, 278
single cell, 110
multiple cell, 115
Desorption, 85, 284
Deuterium (equilibrium, e-D_2; normal, n-D_2), 55, 71-72, 88, 230, 285
as SRM, 140
heat of spin conversion, 75
properties, 511, 522, 524
spin conversion, 74-76, 257
triple point, 71-72, 74-76, 86, 89
in approximating the ITS-90, 136-37, 139, 141
sealed cell, 47, 98, 117-18, 143-44
Device, *see also* Cell
Device, 27, 37, 44, 47, 50, 77, 86, 95-98, 101, 115-19, 123-28, 135, 136-40, 172, 193, 196, 209, 240, 265-68, 277, 279, 282
Dew
line, 53, 224-25
point, 53, 193, 241, 260, 285, 354
Diaphragm, 193
pressure transducer, 121, 150, 160, 164, 172-74, 176-77, 190, 193-97, 215, 234, 236, 256, 267, 279, 315, 394
zero calibration, 196-97, 237-39, 405, 412-413
Diameter measurements, 340-341, 367
Diatomic, 71, 229
Dielectric constant, *see also* Permittivity, 24, 174-175, 201-205
Dielectric virial coefficient, *see* Coefficient, virial
Dielectric constant gas thermometer (DCGT), *see also* Gas thermometer
Dielectric constant gas thermometer (DCGT), 201
Differential
pressure measurement, 295
measurement by twin pressure balances, 335, 370-374
pressure transducer, 412, 415
at high line pressure, 412-416
used as null detectors, 416-418
thermocouple, 122, 145, 192, 218, 275, 279, 303
Diffusivity, thermal, 69, 79, 82, 93, 97, 115, 187, 213, 256
Dilution, 60, 62, 64, 224, 231, 255, 265, 267, 273, 275, 286
Discontinuity, 39-42, 70-71, 123, 193, 229, 241, 507
Discontinuous, *see* Discontinuity
Dispersion, 39, 42, 72, 102, 113-14, 155, 228, 325
Distillation, 66, 72, 74, 86, 230, 242, 317
Distortion, *see also* Elastic distortion calculations, Pressure distortion coefficient, 344, 355
Distortion, coefficient of piston and cylinder, 337, 344-349, 355-360
of piston and cylinder, 344-349
Distribution coefficient (k0), 65-66, 70, 106, 516

Drift, 75, 86, 91, 93, 103, 105-06, 127, 209, 303, 383
Driving capability, 98, 113
Dynamic technique, 77, 81, 100, 122
Dynamic thermal error, 92
Dynamic viscosity, 266, 348, 554

E
Effective area (of a piston-cylinder unit), 339-344, 346-348, 361-362
  calculations by analytical methods, 339-344, 346-348, 355
  calculated by dimensional measurements, 339-340
  obtained from comparisons, 374, 464-478
  pressure distortions by Finite Element Methods, 358-361
  variation with pressure and temperature, 344, 348-350
Efficiency, 7-9, 76
Elastic, 18, 173, 193, 331
Elastic deformation, *see* Deformation
Elastic distortion
  calculations by analytical methods, 339-344, 346-348, 355
  calculations by Finite Element Methods, 358-361
  of piston and cylinder, 339-344
Elastic distortion, *see also* Elastic distortion calculations, Pressure distortion coefficient
Elastic distortion calculations, 339-344
Elastic distortion coefficient, 344
  by analytical methods, 339-344, 346-348, 355
  by calculation for free deformation piston-cylinder, 342, 345
  by calculation for re-entrant piston-cylinder, 355
  by calculation for controlled clearance piston-cylinder, 355-356
  by Finite Element Methods, 358-361
Elasticity, 162-63, 203, 207, 217, 344
  adiabatic modulus, 207
Electrical noise, 102-04, 108, 399
Electrolysis, 67
Electromagnetic force-balance pressure transducers, *see also* Pressure transducers, 397, 398, 406
Electrostatic charge measurements in pressure balances, 388
Empirical (also semi-), temperature (also -scale), 5-6, 12-13, 16, 18-21, 24-30, 35-38, 44, 46-47, 86, 106, 147, 157, 176, 222-23, 243-44, 247, 249, 253, 298
Energy, 4, 8, 10-15, 19, 49, 59-60, 91-92, 155, 207, 280, 295
  thermal, 18-19, 80-81, 91, 97, 116, 119, 126, 154, 166, 239, 277-78, 282
Engine, 5, 7-8, 330
Enthalpy, 50, 59, 60, 97, 139, 168, 276, 508
Enthalpy (change) of
  evaporation, 80, 83
  fusion, melting (solidification), 45, 53-54, 61, 91-92, 101, 110, 140, 281
    molar, 55, 57, 60, 97
  high (cells), 110, 118-19, 280-82
  spin conversion
    molar, 55, 276
  transition, 124, 130-31
  vaporization, 239
    molar, 55, 158, 221, 249
Entropy, 5, 8, 12, 14-17, 49, 59-62, 124, 222, 295, 412
  molar, 221
EPT-76, *see also* T_{76}, 147, 160, 199, 247, 250, 253, 507, 509, 543, 547
Equation, *see also* Function
Equation, 5, 12, 19, 24, 26, 27, 39, 57, 68, 73, 132, 137-38, 148, 150-51, 154, 166, 168-69, 179, 198-99, 201-02, 212, 217-19, 222-23, 226, 228, 243-46, 253, 263, 282-84, 288
Equilibrium, 3, 5-6, 8, 10-11, 13-17, 44-46, 48-55, 61-66, 69, 74-77, 80-84, 85, 88-93, 97-98, 101-03, 105-06, 145-46, 166, 175, 224, 230-31, 241, 243, 266, 292
  quasi-, 17
Equivalent, non-, 16-17, 97, 243
Error, 25, 27-28, 31, 35, 39, 65, 90, 102, 169, 184-85, 197, 205, 209, 248, 252-55, 296
  absolute
  adsorption, 175
  due to impurities, 59, 66, 86, 158-59, 224, 226-28, 231
    influence quantities
  dynamic thermal, 90, 92
  film reflux, 251-52
  immersion, 99, 135
  in calibration (and due to interpolation), 196-97, 199, 248
  Kapitza resistance
  nonuniqueness, 177

of measurement
random, 24, 29
relative, 205
stationary, 90-91
systematic (nonrandom), 28, 33, 35, 185, 203, 209, 211, 218, 296
thermal, 55, 89, 251
Ethane (C_2H_6), 55, 86
properties, 537
triple point, 98, 514
sealed cell, 98, 130
solid-solid transition, 130
vapor pressure, 243
Ethyl benzoate, 281-82
Eutectic, 56, 69, 522, 524, 527, 529, 530-31, 532-33, 534-40
Evaporation, *see* Vaporization; Vapor; Vapor pressure
Exchange
gas, 77, 122, 126, 197, 271-72, 275, 280
thermal, 14, 77, 97, 119, 235-36, 278, 281
Experimental chamber, 209, 266-67, 270-76, 280, 209, 266-67, 270-76, 280
Extrapolation, 59, 65, 69, 83-86, 106, 125, 146, 157, 176, 217, 218, 231, 248, 280, 362

F

Fabrication, 28, 44, 98, 110, 114, 117, 127, 143, 175, 184, 252, 259, 280, 282, 333
Factor, 15, 64-65, 68, 154, 157, 171, 175, 183, 195, 211, 213, 236-37, 239, 252, 296
gauge, 407-408
integrating, 6, 12
of calibration, 413-414, 432
Factor, *see also* Gauge factor, Calibration factor
$Fe_2O_3 \times (H_2O)_n$, 76
Film, 44, 252, 276, 284, 396
adsorbed, 158, 205
evaporation, 253
reflux of superfluid helium, 251-53
surface, 205
Fin, 82, 98, 141
Finite Element Methods, 346, 359-361
Fixed point, *see also* Pressure fixed points, Temperature fixed points, 438
Fixed point, 21, 23-24, 26-28, 46-47
calibrating, 47
for pressure measurements, 46, 50, 298, 433, 435-436, 511-514
criteria for use, 438
for temperature measurements, 45
boiling point, 6, 20-22, 30, 38, 45, 50, 74-75, 132, 197-98, 221, 226, 243-44, 253, 279, 285, 495, 511, 520
critical point, 50
definition, 26, 28, 46
in sealed cells, 94-123, 125-129
in vapor-pressure thermometry, 221-23, 243-46, 495
liquid-to-liquid transition (^{4}He lambda), 123-25
of the interpolating CVGT, 176-82, 253
of the ITS-90 below 273.16 K, 495
of scales approximating the ITS-90, 37, 136-38
solid-to-solid transition, 130-31
triple point, 50-54, 55-66, 69-76
Fixed points, in condensed ^{4}He and PLTS-2000, 51, 262-63
Flow, *see* Vapor flow
Flow, cryostat, 170, 189, 277-78, 280, 286
Flowrate, 278, 280, 285, 359
molar film, 252
Fluid
buoyancy, 338, 352
normal, 127-29
properties in manometry, 549-551, 554
properties in pressure balances, 323, 348, 353-355, 554-558
super-, 124-29, 246, 250-54, 262, 275-76
Force, balance principle, 364, 397, 409
FPG (Force-balance pressure balance), 364-366
Fraction, 31, 74, 89, 97, 101, 138, 225, 292
frozen, 78
liquid, 56, 58-60, 82, 84, 141, 225, 233
melted, 56, 58, 81-84, 90-92, 97-98, 116, 146
inverse, 58
molar (amount), 60, 67, 128, 158, 214
Fraction of
impurity (amount), 58, 60, 67, 68, 159, 227, 253, 255
solid, 53
solute, 57
vapor, 54
Free deformation piston-cylinder units, 332, 334, 336, 344, 376, 559-560
Freezing, *see also* Solidification
Freezing, plateau, 55, 64-66, 77, 80, 145, 525
Frequency, resonance pressure transducers, 397, 399, 400-402, 426
Frequency of, resonance, *see* Resonance
revolution (in pressure balances), 333

Function, 6, 8, 11-13, 15, 27-29, 33, 38-41, 44, 91-92, 106-08, 132, 150, 154-55, 177-80, 212, 222, 225, 229, 295
correction, 39, 71, 73
deviation (residual), 131, 136, 179-80
ICVGT
linear, 177-78
other, 182
quadratic, 180-81
interpolating, 38-42, 131-32, 176-77, 180-81, 195
model, 37, 108-09
reference, 39, 131, 199-200
stipulated, 37, 176, 179
vapor pressure, 242
virial, 180-81
ITS-90 stipulation, 180-81
Fusion (or solidification), *see also* Enthalpy of, Triple point, 51, 54-56, 59, 79, 132, 276

G

Gallium manometers, 329-330
Gadolinium oxide, *see* Gd_2O_3
Gas, *see also* Vapor
Gas
adsorption on the walls, 179, 184, 201, 216-17
as quantum fluid, 14
as reference material, 85, 137
based reference points
condensed, 75, 77, 80, 88, 90-91, 94-97, 117-21, 224, 229-30, 252, 262, 267, 274, 292
constant R, *see* Constant R, 148, 322, 353, 555
cubic thermal expansion coefficient of, 21, 124
density, *see* Density of a gas
handling system, 85, 86-88, 100, 141, 216, 257, 259-60
ideal, 13, 18, 19
kinetic theory of, 6, 13, 19, 297
leak, 85, 98, 144, 158, 173, 215-17, 237, 256, 259, 301
pressure measurements, 299, 334, 370, 403, 443, 448, 465
properties, 520-540
purge, 119, 273
reference data, 515
solid plug, 265-67
supercritical, 55
thermometer, 147
absolute-mode (primary), 149, 176, 183, 185, 192-93, 203-06, 214
acoustic, 207
constant-volume, 148
dielectric constant, 201
filling density, 171
in the ITS-90, 198, 495
lower accuracy, 193
realizations, 183, 195
refraction index, 205
two-bulb, 169, 192-93
with cryogenic pressure measurement, 193
with reference at 273.16 K, 191
velocity in, 207-12
Gas chromatograph, 213-14
Gauge factor, 407-408
Gas thermometry, *see* Gas thermometer
Gauge pressure, measurement, 294, 351-363, 406, 490
Geometric, 85, 158, 164, 175, 184-85, 188, 209, 216-18, 282, 296
Gd_2O_3, 76, 143
Gibb, 10, 14, 59
Gibb's chemical potential, 230
Gibb's rule, 45-46, 69
Glass, 18, 23-25, 89, 115, 122, 133, 135, 158, 162, 184, 281
Gradient
hydrostatic (aerostatic), 88, 248
of gravity, 321
of temperature (thermal), 3, 5, 78-82, 90, 97, 119, 125, 163, 168, 185, 195, 235-36, 239, 251, 279, 293
Gravimeter
absolute, 320-321
relative, 320-321
Gravity, *see also* Acceleration of gravity
GUM, 67-68, 326

H

Handling, *see* Gas-handling system
He-I, 124, 251
He-II, 124, 251
^{3}He, melting-line thermometry, *see* Helium-3
Head correction, 163, 321-323, 351
Heat, *see* Energy (thermal)
capacity, 55, 77, 80, 82, 89, 91, 108, 115, 129-30, 168, 212, 222, 412
exchange, 14, 77, 97, 119, 235-36, 278, 281
exchanger, 80, 83-84, 95, 112, 122, 238, 248, 412
flux (flow), 5, 16-18, 80-82, 90-92, 125-29, 167, 185-88, 239, 251-52
of melting, *see* Enthalpy of melting

of spin conversion, *see* Enthalpy of spin conversion
of transition, *see* Enthalpy of transition
of vaporization, *see* Enthalpy of vaporization
latent, 8, 61
parasitic, 91
switch, 270, 282
gas-type, 282
mechanical, 271
ON/OFF, 282-83
thermosiphon type, 284
switching ratio, 282-83
transport, 124-126, 285
Heater, 77, 79-82, 98, 102, 104, 119, 124, 127, 145, 267, 270, 277, 284, 286
Heating, 18, 55, 63-64, 79, 81-82, 90-92, 101-04, 122-23, 125-27, 129-30, 184, 249, 255, 397
continuous, 79, 122-23, 126
intermittent (stepwise or by steps), 81, 122
over- or super-, 56, 79-82, 84, 91-92, 99, 101-04, 131, 249, 255
pulse, 90, 102, 104, 106
rate, 81-82
self- (Joule), 103-04, 126
Height, correction for primary and secondary standards, 299, 321, 351
measurements in liquid columns, 299-316
capacitance and gauge blocks, 310-311
capacitance measurements, 300, 311-312
electrical continuity, 300
laser interferometry, 300, 306-310
photocell detectors, 300
telescope cathetometer, 299
ultrasonic interferometry, 300, 313-315
white-light interferometry, 300, 302-306
Helium, (unspecified, i.e. ^{4}He), 37, 100, 119, 124-25, 147, 154-55, 157-59, 162, 173-75, 201, 203-05, 208-14, 222, 236, 239, 245-47, 249-50, 252-53, 270, 274-79, 284-85
absence of triple point, 50
as thermal-exchange gas, 94, 99, 119, 121, 129
bath, 88, 191
in (interpolating) CVGT, 195
isotopes, 14, 50, 150, 154, 160, 165, 175, 180, 231, 233-34, 240, 243, 248-49
Helium-3 (^{3}He), 14, 30, 155, 233, 262-63, 427, 541, 544
as impurity, 125, 129, 158-60, 226, 231
gas thermometry, 148, 155-57, 168-71, 173, 178-81, 189-91, 193, 196, 199, 203
in acoustic gas thermometry, 209
in dielectric constant gas thermometry, 203
in refractive index gas thermometry, 206
in the ITS-90 and PLTS-2000, 268, 495
in the interpolating CVGT definition, 182, 196, 199
melting line, 262-63
purity, 158-60, 226, 231
properties, 14, 262-63, 520
refrigerator, 273-75
Scale, 30, 182, 246-47, 253, 268, 495
sealed cell, 262-63
solid, 14, 262-63
state diagram, 14, 262-63
thermal acoustic oscillations, 249
vapor pressure, 39-40, 147, 156-57, 222, 233, 247-52, 253-55, 261, 495
effect of magnetic fields, 232
impurity effects, 231
scale (equation), 246, 247-48, 541, 544
virials, 148, 151-55, 170-71, 178-80, 181, 189-91, 199
Helium-4 (^{4}He), 14, 20, 30, 155, 233, 262-63, 284, 323, 521, 541, 544
as impurity, 158-60, 226, 231, 226
gas thermometry, 148, 155-57, 167-72, 173, 178-81, 189-91, 195-98, 199, 203
in acoustic gas thermometry, 209
in dielectric constant gas thermometry, 203
in refractive index gas thermometry, 206
in the ITS-90, 38
in the interpolating CVGT definition, 182, 196, 199
λ-transition, 123-25, 127-29, 251
purity, 125, 129, 158-60, 195, 226, 231, 255
properties, 14, 51, 521
refrigerator, 270-82
sealed cell, 123-25, 127-28, 251
Scale, 38, 148, 242-45, 253
state diagram, 51
superfluid, 124-25
thermal acoustic oscillations, 249
vapor pressure, 148, 156-57, 222, 233, 241, 246, 249-55
effect of magnetic fields, 232
scale, 249-53, 495
superfluid helium, 122, 250-53
virials, 148, 150-55, 159, 170-71, 178-80
Henry's Law, 66
High pressure separators, 412, 416, 430
Hotness, 6, 12-13

Humidity, 354, 555-557
of air, 354, 555-557
relative, 354, 555-557
Hydrate, 76, 101, 143-45
Hydrogen, 20, 29-30, 50, 56, 86, 89, 175, 233, 242, 242, 288
isotope, isomer, 33, 71-72, 228
heat switch, 285
Hydrogen (equilibrium, e-H_2), 55, 70-72, 74, 88, 98
as impurity, 63, 66, 73, 158-60, 195, 214, 229
as liquid refrigerant, 274
as solid refrigerant, 276
gas thermometer (and ICVGT), 147, 198
heat of spin conversion, 75
properties, 55, 88, 98, 233, 511-13, 516-19, 522
purity, 66, 86, 226-27
refrigerator, 271, 274
scale, 30, 115-16, 132, 198, 242, 495
slush, 276
spin conversion, 74-76, 85
thermal acoustic oscillations, 249
triple point, 90-92, 98, 113, 115-16
distillation effect, 74
in the ITS-90, 115, 495
in approximating the ITS-90, 136-39, 230
in the interpolating CVGT definition, 180, 197
sealed cell, 98, 113, 117-18
vapor pressure, 72, 132, 198, 230-31, 242, 284, 541-42, 544-45
impurity effects, 227
solid, 241-42, 244, 276, 284
in heat switch, 285
Hydrogen (normal, n-H_2), 74-76
Hydrogen deuteride (HD), 48, 71, 76, 86, 140, 228, 230, 522-24
Hydrostatic, 291-294
conditions, 291-294
temperature gradient (head), 88, 125, 236, 248, 251, 266, 279, 291
compression, 206
Hydrous ferric oxide, *see* $Fe_2O_3 \times (H_2O)_n$
Hysteresis in pressure transducers, 174, 393-395, 576

I

Immersion, 50, 99, 276, 498
Implementation, 24, 30, 33-36, 36-38, 115, 133, 160, 177-80, 183, 186, 196, 204-06, 222, 234, 243, 273, 362
Impure sample, 58-59
Impurity, *see also* Air; Argon; Carbon dioxide; Deuterium; Error; Gas; Helium-3; Helium-4; Hydrogen; Hydrogen deuteride; Methane; Neon; Nitrogen; Oxygen; Triple point; Vapor; Water
Impurity, 47, 57, 60, 62-66, 70, 84-86, 106-07, 124, 127, 129, 138, 149, 157-59, 174, 184, 190, 192, 195, 205, 209, 213-14, 224-25, 228, 232, 252, 255, 284, 317
backflow, 255
chemical, 66-68, 73, 213, 226
isotopic/isomeric, 73, 86, 230
(molar) concentration, 57-58, 60-61, 63-65, 159, 224-25
molar fraction, 60, 68, 158-60, 190, 227
paramagnetic, 75
soluble/insoluble, 64, 225
volatile, 225-26, 232, 285
Impurity effect, 59-60, 62, 64, 84-86, 125, 159, 206, 224, 226-27, 232, 253
Inconsistency, (and inconsistent)
Inflection point, 56, 59, 84, 130-31, 262
Influence parameter, effect, *see* Systematic effect, Correction
Integrating factor, 6, 12
Intercomparison, *see also* Comparison
Intercomparison, 47, 71, 111, 113, 117-18, 121, 131, 228, 246-47, 250, 255
of pressure transducers, 474-476
using pressure fixed points, 438-444
Interface, 79-82, 89-90, 96-98, 116, 125-30, 169, 212, 238, 241, 249-52, 266, 416
Interferometer, 206, 209-10, 212, 300
fringe
Interferometric liquid-column manometers, 306-315
Interpolating, constant-volume gas thermometer, *see* Gas thermometer, Gas thermometry
Interpolating
device, *see* Device, 35, 138, 147
function, 38-39, 40-41, 133
instrument, 27-28, 30, 33-35, 37, 44, 133, 147
Interpolation, 131
IPTS-68, *see also* T68
Irreversible, 5, 11, 17, 48, 454
Isobar (Isobaric), 49-54, 225
Isochore, 53-55, 267
Iso-enthalpic, 49
Isomeric, 85, 228

Isotherm (Isothermal), (and non-), 7, 8, 28, 34, 49, 53-57, 77, 79-80, 91, 97, 111, 122, 156-57, 168, 185-87, 190, 193, 203-05, 212, 238, 267, 279, 295
Isothermal compressibility of mercury, 319-320, 550
Isotope, 14, 70, 140
Isotopic
  amount-of-substance, 70-71
  composition, 31, 41, 47, 55-56, 59, 70-73, 88, 108-09, 113, 118, 228, 315
  correction, 71-74, 118
  distillation, 74, 230, 242
  effect, 50, 72, 107, 228
    in helium, 50, 148, 157, 160, 165, 175, 180, 198
  in hydrogen, 33, 71-72, 89, 175
  in neon, 72-73, 229
  in other gases, 72-74, 214, 229, 242
  in water, 33
  on triple point, 70-71
  impurity, 62, 73, 86
ITS-90, *see also* T_{90}

J

Jacket, 119, 187
  vacuum, 83, 95, 122, 187, 190, 238, 249, 252, 334
Jacket pressure, distortion coefficient, 362
  experimental determination for pressure balances, 361-363
  values for controlled clearance piston-cylinder, 334, 361-363
Jeevanandam result, 229
Joule, 4, 9, 11, 126, 273

K

Kapitza effect, 3, 124, 251-52, 268, 273
KCDB FAQs, 493
KCDB Newsletter, 493
kelvin (SI unit of temperature), 6, 21-22, 23, 26, 30-32, 35, 37, 44, 71, 138, 199, 214, 261, 301
Kelvin
Kelvin, first temperature definition, 8, 19
  Lord, 8, 11, 15, 18-19
  second temperature definition, 9, 19
Key Comparison Database (KCDB), *see also* BIPM-KCDB, 491-493
Key comparison
  related to gas pressure measurements, 464-478
  related to temperature measurements, 479-81, 485-488, 459
Kinetic, 10, 13, 15, 19, 59-60, 297
  temperature, 13
  theory, 6, 13, 19
Knudsen number, 283
Knudsen regime, 283, 448
Krypton (Kr), 142
  as impurity, 70
  isotope, 56, 70, 73, 230
  triple point, 55, 73, 88
    sealed cell, 70, 73, 98
  properties, 55, 88, 98, 233
  vapor pressure, 230, 436
    solid, 242, 284
Kundt's tube, 209

L

Lambda, plate, 125, 275
  transition (point) in ^{4}He, *see* Transition, lambda
Laplace, 208
Layer, 78-79, 175, 280
  absorbed, 175-76
  boundary, 209, 211-12
  liquid, 80, 91-93, 239, 255
  molecule, 85, 158, 174-75, 190, 301
  mono, 158, 175, 205
  multi, 186, 275, 278
  solid, 79-80
  thin, 82, 239
Layering, thermal, 125, 209
Law, 5, 14-18, 22-25, 44, 48, 58, 64-66, 69-71, 92, 106, 147, 150, 205, 225-26, 231, 264, 435
Leak(-age), gas and vacuum, 85, 98, 144, 158, 173, 215-17, 238, 256, 301, etc
  thermal, 59, 83, 91, 126, 128, 259
Level, 6, 12, 15, 18, 19, 31, 33, 35-37, 47, 50, 72, 86, 101-04, 121, 126, 129, 136-38, 156, 159-60, 170, 177, 180, 190, 195, 204, 214, 240, 243, 248, 254, 264, 270-71, 277, 279, 288
LSMFE, 72, 103-04, 106-09, 115
Liang equation, *see also* Thermomolecular pressure difference effect
Liang equation, 450-451
Line pressure, 335, 370-374, 412-418
Linear, 15, 18, 24, 65, 106-09, 116, 146, 150, 162, 166, 170, 177-78, 182, 198, 203-04, 222, 225-26, 231, 243, 250, 256, 304
  non-, 25-26, 153, 178, 193, 195-96, 205, 227, 246, 263
Linear compression modulus, 216

Linear thermal expansion coefficients, 337, 348-349, 391, 549
for piston-cylinder materials, 337, 348-349
of copper
Linearity, 150, 174, 178, 215
Liquefied (and liquefaction), 53, 76, 78, 121
gas properties, 270, 273
Liquid, 23, 46, 49-66, 69, 71-76, 78-82, 84-86, 88-90, 91-102, 107, 119-127, 129-133, 135, 140, 171, 177, 187, 206, 213, 221, 223-26, 229-30, 232-34, 236-39, 241-45, 248-49, 251-53, 255, 262, 264, 266-67, 269-70, 273-82, 284-285, 291
fraction, 56, 58-59, 64, 82, 84, 225, 233
(un-)saturated, 53-54
Liquid-column manometers, 298-330
absolute pressures, 299-301
capacitance, 311-312
capacitance/gauge block, 310-311
differential pressures, 328
gallium, 329-330, 549
laser interferometry, 306-310
mercury, 317-320
oil, 554
reference data, 316, 549-554
small gas pressure, 329-330
ultrasonic, 313-315
very high gas pressure, 327-328
water, 554
white-light interferometry, 302-306
Liquid refrigerant, 269, 274, 277, 285
Liquid-refrigerant cryostats
Liquidus (point and line), 53, 58, 61, 63-65, 67-70, 84, 88, 90, 103-08
Load, corrections, 338
due to masses in gravitational field, 337-339, 352
Long stem, *see* Thermometer
Lorenz-Lorenz law, 205

M

Macroscopic, 5, 7, 13-15, 18
Magnetic (also electro-), 26, 210, 254-55, 262-64, 292
Magnetic field (also electro-), 213, 231-32, 388
effect, 231
Magnetic field influence in piston-cylinder, 388
on pressure transducers at cryogenic temperatures, 422-423
on pressure transducers at room temperatures, 422-426
Magnetic thermometry, 147, 247-49, 255, 263
Manometers, 215, 236, 298-330, 379-392, 549-554
mercury, 298-330, 379
see also Barometers
see also Liquid-Column manometers
Manometric fluids, 317, 329, 549-551, 554
Mass, 337-339
materials, 338-339
measurements, 338-339, 352, 369, 392, 559-560
molar, 110, 208, 284, 322
Material, aluminum, 124, 211, 213, 217, 303
beryllium copper, 196, 265, 426
bulk, 14, 19, 27, 86, 89, 125, 251-55
coin silver, 194
copper, 38, 55, 77-79, 84, 91-93, 96-98, 110, 112-14, 117-19, 121-23, 125-29, 161-63, 175, 184-85, 189-97, 199, 205-06, 213, 238, 252, 264-66, 280, 303
glass, 18, 23-25, 89, 115, 123, 133, 135, 158, 162, 184, 281
gold, 110, 163, 175, 184-85, 189-91, 276
indium, 96, 98, 110, 124, 180, 184-05, 196, 272, 512
sapphire, 190, 194, 197, 427
silver, 110, 117, 497
stainless steel, 91-93, 98, 110-14, 117, 123-26, 129, 166, 187, 190-92, 213, 278, 281-83, 301
Invar, 304
VAR, 114
Materials, *see also* Gases
Materials, for piston and cylinders (pressure balances), 558
Mathematical, 27, 30, 33, 44, 66, 132, 136, 177, 217, 243, 354
Maxwell, equation, 5, 8, 13-14
Mean free path, 282-83, 448
Measurement
Measurement accuracy, definition, 576
liquid column manometers, 297, 316, 325-327, 391, 553-554
pressure balances, 297, 368-370, 392, 559-560
pressure transducers, 396, 407-408
Measurement precision, definition, 576-77
Measurement procedure, 26, 145, 219, 260, 336, 577-78
Measurement uncertainty, *see* Uncertainty
Melted fraction, 56-58, 81-84, 90-92, 97-98, 146, 439
Melting, *see also* Fusion

Melting
curve, 30, 59, 91, 108
line of ^{3}He thermometry, 51, 261-68, 436
plateau, 56-59, 64-66, 80-86, 89-91, 100, 104-09, 116-18, 123, 282, 440
range definition, 59
Mercury (Hg), 23, 55, 115, 279
boiling point, 551
compressibility, 550
density, 317-320, 391, 549
density versus temperature and pressure, 550
for approximating the ITS-90, 136-37
for volume measurements, 185, 187, 209, 212, 218
freezing point, 551
manometer, 191-97, 238, 295
melting line, 436, 438, 445
surface tension, 551
triple point, 38-39, 73, 88, 112, 133, 135, 281-82, 551
thermal expansion, 549
vapor pressure, 550-551
Methane (CH_4), 418
as impurity, 517
for approximating the ITS-90, 136-38, 139
properties, 55, 88, 98, 233, 511, 532, 546
spin conversion, 76, 85
triple point and s.s.t., 76, 110, 117, 121, 130
as pressure fixed point, 418
sealed cell, *see* triple point and s.s.t.
vapor pressure, 243, 245
solid, 76, 242
Method
dynamic, 97, 119, 122
calorimetric, 123
Mise en pratique, 23, 30-38, 71, 137, 199
Mixture, 23, 45-48, 56-59, 61, 69-70, 85, 224-25, 524
artificial certified, 73, 118
binary, 64, 66, 69
ideal, 61, 224
diluted, 54, 57, 63, 66, 224
isotopic or isomer, 74, 107, 225, 242
Model, *see* Mathematical
Molar, *see* all entries with "molar"
Mole (mol), definition, 22
Molecule (also molecular), 5, 10, 13-15, 19, 50, 56, 59, 74, 85-88, 149-50, 154-61, 168-75, 178-81, 187-88, 195, 204-05, 229, 236-38, 242, 248-49, 252, 254-55, 282-83, 297
Molecule, monolayer, 158, 175, 205
Monte Carlo method, 72, 326, 368, 552
Moving bodies, fast, 16-17
Mutual recognition arrangement (MRA), *see* full text in Appendix G, 463-493, 561-573

N

Negative, 14, 16, 19, 62, 69, 102, 106, 197, 225, 239, 262, 266, 291
Nitrogen (N_2), 50, 191, 323
as adsorbed gas, 158
as impurity, 62-63, 66, 73, 195, 214, 226-28, 517
as liquid refrigerant, 99-100, 119-21, 133, 171, 274, 281
as solid refrigerant, 240, 275-76, 279
properties, 55, 88, 98, 233, 511, 513, 527, 542, 545-46
triple point and s.s.t., 110, 119, 130
in approximating the ITS-90, 136-37, 139
sealed cell, 117
vapor pressure, 121, 244
impurity effects, 227
magnetic field effects, 232
solid, 241-43, 284
in heat switch, 285
Noise, electrical, *see* Electrical noise
Non equilibrium, 455
Non linearity, 263, 406
Non repeatability of pressure transducers, *see also* Pressure transducers, 393, 576, 578
Non uniqueness, 132-34, 136-37, 512-13
Type 1, 133
Type 2, 133
Null detector, *see also* Pressure transducers, 412-418

O

Official (also un-), 29, 32, 40, 47, 73, 137, 180, 189, 199, 243, 495
Oil
lubricated piston-cylinder units, 328, 334
manometers, 309
properties, 554
Open cell, 80
Operating p_j values (for controlled clearance piston-cylinder units), 362
Ordering, 19, 103, 262
Ortho, 74-76, 230
to para (and the reverse) conversion in H2, 74

Osmosis, 61
Overheating, *see* Heating, over-
Oxygen (O_2), 50
  Ar impurity, 66, 70, 131, 138
  as catalyst, 75
  as impurity, 62-63, 66, 226-27
  isotopic, 72, 74
  properties, 55, 88, 98, 233
  purity, 63, 226
  triple point and s.s.t., 92, 110, 113, 115, 130, 276
    as pressure fixed point, 418
    in the ITS-90, 30, 115, 117-18
    in approximating the ITS-90, 136-138, 139
    sealed cell, 113, 116
  vapor pressure, 237, 244
    impurity effects, 227-28
    magnetic field effects, 232
    solid, 284

P

Para, 74-76, 230
  to ortho converison in D2, 74
Paramagnetic, 26, 75, 232, 247
Parameter, 5, ott-16, 19-20, 24-27, 37, 40, 44, 46-47, 55, 82, 90, 93, 97, 98, 101, 107-10, 112, 115, 149, 164, 169, 174, 177-81, 183, 186, 194-95, 199, 203-4, 213, 222, 232, 234, 238, 245-47, 263, 282-83, 299
  physical, 150, 224
  technical, 160-61, 176-77, 180, 234
pascal (SI unit for pressure), 288-289
Passive
  shield, 122, 280
  temperature control, 281
Passive thermostat, 118, 280-81
Peritectic, 69, 527-31
Peritectic point, *see also* Oxygen, impurities in
Permeability, 158, 162, 283
Permittivity, 201-02
  of vacuum, 202, 206
  virial coefficient, 206
Phase, 8, 10-11, 46, 57, 59-63, 80, 82, 88, 91, 130, 155, 229-30, 262-63
  boundary, 129
  diagram, 48, 53, 59, 61, 63, 69, 261-62
  gas, 48, 54, 175
  liquid, 46, 50, 53, 55, 60-64, 66, 71, 77, 82, 84, 86, 90-93, 99, 124, 130, 221, 224-27, 230, 233, 248, 267, 277, 285
  solid, 46, 50, 53, 56, 60-64, 66, 71, 78-80, 82, 84, 90-91, 98, 124, 130, 225, 241, 266-67, 285
  superfluid, 124, 262, 275
  transition, 48-49, 50, 54, 59, 97, 119, 123, 247, 261, 281-82, 298
  vapor, 46, 50, 53, 82, 86, 130, 224, 227, 229, 232, 251
Phase transition, *see also* Lambda point; Triple point; Vapor pressure
Phonon
Physical properties of manometric fluids, 14, 252, 317-320, 348, 353-355, 443-445, 511-514, 515-540, 549-551, 554, 555-558
Piezoresistive effects, 407-408
Piston fall rate measurements, 293, 333, 336, 359-360, 362, 375
Piston-Cylinder, 294
  controlled clearance type, 332, 334, 361-363
  distortion of (*see also* Elastic distortion calculations), 344-348, 355-361
  effective area, 339-344
  FPG type, 364-366
  free deformation (simple) type, 332, 334
  ideal, 331-333
  materials, 558
  mixed type, 352
  large diameters, 364-368
  main piston-cylinder types, 332, 334-336
  of pressure balance, 294, 331-392
  principle of operation, 294
Plank gas, 5
Plateau, *see* Melting plateau or Freezing plateau
Plateau
  fit, 102-03, 106-09, 116
  slope, 106
Platform, 125, 127-28
Point, boiling, *see* Boiling point
  critical, *see* Critical point
  dew, *see* Dew point
  eutecitc, *see* Eutectic
  fusion, *see* Fusion
  inflection, *see* Inflection point
  liquidus, *see* Liquidus point
  peritectic, *see* Peritectic
  reference, *see* Reference point
  solidus, *see* Solidus point
  triple, *see* Triple point
Poisson coefficient of materials, 333, 558
Polarizability, 24, 175, 204, 206
  molar, 201, 203, 206

Positive
Pot, 126, 173, 274
Potential, 60, 154-155, 199, 263
  energy, 14, 59-60, 155
  chemical, 74, 230
  thermodynamic, 60-61
Pre-melting, 81, 89-90, 145, 525, 536
Pressure
  built-in device, 163, 172, 193, 195
  bulb, 77
  critical, 50, 53, 236, 520
  difference, 160-162, 169, 236, 251, 265, 279, 297
  aerostatic/hydrostatic gradient, *see* Aerostatic, Hydrostatic
  line, 49-51, 97, 124, 164, 169, 203, 221, 233, 262, 372
  partial, 225, 285
  scale, 30, 39, 95, 132, 148, 179-80, 222-28, 241-43, 247-57, 261, 268, 295-298, 435-436
  tube (as opposite to capillary tube), 96, 173, 204, 234, 238, 249, 435
  units, 288-289
Pressure balances
  absolute pressure measurements, 294, 297-298, 336-351
  gauge pressure measurements, 294, 297, 351-363
  differential pressure measurements, 294, 370
  differential pressure measurements at high line pressure, 370-374
  large diameters, 364-368
  non rotating, *see also* FPG (Force-balance pressure balance), 364-366
Pressure distortion coefficient, by FEM calculations, 346, 359-361
  see also Elastic distortion calculations, 344-348, 355-359
Pressure distortion coefficient of piston-cylinder units, *see also* Elastic distortion coefficent, 344-348
Pressure fixed points
Pressure fixed points, *see also* Pressure scale, 433-445
Pressure measurement, 132, 149, 157, 168, 171, 174, 179, 188, 193, 230, 234, 236, 239-241, 244, 247, 261, 264-65
  bulb level, 177
Pressure transducers, 393-432
  capacitance type, 397, 403-406, 426-427
  for cryogenic environments, 418-429
  electromagnetic-force balance type, 397-398
  LVDT type, 408
  optical type, 397
  piezoresistive type, 396, 408, 413
  resonant oscillator type, 411, 426
  semiconductor type, 408
  variable reluctance type, 425
  vibrating element or structure type, 397, 399
  see also Pressure transfer standards
Pressure transfer standards
  absolute pressure measurements, 395-398, 403-406
  atmospheric pressure measurements, 398-403
  cryogenic environment, 418-429
  differential pressure measurements, 412-416
  differential pressure measurements at high line pressures, 411, 416-418
  gauge pressure measurements, 406-412
  using pressure fixed points, 438-443
Primary, 12, 24-26, 31-32, 192, 197, 203-06, 263
Procedures for
  static calibration of a pressure transducer, 430-432
  static calibration of a pressure transducer in cryogenic conditions, 418-421
  use of triple points as pressure transfer standards, 438-443
  performing differential pressure measurements, 416-418
Propane (C_3H_8), 56
  properties, 55, 514, 539
  triple point and s.s.t., 98, 130
    sealed cell, 130
  vapor pressure, 243
Protium, 86, 114, 230
Pump, turbomolecular, 87, 143, 324
Purity, 27, 44-47, 54-55, 66-67, 73, 76-78, 82-86, 94-95, 108, 118, 128, 140, 148-150, 157-58, 162, 174, 177-79, 184, 188-90, 213, 224, 234, 239-43, 264, 317
  nominal, 68, 73, 84, 118, 128
Purification, 86, 189, 216, 259, 317

Q

Quality, 33-37, 47, 73, 77, 85-87, 97, 106-110, 115, 123, 130, 136-39, 146, 195, 240, 263, 275, 294
  certified, 138, 144

Quantum, 14-15, 74, 154, 229
fluid, 14
gas, 19
mechanics, 14, 59, 390
state, 14
Quartz transducers for pressure measurements, 397-403, 411, 413-414
Quasi-spherical, 210-13
Quasi-static process, 11, 17

R
Random, (and non-), 24, 29, 108, 199-203, 209-10, 218, 264, 315
Range, 1-3, 6, 12, 24, 27-28, 32-44, 54, 57-59, 64-66, 69-74, 77, 84-87, 91, 97-98, 109-12, 114-15, 122-24, 127, 131-133, 136-139, 147-48, 151-52, 156-57, 161, 166-67, 172, 179-80, 182-84, 189-93, 195-201, 203-05, 209-14, 223, 230-31, 234-41, 243-48, 252-55, 261-68, 271, 276, 282, 285
Raoult law, 58, 64-65, 69, 106, 225, 231
Rate, 6, 19, 55-56, 65, 75, 78-82, 100, 119, 128, 187, 237, 251-52, 277, 280, 285, 293
Rate of, fall of piston (in pressure balance), 293, 333, 336, 359-360, 362, 375
rotation of a piston (in pressure balance), 333, 368, 382, 385-386
Reactive substances, 85-86
Real, area, 184
gas, 54-55, 77, 147, 150, 177, 201, 208, 224
surface, 175, 184
Realization, 23, 28, 31-39, 45-48, 50, 53-54, 57, 66, 71-78, 81-85, 90, 94-96, 100-01, 109, 115, 119-23, 126-28, 130-33, 135-38, 141, 147-50, 161, 179, 183, 189-93, 195-99, 201, 221-23, 226, 234, 242-48, 250-55, 264, 276-79, 281-82
Recommendation
CCT, 36, 214, 244-45, 325
CIPM on measurement uncertainty, *see also* GUM, 521-522
on terminology, *see* Appendix H and VIM, 575-579
Recovery time (to thermal equilibrium), 82, 90, 93
Reentrant piston-cylinder units, 332, 351-352, 355-356
Reference
composition
isotopic, 71, 73
condition, 148, 161, 192, 198, 261-67
(fixed) point, 23, 45-46, 50, 56, 59, 69, 76, 84-86, 94, 110, 123, 125, 131
function, 495
ITS-90, 32, 39, 100, 131, 199-200
level, 321-324, 337-338, 351
material, *see* Standard reference material
point, *see* Reference temperature
pressure, *see also* Vacuum reference pressure; Residual pressure, 197, 261, 294, 301, 304, 324-325, 337, 350, 553
temperature, 9, 17, 20, 24, 26-28, 149, 154, 163, 183, 185, 189, 191-92, 196, 204, 206, 208, 228
value, 466
of a comparison, 471-473, 475-478, 480, 482-483, 485-488, 563-569, 572
volume (in gas thermometry), 187
Reference data, 515-540, 549-560
for liquid column manometers, 549-554
for pressure balances, 555-560
for thermometry, 495, 511, 520, 541
Reference point, *see* Fixed point, Reference pressure
Reflux, *see also* Film reflux, 251-53
Refractive index gas thermometer (RIGT), *see* Gas thermometer
Refractive index, 200, 206, 304
correction, 305-306, 390-391
Refrigerant, 53, 79, 83-84, 100, 119, 125, 192, 238-39, 277
bath, *see* Bath
liquid, 50, 100, 269, 274
slush, 135, 264, 266-67, 276
solid, 240, 276
Refrigeration, 54, 83, 124, 127, 183, 253, 263, 270, 273, 276, 280-81
enthalpy, 276
Refrigerator, *see also* Cryocooler
Refrigerator, 77-78, 123, 133-34, 170, 173, 265-67, 269-79, 285
Relative, 70-71, 91, 101, 148, 156, 162, 168-69, 171, 175, 191, 196, 201-08, 214, 229, 236, 264-65, 294
Relative molecular mass of some gases, 520-522, 524, 526-528, 530, 532, 534-537, 539
Relativistic, 17-18
Repeatability, 393, 576, 578

Reproducibility, 101, 136, 418, 435, 443, 577-578
Requirements for pressure balance optimum operations, 291, 331-333, 342
  electrostatic forces, 388-389
  fluid selection, 334, 520-540
  leaks, 333
  magnetization, 388-389
  mounting and levelling, 332-333
  piston fall rate, 333
  rotational frequency of piston and masses, 333
Residual gas analyser, *see* RGA
Residual pressure, for absolute measurements in pressure balances, 337, 350-351
Residual pressure, *see also* Vacuum reference pressure, 350-351
Resonance, 209-13, 222, 390
Resonant frequency, 397, 403, 421
Resolution, 579
Resonant pressure transducers, *see also* Pressure transducers, 397, 399-403, 411, 426
Resonant cavity, 209, 394
Resonant gas thermometer, *see also* Acoustic gas thermometer
Resonator, 193, 210-13, 249, 267, 284
  cylindrical, 209, 211
  quasi-spherical, 210-11, 213
  spherical, 209, 210-12
Reversible, 7-8, 17, 118, 433
Revolution frequency, *see also* Requirements for pressure balance optimum operations, 333, 379
RGA, 87-88, 143
Rotational decay, *see also* Requirements for pressure balance optimum operations, 333
Rotational influence on effective area of a pressure balance, *see also* Rotational decay, 380, 385

S

Sample, 21, 33, 47, 51-59, 66, 71-73, 75-85, 87-92, 94-102, 104-08, 110-12, 117-19, 133, 140, 162, 190, 195, 225, 228, 232, 240, 264, 267-68, 317
Sample, impure, 58-59
Saturated liquid, 53-54, 245
Saturation line, 53, 221
Scale approximation, *see* Temperature scale; Uncertainty
Scale, *see also* Pressure scale; Temperature scale; Vapor pressure scale
Scale, alternative, 31, 36-37, 136-38, 253
  approximation, *see* Approximation, of a scale
  conversion, 25
  definition, 26, 28, 32-33, 44, 180, 223, 246-47, 249, 255, 298
  realization, 28, 30-31, 72, 138, 223, 227
Seal, 95-96, 98-100, 111, 142-44, 184, 196, 270, 272, 286, 332
  indium, 96, 98, 110, 124, 180, 184-85, 196, 273
  permanent, 86, 94-99, 109, 142, 174, 239
  pinch, 96, 98, 100, 110, 112, 117, 142-44, 239
Sealed cell, *see also* Triple point
Sealed cell, *see* Cell, sealed
Sealed cell
  for capsule thermometers, *see* Cell, for capsule thermometers
  for long stem thermometers, *see* Cell, for long stem thermometers
  weighing, 101, 140, 143-44, 185
Sealing, 94-98, 100-01, 109-10, 117, 139, 143-44, 184, 189, 192, 194, 216, 239-40, 257, 265, 267, 273
Secondary, *see also* Calibration, Pressure transfer standard, Pressure scale
Secondary fixed point, 36, 140, 244, 437-438
Segregation, 62, 64
Self-regulating shields, 122, 280, 282
Sensitivity, 66-70, 73, 157, 160, 171-73, 179, 181, 192, 195, 216, 236-37, 242-43, 253, 255, 264-68, 296, 579
Separator, *see also* Null detectors
Series expansion systems, 297, 405-406
Shield, 77, 96, 122, 271, 275, 277-80, 287
  adiabatic, 101-02, 192, 271-72
  high-enthalpy, 280-81
  isothermal, 111, 122, 185, 190, 279
  radiation, 186
Shift, of zero signal of a pressure transducer, 413, 416-418
Similarity method, 344, 355, 363
Simple type of a piston-cylinder unit, *see also* free deformation piston-cylinder units, 332, 334, 336
Siu equation, *see also* Thermomolecular pressure difference effect, 454-455
SLAP, 71
Slope, 53, 61-63, 66, 69, 71-72, 103, 106-08, 123, 193, 241, 266, 516-19

Slope of, isotopic T vs x(HD) relationship for e-H_2, 71
isotopic T vs $x(^{22}Ne)$ relationship for Ne, 73
liquidus line (initial), 61, 67-68
solidus line (initial), 61
Smoothness, 28, 255
Soldering, 98, 117, 143, 184, 428
Soldering, flux, 99, 143
Solid, 46, 49-51, 53-54, 56, 59-65, 69, 71, 76, 78-80, 82, 84-85, 88-91, 97-98, 107, 115, 123-24, 205, 223, 233, 240-45, 252, 256, 262, 265-68, 276, 285, 291
insoluble, 57, 59-66
soluble, 58-66
Solidification, *see also* Fusion; Triple point, 51, 54-56, 78-79, 276
Solidified gas properties
Solidus, line, 59, 61, 63-65, 69-70
Solidus, point, 53, 58, 108
Solid-to-solid transition (s.s.t., sst), 50, 56, 110, 115, 123, 130-31, 137-39, 242
first order, 130
second order, 131
Solute, 57, 60, 62, 66, 69
Solution, 57-61, 72, 224
Solution, ideal, 74
Solvent, 57, 61-63, 66-68, 86-87, 225
Sound velocity, *see* Velocity of sound, 208, 209, 313-315
Space, 12, 18-19, 25, 95, 118, 120, 174, 185-87, 192, 197, 225-26, 233, 237-39, 248, 269, 276, 280
Specific heat, 5, 16, 19, 25, 45, 55-57, 97, 124, 140, 222, 295, 508
Spin, composition, 3, 14, 19, 74-76, 85, 257
conversion, 75
equilibrium, 55, 74-76, 88, 98, 230, 257
nuclear, 74, 76, 221-22, 264
Spline function, 28, 40-42
SRM, 37, 47-48, 56, 139
Stability (and in-), 16, 83, 91, 97, 116, 118, 133, 172-74, 184, 187, 190, 193, 204-05, 237, 264, 271, 280, 286-87, 579
in time, 46, 48, 86, 103
long term, 94, 110, 133, 138
Stainless steel, *see* Material, stainless steel
Stainless steel, 304L, 143
Standard Mean Ocean Water (SMOW), 31
Standard uncertainty, 39, 42, 71-72, 101, 129
Standard reference materials (for gases), *see* SRM, 46-48, 85, 139-40, 244
Standards, 30, 32-34, 38, 44, 46, 96, 132, 138, 176, 183, 195, 214, 242, 246, 153, 263, 268, 495
State, *see also* Equilibrium, 8, 11, 13-15, 17, 19, 27, 45-49, 149, 156, 201, 221, 261
State
metastable, 55, 74, 130, 540
of the art, 26, 31, 33-35, 44, 77, 101, 140, 160, 204, 297
Static, *see* Stationary
Stationary, 13, 90, 237, 427
Statistic (also statistical), 6, 13-14, 107, 109, 155, 454
Bose-Einstein, 14
Fermi-Dirac, 14
Maxwell–Boltzmann, 14
Stipulated, *see* Stipulation
Stipulation, 23, 25, 37, 152, 176-77, 179-82, 196, 217, 243
Storage, 50, 85, 87, 94, 97, 121, 138, 140, 224, 251, 270, 275, 277
Strain, 184, 315
free, 28
Stress tensor, 291-292
Subcooling, 55-56, 59, 79-80, 277, 279, 284, 525
Sublimation, 49, 55, 123, 276, 513
Subrange, 33, 131-34, 250
Substance, 1, 4, 7-9, 18-19, 23, 27, 44, 46, 49, 50, 54-56, 85, 148-50, 157, 221-24, 232, 265
active, 157
amount of, *see* Amount
impure, 54
pure, 45, 47, 50, 55-59, 69, 221-22, 237, 433
reactive, 86
Superconducting, 37, 47, 123-24, 180, 217, 241, 419
Supercritical, 55
Superfluid, 124-25, 127, 129, 246, 250-54, 262, 275-76, 426
transition (in ^{4}He), *see* Transition, lambda
Surface, geometric versus real, 85, 224
Surface, tension of fluids, 224, 325, 551, 554
Surface effects, *see* Thermomolecular pressure difference effect, 459-462
Systematic, effect (or error), 28-29, 33-34, 44, 66-67, 70, 122, 155, 185, 211, 296

T
T_{48}, 21, 509, 515, 526, 530, 534-35, 537
T_{58}, 30, 222, 246-47, 249-50, 253, 497, 544, 547
T_{62}, 30, 222, 231, 246-47, 253, 268, 497, 544, 547
T_{68}, 244, 246, 319, 496-97, 507-08, 512, 515, 522, 524, 526-28, 530, 532, 536, 539, 543, 546, 548
T_{76}, 507, 509, 543-44, 547
T_{90}, 28, 32, 38-42, 71, 136, 191, 200, 231, 244, 246-48, 250, 253, 260, 282, 318, 395, 507-09, 511-12, 514-15, 520-22, 541-47
T_{2000}, 32, 40
T_{2006}, 39-40, 247-48, 255
Takaishi-Sensui equation, *see also* Thermomolecular pressure difference effect, 451-452, 457
Technical Annex to the mise en pratique of the kelvin, 23, 30, 32-33, 71-72
Technique, 26, 36, 44, 57, 72, 76-77, 80-81, 94, 100, 108-09, 110, 114, 123, 157, 194, 196-97, 201, 208-09, 211-12, 239, 246, 261, 263-64, 276, 279-80
  calorimetric, 84
  equilibrium, 77, 80, 82
Temperature, absolute, *see* Absolute, temperature
  coefficient, 172, 315
    of gauge factor, 408
    of materials, 163, 304, 319, 333, 348-349, 549, 554, 558
  concept, 5
  critical, *see* Critical, temperature
  definition, *see* Definition, of temperature
    first Lord Kelvin definition, *see* Kelvin
    second Lord Kelvin definition, *see* Kelvin
  depression, *see* Depression
  distribution, 99, 157, 164-68, 170, 176, 186-88, 190, 192, 216-19, 233, 239, 249-51, 259-60, 265, 440
  empirical (semi), *see* Empirical and semi-empirical
  equilibrium, *see* Equilibrium
  generator (T-Gen), 96, 111, 116, 118-19
  gradient, *see* Gradient, of temperature
    hydrostatic, aerostatic
  jump (Kapitza), *see* Kapitza effect
  kinetic, *see* Kinetic, temperature
  measurements
    on liquid-column manometers, 318-319, 391
    on pressure balances, 349, 392
  negative, *see* Negative
  nonequilibrium, 16-17
  of piston and cylinder, 349, 392
  room, 2, 19, 51-55, 74-76, 80-82, 85, 94-100, 118-20, 121-23, 125, 132, 135, 141-45, 149-51, 157-65, 170-74, 183-93, 196, 206, 209-10, 215-18, 232-35, 237-42, 249, 255-60, 265-67, 270-73, 276-77, 282-85
  Scale, *see* Scale
  statistical mechanics, *see* Statistic
  thermodynamic, 5-6, 9, 12, 13-16, 20-22, 24-28, 30-35, 38-40, 44, 131, 147-48, 176-77, 183-84, 189, 199, 203, 207-12, 221-22, 246-47, 249-50, 253-55, 261-64, 268
Temperature control
  passive, *see* Passive, temperature control
  self-regulating, *see* Self-regulating shields
  via cryogen bath pressure control, 279
  via flowrate control, 280
Temperature effect in gauge factor of pressure transducers, 408
Temperature measurement, key comparisons, 479
Temperature scale, international (ITS), 23, 27-40, 44, 55, 71-74, 88, 98, 100, 109-10, 113-16, 123, 130-38, 147-48, 152, 170, 176-82, 189-90, 196-200, 203, 211, 216-17, 222, 230, 244-48, 250, 253, 261-63, 268, 271, 276-77, 495
  IPTS-68 (T_{68}), *see* T_{68}
  ITS-90 (T_{90}), *see* T_{90}
  PLTS-2000 (T_{2000}), *see* T_{2000}
Tension, *see* Surface tension, 224, 325, 551, 554
Terminology, 326-327, 429-430, 575-579
T-Gen, *see* Temperature, T-gen
Thermal acoustic oscillations, 249, 259
Thermal conductivity, 55, 78-80, 93, 98, 115-16, 119, 124-29, 145, 166, 184-86, 212, 239, 249, 259, 266, 282-85, 287
  of superfluid helium, 124
Thermal expansion coefficients
  of materials, 163, 304, 319, 333, 348-349, 549, 554, 558

liquids used in manometry, 304, 319, 549, 554
materials in pressure balances, 333, 558
Thermal
analysis, 70, 529
anchoring, 119, 167, 171, 177, 190, 196, 238, 272-73, 277, 419
contact, 8, 79-84, 91, 94, 97-99, 115-17, 130, 141, 275-77, 280
dry, 277, 282
movable or removable, 275, 277, 282
wetted, 80
cycling, 98, 173-74, 193, 205, 267, 287, 427
diffusivity, 69, 79, 82, 93, 97, 115, 187, 213, 256
drift, *see* Drift
dynamic error, *see* Dynamic thermal error
equilibrium, *see* Equilibrium
error, 55, 89
exchange, *see* Exchange, thermal and Helium
expansion, 21, 23, 51, 124, 161-63, 184, 190-91, 196, 199, 205, 209-12, 216-17, 262, 301
mass, 78, 96, 98, 141
problems, *see* Error, Thermal exchange
properties, 323
resistance (R_{cs}), 82, 84, 90, 97, 103, 126, 129
static (stationary) error, *see* Stationary
tie-down, *see also* Thermal, contact, 83, 100, 145, 238
sliding, movable, 259, 287
transient, 79, 90, 168, 237
Thermally decoupled, 126, 145
Thermocouple, 23, 36-37, 186, 190, 303
differential, 121, 145, 192, 218, 275, 279
Thermodynamics, 5-6, 10-12, 15-17, 48, 454
Thermodynamic
potential, 59-61
state, *see* State
Thermometer, 18, 23-28, 34, 44, 77-80, 160, 278
absolute, *see* Absolute thermometer
calibration, 27, 34, 46, 94, 103-04, 115, 135, 183, 189, 218, 221, 243, 263, 268
capsule, 96, 98-100, 110, 113, 122, 135, 141
dial, 25
external, 98, 117
gas (also interpolating), *see also* Gas, thermometer, 20, 24, 35, 133, 147
^{3}He melting line, *see* Helium-3, melting line
internal, 80-81, 110
liquid-in-glass (or glass), 18, 23, 25
long stem, 88, 99-100, 119, 121-22, 133, 135, 141
nonuniqueness, *see* Non uniqueness, 28, 39, 134
other type, 28, 36-37, 46, 138, 147, 231, 255, 264
platinum resistance, 27-30, 46, 131-32, 134, 147, 176, 244, 271
primary, 24, 31-32, 203-04, 206, 263
radiation, 23, 37
RhFe, 129, 197
self heating, 103-04, 126
stability, *see* Thermometer, calibration
thermoelectric, *see* Thermocouple
thermodynamic, 24, 35, 199, 222, 255
vapor-pressure, 24, 33, 132-33, 204, 232-35, 237-43, 252, 273
volume, 175, 212, 234
Thermometry, absolute, *see* Absolute thermometer
Thermostatics, 6, 17
Thermomolecular pressure difference effect, *see also* Transpiration effect
Thermomolecular pressure difference effect, 157, 160-61, 168-73, 178-81, 187-88, 195, 204, 216-18, 236-38, 248-49, 254-55, 259-60, 297, 447-462
Thickness, 91, 93, 158, 162, 166, 175, 184, 205, 239, 427
Tie-down, *see* Thermal tie-down
Time
arrow, 5, 17
constant, 79, 90, 92-93, 102, 106, 115, 130, 235, 284
recovery, 82, 90, 93
TPIE, 70-71, 228-30
Traceability, 135, 577
Transducers, *see also* Pressure transducers, Pressure transfer standards, 393
Transfer standards, *see also* Pressure transfer standards, 395, 406
Transient, 79, 90, 102, 168, 187, 224, 237
Transition, *see* Phase, transition
Transition
in ^{3}He melting line, 262-68
A, 262-63
B, 261-63
first order, *see* Solid-to-solid transition (s.s.t.)

liquid-liquid, *see* Lambda, transition
martensitic, 130
Néel, 261
regime, 283, 388
second order, *see* Solid-to-solid transition (s.s.t.)
solid-liquid-vapor, *see* Triple point
solid-solid, 46, 110, 129-30
superconducting, *see* Superconducting
Transpiration effect, 447
calculations, 448-455
experimental measurements, 456-461
theories, 461-462
Triple point, (or line), 6, 30, 45-49, 50, 53, 55, 76, 223
argon, 83, 100, 113, 116, 119, 136-38, 141-42, 230, 235, 241-42, 279, 418, 434, 436-437, 439-441, 530
carbon dioxide, 119, 123, 136, 241-42, 436, 443, 511, 536
chemical-physical problems, 50, 85
constant, 71
cryoscopic constant, *see* Kryoscopic, constant
deuterium, 74-75, 86, 136-38, 141-42
definition, 59, 84
ethane, 55, 86, 98
hydrogen, 74-75, 113, 115, 116, 136-38, 141-42, 180, 198, 228, 241, 436, 522
in interpolating CVGT definition, 180-82
krypton, 141-42, 230, 436, 534
melting range definition, *see* Melting, range definition, 59
mercury, 38, 73, 115, 133, 133-36, 281-82, 436, 551
methane, 76, 136-38, 436, 532
neon, 73, 93, 113, 115, 116, 137, 141-42, 180, 191, 198, 228, 230, 241-42, 436, 526
(none), 53, 54
nitrogen, 136-37, 141-42, 241-42, 276, 436, 527
of eutectic mixtures, 69
of impure substance, 54, 58
of peritectic mixtures, 69
of pure substance, 50, 56-58
oxygen, 113, 116, 129-30, 136-37, 141-42, 276, 436, 528
propane, 55, 86, 98
pure substance, 56
sealed cell, 94
use in the ITS-90, 495
used in pressure measurements, 435-437
water, 21-24, 31-33, 44, 72, 115, 123, 133, 135, 141-42, 206-13, 436
xenon, 133, 136, 141-42, 230, 436, 535
Tube, pressure, 96, 173, 204, 234, 238, 249, 435
capillary, 126, 164, 168, 185-86, 283-84, 455
isothermal, 186
temperature distribution, 165-67, 187
capillary volume
by mercury filling, 209, 218
by volumetric expansion, 187
manometric, 195
Tube, *see also* Vapor pressure
Turbomolecular pump, *see* Pump, turbomolecular
Two-phase, 48-50, 53, 61-62, 229, 434

U

Ultrasonic interferometer manometers, 300, 313-315
Uncertainty, *see also* GUM, 521-522, 577-578
Uncertainty, 21, 24, 27, 31-34, 35-39, 42, 47, 57, 66, 72, 84, 91, 130, 132, 140, 149, 157, 161-62, 164, 168-69, 173-74, 178-81, 185-87, 190-95, 200-04, 207-08, 211-13, 222, 236-43, 248, 255
absolute pressure measurements, 297, 316
expanded, 67-68, 73, 104, 106, 115, 148, 198, 214, 578
for transfer standards, 396, 403, 407, 432
for pressure transducers, 393-395
liquid column manometers
absolute pressure measurements, 316, 325, 391, 553-554
gauge pressure measurements, 325, 553-554
related to density of fluid, 317-320, 549-551
related to gravity acceleration, 320-321
related to height, 316
related to temperature, 319, 550
of reference value, 568, 572
pressure balances
related to absolute pressure measurements, 297, 368-370, 559
related to gauge pressure measurements, 297, 368-370, 392, 559-560
related to differential pressure measurements, 373
related to density, 348, 353-355
related to effective area, 339-344

related to elastic distortion coefficient, 344-348, 355-363
related to gravity acceleration, 320-321, 339
related to mass, 338-339
related to reference pressure, 324-325, 350-351
related to temperature, 349
related to thermal expansion coefficients, 348-349
recommendation for calculations, 325-327, 368-370
standard, 34, 39, 42, 67-68, 71, 72, 101, 118, 122-23, 129, 139-40, 151, 153-57, 159, 162-65, 170-71, 179, 181, 185, 191, 197, 205-06, 209-11, 226, 254, 577
Uncertainty in
temperature
scale approximations, 135-37
weighing of cell, 101

V

Vacuum, 22, 126, 138, 166, 184-87, 197, 202, 213, 270-79, 282-84
clean, 143
high, 86-87, 143, 145, 185, 271, 275
jacketing, 83, 95, 186, 190, 238, 249, 252, 259
measurements, 271, 294, 297, 324-325
pressure, *see also* Residual pressure, Vacuum reference pressure
rough, 275
static, 143, 174, 237
Vacuum reference pressure, 337, 350-351, 478
Valve, 85, 94, 121, 164, 191, 224, 238-40, 277, 279
bypass, 173, 189, 194, 237, 240
constant volume, 188, 190, 192, 236
cryogenic, 173, 194, 204, 241, 265-67
ball-and-edge
high-pressure, 100, 240
room temperature, 81
sealing, 95
throttling, 204
van Laar equation, 57
van't Hoff model, 59-61, 70
Vapor, 6
column, 77, 80, 82, 238
definition, 52
flow, 233, 280
phase, 46, 50, 53, 82, 86, 129, 224, 227-29, 232, 251, 436
pressure
boundary in gas thermometer, 156
data, 541
equations, 243, 541
impurity effects, 226-28
in heat switch, 284-85
in ITS-90, 495
in magnetic fields, 231-32
isotopic effect (VPIE), 71, 228-30
of mercury, 550
saturated line, 224
scale, 242
thermometry, 24-26, 30, 33, 37-40, 44, 48-54, 69-72, 76-83, 86, 95-97, 123-24, 130-133, 137, 147-48, 156, 159-61, 173, 179-80, 187, 196, 204, 221, 261-63, 268
solid equilibria, 241
space (as opposite to dead volume), 95, 121, 225-26, 233, 237-39, 248
temperature distribution, 233, 239, 249-51, 259-60, 265, 440
Vaporization, *see* Enthalpy of
Velocity of sound
in gases, 200, 214
in mercury, 313-315
Vibration, 88, 271
VIM-International Vocabulary of Metrology, 34, 326, 429-30, 575
Virial (coefficient), *see* Coefficient of virial
Viscosity, *see* Dynamic viscosity, 348, 361, 387, 450, 551, 554
Viscous regime, 388, 448
Volume, 7-12, 21, 51-54, 80, 110, 126, 141-44
at room temperature, 80, 96, 234, 239, 257
ballast, 95-96, 119, 122, 141-43, 190, 232, 240, 257-59
bulb, 157, 160-63, 174, 183-85, 188, 191-93, 215-18, 232-35, 258
cell, 97, 240, 248
constant, 21, 24, 35, 148, 160
contraction, 162
dead, *see* Dead volume
zero, *see* Dead volume, zero
guard, 162, 194, 216
molar, 71, 131, 158, 202, 229
working, 209

W

Wall-gas interaction, *see* Coefficient of washing
Water (H_2O), 76
as an impurity, 195, 214
in liquid-column manometers, 328-330, 554
triple point, 72, 436, 444

vapor pressure, 72, 284
Wavelenght, (wave), 14, 209
Wave
high-frequency, 209
low-frequency, 300
micro, 193, 210-13, 267
Weber-Schmidt equation, 168-69, 189, 449-450, 459-460
Weight, 333-334
buoyancy effects, 352
calibration, 338-339, 369-370
density of air effect, 352-355, 555-558
density of materials effect, 338-339
Welding, 96, 98-100, 110, 117, 142-43, 429
Well, 60, 80, 82-84, 87, 99-100, 110-12, 116-17, 119-21, 126, 135, 142, 145, 155, 187, 234, 273, 276, 286-87
White light interferometers, 302-306
Work, 5-7, 10-11, 17
mechanical, 7-8, 18

X

Xenon (Xe)
triple point, 136
in approximating the ITS-90
properties, 55-56, 70, 73, 88, 98, 133, 233, 436, 444, 511, 514, 535, 547
vapor pressure, 547

Y

Young modulus, 333, 360, 558

Z

Zero, in temperature definitions, 495
Zero clearance jacket pressure, *see also* Jacket pressure, 361-363
Zero shift
differential pressure transducer at high line pressure, 411, 416-418
pressure transducer due to temperature, 405, 408, 424
Zhokhovskii equation, 245-47, 250, 437, 544-47
Zone melting, 86